frontiers | Research Topics

The interconnection between the tumor microenvironment and immunotherapy in brain tumors

Edited by
Quan Cheng, Wen Cheng, Junxia Zhang and Longbo Zhang

Published in
Frontiers in Immunology
Frontiers in Oncology

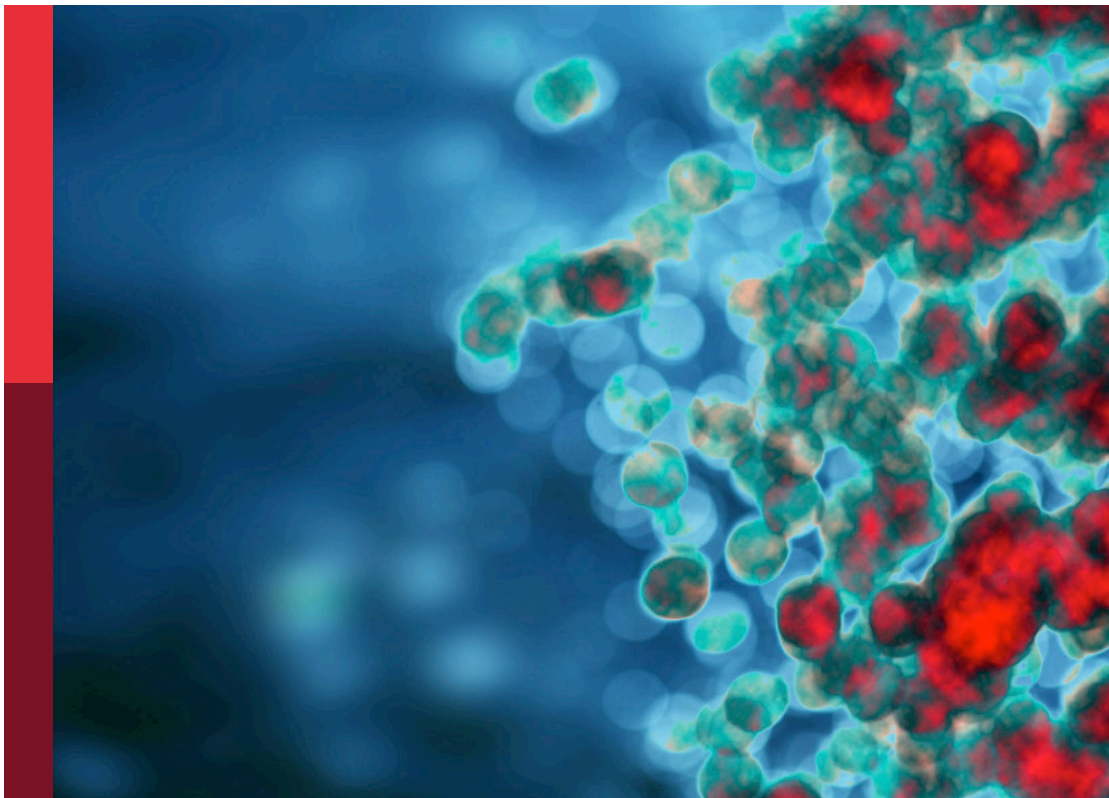

FRONTIERS EBOOK COPYRIGHT STATEMENT

The copyright in the text of individual articles in this ebook is the property of their respective authors or their respective institutions or funders. The copyright in graphics and images within each article may be subject to copyright of other parties. In both cases this is subject to a license granted to Frontiers.

The compilation of articles constituting this ebook is the property of Frontiers.

Each article within this ebook, and the ebook itself, are published under the most recent version of the Creative Commons CC-BY licence. The version current at the date of publication of this ebook is CC-BY 4.0. If the CC-BY licence is updated, the licence granted by Frontiers is automatically updated to the new version.

When exercising any right under the CC-BY licence, Frontiers must be attributed as the original publisher of the article or ebook, as applicable.

Authors have the responsibility of ensuring that any graphics or other materials which are the property of others may be included in the CC-BY licence, but this should be checked before relying on the CC-BY licence to reproduce those materials. Any copyright notices relating to those materials must be complied with.

Copyright and source acknowledgement notices may not be removed and must be displayed in any copy, derivative work or partial copy which includes the elements in question.

All copyright, and all rights therein, are protected by national and international copyright laws. The above represents a summary only. For further information please read Frontiers' Conditions for Website Use and Copyright Statement, and the applicable CC-BY licence.

ISSN 1664-8714
ISBN 978-2-8325-2565-4
DOI 10.3389/978-2-8325-2565-4

About Frontiers

Frontiers is more than just an open access publisher of scholarly articles: it is a pioneering approach to the world of academia, radically improving the way scholarly research is managed. The grand vision of Frontiers is a world where all people have an equal opportunity to seek, share and generate knowledge. Frontiers provides immediate and permanent online open access to all its publications, but this alone is not enough to realize our grand goals.

Frontiers journal series

The Frontiers journal series is a multi-tier and interdisciplinary set of open-access, online journals, promising a paradigm shift from the current review, selection and dissemination processes in academic publishing. All Frontiers journals are driven by researchers for researchers; therefore, they constitute a service to the scholarly community. At the same time, the *Frontiers journal series* operates on a revolutionary invention, the tiered publishing system, initially addressing specific communities of scholars, and gradually climbing up to broader public understanding, thus serving the interests of the lay society, too.

Dedication to quality

Each Frontiers article is a landmark of the highest quality, thanks to genuinely collaborative interactions between authors and review editors, who include some of the world's best academicians. Research must be certified by peers before entering a stream of knowledge that may eventually reach the public - and shape society; therefore, Frontiers only applies the most rigorous and unbiased reviews. Frontiers revolutionizes research publishing by freely delivering the most outstanding research, evaluated with no bias from both the academic and social point of view. By applying the most advanced information technologies, Frontiers is catapulting scholarly publishing into a new generation.

What are Frontiers Research Topics?

Frontiers Research Topics are very popular trademarks of the *Frontiers journals series*: they are collections of at least ten articles, all centered on a particular subject. With their unique mix of varied contributions from Original Research to Review Articles, Frontiers Research Topics unify the most influential researchers, the latest key findings and historical advances in a hot research area.

Find out more on how to host your own Frontiers Research Topic or contribute to one as an author by contacting the Frontiers editorial office: frontiersin.org/about/contact

The interconnection between the tumor microenvironment and immunotherapy in brain tumors

Topic editors

Quan Cheng — Central South University, China
Wen Cheng — The First Affiliated Hospital of China Medical University, China
Junxia Zhang — Nanjing Medical University, China
Longbo Zhang — Yale University, United States

Citation

Cheng, Q., Cheng, W., Zhang, J., Zhang, L., eds. (2023). *The interconnection between the tumor microenvironment and immunotherapy in brain tumors*. Lausanne: Frontiers Media SA. doi: 10.3389/978-2-8325-2565-4

Table of contents

06 Editorial: The interconnection between the tumor microenvironment and immunotherapy in brain tumors
Chunrun Qu, Longbo Zhang, Wen Cheng, Quan Cheng and Junxia Zhang

10 A Systematic Review of the Tumor-Infiltrating CD8+ T-Cells/PD-L1 Axis in High-Grade Glial Tumors: Toward Personalized Immuno-Oncology
Mahdi Abdoli Shadbad, Zahra Asadzadeh, Negar Hosseinkhani, Afshin Derakhshani, Nazila Alizadeh, Oronzo Brunetti, Nicola Silvestris and Behzad Baradaran

23 *Breaking Bad*: Autophagy Tweaks the Interplay Between Glioma and the Tumor Immune Microenvironment
Yuxiang Fan, Yubo Wang, Jian Zhang, Xuechao Dong, Pu Gao, Kai Liu, Chengyuan Ma and Gang Zhao

42 NK Cell-Based Immunotherapy and Therapeutic Perspective in Gliomas
Changqing Pan, You Zhai, Guanzhang Li, Tao Jiang and Wei Zhang

54 Integrin Alpha-2 as a Potential Prognostic and Predictive Biomarker for Patients With Lower-Grade Glioma
Li Lin, Kai Huang, Zewei Tu, Xingen Zhu, Jingying Li, Kunjian Lei, Min Luo, Peng Wang, Chuandong Gong, Xiaoyan Long and Lei Wu

70 HOTAIR Up-Regulation Activates NF-κB to Induce Immunoescape in Gliomas
Yunfei Wang, Kaikai Yi, Xing Liu, Yanli Tan, Weili Jin, Yansheng Li, Junhu Zhou, Hongjun Wang and Chunsheng Kang

83 Galectin-9/TIM-3 as a Key Regulator of Immune Response in Gliomas With Chromosome 1p/19q Codeletion
Guanzhang Li, Ruoyu Huang, Wenhua Fan, Di Wang, Fan Wu, Fan Zeng, Mingchen Yu, You Zhai, Yuanhao Chang, Changqing Pan, Tao Jiang, Wei Yan, Hongjun Wang and Wei Zhang

95 PTRF/Cavin-1 as a Novel RNA-Binding Protein Expedites the NF-κB/PD-L1 Axis by Stabilizing lncRNA NEAT1, Contributing to Tumorigenesis and Immune Evasion in Glioblastoma
Kaikai Yi, Xiaoteng Cui, Xing Liu, Yunfei Wang, Jixing Zhao, Shixue Yang, Can Xu, Eryan Yang, Menglin Xiao, Biao Hong, Chuan Fang, Chunsheng Kang, Yanli Tan and Qixue Wang

110 DNA Damage Repair in Brain Tumor Immunotherapy
Shihong Zhao, Boya Xu, Wenbin Ma, Hao Chen, Chuanlu Jiang, Jinquan Cai and Xiangqi Meng

126 Current Understanding of Exosomal MicroRNAs in Glioma Immune Regulation and Therapeutic Responses
Jinwu Peng, Qiuju Liang, Zhijie Xu, Yuan Cai, Bi Peng, Jianbo Li, Wenqin Zhang, Fanhua Kang, Qianhui Hong, Yuanliang Yan and Mingyu Zhang

143 The Non-N^6-Methyladenosine Epitranscriptome Patterns and Characteristics of Tumor Microenvironment Infiltration and Mesenchymal Transition in Glioblastoma
Jianye Xu, Zijie Gao, Kaining Liu, Yang Fan, Zongpu Zhang, Hao Xue, Xing Guo, Ping Zhang, Lin Deng, Shaobo Wang, Huizhi Wang, Qingtong Wang, Rongrong Zhao and Gang Li

164 Tumor Immune Microenvironment and Immunotherapy in Brain Metastasis From Non-Small Cell Lung Cancer
Yuchang Wang, Rui Chen, Yue Wa, Shikuan Ding, Yijian Yang, Junbo Liao, Lei Tong and Gelei Xiao

176 Diverse Macrophages Constituted the Glioma Microenvironment and Influenced by PTEN Status
Fengqi Zhou, Qinyu Shi, Xiao Fan, Ruilei Yu, Zhiqiang Wu, Binbin Wang, Wei Tian, Tianfu Yu, Minhong Pan, Yongping You and Yingyi Wang

186 Matrix Remodeling-Associated Protein 8 as a Novel Indicator Contributing to Glioma Immune Response by Regulating Ferroptosis
Zhijie Xu, Xi Chen, Liying Song, Fang Yuan and Yuanliang Yan

202 The AlkB Family: Potential Prognostic Biomarkers and Therapeutic Targets in Glioblastoma
Songshan Feng, Zhijie Xu, Jinwu Peng and Mingyu Zhang

215 ITGA5 Is a Novel Oncogenic Biomarker and Correlates With Tumor Immune Microenvironment in Gliomas
Shuyu Li, Nan Zhang, Shiyang Liu, Hao Zhang, Jiajing Liu, Yiwei Qi, Qi Zhang and Xingrui Li

230 The Role of m5C-Related lncRNAs in Predicting Overall Prognosis and Regulating the Lower Grade Glioma Microenvironment
Hongshu Zhou, Ming Meng, Zeyu Wang, Hao Zhang, Liting Yang, Chuntao Li and Liyang Zhang

245 Pan-Cancer Analysis Shows That ALKBH5 Is a Potential Prognostic and Immunotherapeutic Biomarker for Multiple Cancer Types Including Gliomas
Cheng Wei, Bo Wang, Dazhao Peng, Xiaoyang Zhang, Zesheng Li, Lin Luo, Yingjie He, Hao Liang, Xuezhi Du, Shenghui Li, Shu Zhang, Zhenyu Zhang, Lei Han and Jianning Zhang

268 Characterising Distinct Migratory Profiles of Infiltrating T-Cell Subsets in Human Glioblastoma
Paris M. Kollis, Lisa M. Ebert, John Toubia, Cameron R. Bastow, Rebecca J. Ormsby, Santosh I. Poonnoose, Sakthi Lenin, Melinda N. Tea, Stuart M. Pitson, Guillermo A. Gomez, Michael P. Brown and Tessa Gargett

287 Immune Gene Signatures and Immunotypes in Immune Microenvironment Are Associated With Glioma Prognose
Xiang-Xu Wang, Haiyan Cao, Yulong Zhai, Shi-Zhou Deng, Min Chao, Yaqin Hu, Yueyang Mou, Shaochun Guo, Wenjian Zhao, Chen Li, Yang Jiao, Guolian Xue, Liying Han, Hong-Mei Zhang and Liang Wang

301 Roles of the m^{6}A Modification of RNA in the Glioblastoma Microenvironment as Revealed by Single-Cell Analyses
Feng Yuan, Xiangming Cai, Zixiang Cong, Yingshuai Wang, Yuanming Geng, Yiliyaer Aili, Chaonan Du, Junhao Zhu, Jin Yang, Chao Tang, Aifeng Zhang, Sheng Zhao and Chiyuan Ma

318 Recurrence- and Malignant Progression-Associated Biomarkers in Low-Grade Gliomas and Their Roles in Immunotherapy
Chubei Teng, Yongwei Zhu, Yueshuo Li, Luohuan Dai, Zhouyang Pan, Siyi Wanggou and Xuejun Li

336 The Identification of Necroptosis-Related Subtypes, the Construction of a Prognostic Model, and the Characterization of the Tumor Microenvironment in Gliomas
Yueyang Ba, Jiahao Su, Shuangqi Gao, Zhi Liao, Zhimin Wu, Chengan Cao, Chaofeng Liang, Jin Gong and Ying Guo

355 PD-L2 Serves as a Potential Prognostic Biomarker That Correlates With Immune Infiltration and May Predict Therapeutic Sensitivity in Lower-Grade Gliomas
Qijun Xie, Xianlong Huang, Wu Huang and Fang Liu

369 Characterization of Fatty Acid Metabolism-Related Genes Landscape for Predicting Prognosis and Aiding Immunotherapy in Glioma Patients
Feng Jiang, Fei Luo, Ni Zeng, Yan Mao, Xinfang Tang, Jimei Wang, Yifang Hu and Chuyan Wu

386 Identification of the novel prognostic biomarker, MLLT11, reveals its relationship with immune checkpoint markers in glioma
Long Chen, Zujian Xiong, Hongyu Zhao, Chubei Teng, Hongwei Liu, Qi Huang, Siyi Wanggou and Xuejun Li

401 Pan-cancer analysis of ASB3 and the potential clinical implications for immune microenvironment of glioblastoma multiforme
Long Mu, Zhibin Han, Shengkun Yu, Aowen Wang, Dongjiang Chen, Sijia Kong, Yifei Gu, Lin Xu, Axiang Liu, Ruohan Sun and Yu Long

frontiers | Frontiers in Oncology

TYPE Editorial
PUBLISHED 13 March 2023
DOI 10.3389/fonc.2023.1147883

Check for updates

OPEN ACCESS

EDITED BY
Darya Alizadeh,
City of Hope, United States

REVIEWED BY
Soma Sengupta,
University of Cincinnati, United States
Crismita Dmello,
Northwestern University, United States

*CORRESPONDENCE
Junxia Zhang
zjx232@njmu.edu.cn
Wen Cheng
cmu071207@163.com
Longbo Zhang
longbo.zhang@yale.edu
Quan Cheng
chengquan@csu.edu.cn

SPECIALTY SECTION
This article was submitted to Cancer Immunity and Immunotherapy, a section of the journal Frontiers in Oncology

RECEIVED 19 January 2023
ACCEPTED 03 March 2023
PUBLISHED 13 March 2023

CITATION
Qu C, Zhang L, Cheng W, Cheng Q and Zhang J (2023) Editorial: The interconnection between the tumor microenvironment and immunotherapy in brain tumors.
Front. Oncol. 13:1147883.
doi: 10.3389/fonc.2023.1147883

COPYRIGHT
© 2023 Qu, Zhang, Cheng, Cheng and Zhang. This is an open-access article distributed under the terms of the Creative Commons Attribution License (CC BY). The use, distribution or reproduction in other forums is permitted, provided the original author(s) and the copyright owner(s) are credited and that the original publication in this journal is cited, in accordance with accepted academic practice. No use, distribution or reproduction is permitted which does not comply with these terms.

Editorial: The interconnection between the tumor microenvironment and immunotherapy in brain tumors

Chunrun Qu[1,2,3], Longbo Zhang[4,5]*, Wen Cheng[6]*, Quan Cheng[1,3]* and Junxia Zhang[7]*

[1]Department of Neurosurgery, Xiangya Hospital, Central South University, Changsha, Hunan, China, [2]Xiangya School of Medicine, Central South University, Changsha, Hunan, China, [3]National Clinical Research Center for Geriatric Disorders, Xiangya Hospital, Central South University, Changsha, Hunan, China, [4]Department of Neurosurgery, Yale University School of Medicine, New Haven, CT, United States, [5]Department of Cellular & Molecular Physiology, Yale University School of Medicine, New Haven, CT, United States, [6]Department of Neurosurgery, Shengjing Hospital of China Medical University, Shenyang, China, [7]Department of Neurosurgery, The First Affiliated Hospital of Nanjing Medical University, Nanjing, Jiangsu, China

KEYWORDS

immunity, brain tumor, tumor microenevironment, immunity checkpoint, tumor infiltrating cell

Editorial on the Research Topic
The interconnection between the tumor microenvironment and immunotherapy in brain tumors

The tumor microenvironment (TME) is an essential part of cancer and plays a key role in regulating tumor growth, progression, migration, and response to therapy in several types of cancer, including brain tumors. The TME is a complex network of cancer cells, stromal cells, and tumor-infiltrating immune cells (TIICs), in which tumor cells communicate not only with each other but also with stromal cells and immune cells. A deep understanding of the interactions between tumour cells and the TME will help us to predict patient prognosis, reduce drug resistance and develop new therapies. Immunotherapy, represented by immune checkpoint (ICP) blockade and chimeric antigen receptor (CAR)-T-cell therapy, has revolutionized cancer treatment (1, 2). However, few clinical trials have demonstrated the beneficial effects of immunotherapy on survival in brain tumor patients.

Gliomas are the most common malignant primary brain tumours in adults and are characterized by recurrence, poor prognosis, and treatment resistance. The main reason for the poor prognosis is the high heterogeneity of tumor cells and their immunosuppressive TME. TIICs are currently thought to be abundant in the immunosuppressive TME of brain tumours and are associated with prognosis. Several key roles for TIICs in brain tumours have also been reported. Current conventional therapies have failed to improve the clinical prognosis, and innovative therapeutic approaches are needed.

The Research Topic consists of 26 manuscripts focusing on various aspects related to "The Interconnection Between the Tumor Microenvironment and Immunotherapy in Brain Tumors". We have summarized what is of particular interest in these manuscripts,

including the following sections: (i) TIIcs in the TME; (ii) the relationship between ICPs and immunotherapy; and (iii) modification of RNA.

TIICs in TME

TIICs play an important role in promoting or inhibiting tumour growth. The study of TIICs has been instrumental in improving the understanding of the TME in glioma and improving the effectiveness of immunotherapy.

Macrophages are an important population of immune cells in the TME of gliomas that have immune functions and can be involved in tumour development through the release of a variety of cytokines and growth factors. Activated macrophages are usually divided into M1 macrophages, which have a predominantly antitumour response, and M2 macrophages, which promote tumour cell development and metastasis. Zhou et al. found that M2 macrophages were abundant in malignant gliomas and were associated with poor prognosis. PTEN is the most often lost tumour suppressor in primary gliomas. They also found that high PTEN expression was associated with prolonged survival in glioma patients and polarization of macrophages. This suggests that the detection of changes in PTEN status will play an important role in predicting a patient's response to immunotherapy.

Autophagy is a key regulatory point for the interaction between glioma and the TME. Autophagy enhances the drug resistance and invasiveness of glioma cells and differentiates major macrophages to the M2 phenotype, inhibiting their phagocytosis and promoting glioma progression. Recent findings on glioma and the TME presented by Fan et al. from the perspective of autophagy may enhance the understanding of the TME and stimulate more applicable and effective strategies for targeting the TME while using autophagy to synergistically fight cancer.

Although specific markers of T cell exhaustion and activation have been studied in glioblastoma (GBM), the migration receptors they require in homing remain unknown. The expression profiles of integrin and chemokine receptors in endogenous GBM-infiltrating T cells were described and validated by Kollis et al. through single-cell RNA sequencing. This has very positive implications for improving the efficacy of T-cell immunotherapy.

Natural killer (NK) cells are a possible next research hotspot. Pan et al. summarized the characteristics of NK cell therapy in glioma treatment. The low incidence of cytokine release syndrome in patients with CAR-NK therapy significantly compensates for the disadvantages of CAR-T cell therapy. CAR-NK cells cause very little graft-versus-host disease. In addition, CAR-NK cells can kill their targets in a CAR-independent manner. They also summarized ways in which the effectiveness of the treatment may be further improved.

MXRA8 is thought to be associated with iron death and is a novel prognostic indicator. Xu et al. found that MXRA8 was significantly associated with various infiltrating immune cells, and played a key role in ferroptosis and the TME in gliomas, promoting tumour progression.

ICPs

Evolving tumour immune evasion mechanisms play an important role in the development and progression of tumours. One of the main mechanisms is related to the immune checkpoint pathway. Immune checkpoint molecules regulate the immune system and maintain its stability by stimulating and suppressing immune responses in physiological situations, but they may also be involved in cancer development. Programmed death protein 1 (PD-1) and cytotoxic T lymphocyte-associated protein 4 are two extremely important immune checkpoint proteins.

PD-1 is expressed on many immune cells and interacts with its ligands, programmed death-ligand (PD-L)1 and PD-L2, upon binding to suppress immune responses. The antitumour immune responses mediated by CD8+ T cells are suppressed by PD-L1. The tumor-infiltrating CD8+ T cell/PD-L1 axis is significant for GBM therapy, but its exact role is not clear. According to a meta-analysis by Shadbad et al., patients with untreated GBM who have PD-L1 overexpression may have a poor prognosis. Increased tumour-infiltrating CD8+ T cells in tumour tissue of patients receiving anticancer therapy may be linked to a worse prognosis because radiotherapy/chemotherapy can upregulate PD-1 expression in tumour-infiltrating CD8+ T cells as well as induce immune cells in a state of exhaustion. lncRNAs are thought to play a critical role in regulating tumour immunity, influencing the activation and function of T cells and macrophages. Polymerase 1 and transcript release factor (PTRF) expression is increased in mesenchymal phenotype GBM (3). According to Yi et al., PTRF interacts with the long noncoding RNA (lncRNA) NEAT1 to stabilize its mRNA, and through NEAT1, PTRF inhibits the expression of UBXN1, which in turn enhances NF-κB activity and, through this pathway, PD-L1 expression. Ultimately, PTRF promotes GBM immune evasion by affecting PD1-PD-L1 interactions. The PTRF-NEAT1-PD-L1 axis may be a novel immunotherapeutic target in GBM. In various cancer types, the lncRNA HOTAIR is highly expressed and linked to tumor metastasis. HOTAIR expression is also elevated in the mesenchymal phenotype of GBM (4). Wang et al. reported that HOTAIR was an activator of the NF-κB pathway lncRNA, its levels positively correlated with PD-L1 levels, and its apparent upregulation promoted inflammatory signaling and immune escape in glioma cells.

PD-L2 is also a PD-1 ligand that can mediate cancer cell immune escape. Xie et al. showed that PD-L2 was overexpressed in glioma tissue and was associated with poor prognosis and immune cell infiltration. In addition, PD-L2 may be a promising predictive biomarker for selecting the best individualized treatment strategy.

Modification of RNA

The study of RNA epitranscriptomics is at the forefront of the field of specific chemical modifications of biomolecules. RNA can have multiple chemical modifications that affect gene expression to varying degrees. Their importance in cancer is gradually being

discovered, opening up new possibilities for cancer therapy. Important internal RNA modifications include 5-methylcytosine (m5C), N6-methyladenosine (m6A), 7-methylguanosine, N1-methyladenosine and others (5).

The most widespread internal modification of RNA is the methylation of adenosine at the 6-position to give m6A. Proteins involved in this process are m6A "writers", m6A "erasers" and m6A "readers". The "writers" are responsible for the installation of m6A, including METTL3 and METTL14, among others (6). The "erasers" have demethylation capabilities and are responsible for the deletion of m6A, including ALKBH5 and FTO, among others (7, 8). "Readers" regulate m6A expression, including YTHDF1 and YTHDF2 (9, 10). m6A modification has been shown to affect the progression of many cancers; for example, in breast cancer, METTL3, HBXIP and let-7g miRNAs form a positive feedback loop to promote cell proliferation (11). However, the relationship between m6A modifications and the TME in GBM is not fully understood at present. The relationship between m6A regulators and other factors was examined by Yuan et al. using bioinformatics and statistical methods. They discovered that at the single-cell level, m6A alterations promote GBM cancer cells to be in a stem cell state and, through ICPs and the GALECTIN signaling pathway, support the development of an immunosuppressive TME. They also identified two m6A-ICP expression patterns (high m6A/low ICP and low m6A/high ICP). ALKBH5 is a m6A "eraser" located in the nucleus, and overexpression of ALKBH5 results in low levels of m6A. Gene Ontology and Kyoto Encyclopedia of Genes and Genomes enrichment analysis by Wei et al. showed that ALKBH5 is associated with inflammatory, metabolic and immune processes in gliomas. ALKBH5 expression also affects sensitivity to immunotherapy and is associated with ICP expression. The ALKB family in GBM underwent thorough analysis by Feng et al. They found that the expression levels of ALKBH2 and ALKBH8 were significantly increased in GBM compared to normal tissues and that greater expression was associated with higher levels of mRNA processing and poorer patient prognosis. This study also showed a close link between DNA damage repair in GBM and the biological activity of members of the ALKB family.

Based on 32 regulatory genes, Xu et al. comprehensively assessed 539 non-m6A RNA modification patterns in GBM and connected these changes to TME invasion and mesenchymal conversion traits. They ultimately identified three patterns of non-m6A RNA modifications associated with different clinical features and biological pathways. This investigation uncovered possible connections between non-m6A RNA modification regulators and clinical characteristics, TME status, and GBM subtypes and clarified their therapeutic potential.

Although the prognosis for patients with lower-grade glioma (LGG) is relatively good, patients frequently relapse and tend to progress to higher grade gliomas, ultimately leading to treatment failure. Eight lncRNA m5C-associated prognostic signatures were established and validated by Zhou et al. for predicting prognosis and treatment response in LGG patients. This provides a promising target for further research.

Prospective

This editorial summarizes the key findings of the Research Topic "*The Interconnection Between the Tumor Microenvironment and Immunotherapy in Brain Tumors*". Here, we present an

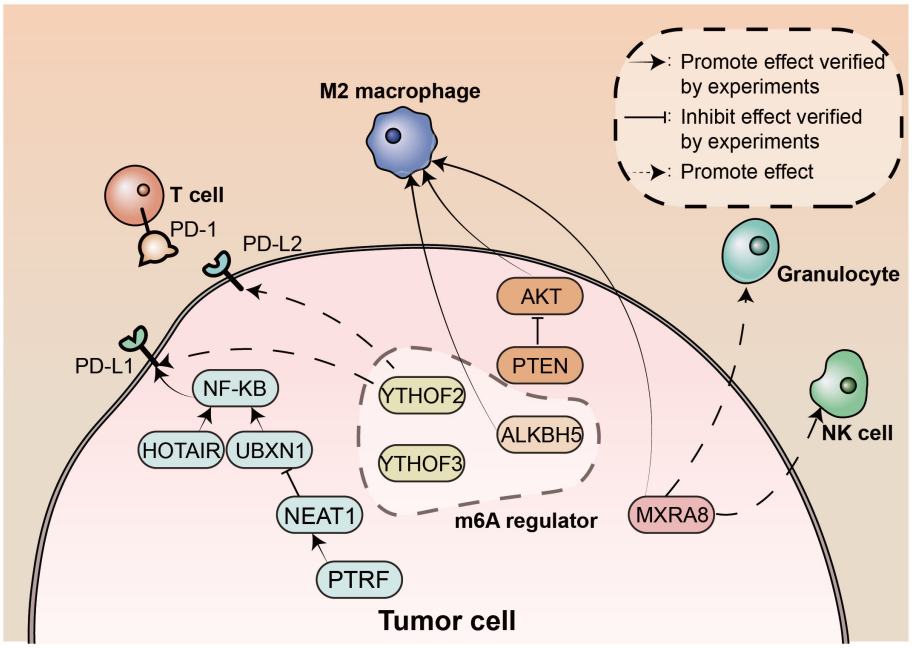

FIGURE 1
The landscape of tumor microenvironment in brain tumors. m6A, N6-methyladenosine; NK, natural killer; PD-1, Programmed death protein 1; PD-L1, programmed death-ligand 1; PD-L2, programmed death-ligand 2; PTRF, polymerase 1 and transcript release factor.

understanding of the interactions between TIICs in the TME of brain tumours, the potential prognostic factors in the TME that predict patient survival, and the impact of specific components of the TME on the efficacy of immunotherapy or other oncological treatments. Important findings are summarised in Figure 1. Immunotherapy has shown great potential in a variety of cancers, and we hope that this Research Topic will contribute to an increased awareness and understanding of the link between the tumour microenvironment and immunotherapy in brain tumours, providing an opportunity to improve treatments and improve patient prognosis.

Author contributions

All authors listed have made a substantial, direct, and intellectual contribution to the work and approved it for publication.

Conflict of interest

The authors declare that the research was conducted in the absence of any commercial or financial relationships that could be construed as a potential conflict of interest.

Publisher's note

All claims expressed in this article are solely those of the authors and do not necessarily represent those of their affiliated organizations, or those of the publisher, the editors and the reviewers. Any product that may be evaluated in this article, or claim that may be made by its manufacturer, is not guaranteed or endorsed by the publisher.

References

1. Wang Y, Zhang H, Liu C, Wang Z, Wu W, Zhang N, et al. Immune checkpoint modulators in cancer immunotherapy: Recent advances and emerging concepts. *J Hematol Oncol* (2022) 15:111. doi: 10.1186/s13045-022-01325-0

2. Qu C, Zhang H, Cao H, Tang L, Mo H, Liu F, et al. Tumor buster - where will the CAR-T cell therapy 'missile' go. *Mol Cancer.* (2022) 21:201. doi: 10.1186/s12943-022-01669-8

3. Huang K, Fang C, Yi K, Liu X, Qi H, Tan Y, et al. The role of PTRF/Cavin1 as a biomarker in both glioma and serum exosomes. *Theranostics.* (2018) 8:1540–57. doi: 10.7150/thno.22952

4. Zhang JX, Han L, Bao ZS, Wang YY, Chen LY, Yan W, et al. HOTAIR, a cell cycle-associated long noncoding RNA and a strong predictor of survival, is preferentially expressed in classical and mesenchymal glioma. *Neuro Oncol* (2013) 15:1595–603. doi: 10.1093/neuonc/not131

5. Barbieri I, Kouzarides T. Role of RNA modifications in cancer. *Nat Rev Cancer.* (2020) 20:303–22. doi: 10.1038/s41568-020-0253-2

6. Liu J, Yue Y, Han D, Wang X, Fu Y, Zhang L, et al. A METTL3-METTL14 complex mediates mammalian nuclear RNA N6-adenosine methylation. *Nat Chem Biol* (2014) 10:93–5. doi: 10.1038/nchembio.1432

7. Zheng G, Dahl JA, Niu Y, Fedorcsak P, Huang CM, Li CJ, et al. ALKBH5 is a mammalian RNA demethylase that impacts RNA metabolism and mouse fertility. *Mol Cell* (2013) 49:18–29. doi: 10.1016/j.molcel.2012.10.015

8. Jia G, Fu Y, Zhao X, Dai Q, Zheng G, Yang Y, et al. N6-methyladenosine in nuclear RNA is a major substrate of the obesity-associated FTO. nat chem biol. *Nat. Chem. Biol* (2011) 7:885–7. doi: 10.1038/nchembio.687

9. Wang X, Lu Z, Gomez A, Hon GC, Yue Y, Han D, et al. N6-methyladenosine-dependent regulation of messenger RNA stability. *Nature.* (2014) 505:117–20. doi: 10.1038/nature12730

10. Wang X, Zhao BS, Roundtree IA, Lu Z, Han D, Ma H, et al. N(6)-methyladenosine modulates messenger RNA translation efficiency. *Cell.* (2015) 161:1388–99. doi: 10.1016/j.cell.2015.05.014

11. Cai X, Wang X, Cao C, Gao Y, Zhang S, Yang Z, et al. HBXIP-elevated methyltransferase METTL3 promotes the progression of breast cancer *via* inhibiting tumor suppressor let-7g. *Cancer Lett* (2018) 415:11–9. doi: 10.1016/j.canlet.2017.11.018

frontiers in Immunology

SYSTEMATIC REVIEW
published: 17 September 2021
doi: 10.3389/fimmu.2021.734956

A Systematic Review of the Tumor-Infiltrating CD8$^+$ T-Cells/PD-L1 Axis in High-Grade Glial Tumors: Toward Personalized Immuno-Oncology

Mahdi Abdoli Shadbad[1,2,3], *Zahra Asadzadeh*[2†], *Negar Hosseinkhani*[2†], *Afshin Derakhshani*[4], *Nazila Alizadeh*[2], *Oronzo Brunetti*[5], *Nicola Silvestris*[5,6*‡] *and Behzad Baradaran*[2,7*‡]

[1] Research Center for Evidence-Based Medicine, Faculty of Medicine, Tabriz University of Medical Sciences, Tabriz, Iran, [2] Immunology Research Center, Tabriz University of Medical Sciences, Tabriz, Iran, [3] Student Research Committee, Tabriz University of Medical Sciences, Tabriz, Iran, [4] Laboratory of Experimental Pharmacology, Istituto Di Ricovero e Cura a Carattere Scientifico (IRCCS) Istituto Tumori Giovanni Paolo II, Bari, Italy, [5] Medical Oncology Unit, IRCCS Istituto Tumori Giovanni Paolo II, Bari, Italy, [6] Department of Biomedical Sciences and Human Oncology, University of Bari "Aldo Moro", Bari, Italy, [7] Department of Immunology, Faculty of Medicine, Tabriz University of Medical Sciences, Tabriz, Iran

Based on preclinical findings, programmed death-ligand 1 (PD-L1) can substantially attenuate CD8$^+$ T-cell-mediated anti-tumoral immune responses. However, clinical studies have reported controversial results regarding the significance of the tumor-infiltrating CD8$^+$ T-cells/PD-L1 axis on the clinical picture and the response rate of patients with high-grade glial tumors to anti-cancer therapies. Herein, we conducted a systematic review according to the preferred reporting items for systematic reviews and meta-analyses (PRISMA) statements to clarify the clinical significance of the tumor-infiltrating CD8$^+$ T-cells/PD-L1 axis and elucidate the impact of this axis on the response rate of affected patients to anti-cancer therapies. Indeed, a better understanding of the impact of this axis on the response rate of affected patients to anti-cancer therapies can provide valuable insights to address the futile response rate of immune checkpoint inhibitors in patients with high-grade glial tumors. For this purpose, we systematically searched Scopus, Web of Science, Embase, and PubMed to obtain peer-reviewed studies published before 1 January 2021. We have observed that PD-L1 overexpression can be associated with the inferior prognosis of glioblastoma patients who have not been exposed to chemo-radiotherapy. Besides, exposure to anti-cancer therapies, e.g., chemo-radiotherapy, can up-regulate inhibitory immune checkpoint molecules in tumor-infiltrating CD8$^+$ T-cells. Therefore, unlike unexposed patients, increased tumor-infiltrating CD8$^+$ T-cells in anti-cancer therapy-exposed tumoral tissues can be associated with the inferior prognosis of affected patients. Because various inhibitory immune checkpoints can regulate anti-tumoral immune responses, the single-cell sequencing of the cells residing in the tumor microenvironment can provide valuable insights into the expression patterns of inhibitory immune checkpoints in the tumor micromovement. Thus, administrating immune checkpoint inhibitors based on the data

OPEN ACCESS

Edited by:
Junxia Zhang,
Nanjing Medical University, China

Reviewed by:
Zhijun Zhou,
University of Oklahoma Health Sciences Center, United States
Dipongkor Saha,
Texas Tech University Health Sciences Center, United States
Daniele Santini,
Campus Bio-Medico University, Italy

***Correspondence:**
Behzad Baradaran
baradaranb@tbzmed.ac.ir
Nicola Silvestris
n.silvestris@oncologico.bari.it

†*These authors have contributed equally to this work*

‡*These authors share last authorship*

Specialty section:
This article was submitted to Cancer Immunity and Immunotherapy, a section of the journal Frontiers in Immunology

Received: *01 July 2021*
Accepted: *02 September 2021*
Published: *17 September 2021*

Citation:
Shadbad MA, Asadzadeh Z, Hosseinkhani N, Derakhshani A, Alizadeh N, Brunetti O, Silvestris N and Baradaran B (2021) A Systematic Review of the Tumor-Infiltrating CD8$^+$ T-Cells/PD-L1 Axis in High-Grade Glial Tumors: Toward Personalized Immuno-Oncology. Front. Immunol. 12:734956. doi: 10.3389/fimmu.2021.734956

from the single-cell sequencing of these cells can increase patients' response rates, decrease the risk of immune-related adverse events development, prevent immune-resistance development, and reduce the risk of tumor recurrence.

Keywords: glioma, tumor-infiltrating lymphocytes, tumor-infiltrating CD8+ T-cells, PD-L1, single-cell sequencing, personalized medicine, immune checkpoint, tumor microenvironment

INTRODUCTION

High-grade glial tumors, e.g., glioblastoma, are among the frequently diagnosed primary brain tumors; however, the prognosis of affected patients with the current treatment is dismal. Although surgery and radio/chemotherapy are considered the first-line therapies for these patients, their response rates have not led to desired outcomes for affected patients. Indeed, a better understanding of the biology of immune cells and the impact of surgery and radio/chemotherapy on the phenotype of immune cells can be essential in increasing their response rates (1).

Traditionally, glial tumors were considered "cold tumors." The common belief was that immune cells could not cross the blood-brain barrier to develop anti-tumoral immune responses. However, it has been shown that immune cells can cross the blood-brain barrier, and indeed, they have substantial roles in determining the response rates of radiotherapy (2). Recent advances in immuno-oncology have shown that immunotherapy can be a promising approach for treating patients with high-grade glial tumors (3). Nevertheless, the immunosuppressive tumor microenvironment impedes the development of anti-tumoral immune responses. Besides facilitating immune evasion, the immunosuppressive tumor microenvironment can pave the way for tumor proliferation and migration (4).

Inhibitory immune checkpoint axes are among the well-studied culprits in transforming the pro-inflammatory tumor microenvironment to the immunosuppressive one. The PD-L1/programmed cell death protein 1 (PD-1) axis is a well-known inhibitory immune checkpoint axis that can be established between immune cells and tumoral cells. The expression of PD-1 and PD-L1 in the tumor microenvironment have been associated with tumor development (5). Furthermore, growing evidence indicates remarkable associations between PD-1 and other inhibitory immune checkpoints, e.g., V-domain immunoglobulin suppressor of T cell activation (VISTA) and T cell immunoreceptor with Ig and ITIM domains (TIGIT), which can further attenuate anti-tumoral immune responses (6–9).

Accumulating evidence indicates that anti-cancer therapy can substantially alter the tumor microenvironment. Recent findings have demonstrated that chemo-radiotherapy can up-regulate inhibitory immune checkpoints expression and induce a state of exhaustion in tumor infiltration immune cells, e.g., tumor-infiltrating $CD8^+$ T-cells (10). Besides, the administration of immune checkpoint inhibitors, e.g., anti-PD-1, has been associated with an increased response rate of anti-cancer therapies in patients with high-grade glial tumors (11). However, the response rates among the affected patients considerably vary. Indeed, some clinical trials have failed to report meaningful benefits of immune checkpoint inhibitors administration in patients with glioblastoma (11, 12). Moreover, despite the well-established anti-tumoral function of $CD8^+$ T-cells in eliminating tumoral cells in preclinical studies, there have been controversial results regarding the significance of tumor-infiltrating $CD8^+$ T-cells in patients with high-grade glial tumors (13–16). In light of these controversial results, there is a need to clarify the significance of the tumor-infiltrating $CD8^+$ T-cells/PD-L1 axis in patients with high-grade glial tumors.

The current study aims to systematically review and sort out the current evidence on the cross-talk between tumor-infiltrating $CD8^+$ T-cells with PD-L1 and their impacts on the prognosis, the clinicopathological features, and the response rate of patients with high-grade glial tumors to anti-cancer therapies. Based on the current clinical and preclinical evidence, we also propose a novel strategy for immune checkpoint inhibitor administration, based on single-cell sequencing and personalized medicine principles, to increase the response rates and ameliorate the prognosis of affected patients.

METHODS

The present study was performed according to the PRISMA statements (17). Concerning the PICO, the studied population is patients with high-grade glial tumors. The intervention/exposure is the level of tumor-infiltrating $CD8^+$ T-cells/tumoral PD-L1 expression with regard to the prognosis/clinicopathological feature of affected patients. The comparator is the patients with the low level of tumor-infiltrating $CD8^+$ T-cells/high PD-L1 expression. The outcome is a better understanding of the impact of the tumor-infiltrating $CD8^+$ T-cells/PD-L1 axis on the response rate to anti-cancer therapies and the clinical picture of affected patients.

Search Strategy

Without restricting to any languages or time, the Web of Science, Scopus, PubMed, and Embase databases were systematically searched to obtain the peer-reviewed records published before 1 January 2021. For this purpose, all fields of records were systematically searched with the following keywords: ("glioma" OR "glioblastoma multiforme" OR "glioblastoma" OR "astrocytoma" OR "ependymoma" OR "subependymoma" OR "oligodendroglioma" OR "oligoastrocytoma" OR "sub-ependymoma" OR "sub ependymoma") and ("programmed death-ligand 1" OR "PD-L1" OR "PD L1" OR "PDL1" OR "B7-H1" OR "B7 H1" OR "B7H1" OR "CD274" OR "cluster of differentiation 274" OR "CD 274" OR "cluster of differentiation274" OR "B7 homolog 1" OR "PDCD1

Ligand 1" OR "PDCD1LG1" OR "PDCD1L1" OR "HPD-L1") and ("CD8" OR "CD 8" OR "Cluster of differentiation 8" OR "Cluster of differentiation-8" OR "Cluster of differentiation8" OR "CD8A" OR "T-lymphocyte differentiation antigen T8/Leu-2" OR "CD8 antigen" OR "CD 8 antigen" OR "Leu2 T-Lymphocyte antigen" OR "CD8a molecule" OR "T-cell antigen Leu2" OR "cytotoxic T cell" OR "cytotoxic T lymphocyte" OR "CTL" OR "T-killer cell" OR "cytolytic T cell" OR "CD8+ T-cell" OR "killer T cell").

Study Selection

Following the systematic search, the obtained records were reviewed in two phases. In phase I, two authors (NH and ZA) independently screened the relevant papers based on their titles and abstracts. In phase II, the same authors independently reviewed the full text of the remaining papers, along with their supplementary data. Any disagreements were resolved *via* consulting with B.B and consensus.

Eligibility Criteria

Records with the following eligibility criteria were included in this study : (1) clinical studies, (2) investigations with the objective of assessing the tumor-infiltrating $CD8^+$ T-cells and the protein expression of PD-L1 in patients with high-grade glial tumors, (3) studies, which investigated and published the quantified relationship between PD-L1 and tumor-infiltrating $CD8^+$ T-cells or the clinicopathological significance of PD-L1 and tumor-infiltrating $CD8^+$ T-cells or the prognostic values of PD-L1 and tumor-infiltrating $CD8^+$ T-cells in patients with high-grade glial tumors, and (4) studies, which were published in English.

Based on the following criteria, records were excluded from this study: (1) studies that investigated the tumor-infiltrating $CD8^+$ T-cells and the protein expression of PD-L1 in patients with low-grade glial tumors, (2) studies that investigated the tumor-infiltrating $CD8^+$ T-cells and the expression of tumoral PD-L1 in glial tumors without considering tumor grades, (3) studies that investigated the cross-talk between PD-L1 and circulating $CD8^+$ T-cells in the blood of the affected patients, (4) studies that investigated the $CD8^+$ T-cells and PD-L1 in a co-culture system, and (5) studies that were based on the data from databases, like The Cancer Genome Atlas (TCGA).

Data Extraction

The following data were extracted from the included studies: (1) the first author, (2) publication year, (3) the used antibody, (4) the endpoint, (5) the country, (6) the type of high-grade glial tumor, (7) the sample size, (8) the treatment of affected patients, (9) the prognostic values of protein expression of PD-L1/tumor-infiltrating $CD8^+$ T-cells, (10) the association between protein expression of PD-L1/tumor-infiltrating $CD8^+$ T-cells, (11) the clinicopathological significance of protein expression of PD-L1/tumor-infiltrating $CD8^+$ T-cells, and (12) and the cut-off for PD-L1 and tumor-infiltrating $CD8^+$ T-cells.

Quality Assessment of the Included Studies

We applied the criteria of Hayden et al. statements for assessing the quality of the prognostic studies (18). We also utilized the Joanna Briggs Institute (JBI) checklist for assessing the studies that investigated the relationship between PD-L1 and tumor-infiltrating $CD8^+$ T-cells in patients with high-grade glial tumors (19).

RESULTS

Selected Studies

Our systematic search on PubMed, Scopus, Embase, and Web of Science retrieved 7468 records. After removing duplication records, 7142 records remained. Based on the independent review of two authors in phase I, 5983 studies were excluded. In phase II, two authors independently reviewed the full text of 1159 studies, along with their supplementary data. Finally, based on the full-text assessment of studies, seven papers were included in the qualitative synthesis. **Figure 1** demonstrates the flowchart of literature identification, inclusion, and exclusion.

Study Characteristics

The included studies were published between 2015 to 2020. Six out of seven studies have investigated high-grade glioma patients (15, 16, 20–23), and one study has investigated high-grade ependymoma patients (24). **Table 1**. demonstrates the general characteristics of the included studies.

We have found a significant increase in the level of tumor-infiltrating $CD8^+$ T-cells in the second surgery of glioblastoma patients treated with surgery/fractionated radiotherapy/

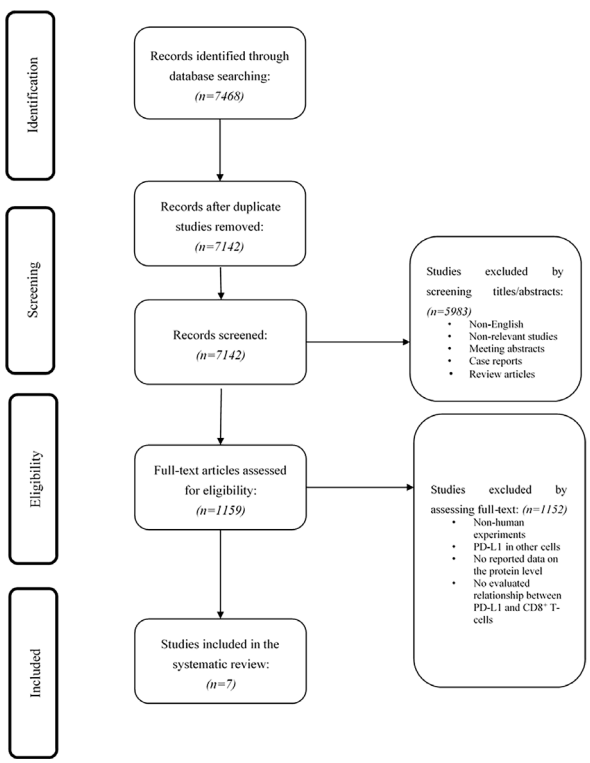

FIGURE 1 | The flow chart of the study selection process.

temozolomide compared to the first resected tumor (P-value=0.009) (**Table 2**). Besides, membranous PD-L1 expression has been more pronounced in the newly diagnosed glioblastoma tissues compared to recurrent glioblastoma tissues (P-value=0.034) (**Table 2**).

The increased level of tumor-infiltrating $CD8^+$ T-cells has been associated with improved overall survival (OS) in high-grade glioma patients who have not been exposed to anti-cancer therapies (P-value<0.05) (**Table 3**). However, increased level of tumor-infiltrating $CD8^+$ T-cells has been associated with worse OS from the second surgery glioblastoma patients who have been exposed to anti-cancer therapies (P-value=0.017) (**Table 3**). Besides, the increased level of tumor-infiltrating $CD8^+$ T-cells has been associated with inferior survival from the second surgery in glioblastoma patients who have been exposed to anti-cancer therapies (P-value=0.005) (**Table 3**). We have observed that PD-L1 overexpression is associated with inferior OS in glioblastoma patients who have not been exposed to anti-cancer therapies (P-value=0.0119) (**Table 3**).

We have found that PD-L1 expression is inversely correlated with tumor-infiltrating $CD8^+$ T-cells in glioblastoma patients who have not been exposed to anti-cancer therapies (r = -0.5064, and P-value= 0.0003) (**Table 4**). Also, we have observed that there is a remarkable relationship between the tumor-infiltrating $CD8^+$ PD-1^+ T-cells with tumor-infiltrating PD-1^+ lymphocytes in glioblastoma patients (P<0.001) (**Table 4**). Besides, increased PD-1^+/tumor-infiltrating $CD8^+$ T-cell ratio is associated with worse OS and progression-free survival (PFS) in glioblastoma patients (P-value<0.001, and P-value=0.01, respectively) (**Table 4**). The survival of patients with low PD-L1 expression and low $CD8^+$ infiltration is similar to those with high PD-L1 expression and low $CD8^+$ infiltration in glioblastoma patients who have not been exposed to anti-cancer therapies (P-value<0.05) (**Table 4**). Moreover, the low expression of PD-L1 and high level of tumor-infiltrating $CD8^+$ T-cells are associated with improved OS in glioblastoma patients who have not been exposed to anti-cancer therapies (P-value<0.05) (**Table 4**). Furthermore, a high PD-1^+/tumor-infiltrating $CD8^+$ T-cells ratio is negatively associated with improved PFS and OS of glioblastoma patients (r =-0.444, P-value<0.02, and r=-0.655, P-value<0.001, respectively) (**Table 4**). We have observed a strong positive association between PD-L1 expression and tumor-infiltrating $CD8^+$ T-cell in patients with high-grade ependymomas (P-value=0.03) (**Table 3S**).

Evaluating the Bias in the Included Studies

We assessed the included studies concerned with the prognostic values of the PD-L1/tumor-infiltrating $CD8^+$ T-cells axis based on the Hayden et al. statement (18). The main risk areas were confounding measurement and outcome measurement (**Table 1S**). Furthermore, we evaluated the remaining studies based on the JBI checklists (19). The main risk areas were addressing potential cofounders (**Table 2S**).

DISCUSSION

Tumor-infiltrating $CD8^+$ T-cells are pivotal cells in eliminating tumoral cells; however, the immunosuppressive tumor

TABLE 1 | The general characteristics of the included studies.

First author, year	Country	Sample	Glial tumor	Endpoint (s)	Cancer treatment record	CD8+ T-cells cut-off	PD-L1 cut-off	PD-L1 antibody for staining
Su, 2020 (16)	China	47	Glioblastoma	OS of tumor-infiltrating $CD8^+$ T-cells and PD-L1 and the association between PD-L1 and tumor-infiltrating $CD8^+$ T-cells	Surgery	More than 10 CD8+ T-cells in high-power field	Based on intensity and reactivity	EPR1161 (2)
Nambirajan, 2019 (24)	India	52	High-grade ependymoma	The association between PD-L1 and tumor-infiltrating $CD8^+$ T-cells	Radio/chemotherapy	More than 6 $CD8^+$ T-cells/mm^2 in high power filed	1%	SP263
Jan, 2018 (21)	Taiwan	47	Glioblastoma	The OS and PFS of tumor-infiltrating $CD8^+$ T-cells and PD-L1	Resection, chemo-radiotherapy, with/without autologous dendritic cell/tumor antigen vaccine	Not clearly mentioned	5%	EPR1161
Plant, 2018 (22)	USA	27	High-grade glioma	The OS of PD-L1 and tumor-infiltrating $CD8^+$ T-cells	Not appropriately provided.	Not clearly mentioned	Based on positivity intensity	29E.2A3
Zhang, 2017 (23)	China	17	Glioblastoma	The association between PD-L1 and tumor-infiltrating $CD8^+$ T-cells	Not specifically categorized.	Based on pathological scoring	Not clearly defined	28-8
Miyazaki, 2017 (15)	Japan	16	Glioblastoma	The clinical significance, OS, PFS, and survival from the second surgery of PD-L1 and tumor-infiltrating $CD8^+$ T-cells	Treated with surgery, radiation, temozolomide, and four patients received a cancer vaccine	Based on pathological scoring	25%	28-8
Berghoff, 2015 (20)	Austria	135	Glioblastoma	The association and clinical significance of tumor-infiltrating $CD8^+$ T-cells and PD-L1	Except for the five unknown patients, others were on chemotherapy/investigational agents.	Based on pathological scoring	5%	5H1

OS, Overall survival; PD-L1, Programmed death-ligand 1; PFS, Progression-free survival; and CD, Cluster of differentiation.

TABLE 2 | The clinical significance of tumor-infiltrating CD8+ T-cells/PD-L1 axis in high-grade glioma patients.

First author, year	Country	Sample size	Clinical significance of the axis	P-value	Cancer treatment history
Berghoff, 2015 (20)	Austria	135	The level of tumor-infiltrating CD8+ T-cells is not statistically significantly different in newly diagnosed and recurrent tumors.	0.103	Except for the five unknown patients, others were on chemotherapy/investigational agents.
Berghoff, 2015 (20)	Austria	135	There is no statistically significant correlation between being older/younger than 65 years old and the level of tumor-infiltrating CD8+ cells.	0.376	Except for the five unknown patients, others were on chemotherapy/investigational agents.
Miyazaki, 2017 (15)	Japan	16	The level of tumor-infiltrating CD8+ cells is significantly increased in the second removal.	0.009	Treated with surgery, radiation, temozolomide, and four patients received a cancer vaccine
Berghoff, 2015 (20)	Austria	135	Diffuse/fibrillary PD-L1 is not statistically associated with tumor recurrence.	0.411	Except for the five unknown patients, others were on chemotherapy/investigational agents.
Berghoff, 2015 (20)	Austria	135	There is no statistical correlation between being older/younger than 65 years old and diffuse/fibrillary PD-L1 expression.	0.383	Except for the five unknown patients, others were on chemotherapy/investigational agents.
Berghoff, 2015 (20)	Austria	135	There is no statistical correlation between being older/younger than 65 years old and membranous PD-L1 expression.	0.612	Except for the five unknown patients, others were on chemotherapy/investigational agents.
Berghoff, 2015 (20)	Austria	135	Membranous PD-L1 expression is more pronounced in initial glioblastoma tumors than recurrent ones.	0.034	Except for the five unknown patients, others were on chemotherapy/investigational agents.
Miyazaki, 2017 (15)	Japan	16	There is no statistically significant difference between membranous PD-L1 in the initial and second resection.	0.187	Treated with surgery, radiation, temozolomide, and four patients received a cancer vaccine

PD-L1, Programmed death-ligand 1; and CD, Cluster of differentiation.

microenvironment of solid cancers impedes the development of anti-tumoral immune responses. Indeed, establishing co-inhibitory signals between the tumor-infiltrating immune cells can substantially transform the pro-inflammatory tumor microenvironment into an immunosuppressive one. Besides, the immunosuppressive tumor microenvironment has been implicated in tumor development (5, 25, 26). The PD-L1/PD-1 axis is a well-established inhibitory axis that can attenuate the anti-tumoral immune responses. Besides facilitating immune evasion, tumoral PD-L1 has been implicated in tumor proliferation and migration in glioblastoma. Indeed, PD-L1 knockdown can inhibit tumor growth in mice bearing glioblastoma (27). In the first and second sections, we aim to discuss the clinical significance and prognostic value of this axis and compare our observed results with preclinical and clinical studies. In the third section, we intend to discuss the association between tumor-infiltrating CD8+ T-cells with PD-L1 expression in high-grade glial tumors. Finally, we propose a novel strategy to address the shortcomings of immune checkpoint inhibitors that have been reflected in unfavorable objective response rates in multiple clinical trials.

The Clinical Significance of the Tumor-Infiltrating CD8+ T-Cells/PD-L1 Axis

We have found a significant increase in the level of tumor-infiltrating CD8+ T-cells in the second resected glioblastoma tumors treated with anti-cancer therapies (paired data). However, there has been no statistically significant change in the level of tumor-infiltrating CD8+ T-cells in recurrent glioblastoma patients and newly diagnosed glioblastoma patients treated with chemotherapy/investigational agents (unpaired data) (**Table 2**). Consistent with our results, Yue et al. have reported a strong positive association between increased CD8+ T-cells infiltration and positive O^6-methylguanine DNA methyltransferase (MGMT) expression in glioblastoma patients (28). Indeed, positive MGMT has been associated with chemoresistant tumors in glioblastoma patients (29). These findings are consistent with our observed results regarding the increased infiltration of CD8+ T-cells in recurrent glioblastomas. In line with these, preclinical studies have also indicated that anti-cancer therapy of glioma can pave the way for T-cells infiltration. Weichselbaum et al. have shown that radiotherapy can facilitate T-cell infiltration *via* the release of tumor antigens and danger-associated molecular patterns. Indeed, radiotherapy can up-regulate the expression of C-X-C motif ligand 9 (CXCL9) and C-X-C motif ligand 10 (CXCL10), leading to the recruitment of immune cells (30). Moreover, recent findings indicate that radiation can induce major histocompatibility complex (MHC)-I expression, associated with the infiltration of CD8+ T-cells into the microenvironment (31).

We have found a remarkable upregulation in PD-L1 in the newly diagnosed glioblastomas compared to the recurrent glioblastomas treated with chemotherapy/investigational agents (**Table 2**). Consistent with this, Heynckes et al. have indicated that temozolomide can inhibit PD-L1 expression in recurrent glioblastoma (32). Besides, it has been reported that PD-L1 expression in recurrent glioblastoma is substantially downregulated following treatment with temozolomide in affected patients (33). Therefore, the insignificant result of the study by Miyazaki et al. might be stemmed from their low sample size. Collectively, based on the current evidence, the level of tumor-infiltrating CD8+ T-cells and the expression level of PD-L1 are substantially increased and decreased in the recurrent glioblastomas compared to newly diagnosed glioblastomas.

The Prognostic Value of Tumor-Infiltrating CD8+ T-Cells/PD-L1 Axis

We have found that PD-L1 overexpression can be associated with inferior OS in glioblastoma patients who have not been

TABLE 3 | The prognostic value of tumor-infiltrating $CD8^+$ T-cells/PD-L1 axis in high-grade glioma patients.

First author, year	Country	Sample size	Prognostic value	P-value	HR and 95%CI	Endpoint	Cancer treatment history
Plant, 2018 (22)	USA	27	The level of tumor-infiltrating $CD8^+$ T-cells is not statistically associated with OS.	P=0.8	1.0190, and 0.8743-1.1637	OS	Not provided.
Jan, 2018 (21)	Taiwan	20	The level of tumor-infiltrating $CD8^+$ T-cells is not statistically associated with OS.	P=0.5	0.725, and 0.284–1.853	OS	Resection and chemo-radiotherapy
Jan, 2018 (21)	Taiwan	20	The level of tumor-infiltrating $CD8^+$ T-cells is not statistically associated with PFS.	P=0.73	1.082, and 0.688–1.703	PFS	Resection and chemo-radiotherapy
Jan, 2018 (21)	Taiwan	27	The level of tumor-infiltrating $CD8^+$ T-cells is not statistically associated with OS.	P=0.31	1.55, and 0.667–3.601	OS	Resection, chemo-radiotherapy, and autologous dendritic cell/tumor antigen vaccine
Jan, 2018 (21)	Taiwan	27	The level of tumor-infiltrating $CD8^+$ T-cells is not statistically associated with PFS.	P=0.36	1.489, and 0.640–3.461	PFS	Resection, chemo-radiotherapy, and autologous dendritic cell/tumor antigen vaccine
Su, 2020 (16)	China	47	The higher level of tumor-infiltrating $CD8^+$ T-cells is associated with improved OS.	P<0.05	Not provided	OS	Surgery
Miyazak, 2017 (15)	Japan	16	The higher level of Tumor-infiltrating $CD8^+$ T-cells is not associated with PFS.	P=0.495	Not provided	PFS	Treated with surgery, radiation, temozolomide, and four patients received a cancer vaccine
Miyazak, 2017 (15)	Japan	16	The higher level of tumor-infiltrating $CD8^+$ T-cells is associated with inferior OS.	P=0.017	Not provided	OS	Treated with surgery, radiation, temozolomide, and four patients received a cancer vaccine
Miyazak, 2017 (15)	Japan	16	The higher level of tumor-infiltrating $CD8^+$ T-cells is associated with inferior survival from the second surgery.	P=0.005	Not provided	Survival from the second surgery	Treated with surgery, radiation, temozolomide, and four patients received a cancer vaccine
Berghoff, 2015 (20)	Austria	135	The membranous PD-L1 is not statistically associated with OS.	P=0.724	Not provided	OS	Except for the five unknown patients, others were on chemotherapy/investigational agents.
Berghoff, 2015 (20)	Austria	135	The diffuse/fibrillary PD-L1 is not statistically associated with OS.	P=0.921	Not provided	OS	Except for the five unknown patients, others were on chemotherapy/investigational agents.
Plant, 2018 (22)	USA	27	The tumoral PD-L1 is not statistically associated with OS.	P=0.6	1.0080, and 0.9789 - 1.0371	OS	Not appropriately provided.
Jan, 2018 (21)	Taiwan	20	The fibrillary/membranous PD-L1 is not statistically associated with OS.	P=0.38	0.654, and 0.254 - 1.685	OS	Resection and chemoradiotherapy
Jan, 2018 (21)	Taiwan	20	The fibrillary/membranous PD-L1 is not statistically associated with PFS.	P=0.5	1.435, and 0.498 - 4.137	PFS	Resection and chemoradiotherapy
Jan, 2018 (21)	Taiwan	27	The fibrillary/membranous PD-L1 is not statistically associated with OS.	P=0.1	0.354, and 0.103 - 1.219	OS	Resection, chemo-radiotherapy, and autologous dendritic cell/tumor antigen vaccine
Jan, 2018 (21)	Taiwan	27	The fibrillary/membranous PD-L1 is not statistically associated with PFS.	P=0.248	0.528, and 0.178 - 1.563	PFS	Resection, chemo-radiotherapy, and autologous dendritic cell/tumor antigen vaccine
Su, 2019 (16)	China	47	The PD-L1 overexpression is associated with inferior OS.	P=0.0119	Not provided	OS	Surgery
Miyazak, 2017 (15)	Japan	16	The tumoral PD-L1 is not statistically associated with PFS.	P=0.095	Not provided	PFS	Treated with surgery, radiation, temozolomide, and four patients received a cancer vaccine
Miyazak, 2017 (15)	Japan	16	The tumoral PD-L1 is not statistically associated with OS.	P=0.356	Not provided	OS	Treated with surgery, radiation, temozolomide, and four patients received a cancer vaccine
Miyazak, 2017 (15)	Japan	16	The tumoral PD-L1 is not statistically associated with survival from the second surgery.	P=0.418	Not provided	Survival from the second surgery	Treated with surgery, radiation, temozolomide, and four patients received a cancer vaccine

OS, Overall survival; PD-L1, Programmed death-ligand 1; PFS, Progression-free survival; HR, Hazard ratio; CI, Confidence interval; and CD, Cluster of differentiation.

TABLE 4 | The cross-talk between the PD-L1/PD-1 axis and tumor-infiltrating $CD8^+$ T-cells in glioblastoma.

First author, year	Country	Sample size	Tumor type	Cross-talk between the PD-L1/PD-1 axis and tumor-infiltrating $CD8^+$ T-cells	P-value	HR, and 95% CI	OR, CI 95%	r
Berghoff, 2015 (20)	Austria	135	Glioblastoma	Tumor-infiltrating PD-1^+ lymphocytes are correlated with tumor-infiltrating $CD8^+$ PD-1^+ cells.	P<0.001	Not applicable	Not applicable	Not provided
Berghoff, 2015 (20)	Austria	135	Glioblastoma	There is no statistically significant association between diffuse/fibrillary PD-L1 and tumor-infiltrating $CD8^+$ T-cells.	P=0.068	Not applicable	Not applicable	Not provided
Berghoff, 2015 (20)	Austria	135	Glioblastoma	There is no statistically significant association between membranous PD-L1 and tumor-infiltrating $CD8^+$ T-cells.	P=0.380	Not applicable	Not applicable	Not provided
Zhang, 2017 (23)	China	17	Glioblastoma	There is no statistically significant association between tumoral PD-L1 and tumor-infiltrating $CD8^+$ T-cells.	P=0.4959	Not applicable	3, and 0.1270 - 70.8770	Not provided
Su, 2019 (16)	China	47	Glioblastoma	The PD-L1 expression is inversely correlated with tumor-infiltrating $CD8^+$ T-cells.	P=0.0003	Not applicable	Not applicable	r = -0.5064
Su, 2019 (16)	China	47	Glioblastoma	The low expression of PD-L1 and high level of tumor-infiltrating $CD8^+$ T-cells are associated with improved OS.	P<0.05	Not provided	Not applicable	Not applicable
Su, 2019 (16)	China	47	Glioblastoma	The survival rate of patients with low PD-L1 expression and low $CD8^+$ infiltration is similar to those with high PD-L1 expression and low $CD8^+$ infiltration.	P<0.05	Not provided	Not applicable	Not applicable
Jan, 2018 (21)	Taiwan	20	Glioblastoma	A high PD-1^+/tumor-infiltrating $CD8^+$ T-cell ratio is associated with worse OS.	P<0.001	11.382, and 3.320–35.707	Not applicable	Not applicable
Jan, 2018 (21)	Taiwan	20	Glioblastoma	A high PD-1^+/tumor-infiltrating $CD8^+$ T-cell ratio is associated with worse PFS.	P=0.01	3.458, and 1.304–9.174	Not applicable	Not applicable
Jan, 2018 (21)	Taiwan	27	Glioblastoma	A high PD-1^+/tumor-infiltrating $CD8^+$ T-cell ratio is not statistically associated with OS.	P-value = 0.23	0.567, and 0.224–1.437	Not applicable	Not applicable
Jan, 2018 (21)	Taiwan	27	Glioblastoma	A high PD-1^+/tumor-infiltrating $CD8^+$ T-cell ratio is not statistically associated with PFS.	P=0.44	1.205, and 0.753–1.929	Not applicable	Not applicable
Jan, 2018 (21)	Taiwan	27	Glioblastoma	The PD-1^+/tumor-infiltrating $CD8^+$ T-cell ratio is inversely associated with OS.	P<0.001	Not applicable	Not applicable	r = -0.655
Jan, 2018 (21)	Taiwan	27	Glioblastoma	The PD-1^+/tumor-infiltrating $CD8^+$ T-cell ratio is inversely associated with PFS.	P=0.02	Not applicable	Not applicable	r = -0.444

OS, Overall survival; PD-L1, Programmed death-ligand 1; PFS, Progression-free survival; PD-1, Programmed cell death protein 1; HR, Hazard ratio; CI, Confidence interval; and CD, Cluster of differentiation.

exposed to anti-cancer therapies (**Table 3**). Consistent with our detected results, Xue et al. have pooled the data from the patients who underwent chemo/radiotherapy after resection with patients treated with other therapeutic modalities and have indicated that PD-L1 can be associated with worse OS in patients with gliomas (34). Nduom et al. have shown that PD-L1 overexpression can be associated with shorter survival in glioblastoma patients (35). Han et al. have indicated that the overexpression of PD-L1 in resected glioblastoma tissues is remarkably associated with the inferior survival of affected patients (36). Besides, Lee et al. have indicated that PD-L1 expression in resected unexposed glioblastoma tissues is associated with worse OS in glioblastoma patients (37).

Regarding the prognostic value of tumor-infiltrating $CD8^+$ T-cells, the level of tumor-infiltrating $CD8^+$ T-cells might be associated with improved OS in glioblastoma patients who have not been exposed to anti-cancer therapies before. However, tumor-infiltrating $CD8^+$ T-cells might be associated with inferior OS and worse survival from the second surgery in glioblastoma patients who were previously exposed to anti-cancer therapies (**Table 3**). Consistent with our detected results, Madkouri et al. have indicated increased infiltration of $CD8^+$ T-cells is associated with improved OS of glioblastoma patients who have not been exposed to anti-cancer therapies before (13). Moreover, Kim et al. have demonstrated that increased infiltration of $CD8^+$ T-cells in the resected glioblastoma tissues, which have not been exposed to anti-cancer therapies before, can improve the survival of glioblastoma patients (14). In other words, these results have indicated that anti-cancer therapies can continuously lead to the exhaustion of tumor infiltrated $CD8^+$ T-cells and pave the way for the transformation of the pro-inflammatory tumor microenvironment into the immunosuppressive one.

Our observed results are also consistent with the preclinical findings. Dai et al. have shown that the combination of anti-PD-1 and temozolomide can substantially decrease tumor size and increase the survival of mice bearing gliomas (10). In mice models of glioblastoma, anti-PD-1 has also remarkably increased the anti-tumoral proprieties of temozolomide *via* down-regulating the expression of lymphocyte-activation gene 3 (LAG-3) and PD-1 (11). Grapin et al. have indicated that radiotherapy can lead to the TIGIT upregulation in the tumor-infiltrating $CD8^+$ T-cells (38). In line with this, the combination of fractionated radiotherapy and the administration of immune checkpoint inhibitors can lead to the abscopal effect, resulting in tumor rejection (31). Besides, it has been reported that anti-PD-1 with localized radiation can substantially increase the survival of mice bearing gliomas compared to monotherapy with radiation (39). Consistent with these, Li et al. have highlighted a remarkable PD-1 upregulation in $CD8^+$ T-cells following radiation therapy (40). Besides, Dovedi et al. have shown that fractionated radiotherapy can up-regulate PD-1 expression in $CD8^+$ T-cells, and the administration of immune checkpoint inhibitors can considerably increase the survival of affected mice (41). Moreover, accumulating evidence indicates that radiation can facilitate the recruitment of regulatory T-cells (Tregs) into the tumor microenvironment. Tregs can up-regulate the expression of interleukin (IL)-10 and transforming growth factor-beta (TGF-β) in the tumor microenvironment. Sharabi et al. have shown that the anti-PD-1 or Treg depletion can substantially increase radiation efficacy in eliminating tumoral cells (42). Besides, Tregs can up-regulate cytotoxic T-lymphocyte-associated protein 4 (CTLA-4) expression and further attenuate the anti-tumoral immune responses. Indeed, CTLA-4 upregulation might be one of the reasons for developing resistance in immune-radiotherapy (43). Besides the beneficial effect of immune checkpoint inhibition on the response rate of glioma radiotherapy, radiotherapy can also increase the permeability of the blood-brain barrier for immune checkpoint inhibitors (44, 45). Therefore, the administration of immune checkpoint inhibitors can increase radiotherapy efficacy and vice versa (41, 42). Collectively, the current evidence indicates that exposure to anti-cancer therapies, e.g., chemo-radiotherapy, can up-regulate inhibitory immune checkpoint molecules in tumor-infiltrating $CD8^+$ T-cells, and unlike unexposed patients, increased tumor-infiltrating $CD8^+$ T-cells in anti-cancer therapy-exposed tumoral tissues can be associated with the inferior prognosis of affected patients.

The Cross-Talk Between the PD-L1/PD-1 Axis and Tumor-Infiltrating $CD8^+$ T-Cells in High-Grade Glial Tumors

We have observed a significant association between tumor-infiltrating $PD\text{-}1^+$ lymphocytes with tumor-infiltrating $CD8^+$ $PD\text{-}1^+$ T-cells in glioblastoma patients treated with chemotherapy/investigational agents. Su et al. have shown a significant inverse relationship between PD-L1 expression and the intensity of tumor-infiltrating $CD8^+$ T-cells in glioblastoma patients who have not been exposed to anti-cancer therapies (**Table 4**). Nambirajan et al. have reported a strong positive association between PD-L1 expression and the level of tumor-infiltrating $CD8^+$ T-cells in patients with high-grade ependymoma (**Table 3S**).

We have found that the combination of low PD-L1 expression and high infiltration of $CD8^+$ T-cells is associated with improved OS in glioblastoma patients who have not been exposed to anti-cancer therapies. Also, the survival rate of glioblastoma patients with low PD-L1 expression and low level of tumor-infiltrating $CD8^+$ T-cells has been similar to the survival rate of glioblastoma patients with high PD-L1 expression and low level of tumor-infiltrating $CD8^+$ T-cells, indicating the critical prognostic value of $CD8^+$ T-cells and its phenotype in determining the survival of glioblastoma patients who have not been exposed to anti-cancer therapies. Besides, a high $PD\text{-}1^+$/tumor-infiltrating $CD8^+$ T-cell ratio has been associated with substantially inferior PFS and OS in glioblastoma patients (**Table 4**). Collectively, the presence phenotype of tumor-infiltrating $CD8^+$ T-cells has an essential role in determining the survival of glioblastoma patients.

Single-Cell Sequencing: A Novel Strategy to Address the Daunting Challenges?

Although PD-1 expression in the tumor-infiltrating $CD8^+$ T-cells can substantially attenuate anti-tumoral effects of cancer therapies, the tumor microenvironment of glioblastoma is more complicated

than its direction can be determined by the expression level of a single inhibitory immune checkpoint molecule. Indeed, various axes, which the PD-L1/PD-1 axis is one of them, determine the fate of anti-tumoral immune responses. Besides the remarkable association between CTLA-4 and PD-1, recent findings have indicated remarkable associations between other inhibitory immune checkpoints, e.g., TIGIT, in gliomas (46). Thus, immunotherapies for glioblastoma patients should be focused on disrupting these inhibitory checkpoints to restore anti-tumoral immune responses.

Furthermore, the low response rate of glioblastoma patients to immune-checkpoint inhibitors compared to melanoma patients also indicates that the glioblastoma tumor microenvironment might not be regulated by a single inhibitory molecule rather a network of the inhibitory immune checkpoints. Nayak et al. have reported that the objective response rate of glioblastoma patients to monotherapy with pembrolizumab is 0% (47). Reardon et al. have shown that the objective response rate of glioblastoma patients to monotherapy with nivolumab is approximately 7.8% (12). Blumenthal et al. have found that monotherapy with pembrolizumab does not bring clinical benefits for patients with brain tumors (48). In contrast to these dismal results, a meta-analysis by Li et al. has shown that PD-1 inhibitors can remarkably improve the OS of melanoma patients (49).

Moreover, the current method of immune checkpoint inhibitors administration can increase the risk of immune-related adverse events development. Administrating immune checkpoint inhibitors without considering the expression patterns of immune checkpoint molecules in the tumor microenvironment cannot effectively stimulate anti-tumoral immune responses in the tumor microenvironment rather can increase the risk of autoimmunity development in healthy tissues (50, 51). Simonelli et al. have reported a glioblastoma patient that nivolumab administration led to severe liver damage (52). Comito et al. have reported a glioblastoma patient that developed aplastic anemia following treatment with nivolumab (53). Therefore, immune checkpoint inhibitors should be administrated according to the immune checkpoints expression patterns in the cells residing in the tumor microenvironment to minimize the risk of immune-related adverse events development (6–8).

Single-cell sequencing technology has allowed us to study the cells at the single-cell level. The single-cell sequencing of immune cells, e.g., tumor-infiltrating $CD8^+$ T-cells, enables us to demonstrate the expression patterns of various inhibitory immune checkpoint molecules (54). Indeed, the expression profile of the cells in the tumor microenvironment can allow us to design a precise regimen for each patient to increase the response rate of immune checkpoint inhibitors and decrease the risk of immune-related adverse events development following the administration of immune checkpoint inhibitors (54, 55) (**Figure 2**).

Besides, single-cell sequencing can provide valuable insights for predicting the response rate of affected patients to immune checkpoint inhibitors. Although there are established biomarkers for predicting the response rate of patients with solid cancers to immune checkpoint inhibitors, e.g., *BRCA1/2* alteration and mismatch-repair status, the data from single-cell sequencing can study the cells and their origins at the single-cell level and provide with more valuable prognostic biomarkers (56, 57). In this regard, it has been identified that the expression of TCF7 in $CD8^+$ T-cells can be a prognostic factor for predicting the response rate of melanoma patients to anti-PD-1 therapy (58).

Zhai et al. have applied single-cell sequencing techniques to investigate the expression of immune checkpoints in resected high-grade glioma. They have found that the expression of the inhibitory immune checkpoints and their pertained ligands in tumoral cells is substantially increased during tumorigenesis (59). Huang et al. have used bioinformatic single-cell sequencing data of immune cells and have demonstrated that CTLA-4 is remarkably up-regulated in natural killer cells (60). Besides the potentiality of this technology in profiling the expression of known inhibitory immune checkpoint molecules and their expression intensities, this technology can also provide new insights about novel inhibitory immune checkpoints in high-grade glial tumors. Li et al. have reported that the sialic acid-binding Ig-like lectin family is a novel inhibitory immune checkpoint in glioma. They have shown that sialic acid-binding Ig-like lectin-16 is functionally similar to PD-L1 and sialic acid-binding Ig-like lectin-5/-7/-9 are functionally similar to immunoglobulin mucin-3 (TIM-3). Besides, their expression levels have been associated with advanced tumor grades in patients with glioma (61). Tan et al. have used bioinformatic single-cell sequencing data of immune cells and have indicated that the expression of sialic acid-binding Ig like lectin 1 is positively correlated with PD-1 and CTLA-4 in glioma (62). A recent clinical trial has used cytometry by time-of-flight technique to identify the reason for the low response rate of glioblastoma patients to pembrolizumab. They have found that the overexpression of CD68 in the tumor microenvironment can be the culprit for the low response rate of glioblastoma patients to pembrolizumab (63). Indeed, the application of single-cell sequencing can provide ample opportunities to investigate the factors that are implicated in immune resistance. Besides, radio/chemotherapy can augment the inhibitory immune checkpoint axes in glioblastoma patients; thus, integrating the results of single-cell sequencing to proscribe immune checkpoint inhibitors can also effectively and precisely improve the response rates of glioblastoma patients.

Despite the promising future of this approach for patients with high-grade glial tumors, this approach has some limitations. The most noticeable limitation of this approach is its complex nature that requires the implantation of high technologies. Its second limitation might be stemmed from the fact that the expression level obtained from sequencing RNAs does not always correlate with their protein expressions because the post-transcriptional modifications can substantially alter the protein expressions. Nevertheless, the recent advances in antibody sequencing and RNA expression and protein sequencing (REAP-seq) technologies can overcome this issue and provide a better insight into the phenotype of cells (55). Its third limitation is that the tumor-microenvironment is highly dynamic, and serial sequencing might be required for optimal

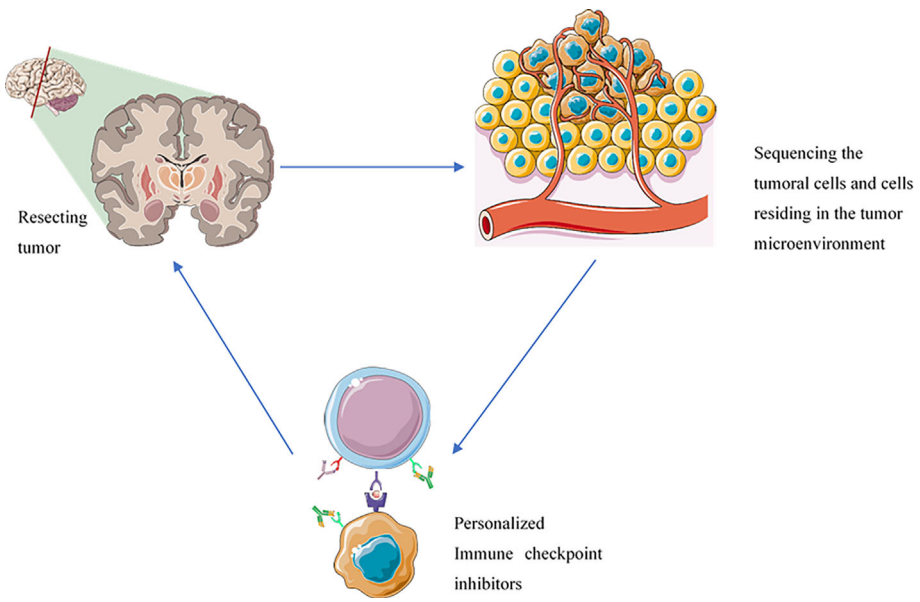

FIGURE 2 | The administration of immune checkpoint inhibitors based on the inhibitory immune checkpoint expression profile of each patient can improve patients' response rates, decrease the risk of immune-related adverse events development, prevent the immune-resistance development, and reduce the risk of tumor recurrence. The components of this figure were obtained from https://smart.servier.com/.

results. Thus, follow-up sequencing might be needed. Nevertheless, the promising preclinical results and the recent advances in deep learning might justify its translation and open a new era in the neuro-oncology field (64).

Collectively, PD-L1 overexpression can be associated with the poor prognosis of glioblastoma patients who have not been exposed to anti-cancer therapies. Since anti-cancer therapies, like chemo-radiotherapy, can increase the expression of inhibitory immune checkpoint molecules in tumor-infiltrating $CD8^+$ T-cells, exposed glioblastoma tissues to anti-cancer therapies can exhaust tumor-infiltrating $CD8^+$ T-cells and these exhausted tumor-infiltrating $CD8^+$ T-cells are associated with the inferior prognosis of glioblastoma patients. Nevertheless, the increased infiltration of tumor-infiltrating $CD8^+$ T-cells is associated with the improved prognosis of glioblastoma patients who have not been exposed to anti-cancer therapies. Therefore, profiling the expression pattern of inhibitory immune checkpoints in the tumor microenvironment *via* single-cell sequencing technologies and administrating related immune checkpoint inhibitors based on these data can pave the way to increase the response rate of anti-cancer therapies, enhance the efficacy of immune checkpoint inhibitors, decrease the risk of tumor recurrence, improve the immune-resistance state, and reduce the risk of autoimmunity development in the affected patients.

The current systematic review has some strengths: First, all fields of the major electronic databases, i.e., Web of Science, Scopus, PubMed, and Embase, have been searched to minimize the risk of not including eligible studies. Second, the current systematic review has shed light on the controversial results accumulating during the past decade and, *via* a systematic and unbiased approach, have elucidated the significance of the tumor-infiltrating $CD8^+$ T-cells/PD-L1 axis in the affected patients. Third, the current systemic review has sorted out the inconsistencies between preclinical and clinical studies and presented novel insights into the tumor microenvironment. Fourth, along with the recent phase II "window-of-opportunity" clinical trial, we have highlighted the potential role of single-cell sequencing in increasing the response rates of anti-cancer therapies, decreasing the risk of immune-related adverse events development, preventing the immune-resistance development, and reducing the risk of tumor recurrence in affected patients. Nevertheless, the current systematic review has some limitations as well. First, the number of included studies has been low because high-grade glial tumors are not as prevalent as other cancers, like breast and lung cancers. Second, our included studies have been limited to the investigations that have been published in English. Third, ideally, studies would apply novel single-cell sequencing-based approaches, e.g., mass cytometry, to study the expression profile of well-established inhibitory immune checkpoints on immune cells; however, so far, the main detection method has been immunohistochemistry (IHC). Therefore, more investigations on the promising potentiality of single-cell sequencing on the profiling of inhibitory immune checkpoints expression are recommended to ameliorate affected patients' prognosis.

CONCLUSION

PD-L1 overexpression can be associated with inferior prognosis in glioblastoma patients unexposed to anti-cancer therapies, e.g.,

chemo-radiotherapy. We have found that the level of tumor-infiltrating $CD8^+$ T-cells can be associated with improved prognosis in glioblastoma patients who have not been exposed to chemo-radiotherapy. Nevertheless, their infiltration level is associated with inferior prognosis in glioblastoma patients who underwent radio/chemotherapy because radio/chemotherapy can up-regulate the expression of inhibitory immune checkpoint molecules, e.g., PD-1, in tumor-infiltrating $CD8^+$ T-cells and induce a state of exhaustion in immune cells. Indeed, the expression of inhibitory immune checkpoint molecules in tumor-infiltrating $CD8^+$ T-cells decreases the response rate of anti-cancer therapies; thus, the administration of immune checkpoint inhibitors can improve the response rates of radio/chemotherapy approaches. Single-cell sequencing of the cells that reside in the tumor microenvironment can allow us to identify the profile of expressed inhibitory immune checkpoint molecules, which can be used to prescribe related immune checkpoint inhibitors. In this approach, the response rate of affected patients can be improved, and the risk of immune-related adverse events development following administration of immune checkpoint inhibitors can be decreased. However, the technical challenges and the cost of the suggested approach requires further studies to evaluate its cost-effectiveness before its translation into the clinics.

AUTHOR CONTRIBUTIONS

MA has come up with the topic, extracted data, and interpreted the data. ZA, NH, AD, NA, and OB have developed the syntax, ran the search, selected the studies, and assessed the quality of included studies. NS and BB have supervised and helped to develop the research question. All authors contributed to the article and approved the submitted version.

ACKNOWLEDGMENTS

We appreciate the researchers of the Immunology Research Center, Tabriz University of Medical Sciences, Tabriz, Iran. We also thank the professional researchers of the Research Center for Evidence-Based Medicine, Tabriz University of Medical Sciences, Tabriz, Iran (number=67552).

SUPPLEMENTARY MATERIAL

The Supplementary Material for this article can be found online at: https://www.frontiersin.org/articles/10.3389/fimmu.2021.734956/full#supplementary-material

REFERENCES

1. Brown NF, Carter TJ, Ottaviani D, Mulholland P. Harnessing the Immune System in Glioblastoma. *Br J Cancer* (2018) 119(10):1171–81. doi: 10.1038/s41416-018-0258-8
2. Qi Y, Liu B, Sun Q, Xiong X, Chen Q. Immune Checkpoint Targeted Therapy in Glioma: Status and Hopes. *Front Immunol* (2020) 11.
3. Dutoit V, Migliorini D, Dietrich P-Y, Walker PR. Immunotherapy of Malignant Tumors in the Brain: How Different From Other Sites? *Front Oncol* (2016) 6:256. doi: 10.3389/fonc.2016.00256
4. DeCordova S, Shastri A, Tsolaki AG, Yasmin H, Klein L, Singh SK, et al. Molecular Heterogeneity and Immunosuppressive Microenvironment in Glioblastoma. *Front Immunol* (2020) 11:1402. doi: 10.3389/fimmu.2020.01402
5. Hosseinkhani N, Derakhshani A, Kooshkaki O, Abdoli Shadbad M, Hajiasgharzadeh K, Baghbanzadeh A, et al. Immune Checkpoints and CAR-T Cells: The Pioneers in Future Cancer Therapies? *Int J Mol Sci* (2020) 21(21):8305. doi: 10.3390/ijms21218305
6. Sun Y, Luo J, Chen Y, Cui J, Lei Y, Cui Y, et al. Combined Evaluation of the Expression Status of CD155 and TIGIT Plays an Important Role in the Prognosis of LUAD (Lung Adenocarcinoma). *Int Immunopharmacol* (2020) 80:106198. doi: 10.1016/j.intimp.2020.106198
7. Wang L, Jia B, Claxton DF, Ehmann WC, Rybka WB, Mineishi S, et al. VISTA is Highly Expressed on MDSCs and Mediates an Inhibition of T Cell Response in Patients With AML. *Oncoimmunology* (2018) 7(9):e1469594. doi: 10.1080/2162402X.2018.1469594
8. Xie X, Zhang J, Shi Z, Liu W, Hu X, Qie C, et al. The Expression Pattern and Clinical Significance of the Immune Checkpoint Regulator VISTA in Human Breast Cancer. *Front Immunol* (2020) 11:2808. doi: 10.3389/fimmu.2020.563044
9. Hosseinkhani N, Derakhshani A, Abdoli Shadbad M, Argentiero A, Racanelli V, Kazemi T, et al. The Role of V-Domain Ig Suppressor of T Cell Activation (VISTA) in Cancer Therapy: Lessons Learned and the Road Ahead. *Front Immunol* (2021) 12:1797. doi: 10.3389/fimmu.2021.676181
10. Dai B, Qi N, Li J, Zhang G. Temozolomide Combined With PD-1 Antibody Therapy for Mouse Orthotopic Glioma Model. *Biochem Biophys Res Commun* (2018) 501(4):871–6. doi: 10.1016/j.bbrc.2018.05.064
11. Park J, Kim CG, Shim J-K, Kim JH, Lee H, Lee JE, et al. Effect of Combined Anti-PD-1 and Temozolomide Therapy in Glioblastoma. *Oncoimmunology* (2019) 8(1):e1525243. doi: 10.1080/2162402X.2018.1525243
12. Reardon DA, Brandes AA, Omuro A, Mulholland P, Lim M, Wick A, et al. Effect of Nivolumab vs Bevacizumab in Patients With Recurrent Glioblastoma: The CheckMate 143 Phase 3 Randomized Clinical Trial. *JAMA Oncol* (2020) 6(7):1003–10. doi: 10.1001/jamaoncol.2020.1024
13. Madkouri R, Kaderbhai CG, Bertaut A, Truntzer C, Vincent J, Aubriot-Lorton MH, et al. Immune Classifications With Cytotoxic CD8+ and Th17 Infiltrates Are Predictors of Clinical Prognosis in Glioblastoma. *Oncoimmunology* (2017) 6(6):e1321186. doi: 10.1080/2162402X.2017.1321186
14. Kim Y-H, Jung T-Y, Jung S, Jang W-Y, Moon K-S, Kim I-Y, et al. Tumour-Infiltrating T-Cell Subpopulations in Glioblastomas. *Br J Neurosurg* (2012) 26 (1):21–7. doi: 10.3109/02688697.2011.584986
15. Miyazaki T, Ishikawa E, Matsuda M, Akutsu H, Osuka S, Sakamoto N, et al. Assessment of PD-1 Positive Cells on Initial and Secondary Resected Tumor Specimens of Newly Diagnosed Glioblastoma and Its Implications on Patient Outcome. *J Neuro-Oncol* (2017) 133(2):277–85. doi: 10.1007/s11060-017-2451-7
16. Su L, Guo W, Lou L, Nie S, Zhang Q, Liu Y, et al. EGFR-ERK Pathway Regulates CSN6 to Contribute to PD-L1 Expression in Glioblastoma. *Mol Carcinogene* (2020) 59(5):520–32. doi: 10.1002/mc.23176
17. Moher D, Liberati A, Tetzlaff J, Altman DG, Group P. Preferred Reporting Items for Systematic Reviews and Meta-Analyses: The PRISMA Statement. *PloS Med* (2009) 6(7):e1000097.
18. Hayden JA, Côté P, Bombardier C. Evaluation of the Quality of Prognosis Studies in Systematic Reviews. *Ann Internal Med* (2006) 144(6):427–37. doi: 10.7326/0003-4819-144-6-200603210-00010
19. Ma L-L, Wang Y-Y, Yang Z-H, Huang D, Weng H, Zeng X-T. Methodological Quality (Risk of Bias) Assessment Tools for Primary and Secondary Medical Studies: What Are They and Which is Better? *Military Med Res* (2020) 7(1):1–11. doi: 10.1186/s40779-020-00238-8
20. Berghoff AS, Kiesel B, Widhalm G, Rajky O, Ricken G, Wöhrer A, et al. Programmed Death Ligand 1 Expression and Tumor-Infiltrating Lymphocytes in Glioblastoma. *Neuro-Oncology* (2015) 17(8):1064–75. doi: 10.1093/neuonc/nou307
21. Jan C-I, Tsai W-C, Harn H-J, Shyu W-C, Liu M-C, Lu H-M, et al. Predictors of Response to Autologous Dendritic Cell Therapy in Glioblastoma Multiforme. *Front Immunol* (2018) 9:727. doi: 10.3389/fimmu.2018.00727

22. Plant AS, Koyama S, Sinai C, Solomon IH, Griffin GK, Ligon KL, et al. Immunophenotyping of Pediatric Brain Tumors: Correlating Immune Infiltrate With Histology, Mutational Load, and Survival and Assessing Clonal T Cell Response. *J Neuro-oncol* (2018) 137(2):269–78. doi: 10.1007/s11060-017-2737-9
23. Zhang Y, Pan C, Wang J, Cao J, Liu Y, Wang Y, et al. Genetic and Immune Features of Resectable Malignant Brainstem Gliomas. *Oncotarget* (2017) 8 (47):82571. doi: 10.18632/oncotarget.19653
24. Nambirajan A, Malgulwar PB, Sharma A, Boorgula MT, Doddamani R, Singh M, et al. Clinicopathological Evaluation of PD-L1 Expression and Cytotoxic T-Lymphocyte Infiltrates Across Intracranial Molecular Subgroups of Ependymomas: Are These Tumors Potential Candidates for Immune Check-Point Blockade? *Brain Tumor Pathol* (2019) 36(4):152–61. doi: 10.1007/s10014-019-00350-1
25. Shadbad MA, Hajiasgharzadeh K, Derakhshani A, Silvestris N, Baghbanzadeh A, Racanelli V, et al. From Melanoma Development to RNA-Modified Dendritic Cell Vaccines: Highlighting the Lessons From the Past. *Front Immunol* (2021) 12:331. doi: 10.3389/fimmu.2021.623639
26. Baghbani E, Noorolyai S, Shanehbandi D, Mokhtarzadeh A, Aghebati-Maleki L, Shahgoli VK, et al. Regulation of Immune Responses Through CD39 and CD73 in Cancer: Novel Checkpoints. *Life Sci* (2021) 119826.
27. Qiu XY, Hu DX, Chen W-Q, Chen RQ, Qian SR, Li CY, et al. PD-L1 Confers Glioblastoma Multiforme Malignancy via Ras Binding and Ras/Erk/EMT Activation. *Biochim Biophys Acta (BBA)-Mol Basis Dis* (2018) 1864(5):1754–69. doi: 10.1016/j.bbadis.2018.03.002
28. Yue Q, Zhang X, Ye H-x, Wang Y, Du Z-G, Yao Y, et al. The Prognostic Value of Foxp3+ Tumor-Infiltrating Lymphocytes in Patients With Glioblastoma. *J Neuro-Oncol* (2014) 116(2):251–9. doi: 10.1007/s11060-013-1314-0
29. Li Q, Guo J, Wang W, Wang D. Relationship Between MGMT Gene Expression and Treatment Effectiveness and Prognosis in Glioma. *Oncol Lett* (2017) 14(1):229–33. doi: 10.3892/ol.2017.6123
30. Weichselbaum RR, Liang H, Deng L, Fu Y-X. Radiotherapy and Immunotherapy: A Beneficial Liaison? *Nat Rev Clin Oncol* (2017) 14 (6):365. doi: 10.1038/nrclinonc.2016.211
31. Zeng H, Zhang W, Gong Y, Xie C. Radiotherapy Activates Autophagy to Increase CD8+ T Cell Infiltration by Modulating Major Histocompatibility Complex Class-I Expression in Non-Small Cell Lung Cancer. *J Int Med Res* (2019) 47(8):3818–30. doi: 10.1177/0300060519855595
32. Heynckes S, Daka K, Franco P, Gaebelein A, Frenking JH, Doria-Medina R, et al. Crosslink Between Temozolomide and PD-L1 Immune-Checkpoint Inhibition in Glioblastoma Multiforme. *BMC Cancer* (2019) 19(1):1–7. doi: 10.1186/s12885-019-5308-y
33. Heynckes S, Gaebelein A, Haaker G, Grauvogel J, Franco P, Mader I, et al. Expression Differences of Programmed Death Ligand 1 in De-Novo and Recurrent Glioblastoma Multiforme. *Oncotarget* (2017) 8(43):74170. doi: 10.18632/oncotarget.18819
34. Xue S, Song G, Yu J. The Prognostic Significance of PD-L1 Expression in Patients With Glioma: A Meta-Analysis. *Sci Rep* (2017) 7(1):1–8. doi: 10.1038/s41598-017-04023-x
35. Nduom EK, Wei J, Yaghi NK, Huang N, Kong L-Y, Gabrusiewicz K, et al. PD-L1 Expression and Prognostic Impact in Glioblastoma. *Neuro-Oncology* (2015) 18(2):195–205.
36. Han J, Hong Y, Lee YS. PD-L1 Expression and Combined Status of PD-L1/PD-1–Positive Tumor Infiltrating Mononuclear Cell Density Predict Prognosis in Glioblastoma Patients. *J Pathol Trans Med* (2017) 51(1):40. doi: 10.4132/jptm.2016.08.31
37. Lee KS, Lee K, Yun S, Moon S, Park Y, Han JH, et al. Prognostic Relevance of Programmed Cell Death Ligand 1 Expression in Glioblastoma. *J Neuro-Oncol* (2018) 136(3):453–61. doi: 10.1007/s11060-017-2675-6
38. Grapin M, Richard C, Limagne E, Boidot R, Morgand V, Bertaut A, et al. Optimized Fractionated Radiotherapy With Anti-PD-L1 and Anti-TIGIT: A Promising New Combination. *J Immunother Cancer* (2019) 7(1):1–12. doi: 10.1186/s40425-019-0634-9
39. Zeng J, See AP, Phallen J, Jackson CM, Belcaid Z, Ruzevick J, et al. Anti-PD-1 Blockade and Stereotactic Radiation Produce Long-Term Survival in Mice With Intracranial Gliomas. *Int J Radiat Oncol Biol Phys* (2013) 86(2):343–9. doi: 10.1016/j.ijrobp.2012.12.025
40. Li D, Chen R, Wang Y-W, Fornace AJJr., Li H-H. Prior Irradiation Results in Elevated Programmed Cell Death Protein 1 (PD-1) in T Cells. *Int J Radiat Biol* (2018) 94(5):488–94. doi: 10.1080/09553002.2017.1400192
41. Dovedi SJ, Adlard AL, Lipowska-Bhalla G, McKenna C, Jones S, Cheadle EJ, et al. Acquired Resistance to Fractionated Radiotherapy Can be Overcome by Concurrent PD-L1 Blockade. *Cancer Res* (2014) 74(19):5458–68. doi: 10.1158/0008-5472.CAN-14-1258
42. Sharabi AB, Nirschl CJ, Kochel CM, Nirschl TR, Francica BJ, Velarde E, et al. Stereotactic Radiation Therapy Augments Antigen-Specific PD-1–Mediated Antitumor Immune Responses via Cross-Presentation of Tumor Antigen. *Cancer Immunol Res* (2015) 3(4):345–55. doi: 10.1158/2326-6066.CIR-14-0196
43. Twyman-Saint Victor C, Rech AJ, Maity A, Rengan R, Pauken KE, Stelekati E, et al. Radiation and Dual Checkpoint Blockade Activate Non-Redundant Immune Mechanisms in Cancer. *Nature* (2015) 520(7547):373–7. doi: 10.1038/nature14292
44. Sanders S, Debinski W. Challenges to Successful Implementation of the Immune Checkpoint Inhibitors for Treatment of Glioblastoma. *Int J Mol Sci* (2020) 21(8):2759. doi: 10.3390/ijms21082759
45. Farber SH, Tsvankin V, Narloch JL, Kim GJ, Salama AK, Vlahovic G, et al. Embracing Rejection: Immunologic Trends in Brain Metastasis. *Oncoimmunology* (2016) 5(7):e1172153. doi: 10.1080/2162402X.2016.1172153
46. Liu F, Huang J, Liu X, Cheng Q, Luo C, Liu Z. CTLA-4 Correlates With Immune and Clinical Characteristics of Glioma. *Cancer Cell Int* (2020) 20 (1):1–10. doi: 10.1186/s12935-019-1085-6
47. Nayak L, Molinaro AM, Peters K, Clarke JL, Jordan JT, de Groot J, et al. Randomized Phase II and Biomarker Study of Pembrolizumab Plus Bevacizumab Versus Pembrolizumab Alone for Patients With Recurrent Glioblastoma. *Clin Cancer Res* (2021) 27(4):1048–57. doi: 10.1158/1078-0432.CCR-20-2500
48. Blumenthal DT, Yalon M, Vainer GW, Lossos A, Yust S, Tzach L, et al. Pembrolizumab: First Experience With Recurrent Primary Central Nervous System (CNS) Tumors. *J Neuro-Oncol* (2016) 129(3):453–60. doi: 10.1007/s11060-016-2190-1
49. Li J, Gu J. Efficacy and Safety of PD-1 Inhibitors for Treating Advanced Melanoma: A Systematic Review and Meta-Analysis. *Immunotherapy* (2018) 10(15):1293–302. doi: 10.2217/imt-2018-0116
50. Shadbad MA, Safaei S, Brunetti O, Derakhshani A, Lotfinejad P, Mokhtarzadeh A, et al. A Systematic Review on the Therapeutic Potentiality of PD-L1-Inhibiting MicroRNAs for Triple-Negative Breast Cancer: Toward Single-Cell Sequencing-Guided Biomimetic Delivery. *Genes* (2021) 12(8):1206.
51. Kooshkaki O, Derakhshani A, Hosseinkhani N, Torabi M, Safaei S, Brunetti O, et al. Combination of Ipilimumab and Nivolumab in Cancers: From Clinical Practice to Ongoing Clinical Trials. *Int J Mol Sci* (2020) 21 (12):4427. doi: 10.3390/ijms21124427
52. Simonelli M, Di Tommaso L, Baretti M, Santoro A. Pathological Characterization of Nivolumab-Related Liver Injury in a Patient With Glioblastoma. *Immunotherapy* (2016) 8(12):1363–9. doi: 10.2217/imt-2016-0057
53. Comito RR, Badu LA, Forcello N. Nivolumab-Induced Aplastic Anemia: A Case Report and Literature Review. *J Oncol Pharm Pract* (2019) 25(1):221–5. doi: 10.1177/1078155217726159
54. Derakhshani A, Rostami Z, Safarpour H, Shadbad MA, Nourbakhsh NS, Argentiero A, et al. From Oncogenic Signaling Pathways to Single-Cell Sequencing of Immune Cells: Changing the Landscape of Cancer Immunotherapy. *Molecules* (2021) 26(8):2278.
55. Gibellini L, De Biasi S, Porta C, Lo Tartaro D, Depenni R, Pellacani G, et al. Single-Cell Approaches to Profile the Response to Immune Checkpoint Inhibitors. *Front Immunol* (2020) 11:490. doi: 10.3389/fimmu.2020.00490
56. Le DT, Uram JN, Wang H, Bartlett BR, Kemberling H, Eyring AD, et al. PD-1 Blockade in Tumors With Mismatch-Repair Deficiency. *New Engl J Med* (2015) 372(26):2509–20. doi: 10.1056/NEJMoa1500596
57. Zhou Z, Li M. Evaluation of BRCA1 and BRCA2 as Indicators of Response to Immune Checkpoint Inhibitors. *JAMA Network Open* (2021) 4(5):e217728–e. doi: 10.1001/jamanetworkopen.2021.7728
58. Sade-Feldman M, Yizhak K, Bjorgaard SL, Ray JP, de Boer CG, Jenkins RW, et al. Defining T Cell States Associated With Response to Checkpoint

Immunotherapy in Melanoma. *Cell* (2018) 175(4):998–1013.e20. doi: 10.1016/j.cell.2018.10.038
59. Zhai Y, Li G, Li R, Chang Y, Feng Y, Wang D, et al. Single-Cell RNA-Sequencing Shift in the Interaction Pattern Between Glioma Stem Cells and Immune Cells During Tumorigenesis. *Front Immunol* (2020) 11:2475. doi: 10.3389/fimmu.2020.581209
60. Huang S, Song Z, Zhang T, He X, Huang K, Zhang Q, et al. Identification of Immune Cell Infiltration and Immune-Related Genes in the Tumor Microenvironment of Glioblastomas. *Front Immunol* (2020) 11.
61. Li G-Z, Zhang K-N, Wang Z, Hu H-M, Wang Z-L, Huang R-Y, et al. Siglecs, Novel Immunotherapy Targets, Potentially Enhance the Effectiveness of Existing Immune Checkpoint Inhibitors in Glioma Immunotherapy. *OncoTargets Ther* (2019) 12:10263. doi: 10.2147/OTT.S223406
62. Tan YQ, Li YT, Yan TF, Xu Y, Liu BH, Yang JA, et al. Six Immune Associated Genes Construct Prognostic Model Evaluate Low-Grade Glioma. *Front Immunol* (2020) 11.
63. De Groot J, Penas-Prado M, Alfaro-Munoz K, Hunter K, Pei BL, O'Brien B, et al. Window-Of-Opportunity Clinical Trial of Pembrolizumab in Patients With Recurrent Glioblastoma Reveals Predominance of Immune-Suppressive Macrophages. *Neuro-Oncology* (2020) 22(4):539–49. doi: 10.1093/neuonc/noz185
64. Fortelny N, Bock C. Knowledge-Primed Neural Networks Enable Biologically Interpretable Deep Learning on Single-Cell Sequencing Data. *Genome Biol* (2020) 21(1):1–36. doi: 10.1186/s13059-020-02100-5

Conflict of Interest: The authors declare that the research was conducted in the absence of any commercial or financial relationships that could be construed as a potential conflict of interest.

Publisher's Note: All claims expressed in this article are solely those of the authors and do not necessarily represent those of their affiliated organizations, or those of the publisher, the editors and the reviewers. Any product that may be evaluated in this article, or claim that may be made by its manufacturer, is not guaranteed or endorsed by the publisher.

Copyright © 2021 Shadbad, Asadzadeh, Hosseinkhani, Derakhshani, Alizadeh, Brunetti, Silvestris and Baradaran. This is an open-access article distributed under the terms of the Creative Commons Attribution License (CC BY). The use, distribution or reproduction in other forums is permitted, provided the original author(s) and the copyright owner(s) are credited and that the original publication in this journal is cited, in accordance with accepted academic practice. No use, distribution or reproduction is permitted which does not comply with these terms.

frontiers in Immunology

REVIEW
published: 04 October 2021
doi: 10.3389/fimmu.2021.746621

Breaking Bad: Autophagy Tweaks the Interplay Between Glioma and the Tumor Immune Microenvironment

Yuxiang Fan, Yubo Wang, Jian Zhang, Xuechao Dong, Pu Gao, Kai Liu, Chengyuan Ma and Gang Zhao**

Department of Neurosurgery, The First Hospital of Jilin University, Changchun, China

Though significant strides in tumorigenic comprehension and therapy modality have been witnessed over the past decades, glioma remains one of the most common and malignant brain tumors characterized by recurrence, dismal prognosis, and therapy resistance. Immunotherapy advance holds promise in glioma recently. However, the efficacy of immunotherapy varies among individuals with glioma, which drives researchers to consider the modest levels of immunity in the central nervous system, as well as the immunosuppressive tumor immune microenvironment (TIME). Considering the highly conserved property for sustaining energy homeostasis in mammalian cells and repeatedly reported links in malignancy and drug resistance, autophagy is determined as a cutting angle to elucidate the relations between glioma and the TIME. In this review, heterogeneity of TIME in glioma is outlined along with the reciprocal impacts between them. In addition, controversies on whether autophagy behaves cytoprotectively or cytotoxically in cancers are covered. How autophagy collapses from its homeostasis and aids glioma malignancy, which may depend on the cell type and the cellular context such as reactive oxygen species (ROS) and adenosine triphosphate (ATP) level, are briefly discussed. The consecutive application of autophagy inducers and inhibitors may improve the drug resistance in glioma after overtreatments. It also highlights that autophagy plays a pivotal part in modulating glioma and the TIME, respectively, and the intricate interactions among them. Specifically, autophagy is manipulated by either glioma or tumor-associated macrophages to conform one side to the other through exosomal microRNAs and thereby adjust the interactions. Given that some of the crosstalk between glioma and the TIME highly depend on the autophagy process or autophagic components, there are interconnections influenced by the status and well-being of cells presumably associated with autophagic flux. By updating the most recent knowledge concerning glioma and the TIME from an autophagic perspective enhances comprehension and inspires more applicable and effective strategies targeting TIME while harnessing autophagy collaboratively against cancer.

Keywords: autophagy, glioma, MDSC, neutrophil, tumor-associated macrophage, tumor immune microenvironment

OPEN ACCESS

Edited by:
Quan Cheng,
Central South University, China

Reviewed by:
Hao Zhang,
Xiangya Hospital Central South University, China
Ming-Zhu Jin,
Shanghai Jiao Tong University, China

****Correspondence:***
Gang Zhao
zhaogjdyy@126.com
Chengyuan Ma
macyjdyy@126.com

Specialty section:
This article was submitted to Cancer Immunity and Immunotherapy, a section of the journal Frontiers in Immunology

Received: *24 July 2021*
Accepted: *17 September 2021*
Published: *04 October 2021*

Citation:
Fan Y, Wang Y, Zhang J, Dong X, Gao P, Liu K, Ma C and Zhao G (2021) Breaking Bad: Autophagy Tweaks the Interplay Between Glioma and the Tumor Immune Microenvironment. Front. Immunol. 12:746621. doi: 10.3389/fimmu.2021.746621

INTRODUCTION

Gliomas originate from supportive glial cells in people with dichotomy prognosis and limited treatment responses (1). Generally, its prognosis depends on the pathologic grade and genetic mutation profile, whose level of concern is checked through isocitrate dehydrogenase (IDH) and *1p/19q* status (2). Lower-grade glioma (LGG, WHO II-III grade) with prognostically favorable mutations yields the most benefits from multimodality approaches like early surgical resection, radiotherapies, chemotherapies, and other anti-tumor comprehensive therapies, while it remains a challenge to extend survival for other malignant types (3). The median survival time of patients with glioblastoma multiforme (GBM, WHO IV grade) is merely 14 months and the H3 Lys27Met-mutant glioma holds the worst prognosis: a 2-year survival rate less than 10%, among all diffuse gliomas (4). Recent advances have been made in exploring potential therapies by targeting the tumor immune microenvironment (TIME) in glioma.

As immunotherapies prevail in cancers, the limited responses in glioma to treatment lead to a reexamination of the core of immunotherapy: the infiltrating immunocytes and their local microenvironment. Immune infiltration in glioma through the disrupted blood-brain barrier (BBB) deprives the central nervous system (CNS) of "immune privilege" - restrictive entry of circulatory immune cells (5, 6). It is reported to be pertinent to glioma oncogenesis, progression, and therapy resistance (7, 8). The infiltrative immune cells, including tumor-associated macrophages/microglia (TAM), myeloid-derived suppressor cells (MDSCs), dendritic cells (DCs), neutrophils, and tumor-infiltrating lymphocytes, are meant to maintain intercellular homeostasis by eliminating abnormalities though the initial targets which ultimately somehow compromise (5, 9). Together with a few exhausted T cells, nonfunctional natural killer cells (NK cells), inflammatory mast cells, cancer-associated fibroblasts, diffusely distributed astrocytes, immunosuppressive cytokines, insufficient nutrient supply, and hypoxia, the glioma immune microenvironment is roughly characterized (10).

The immune microenvironment plays a dual role in glioma. Both innate and adaptive immune responses exert influence to retain control of glioma, whilst glioma inversely manipulates immune cells to attain immune suppression and evasion (11). It warrants more studies unraveling the potential mechanisms that glioma utilizes to shift functional immune cells towards being tumorigenic. Thus, it becomes possible to restore immune efficacy and revive the success of immunotherapies. Specifically, one way that could be employed not only by glioma but also by immune cells to adapt to both intrinsic and extrinsic alterations is autophagy.

Autophagy ensures cellular homeostasis and recycles cytoplasmic entities for energy supply when under stress (1). It typically includes three primary subtypes: macroautophagy, microautophagy, and chaperone-mediated autophagy (CMA). Despite the three morphologically unique forms, they all end up in the degradation of targets within lysosomes consonantly (12). In brief, macroautophagy, widely known as autophagy, uses autophagy adaptor proteins like p62/SQSTM1 to label cytoplasmic cargo for a double-membrane vesicle called autophagosome and lysosome degradation (13). In contrast, microautophagy directly encapsulates cellular cargos with endosomal membranes or invagination of lysosomal. CMA is characterized by the chaperone-binding cargos with Lys-Phe-Glu-Arg-Gln (KFERQ) -like pentapeptide motif entering lysosomes *via* lysosomal-associated membrane protein 2a (LAMP2a) (14). The detailed autophagy phases and machinery for each subtype are beyond the scope of this review and have already been extensively reviewed (15).

A myriad of evidence show that autophagy is exploited by glioma to resist therapies and by immune cells to dampen anti-tumor responses (16, 17). A study manifests that it is autophagy that is blocked by chloroquine (CQ), thereby enhancing cytotoxicity of temozolomide (TMZ) to glioma cells (18). Additionally, by analogy to the mammalian target of rapamycin (mTOR) inhibitor rapamycin, indoleamine 2,3-dioxygenase (IDO) -mediated tryptophan depletion educates T cells towards immune tolerance through triggering autophagy (19). Concerning the complex nature, it might be more informative and illuminating to integrate into a summary with the updated works of literature relative to autophagy in the glioma immune microenvironment.

In this review, the heterogeneity of tumor immune microenvironment in glioma is discussed, along with the reciprocal impacts on both sides. It also unveils the way that autophagy aids malignancy by switching itself between a cytoprotective role and a cytotoxic one within glioma. The fact that autophagy plays a pivotal part in modulating glioma cells and the members in the TIME, and thereby influencing the subtle interactions among the components of the microenvironment, are specifically highlighted. Overall, this review aims to pave the way for a resounding success of immunotherapies adjuvant with autophagy modulators for glioma in the near future.

THE INTERACTIVE TUMOR IMMUNE MICROENVIRONMENT IN GLIOMA

Despite a paucity of immune cells and limited lymphatic drainage, immunosurveillance within a healthy brain with brain-specific microglia is capable of stimulating a modest and highly regulated immune response (20). Circulating immune cells should have infiltrated in the CNS across the impaired BBB in the presence of glioma (21). Still, glioma displays a "cold tumor" phenotype with a low number of immunogenic effector immune cells compared with other tumors, which might be related to the limited efficacy of immunotherapies (22). Given the paradox of immune responses before and after glioma development, the intricate regulations of the immune microenvironment involved with both cellular and molecular mechanisms deserve more attention and discussion (**Figure 1**).

Tumor-Associated Macrophage/Microglia

TAMs dominate the infiltrative immune cells, which comprise up to 30% ~ 50% of glioma constituents (23, 24). It is initially conceived that TAMs shoulder tumor clearance through pro-inflammatory cytokine release and phagocytosis, which is validated by a recent study that uses activated TAMs for tumor containment (25). However, TAMs are one of the numerous

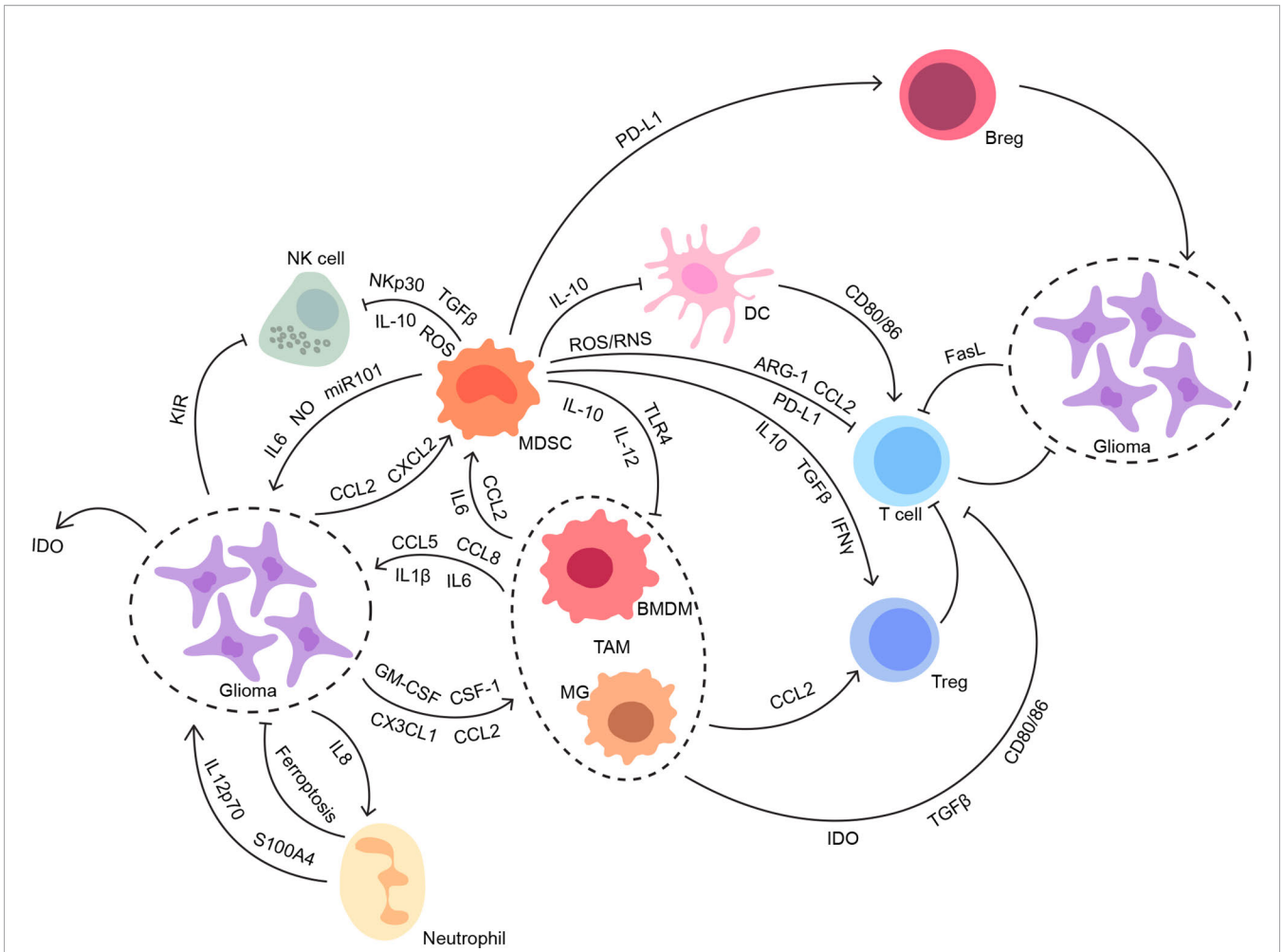

FIGURE 1 | The interconnections between glioma and its immune microenvironment. Both innate and adaptive immune systems contribute to the suppressive immune microenvironment in glioma. The intricate interconnections among the members of the glioma immune microenvironment work synergistically to facilitate tumor progression without disturbance, especially from anti-tumor immunity.

culprits to be blamed in the immunosuppressive TIME glioma, whose reasons may lie in its components (26). The bone-marrow-derived macrophages (BMDMs) appear to be defined as $CD11b^{+-}$ $CD45^{+}$ $CD49d^{+}$ macrophage population and recruited from peripheral circulating monocytes by glioma, whereas the tissue-resident $CD11b^{+}$ $CD45^{-}$ $CD49d^{-}$ microglia (MG) are derived from erythro-myeloid progenitors (EMPs) in embryonic yolk sac without postnatal replenishment from peripheral mononuclear hematopoiesis (5, 8, 27). Of distinct ontogenies, infiltrating TAMs may lead to varying outcomes in patients (28). The gene signature of BMDM, rather than MG, is observed to be negatively associated with survival in LGG (29). To better comprehend the complex mechanisms, further studies are conducted concerning the interplay between TAMs and glioma.

Glioma attracts TAMs, especially BMDMs, by secreting chemoattractants, including C-C motif chemokine ligand 2 (CCL2), C-C motif chemokine ligand 3 (CCL3), C-X-C motif chemokine ligand 12 (CXCL12), C-X3-C motif chemokine ligand 1(CX3CL1), colony-stimulating factor 1 (CSF-1), and granulocyte-macrophage colony-stimulating factor (GM-CSF) (30–33). Typically, CCL2 and CX3CL1 are regarded as the two of the most important chemokines in directing BMDMs and MG migration, respectively. A study reports that low-grade glioma stem-like cells (GSCs) harboring *BRAF* kinase gene mutations (*KIAA1549:BRAF* fusion) express Ccl2 for circulating monocytes recruitment (34). In parallel, MG highly expressing Cx3cr1 are led towards glioma by Cx3cl1, which is secreted by glioma cells with NF1 mutation (35). Moreover, intercellular adhesion molecule 1 (ICAM1) silencing in the *IDH1* wild-type glioma cells is demonstrated to increase macrophage infiltration and potentially enhance anti-tumor functions like phagocytosis. There are alternative ways for TAMs to be recruited, of which the composition could be chemokine-dependent (8). For example, lysyl oxidase (LOX) expression is activated by yes1 associated transcriptional regulator (YAP1) in a PTEN-deficient GBM model to recruit macrophages, which in turn supports the GBM with Secreted Phosphoprotein 1 (SPP1) (36).

Heavily dependent on the specific environmental signals, such as interferon-γ (IFN-γ), tumor necrosis factor (TNF), and IL-4, macrophages usually polarize but are not confined to binary phenotypes, antitumor M1 and protumor M2 subtypes (37). $CD68^+$ and $CD163^+$ M2 polarized cells are more prevalent in the TIME, which is in line with their immunosuppressive properties (38). However, there are difficulties in applying the predefined dual classification to TAMs. The expression profiles of TAMs in the GL261 glioma model and RCAS transgenic system, known as murine glioma models, resemble other specialized macrophage subgroups rather than matching with either the M1 or the M2 polarity (39). Consistently, TAMs isolated from the patients' biopsies co-express M1 and M2 genes frequently (29, 40). It may give rise to a novel classification suitable for TAMs, but the current paradigm distinguishing M1/M2 lays a solid basis for future refinement, which is CD40, CD74, CD80, CD86, MHC-II, and phosphorylated Signal Transducer and Activator Of Transcription 1 (STAT1) for the M1-like, while it is CD163, CD204, CD206, arginase-1(ARG-1), and phosphorylated STAT3 and STAT6 for the M2-like (30, 41).

Not only do the genetic alterations in TAMs result in new lineages, but they also involve glioma progression and lead to immunosuppression in the glioma microenvironment. The finding that the mouse GL261 glioma cells inoculated in *Tlr2* knockout mice grow a smaller tumor leading to longer survival of the host compared to the control indicates that the TAMs promote glioma progression *via* TLR2 signaling (42). TLR2 upregulates membrane type 1 matrix metalloprotease (MT1-MMP) and metallopeptidase 14 (MMP14) in MG to activate glioma-sourced MMP2 when responding to TLR2 endogenous ligands and thereby facilitate glioma invasion (43). TLR2 also increases matrix metalloproteinase 9 (MMP9) production, resulting in extracellular matrix (ECM) degradation (44). Of note, platelet-derived growth factor receptor (PDGFR) in glioma cells is induced by MG exclusively, which also promotes glioma progression (45). As for immunosuppression, TAMs produce CCL2 for recruiting $CCR2^+$ MDSCs and $CCR4^+$ Tregs (46).

Apart from the genetic influences, the distinct distribution of TAM components in glioma could be listed as a major factor contributing to immunosuppression as well. Recent single-cell RNA sequencing analyses reiterates that the BMDMs are more responsible for immunosuppression and unfavorable outcomes in glioma in contrast to the MG that mostly resides in the tumor periphery (29, 47–49). It also indicates that IDH mutation may correlate with TAM infiltration when the critical shift in the proportion of MG to BMDM between IDH mutation and IDH wild type is observed (49). Consistent with previous findings, it is ascribed to the BMDMs in the glioma center rather than the brain-resident MG occupying the peritumor area in terms of inhibited immunity in glioma (50). It leaves MG a dearth of credits since most effects are pinned on migratory macrophages. Indeed, the resident MG is capable of phagocytosis when meeting with glioma cells in response to myeloid checkpoint CD47- Signal regulatory proteinα (SIRPα) blockade *in vivo*. The MG even shows a dampened inflammatory response, making specific reeducation of the MG a promising strategy in glioma management (51). These reports indicate that specific and distinct roles of the TAM compartments are emerging with more in-depth investigations ongoing at single-cell resolution.

Moreover, studies reveal the crucial role of TAMs in glioma tumorigenesis, stemness, angiogenesis, invasion, and migration (52–55). Interleukin 1β (IL-1β) released by TAMs reprograms cellular metabolism by boosting glycolysis of glioma through the IL-1β-protein kinase-delta (PKCδ)-glycolytic enzyme glycerol-3-phosphate dehydrogenase (GPD2) axis, which promotes tumor proliferation and tumorigenesis (56). Specifically, it is C-C motif chemokine ligand 8 (CCL8) highly expressed by TAMs that promotes stem-like traits of GBM cells *via* the activation of ERK1/2 (54). Glioma angiogenesis is induced *via* vascular endothelial growth factor (VEGF) secretion (57). The fact that C-C motif chemokine ligand 5 (CCL5) modulates invasive and migratory behaviors of glioma through the phosphorylation of calmodulin-dependent protein kinase II (CaMKII) renders CCL5 and CaMKII interesting targets to halt glioma progression (55). More related reports are needed for an improved understanding of how TAMs interact with glioma and modulate the TIME so that therapies targeting TAMs would be boosted.

Myeloid-Derived Suppressive Cells

As a critical part of the suppressive network, myeloid-derived suppressive cells usually accumulate under pathologic conditions (58). The enrichment of MDSCs predicts glioma malignancy, poor prognosis, and low responses to treatments (59). Interestingly, the Bruyère group finds that the inhibition of chemokine C-X-C motif chemokine ligand 2 (CXCL2) expression in Hs683 glioma cells results in impaired cell proliferation (60). There is a related report showing that it is the CXCL2-CXCR2 axis that mediates MDSCs recruitment in the tumor (61). Targeting CCR2 with CCX872 not only reduces infiltrated MDSCs but also augments immunotherapy efficacy (62). Still, more mechanism studies uncovering how MDSCs are recruited to glioma are encouraged.

MDSCs mainly consist of $CD14^+$ $CD15^-$ monocytic MDSCs (M-MDSCs) and $CD14^-$ $CD15^+$ granulocytic or polymorphonuclear MDSCs (PMN-MDSCs). Some evidence shows that PMN-MDSCs predominates the blood and M-MDSCs mainly distribute throughout glioma tissue, while others supported the opposite, which may require more studies to corroborate (63–65). The two subsets of MDSCs could be differentiated from each other based on genomic entities, biochemical markers, and biological functions, especially the capacity to inhibit immune responses. Interestingly, hypoxia-stimulated glioma-derived exosomes containing microRNAs are reportedly associated with MDSC proliferation, differentiation, and activation (66, 67).

MDSCs suppress immunological reactivities in a variety of ways. They cripple TAMs and DCs for antigen presentation impairment, inhibit anti-tumor responses by NK cells and cytotoxic T cells, and induce inhibitory regulatory T cells (Tregs) (68–71). MDSCs modulate TAMs, the most common immune cells in glioma, to attain the suppressive goal. Through crosstalk with MDSCs releasing IL-10, macrophages are skewed towards the M2 phenotype producing less IL-12 and more

IL-10 (72). Similarly, it claims that MDSCs also disturb DC-mediated T cell stimulation by IL-10 (73). MDSCs additionally inhibited NK cells with ROS, TGF-β1, and NKp30 (74–76). The main strategy that MDSCs employed to interfere with T cells is through signal transducer and activator of transcription 3 (STAT3)-induced ROS and reactive nitrogen species (RNS) as oxidative stress, which leads to an increased level of arginase 1 (ARG1) and inducible nitric oxide synthase (iNOS) and thereafter L-arginine depletion, cell cycle arrest, and even apoptosis (70, 77, 78). The oxidative stress additionally renders T cells anergic and suppressive by reducing CD3 ζ chain expression and inducing nitrosylation of the IL-2 pathway (78). It also inhibited T cell migration when CCL2 is under nitration (70).

Beyond modulation of immune cells, some molecules, like nitric oxide (NO), prostaglandin E2 (PGE2), and programmed cell death 1 ligand 1 (PD-L1), are also associated with MDSC-mediated immunosuppression (79–82). The suppressive function of regulatory B cells (Bregs) is augmented by PD-L1 derived from MDSCs and thereby impeding $CD8^+$ T cell activation (82). Moreover, tumor-associated macrophages (TAM) can be renewed by M-MDSCs or monocytes differentiation, which is facilitated by HIF-1α along with CD45 tyrosine phosphate and STAT3 regulation in hypoxia (83–85).

Neutrophils

As the first-line sentinel of host defense for tissue homeostasis, neutrophils rapidly migrate to the tumor site in response to many signals like IL-8 and IL-1β (86). Glioma-derived IL-8 recruits neutrophils to infiltrate, while the recruited ones produce a magnitude of neutrophil extracellular traps (NETs) stimulating the NF-κB signaling pathway in GBM cells and promote IL-8 secretion *via* HMGB1 binding to the receptor for advanced glycation end products (RAGE) (87). Glioma progression accompanying neutrophil recruitment is also mediated by the long non-coding RNA LINC01116-triggered IL-1β upregulation (88). It is observed that both circulating and infiltrative neutrophils increase with glioma pathological grade, which predicts poor prognosis for patients (78). Besides, a recent study proposes that ferroptosis could be the nature of "necrosis" typically identified in GBM, which is mediated by the infiltrating neutrophils and the myeloperoxidase-containing granules (89). In contrast to their proinflammatory role, activated neutrophils (or granulocytic MDSCs) characterized by high plasma levels of IL12p70 promote glioma malignancy (90). Elastases secreted by infiltrative neutrophils nearby also accelerate the infiltration in glioma (91).

When treating glioblastoma with anti-VEGF therapy, increased neutrophil infiltration advances glioma mesenchymal transition and promotes proliferation of GSCs through upregulation of S100A4 (92). Targeting S100A4 can also sensitize glioma cells to bevacizumab treatment. The protumor role of neutrophils is further strengthened since depleting glioma-associated neutrophils with a monoclonal antibody against $Ly6G^+$ neutrophils prolongs survival in a preclinical GBM murine model (93). Neutrophils are also involved in the resistance to PD-1 inhibitors, which is revealed by the improved therapeutic efficacy of combinational treatment with antineutrophil and PD-1 inhibitors (94). However, more in-depth studies concerning the molecular mechanism mediated by neutrophils would provide better comprehension for the development of glioma therapy resistance.

Yet the detailed mechanism for neutrophil recruitment to glioma remains largely elusive. How the interaction between neutrophils and glioma in the local immune microenvironment works still needs to be intensively investigated. Since tumor-associated neutrophils generally exhibit functional plasticity and polarization, represented by anti-tumor N1-like and pro-tumor N2-like states, it would inspire more treatment strategies if the stimuli for neutrophil reprogramming and differentiation were uncovered.

Dendritic Cells

Due to the overestimation of MG as major antigen-presenting cells in CNS, DCs have not been gaining sufficient attention until recently (95, 96). DCs serve as indispensable sentinels of adaptive immune responses through internalizing surrounding antigens for presentation (97, 98). DCs are well-known for their activation of NK cells, T cells, and Tregs. One majority subtype of DCs is mostly $CD11c^+$ myeloid conventional dendritic cells (cDCs), another group is $CD11c^-$ plasmacytoid dendritic cells (pDCs) (99, 100). Relative to cDCs aiding $CD4^+$ Th1 differentiation and $CD8^+$ T cell activation, pDCs are more of interest because of their secretion of IFN-α, which directly stimulates antitumor immunity (100, 101).

Nonetheless, there are some studies casting doubts on immunogenicity generated by pDCs. The compromised elaboration of IFN-α, impaired antigen presentation, and increased Treg infiltration are witnessed in a murine glioma model (96). As restoration, the survival of the tumor-bearing mice extends and infiltrative Treg cells diminish when pDCs are selectively excluded. A similar report also argues that pDCs are at play in promoting tumor progression and immunosuppression under the influence of granulocyte-macrophage colony-stimulating factor (GM-CSF) (102). DCs are induced to produce IL-10 and thereby inhibit T cell *via* its poliovirus receptor (PVR) -immunoreceptor tyrosine-based inhibitory motif (ITIM) interaction with T cells (103). Further, immature DCs characterized by low expression of CD80 and CD86 contribute to tolerance in T cells (104).

Mast Cells

The presence of mast cell (MC) in mouse and human glioma mirrors the entanglement of inflammation and cancer (105). It is demonstrated that the endogenous stem cell factor (SCF) largely contributes not only to the expansion of the glioma-associated MCs but also to the localization of the MCs in the vicinity of the tumor blood vessel and glioma cells along with the CXCL12/CXCR4 axis (105). Glioma-derived macrophage migration inhibitory factor (MIF) also recruits MCs to glioma through signal transducer and activator of transcription 5 (STAT5) signaling in a malignancy-dependent manner (106). Interactively, recruited MCs release a variety of mediators to inhibit glioma progression and induce tumor differentiation by downregulating GSK3β expression (107).

T Cells and Regulatory T Cells

Standing in as infiltrative T cells are $CD4^+$ helper T cells (Th), $CD8^+$ cytotoxic T cells, and $CD4^+/CD25^+/FoxP3^+$ Tregs which lead an exhausting life in the suppressive microenvironment of

glioma (9). Although constantly releasing quantities of proinflammatory IFN-γ for T cell recruitment, $CD4^+$ T cells upregulate the expression of inhibitory co-receptors like programmed cell death protein 1 (PD-1), cytotoxic T lymphocyte-associated antigen (CTLA), lymphocyte-activation-gene-3 (LAG-3), and T cell immunoglobulin domain and mucin domain-3 (TIM-3) (108). $CD8^+$ T cells remained largely inactive, being in line with their counterparts. The inactivation of T cells may also come from IL-10 and TGF-β released by glioma cells (9). In addition, attracted by mediators such as CCL2 and IDO, Tregs contribute greatly to immunosuppression (108, 109).

Increased T cell infiltration is related to favorable outcomes in glioblastoma patients (110). However, only limited immune response mediated by T cells is permitted in CNS, especially in the glioma microenvironment. The maturation of T cells is inhibited by tumor-derived Fas ligand (111). The activation of T cells is also inhibited by the IDO and TGF-β released from MG. Lack of co-stimulatory CD40, CD80, and CD86 expression on TAMs and glioma cell surface disengage T cell binding (112). T cell-mediated immunity in glioma is further drained through apoptosis induced by PD-1 and CTLA (9). An additional observation shows that GCN2 kinase results in T cell anergy and lack of proliferation in response to tryptophan depletion by IDO (113). Another GCN2-focused report highlights the importance of GCN2 as an amino acid sensor preventing CD8+ T cell apoptosis under amino acid stress in a murine glioma model (114).

Like two sides of the same coin, regulatory T cells ordinarily orchestrate balance and keep hyperactive immunity, including overactivated T cells, in control. In contrast to the T cells, infiltrative Tregs increase with glioma grade, predicts poor survival, and relates to recurrence (115, 116). It recruits Treg cells towards glioma using attractants such as CCL2 and IDO (46). The IDO expression not only involves Treg recruitment and immunosuppression thereafter but also plays a critical role in the Treg cell expansion by interacting with mTOR (117). Although it seems obvious and solid to conclude the interplay between the Treg and glioma, it is of great importance to dig deeper into the encouraging topic.

Furthermore, largely dependent on Tregs for either pro- or anti-tumor polarization are T helper 17 (Th17) cells (118). Tregs may induce Th17 polarization towards IL-10 producing cells rather than IFN-γ secretion in the context of TGF-β *in vitro* (118). Another Th17 study consistently reports that the TGF-β1 stimulated Th17 cells may lead to the permissive TIME in glioma by releasing IL-10 (119). The confirmation of Th17 cell infiltration in the glioma tissues gives rise to the investigation of the role of IL-17, one of the major mediators and hallmarks of the Th17 cells, which promotes glioma proliferation and migration through the activation of PI3K/Akt1/NF-κB-p65 axis (120).

Natural Killer Cells

NK cells detect and precisely execute cancer cells. They act under the balance between activating and inhibitory signals once approaching the susceptible (75). Given the minor proportion of infiltrative $CD45^+$ cells, NK cell activity is blunted close to non-functional. Glioma cells utilize MHC-I molecules binding with the inhibitory killer cell immunoglobulin-like receptor (KIR) to evade termination (121). As previously mentioned, NK cells are also inhibited by MDSCs *via* NKp30/NRC3 or NKG2D, and ensuing reduced IFN-γ production (75).

Cancer-Associated Fibroblasts

Given the fact that fibroblasts are associated with the progression and metastasis of many malignancies, it is reasonable to postulate that the cancer-associated fibroblasts (CAF) in the tumor niche of glioma may contribute to the proliferation or invasion of glioma (122–124). However, pieces of evidence related to fibroblast entities and existence in the brain remain scarce. A study claims that tumor-associated mesenchymal stem-like cells (tMSLCs), presumably as reminiscent of fibroblasts in other tumors, correlate with the poor prognosis of the GBM and enhance the invasiveness of GBM by force-mediated ECM remodeling through CCL2/JAK1/MLC2 signaling (125). And this pro-invasive effect brought by CAFs in glioma could also be mediated by the secretion of CXCL14 (126). Furthermore, it reveals that long non-coding RNA (lncRNA) HOXA transcript antisense RNA, myeloid-specific 1 (HOTAIRM1), is upregulated in the malignantly transformed fibroblasts derived from an orthotopic model and regulates TGF-β *via* miR-133b-3p to promote malignancy (127).

Cytokines, Chemokines, and Extracellular Molecules

Elevated levels of inhibitory cytokines, such as IL-10 and TGF-β, overthrow the balance with proinflammatory molecules contributing to the immunosuppressive microenvironment around glioma. It is interesting that IDO produced by glioma cells or pDC activates Treg cells and impedes T cell activity through tryptophan depletion (109). Besides, kynurenine, a metabolite of tryptophan, induces T cell apoptosis and polarizes Tregs by upregulating Foxp3 expression (128, 129). However, preclinical trials targeting IDO hold less promise than is expected (130).

Moreover, interference with *LGALS1* expression, which encoded Galectin-1 in the immune system, reduces MDSCs infiltration and immunosuppressive cytokine secretion (131). LAG3 binds to Galectin-3 (Gal-3) and MHC-II for $CD8^+$ T cell inhibition and inhibitory signal transmission, respectively (132, 133). It is reported that LAG-3 overexpression depletes CD8+ T cells (134). By binding to Galectin-9 (Gal-9), TIM-3 regulates T cell depletion and contributes to immunosuppression and even immune evasion. Limited arginine resulted from high levels of infiltrative myeloid cells-derived arginase also restrains immunocytes' survival.

AUTOPHAGY MODIFIES THE INTERPLAY BETWEEN GLIOMA AND THE TUMOR IMMUNE MICROENVIRONMENT

Autophagy becomes an interesting element in glioma due to paradoxical roles in glioma oncogenesis, progression, metastasis, and therapy resistance. Whether autophagy favors or hinders tumors may highly depend on stimuli, cell type, and specific stage of tumor cells. As a physiological part working at a base

level, autophagy degrades misfolded proteins and recycles organelles to reduce unsolicited ROS production, protein aggregates, and further damages DNA especially under stress (135). Ironically, it may apply the used tricks for normal survival to nurture tumor growth once the cells trend towards malignancy (136, 137). Herein, autophagy in glioma cells per se suits the case, as well as each component of its surrounding immune microenvironment, and thereby tweaking the interplay between glioma and the TIME (**Figure 2**).

Autophagy in Glioma Cells

As one hypothesizes an "inhibition-loss-promotion" model in an attempt to unify the conflicting roles of autophagy in cancer development, the model may apply to glioma with some revisions (12). Proficient autophagy may counteract the accumulated genetic defects when glioma cells are undergoing malignant transformation. Autophagy exhibits suppression on oncogenesis by degrading p62, so that mitochondrial damages, ROS-mediated oxidized molecules, and unstable genome mutations are averted (138, 139). Given that autophagy degrades carbohydrates, proteins, and lipids into sugars, amino acids, and fatty acids, respectively, to fuel cellular metabolism maintaining homeostasis, it still displays bipolar effects in glioma initiation after transitory "loss" or compromises at a very early phase of malignant transformation from healthy cells (140). Once glioma is established, autophagy responds more variably to cellular and environmental stimuli than expected with glioma growing and progressing.

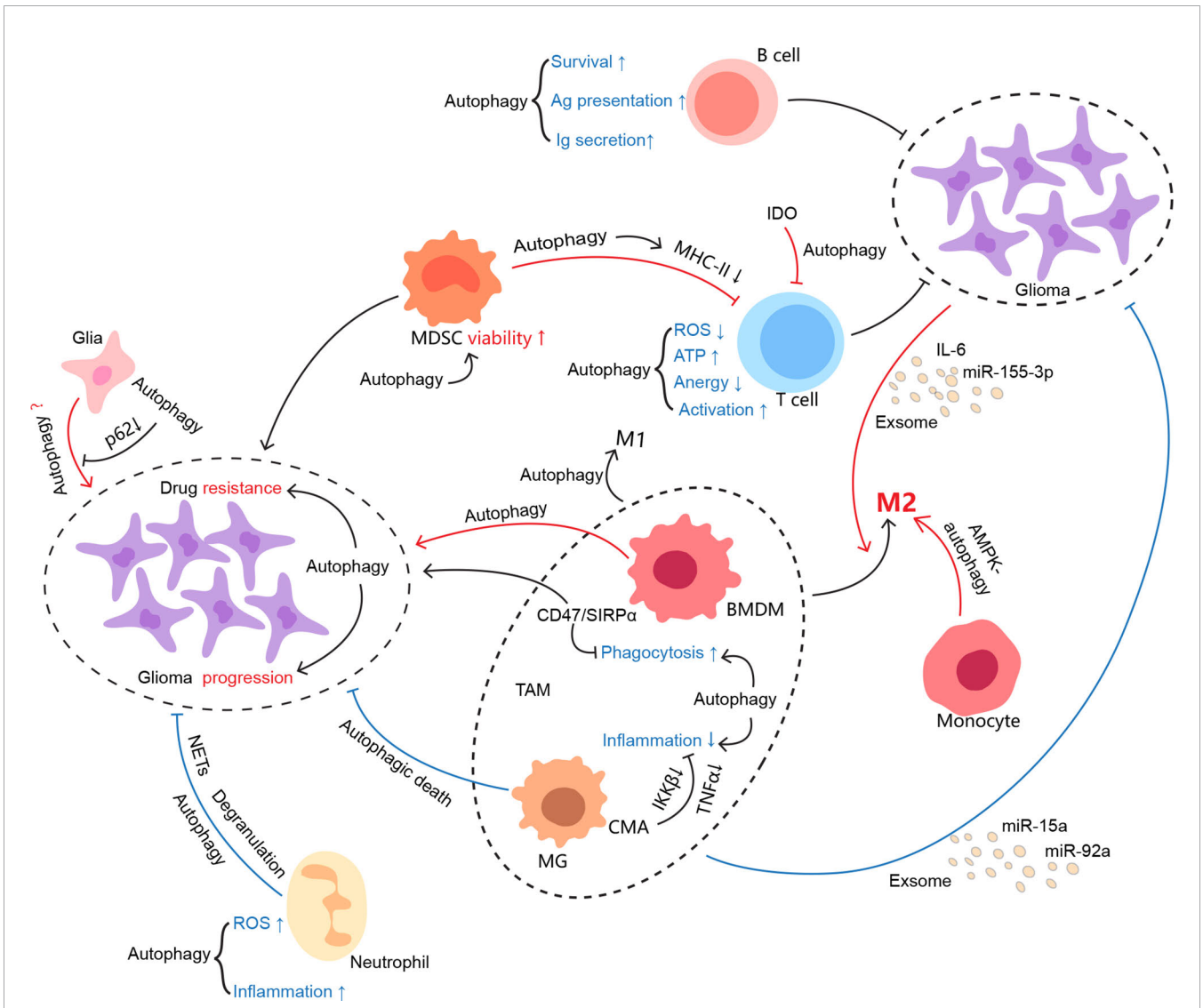

FIGURE 2 | Autophagy involvement in the regulation of the glioma immune microenvironment. As one of the evolutionarily conserved processes, autophagy keeps cellular homeostasis not only for immunocytes but also for tumor cells. It may be manipulated by conflicting sides in favor of their profits. However, it seems that autophagy somehow is not capable of either ensuring the physiological function of immune cells or restraining glioma growth in the glioma immune microenvironment. The interconnections between the cells in the TIME are colored if autophagy is involved, where red indicates protumor effects and blue indicates antitumor effects.

In a KRAS-driven GBM mouse model, autophagy inhibited by downregulating *Ulk1*, *Atg7*, and *Atg13* disrupts tumor growth and development. The capacity of KRAS-expressing glial cells for colony formation and survival in low-serum conditions is inhibited when autophagy is inhibited (141). It indicates that autophagy is vital to facilitate oncogenic transformation. The malignant, heterogeneous, and recurrent properties of GBM may source from GSCs, whose pluripotency and proliferation highly implicate autophagy (142–145). For instance, autophagy is manifested to degrade Notch1 and thereby modulate GSC tumorigenicity (146). The GSC tumorigenicity is also restrained by the overexpression of microRNA-93 (miR-93) targeting autophagic regulators, including Beclin-1, ATG5, ATG4B, and p62 (147).

Furthermore, GSCs activate autophagy through Bcl-2 nineteen-kilodalton interacting protein 3 (BNIP3) to habituate themselves to hypoxia (148, 149). More than adapting to hypoxia, BNIP-3-mediated autophagy facilitates GBMs thriving and contributes to resistance to chemotherapies *via* the MT1-MMP-JAK-STAT axis (150). As confirmation of autophagy modifying GSC survival, autophagy inhibitor quinacrine sensitizes GSCs to TMZ by triggering ferroptosis (146). However, autophagy induction *via* mTOR inhibition in GSCs promotes differentiation and disrupted autophagy increases stemness, which suggests that manipulation of autophagy influences GSCs formation and further GBM malignancy (151–153).

Emerging evidence shows that autophagy is implicated in glioma progression. Autophagy-related protein LC3 and p62 expression levels are negatively associated with glioma prognosis, especially with high-grade glioma prognosis, suggesting potential links between autophagy and glioma progression (154). Knockdown of autophagy-related 4C cysteine peptidase (ATG4C) repressed glioma progression by arresting tumor cells at the G1 phase and promoting apoptosis (155). Overexpression of maternal expression gene 3 (Meg3) encoding a critical non-coding RNA promotes epithelial to mesenchymal transition, migration, invasion, and autophagy in glioma. The employment of autophagy inhibitor CQ partially hampers glioma progression, suggesting autophagy involvement (156). Silencing of lysosome enzyme alpha-l-fucosidase 1 (FUCA1) impedes U87 and U251 glioma cell proliferation, whereas the growth inhibition appears less significant when the cells are co-incubating with 3-MA (157). It implies that downregulation of FUCA1 may lead to autophagy-associated cell death, considering increased LC3-II/LC3-I ratio, Beclin-1, and ATG-12 expression level. Interestingly, antidepressant imipramine augmented with P2Y12 inhibitor ticlopidine elicits autophagy-associated cell death, which limits glioma cell growth *in vitro*, hinders tumor progression *in vivo*, and prolongs survival of glioma-bearing mice (158). Together, autophagy closely involves glioma progression, while its reputation mostly lies in therapy resistance.

The point that autophagy mainly contributes to glioma resistance to therapies prevails and is corroborated by a majority of studies. TMZ stands as a clinical routine for GBM treatment because of its high efficacy, BBB permeation, and tolerable adverse effects (16, 159). As suggested, cytoprotective autophagy saves cells from stresses, including drug, radiation, and hypoxia cytotoxicity from death (160–162). In the case of drug resistance, for instance, GSC–derived PD–L1–containing exosomes activate AMPK/ULK1-mediated autophagy to increase TMZ–resistance in GBM (163). And ATG4C depletion impairs TMZ-resistance and improves the susceptibility of glioma to TMZ (155). Similarly, autophagy is transiently induced by acute TMZ treatment *via* transitory activation of the AMPK-ULK1 axis, while CQ blocks the autophagy and enhances the efficacy of TMZ in glioma cells (18, 164). CQ and its analogs have therefore been an alternative adjuvant to potentiate the TMZ treatment. Moreover, T-LAK cell-originated protein kinase (TOPK) inhibits autophagy by phosphorylating ULK1 in glioma cells and promotes glioma resistance to TMZ (165). TMZ-stimulated autophagy is also inhibited by the lncRNA DLEU1 knockdown, which increases glioma susceptibility to the drug cytotoxicity at the same time (166). In addition, lncRNA CASC2 sponges miR-193a-5p to reduce autophagy and potentiate TMZ efficacy *via* mTOR upregulation (167). LncRNA AC023115.3 induced by chemotherapy, in turn, improves chemosensitivity of glioma to cisplatin by competing with miR-26a, thereby releasing GSK3β to inhibit autophagy (168).

The role of autophagy in glioma radiation therapy is currently controversial. Autophagy is triggered to shelter glioma cells from death due to the toxicity of free radicals, misfolded proteins, and damaged organelles mediated by radiotherapy (169–171). It is demonstrated that radiation augments autophagic flux by upregulating mammalian sterile-20-like kinase 4 (MST4), which phosphorylates and motivates ATG4B in GBM, whereas inhibition of autophagy *via* ATG4B blockade improves sensitivity to radiation (170). Targeting Beclin-1-mediated autophagy with miR-17-5p expression also improves the radiosensitivity of glioma (172). However, radiation-induced autophagy may also promote apoptosis in glioma (173). There could be an explanation for the conflicting results that glioma cells respond variably to radiation simply out of distinct individual sensitivity, but the intensity and duration of radiation should also be considered (174).

A large body of literature regarding autophagy-mediated therapy resistance predisposes autophagy to be cytoprotective, but the fact that overactivated or insufficient autophagy under drug perturbation drives glioma cells to death should not be neglected. It is demonstrated that autophagy-associated cell death after TMZ or ionizing radiation treatment is relieved by downregulation of Beclin-1 or ATG7 with siRNA (175). In light of the extent of triggering autophagy-associated death, coordinated autophagy modulation with autophagy inducers followed by inhibitors and TMZ treatment may overcome chemotherapeutic resistance in GBM. It is noticeable that mitochondrial respiration and oxidative phosphorylation is greatly interfered with by the disrupted autophagic system under autophagy modulation (176). Though more clinical translation is in need, tweaks in the autophagic system using autophagy inducers and consecutive inhibitors would doubtlessly galvanize autophagic intervention for chemoresistance.

How autophagy shuttles between cytoprotective and cytotoxic roles in glioma, especially in terms of therapeutic resistance, probably depends on doses and duration of treatment to decide a compatible pathway (16). It indicates that autophagy may act as a survival strategy under relatively mild therapies, such as low dose and short term, but consistent treatment with maximum dosage

could induce autophagy-associated cell death (164). Of all the possible mediators for protective autophagy initiation, surging adenosine triphosphate (ATP) is observed to have a key role in promoting autophagy for drug toxicity adaption, especially in glioma cells on TMZ administration (177). Disruption of energy balance with drug targeting mitochondria activity is demonstrated to induce AMPK phosphorylation and inactivate mTORC1 and thereby suppress aggressive properties of glioma cells (178). Since TMZ in co-treatment with autophagy inhibitor CQ induces ROS production and augments cytotoxicity, it is also reasonable to hypothesize that ROS level may drive the shift of autophagy from cytoprotection to cytotoxicity with the additional consideration that hydrogen peroxide accumulation leads to apoptosis or necrosis (179, 180).

Although the hypothetical theory seems to coordinate autophagy's conflicting roles in therapy resistance, autophagy in glioma development remains misunderstood. How to determine any mediators or specific markers for autophagy altering from the beneficial to the lethal is yet to be answered in glioma progression. It may display context-dependency, such as the ROS and ATP level in the intra- or intercellular microenvironment (181). Or, it is reasonable to speculate that mild stimuli give rise to cytoprotective autophagy, whereas harsher conditions lead to autophagy-associated death.

Autophagy in TAMs

It remains controversial to assess the contribution of autophagy in the components of the glioma-related immune microenvironment. Based on the currently incomplete understanding, autophagy mainly involves TAM generation, function, and polarization (182, 183). Autophagy induced by c-Jun N-terminal Kinase (JNK) activation and disruption of ATG5 cleavage promotes monocytes differentiation into macrophages, produces cytokines, and prevents monocyte apoptosis (184). For phagocytosis of debris, macrophages degrade phagocytosed cells *via* LC3-associated phagocytosis, of which blockade would improve anti-tumor immunity (185). Interestingly, disrupting the CD47-SIRPα axis ("don't eat me" signal) with specific fusion protein binding augments phagocytosis of macrophages, triggers cytoprotective autophagic flux in glioma cells, and further improves not only macrophage but also CD8+ T cell infiltration if combined with autophagy inhibitors (186, 187).

Impairment of the autophagy-mediated phagocytosis in MG also stimulates inflammation (188). A study shows that Beclin-1-mediated autophagy may regulate neuroinflammation *via* NRLP3 degradation in murine MG (189). On top of that, rapid loss of IKKβ protein and TNF-α is mediated by CMA in microglia, indicating the critical role of CMA in controlling inflammation (190). These discussed studies suggest that impaired autophagy in TAMs may enhance inflammation, but it should be reconsidered for the simultaneous inhibition of phagocytosis.

In an immunosuppressive microenvironment, TAMs incline to polarize toward the M2 phenotype facilitating tumor progression and metastasis. Interestingly, autophagy contributes greatly to the M2 polarization, namely *via* the STAT3 pathway (191–193). Several studies modify the TAM state into a specific activation state by targeting autophagy (194–196). Monocytes respond to colony-stimulating factor-1 (CSF-1) through AMPK-mediated autophagy activation and differentiate into M2 macrophages (188, 197). Nonetheless, there are always exceptions to predisposing TAM to the M2 phenotype, which presumably depends on tumor types and local milieu. For instance, it is reported that inhibition of mTOR, a key switch of the autophagy pathway, skews TAM polarization to the M1 phenotype, resulting in increased IL-12, decreased IL-10, and reduced tumor angiogenesis (195). Collectively, it may hold promise in targeting autophagy to modulate TAM polarization and function, but more investigations are required.

Autophagy in MDSCs and Neutrophils

MDSCs contribute greatly to the suppressive environment around glioma and contrive autophagy to maintain themselves under inhospitable conditions. It is understood that autophagy promotes MDSC viability. Either neutralization of high mobility group box protein-1 (HMGB1), a damage-associated molecular pattern, induces autophagy, or inhibiting autophagy directly increases apoptosis in MDSCs. Furthermore, interference with autophagy in MDSCs hampers tumor growth by endorsing antitumor responses. MDSCs enhance MHC II expression due to compromised autophagy and reduced lysosomal degradation so that tumor-specific $CD4^+$ T cells are efficiently activated (198).

Neutrophils exist and survive in the suppressed environment of glioma although the mechanisms of neutrophil recruitment to glioma are poorly defined (199). The specific role that autophagy plays in the context of glioma is worthy of reevaluation, even if the implication of autophagy in neutrophil granulopoiesis, phagocytosis, degranulation, and neutrophil extracellular trap (NET) formation is well-documented (200). In particular, neutrophils also require autophagy as a key regulator for building NADPH-oxidase-mediated reactive oxygen species (ROS) and inflammatory activity (201).

Autophagy in Tumor-Infiltrating Lymphocytes

Autophagy generally maintains cellular homeostasis and relieves lymphocytes from accumulating stress (202, 203). Notably, reports are claiming that autophagy-mediated metabolism in T cells modulates T cell activity (204, 205). That T cells heavily rely on autophagy for ATP supply is not limited to survival guarantee, but is also essential when T cell receptor (TCR) engagement and $CD4^+$ The cell activation cause an increased demand for energy (205). Following activation of $CD4^+$ Th cell, common γ-chain cytokines represented by IL-2 and IL-4 also mediate regulation of autophagy in Th cell with JAK signaling involvement (206). It indicates that induction of autophagy in $CD4^+$ T cells in response to TCR activation secures the T cell engaging in effector responses accordingly, and exempts itself from the energy otherwise (207). Upon TCR stimulation, however, the planned entry to the S phase is unexpectedly perturbed thanks to accumulated cyclin-dependent kinase inhibitor CDKN1B in autophagy-deficient T cell, suggesting a key role of autophagy in T cell proliferation (208).

Autophagy fuels $CD4^+$ T cells and it meets the energy demands of other T cell populations as well. It is dynamically regulated throughout $CD8^+$ T cell activities, including proliferation, memory generation, function, and survival (209). In particular, $CD8^+$ T cells

depleted of *Atg5* or *Atg14* are metabolically reprogrammed to glycolytic consumption and display an enhanced effector memory cell activity against the tumor (210, 211). The report implies that the shift towards glycolytic metabolism instead of autophagy in *Atg5*$^{-/-}$ T cells leaves less carbon available for methylation and results in epigenetic alterations.

Not does autophagy only adjust to activity or environmental cues but also to distinct T cell lineages (212). Tregs depleted of *Atg5* or *Atg7* show upregulation of mTOR complex 1(mTORC1) and glycolysis, defective functional integrity, and increased apoptosis (213). Interestingly, it rescued the Foxp3 instability phenotype in autophagy-deficient Tregs by inhibiting pyruvate dehydrogenase kinase and glycolysis.

Overall, those studies imply that autophagy fulfilling the energy needs of lymphocytes is subject to specific environmental context, or exact activity, or cell type in a variety of pathways (212). It is plausible to hypothesize that autophagy in those infiltrating T cells is occluded, at least partially, or are diverted to degrade anti-tumor molecules only, or other undiscovered mechanisms contribute to the "non-functional" T cells in the glioma immune microenvironment. Therefore, studies at a single-cell resolution are required for a complete understanding of autophagy in shaping the protumor microenvironment.

REDEFINE THE INTERCONNECTION BETWEEN GLIOMA AND THE IMMUNE MICROENVIRONMENT FROM AN AUTOPHAGIC PERSPECTIVE

Autophagy is generally deployed by multiple types of cells in glioma not only for energy gratification and integrity maintenance, but also for essential functions, such as cytokine production, phagocytosis, and antigen presentation (182). Therefore, the interconnections between glioma and the TIME would be impacted if the energy supply or the cellular context of these cells alters with malignancy progressing. Substantial bioinformatic analyses raise awareness of the autophagy-associated links between glioma and the components of TIME predicting a wide area of intensive basic research (214–219). It has been anticipated by distinct autophagy gene signature-based prognostic risk models that there is more immune cells infiltration in the sets with higher autophagy risk scores, implying latent autophagy-involved associations between autophagy and immunity in glioma (214, 218, 220). However, interpretation for the "coincidental" intertwinement between autophagy and immune responses may require future experimental evidence. It is also worthy of investigation to determine whether it is a cause-effect relation or coincidence and to identify specific cell populations that manipulate autophagy and thereby renovate the immune microenvironment in glioma.

Hypoxia stimulates glioma cells to release exosomes into the peritumor area for intercellular communication. Since TAMs dominates the infiltrating immunocytes and autophagy is highly involved in M2-like macrophage, a piece of evidence illustrates that the glioma-derived exosomes mainly containing IL-6 and miR-155-3p initiate autophagic activities in TAMs and promote M2-like polarization *via* IL-6-pSTAT3-miR-155-3p-autophagy-pSTAT3 positive feedback loop (221, 222). It exposes the bridging role that autophagy plays in glioma-sourced immunosuppression. M2 macrophage-sourced exosomal miR-15a and miR-92a are reversely corroborated to inhibit glioma invasion and migration *via* phosphatidylinositol-3-kinase (PI3K)-AKT-mTOR pathway (223). On the other hand, LPS/IFN-γ-stimulated MG can trigger autophagy-dependent death in glioma cells that are resistant to death ligands, like TNF α and TRAIL (224). Although the specific molecular elements restoring the anti-tumor function of MG are of utmost interest, the report exposes that MG-mediated autophagic death may overcome apoptosis resistance in glioma (225).

In addition to exosomal microRNA-mediated autophagic activities, the researchers shed light on the employment of classic autophagy modulators to improve the therapeutic efficacy of immune checkpoint inhibitors (41). According to the report, rapamycin treatment combined with hydroxychloroquine (HCQ) reduces M2-like polarized macrophages *in vitro* and augments both M1/M2 and CD8/CD4 ratio in the GL261 model. The phagocytic capacity of treated macrophages is also enhanced (41). Further, dropping the expression level of CD47 and SIRPα on glioma cells and macrophages resulted from the combination treatment suggests the deteriorating anti-phagocytic ability of glioma (41, 186). Other mechanisms influencing the TIME may include the evidence that glioblastoma promotes CMA and thereby wearing off the immunogenicity of pericytes, which is reversed by the CMA inhibition (226).

Besides, a novel nanodiamond carrying doxorubicin (Nano-DOX) is designed and corroborated to trigger autophagy instead of apoptosis in GBM. The Nano-DOX further stimulates GBM cells to emit antigens and damage-associated molecular patterns (DAMPs) leading to the boosted activation of DCs (227). Moreover, the liposomal honokiol and disulfiram/copper codelivery system (CDX-LIPO) is demonstrated to be a remarkable autophagy initiator in glioma cells and induces immunogenic cell death which results in enhanced activation of anti-tumor immunity. The CDX-LIPO is developed to inhibit the mTOR signaling pathway to promote autophagy, shift the M2 TAM towards the M1 type, and even interfere with glucose metabolism and lactate production. It also triggers immunogenic cell death, promoting the maturation of antigen-presenting cells and, further, the activation of T cells. The TIME in glioma is thus remodeled, marked by M2-polarized TAMs, matured DCs and NK cells, activated cytotoxic T cells, and repressed MDSCs, along with diminished glycolysis and lactate metabolism (228).

Current Autophagy-Adjuvant and Autophagy-Related Therapies Against Glioma

As is shown in the extensive studies discussed previously, there are generally two directions to manipulate autophagy against glioma. One method of autophagy intervention is to overcome protective autophagy stimulated by drugs and repurpose the lethal condition to induce cell death. For instance, it has long been discussed that TMZ treatment at clinically available dosage induces autophagy in glioma cells for survival in adverse conditions (229). The TMZ-induced autophagy may require

ERK1/2 signaling (230). The therapeutic efficacy of TMZ is further improved with later autophagy inhibitor bafilomycin or CQ administration. Recent studies unravel the mechanisms of TMZ-stimulated autophagy including, but not limited to, mitochondrial and endoplasmic stress, O^6-methylguanine adducts generation, and ATP surge (177, 231, 232).

The addition of CQ or HCQ to the conventional glioma treatment TMZ represents a breakthrough. These quinolone derivatives initially used as antimalarial and rheumatological drugs are the only autophagy modulators that have been extensively researched and even tested in clinical trials for glioma combinational therapies (NCT02378532 and NCT00486603) (233, 234). Particularly, CQ in combination with TMZ renders U87, U251, and LN229 cells susceptible to TMZ by interfering with GRP78-dependent and PI3KC3-BECN1-dependent autophagy and cleaving poly ADP-ribose polymerase (PARP) (18). It is revealed that mitophagy is additionally inhibited by the CQ cotreatment with TMZ resulting in ROS accumulation (179). Other synergistic effects of combinations of CQ and TMZ may lie in the p53-mediated apoptosis induction or p53-independent cell cycle arrest in glioma cell lines (235). However, CQ- or HCQ-based conclusions merit further consideration due to their autophagy-independent off-target effects (137). Research focusing on more precisely targeted inhibitors of autophagy are highly welcomed for antitumor drug development.

However, a few clinical trials have been conducted to translate the promising treatment efficacy of CQ and TMZ into the application. A total of 30 postoperative GBM patients are recruited into a randomized, double-blinded, and placebo-controlled trial to evaluate the efficacy of CQ as adjuvant therapy for glioma (234). Despite the lack of statistical significance, the median survival of CQ-treated patients being 24 months is approximately two times longer than the control group being 11 months, which may be more definitive and more generalized if enlarging the sample size is permitted. A more recent phase I/II cohort focuses on the efficacy of HCQ along with concurrent radiotherapy and TMZ administration in newly diagnosed GBM (233). Nevertheless, the maximum tolerated dose for HCQ is 600 mg/d due to severe dose-limiting toxicity, at which autophagy may not be sufficiently and consistently inhibited in patients. As a result, any significant improvement in overall survival is hardly detected (233). The conflicting results between basic studies and clinical trials encourage the development of more tolerable, BBB-penetrable, and potent autophagy modulators. More novel options in conjunction with TMZ for glioma management are currently being explored and evaluated, such as combined TMZ/SAHA therapy (**Table 1**) (236).

Apart from inhibiting protective autophagy, another direction may involve the agents triggering cytotoxic autophagy. Delta-9-tetrahydrocannabinol (THC) and cannabidiol (CBD) are both cannabinoids utilized as anticancer agents due to their ability to induce lethal autophagy (244). The systemic administration of THC + CBD at a 1:1 ratio in combination with TMZ strongly reduces the subcutaneous and the intracranial tumor volume in the preclinical models of glioma, which results in complete tumor regression in over half of the animals (237). Indeed, the TMZ/THC/CBD therapy has already been proposed to be evaluated through a clinical trial (NCT03529448). Although microRNAs are mostly regarded as biomarkers for diagnosis or prognosis, the synergistic effect of miR-450a-5p overexpression combined with epidermal growth factor receptor (EGFR) inhibitor gefitinib confers the sensitivity to chemotherapy in glioma through the EGFR-stimulated PI3K/AKT/mTOR signaling pathway and further pro-death autophagy activation (245). Furthermore, the application of rapamycin induces autophagy and results in an increase of radiosensitivity in EGFR-silencing GBM cell lines (246).

With the addition of carnosic acid (CA), an abietane diterpenoid extracted from rosemary or common sage, the U251 and LN229 cells are resensitized to TMZ incubation showing Cyclin B1-mediated cell cycle arrest, cellular apoptosis induction by cleavage of PARP and Caspase-3, and enhanced autophagy through inhibition of phosphorylated AKT (238). This is similar to how pan-PI3K inhibitor GDC-0941 combined with TMZ arrests cell cycle, exerts a pro-apoptotic effect, and augments autophagy mainly through the PI3K-AKT signaling pathway (239). The Janus kinase (JAK) inhibitor momelotinib (MTB) also potentiates TMZ efficacy *via* apoptosis and autophagy induction (240). Although TMZ/CA, the TMZ/GDC-0941, and the TMZ/MTB therapy fail to identify the relation between the relationship between apoptosis and autophagy, it is plausible to think that the "apoptotic" cell death could be ascribed to autophagy-associated impacts. Some of the autophagy-related agents treating glioma are summarized in **Table 1**, while the other autophagy modulating chemicals or autophagy-related molecular targets have been discussed elsewhere (181, 247, 248).

CONCLUSION AND FUTURE PERSPECTIVE

Autophagy represents not merely a way for cellular maintenance, but also a key point of regulation in finely adjusting interplays between glioma and the TIME. It supports glioma typically by enhancing the adaptability of glioma cells to the extent of progressive, invasive, and drug-resistant malignancy, and also by rendering prevailing TAMs differentiating towards the M2 phenotype through exosomes and reduce phagocytosis. Neutrophils use autophagy for proper immunity against glioma. The intercellular engagement, activation, and anti-glioma activities of T cells are ensured with autophagy involvement.

Conclusively, the ultimate effect of autophagy in glioma and the TIME may highly depend on the cell type, the intensity of the surrounding signal, and the stage of the lesion and progression. Autophagy can be utilized to cater to a variety of demands, but it seemingly turned out to be tumor-promoting cumulatively with glioma progression. It also should be reiterated that autophagy may influence the status and well-being of glioma cells and the members of TIME, and thereby modulate their interconnections in the permissive environment. Some interplays may rely on the whole process of autophagy while others are involved with some of the autophagic components instead of the entire flux.

Beyond glioma cells, autophagy in any peritumor cells would be influenced when autophagy is manipulated systemically. Considering the promising efficacy of autophagy modulators and the definite number of related clinical trials and basic studies, it is of great importance to shed more light on the entire supervision of glioma cells and their environment at a single-cell level, of which the

TABLE 1 | Autophagy-related therapy against glioma.

Autophagy-Related Therapy	Mechanism	Effects on Autophagy	Autophagy Type	Experiment Setting	Refs
TMZ	ROS induction	Activation	Protective autophagy	*In vitro*: U87 and U251	(177)
TMZ + CQ	PARP cleavage, apoptosis induction	Inhibition	Protective autophagy	*In vitro*: LN229 and U251 *In vivo*: U251	(18)
	ROS induction	Inhibition	Protective autophagy	In vitro: U87 and C6	(179)
	Induction of p53-dependent apoptosis and cell cycle arrest	Inhibition	Protective autophagy	*In vitro*: U87 and U373	(235)
	Induction of toxicity	Inhibition	Protective autophagy	Clinical trial Phase I	(234)
TMZ + HCQ	Induction of toxicity	Inhibition	Protective autophagy	Clinical trial Phase I/II	(233)
TMZ + SAHA + CQ	Induction of apoptosis, H3 and H4 histone acetylation	Inhibition	Protective autophagy	*In vitro*: U251	(236)
TMZ + Curcumin + CQ	Induction of DNA damage, inhibition of PI3K/AKT ERK1/2	Inhibition	Protective autophagy	*In vitro*: U87, C6, and U251*In vivo*: C6	(230)
TMZ + Irradiation	Increase of Beclin-1, ATG5	Activation	Lethal autophagy	*In vitro*: T98 and U373	(175)
TMZ + THC + CBD	Induction of autophagy-associated apoptosis and toxicity	Activation	Lethal autophagy	*In vivo*: U87	(237)
TMZ + CA	Induction cell cycle arrest and apoptosis, inhibition of p-AKT	Activation	–	*In vitro*: U251 and LN229	(238)
TMZ + GDC-0941	Induction of cell cycle arrest and apoptosis, inhibition of p-AKT and MGMT	Activation	–	*In vitro*: A172, T98, and SHG44	(239)
TMZ + MTB	Induction of apoptosis, inhibition of JAK2/STAT3	Activation	–	In vivo: U251	(240)
CQ + Galunisertib	Inhibition of TGF-β2-induced autophagy	Inhibition	Protective autophagy	*In vitro*: U87, T98, and U251 *In vivo*: U87	(241)
CQ + BAFA1	ROS induction	Inhibition	Protective autophagy	*In vitro*: U87 and C6	(179)
2DG + CP	ER stress induction, induction of apoptosis	Inhibition	Protective autophagy	*In vitro*:LN229 and A172	(242)
IM + TIC	Induction of non-apoptosis cell death *via* AC/cAMP/EPAC1 signaling pathway	Activation	Lethal autophagy	*In vitro*: LN71, LN229, and LN443 *In vivo*: LN229	(158)
Erlotinib + Sorafenib	Inhibition AKT and ERK signaling	Activation	Lethal autophagy	*In vitro*: U87, LNZ308, LN428, and GSC	(243)

TMZ, temozolomide; CQ, chloroquine; HCQ, hydroxychloroquine; SAHA, suberoylanilide hydroxamic acid; THC, delta-9-Tetrahydrocannabinol; CBD, cannabidiol; CA, carnosic acid; MTB, momelotinib; BAFA1, bafilomycin A1; 2DG, 2-deoxy-D-glucose; CP, cisplatin; IM, imipramine; TIC, ticlopidin.

members in the suppressive immune environment should be prioritized. Therefore, more profound insights will be acquired for novel autophagy-related therapy development.

The reason why it deserves more attention not only comes from the trend that autophagy modulators might be part of regular use for glioma treatment one day but also lies in the autophagy-related drugs that are being clinically employed. However, the mechanism challenges regarding autophagy in glioma and its TIME are pressing. How autophagy contributes to oncosuppression and turns itself into an indispensable part of glioma malignancy remains to be determined. It is also critical to identify specific and easily-tested indicators for autophagy status so that the dependency on autophagy for a certain type of cells in glioma is characterized before autophagy therapies.

AUTHOR CONTRIBUTIONS

The study and conception were designed by YF, CM, and GZ. The manuscript was drifted by YF, YW, JZ, XD, PG, and KL. Figures were prepared by YF, YW, JZ, and XD. Reviewing and editing was completed by CM and GZ. All authors contributed to the article and approved the submitted version.

FUNDING

We acknowledge the funding support from National Nature and Science Foundation of China (Grant Number: 81772684 and 81872050), the S&T Development Planning Program of Jilin Province (Grant Number: 20200201469JC, 20200201613JC, and 20200201388JC), and Foundation from the Development and Reform Commission of Jilin Province (Grant Number: 2017C059-2, and Chinese People's Brain Neural Network Research and Innovation Cooperation Platform Construction Project).

ACKNOWLEDGMENTS

We appreciate the clinical supervision and instruction of Dr. Hongquan Yu and Dr. Haiyang Xu.

REFERENCES

1. Zhang X, Deibert CP, Kim WJ, Jaman E, Rao AV, Lotze MT, et al. Autophagy Inhibition Is the Next Step in the Treatment of Glioblastoma Patients Following the Stupp Era. *Cancer Gene Ther* (2020) 28(9):971–83. doi: 10.1038/s41417-020-0205-8
2. Louis DN, Perry A, Reifenberger G, von Deimling A, Figarella-Branger D, Cavenee WK, et al. The 2016 World Health Organization Classification of Tumors of the Central Nervous System: A Summary. *Acta Neuropathol* (2016) 131(6):803–20. doi: 10.1007/s00401-016-1545-1
3. Schiff D, Van den Bent M, Vogelbaum MA, Wick W, Miller CR, Taphoorn M, et al. Recent Developments and Future Directions in Adult Lower-Grade Gliomas: Society for Neuro-Oncology (SNO) and European Association of Neuro-Oncology (EANO) Consensus. *Neuro Oncol* (2019) 21(7):837–53. doi: 10.1093/neuonc/noz033
4. Lapointe S, Perry A, Butowski NA. Primary Brain Tumours in Adults. *Lancet* (2018) 392(10145):432–46. doi: 10.1016/s0140-6736(18)30990-5
5. Quail DF, Joyce JA. The Microenvironmental Landscape of Brain Tumors. *Cancer Cell* (2017) 31(3):326–41. doi: 10.1016/j.ccell.2017.02.009
6. Weiss N, Miller F, Cazaubon S, Couraud PO. The Blood-Brain Barrier in Brain Homeostasis and Neurological Diseases. *Biochim Biophys Acta* (2009) 1788(4):842–57. doi: 10.1016/j.bbamem.2008.10.022
7. Domingues P, González-Tablas M, Otero Á, Pascual D, Miranda D, Ruiz L, et al. Tumor Infiltrating Immune Cells in Gliomas and Meningiomas. *Brain Behav Immun* (2016) 53:1–15. doi: 10.1016/j.bbi.2015.07.019
8. Gutmann DH, Kettenmann H. Microglia/Brain Macrophages as Central Drivers of Brain Tumor Pathobiology. *Neuron* (2019) 104(3):442–9. doi: 10.1016/j.neuron.2019.08.028
9. Gieryng A, Pszczolkowska D, Walentynowicz KA, Rajan WD, Kaminska B. Immune Microenvironment of Gliomas. *Lab Invest J Tech Methods Pathol* (2017) 97(5):498–518. doi: 10.1038/labinvest.2017.19
10. Zhang H, Zhou Y, Cui B, Liu Z, Shen H. Novel Insights Into Astrocyte-Mediated Signaling of Proliferation, Invasion and Tumor Immune Microenvironment in Glioblastoma. *Biomed Pharmacother* (2020) 126:110086. doi: 10.1016/j.biopha.2020.110086
11. Gargini R, Segura-Collar B, Sánchez-Gómez P. Cellular Plasticity and Tumor Microenvironment in Gliomas: The Struggle to Hit a Moving Target. *Cancers (Basel)* (2020) 12(6):1622. doi: 10.3390/cancers12061622
12. Gerada C, Ryan KM. Autophagy, the Innate Immune Response and Cancer. *Mol Oncol* (2020) 14(9):1913–29. doi: 10.1002/1878-0261.12774
13. Dikic I, Elazar Z. Mechanism and Medical Implications of Mammalian Autophagy. *Nat Rev Mol Cell Biol* (2018) 19(6):349–64. doi: 10.1038/s41580-018-0003-4
14. Tekirdag K, Cuervo AM. Chaperone-Mediated Autophagy and Endosomal Microautophagy: Joint by a Chaperone. *J Biol Chem* (2018) 293(15):5414–24. doi: 10.1074/jbc.R117.818237
15. Mizushima N, Komatsu M. Autophagy: Renovation of Cells and Tissues. *Cell* (2011) 147(4):728–41. doi: 10.1016/j.cell.2011.10.026
16. Yan Y, Xu Z, Dai S, Qian L, Sun L, Gong Z. Targeting Autophagy to Sensitive Glioma to Temozolomide Treatment. *J Exp Clin Cancer Res* (2016) 35:23. doi: 10.1186/s13046-016-0303-5
17. Molina ML, Garcia-Bernal D, Martinez S, Valdor R. Autophagy in the Immunosuppressive Perivascular Microenvironment of Glioblastoma. *Cancers (Basel)* (2019) 12(1):102. doi: 10.3390/cancers12010102
18. Golden EB, Cho HY, Jahanian A, Hofman FM, Louie SG, Schonthal AH, et al. Chloroquine Enhances Temozolomide Cytotoxicity in Malignant Gliomas by Blocking Autophagy. *Neurosurg Focus* (2014) 37(6):E12. doi: 10.3171/2014.9.FOCUS14504
19. Metz R, Rust S, Duhadaway JB, Mautino MR, Munn DH, Vahanian NN, et al. IDO Inhibits a Tryptophan Sufficiency Signal That Stimulates mTOR: A Novel IDO Effector Pathway Targeted by D-1-Methyl-Tryptophan. *Oncoimmunology* (2012) 1(9):1460–8. doi: 10.4161/onci.21716
20. Desland FA, Hormigo A. The CNS and the Brain Tumor Microenvironment: Implications for Glioblastoma Immunotherapy. *Int J Mol Sci* (2020) 21(19):7358. doi: 10.3390/ijms21197358
21. Sampson JH, Gunn MD, Fecci PE, Ashley DM. Brain Immunology and Immunotherapy in Brain Tumours. *Nat Rev Cancer* (2020) 20(1):12–25. doi: 10.1038/s41568-019-0224-7
22. Pires-Afonso Y, Niclou SP, Michelucci A. Revealing and Harnessing Tumour-Associated Microglia/Macrophage Heterogeneity in Glioblastoma. *Int J Mol Sci* (2020) 21(3):689. doi: 10.3390/ijms21030689
23. Wei J, Chen P, Gupta P, Ott M, Zamler D, Kassab C, et al. Immune Biology of Glioma-Associated Macrophages and Microglia: Functional and Therapeutic Implications. *Neuro Oncol* (2020) 22(2):180–94. doi: 10.1093/neuonc/noz212
24. Fu W, Wang W, Li H, Jiao Y, Huo R, Yan Z, et al. Single-Cell Atlas Reveals Complexity of the Immunosuppressive Microenvironment of Initial and Recurrent Glioblastoma. *Front Immunol* (2020) 11:835. doi: 10.3389/fimmu.2020.00835
25. Huang Y, Zhang Q, Lubas M, Yuan Y, Yalcin F, Efe IE, et al. Synergistic Toll-Like Receptor 3/9 Signaling Affects Properties and Impairs Glioma-Promoting Activity of Microglia. *J Neurosci* (2020) 40(33):6428–43. doi: 10.1523/JNEUROSCI.0666-20.2020
26. Zhang H, Luo YB, Wu W, Zhang L, Wang Z, Dai Z, et al. The Molecular Feature of Macrophages in Tumor Immune Microenvironment of Glioma Patients. *Comput Struct Biotechnol J* (2021) 19:4603–18. doi: 10.1016/j.csbj.2021.08.019
27. Muller A, Brandenburg S, Turkowski K, Muller S, Vajkoczy P. Resident Microglia, and Not Peripheral Macrophages, Are the Main Source of Brain Tumor Mononuclear Cells. *Int J Cancer* (2015) 137(2):278–88. doi: 10.1002/ijc.29379
28. Bowman RL, Klemm F, Akkari L, Pyonteck SM, Sevenich L, Quail DF, et al. Macrophage Ontogeny Underlies Differences in Tumor-Specific Education in Brain Malignancies. *Cell Rep* (2016) 17(9):2445–59. doi: 10.1016/j.celrep.2016.10.052
29. Muller S, Kohanbash G, Liu SJ, Alvarado B, Carrera D, Bhaduri A, et al. Single-Cell Profiling of Human Gliomas Reveals Macrophage Ontogeny as a Basis for Regional Differences in Macrophage Activation in the Tumor Microenvironment. *Genome Biol* (2017) 18(1):234. doi: 10.1186/s13059-017-1362-4
30. Roesch S, Rapp C, Dettling S, Herold-Mende C. When Immune Cells Turn Bad-Tumor-Associated Microglia/Macrophages in Glioma. *Int J Mol Sci* (2018) 19(2):436. doi: 10.3390/ijms19020436
31. Wang SC, Hong JH, Hsueh C, Chiang CS. Tumor-Secreted SDF-1 Promotes Glioma Invasiveness and TAM Tropism Toward Hypoxia in a Murine Astrocytoma Model. *Lab Invest* (2012) 92(1):151–62. doi: 10.1038/labinvest.2011.128
32. Komohara Y, Ohnishi K, Kuratsu J, Takeya M. Possible Involvement of the M2 Anti-Inflammatory Macrophage Phenotype in Growth of Human Gliomas. *J Pathol* (2008) 216(1):15–24. doi: 10.1002/path.2370
33. Platten M, Kretz A, Naumann U, Aulwurm S, Egashira K, Isenmann S, et al. Monocyte Chemoattractant Protein-1 Increases Microglial Infiltration and Aggressiveness of Gliomas. *Ann Neurol* (2003) 54(3):388–92. doi: 10.1002/ana.10679
34. Chen R, Keoni C, Waker CA, Lober RM, Chen YH, Gutmann DH. KIAA1549-BRAF Expression Establishes a Permissive Tumor Microenvironment Through NFkappaB-Mediated CCL2 Production. *Neoplasia (New York NY)* (2019) 21(1):52–60. doi: 10.1016/j.neo.2018.11.007
35. Chen Z, Feng X, Herting CJ, Garcia VA, Nie K, Pong WW, et al. Cellular and Molecular Identity of Tumor-Associated Macrophages in Glioblastoma. *Cancer Res* (2017) 77(9):2266–78. doi: 10.1158/0008-5472.CAN-16-2310
36. Chen P, Zhao D, Li J, Liang X, Li J, Chang A, et al. Symbiotic Macrophage-Glioma Cell Interactions Reveal Synthetic Lethality in PTEN-Null Glioma. *Cancer Cell* (2019) 35(6):868–84 e6. doi: 10.1016/j.ccell.2019.05.003
37. Mantovani A, Sica A, Locati M. Macrophage Polarization Comes of Age. *Immunity* (2005) 23(4):344–6. doi: 10.1016/j.immuni.2005.10.001
38. Vidyarthi A, Agnihotri T, Khan N, Singh S, Tewari MK, Radotra BD, et al. Predominance of M2 Macrophages in Gliomas Leads to the Suppression of Local and Systemic Immunity. *Cancer Immunol Immunother* (2019) 68(12):1995–2004. doi: 10.1007/s00262-019-02423-8
39. Szulzewsky F, Pelz A, Feng X, Synowitz M, Markovic D, Langmann T, et al. Glioma-Associated Microglia/Macrophages Display an Expression Profile Different From M1 and M2 Polarization and Highly Express Gpnmb and Spp1. *PloS One* (2015) 10(2):e0116644. doi: 10.1371/journal.pone.0116644
40. Szulzewsky F, Arora S, de Witte L, Ulas T, Markovic D, Schultze JL, et al. Human Glioblastoma-Associated Microglia/Monocytes Express a Distinct

RNA Profile Compared to Human Control and Murine Samples. *Glia* (2016) 64(8):1416–36. doi: 10.1002/glia.23014
41. Hsu SPC, Chen YC, Chiang HC, Huang YC, Huang CC, Wang HE, et al. Rapamycin and Hydroxychloroquine Combination Alters Macrophage Polarization and Sensitizes Glioblastoma to Immune Checkpoint Inhibitors. *J Neurooncol* (2020) 146(3):417–26. doi: 10.1007/s11060-019-03360-3
42. Hu F, Dzaye O, Hahn A, Yu Y, Scavetta RJ, Dittmar G, et al. Glioma-Derived Versican Promotes Tumor Expansion *via* Glioma-Associated Microglial/Macrophages Toll-Like Receptor 2 Signaling. *Neuro Oncol* (2015) 17(2):200–10. doi: 10.1093/neuonc/nou324
43. Vinnakota K, Hu F, Ku MC, Georgieva PB, Szulzewsky F, Pohlmann A, et al. Toll-Like Receptor 2 Mediates Microglia/Brain Macrophage MT1-MMP Expression and Glioma Expansion. *Neuro Oncol* (2013) 15(11):1457–68. doi: 10.1093/neuonc/not115
44. Hu F, Ku MC, Markovic D, Dzaye O, Lehnardt S, Synowitz M, et al. Glioma-Associated Microglial MMP9 Expression is Upregulated by TLR2 Signaling and Sensitive to Minocycline. *Int J Cancer* (2014) 135(11):2569–78. doi: 10.1002/ijc.28908
45. Wallmann T, Zhang XM, Wallerius M, Bolin S, Joly AL, Sobocki C, et al. Microglia Induce PDGFRB Expression in Glioma Cells to Enhance Their Migratory Capacity. *iScience* (2018) 9:71–83. doi: 10.1016/j.isci.2018.10.011
46. Chang AL, Miska J, Wainwright DA, Dey M, Rivetta CV, Yu D, et al. CCL2 Produced by the Glioma Microenvironment Is Essential for the Recruitment of Regulatory T Cells and Myeloid-Derived Suppressor Cells. *Cancer Res* (2016) 76(19):5671–82. doi: 10.1158/0008-5472.CAN-16-0144
47. Darmanis S, Sloan SA, Croote D, Mignardi M, Chernikova S, Samghababi P, et al. Single-Cell RNA-Seq Analysis of Infiltrating Neoplastic Cells at the Migrating Front of Human Glioblastoma. *Cell Rep* (2017) 21(5):1399–410. doi: 10.1016/j.celrep.2017.10.030
48. Friebel E, Kapolou K, Unger S, Núñez NG, Utz S, Rushing EJ, et al. Single-Cell Mapping of Human Brain Cancer Reveals Tumor-Specific Instruction of Tissue-Invading Leukocytes. *Cell* (2020) 181(7):1626–42.e20. doi: 10.1016/j.cell.2020.04.055
49. Klemm F, Maas RR, Bowman RL, Kornete M, Soukup K, Nassiri S, et al. Interrogation of the Microenvironmental Landscape in Brain Tumors Reveals Disease-Specific Alterations of Immune Cells. *Cell* (2020) 181(7):1643–60.e17. doi: 10.1016/j.cell.2020.05.007
50. Pinton L, Masetto E, Vettore M, Solito S, Magri S, D'Andolfi M, et al. The Immune Suppressive Microenvironment of Human Gliomas Depends on the Accumulation of Bone Marrow-Derived Macrophages in the Center of the Lesion. *J Immunother Cancer* (2019) 7(1):58. doi: 10.1186/s40425-019-0536-x
51. Hutter G, Theruvath J, Graef CM, Zhang M, Schoen MK, Manz EM, et al. Microglia are Effector Cells of CD47-Sirpα Antiphagocytic Axis Disruption Against Glioblastoma. *Proc Natl Acad Sci USA* (2019) 116(3):997–1006. doi: 10.1073/pnas.1721434116
52. Hambardzumyan D, Gutmann DH, Kettenmann H. The Role of Microglia and Macrophages in Glioma Maintenance and Progression. *Nat Neurosci* (2016) 19(1):20–7. doi: 10.1038/nn.4185
53. Pyonteck SM, Akkari L, Schuhmacher AJ, Bowman RL, Sevenich L, Quail DF, et al. CSF-1R Inhibition Alters Macrophage Polarization and Blocks Glioma Progression. *Nat Med* (2013) 19(10):1264–72. doi: 10.1038/nm.3337
54. Zhang X, Chen L, Dang WQ, Cao MF, Xiao JF, Lv SQ, et al. CCL8 Secreted by Tumor-Associated Macrophages Promotes Invasion and Stemness of Glioblastoma Cells *via* ERK1/2 Signaling. *Lab Invest J Tech Methods Pathol* (2020) 100(4):619–29. doi: 10.1038/s41374-019-0345-3
55. Yu-Ju Wu C, Chen CH, Lin CY, Feng LY, Lin YC, Wei KC, et al. CCL5 of Glioma-Associated Microglia/Macrophages Regulates Glioma Migration and Invasion *via* Calcium-Dependent Matrix Metalloproteinase 2. *Neuro Oncol* (2020) 22(2):253–66. doi: 10.1093/neuonc/noz189
56. Lu J, Xu Z, Duan H, Ji H, Zhen Z, Li B, et al. Tumor-Associated Macrophage Interleukin-β Promotes Glycerol-3-Phosphate Dehydrogenase Activation, Glycolysis and Tumorigenesis in Glioma Cells. *Cancer Sci* (2020) 111(6):1979–90. doi: 10.1111/cas.14408
57. Chen X, Zhang L, Zhang IY, Liang J, Wang H, Ouyang M, et al. RAGE Expression in Tumor-Associated Macrophages Promotes Angiogenesis in Glioma. *Cancer Res* (2014) 74(24):7285–97. doi: 10.1158/0008-5472.CAN-14-1240
58. De Leo A, Ugolini A, Veglia F. Myeloid Cells in Glioblastoma Microenvironment. *Cells* (2020) 10(1):18. doi: 10.3390/cells10010018
59. Alban TJ, Alvarado AG, Sorensen MD, Bayik D, Volovetz J, Serbinowski E, et al. Global Immune Fingerprinting in Glioblastoma Patient Peripheral Blood Reveals Immune-Suppression Signatures Associated With Prognosis. *JCI Insight* (2018) 3(21):e122264. doi: 10.1172/jci.insight.122264
60. Bruyère C, Mijatovic T, Lonez C, Spiegl-Kreinecker S, Walter Berger REK, Ruysschaert J-M, et al. Temozolomide-Induced Modification of the CXC Chemokine Network in Experimental Gliomas. *Int J Oncol* (2011) 38(5):1453–64. doi: 10.3892/ijo.2011.964
61. Zhang H, Ye YL, Li MX, Ye SB, Huang WR, Cai TT, et al. CXCL2/MIF-CXCR2 Signaling Promotes the Recruitment of Myeloid-Derived Suppressor Cells and Is Correlated With Prognosis in Bladder Cancer. *Oncogene* (2017) 36(15):2095–104. doi: 10.1038/onc.2016.367
62. Flores-Toro JA, Luo D, Gopinath A, Sarkisian MR, Campbell JJ, Charo IF, et al. CCR2 Inhibition Reduces Tumor Myeloid Cells and Unmasks a Checkpoint Inhibitor Effect to Slow Progression of Resistant Murine Gliomas. *Proc Natl Acad Sci USA* (2020) 117(2):1129–38. doi: 10.1073/pnas.1910856117
63. Mi Y, Guo N, Luan J, Cheng J, Hu Z, Jiang P, et al. The Emerging Role of Myeloid-Derived Suppressor Cells in the Glioma Immune Suppressive Microenvironment. *Front Immunol* (2020) 11:737. doi: 10.3389/fimmu.2020.00737
64. Raychaudhuri B, Rayman P, Ireland J, Ko J, Rini B, Borden EC, et al. Myeloid-Derived Suppressor Cell Accumulation and Function in Patients With Newly Diagnosed Glioblastoma. *Neuro Oncol* (2011) 13(6):591–9. doi: 10.1093/neuonc/nor042
65. Gielen PR, Schulte BM, Kers-Rebel ED, Verrijp K, Petersen-Baltussen HMJM, ter Laan M, et al. Increase in Both CD14-Positive and CD15-Positive Myeloid-Derived Suppressor Cell Subpopulations in the Blood of Patients With Glioma But Predominance of CD15-Positive Myeloid-Derived Suppressor Cells in Glioma Tissue. *J Neuropathol Exp Neurol* (2015) 74(5):390–400. doi: 10.1097/NEN.0000000000000183
66. Guo X, Qiu W, Liu Q, Qian M, Wang S, Zhang Z, et al. Immunosuppressive Effects of Hypoxia-Induced Glioma Exosomes Through Myeloid-Derived Suppressor Cells *via* the miR-10a/Rora and miR-21/Pten Pathways. *Oncogene* (2018) 37(31):4239–59. doi: 10.1038/s41388-018-0261-9
67. Guo X, Qiu W, Wang J, Liu Q, Qian M, Wang S, et al. Glioma Exosomes Mediate the Expansion and Function of Myeloid-Derived Suppressor Cells Through microRNA-29a/Hbp1 and microRNA-92a/Prkar1a Pathways. *Int J Cancer* (2019) 144(12):3111–26. doi: 10.1002/ijc.32052
68. Ugolini A, Tyurin VA, Tyurina YY, Tcyganov EN, Donthireddy L, Kagan VE, et al. Polymorphonuclear Myeloid-Derived Suppressor Cells Limit Antigen Cross-Presentation by Dendritic Cells in Cancer. *JCI Insight* (2020) 5(15):e138581. doi: 10.1172/jci.insight.138581
69. Li H, Han Y, Guo Q, Zhang M, Cao X. Cancer-Expanded Myeloid-Derived Suppressor Cells Induce Anergy of NK Cells Through Membrane-Bound TGF-Beta 1. *J Immunol* (2009) 182(1):240–9. doi: 10.4049/jimmunol.182.1.240
70. Raber PL, Thevenot P, Sierra R, Wyczechowska D, Halle D, Ramirez ME, et al. Subpopulations of Myeloid-Derived Suppressor Cells Impair T Cell Responses Through Independent Nitric Oxide-Related Pathways. *Int J Cancer* (2014) 134(12):2853–64. doi: 10.1002/ijc.28622
71. Huang B, Pan PY, Li Q, Sato AI, Levy DE, Bromberg J, et al. Gr-1+CD115+ Immature Myeloid Suppressor Cells Mediate the Development of Tumor-Induced T Regulatory Cells and T-Cell Anergy in Tumor-Bearing Host. *Cancer Res* (2006) 66(2):1123–31. doi: 10.1158/0008-5472.CAN-05-1299
72. Ostrand-Rosenberg S, Sinha P, Beury DW, Clements VK. Cross-Talk Between Myeloid-Derived Suppressor Cells (MDSC), Macrophages, and Dendritic Cells Enhances Tumor-Induced Immune Suppression. *Semin Cancer Biol* (2012) 22(4):275–81. doi: 10.1016/j.semcancer.2012.01.011
73. Hu CE, Gan J, Zhang RD, Cheng YR, Huang GJ. Up-Regulated Myeloid-Derived Suppressor Cell Contributes to Hepatocellular Carcinoma Development by Impairing Dendritic Cell Function. *Scand J Gastroenterol* (2011) 46(2):156–64. doi: 10.3109/00365521.2010.516450
74. Fortin C, Huang X, Yang Y. NK Cell Response to Vaccinia Virus Is Regulated by Myeloid-Derived Suppressor Cells. *J Immunol* (2012) 189(4):1843–9. doi: 10.4049/jimmunol.1200584
75. Li H, Han Y, Guo Q, Zhang M, Cao X. Cancer-Expanded Myeloid-Derived Suppressor Cells Induce Anergy of NK Cells Through Membrane-Bound TGF-Beta 1. *J Immunol* (2009) 182(1):240–9. doi: 10.4049/jimmunol.182.1.240

76. Hoechst B, Voigtlaender T, Ormandy L, Gamrekelashvili J, Zhao F, Wedemeyer H, et al. Myeloid Derived Suppressor Cells Inhibit Natural Killer Cells in Patients With Hepatocellular Carcinoma *via* the NKp30 Receptor. *Hepatology* (2009) 50(3):799–807. doi: 10.1002/hep.23054
77. Liu Y, Wei J, Guo G, Zhou J. Norepinephrine-Induced Myeloid-Derived Suppressor Cells Block T-Cell Responses *via* Generation of Reactive Oxygen Species. *Immunopharmacol Immunotoxicol* (2015) 37(4):359–65. doi: 10.3109/08923973.2015.1059442
78. Khan S, Mittal S, McGee K, Alfaro-Munoz KD, Majd N, Balasubramaniyan V, et al. Role of Neutrophils and Myeloid-Derived Suppressor Cells in Glioma Progression and Treatment Resistance. *Int J Mol Sci* (2020) 21 (6):1954. doi: 10.3390/ijms21061954
79. Veglia F, Perego M, Gabrilovich D. Myeloid-Derived Suppressor Cells Coming of Age. *Nat Immunol* (2018) 19(2):108–19. doi: 10.1038/s41590-017-0022-x
80. Jia W, Jackson-Cook C, Graf MR. Tumor-Infiltrating, Myeloid-Derived Suppressor Cells Inhibit T Cell Activity by Nitric Oxide Production in an Intracranial Rat Glioma + Vaccination Model. *J Neuroimmunol* (2010) 223 (1-2):20–30. doi: 10.1016/j.jneuroim.2010.03.011
81. Fujita M, Kohanbash G, Fellows-Mayle W, Hamilton RL, Komohara Y, Decker SA, et al. COX-2 Blockade Suppresses Gliomagenesis by Inhibiting Myeloid-Derived Suppressor Cells. *Cancer Res* (2011) 71(7):2664–74. doi: 10.1158/0008-5472.CAN-10-3055
82. Lee-Chang C, Rashidi A, Miska J, Zhang P, Pituch KC, Hou D, et al. Myeloid-Derived Suppressive Cells Promote B Cell-Mediated Immunosuppression *via* Transfer of PD-L1 in Glioblastoma. *Cancer Immunol Res* (2019) 7(12):1928–43. doi: 10.1158/2326-6066.Cir-19-0240
83. Shand FH, Ueha S, Otsuji M, Koid SS, Shichino S, Tsukui T, et al. Tracking of Intertissue Migration Reveals the Origins of Tumor-Infiltrating Monocytes. *Proc Natl Acad Sci USA* (2014) 111(21):7771–6. doi: 10.1073/pnas.1402914111
84. Kumar V, Cheng P, Condamine T, Mony S, Languino LR, McCaffrey JC, et al. CD45 Phosphatase Inhibits STAT3 Transcription Factor Activity in Myeloid Cells and Promotes Tumor-Associated Macrophage Differentiation. *Immunity* (2016) 44(2):303–15. doi: 10.1016/j.immuni.2016.01.014
85. Corzo CA, Condamine T, Lu L, Cotter MJ, Youn JI, Cheng P, et al. HIF-1alpha Regulates Function and Differentiation of Myeloid-Derived Suppressor Cells in the Tumor Microenvironment. *J Exp Med* (2010) 207 (11):2439–53. doi: 10.1084/jem.20100587
86. Hor WS, Huang WL, Lin YS, Yang BC. Cross-Talk Between Tumor Cells and Neutrophils Through the Fas (APO-1, CD95)/FasL System: Human Glioma Cells Enhance Cell Viability and Stimulate Cytokine Production in Neutrophils. *J Leukoc Biol* (2003) 73(3):363–8. doi: 10.1189/jlb.0702375
87. Zha C, Meng X, Li L, Mi S, Qian D, Li Z, et al. Neutrophil Extracellular Traps Mediate the Crosstalk Between Glioma Progression and the Tumor Microenvironment *via* the HMGB1/RAGE/IL-8 Axis. *Cancer Biol Med* (2020) 17(1):154–68. doi: 10.20892/j.issn.2095-3941.2019.0353
88. Wang T, Cao L, Dong X, Wu F, De W, Huang L, et al. LINC01116 Promotes Tumor Proliferation and Neutrophil Recruitment *via* DDX5-Mediated Regulation of IL-1beta in Glioma Cell. *Cell Death Dis* (2020) 11(5):302. doi: 10.1038/s41419-020-2506-0
89. Yee PP, Wei Y, Kim SY, Lu T, Chih SY, Lawson C, et al. Neutrophil-Induced Ferroptosis Promotes Tumor Necrosis in Glioblastoma Progression. *Nat Commun* (2020) 11(1):5424. doi: 10.1038/s41467-020-19193-y
90. Rahbar A, Cederarv M, Wolmer-Solberg N, Tammik C, Stragliotto G, Peredo I, et al. Enhanced Neutrophil Activity Is Associated With Shorter Time to Tumor Progression in Glioblastoma Patients. *Oncoimmunology* (2016) 5(2):e1075693. doi: 10.1080/2162402X.2015.1075693
91. Iwatsuki K, Kumara E, Yoshimine T, Nakagawa H, Sato M, Hayakawa T. Elastase Expression by Infiltrating Neutrophils in Gliomas. *Neurol Res* (2000) 22(5):465–8. doi: 10.1080/01616412.2000.11740701
92. Liang J, Piao Y, Holmes L, Fuller GN, Henry V, Tiao N, et al. Neutrophils Promote the Malignant Glioma Phenotype Through S100A4. *Clin Cancer Res* (2014) 20(1):187–98. doi: 10.1158/1078-0432.CCR-13-1279
93. Fujita M, Scheurer ME, Decker SA, McDonald HA, Kohanbash G, Kastenhuber ER, et al. Role of Type 1 IFNs in Antiglioma Immunosurveillance–Using Mouse Studies to Guide Examination of Novel Prognostic Markers in Humans. *Clin Cancer Res* (2010) 16 (13):3409–19. doi: 10.1158/1078-0432.CCR-10-0644
94. Wang P-F, Zhang Y-X, Su J, Yao K, Li S-W, Huang G-R, et al. Neutrophil Depletion Enhances the Therapeutic Effect of PD-1 Antibody on Glioma. *Aging* (2020) 12(15):15290–301. doi: 10.18632/aging.103428
95. Filley AC, Dey M. Dendritic Cell Based Vaccination Strategy: An Evolving Paradigm. *J Neurooncol* (2017) 133(2):223–35. doi: 10.1007/s11060-017-2446-4
96. Dey M, Chang AL, Miska J, Wainwright DA, Ahmed AU, Balyasnikova IV, et al. Dendritic Cell-Based Vaccines That Utilize Myeloid Rather Than Plasmacytoid Cells Offer a Superior Survival Advantage in Malignant Glioma. *J Immunol* (2015) 195(1):367–76. doi: 10.4049/jimmunol.1401607
97. Anguille S, Smits EL, Lion E, van Tendeloo VF, Berneman ZN. Clinical Use of Dendritic Cells for Cancer Therapy. *Lancet Oncol* (2014) 15(7):e257–e67. doi: 10.1016/s1470-2045(13)70585-0
98. Palucka K, Banchereau J. Cancer Immunotherapy *via* Dendritic Cells. *Nat Rev Cancer* (2012) 12(4):265–77. doi: 10.1038/nrc3258
99. Banchereau J, Briere F, Caux C, Davoust J, Lebecque S, Liu YJ, et al. Immunobiology of Dendritic Cells. *Annu Rev Immunol* (2000) 18:767–811. doi: 10.1146/annurev.immunol.18.1.767
100. Collin M, Bigley V. Human Dendritic Cell Subsets: An Update. *Immunology* (2018) 154(1):3–20. doi: 10.1111/imm.12888
101. Candolfi M, King GD, Yagiz K, Curtin JF, Mineharu Y, Muhammad AK, et al. Plasmacytoid Dendritic Cells in the Tumor Microenvironment: Immune Targets for Glioma Therapeutics. *Neoplasia (New York NY)* (2012) 14(8):757–70. doi: 10.1593/neo.12794
102. Ghirelli C, Reyal F, Jeanmougin M, Zollinger R, Sirven P, Michea P, et al. Breast Cancer Cell-Derived GM-CSF Licenses Regulatory Th2 Induction by Plasmacytoid Predendritic Cells in Aggressive Disease Subtypes. *Cancer Res* (2015) 75(14):2775–87. doi: 10.1158/0008-5472.CAN-14-2386
103. Yu X, Harden K, Gonzalez LC, Francesco M, Chiang E, Irving B, et al. The Surface Protein TIGIT Suppresses T Cell Activation by Promoting the Generation of Mature Immunoregulatory Dendritic Cells. *Nat Immunol* (2009) 10(1):48–57. doi: 10.1038/ni.1674
104. Waisman A, Lukas D, Clausen BE, Yogev N. Dendritic Cells as Gatekeepers of Tolerance. *Semin Immunopathol* (2017) 39(2):153–63. doi: 10.1007/s00281-016-0583-z
105. Polajeva J, Sjosten AM, Lager N, Kastemar M, Waern I, Alafuzoff I, et al. Mast Cell Accumulation in Glioblastoma With a Potential Role for Stem Cell Factor and Chemokine CXCL12. *PloS One* (2011) 6(9):e25222. doi: 10.1371/journal.pone.0025222
106. Polajeva J, Bergstrom T, Edqvist PH, Lundequist A, Sjosten A, Nilsson G, et al. Glioma-Derived Macrophage Migration Inhibitory Factor (MIF) Promotes Mast Cell Recruitment in a STAT5-Dependent Manner. *Mol Oncol* (2014) 8(1):50–8. doi: 10.1016/j.molonc.2013.09.002
107. Attarha S, Roy A, Westermark B, Tchougounova E. Mast Cells Modulate Proliferation, Migration and Stemness of Glioma Cells Through Downregulation of GSK3beta Expression and Inhibition of STAT3 Activation. *Cell Signal* (2017) 37:81–92. doi: 10.1016/j.cellsig.2017.06.004
108. Woroniecka K, Chongsathidkiet P, Rhodin K, Kemeny H, Dechant C, Farber SH, et al. T-Cell Exhaustion Signatures Vary With Tumor Type and Are Severe in Glioblastoma. *Clin Cancer Res* (2018) 24(17):4175–86. doi: 10.1158/1078-0432.Ccr-17-1846
109. Wainwright DA, Balyasnikova IV, Chang AL, Ahmed AU, Moon KS, Auffinger B, et al. IDO Expression in Brain Tumors Increases the Recruitment of Regulatory T Cells and Negatively Impacts Survival. *Clin Cancer Res* (2012) 18(22):6110–21. doi: 10.1158/1078-0432.CCR-12-2130
110. Lohr J, Ratliff T, Huppertz A, Ge Y, Dictus C, Ahmadi R, et al. Effector T-Cell Infiltration Positively Impacts Survival of Glioblastoma Patients and Is Impaired by Tumor-Derived TGF-Beta. *Clin Cancer Res* (2011) 17 (13):4296–308. doi: 10.1158/1078-0432.CCR-10-2557
111. Jansen T, Tyler B, Mankowski JL, Recinos VR, Pradilla G, Legnani F, et al. FasL Gene Knock-Down Therapy Enhances the Antiglioma Immune Response. *Neuro Oncol* (2010) 12(5):482–9. doi: 10.1093/neuonc/nop052
112. Perng P, Lim M. Immunosuppressive Mechanisms of Malignant Gliomas: Parallels at Non-CNS Sites. *Front Oncol* (2015) 5:153. doi: 10.3389/fonc.2015.00153
113. Munn DH, Sharma MD, Baban B, Harding HP, Zhang Y, Ron D, et al. GCN2 Kinase in T Cells Mediates Proliferative Arrest and Anergy Induction in Response to Indoleamine 2,3-Dioxygenase. *Immunity* (2005) 22(5):633–42. doi: 10.1016/j.immuni.2005.03.013

114. Rashidi A, Miska J, Lee-Chang C, Kanojia D, Panek WK, Lopez-Rosas A, et al. GCN2 Is Essential for CD8(+) T Cell Survival and Function in Murine Models of Malignant Glioma. *Cancer Immunol Immunother* (2020) 69 (1):81–94. doi: 10.1007/s00262-019-02441-6
115. Heimberger AB, Abou-Ghazal M, Reina-Ortiz C, Yang DS, Sun W, Qiao W, et al. Incidence and Prognostic Impact of FoxP3+ Regulatory T Cells in Human Gliomas. *Clin Cancer Res* (2008) 14(16):5166–72. doi: 10.1158/1078-0432.CCR-08-0320
116. Sayour EJ, McLendon P, McLendon R, De Leon G, Reynolds R, Kresak J, et al. Increased Proportion of FoxP3+ Regulatory T Cells in Tumor Infiltrating Lymphocytes Is Associated With Tumor Recurrence and Reduced Survival in Patients With Glioblastoma. *Cancer Immunol Immunother* (2015) 64(4):419–27. doi: 10.1007/s00262-014-1651-7
117. Folgiero V, Miele E, Carai A, Ferretti E, Alfano V, Po A, et al. IDO1 Involvement in mTOR Pathway: A Molecular Mechanism of Resistance to mTOR Targeting in Medulloblastoma. *Oncotarget* (2016) 7(33):52900–11. doi: 10.18632/oncotarget.9284
118. Cantini G, Pisati F, Mastropietro A, Frattini V, Iwakura Y, Finocchiaro G, et al. A Critical Role for Regulatory T Cells in Driving Cytokine Profiles of Th17 Cells and Their Modulation of Glioma Microenvironment. *Cancer Immunol Immunother* (2011) 60(12):1739–50. doi: 10.1007/s00262-011-1069-4
119. Paladugu M, Thakur A, Lum LG, Mittal S, Parajuli P. Generation and Immunologic Functions of Th17 Cells in Malignant Gliomas. *Cancer Immunol Immunother* (2013) 62(1):75–86. doi: 10.1007/s00262-012-1312-7
120. Wang B, Zhao CH, Sun G, Zhang ZW, Qian BM, Zhu YF, et al. IL-17 Induces the Proliferation and Migration of Glioma Cells Through the Activation of PI3K/Akt1/NF-kappaB-P65. *Cancer Lett* (2019) 447:93–104. doi: 10.1016/j.canlet.2019.01.008
121. Wiendl H, Mitsdoerffer M, Hofmeister V, Wischhusen J, Bornemann A, Meyermann R, et al. A Functional Role of HLA-G Expression in Human Gliomas: An Alternative Strategy of Immune Escape. *J Immunol* (2002) 168 (9):4772–80. doi: 10.4049/jimmunol.168.9.4772
122. Orimo A, Gupta PB, Sgroi DC, Arenzana-Seisdedos F, Delaunay T, Naeem R, et al. Stromal Fibroblasts Present in Invasive Human Breast Carcinomas Promote Tumor Growth and Angiogenesis Through Elevated SDF-1/CXCL12 Secretion. *Cell* (2005) 121(3):335–48. doi: 10.1016/j.cell.2005.02.034
123. Sugihara H, Ishimoto T, Yasuda T, Izumi D, Eto K, Sawayama H, et al. Cancer-Associated Fibroblast-Derived CXCL12 Causes Tumor Progression in Adenocarcinoma of the Esophagogastric Junction. *Med Oncol (Northwood London England)* (2015) 32(6):618. doi: 10.1007/s12032-015-0618-7
124. Whipple CA, Brinckerhoff CE. BRAF(V600E) Melanoma Cells Secrete Factors That Activate Stromal Fibroblasts and Enhance Tumourigenicity. *Br J Cancer* (2014) 111(8):1625–33. doi: 10.1038/bjc.2014.452
125. Lim EJ, Suh Y, Kim S, Kang SG, Lee SJ. Force-Mediated Proinvasive Matrix Remodeling Driven by Tumor-Associated Mesenchymal Stem-Like Cells in Glioblastoma. *BMB Rep* (2018) 51(4):182–7. doi: 10.5483/bmbrep.2018.51.4.185
126. Fazi B, Proserpio C, Galardi S, Annesi F, Cola M, Mangiola A, et al. The Expression of the Chemokine CXCL14 Correlates With Several Aggressive Aspects of Glioblastoma and Promotes Key Properties of Glioblastoma Cells. *Int J Mol Sci* (2019) 20(10):2496. doi: 10.3390/ijms20102496
127. Wang H, Li H, Jiang Q, Dong X, Li S, Cheng S, et al. HOTAIRM1 Promotes Malignant Progression of Transformed Fibroblasts in Glioma Stem-Like Cells Remodeled Microenvironment *via* Regulating miR-133b-3p/TGFbeta Axis. *Front Oncol* (2021) 11:603128. doi: 10.3389/fonc.2021.603128
128. Mbongue JC, Nicholas DA, Torrez TW, Kim NS, Firek AF, Langridge WH. The Role of Indoleamine 2, 3-Dioxygenase in Immune Suppression and Autoimmunity. *Vaccines (Basel)* (2015) 3(3):703–29. doi: 10.3390/vaccines3030703
129. Mellor AL, Munn DH. Physiologic Control of the Functional Status of Foxp3 + Regulatory T Cells. *J Immunol* (2011) 186(8):4535–40. doi: 10.4049/jimmunol.1002937
130. Hanihara M, Kawataki T, Oh-Oka K, Mitsuka K, Nakao A, Kinouchi H. Synergistic Antitumor Effect With Indoleamine 2,3-Dioxygenase Inhibition and Temozolomide in a Murine Glioma Model. *J Neurosurg* (2016) 124 (6):1594–601. doi: 10.3171/2015.5.JNS141901
131. Chen Q, Han B, Meng X, Duan C, Yang C, Wu Z, et al. Immunogenomic Analysis Reveals LGALS1 Contributes to the Immune Heterogeneity and Immunosuppression in Glioma. *Int J Cancer* (2019) 145(2):517–30. doi: 10.1002/ijc.32102
132. Kouo T, Huang L, Pucsek AB, Cao M, Solt S, Armstrong T, et al. Galectin-3 Shapes Antitumor Immune Responses by Suppressing CD8+ T Cells via LAG-3 and Inhibiting Expansion of Plasmacytoid Dendritic Cells. *Cancer Immunol Res* (2015) 3(4):412–23. doi: 10.1158/2326-6066.CIR-14-0150
133. Workman CJ, Vignali DAA. The CD4-Related Molecule, LAG-3 (CD223), Regulates the Expansion of Activated T Cells. *Eur J Immunol* (2003) 33 (4):970–9. doi: 10.1002/eji.200323382
134. Andrews LP, Marciscano AE, Drake CG, Vignali DA. LAG3 (CD223) as a Cancer Immunotherapy Target. *Immunol Rev* (2017) 276(1):80–96. doi: 10.1111/imr.12519
135. Liu EY, Ryan KM. Autophagy and Cancer–Issues We Need to Digest. *J Cell Sci* (2012) 125(Pt 10):2349–58. doi: 10.1242/jcs.093708
136. Poillet-Perez L, Xie X, Zhan L, Yang Y, Sharp DW, Hu ZS, et al. Autophagy Maintains Tumour Growth Through Circulating Arginine. *Nature* (2018) 563(7732):569–73. doi: 10.1038/s41586-018-0697-7
137. Galluzzi L, Pietrocola F, Bravo-San Pedro JM, Amaravadi RK, Baehrecke EH, Cecconi F, et al. Autophagy in Malignant Transformation and Cancer Progression. *EMBO J* (2015) 34(7):856–80. doi: 10.15252/embj.201490784
138. Mathew R, Karp CM, Beaudoin B, Vuong N, Chen G, Chen HY, et al. Autophagy Suppresses Tumorigenesis Through Elimination of P62. *Cell* (2009) 137(6):1062–75. doi: 10.1016/j.cell.2009.03.048
139. Filomeni G, De Zio D, Cecconi F. Oxidative Stress and Autophagy: The Clash Between Damage and Metabolic Needs. *Cell Death Differ* (2015) 22 (3):377–88. doi: 10.1038/cdd.2014.150
140. Kimmelman AC, White E. Autophagy and Tumor Metabolism. *Cell Metab* (2017) 25(5):1037–43. doi: 10.1016/j.cmet.2017.04.004
141. Gammoh N, Fraser J, Puente C, Syred HM, Kang H, Ozawa T, et al. Suppression of Autophagy Impedes Glioblastoma Development and Induces Senescence. *Autophagy* (2016) 12(9):1431–9. doi: 10.1080/15548627.2016.1190053
142. Inda MM, Bonavia R, Seoane J. Glioblastoma Multiforme: A Look Inside its Heterogeneous Nature. *Cancers (Basel)* (2014) 6(1):226–39. doi: 10.3390/cancers6010226
143. Galan-Moya EM, Le Guelte A, Lima Fernandes E, Thirant C, Dwyer J, Bidere N, et al. Secreted Factors From Brain Endothelial Cells Maintain Glioblastoma Stem-Like Cell Expansion Through the mTOR Pathway. *EMBO Rep* (2011) 12(5):470–6. doi: 10.1038/embor.2011.39
144. Jhanwar-Uniyal M, Albert L, McKenna E, Karsy M, Rajdev P, Braun A, et al. Deciphering the Signaling Pathways of Cancer Stem Cells of Glioblastoma Multiforme: Role of Akt/mTOR and MAPK Pathways. *Adv Enzyme Regul* (2011) 51(1):164–70. doi: 10.1016/j.advenzreg.2010.09.017
145. Galli R, Binda E, Orfanelli U, Cipelletti B, Gritti A, De Vitis S, et al. Isolation and Characterization of Tumorigenic, Stem-Like Neural Precursors From Human Glioblastoma. *Cancer Res* (2004) 64(19):7011–21. doi: 10.1158/0008-5472.CAN-04-1364
146. Buccarelli M, Marconi M, Pacioni S, De Pascalis I, D'Alessandris QG, Martini M, et al. Inhibition of Autophagy Increases Susceptibility of Glioblastoma Stem Cells to Temozolomide by Igniting Ferroptosis. *Cell Death Dis* (2018) 9(8):841. doi: 10.1038/s41419-018-0864-7
147. Huang T, Wan X, Alvarez AA, James CD, Song X, Yang Y, et al. MIR93 (microRNA -93) Regulates Tumorigenicity and Therapy Response of Glioblastoma by Targeting Autophagy. *Autophagy* (2019) 15(6):1100–11. doi: 10.1080/15548627.2019.1569947
148. Jawhari S, Ratinaud MH, Verdier M. Glioblastoma, Hypoxia and Autophagy: A Survival-Prone 'Ménage-À-Trois'. *Cell Death Dis* (2016) 7(10):e2434. doi: 10.1038/cddis.2016.318
149. Kahlert UD, Maciaczyk D, Dai F, Claus R, Firat E, Doostkam S, et al. Resistance to Hypoxia-Induced, BNIP3-Mediated Cell Death Contributes to an Increase in a CD133-Positive Cell Population in Human Glioblastomas *In Vitro*. *J Neuropathol Exp Neurol* (2012) 71(12):1086–99. doi: 10.1097/NEN.0b013e3182772d83
150. Pratt J, Annabi B. Induction of Autophagy Biomarker BNIP3 Requires a JAK2/STAT3 and MT1-MMP Signaling Interplay in Concanavalin-A-Activated U87 Glioblastoma Cells. *Cell Signal* (2014) 26(5):917–24. doi: 10.1016/j.cellsig.2014.01.012
151. Sunayama J, Sato A, Matsuda K, Tachibana K, Suzuki K, Narita Y, et al. Dual Blocking of Mtor and PI3K Elicits a Prodifferentiation Effect on

Glioblastoma Stem-Like Cells. *Neuro Oncol* (2010) 12(12):1205–19. doi: 10.1093/neuonc/noq103
152. Zhuang W, Li B, Long L, Chen L, Huang Q, Liang Z. Induction of Autophagy Promotes Differentiation of Glioma-Initiating Cells and Their Radiosensitivity. *Int J Cancer* (2011) 129(11):2720–31. doi: 10.1002/ijc.25975
153. Hu X, Pandolfi PP, Li Y, Koutcher JA, Rosenblum M, Holland EC. mTOR Promotes Survival and Astrocytic Characteristics Induced by Pten/AKT Signaling in Glioblastoma. *Neoplasia (New York NY)* (2005) 7(4):356–68. doi: 10.1593/neo.04595
154. Tamrakar S, Yashiro M, Kawashima T, Uda T, Terakawa Y, Kuwae Y, et al. Clinicopathological Significance of Autophagy-Related Proteins and Its Association With Genetic Alterations in Gliomas. *Anticancer Res* (2019) 39(3):1233–42. doi: 10.21873/anticanres.13233
155. Wen ZP, Zeng WJ, Chen YH, Li H, Wang JY, Cheng Q, et al. Knockdown ATG4C Inhibits Gliomas Progression and Promotes Temozolomide Chemosensitivity by Suppressing Autophagic Flux. *J Exp Clin Cancer Res* (2019) 38(1):298. doi: 10.1186/s13046-019-1287-8
156. Yang Z, Bian E, Xu Y, Ji X, Tang F, Ma C, et al. Meg3 Induces EMT and Invasion of Glioma Cells *via* Autophagy. *Onco Targets Ther* (2020) 13:989–1000. doi: 10.2147/ott.S239648
157. Xu L, Li Z, Song S, Chen Q, Mo L, Wang C, et al. Downregulation of Alpha-L-Fucosidase 1 Suppresses Glioma Progression by Enhancing Autophagy and Inhibiting Macrophage Infiltration. *Cancer Sci* (2020) 111(7):2284–96. doi: 10.1111/cas.14427
158. Shchors K, Massaras A, Hanahan D. Dual Targeting of the Autophagic Regulatory Circuitry in Gliomas With Repurposed Drugs Elicits Cell-Lethal Autophagy and Therapeutic Benefit. *Cancer Cell* (2015) 28(4):456–71. doi: 10.1016/j.ccell.2015.08.012
159. Hombach-Klonisch S, Mehrpour M, Shojaei S, Harlos C, Pitz M, Hamai A, et al. Glioblastoma and Chemoresistance to Alkylating Agents: Involvement of Apoptosis, Autophagy, and Unfolded Protein Response. *Pharmacol Ther* (2018) 184:13–41. doi: 10.1016/j.pharmthera.2017.10.017
160. Ito H, Daido S, Kanzawa T, Kondo S, Kondo Y. Radiation-induced autophagy Is associated with LC3 and its inhibition sensitizes malignant glioma cells. *Int J Oncol* (2005) 26(5):1401–10. doi: 10.3892/ijo.26.5.1401
161. Ryabaya OO, Inshakov AN, Egorova AV, Emelyanova MA, Nasedkina TV, Zasedatelev AS, et al. Autophagy Inhibitors Chloroquine and LY294002 Enhance Temozolomide Cytotoxicity on Cutaneous Melanoma Cell Lines *In Vitro*. *Anticancer Drugs* (2017) 28(3):307–15. doi: 10.1097/CAD.0000000000000463
162. Yang L, Lin C, Wang L, Guo H, Wang X. Hypoxia and Hypoxia-Inducible Factors in Glioblastoma Multiforme Progression and Therapeutic Implications. *Exp Cell Res* (2012) 318(19):2417–26. doi: 10.1016/j.yexcr.2012.07.017
163. Zheng Y, Liu L, Wang Y, Xiao S, Mai R, Zhu Z, et al. Glioblastoma Stem Cell (GSC)-Derived PD-L1-Containing Exosomes Activates AMPK/ULK1 Pathway Mediated Autophagy to Increase Temozolomide-Resistance in Glioblastoma. *Cell Biosci* (2021) 11(1):63. doi: 10.1186/s13578-021-00575-8
164. Filippi-Chiela EC, Bueno e Silva MM, Thome MP, Lenz G. Single-Cell Analysis Challenges the Connection Between Autophagy and Senescence Induced by DNA Damage. *Autophagy* (2015) 11(7):1099–113. doi: 10.1080/15548627.2015.1009795
165. Lu H, Xiao J, Ke C, Ni X, Xiu R, Tian Q, et al. TOPK Inhibits Autophagy by Phosphorylating ULK1 and Promotes Glioma Resistance to TMZ. *Cell Death Dis* (2019) 10(8):583. doi: 10.1038/s41419-019-1805-9
166. Lv QL, Wang LC, Li DC, Lin QX, Shen XL, Liu HY, et al. Knockdown lncRNA DLEU1 Inhibits Gliomas Progression and Promotes Temozolomide Chemosensitivity by Regulating Autophagy. *Front Pharmacol* (2020) 11:560543. doi: 10.3389/fphar.2020.560543
167. Jiang C, Shen F, Du J, Fang X, Li X, Su J, et al. Upregulation of CASC2 Sensitized Glioma to Temozolomide Cytotoxicity Through Autophagy Inhibition by Sponging miR-193a-5p and Regulating mTOR Expression. *Biomed Pharmacother* (2018) 97:844–50. doi: 10.1016/j.biopha.2017.10.146
168. Ma B, Yuan Z, Zhang L, Lv P, Yang T, Gao J, et al. Long Non-Coding RNA AC023115.3 Suppresses Chemoresistance of Glioblastoma by Reducing Autophagy. *Biochim Biophys Acta Mol Cell Res* (2017) 1864(8):1393–404. doi: 10.1016/j.bbamcr.2017.05.008
169. Gewirtz DA. When Cytoprotective Autophagy Isn't... And Even When It Is. *Autophagy* (2014) 10(3):391–2. doi: 10.4161/auto.27719
170. Huang T, Kim CK, Alvarez AA, Pangeni RP, Wan X, Song X, et al. MST4 Phosphorylation of ATG4B Regulates Autophagic Activity, Tumorigenicity, and Radioresistance in Glioblastoma. *Cancer Cell* (2017) 32(6):840–55 e8. doi: 10.1016/j.ccell.2017.11.005
171. Singer E, Judkins J, Salomonis N, Matlaf L, Soteropoulos P, McAllister S, et al. Reactive Oxygen Species-Mediated Therapeutic Response and Resistance in Glioblastoma. *Cell Death Dis* (2015) 6:e1601. doi: 10.1038/cddis.2014.566
172. Hou W, Song L, Zhao Y, Liu Q, Zhang S. Inhibition of Beclin-1-Mediated Autophagy by MicroRNA-17-5p Enhanced the Radiosensitivity of Glioma Cells. *Oncol Res* (2017) 25(1):43–53. doi: 10.3727/096504016X14719078133285
173. Jo GH, Bogler O, Chwae YJ, Yoo H, Lee SH, Park JB, et al. Radiation-Induced Autophagy Contributes to Cell Death and Induces Apoptosis Partly in Malignant Glioma Cells. *Cancer Res Treat* (2015) 47(2):221–41. doi: 10.4143/crt.2013.159
174. Koukourakis MI, Mitrakas AG, Giatromanolaki A. Therapeutic Interactions of Autophagy With Radiation and Temozolomide in Glioblastoma: Evidence and Issues to Resolve. *Br J Cancer* (2016) 114(5):485–96. doi: 10.1038/bjc.2016.19
175. Palumbo S, Pirtoli L, Tini P, Cevenini G, Calderaro F, Toscano M, et al. Different Involvement of Autophagy in Human Malignant Glioma Cell Lines Undergoing Irradiation and Temozolomide Combined Treatments. *J Cell Biochem* (2012) 113(7):2308–18. doi: 10.1002/jcb.24102
176. Kriel J, Muller-Nedebock K, Maarman G, Mbizana S, Ojuka E, Klumperman B, et al. Coordinated Autophagy Modulation Overcomes Glioblastoma Chemoresistance Through Disruption of Mitochondrial Bioenergetics. *Sci Rep* (2018) 8(1):10348. doi: 10.1038/s41598-018-28590-9
177. Katayama M, Kawaguchi T, Berger MS, Pieper RO. DNA Damaging Agent-Induced Autophagy Produces a Cytoprotective Adenosine Triphosphate Surge in Malignant Glioma Cells. *Cell Death Differ* (2007) 14(3):548–58. doi: 10.1038/sj.cdd.4402030
178. Hegazy AM, Yamada D, Kobayashi M, Kohno S, Ueno M, Ali MA, et al. Therapeutic Strategy for Targeting Aggressive Malignant Gliomas by Disrupting Their Energy Balance. *J Biol Chem* (2016) 291(41):21496–509. doi: 10.1074/jbc.M116.734756
179. Hori YS, Hosoda R, Akiyama Y, Sebori R, Wanibuchi M, Mikami T, et al. Chloroquine Potentiates Temozolomide Cytotoxicity by Inhibiting Mitochondrial Autophagy in Glioma Cells. *J Neurooncol* (2015) 122(1):11–20. doi: 10.1007/s11060-014-1686-9
180. Hampton MB, Orrenius S. Dual Regulation of Caspase Activity by Hydrogen Peroxide: Implications for Apoptosis. *FEBS Lett* (1997) 414(3):552–6. doi: 10.1016/s0014-5793(97)01068-5
181. Ulasov I, Fares J, Timashev P, Lesniak MS. Editing Cytoprotective Autophagy in Glioma: An Unfulfilled Potential for Therapy. *Trends Mol Med* (2020) 26(3):252–62. doi: 10.1016/j.molmed.2019.11.001
182. Germic N, Frangez Z, Yousefi S, Simon HU. Regulation of the Innate Immune System by Autophagy: Monocytes, Macrophages, Dendritic Cells and Antigen Presentation. *Cell Death Differ* (2019) 26(4):715–27. doi: 10.1038/s41418-019-0297-6
183. Chen P, Cescon M, Bonaldo P. Autophagy-Mediated Regulation of Macrophages and Its Applications for Cancer. *Autophagy* (2014) 10(2):192–200. doi: 10.4161/auto.26927
184. Zhang Y, Morgan MJ, Chen K, Choksi S, Liu ZG. Induction of Autophagy Is Essential for Monocyte-Macrophage Differentiation. *Blood* (2012) 119(12):2895–905. doi: 10.1182/blood-2011-08-372383
185. Cunha LD, Yang M, Carter R, Guy C, Harris L, Crawford JC, et al. LC3-Associated Phagocytosis in Myeloid Cells Promotes Tumor Immune Tolerance. *Cell* (2018) 175(2):429–41 e16. doi: 10.1016/j.cell.2018.08.061
186. Zhang X, Chen W, Fan J, Wang S, Xian Z, Luan J, et al. Disrupting CD47-Sirpα Axis Alone or Combined With Autophagy Depletion for the Therapy of Glioblastoma. *Carcinogenesis* (2018) 39(5):689–99. doi: 10.1093/carcin/bgy041
187. Zhang X, Wang S, Nan Y, Fan J, Chen W, Luan J, et al. Inhibition of Autophagy Potentiated the Anti-Tumor Effects of VEGF and CD47 Bispecific Therapy in Glioblastoma. *Appl Microbiol Biotechnol* (2018) 102(15):6503–13. doi: 10.1007/s00253-018-9069-3
188. Clarke AJ, Simon AK. Autophagy in the Renewal, Differentiation and Homeostasis of Immune Cells. *Nat Rev Immunol* (2019) 19(3):170–83. doi: 10.1038/s41577-018-0095-2

189. Houtman J, Freitag K, Gimber N, Schmoranzer J, Heppner FL, Jendrach M. Beclin1-Driven Autophagy Modulates the Inflammatory Response of Microglia *via* NLRP3. *EMBO J* (2019) 38(4):e99430. doi: 10.15252/embj.201899430
190. Liu L, An D, Xu J, Shao B, Li X, Shi J. Ac2-26 Induces IKKbeta Degradation Through Chaperone-Mediated Autophagy *Via* HSPB1 in NCM-Treated Microglia. *Front Mol Neurosci* (2018) 11:76. doi: 10.3389/fnmol.2018.00076
191. Liu K, Zhao E, Ilyas G, Lalazar G, Lin Y, Haseeb M, et al. Impaired Macrophage Autophagy Increases the Immune Response in Obese Mice by Promoting Proinflammatory Macrophage Polarization. *Autophagy* (2015) 11(2):271–84. doi: 10.1080/15548627.2015.1009787
192. Yang M, Liu J, Shao J, Qin Y, Ji Q, Zhang X, et al. Cathepsin S-Mediated Autophagic Flux in Tumor-Associated Macrophages Accelerate Tumor Development by Promoting M2 Polarization. *Mol Cancer* (2014) 13:43. doi: 10.1186/1476-4598-13-43
193. Qian M, Wang S, Guo X, Wang J, Zhang Z, Qiu W, et al. Hypoxic Glioma-Derived Exosomes Deliver microRNA-1246 to Induce M2 Macrophage Polarization by Targeting TERF2IP *via* the STAT3 and NF-κb Pathways. *Oncogene* (2020) 39(2):428–42. doi: 10.1038/s41388-019-0996-y
194. Lin JC, Liu CL, Lee JJ, Liu TP, Ko WC, Huang YC, et al. Sorafenib Induces Autophagy and Suppresses Activation of Human Macrophage. *Int Immunopharmacol* (2013) 15(2):333–9. doi: 10.1016/j.intimp.2013.01.006
195. Chen W, Ma T, Shen XN, Xia XF, Xu GD, Bai XL, et al. Macrophage-Induced Tumor Angiogenesis Is Regulated by the TSC2-mTOR Pathway. *Cancer Res* (2012) 72(6):1363–72. doi: 10.1158/0008-5472.CAN-11-2684
196. Chang CP, Su YC, Lee PH, Lei HY. Targeting NFKB by Autophagy to Polarize Hepatoma-Associated Macrophage Differentiation. *Autophagy* (2013) 9(4):619–21. doi: 10.4161/auto.23546
197. Jacquel A, Obba S, Boyer L, Dufies M, Robert G, Gounon P, et al. Autophagy is Required for CSF-1-Induced Macrophagic Differentiation and Acquisition of Phagocytic Functions. *Blood* (2012) 119(19):4527–31. doi: 10.1182/blood-2011-11-392167
198. Alissafi T, Hatzioannou A, Mintzas K, Barouni RM, Banos A, Sormendi S, et al. Autophagy Orchestrates the Regulatory Program of Tumor-Associated Myeloid-Derived Suppressor Cells. *J Clin Invest* (2018) 128(9):3840–52. doi: 10.1172/JCI120888
199. Fossati G, Ricevuti G, Edwards SW, Walker C, Dalton A, Rossi ML. Neutrophil Infiltration Into Human Gliomas. *Acta Neuropathol* (1999) 98:349–54. doi: 10.1007/s004010051093
200. Skendros P, Mitroulis I, Ritis K. Autophagy in Neutrophils: From Granulopoiesis to Neutrophil Extracellular Traps. *Front Cell Dev Biol* (2018) 6:109. doi: 10.3389/fcell.2018.00109
201. Bhattacharya A, Wei Q, Shin JN, Abdel Fattah E, Bonilla DL, Xiang Q, et al. Autophagy Is Required for Neutrophil-Mediated Inflammation. *Cell Rep* (2015) 12(11):1731–9. doi: 10.1016/j.celrep.2015.08.019
202. Pua HH, He YW. Mitophagy in the Little Lymphocytes: An Essential Role for Autophagy in Mitochondrial Clearance in T Lymphocytes. *Autophagy* (2009) 5(5):745–6. doi: 10.4161/auto.5.5.8702
203. Jia W, He YW. Temporal Regulation of Intracellular Organelle Homeostasis in T Lymphocytes by Autophagy. *J Immunol* (2011) 186(9):5313–22. doi: 10.4049/jimmunol.1002404
204. Zheng Y, Delgoffe GM, Meyer CF, Chan W, Powell JD. Anergic T Cells are Metabolically Anergic. *J Immunol* (2009) 183(10):6095–101. doi: 10.4049/jimmunol.0803510
205. Hubbard VM, Valdor R, Patel B, Singh R, Cuervo AM, Macian F. Macroautophagy Regulates Energy Metabolism During Effector T Cell Activation. *J Immunol* (2010) 185(12):7349–57. doi: 10.4049/jimmunol.1000576
206. Botbol Y, Patel B, Macian F. Common Gamma-Chain Cytokine Signaling is Required for Macroautophagy Induction During CD4+ T-Cell Activation. *Autophagy* (2015) 11(10):1864–77. doi: 10.1080/15548627.2015.1089374
207. Mocholi E, Dowling SD, Botbol Y, Gruber RC, Ray AK, Vastert S, et al. Autophagy Is a Tolerance-Avoidance Mechanism That Modulates TCR-Mediated Signaling and Cell Metabolism to Prevent Induction of T Cell Anergy. *Cell Rep* (2018) 24(5):1136–50. doi: 10.1016/j.celrep.2018.06.065
208. Jia W, He MX, McLeod IX, Guo J, Ji D, He YW. Autophagy Regulates T Lymphocyte Proliferation Through Selective Degradation of the Cell-Cycle Inhibitor CDKN1B/P27kip1. *Autophagy* (2015) 11(12):2335–45. doi: 10.1080/15548627.2015.1110666
209. Xu X, Araki K, Li S, Han JH, Ye L, Tan WG, et al. Autophagy Is Essential for Effector CD8(+) T Cell Survival and Memory Formation. *Nat Immunol* (2014) 15(12):1152–61. doi: 10.1038/ni.3025
210. DeVorkin L, Pavey N, Carleton G, Comber A, Ho C, Lim J, et al. Autophagy Regulation of Metabolism Is Required for CD8(+) T Cell Anti-Tumor Immunity. *Cell Rep* (2019) 27(2):502–13 e5. doi: 10.1016/j.celrep.2019.03.037
211. Puleston DJ, Zhang H, Powell TJ, Lipina E, Sims S, Panse I, et al. Autophagy Is a Critical Regulator of Memory CD8(+) T Cell Formation. *eLife* (2014) 3: e03706. doi: 10.7554/eLife.03706
212. Dowling SD, Macian F. Autophagy and T Cell Metabolism. *Cancer Lett* (2018) 419:20–6. doi: 10.1016/j.canlet.2018.01.033
213. Wei J, Long L, Yang K, Guy C, Shrestha S, Chen Z, et al. Autophagy Enforces Functional Integrity of Regulatory T Cells by Coupling Environmental Cues and Metabolic Homeostasis. *Nat Immunol* (2016) 17(3):277–85. doi: 10.1038/ni.3365
214. Xu Y, Li R, Li X, Dong N, Wu D, Hou L, et al. An Autophagy-Related Gene Signature Associated With Clinical Prognosis and Immune Microenvironment in Gliomas. *Front Oncol* (2020) 10:571189. doi: 10.3389/fonc.2020.571189
215. Lin JZ, Lin N. A Risk Signature of Three Autophagy-Related Genes for Predicting Lower Grade Glioma Survival Is Associated With Tumor Immune Microenvironment. *Genomics* (2021) 113(1 Pt 2):767–77. doi: 10.1016/j.ygeno.2020.10.008
216. Xu S, Tang L, Liu Z, Yang K, Cheng Q. Bioinformatic Analyses Identify a Prognostic Autophagy-Related Long Non-Coding RNA Signature Associated With Immune Microenvironment in Diffuse Gliomas. *Front Cell Dev Biol* (2021) 9:694633. doi: 10.3389/fcell.2021.694633
217. Wang Y, Zhao W, Xiao Z, Guan G, Liu X, Zhuang M. A Risk Signature With Four Autophagy-Related Genes for Predicting Survival of Glioblastoma Multiforme. *J Cell Mol Med* (2020) 24(7):3807–21. doi: 10.1111/jcmm.14938
218. Wang QW, Liu HJ, Zhao Z, Zhang Y, Wang Z, Jiang T, et al. Prognostic Correlation of Autophagy-Related Gene Expression-Based Risk Signature in Patients With Glioblastoma. *Onco Targets Ther* (2020) 13:95–107. doi: 10.2147/OTT.S238332
219. Zhang N, Dai Z, Wu W, Wang Z, Cao H, Zhang Y, et al. The Predictive Value of Monocytes in Immune Microenvironment and Prognosis of Glioma Patients Based on Machine Learning. *Front Immunol* (2021) 12:656541. doi: 10.3389/fimmu.2021.656541
220. Fan Y, Peng X, Li B, Zhao G. Development of Autophagy Signature-Based Prognostic Nomogram for Refined Glioma Survival Prognostication. *BioMed Res Int* (2020) 2020:1872962. doi: 10.1155/2020/1872962
221. Xu J, Zhang J, Zhang Z, Gao Z, Qi Y, Qiu W, et al. Hypoxic Glioma-Derived Exosomes Promote M2-Like Macrophage Polarization by Enhancing Autophagy Induction. *Cell Death Dis* (2021) 12(4):373. doi: 10.1038/s41419-021-03664-1
222. Xue H, Yuan G, Guo X, Liu Q, Zhang J, Gao X, et al. A Novel Tumor-Promoting Mechanism of IL6 and the Therapeutic Efficacy of Tocilizumab: Hypoxia-Induced IL6 is a Potent Autophagy Initiator in Glioblastoma *via* the P-STAT3-MIR155-3p-CREBRF Pathway. *Autophagy* (2016) 12(7):1129–52. doi: 10.1080/15548627.2016.1178446
223. Yao J, Wang Z, Cheng Y, Ma C, Zhong Y, Xiao Y, et al. M2 Macrophage-Derived Exosomal microRNAs Inhibit Cell Migration and Invasion in Gliomas Through PI3K/AKT/mTOR Signaling Pathway. *J Transl Med* (2021) 19(1):99. doi: 10.1186/s12967-021-02766-w
224. Mora R, Abschuetz A, Kees T, Dokic I, Joschko N, Kleber S, et al. TNF-Alpha- and TRAIL-Resistant Glioma Cells Undergo Autophagy-Dependent Cell Death Induced by Activated Microglia. *Glia* (2009) 57(5):561–81. doi: 10.1002/glia.20785
225. Mora R, Régnier-Vigouroux A. Autophagy-Driven Cell Fate Decision Maker: Activated Microglia Induce Specific Death of Glioma Cells by a Blockade of Basal Autophagic Flux and Secondary Apoptosis/Necrosis. *Autophagy* (2009) 5(3):419–21. doi: 10.4161/auto.5.3.7881
226. Valdor R, García-Bernal D, Riquelme D, Martinez CM, Moraleda JM, Cuervo AM, et al. Glioblastoma Ablates Pericytes Antitumor Immune Function Through Aberrant Up-Regulation of Chaperone-Mediated Autophagy. *Proc Natl Acad Sci USA* (2019) 116(41):20655–65. doi: 10.1073/pnas.1903542116
227. Li TF, Xu YH, Li K, Wang C, Liu X, Yue Y, et al. Doxorubicin-Polyglycerol-Nanodiamond Composites Stimulate Glioblastoma Cell Immunogenicity

Through Activation of Autophagy. *Acta Biomater* (2019) 86:381–94. doi: 10.1016/j.actbio.2019.01.020
228. Zheng Z, Zhang J, Jiang J, He Y, Zhang W, Mo X, et al. Remodeling Tumor Immune Microenvironment (TIME) for Glioma Therapy Using Multi-Targeting Liposomal Codelivery. *J Immunother Cancer* (2020) 8(2): e000207. doi: 10.1136/jitc-2019-000207
229. Kanzawa T, Germano IM, Komata T, Ito H, Kondo Y, Kondo S. Role of Autophagy in Temozolomide-Induced Cytotoxicity for Malignant Glioma Cells. *Cell Death Differ* (2004) 11(4):448–57. doi: 10.1038/sj.cdd.4401359
230. Zanotto-Filho A, Braganhol E, Klafke K, Figueiro F, Terra SR, Paludo FJ, et al. Autophagy Inhibition Improves the Efficacy of Curcumin/Temozolomide Combination Therapy in Glioblastomas. *Cancer Lett* (2015) 358(2):220–31. doi: 10.1016/j.canlet.2014.12.044
231. Lin CJ, Lee CC, Shih YL, Lin CH, Wang SH, Chen TH, et al. Inhibition of Mitochondria- and Endoplasmic Reticulum Stress-Mediated Autophagy Augments Temozolomide-Induced Apoptosis in Glioma Cells. *PloS One* (2012) 7(6):e38706. doi: 10.1371/journal.pone.0038706
232. Knizhnik AV, Roos WP, Nikolova T, Quiros S, Tomaszowski KH, Christmann M, et al. Survival and Death Strategies in Glioma Cells: Autophagy, Senescence and Apoptosis Triggered by a Single Type of Temozolomide-Induced DNA Damage. *PloS One* (2013) 8(1):e55665. doi: 10.1371/journal.pone.0055665
233. Rosenfeld MR, Ye X, Supko JG, Desideri S, Grossman SA, Brem S, et al. A Phase I/II Trial of Hydroxychloroquine in Conjunction With Radiation Therapy and Concurrent and Adjuvant Temozolomide in Patients With Newly Diagnosed Glioblastoma Multiforme. *Autophagy* (2014) 10(8):1359–68. doi: 10.4161/auto.28984
234. Sotelo J, Briceño E, López-González MA. Adding Chloroquine to Conventional Treatment for Glioblastoma Multiforme: A Randomized, Double-Blind, Placebo-Controlled Trial. *Ann Intern Med* (2006) 144 (5):337–43. doi: 10.7326/0003-4819-144-5-200603070-00008
235. Lee SW, Kim HK, Lee NH, Yi HY, Kim HS, Hong SH, et al. The Synergistic Effect of Combination Temozolomide and Chloroquine Treatment Is Dependent on Autophagy Formation and P53 Status in Glioma Cells. *Cancer Lett* (2015) 360(2):195–204. doi: 10.1016/j.canlet.2015.02.012
236. Goncalves RM, Agnes JP, Delgobo M, de Souza PO, Thome MP, Heimfarth L, et al. Late Autophagy Inhibitor Chloroquine Improves Efficacy of the Histone Deacetylase Inhibitor SAHA and Temozolomide in Gliomas. *Biochem Pharmacol* (2019) 163:440–50. doi: 10.1016/j.bcp.2019.03.015
237. Lopez-Valero I, Torres S, Salazar-Roa M, Garcia-Taboada E, Hernandez-Tiedra S, Guzman M, et al. Optimization of a Preclinical Therapy of Cannabinoids in Combination With Temozolomide Against Glioma. *Biochem Pharmacol* (2018) 157:275–84. doi: 10.1016/j.bcp.2018.08.023
238. Shao N, Mao J, Xue L, Wang R, Zhi F, Lan Q. Carnosic Acid Potentiates the Anticancer Effect of Temozolomide by Inducing Apoptosis and Autophagy in Glioma. *J Neurooncol* (2019) 141(2):277–88. doi: 10.1007/s11060-018-03043-5
239. Shi F, Guo H, Zhang R, Liu H, Wu L, Wu Q, et al. The PI3K Inhibitor GDC-0941 Enhances Radiosensitization and Reduces Chemoresistance to Temozolomide in GBM Cell Lines. *Neuroscience* (2017) 346:298–308. doi: 10.1016/j.neuroscience.2017.01.032
240. Liu T, Li A, Xu Y, Xin Y. Momelotinib Sensitizes Glioblastoma Cells to Temozolomide by Enhancement of Autophagy *via* JAK2/STAT3 Inhibition. *Oncol Rep* (2019) 41(3):1883–92. doi: 10.3892/or.2019.6970
241. Zhang C, Zhang X, Xu R, Huang B, Chen AJ, Li C, et al. TGF-β2 Initiates Autophagy *via* Smad and Non-Smad Pathway to Promote Glioma Cells' Invasion. *J Exp Clin Cancer Res* (2017) 36(1):162. doi: 10.1186/s13046-017-0628-8
242. Jalota A, Kumar M, Das BC, Yadav AK, Chosdol K, Sinha S. Synergistic Increase in Efficacy of a Combination of 2-Deoxy-D-Glucose and Cisplatin in Normoxia and Hypoxia: Switch From Autophagy to Apoptosis. *Tumour Biol* (2016) 37(9):12347–58. doi: 10.1007/s13277-016-5089-8
243. Shingu T, Holmes L, Henry V, Wang Q, Latha K, Gururaj AE, et al. Suppression of RAF/MEK or PI3K Synergizes Cytotoxicity of Receptor Tyrosine Kinase Inhibitors in Glioma Tumor-Initiating Cells. *J Transl Med* (2016) 14:46. doi: 10.1186/s12967-016-0803-2
244. Salazar M, Carracedo A, Salanueva IJ, Hernandez-Tiedra S, Lorente M, Egia A, et al. Cannabinoid Action Induces Autophagy-Mediated Cell Death Through Stimulation of ER Stress in Human Glioma Cells. *J Clin Invest* (2009) 119(5):1359–72. doi: 10.1172/jci37948
245. Liu Y, Yang L, Liao F, Wang W, Wang ZF. MiR-450a-5p Strengthens the Drug Sensitivity of Gefitinib in Glioma Chemotherapy *via* Regulating Autophagy by Targeting EGFR. *Oncogene* (2020) 39(39):6190–202. doi: 10.1038/s41388-020-01422-9
246. Palumbo S, Tini P, Toscano M, Allavena G, Angeletti F, Manai F, et al. Combined EGFR and Autophagy Modulation Impairs Cell Migration and Enhances Radiosensitivity in Human Glioblastoma Cells. *J Cell Physiol* (2014) 229(11):1863–73. doi: 10.1002/jcp.24640
247. Feng F, Zhang M, Yang C, Heng X, Wu X. The Dual Roles of Autophagy in Gliomagenesis and Clinical Therapy Strategies Based on Autophagic Regulation Mechanisms. *Biomed Pharmacother* (2019) 120:109441. doi: 10.1016/j.biopha.2019.109441
248. Taylor MA, Das BC, Ray SK. Targeting Autophagy for Combating Chemoresistance and Radioresistance in Glioblastoma. *Apoptosis* (2018) 23(11-12):563–75. doi: 10.1007/s10495-018-1480-9

Conflict of Interest: The authors declare that the research was conducted in the absence of any commercial or financial relationships that could be construed as a potential conflict of interest.

Publisher's Note: All claims expressed in this article are solely those of the authors and do not necessarily represent those of their affiliated organizations, or those of the publisher, the editors and the reviewers. Any product that may be evaluated in this article, or claim that may be made by its manufacturer, is not guaranteed or endorsed by the publisher.

Copyright © 2021 Fan, Wang, Zhang, Dong, Gao, Liu, Ma and Zhao. This is an open-access article distributed under the terms of the Creative Commons Attribution License (CC BY). The use, distribution or reproduction in other forums is permitted, provided the original author(s) and the copyright owner(s) are credited and that the original publication in this journal is cited, in accordance with accepted academic practice. No use, distribution or reproduction is permitted which does not comply with these terms.

frontiers in Oncology

REVIEW
published: 26 October 2021
doi: 10.3389/fonc.2021.751183

NK Cell-Based Immunotherapy and Therapeutic Perspective in Gliomas

Changqing Pan[1], *You Zhai*[2], *Guanzhang Li*[2], *Tao Jiang*[1,2,3,4*] *and Wei Zhang*[1,2,3,4*]

[1] Department of Neurosurgery, Beijing Tiantan Hospital, Capital Medical University, Beijing, China, [2] Beijing Neurosurgical Institute, Capital Medical University, Beijing, China, [3] China National Clinical Research Center for Neurological Diseases, Beijing, China, [4] Chinese Glioma Genome Atlas (CGGA) and Asian Glioma Genome Atlas (AGGA), Beijing, China

Glioma is the most common malignant primary brain tumor diagnosed in adults. Current therapies are unable to improve its clinical prognosis, imposing the need for innovative therapeutic approaches. The main reason for the poor prognosis is the great cell heterogeneity of the tumor and its immunosuppressive microenvironment. Development of new therapies that avoid this immune evasion could improve the response to the current treatments. Natural killer (NK) cells are an intriguing candidate for the next wave of therapies because of several unique features that they possess. For example, NK cell-based immunotherapy causes minimal graft-*versus*-host disease. Cytokine release syndrome is less likely to occur during chimeric antigen receptor (CAR)-NK therapy, and CAR-NK cells can kill targets in a CAR-independent manner. However, NK cell-based therapy in treating glioma faces several difficulties. For example, CAR molecules are not sufficiently well designed so that they will thoroughly release functioning NK cells. Compared to hematological malignancies, the application of many potential NK cell-based therapies in glioma lags far behind. Here, we review several issues of NK cells and propose several strategies that will improve the efficacy of NK cell-based cancer immunotherapy in the treatment of glioma.

Keywords: natural killer cells, alloreactivity, chimeric antigen receptor, adoptive cell immunotherapy, glioma

OPEN ACCESS

Edited by:
Quan Cheng,
Central South University, China

Reviewed by:
Zhijun Zhou,
University of Oklahoma Health Sciences Center, United States
Wen-Jing Zeng,
Central South University, China

****Correspondence:***
Tao Jiang
taojiang1964@163.com
Wei Zhang
zhangwei_vincent@126.com

Specialty section:
This article was submitted to Cancer Immunity and Immunotherapy, a section of the journal Frontiers in Oncology

Received: *31 July 2021*
Accepted: *08 October 2021*
Published: *26 October 2021*

Citation:
Pan C, Zhai Y, Li G, Jiang T and Zhang W (2021) NK Cell-Based Immunotherapy and Therapeutic Perspective in Gliomas. Front. Oncol. 11:751183. doi: 10.3389/fonc.2021.751183

INTRODUCTION

Gliomas are the most common intracranial primary malignant tumor (1). The incidence of gliomas is approximately of six cases per 100,000 individuals worldwide. Glioblastoma (GBM), the most common glioma histology, has a 5-year relative survival of ~5%. While the majority of cases are sporadic, a small portion of these tumors are associated with neurofibromatosis type I, tuberous sclerosis, and Li-Fraumeni syndrome. Standard medical care, including the most extensive tumor resection followed by radiotherapy and chemotherapy. Surgery is commonly performed with both diagnostic and therapeutic intent. The therapeutic goal of surgery is to remove as much tumor tissue while preserving neurological function. Even for diffuse gliomas, a biopsy is recommended to acquire tissue specimens for molecular profiling (IDH mutations,1p/19q codeletion, MGMT promoter methylation, EGFR amplification et al) (2). Most patients receive chemotherapy. Classic schemes including Stupp (NCT00006353) and PCV (Procarbazine, CCNU, and Vincristine) (3). The strategies of radiotherapy are determined by the disease subtype and prognostic factors, including residual tumor volume, age, KPS. The details of novel strategies

including tumor-treating fields (TTFields), checkpoint inhibitor, vaccine and oncolytic virus are described in **Table 1**. In general, the prognosis of high-grade glioma is still unpleasant, which calls for more efficient approaches.

Adoptive cell therapy (ACT), especially CAR-armed cell therapy, has great potential due to its high cytotoxicity and precise strikes. ACT consists of a series of infusions of autologous or allogeneic immune cells to kill targets, and T cell-based immunotherapy is an example of a mainstream form of ACT that is well-studied. Chimeric antigen receptor (CAR) T cells targeting CD19 is one therapy that has resulted in encouraging success in patients with B cell malignancies and has been approved by the US Food and Drug Administration (FDA) (5–7). However, there are numerous logistic and clinical limitations to the use of autologous CAR-modified T cells. Personalized CAR-T products are time-consuming and expensive to produce. Allogeneic T cell-based therapy can cause substantial toxic effects, such as graft-*versus*-host disease (GvHD) and cytokine release syndrome (CRS) (8). Furthermore, the results of CAR-T cell therapy for solid tumors are suboptimal. These shortcomings of CAR-T cells have called for interest in other candidate.

NK cells are a subpopulation of the innate immune system (9, 10). NK cells can be identified by CD3(-) CD56(+). Depending on the level of CD56 and CD16 expression, NK cells can be divided into $CD16^{+}CD56^{dim}$ and $CD16^{-}CD56^{bright}$ cells. $CD16^{+}CD56^{dim}$ NK cells predominate in peripheral blood while $CD16^{-}CD56^{bright}$ NK cells are distributed into secondary lymphoid organs (11). $CD16^{-}CD56^{bright}$ NK cells are robust cytokine producers and are weakly cytotoxic while the $CD16^{+}CD56^{dim}$ NK cell population can mediate serial killing of infected and/or malignant cells. NK cell receptors are germline-encoded without a requirement for 'V(D)J' recombination. Natural killer (NK) cells have gained attention as a promising alternative candidate for ACT owing to their unique biological attributes.

NK cells do not require any prior antigen and can rapidly recognize and kill cells for which major histocompatibility complex (MHC) class I molecular expression is compromised by infection or transformation (9). Once activated, NK cells can release perforin and granzyme, contributing to target cell lysis. NK cells upregulate death ligands on their surface, such as FAS ligand and TRAIL, and initiate the caspase pathway of tumor cells and induce apoptosis when binding to death receptors on target cells. NK cells can eradicate cancer cells through antibody-dependent cellular cytotoxicity (ADCC) mediated by FcγRIIIA/CD16a. Furthermore, NK cells produce interferon gamma (IFN-γ), regulating and activating the adaptive immune response.

NK cell-based therapy is safe and has potential generated as off-the-shelf cellular therapy products. Autologous NK cells exert limited cytotoxicity against autologous tumors, while allogeneic NK cells are highly cytotoxic and cause minimal risk of GvHD (12–16). Thus, NK cells can originate from different sources, such as peripheral blood NK cells (PBNK), induced pluripotent stem cells (iPSCs), umbilical cord blood (UCB) and NK-92 cells, and this eliminates the need to produce a personalized CAR-NK product. However, the claim that allogeneic NK cells cause no or minimal GvHD and CRS is controversial and originated from observations obtained during clinical trials, especially in the setting of hematopoietic cell transplantation (HCT), the mechanism of which has not been thoroughly discussed. Here, we review important issues regarding NK cells and glioma and discuss several options that can be used to improve the efficacy of CAR-NK in glioma treatment.

THE SAFETY OF NK CELL-BASED IMMUNOTHERAPY

NK Cell Alloreactivity

All NK cells are non-responsive towards healthy autologous cells, which involves the interaction of at least inhibitory killer immunoglobulin-like receptors (KIRs) or CD94-NKG2A with one autologous MHC class I molecule. KIRs can be classified based on two factors: the number of immunoglobulin-like

TABLE 1 | Applications of novel strategies in glioma.

Strategies	Interventions	Results	Tumors	Phase	Reference/ NCT
TTFields	TTFields plus temozolomide VS temozolomide alone	TTFields plus temozolomide improve PFS and OS significantly	Glioblastoma	III	NCT00916409
Checkpoint Inhibitor	nivolumab VS bevacizumab	Nivolumab failed to improve OS	Recurrent Glioblastoma	III	NCT02017717
	Neoadjuvant pembrolizumab	Neoadjuvant extended OS and enhanced both the local and systemic antitumor immune response	Recurrent Glioblastoma	/	Cloughesy et al. (4)
Vaccine	Rindopepimut (CDX-110), a vaccine targeting EGFRvIII	Rindopepimut did not increase OS	Glioblastoma	III	NCT01480479
	peptide vaccine (IDH1-vac) targeting mutant IDH1	IDH1-vac increased PFS and immune responses, but accompanied by a high frequency of pseudoprogression	Grade III and IV Astrocytomas	I	NCT02454634
	autologous dendritic cell vaccine ICT-107	ICT-107 significantly improved PFS	Glioblastoma	II	NCT01280552
Oncolytic Virus	intratumoral infusion of polio-rhinovirus chimera (PVSRIPO)	PVSRIPO therapy increased OS	Recurrent malignant Glioma	I	NCT01491893
	intratumoral injection of oncolytic adenovirus (DNX-2401)	DNX-2401 resulted in dramatic responses with long-term survival	Recurrent malignant Glioma	I	NCT00805376

domains (2D and 3D) and the length of the intracytoplasmic tail (L or S). Inhibitory KIRs usually possess a long cytoplasmic tail (KIR2DL), whereas activating KIR possess a short one (KIR2DS), except for the activating KIR2DL4, which has a long cytoplasmic tail. Inhibitory KIRs contain immunoreceptor tyrosine-based inhibition motif (ITIM) sequences responsible for the inhibitory signal. Unlike cytotoxic CD8+ T cells, which are highly specific for antigens, NK cells express clonally distributed inhibitory receptors termed KIRs that recognize determinants (KIR ligands) shared by subsets of HLA-B or -C allotypes (17–20). More than fifty KIR family members have been identified, and each of these genes is highly polymorphic and has thousands of alleles (21). Three subfamilies and associated inhibitory specificities are well determined (**Table 2**). The CD94-NKG2A heterodimer, belonging to C-type lectins, is specific for HLA-E (24–26).

Major models used to predict NK cell alloreactivity include 'missing self' and 'missing ligand' (**Figure 1**). Missing self-recognition (the 'ligand–ligand' model) was proposed by Karre et al. and occurs under HLA haplotype-mismatched transplants in the graft-*versus*-host direction (27). Donor NK cells express a KIR for the self HLA class I group that is absent in the recipient, which mediates alloreactions (28–30). HLA testing is required to predict NK cell alloreactivity due to the missing self-model.

Because the genes for KIR, HLA, and CD94–NKG2 are located on different chromosomes (31–33), KIR genes segregate independently of the HLA genes, and thus, KIR mismatches can exist in two HLA-matched individuals. Also, it was found that many individuals have 3 inhibitory KIRs (for HLA-C1 and -C2 and for HLA-Bw4 alleles), while their own cells only express 1 or 2 HLA KIR ligands (22, 34, 35). KIR expression is donor specific, but not related to the donor or recipient HLA and is not affected by the recipient's HLA groups (36). The missing ligand model (the 'receptor-ligand' model) was based on these. According to this model, NK cell alloreactivity occurs not only in HLA haplotype-mismatched transplants, but also in HLA haplotype-matched transplants from donors possessing 'extra' KIR(s), for which neither donor nor recipient possess HLA ligand(s) (35–37). The donor's potentially self-reactive NK cells can trigger an alloreactive effect in the recipient while maintaining anergy in the donor. Analysis of the KIR expression on the donor's NK cells and HLA testing of the recipient's cells are required to predict NK cell alloreactivity due to the missing ligand model.

The missing self and missing ligand models can be used to predict NK cell alloreactivity. Although alloreactive NK cells can eradicate tumor cells, the anti-tumor effect is not confined to alloreactive NK cells. NK cell activity depends on the balance between inhibitory and stimulatory receptors. An anti-tumor effect can be mediated by NK cells expressing stimulatory receptors, such as activating KIR and NKG2D (38–40).

TABLE 2 | Three subfamilies of KIRs and specific ligands.

Group[a]	HLA-class I specificity[b]
KIR2DL1(CD158a)	C2(-Cw2, -Cw4, -Cw5, -Cw6)
KIR2DL2/3(CD158b1/b2)	C1(-Cw1, -Cw3, -Cw7, -Cw8)
KIR3DL1(CD158e1)	Bw4(-B27, -B51)

[a]*Each group compromises different numbers of alleles, which differ by 1-9 nucleotide substitutions (22).*

[b]*Two groups of HLA-C alleles are distinguished by dimorphic positions Ser 77–Asn 80 (C1) and Asn 77–Lys 80 (C2) of the α1 helix (23). HLA-B allotypes share the Bw4 sequence motif at positions 77–83 of the α1 helix (22).*

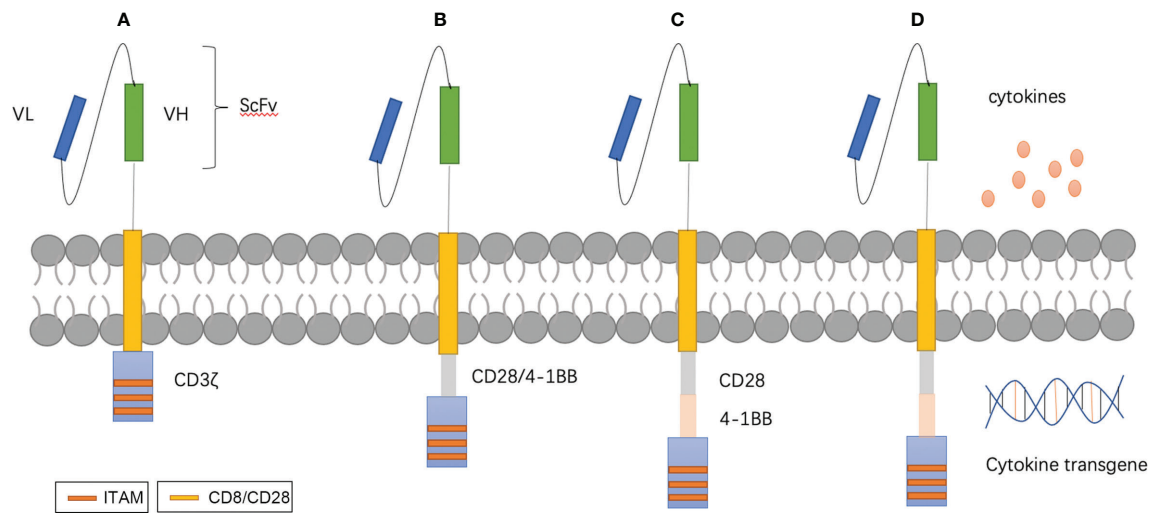

FIGURE 1 | T-CAR designs. **(A–D)** show the four generations of T-CAR. In brief, CAR contains three parts: extracellular domains are comprised of a single-chain variable fragment (scFv) for recognizing targeted antigen and transmembrane domains, and endocellular domains for transducing signals. First generation CARs consist of the basic structure with CD3ζ **(A)**. Second generation CARs contain an additional costimulatory domain such as CD28 or 4–1BB **(B)**. Third generation CARs possess multiple costimulatory domains **(C)**. Fourth-generation CARs, also known as 'armored CARs' can be designed to secret cytokines to improve the proliferation, persistence.

NK CELL-BASED IMMUNOTHERAPY CAUSES MINIMAL GvHD AND CRS

GvHD refers to a condition resulting from the systemic attack of allogenic T cells on recipient tissues after allogeneic hematopoietic stem cell transplantation or infusion of allogeneic T cells (41–43). The effects of GvHD are commonly manifested in the gastrointestinal tract, liver, and skin (44), and severe GvHD can be fatal. The role of alloreactive NK cells on GvHD in the setting of HCT varies among studies. Some investigations found that alloreactive NK cells were related to decreased GvHD (36, 45, 46), which was partially attributed to the observations that allogeneic NK cells would be expected to kill host dendritic cells (DCs) and donor T cells (46, 47). Miller et al. analyzed 2,062 patients undergoing unrelated donor HCT (48). They found that one or more KIR ligands were missing *versus* the presence of all ligands, which is associated with a low relapse rate in patients with early myeloid leukemia. This omission predicted a greater risk of developing grade 3-4 GvHD in the setting of chronic myeloid leukemia (CML) patients. Miller et al. attributed the higher rate of acute GvHD in CML to the expanded myeloid pool with more host antigen-presenting cells (APCs) capable of presenting alloantigen to donor T cells (48).

HCT after ablation of bone marrow is used to cure hematological malignancies and results in less cancer relapse compared to chemoradiotherapy (49). T cells of allogeneic hematopoietic grafts for treating leukemia mediate the antileukemia effect as well as lethal GvHD. In many studies, it was attempted to prevent GvHD by depleting the T cells from the graft and infusing large numbers of hematopoietic stem cells to overcome rejection (50), which was at the expense of immunity reconstitution failure and infection. Later, NK cells from alloreactive donors were found to protect patients against rejection and GvHD in the setting of HCT (46). Interestingly, we found the idea that NK cell-based therapy caused GvHD mostly happened in the setting of HCT. But we should not evaluate the effects of alloreactive NK cells on GvHD in the setting of HCT because the effect of T cells in the grafts is negligible. It is likely that T cell interference is the most important controversial element with respect to the alloreactive NK cell effects on GvHD.

In fact, NK cell-based immunotherapy is safe and causes minimal GvHD. GvHD most likely occurs when NK cells from donors with several KIR subfamilies are infused into recipients possessing one group HLA ligand. Valiante et al. analyzed NK cell receptor repertoires in the peripheral blood of two human donors (donor PP only possessed group 1 HLA-C ligand, and donor NV possessed group 1 and 2 HLA-C ligands and the Bw4 HLA-B ligand, both of which have three KIR subfamilies as demonstrated in **Table 2**) (51). They found that more than 98% of NK clones were inhibited self-HLA class I allotypes, and no NK cell from either donor was able to lyse the autologous B cell line (51). Interestingly, NV possessed approximately 15% of the analyzed NK cell clones, did not express KIR2DL2 or CD94: NKG2a, and was able to lyse the B cell line from PP, whereas the NK cell clones from PP failed to lyse the B cell line from NV (51). Ruggeri adopted functional analysis to evaluate the NK cell alloreactivity in more than 200 NK clones (46). Alloreactivity was defined as positive when the frequency of lytic clones was no less than 1 in 50 (46). In addition, the expression of CD94: NKG2a is inversely related to KIR levels (51). Approximately, 50% of NK cells in an individual express CD94:NKG2a (51, 52). Cell-surface HLA-E expression depends on many peptides, including the leader peptides of HLA-A, -B, or -C, and downregulation of HLA-E expression requires the elimination of three types of HLA molecules (53, 54). Thus, NK cells expressing CD94–NKG2A display no alloreactivity because all individuals express HLA-E molecules. Therefore, NK cell-based immunotherapy is safe most of the time and will cause minimal GvHD because alloreactive NK cells only account for a small proportion. In addition, healthy cells express high levels of MHC class I molecules, but they express no or minimal level of ligands for NK cell activating receptors. Conversely, tumorigenic cells downregulate MHC class I expression but upregulate the expression of ligands for NK cell activating receptors. For example, MICA/MICB and ULBP, ligands for NKG2D, are often induced by stress or transformation (55, 56). The integration of the activating and inhibitory signals from the ligand/receptor determines NK cell activity. Some studies indicated that the positive signal delivered by NKG2D could override inhibition. Therefore, NK cells become alloreactive prior to killing tumor cells.

CRS involves elevated levels of circulating cytokines, especially interferons and immune-cell hyperactivation, which manifests as an influenza-like syndrome, organ failure, and even death (57). CAR-NK is less likely to induce CRS and neurotoxicity partially because of a different spectrum of secreted cytokines consisting of activated NK cells that produce IFN-gamma and GM-CSF, and CAR-T cells that predominantly release tumor necrosis factor (TNF)-a and interleukins, such as IL-1, IL-2, and IL-6 (57, 58). The mechanism was validated by clinical trials. Liu et al. launched a clinical trial (NCT03056339) that administered HLA-mismatched anti-CD19 CAR-NK cells to 11 patients with high-risk lymphoid malignancies (16). The administration of CAR-NK cells was not associated with the development of cytokine release syndrome and there was no increase in the levels of inflammatory cytokines, including interleukin-6, over baseline (16).

NK EXPANSION TECHNIQUES

Large numbers of cells are essential for successful adoptive transfer cell therapy. It has been proved that high doses of NK cells from10^7cells/kg to 4.7×10^10 total NK cells can be well tolerated (16, 59, 60). NK cells only account for approximately 10% of peripheral blood mononuclear cells. The NK92 cell line is used in current clinical trials with CAR-NK because of their unlimited proliferation ability *in vitro*. However, the NK92 cell line is tumorigenic and lacks CD16 and NKp44 expression, and additionally, these cells will lose their proliferation ability due to

lethal irradiation infusion (61, 62). Because of these drawbacks, it is unlikely that they will be an ideal cell source for CAR-NK cell therapy.

Expansion protocols possess considerable heterogeneity. The expansion process often takes 2-3 weeks of culture in the presence of mitogenic cytokines, and engineered feeder cells can optimize the expansion process. K562 cells engineered to express membrane-bound IL-15 or IL-21 along with the adhesion molecule 4-1BBL are adopted as feeder cells in many clinical trials (63, 64). There have been reports of 300-fold expansions combined with IL-2 and IL-15. IL-15 is important to NK cell survival and function (65, 66), and 4-1BBL provides a cell to cell contact-dependent co-stimulatory signal (67). We observed that low density less than 10^5cells/mL is not ideal for NK expansion. We recommend that the ratio of engineered K562 feeder cells and NK cells is 1:1 to 2:1. The K562 cell line possesses unique properties and lacks HLA expression. As described above, inhibitory KIRs recognizing corresponding HLA ligands can inactivate NK cells. This can be proved by our laboratory findings that other cell lines engineered to express IL-21 and 4-1BBL failed to achieve high-fold NK expansion. Some studies used RetroNectin-stimulated T (RN-T) cells as feeder cells (68, 69). Briefly, the procedure for this is to culture T cells from autologous peripheral blood mononuclear cells (PBMCs) with RetroNectin and anti-CD3 monoclonal antibody. In approximately 2 weeks, RN-T cells can serve as feeder cells after irradiation. RetroNectin plays a role in cell adhesion (70). The anti-CD3 monoclonal antibody leads to T-cell activation and cytokine secretion, and activated T cells express ligands of NKG2D (47, 71). Irradiated PBMCs as feeder cells were utilized by Parkhurst et al. and share a similar mechanism with RN-T in NK cell expansion (60, 72). The CD14+ monocyte fraction of irradiated PBMCs function in cell-cell contact (73). Feeder cells derived from autologous PBMCs eliminate the need for infusion of viable malignant feeder cells into the NK cell product. Feeder-free expansion approaches have also been tested. Li et al. cultured NK cells in an anti-CD16 (Beckman Coulter)-coated flask (74). Antibody-coated beads targeting CD2 and NKp46 (CD335) are commercially available. However, not everyone or each NK cell expresses these stimulatory receptors, and feeder-free expansion protocols lose cell-to-cell contact effects. For example, only a part of NK cells of an individual expresses CD16 on blood NK cells (75, 76).

ADOPTIVE CELL THERAPY AND CAR-NK CELLS

There are several developmental stages in ACT. Lymphokine-activated killer (LAK) cells, which consist of a mixture of NK cells, NKT cells, and T cells, were adopted to overcome insufficient quantities of immune cells (77). An unwanted side effect of a high dose of IL-2 is that it induces capillary leak syndrome and neuropsychiatric diseases in a manner similar to that of CRS. To obtain immune cells that can effectively respond to tumors, Rosenberg introduced the concept of tumor-infiltrating lymphocytes (TILs) (78), which have many similarities with LAK cells except the origin of lymphocytes. The former is isolated from the stroma of tumors, while the latter is acquired from PBMCs. Success with TILs has been achieved in many solid tumors, including breast cancer tumors (79, 80). With TCR engineering, tumor-specific TCR α and β chains are identified and integrated with T cells *via* viral vectors (81). There must be specificity with T-cell engineering and CAR-T. Compared to CAR-T therapy, there are limited choices for physiological receptors with TCR engineering. Effective CAR-T cell therapy relies on optimal CAR molecular design. The CAR construct is becoming increasingly sophisticated with the understanding of T cell activation and tumor-specific and -associated antigens (82). Four generations of CAR designs have been developed that are mainly different in categories and number of co-stimulation factors (**Figure 1**). For safety and effectiveness, many novel designs have been tested, such as 'inverted CAR,' 'off-switch CAR' and 'logic-gate CAR' (83–85).

NK cell-based immunotherapy is a subset of ACT and is similar to adoptive T therapy, especially with respect to CAR therapy. CAR-NK-related clinical trials show that the most adopted CAR design corresponds with first and second generation T-CAR (86). Most NK-CARs use CD28 and 4-1BB, which are more specific to T cells, as their transmembrane and intracellular domain, respectively (87, 88). Later studies began to design CARs specific to NK cells. For example, intracellular domains replaced CD28 with 2B4, DAP12, or DAP10 (89, 90). Li et al. proved that the signaling domains of CAR-NK, such as NKG2D-2B4, exhibited superior *in vitro* and *in vivo* anti-tumor activities compared to that which contains CD28-4-1BB (91). The revolution of CAR-NK therapy is described in **Figures 2A–D**, and it is clear that the CAR construct is becoming increasingly sophisticated with the growing understanding of T cell activation and tumor-specific and -associated antigens that are also suitable for NK cells.

IMMUNOSUPPRESSIVE MECHANISMS OF GLIOMA

Glioma, especially GBM, shows an extreme cell heterogeneity, diffuse growth patterns and high invasiveness. Gliomas were thought to be "immune cold" tumors with low infiltration of lymphocytes (95). Furthermore, microenvironment of the glioma has the ability to suppress immune response systematically and locally.

Mahaley et al. first reported the presence of lymphopenia in GBM (96). Studies have found patient-derived peripheral blood lymphocytes shows immune defects that exhibited varying levels of proliferative unresponsiveness to the T-cell mitogens concanavalin A (ConA), phytohemagglutinin (PHA) and anti-CD3 monoclonal antibody as well as with the T-dependent B-cell mitogen, pokeweed mitogen (PWM) (97, 98). A selective impairment of the IL-2 system and T cell receptor-mediated signaling in lymphocytes of patients with glioblastomas may contribute to the unresponsiveness (99, 100). Compared to healthy individuals,

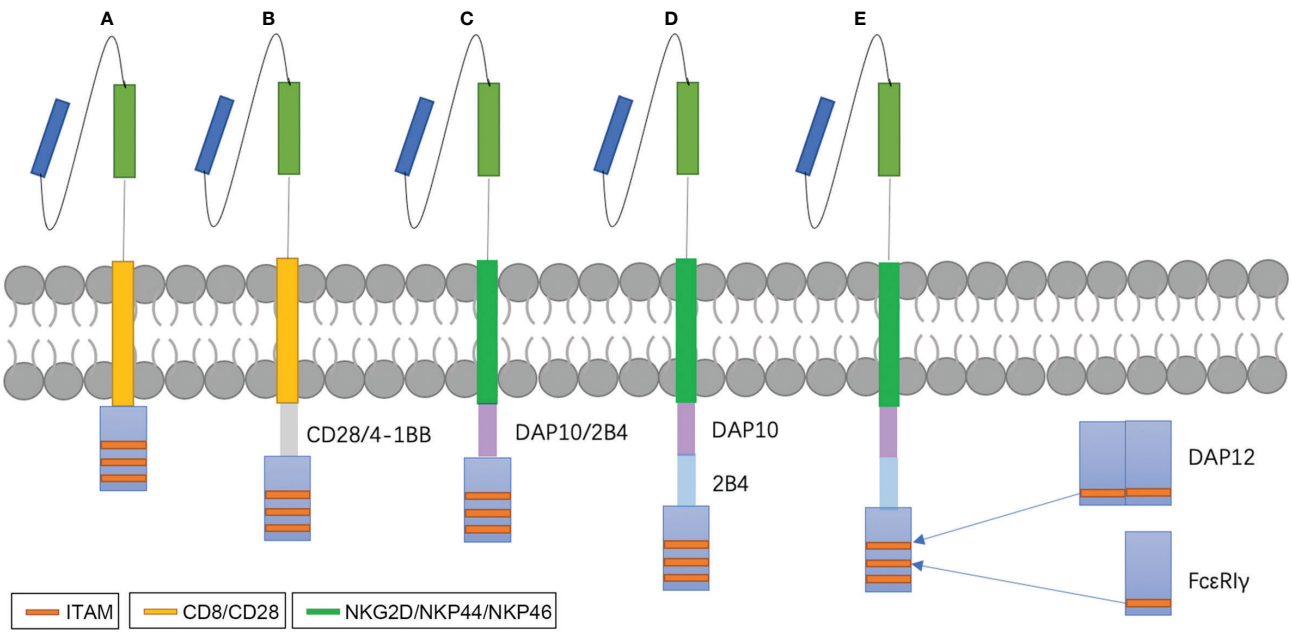

FIGURE 2 | NK-CAR designs. Early studies exploring CAR-NK cells used CAR constructs optimized for T cell signaling and function **(A, B)**. Later, many investigators begin to study costimulatory domains specific for NK cell signaling, such as DAP10, DAP12 or 2B4 **(C, D)**. DAP10 is the adaptor molecule of NKG2D and acts *via* a Syk-independent regulatory pathway (92). DAP12 is the adaptor molecules of NKG2C, NKp44 and activating killer immunoglobulin receptors (KIRs) and contain immunoreceptor tyrosine-based activation motifs (ITAMs) (93). 2B4, an important co-stimulation factor of NK activation, contains immunoreceptor tyrosine-based switch motifs (ITSMs) that recruit adaptor molecules such as SLAM-associated protein (SAP) to mediate signal transduction (94). We design a new CARs that replace ITAMs of CD3ζ with FcεRIγ and DAP12 **(E)**.

accumulation of myeloid-derived suppressor cells (MDSCs) in the peripheral blood of patients with glioma was found (101, 102). MDSCs impair tumor immunity by interacting with macrophages to increase IL-10 and decrease IL-12 production, driving a tumor-promoting type 2 response (103). Inhibitory soluble factors secreted by glioma can suppress lymphocyte's function. Transforming growth factor beta (TGF-β) can impair peripheral blood NK cell function by downregulating NKG2D (104–107). Therefore, the immune responses are suppressed systematically in glioma microenvironment.

Gliomas often overexpress phosphorylated signal transducer and activator of transcription 3 (p-STAT3) that induces a variety of immunosuppressive factors including IL-10, prostaglandin E2 (PGE2), vascular endothelial growth factor (VEGF) and TGF-β (108). These soluble factors can suppress cytotoxic T lymphocytes activity and proliferation (108). TGF-β and IL-10 can induce Tregs that inversely modulate immune response (109). Chemokines and cytokines, such as CX3CL1 and CCL5 can recruit tumor-associated macrophages to GBM microenvironment and contribute to abnormal angiogenesis (110, 111). Most GBM cells express high levels of MHC class I molecules that can inhibit NK cells by interacting with inhibitory KIRs (112). Absolute survival advantages of tumor depriving of nutrition and oxygen might suppress NK cell metabolism and antitumor activity (113). N6-methyladenosine (m6A) modification is an emerging field in the study of tumorigenicity and therapy resistance of glioma (114, 115). The relationship between m6A states and immune infiltration and function in glioma is still unclear. Studies found higher m6Ascore was associated with T cells exhaustion and lower NK cells in the m6Ascore-high pancreatic ductal adenocarcinoma (116). So, the immune responses are suppressed locally in glioma microenvironment.

APPLICATIONS OF NK CELLS FOR GLIOMA TREATMENT

Except for unique advantages of NK cells, there is still a potential of NK cells in treating glioma. Cózar et al. analyzed RNA-seq datasets from the TCGA database and found NK-cell infiltration in both low grade glioma and GBM and even had higher scores compared to T-cell infiltration, which paved the way for the use of treatments targeting NK cells in glioma (117). Similar to adoptive T therapy, NK cell-based immunotherapy mainly concentrates on hematological malignancies. Thus far, the therapeutic utility of NK cell-based immunotherapy for the treatment of glioma has mainly been investigated in preclinical studies (**Table 3**). These trials most utilize either PBNK cells or NK92 cells, as well as first and second generation CARs designed for T cells and not optimized for NK cell signaling. Furthermore, clinical trials pay more attention to evaluate the safety of CAR-NK therapy. Although preclinical studies began to test the efficiency of DAP12 specific for NK cell signaling. Most of

TABLE 3 | Applications of NK cells in glioma.

Targets	NK Source	CAR construct	Tumors	Phase	Reference/NCT
EGFRvIII	NK92 cell line	scFv-CD28TM+IC-CD3ζ	Glioblastoma	/	Genßler et al. (118)
EGFRvIII	YTS NK cell line	scFv-DAP12 TM+IC	Glioblastoma	/	Müller et al. (90)
EGFRvIII	KHYG-1 NK cell line	scFv-CD28 TM+IC-CD137-CD3ζ	Glioblastoma	/	Murakami et al. (119)
EGFRvIII	NK92 cell line	scFv-CD28 TM+IC-CD3ζ	Glioblastoma	/	Han et al. (120)
HER2	NK92 cell line	scFv-CD3 TM+IC	Glioblastoma	/	Alkins et al. (121)
HER2	NK92 cell line	scFv-CD28 TM+IC-CD3ζ	Glioblastoma	/	Zhang et al. (122)
HER2	NK92 cell line	scFv-CD28-CD3ζ	Glioblastoma	I	NCT03383978
HER2	NK92 cell line	Unknown	Glioblastoma	I	NCT03383978
MUC1	Unknown	Unknown	High Grade Glioma	I/II	NCT02839954
None	PBMCs	None	High Grade Glioma	I	NCT04254419
None	PBMCs	None	Glioma	I	NCT00909558
None	Placenta	None	High Grade Glioma	I	NCT04489420

them adopted similar CARs as used in clinical trials. Compared to hematological malignancies, both in the quantity and CARs design, the application of NK cell-based therapies in glioma lags far behind.

FUTURE PERSPECTIVES

Compared to T cell-based therapy, the development of NK cell-based therapy falls behind to some degree in the treatment of glioma. Adoptive NK cell therapy is lack of *in vivo* persistence without cytokine support, which may limit the efficacy of the NK cell immunotherapy. System administration of cytokines is associated with undesirable toxicities as described above. Trafficking to tumor beds is critical for the efficacy of adoptive cellular therapy. Müler et al. observed an infiltration increase of anti-EGFRvIII CAR-NK cells engineered to express CXCR4 to CXCL12/SDF-1α secreting glioblastoma cells, leading to improved tumor regression and survival in a mouse model of glioblastoma (90). The difficulty may be resolved by intratumoral administration of NK cells products. In general, there is much room for the development of CAR-NK therapy in the field of glioma treatment. Much more pressing for NK cell-based therapy is designing more efficient products in treating glioma. Therefore, we try to put up several strategies to achieve the goal on the base of the knowledge of NK cells and glioma.

NK cell therapy is the lack of *in vivo* persistence in the absence of cytokine support. IL-15 is essential for NK cell function and homeostasis and can be added to CAR molecules to mimic the fourth generation of T-CAR. TGF-β plays an essential role in impairing NK cell function. Inverted CAR may be applied to reverse the situation by fusing the ectodomain of the TGF-β receptor to the endodomain of an activating receptor. CD3ζ is found in the intracellular domains of T-CAR and NK-CAR. Furthermore, CD3ζ, containing three immunoreceptor tyrosine-based activation motifs (ITAMs; YxxL/Ix6-8YxxL/I, with 29 amino acids), has a limited impact on the effectiveness of CAR-NK (123).

Modification targeting CD3ζ has been tested in CAR-T therapy. Wu et al. found that CD3ϵ recruits Csk and p85 *via* its mono-phosphorylated ITAM and BRS motif, respectively (124). Incorporation of the ITAM of CD3ϵ into a second-generation CAR increased the antitumor activity of CAR-T cells by reducing the cytokine production and promoting the persistence of CAR-T (124). NK cells possess many types of stimulatory receptors, such as CD16, NKp46, and NKG2D, and these stimulatory receptors do not act separately. In fact, apart from CD16, which is sufficient for activation of resting NK cells, it is necessary for all activating receptors to cooperate and synergize with one another for NK activation (125). Interestingly, the ITAM of many stimulatory receptors or their related adaptors, such as FcϵRIγ and DAP12, also consists of 29 amino acids with different sequences. Therefore, an exchange may produce more effective CAR-NK cells (**Figure 2E**) with mild changes in CD3ζ structure.

CAR-NK cells can kill targets in a CAR-independent manner. Combination therapy with monoclonal antibodies is promising, and it was observed that trifunctional antibodies recognized targets and simultaneously engaged NKP46 and CD16, which controlled tumor growth in mouse models (126). A team used antibodies to prevent the loss of cell surface MICA and MICB in human cancer cells, which stabilizes the bond between NKG2D and its ligands. These antibodies inhibit tumor growth in mouse models, and the antitumor effect is mediated mainly by the activation of NKG2D and CD16 (127). Apart from the activating receptors, antibodies blocking the inhibitory receptors of NK cells, such as KIR, NKG2A, TIM3, and TIGIT have been studied (52, 128–130). NK cells can express FcγRIIIA/CD16a and/or FcγRIIC, which bind to the Fc portion of human immunoglobulins. Once antibodies bind to targets, NK cells are able to recognize the Fc portion and lyse target cells through antibody-dependent cell-mediated cytotoxicity (ADCC) (131). So, the combination of immune checkpoint inhibitors and NK cell-based therapy may be potential. Although, Nivolumab failed to improve overall survival of patients with recurrent glioblastoma. Studies have found that cancer type 1 or 2 susceptibility gene (BRCA1/2) alteration was associated with higher tumor mutation burden(TMB) and may serve as a novel indicator associated with better treatment outcomes of immune checkpoint inhibitors (132). The function of BRCA1/2 and other DNA mismatch repair gene alteration are worth being investigated in glioma. Most GBM cells express high levels of MHC class I molecules (112). Thus, blockade of such KIRs with antibodies may enhance NK-cell mediated killing.

NK cells and T cells originate from a common ancestor and share many similarities. Both interact with MHC class I molecules, contributing to innate and adaptive immunity. They have similar cell-surface phenotypes and cellular functions, such as cytotoxicity, secretion of cytokines, and interaction with DCs (133). NK cells also play a role in regulating T cell response. For example, NK cells can produce IFN-gamma, which promotes CD4+ T cell differentiation into TH1 helper cells (134). The latter contributes to an enhanced CD8+ T cell response (135). NK cells produce IFN-gamma, leading to DC maturation and IL-12 secretion, which is sufficient for CD8+ T cell activation independent of CD4+ T cell (136). As an important constituent of the innate immunity response, NK cells can kill target cells and release antigen for cross-presentation and activation of T cells (137). NK cells can also negatively regulate a T cell response as described above or in the setting of acute viral infections (138, 139). A combination of NK cells and T cells comprise an ideal potential therapy for tumor treatment. A study has reported that CAR-NK cells can eliminate myeloid-derived suppressor cells and rescue impaired CAR-T cell activity against solid tumors (140). Moreover, CAR-NK cells can improve the infiltration and functions of subsequently infused CAR-T cells by secreting proinflammatory cytokines and chemokines (140). Cózar et al. found marked NK-cell infiltration in solid tumors were also infiltrated with T cells (117).Anti-IL13Rα, anti-HER2, and anti-EGFRvIII CAR-T have been tested in glioma (141–143). Utilizing the safety of CAR-NK cells and the high efficacy of CAR-T cells is worth exploring in gliomas.

Oncolytic virus (OV) OVs have a double oncolytic action by both directly attacking the cancer cells and inspiring a tumor specific immune response. OVs can be engineered to repress antibodies targeting tumor antigen and/or secret cytokines activating immune response. Xilin Chen et al. observed that the combination of EGFR-CAR NK-92 cells with oHSV-1 resulted in more efficient killing of MDA-MB-231 tumor cells and significantly longer survival of tumor-bearing mice (144). Rui Ma et al. (145) generated a therapy that combined off-the-shelf EGFR-CAR NK cells and an Oncolytic virus OV called OV-IL15C. OV-IL15C-infected GBM cells can secrete soluble IL15/IL15Rα complex. GBM-bearing mice models exhibited that the therapy synergistically suppressed tumor growth. These potential therapies are anticipated to be further investigated in clinical trials. Combination therapies are based on the knowledge of NK cell biology. An evolving understanding of gliomas can inspire treatment strategies targeting the basic elements of these malignant cells and their microenvironments. We believe NK cell-based immunotherapy will have a better performance in treating glioma in the future.

AUTHOR CONTRIBUTIONS

CP conceived the article. YZ compiled the review and prepared the draft of the manuscript. GL, TJ, and WZ reviewed and edited the manuscript. All authors contributed to the article and approved the submitted version.

FUNDING

This work was supported by grants from National Natural Science Foundation of China (No.82072768), Construction Project of Multi Omics Platform for Major Brain Diseases (PXM2019_026280_000002), Sino German Cooperation and Exchange Project (Mobility Programme, M-0020), Research Fund for Clinical and Translational Medicine of Chinese Academy of Medical Sciences (2020-I2M-C&T-A-024).

REFERENCES

1. Janjua TI, Rewatkar P, Ahmed-Cox A, Saeed I, Mansfeld FM, Kulshreshtha R, et al. Frontiers in the Treatment of Glioblastoma: Past, Present and Emerging. *Adv Drug Delivery Rev* (2021) 171:108–38. doi: 10.1016/j.addr.2021.01.012
2. Hamisch CA, Minartz J, Blau T, Hafkemeyer V, Rueß D, Hellerbach A, et al. Frame-Based Stereotactic Biopsy of Deep-Seated and Midline Structures in 511 Procedures: Feasibility, Risk Profile, and Diagnostic Yield. *Acta Neurochir (Wien)* (2019) 161(10):2065–71. doi: 10.1007/s00701-019-04020-1
3. Buckner JC, Shaw EG, Pugh SL, Chakravarti A, Gilbert MR, Barger GR, et al. Radiation Plus Procarbazine, CCNU, and Vincristine in Low-Grade Glioma. *N Engl J Med* (2016) 374(14):1344–55. doi: 10.1056/NEJMoa1500925
4. Cloughesy TF, Mochizuki AY, Orpilla JR, Hugo W, Lee AH, Davidson TB, et al. Neoadjuvant Anti-PD-1 Immunotherapy Promotes a Survival Benefit With Intratumoral and Systemic Immune Responses in Recurrent Glioblastoma. *Nat Med* (2019) 25(3):477–86. doi: 10.1038/s41591-018-0337-7
5. June CH, O'Connor RS, Kawalekar OU, Ghassemi S, Milone MC. CAR T Cell Immunotherapy for Human Cancer. *Science* (2018) 359(6382):1361–5. doi: 10.1126/science.aar6711
6. Kochenderfer JN, Dudley ME, Kassim SH, Somerville RP, Carpenter RO, Stetler-Stevenson M, et al. Chemotherapy-Refractory Diffuse Large B-Cell Lymphoma and Indolent B-Cell Malignancies can be Effectively Treated With Autologous T Cells Expressing an Anti-CD19 Chimeric Antigen Receptor. *J Clin Oncol* (2015) 33(6):540–9. doi: 10.1200/jco.2014.56.2025
7. Park JH, Rivière I, Gonen M, Wang X, Sénéchal B, Curran KJ, et al. Long-Term Follow-Up of CD19 CAR Therapy in Acute Lymphoblastic Leukemia. *N Engl J Med* (2018) 378(5):449–59. doi: 10.1056/NEJMoa1709919
8. Singh AK, McGuirk JP. CAR T Cells: Continuation in a Revolution of Immunotherapy. *Lancet Oncol* (2020) 21(3):e168–e78. doi: 10.1016/s1470-2045(19)30823-x
9. Vivier E, Tomasello E, Baratin M, Walzer T, Ugolini S. Functions of Natural Killer Cells. *Nat Immunol* (2008) 9(5):503–10. doi: 10.1038/ni1582
10. Zhang Y, Wallace DL, de Lara CM, Ghattas H, Asquith B, Worth A, et al. *In Vivo* Kinetics of Human Natural Killer Cells: The Effects of Ageing and Acute and Chronic Viral Infection. *Immunology* (2007) 121(2):258–65. doi: 10.1111/j.1365-2567.2007.02573.x
11. Keating SE, Zaiatz-Bittencourt V, Loftus RM, Keane C, Brennan K, Finlay DK, et al. Metabolic Reprogramming Supports IFN-γ Production by CD56bright NK Cells. *J Immunol* (2016) 196(6):2552–60. doi: 10.4049/jimmunol.1501783
12. Stringaris K, Sekine T, Khoder A, Alsuliman A, Razzaghi B, Sargeant R, et al. Leukemia-Induced Phenotypic and Functional Defects in Natural Killer Cells Predict Failure to Achieve Remission in Acute Myeloid Leukemia. *Haematologica* (2014) 99(5):836–47. doi: 10.3324/haematol.2013.087536
13. Rubnitz JE, Inaba H, Ribeiro RC, Pounds S, Rooney B, Bell T, et al. NKAML: A Pilot Study to Determine the Safety and Feasibility of Haploidentical

Natural Killer Cell Transplantation in Childhood Acute Myeloid Leukemia. *J Clin Oncol* (2010) 28(6):955–9. doi: 10.1200/jco.2009.24.4590
14. Miller JS, Soignier Y, Panoskaltsis-Mortari A, McNearney SA, Yun GH, Fautsch SK, et al. Successful Adoptive Transfer and In Vivo Expansion of Human Haploidentical NK Cells in Patients With Cancer. *Blood* (2005) 105 (8):3051–7. doi: 10.1182/blood-2004-07-2974
15. Morvan MG, Lanier LL. NK Cells and Cancer: You can Teach Innate Cells New Tricks. *Nat Rev Cancer* (2016) 16(1):7–19. doi: 10.1038/nrc.2015.5
16. Liu E, Marin D, Banerjee P, Macapinlac HA, Thompson P, Basar R, et al. Use of CAR-Transduced Natural Killer Cells in CD19-Positive Lymphoid Tumors. *N Engl J Med* (2020) 382(6):545–53. doi: 10.1056/NEJMoa1910607
17. Colonna M, Samaridis J. Cloning of Immunoglobulin-Superfamily Members Associated With HLA-C and HLA-B Recognition by Human Natural Killer Cells. *Science* (1995) 268(5209):405–8. doi: 10.1126/science.7716543
18. Ruggeri L, Mancusi A, Capanni M, Urbani E, Carotti A, Aloisi T, et al. Donor Natural Killer Cell Allorecognition of Missing Self in Haploidentical Hematopoietic Transplantation for Acute Myeloid Leukemia: Challenging Its Predictive Value. *Blood* (2007) 110(1):433–40. doi: 10.1182/blood-2006-07-038687
19. Storkus WJ, Howell DN, Salter RD, Dawson JR, Cresswell P. NK Susceptibility Varies Inversely With Target Cell Class I HLA Antigen Expression. *J Immunol* (1987) 138(6):1657–9.
20. Moretta A, Vitale M, Bottino C, Orengo AM, Morelli L, Augugliaro R, et al. P58 Molecules as Putative Receptors for Major Histocompatibility Complex (MHC) Class I Molecules in Human Natural Killer (NK) Cells. Anti-P58 Antibodies Reconstitute Lysis of MHC Class I-Protected Cells in NK Clones Displaying Different Specificities. *J Exp Med* (1993) 178(2):597–604. doi: 10.1084/jem.178.2.597
21. Pende D, Falco M, Vitale M, Cantoni C, Vitale C, Munari E, et al. Killer Ig-Like Receptors (KIRs): Their Role in NK Cell Modulation and Developments Leading to Their Clinical Exploitation. *Front Immunol* (2019) 101179:1179. doi: 10.3389/fimmu.2019.01179
22. Uhrberg M, Valiante NM, Shum BP, Shilling HG, Lienert-Weidenbach K, Corliss B, et al. Human Diversity in Killer Cell Inhibitory Receptor Genes. *Immunity* (1997) 7(6):753–63. doi: 10.1016/s1074-7613(00)80394-5
23. Colonna M, Brooks EG, Falco M, Ferrara GB, Strominger JL. Generation of Allospecific Natural Killer Cells by Stimulation Across a Polymorphism of HLA-C. *Science* (1993) 260(5111):1121–4. doi: 10.1126/science.8493555
24. López-Botet M, Pérez-Villar JJ, Carretero M, Rodríguez A, Melero I, Bellón T, et al. Structure and Function of the CD94 C-Type Lectin Receptor Complex Involved in Recognition of HLA Class I Molecules. *Immunol Rev* (1997) 155:165–74. doi: 10.1111/j.1600-065x.1997.tb00949.x
25. Brooks AG, Posch PE, Scorzelli CJ, Borrego F, Coligan JE. NKG2A Complexed With CD94 Defines a Novel Inhibitory Natural Killer Cell Receptor. *J Exp Med* (1997) 185(4):795–800. doi: 10.1084/jem.185.4.795
26. Carretero M, Cantoni C, Bellón T, Bottino C, Biassoni R, Rodríguez A, et al. The CD94 and NKG2-A C-Type Lectins Covalently Assemble to Form a Natural Killer Cell Inhibitory Receptor for HLA Class I Molecules. *Eur J Immunol* (1997) 27(2):563–7. doi: 10.1002/eji.1830270230
27. Kärre K, Ljunggren HG, Piontek G, Kiessling R. Selective Rejection of H-2-Deficient Lymphoma Variants Suggests Alternative Immune Defence Strategy. *Nature* (1986) 319(6055):675–8. doi: 10.1038/319675a0
28. Farag SS, Fehniger TA, Ruggeri L, Velardi A, Caligiuri MA. Natural Killer Cell Receptors: New Biology and Insights Into the Graft-*Versus*-Leukemia Effect. *Blood* (2002) 100(6):1935–47. doi: 10.1182/blood-2002-02-0350
29. Kärre K. NK Cells, MHC Class I Molecules and the Missing Self. *Scand J Immunol* (2002) 55(3):221–8. doi: 10.1046/j.1365-3083.2002.01053.x
30. Ruggeri L, Capanni M, Casucci M, Volpi I, Tosti A, Perruccio K, et al. Role of Natural Killer Cell Alloreactivity in HLA-Mismatched Hematopoietic Stem Cell Transplantation. *Blood* (1999) 94(1):333–9. doi: 10.1182/blood.V94.1.333.413a31_333_339
31. Yabe T, McSherry C, Bach FH, Fisch P, Schall RP, Sondel PM, et al. A Multigene Family on Human Chromosome 12 Encodes Natural Killer-Cell Lectins. *Immunogenetics* (1993) 37(6):455–60. doi: 10.1007/bf00222470
32. Gumperz JE, Valiante NM, Parham P, Lanier LL, Tyan D. Heterogeneous Phenotypes of Expression of the NKB1 Natural Killer Cell Class I Receptor Among Individuals of Different Human Histocompatibility Leukocyte Antigens Types Appear Genetically Regulated, But Not Linked to Major Histocompatibililty Complex Haplotype. *J Exp Med* (1996) 183(4):1817–27. doi: 10.1084/jem.183.4.1817
33. Vilches C, Parham P. KIR: Diverse, Rapidly Evolving Receptors of Innate and Adaptive Immunity. *Annu Rev Immunol* (2002) 20:217–51. doi: 10.1146/annurev.immunol.20.092501.134942
34. Hsu KC, Keever-Taylor CA, Wilton A, Pinto C, Heller G, Arkun K, et al. Improved Outcome in HLA-Identical Sibling Hematopoietic Stem-Cell Transplantation for Acute Myelogenous Leukemia Predicted by KIR and HLA Genotypes. *Blood* (2005) 105(12):4878–84. doi: 10.1182/blood-2004-12-4825
35. Leung W, Iyengar R, Triplett B, Turner V, Behm FG, Holladay MS, et al. Comparison of Killer Ig-Like Receptor Genotyping and Phenotyping for Selection of Allogeneic Blood Stem Cell Donors. *J Immunol* (2005) 174 (10):6540–5. doi: 10.4049/jimmunol.174.10.6540
36. Leung W, Iyengar R, Turner V, Lang P, Bader P, Conn P, et al. Determinants of Antileukemia Effects of Allogeneic NK Cells. *J Immunol* (2004) 172 (1):644–50. doi: 10.4049/jimmunol.172.1.644
37. Hsu KC, Gooley T, Malkki M, Pinto-Agnello C, Dupont B, Bignon JD, et al. KIR Ligands and Prediction of Relapse After Unrelated Donor Hematopoietic Cell Transplantation for Hematologic Malignancy. *Biol Blood Marrow Transplant* (2006) 12(8):828–36. doi: 10.1016/j.bbmt.2006.04.008
38. Verheyden S, Schots R, Duquet W, Demanet C. A Defined Donor Activating Natural Killer Cell Receptor Genotype Protects Against Leukemic Relapse After Related HLA-Identical Hematopoietic Stem Cell Transplantation. *Leukemia* (2005) 19(8):1446–51. doi: 10.1038/sj.leu.2403839
39. Sconocchia G, Lau M, Provenzano M, Rezvani K, Wongsena W, Fujiwara H, et al. The Antileukemia Effect of HLA-Matched NK and NK-T Cells in Chronic Myelogenous Leukemia Involves NKG2D-Target-Cell Interactions. *Blood* (2005) 106(10):3666–72. doi: 10.1182/blood-2005-02-0479
40. Verheyden S, Demanet C. NK Cell Receptors and Their Ligands in Leukemia. *Leukemia* (2008) 22(2):249–57. doi: 10.1038/sj.leu.2405040
41. Shimasaki N, Jain A, Campana D. NK Cells for Cancer Immunotherapy. *Nat Rev Drug Discovery* (2020) 19(3):200–18. doi: 10.1038/s41573-019-0052-1
42. Weiden PL, Flournoy N, Thomas ED, Prentice R, Fefer A, Buckner CD, et al. Antileukemic Effect of Graft-*Versus*-Host Disease in Human Recipients of Allogeneic-Marrow Grafts. *N Engl J Med* (1979) 300(19):1068–73. doi: 10.1056/nejm197905103001902
43. Horowitz MM, Gale RP, Sondel PM, Goldman JM, Kersey J, Kolb HJ, et al. Graft-*Versus*-Leukemia Reactions After Bone Marrow Transplantation. *Blood* (1990) 75(3):555–62. doi: 10.1182/blood.V75.3.555.555
44. Ferrara JL, Levine JE, Reddy P, Holler E. Graft-*Versus*-Host Disease. *Lancet* (2009) 373(9674):1550–61. doi: 10.1016/s0140-6736(09)60237-3
45. Giebel S, Locatelli F, Lamparelli T, Velardi A, Davies S, Frumento G, et al. Survival Advantage With KIR Ligand Incompatibility in Hematopoietic Stem Cell Transplantation From Unrelated Donors. *Blood* (2003) 102 (3):814–9. doi: 10.1182/blood-2003-01-0091
46. Ruggeri L, Capanni M, Urbani E, Perruccio K, Shlomchik WD, Tosti A, et al. Effectiveness of Donor Natural Killer Cell Alloreactivity in Mismatched Hematopoietic Transplants. *Science* (2002) 295(5562):2097–100. doi: 10.1126/science.1068440
47. Cerboni C, Zingoni A, Cippitelli M, Piccoli M, Frati L, Santoni A. Antigen-Activated Human T Lymphocytes Express Cell-Surface NKG2D Ligands *via* an ATM/ATR-Dependent Mechanism and Become Susceptible to Autologous NK- Cell Lysis. *Blood* (2007) 110(2):606–15. doi: 10.1182/blood-2006-10-052720
48. Miller JS, Cooley S, Parham P, Farag SS, Verneris MR, McQueen KL, et al. Missing KIR Ligands are Associated With Less Relapse and Increased Graft-*Versus*-Host Disease (GVHD) Following Unrelated Donor Allogeneic HCT. *Blood* (2007) 109(11):5058–61. doi: 10.1182/blood-2007-01-065383
49. Barnes DW, Corp MJ, Loutit JF, Neal FE. Treatment of Murine Leukaemia With X Rays and Homologous Bone Marrow; Preliminary Communication. *Br Med J* (1956) 2(4993):626–7. doi: 10.1136/bmj.2.4993.626
50. Bachar-Lustig E, Rachamim N, Li HW, Lan F, Reisner Y. Megadose of T Cell-Depleted Bone Marrow Overcomes MHC Barriers in Sublethally Irradiated Mice. *Nat Med* (1995) 1(12):1268–73. doi: 10.1038/nm1295-1268
51. Valiante NM, Uhrberg M, Shilling HG, Lienert-Weidenbach K, Arnett KL, D'Andrea A, et al. Functionally and Structurally Distinct NK Cell Receptor

Repertoires in the Peripheral Blood of Two Human Donors. *Immunity* (1997) 7(6):739–51. doi: 10.1016/s1074-7613(00)80393-3
52. André P, Denis C, Soulas C, Bourbon-Caillet C, Lopez J, Arnoux T, et al. Anti-NKG2A mAb Is a Checkpoint Inhibitor That Promotes Anti-Tumor Immunity by Unleashing Both T and NK Cells. *Cell* (2018) 175(7):1731–43.e13. doi: 10.1016/j.cell.2018.10.014
53. Braud V, Jones EY, McMichael A. The Human Major Histocompatibility Complex Class Ib Molecule HLA-E Binds Signal Sequence-Derived Peptides With Primary Anchor Residues at Positions 2 and 9. *Eur J Immunol* (1997) 27(5):1164–9. doi: 10.1002/eji.1830270517
54. Braud VM, Allan DS, Wilson D, McMichael AJ. TAP- and Tapasin-Dependent HLA-E Surface Expression Correlates With the Binding of an MHC Class I Leader Peptide. *Curr Biol* (1998) 8(1):1–10. doi: 10.1016/s0960-9822(98)70014-4
55. Bauer S, Groh V, Wu J, Steinle A, Phillips JH, Lanier LL, et al. Activation of NK Cells and T Cells by NKG2D, a Receptor for Stress-Inducible MICA. *Science* (1999) 285(5428):727–9. doi: 10.1126/science.285.5428.727
56. Cosman D, Müllberg J, Sutherland CL, Chin W, Armitage R, Fanslow W, et al. ULBPs, Novel MHC Class I-Related Molecules, Bind to CMV Glycoprotein UL16 and Stimulate NK Cytotoxicity Through the NKG2D Receptor. *Immunity* (2001) 14(2):123–33. doi: 10.1016/s1074-7613(01)00095-4
57. Fajgenbaum DC, June CH. Cytokine Storm. *N Engl J Med* (2020) 383 (23):2255–73. doi: 10.1056/NEJMra2026131
58. Klingemann H. Are Natural Killer Cells Superior CAR Drivers? *Oncoimmunology* (2014) 3:e28147. doi: 10.4161/onci.28147
59. Tang X, Yang L, Li Z, Nalin AP, Dai H, Xu T, et al. First-In-Man Clinical Trial of CAR NK-92 Cells: Safety Test of CD33-CAR NK-92 Cells in Patients With Relapsed and Refractory Acute Myeloid Leukemia. *Am J Cancer Res* (2018) 8(6):1083–9.
60. Parkhurst MR, Riley JP, Dudley ME, Rosenberg SA. Adoptive Transfer of Autologous Natural Killer Cells Leads to High Levels of Circulating Natural Killer Cells But Does Not Mediate Tumor Regression. *Clin Cancer Res* (2011) 17(19):6287–97. doi: 10.1158/1078-0432.Ccr-11-1347
61. Maki G, Klingemann HG, Martinson JA, Tam YK. Factors Regulating the Cytotoxic Activity of the Human Natural Killer Cell Line, NK-92. *J Hematother Stem Cell Res* (2001) 10(3):369–83. doi: 10.1089/152581601750288975
62. Schönfeld K, Sahm C, Zhang C, Naundorf S, Brendel C, Odendahl M, et al. Selective Inhibition of Tumor Growth by Clonal NK Cells Expressing an ErbB2/HER2-Specific Chimeric Antigen Receptor. *Mol Ther* (2015) 23 (2):330–8. doi: 10.1038/mt.2014.219
63. Vela M, Corral D, Carrasco P, Fernández L, Valentín J, González B, et al. Haploidentical IL-15/41BBL Activated and Expanded Natural Killer Cell Infusion Therapy After Salvage Chemotherapy in Children With Relapsed and Refractory Leukemia. *Cancer Lett* (2018) 422:107–17. doi: 10.1016/j.canlet.2018.02.033
64. Ciurea SO, Schafer JR, Bassett R, Denman CJ, Cao K, Willis D, et al. Phase 1 Clinical Trial Using Mbil21 Ex Vivo-Expanded Donor-Derived NK Cells After Haploidentical Transplantation. *Blood* (2017) 130(16):1857–68. doi: 10.1182/blood-2017-05-785659
65. Huntington ND, Puthalakath H, Gunn P, Naik E, Michalak EM, Smyth MJ, et al. Interleukin 15-Mediated Survival of Natural Killer Cells Is Determined by Interactions Among Bim, Noxa and Mcl-1. *Nat Immunol* (2007) 8 (8):856–63. doi: 10.1038/ni1487
66. Guo Y, Luan L, Patil NK, Sherwood ER. Immunobiology of the IL-15/IL-15rα Complex as an Antitumor and Antiviral Agent. *Cytokine Growth Factor Rev* (2017) 38:10–21. doi: 10.1016/j.cytogfr.2017.08.002
67. Robertson MJ, Cameron C, Lazo S, Cochran KJ, Voss SD, Ritz J. Costimulation of Human Natural Killer Cell Proliferation: Role of Accessory Cytokines and Cell Contact-Dependent Signals. *Nat Immun* (1996) 15(5):213–26.
68. Sakamoto N, Ishikawa T, Kokura S, Okayama T, Oka K, Ideno M, et al. Phase I Clinical Trial of Autologous NK Cell Therapy Using Novel Expansion Method in Patients With Advanced Digestive Cancer. *J Transl Med* (2015) 13:277. doi: 10.1186/s12967-015-0632-8
69. Ishikawa T, Okayama T, Sakamoto N, Ideno M, Oka K, Enoki T, et al. Phase I Clinical Trial of Adoptive Transfer of Expanded Natural Killer Cells in Combination With IgG1 Antibody in Patients With Gastric or Colorectal Cancer. *Int J Cancer* (2018) 142(12):2599–609. doi: 10.1002/ijc.31285
70. Ruoslahti E. Fibronectin and its Receptors. *Annu Rev Biochem* (1988) 57:375–413. doi: 10.1146/annurev.bi.57.070188.002111
71. Rabinovich BA, Li J, Shannon J, Hurren R, Chalupny J, Cosman D, et al. Activated, But Not Resting, T Cells can be Recognized and Killed by Syngeneic NK Cells. *J Immunol* (2003) 170(7):3572–6. doi: 10.4049/jimmunol.170.7.3572
72. Lee HR, Son CH, Koh EK, Bae JH, Kang CD, Yang K, et al. Expansion of Cytotoxic Natural Killer Cells Using Irradiated Autologous Peripheral Blood Mononuclear Cells and Anti-CD16 Antibody. *Sci Rep* (2017) 7(1):11075. doi: 10.1038/s41598-017-09259-1
73. Miller JS, Oelkers S, Verfaillie C, McGlave P. Role of Monocytes in the Expansion of Human Activated Natural Killer Cells. *Blood* (1992) 80 (9):2221–9. doi: 10.1182/blood.V80.9.2221.2221
74. Li L, Li W, Wang C, Yan X, Wang Y, Niu C, et al. Adoptive Transfer of Natural Killer Cells in Combination With Chemotherapy Improves Outcomes of Patients With Locally Advanced Colon Carcinoma. *Cytotherapy* (2018) 20(1):134–48. doi: 10.1016/j.jcyt.2017.09.009
75. Lehrnbecher T, Foster CB, Zhu S, Leitman SF, Goldin LR, Huppi K, et al. Variant Genotypes of the Low-Affinity Fcgamma Receptors in Two Control Populations and a Review of Low-Affinity Fcgamma Receptor Polymorphisms in Control and Disease Populations. *Blood* (1999) 94 (12):4220–32. doi: 10.1182/blood.V94.12.4220.424k08_4220_4232
76. Freud AG, Mundy-Bosse BL, Yu J, Caligiuri MA. The Broad Spectrum of Human Natural Killer Cell Diversity. *Immunity* (2017) 47(5):820–33. doi: 10.1016/j.immuni.2017.10.008
77. Grimm EA, Mazumder A, Zhang HZ, Rosenberg SA. Lymphokine-Activated Killer Cell Phenomenon. Lysis of Natural Killer-Resistant Fresh Solid Tumor Cells by Interleukin 2-Activated Autologous Human Peripheral Blood Lymphocytes. *J Exp Med* (1982) 155(6):1823–41. doi: 10.1084/jem.155.6.1823
78. Rosenberg SA, Spiess P, Lafreniere R. A New Approach to the Adoptive Immunotherapy of Cancer With Tumor-Infiltrating Lymphocytes. *Science* (1986) 233(4770):1318–21. doi: 10.1126/science.3489291
79. Restifo NP, Dudley ME, Rosenberg SA. Adoptive Immunotherapy for Cancer: Harnessing the T Cell Response. *Nat Rev Immunol* (2012) 12 (4):269–81. doi: 10.1038/nri3191
80. Zacharakis N, Chinnasamy H, Black M, Xu H, Lu YC, Zheng Z, et al. Immune Recognition of Somatic Mutations Leading to Complete Durable Regression in Metastatic Breast Cancer. *Nat Med* (2018) 24(6):724–30. doi: 10.1038/s41591-018-0040-8
81. Morgan RA, Dudley ME, Wunderlich JR, Hughes MS, Yang JC, Sherry RM, et al. Cancer Regression in Patients After Transfer of Genetically Engineered Lymphocytes. *Science* (2006) 314(5796):126–9. doi: 10.1126/science.1129003
82. Zhai Y, Li G, Jiang T, Zhang W. CAR-Armed Cell Therapy for Gliomas. *Am J Cancer Res* (2019) 9(12):2554–66.
83. Leen AM, Sukumaran S, Watanabe N, Mohammed S, Keirnan J, Yanagisawa R, et al. Reversal of Tumor Immune Inhibition Using a Chimeric Cytokine Receptor. *Mol Ther* (2014) 22(6):1211–20. doi: 10.1038/mt.2014.47
84. Wang Y, Jiang H, Luo H, Sun Y, Shi B, Sun R, et al. An IL-4/21 Inverted Cytokine Receptor Improving CAR-T Cell Potency in Immunosuppressive Solid-Tumor Microenvironment. *Front Immunol* (2019) 10:1691. doi: 10.3389/fimmu.2019.01691
85. Han X, Wang Y, Wei J, Han W. Multi-Antigen-Targeted Chimeric Antigen Receptor T Cells for Cancer Therapy. *J Hematol Oncol* (2019) 12(1):128. doi: 10.1186/s13045-019-0813-7
86. Xie G, Dong H, Liang Y, Ham JD, Rizwan R, Chen J. CAR-NK Cells: A Promising Cellular Immunotherapy for Cancer. *EBioMedicine* (2020) 59:102975. doi: 10.1016/j.ebiom.2020.102975
87. Klöß S, Oberschmidt O, Morgan M, Dahlke J, Arseniev L, Huppert V, et al. Optimization of Human NK Cell Manufacturing: Fully Automated Separation, Improved Ex Vivo Expansion Using IL-21 With Autologous Feeder Cells, and Generation of Anti-CD123-CAR-Expressing Effector Cells. *Hum Gene Ther* (2017) 28(10):897–913. doi: 10.1089/hum.2017.157
88. Tseng HC, Xiong W, Badeti S, Yang Y, Ma M, Liu T, et al. Efficacy of Anti-CD147 Chimeric Antigen Receptors Targeting Hepatocellular Carcinoma. *Nat Commun* (2020) 11(1):4810. doi: 10.1038/s41467-020-18444-2

89. Altvater B, Landmeier S, Pscherer S, Temme J, Schweer K, Kailayangiri S, et al. 2b4 (CD244) Signaling by Recombinant Antigen-Specific Chimeric Receptors Costimulates Natural Killer Cell Activation to Leukemia and Neuroblastoma Cells. *Clin Cancer Res* (2009) 15(15):4857–66. doi: 10.1158/1078-0432.Ccr-08-2810
90. Müller N, Michen S, Tietze S, Töpfer K, Schulte A, Lamszus K, et al. Engineering NK Cells Modified With an EGFRvIII-Specific Chimeric Antigen Receptor to Overexpress CXCR4 Improves Immunotherapy of CXCL12/SDF-1α-Secreting Glioblastoma. *J Immunother* (2015) 38(5):197–210. doi: 10.1097/cji.0000000000000082
91. Li Y, Hermanson DL, Moriarity BS, Kaufman DS. Human iPSC-Derived Natural Killer Cells Engineered With Chimeric Antigen Receptors Enhance Anti-Tumor Activity. *Cell Stem Cell* (2018) 23(2):181–92.e5. doi: 10.1016/j.stem.2018.06.002
92. Billadeau DD, Upshaw JL, Schoon RA, Dick CJ, Leibson PJ. NKG2D-DAP10 Triggers Human NK Cell-Mediated Killing via a Syk-Independent Regulatory Pathway. *Nat Immunol* (2003) 4(6):557–64. doi: 10.1038/ni929
93. Bryceson YT, March ME, Ljunggren HG, Long EO. Activation, Coactivation, and Costimulation of Resting Human Natural Killer Cells. *Immunol Rev* (2006) 214:73–91. doi: 10.1111/j.1600-065X.2006.00457.x
94. Eissmann P, Beauchamp L, Wooters J, Tilton JC, Long EO, Watzl C. Molecular Basis for Positive and Negative Signaling by the Natural Killer Cell Receptor 2B4 (CD244). *Blood* (2005) 105(12):4722–9. doi: 10.1182/blood-2004-09-3796
95. Chakravarthy A, Furness A, Joshi K, Ghorani E, Ford K, Ward MJ, et al. Pan-Cancer Deconvolution of Tumour Composition Using DNA Methylation. *Nat Commun* (2018) 9(1):3220. doi: 10.1038/s41467-018-05570-1
96. Mahaley MSJr., Gentry RE, Bigner DD. Immunobiology of Primary Intracranial Tumors. *J Neurosurg* (1977) 47(1):35–43. doi: 10.3171/jns.1977.47.1.0035
97. Elliott LH, Brooks WH, Roszman TL. Activation of Immunoregulatory Lymphocytes Obtained From Patients With Malignant Gliomas. *J Neurosurg* (1987) 67(2):231–6. doi: 10.3171/jns.1987.67.2.0231
98. McVicar DW, Davis DF, Merchant RE. *In Vitro* Analysis of the Proliferative Potential of T Cells From Patients With Brain Tumor: Glioma-Associated Immunosuppression Unrelated to Intrinsic Cellular Defect. *J Neurosurg* (1992) 76(2):251–60. doi: 10.3171/jns.1992.76.2.0251
99. Ashkenazi E, Deutsch M, Tirosh R, Weinreb A, Tsukerman A, Brodie C. A Selective Impairment of the IL-2 System in Lymphocytes of Patients With Glioblastomas: Increased Level of Soluble IL-2R and Reduced Protein Tyrosine Phosphorylation. *Neuroimmunomodulation* (1997) 4(1):49–56. doi: 10.1159/000097315
100. Morford LA, Elliott LH, Carlson SL, Brooks WH, Roszman TL. T Cell Receptor-Mediated Signaling is Defective in T Cells Obtained From Patients With Primary Intracranial Tumors. *J Immunol* (1997) 159(9):4415–25.
101. Raychaudhuri B, Rayman P, Ireland J, Ko J, Rini B, Borden EC, et al. Myeloid-Derived Suppressor Cell Accumulation and Function in Patients With Newly Diagnosed Glioblastoma. *Neuro Oncol* (2011) 13(6):591–9. doi: 10.1093/neuonc/nor042
102. Rodrigues JC, Gonzalez GC, Zhang L, Ibrahim G, Kelly JJ, Gustafson MP, et al. Normal Human Monocytes Exposed to Glioma Cells Acquire Myeloid-Derived Suppressor Cell-Like Properties. *Neuro Oncol* (2010) 12(4):351–65. doi: 10.1093/neuonc/nop023
103. Sinha P, Clements VK, Bunt SK, Albelda SM, Ostrand-Rosenberg S. Cross-Talk Between Myeloid-Derived Suppressor Cells and Macrophages Subverts Tumor Immunity Toward a Type 2 Response. *J Immunol* (2007) 179(2):977–83. doi: 10.4049/jimmunol.179.2.977
104. Friese MA, Wischhusen J, Wick W, Weiler M, Eisele G, Steinle A, et al. RNA Interference Targeting Transforming Growth Factor-Beta Enhances NKG2D-Mediated Antiglioma Immune Response, Inhibits Glioma Cell Migration and Invasiveness, and Abrogates Tumorigenicity *In Vivo*. *Cancer Res* (2004) 64(20):7596–603. doi: 10.1158/0008-5472.Can-04-1627
105. Castriconi R, Cantoni C, Della Chiesa M, Vitale M, Marcenaro E, Conte R, et al. Transforming Growth Factor Beta 1 Inhibits Expression of NKp30 and NKG2D Receptors: Consequences for the NK-Mediated Killing of Dendritic Cells. *Proc Natl Acad Sci USA* (2003) 100(7):4120–5. doi: 10.1073/pnas.0730640100
106. Viel S, Marçais A, Guimaraes FS, Loftus R, Rabilloud J, Grau M, et al. TGF-β Inhibits the Activation and Functions of NK Cells by Repressing the mTOR Pathway. *Sci Signal* (2016) 9(415):ra19. doi: 10.1126/scisignal.aad1884
107. Close HJ, Stead LF, Nsengimana J, Reilly KA, Droop A, Wurdak H, et al. Expression Profiling of Single Cells and Patient Cohorts Identifies Multiple Immunosuppressive Pathways and an Altered NK Cell Phenotype in Glioblastoma. *Clin Exp Immunol* (2020) 200(1):33–44. doi: 10.1111/cei.13403
108. Wei J, Barr J, Kong LY, Wang Y, Wu A, Sharma AK, et al. Glioblastoma Cancer-Initiating Cells Inhibit T-Cell Proliferation and Effector Responses by the Signal Transducers and Activators of Transcription 3 Pathway. *Mol Cancer Ther* (2010) 9(1):67–78. doi: 10.1158/1535-7163.Mct-09-0734
109. Kinjyo I, Inoue H, Hamano S, Fukuyama S, Yoshimura T, Koga K, et al. Loss of SOCS3 in T Helper Cells Resulted in Reduced Immune Responses and Hyperproduction of Interleukin 10 and Transforming Growth Factor-Beta 1. *J Exp Med* (2006) 203(4):1021–31. doi: 10.1084/jem.20052333
110. Laudati E, Currò D, Navarra P, Lisi L. Blockade of CCR5 Receptor Prevents M2 Microglia Phenotype in a Microglia-Glioma Paradigm. *Neurochem Int* (2017) 108:100–8. doi: 10.1016/j.neuint.2017.03.002
111. Held-Feindt J, Hattermann K, Müerköster SS, Wedderkopp H, Knerlich-Lukoschus F, Ungefroren H, et al. CX3CR1 Promotes Recruitment of Human Glioma-Infiltrating Microglia/Macrophages (GIMs). *Exp Cell Res* (2010) 316(9):1553–66. doi: 10.1016/j.yexcr.2010.02.018
112. Golán I, Rodríguez de la Fuente L, Costoya JA. NK Cell-Based Glioblastoma Immunotherapy. *Cancers (Basel)* (2018) 10(12):522. doi: 10.3390/cancers10120522
113. O'Brien KL, Finlay DK. Immunometabolism and Natural Killer Cell Responses. *Nat Rev Immunol* (2019) 19(5):282–90. doi: 10.1038/s41577-019-0139-2
114. Tassinari V, Cesarini V, Tomaselli S, Ianniello Z, Silvestris DA, Ginistrelli LC, et al. ADAR1 is a New Target of METTL3 and Plays a Pro-Oncogenic Role in Glioblastoma by an Editing-Independent Mechanism. *Genome Biol* (2021) 22(1):51. doi: 10.1186/s13059-021-02271-9
115. Chang YZ, Chai RC, Pang B, Chang X, An SY, Zhang KN, et al. METTL3 Enhances the Stability of MALAT1 With the Assistance of HuR *via* M6a Modification and Activates NF-κb to Promote the Malignant Progression of IDH-Wildtype Glioma. *Cancer Lett* (2021) 511:36–46. doi: 10.1016/j.canlet.2021.04.020
116. Zhou Z, Zhang J, Xu C, Yang J, Zhang Y, Liu M, et al. An Integrated Model of N6-Methyladenosine Regulators to Predict Tumor Aggressiveness and Immune Evasion in Pancreatic Cancer. *EBioMedicine* (2021) 65:103271. doi: 10.1016/j.ebiom.2021.103271
117. Cózar B, Greppi M, Carpentier S, Narni-Mancinelli E, Chiossone L, Vivier E. Tumor-Infiltrating Natural Killer Cells. *Cancer Discovery* (2021) 11(1):34–44. doi: 10.1158/2159-8290.Cd-20-0655
118. Genßler S, Burger MC, Zhang C, Oelsner S, Mildenberger I, Wagner M, et al. Dual Targeting of Glioblastoma With Chimeric Antigen Receptor-Engineered Natural Killer Cells Overcomes Heterogeneity of Target Antigen Expression and Enhances Antitumor Activity and Survival. *Oncoimmunology* (2016) 5(4):e1119354. doi: 10.1080/2162402x.2015.1119354
119. Murakami T, Nakazawa T, Natsume A, Nishimura F, Nakamura M, Matsuda R, et al. Novel Human NK Cell Line Carrying CAR Targeting EGFRvIII Induces Antitumor Effects in Glioblastoma Cells. *Anticancer Res* (2018) 38(9):5049–56. doi: 10.21873/anticanres.12824
120. Han J, Chu J, Keung Chan W, Zhang J, Wang Y, Cohen JB, et al. CAR-Engineered NK Cells Targeting Wild-Type EGFR and EGFRvIII Enhance Killing of Glioblastoma and Patient-Derived Glioblastoma Stem Cells. *Sci Rep* (2015) 5:11483. doi: 10.1038/srep11483
121. Alkins R, Burgess A, Kerbel R, Wels WS, Hynynen K. Early Treatment of HER2-Amplified Brain Tumors With Targeted NK-92 Cells and Focused Ultrasound Improves Survival. *Neuro Oncol* (2016) 18(7):974–81. doi: 10.1093/neuonc/nov318
122. Zhang C, Burger MC, Jennewein L, Genßler S, Schönfeld K, Zeiner P, et al. ErbB2/HER2-Specific NK Cells for Targeted Therapy of Glioblastoma. *J Natl Cancer Inst* (2016) 108(5). doi: 10.1093/jnci/djv375
123. Burger MC, Zhang C, Harter PN, Romanski A, Strassheimer F, Senft C, et al. CAR-Engineered NK Cells for the Treatment of Glioblastoma: Turning

Innate Effectors Into Precision Tools for Cancer Immunotherapy. *Front Immunol* (2019) 10:2683. doi: 10.3389/fimmu.2019.02683
124. Wu W, Zhou Q, Masubuchi T, Shi X, Li H, Xu X, et al. Multiple Signaling Roles of CD3ε and Its Application in CAR-T Cell Therapy. *Cell* (2020) 182 (4):855–71.e23. doi: 10.1016/j.cell.2020.07.018
125. Bryceson YT, March ME, Ljunggren HG, Long EO. Synergy Among Receptors on Resting NK Cells for the Activation of Natural Cytotoxicity and Cytokine Secretion. *Blood* (2006) 107(1):159–66. doi: 10.1182/blood-2005-04-1351
126. Gauthier L, Morel A, Anceriz N, Rossi B, Blanchard-Alvarez A, Grondin G, et al. Multifunctional Natural Killer Cell Engagers Targeting NKp46 Trigger Protective Tumor Immunity. *Cell* (2019) 177(7):1701–13.e16. doi: 10.1016/j.cell.2019.04.041
127. Ferrari de Andrade L, Tay RE, Pan D, Luoma AM, Ito Y, Badrinath S, et al. Antibody-Mediated Inhibition of MICA and MICB Shedding Promotes NK Cell-Driven Tumor Immunity. *Science* (2018) 359(6383):1537–42. doi: 10.1126/science.aao0505
128. da Silva IP, Gallois A, Jimenez-Baranda S, Khan S, Anderson AC, Kuchroo VK, et al. Reversal of NK-Cell Exhaustion in Advanced Melanoma by Tim-3 Blockade. *Cancer Immunol Res* (2014) 2(5):410–22. doi: 10.1158/2326-6066.Cir-13-0171
129. Zhang Q, Bi J, Zheng X, Chen Y, Wang H, Wu W, et al. Blockade of the Checkpoint Receptor TIGIT Prevents NK Cell Exhaustion and Elicits Potent Anti-Tumor Immunity. *Nat Immunol* (2018) 19(7):723–32. doi: 10.1038/s41590-018-0132-0
130. Benson DM Jr, Hofmeister CC, Padmanabhan S, Suvannasankha A, Jagannath S, Abonour R, et al. A Phase 1 Trial of the Anti-KIR Antibody IPH2101 in Patients With Relapsed/Refractory Multiple Myeloma. *Blood* (2012) 120(22):4324–33. doi: 10.1182/blood-2012-06-438028
131. Wang W, Erbe AK, Hank JA, Morris ZS, Sondel PM. NK Cell-Mediated Antibody-Dependent Cellular Cytotoxicity in Cancer Immunotherapy. *Front Immunol* (2015) 6:368. doi: 10.3389/fimmu.2015.00368
132. Zhou Z, Li M. Evaluation of BRCA1 and BRCA2 as Indicators of Response to Immune Checkpoint Inhibitors. *JAMA Netw Open* (2021) 4(5):e217728. doi: 10.1001/jamanetworkopen.2021.7728
133. Parham P. MHC Class I Molecules and KIRs in Human History, Health and Survival. *Nat Rev Immunol* (2005) 5(3):201–14. doi: 10.1038/nri1570
134. Martín-Fontecha A, Thomsen LL, Brett S, Gerard C, Lipp M, Lanzavecchia A, et al. Induced Recruitment of NK Cells to Lymph Nodes Provides IFN-Gamma for T(H)1 Priming. *Nat Immunol* (2004) 5(12):1260–5. doi: 10.1038/ni1138
135. Mocikat R, Braumüller H, Gumy A, Egeter O, Ziegler H, Reusch U, et al. Natural Killer Cells Activated by MHC Class I(low) Targets Prime Dendritic Cells to Induce Protective CD8 T Cell Responses. *Immunity* (2003) 19 (4):561–9. doi: 10.1016/s1074-7613(03)00264-4
136. Adam C, King S, Allgeier T, Braumüller H, Lüking C, Mysliwietz J, et al. DC-NK Cell Cross Talk as a Novel CD4+ T-Cell-Independent Pathway for Antitumor CTL Induction. *Blood* (2005) 106(1):338–44. doi: 10.1182/blood-2004-09-3775
137. Krebs P, Barnes MJ, Lampe K, Whitley K, Bahjat KS, Beutler B, et al. NK-Cell-Mediated Killing of Target Cells Triggers Robust Antigen-Specific T-Cell-Mediated and Humoral Responses. *Blood* (2009) 113(26):6593–602. doi: 10.1182/blood-2009-01-201467
138. Cook KD, Whitmire JK. The Depletion of NK Cells Prevents T Cell Exhaustion to Efficiently Control Disseminating Virus Infection. *J Immunol* (2013) 190(2):641–9. doi: 10.4049/jimmunol.1202448
139. Andrews DM, Estcourt MJ, Andoniou CE, Wikstrom ME, Khong A, Voigt V, et al. Innate Immunity Defines the Capacity of Antiviral T Cells to Limit Persistent Infection. *J Exp Med* (2010) 207(6):1333–43. doi: 10.1084/jem.20091193
140. Parihar R, Rivas C, Huynh M, Omer B, Lapteva N, Metelitsa LS, et al. NK Cells Expressing a Chimeric Activating Receptor Eliminate MDSCs and Rescue Impaired CAR-T Cell Activity Against Solid Tumors. *Cancer Immunol Res* (2019) 7(3):363–75. doi: 10.1158/2326-6066.Cir-18-0572
141. Brown CE, Alizadeh D, Starr R, Weng L, Wagner JR, Naranjo A, et al. Regression of Glioblastoma After Chimeric Antigen Receptor T-Cell Therapy. *N Engl J Med* (2016) 375(26):2561–9. doi: 10.1056/NEJMoa1610497
142. Ahmed N, Brawley V, Hegde M, Bielamowicz K, Kalra M, Landi D, et al. HER2-Specific Chimeric Antigen Receptor-Modified Virus-Specific T Cells for Progressive Glioblastoma: A Phase 1 Dose-Escalation Trial. *JAMA Oncol* (2017) 3(8):1094–101. doi: 10.1001/jamaoncol.2017.0184
143. O'Rourke DM, Nasrallah MP, Desai A, Melenhorst JJ, Mansfield K, Morrissette JJD, et al. A Single Dose of Peripherally Infused EGFRvIII-Directed CAR T Cells Mediates Antigen Loss and Induces Adaptive Resistance in Patients With Recurrent Glioblastoma. *Sci Transl Med* (2017) 9(399):eaaa0984. doi: 10.1126/scitranslmed.aaa0984
144. Chen X, Han J, Chu J, Zhang L, Zhang J, Chen C, et al. A Combinational Therapy of EGFR-CAR NK Cells and Oncolytic Herpes Simplex Virus 1 for Breast Cancer Brain Metastases. *Oncotarget* (2016) 7(19):27764–77. doi: 10.18632/oncotarget.8526
145. Ma R, Lu T, Li Z, Teng KY, Mansour AG, Yu M, et al. An Oncolytic Virus Expressing Il15/Il15rα Combined With Off-The-Shelf EGFR-CAR NK Cells Targets Glioblastoma. *Cancer Res* (2021) 81(13):3635–48. doi: 10.1158/0008-5472.Can-21-0035

Conflict of Interest: The authors declare that the research was conducted in the absence of any commercial or financial relationships that could be construed as a potential conflict of interest.

Publisher's Note: All claims expressed in this article are solely those of the authors and do not necessarily represent those of their affiliated organizations, or those of the publisher, the editors and the reviewers. Any product that may be evaluated in this article, or claim that may be made by its manufacturer, is not guaranteed or endorsed by the publisher.

Copyright © 2021 Pan, Zhai, Li, Jiang and Zhang. This is an open-access article distributed under the terms of the Creative Commons Attribution License (CC BY). The use, distribution or reproduction in other forums is permitted, provided the original author(s) and the copyright owner(s) are credited and that the original publication in this journal is cited, in accordance with accepted academic practice. No use, distribution or reproduction is permitted which does not comply with these terms.

frontiers in Oncology

ORIGINAL RESEARCH
published: 27 October 2021
doi: 10.3389/fonc.2021.738651

Integrin Alpha-2 as a Potential Prognostic and Predictive Biomarker for Patients With Lower-Grade Glioma

Li Lin[1†], Kai Huang[1,2,3†], Zewei Tu[1,3†], Xingen Zhu[1,3], Jingying Li[4], Kunjian Lei[1], Min Luo[1], Peng Wang[1], Chuandong Gong[1], Xiaoyan Long[2] and Lei Wu[1,3]*

[1] Department of Neurosurgery, The Second Affiliated Hospital of Nanchang University, Nanchang, China, [2] Department of Scientific Research, East China Institute of Digital Medical Engineering, Shangrao, China, [3] Institute of Neuroscience, Nanchang University, Nanchang, China, [4] Department of Comprehensive Intensive Care Unit, The Second Affiliated Hospital of Nanchang University, Nanchang, China

OPEN ACCESS

Edited by:
Longbo Zhang,
Yale University, United States

Reviewed by:
Gefei Guan,
The First Affiliated Hospital of China Medical University, China
Hao Zhang,
Xiangya Hospital Central South University, China

***Correspondence:**
Lei Wu
doctorleiming@163.com

[†]These authors have contributed equally to this work and share first authorship

Specialty section:
This article was submitted to Cancer Immunity and Immunotherapy, a section of the journal Frontiers in Oncology

Received: 09 July 2021
Accepted: 06 October 2021
Published: 27 October 2021

Citation:
Lin L, Huang K, Tu Z, Zhu X, Li J, Lei K, Luo M, Wang P, Gong C, Long X and Wu L (2021) Integrin Alpha-2 as a Potential Prognostic and Predictive Biomarker for Patients With Lower-Grade Glioma. Front. Oncol. 11:738651. doi: 10.3389/fonc.2021.738651

Diffuse gliomas are the most common malignant brain tumors with the highest mortality and recurrence rate in adults. Integrin alpha-2 (ITGA2) is involved in a series of biological processes, including cell adhesion, stemness regulation, angiogenesis, and immune/blood cell functions. The role of ITGA2 in lower-grade gliomas (LGGs) is not well defined. Firstly, we downloaded RNA sequencing and relevant clinical information from The Cancer Genome Atlas cohort, the Chinese Glioma Genome Atlas cohort, and related immune cohorts. Next, prognosis analysis, difference analysis, clinical model construction, enrichment analysis, and immune infiltration analysis are performed for this study. These analyses indicated that ITGA2 may have clinical application value and research value in LGG immunotherapy. We also detected the mRNA and protein expression of ITGA2 in three LGG cell lines and normal glial cells using quantitative real-time polymerase chain reaction assay and western blot assay. Our study not only offers a novel target for LGG immunotherapy but also can better comprehend the mechanism of the development and progression of patients with LGG. This study revealed that ITGA2 may be a potential prognostic and predictive biomarker for LGG, which can bring new insights into targeted immunotherapy.

Keywords: immune infiltration, prognostic signature, overall survival (OS), lower grade gliomas, integrin alpha-2 (ITGA2)

INTRODUCTION

According to the malignant degree of gliomas, the World Health Organization has classified them into grade I to IV, which is judged by a variety of histological features accompanied by genetic changes (1). Diffuse gliomas, which include WHO grade II and III gliomas, are the most common malignant brain tumors with the highest mortality and recurrence rate in adults. It is also known as lower-grade gliomas (LGGs) in studies (2). LGG is a diverse primary and malignant brain tumor that frequently arises in young patients and has an indolent course, with a better survival rate than glioblastoma (3), but it always recurs and progresses into glioblastoma. The poor prognosis for patients with LGG shows the diversity of this malignant glioma; therefore, new treatment strategies are needed to continuously improve the prognosis of LGG patients (4). Although radiotherapy and chemotherapy are used to

treat patients with glioma, their effectiveness against glioma is not remarkable (5). Therefore, it is very pivotal to find a new prognostic biomarker to enhance the treatment of glioma and increase the understanding of glioma treatment. Integrin alpha-2 (ITGA2), as an important influencing factor on the tumor immune microenvironment, has the potential to become a molecular marker for targeted therapy and the diagnosis of LGG.

ITGA2 belongs to the integrin family, which is pivotal to sustain the integrity of the cytoskeletal–extracellular matrix linkage among all cell adhesion receptors (6). Some research had shown that ITGA2 is a cell transmembrane receptor that assists the adhesion of other several cells to the extracellular matrix (7). In addition, changes of ITGA2 expression affect the immune microenvironment and immunogenicity of tumors (8). A solid tumor is composed not only of cancer cells but also of immune cells, stromal cells, and more, which all may make a difference to LGG progression in a subtle and dynamic way. ITGA2 reportedly is involved in the occurrence and progress of multiple cancers, including colorectal cancer, hepatocellular carcinoma, and breast cancer (9–11). Experts have studied the ITGA2 ligand blockade that significantly obstructed cell migration in glioblastoma (12), but research in LGG has not yet been carried out. To fill this gap, we suggested that ITGA2 can be a robust prognostic and predictive biomarker for LGG.

We investigated the prognostic significance of ITGA2 by bioinformatic analysis in The Cancer Genome Atlas (TCGA) cohort (n = 407); the subgroup of patients with high ITGA2 expression usually induced poor overall survival (OS) times and rates. Similar results were obtained in the Chinese Glioma Genome Atlas (CGGA) cohorts, CGGAseq1 (n = 420) and CGGAseq2 (n = 171). Using clinical patient information, we performed a correlation analysis with ITGA2 expression and established a clinical nomogram to estimate the OS of patients with LGG. Gene Ontology (GO) analysis was implemented to annotate the function of differentially expressed genes, using ITGA2 expression as a boundary. Analysis of the Kyoto Encyclopedia of Genes and Genomes (KEGG) pathway enrichment was also performed as well as Gene Set Enrichment Analysis (GSEA). A single-sample GSEA (ssGSEA) algorithm investigated the relationship between the enrichment level of the 29 immune-associated gene sets and ITGA2 expression. A study on correlation was applied to explore the relationship between ITGA2 and several known immune checkpoints. Our experiments verified that LGG has a higher protein expression and mRNA expression of ITGA2 than normal glial cells. In brief, through a range of comprehensive analyses, we suggested that ITGA2 can be used as a robust prognostic biomarker for patients with LGG to enhance the outcome of LGG.

MATERIALS AND METHODS

Data Acquisition and Pre-processing

In this study, three independent LGG cohorts—TCGA cohort and CGGA seq1 and CGGA seq2 cohorts—were downloaded and used for analysis. Data of immunotherapeutic cohorts were downloaded from IMvigor210 cohort (a BLCA immunotherapy cohort, n = 398) (13) and two melanoma immunotherapy cohorts, including GSE78220 cohort (n = 26) and GSE91061 cohort (pre-treatment, n = 51) (14). Data of single-cell RNA sequencing analysis was downloaded from GSE84465 cohort. The RNA sequencing and relevant clinical information of TCGA cohort were downloaded from the Genomic Data Commons Data Portal website (https://portal.gdc.cancer.gov/). The mRNA expression and clinical data were obtained from the CGGA website (http://www.cgga.org.cn/), and the CGGAseq1 and CGGAseq2 cohorts obtained were regarded as the two external validation sets. The RNA sequencing and relevant clinical information of IMvigor210 cohort were downloaded from https://www.nature.com/articles/nature25501, and other cohorts were downloaded from GEO database. The inclusion criteria for LGG were as follows: (1) patients with WHO grade II or III glioma, (2) patients diagnosed with glioma with OS of more than 30 days, (3) patients with expression data, and (4) patients with primary glioma. After filtering, we screened for LGGs that could be used for additional analysis from the three independent datasets (TCGA, CGGAseq1, and CGGAseq2), which resulted in 407, 420, and 171 patients with LGG, respectively. The transcripts per kilobase million of the three RNA sequence cohorts were converted from fragments per kilobase per million using a previously published formula (15, 16). In addition, we deleted 50 data from IMvigor210 cohort, which were not available (NA) for PDL1 treatment (n = 398). Then, the transcripts per kilobase million values were analyzed in the follow-up work.

Prognostic Role of ITGA2 and Validation

Patients with LGG were split into subgroups of low and high ITGA2 expression on the basis of the median ITGA2 expression in the TCGA and CGGA cohorts. Receiver operating characteristic (ROC) curves and area under the curve (AUC) values were used to estimate the prognostic predictive ability of ITGA2 expression in the three cohorts. Univariate and multivariate Cox regression analyses were conducted to estimate the independent prognostic value of ITGA2 expression.

Functional Enrichment Analysis

In the TCGA cohort, the "limma" package, with the standards of $|\log2 \text{ (fold change)}| > 1$ and $P < .05$, was used to identify differentially expressed genes (DEGs) between LGG subgroups of low and high ITGA2 expression (17). Overall, 2,486 DEGs were screened out, and GO biological processes (GO-BP) analysis and KEGG analysis were performed on the basis of selected DEGs using the "clusterProfiler" R package (18). In addition, to identify tumor hallmarks enriched in LGG with higher ITGA2 expression, GSEA was performed by the GSEA software platform (version 4.0.1, https://www.gsea-msigdb.org/gsea/index.jsp) (19).

Construction and Validation of the Nomogram Predictive Model

Univariate and multivariate Cox regression analyses were conducted to validate the independent prognostic factors

among ITGA2 expression and included the following clinical factors: 40 → median age WHO grade (II or III), O(6)-methylguanine-DNA methyltransferase (MGMT) promoter methylation status (methylated or unmethylated), isocitrate dehydrogenase (IDH) mutation status (mutant or wild-type IDH), and 1p/19q co-deletion status (co-deletion or non-co-deletion). A nomogram model was established depending on the outcomes of the multivariate Cox regression, using the R package "rsm." Continuous variables, the WHO grade of the LGG of the patient, and the ITGA2 expression level were contained in the nomogram model. Calibration curves were formed by means of the "calibrate" function of the "rms" package in TCGA cohort and were validated in the CGGA cohorts. Discrimination was evaluated by calculating Harrell's C-index. To assess the clinical utility of the nomogram model, decision curve analysis (DCA) was used to compare the benefits of different factors.

ssGSEA

Using an ssGSEA algorithm to quantify the enrichment of the 29 immune-associated signatures, downloaded from previous research (20, 21), and the R package " GSVA," we examined the infiltration of each immune cell type in the LGG tumor microenvironment (TME) (22). On the basis of the median expression of ITGA2, the samples were split into high- and low-expression groups for ssGSEA analysis in the TCGA cohort. The estimate algorithm was conducted to calculate tumor purity, estimate scores, immune scores, and stromal scores of LGGs using the "estimate" package (23). The relevant abundance of each infiltrating immune cell was calculated using the ssGSEA algorithm.

Single-Cell RNA Sequencing Analysis

The distribution and abundance of ITGA2 in different cells, such as vascular cell, immune cell, neuron cell, astrocyte cell, neoplastic cell, oligodendrocyte cell, and oligodendrocyte precursor cell (OPC), were obtained by single-cell RNA analysis, implemented by R package "limma", "Seurat", "dplyr", and "magrittr".

Tumor Immune Dysfunction and Exclusion

Tumor immune dysfunction and exclusion (TIDE) algorithm, based on the database of melanoma and non-small cell lung cancer, can predict the immune response of the patients in other cancer types (24). It mainly depends on two mechanisms: inducing the dysfunction of T cell in tumors with high cytotoxic T lymphocyte (CTL) abundance and preventing the infiltration of T cell in tumors with low CTL levels (25). TIDE algorithm was performed by the website http://tide.dfci.harvard.edu/. Depending on the expression data in the TCGA database, we estimate the immune response of patients with gliomas by utilizing the TIDE algorithm.

Cell Culture

Bt142 mut/-, SW-1783, and SW-1088 human glioma cell lines were received from the American Type Culture Collection (ATCC). A normal human astrocyte (NHA) cell line was acquired from the Culture Collection of the Chinese Academy of Sciences (Shanghai, China). Leibovitz's L-15 medium (ATCC), with 10% fetal bovine serum (Gibco) added, was used to culture SW-1783 and SW-1088 cell lines. Dulbecco's modified Eagle's medium/F12 (ATCC) medium was used to culture Bt142-mut and NHA cell lines. All cell lines were incubated in an incubator with 5% CO_2 at 37°C.

Western Blot Analysis and Quantitative Real-Time PCR

The use of human tissue was approved by the Ethics Committee of the Second Affiliated Hospital of Nanchang University. Cell and human tissue lysates were extracted with a radioimmunoprecipitation assay buffer (Solarbio, China) with a mixture of protease inhibitors. Western blot analysis was conducted using ITGA2 (1:1,000, 24552-1-AP, Proteintech, China) and glyceraldehyde-3-phosphate dehydrogenase (GAPDH) antibodies (1:5,000, 10494-1-AP, Proteintech, China). Briefly, the total cell lysates were isolated by 5–12% sodium dodecyl sulfate polyacrylamide gel electrophoresis and then transferred to polyvinylidene difluoride membranes (PVDF membranes, Millipore, MA, USA). The PVDF membranes were incubated with primary antibodies. Enhanced chemiluminescence was used to visualize specific proteins by GV6000M (GelView 6000pro; China). Total RNA was separated from cells using Simply P Total RNA Extraction Kit (Bioflux China), and then extracted RNA was reverse-transcribed to cDNA with Prime Script RTase (Ribobio, Guangzhou). FastStart Universal SYBR Green Master (Roche Diagnostics, Basel, Switzerland) was applied to conduct qRT-PCR. The nucleotide primer sequences are as follows: the forward primer for ITGA2 is 5′-TCCAGATGAGATTGATGAGACCAC-3′; the reverse primer for ITGA2 is 5′-AATCCATTCACGCAAACA GCA-3′; the forward primer for GAPDH is 5′-CTCAC CGGATGCACCAATGTT-3′; and the reverse primer for GAPDH is 5′-CGCGTTGCTCACAATGTTCAT-3′.

Immunofluorescence

SW-1088 glioma cell lines were fixed in methanol (Xilong Scientific, China), then permeabilized with 0.1% tween-20 (Solarbio, T8220, China), and blocked with 5% goat serum for 40 min. We stained SW-1088 cell using rabbit anti-ITGA2 (ITGA2, 1:200, 24552-1-AP, Proteintech, China). Then, we incubated it with AffiniPure Alpaca Anti-Rabbit IgG (H+L) antibody (1:200, min X Bov, Hu, Ms Sr Prot, Jackson ImmunoResearch, Japan), and the nucleus was stained by DAPI. The cells were measured by confocal laser scanning microscopy (Nikon, C2si/C2, Japan).

Cell Proliferation Experiment

We designed the siRNA (http://biodev.extra.cea.fr/DSIR/DSIR.html) that target ITGA2 mRNA, transfected it into the SW1088 cell line using Lipofectamine™ 3000 Transfection Reagent (Thermo Fisher, L3000075, USA), and then incubated it in an incubator with 5% CO_2 at 37°C. After transfection for 24 h, the SW1088 cell line was planted in a 96-well plate with a density of 2,000 cells/per well; 10 ul of CCK8 (Beyotime, C0037, China) was added to each well at 1, 2, and 3 days respectively, and the optical

density value was measured at 450 nm after 2 h. The nucleotide siRNA sequence is 5′- GGAAGAGUCUACCUGUUUACU-3′ (sense strand).

Cell Transwell Invasion Assays

Invasion analysis was performed using a Corning Transwell chamber and membrane with a pore size of 8 μM (Corning, 3524, USA). The chambers were coated with 500 ug/ml Matrigel (Corning, 356234 USA), spread with 30,000 cells on each chamber, and cultured with serum-free medium. Then, medium with 10% fetal bovine serum and 1% antibiotic/antimycotic was filled in the lower chamber of the transwell, and the 24-well plate was incubated in an incubator for 24 h. Next, we wiped the non-invasive cells on the surface of the chambers with a cotton swab, fixed the invasive cells with 4% paraformaldehyde (Solarbio, P1110, China) for 30 min, and dye them with Crystal Violet stain (Solarbio, G1075, China). Leica Microsystems D-35578 microscope was used to take the images of the invasion cells. The experiments were performed in duplicate.

Statistical Analysis

The Kaplan–Meier method and two-sided log-rank test were employed to contrast the clinical outcomes between LGG subgroups with low and high ITGA2 expressions. The Kaplan–Meier method was adopted to execute survival analyses, which were compared with the log-rank test. The Student's *t*-test or chi-square test was utilized to determine the differential expression of ITGA2 between different subgroups by clinical features, and these tests were also performed to probe the expression of various immune checkpoint genes in different subgroups (grouped by ITGA2 expression). A correlation analysis was implemented to confirm the relationship between ITGA2 expression and several immune checkpoint genes. On account of nonlinear dimensionality reduction, *t*-distributed stochastic neighbor embedding (tSNE) single-cell profiling was implemented by using the R package "Rtsne". All statistical analyses were conducted by SPSS Statistics, version 25 (https://www.ibm.com/products/software; IBM, USA) and R programming, version 3.6.1 (https://www.r-project.org/). *P*-values less than.05 were considered as statistically significant.

RESULTS

Clinical Relevance of ITGA2 in Patients With LGG

We screened out 407 patients with LGG in the TCGA cohort and 420 and 171 patients with LGG in the CGGAseq1 and CGGAseq2 cohorts, respectively. The related clinical information of selected patients with LGG are shown in **Supplementary Table S1**. A heat map displays the associations between ITGA2 expression and clinicopathological features in the TCGA dataset (**Figure 1A**). We then divided patients with LGG into subgroups of high and low ITGA2 expression in view of the median value of ITGA2 expression in the three independent cohorts and analyzed the relationship between ITGA2 expression and clinical information, including 1p/19q status, WHO grade, age, IDH status, MGMT status, and gender, in the three datasets. The results showed that the clinical characteristics had robust statistical differences, except for age and gender in the TCGA cohort (**Figure 1B**), and similar results were also observed in the CGGA cohorts (**Supplementary Figure S1**). These results suggested that the level of ITGA2 expression can influence the clinical characteristics of patients with LGG to some extent. Furthermore, we conducted a prognostic survival study on account of ITGA2 gene expression in the TCGA cohort and the CGGA cohorts (CGGAseq1 and CGGAseq2). The three independent cohorts displayed significant differences in survival outcomes (P <.001, **Figure 1C**), and the Kaplan–Meier survival curves suggested a consistent trend that patients with LGG had poor outcomes, usually accompanied with a high ITGA2 expression. These preliminarily data show that ITGA2 should be studied in more detail in patients with LGG.

Verification of the Prognostic Value of ITGA2 in Three Cohorts

We also performed a Kaplan–Meier analysis in each LGG subgroup, divided by clinical features, and the results indicated that the OS of the subgroup with low ITGA2 expression was always higher than the subgroup with high ITGA2 expression (**Figure 2A**). Similar results were obtained in the CGGAseq1 (n = 420) and CGGAseq2 (n = 171) cohorts (**Supplementary Figure S2**). Furthermore, we used the time-dependent ROC curves to analyze the accuracy of the prognostic model of patients with LGG in the TCGA, CGGAseq1, and CGGAseq2 datasets. As shown in **Figure 2**, the prognostic model of the TCGA cohort had outstanding accuracy with regard to 1-, 3-, and 5-year OS. The AUCs were 0.779, 0.785, and 0.681, respectively (**Figure 2B**). In addition, the AUCs of the prognostic model for 1-, 3-, and 5-year OS were 0.533, 0.610, and 0.658, respectively, in the CGGAseq1 dataset, and they were 0.755, 0.679, and 0.728, respectively, in the CGGAseq2 dataset (**Figure 2B**). These reliable results strongly displayed that ITGA2 could be a robust prognostic and predictive biomarker for patients with LGG.

ITGA2 Is a Risk Factor in LGGs and *In Vitro* Experiments of ITGA2

Firstly, the tSNE single-cell profiling demonstrated that ITGA2 was more expressed in neoplastic cell than in other cell types, including immune cell, OPC, oligodendrocyte cell, astrocyte cell, vascular cell, and neuron cell (**Figure 3A**). Then, we detected the protein expression and mRNA expression in three LGG cell lines (SW1088, SW1783, and BT142) and in an NHA cell line (**Figures 3B, C**), which showed that ITGA2 expression was high in LGG cell lines compared with the NHA line. In addition, we collected LGG tissues and para-cancerous tissues from six patients in the Second Affiliated Hospital of Nanchang

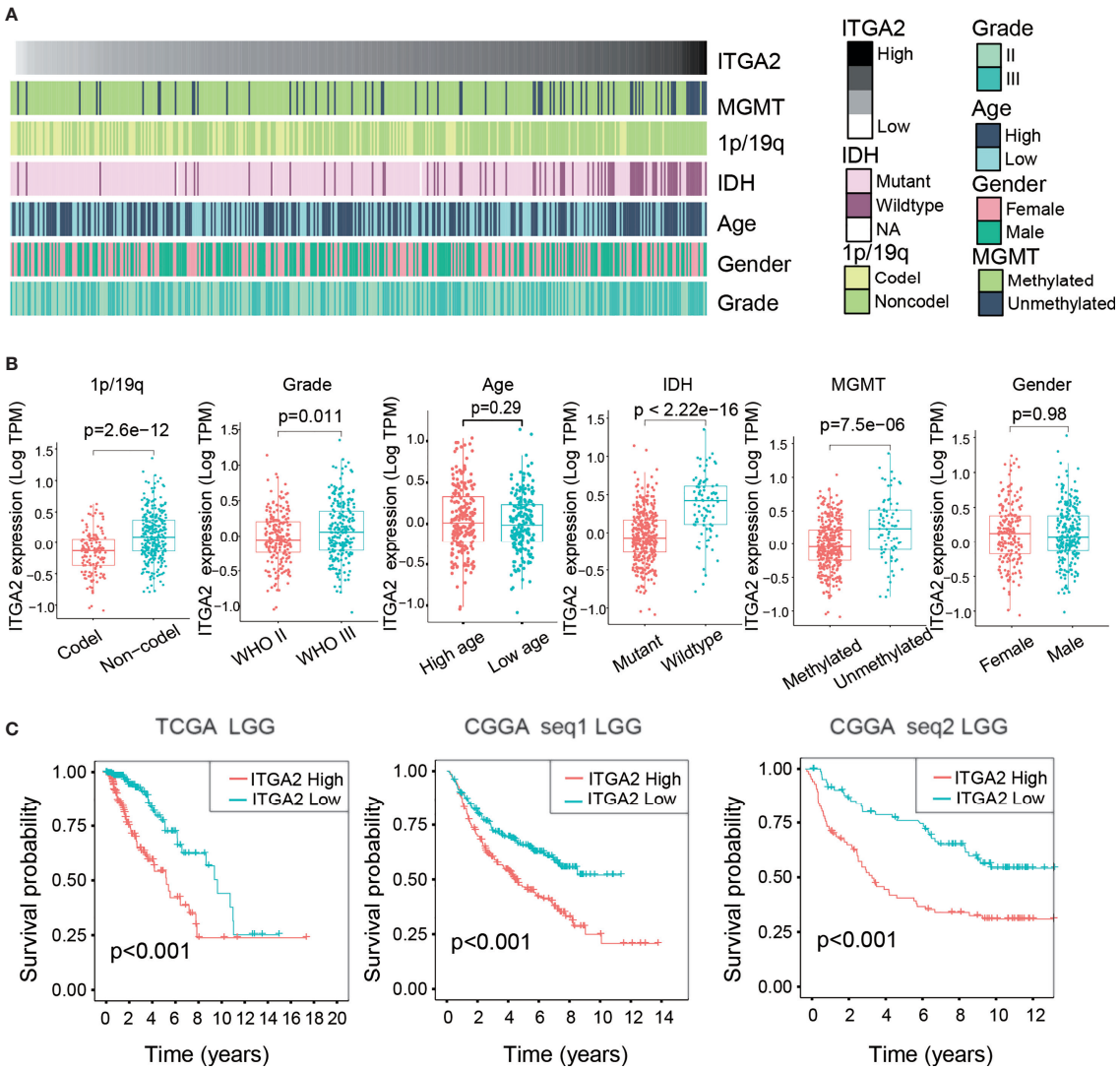

FIGURE 1 | Clinical relevance of integrin alpha-2 (ITGA2) in patients with lower-grade glioma. **(A)** Relationship between ITGA2 expression profiles and clinical features of gliomas. **(B)** Variance analysis of ITGA2 expression in various clinical traits [gender, age, grade, *IDH*, 1p/19q, and O(6)-methylguanine-DNA methyltransferase] in The Cancer Genome Atlas (TCGA) cohort. **(C)** Prognostic analysis of different ITGA2 groups in a cohort from TCGA and two cohorts from the Chinese Glioma Genome Atlas, CGGAseq1 and CGGAseq2.

University. Compared with the matched para-cancerous tissue, ITGA2 proteins were overexpressed in LGG tissues, and the ITGA2 protein levels were also measured by ImageJ software (**Figure 3D**). We found that the knockdown of ITGA2 did not induce any statistically meaningful change in SW-1088 cell proliferation (**Figure 3E**). However, it reduced the invasion ability of SW-1088 cell. The number of invasion cells was qualified by Image J software (**Figure 3F**). The verification that ITGA2 was knocked down by siRNA at the protein level is shown in **Supplementary Figure S4**. Lastly, ITGA2 protein expressions were revealed by immunofluorescence staining. It was found that ITGA2 was mainly located in the cytoplasm and cell membrane (**Figure 3G**). These results demonstrated that ITGA2 was a risk factor in LGGs.

Enrichment Analysis of ITGA2-Related Genes

To explore the impact of ITGA2 on the prognosis of LGGs in more detail, we made a differential expression analysis of all genes according to the ITGA2 expression, and we screened out the 2,486 DEGs [|log2 (fold change)| >1 and P <.05]. These DEGs were mainly used for GO-BP and KEGG analyses. The GO-BP study indicated that these DEGs enriched in co-translational protein biomarkers to membrane pathways, viral gene expression, and neutrophil activation involved in the immune response process, oxidative phosphorylation, and more (**Figure 4A**). The KEGG pathway research manifested that these DEGs were related to coronavirus disease of 2019, the severe acute respiratory syndrome coronavirus that has

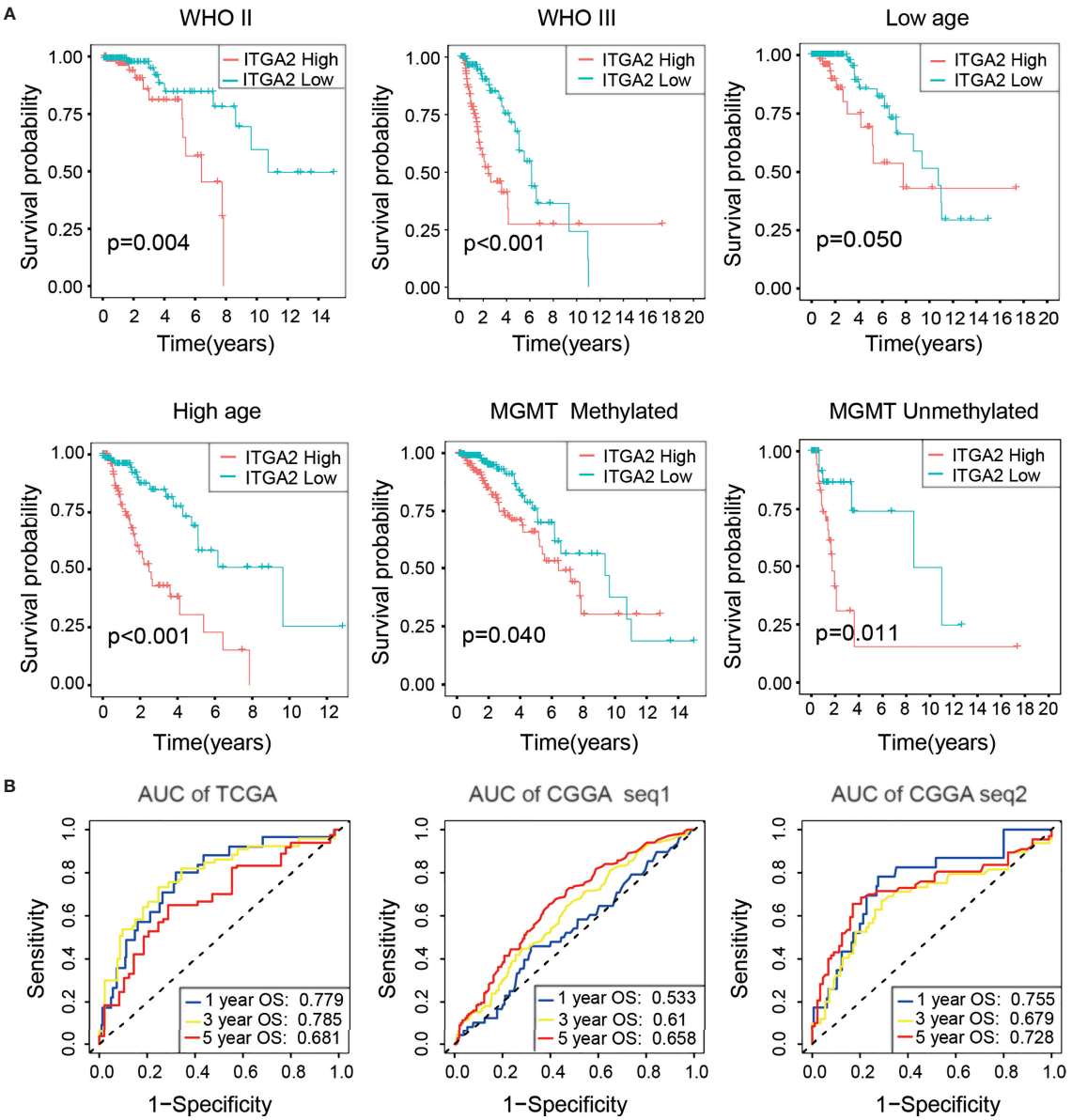

FIGURE 2 | Verification of the prognostic value of integrin alpha-2 in three cohorts. **(A)** Kaplan–Meier overall survival curves of patients with lower-grade glioma grouped by integrin alpha-2 expression in The Cancer Genome Atlas (TCGA) dataset and stratified by World Health Organization grade, age, and O(6)-methylguanine-DNA methyltransferase status. **(B)** Time-dependent receiver operating characteristic curves for the prognostic model in a cohort from TCGA and two cohorts from the Chinese Glioma Genome Atlas, CGGAseq1 and CGGAseq2 (for predicting 1-, 3-, and 5-year overall survival).

spread across the world (26) and associated with regulation of the actin cytoskeleton, proteoglycans in cancer, hypoxia-inducible factor 1 signaling pathway, and cell adhesion molecules (**Figure 4B**). The GSEA analysis indicated that tumor hallmarks were enriched in high ITGA2 expression subgroup, such as the ensheathment of neurons pathway, regulation of lamellipodium organization pathway, tissue regeneration pathway, cortical actin cytoskeleton organization pathway, glial cell development pathway, and fucose metabolic process pathway (**Figure 4C**). These data may offer some clues that could find the potential mechanisms of ITGA2 in LGG.

ITGA2 as an Independent Prognostic Factor in Patients With LGG

We applied univariate and multivariate Cox regression analyses to estimate whether ITGA2 could be an independent prognostic factor in the training set and validating sets. Univariate Cox regression analysis indicated that ITGA2 was meaningfully

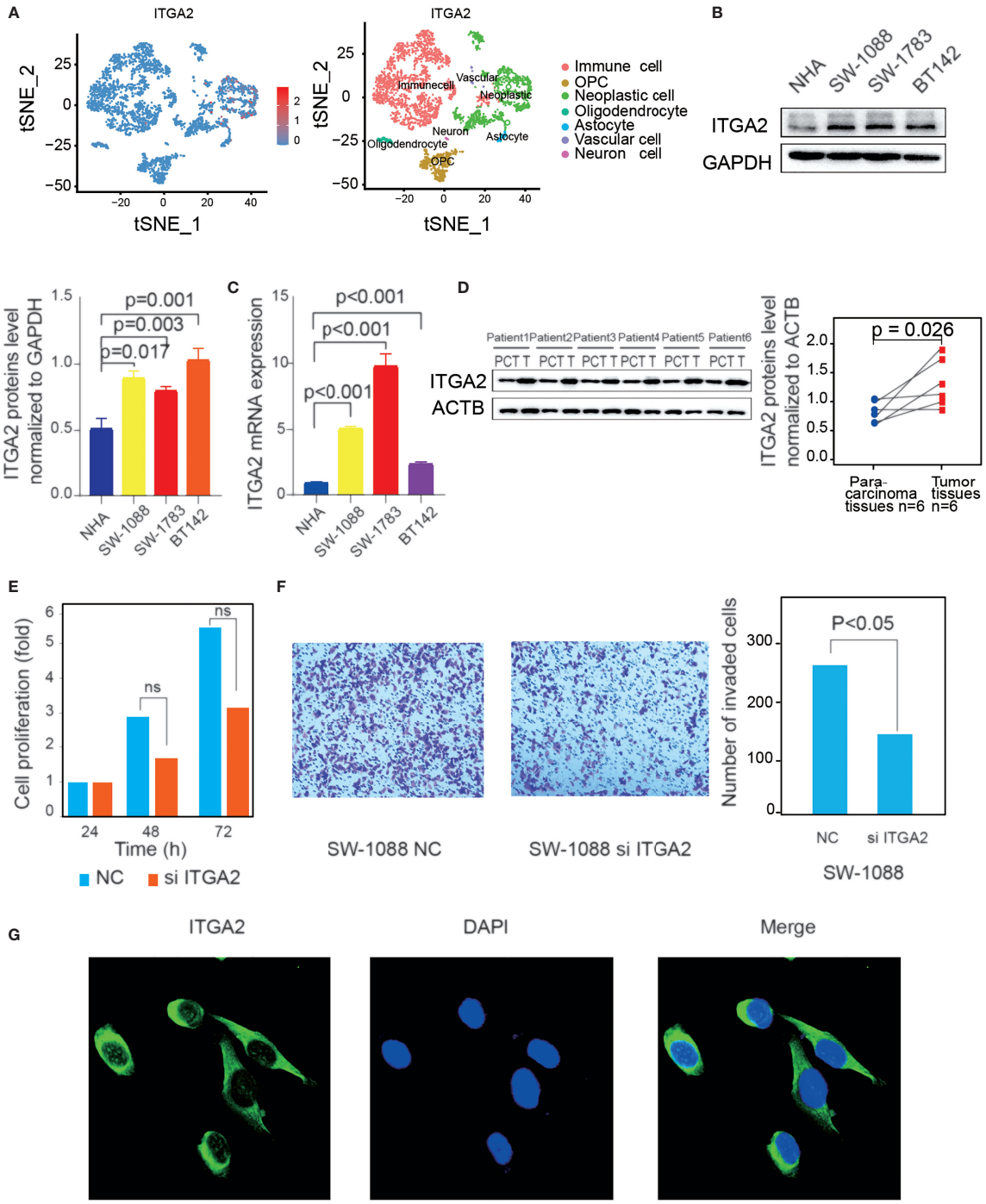

FIGURE 3 | Verification of the high expression of integrin alpha-2 (ITGA2) in lower-grade gliomas (LGGs) and immunofluorescence of ITGA2. **(A)** Expression abundance of ITGA2 gene in different color-labeled cell types. **(B)** Western blot (WB) and **(C)** quantitative real-time polymerase chain reaction analysis of ITGA2 expression in LGG cell lines and normal glial cells (NHA). WB was repeated in three independent experiments. **(D)** Western blot analysis of ITGA2 expression in six paired LGG tissues and the match para-carcinoma tissue of the same patient. The ITGA2 protein expression levels were quantified by ImageJ software. WB was repeated in three independent experiments. **(E)** The effect of ITGA2 knockdown on SW1088 cell proliferation. Paired *t*-test was used to analyze. [ns (nonsense)] **(F)** The trans-well assays of SW1088 cell line under the knockdown of the ITGA2. The quantitative analysis of the transwell invasion assays performed by Image J Paired *t*-test was used to analyze. **(G)** SW-1088 cells were treated with the rabbit anti-ITGA2 (green) at 4°C overnight, and nucleus stained by DAPI. The protein plots were cut by the original bands.

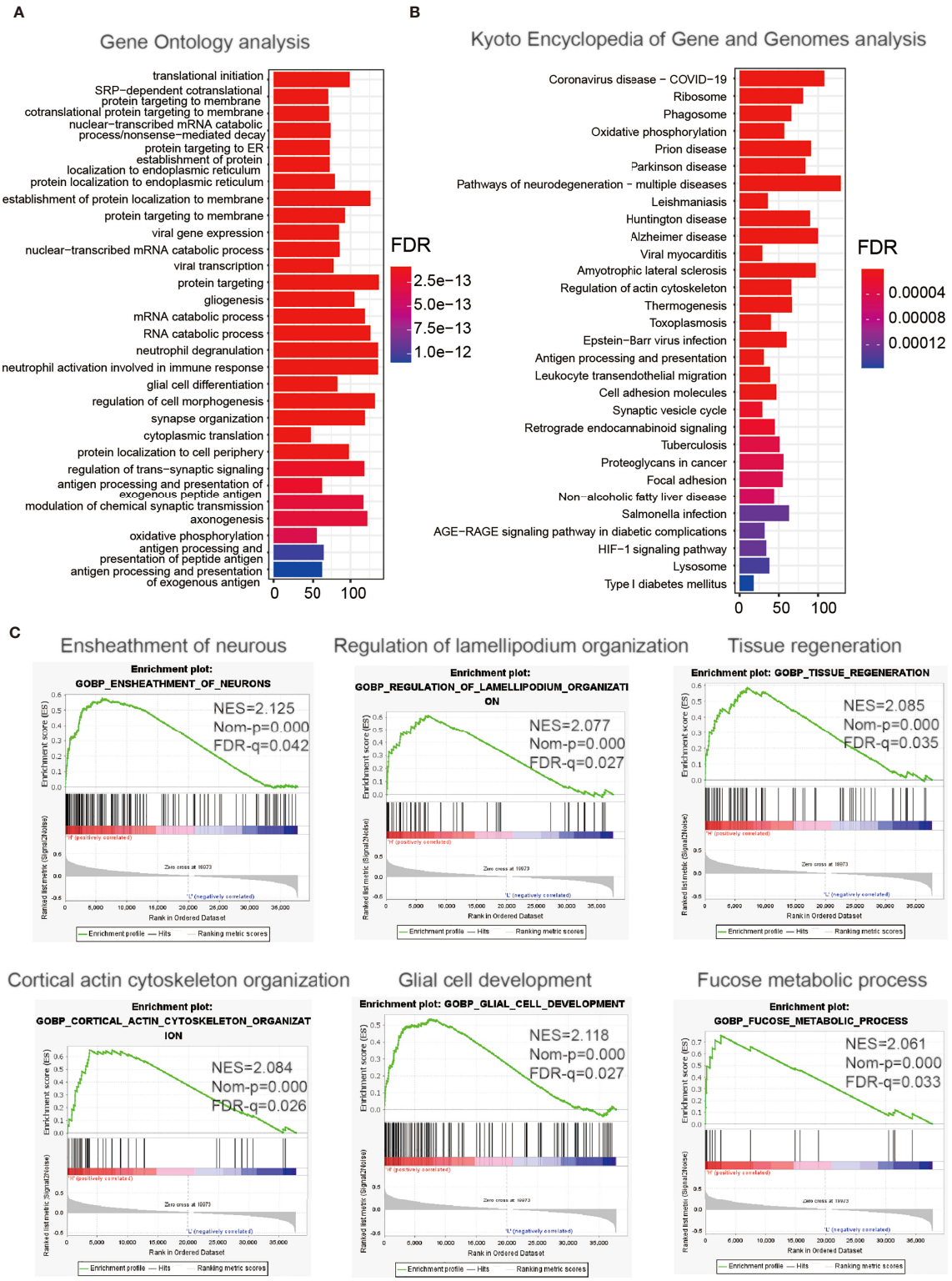

FIGURE 4 | Enrichment analysis of integrin alpha-2-related genes. Functional analysis of 2,486 differentially expressed genes between the low- and high-expression groups. **(A)** Gene Ontology analysis of biological processes. **(B)** Kyoto Encyclopedia of Genes and Genomes pathway analysis. **(C)** Gene Set Enrichment Analysis.

correlated with clinical prognosis in patients with LGG in the TCGA cohort (hazard ratio, 2.2268; 95% CI, 1.7136–2.8936; P <.001; **Supplementary Table S2**). The multivariate Cox regression analysis then revealed that ITGA2 is an independent and powerful prognostic factor in TCGA datasets (hazard ratio, 2.0269; 95% CI, 1.1782–3.4871; P <.05; **Supplementary Table S2**). Similar results were obtained from the CGGA datasets (**Supplementary Table S2**). These results suggest that ITGA2 can be used as an independent clinical prognostic factor to predict OS for patients with LGG depending on the outcomes of the multivariate Cox regression analysis.

Construction and Confirmation Clinical Nomogram in Patients With LGG

To produce a clinically usable and quantitative tool to predict the 1-, 3-, and 5-year OS of patients with LGG, we created a nomogram model using the ITGA2 expression and the WHO grade along with the outcomes of the multivariate Cox regression analysis (**Figure 5A**). The total points in the nomogram model forecast the 1-, 3-, and 5-year OS for patients with LGG. Then, we performed calibration curves to estimate the predictive ability of the nomogram model, and DCA was used to judge the net benefit for patients with LGG. The calibration curves of the nomogram model had a significant prediction accuracy for forecasting the 1-, 3-, and 5-year OS in the TCGA dataset (**Figure 5B**). The C-index reflects the predictive power of the nomogram between the TCGA dataset and the CGGA datasets; the results displayed a steady and powerful predictive power (**Figures 5C, D)**. The C-index for the TCGA dataset was 0.804; for the CGGAseq1 dataset, 0.716; and for the CGGAseq2 dataset, 0.794. The DCA curves revealed that the clinical nomogram had robust accuracy for 1-, 3-, and 5-year OS compared with the other predictors in the TCGA cohort. In addition, the net benefit of the nomogram model was usually better than that of other predictors at various thresholds (**Figures 5E–G**). These powerful results prove that the nomogram model is accurate for use in patients with LGG, so this model may help identify high-risk patients in the future.

The Correlation Analysis of Immune Infiltration

To explore the relationship between immune infiltration and ITGA2 expression, we carried out the ssGSEA algorithm to quantify the enrichment of the 29 immune-associated signatures. Compared with the low-ITGA2-expression group, we found that the fraction of most immune-related signatures in the high-ITGA2-expression group was relatively higher (P < 0.05, **Figure 6A**). In addition, most of the immune features, such as presence of major histocompatibility class I, type I interferon response, and human leukocyte antigen status, were positively correlated with ITGA2 expression. The relevant abundance of the most of infiltrating immune cells increased as ITGA2 expression increased in the TCGA datasets (**Figure 6B**). Next, using the estimate algorithm to acquire the immune scores and stromal scores of patients with LGG, we implemented a differential analysis between the immune-related scores and ITGA2 expression. The results elucidated that ITGA2 was markedly correlated with immune infiltration: the immune-related scores were significantly different (P <.001) between the low- and high-ITGA2-expression subgroups (**Figure 6C**). These results indicated that ITGA2 is an immune gene that may have a certain impact on the prognosis of LGG.

Analysis of the Correlation Between Immune Checkpoint and ITGA2 Expression Level

To detect the expression differences of various immune checkpoints between the subgroups with high and low ITGA2 expression in patients with LGG, we performed a differential study in the TCGA cohort. The result showed that most of the immune checkpoints, except the cluster of differentiation 163 and lymphocyte-activation-gene-3, differed significantly between the two subgroups (**Figure 7A**). To better understand the internal relationship between ITGA2 and known immune checkpoints, a correlation analysis was performed between ITGA2 and immune checkpoint expression in the TCGA cohort; we found that ITGA2 was prominently correlated with C-C motif ligand 2, programmed cell death 1 ligand 1 (PD-L1), cluster of differentiation 276, interleukin 1 A, programmed death 1 (PD1), cytotoxic lymphocyte antigen 4 (CTLA4), programmed cell death 1 ligand 2, and transforming growth factor beta 1 (**Figure 7B**). However, the correlation is insufficient, and the mechanism of ITGA2 at the immunosuppressive point still needs to be further explored.

The Prediction of Clinical Immune Response Patients With Gliomas

More independent cohorts ought to take for reverification the validated prognostic value of ITGA2. Therefore, we took the anti-PDL1 (IMvigor210) cohort for further validating the prognostic value of ITGA2. The anti-PD-L1 clinical response was grouped in progressive disease (PD), stable disease (SD), partial response (PR), and complete response (CR). Compared with the high-ITGA2 group, the prominent intensity of treatment and anti-PD-L1 immunotherapy response of the low-ITGA2 group were also validated (**Figures 8A–C**). The Kaplan–Meier survival curves suggested a consistent trend that patients with high ITGA2 expression level had poor outcomes (**Figure 8A**). We discovered that ITGA2 had significant differences between the CR and PD groups (P <.05, **Figure 8B**). ITGA2 had also meaningful differences between the CR/PR and SD/PD groups (P <.05, **Figure 8C**). In the anti-PD-L1 cohort, the proportions of CR, PR, SD, and PD were 10.11, 16.85, 21.35, and 51.69% in the low-ITGA2 group and 5.83, 10.83, 20.83, and 62.50% in the high-ITGA2 group, respectively. The proportions of CR/PR and SD/PD were 73.03 and 26.97% in the low-ITGA2 group and 83.33 and 16.67% in the high-ITGA2 group, respectively. The proportions of high ITGA2 expression in the CR, PR, SD, and PD groups were 28.00, 30.23, 28.00, and 44.91%, and the proportions of low ITGA2 expression in the CR, PR, SD, and PD groups were 72.00, 69.77, 30.32, and 55.09%, respectively (**Figure 8D**). In addition, we also

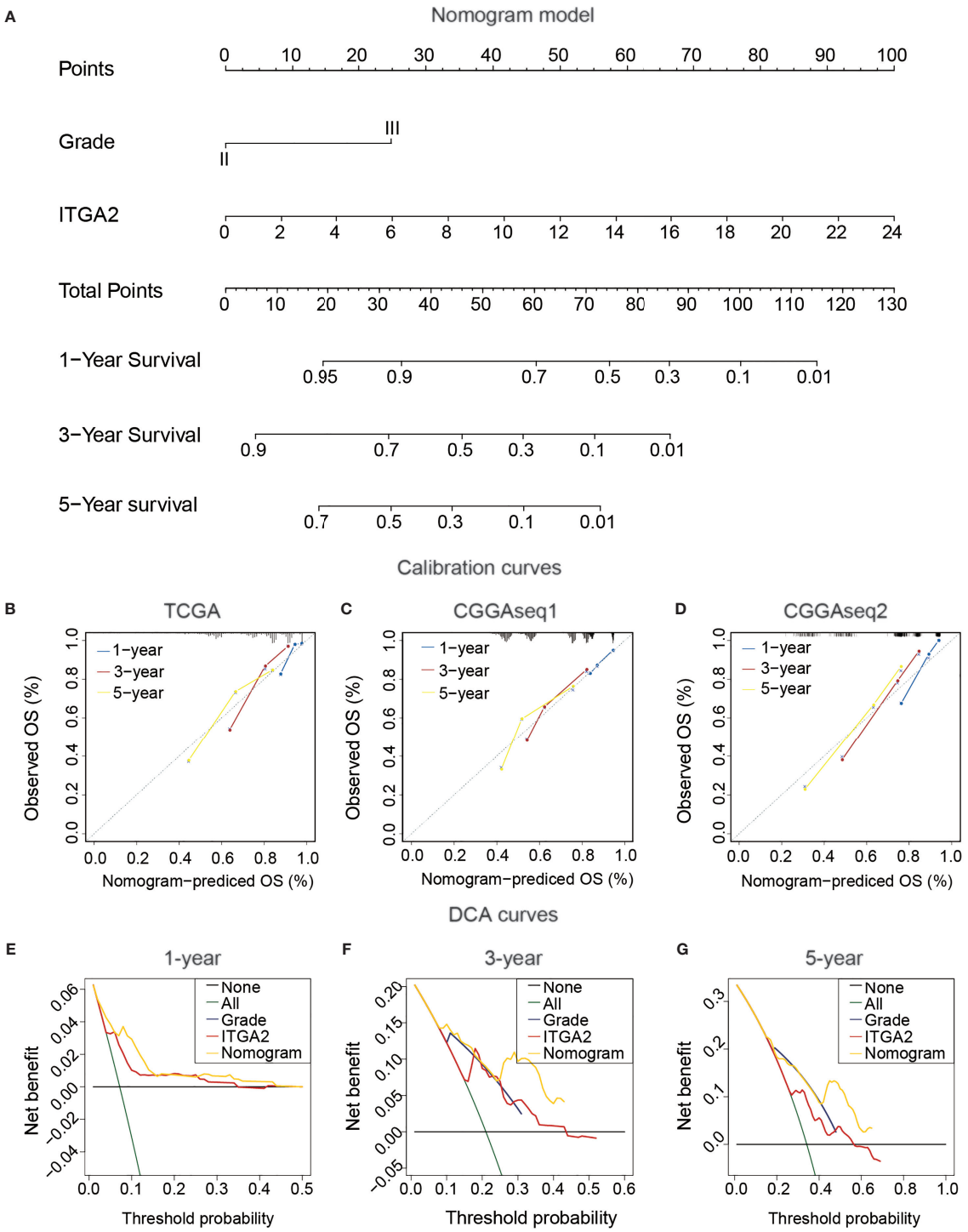

FIGURE 5 | Construction and confirmation clinical nomogram in patients with lower-grade glioma. **(A)** The Cancer Genome Atlas (TCGA) nomogram model of clinical features, including *IDH* status, 1p19q status, grade, and integrin alpha-2 expression. **(B)** TCGA calibration plots of the nomogram. **(C, D)** The validation of the TCGA nomogram in Chinese Glioma Genome Atlas CGGAseq1 and CGGAseq2. **(E–G)** The validation of Decision Curves Analysis (DCA) in TCGA cohort. (for estimating 1, 3, and 5-year OS).

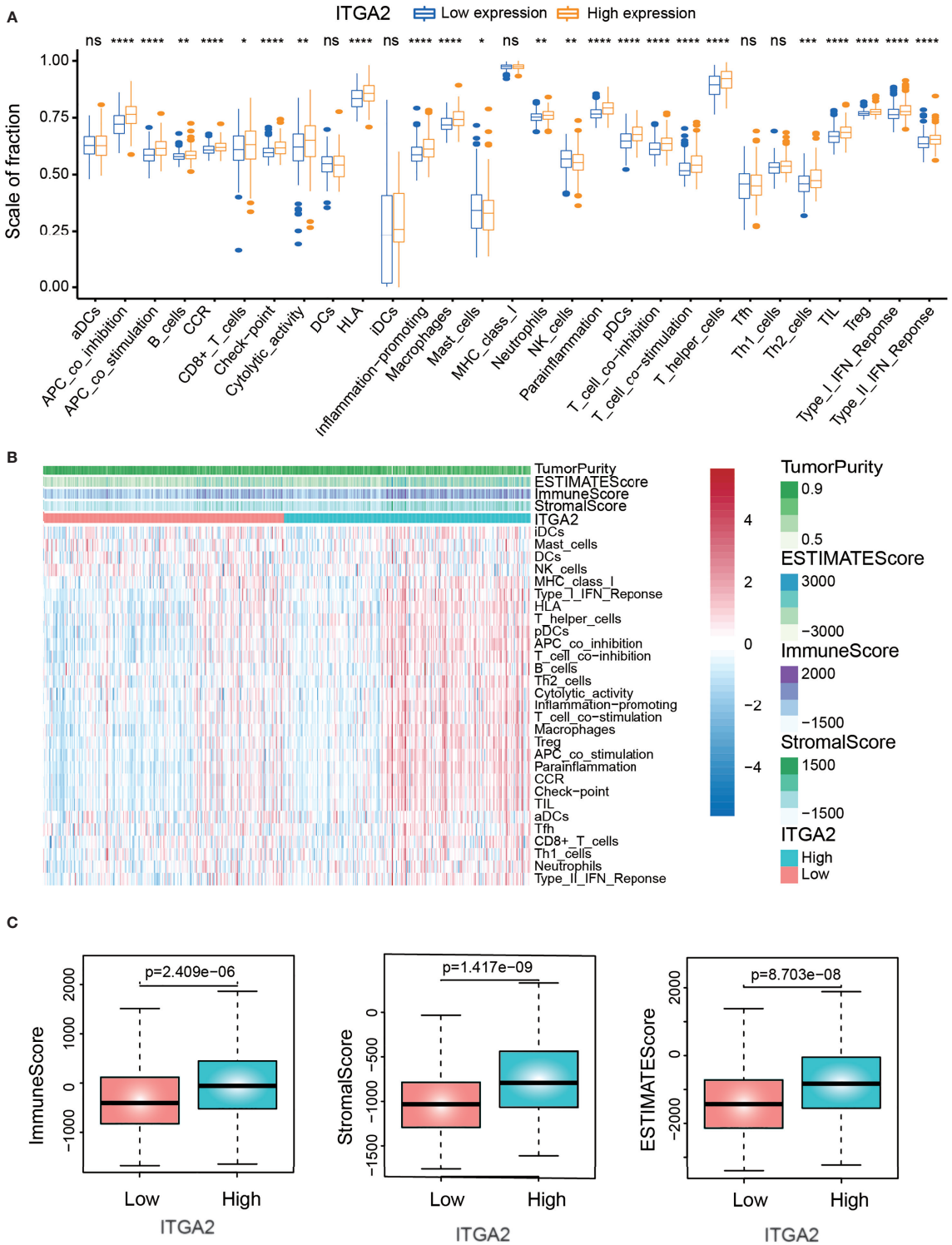

FIGURE 6 | The correlation analysis of immune infiltration. **(A)** The differences of immune-related cells between low-expression integrin alpha-2 (ITGA2) and high-expression ITGA2 groups. **(B)** Heat map demonstrating the correlation between the expression of the ITGA2 genes and immune infiltration. **(C)** Correlation analysis between the expression of the ITGA2 gene and immune-related score (immune score, stromal score, and estimate score). *p < 0.05, **p < 0.01, ***p < 0.001, ****p < 0.0001. ns (nonsense)

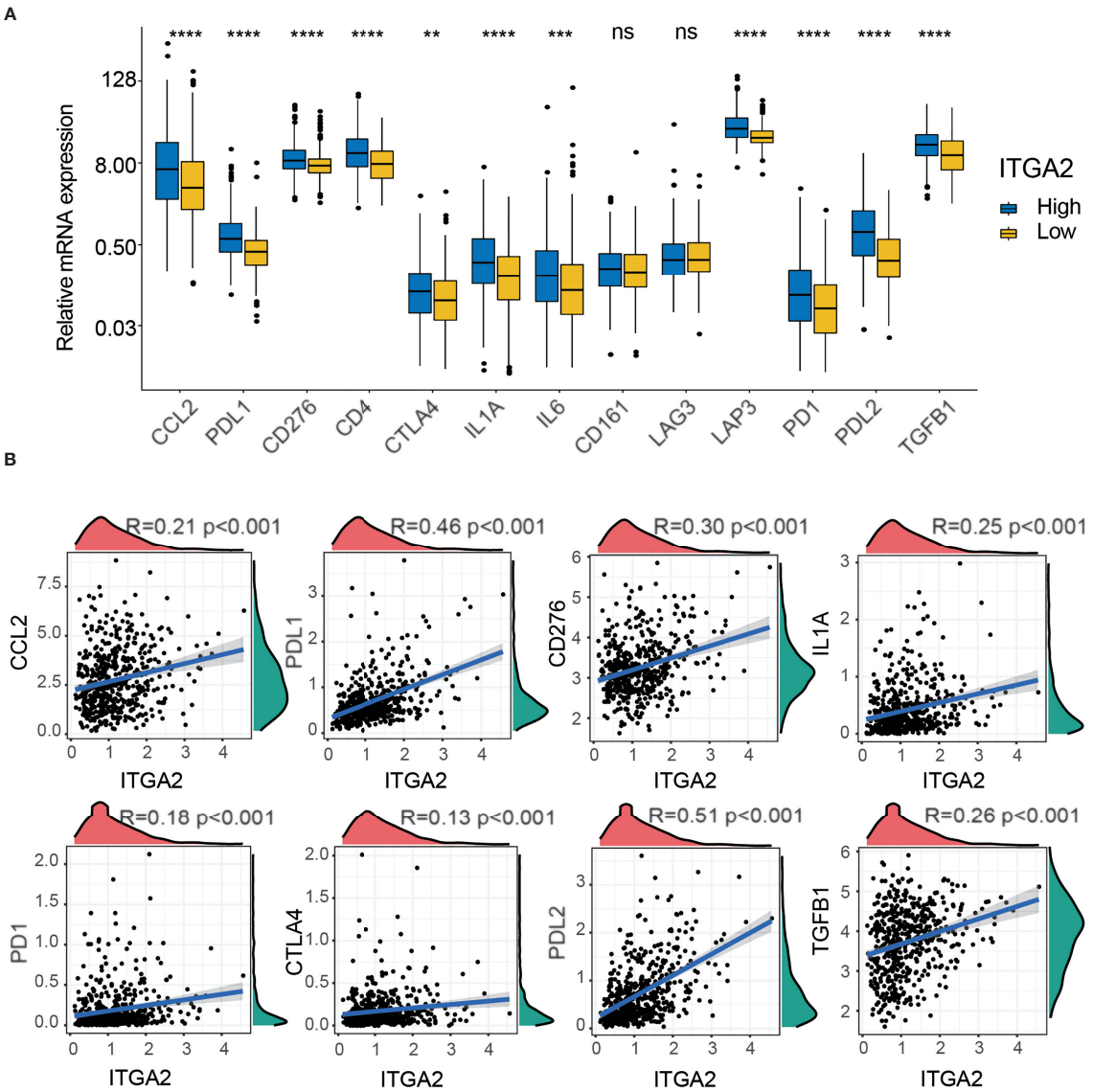

FIGURE 7 | The correlation profiling of immune checkpoints. **(A)** Differential analysis of several immune checkpoint expression levels between high- and low-integrin alpha-2 (ITGA2) expression levels. **(B)** Correlation analysis between ITGA2 and eight selected immune checkpoint expression levels. **p < 0.01, ***p < 0.001, and ****p < 0.0001. ns (nonsense).

took the GSE78220 cohort and the GSE91061 cohort to predict the prognosis of ITGA2 in melanoma (**Supplementary Figure S3**). Due to the small sample size in the GSE78220 cohort, its results were not significant (**Supplementary Figure S3A**). In the GSE91061 cohort, the patients with high ITGA2 expression level have a poor outcome (**Supplementary Figure S3B**). Although the proportion analysis was not meaningless, the data were still different (**Supplementary Figure S3B**).

Based on the TCGA database, we also performed TIDE algorithm to reflect the different responses of patients to immunotherapy. In the previous study, the abundance of cancer-associated fibroblasts cells (CAFs), myeloid-derived suppressor cells (MDSCs), and the M2 subtype of tumor-associated macrophages (TAMs) can reflect the degree of T cell exclusion (24). Firstly, ITGA2 was positively interrelated to the T cell exclusion score (**Figure 8E**). Meanwhile, CAFs, MDSCs, and TAMs were also significantly different in the low- and high-ITGA2 groups (**Figure 8F**). Additionally, the results suggested that the higher TIDE score was accompanied by a negative clinical immune response, and the patients with low ITGA2 expression level had a more excellent clinical response than the high-ITGA2 group (**Figure 8G**). The proportions of response (R) and no-response (NR) were 31.03 and 68.97% in the low-ITGA2 group and 23.15 and 76.85% in the high-ITGA2 group, respectively. The proportions of low ITGA2 expression in the R and NR groups were 57.27 and 47.30%, and the proportions of

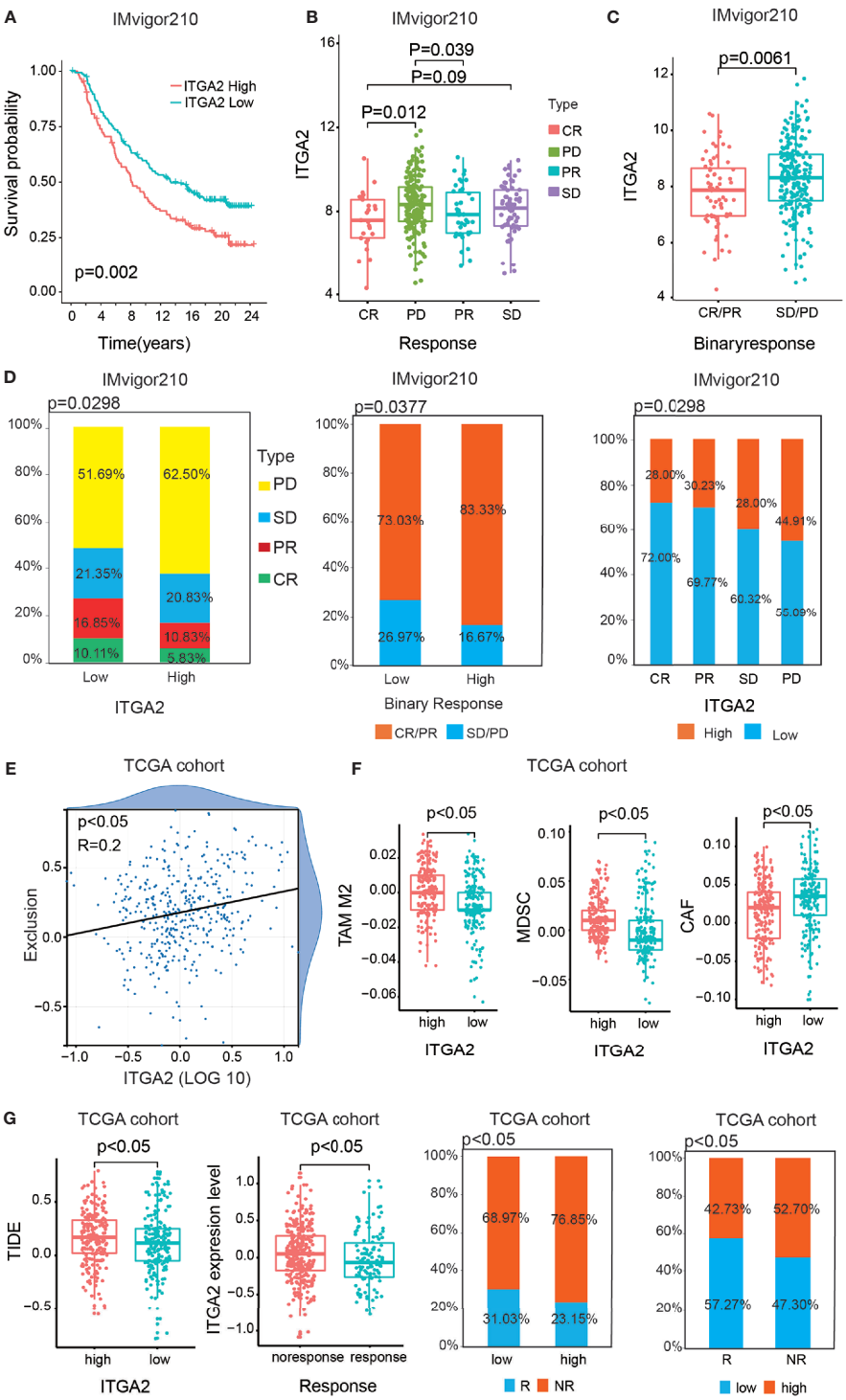

FIGURE 8 | The statistics analysis of ITGA2 in the anti-PD-L1 (IMvigor210) cohort. **(A)** Kaplan–Meier overall survival (OS) curves of patients regarding the response of anti-PD-L1 (IMvigor210) cohort grouped by integrin alpha-2 (ITGA2) expression. **(B)** The variance analysis of ITGA2 in the distinct anti-PD-L1 clinical response groups. **(C)** The variance analysis of ITGA2 in the binary response. **(D)** The proportion analysis between ITGA2 subgroups and the distinct anti-PD-L1 clinical response groups. Chi-square test was used for data analysis. **(E)** The correlation analysis between ITGA2 expression level and the abundance of T cell exclusion. **(F)** The variance analysis of the TAM M2, MDSC, and CAF cells in the low- and high-ITGA2 groups. **(G)** The variance analysis of ITGA2 in the clinical responses and the variance analysis between ITGA2 subgroups and TIED score. The proportion analysis between clinical response groups and ITGA2 subgroups. Chi-square test was used for data analysis.

high ITGA2 expression in the R and NR groups were 42.73 and 52.70%, respectively. These results indicate that LGG was realized as immune escape by preventing T cell infiltration, and the patients with low ITGA2 expression have a considerable immunotherapeutic response, which may be related to tumorigenesis and benefit by immunotherapies (27).

DISCUSSION

We studied 998 glioma samples from TCGA and CGGA cohorts to validate ITGA2 as a novel biomarker for LGG in both cohorts. The treatment of glioma demands on a multidisciplinary method, including neuroimaging, surgery, neuropathology, radiotherapy, chemotherapy, and supportive therapy (28). Clinical data from LGG patients are rare because of the low incidence rate, high mortality rate, and heterogeneity of multiple tumor subtypes (29). Therefore, traditional treatment is not always successful for patients with glioma, so it is urgent and pivotal to search for new molecular biomarkers to improve the prognostic outcome of patients with glioma. We undertook a series of systematic analyses to verify the prognostic value of ITGA2. First, we conducted a prognostic survival analysis and a relevant analysis of clinical and molecular characteristics for patients with LGG from three datasets. The patients with LGG with a higher ITGA2 expression had a worse prognostic clinical outcome compared with patients in the low-expression group. Next, ROC curves were used to judge the predictive power of the prognostic robustness in patients with LGG.

We then performed GO analysis, KEGG analysis, and GSEA. We found that the cancer-related indicators were more enriched in the LGG subgroup with high ITGA2 expression compared with the subgroup of low expression. Univariate and multivariate Cox regression analyses were used to prove the independent prognostic role of ITGA2 in LGG. In addition, we set up a nomogram model to forecast the prognosis outcome for patients with LGG depending on the outcomes of the multivariate Cox regression analysis; this model was validated by calibration curves and DCA. DCA is a novel statistical method that graphically describes the net benefit for patients at various thresholds. DCA was used to evaluate whether the nomogram model had utility in supporting clinical decisions and to determine which factors led to the best decisions. Therefore, DCA was an essential validation tool for clinical usefulness (30). Using the nomogram model, a neurosurgeon can better forecast the outcome of patients with LGG. To better comprehend the internal connections between immune infiltration and ITGA2 expression, we analyzed the levels of the immune score, stromal score, and estimate score between subgroups with low and high ITGA2 expression. The results suggest that ITGA2 is clearly related to immune cell infiltration. Finally, RT-qPCR and western blot were utilized to detect ITGA2 protein expression and mRNA expression in all three LGG cell lines (SW1088, SW1783, and Bt142) and in the NHA cell line; the results indicate that ITGA2 was expressed more in LGG.

The advantages of this study included the analysis of comprehensive clinical data from 999 LGG patients and IMvigor210 (n = 298) cohort. The construct of a nomogram model was validated in two external, independent LGG cohorts. The ITGA2-related signature has a strong and steady prognostic value, so it may be successful for clinical application. This study provides a powerful clue about predicting the prognosis and diagnosis of LGG patients. Nevertheless, the study has some limitations. More independent LGG cohorts ought to be taken for reverification of the validated prognostic value of ITGA2. For an expanded clinical application, the mechanism explaining the role that ITGA2 plays in affecting tumorigenesis and LGG development, specifically, must be determined. In addition, experimental studies, *in vitro* and *in vivo*, should be accomplished to explore the correlation between ITGA2-related signatures and outcome in patients with LGG.

It is now clear that TME contains not only cancer cells but also immune cells, stromal cells, endothelial cells, and cancer-related fibroblasts (31). After TME is formed, numerous immune cells can chemotax to there (32). Immunocytes may also produce a certain effect on tumors in a subtle way. TME has progressively been shown to indicate abnormal tissue function and to play a vital role in the subsequent progress of malignancies (33). In the recent years, immunotherapy has become a new research hotspot that can stimulate the actions of some immune cells in the TME to engender unknown effects on tumors. In addition, immune checkpoints block (ICB) treatment has become a new method to treat all kinds of cancers (34), especially the study of CTLA-4 and PD-1/PD-L1 molecules. In previous studies, some experts have already investigated a new mechanism by which ITGA2 plays a key role in regulating cancer immune response (35). Besides this, clinical studies have been carried out in lung cancer, prostate cancer, colorectal cancer, and melanoma treatment by ICB (36). It brings new challenges to the immunotherapy of gliomas. We found that ITGA2 may be interrelated to the immune response mechanism of cancer cells and was interrelated with TME. The proportion of immune cell infiltration in LGG was significantly correlated with clinical outcome. These details suggested that targeting ITGA2 may be an effective approach to improve the curative effect of cancer checkpoint immunotherapy. The results may offer some ideas for future research, concentrating on the mechanism of immune response processes.

It is reported that the abnormal expression of ITGA2 is involved in many cancers. One study indicates that a higher ITGA2 protein level was detected in breast cancers and that an increased expression of ITGA2 was positively bound up with increased metastatic ability in breast cancer (35). Another study showed that ITGA2 was highly expressed and may have had an extensive impact on colon cancer through interacting with transcription factors (37). In contrast to the expression in normal tissues, experts found that the mRNA expression of ITGA2 in gastric cancer was obviously increased. These results verified that targeting ITGA2 with antibodies not only inhibited cell migration but also induced an effect of apoptosis on gastric cancer cells (38). In contrast to normal glial cells, we also discovered that ITGA2 was notably upregulated in human LGG tumor cell lines. Growing evidence indicates that ITGA2 participates in the process of cancer pathogenesis and development. Therefore, we predict that

ITGA2 may exert an influence on apoptosis, proliferation, and invasion in LGG. The existing standard treatments for LGG have limited effectiveness because of the aggressiveness of LGG and its resistance to chemotherapy. Thus, the discovery of a novel biomarker for patients with LGG is urgently needed. Comprehensive and systematic analyses revealed that ITGA2 may be a potential prognostic and predictive biomarker for LGG, which can bring new insights into targeted therapy. Moreover, ITGA2 was connected to immune infiltration; these data can provide researchers with new ideas about immunity in relation to the prognosis and diagnosis of patients with LGG. In conclusion, targeting ITGA2 may be a prospective immunotherapy to enhance the survival outcomes of patients with LGG.

CONCLUSION

We suggested that ITGA2 can be a prognostic and predictive biomarker for patients with LGG. This study offered some ideas for future research, concentrating on the mechanism of glioma progression.

DATA AVAILABILITY STATEMENT

The datasets presented in this study can be found in online repositories. The names of the repository/repositories and accession number(s) can be found in the article/**Supplementary Material**.

ETHICS STATEMENT

The studies involving human participants were reviewed and approved by the Ethics Committee of the Second Affiliated Hospital of Nanchang University. The patients/participants provided their written informed consent to participate in this study. Written informed consent was obtained from the individual(s) for the publication of any potentially identifiable images or data included in this article.

AUTHOR CONTRIBUTIONS

LL and ZT took the lead in writing the manuscript and figure production. LW, XZ, and KH supervised the work. JL contributed to data collection. KL, PW, ML, CG, and XL made important revisions to the paper. All authors contributed to the article and approved the submitted version.

FUNDING

The current study was funded by the National Natural Science Foundation (grant nos. 81860448 and 82002660), the Natural Science Foundation of Jiangxi Province (grant no. 20192BAB205077), and the Jiangxi Province Department of Education Science and Technology Research Project, China (grant no. GJJ190018).

SUPPLEMENTARY MATERIAL

The Supplementary Material for this article can be found online at: https://www.frontiersin.org/articles/10.3389/fonc.2021.738651/full#supplementary-material

Supplementary Table 1 | Clinical molecular information of patients with glioma involved in this study.

Supplementary Table 2 | Univariate and multivariate Cox regression analyses based on clinical features (gender, age, grade, *IDH*, 1p/19q, and ITGA2) in three cohorts.

Supplementary Figure 1 | Variance analysis of ITGA2 expression in various clinical traits. **(A, B)** Variance analysis of integrin alpha-2 (ITGA2) expression in various clinical traits (gender, age, grade, *IDH*, 1p/19q, and MGMT) in Chinese Glioma Genome Atlas CGGAseq1 and CGGAseq2 cohorts.

Supplementary Figure 2 | The prognostic analysis of integrin alpha-2 in the Chinese Glioma Genome Atlas (CGGA) cohorts. **(A, B)** Kaplan–Meier overall survival curves of patients with lower-grade glioma grouped by integrin alpha-2 (ITGA2) expression in the CGGA CGGAseq1 and CGGAseq2 datasets, stratified by World Health Organization grade, age, and O(6)-methylguanine-DNA methyltransferase status.

Supplementary Figure 3 | The statistics analysis of integrin alpha-2 in GSE78220 and GSE91061 cohorts. **(A)** Kaplan–Meier overall survival (OS) curves of patients regarding the response of the anti-PD1 (GSE78220) cohort grouped by ITGA2 expression and the proportion analysis between clinical responses and ITGA2 subgroups. **(B)** Kaplan–Meier OS curves of patients regarding the response of the anti-PD1 and anti-CTLA4 (GSE91061) cohort grouped by ITGA2 expression and the proportion analysis between clinical responses and ITGA2 subgroups.

Supplementary Figure 4 | The verification of integrin alpha-2 knockdown at the protein level.

REFERENCES

1. Furnari FB, Fenton T, Bachoo RM, Mukasa A, Stommel JM, Stegh A, et al. Malignant Astrocytic Glioma: Genetics, Biology, and Paths to Treatment. *Genes Dev* (2007) 21(21):2683–710. doi: 10.1101/gad.1596707
2. Miller AM, Shah RH, Pentsova EI, Pourmaleki M, Briggs S, Distefano N, et al. Tracking Tumour Evolution in Glioma Through Liquid Biopsies of Cerebrospinal Fluid. *Nature* (2019) 565(7741):654–8. doi: 10.1038/s41586-019-0882-3
3. Forst DA, Nahed BV, Loeffler JS, Batchelor TT. Low-Grade Gliomas. *Oncologist* (2014) 19(4):403–13. doi: 10.1634/theoncologist.2013-0345
4. Taylor MA, Das BC, Ray SK. Targeting Autophagy for Combating Chemoresistance and Radioresistance in Glioblastoma. *Apoptosis* (2018) 23 (11-12):563–75. doi: 10.1007/s10495-018-1480-9
5. Pan Q, Wang L, Chai S, Zhang H, Li B. The Immune Infiltration in Clear Cell Renal Cell Carcinoma and Their Clinical Implications: A Study Based on TCGA and GEO Databases. *J Cancer* (2020) 11(11):3207–15. doi: 10.7150/jca.37285

6. Adorno-Cruz V, Liu H. Regulation and Functions of Integrin Alpha2 in Cell Adhesion and Disease. *Genes Dis* (2019) 6(1):16–24. doi: 10.1016/j.gendis.2018.12.003
7. . <Integrin α2 I-domain Is a binding site for collagens.pdf>.
8. Yang Q, Bavi P, Wang JY, Roehrl MH. Immuno-Proteomic Discovery of Tumor Tissue Autoantigens Identifies Olfactomedin 4, CD11b, and Integrin Alpha-2 as Markers of Colorectal Cancer With Liver Metastases. *J Proteomics* (2017) 168:53–65. doi: 10.1016/j.jprot.2017.06.021
9. Ferraro A, Boni T, Pintzas A. EZH2 Regulates Cofilin Activity and Colon Cancer Cell Migration by Targeting ITGA2 Gene. *PloS One* (2014) 9(12): e115276. doi: 10.1371/journal.pone.0115276
10. Wang L, Gao Y, Zhao X, Guo C, Wang X, Yang Y, et al. HOXD3 was Negatively Regulated by YY1 Recruiting HDAC1 to Suppress Progression of Hepatocellular Carcinoma Cells *via* ITGA2 Pathway. *Cell Prolif* (2020) 53(8): e12835. doi: 10.1111/cpr.12835
11. Ding W, Fan XL, Xu X, Huang JZ, Xu SH, Geng Q, et al. Epigenetic Silencing of ITGA2 by MiR-373 Promotes Cell Migration in Breast Cancer. *PloS One* (2015) 10(8):e0135128. doi: 10.1371/journal.pone.0135128
12. Guo P, Moses-Gardner A, Huang J, Smith ER, Moses MA. ITGA2 as a Potential Nanotherapeutic Target for Glioblastoma. *Sci Rep* (2019) 9(1):6195. doi: 10.1038/s41598-019-42643-7
13. Mariathasan S, Turley SJ, Nickles D, Castiglioni A, Yuen K, Wang Y, et al. Tgfβ Attenuates Tumour Response to PD-L1 Blockade by Contributing to Exclusion of T Cells. *Nature* (2018) 554(7693):544–8. doi: 10.1038/nature25501
14. Wang X, Chai Z, Li Y, Long F, Hao Y, Pan G, et al. Identification of Potential Biomarkers for Anti-PD-1 Therapy in Melanoma by Weighted Correlation Network Analysis. *Genes (Basel)* (2020) 11(4):435. doi: 10.3390/genes11040435
15. Li B, R V, Stewart RM, Thomson JA, Dewey CN. Measurement of mRNA Abundance Using RNA-Seq Data: RPKM Measure Is Inconsistent Among Samples. *Bioinformatics* (2010) 26:493–500. doi: 10.1093/bioinformatics/btp692
16. Li B, Ruotti V, Stewart RM, Thomson JA, Dewey CN. RNA-Seq Gene Expression Estimation With Read Mapping Uncertainty. *Bioinformatics* (2010) 26(4):493–500. doi: 10.1093/bioinformatics/btp692
17. Ritchie ME, Phipson B, Wu D, Hu Y, Law CW, Shi W, et al. Limma Powers Differential Expression Analyses for RNA-Sequencing and Microarray Studies. *Nucleic Acids Res* (2015) 43:e47. doi: 10.1093/nar/gkv007
18. Yu G, Wang LG, Han Y, He QY. Clusterprofiler: An R Package for Comparing Biological Themes Among Gene Clusters. *OMICS* (2012) 16(5):284–7. doi: 10.1089/omi.2011.0118
19. Subramanian A, Tamayo P, Mootha VK, Mukherjee S, Ebert BL, Gillette MA, et al. Gene Set Enrichment Analysis: A Knowledge-Based Approach for Interpreting Genome-Wide Expression Profiles. *Proc Natl Acad Sci USA* (2005) 102:15545–50. doi: 10.1073/pnas.0506580102
20. Barbie DA, Tamayo P, Boehm JS, Kim SY, Moody SE, Dunn IF, et al. Systematic RNA Interference Reveals That Oncogenic KRAS-Driven Cancers Require TBK1. *Nature* (2009) 462:108–12. doi: 10.1038/nature08460
21. Charoentong FF, Angelova M, Mayer C, Efremova M, Rieder D, Hackl H, et al. Pan-Cancer Immunogenomic Analyses Reveal Genotype-Immunophenotype Relationships and Predictors of Response to Checkpoint Blockade. *Cell Rep* (2017) 18:248–62. doi: 10.1016/j.celrep.2016.12.019
22. Hanzelmann S, Castelo R, Guinney J. GSVA: Gene Set Variation Analysis for Microarray and RNA-Seq Data. *BMC Bioinf* (2013) 14:7. doi: 10.1186/1471-2105-14-7
23. Yoshihara K, Shahmoradgoli M, Martinez E, Vegesna R, Kim H, Torres-Garcia W, et al. Inferring Tumour Purity and Stromal and Immune Cell Admixture From Expression Data. *Nat Commun* (2013) 4:2612. doi: 10.1038/ncomms3612
24. Jiang P, Gu S, Pan D, Fu J, Sahu A, Hu X, et al. Signatures of T Cell Dysfunction and Exclusion Predict Cancer Immunotherapy Response. *Nat Med* (2018) 24(10):1550–8. doi: 10.1038/s41591-018-0136-1
25. Wang P, Li J, Wu M, Ye M, Huang K, Zhu X. Human Mitochondrial Ribosomal RNA Modification-Based Classification Contributes to Discriminate the Prognosis and Immunotherapy Response of Glioma Patients. *Front Immunol* (2021) 12:722479. doi: 10.3389/fimmu.2021.722479
26. Reza-Zaldivar EE, Hernandez-Sapiens MA, Minjarez B, Gomez-Pinedo U, Marquez-Aguirre AL, Mateos-Diaz JC, et al. Infection Mechanism of SARS-COV-2 and Its Implication on the Nervous System. *Front Immunol* (2020) 11:621735. doi: 10.3389/fimmu.2020.621735
27. Zhang H, He J, Dai Z, Wang Z, Liang X, He F, et al. PDIA5 Is Correlated With Immune Infiltration and Predicts Poor Prognosis in Gliomas. *Front Immunol* (2021) 12:628966. doi: 10.3389/fimmu.2021.628966
28. Jiang T, Mao Y, Ma W, Mao Q, You Y, Yang X, et al. CGCG Clinical Practice Guidelines for the Management of Adult Diffuse Gliomas. *Cancer Lett* (2016) 375(2):263–73. doi: 10.1016/j.canlet.2016.01.024
29. Rasmussen BK, Hansen S, Laursen RJ, Kosteljanetz M, Schultz H, Norgard BM, et al. Epidemiology of Glioma: Clinical Characteristics, Symptoms, and Predictors of Glioma Patients Grade I-IV in the the Danish Neuro-Oncology Registry. *J Neurooncol* (2017) 135(3):571–9. doi: 10.1007/s11060-017-2607-5
30. Van Calster B, Wynants L, Verbeek JFM, Verbakel JY, Christodoulou E, Vickers AJ, et al. Reporting and Interpreting Decision Curve Analysis: A Guide for Investigators. *Eur Urol* (2018) 74(6):796–804. doi: 10.1016/j.eururo.2018.08.038
31. Lei X, Lei Y, Li JK, Du WX, Li RG, Yang J, et al. Immune Cells Within the Tumor Microenvironment: Biological Functions and Roles in Cancer Immunotherapy. *Cancer Lett* (2020) 470:126–33. doi: 10.1016/j.canlet.2019.11.009
32. Wei Q, Xu Q, Yuan X, Li J-J, Chen L, Luo C, et al. Immunological Impact of Chemotherapy on the Tumor Microenvironment in Gastric Cancer. *J Surg Oncol* (2021) 123(8):1708–15. doi: 10.1002/jso.26449
33. Roma-Rodrigues C, Mendes R, Baptista PV, Fernandes AR. Targeting Tumor Microenvironment for Cancer Therapy. *Int J Mol Sci* (2019) 20(4):840. doi: 10.3390/ijms20040840
34. Pitt JM, Marabelle A, Eggermont A, Soria JC, Kroemer G, Zitvogel L. Targeting the Tumor Microenvironment: Removing Obstruction to Anticancer Immune Responses and Immunotherapy. *Ann Oncol* (2016) 27 (8):1482–92. doi: 10.1093/annonc/mdw168
35. Ren D, Zhao J, Sun Y, Li D, Meng Z, Wang B, et al. Overexpressed ITGA2 Promotes Malignant Tumor Aggression by Up-Regulating PD-L1 Expression Through the Activation of the STAT3 Signaling Pathway. *J Exp Clin Cancer Res* (2019) 38(1):485. doi: 10.1186/s13046-019-1496-1
36. Topalian SL, Hodi FS, Brahmer JR, Gettinger SN, Smith DC, McDermott DF, et al. Safety, Activity, and Immune Correlates of Anti-PD-1 Antibody in Cancer. *N Engl J Med* (2012) 366(26):2443–54. doi: 10.1056/NEJMoa1200690
37. Ruan Z, Deng H, Liang M, Xu Z, Lai M, Ren H, et al. Overexpression of Long non-Coding RNA00355 Enhances Proliferation, Chemotaxis, and Metastasis in Colon Cancer *via* Promoting GTF2B-Mediated ITGA2. *Transl Oncol* (2021) 14(1):100947. doi: 10.1016/j.tranon.2020.100947
38. Chuang YC, Wu HY, Lin YL, Tzou SC, Chuang CH, Jian TY, et al. Blockade of ITGA2 Induces Apoptosis and Inhibits Cell Migration in Gastric Cancer. *Biol Proced Online* (2018) 20:10. doi: 10.1186/s12575-018-0073-x

Conflict of Interest: The authors declare that the research was conducted in the absence of any commercial or financial relationships that could be construed as a potential conflict of interest.

Publisher's Note: All claims expressed in this article are solely those of the authors and do not necessarily represent those of their affiliated organizations, or those of the publisher, the editors and the reviewers. Any product that may be evaluated in this article, or claim that may be made by its manufacturer, is not guaranteed or endorsed by the publisher.

Copyright © 2021 Lin, Huang, Tu, Zhu, Li, Lei, Luo, Wang, Gong, Long and Wu. This is an open-access article distributed under the terms of the Creative Commons Attribution License (CC BY). The use, distribution or reproduction in other forums is permitted, provided the original author(s) and the copyright owner(s) are credited and that the original publication in this journal is cited, in accordance with accepted academic practice. No use, distribution or reproduction is permitted which does not comply with these terms.

frontiers in Immunology

ORIGINAL RESEARCH
published: 23 November 2021
doi: 10.3389/fimmu.2021.785463

HOTAIR Up-Regulation Activates NF-κB to Induce Immunoescape in Gliomas

Yunfei Wang[1,2†], Kaikai Yi[1,2,3,4†], Xing Liu[5†], Yanli Tan[6,7], Weili Jin[1,2], Yansheng Li[1,2], Junhu Zhou[1,2], Hongjun Wang[8] and Chunsheng Kang[1,2*]*

[1] Laboratory of Neuro-Oncology, Department of Neurosurgery, Tianjin Neurological Institute, Tianjin Medical University General Hospital, Tianjin, China, [2] Key Laboratory of Post-Neuro Injury Neuro-Repair and Regeneration in Central Nervous System, Ministry of Education and Tianjin City, Tianjin, China, [3] Department of Neuro-Oncology and Neurosurgery, Tianjin Medical University Cancer Institute and Hospital, Tianjin, China, [4] National Clinical Research Center for Cancer, Key Laboratory of Cancer Prevention and Therapy of Tianjin, Tianjin Clinical Research Center for Cancer, Tianjin, China, [5] Beijing Neurosurgical Institute, Capital Medical University, Beijing, China, [6] Department of Pathology, Hebei University Medical College, Baoding, China, [7] Department of Pathology, Affiliated Hospital of Hebei University, Baoding, China, [8] Department of Neurosurgery, The Second Affiliated Hospital of Harbin Medical University, Harbin, China

OPEN ACCESS

Edited by:
Wen Cheng,
The First Affiliated Hospital of China Medical University, China

Reviewed by:
Weiwei Tao,
Huazhong Agricultural University, China
Ailiang Zeng,
University of Texas MD Anderson Cancer Center, United States

***Correspondence:**
Chunsheng Kang
kang97061@tmu.edu.cn
Hongjun Wang
wanghongjun8000@sina.com

[†]These authors share first authorship

Specialty section:
This article was submitted to Cancer Immunity and Immunotherapy, a section of the journal Frontiers in Immunology

Received: *29 September 2021*
Accepted: *05 November 2021*
Published: *23 November 2021*

Citation:
Wang Y, Yi K, Liu X, Tan Y, Jin W, Li Y, Zhou J, Wang H and Kang C (2021) HOTAIR Up-Regulation Activates NF-κB to Induce Immunoescape in Gliomas. Front. Immunol. 12:785463. doi: 10.3389/fimmu.2021.785463

Background: Checkpoint blockade therapies targeting programmed death ligand 1 (PD-L1) and its receptor programmed cell death 1 promote T cell-mediated immune surveillance against tumors and have been associated with significant clinical benefit in cancer patients. The long-stranded non-coding RNA HOTAIR is highly expressed and associated with metastasis in a variety of cancer types and promotes tumor metastasis at least in part through association with the PRC2 complex that induces redirection to hundreds of genes involved in tumor metastasis. Here, we report that HOTAIR is an activator lncRNA of the NF-κB pathway and demonstrate that its apparent upregulation promotes inflammatory signaling and immune escape in glioma cells.

Methods: Bioinformatics analysis was used to elucidate the relationship between HOTAIR and NF-κB pathway in HOTAIR knockdown glioma cells. At the cytological level, protein hybridization and immunofluorescence were used to detect the response of proteins in the NF-κB signaling pathway to HOTAIR regulation. ChIP and ChIRP experiments identified HOTAIR target genes. Animal experiments verified alterations in inflammation and immune escape following HOTAIR knockdown and activity inhibition.

Results: HOTAIR activated the expression of proteins involved in NF-κB, TNFα, MAPK and other inflammatory signaling pathways. In addition, HOTAIR induced various proteins containing protein kinase structural domains and promoted the enrichment of proteins and complexes of important inflammatory signaling pathways, such as the TNFα/NF-κB signaling protein complex, the IκB kinase complex, and the IKKA-IKKB complex. In addition, HOTAIR aberrantly activated biological processes involved in glioma immune responses, T-cell co-stimulation and transcription initiation by RNA polymerase II. HOTAIR facilitated the induction of IκBα phosphorylation by suppressing the expression of the NF-κB upstream protein UBXN1, promoting NF-κB phosphorylation and nuclear

translocation. *In vivo*, reduction of HOTAIR decreased PD-L1 protein expression, indicating that cells are more likely to be targeted by immune T cells.

Conclusion: In conclusion, our results provide convincing evidence that lncRNA HOTAIR drives aberrant gene transcription and immune escape from tumor cells through the NF-κB pathway.

Keywords: HOTAIR, chromatin structure, NF-κB activation, immunoescape, inflammatory signaling pathway

INTRODUCTION

The role of the immune system in carcinogenesis remains unclear. Checkpoints are negatively regulated pathways in the immune regulatory system and the malignant evolution of tumors effectively suppresses the immune response by activating the expression of checkpoints that enable them to actively evade detection. Of the many checkpoint proteins, cytotoxic T lymphocyte protein 4 (CTLA4) and programmed cell death protein 1 (PD-1) have been the most studied. PD-1 is a cytokine receptor on the surface of T cells that is expressed on the surface of activated T cells and is capable of binding to two ligands, PD-L1 or PD-L2. Many cell types express PD-L1, including tumor cells and immune cells regulated by cytokines such as interferon (IFN)-γ. The binding of PD-1 to PD-L1 or PD-L2 impairs T-cell activity (1). In a study of brain tumor samples from 284 clinical glioma cases, Han et al. found that the ratio of CD4(+) tumor-infiltrating lymphocytes to CD8(+) tumor-infiltrating lymphocytes was inversely correlated with overall survival and that high expression of the transcription factor FoxP3 by regulatory T cells could be found in high-grade gliomas, whereas it was not observed in low-grade gliomas (2). In addition, tumor shrinkage was evident in high-grade gliomas after treatment with nivolumab, suggesting that, similar to other solid tumors, immunotherapy could be applied to the treatment of gliomas (3).

HOX antisense intergenic RNA (HOTAIR), originally identified by Rinn et al. in 2007, is an lncRNA that is overexpressed in a variety of human cancers (4). It located in the HOXC cluster on chromosome 12, and regulates the HOXD gene cluster on chromosome 2 (5). HOTAIR silences the transcription of genes located in distant chromosomal regions at the epigenetic level by interacting with the polycomb protein complex 2 (PRC2). This interaction allows the Zeste 2 enhancer (EZH2) to occupy specific gene themes, such as the HOXD theme and undergo H3K27me3 (trimethylation of histone H3 lysine K27) modification, leading to gene repression (6, 7). Other interchromosomal targets of HOTAIR include cancer-related genes such as pro-calmodulin (PCDH), hepatic ligand protein receptor (EPHA1) and NF-κB inhibitory protein IκBα (5, 8). Although epigenetic processes have been reported to have a key role in immunosuppression, including aberrant histone methylation induced by EZH2 (9–12), the direct role of HOTAIR in immunosuppression has not been investigated. However, enhanced HOTAIR activation has been observed in solid tumors, including mesenchymal glioma (13–15). Furthermore, according to the TCGA transcriptional classification scheme, PD-L1 appears to be expressed more in the mesenchymal subtype and may contribute as a potential marker for the mesenchymal subtype of glioblastoma (16), suggesting a potential interaction between PD-L1-dependent immunosuppression and HOTAIR.

As a widely expressed transcription factor with a rapid response, NF-κB regulates the cellular immune response and inflammatory signaling pathway under cytokine stimulation, and its downstream regulatory genes include a variety of immune-related cytokines. Following these stimuli, NF-κB inhibitor α (IκBα), which is coupled to NF-κB, is phosphorylated and then degraded by proteases. NF-κB is thus released and translocated to the nucleus, where it activates the expression of target genes. The underlying inflammation due to the presence of a tumor leads to aberrant NF-κB activation and promotes cancer invasion and metastasis, and such a phenomenon has been observed in many tumor types, including lung cancer, breast cancer, and glioma (17–19). In previous studies (20), ubiquitin regulatory X (UBX) domain-containing protein UBXN1 interacts with inhibitor of apoptosis proteins (cIAPs), the E3 ubiquitin ligase of RIP1 in the TNFα receptor complex, blocks cIAP1 recruitment to TNFα receptor 1 (TNFR1) and sequentially inhibits RIP1 polyubiquitin chain modifications. This is important for the recruitment of TGFβ-activated kinase 1 (TAK1) and TAK1-binding protein 2/3 (TAB2/3) heterodimeric complexes and IKK heterodimeric complexes. Activated TAK1 phosphorylates and activates IKKβ, which phosphorylates IκBα and leads to its degradation and NF-κB nuclear translocation (21, 22)

In our ongoing efforts to understand the biological and pathological role of lncRNA, a previous sequencing analysis of HOTAIR-related proteome and clinical samples determined that HOTAIR activates a variety of proteins containing protein kinase domains and promotes the enrichment of important inflammatory signaling pathway proteins and their complexes, such as the TNFα/NF-κB signaling protein complex, I-kappaB kinase complex, and IKKα-IKKβ complex. Moreover, HOTAIR upregulates the expression of several inflammatory signaling

Abbreviations: LncRNAs, long noncoding RNAs; HOTAIR, HOX antisense intergenic RNA; PRC2, polycomb repressive complex 2; EZH2, enhancer Of zeste 2 polycomb repressive complex 2; NF-κB, nuclear factor-κB; IκBα, inhibitor of NF-κB alpha; IKK, IκB kinases; NKRF, NFκB repressing factor; PRKCQ, protein kinase C theta; UBXN1, ubiquitin-associated and ubiquitin regulatory X domain-containing protein 1; PD-L1, Programmed Cell Death 1 Ligand 1; TCGA, the cancer genome atlas; CGGA, Chinese Glioma Genome Atlas; KEGG, Kyoto encyclopedia of genes and genomes; SD, standard deviation.

proteins, such as TNFα, and MAPK. An analysis of clinical samples found abnormal HOTAIR expression in stromal glioblastoma, which was correlated with the malignancy degree of the glioma. HOTAIR abnormally activated biological processes involved in the immune response, T cell synergistic stimulation, and RNA polymerase II transcription initiation in glioma. Simultaneously, HOTAIR was highly positively correlated with the tumor immune escape related protein PD-L1; furthermore, it was negatively correlated with the expression of NFκB repressing factor (NKRF), Protein Kinase C Theta (PRKCQ) and ubiquitin-associated and ubiquitin regulatory X domain-containing protein 1 (UBXN1), which are repressors of the NF-κB signaling pathway. Therefore, we concluded that HOTAIR might regulate the gene transcription of key repressors of the NF-κB activation pathway through epigenetic modulation, thereby participating in the immune escape biological process in glioma cells.

MATERIALS AND METHODS

Cell Lines and Culture Conditions

The human epithelial glioma cell line U87 MG was obtained from the American Type Culture Collection (ATCC, Manassas, VA, USA) in May 2015. Its short tandem repeat (STR) profile is presented on the ATCC website (https://www.atcc.org/products/all/HTB-14.aspx#specifications); furthermore, we performed a reauthentication by STR analysis in June 2017. The primary cell line TBD was derived from a GBM patient with recurrent lesions undergoing surgery at the Hebei University Affiliated Hospital according to a protocol reported by Dong et al. (23). After the three cell lines were obtained, they were immediately proliferated, amplified, and frozen in liquid nitrogen. All cells used in subsequent experiments were recovered from these cryopreserved cell lines. The U87 MG and TBD cells were cultured in Dulbecco's modified Eagle's medium (DMEM) containing 10% fetal bovine serum (FBS). The U87 cells were cultured in DMEM/F12 supplemented with 10% FBS. All cells were proliferated at 37°C in a humidified atmosphere of 5% CO_2. All glioma cells with the exception of *in vivo* cultures were maintained for less than eight passages. Cells in the logarithmic growth phase or at 80% confluence were used for subsequent experiments.

Cell Culture and Labeling

To profile protein expression in response to HOTAIR knockdown, U87 cells transfected with lentivirus-siRNA of HOTAIR (siHOTAIR-U87) or a negative control (siNC-U87) were labeled with the SILAC Protein Quantitation Kit (Invitrogen, Carlsbad, CA) according to manufacturer's instructions. siHOTAIR-U87 cells and siNC-U87 cells were cultured separately in DMEM supplemented with 10% FBS and either the light isotopic forms of [U-$^{12}C_6$]-L-lysine and [U $-^{12}$ $C_6^{14}N_4$]-L-arginine or the heavy isotopic forms of [U-$^{13}C_6$]-L-lysine and [U $-^{13}$ $C_6^{15}N_4$]-L-arginine. After six passages, the heavy labeling efficiency of [U-$^{13}C_6$]-L-lysine and [U $-^{13}$ $C_6^{15}N_4$]-L-arginine in control cells was evaluated by mass spectrometry to confirm a greater than 99% labeling efficiency. Then, cells were continuously expanded in SILAC medium until reaching the desired confluence. Finally, cells from both the heavy- or light-labeled pool were harvested separately and combined in equal amounts.

Nondenatured protein lysates were obtained from the harvested cells and were centrifuged to collect protein precipitates. The collected fractions were combined, vacuum-dried, and analyzed by high-performance liquid chromatography with tandem mass spectrometry (HPLC-MS/MS).

Proteomic and Transcriptome Profiling

Based on the SILAC labeling-based proteomics, we comparatively quantified the host proteome of siHOTAIR-U87 and siNC-U87 cells. We analyzed the quantifiable proteome dataset for three enrichment gene ontology (GO) categories: Biological Process, Protein Complex, and Protein Domains. Pathway clustering was conducted using the KEGG. Fisher's exact/chi-squared tests and false discovery rates (FDRs) were used to determine significance, denoted by the *P*-value between the GO term and the pathway correlated to the experimental conditions. Lower FDRs indicated smaller errors in the determination of the *P*-value.

Triplicate RNA samples from four sets of U87 cells transfected with lenti-HOTAIR or lenti-NC for 48 h were randomly selected for RNA-sequencing. For mRNA network analysis, biological process (BP) analysis through gene ontology and pathway clustering through KEGG were performed. Furthermore, two large cohorts were used for gene ontology and correlation analysis: the Chinese Glioma Genome Atlas cohort (CGGA, http://www.cgcg.org.cn/, n=301) and The Cancer Genome Atlas cohort (TCGA, https://tcga-data.nci.nih.gov/docs/publications/gbm_2013/, including the transcriptome of 164 RNA samples profiled by RNA-seq).

RNA Extraction and RT-PCR

Total RNA was isolated from cells using the TRIzol reagent (Invitrogen). Next, 1 μg total RNA was reverse transcribed into cDNA using the GoScript™ reverse transcription system (Promega, USA) according to the manufacturer's instructions. Analyses were performed utilizing PowerUp™ SYBR™ Green on a ABI QuantStudio 5 real-time fluorescence detection PCR system. The expression levels of specific genes are reported as ratios to GAPDH expression in the same master reaction. The primers used for real-time RT-PCR are listed in the **Supplementary Table 1**.

Luciferase Reporter Assays

Dual-luciferase assays were performed 48 h post-transfection following the manufacturer's protocol (Dual-Luciferase Reporter Assay System, Promega, USA), and expression was detected with a microplate reader (Synergy2, BioTek, USA). All cell lines were transfected with 0.1 μg of the luciferase reporter p-NF-κB-Luc plus 0.01 μg of the Renilla reporter pRL-TK. After AQB treatment for 48 h, the transfected cells were collected. The

luciferase assays were performed using a dual-specific luciferase assay kit (Promega, USA).

T Lymphocyte Purification and Flow Cytometry

Female C57BL/6 mice (8-10 weeks old) with GL261-induced tumor xenografts were treated parenterally with DMSO or AQB and were used for T lymphocyte purification and flow cytometry. The lymph nodes were removed aseptically, minced, and suspended in RPMI 1640 medium. Single cell suspensions were prepared *via* filtration through a sterile sieve mesh. Blood was collected from the eyeballs of C57BL/6 mice, and heparin was added for anticoagulation. Erythrocytes were lysed with a red blood cell lysis buffer, and the cells were washed twice with cold PBS supplemented with 2% FBS. After washing, T lymphocytes harvested from spleens and blood were stained with PE-conjugated-CD8α, FITC conjugated-CD4, and APC conjugated-CD3 (eBioscience). The samples were acquired using an LSR II (BD Biosciences) flow cytometer, and the data were analyzed with Kaluza Analysis Software (Beckman Coulter, Brea).

Laser Confocal Immunofluorescence Assay

Cells seeded on glass-covered slides were fixed with 4% paraformaldehyde, permeabilized with 0.25% Triton X-100, and blocked with 1% bovine serum albumin (BSA). Next, the cells were probed with primary antibodies diluted in 1% BSA solution overnight at 4°C. Rabbit or mouse IgG antibodies coupled with Alexa (1:100 dilution, Invitrogen) were used as secondary antibodies followed by nuclear staining with DAPI. The images were visualized and captured by laser confocal scanning microscopy (Olympus, Tokyo, Japan). Antibodies against human NF-κB, pNF-κB, H3K27me3 (1:100 dilution, Cell Signaling Technology), and PD-L1 (1:1000, Abcam) were utilized as primary antibodies.

Western Blot Analysis

Western blot was performed as described previously. Thirty μg protein were loaded per lane. Cell lysates were separated on analytical 10% SDS-PAGE gels and transferred onto poly vinylidene difluoride (PVDF) membranes. Non-specific binding was blocked by incubation with 5% skim milk. Antibodies against human NF-κB, pNF-κB, H3K27me3, IKKα, IKKβ, IκBα, pIKKα, pIKKβ (1:1000 dilution, Cell Signaling Technology), PD-L1 (1:1000, Abcam), and GAPDH (1: 4000 dilution, Proteintech) were used as primary antibodies.

Rabbit or mouse IgG antibodies coupled to horseradish peroxidase (1:10000 dilution, Promega) were utilized as secondary antibodies. Antibody-labeled protein bands on the membranes were detected with a G:BOXiChemi XT chemiluminescence and fluorescence imaging system (Syngene). Band densities were determined using the Image J software.

Chromatin Immunoprecipitation (ChIP)

ChIP assays were performed using the EZ-ChIP kit (Millipore). Briefly, cells were fixed with 1% formaldehyde, and then formaldehyde was neutralized with 0.125 M glycine. Cells were then lysed with SDS and protease inhibitor lysis buffer. Soluble chromatin of 200-1000 bp was collected after sonication, pre-cleared in 1:10 dilution buffer, and incubated overnight with IgG, H3K27me3, and NF-κB antibodies in a rotating platform at 4°C. After washing the immune complexes captured by G-Sepharose protein beads, the bound DNA fragments were eluted and analyzed by real-time quantitative pcr using ChIP primers. The primers used for real-time RT-PCR are listed in the **Supplementary Table 2**.

Chromatin Isolation by RNA Purification (ChIRP)

The ChIRP assay was performed using the Magna ChIRP RNA Interactome Kit (Millipore, USA) following the manufacturer's guidelines. Briefly, a total of 1×10^7 cells was lysed in complete lysis buffer for each reaction, and the DNA was then sheared into small fragments through sonication. Then the lysate was incubated with biotin-labeled probes that could hybridize with HOTAIR or control probe. Finally, the probes were extracted by streptavidin magnetic beads, the combined protein was isolated for immunoblotting analysis, and the RNAs and DNAs samples were enriched for agarose electrophoresis. The probes used are listed in the **Supplementary Table 3**.

Tumor Xenografts

Bagg albino (BALB)/c nude mice (4 weeks old) and C57BL/6 black mice (4-6 weeks old) were purchased from the Animal Center at the Cancer Institute of the Chinese Academy of Medical Science (Beijing, China). All experimental protocols were approved by the Tianjin Medical University Animal Care and Use Committee. To establish orthotopic models, glioma cells transduced with a luciferase lentivirus were implanted stereotactically: anthropogenic U87 or TBD in BALB/c nude mice and murine GL261 in C57BL/6 black mice. The mice were randomly assigned into six groups (n = 8 per group). Twenty-one days after implantation, PBS or AQB (5 mg/kg) was administered by intraperitoneal injection every other day for 14 days. The nude mice were imaged for luciferase activity once per week. The mice were sacrificed on day 42, and their brains were removed for paraffin-embedding. The ratio of CD4/CD8 T cells was measured in blood and lymph node specimens of black mice, and the brain tissues were used to prepare paraffin sections for immunohistochemical and hematoxylin-eosin staining.

Immunohistochemistry

Brain tumor tissues in paraffin were sectioned at 4 μm and mounted on slides. Paraffin slices were dewaxed and incubated with primary antibodies. Primary antibodies against human NF-κB, pNF-κB (1: 200 dilution, Cell Signaling Technology), and PD-L1 (1:200, Abcam) were used for antigen recognition; secondary antibodies were conjugated with biotin labels. DAB was utilized as a developing method to detect the biotin reporter, and hematoxylin was utilized for counterstaining. Next, sections were rinsed with PBS, re-stained with ammonia, stained with hematoxylin, and observed by microscopy. The results were analyzed using the National Institutes of Health (NIH) ImageJ software.

Hematoxylin-Eosin Staining

Paraffin-embedded tissue sections were subjected to hematoxylin-eosin staining. After blocking with 3% H_2O_2 and non-immune rabbit serum, sections were incubated with primary antibodies (1:200 dilutions) overnight at 4°C followed by an incubation with a streptavidin-biotinylated secondary antibody (ZSGB-BIO) for 1 h at 37°C. The chromogenic substrate used was 3,3'-diaminobenzidine, and hematoxylin was utilized as the counterstain. The sections were visualized under a light microscope.

Statistical Analyses

Statistical analyses were performed utilizing Kaplan-Meier survival curves, the long-rank test, and univariate and multivariate Cox proportional hazards regression analysis with SPSS 16.0 (IBM, USA). All values are presented as the mean ± standard deviation (SD). Statistical comparisons between two groups were performed using Student's *t*-test. Differences among three or more groups were determined by two-way ANOVA followed by Dunnett's test. Significance was set to $^{*}P < 0.05$, $^{**}P < 0.01$.

RESULTS

Proteomics Analysis Revealed That HOTAIR Regulates Proteins in Glioma Cells

An abnormally high expression of the lncRNA HOTAIR has been previously demonstrated in glioma cells. HOTAIR regulates genes by anchoring epigenetic modification proteins and causes abnormalities in multiple signaling pathways (5, 13, 24, 25). We knocked down HOTAIR in glioma cells by siRNA with SILAC labeling, and then total protein was extracted for proteome mass spectrometry. A proteomics analysis showed that in HOTAIR knockdown glioma cells, 1074 proteins were up-regulated, whereas 390 proteins were inhibited (**Figure 1A**, **Supplementary Table 4**). Among these proteins, 434 protein correlations were enriched in one protein network (**Figure 1B**). HOTAIR was associated with two main cluster networks of biological processes (**Figure 1C**, **Supplementary Table 5**). Next, proteins were annotated with the Kyoto Encyclopedia of Genes and Genomes (KEGG), and a significant association of HOTAIR with proteins in metabolic pathways and in the MAPK and PI3K-Akt

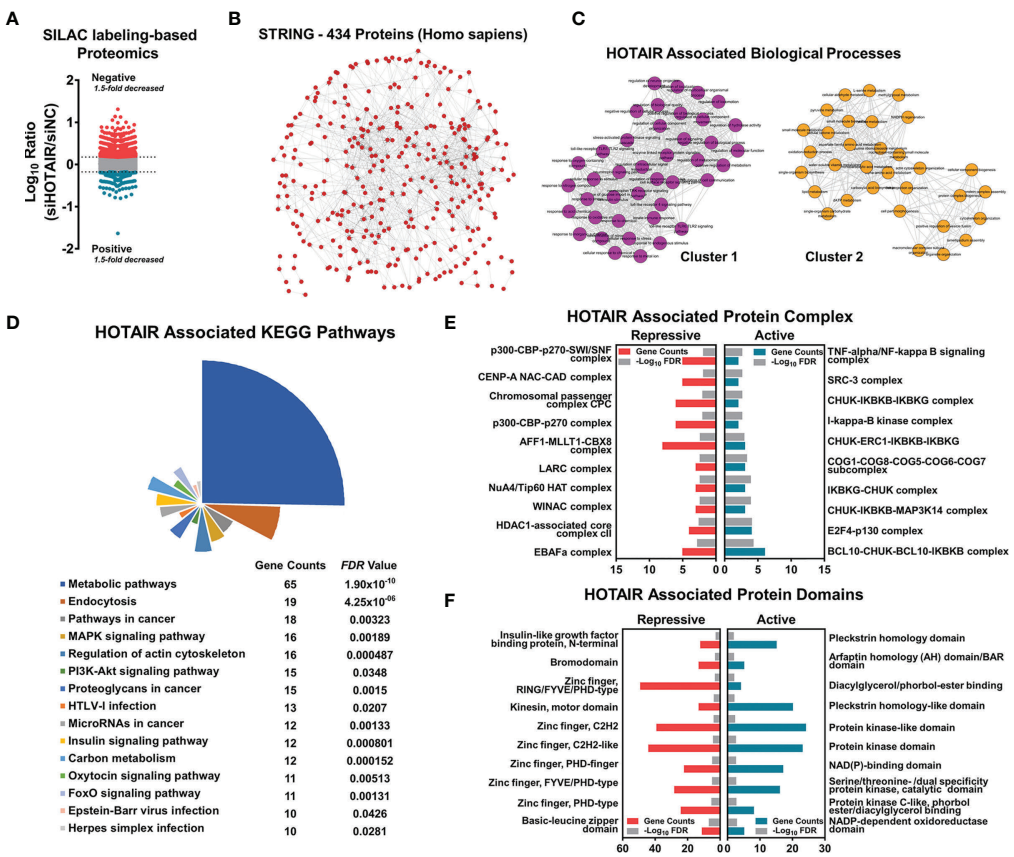

FIGURE 1 | HOTAIR regulated protein level associated with multiple biological progress, when applied to SILAC labeling-based proteome of U87 cells. **(A)** The scatter plot shows the number of differential proteins detected by proteome sequencing, with a difference ratio greater than 1.5. **(B)** STRING protein network shows that 434 proteins had high correlation. **(C–F)** Enrichment and clustering analysis of the quantifiable proteomics data set including HOTAIR associated biological processes clustering **(C)**, KEGG pathway analysis **(D)**, protein complex enrichment **(E)** and protein domains enrichment **(F)**.

signaling pathways was identified (**Figure 1D**). An InterPro database protein complex analysis demonstrated that proteins annotated in complexes with histone acetyltransferases were repressed by HOTAIR, including the p300-CBP-p270-SWI/SNF, CENP-A NAD-CAD, and NuA4/Tip60 HAT complexes with enrichment *P* values 0.001765, 0.003027, and 0.011090, respectively. HOTAIR activated the TNF-α/NF-κB, CHUK-IKBKB-IKBKG, and IκB kinase complexes, which are involved in the NF-κB signaling activation process, with enrichment *P* values 0.000053, 0.000131, and 0.000131, respectively (**Figure 1E**). To investigate the HOTAIR-associated proteins domains, we analyzed their profiles in the CORUM database. The expression of proteins containing an IGF binding domain, a bromodomain, and a zinc finger was repressed by HOTAIR (*P* values 0.003775, 0.001489, and 0.001130, respectively). Proteins activated by HOTAIR mostly contained a protein kinase domain or a kinase-like domain (enrichment *P* values 0.003446 and 0.006261, respectively) (**Figure 1F**).

To elucidate HOTAIR's effects, we analyzed different databases and datasets including samples from glioma cell lines and clinical glioma samples. Microarray mRNA datasets, in which HOTAIR was overexpressed for 6 h or 48 h in U87 glioma cells, exhibited 1920 upregulated and 470 downregulated genes at both timepoints (**Figures 2A, B**). HOTAIR was positively associated with biological processes, including cell cycle and intracellular signal transduction and with multiple pathways (**Figures 2C, D**). A CGGA database analysis based on 301 patients revealed high HOTAIR expression in WHO III and IV grade glioblastoma samples, especially in classical and mesenchymal glioblastomas (**Figures 2E, F**). Quantifiable genes associated with HOTAIR in glioblastoma samples in the CGGA RNAseq dataset were classified by an ontology annotation based on biological processes. The findings demonstrated that HOTAIR regulates the immune response, T cell co-stimulation, and adaptive immune response (**Figure 2G**). As shown in **Figure 3A**, multiple genes which were participated in IL6-JAK-STAT3 signaling and TNFα/NF-κB

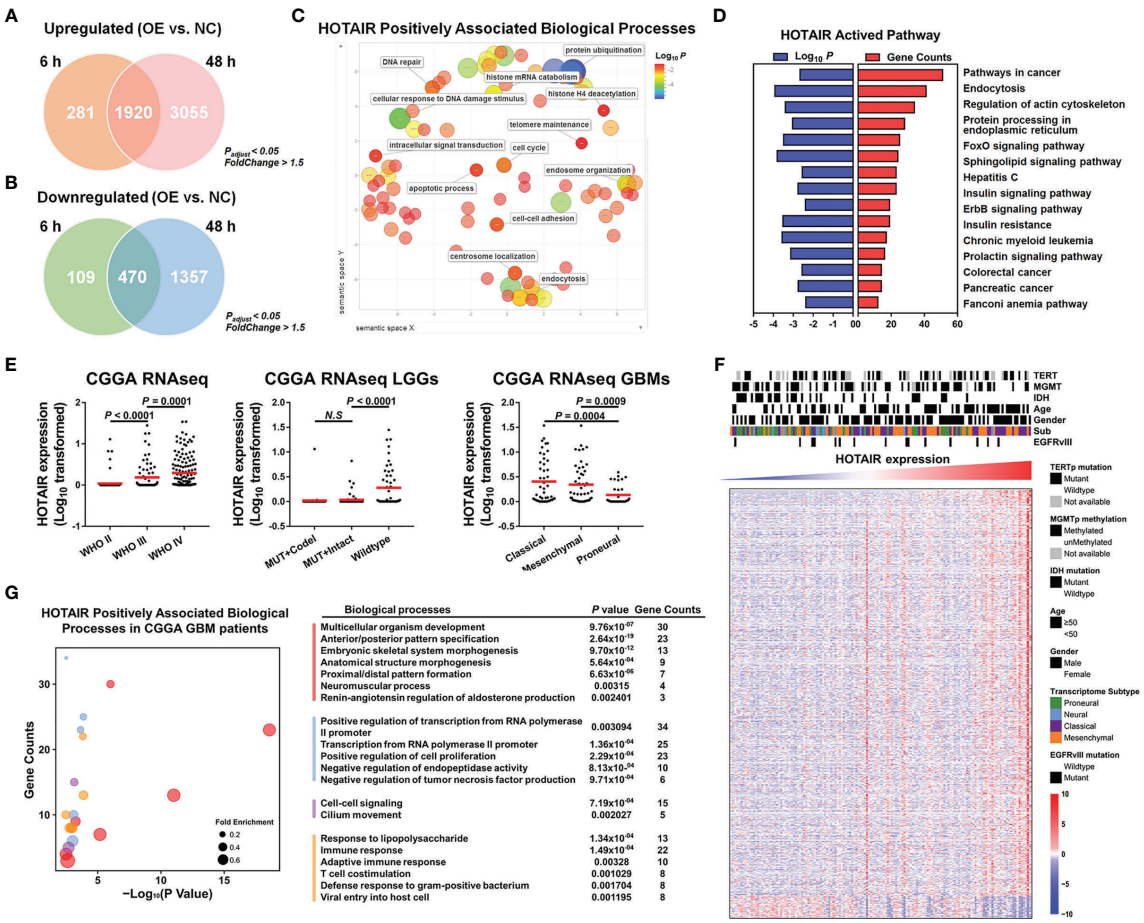

FIGURE 2 | HOTAIR regulated gene expression participated in multiple biological processes in different dataset. **(A)** HOTAIR upregulated 2201 genes after 6h expressing in U87 and 4975 genes after 48h, respectively, and there were 1920 overlapping genes. **(B)** HOTAIR downregulated 579 genes and 1827 genes when HOTAIR were expressed for 6h and 48h in U87 respectively, and the overlapping genes reached 470. **(C, D)** HOTAIR regulated genes were enriched in several biological processes **(C)** and pathways **(D)**. **(E)** HOTAIR expression in CGGA RNAseq dataset (n=301). **(F)** Cluster heatmap showed the gene expression level correlated with HOTAIR expression in glioma based on CGGA RNAseq dataset (n=301). **(G)** Quantifiable genes of GBM patients in CGGA RNAseq dataset associated with HOTAIR were classified by ontology annotation based on biological processes.

signaling pathways, significantly enriched in HOTAIR positively correlated gene group. The expression of HOTAIR was positively correlated with the messenchymal subtype of glioma, but negatively correlated with the subtype of proneural (**Figure 3A**). Similar conclusions can also be drawn from the sequencing data published by several teams that the activity of NF-κB and downstream pathways is significantly positively correlated with the malignant messenchymal subtype of glioma (**Figure 3B**).

AQB Inhibited Inflammatory Signaling Pathways and the Checkpoint Protein Downstream of NF-κB

To verify the database analysis results regarding a relationship between HOTAIR and NF-κB, the regulatory effect of HOTAIR on the NF-κB pathway was verified by *in vitro* experiments. In previous study, we identified a small molecule compound AC1Q3QWB (AQB) as an efficient disruptor of HOTAIR-EZH2 interaction, resulting in blocking of PRC2 recruitment (14, 26). First, we treated U87 and TBD human glioma cells with AQB. We found that AQB significantly reduced the levels of the inflammatory associated proteins including XIAP, Bcl2, IL-8, IL-1B and TNFα, compared with DMSO treatment in the control group (**Figures 3C, D**). After treatment with 40uM and 80uM AQB, there was a subtle decrease in the total amount of NF-kB, especially after 80μM AQB treatment, while the level of phosphorylated NF-kB decreased significantly (**Figure 3E**). Furthermore, PD-L1 expression was inhibited by AQB. With AQB interfering with the EZH2/HOTAIR combination,

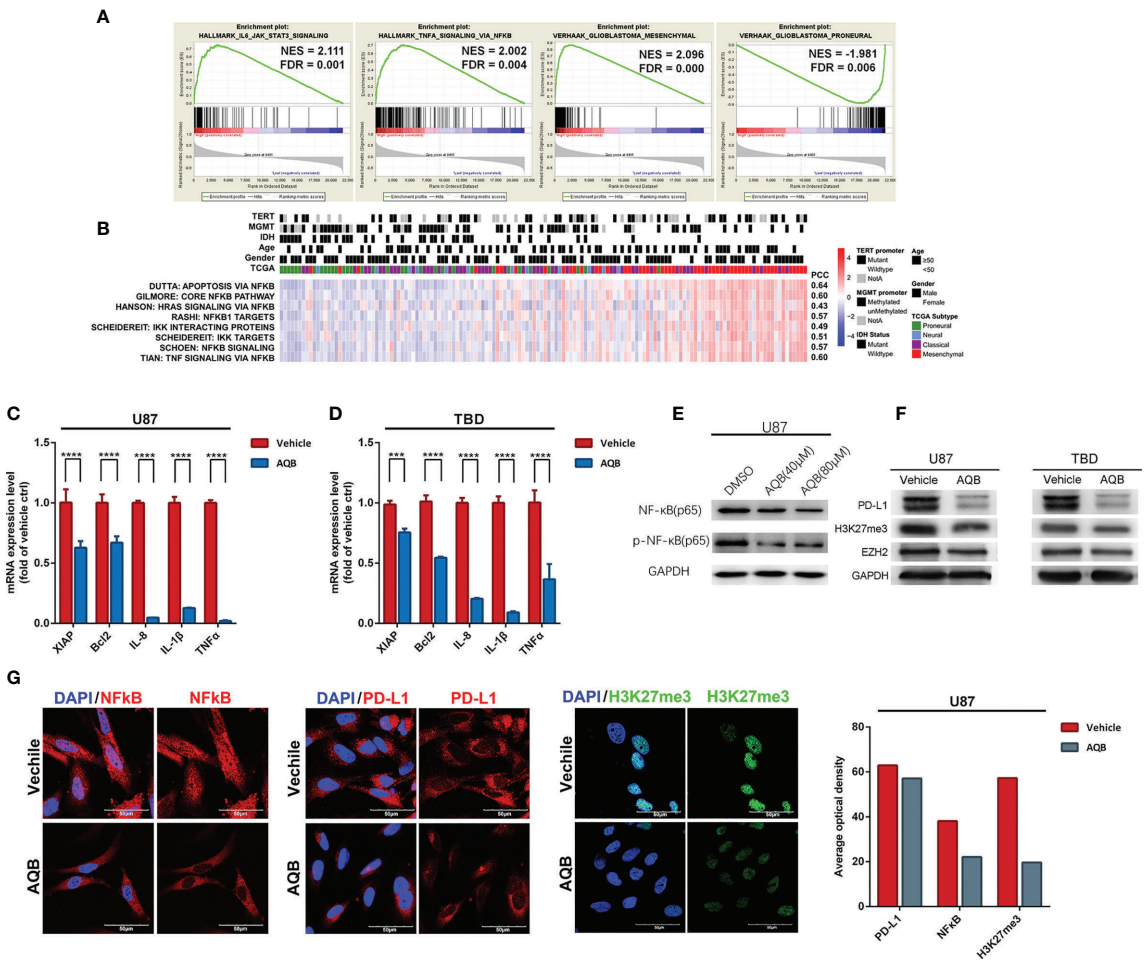

FIGURE 3 | HOTAIR may regulate gene expression pattern in an NF-κB-dependent manner in glioma. **(A)** The enrichment plots of gene expression signatures of HOTAIR-induced IL6-JAK-STAT3 signaling and TNFα signaling *via* NF-κB, and the signatures of samples annotated in mesenchymal glioma and proneural glioma, sorted according to the differences between the samples with high and low level HOTAIR expression. **(B)** Enrichment heatmap showed the NFκB-dependent biological processes associated with the grade of samples. **(C, D)** NF-κB regulated gene expression levels in U87 **(C)** and TBD **(D)** at 24 hours after treatment with AQB. Values are means ± s.d. from n = 3 independent experiments. The *P* value was determined by two-sided Student's t-test. **(E)** Immunobolts detect the protein level of NF-κB and pNF-κB, using GAPDH as control in U87 cells treated with AQB at the concertration of 40μM and 80μM. **(F)** Immunoblots showing the effect of AQB on expression of PD-L1 and EZH2 in U87 and TBD cells, using GAPDH as control. **(G)** Immunoflourescence showing the protein level and protein distribution of H3K27me3, NF-κB and PD-L1 in DMSO or AQB treated U87 cells. The bar chart indicates differences in the mean optical densities of NF-κB, PD-L1, and H3K27me3 proteins in DMSO or AQB-treated U87 cells. Scale bar, 50μm. ***$P < 0.001$, ****$P < 0.0001$.

H3K27me3 levels decreased, but the EZH2 protein level did not change significantly (**Figure 3F**). The same phenomenon can be significantly observed in the immunofluorescence staining experiment, PD-L1, nuclear NF-κB and H3K27me3 in U87 cells treated with AQB decreased significantly (**Figure 3G**). This suggests that HOTAIR functional inhibition can regulate the downstream of the NF-κB signaling pathway.

The Stock of HOTAIR Is Positively Associated to the Positioning and Function of NF-κB

To test the effect of HOTAIR on NF-κB, we used AQB to inhibit the function of HOTAIR or varied the stock of HOTAIR using distinct siRNAs or lenti-HOTAIR virus. In U87 and TBD cells treated with DMSO or 40μM AQB, fewer NF-κB proteins entered into the nucleus, while phosphorylated-NF-κB proteins in the cytoplasm and nucleus decreased (**Figure 4A**). Knocking down HOTAIR through distinct siRNAs caused decreased mRNA expression of IL-8 and TNFα in both U87 and TBD cells. It caused decreases in phosphorylated NF-κB, which is the same as knocking down EZH2 (**Figure 4B**). In siHOTAIR U87 cells, western blotting showed that NF-κB in the cytoplasm increased, but less in the nucleus. Correspondingly, phosphorylated NF-κB decreased in both the cytoplasm and the nucleus. And the phosphorylated IκB decreased in nuclear. (**Figure 4B**). Correspondingly, when we transferred HOTAIR overexpressed lentivirus into U87 and TBD cells, the level of phosphorylated NF-κB increased, the content of nuclear NF-κB protein and phosphorylated NF-κB protein increased, and the phosphorylated IκB increased. The mRNA of IL-8 and TNFα were all increased induced by overexpressed HOTAIR lncRNA (**Figure 4C**). It suggested that inhibiting the function of HOTAIR or reducing the stock of HOTAIR can reduce the phosphorylation modification of NF-κB, thereby affecting the expression of NF-κB regulatory protein. We then tested the results of overexpression of HOTAIR in glioma cells treated with AQB. mRNA expression level showed that HOTAIR could restore the expression of suppressed IL-8, IL-1β and TNFα. Western blotting showed that overexpression of HOTAIR in TBD cells could restore the level of phosphorylated NF-κB inhibited by AQB, but the effect was not significant in U87 (**Figure 4D**). This means that the combination of HOTAIR and EZH2 to regulate epigenetic modification is the key to regulating NF-κB phosphorylation.

Furthermore, in luciferase reporter assays detecting NF-κB transcription activity, AQB inhibited the transcriptional regulatory activity of NF-κB similarly to the NF-κB inhibitor JSH-23, and this inhibition was reversed by overexpression of HOTAIR (**Figure 4F**).

HOTAIR Regulation on NF-κB Signal Pathway Through the Negative Regulator UBXN1

In order to further clarify the intermediate factors of HOTAIR regulating NF-κB pathway activation, we tested several factors involved in the regulation of NF-κB signaling pathway. NKRF encodes a transcriptional inhibitor that binds to negative regulatory elements to inhibit the transcriptional regulation of NF-κB (27). PRKCQ encodes a serine/threonine protein kinase that can activate the IKK complex, thus activating NF-κB resulting in nuclear translocation and activation (28, 29). As shown in **Figure 4D**, in U87 and TBD cells treated with AQB, the mRNA expression of NKRF and PRKCQ were both inhibited by AQB, suggesting that their gene expression may not be regulated by HOTAIR through H3K27 trimethylation. But we found another protein, UBXN1, which was reported as negative regulator of NF-κB pathway decreased in LV-HOTAIR treated U87 and TBD cells (**Figure 4C**). As shown in **Figure 4E**, both the mRNA and protein of UBXN1 were induced by AQB in U87 and TBD cells. These results suggest that UBXN1 could be a possible bridge for HOTAIR to regulate the activation of NF-κB.

The modification of H3K27me3 in UBXN1 promoter region decreased when the function of HOTAIR was inhibited by AQB. On the contrary, overexpression of HOTAIR can restore the modification level of H3K27me3. It indicated that HOTAIR can directly regulate the expression level of UBXN1 by regulating histone modification (**Figure 5A**). In the ChIRP experiment, we observed that when AQB acted, HOTAIR bound to chromatin decreased, and HOTAIR bound to chromatin DNA in the UBXN1 promoter region decreased (**Figure 5B**).

HOTAIR Regulation on PD-L1 Expression Affected T Cell-Dependent Toxicity

It has been demonstrated that PD-L1 on tumor cells is sufficient to mediate T cell tolerance, and inhibition of PD-L1 on tumor cells can effectively activate anti-tumor immunity (30). As the transcription regulation target of NF-κB, we found that the gene expression of PD-L1 was positively regulated by HOTAIR (**Figure 4D**). Moreover, a genome immune coprecipitation experiment revealed that AQB significantly inhibited NF-κB in the *CD274* gene promoter region, and that HOTAIR overexpression reversed and promoted NF-κB enrichment in this area, implying that AQB may regulate the immune sensitivity of tumor cells by inhibiting the transcriptional regulation of *CD274* gene by NF-κB (**Figure 5C**). Moreover, NF-κB recognized the promoter region of *HOTAIR*, suggesting that there might be regulatory feedback circuits involving lncRNA and transcription factors (**Figure 5D**).

To test whether the inhibition of PD-L1 mediated by HOTAIR affects the immune sensitivity of tumor cells, we co-cultured glioma cells treated with EZH2 siRNA or HOTAIR siRNA with activated human peripheral blood mononuclear cells (PBMCs). As expected, disruption of EZH2 or HOTAIR increased the sensitivity of tumor cells to T cell killing (**Figure 5E**). These results suggested that HOTAIR alters PD-L1 gene expression and T cell toxicity through NF-κB signaling pathway and highlight HOTAIR as a promising target for tumor immunotherapy.

Blockade of HOTAIR Function Activated Anti-Cancer Immunity *In Vivo*

To further confirm the regulation of HOATIR on PD-L1 dependent on the NF-kB pathway, we performed *in vivo* tests.

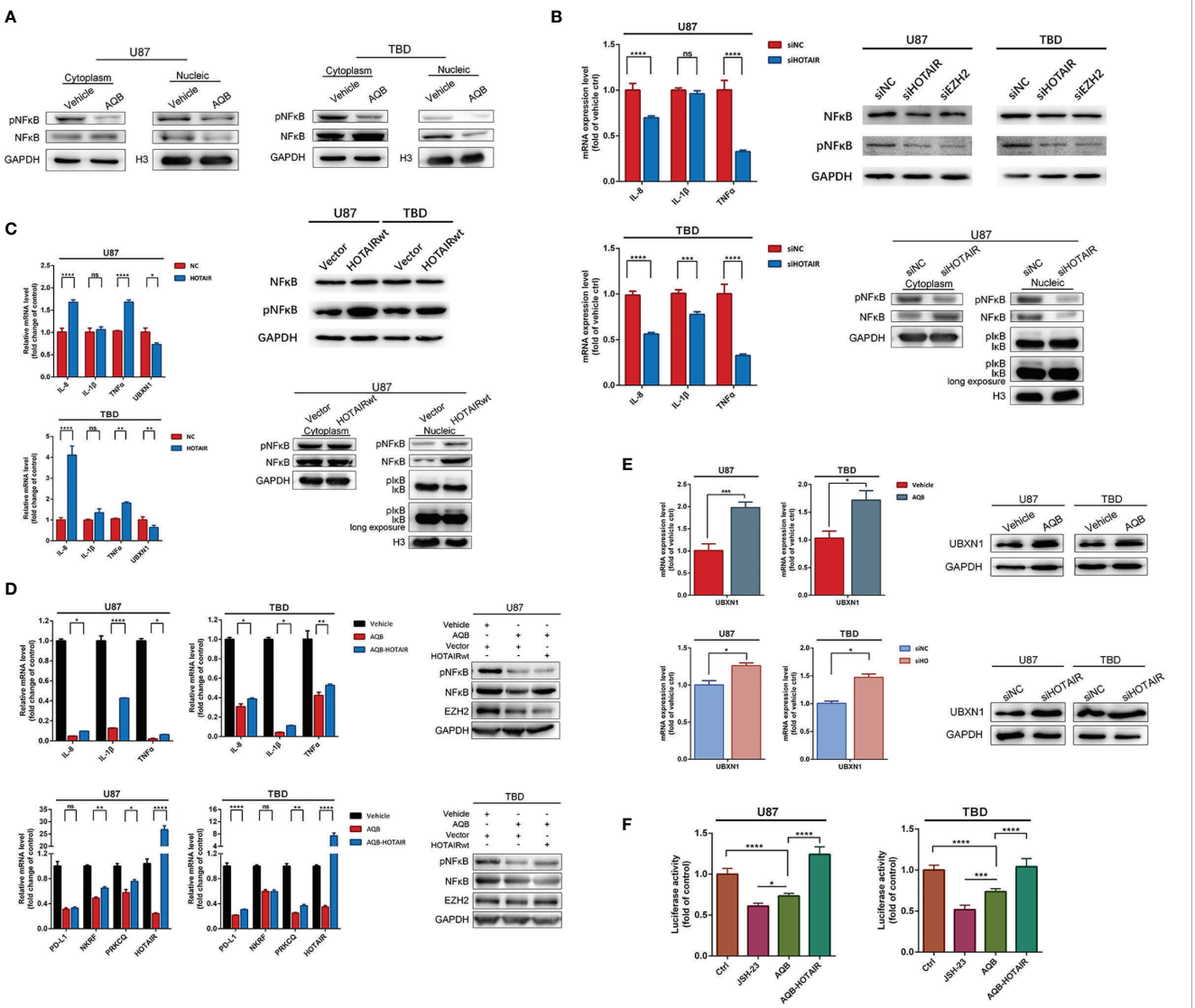

FIGURE 4 | Inhibition of H3K27me3 modification can regulate the activation and function of NF-κB. **(A)** Immunoblots showing the distribution of NF-κB and pNF-κB proteins in the nucleus and cytoplasm, with GAPDH as the cytoplasmic protein control and histone H3 as the nuclear protein control. **(B)** Quantitative PCR to detect mRNA expression levels of IL-8, IL-1β, and TNFα in U87 and TBD cells treated with HOTAIR knockdown. The protein expression levels of NF-κB and pNF-κB in U87 and TBD cells with HOTAIR knockdown and EZH2 knockdown were detected by immunoblots. **(C)** Quantitative PCR to detect mRNA expression levels of IL-8, IL-1β, TNFα and UBXN1 in U87 and TBD cells overexpressing HOTAIR. Immunoblots detected the protein expression levels of NF-κB and pNF-κB in U87 and TBD cells overexpressing HOTAIR. **(D)** Quantitative PCR detecting mRNA expression levels of IL-8, IL-1β, TNFα, PD-L1, NKRF, PRKCQ and HOTAIR in U87 and TBD cells treated with AQB or AQB deals with joint HOTAIR overexpression. Immunoblots detected the protein expression levels of NF-κB and pNF-κB in U87 and TBD cells treated with AQB or AQB deals with joint HOTAIR overexpression. **(E)** Quantitative PCR and immunoblots showing the message RNA and protein level of UBXN1 in U87 and TBD cells treated with AQB using vehicle as control. **(F)** NFκB function was analysis using NFκB binding domain fused luciferase reporter vector in U87 and TBD cells treated with JSH-23, or AQB or AQB joint HOTAIR overexpression. For all the statistical histograms above, values are means ± s.d. from n = 3 independent experiments. The *P* value was determined by two-sided Student's t-test. ns, not statistically significant, $^{*}P < 0.05$, $^{**}P < 0.01$, $^{***}P < 0.001$, $^{****}P < 0.0001$.

We evaluated lentivirus-mediated HOTAIR overexpression and anti-HOTAIR AQB treatment alone or combination in TBD orthotopic tumor model established in Bagg albino (BALB)/c nude mice. AQB treatment resulted in a significant reduction of the intracranial tumor volume compared with the DMSO group (43% reduction with $P < 0.05$), contrarily, overexpression of HOTAIR increased the malignant progression of the tumor (52% enhancement in nude mice, $P < 0.05$; **Figures 6A, C**). Morphologically, hematoxylin-eosin-stained slides indicated that AQB induced shrinkage of tumor cell nuclei (**Figure 6B**). Compared with the control group (median survival: 19 days), AQB treatment group (median survival: 23 days) showed prolonged survival in Kaplan-Meier survival curves ($P < 0.05$; **Figure 6D**). The same results appeared in the HOTAIRwt group

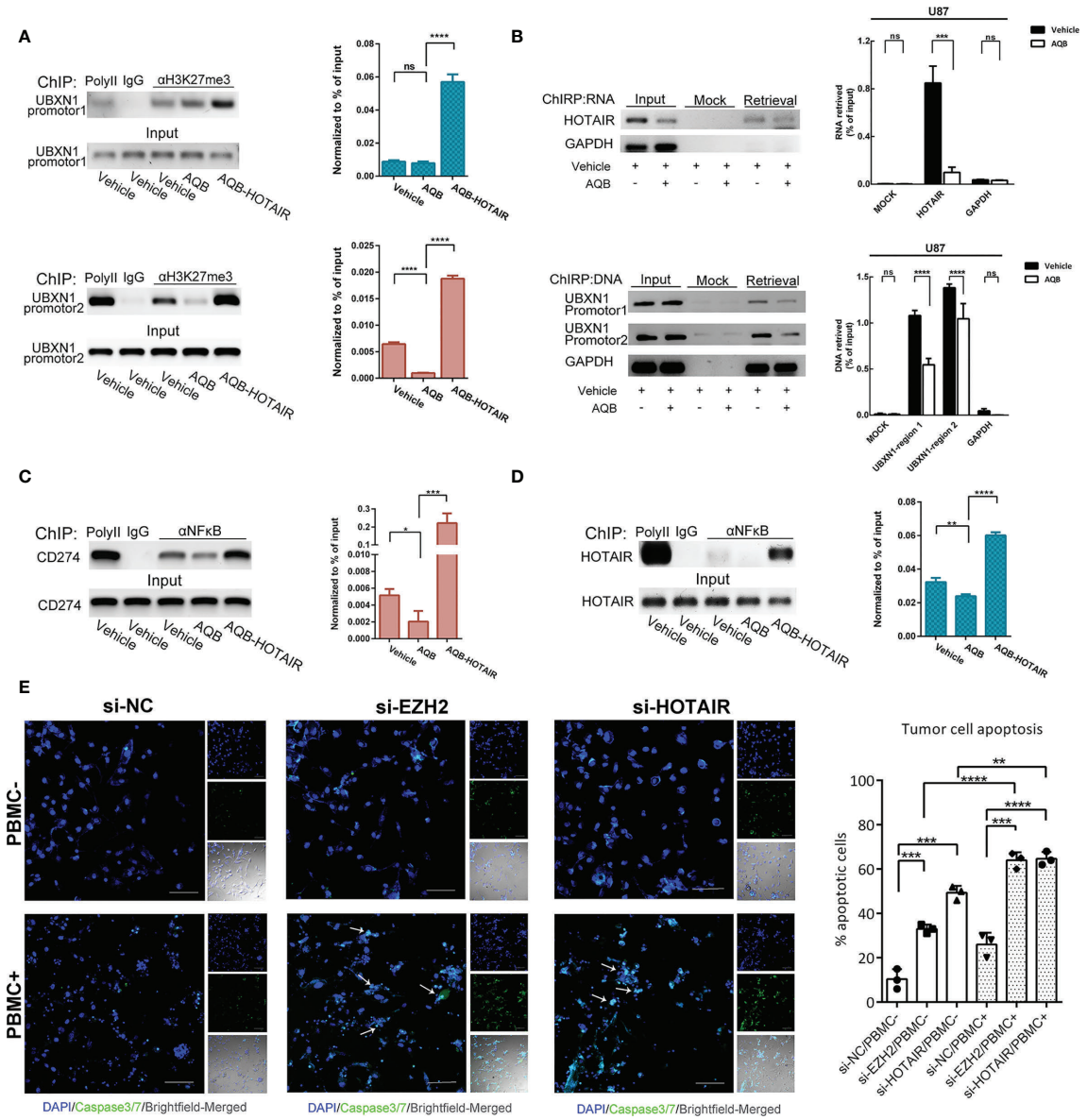

FIGURE 5 | HOTAIR inhibited the expression of UBXN1 by epigenetic modification. **(A)** ChIP assay detected the H3K27me3 modification on the promotor region of *UBXN1*. **(B)** Upper: ChIRP assay enriches HOTAIR RNA with high yield and specificity. Lower: ChIRP assay detect the HOTAIR binding region on the promotor of *UBXN1*. **(C)** ChIP assay detected NF-κB binding on the promotor of *CD274* in U87 treated with AQB or vehicle as control. **(D)** ChIP assay detected NF-κB binding on the promotor of *HOTAIR* in U87 cells treated with AQB or vehicle as control. **(E)** T cell killing assay of TBD cells treated with siRNAs for EZH2 and HOTAIR. Cell nuclei were stained by DAPI in blue, and apoptotic cells were displayed by fluorescent products of caspase 3/7 cleavage (green). For all the statistical histograms above, values are means ± s.d. from n = 3 independent experiments. The *P* value was determined by two-sided Student's t-test.

(median survival of HOTAIRwt: 17 days and HOTAIRwt-AQB: 21 days; **Figure 6D**). Moreover, immunohistochemistry staining showed the reduction in nuclear NF-κB and phospho-NF-κB levels in the AQB group (**Figure 6B**).

Next, we constructed TBD cell xenograft tumors in C57BL/6 black mice to established immunocompetent mouse model (**Figure 6G**). The *in vivo* bioluminescence imaging showed that AQB could dramatically inhibit the tumor growth of both the control group (72% reduction with $P < 0.05$) and the HOTAIRwt group (61% reduction with $P < 0.05$; **Figure 6E**). AQB treatment significantly prolonged the survival of glioma bearing mice both in control group and HOTAIRwt group (36.2% and 42% respectively; **Figure 6F**). Moreover, immunohistochemical staining showed that the infiltration of CD45 labeled leukocytes in tumor increased under AQB treatment, while the infiltration of CD14 labeled macrophages decreased, as well as the small amount of perforin and granzyme B staining was present in the tumor portion (**Figure 6H**). Taken together, these

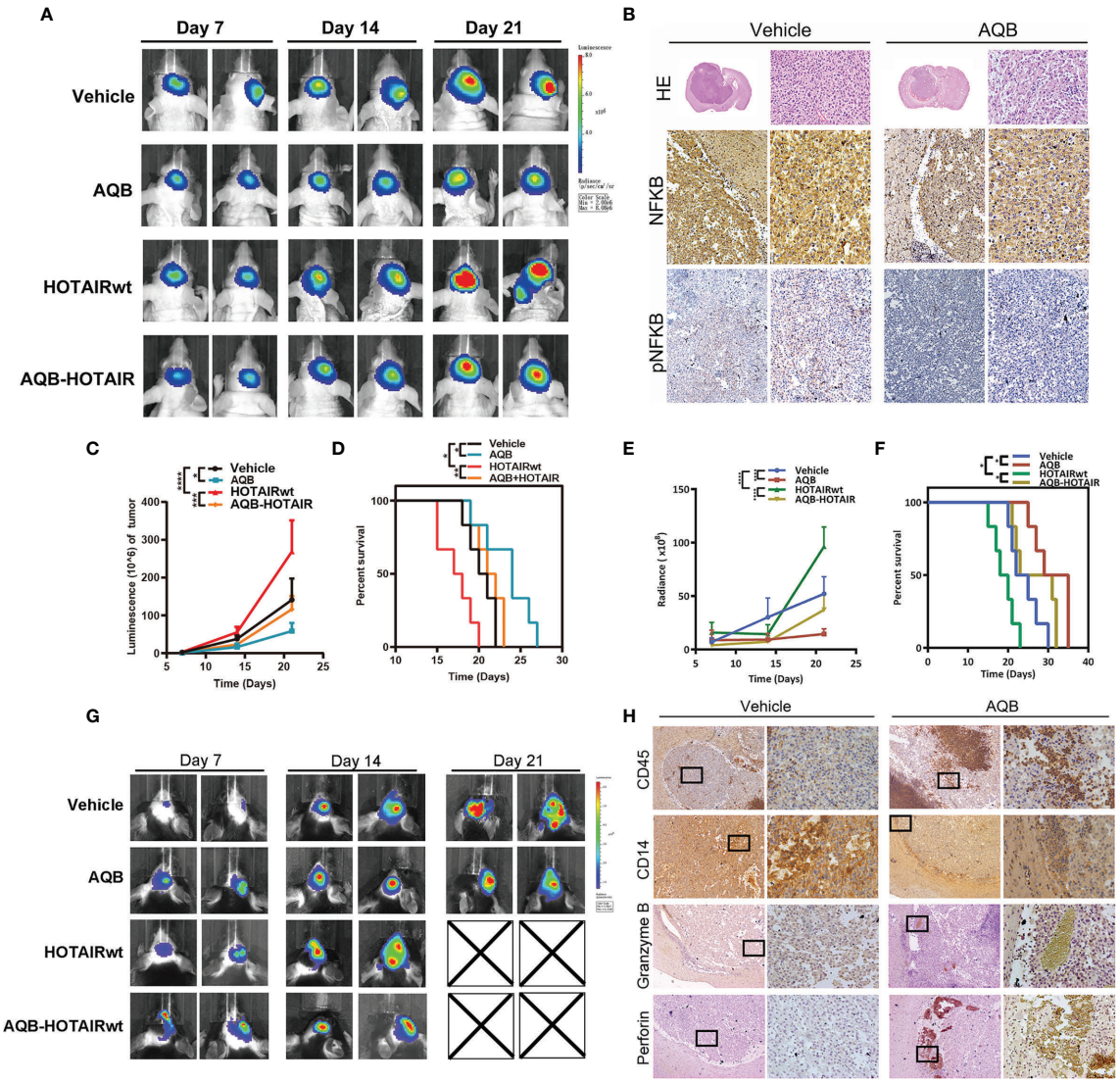

FIGURE 6 | Apparent inhibition of UBXN1 expression levels activated tumor growth and tumor growth regulated by NF-κB *in vivo*. **(A)** Representative pseudocolor bioluminescence images of mice implanted with intracranial tumors infected with HOTAIR overexpressing lentivirus or control lentivirus, and heal every other day with vehicle or AQB. **(B)** Representative images of the H&E-stained mice brain tissue and the immunohistochemical staining of NF-κB and pNF-κB in brain tissues. Nuclei were stained by DAPI. **(C)** The tumor growth curve with time in xenotypic *in situ* tumor model animal was calculated by corresponding light value in **(A)**. **(D)** Kaplan-Meier survival plot shows the overall survival of glioblastoma TBD mice treated with regime describe previously. **(E)** In heterotypic *in situ* tumor-bearing black mice, the tumor growth curve over time was calculated from the corresponding light values in **(G)**. **(F)** Kaplan-Meier survival plot shows the overall survival of glioblastoma TBD mice with same treatment. **(G)** Representative pseudocolor bioluminescence images of tumor-bearing C57BL/6 mice as shown previously, and heal every other day with vehicle or AQB. **(H)** Representative images of the immunohistochemical staining of CD45, CD14, perforin and Granzyme B in brain tissues. For all the statistical collapsed line graph above, values are means ± s.d. from n = 3 independent experiments. The P value was determined by two-sided Student's t-test.

findings indicate that the inhibition of HOTAIR function blocks the expression of PD-L1 to a certain extent on the surface of glioma cells, thereby further promotes the infiltration of tumor-related immune cells. Collectively, these experiments supported the notion that HOTAIR silencing the expression of UBXN1 can regulate the activation of NF-kB pathway and induce the expression of checkpoint protein PD-L1 on surface of glioma cells, thereby initiating glioma to escape T cell recognition and killing.

DISCUSSION

HOTAIR expression is commonly altered in glioblastoma and is especially abnormally elevated in mesenchymal glioma. Furthermore, HOTAIR promotes tumor progression through activation of β-catenin, PKM2, and other pathways (13, 24, 25). We have previously demonstrated that HOTAIR is a positive factor in the progression of malignant glioma and is directly related to poor prognosis in glioma patients. Moreover, we have

shown that HOTAIR exhibits a pro-oncogenic activity by modulating the cell cycle, and its main function of is to inhibit the expression of the target genes *via* H3K27 histone methylation and mediation of the PRC2 complex activity and to promote tumor progression (13, 24, 25). However, it is unclear whether HOTAIR is involved in the regulation of inflammation and immune escape in glioma cells. In the present study, we demonstrated the role of HOTAIR in the regulation of the NF-κB pathway, which is associated with inflammation and immunity. The analysis of protein spectrum data from HOTAIR knockdown cell lines revealed that HOTAIR expression was closely associated with the expression of NF-κB pathway proteins. *In vitro* experiments demonstrated that HOTAIR regulates the phosphorylation and nucleation of NF-κB, which was dependent on the epigenetic modulation of NF-κB negative regulators by HOTAIR. Furthermore, *in vivo* and *in vitro* experiments demonstrated that AQB inhibits tumor growth and reduces NF-κB and phospho-NF-κB levels in the xenograft model. Furthermore, AQB improved the immune sensitivity of tumor cells similarly to the effect exerted by a HOTAIR siRNA. These results provide evidence that HOTAIR regulates tumor cell inflammatory responses and immune escape *via* the NF-κB pathway in glioblastoma.

In a variety of malignancies with aberrant NF-κB activity, only a fraction of them are due to mutations in NF-κB genes. Abnormal activation of NF-κB in many malignant solid tumor cells may be due to inflammatory cytokine stimulation in the tumor microenvironment (18, 31). Herein, our data indicate that the lncRNA HOTAIR promotes NF-κB activity in malignant glioma cells, whereas its overexpression leads to aberrant NF-κB activation even without inflammatory stimulation. These findings suggest that the lncRNA HOTAIR is an essential "driver" of NF-κB signaling in malignant glioma cells. NF-κB is constitutively active in many tumor types and is considered a key factor in cancer development (18, 31). A number of negative regulators of the NF-κB pathway such as the deubiquitinases (DUB) A20 (32) and CYLD (33), ubiquitin ligase SOCS-1 (19), and a group of miRNAs (34), etc., have been identified as tumor suppressors. Many of these regulators are transcribed by NF-κB but participate in negative feedback loops to prevent a sustained or excessive activation of the NF-κB pathway (19). The activation and release of NF-κB depend on the phosphorylation of IκBα by the classical IKKα/IKKβ/CHUK complex. A cytoplasmic, NF-κB-interacting lncRNA reportedly blocks IκB phosphorylation and suppresses breast cancer metastasis (35). In our study, the lncRNA HOTAIR was implicated in the abnormal activation of the NF-κB pathway. Furthermore, protein spectrum data and *in vitro* experiments showed that HOTAIR activates the protein expression of the TNFα/NF-κB signaling complex and IκBα kinase complex. This abnormal activation may lead to high PD-L1 expression, which may block the tumor cell killing by T cells.

CONCLUSIONS

In summary, our data demonstrated that HOTAIR activates the implicated in inflammatory responses NF-κB pathway in mesenchymal glioma cells and promotes immune escape *via* an aberrant PD-L1 expression. Furthermore, *in vivo* and *vitro* data showed that HOTAIR inhibits the NF-κB repressors UBXN1 *via* an H3K27me3 modification, which promotes IKKα/IKKβ/IKKγ-IκBα-induced NF-κB activation and transmission and forms an HOTAIR-NF-κB axis.

DATA AVAILABILITY STATEMENT

The data presented in the study are deposited in the iProX repository, accession number IPX0003692000.

ETHICS STATEMENT

The animal study was reviewed and approved by Tianjin Medical University General Hospital Experimental Animal Welfare Ethics Committee.

AUTHOR CONTRIBUTIONS

YW, KY, and XL designed experiments, analyzed data and wrote the paper. YW, KY, WJ, JZ, YL, and YT performed experiments and contributed to writing. HW and CK supervised the study. All authors contributed to the article and approved the submitted version.

FUNDING

This work was supported by grants from National Nature Science Foundation of China (82073322) and Tianjin Key R&D Plan of Tianjin Science and Technology Plan Project (20YFZCSY00360).

SUPPLEMENTARY MATERIAL

The Supplementary Material for this article can be found online at: https://www.frontiersin.org/articles/10.3389/fimmu.2021.785463/full#supplementary-material

REFERENCES

1. Freeman GJ, Long AJ, Iwai Y, Bourque K, Chernova T, Nishimura H, et al. Engagement of the PD-1 Immunoinhibitory Receptor by a Novel B7 Family Member Leads to Negative Regulation of Lymphocyte Activation. *J Exp Med* (2000) 192(7):1027–34. doi: 10.1084/jem.192.7.1027
2. Han S, Zhang C, Li Q, Dong J, Liu Y, Huang Y, et al. Tumour-Infiltrating CD4(+) and CD8(+) Lymphocytes as Predictors of Clinical Outcome in Glioma. *Br J Cancer* (2014) 110(10):2560–8. doi: 10.1038/bjc.2014.162
3. Bouffet E, Larouche V, Campbell BB, Merico D, de Borja R, Aronson M, et al. Immune Checkpoint Inhibition for Hypermutant Glioblastoma Multiforme Resulting From Germline Biallelic Mismatch Repair

Deficiency. *J Clin Oncol* (2016) 34(19):2206–11. doi: 10.1200/JCO.2016.66.6552
4. Tsai MC, Spitale RC, Chang HY. Long Intergenic Noncoding RNAs: New Links in Cancer Progression. *Cancer Res* (2011) 71(1):3–7. doi: 10.1158/0008-5472.can-10-2483
5. Gupta RA, Shah N, Wang KC, Kim J, Horlings HM, Wong DJ, et al. Long non-Coding RNA HOTAIR Reprograms Chromatin State to Promote Cancer Metastasis. *Nature* (2010) 464(7291):1071–6. doi: 10.1038/nature08975
6. Guttman M, Amit I, Garber M, French C, Lin MF, Feldser D, et al. Chromatin Signature Reveals Over a Thousand Highly Conserved Large non-Coding RNAs in Mammals. *Nature* (2009) 458(7235):223–7. doi: 10.1038/nature07672
7. Guil S, Soler M, Portela A, Carrere J, Fonalleras E, Gomez A, et al. Intronic RNAs Mediate EZH2 Regulation of Epigenetic Targets. *Nat Struct Mol Biol* (2012) 19(7):664–70. doi: 10.1038/nsmb.2315
8. Chu C, Qu K, Zhong FL, Artandi SE, Chang HY. Genomic Maps of Long Noncoding RNA Occupancy Reveal Principles of RNA-Chromatin Interactions. *Mol Cell* (2011) 44(4):667–78. doi: 10.1016/j.molcel.2011.08.027
9. Karin M, Shalapour S. Regulation of Antitumor Immunity by Inflammation-Induced Epigenetic Alterations. *Cell Mol Immunol* (2021). doi: 10.1038/s41423-021-00756-y
10. Li J, Wang W, Zhang Y, Cieslik M, Guo J, Tan M, et al. Epigenetic Driver Mutations in ARID1A Shape Cancer Immune Phenotype and Immunotherapy. *J Clin Invest* (2020) 130(5):2712–26. doi: 10.1172/JCI134402
11. Guo W, Wang Y, Yang M, Wang Z, Wang Y, Chaurasia S, et al. LincRNA-Immunity Landscape Analysis Identifies EPIC1 as a Regulator of Tumor Immune Evasion and Immunotherapy Resistance. *Sci Adv* (2021) 7(7). doi: 10.1126/sciadv.abb3555
12. Ratnam NM, Sonnemann HM, Frederico SC, Chen H, Hutchinson MND, Dowdy T, et al. Reversing Epigenetic Gene Silencing to Overcome Immune Evasion in CNS Malignancies. *Front Oncol* (2021) 11:719091. doi: 10.3389/fonc.2021.719091
13. Zhang JX, Han L, Bao ZS, Wang YY, Chen LY, Yan W, et al. HOTAIR, a Cell Cycle-Associated Long Noncoding RNA and a Strong Predictor of Survival, is Preferentially Expressed in Classical and Mesenchymal Glioma. *Neuro-oncology* (2013) 15(12):1595–603. doi: 10.1093/neuonc/not131
14. Shi J, Lv S, Wu M, Wang X, Deng Y, Li Y, et al. HOTAIR-EZH2 Inhibitor AC1Q3QWB Upregulates CWF19L1 and Enhances Cell Cycle Inhibition of CDK4/6 Inhibitor Palbociclib in Glioma. *Clin Trans Med* (2020) 10(1):182–98. doi: 10.1002/ctm2.21
15. Zhang L, He A, Chen B, Bi J, Chen J, Guo D, et al. A HOTAIR Regulatory Element Modulates Glioma Cell Sensitivity to Temozolomide Through Long-Range Regulation of Multiple Target Genes. *Genome Res* (2020) 30(2):155–63. doi: 10.1101/gr.251058.119
16. Wang Z, Zhang C, Liu X, Wang Z, Sun L, Li G, et al. Molecular and Clinical Characterization of PD-L1 Expression at Transcriptional Level via 976 Samples Brain Glioma. *Oncoimmunol* (2016) 5(11):e1196310. doi: 10.1080/2162402X.2016.1196310
17. Akca H, Demiray A, Tokgun O, Yokota J. Invasiveness and Anchorage Independent Growth Ability Augmented by PTEN Inactivation Through the PI3K/AKT/NFkB Pathway in Lung Cancer Cells. *Lung Cancer* (2011) 73(3):302–9. doi: 10.1016/j.lungcan.2011.01.012
18. DiDonato JA, Mercurio F, Karin M. NF-kappaB and the Link Between Inflammation and Cancer. *Immunol Rev* (2012) 246(1):379–400. doi: 10.1111/j.1600-065X.2012.01099.x
19. Ruland J. Return to Homeostasis: Downregulation of NF-kappaB Responses. *Nat Immunol* (2011) 12(8):709–14. doi: 10.1038/ni.2055
20. Chernorudskiy AL, Gainullin MR. Ubiquitin System: Direct Effects Join the Signaling. *Sci Signaling* (2013) 6(280):pe22. doi: 10.1126/scisignal.2004251
21. Ghosh S, Hayden MS. Celebrating 25 Years of NF-κb Research. *Immunol Rev* (2012) 246(1):5–13. doi: 10.1111/j.1600-065X.2012.01111.x
22. Chen G, Goeddel DV. TNF-R1 Signaling: A Beautiful Pathway. *Sci (New York NY)* (2002) 296(5573):1634–5. doi: 10.1126/science.1071924
23. Dong F, Eibach M, Bartsch JW, Dolga AM, Schlomann U, Conrad C, et al. The Metalloprotease-Disintegrin ADAM8 Contributes to Temozolomide Chemoresistance and Enhanced Invasiveness of Human Glioblastoma Cells. *Neuro-oncology* (2015) 17(11):1474–85. doi: 10.1093/neuonc/nov042
24. Zhang K, Sun X, Zhou X, Han L, Chen L, Shi Z, et al. Long non-Coding RNA HOTAIR Promotes Glioblastoma Cell Cycle Progression in an EZH2 Dependent Manner. *Oncotarget* (2015) 6(1):537–46. doi: 10.18632/oncotarget.2681
25. Zhou X, Ren Y, Zhang J, Zhang C, Zhang K, Han L, et al. HOTAIR is a Therapeutic Target in Glioblastoma. *Oncotarget* (2015) 6(10):8353–65. doi: 10.18632/oncotarget.3229
26. Li Y, Ren Y, Wang Y, Tan Y, Wang Q, Cai J, et al. A Compound AC1Q3QWB Selectively Disrupts HOTAIR-Mediated Recruitment of PRC2 and Enhances Cancer Therapy of DZNep. *Theranostics* (2019) 9(16):4608–23. doi: 10.7150/thno.35188
27. Niedick I, Froese N, Oumard A, Mueller PP, Nourbakhsh M, Hauser H, et al. Nucleolar Localization and Mobility Analysis of the NF-kappaB Repressing Factor NRF. *J Cell Sci* (2004) 117(Pt 16):3447–58. doi: 10.1242/jcs.01129
28. Klemm S, Gutermuth J, Hültner L, Sparwasser T, Behrendt H, Peschel C, et al. The Bcl10-Malt1 Complex Segregates Fc Epsilon RI-Mediated Nuclear Factor Kappa B Activation and Cytokine Production From Mast Cell Degranulation. *J Exp Med* (2006) 203(2):337–47. doi: 10.1084/jem.20051982
29. Nicolle A, Zhang Y, Belguise K. The Emerging Function of PKCtheta in Cancer. *Biomolecules* (2021) 11(2):221–32. doi: 10.3390/biom11020221
30. Juneja VR, McGuire KA, Manguso RT, LaFleur MW, Collins N, Haining WN, et al. PD-L1 on Tumor Cells is Sufficient for Immune Evasion in Immunogenic Tumors and Inhibits CD8 T Cell Cytotoxicity. *J Exp Med* (2017) 214(4):895–904. doi: 10.1084/jem.20160801
31. Fornier MN, Rathkopf D, Shah M, Patil S, O'Reilly E, Tse AN, et al. Phase I Dose-Finding Study of Weekly Docetaxel Followed by Flavopiridol for Patients With Advanced Solid Tumors. *Clin Cancer Res* (2007) 13(19):5841–6. doi: 10.1158/1078-0432.ccr-07-1218
32. Cake MA, Appleyard RC, Read RA, Ghosh P, Swain MV, Murrell GC. Topical Administration of the Nitric Oxide Donor Glyceryl Trinitrate Modifies the Structural and Biomechanical Properties of Ovine Articular Cartilage. *Osteoarthritis cartilage* (2003) 11(12):872–8. doi: 10.1016/j.joca.2003.08.003
33. Brummelkamp TR, Nijman SM, Dirac AM, Bernards R. Loss of the Cylindromatosis Tumour Suppressor Inhibits Apoptosis by Activating NF-kappaB. *Nature* (2003) 424(6950):797–801. doi: 10.1038/nature01811
34. Boldin MP, Baltimore D. MicroRNAs, New Effectors and Regulators of NF-kappaB. *Immunol Rev* (2012) 246(1):205–20. doi: 10.1111/j.1600-065X.2011.01089.x
35. Liu B, Sun L, Liu Q, Gong C, Yao Y, Lv X, et al. A Cytoplasmic NF-kappaB Interacting Long Noncoding RNA Blocks IkappaB Phosphorylation and Suppresses Breast Cancer Metastasis. *Cancer Cell* (2015) 27(3):370–81. doi: 10.1016/j.ccell.2015.02.004

Conflict of Interest: The authors declare that the research was conducted in the absence of any commercial or financial relationships that could be construed as a potential conflict of interest.

Publisher's Note: All claims expressed in this article are solely those of the authors and do not necessarily represent those of their affiliated organizations, or those of the publisher, the editors and the reviewers. Any product that may be evaluated in this article, or claim that may be made by its manufacturer, is not guaranteed or endorsed by the publisher.

Copyright © 2021 Wang, Yi, Liu, Tan, Jin, Li, Zhou, Wang and Kang. This is an open-access article distributed under the terms of the Creative Commons Attribution License (CC BY). The use, distribution or reproduction in other forums is permitted, provided the original author(s) and the copyright owner(s) are credited and that the original publication in this journal is cited, in accordance with accepted academic practice. No use, distribution or reproduction is permitted which does not comply with these terms.

frontiers in Immunology

ORIGINAL RESEARCH
published: 08 December 2021
doi: 10.3389/fimmu.2021.800928

Galectin-9/TIM-3 as a Key Regulator of Immune Response in Gliomas With Chromosome 1p/19q Codeletion

Guanzhang Li[1,2†], Ruoyu Huang[1,2†], Wenhua Fan[1,2†], Di Wang[2†], Fan Wu[1], Fan Zeng[1], Mingchen Yu[1], You Zhai[1], Yuanhao Chang[1], Changqing Pan[2], Tao Jiang[1,2,3,4,5], Wei Yan[6], Hongjun Wang[7*] and Wei Zhang[1,2,4,5*]*

[1] Department of Molecular Neuropathology, Beijing Neurosurgical Institute, Capital Medical University, Beijing, China, [2] Department of Neurosurgery, Beijing Tiantan Hospital, Capital Medical University, Beijing, China, [3] Center of Brain Tumor, Beijing Institute for Brain Disorders, Beijing, China, [4] China National Clinical Research Center for Neurological Diseases, Beijing, China, [5] Chinese Glioma Genome Atlas Network (CGGA) and Asian Glioma Genome Atlas Network (AGGA), Beijing, China, [6] Department of Neurosurgery, The First Affiliated Hospital of Nanjing Medical University, Nanjing, China, [7] Department of Neurosurgery, The Second Affiliated Hospital of Harbin Medical University, Harbin, China

Gliomas with chromosome 1p/19q codeletion were considered a specific tumor entity. This study was designed to reveal the biological function alterations tightly associated with 1p/19q codeletion in gliomas. Clinicopathological and RNA sequencing data from glioma patients were obtained from The Cancer Genome Atlas and Chinese Glioma Genome Atlas databases. Gene set variation analysis was performed to explore the differences in biological functions between glioma subgroups stratified by 1p/19q codeletion status. The abundance of immune cells in each sample was detected using the CIBERSORT analytical tool. Single-cell sequencing data from public databases were analyzed using the t-distributed stochastic neighbor embedding (t-SNE) algorithm, and the findings were verified by *in vitro* and *in vivo* experiments and patient samples.We found that the activation of immune and inflammatory responses was tightly associated with 1p/19q codeletion in gliomas. As the most important transcriptional regulator of Galectin-9 in gliomas, the expression level of CCAAT enhancer-binding protein alpha in samples with 1p/19q codeletion was significantly decreased, which led to the downregulation of the immune checkpoints Galectin-9 and TIM-3. These results were validated in three independent datasets. The t-SNE analysis showed that the loss of chromosome 19q was the main reason for the promotion of the antitumor immune response. IHC protein staining, *in vitro* and *in vivo* experiments verified the results of bioinformatics analysis. In gliomas, 1p/19q codeletion can promote the antitumor immune response by downregulating the expression levels of the immune checkpoint TIM-3 and its ligand Galectin-9.

Keywords: glioma, 1p/19q codeletion, DNA repair functions, immune checkpoint, prognosis prediction

OPEN ACCESS

Edited by:
Quan Cheng,
Central South University, China

Reviewed by:
Jie Ding,
Stanford University, United States
Lei Han,
Tianjin Medical University General Hospital, China

***Correspondence:**
Wei Zhang
zhangwei_vincent@126.com
Hongjun Wang
wanghongjun8000@sina.com
Wei Yan
neuro_yw@njmu.edu.cn

[†]These authors have contributed equally to this work

Specialty section:
This article was submitted to Cancer Immunity and Immunotherapy, a section of the journal Frontiers in Immunology

Received: *24 October 2021*
Accepted: *24 November 2021*
Published: *08 December 2021*

Citation:
Li G, Huang R, Fan W, Wang D, Wu F, Zeng F, Yu M, Zhai Y, Chang Y, Pan C, Jiang T, Yan W, Wang H and Zhang W (2021) Galectin-9/TIM-3 as a Key Regulator of Immune Response in Gliomas With Chromosome 1p/19q Codeletion. Front. Immunol. 12:800928. doi: 10.3389/fimmu.2021.800928

INTRODUCTION

Gliomas, the most common and lethal primary intracranial tumor in adults, are characterized by strong invasiveness and a high recurrence rate (1–3). Tumor-specific molecular alterations, such as isocitrate dehydrogenase 1 (IDH1) mutation and the codeletion of chromosome arms 1p and 19q (1p/19q codeletion), could serve as prognostic indicators or therapeutic targets for glioma patients (4–6). These biomarkers were also included in the 2016 World Health Organization (WHO) Classification of Tumors of the Central Nervous System (CNS), providing an important theoretical foundation for the diagnosis and individualized treatment of gliomas (7). However, the specific molecular mechanism by which 1p/19q codeletion affects the biological characteristics and clinical prognosis of gliomas remains unclear.

Chromosome 1p/19q codeletion is a representative event in the oligodendroglial histologic type of gliomas and is strongly associated with overall survival of glioma patients (8–10). In general, glioma patients with 1p/19q codeletion tend to have a better prognosis (8, 11). Patients with 1p/19q codeletion are more sensitive to chemotherapy with alkylating agents such as temozolomide (TMZ) (12). The loss of chromosome 1p or 19q inevitably results in significant reductions in the expression of multiple genes located on these regions; thus, 1p/19q codeletion can cause significant abnormalities in the biological function of gliomas (13). The remolding of the tumor immune environment plays an essential role in chemotherapy resistance of various cancers (14). Thus, we hypothesized that 1p/19q codeletion may improve glioma sensitivity to postoperative treatment by regulating the tumor immune microenvironment.

This study comprehensively analyzed the alterations in biological functions associated with 1p/19q codeletion in gliomas by gene set variation analysis (GSVA) (15). We observed differences in immune system process between patients according to 1p/19q codeletion status. To further clarify the specific molecular mechanism of 1p/19q codeletion remodeling of the immune microenvironment of gliomas, CIBERSORT was applied, revealing seven immune metagenes (16, 17). The results suggested that 1p/19q codeletion upregulated immune response by reducing the expression of TIM-3 and its ligand Galectin-9 but had no significant effect on immune cell infiltration. We also found that the transcription factor CCAAT enhancer-binding protein alpha (CEBPA), located on chromosome 19q, played a key role in regulating the expression level of Galectin-9 in both lower-grade glioma (LGG) and glioblastoma (GBM). These results indicate that the loss of chromosome 19q in glioma patients with 1p/19q codeletion could significantly inhibit Galectin-9 expression and the immunosuppressive function of TIM-3. In conclusion, this is the first integrative study to illustrate the association between 1p/19q codeletion and the immune microenvironment of gliomas, which may provide a more accurate assessment of individualized clinical management in patients with gliomas.

METHODS

Sample and Databases

This study was approved by Beijing Tiantan Hospital Institutional Review Board (IRB). Written informed consents were obtained from the patients (or their families).

This study included a total of 368 patients with data on transcriptome sequencing and 1p/19q codeletion status. The details of sample acquisition and sequencing were described previously (18). Pathological diagnosis was confirmed by at least two neuropathology experts in the Neuropathology Department of Beijing Neurosurgical Institute. The tumor 1p36 and 19q13 statuses were determined using fluorescent *in situ* hybridization analysis of formalin-fixed, paraffin-embedded blocks. The CGGA project performed transcriptome sequencing on two batches of glioma samples at different periods, named the CGGA database and the CGGA New database respectively. These two databases are mutually independent databases and can be used as an independent verification database for each other. Sequence data from the Cancer Genome Atlas (TCGA) mRNA-seq database were downloaded from public databases (https://cancergenome.nih.gov). The clinical information of the patients is summarized in **Table 1**.

Availability of Data and Material

The sequencing data, clinical data and molecular pathology data of all patients were uploaded to the CGGA portal (http://cgga.org.cn/). All data related to this research are available on reasonable request from the first and corresponding authors.

GSVA

A total of 7,345 biological functional enrichment scores calculated independently for each patient were generated based on default parameters in the *gsva* package in R, as described previously (19). Subsequently, all negatively regulated BPs have been removed. Based on the remaining 6613 biological processes, the biological functions related to 1p/19q codel status were examined. The gene list for each biological function is available from the AmiGO 2 Web portals (http://amigo.geneontology.org).

Immune Cells and Cytokine Enrichment Scores

The abundance of immune cells in each patient was estimated from transcriptome sequencing data using CIBERSORT analytical tool developed by Newman et al. (16). The calculation was performed online using default parameters (https://cibersort.stanford.edu). The calculation of cytokines scores and the corresponding gene list were calculated by the GSVA algorithm as described previously (18, 20). Subsequently, the significance of the difference between the enrichment score of two groups was verified by *Student's t-test*.

Single-Cell Sequencing Analysis

Single-cell sequencing and molecular pathology data were downloaded from the Gene Expression Omnibus databases (https://www.ncbi.nlm.nih.gov/gds/?term=GSE70630 and https://www.ncbi.nlm.nih.gov/gds/?term=GSE89567). Based on

TABLE 1 | Clinical information of patients.

Characteristics	No. of Patients (CGGA)		No. of Patients (CGGA New)		No. of Patients (TCGA)	
	Codel	Non-Codel	Codel	Non-Codel	Codel	Non-Codel
Age at diagnosis						
Mean	38.5	38.1	41.3	38.9	43.5	37.8
Standard Deviation	7.4	8.2	9.3	8.9	12.3	11.7
Gender						
Male	29	27	25	46	44	61
Female	15	19	26	24	38	59
Histology						
Astrocytoma	0	31	5	30	2	44
Oligodendroglioma	22	1	16	3	63	31
Oligoastrocytoma	22	14	30	37	17	45
WHO Grade						
II	44	46	51	70	82	120
III or IV	0	0	0	0	0	0
IDH1 Mutation						
Mutation	44	46	51	70	82	120
Wildtype	0	0	0	0	0	0
Survival Time						
Range (Days)	181-4143	19-4163	127-4075	41-4374	2-5466	1-6331
Median (Days)	3197	552.5	2703	664	439	373

the cell markers from the Cellmarker website (http://biocc.hrbmu.edu.cn/CellMarker), the cells for each patient were grouped independently using the t-distributed stochastic neighbor embedding (t-SNE) algorithm in the R environment.

Immunohistochemical (IHC) Staining

Paraffin-embedded tissues were obtained from the CGGA sample bank. The IHC experimental procedures and scoring methods were as reported previously (21). The antibodies for IHC staining included those for CEBPA (Abcam, ab140479, 1:200), Galectin-9 (Proteintech, 17938-1-AP, 1:100), and TIM-3 (Proteintech, 60355-1-lg, 1:1000).

Cell Isolation and Culture

293T and U87 cell lines were obtained from the Institute of Biochemistry and Cell Biology, Chinese Academy of Science. 293T and U87 cell lines were cultured in medium containing DMEM (Gibco) supplemented with 10% FBS (Gibco). T cells were obtained from a healthy adult male donor. Isolation and culture of T cells was performed following the protocol as previously described (22).

siRNA Transfection

The CEBPA siRNA and the corresponding negative control plasmid were purchased from syngentech (Beijing, China). 293T cells were transfected with siRNA using X-tremeGENE HP DNA Transfection Reagent (Roche, Switzerland) according to instructions exactly. The transfection efficiency was determined by the proportion of fluorescence-labeled cells.

Western Blotting

The extraction of total cell protein and the Western Blotting experiment were carried out as previous described (23). Antibodies for Western Blotting: CEBPA antibody (Abcam, ab140479, 1:1000), Galectin-9 antibody (proteintech, 17938-1-AP, 1:500), TIM-3 antibody (proteintech, 60355-1-lg, 1:1000), GAPDH antibody (proteintech, 60004-1-lg, 1:5000).

Flow Cytometry

The surgically removed tumor tissue was washed with phosphate-buffered saline and immediately immersed in DMEM medium and transported to the laboratory within half an hour. Then, the tumor sample was fully mechanical and enzymatic dissociated into single cells. After the dead cells removed by Dead Cell Removal Kit (miltenyi, 130-090-101), the remaining cells were used for flow cytometry. Antibodies for flow cytometry: TIM-3 antibody (1:100, BioLegend, 345012), Galectin-9 antibody (1:100, BioLegend, 348911), CD3 antibody (1:100, STEMCELL, 60011AZ.1).

In Vivo Xenograft Growth

Animal experiments were performed at the animal laboratory of Beijing Neurosurgical Institute according to NIH guidelines. Luciferase labeled glioma tumor cells with/without CEBPA knock down and T cells were mixed (1:1, totally 4×10^5 cells in 5 μL of PBS) and then transplanted into the right hemisphere of NOD-Prkdcs^{cid} Il2rg^{null} mice (23). The growth of intracranial tumors in mice was monitored weekly by *in vivo* fluorescence imaging.

Statistical Analysis

The statistical analysis and visualization in this study were performed using R (https://www.r-project.org/, v3.5.0), IBM SPSS Statistics for Windows, version 25.0 (IBM Corp., Armonk, NY) and GraphPad Prism version 8.0 (La Jolla, CA). After applying the homogeneity test of variance, significant differences between two groups of normally distributed data were verified by the Student's t-test. Significant correlations between two groups of normally distributed data were verified

using the Pearson's correlation analysis. For all statistical methods, $p<0.05$ indicated significant differences.

RESULTS

Gliomas With 1p/19q Codeletion Show a Unique Tumor Immune Status

Chromosomal 1p/19q codeletion, as a genomic variation at the chromosome level, contribute to dysfunction in tumor biological processes (11, 24). To explore the potential functional characteristics of 1p/19q codeleted tumors, the enrichment scores of 6,613 biological functions were obtained through GSVA of the CGGA and TCGA RNA-seq databases. As shown in **Figures 1A–C**, more than 3,000 biological functions showed significant differences between 1p/19q codeleted and non-codeleted tumors. After classifying these functions, we found that the immune system process was most tightly correlated with the 1p/19q codeletion status in the glioma samples (**Figures 1D–F**). These results indicated that 1p/19q codeletion may play an essential role in the regulation of the tumor immune microenvironment of gliomas.

Overview of the Immune Process in Tumors With Different 1p/19q Codeletion Statuses

To overview the differences in immune response between 1p/19q codeleted and non-codeleted samples, we included the top 11 critical immune system processes. Student's t-tests were performed to evaluate the differences in enrichment scores between stratified patients. The results suggested that most tumor-related immune responses were tightly correlated with 1p/19q codeletion status in the CGGA database, especially the activation of T lymphocytes, T cell and natural killer (NK) cell-mediated immune response to tumor cells, as well as the production and secretion of cytokines (**Figure 2A**). These analyses were also performed in the CGGA NEW and TCGA RNA-seq database for validation, with similar results (**Figures 2B, C**). These results indicated that 1p/19q codeletion status had a significant effect on T lymphocytes, NK cells, and cytokine-mediated antitumor immunity.

1p/19q Codeletion Status Was Associated With Tumor Inflammatory Activities

Infiltrating immune cells are a vital component of the tumor microenvironment, which has diverse roles in glioma biology (25).

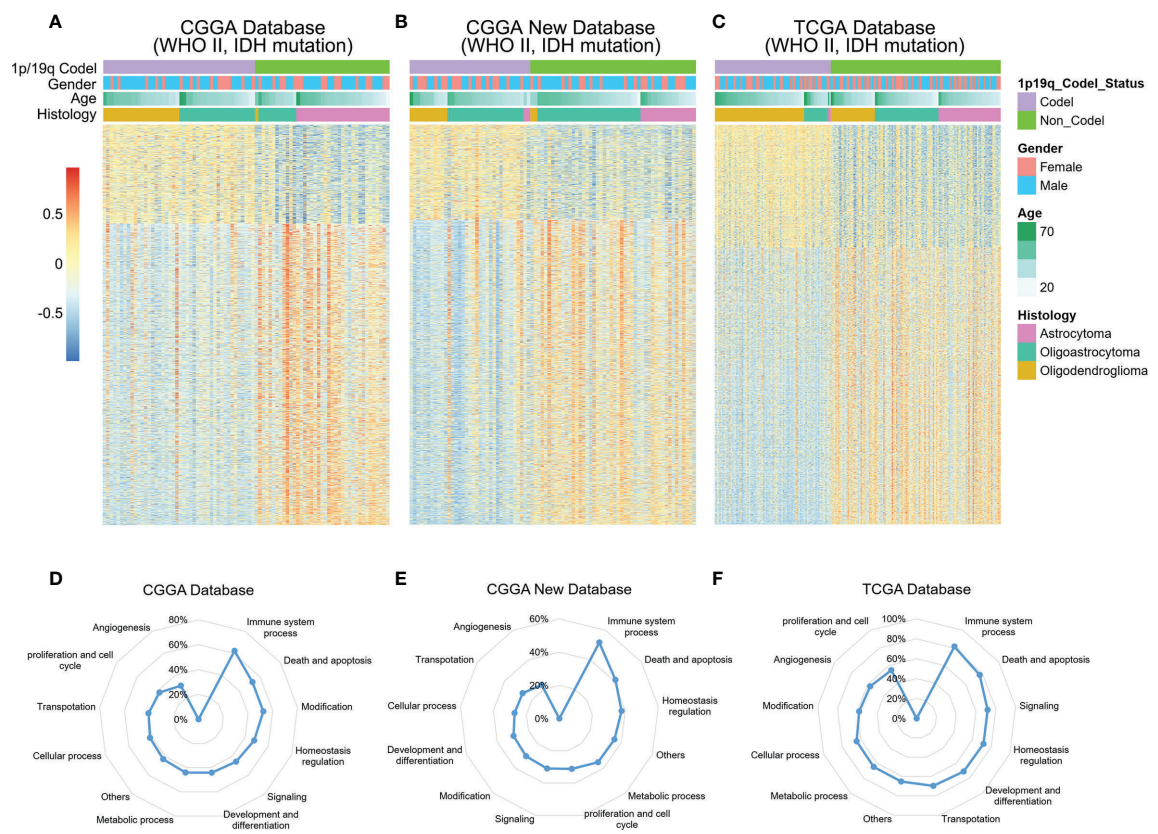

FIGURE 1 | Relationships between chromosome 1p/19q codeletion and altered biological processes in glioma. **(A–C)** Heatmap showing the enrichment patterns of biological processes associated with 1p/19q codeletion status in the CGGA, CGGA New and TCGA databases. **(D–F)** Alterations in different classifications of biological functions in gliomas samples with 1p/19q codeletion.

Thus, to further explore whether there was a significant difference in immune cell infiltration between 1p/19q codeletion and 1p/19q non-codeletion samples, we evaluated the abundance of various types of immune cells in the CGGA and TCGA databases by CIBERSORT. The results showed significant differences between stratified patients for only a few types of immune cells; however, these differences could not be mutually verified in the three databases (**Supplementary Figures 1A–C**). This finding indicates that 1p/19q codeletion status may not regulate the tumor immune microenvironment by affecting the infiltration of immune cells in gliomas. To further investigate the function of 1p/19q codeletion in the tumor immune microenvironment of gliomas, we assessed seven metagenes. As we described previously, these seven metagenes represent several types of inflammation and immune responses (18). The results showed significantly reduced enrichment scores for hematopoietic cell kinase, lymphocyte-specific protein tyrosine kinase, and major histocompatibility complex II (MHC-II) in patients with 1p/19q codeletion (**Figures 3A–C**), suggesting the activation of the immunological functions of lymphocyte and antigen-presenting cells.

Specific Reduction in the Expression of TIM-3 and Its Ligands in Gliomas With 1p/19q Codeletion

Our previous studies showed that immune checkpoints such as programmed cell death protein 1 (PD1) and TIM-3 play a crucial role in the regulation of the immune and inflammatory response in glioma (18, 20). This study investigated multiple immune checkpoint receptors and their ligands to further explore the

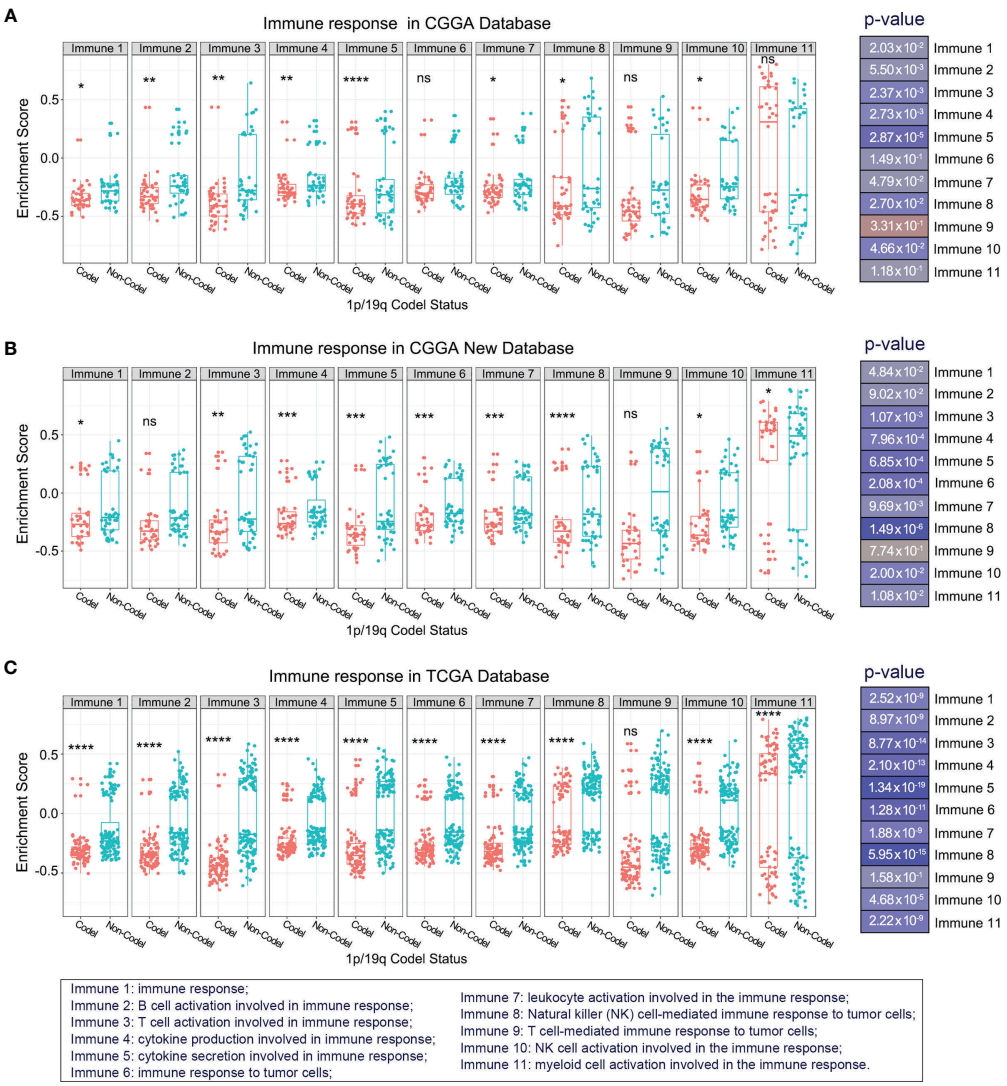

FIGURE 2 | Overview of the differences in kernel immune response in glioma patients stratified by 1p/19q codeletion status in the CGGA **(A)**, CGGA New **(B)**, and TCGA **(C)** databases. The significance of the difference between the two groups was verified by *Student's t-test*. $^{ns}p > 0.05$, $^{*}p < 0.05$, $^{**}p < 0.01$, $^{***}p < 0.001$, $^{****}p < 0.0001$.

effect of 1p/19q codeletion on the expression level of immune checkpoints. We observed significant differences in some immune checkpoint receptors and their ligands in patients stratified according to 1p/19q codeletion status in the CGGA database (**Figures 4A, B**). For further validation, similar analyses were performed in the CGGA NEW database and TCGA database (**Figures 4C–F**). The results showed that only TIM-3 and DNAX accessory molecule-1 (DNAM-1) with their respective ligands showed consistent expression differences between stratified patients across all databases (**Figures 4A–F**). However, the expression level of DNAM-1 and its ligand CD155 in glioma was very low, indicating that they may play a limited role in regulating the glioma tumor immune microenvironment (**Figures 4G–I**). In contrast, high expression levels of TIM-3 and its ligand Galectin-9 were observed in glioma samples (**Figures 4G–I** and **Supplementary Figure 2**). Thus, we

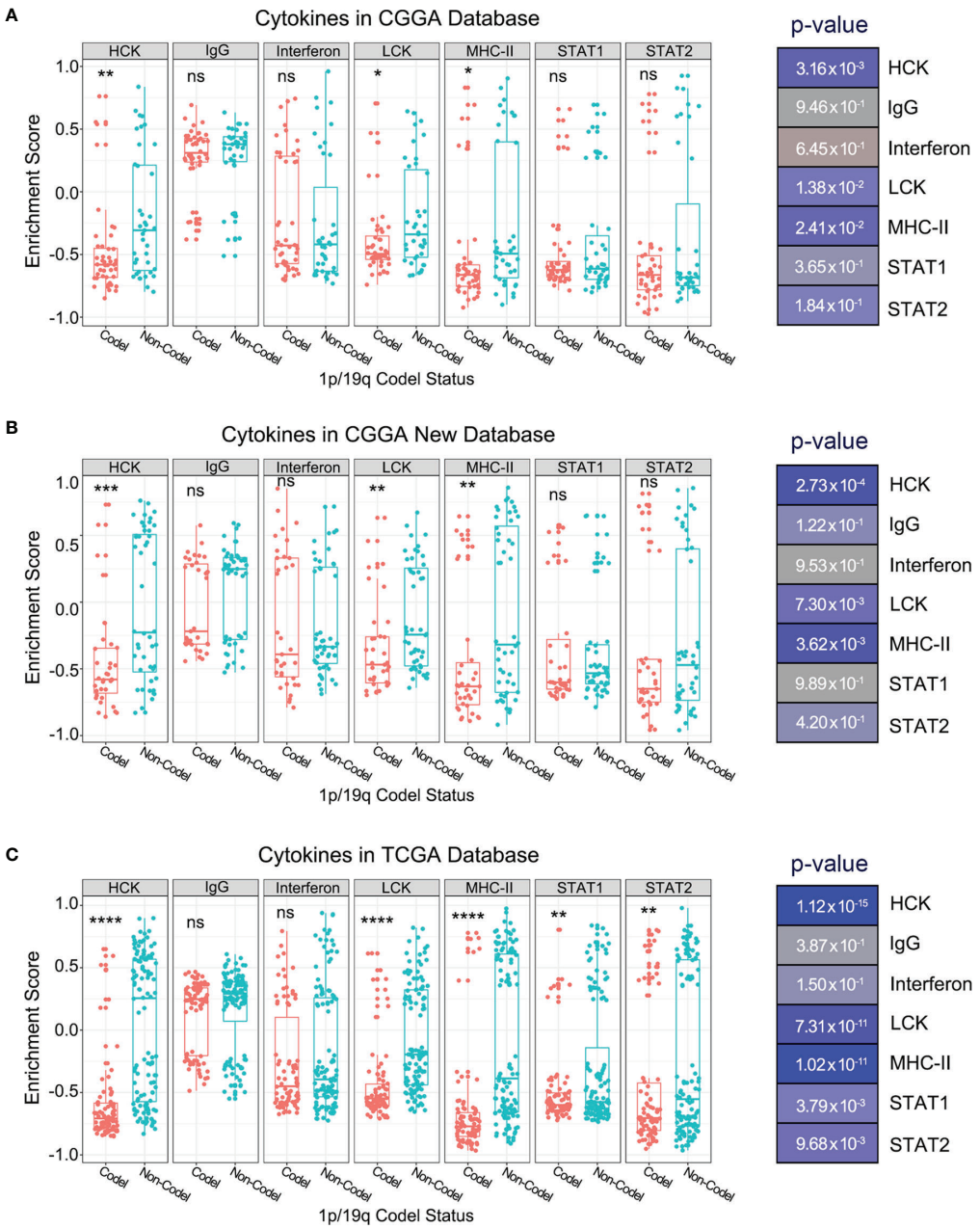

FIGURE 3 | Enrichment scores of seven immune and inflammatory-related metagenes in glioma patients with different 1p/19q codeletion status in the CGGA **(A)**, CGGA New **(B)**, and TCGA **(C)** databases. The significance of the difference between the two groups was verified by *Student's t-test*. $^{ns}p > 0.05$, $^{*}p < 0.05$, $^{**}p < 0.01$, $^{***}p < 0.001$, $^{****}p < 0.0001$.

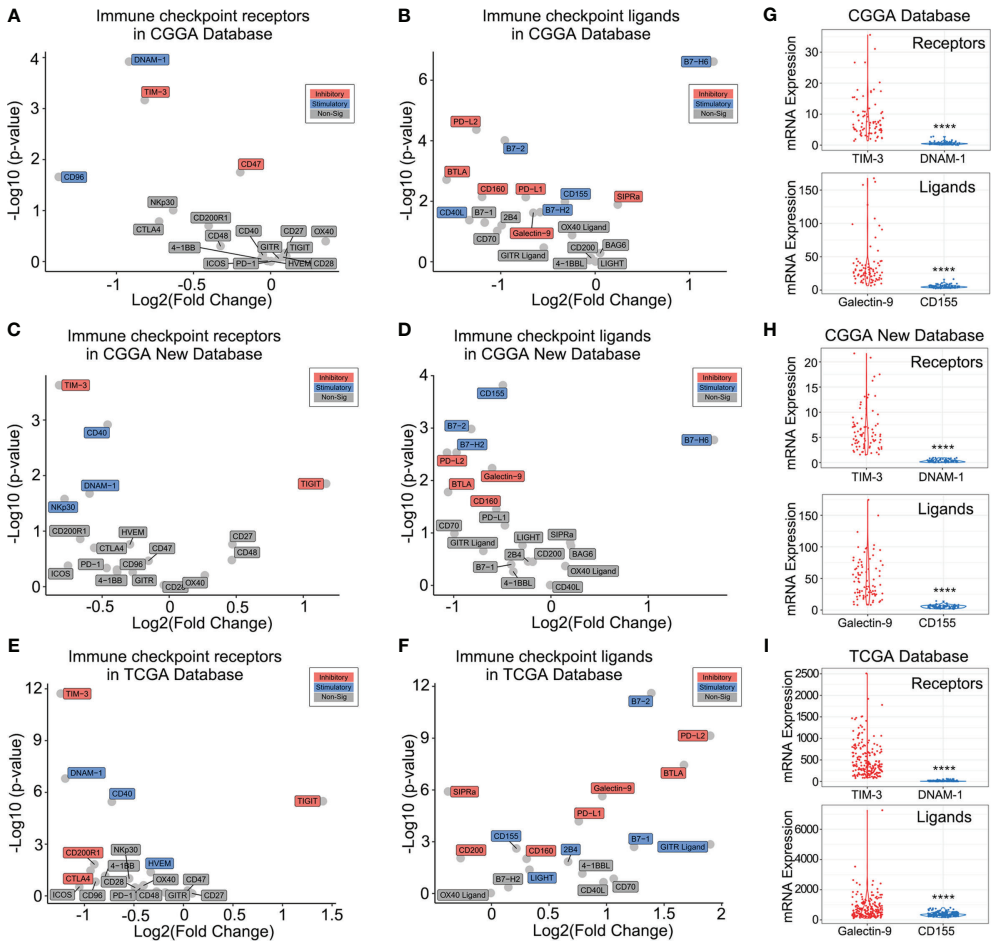

FIGURE 4 | Association between 1p/19q codeletion and immune checkpoints. **(A–F)** Differences in immune checkpoint expression in glioma patients with different 1p/19q codeletion status in the CGGA **(A, B)**, CGGA New **(C, D)**, and TCGA databases **(E, F)** databases. **(G–I)** TIM-3/Galectin-9 and DNAM-1/CD155 expression levels in the CGGA **(G)**, CGGA New **(H)**, and TCGA **(I)**. The significance of the difference between the two groups was verified by *Student's t-test*. *****p* < *0.0001*.

hypothesized that 1p/19q codeletion may change the immune microenvironment of glioma by affecting TIM-3 or Galectin-9 expression levels.

Decreased Expression of TIM-3 and Its Ligands in 1p/19q Codeletion Tumors Owing to Decreased CEBPA

To explore whether the differential expression of TIM-3 and its ligands in different 1p/19q codeletion status was independent of clinical characteristics, the relationship between them was studied. The results showed that gender, age, total number of tumor involved regions, and the degree of surgical resection are not related to the expression of Galectin-9 and TIM-3 (**Supplementary Figures 3–5**). We further investigated the specific molecular mechanism by which 1p/19q codeletion affected TIM-3 and Galectin-9 expression levels. Relevant studies confirmed that four transcription factors (AR, CEBPA, CEBPB, and TFAP2C) are involved in the regulation of Galectin-9 gene expression (26–28). We found that, among these four transcription factors, only CEBPA located on chromosome 19q13.11 was tightly correlated with Galectin-9 expression level in both CGGA and TCGA databases (**Figure 5A** and **Supplementary Figure 6**). Furthermore, we downloaded a pan-cancer database from a public website to further explore whether there are similar phenomena in other kinds of tumor tissues. As shown in **Figure 5B**, compared with other tumor samples, CEBPA and Galectin-9 were most closely correlated in lower-grade glioma (LGG, WHO grades II and III). They were also tightly correlated in glioblastoma multiforme (GBM, WHO grade IV). These results indicated differences in the transcription factors regulating Galectin-9 expression in different tumor tissues. Among them, CEBPA played a key role in the regulation of Galectin-9 expression in gliomas. As CEBPA is located on chromosome 19q13.11, the deletion of chromosome 19q likely inhibits Galectin-9 transcription by downregulating CEBPA expression. Due to the absence of ligands, the immunosuppressive effect of TIM-3 was significantly attenuated. This may explain the better prognosis of glioma

patients with 1p/19q codeletion. To further investigate whether the chromosome 1p deletion also participated in the regulation of CEBPA and Galectin-9 expression, we also analyzed single-cell sequencing data from the GSE70630 and GSE89567 databases. t-SNE was performed to evaluate CEBPA and Galectin-9 expression levels in glioma cells with different 1p/19q codeletion statuses. The results revealed significantly reduced CEBPA and Galectin-9 expression levels in most glioma cells with 1p/19q codeletion (**Figure 5C**). The same phenomenon was found in glioma cells with only chromosome 19q deletion (**Figure 5C**). However, glioma cells with intact chromosome 1p/19q showed a significantly increased proportion of cells with high CEBPA and Galectin-9 expression levels (**Figure 5C**).

CEBPA, Galectin-9, and TIM-3 Protein Expression Levels by IHC

To further verify the results of the bioinformatics analyses described above, IHC protein staining was performed in an independent group of glioma patients from the CGGA database. After stratifying glioma samples according to WHO grade and 1p/19q codeletion status, we found lower expression levels of CEBPA, Galectin-9, and TIM-3 proteins in whole grade glioma samples with 1p/19q codeletion compared with those in samples with retained 1p/19q or normal tissues (**Figures 6A, B**). Collectively, we proved that 1p/19q codeletion status had a significant impact on the tumor immune microenvironment of gliomas at mRNA and protein levels.

The Decreased Galectin-9 Regulated by CEBPA Can Improve the Efficacy of Cytotherapy

To further verify the regulatory relationship between CEBPA and Galectin-9, biochemical studies were performed. *In vitro* experiments confirmed that knockdown of CEBPA can significantly decrease in expression of Galectin-9 at the transcriptome level and protein level (**Figures 7A, B**). Furthermore, 4 samples from 1p/19q codel LGG and 5 samples from 1p/19q non-codel LGG were collected for flow cytometry experiments. The proportion of cells expressing CD3, TIM-3 and Galectin-9 were tested by Flow Cytometer. The results showed that the proportion of CD3+ cells was no significant correlated with the 1p/19q codel status of LGG, and the positive ratio of TIM-3 and Galectin-9 were significantly lower in 1p/19q codel LGG (**Figure 7C**).

Cytotherapy, as a new type of tumor immunotherapy, is coming into focus recently (29). Therefore, the difference in efficacy of cytotherapy in 1p/19q codel and non-codel tumors were explored. Luciferase labeled glioma tumor cells with/

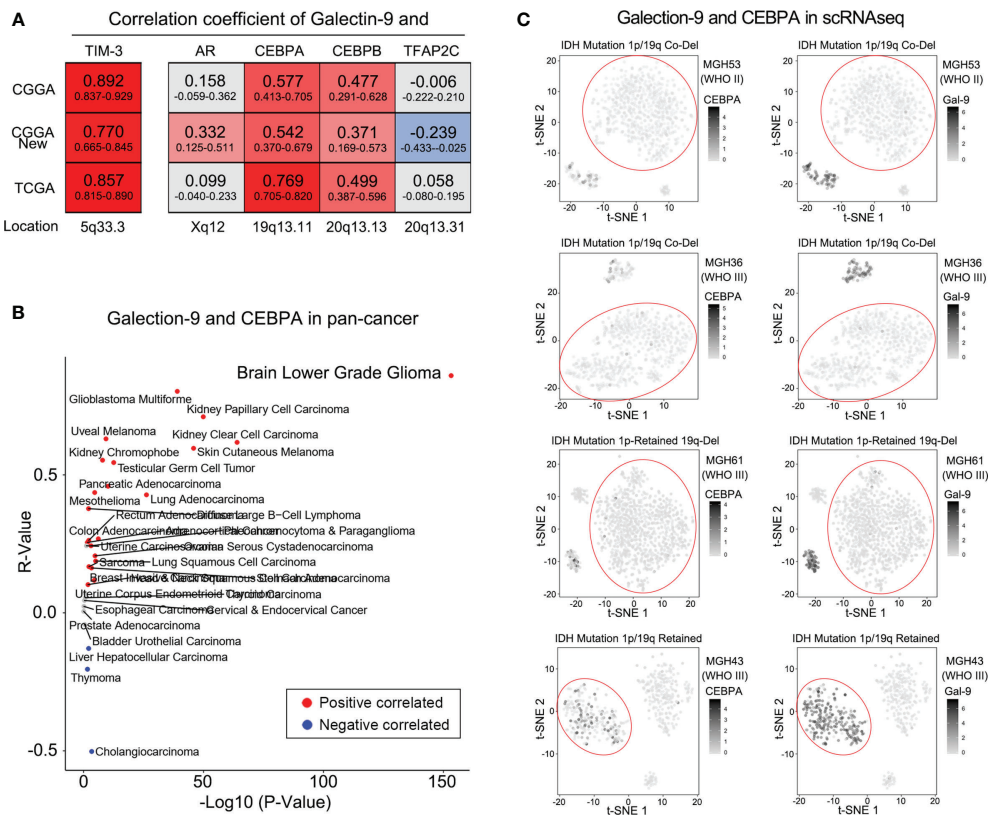

FIGURE 5 | 1p/19q codeletion downregulated Galectin-9 expression *via* CEBPA. **(A)** Correlations between Galectin-9 and transcription factors by Pearson correlation analysis in the CGGA and TCGA databases. **(B)** Correlation between Galectin-9 and CEBPA detected by Pearson correlation analysis in the TCGA pan-cancer database. **(C)** t-SNE analysis performed to evaluate the association between Galectin-9 expression and the loss of chromosome 19q.

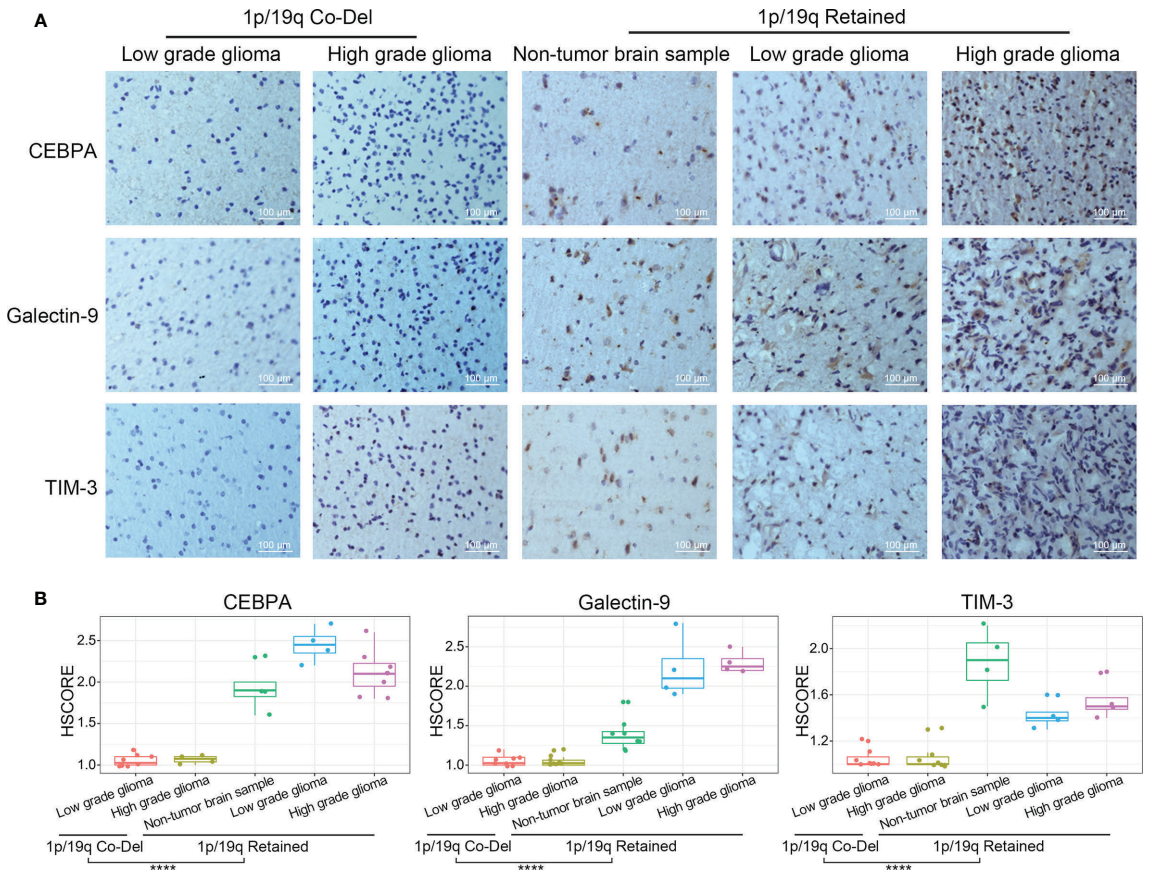

FIGURE 6 | TIM-3, Galectin-9, and CEBPA expression levels evaluated by IHC protein staining in glioma samples stratified by WHO grade and 1p/19q codeletion status. **(A)** IHC staining of CEBPA, Galectin-9 and TIM-3 in glioma samples stratified by WHO grade and 1p/19q codeletion status. **(B)** Differential analysis of HScore of IHC staining of CEBPA, Galectin-9 and TIM-3 in glioma samples. The significance of the difference between the two groups was verified by *Student's t-test*. *****p* < 0.0001*.

without CEBPA knock down and T cells were mixed (1:1) and then transplanted into the intracranial of immunodeficient mice. The growth of intracranial tumors in mice was monitored weekly by *in vivo* fluorescence imaging. The results showed that tumors with CEBPA knock down (simulate the 1p/19q codel tumor) can improve the inhibition of T cells on tumor cells (**Figure 7D**).

DISCUSSION

The 2016 WHO Classification of Tumors of the CNS included several tumor-specific molecular alterations in its classification and diagnosis of gliomas (7). Among them, 1p/19q codeletion status was included in the stratification of oligodendroglioma. Several studies have demonstrated the significant prognostic value of 1p/19q codeletion in WHO subgroups of oligodendrocytoma (10, 12). In recent years, immunotherapy has been widely applied in tumors, but many solid tumors show poor immunotherapy effects due to the special immunosuppressive microenvironment (30). Glioma, as an immunologically "cold tumor", is considered to be highly resistant to immunotherapy (31). However, our study found that patients with 1p/19q co-deleted glioma may benefit from immunotherapy. Our research provided a theoretical basis for the application of immunotherapy in these glioma patients.

The tumor immune microenvironment, including immune cells and immune-related molecules, plays an essential role in glioma occurrence and development (32). The present study mainly explored the association between 1p/19q codeletion and glioma tumor immune microenvironment. In this study, we found that 1p/19q codeletion status did not significantly affect immune cell infiltration. However, the expression levels of immune checkpoint TIM-3 and its ligand Galectin-9 were tightly associated with 1p/19q codeletion. To further explore the specific molecular mechanism of this phenomenon, we assessed four transcription factors of Galectin-9 (AR, CEBPA, CEBPB, and TFAP2C) and found that CEBPA on chromosome 19q played a leading role in the transcriptional regulation of Galectin-9 in gliomas. Moreover, t-SNE analysis in single-cell RNA sequencing data indicated that the loss of chromosome 19q rather than chromosome 1p caused decreased Galectin-9 expression and abnormal TIM-3 function. CEBPA's regulation of Galectin-9's transcription and protein has been verified by experimental and clinical samples. Importantly, the killing effect of T cells on CEBPA-decreased tumor cells was significantly

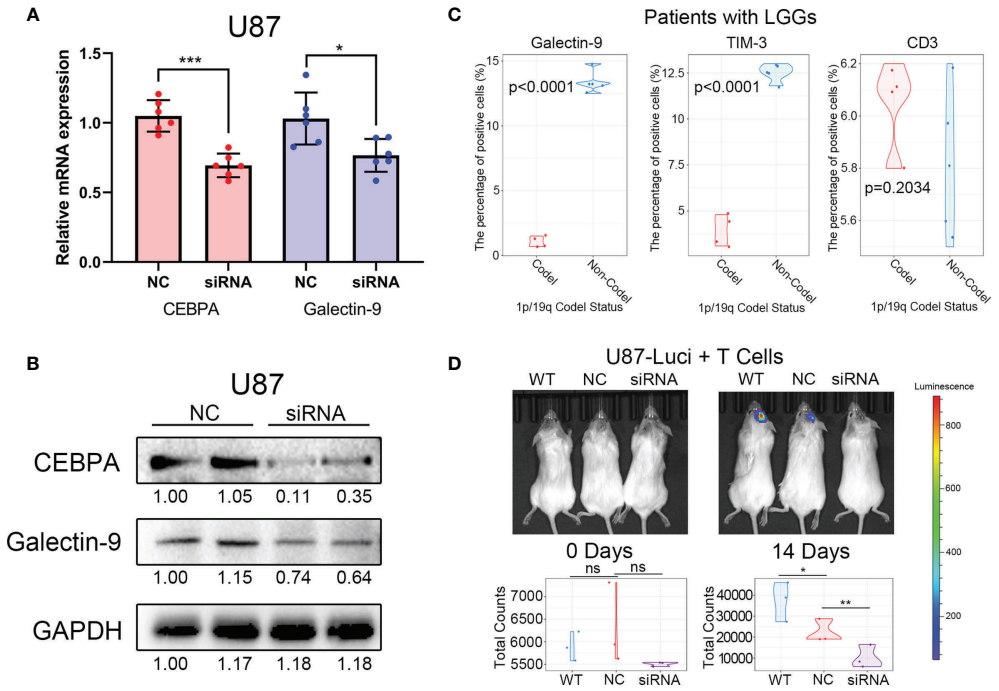

FIGURE 7 | Decreased CEBPA expression leads to a decrease in Galectin-9 expression and an increase in the efficacy of cytotherapy. **(A)** Results of RT-PCR showed that the decrease of CEBPA leads to a significant decrease in the mRNA expression of Galectin-9 in U87. **(B)** Results of western blot showed that the decrease of CEBPA leads to a significant decrease in protein expression of Galectin-9 in U87. **(C)** Results of flow cytometry showed that the proportion of Galectin-9 and TIM-3 positive cells in patients with 1p/19q codel LGGs was significantly lower than that in patients with 1p/19q non-codel LGGs. There was no significant difference in the proportion of CD3 positive cells between the two groups. **(D)** Results of *in vivo* fluorescence imaging showed that the decrease of CEBPA can enhance the killing effect of T cells on tumor cells. The significance of the difference between the two groups was verified by *Student's t-test*. $^{ns}p > 0.05$, $^{*}p < 0.05$, $^{**}p < 0.01$, $^{***}p < 0.001$.

increased *in vivo*. This result suggests that patients with 19q deletion may be insensitive to immune checkpoint inhibitors due to TIM-3 and Galectin-9 dysfunction. In contrast, patients with intact chromosome 19q could benefit from cytotherapy.

In addition to TMZ, limited breakthroughs in recent decades have been reported to improve the outcome in the conventional treatment of gliomas (33–36). To change this situation, many efforts have been made to identify novel molecular markers and therapeutic methods for managing gliomas (5, 6, 8, 37–39). However, limited studies have focused on the effect of 1p/19q codeletion on the biological processes and tumor immune microenvironment of gliomas.

Gliomas with 1p/19q codeletion tend to show characteristics of weaker invasive ability and higher therapy sensitivity (40–42). This is one of the main reasons that oligodendrogliomas characterized by 1p/19q codeletion show a clear boundary on magnetic resonance imaging and better clinical prognosis (43). Recently, Chai et al. reported a significant correlation between 1p/19q codeletion and genes involved in cell proliferation, the extracellular matrix, angiogenesis, and DNA injury response (13). Moreover, the oligodendroglioma cells are deficient in microtube-associated gap junction-mediated tumor cell interactions essential for astrocyte invasion, proliferation, and radioresistance (44). However, these studies failed to provide treatment guidance for patients with 1p/19q codeletion, especially immunotherapy. The tumor immune microenvironmental status in many malignant tumors significantly impacts immunotherapy sensitivity (45–47). Our previous studies showed that immune checkpoints such as PD-LI and TIM-3 could suppress T cell function and macrophage-related immune response in gliomas and lead to worse patient prognosis (18, 20). Thus, the negative correlation between TIM-3 and 1p/19q codeletion indicated that gliomas with the loss of chromosome 1p or/and 19q may benefit more from immunotherapy due to the altered immune microenvironment. Our study initially confirmed the above viewpoint and could be applied to guide the immunotherapy of patients with glioma.

This study has several limitations. First, although only patients with IDH mutation and WHO II glioma were included in this study, the bias caused by other genetic differences in the results still cannot be eliminated. Second, the directionality of most biological functions cannot be reflected by the corresponding enrichment scores. Therefore, the difference analysis of enrichment scores in different 1p/19q status in this study only indicated the strength of the correlation. The directionality of the correlation still needs further experimental verification. Third, since 1p/19q co-deleted glioma cell lines cannot be established *in vitro*, the results of *in vivo* and *in vitro* experiments in this study need to be further verified in transgenic mice or patients.

In conclusion, to the best of our knowledge, this was the first study to investigate the association between 1p/19q codeletion and glioma tumor immune microenvironment. Comprehensive analysis of RNA sequencing data from the CGGA and TCGA databases and single-cell sequencing data from the GSE70630 and GSE89567 databases showed that the loss of chromosome 19q altered the tumor immune microenvironment by downregulating the immunosuppressive function of TIM-3 and its ligand Galectin-9 in glioma patients with 1p/19q codeletion, which may further affect the tumor sensitivity to chemotherapy and immunotherapy. These conclusions provided new insight into the biological functions of 1p/19q codeletion in glioma and might be an important reference for individualized immunotherapy in glioma patients.

DATA AVAILABILITY STATEMENT

The original contributions presented in the study are included in the article/**Supplementary Material**. Further inquiries can be directed to the corresponding authors.

ETHICS STATEMENT

The studies involving human participants were reviewed and approved by Beijing Tiantan Hospital Institutional Review Board (IRB). The patients/participants provided their written informed consent to participate in this study. The animal study was reviewed and approved by Beijing Neurosurgical Institute Review Board (IRB).

AUTHOR CONTRIBUTIONS

WZ, HW, and WY: conception, supervision, and design of this article. GL, RH, WF, and DW: data analysis and editing the manuscript. FW, MY, and YZ: data collection and organization of Single-Cell RNA-Sequencing data. YC, CP, and TJ: *in vitro* and *in vivo* experiment. All authors contributed to the article and approved the submitted version.

FUNDING

This work was supported by grants from National Natural Science Foundation of China (No. 82072768, 81802994), Construction of the Genomics Platform for Chinese People's Brain Diseases (No. PXM2019_026280_000002), Sino-German Center Cooperation and Exchanges Program (M-0020) and The Medical and Health Technology Innovation Project of the Chinese Academy of Medical Sciences (2020-I2M-C&T-A-024).

ACKNOWLEDGMENTS

We thank Ms. Shuqing Sun and Hua Huang for tissue sample collection and clinical data retrieval.

SUPPLEMENTARY MATERIAL

The Supplementary Material for this article can be found online at: https://www.frontiersin.org/articles/10.3389/fimmu.2021.800928/full#supplementary-material

REFERENCES

1. Jiang T, Mao Y, Ma W, Mao Q, You Y, Yang X, et al. CGCG Clinical Practice Guidelines for the Management of Adult Diffuse Gliomas. *Cancer Lett* (2016) 375(2):263–73. doi: 10.1016/j.canlet.2016.01.024
2. Ricard D, Idbaih A, Ducray F, Lahutte M, Hoang-Xuan K, Delattre JY. Primary Brain Tumours in Adults. *Lancet* (2012) 379(9830):1984–96. doi: 10.1016/s0140-6736(11)61346-9
3. Ostrom QT, Gittleman H, Liao P, Rouse C, Chen Y, Dowling J, et al. CBTRUS Statistical Report: Primary Brain and Central Nervous System Tumors Diagnosed in the United States in 2007-2011. *Neuro Oncol* (2014) 16(Suppl 4):iv1–63. doi: 10.1093/neuonc/nou223
4. Yan H, Parsons DW, Jin G, McLendon R, Rasheed BA, Yuan W, et al. IDH1 and IDH2 Mutations in Gliomas. *N Engl J Med* (2009) 360(8):765–73. doi: 10.1056/NEJMoa0808710
5. Sabha N, Knobbe CB, Maganti M, Al Omar S, Bernstein M, Cairns R, et al. Analysis of IDH Mutation, 1p/19q Deletion, and PTEN Loss Delineates Prognosis in Clinical Low-Grade Diffuse Gliomas. *Neuro Oncol* (2014) 16 (7):914–23. doi: 10.1093/neuonc/not299
6. Wiestler B, Capper D, Hovestadt V, Sill M, Jones DT, Hartmann C, et al. Assessing CpG Island Methylator Phenotype, 1p/19q Codeletion, and MGMT Promoter Methylation From Epigenome-Wide Data in the Biomarker Cohort of the NOA-04 Trial. *Neuro Oncol* (2014) 16(12):1630–8. doi: 10.1093/neuonc/nou138
7. Louis DN, Perry A, Reifenberger G, von Deimling A, Figarella-Branger D, Cavenee WK, et al. The 2016 World Health Organization Classification of Tumors of the Central Nervous System: A Summary. *Acta Neuropathol* (2016) 131(6):803–20. doi: 10.1007/s00401-016-1545-1
8. Eckel-Passow JE, Lachance DH, Molinaro AM, Walsh KM, Decker PA, Sicotte H, et al. Glioma Groups Based on 1p/19q, IDH, and TERT Promoter Mutations in Tumors. *N Engl J Med* (2015) 372(26):2499–508. doi: 10.1056/NEJMoa1407279
9. Gelpi E, Ambros IM, Birner P, Luegmayr A, Drlicek M, Fischer I, et al. Fluorescent *In Situ* Hybridization on Isolated Tumor Cell Nuclei: A Sensitive Method for 1p and 19q Deletion Analysis in Paraffin-Embedded Oligodendroglial Tumor Specimens. *Mod Pathol* (2003) 16(7):708–15. doi: 10.1097/01.MP.0000076981.90281.BF
10. Cahill DP, Louis DN, Cairncross JG. Molecular Background of Oligodendroglioma: 1p/19q, IDH, TERT, CIC and FUBP1. *CNS Oncol* (2015) 4(5):287–94. doi: 10.2217/cns.15.32
11. Chen R, Smith-Cohn M, Cohen AL, Colman H. Glioma Subclassifications and Their Clinical Significance. *Neurotherapeutics* (2017) 14(2):284–97. doi: 10.1007/s13311-017-0519-x
12. Panageas KS, Iwamoto FM, Cloughesy TF, Aldape KD, Rivera AL, Eichler AF, et al. Initial Treatment Patterns Over Time for Anaplastic Oligodendroglial Tumors. *Neuro Oncol* (2012) 14(6):761–7. doi: 10.1093/neuonc/nos065
13. Chai RC, Zhang KN, Chang YZ, Wu F, Liu YQ, Zhao Z, et al. Systematically Characterize the Clinical and Biological Significances of 1p19q Genes in 1p/19q Non-Codeletion Glioma. *Carcinogenesis* (2019) 40(10):1229–39. doi: 10.1093/carcin/bgz102
14. Dzobo K. Taking a Full Snapshot of Cancer Biology: Deciphering the Tumor Microenvironment for Effective Cancer Therapy in the Oncology Clinic. *OMICS* (2020) 24(4):175–9. doi: 10.1089/omi.2020.0019
15. Hanzelmann S, Castelo R, Guinney J. GSVA: Gene Set Variation Analysis for Microarray and RNA-Seq Data. *BMC Bioinf* (2013) 14:7. doi: 10.1186/1471-2105-14-7

16. Newman AM, Liu CL, Green MR, Gentles AJ, Feng W, Xu Y, et al. Robust Enumeration of Cell Subsets From Tissue Expression Profiles. *Nat Methods* (2015) 12(5):453–7. doi: 10.1038/nmeth.3337
17. Rody A, Holtrich U, Pusztai L, Liedtke C, Gaetje R, Ruckhaeberle E, et al. T-Cell Metagene Predicts a Favorable Prognosis in Estrogen Receptor-Negative and HER2-Positive Breast Cancers. *Breast Cancer Res* (2009) 11(2):R15. doi: 10.1186/bcr2234
18. Li G, Wang Z, Zhang C, Liu X, Cai J, Wang Z, et al. Molecular and Clinical Characterization of TIM-3 in Glioma Through 1,024 Samples. *Oncoimmunology* (2017) 6(8):e1328339. doi: 10.1080/2162402X.2017.1328339
19. Wang K, Huang R, Li G, Zeng F, Zhao Z, Liu Y, et al. CKAP2 Expression Is Associated With Glioma Tumor Growth and Acts as a Prognostic Factor in Highgrade Glioma. *Oncol Rep* (2018) 40(4):2036–46. doi: 10.3892/or.2018.6611
20. Wang Z, Zhang C, Liu X, Wang Z, Sun L, Li G, et al. Molecular and Clinical Characterization of PD-L1 Expression at Transcriptional Level *via* 976 Samples of Brain Glioma. *Oncoimmunology* (2016) 5(11):e1196310. doi: 10.1080/2162402X.2016.1196310
21. McCarty KSJr., Szabo E, Flowers JL, Cox EB, Leight GS, Miller L, et al. Use of a Monoclonal Anti-Estrogen Receptor Antibody in the Immunohistochemical Evaluation of Human Tumors. *Cancer Res* (1986) 46(8 Suppl):4244s–8s.
22. Li D, Hu Y, Jin Z, Zhai Y, Tan Y, Sun Y, et al. TanCAR T Cells Targeting CD19 and CD133 Efficiently Eliminate MLL Leukemic Cells. *Leukemia* (2018) 32(9):2012–6. doi: 10.1038/s41375-018-0212-z
23. Li G, Li Y, Liu X, Wang Z, Zhang C, Wu F, et al. ALDH1A3 Induces Mesenchymal Differentiation and Serves as a Predictor for Survival in Glioblastoma. *Cell Death Dis* (2018) 9(12):1190. doi: 10.1038/s41419-018-1232-3
24. Aldape K, Burger PC, Perry A. Clinicopathologic Aspects of 1p/19q Loss and the Diagnosis of Oligodendroglioma. *Arch Pathol Lab Med* (2007) 131(2):242–51. doi: 10.1043/1543-2165(2007)131[242:CAOQLA]2.0.CO;2
25. Zou MX, Zheng BW, Liu FS, Wang XB, Hu JR, Huang W, et al. The Relationship Between Tumor-Stroma Ratio, the Immune Microenvironment, and Survival in Patients With Spinal Chordoma. *Neurosurgery* (2019) 85(6):E1095–110. doi: 10.1093/neuros/nyz333
26. Tan SK, Lin ZH, Chang CW, Varang V, Chng KR, Pan YF, et al. AP-2gamma Regulates Oestrogen Receptor-Mediated Long-Range Chromatin Interaction and Gene Transcription. *EMBO J* (2011) 30(13):2569–81. doi: 10.1038/emboj.2011.151
27. Schmidt SF, Jorgensen M, Chen Y, Nielsen R, Sandelin A, Mandrup S. Cross Species Comparison of C/EBPalpha and PPARgamma Profiles in Mouse and Human Adipocytes Reveals Interdependent Retention of Binding Sites. *BMC Genomics* (2011) 12:152. doi: 10.1186/1471-2164-12-152
28. Takayama K, Suzuki T, Fujimura T, Urano T, Takahashi S, Homma Y, et al. CtBP2 Modulates the Androgen Receptor to Promote Prostate Cancer Progression. *Cancer Res* (2014) 74(22):6542–53. doi: 10.1158/0008-5472.CAN-14-1030
29. Zhai Y, Li G, Jiang T, Zhang W. CAR-Armed Cell Therapy for Gliomas. *Am J Cancer Res* (2019) 9(12):2554–66.
30. Heidegger S, Wintges A, Stritzke F, Bek S, Steiger K, Koenig PA, et al. RIG-I Activation Is Critical for Responsiveness to Checkpoint Blockade. *Sci Immunol* (2019) 4(39). doi: 10.1126/sciimmunol.aau8943
31. Jackson CM, Choi J, Lim M. Mechanisms of Immunotherapy Resistance: Lessons From Glioblastoma. *Nat Immunol* (2019) 20(9):1100–9. doi: 10.1038/s41590-019-0433-y
32. Wang Q, Hu B, Hu X, Kim H, Squatrito M, Scarpace L, et al. Tumor Evolution of Glioma-Intrinsic Gene Expression Subtypes Associates With Immunological Changes in the Microenvironment. *Cancer Cell* (2017) 32(1):42–56 e6. doi: 10.1016/j.ccell.2017.06.003
33. Van Meir EG, Hadjipanayis CG, Norden AD, Shu HK, Wen PY, Olson JJ. Exciting New Advances in Neuro-Oncology: The Avenue to a Cure for Malignant Glioma. *CA Cancer J Clin* (2010) 60(3):166–93. doi: 10.3322/caac.20069
34. Yang P, Zhang W, Wang Y, Peng X, Chen B, Qiu X, et al. IDH Mutation and MGMT Promoter Methylation in Glioblastoma: Results of a Prospective Registry. *Oncotarget* (2015) 6(38):40896–906. doi: 10.18632/oncotarget.5683
35. Cairncross JG, Ueki K, Zlatescu MC, Lisle DK, Finkelstein DM, Hammond RR, et al. Specific Genetic Predictors of Chemotherapeutic Response and Survival in Patients With Anaplastic Oligodendrogliomas. *J Natl Cancer Inst* (1998) 90(19):1473–9. doi: 10.1093/jnci/90.19.1473
36. Zaazoue MA, Manley PE, Mehdar MA, Ullrich NJ, Dasenbrock HH, Chordas CA, et al. Optimizing Postoperative Surveillance of Pediatric Low-Grade Glioma Using Tumor Behavior Patterns. *Neurosurgery* (2020) 86(2):288–97. doi: 10.1093/neuros/nyz072
37. Pekmezci M, Rice T, Molinaro AM, Walsh KM, Decker PA, Hansen H, et al. Adult Infiltrating Gliomas With WHO 2016 Integrated Diagnosis: Additional Prognostic Roles of ATRX and TERT. *Acta Neuropathol* (2017) 133(6):1001–16. doi: 10.1007/s00401-017-1690-1
38. Li GZ, Zhang KN, Wang Z, Hu HM, Wang ZL, Huang RY, et al. Siglecs, Novel Immunotherapy Targets, Potentially Enhance The Effectiveness of Existing Immune Checkpoint Inhibitors in Glioma Immunotherapy. *Onco Targets Ther* (2019) 12:10263–73. doi: 10.2147/OTT.S223406
39. Barritault M, Picart T, Poncet D, Fenouil T, d'Hombres A, Gabut M, et al. Avoiding New Biopsies by Identification of IDH1 and TERT Promoter Mutation in Nondiagnostic Biopsies From Glioma Patients. *Neurosurgery* (2020) E513–9. doi: 10.1093/neuros/nyaa025
40. Cairncross G, Jenkins R. Gliomas With 1p/19q Codeletion: a.K.a. Oligodendroglioma. *Cancer J* (2008) 14(6):352–7. doi: 10.1097/PPO.0b013e31818d8178
41. Buckner JC, Shaw EG, Pugh SL, Chakravarti A, Gilbert MR, Barger GR, et al. Radiation Plus Procarbazine, CCNU, and Vincristine in Low-Grade Glioma. *N Engl J Med* (2016) 374(14):1344–55. doi: 10.1056/NEJMoa1500925
42. Wang Y, Jiang T. Understanding High Grade Glioma: Molecular Mechanism, Therapy and Comprehensive Management. *Cancer Lett* (2013) 331(2):139–46. doi: 10.1016/j.canlet.2012.12.024
43. Lasocki A, Gaillard F, Gorelik A, Gonzales M. MRI Features Can Predict 1p/19q Status in Intracranial Gliomas. *AJNR Am J Neuroradiol* (2018) 39(4):687–92. doi: 10.3174/ajnr.A5572
44. Osswald M, Jung E, Sahm F, Solecki G, Venkataramani V, Blaes J, et al. Brain Tumour Cells Interconnect to a Functional and Resistant Network. *Nature* (2015) 528(7580):93–8. doi: 10.1038/nature16071
45. Sokratous G, Polyzoidis S, Ashkan K. Immune Infiltration of Tumor Microenvironment Following Immunotherapy for Glioblastoma Multiforme. *Hum Vaccin Immunother* (2017) 13(11):2575–82. doi: 10.1080/21645515.2017.1303582
46. Wu T, Dai Y. Tumor Microenvironment and Therapeutic Response. *Cancer Lett* (2017) 387:61–8. doi: 10.1016/j.canlet.2016.01.043
47. Friedmann Angeli JP, Krysko DV, Conrad M. Ferroptosis at the Crossroads of Cancer-Acquired Drug Resistance and Immune Evasion. *Nat Rev Cancer* (2019) 19(7):405–14. doi: 10.1038/s41568-019-0149-1

Conflict of Interest: The authors declare that the research was conducted in the absence of any commercial or financial relationships that could be construed as a potential conflict of interest.

Publisher's Note: All claims expressed in this article are solely those of the authors and do not necessarily represent those of their affiliated organizations, or those of the publisher, the editors and the reviewers. Any product that may be evaluated in this article, or claim that may be made by its manufacturer, is not guaranteed or endorsed by the publisher.

Copyright © 2021 Li, Huang, Fan, Wang, Wu, Zeng, Yu, Zhai, Chang, Pan, Jiang, Yan, Wang and Zhang. This is an open-access article distributed under the terms of the Creative Commons Attribution License (CC BY). The use, distribution or reproduction in other forums is permitted, provided the original author(s) and the copyright owner(s) are credited and that the original publication in this journal is cited, in accordance with accepted academic practice. No use, distribution or reproduction is permitted which does not comply with these terms.

frontiers in Immunology

ORIGINAL RESEARCH
published: 06 January 2022
doi: 10.3389/fimmu.2021.802795

PTRF/Cavin-1 as a Novel RNA-Binding Protein Expedites the NF-κB/PD-L1 Axis by Stabilizing lncRNA NEAT1, Contributing to Tumorigenesis and Immune Evasion in Glioblastoma

Kaikai Yi[1,2†], Xiaoteng Cui[1†], Xing Liu[3], Yunfei Wang[1], Jixing Zhao[1], Shixue Yang[1], Can Xu[4], Eryan Yang[1], Menglin Xiao[4,5], Biao Hong[1], Chuan Fang[4,5], Chunsheng Kang[1,6], Yanli Tan[5,7,8] and Qixue Wang[1*]*

[1] Laboratory of Neuro-oncology, Tianjin Neurological Institute, Tianjin Medical University General Hospital, Key Laboratory of Post-Neuro Injury Neuro-repair and Regeneration in Central Nervous System, Ministry of Education, Tianjin, China, [2] Department of Neuro-Oncology and Neurosurgery, Tianjin Medical University Cancer Institute and Hospital, National Clinical Research Center for Cancer, Key Laboratory of Cancer Prevention and Therapy of Tianjin, Tianjin's Clinical Research Center for Cancer, Tianjin, China, [3] Beijing Neurosurgical Institute, Department of Neurosurgery, Beijing Tiantan Hospital, Capital Medical University, Beijing, China, [4] Department of Neurosurgery, Affiliated Hospital of Hebei University, Baoding, China, [5] Key Laboratory of Precise Diagnosis and Treatment of Glioma in Hebei Province, Baoding, China, [6] Department of Neurosurgery, Tianjin Medical University General Hospital, Tianjin, China, [7] Department of Pathology, Affiliated Hospital of Hebei University, Baoding, China, [8] Department of Pathology, Hebei University School of Basic Medical Sciences, Baoding, China

Background: Immunotherapy, especially checkpoint inhibitors targeting PD-1 or PD-L1, has revolutionized cancer therapy. However, PD-1/PD-L1 inhibitors have not been investigated thoroughly in glioblastoma (GBM). Studies have shown that polymerase 1 and transcript release factor (PTRF/Cavin-1) has an immune-suppressive function in GBM. Thus, the relationship between PTRF and PD-L1 and their role in immune suppression requires further investigation in GBM.

Methods: We used public databases and bioinformatics analysis to investigate the relationship between PTRF and PD-L1. We next confirmed the predicted relationship between PTRF and PD-L1 in primary GBM cell lines by using different experimental approaches. RIP-Seq, RIP, ChIP, and qRT-PCR were conducted to explore the molecular mechanism of PTRF in immunosuppression.

Results: We found that PTRF stabilizes lncRNA *NEAT1* to induce NF-κB and PD-L1 and promotes immune evasion in GBM. PTRF was found to correlate with immunosuppression in the public GBM databases. PTRF increased the level of PD-L1 in primary cell lines from GBM patients. We carried out RIP-Seq of GBM cells and found

OPEN ACCESS

Edited by:
Junxia Zhang,
First Affiliated Hospital, Nanjing Medical University, China

Reviewed by:
Xiuping Zhou,
Xuzhou Medical University, China
Xudong Zhao,
Sichuan University, China
Ailiang Zeng,
University of Texas MD Anderson Cancer Center, United States

***Correspondence:**
Qixue Wang
qixue_wang@tmu.edu.cn
Yanli Tan
tanyanli5536@126.com

†These authors have contributed equally to this work and share first authorship

Specialty section:
This article was submitted to Cancer Immunity and Immunotherapy, a section of the journal Frontiers in Immunology

Received: *27 October 2021*
Accepted: *14 December 2021*
Published: *06 January 2022*

Citation:
Yi K, Cui X, Liu X, Wang Y, Zhao J, Yang S, Xu C, Yang E, Xiao M, Hong B, Fang C, Kang C, Tan Y and Wang Q (2022) PTRF/Cavin-1 as a Novel RNA-Binding Protein Expedites the NF-κB/PD-L1 axis by Stabilizing lncRNA NEAT1, Contributing to Tumorigenesis and Immune Evasion in Glioblastoma. Front. Immunol. 12:802795. doi: 10.3389/fimmu.2021.802795

that PTRF interacts with lncRNA *NEAT1* and stabilizes its mRNA. PTRF also promoted the activity of NF-κB by suppressing UBXN1 expression *via NEAT1* and enhanced the transcription of PD-L1 through NF-κB activation. Finally, PTRF promoted immune evasion in GBM cells by regulating PD-1 binding and PD-L1 mediated T cell cytotoxicity.

Conclusions: In summary, our study identified the PTRF-*NEAT1*-PD-L1 axis as a novel immune therapeutic target in GBM.

Keywords: glioblastoma, PTRF, lncRNA *NEAT1*, PDL1, immunosuppression

INTRODUCTION

Glioblastoma (GBM) is the most aggressive primary brain tumor in adults (1). Standard treatment regimens, including surgery, temozolomide chemotherapy, and radiation therapy, fail to improve patient survival (2). Immunotherapy, particularly immune checkpoint blockade with anti-programmed death 1 (PD-1)/PD-1 ligand (PD-L1) antibodies, has radically changed the treatment of multiple tumors (3–5). However, clinical studies investigating the use of anti-PD-1/PD-L1 in GBM remain are limited (6).

PD-L1 is an important immune checkpoint molecule on cancer cells which plays a critical role in immune surveillance and immune evasion. The majority of GBM patients are resistant to anti-PD-1/PD-L1 therapy, and only a minority of patients respond to this immunotherapy (7). The response to PD-1/PD-L1 blockade is correlated with PD-L1 expression in tumor cells (8, 9). Previous studies demonstrated that PD-L1 protein levels are associated with glioma grades, with elevated levels on tumor cells facilitating immune evasion in glioma patients (10, 11). Thus, one possible mechanism of immune evasion in GBM is the upregulation of PD-L1 which requires an in-depth investigation. Recent studies show that the expression of PD-L1 in tumors is regulated by signaling pathways, transcription factors and epigenetic factors, such as the Wnt/β-catenin pathway (12), STAT3 (13), and NF-κB (14). To develop an effective strategy to enhance antitumor immunity, the underlying mechanisms of PD-L1 regulation in GBM need to be elucidated.

Polymerase 1 and Transcript Release Factor (PTRF, also known as Cavin-1) is upregulated in GBM with mesenchymal phenotype compared with other subtypes of GBM (15). The prognosis of GBM patients with high PTRF expression is also worse (15). Previous studies found that PTRF protects vascular endothelial cells from cytotoxic T cell-mediated lysis (16). Further, in the challenge phase of asthma, loss of PTRF led to intense airway inflammation and potent type 2 immune responses (17). In GBM, bioinformatics analysis showed a negative correlation between PTRF expression and cytotoxic lymphocytes (18). We also demonstrated that PTRF overexpression increased tumor proliferation and decreased tumor-infiltrating $CD8^+$ T cells mediated anti-tumor immunity (19). However, the mechanism by which PTRF influences immunosuppression, particularly PD-L1 expression, in GBM needs further research.

Here, we show that PTRF correlates with immunosuppression and increases the expression of PD-L1 in GBM. Further we found that PTRF interacts with lncRNA *NEAT1* and maintains the mRNA stability of *NEAT1*, increasing H3K27me3 level on the UBXN1 promoter, which results in the binding of NF-κB to the PD-L1 promoter. These findings highlight the role of the PTRF-*NEAT1*-PD-L1 axis in immune evasion in GBM; this immune-suppressive axis may be targeted as a novel immunotherapeutic strategy.

MATERIALS AND METHODS

Cell Culture, Lentiviruses, and Chemicals

N9 cell lines derived from GBM patients, were established by Professor Fan of Beijing Normal University. TBD0220 cell lines derived from GBM patients, were established by Professor Kang of Tianjin Medical University (20, 21). N9 and TBD0220 cells were cultured in DMEM/F12 supplemented with 1% Penicillin-Streptomycin and 10% FBS. Cells were maintained at 37°C in a humidified 5% CO2 atmosphere. All GBM cells, except *in vivo* cultures, were maintained for less than eight generations. Lentiviruses encoding the PTRF-EGFP fusion protein (GOSL87854) and luciferase (GCNL84615) were purchased from GENECHEM (Shanghai, China). Small interfering RNAs targeting PTRF were synthesized by GenePharma (Shanghai, China). Sequences of siRNAs were as follows: PTRF siRNA#1 5'-GCCGCAACUUUAAAGUCAUGAUCUA; PTRF siRNA#2 5'-AGGAGUCCCGCGCAGAGCGUAUCAA. Small interfering RNAs targeting *NEAT1* were synthesized by GenePharma (Shanghai, China). Sequences of siRNAs were as follows: *NEAT1* siRNA 5'- GAACUUUACUUCGUUAGAUTT. We treated cells with Actinomycin D (Selleck, S7418) at a final concentration of 1 μM.

Western Blot Analysis

The protein was extracted GBM cells by RIPA protein lysis buffer (Solarbio, R0010), with a freshly added mixture of protease inhibitor cocktail and PMSF. Then, 20 μg of protein was run on an SDS-PAGE gel, separated by electrophoresis and transferred to PVDF membranes. The membrane was first blocked by 5% BSA for 1-2 hours at room temperature, followed by incubation with primary antibodies at 4°C overnight. After washing three times with PBST, the membrane was blocked with secondary antibodies (Promega, 1:10000). Protein bands were detected was performed using G:BOXF3 (Syngene, UK) with Western HRP Substrate (Millipore, WBLUF0500). The antibodies used for western blots were: PD-L1 (Abcam, ab58810, 1:500), NF-κB (Cell Signaling

Technology, 8242, 1:1000), Phospho-NF-κB (Cell Signaling Technology, 3033, 1:1000), UBXN1 (Proteintech, 16135-1-AP, 1:1000), GAPDH (Proteintech, 60004-1-Ig, 1:1000).

Quantitative RT-PCR

Cells were lysed in TRIzol Reagent and mixed with chloroform, then centrifuged at 12000 rpm for 10 minutes at 4°C. The upper aqueous phase was transferred to a clean tube and an equal volume of isopropanol was added. The samples were mixed and stored at −20°C overnight. The concentration of total RNA was measured by NanoDrop 2000 (Thermo Scientific, USA). cDNA was synthesized from 1 μg of RNA using a reverse transcription kit (Promega, USA), according to the manufacturer's protocol. qRT-PCR was performed using the DNA Engine Opticon 2 Two-Color qRT-PCR detection system (Bio-Rad Laboratories, USA) and the results were normalized to the GAPDH. The following primers were used:

PD-L1-F: AGGAGTACCTTGGCTTTGCC
PD-L1-R: GCCTTGCTCAGCCACAATTC
NEAT1-1F: CCAGTTTTCCGAGAACCAAA
NEAT1-1R: ATGCTGATCTGCTGCGTATG
NEAT1-2F: CTAGAGGCTCGCATTGTGTG
NEAT1-2R: GCCCACACGAAACCTTACAT
UBXN1-F: AGTGAAGAGGAAAGACAGGAA
UBXN1-R: TTTGTCCCTCTCGATCTTTTC
TNFα-F: CCCAGGCAGTCAGATCATCTTC
TNFα-R: GGTTTGCTACAACATGGGCTACA
IL1β-F: CCACAGACCTTCCAGGAGAATG
IL1β-R: GTGCAGTTCAGTGATCGTACAGG
IL8-F: GAGTGATTGAGAGTGGACCACACT
IL8-R: AGACAGAGCTCTCTTCCATCAGAAA
GAPDH-F: TGCACCACCAACTGCTTAGC
GAPDH-R: GGCATGGACTGTGGTCATGAG

Flow Cytometry

For the detection of cell-surface PD-L1, cells were trypsinized and collected into a flow tube. The cells were incubated with 100 μL PBS by adding PE anti-human PD-L1 Antibody (329705, BioLegend; the dilution ratio is 1: 100) at room temperature for 1 hour. Then, the cells were analyzed *via* flow cytometer after washing with PBS.

RNA-Binding Protein Immunoprecipitation

RIP experiment was performed using the Magna RIP RNA-Binding Protein Immunoprecipitation Kit (Millipore, No.17-701) according to the manufacturer's instructions. For high-throughput sequencing (RIP-Seq), the libraries were prepared following the manufacturer's instructions and applied to the Illumina HiSeq X Ten system by ABlife. Inc (Wuhan, China). To further validate the RIP-Seq results, the RNA fraction, precipitated by RIP, was analyzed *via* RT-qPCR. The data presented in the study are deposited in the SRA repository, accession number PRJNA777377

Chromatin Immunoprecipitation

ChIP experiment was performed using the Magna ChIP Chromatin Immunoprecipitation Kit (Millipore, No.17-10085) according to the manufacturer's instructions. The antibodies against H3K27me3 and NF-κB were purchased from Cell Signaling Technology (Denver, MA, USA). The primers used for UBXN1 have been described. The primers used for UBXN1 and PDL1 were as follows:

UBXN1-F: GGCAGGGGAAATGATGGATA
UBXN1-R: TAACCTGCCCACTCCATTAC
PD-L1-1F: ACTGAAAGCTTCCGCCGATT
PD-L1-1R: GAGGAACAACGCTCCCTACC
PD-L1-2F: GGGTGGCAGAATATCAGGGAC
PD-L1-2R: CGTGGATTCTGTGACTTCCTC
PDL1-3F: ACCTGTAAACTGTATTGCCACA
PDL1-3R: TGGTGACTGTAAGTTTGGGTGA
PDL1-4F: AGGGTAGAAACAGGTGGGAA
PDL1-4R: GAAAGCAGTGTTCAGGGTCTAC

Luciferase Reporter Assay

The expression vectors encoding PGL3-Basic-PD-L1^{WT} and PGL3-Basic-PD-L1^{MUT} were synthesized by Integrated Biotech Solutions (Shanghai, China). Briefly, the GBM cells were transfected with 0.5 μg of PGL3-Basic empty vector, PGL3-Basic-PD-L1^{WT} and PGL3-Basic-PD-L1^{MUT} by Lipofectamine 3000 (Invitrogen) separately. After incubation for 48 hours, luciferase activity was measured using the luciferase assay system (E1501, Promega) according to the manufacturer's protocol.

In Situ Hybridization Histochemistry

The glioma tissues were surgically resected from patients at the Beijing Tiantan Hospital. The ISH experiments for *NEAT1* were performed using the RNA ISH kit (Boster, China) according to the manufacturer's instructions. The probes were designed and synthesized by Boster (Wuhan, China).

In Vivo Intracranial Patient-Derived Xenografts Model

Female BALB/C nude mice (4 weeks old) were used for intracranial GBM Patient-derived xenografts, and TBD0220 cells were used to construct the intracranial model. The cells were injected into the mice under the guidance of a stereotactic instrument at coordinates relative to bregma. Bioluminescence imaging was used to detect intracranial tumor growth by *In Vivo* Imaging System (IVIS) Spectrum. On day 21, the mice were sacrificed, and the brain tissues were removed. The brain tissue was then fixed in 10% formalin for 24 h, embedded in paraffin, and sectioned into 8 μm slices. All experiments were approved by the Animal Ethical and Welfare Committee of Tianjin Medical University. Kaplan-Meier survival curves were plotted to analyze the survival.

HE and Immunohistochemical Staining

The glioma tissues were surgically resected from patients at the Beijing Tiantan Hospital. The tissues were embedded in paraffin,

sectioned, and stained with HE. IHC staining was performed as described previously. Staining intensity was quantified by a pathologist. Antibodies include Ki-67 (ZSGB-BIO, ZM-0167, 1: 100), Phospho-NF-κB (Cell Signaling Technology, 3033, 1:400), UBXN1 (Proteintech, 16135-1-AP, 1:200), PTRF (Proteintech, 18892-1-AP, 1:200), PD-L1 (Cell Signaling Technology, 13684, 1:400), CD8 (Proteintech, 66868-1-lg, 1:200).

PD-L1/PD-1–Binding Assay

Confocal laser scanning microscopy (CLSM) and flow cytometry were used to study the PD-L1/PD-1–binding in GBM cells. Cells were trypsinized and collected into a flow tube. Control and PTRF overexpressing TBD0220 cells were incubated with 5 μg/mL recombinant human PD-1 FC chimera protein (1086-PD-050, R&D Systems) at room temperature for 1 hour. After incubation, the cells were washed three times with PBS and incubated with anti-Human IgG (H+L) Cross-Adsorbed Secondary Antibody (Alexa Fluor 488) (A-11013, Thermo Fisher) for 1 hour at room temperature. For CLSM analysis, the cells were fixed with paraformaldehyde for 15 minutes at room temperature and further stained with DAPI for detecting the cell nucleus. CLSM images were observed by FV-1200 laser scanning confocal microscope (Olympus Corporation, Japan). For flow cytometry analysis, the cells were trypsinized and collected by centrifugation, then resuspended in PBS. The data were analyzed by FlowJo v10.6.2.

T Cell Cytotoxicity Assay

Control and PTRF overexpressing TBD0220 cells were separately transfected with siRNA for *NEAT1* in DMEM/F12 medium. Human peripheral blood mononuclear cells (PBMC; CBP-002, StemEry) were maintained in DMEM/F12 medium. The PBMC cells were activated with 100 ng/mL CD3 antibody (317325, BioLegend), 100 ng/mL CD28 antibody (302933, BioLegend), and 10 ng/mL IL2 (589102, BioLegend) for 24 h. Then, activated PBMC cells were incubated with TBD0220 cells at 10:1 ratio in the presence of caspase-3/7 green detection reagent (C10723, Thermo Fisher, 1:1000) at 37°C for 12 hours according to the manufacturer's protocol. The cell nuclei were visualized by staining with DAPI. All the images were observed using FV-1200 laser scanning confocal microscope (Olympus Corporation, Japan).

Clinical Information And Transcriptome Data of Glioma Patients

The clinical and RNA sequencing data sets of glioma patients in TCGA database were downloaded from the University of California Santa Cruz (UCSC) Xena Functional Genomics Explorer (https://xenabrowser.net/). CGGA-693 RNA sequencing data sets and Rembrandt microarray data were obtained from the Chinese Glioma Genome Atlas (CGGA) (http://www.cgga.org.cn/). All the RNA sequencing data were transformed by log2 (normalized count + 1).

PTRF-correlated genes were obtained by a filtering condition: Pearson correlation coefficients between the expression of PTRF and other genes ≥ 0.3 and p-value ≤ 0.05. GO-BP analysis of PTRF-correlated genes was performed by the cluster Profiler v3.18.0 R package and visualized by bubble charts. Tumor purity of glioma data in TCGA, CGGA, and Rembrandt databases was measured by estimate v1.0.13 R package. The univariant and multivariant cox analyses were employed by survival v3.1.12 R package and displayed as forest maps. The PNP score of each patient was calculated by the formula below, and overall survival data of patients with PNP score-high or low were shown as survival curves.

$$\beta\text{-value}_{(PTRF)} \times \text{expression data}_{(PTRF)} + \beta\text{-value}_{(NEAT1)} \times \text{expression data}_{(NEAT1)} + \beta\text{-value}_{(PD\text{-}L1)} \times \text{expression data}_{(PD\text{-}L1)}$$

Statistical Analysis

All data visualization was performed using Microsoft Excel, GraphPad Prism 8 software, and R. Two-tail unpaired Student's t-test was used to compare two experimental groups, and one-way or two-way ANOVA was used when comparing three or more experimental groups. All data represent the mean ± SD. A p-value less than 0.05 was considered statistically significant, ns = not significant. Significance was defined as *p < 0.05, **p < 0.01, ***p < 0.001, ****p < 0.0001.

RESULTS

PTRF Increases PD-L1 Levels and Correlates With Immunosuppression in GBM

In this study, considering the immune-regulation function of PTRF, we assessed the relationships between PTRF and immune responses in GBM by examining GBM cases in public databases. We acquired the transcriptome data of glioma in CGGA, TCGA, and Rembrandt databases, and calculated the correlation between PTRF and other genes. The PTRF co-expression gene sets (r>0.3) were filtered out and interrogated by gene ontology (GO) enrichment analysis. GO-biological process (GO-BP) results show that the functions associated with T cell activation was significantly enriched (**Figure 1A** and **Supplemental Figure 1A**). Elevated expression of PTRF was associated with low tumor purity and had a positive correlation with the expressions of genes, involved in tumor immunity (**Figure 1B**, **Supplemental Figure 1B**). The correlation between PTRF and the representative genes of immune cells in TCGA, CGGA, and Rembrandt databases, were calculated and visualized as scatter maps (**Figure 1C** and **Supplemental Figure 1C**). We found that the expression of PTRF positively correlated with PD-L1 (correlation coefficient of 0.56), suggesting that PTRF may regulate PD-L1. To investigate the regulation of PD-L1 by PTRF, we stably overexpressed PTRF in primary GBM cell lines (N9 and TBD0220) by transfecting lentivirus. We conducted immunoblotting analysis of cultured N9 and TBD0220 cells and found that PTRF overexpression promoted the increase of PD-L1 protein levels in N9 PTRF and TBD0220 PTRF cells compared with their respective control cells (**Figure 1D** and **Supplemental Figure 1D**). Real-time quantitative PCR (RT-qPCR) determined that the mRNA level of PD-L1 was increased in N9 PTRF and TBD0220 PTRF cells compared with the control cells (**Figure 1E**).

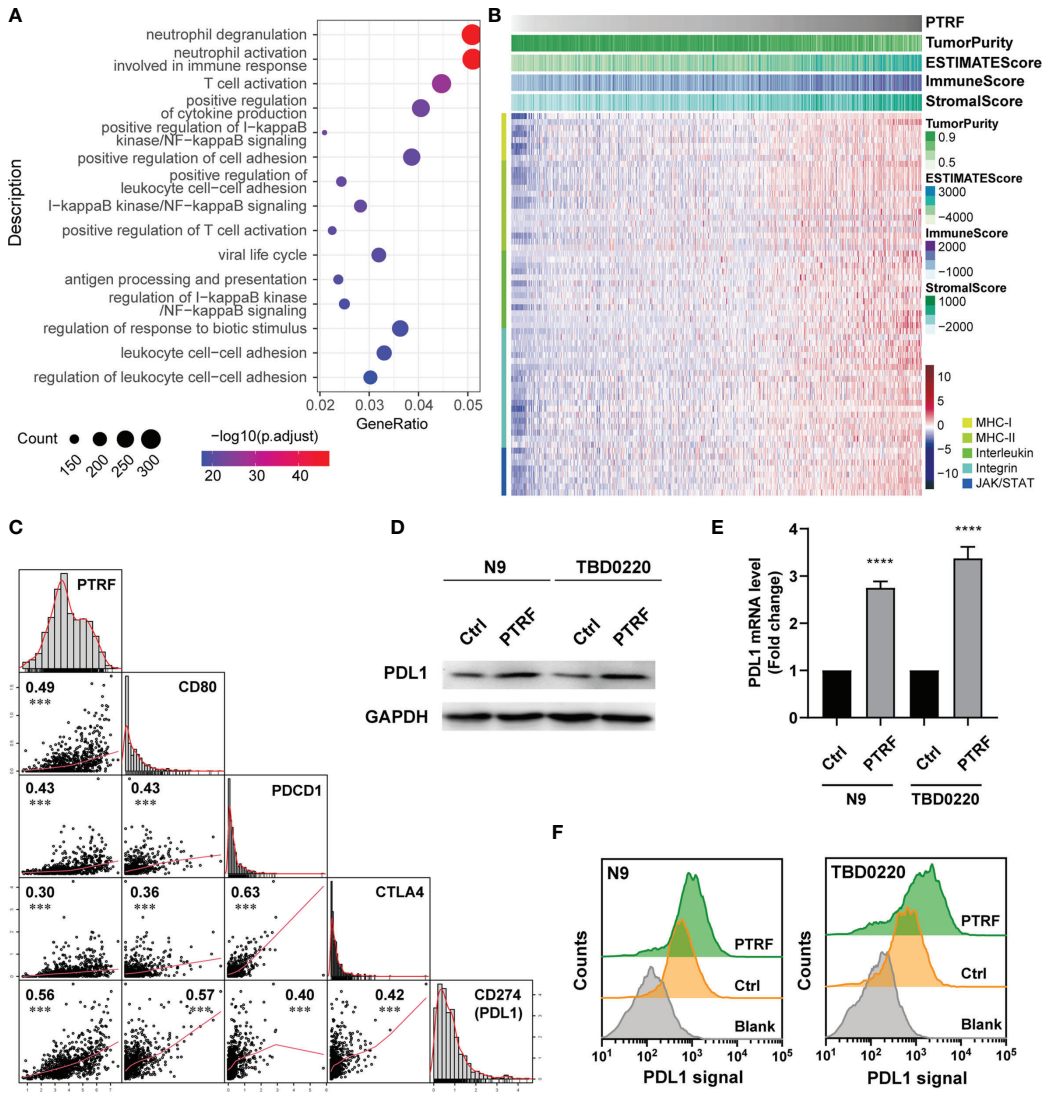

FIGURE 1 | PTRF increases PD-L1 levels and correlates with immunosuppression in GBM. **(A)** Gene ontology enrichment analysis of genes that are positively associated with PTRF in the CGGA GBM database. **(B)** Heatmap showing the relationship between PTRF, low tumor purity, and genes regulating immunity in the CGGA GBM database. **(C)** The correlation between PTRF, CD80, PDCD1, CTLA4, and PD-L1 levels in the CGGA GBM database, measured by Pearson's correlation test. **(D)** Western blot analysis of PD-L1 expression in primary GBM cells (N9 and TBD0220; both control and PTRF overexpression cells). **(E)** Relative mRNA level of PD-L1 in control and PTRF overexpressing cells. **(F)** Flow cytometry analysis of PD-L1 in control and PTRF overexpressing cells. ****$p \leq 0.001$.

We further employed flow cytometry to interrogate the PD-L1 level changes on the cell membranes of N9 and TBD0220 cells overexpressed PTRF. We confirmed that PD-L1 protein levels were higher in the PTRF overexpressing cells compared with the control cells (**Figure 1F**). We verified the effect of PTRF on PD-L1 by PTRF knock-down in N9 and TBD0220 cells. The mRNA and protein level of PD-L1 was significantly decreased by PTRF knockdown in N9 and TBD0220 cells compared with their respective control cells (**Supplemental Figures 1E, F**). These results show that PTRF regulates the expression of PD-L1 at the transcription level in GBM cells.

PTRF Maintains mRNA Stability of lncRNA *NEAT1*

PTRF is a novel non-canonical RNA-binding protein (RBP) (22) and participates in the transcription regulation of PD-L1 in GBM. To investigate the potential mechanism of PTRF as an RBP affecting the expression of PD-L1, we performed RBP immunoprecipitation-coupled high-throughput sequencing (RIP-Seq) by Illumina HiSeq X Ten system in N9 cells with PTRF-Flag over-expression (**Figure 2A**). The experiments were biologically repeated twice and the clean reads were mapped to the human reference genome (GRCh38) using TopHat2. The

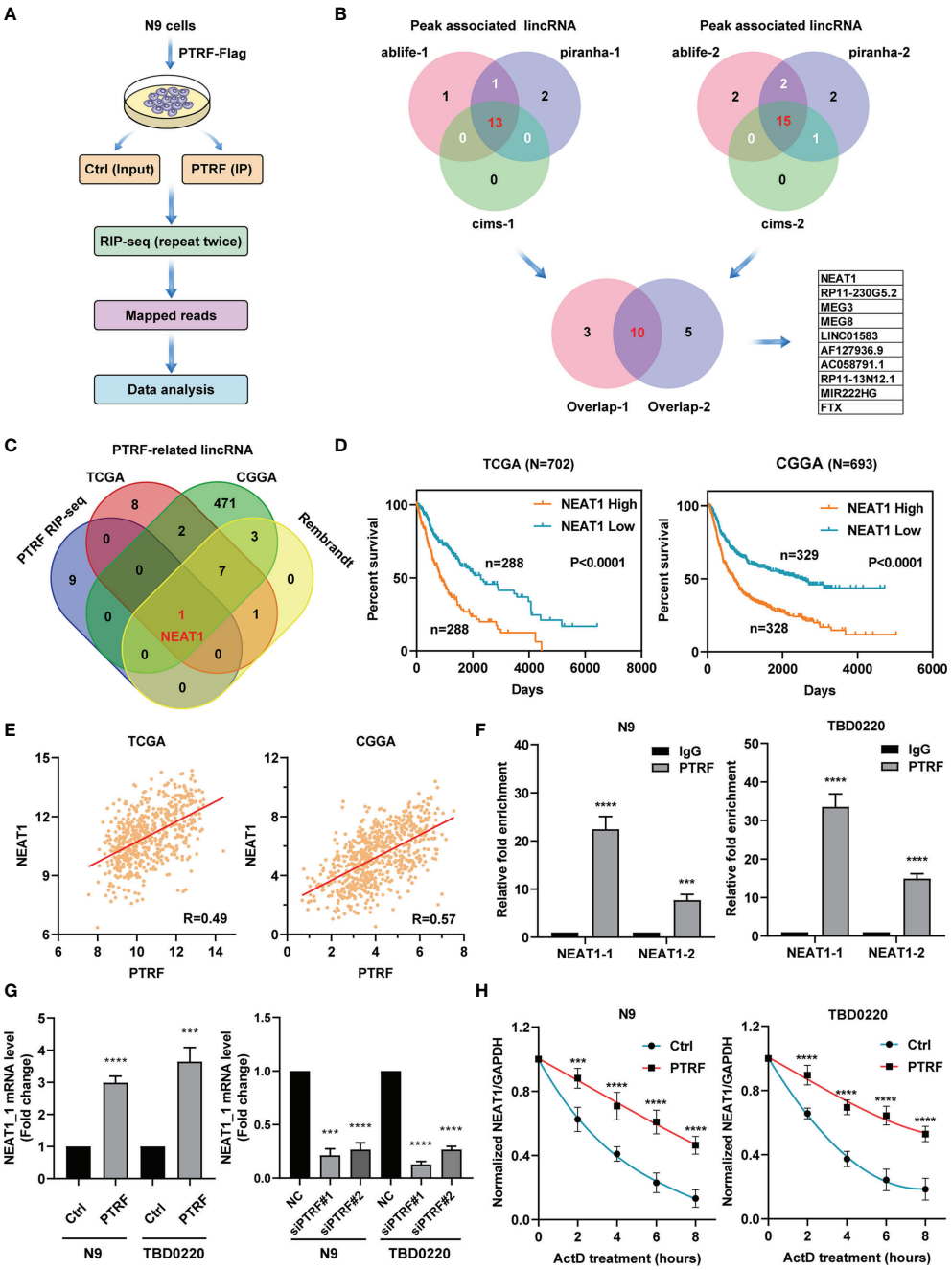

FIGURE 2 | PTRF interacts with LncRNA *NEAT1* and maintains its mRNA stability. **(A)** Schematic of RIP-seq analysis in primary GBM cells with PTRF overexpression. **(B)** Venn diagrams showing the number of peaks associated with lncRNA that overlap between two repeated experiments by three computational methods: (a) CIMS, (b) Piranha, and (c) ABlife. Ten lncRNAs were identified as potential PTRF-associated RNA molecules. **(C)** Venn diagrams of results for potential lncRNAs between PTRF RIP-Seq, TCGA, CGGA, and Rembrandt database. **(D)** The Kaplan–Meier curves of patients with high or low lncRNA *NEAT1* expression (the TCGA database and CGGA database). **(E)** The correlation between PTRF and *NEAT1* levels in the TCGA and CGGA GBM database. **(F)** RIP-qPCR verification of RIP-Seq results with PTRF antibodies for the enrichment of *NEAT1* in N9 and TBD0220 cells. **(G)** The relative level of *NEAT1* in control and PTRF overexpressing cells (left). The level of *NEAT1* after PTRF knockdown in N9 and TBD0220 cells (right). **(H)** RT-qPCR analysis of *NEAT1*, treated with actinomycin D (ActD) at the indicated time points in N9 and TBD0220 cells. ***p ≤ 0.001 and ****p ≤ 0.001.

reads were analyzed for PTRF-associated RNA sequences after normalization by three computational methods: (a) CIMS, (b) Piranha, and (c) ABlife. Based on screening with two replicates by three different computations, we identified ten long noncoding RNAs (lncRNAs) as potential PTRF-associated RNA molecules (**Figure 2B**).

To clarify the function of PTRF as RBP, we performed the co-expression analysis to identify PTRF-related lncRNAs (r > 0.3) in TCGA, CGGA, and Rembrandt glioma databases. We overlapped the lncRNAs data from RIP-Seq results and public GBM databases. The cross-comparison of the four lists revealed that nuclear enriched abundant transcript 1 (*NEAT1*) is the lncRNA that interacts with PTRF (**Figure 2C**). Patients with a high level of *NEAT1* had shorter overall survival times compared with those with low *NEAT1* expression (**Figure 2D** and **Supplemental Figure 2A**). Further, we found a significant correlation between PTRF and *NEAT1* in TCGA (r = 0.49), CGGA (r = 0.57), and Rembrandt (r = 0.49) databases (**Figure 2E** and **Supplemental Figure 2B**). RBP immunoprecipitation–coupled RT-qPCR was performed in N9 and TBD0220 cells in which the cell lysates were followed by IP with the antibody against PTRF. Given that two transcripts of *NEAT1*, *NEAT1*_1 (3.7 kb) and *NEAT1*_2 (23 kb), we designed two pairs of primers for PCR amplification, respectively. Quantitative PCR analysis showed the enrichment of *NEAT1*_1 and *NEAT1*_2 in the PTRF group, compared with the IgG group, validating the RIP-Seq results. The enrichment of *NEAT1*_1 was significantly higher than that of *NEAT1*_2 in RBP immunoprecipitation (**Figure 2F**).

To verify the effect of PTRF on *NEAT1*, we conducted quantitative PCR analysis to determine that the mRNA level of *NEAT1*_1 was increased in N9 PTRF and TBD0220 PTRF cells than control cells. The mRNA level of *NEAT1*_1 was significantly decreased by PTRF knockdown in N9 and TBD0220 cells (**Figure 2G**). The effect of PTRF on *NEAT1*_2 is consistent with the results of *NEAT1*_1 (**Supplemental Figures 2C, D**). Considering the pivotal role of RBP in post-transcriptional regulation, we investigated whether PTRF regulated the stability of *NEAT1* with actinomycin D (ActD) blocking mRNA synthesis. We conducted a quantitative PCR–based time curve (0–8 h) analysis of *NEAT1*, which showed that PTRF resulted in significantly lower degradation of *NEAT1* level (**Figure 2H** and **Supplemental Figure 2E**).

PTRF Suppresses UBXN1 Expression and Promotes the Activity of NF-κB *via NEAT1*

The genes that positively correlated with PTRF were found to be closely related to the NF-κB signaling pathway (**Figure 1A**). Since, NF-κB plays a crucial role in the immune response and PD-L1 regulation, we explored the role of *NEAT1* in the regulation of NF-κB in a PTRF-dependent manner. We previously demonstrated that the PRC2 complex promoted NF-κB activity *via* the trimethylation of H3K27 (H3K27me3) in the UBXN1 promoter (23, 24). Based on the interaction between *NEAT1* and EZH2, we designed siRNA to knock-down *NEAT1* expression. The level of UBXN1 was significantly decreased by PTRF overexpression in N9 and TBD0220 cells, and this decrease was reversed by *NEAT1* knockdown (**Figure 3A**). Further, the level of UBXN1 was significantly increased in PTRF knockdown cells compared with the control cells (**Figure 3B**). We next performed chromatin immunoprecipitation (ChIP)-qPCR analysis to evaluate the chromatin state of the UBXN1 promoter and found that the enrichment levels of H3K27me3 were increased at the UBXN1 promoter region in cells overexpressing PTRF (**Figure 3C**). Further, knockdown of PTRF or *NEAT1* reduced H3K27me3 enrichment at the UBXN1 promoter region in N9 and TBD0220 cells (**Figure 3D**).

We next investigated how PTRF regulates the activity of NF-κB. PTRF overexpression decreased the proteins level of UBXN1 (**Figure 3E** and **Supplemental Figure 3A**) and increased the nuclear levels of p-NF-κB in N9 and TBD0220 cells, which were reversed by knocking down *NEAT1* (**Figure 3E** and **Supplemental Figure 3B**). In contrast, knockdown of PTRF increased the UBXN1 proteins level (**Figure 3F** and **Supplemental Figure 3C**) and decreased the nuclear levels of p-NF-κB (**Figure 3F**). In addition, we cultured N9 and TBD0220 cells with lentivirus vector expressing a NF-κB luciferase construct. Luciferase reporter assay showed that the activity of NF-κB was significantly up-regulated by overexpression of PTRF in N9 and TBD0220 cells and the effect was reversed by *NEAT1* knockdown (**Figure 3G**). Knockdown of PTRF decreased the luciferase activity of NF-κB reporter (**Supplemental Figure 3D**). We also detected the expression of NF-κB target genes, confirming that NF-κB was activated by PTRF overexpression in N9 and TBD0220 cells (**Figure 3H**). PTRF knockdown produced the opposite effects (**Supplemental Figure 3E**). These results suggest that PTRF suppresses UBXN1 expression and promotes the activity of NF-κB *via NEAT1*.

PTRF Contributes to GBM Proliferation Through the UBXN1/NF-κB Axis by Regulating *NEAT1 In Vivo*

To further verify the role of the PTRF/*NEAT1*/NF-κB axis *in vivo*, we established an intracranial GBM patient-derived xenografts model in BALB/c nude mice. We transfected TBD0220 and TBD0220 PTRF cells with *NEAT1* siRNA respectively. The bioluminescence imaging showed that PTRF overexpression resulted in a significant increase in tumor growth. *NEAT1* knockdown reduced the growth of the tumor and attenuated the tumor growth induced by PTRF (**Figures 4A, B**). The mice bearing tumors, derived from the PTRF overexpressing cells, showed poor survival compared with the control group by Kaplan–Meier survival curves. *NEAT1* knockdown group had a longer survival time compared with their respective control groups (**Figure 4C**). Similar results could be found in Hematoxylin-Eosin (H&E) staining that *NEAT1* knockdown partly reverse the promotion of GBM proliferation induced by PTRF (**Figure 4D**). The expression of *NEAT1* was increased in the PTRF overexpressing group compared with the control group (**Figure 4E**). Overexpression of PTRF resulted in a significant decrease in UBXN1 and an increase in Ki-67 and p-NF-κB (**Figure 4E**). *NEAT1* knockdown significantly increased the level of UBXN1 and decreased the level of Ki-67 and p-NF-κB (**Figure 4E**). These data suggest that PTRF regulates *NEAT1* and promotes GBM proliferation through the UBXN1/NF-κB axis.

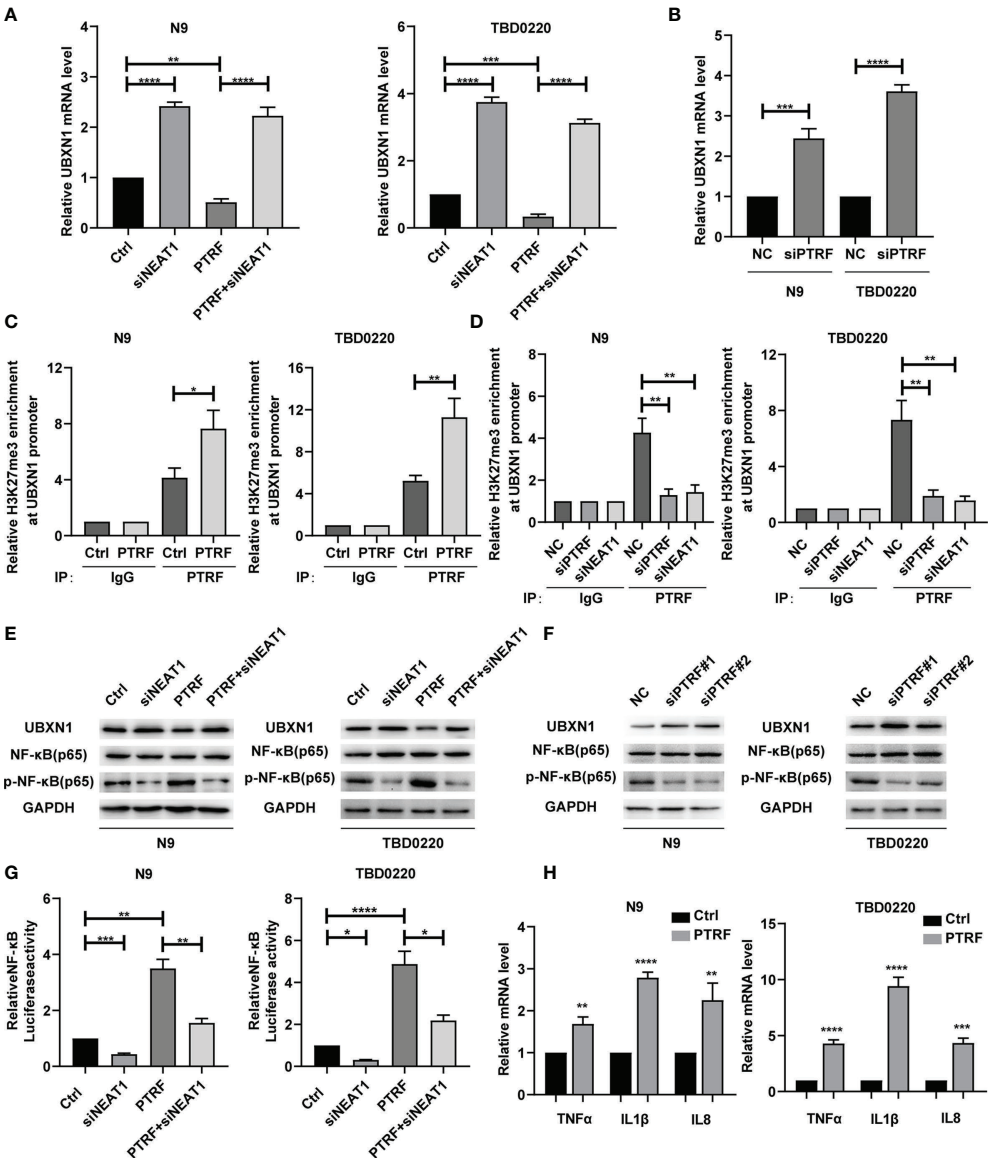

FIGURE 3 | **(A)** RT-qPCR analysis of UBXN1 in N9 and TBD0220 cells with or without PTRF overexpression, as well as treatment with *NEAT1* knockdown. **(B)** The mRNA level of UBXN1 after PTRF knockdown in N9 and TBD0220 cells. **(C)** ChIP-PCR analysis of the ability of H3K27me3 to bind to the UBXN1 promoter using H3K27me3 antibody in N9 and TBD0220 cells with or without PTRF overexpression. **(D)** ChIP-PCR analysis of the ability of H3K27me3 to bind to the UBXN1 promoter normalized to IgG with PTRF or *NEAT1* knockdown in N9 and TBD0220 cells, respectively. **(E)** Western blot analysis of UBXN1, NF-κB, and P-NF-κB expression in primary GBM cells (N9 and TBD0220) with or without PTRF overexpression, as well as treatment with *NEAT1* knockdown respectively. **(F)** Western blot analysis of UBXN1, NF-κB, and P-NF-κB expression with PTRF knockdown in N9 and TBD0220 cells. **(G)** The Luciferase activity of NF-κB in N9 and TBD0220 cells with or without PTRF overexpression, as well as treatment with *NEAT1* knockdown respectively. **(H)** The mRNA level of NF-κB downstream target genes, including TNFα, IL-1β, and IL-8 in N9 and TBD0220 cells with PTRF overexpression. *p ≤ 0.05, **p ≤ 0.01, ***p ≤ 0.001, and ****p ≤ 0.001.

The NF-κB Binds to the PD-L1 Promoter Region in Response to PTRF Activation and Enhances PD-L1 Transcription

To identify the binding sequence of NF-κB in the promoter region of PD-L1, we analyzed the PD-L1 promoter and found four putative binding sites for NF-κB in the PD-L1 promoter region (25). Four pairs of primers with CHIP-qPCR for PD-L1 promoter were designed respectively. The sonicated chromatin from PTRF overexpression in N9 and TBD0220 cells was immunoprecipitated with an anti-NF-κB antibody, and only one fragment was amplified in N9 PTRF and TBD0220 PTRF cells compared with control cells by PCR, indicating (–111)-GGAAAGTCCA- (–102) as a consensus sequence recognized by NF-κB (**Figure 5A**). We constructed a luciferase reporter driven by the PD-L1 promoter that contains the WT or a mutated potential NF-κB-binding sequence (**Figure 5B**). We transfected the luciferase reporter

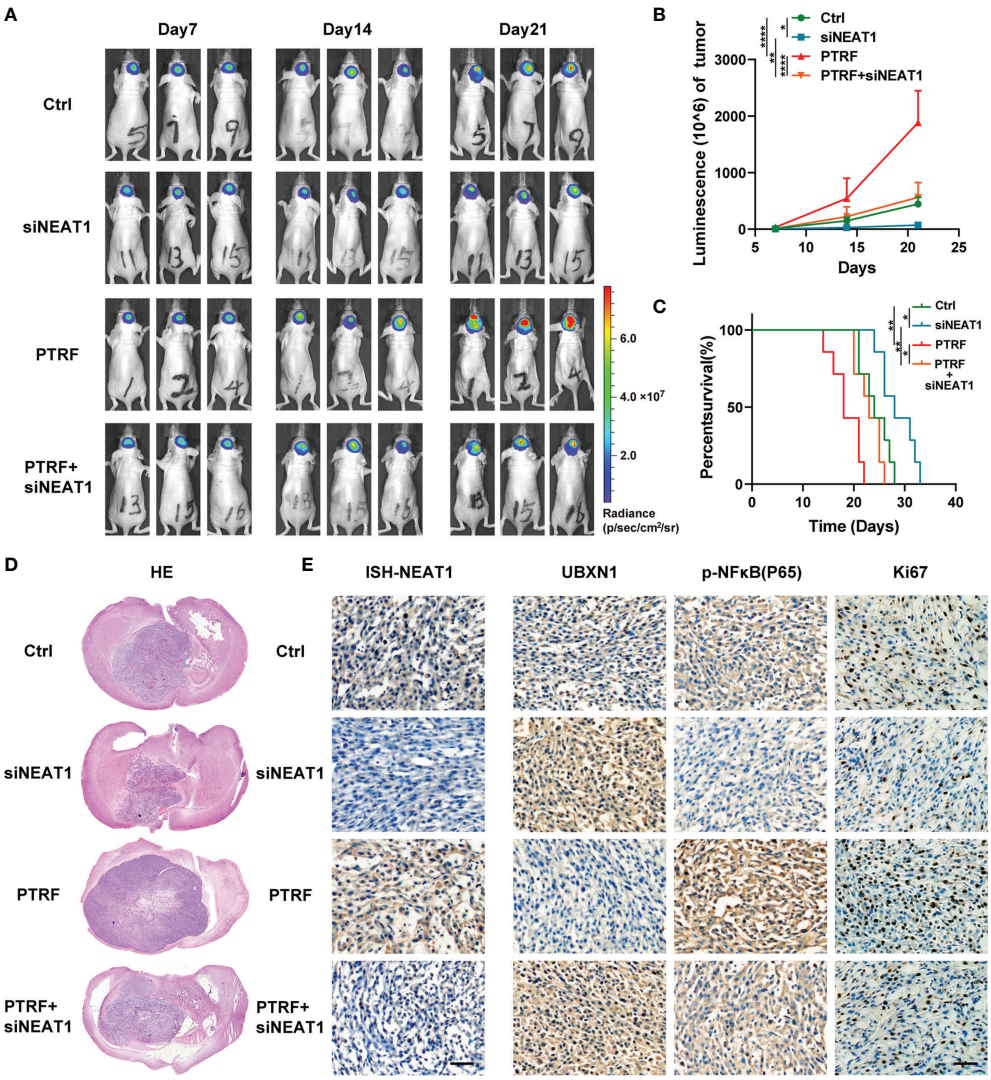

FIGURE 4 | PTRF contributes to GBM proliferation through the UBXN1/NF-κB axis by regulating *NEAT1 In Vivo*. **(A)** Representative tumor bioluminescence images of mice at 7, 14, and 21 days post tumor implantation. **(B)** Tumor growth curves using quantification of bioluminescence imaging signal intensities for mice bearing GBM with or without PTRF overexpression, as well as treatment with *NEAT1* knockdown respectively. **(C)** Kaplan-Meier survival curve of nude mice implanted with TBD0220 cells with or without PTRF overexpression, as well as treatment with *NEAT1* knockdown respectively. **(D)** Representative images of H&E staining of tumors from the nude mice. **(E)** ISH staining of *NEAT1* in tumors (left). IHC staining of UBXN1, P-NF-κB, and Ki-67 in tumors (right). Scale bar, 50 μm. *p ≤ 0.05, **p ≤ 0.01, and ****p ≤ 0.001.

construct into N9 and TBD0220 cells and measured luciferase activity. PTRF overexpression in N9 and TBD0220 cells significantly increased the activity of the WT but not of mutated promoter, indicating that PTRF increased the binding of NF-κB to PD-L1. The knockdown of PTRF reduced the luciferase activity driven by the PD-L1 promoter in N9 and TBD0220 cells (**Figure 5C**). A similar inhibitory effect was also observed by *NEAT1* knockdown in N9 and TBD0220 cells (**Figure 5D**). These results demonstrate that NF-κB binds to the PD-L1 promoter region and enhances the PD-L1 transcription in response to PTRF activation in GBM cells, and this regulation is mediated *via* one of the NF-kB binding sites (-111 to -102 nt region).

PTRF Promotes Immune Evasion of GBM Cells by Affecting PD-1 Binding and PD-L1–Mediated T Cell Toxicity

Previous studies have shown that elevated PD-L1 expression in tumor cells mediates T cell tolerance and activates anti-tumor immunosuppression (10, 12). To determine whether PTRF regulation on PD-L1 may affect its interaction with PD-1, we incubated a recombinant protein containing human PD-1 and Fc fragment of IgG with TBD0220 cells. We found that PTRF overexpression increased PD-1 binding on the TBD0220 cell surface compared with the control cells (**Figures 5E, F**). Immunofluorescence assays revealed that overexpression of

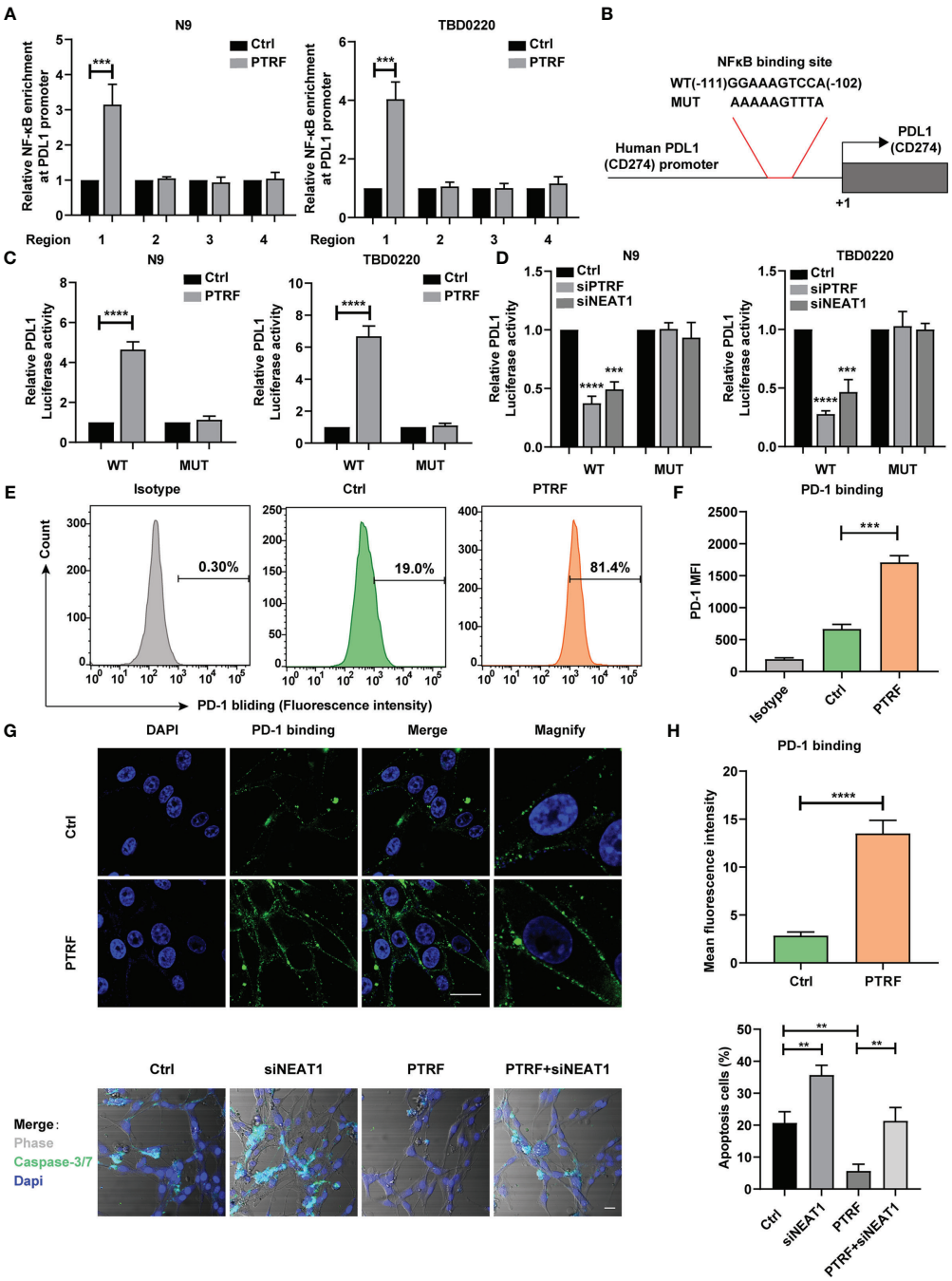

FIGURE 5 | PTRF enhances PD-L1 transcription *via* NF-κB and promotes immune evasion of GBM cells through PD-L1. **(A)** ChIP-PCR analysis of the ability of NF-κB to bind to the PD-L1 promoter in N9 and TBD0220 cells with or without PTRF overexpression. Results are normalized to IgG. **(B)** Schematic illustration of the proximal region of the human PD-L1 promoter. **(C)** N9 and TBD0220 cells (with the expression of empty vector or PTRF) were transfected with a luciferase reporter vector containing WT or mutated NF-κB sequence of PD-L1 promoter. **(D)** N9 and TBD0220 cells with PTRF or *NEAT1* knockdown were transfected with a luciferase reporter vector containing WT or mutated NF-κB sequence of PD-L1 promoter. **(E)** Flow cytometry analysis of PD-1 binding in TBD0220 cells with or without PTRF overexpression. **(F)** Quantification of fluorescence intensity in **(E)**. The y axis represents the mean fluorescence intensity of PD-1. **(G)** Immunofluorescence staining of control and PTRF overexpressing cells. PD-1 (green), Nuclei (blue), scale bar, 20 μm. **(H)** Quantification of fluorescence intensity in **(G)**. **(I)** T cell killing assay of TBD0220 cells with or without PTRF overexpression, as well as treatment with *NEAT1* knockdown respectively. caspase3/7 cleavage (green), Nuclei (blue), scale bar, 20 μm. **p ≤ 0.01, ***p ≤ 0.001, and ****p ≤ 0.001.

PTRF was accompanied by high expression of PD-1 (**Figures 5G, H**), indicating that PTRF significantly increased PD-1 binding on the GBM cell surface, which is consistent with the flow cytometry results. Furthermore, PTRF overexpression decreased the sensitivity of GBM cells to T cell-mediated cytotoxicity. The knockdown of *NEAT1* sensitized GBM cells to T cell-mediated cell death and attenuated the immune evasion induced by PTRF in GBM (**Figure 5I**). These results demonstrate that PTRF alters PD-1 binding and T cell-mediated cytotoxicity through regulation of PD-L1 expression in GBM.

To further assess relationships between PTRF, *NEAT1*, and PD-L1 in GBM, we chose tissue samples of GBM patients with high or low PTRF expression. GBM patients with high PTRF-expression had high levels of *NEAT1* and p-NF-κB, showing that PTRF significantly correlates with *NEAT1* and p-NF-κB (**Figure 6A**). Furthermore, high levels of PTRF positively correlated with PD-L1 expression and inversely correlated with $CD8^+$ T cell infiltration in GBM (**Figure 6A**). These results suggest a role of PTRF in PD-L1 regulation and immune evasion in GBM.

To evaluate the prognostic relevance of PTRF, *NEAT1*, and PD-L1 expression, we analyzed glioma data from TCGA, CGGA, and Rembrandt databases. As shown in **Figure 6B** and **Supplemental Figure 4**, high expressions of PTRF, *NEAT1*, and PD-L1 are independent poor prognostic markers. Next, we integrated the expression levels of these genes and evaluated the suggestive effect of the PNP geneset (PTRF-*NEAT1*-PD-L1) on the prognosis of GBM patients. We show that a higher level of PNP indicates a shorter survival time in patients with glioma in TCGA, CGGA, and Rembrandt databases (**Figure 6C**).

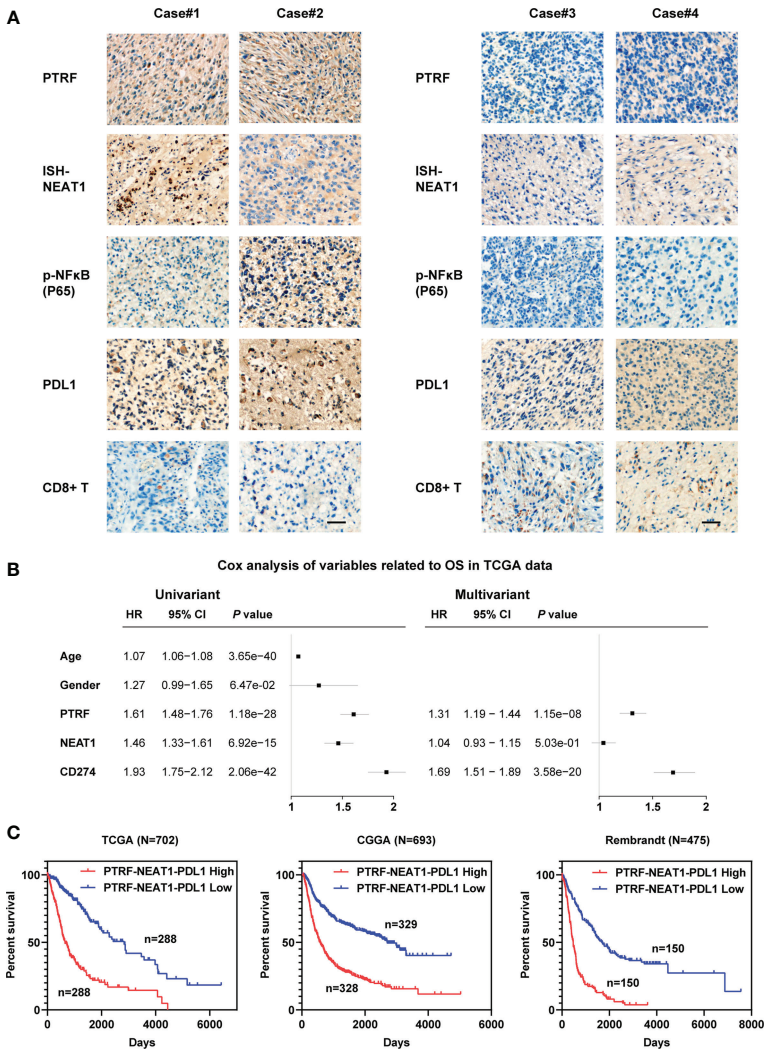

FIGURE 6 | The relationships between PTRF, *NEAT1*, and PD-L1 in GBM. **(A)** IHC or ISH staining of PTRF, *NEAT1*, P-NF-Kb, PD-L1, and CD8 in four representative GBM specimens. Scale bar, 50 μm. **(B)** Univariate and multivariate Cox analyses of PTRF, *NEAT1*, and PD-L1 expression in the TCGA databases. **(C)** The Kaplan–Meier curves for patients with different expressions of PTRF, *NEAT1*, and PD-L1.

DISCUSSION

In this study, we show that PTRF induces the stability of lncRNA *NEAT1* and promotes the activity of NF-κB, leading to PD-L1 mediated immune evasion in GBM (**Figure 7**). According to previous studies, PTRF plays different roles in different types of tumors. PTRF inhibits tumor metastasis in prostate cancer and tumorigenesis in colorectal cancer (26, 27). In contrast, PTRF promotes the progression of pancreatic cancer and proliferation of rhabdomyosarcoma (28, 29). The tumor-promoting effect of PTRF in gliomas is widely recognized. Previously, we showed that the expression of PTRF positively correlates with the WHO grade of glioma, and the prognosis of glioma patients with high PTRF expression is worse (15). We further found a reduction in the number of $CD8^+$ T cells and $CD8^+$ T cells mediated cytotoxic activity in tumor tissues with PTRF overexpression (19). In this study, we demonstrated that PTRF increases the expression of PD-L1 and promotes immune evasion in GBM.

Recently studies have shown that lncRNAs play a crucial roles in regulating immunity, including the activation and function of macrophages and T cells (30). One such lncRNA is *NEAT1*. Previous studies have found that *NEAT1*-knockout mice have abnormalities in their Treg and Th cell differentiation (31). *NEAT1* has also been found to target STAT3 and regulate the differentiation of Th17 cells in rheumatoid arthritis (32). Imamura et al. found that *NEAT1* activate the transcription of IL-8 by removing SFPQ from the IL-8 promoter (33). Knockdown of *NEAT1* also limits the apoptosis of $CD8^+$ T cells through the miR-155/Tim-3 pathway (34). Although *NEAT1* has been studied in immune response, the relationship

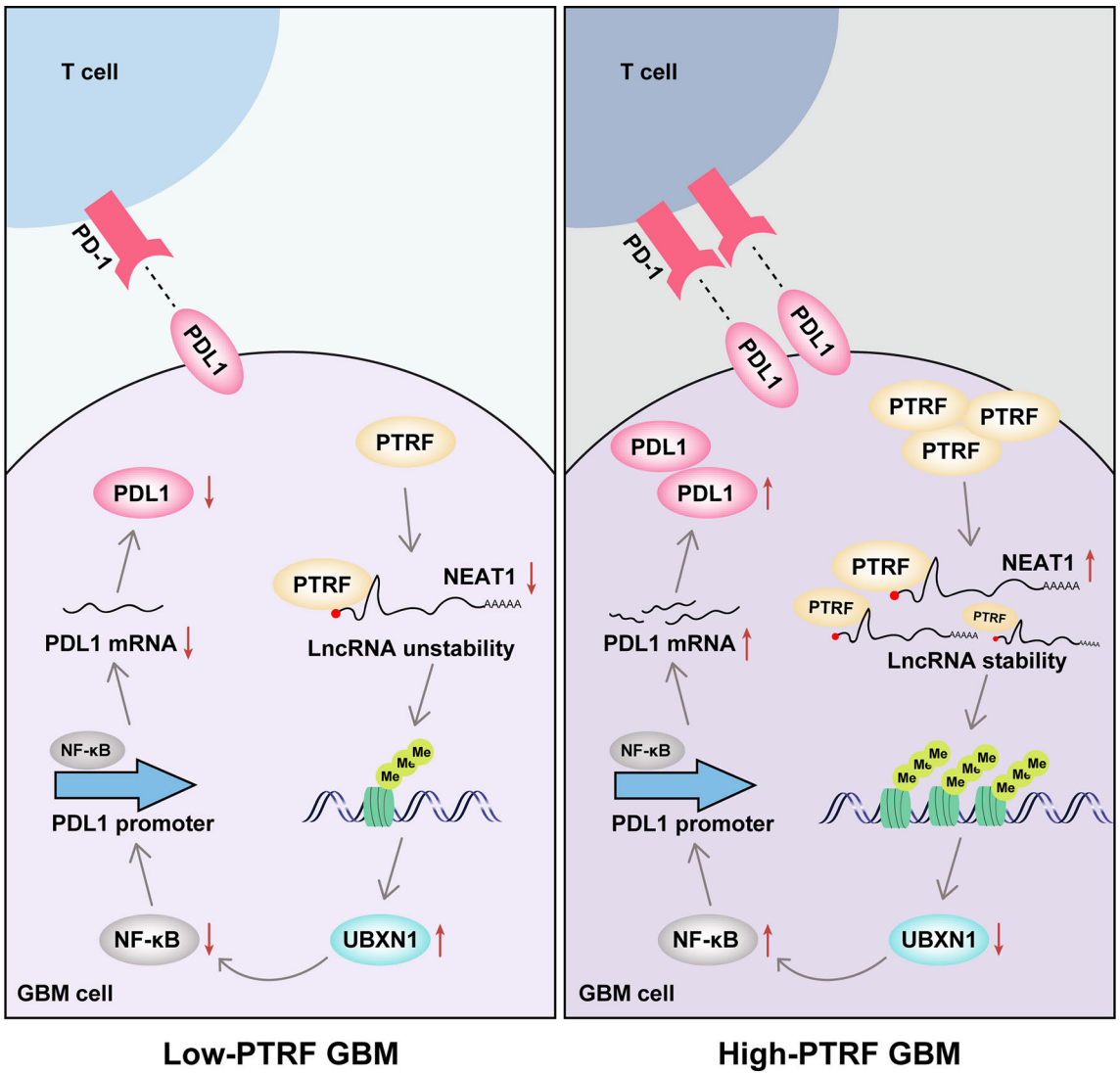

FIGURE 7 | The mechanistic model showing how PTRF/Cavin-1 stabilizes lncRNA *NEAT1* to maintain the activity of NF-κB and promote immune evasion *via* PD-L1 in glioblastoma.

between *NEAT1* and PD-L1 remains unclear. In this study, we found that *NEAT1*, induced by PTRF, mediates PD-L1 regulation and promotes immune evasion in GBM.

UBXN1 is a UBX domain-containing protein which inhibits NF-κB activation. The knockdown of UBXN1 decreases the stability of IκBα and enhances NF-κB signaling (35). In addition, UBXN1 is the negative regulator of NF-κB signaling and interacts with cIAPs through the UBA domain (36). YTHDF2 was also shown to accelerate UBXN1 mRNA degradation *via* METTL3−mediated m6A, promoting the activation of NF−κB (37). Our previous study found that UBXN1 is also a target for EZH2 mediated H3K27me3, and is regulated by EGFR and lncRNA *PRADX* (23, 24). In addition, we also detected that lncRNA *NEAT1* binds to EZH2 and mediates the trimethylation of H3K27 in their promoters (38), which regulated by EGFR pathway activity. From the discussion above, we further demonstrated that PTRF maintains the stability of *NEAT1* to suppresses UBXN1 expression and activate NF-κB activity.

Although the expression of PD-L1 is regulated by multiple mechanisms, transcriptional regulation plays an important part in its regulation in cancer. MYC was shown to directly bind to the promoter of PD-L1 and enhanced the expression of PD-L1, regulating the anti-tumor response in mouse tumors and human tumor cells (39). Interferon regulatory factor-1 (IRF-1), a transcription factor, regulates the constitutive and IFN-γ-mediated PD-L1 expression in human lung cancer cell (40). In classical Hodgkin lymphoma, AP-1-responsive enhancer in the PD-L1 gene binds to the PD-L1 enhancer and increases the activity of PD-L1 promoter (41). Recently, MUC1-C was found to activate PD-L1 transcription by recruiting MYC and NF-κB to the PD-L1 promoter region in triple-negative breast cancer (42). Our study identified another novel mechanism of PD-L1 regulation in cancer—PTRF induces the binding of NF-κB to the PD-L1 gene promoter region and enhances PD-L1 transcription in GBM.

DATA AVAILABILITY STATEMENT

The data presented in the study are deposited in the SRA repository, accession number PRJNA777377.

ETHICS STATEMENT

The animal study was reviewed and approved by the Animal Ethical and Welfare Committee (Protocol # TMUaMEC 2018034). Written informed consent was not obtained from the individual(s) for the publication of any potentially identifiable images or data included in this article.

AUTHOR CONTRIBUTIONS

Developed the study concept and designed the study: YT and QW. Conducted the experiments and acquired the data: KY, XC, XL, YW, JZ, SY, CX, EY, MX, BH, CF, YT and QW. Analyzed the data, generated the figures, and wrote the paper: CK, KY and XC. All authors contributed to the article and approved the submitted version.

FUNDING

This work was supported by the National Natural Science Foundation of China (No. 81772667 and 82002657), the Tianjin Key R&D Plan of Tianjin Science and Technology Plan Project (No. 20YFZCSY00360), the Central Government Guided Local Science and Technology Development fund Project of Hebei Province (No. 216Z7711G), the Hebei Natural Science Foundation Precision Medicine Joint Project (No. H2020201206), the Key Scientific Research Project in Colleges and Universities of Hebei Province (No. ZD2021308), The National Key Research and Development Programs of China (No. 2018YFA0209700), and the Science and Technology Project of Tianjin Municipal Health Commission (No. TJWJ2021QN007 and TJWJ2021QN003).

SUPPLEMENTARY MATERIAL

The Supplementary Material for this article can be found online at: https://www.frontiersin.org/articles/10.3389/fimmu.2021.802795/full#supplementary-material

REFERENCES

1. Ostrom QT, Patil N, Cioffi G, Waite K, Kruchko C, Barnholtz-Sloan JS. CBTRUS Statistical Report: Primary Brain and Other Central Nervous System Tumors Diagnosed in the United States in 2013-2017. *Neuro Oncol* (2020) 22 (12 Suppl 2):iv1–96. doi: 10.1093/neuonc/noaa200
2. Van Meir EG, Hadjipanayis CG, Norden AD, Shu HK, Wen PY, Olson JJ. Exciting New Advances in Neuro-Oncology: The Avenue to a Cure for Malignant Glioma. *CA: Cancer J Clin* (2010) 60(3):166–93. doi: 10.3322/caac.20069
3. Xu F, Jin T, Zhu Y, Dai C. Immune Checkpoint Therapy in Liver Cancer. *J Exp Clin Cancer Res* (2018) 37(1):110. doi: 10.1186/s13046-018-0777-4
4. Reck M, Rodriguez-Abreu D, Robinson AG, Hui R, Csoszi T, Fulop A, et al. Pembrolizumab Versus Chemotherapy for PD-L1-Positive Non-Small-Cell Lung Cancer. *N Engl J Med* (2016) 375(19):1823–33. doi: 10.1056/NEJMoa1606774
5. Ferris RL, Blumenschein GJr., Fayette J, Guigay J, Colevas AD, Licitra L, et al. Nivolumab for Recurrent Squamous-Cell Carcinoma of the Head and Neck. *N Engl J Med* (2016) 375(19):1856–67. doi: 10.1056/NEJMoa1602252
6. Chuntova P, Chow F, Watchmaker PB, Galvez M, Heimberger AB, Newell EW, et al. Unique Challenges for Glioblastoma Immunotherapy-Discussions Across Neuro-Oncology and Non-Neuro-Oncology Experts in Cancer Immunology. Meeting Report From the 2019 SNO Immuno-Oncology Think Tank. *Neuro Oncol* (2021) 23(3):356–75. doi: 10.1093/neuonc/noaa277
7. Sharma P, Allison JP. The Future of Immune Checkpoint Therapy. *Science* (2015) 348(6230):56–61. doi: 10.1126/science.aaa8172
8. Herbst RS, Soria JC, Kowanetz M, Fine GD, Hamid O, Gordon MS, et al. Predictive Correlates of Response to the Anti-PD-L1 Antibody MPDL3280A in Cancer Patients. *Nature* (2014) 515(7528):563–7. doi: 10.1038/nature14011
9. Iwai Y, Ishida M, Tanaka Y, Okazaki T, Honjo T, Minato N. Involvement of PD-L1 on Tumor Cells in the Escape From Host Immune System and Tumor

Immunotherapy by PD-L1 Blockade. *Proc Natl Acad Sci USA* (2002) 99 (19):12293–7. doi: 10.1073/pnas.192461099
10. Garber ST, Hashimoto Y, Weathers SP, Xiu J, Gatalica Z, Verhaak RG, et al. Immune Checkpoint Blockade as a Potential Therapeutic Target: Surveying CNS Malignancies. *Neuro Oncol* (2016) 18(10):1357–66. doi: 10.1093/neuonc/now132
11. Berghoff AS, Kiesel B, Widhalm G, Rajky O, Ricken G, Wohrer A, et al. Programmed Death Ligand 1 Expression and Tumor-Infiltrating Lymphocytes in Glioblastoma. *Neuro Oncol* (2015) 17(8):1064–75. doi: 10.1093/neuonc/nou307
12. Du L, Lee JH, Jiang H, Wang C, Wang S, Zheng Z, et al. Beta-Catenin Induces Transcriptional Expression of PD-L1 to Promote Glioblastoma Immune Evasion. *J Exp Med* (2020) 217(11):e20191115. doi: 10.1084/jem.20191115
13. Xiang Z, Zhou Z, Song S, Li J, Ji J, Yan R, et al. Dexamethasone Suppresses Immune Evasion by Inducing GR/STAT3 Mediated Downregulation of PD-L1 and IDO1 Pathways. *Oncogene* (2021) 40(31):5002–12. doi: 10.1038/s41388-021-01897-0
14. Peng J, Hamanishi J, Matsumura N, Abiko K, Murat K, Baba T, et al. Chemotherapy Induces Programmed Cell Death-Ligand 1 Overexpression *via* the Nuclear Factor-KappaB to Foster an Immunosuppressive Tumor Microenvironment in Ovarian Cancer. *Cancer Res* (2015) 75(23):5034–45. doi: 10.1158/0008-5472.CAN-14-3098
15. Huang K, Fang C, Yi K, Liu X, Qi H, Tan Y, et al. The Role of PTRF/Cavin1 as a Biomarker in Both Glioma and Serum Exosomes. *Theranostics* (2018) 8 (6):1540–57. doi: 10.7150/thno.22952
16. Thommen DS, Schuster H, Keller M, Kapoor S, Weinzierl AO, Chennakesava CS, et al. Two Preferentially Expressed Proteins Protect Vascular Endothelial Cells From an Attack by Peptide-Specific CTL. *J Immunol* (2012) 188 (11):5283–92. doi: 10.4049/jimmunol.1101506
17. Ni Y, Hao J, Hou X, Du W, Yu Y, Chen T, et al. Dephosphorylated Polymerase I and Transcript Release Factor Prevents Allergic Asthma Exacerbations by Limiting IL-33 Release. *Front Immunol* (2018) 9:1422. doi: 10.3389/fimmu.2018.01422
18. Guo Q, Guan GF, Cheng W, Zou CY, Zhu C, Cheng P, et al. Integrated Profiling Identifies Caveolae-Associated Protein 1 as a Prognostic Biomarker of Malignancy in Glioblastoma Patients. *CNS Neurosci Ther* (2019) 25(3):343–54. doi: 10.1111/cns.13072
19. Yi K, Zhan Q, Wang Q, Tan Y, Fang C, Wang Y, et al. PTRF/cavin-1 Remodels Phospholipid Metabolism to Promote Tumor Proliferation and Suppress Immune Responses in Glioblastoma by Stabilizing Cpla2. *Neuro Oncol* (2021) 23(3):387–99. doi: 10.1093/neuonc/noaa255
20. Li X, Qian X, Wang B, Xia Y, Zheng Y, Du L, et al. Programmable Base Editing of Mutated TERT Promoter Inhibits Brain Tumour Growth. *Nat Cell Biol* (2020) 22(3):282–8. doi: 10.1038/s41556-020-0471-6
21. Zhang Y, Li J, Yi K, Feng J, Cong Z, Wang Z, et al. Elevated Signature of a Gene Module Coexpressed With CDC20 Marks Genomic Instability in Glioma. *Proc Natl Acad Sci USA* (2019) 116(14):6975–84. doi: 10.1073/pnas.1814060116
22. Wang Z, Tang W, Yuan J, Qiang B, Han W, Peng X. Integrated Analysis of RNA-Binding Proteins in Glioma. *Cancers (Basel)* (2020) 12(4):892. doi: 10.3390/cancers12040892
23. Li Y, Liu X, Cui X, Tan Y, Wang Q, Wang Y, et al. LncRNA PRADX-Mediated Recruitment of PRC2/DDX5 Complex Suppresses UBXN1 Expression and Activates NF-KappaB Activity, Promoting Tumorigenesis. *Theranostics* (2021) 11(9):4516–30. doi: 10.7150/thno.54549
24. Huang K, Yang C, Wang QX, Li YS, Fang C, Tan YL, et al. The CRISPR/Cas9 System Targeting EGFR Exon 17 Abrogates NF-KappaB Activation *via* Epigenetic Modulation of UBXN1 in EGFRwt/vIII Glioma Cells. *Cancer Lett* (2017) 388:269–80. doi: 10.1016/j.canlet.2016.12.011
25. Huang G, Wen Q, Zhao Y, Gao Q, Bai Y. NF-KappaB Plays a Key Role in Inducing CD274 Expression in Human Monocytes After Lipopolysaccharide Treatment. *PloS One* (2013) 8(4):e61602. doi: 10.1371/journal.pone.0061602
26. Wang F, Zheng Y, Orange M, Yang C, Yang B, Liu J, et al. PTRF Suppresses the Progression of Colorectal Cancers. *Oncotarget* (2017) 8(30):48650–9. doi: 10.18632/oncotarget.9424
27. Moon H, Lee CS, Inder KL, Sharma S, Choi E, Black DM, et al. PTRF/cavin-1 Neutralizes Non-Caveolar Caveolin-1 Microdomains in Prostate Cancer. *Oncogene* (2014) 33(27):3561–70. doi: 10.1038/onc.2013.315
28. Faggi F, Chiarelli N, Colombi M, Mitola S, Ronca R, Madaro L, et al. Cavin-1 and Caveolin-1 Are Both Required to Support Cell Proliferation, Migration and Anchorage-Independent Cell Growth in Rhabdomyosarcoma. *Lab Invest; J Tech Methods Pathol* (2015) 95(6):585–602. doi: 10.1038/labinvest.2015.45
29. Liu L, Xu HX, Wang WQ, Wu CT, Chen T, Qin Y, et al. Cavin-1 Is Essential for the Tumor-Promoting Effect of Caveolin-1 and Enhances Its Prognostic Potency in Pancreatic Cancer. *Oncogene* (2014) 33(21):2728–36. doi: 10.1038/onc.2013.223
30. Chen W, Liu S, Wang F. Potential Impact and Mechanism of Long Non-Coding RNAs on Cancer and Associated T Cells. *J Cancer* (2021) 12 (16):4873–82. doi: 10.7150/jca.58859
31. Gast M, Rauch BH, Haghikia A, Nakagawa S, Haas J, Stroux A, et al. Long Noncoding RNA NEAT1 Modulates Immune Cell Functions and Is Suppressed in Early Onset Myocardial Infarction Patients. *Cardiovasc Res* (2019) 115(13):1886–906. doi: 10.1093/cvr/cvz085
32. Shui X, Chen S, Lin J, Kong J, Zhou C, Wu J. Knockdown of lncRNA NEAT1 Inhibits Th17/CD4(+) T Cell Differentiation Through Reducing the STAT3 Protein Level. *J Cell Physiol* (2019) 234(12):22477–84. doi: 10.1002/jcp.28811
33. Imamura K, Imamachi N, Akizuki G, Kumakura M, Kawaguchi A, Nagata K, et al. Long Noncoding RNA NEAT1-Dependent SFPQ Relocation From Promoter Region to Paraspeckle Mediates IL8 Expression Upon Immune Stimuli. *Mol Cell* (2014) 53(3):393–406. doi: 10.1016/j.molcel.2014.01.009
34. Yan K, Fu Y, Zhu N, Wang Z, Hong JL, Li Y, et al. Repression of lncRNA NEAT1 Enhances the Antitumor Activity of CD8(+)T Cells Against Hepatocellular Carcinoma *via* Regulating miR-155/Tim-3. *Int J Biochem Cell Biol* (2019) 110:1–8. doi: 10.1016/j.biocel.2019.01.019
35. Hu Y, O'Boyle K, Auer J, Raju S, You F, Wang P, et al. Multiple UBXN Family Members Inhibit Retrovirus and Lentivirus Production and Canonical NFkappaBeta Signaling by Stabilizing IkappaBalpha. *PloS Pathog* (2017) 13 (2):e1006187. doi: 10.1371/journal.ppat.1006187
36. Wang YB, Tan B, Mu R, Chang Y, Wu M, Tu HQ, et al. Ubiquitin-Associated Domain-Containing Ubiquitin Regulatory X (UBX) Protein UBXN1 Is a Negative Regulator of Nuclear Factor KappaB (NF-Kappab) Signaling. *J Biol Chem* (2015) 290(16):10395–405. doi: 10.1074/jbc.M114.631689
37. Chai RC, Chang YZ, Chang X, Pang B, An SY, Zhang KN, et al. YTHDF2 Facilitates UBXN1 mRNA Decay by Recognizing METTL3-Mediated M(6)A Modification to Activate NF-KappaB and Promote the Malignant Progression of Glioma. *J Hematol Oncol* (2021) 14(1):109. doi: 10.1186/s13045-021-01124-z
38. Chen Q, Cai J, Wang Q, Wang Y, Liu M, Yang J, et al. Long Noncoding RNA NEAT1, Regulated by the EGFR Pathway, Contributes to Glioblastoma Progression Through the WNT/beta-Catenin Pathway by Scaffolding Ezh2. *Clin Cancer Res* (2018) 24(3):684–95. doi: 10.1158/1078-0432.CCR-17-0605
39. Casey SC, Tong L, Li Y, Do R, Walz S, Fitzgerald KN, et al. MYC Regulates the Antitumor Immune Response Through CD47 and PD-L1. *Science* (2016) 352 (6282):227–31. doi: 10.1126/science.aac9935
40. Lee SJ, Jang BC, Lee SW, Yang YI, Suh SI, Park YM, et al. Interferon Regulatory Factor-1 Is Prerequisite to the Constitutive Expression and IFN-Gamma-Induced Upregulation of B7-H1 (Cd274). *FEBS Lett* (2006) 580 (3):755–62. doi: 10.1016/j.febslet.2005.12.093
41. Green MR, Rodig S, Juszczynski P, Ouyang J, Sinha P, O'Donnell E, et al. Constitutive AP-1 Activity and EBV Infection Induce PD-L1 in Hodgkin Lymphomas and Posttransplant Lymphoproliferative Disorders: Implications for Targeted Therapy. *Clin Cancer Res* (2012) 18(6):1611–8. doi: 10.1158/1078-0432.CCR-11-1942
42. Maeda T, Hiraki M, Jin C, Rajabi H, Tagde A, Alam M, et al. MUC1-C Induces PD-L1 and Immune Evasion in Triple-Negative Breast Cancer. *Cancer Res* (2018) 78(1):205–15. doi: 10.1158/0008-5472.CAN-17-1636

Conflict of Interest: The authors declare that the research was conducted in the absence of any commercial or financial relationships that could be construed as a potential conflict of interest.

Publisher's Note: All claims expressed in this article are solely those of the authors and do not necessarily represent those of their affiliated organizations, or those of the publisher, the editors and the reviewers. Any product that may be evaluated in

this article, or claim that may be made by its manufacturer, is not guaranteed or endorsed by the publisher.

Copyright © 2022 Yi, Cui, Liu, Wang, Zhao, Yang, Xu, Yang, Xiao, Hong, Fang, Kang, Tan and Wang. This is an open-access article distributed under the terms of the Creative Commons Attribution License (CC BY). The use, distribution or reproduction in other forums is permitted, provided the original author(s) and the copyright owner(s) are credited and that the original publication in this journal is cited, in accordance with accepted academic practice. No use, distribution or reproduction is permitted which does not comply with these terms.

frontiers in Immunology

REVIEW
published: 13 January 2022
doi: 10.3389/fimmu.2021.829268

DNA Damage Repair in Brain Tumor Immunotherapy

Shihong Zhao†, Boya Xu†, Wenbin Ma, Hao Chen, Chuanlu Jiang, Jinquan Cai and Xiangqi Meng**

Department of Neurosurgery, The Second Affiliated Hospital of Harbin Medical University, Harbin, China

OPEN ACCESS

Edited by:
Quan Cheng,
Central South University, China

Reviewed by:
Fumio Yamaguchi,
Nippon Medical School, Japan
Sheng Han,
The First Affiliated Hospital of China Medical University, China

***Correspondence:**
Jinquan Cai
caijinquan666777@126.com
Xiangqi Meng
neptune_mxq@126.com

†These authors have contributed equally to this work and share first authorship

Specialty section:
This article was submitted to Cancer Immunity and Immunotherapy, a section of the journal Frontiers in Immunology

Received: *05 December 2021*
Accepted: *22 December 2021*
Published: *13 January 2022*

Citation:
Zhao S, Xu B, Ma W, Chen H, Jiang C, Cai J and Meng X (2022) DNA Damage Repair in Brain Tumor Immunotherapy. Front. Immunol. 12:829268. doi: 10.3389/fimmu.2021.829268

With the gradual understanding of tumor development, many tumor therapies have been invented and applied in clinical work, and immunotherapy has been widely concerned as an emerging hot topic in the last decade. It is worth noting that immunotherapy is nowadays applied under too harsh conditions, and many tumors are defined as "cold tumors" that are not sensitive to immunotherapy, and brain tumors are typical of them. However, there is much evidence that suggests a link between DNA damage repair mechanisms and immunotherapy. This may be a breakthrough for the application of immunotherapy in brain tumors. Therefore, in this review, first, we will describe the common pathways of DNA damage repair. Second, we will focus on immunotherapy and analyze the mechanisms of DNA damage repair involved in the immune process. Third, we will review biomarkers that have been or may be used to evaluate immunotherapy for brain tumors, such as TAMs, RPA, and other molecules that may provide a precursor assessment for the rational implementation of immunotherapy for brain tumors. Finally, we will discuss the rational combination of immunotherapy with other therapeutic approaches that have an impact on the DNA damage repair process in order to open new pathways for the application of immunotherapy in brain tumors, to maximize the effect of immunotherapy on DNA damage repair mechanisms, and to provide ideas and guidance for immunotherapy in brain tumors.

Keywords: DNA damage repair, brain tumor, immunotherapy, TME, TAMs, ICI, biomarker, combination therapy

INTRODUCTION

DNA is a nucleic acid that is a key material essential for the body to function properly. However, DNA is affected by various endogenous and exogenous factors every day, such as ionizing radiation, benzene, Epstein-Barr virus and other physical, chemical and biological factors (1), and internal due to the activation of proto-oncogenes (2). Fortunately, the body has a variety of DNA repair pathways to correct and repair the damaged location in a timely manner to ensure the stability and integrity of the eukaryotic genome. There are currently known DNA damage repair pathways, namely: mismatch repair (MMR), base excision repair (BER), nucleotide excision repair (NER),

homologous recombination repair (HRR), nonhomologous end-joining (NHEJ). Among them, both HRR and NHEJ are used to repair double strand breaks (DSBs) (3). Once the damage mechanism is dysregulated, the stability of the genome will be disrupted and cells will suffer various damages such as inflammation, aging and even cancer (4, 5). For example, MMR defects can increase the risk of hereditary colon cancer (6), and BER defects can increase the risk of lung cancer (7). Meanwhile, the exploration of tumor immunotherapy is rapidly evolving. Unlike traditional tumor treatments, tumor immunotherapy aims to restore the body's normal anti-tumor immune response by initiating the tumor immune cycle to accomplish the recognition and clearance of tumor cells (8). This property allows immunotherapy to maintain longer survival or even achieve clinical cure by the body's own action once the immune system in the body is awakened. Currently, the following immunologic agents are approved by the FDA and used in clinical work (**Table 1**). However, immunotherapy is extremely selective in terms of target populations and not all tumor patients benefit from immunotherapy. For example, brain tumors are a class of "cold tumors" in the immunological sense. Due to their unique tumor immune microenvironment (TME), they are the least sensitive to immunotherapy. Currently, surgery, radiation and chemotherapy are still widely accepted in brain tumors. Meanwhile, neurorestorative treatment have also emerged in recent years and have been shown to repair the function of damaged nerves in some sense (9). For example, olfactory ensheathing cells, with their superior ability to integrate and repair nerves (10, 11), interact with glial scars to stimulate vascular and axonal growth (12), in order to repair brain nerves after tumor damage and help restore brain function (13). In contrast to these rapid developments, immunotherapy, which has achieved superior therapeutic results in other tumors, remains ineffective in brain tumors. But, since tumor cells also depend on DNA damage repair pathways for their survival and reproduction as normal cells do (14), then rational disruption of the DNA damage repair pathways of tumor cells is a major way to overcome tumors. This mechanism has been used in brain tumor cell therapy for a long time, and many radiotherapy and chemotherapy treatments are based on it. Then, the use of DNA damage repair mechanism to improve the effect of brain tumor immunotherapy is a breakthrough, and whether this mechanism can be used to complete the immunotherapy of "cold tumors" is the focus of this paper. The purpose of this paper is to discuss this idea in the following four aspects. First, we review the specific process of DNA damage repair and identify key site that may influence immunotherapy. Second, the repair mechanisms involved in the action of the most common immunotherapy, immune checkpoint inhibitors, will be described. Subsequently, we will screen existing or potential site from the DNA damage repair process, assess their place in brain tumor immunotherapy, and discuss their feasibility and predictiveness as biomarkers for brain tumor immunotherapy. Finally, based on the process of DNA damage repair, it is reasonable to think about the feasibility of combining immunotherapy with other therapeutic approaches applying this principle, which is currently a hot research direction for the rational inclusion of immunotherapy in the brain tumor population. To explore the place of DNA damage repair in immunotherapy of brain tumors and its broad development prospect, and to provide some clinical guidance.

DNA DAMAGE REPAIR PATHWAYS

There are five common DNA damage repair pathways that play a key role in maintaining genome stability, and they are briefly described below (**Figure 1**).

Mismatch Repair (MMR)

The main targets of MMR in the correction of DNA damage are base-base mismatches and insertion/deletion mispairs. Essential proteins in the MMR process, to which MutSα and MutSβ are sensitive to these misconfigurations (15). MutSα (MSH2-MSH6) recognizes mismatches and smaller nucleotide alterations and functions as a molecular switch after identifying the repair pathway to be initiated. MutSβ (MSH2-MSH3) is responsible for detecting larger nucleotide insertion/deletion and bends the DNA double helix after damage is detected, providing the basis for subsequent repair (16). During the execution of MMR, MutSα/MutSβ is the first to spot the damage areas and recruit at the damage sites. In the meantime, MutLα is assigned to exert endonuclease activity to cleave the single strand of DNA at the mismatch site. Subsequently, PCNA, EXO1 and other proteins act on the site to separate the mismatched part from the DNA strand. Finally, polymerase δ and DNA ligase 1 (LIG1) function together to fill the gap that appears after the trimming, completing the MMR process (17).

Base Excision Repair (BER)

The BER pathway is often used to correct the deamidation and alkylation of bases in DNA molecules. The core component of the BER pathway is DNA glycosylase, which can be divided into two categories according to their functions (18). One class is monofunctional DNA glycosylases, such as UNG, MBD4, MYH, etc. The other has both 3'AP lyase activity and glycosylase activity, and the common ones are OGG1, NTH1, etc. (19) The DNA glycosylase then catalyzes the cleavage of the damaged site, exposing an AP site. Apurinic/apyrimidinic endonuclease 1 (APE1) cis-activates the DNA strand at the location of the AP site, yielding an independent 3'-hydroxyl fragment of DNA (16). This fragment will serve as a template to guide XRCC1 and DNA polβ to reinsert the missing bases and complete the filling of the processed deletion site (20). Finally, the break site is ligated by DNA ligase 3 (LIG3), and the whole BER process is completed (21).

Nucleotide Excision Repair (NER)

NER is the only one among all DNA damage repair pathways that can correct UV-photolesions. In addition, NER also plays an important role in the repair of reactive oxygen species (ROS) induced base alterations, and intrastrand crosslinks (22). NER has been divided into two pathways depending on the target audience.

TABLE 1 | FDA-approved immunotherapies.

Immunotherapy category	Mechanism	Therapy	FDA-approved cancers	Year of approval
Checkpoint inhibitors	Anti-CTLA-4	Ipilimumab	Melanoma	2011
			Advanced renal cell carcinoma	2018
			MSI-H/dMMR metastatic colorectal cancer	
			Hepatocellular carcinoma(HCC)	2020
			Metastatic or recurrent non-small cell lung cancer	
			Malignant pleural mesothelioma	
	Anti-PD-1	Pembrolizumab	Melanoma	2014
			Non-small cell lung cancer(NSCLC)	2015
			Head and neck squamous cell carcinoma(HNSCC)	
			Classical Hodgkin lymphoma(CHL)	2017
			Advanced or metastatic urothelial carcinoma	
			MSI-H/dMMR solid tumors	
			Advanced gastric cancer	
			Recurrent or metastatic cervical cancer	2018
			Primary mediastinal large B-cell lymphoma (PMBCL)	
			Advanced or metastatic Merkel cell carcinoma(MCC)	
			Advanced renal cell carcinoma(RCC)	2019
			Esophageal cancer	
			Hepatocellular carcinoma(HCC)	
			Endometrial carcinoma	
			Metastatic small cell lung cancer (SCLC)	
			MSI-H/dMMR metastatic colorectal cancer	2020
			Tumor mutational burden-high (TMB-H) solid tumors	
			Non-muscle invasive bladder cancer (NMIBC)	
			Recurrent or metastatic cutaneous squamous cell carcinoma (cSCC)	
			Advanced esophageal or gastroesophageal (GEJ) carcinoma	2021
			Triple-negative breast cancer (TNBC)	
		Nivolumab	Melanoma	2014
			Non-small-cell lung cancer	2015
			Renal cell carcinoma	
			Classical Hodgkin lymphoma(cHL)	2016
			Head and neck squamous cell carcinoma	
			Urothelial carcinoma(UC)	2017
			MSI-H/dMMR colorectal cancer	
			Hepatocellular carcinoma(HCC)	
			Metastatic small cell lung cancer(SCLC)	2018
			Advanced, recurrent or metastatic esophageal squamous cell carcinoma (ESCC)	2020
			Malignant pleural mesothelioma	
			Metastatic or recurrent non-small cell lung cancer	
			Advanced or metastatic gastric cancer, gastroesophageal junction cancer, and esophageal adenocarcinoma	2021
			Esophageal or gastroesophageal junction (GEJ) cancer	
		Cemiplimab	Metastatic cutaneous squamous cell carcinoma (CSCC)	2018
			Locally advanced basal cell carcinoma (laBCC)	2021
			Advanced non-small cell lung cancer (NSCLC)	
	Anti-PD-L1	Atezolizumab	Advanced or metastatic urothelial carcinoma	2016
			Non-small cell lung cancer (NSCLC)	
			Triple-negative breast cancer(TNBC)	2018
			Small cell lung cancer(SCLC)	2019
			Melanoma	2020
			Hepatocellular carcinoma(HCC)	
		Avelumab	Metastatic Merkel cell carcinoma(MCC)	2017
			Advanced or metastatic urothelial cell carcinoma	
			Advanced renal cell carcinoma(RCC)	2019
		Durvalumab	Urothelial cell carcinoma	2017
			Non-small cell lung cancer (NSCLC)	2018
			Extensive-stage small cell lung cancer (ES-SCLC)	2020
Cytokines modulation	Interferon alfa-2b,recombinant	Intron A	Hairy cell leukaemia	1986
			AIDS-related Kaposi sarcoma	1988
			Melanoma	1995

(Continued)

TABLE 1 | Continued

Immunotherapy category	Mechanism	Therapy	FDA-approved cancers	Year of approval
			Follicular lymphoma	1997
	Interferon alfa-2a,recombinant	Roferon-A	Hairy cell leukaemia	1986
			AIDS-related Kaposi sarcoma	1988
			Chronic myelogenous leukaemia	1997
	Interleukin-2,recombinant	Aldesleukin	Melanoma	1998
			Renal cell carcinoma	1992
	Stimulates TNF, IL-12 and IFNγ	Imiquimod	Basal cell carcinoma	2004
CAR T-cell therapy	CD19-directed	Tisagenlecleucel	B-cell precursor acute lymphoblastic leukemia (ALL)	2017
			Large B-cell lymphoma	2018
		Axicabtagene ciloleucel	Large B-cell lymphoma	2017
			Relapsed or refractory follicular lymphoma (FL)	2021
		Brexucabtagene Autoleucel	Mantle cell lymphoma (MCL)	2020
		Lisocabtagene maraleucel	Diffuse large B-cell lymphoma (DLBCL)	2021
	B-cell maturation antigen (BCMA)-directed	Idecabtagene vicleucel	Relapsed or refractory multiple myeloma	2021
Vaccines	Autologous APCs with recombinant human PAPGM-CSF	Sipuleucel-T	Prostate cancer	2010
Oncolytic viruses	Genetically modified HSV-1 designed to replicate within tumours and produce GM-CSF	Talimogene laherparepvec	Melanoma	2015
Bispecific antibodies	CD19 and CD3 bispecific antibody	Blinatumomab	B cell acute lymphocytic leukaemia	2014
		Amivantamab-vmjw	Advanced or metastatic non-small cell lung cancer (NSCLC)	2021

One is global genomic repair (GG-NER), which plays a role in correcting genome-wide errors. The other is TC-NER, which only targets errors in the transcriptional strand of active genes for repair. These two are different in the early stage but are consistent in the late stage (23). In GG-NER, XPC and UV-DDB are the key genes in the process, DDB can be divided into DDB1 and DDB2 (XPE), and in general, XPC can directly identify DNA molecules with abnormal helix structure (24). However, there exist some complex situations that do not support correction in the above manner. Such cases would require that the damaged site is first identified by DDB2 and subsequently DDB1 is recruited and forms a complex structure with it. XPC can identify the DDB complex anchored to the DNA double helix and through this process complete the exclusion of the abnormal helix and the recruitment of TFIIH. The TC-NER pathway does not use the above-mentioned genes to exclude the distorted helix, but rather RNAP II, CSB, and CSA to initiate the error site recognition mechanism. The next link in both pathways is the same. Both direct the XPA to verify the site of injury and then complete the recruitment of replication protein A (RPA) (25). The role of RPA lies in its ability to bind to the template strand, which is ssDNA complementary to the damaged DNA strand,

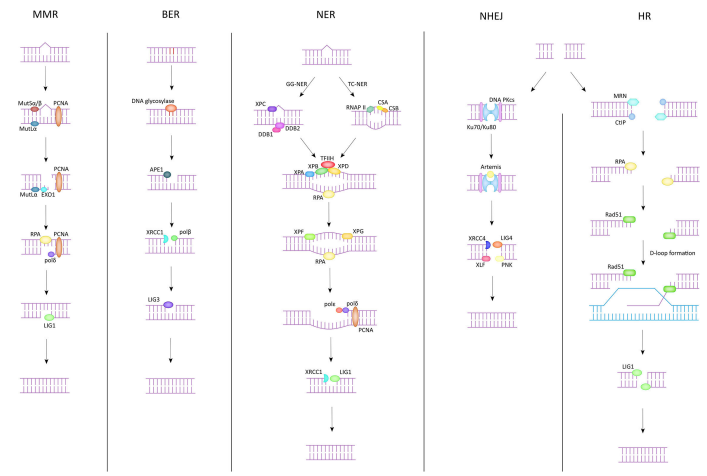

FIGURE 1 | DNA damage repair pathway.

to keep it free from interference by other related factors and to ensure the accuracy of genetic information (26). Immediately afterwards, TFIIH forms a complex with XPB, XPD to unwind the helical structure at the wrong site (27). Subsequently, XPF and XPG incise the 5' and 3' single/double strand junction respectively. Meanwhile, PCNA, polδ, and polε are responsible for reconstructing the correct DNA fragment based on the template strand and filling it in the deletion. Finally, the scattered DNA fragments are connected by LIG1/XRCC1-ligase3 to restore the integrity of the DNA structure (28).

Non-Homologous End Joining (NHEJ)

DSB is one of the most serious types of DNA damage, because it involves a wider region and more damaged fragments, which is more likely to cause damage to genomic stability and enhance susceptibility to many diseases. NHEJ and HR are two common DNA damage repair pathways that target DSBs. NHEJ can function in any process of the cell cycle, thanks to its repair independent of homologous sequences. DNA double-strand breaks are initially recognized by Ku70 (XRCC6)/Ku80 (XRCC5), which binds to the exposed broken ends after damage. This process has several important functions. First, Ku70/Ku80 binds to the break end and protects it from damage by other related enzymes. Second, this process provides the conditions for subsequent anchoring of DNA PKcs, which has a low affinity for the DNA duplex and can reach more than one hundred times the original affinity in the presence of Ku70/Ku80. Furthermore, the binding of Ku70/Ku80 to the broken ends can also improve the binding ability of XRCC4, LIG4, etc. to DNA ends, laying the foundation for the final processing (29). After Ku70/Ku80 binds to DNA broken ends, DNA PKcs interacts with Ku70/Ku80 to form a complex and complete anchoring (30). At the same time, Artemis is activated and given the ability to cut the DNA strand (29). Next, the DNA ends are treated by Artemis by endo-nucleation and XRCC4 activates LIG4 and forms a complex with it to act on the treated broken ends. The ligation of the DNA strand is done with the help of XLF, PNK and other substances. The NHEJ pathway is efficient and convenient for repairing damaged DNA double strands in a short period of time. Unfortunately, this approach is not precise enough, and the repair process is prone to fragment deletion and incorrect insertion.

Homologous Recombination (HR)

The HR pathway is another repair pathway for DSBs besides NHEJ. Compared with NHEJ, the HR pathway can make the genome more precise and even identical to that before the injury. However, in contrast, the HR pathway exists only in S and G2 phases because sister chromatid must be present in the HR process to provide the homologous sequences necessary for repair. First, the damaged DNA ends are recognized by the MRE11-RAD50-NBS1 (MRN) complex, and then the damaged DNA segments are excised along the 5' to 3' direction in association with the C-terminal interacting protein (CtIP) to form single-stranded DNA (31). After this, BLM, EXO1 work together to provide the conditions for RPA anchoring on ssDNA, and the binding of RPA to ssDNA both replaces the faulty part of the structure and ensures the conformational stability of the exposed part of ssDNA. After this process is completed, Rad51, the most important protein in the HR pathway, will play a role in the replacement of RPA with the help of proteins such as BRCA2, Rad52, paralogs of Rad51 (32) and search for a template homologous to the damaged segment on the sister chromatid, which is also known as D-loop formation, which is crucial for the HR pathway to ensure accurate repair. Finally, DNA polymerase is used to synthesize a new DNA fragment based on the selected template, and LIG1 completes the ligation of the newly synthesized fragment to the initial fragment to repair the damaged DNA double strand (33).

DNA DAMAGE REPAIR IS RELATED TO INNATE IMMUNITY AND TUMOR IMMUNE ESCAPE

In **Table 1**, we have listed several methods currently approved by the FDA for tumor immunotherapy. Among them, immune checkpoint inhibitors (ICI) have been shown to have powerful immunotherapeutic activity. The role of DNA damage repair in the process of innate immunity has been confirmed. Next, since

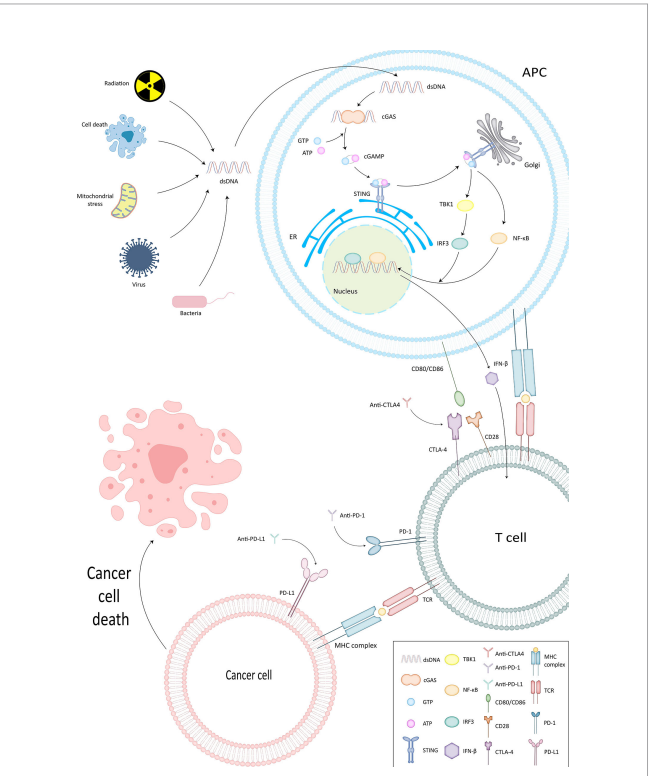

FIGURE 2 | cGAS-STING pathway and ICI mechanism of action. In cGAS-STING pathway, cGAS binds to dsDNA and is subsequently activated to produce cGAMP. The latter interacts and activates STING on the endoplasmic reticulum membrane. STING then further confers TBK1 activity and sets the stage for TBK1 phosphorylation of IRF3, thus completing the recruitment of TBK1 and IRF3 by STING. Type I IFN is generated under the influence of IRF3 and functions to activate the immune system.

this section has already been reviewed by researchers, we will briefly describe important pathways in the immune response, explain the role of DNA damage repair in the process of tumor immune escape, and further analyze the mechanism of ICI targeting PD-1/PD-L1 (**Figure 2**).

cGAS-STING Pathway

STING enables surveillance of tumor cells and participates in the innate anti-tumor immune process by inducing apoptosis. cGAS generates cGAMP that can interact with STING by binding to dsDNA (34). It also confers the ability to phosphorylate IRF3 by TBK1, thus completing the recruitment of TBK1 and IRF3 (35). Subsequently Type I IFN, which has an activating effect on the immune system (36, 37), is produced and exerts direct and indirect antitumor effects by promoting the production of perforin and granzyme by CTL and NK cells (10, 38, 39).

Association of PD-1 and PD-L1 With Tumor Immune Escape

PD-1 is mainly expressed on activated T cells, B cells and macrophages (40). T cells can gain the ability to eliminate tumor cells by expressing PD-1 (41). However, tumor cells and APCs can express PD-L1, the ligand of PD-1 (42, 43) (**Figure 1**). By binding to PD-1, TIL apoptosis is induced on the one hand and CD4+ differentiation into regulatory cells (Treg) is stimulated on the other hand (44, 45). Weakening the recognition of tumor cells by T cells (46) and completing the immune escape (47). Anti-PD-1/PD-L1 destroys this process to wake up the immune response and prevent tumor cells from escaping.

TARGETED DNA DAMAGE REPAIR TO EXPLORE IMMUNOTHERAPY BIOMARKER

Glioblastoma (GBM) in brain tumors, one of the most lethal solid tumors, has a median survival rate of only 12-15 months despite various therapeutic modalities such as surgical resection, radiation therapy chemotherapy, and others have been carried out (48). Aggressive tumors like GBM possess cancer-resistant stem cells (CSCs) with a high capacity for self-renewal. The ability to acquire such strong self-healing characteristics is mainly due to the outstanding DNA damage repair capacity of GBM cells. Then, it is possible to increase the immunotherapy of brain tumors by disrupting the DNA damage repair process of brain tumors. And to identify cells or factors that may have a directive effect on TME, and use them as biomarkers to assess the feasibility and predict the effect of immunotherapy. Therefore, we tried to find biomarkers that have been applied or have potential value in the DNA damage repair pathway to provide guidance for the development of immunotherapy in brain tumors.

Approved Biomarkers

GSCs

Glioma stem cells (GSCs) are a highly treatment-resistant population of GBM microenvironment components that assume a crucial role in tumor initiation, progression, and recurrence (49). During the early stages of tumorigenesis, GSCs have a major role in maintaining the reproductive potential of tumor cells. For example, the overexpression of transcription factors (TFs), Oct4 and Sox2 in GBM has been reported to promote tumor proliferation (50). In addition to this. Compared to the rest of the cells, a higher number of PD-L1 and immunosuppressive factors could be detected on the surface of GSCs, while the degree of CD80/CD86 expression was reduced (51). Moreover, GSCs interact with immune cells both to inhibit the antitumor effects of immune cells in the aforementioned manner (52), and to obscure their recognition by T cells through passive downregulation of MHC-I and antigen processing mechanisms to complete the immune escape process (53, 54). Khosravi et al. also reported similar results that GSCs can help tumor cells escape from the recognition correction of the immune system by upregulating specific immunosuppressive factors (55). Gangoso E et al. have further deepened their understanding. They believe that no matter what kind of treatment, when GSCs are discovered by the immune system, their DNA methylation and transcription processes will respond accordingly, and help them by secreting more chemokines. The DNA methylation and transcriptional processes of GSCs that survive are preserved, completing the process of downward transmission of immune evasion ability (56). In addition, the recruitment of macrophages, Tregs and myeloid-derived suppressor cells (MDSC) in the microenvironment is also inextricably linked to GSCs (57, 58). From this point of view, GSCs is a key biomarker for glioma immunotherapy, and some oncolytic viruses (OVs) targeting the effects of GSCs have been deeply studied. The concept of OVs is to selectively kill tumor cells without accidentally injuring normal cells. This is manifested by weakening or eliminating virulence factors so that they do not pose a threat to the growth and reproduction of normal cells. However, the virus itself retains the ability to fight against tumor cells, which is the most important basis for its function. Additionally, the OVs have the ability to recruit immune cells, that can continue the removal of tumor cells through the immune pathway (59, 60). Zika virus (ZIKV) is a typical example (61). ZIKV acts on the basis of GSCs, to which it is extremely sensitive, and can inhibit the proliferation of glioma cells by inducing apoptosis of GSCs, break the supporting effect of GSCs on immune escape, and further activate CD8+ T cells to complete the clearance of tumor cells (62). Also, because of the high enrichment of integrins $\alpha V\beta 3/\alpha V\beta 5$ in GSCs, OVs can target GSCs by acting on integrins (63). It has also been demonstrated that GSCs achieve tumor cell invasion and metastasis by affecting the extracellular matrix (64). Thus, GSCs and therapies targeting GSCs have become the focus of immunotherapy for brain tumors, and the use of GSCs as biomarkers may provide a major reference for the treatment of brain tumors.

TAMs

Tumor-associated macrophages (TAMs) are the most abundant cells in the GBM microenvironment, accounting for roughly 30%-50% of all cells in TME (65). TAMs strictly include both

microglias and macrophages of embryonic or bone marrow origin. There are numerous literature TAMs have been reported to have immunosuppressive effects on TME (66, 67). TAMs can be stimulated by a variety of cytokines and thus activate differentiation potential into M1-type TAMs, which have suppressive effects on tumor cells, and M2-type TAMs, which promote tumor cell proliferation and metastasis (68, 69). Lipopolysaccharide and IFN-γ, etc. can induce the differentiation of TAMs to M1-type and endow M1-type TAMs with the function of secreting pro-inflammatory cytokines and activating other immune cells, such as natural killer cells (NK) and dendritic cells (DC). M1-type TAMs can both directly induce tumor cell death through their own cytotoxic effects and indirectly serve anti-tumor purposes by phagocytosis, which enables the process of neoantigen presentation on the surface of tumor cells and provides conditions for adaptive immunity to proceed (70). Both have prominent contributions to probing tumor cells and slowing their proliferation. In contrast, M2-type TAMs are strongly associated with the malignant biological behavior of GBM cells (71). M2-type TAMs can be activated by a variety of cytokines, such as interleukin-4 (IL-4), colony-stimulating factor-1 (CSF-1) and tumor growth factor-β (TGF-β). These cytokines play different roles in the biological behavior of GBM cells. For example, tumor cells can achieve the recruitment of microglias by secreting CSF-1 and contribute to their differentiation to M2-type (72). And the function of TGF-β is highlighted in its provision of conditions for tumor cell metastasis (73). In addition, M2-type TAMs have remarkable ability in inducing GBM cytogenesis and immune escape, based on which they assume important functions in the process of tumor cell growth and metastasis. It has been reported that M2-type TAMs contribute to the vascular proliferation of GBM cells by releasing insulin-like growth factor binding protein 1 (IGFBP1) and IL-6 to contribute to the expansion of tumor blood vessels in TME and the enhancement of blood supply to tumor tissues (74). Meanwhile, M2-type TAMs can also secrete IL-10 through the JAK2/STAT3 signaling pathway to induce GBM cell genesis and promote tumor progression (75). Not only that, M2-type TAMs also have the ability to recruit Treg, and the number of Treg in the microenvironment shows a positive correlation with poor prognosis during tumor cell progression (70). As well as the inhibition of CTL cells in TME, which are responsible for the poor response of GBM to immunotherapy based on T-cell principles (70). With the increasing attention to the field involving TAMs, there are more and more reports about the involvement of M2-type TAMs in tissue remodeling, induction of hypersensitivity responses, domination of immune microenvironment formation, and promotion of GBM progression (76–79). TAMs are gradually becoming key targets in the fight against GBM (80, 81). Therefore, there are now a number of therapies targeting TAMs that are continuously being investigated. Basically, they are all based on the principle of blocking the migration of monocytes into TME and inhibiting the production of M2-type TAMs. Lee, Chanhee et al. found that artificially interfering with TAMs to convert them to M1-type and preventing them from converting to M2-type could inhibit the proliferation of GBM (82). This provides a new possibility for controlling GBM growth and attenuating GBM resistance to immunotherapy, and may provide a guiding role in the treatment of GBM.

ATM

The ATM gene encodes a protein that is an important cell cycle checkpoint kinase that phosphorylates important sites such as CHK2, p53, MRN complex and plays a prominent role in the HR pathway (83). ATM, an important factor in DNA damage repair, signals in association with PARP-1 to activate E3 ubiquitin ligase within one hour of recognition of a DNA double-strand break. And further recruit STING to achieve activation of nuclear factor NF-κB. Activated NF-κB has been shown to play an important role in tumor progression and clearance of tumors by the immune system (41, 84). Wang L et al. came to a similar conclusion that the ATM-CHK2 axis could be a potential target during tumor therapy and that selective inhibition of the checkpoint signaling axis ATM-CHK2 could activate the body's intrinsic innate immunity and enhance ICI therapeutic efficacy, which has been demonstrated in ARID1A-deficient tumors (85). In addition, Sato H et al. first elucidated that DNA double-strand breaks can upregulate PD-L1 expression in an ATM-dependent manner (86). Hu et al. demonstrated that ATM inhibition can activate the cGAS-STING pathway by promoting cytoplasmic leakage of mitochondrial DNA and downregulating mitochondrial transcription factor A (TFAM) and in this way enhance the effect of ICI treatment. Therefore, mutations in ATM can be used to predict the clinical efficacy of ICI as an ICI therapeutic target and biomarker (87). In addition, ATM has also been reported to achieve enhancement of ICI therapeutic efficacy through the cGAS-STING-independent pathway (88). In addition, there is the most important point for brain tumors. ATM/ATR has been shown to be an important cause of chemotherapeutic drug resistance in GBM tumors, so could the detoxification of resistance to chemotherapeutic drugs as well as upregulation of immunotherapy sensitivity be achieved by blocking ATM/ATR. Meanwhile, the application of TMZ resulted in replication fork arrest of GBM cells and successive activation of ATR-Chk1 axis and ATM-Chk2 axis, which may be potential targets for combining chemotherapy with immunotherapy (89).

CTLA-4

CTLA-4 is a coinhibitory molecule expressed by Tregs cells that can be regulated by activated CD4+ versus CD8+ T cells and achieve interference with T-cell activation (90, 91). CD28 is expressed by activated CD4+ versus CD8+ and has a role in promoting immune responses and activating T cells. When the T-cell receptor (TCR) is engaged, CTLA-4 increases rapidly at the immune synapse through cytoskeletal reorganization, achieving enrichment. The CTLA-4 that reaches the synaptic site has a higher affinity for CD80 (B7-1) and CD86 (B7-2) than CD28 (92, 93). The above process is extracellular pathway. In addition, CTLA-4 has been shown to function through intracellular pathways, specifically by binding to CD80/CD86 and acting within activated conventional T-cells. CTLA-4

suppresses immune responses by recruiting SHP-2 and PP2A to immune synapses (92, 94). Different routes to the same goal, both of which negatively regulate T-cell proliferation (95, 96). Ensure T-cell activity by fine-tuning the TCR to help safeguard beneficial anti-pathogen and anti-tumor responses, while maintaining tissue integrity, promoting tissue repair, and regulating immune sensitivity (97).

Other Potential Biomarkers

RPA is a ssDNA binding protein, which plays an important role in both NER and HR (98, 99). In the primary GBM cell lines, high-level expression of RPA was detected. RPA expression can also be detected in differentiated GBM cells, and it has been observed that RPA70 and RPA14 have priority in expression. RPA mediates the high invasiveness of GBM. It is believed that blocking the function of RPA may increase the responsiveness of radiotherapy. And RPA can function by interacting with sites such as ATR, Rad51, BRCA1/2, and p53 (100, 101). This may be a potential biomarker for highly aggressive tumors such as GBM (102).

Zhang J et al. supplied a new immune target where DNA-PKcs could influence TGF-β1, a significant factor in the epithelial-mesenchymal transition (EMT) process (103). DNA-PKcs deletion enhances ICI treatment (104). The mutant group had a more satisfactory survival outcome after ICI treatment compared to patients with normal DNA-PKcs (105). Echoing this, Yang H et al. concluded that the combination of immunotherapy with DNA-PKcs as a target can have a synergistic effect, with the result that patients can benefit more from immunotherapy (106). There is also a DNA-PK inhibitor called CC-115, which is able to cross the BBB, whose efficacy in patients with GBM is being tested and CC-115 is being considered in combination with radiotherapy and TMZ for GBM (107).

In recent years, there has also been significant progress in the exploration of protein-coding RNAs, and it is thought that RNA dysfunction can also influence cancer development (108). Subsequently, immunotherapies targeting RNAs have also emerged, particularly LncRNA, whose expression has been shown to be associated with various immune checkpoints such as PD-1/PD-L1 and CTLA-4 (109). It has also been shown that Lnc-talc interferes with the action of temozolomide by affecting the immune microenvironment, leading to GBM resistance (110, 111). In addition to this, epidermal growth factor receptor (EGFR) and mesenchymal-epithelial transition factor (MET) signaling pathways have been demonstrated in temozolomide resistance (112). The experiments conducted for the above new targets provide new therapeutic strategies for GBM and offer the possibility to explore immunotherapy for GBM.

COMBINED DNA DAMAGE REPAIR-BASED THERAPY WITH IMMUNOTHERAPY

A growing number of experiments have shown that therapies that destabilize DNA and disrupt the repair process of tumor cell damage, can reshape the tumor immune microenvironment and offer the possibility of applying immunotherapy to tumor cells that are resistant or less sensitive to immunotherapy. This is particularly important for the application of immunotherapy in brain tumors. On this basis, it becomes feasible and meaningful to combine immunotherapy with other tumor treatment modalities.

Radiotherapy With Immunotherapy

It is well known that radiation therapy corrects tumor mainly through two mechanisms, one is the production of free radicals, which induce oxidative responses in the body and activate damage-associated molecular patterns (DAMPs), and in this way enhance DC function. The other is DNA damage, the vast majority of which is DNA strand breaks, with double-strand breaks (DSBs) being the key damage in radiation-killed cells. The role that radiation therapy plays in the immune process has been discovered step by step in recent years. Its effect on immune response is mainly to enhance tumor immunogenicity by increasing tumor-recognizable neoantigens, expression of MHC molecules, etc. (113) And to recruit CD8+ T cells and DC cells to awaken the body' s anti-tumor immune process (114). Radiotherapy triggers immunogenic cell death by both of these means (115), enhances DC function and further promotes antigenic expression of dendritic cells (DCs) (116), allows DCs to be recruited between tumor tissues. Common DAMPs include HMGB1 and calreticulin, etc. (117) HMGB1 allows DC cells to acquire the ability to process and present antigens by acting on toll-like receptor (TLR) 4 receptors and furthermore induce T cell immune responses (118). Cells expressing calreticulin on the surface can be recognized by DCs and achieve phagocytosis of would-be dead cells. In contrast, DSBs resulting from DNA damage after radiotherapy produce cytosolic DNA fragments and micronuclei that activate the cGAS/STING pathway (119, 120). Further stimulates the production of IFN, increases the expression of MHC molecules on the surface of tumor cells, promotes the maturation of DC cells and drives other immune-related processes (111, 121–124). To achieve the purpose of enhancing the recognition ability of the immune system. Because of this, radiotherapy is also thought to be involved in the DNA damage repair process known as activate mTOR signaling (125). However, the effects of radiotherapy go far beyond this. Radiotherapy has also been reported to induce the expression of adhesion molecules ICAM and VCAM1 on tumors and endothelial cells, and in this way block the binding of adhesion molecules to T cells. Then reduced the incidence of tumor rejection (126). In addition, radiotherapy has been shown to increase the expression of inflammatory chemokines, such as CXCL5 and CXCL2, which recruit suppressive cells in TME while producing TGFβ and participating in the tumor immune process (126, 127). The common outcome of these aforementioned post-radiotherapy alterations is to promote the infiltration of CD8+ T cells in TME and to achieve up-regulation of PD-L1 expression by all of the above (128). Therefore, this behavior is a key part of the therapeutic effect of radiotherapy combined with PD-1/PD-L1 inhibitors (129). More importantly, the increase of MDSCs in TME after radiotherapy, which has been shown to drive tumor growth and angiogenesis, upregulate CTLA-4 expression in Tregs (130) and inhibit cytotoxic T-cell

activation acting as a coordinating immunosuppressive agent (131). Furthermore, it has been suggested that TAMs and regulatory T-cells (Tregs) are more resistant to radiation than T cells, contributing to the enrichment in TME after radiotherapy (132). Radiotherapy can also activate NK cell action by upregulating the NKG2D receptor in the co-stimulatory receptor, achieving immunomodulation by interfering with the innate immune system. Also, radiotherapy has been reported to act on TNF receptors (133). Including FasL, TNF-α receptor, TRAIL-R1 and TRAIL-R2. Since CTL can express ligands of the above receptors, it makes tumor cells more sensitive to the action of CTL after radiotherapy. This also explains from a certain perspective, why some tumors gradually show a more satisfactory sensitivity to immunotherapy after receiving radiotherapy. It may be related to the direct or indirect recruitment and activation of CTL caused after radiotherapy. For example, IFN-γ and TNF-α produced after radiotherapy can induce CXCL9, CXCL16, etc. And then further collect CTL into TME. These reports support that the effect of radiotherapy on DNA damage repair can act on the immune system and provide a theoretical basis for the feasibility of radiotherapy combined with immunotherapy (134). Not only that, there are many animal experiments embarking on the combination of radiotherapy and immunotherapy.

Radiation therapy (RT) is widely used in patients with solid tumors, and GBM is no exception. Several preclinical studies have reported that RT can lay the foundation for immunotherapy and improve the response rate of immunotherapy. The most widely used immunotherapies are ICIs, and three types of ICIs have been approved by the FDA for clinical use, namely anti-CTLA-4, anti-PD-1 and anti-PD-L1. TIM-3 is a negative regulator that is widely expressed on Tregs and NK cells, and blocking TIM-3 can help CD4/CD8+ T cells to restore specific immune function, which is helpful in relieving the immune resistance of tumor cells (135). It has been shown that TIM-3 expression is elevated in glioma patients and can be detected not only on the surface of TIL, but also in circulating blood lymphocytes (136, 137). Kim, Jennifer E et al. attempted to apply anti-TIM-3 along with stereotatic radiosurgery (SRS) and analyzed the role of the combination in the treatment of glioma. The experiment showed that the median survival time of SRS alone was 27 days, while the combined anti-TIM-3 group could extend up to 100 days. Also, the team experimented with the possibility of combining two ICIs, anti-PD-1 and anti-TIM3. It was shown that both PD-1 and TIM-3 have inhibitory effects on the secretion of some cytokines such as IFNγ and TNFα (138). Compared to anti-PD-1 alone, Kim, Jennifer E et al. did not observe an increase in the amount of IFNγ in the combination of anti-PD-1 with anti-TIM-3. However, there was positive feedback from the trinity treatment approach of both ICI combined with SRS compared to the anti-PD-1 combined with SRS group. That is, a trend was detected to promote the secretion of IFNγ, TNFα, and the secretion of such cytokines was widely shown to be associated with prolongation of OS. Although the combination of ICI and RT has been repeatedly reported to have a synergistic effect in saving brain tumors, there are conflicting opinions about the side effects (139). Clausi MG et al. suggested that RT in combination with ICI induced activation of CD8+ T cells and polarization of TAMs. It was reported that CD8+ T cells were not found in normal brain tissue, while traces of CD8+ T cells were detected in the white matter and hippocampus of mice with brain tumors after combined treatment. Meanwhile, in studying the side effects of the combination treatment, they evaluated the cognitive and behavioral performance and neuroinflammation in the mice. The results showed that although the combination therapy reflected better results on tumor control, it also induced cognitive and behavioral, neuroinflammatory and other side effects that affected the quality of survival (140). However, positive side effects of the combination treatment have also been reported, as Qiu B et al. found that RT combined with ICI treatment can lead to permanent depletion of neuroblasts in the subgranular zone (SGZ) of the hippocampal dentate gyrus, which can indirectly protect the function of the hippocampal region. The addition of anti-PD-1 provided a cerebral protective effect relative to RT applied alone (141).

Chemotherapy With Immunotherapy

Chemotherapy is one of the most effective methods of treating tumors. It is used to kill tumor cells through the application of drugs to achieve a therapeutic goal. One of the main advantages of chemotherapy over traditional surgery and radiation therapy is that chemotherapy is a systemic treatment. Chemotherapy drugs can act on most tissues throughout the body through blood circulation, which is an outstanding advantage in treating metastatic cancer. Also for GBM, the application of chemotherapeutic drugs has shown to be extremely superior, and TMZ plays an integral role in GBM treatment. However, in recent years, as chemotherapy has become more widely understood, it has been found that chemotherapy has not only cell-damaging effects, but also significant effects on the immune system. Chemotherapy can expose neoantigens on the surface of tumor cells, which are recognized by DCs and presented to CTL cells, further activating the antitumor immune response. In recent years, the exploration of the relationship between chemotherapy and immune response has gradually become a popular topic. Toll-like receptors (TLRs) mentioned before is one of the cases. Many immune cells activate the relevant immune response through the interaction between receptors called TLRs and pathogens (142). Based on this, molecules that have agonistic effects on TLRs have won widespread attention. One of them is an oligonucleotide called CpG-ODN (143). CpG-ODN is classified as A, B and C according to the type of cells it acts on. Among them, type B CpG-ODN has been shown to inhibit tumor cell growth by acting on TLR9 in several preclinical models, with long-lasting effects and immune memory detected in specific subjects (144). TLR4 has also been found to be induced by paclitaxel and cause immune cell death. But chemotherapy is also thought to activate the immunostimulatory pathway and can be used to kill cancer cells by this mechanism. After the application of drugs such as docetaxel, oxaliplatin and cyclophosphamide (CPA). ATP, HMGB1 and tumor cell surface

calcineurin can be detected. These exposed neoantigens increase the possibility of tumor cells being recognized by immune cells (145, 146). Chemotherapeutic agents can also directly modulate immune cell populations. Cyclophosphamide depletes immunosuppressive myeloid suppressor cells and Treg cells, relieves their inhibitory effects on NK and T cells, elevates the innate immune response, and promotes Th1 cytokine production (147). Cyclophosphamide has been used as a first-line chemotherapeutic agent for many years, and although it has been shown to have excellent anti-tumor performance, experimental feedback suggests that combination therapy can achieve superior results compared to monotherapy. Jordan, M et al. conducted a study in 2016, which showed that the addition of CpG-1826 immunotherapy on day 12 after the application of cyclophosphamide therapy prolonged the duration of immune response prompted by cyclophosphamide and a satisfactory antitumor response was observed. Combining CpG-1826 after cyclophosphamide treatment minimizes the ablation of immune cells by cyclophosphamide and prolongs the duration of response (142). It is well known that temozolomide synchronized chemotherapy is an indispensable and critical part of GBM treatment, so how to use TMZ rationally to enhance the effect of GBM immunotherapy is being paid attention to (148). Although reduction of multiple lymphocytes in TME can be observed after TMZ application, in some cases, TMZ was found to induce anti-tumor immune response (149). Hasan, Md Nabiul et al. focused on the effect of Na/H exchanger 1 in combination with TMZ on immunotherapy. They found that NHE1 was closely related to the immunosuppressive TME of GBM, which is one of the reasons for downregulating the sensitivity of GBM to the immune response (150). And further validated the effect of combination treatment of NHE1 inhibitor HOE642 with TMZ on PD-1. The results showed that the infiltration of GAMs and T cells was significantly increased in the combination treatment group, and Th1 was activated along with enhanced anti-tumor immunity. In addition to this, the combination therapy increased the sensitivity of anti-PD-1 treatment modality, providing the possibility of ICI in GBM treatment (151). The rationale for this therapeutic approach focuses on the metabolic reprogramming of TAMs and T cells that has been discovered in recent years, which plays an important value in the anti-GBM immune response. This is thought to be a pathway for tumor cells to evade surveillance by the immune system, i.e., by upregulating PD-L1 and binding to PD-1 on the surface of T cells to induce T cell apoptosis to complete the immune escape process (152). Although this process is a survival strategy for tumor cells, it also brings an idea for the application of immunotherapy, i.e., the possibility of targeting immune checkpoints for blockade, which is a breakthrough for brain tumors that are part of cold tumors. One trial specifically analyzed the effect of combining TMZ with ICI and reported that when TMZ was administered systemically, the combined ICI treatment did not show any survival advantage. In contrast, when TMZ was administered locally, the survival advantage appeared to be significantly altered with the combined application of ICI. This seems to indicate that the effect of TMZ on anti-tumor immune response is related to factors such as dose and route of administration (153). In addition, the oncolytic virus, which has been widely studied in brain tumors, has shown satisfactory results in joint experiments with TMZ. Sampson JH et al. demonstrated that an enhanced antitumor immune response was observed with the application of TMZ in GBM patients treated with oncolytic virus.

DNA Damage Repair Inhibitors With Immunotherapy

Poly ADP-Ribose Polymerase Inhibitor (PARPi)

PARP, is a DNA repair protein. It maintains genomic stability by repairing damaged DNA single strands during DNA damage repair, PARP is mainly divided into PARP1 and PARP2, with PARP1 playing a key role in the efficient repair of DNA single strand breaks (SSBs) (154). This mechanism is also generalized in tumor cells. A large proportion of antitumor drugs interfere with the normal life activities of tumor cells by damaging their DNA, and in this way, they aim to kill them. Unfortunately, tumor cells can protect themselves through the above damage repair mechanism. Inhibitors of poly ADP-ribose polymerase (PARPi) have emerged as new tumor therapeutic agents (**Table 2**). PARPi applies the concept of synergistic lethality of DNA damage repair by competitively binding to PARP to inhibit HR, resulting in the accumulation of large amounts of single-stranded DNA in tumor cells that are not repaired in time (155).

TABLE 2 | FDA-approved PARPi class drugs.

PARP inhibitors	FDA-approved cancers	Year of approval
Olaparib	Advanced ovarian cancer	2014
	Primary peritoneal cancer	2017
	HER-2 negative metastatic breast cancer	2018
	Metastatic pancreatic adenocarcinoma	2019
	Metastatic castration-resistant prostate cancer(mCRPC)	2020
Rucaparib	Ovarian cancer	2016
	Recurrent epithelial ovarian	2018
	Primary peritoneal cancer	
	Metastatic castration-resistant prostate cancer(mCRPC)	2020
Niraparib	Primary peritoneal cancer	2017
	Advanced ovarian	2019
	Primary peritoneal cancer	
Talazoparib	HER-2 negative locally advanced or metastatic breast cancer	2018

This enhances the efficacy of chemotherapeutic agents. However, PARPi's contribution to tumor therapy goes far beyond this. While inhibiting DNA-SSB repair, PARPi acts with the cofactor NAD+ to anchor PARP1 to damaged DNA, forming a stable PARP-SSB complex. In turn, the replication fork disintegrates upon contact with the PARP-SSB complex and consequently leads to more severe DSBs, which serve to induce tumor cell death (154, 156). More notably, PARPi has a targeted effect on BRCA-deficient tumors. BRCA is also a DNA repair protein, but unlike PARP, BRCA is primarily responsible for the repair of DSBs. Therefore, BRCA1 and BRCA2-deficient tumor cells are very dependent on PARP for repair, and for this reason, PARPi has a significant effect on DNA damage in such tumor cells, showing great cytotoxicity (147, 157). Therefore, it has become a precision drug for cancers with DDR defects in the HR pathway and was approved by the FDA in 2018 for the treatment of BRCA-deficient cancers. Many studies have shown that the antitumor effect of PARPi is related to innate immune response in addition to the induction of DNA strand breaks (158). PARPi accomplishes antitumor efficacy by activating the cGAS-STING pathway, recruiting CD8+ T cells, and inducing type 1 interferon (IFN) signaling, thereby resetting or initiating the tumor microenvironment (159). Currently, most of the clinical trials assessing the role of PARP in GBM neglect to assess BRCA (160), which may be related to the low frequency of BRCA mutations in GBM (161). PARP expression has been reported to be associated with tumor grade as well as poorer survival (162). An increase in tumor radiotherapy sensitivity was observed in *in vitro* experiments applying PARPi against GBM models (163). With a better understanding of the molecular relationship between PARP and GBM (164), PARP may be used as a biomarker to assess prognosis and drug resistance mechanisms.

Other DNA Damage Repair Inhibitors

Heat shock protein 70 (Hsp70) is often expressed on the surface of highly aggressive tumor cells such as GBM, while the upregulation of Hsp70 can also be observed after radiotherapy and chemotherapy (165). Shevtsov M et al. investigated the antitumor effect of a combination therapy consisting of Hsp70-peptide TKD/IL-2-activated NK cells and anti-PD-1 on GBM in mice. The results showed that both alone retarded the growth and migration of tumor cells and prolonged the OS of the GBM mouse model, while the combination therapy further improved the outcome parameters compared to the monotherapy modality. The OS in the combination treatment group was 2.3 times higher than that in the control group. Tumor tissue sections showed increased infiltration of CD8+ T cells and NK cells in the treatment groups, with the most pronounced immune cell infiltration in the combination treatment group and a 1.5-fold increase in anti-tumor cytotoxicity. This is consistent with previous reports that blocking PD-1 on the surface of NK cells can enhance immune responses (166).

In addition, phosphatases are also attracting attention as new brain tumor targets (167). It has been claimed that PP2A can activate CTLA-4 on the surface of T cells through dephosphorylation, which has a potential inhibitory effect on the immune function of CTL (168). Besides, researchers also found that the negative immune regulatory function of Treg was broken in the model of PP2A deficiency, which contributed to the proliferation of TIL (169). Based on this, Maggio D et al. considered to analyze the effect of simultaneously targeting both PP2A and PD-1 checkpoints on tumor control. It was found that simultaneous blockade of PP2A and PD1 significantly improved OS in GBM mice, with a substantial increase in the number of immunoreactive T cells in the group compared to the control group, and resulted in complete regression of GBM in about a quarter of the mice. The team further speculated that this might be related to the activation of the mTORC1 pathway after the application of PP2A inhibitor (170). Another molecule highly expressed in GBM is arginase (ARG), which is more easily detected especially in TAMs with highly aggressive GBM. Some studies have confirmed that ARG has a proliferative effect on CTL, while lower plasma concentrations of ARG are often accompanied by the appearance of significant immunosuppression (171). Inhibition of ARG restored the function of TAMs and NK cells and improved the sensitivity to anti-PD-1. Zhang J et al. applied an anti-ARG called OAT-1746 in combination with anti-PD-1 in a GBM mouse model, and OAT-1746 could penetrate the BBB, which is known for its defensive capabilities. The results observed an increase in the proportion of CD3+ T cells in the TME of mice after the combination treatment, which is important for considering the simultaneous inhibition of ARG and PD-1 in the GBM population for potential feasibility. Meanwhile, decreased expression of CCL2 and CCL7 was detected in the experimental group, and the expression of CCL2 is closely associated with tumor angiogenesis and high invasiveness (172), while CCL7 has a recruitment effect on Treg (173). The positive feedback of combination therapy for TME may be related to OAT-1746 affecting the expression of CCL2 and CCL7-related genes (174).

CONCLUSION

Tumor immunotherapy has evolved rapidly in the past decade. And today, many therapies targeting the immune response have been approved and are used in clinical practice. However, unfortunately, the use of immunotherapy in the field of brain tumors still has not progressed much. Due to the existence of BBB, the intracranial system can protect the brain tissue from damage, but also increase the difficulty of drugs breaking through the barrier. Moreover, brain tumors are immunologically "cold tumors" that do not show satisfactory sensitivity to immunotherapy, and the use of autoimmune response to achieve clearance of brain tumors remains a major challenge. Fortunately, tumors are associated with genomic instability, and DNA damage repair is an important way for the body to maintain and correct genetic information. Therefore, targeting DNA damage repair mechanisms in tumor therapy may be a breakthrough guide in the fight against tumors. This study also focused on this hot topic and analyzed the intrinsic link between immunotherapy and DNA damage repair. We also found that appropriate biomarkers are particularly important for evaluating

immunotherapy. TAMs, as the largest group of cells in brain tumor TME, play an important role in immune regulation of the microenvironment. And biomarkers such as MSI and ATM, which have been widely used in "hot tumors", also seem to guide brain tumors that are not sensitive to immunotherapy. RPA, DNA-PKcs and other proteins in the DNA damage repair process may provide a precursor assessment for the rational implementation of immunotherapy in brain tumors and may serve as a guide for immunotherapy. At the same time, we discuss the feasibility of combining immunotherapy with other treatments. DNA double-strand breaks during radiation therapy, chemotherapy that partially targets DNA damage directly, and targeted therapies that are now used to break the DNA damage repair process in tumor cells all provide favorable premises for the use of immunotherapy. We also describe the current state of research in combination therapy. Even so, little is known about brain tumors and TME and how the promising immunotherapy can be used in the clinic. The application of immunotherapy in brain tumors remains a major challenge that needs to be explored jointly by clinicians, genomics, translational medicine and other multidisciplinary personnel. Together, we will reveal the intrinsic link between DNA damage repair processes and brain tumor immunotherapy, and provide inspiration and support for the application of damage repair in brain tumor immunotherapy.

AUTHOR CONTRIBUTIONS

SZ and BX wrote the article. WM and HC conducted cutting-edge searches and modifications. CJ provided critical perspectives on the article ideas. JC and XM participated in the figure design and article revision. All authors contributed to the article and approved the submitted version.

FUNDING

This study was supported by 1. The National Natural Science Foundation of China (No. 81874204, No. 81772666, No. 81972817, No. 82073298, No. 82003022); 2. Excellent Young Talents Project of Central Government Supporting Local University Reform and Development Fund (0202-300011190006); 3. Karolinska Institute Research Foundation Grants 2020–2021 (No. FS-2020:0007); 4. The China Postdoctoral Science Foundation (2018M640305, 2019M660074, 2020T130157); 5. The Heilongjiang Postdoctoral Science Foundation (LBH-Z18103, LBH-Z19029); 6. The Research Project of the Health and Family Planning Commission of Heilongjiang Province (2019-102); 7. The Young and Middle-aged Innovative Scientific Research Fund of the Second Affiliated Hospital of Harbin Medical University (KYCX2018-08).

REFERENCES

1. Owiti NA, Nagel ZD, Engelward BP. Fluorescence Sheds Light on DNA Damage, DNA Repair, and Mutations. *Trends Cancer* (2021) 7(3):240–8. doi: 10.1016/j.trecan.2020.10.006
2. Ma Q, Wang J, Qi J, Peng D, Guan B, Zhang J, et al. Increased Chromosomal Instability Characterizes Metastatic Renal Cell Carcinoma. *Transl Oncol* (2021) 14(1):100929. doi: 10.1016/j.tranon.2020.100929
3. Scarbrough PM, Weber RP, Iversen ES, Brhane Y, Amos CI, Kraft P, et al. A Cross-Cancer Genetic Association Analysis of the DNA Repair and DNA Damage Signaling Pathways for Lung, Ovary, Prostate, Breast, and Colorectal Cancer. *Cancer Epidemiol Biomarkers Prev* (2016) 25(1):193–200. doi: 10.1158/1055-9965.EPI-15-0649
4. Dianov GL, Hubscher U. Mammalian Base Excision Repair: The Forgotten Archangel. *Nucleic Acids Res* (2013) 41(6):3483–90. doi: 10.1093/nar/gkt076
5. Majidinia M, Yousefi B. DNA Repair and Damage Pathways in Breast Cancer Development and Therapy. *DNA Repair (Amst)* (2017) 54:22–9. doi: 10.1016/j.dnarep.2017.03.009
6. Chen X, Yang Z, Feng J, Duan T, Pan T, Yan L, et al. Combination of Lysine-Specific Demethylase 6A (KDM6A) and Mismatch Repair (MMR) Status is a Potential Prognostic Factor in Colorectal Cancer. *Cancer Med* (2021) 10 (1):317–24. doi: 10.1002/cam4.3602
7. Casal-Mourino A, Ruano-Ravina A, Torres-Duran M, Parente-Lamelas I, Provencio-Pulla M, Castro-Anon O, et al. Polymorphisms in the BER and NER Pathways and Their Influence on Survival and Toxicity in Never-Smokers With Lung Cancer. *Sci Rep* (2020) 10(1):21147. doi: 10.1038/s41598-020-78051-5
8. Waldman AD, Fritz JM, Lenardo MJ. A Guide to Cancer Immunotherapy: From T Cell Basic Science to Clinical Practice. *Nat Rev Immunol* (2020) 20 (11):651–68. doi: 10.1038/s41577-020-0306-5
9. Wang X, Sun N, Meng X, Chen M, Jiang C, Cai J. Review of Clinical Nerve Repair Strategies for Neurorestoration of Central Nervous System Tumor Damage. *J Neurorestoratol* (2020) 8:172–81. doi: 10.26599/JNR.2020.9040018
10. Wang Y, Guo X, Liu Y, Li Y, Liu Y, Chen D, et al. A Pilot Study of Clinical Cell Therapy for Patients With Vascular Dementia. *J Neurorestoratol* (2021) 9(2):137–50. doi: 10.26599/jnr.2021.9040011
11. Silvia G, Ratti OJS, Alvarez EO. Behavioural Multigenerational Effects Induced by the Administration of Very Low Doses of Zinc During Pregnancy, Lactation, and Prepuberal Period in the Rat. *J Neurorestoratol* (2021) 9(1):72–80. doi: 10.26599/jnr.2021.9040004
12. Kuang N, Wang X, Chen Y, Liu G, Fe K, Wang N, et al. Olfactory Ensheathing Cell Transplantation for Chronic Spinal Cord Injury: A Long-Term Follow-Up Study. *J Neurorestoratol* (2021) 9(2):94–105. doi: 10.26599/jnr.2021.9040008
13. Moviglia G. Special Issue on Cell Therapy. *J Neurorestoratol* (2021) 9: (2):81–2. doi: 10.26599/jnr.2021.9040018
14. Jin W, Zhao J, Li S. Research Progress on the Therapeutic Effect of Olfactory Ensheathing Cell Transplantation on Ischemic Stroke. *J Neurorestoratol* (2021) 9(2):83–93. doi: 10.26599/jnr.2021.9040012
15. Larrea AA, Lujan SA, Kunkel TA. SnapShot: DNA Mismatch Repair. *Cell* (2010) 141(4):730.e1. doi: 10.1016/j.cell.2010.05.002
16. Iyama T, Wilson DM3rd. DNA Repair Mechanisms in Dividing and non-Dividing Cells. *DNA Repair (Amst)* (2013) 12(8):620–36. doi: 10.1016/j.dnarep.2013.04.015
17. Li Z, Liu JY, Zhang JT. 14-3-3sigma, the Double-Edged Sword of Human Cancers. *Am J Transl Res* (2009) 1(4):326–40.
18. Viel A, Bruselles A, Meccia E, Fornasarig M, Quaia M, Canzonieri V, et al. A Specific Mutational Signature Associated With DNA 8-Oxoguanine Persistence in MUTYH-Defective Colorectal Cancer. *EBioMedicine* (2017) 20:39–49. doi: 10.1016/j.ebiom.2017.04.022
19. Hazra TK, Hill JW, Izumi T, Mitra S. Multiple DNA Glycosylases for Repair of 8-Oxoguanine and Their Potential *In Vivo* Functions. *Prog Nucleic Acid Res Mol Biol* (2001) 68:193–205. doi: 10.1016/s0079-6603(01)68100-5
20. Caglayan M. Pol Beta Gap Filling, DNA Ligation and Substrate-Product Channeling During Base Excision Repair Opposite Oxidized 5-Methylcytosine Modifications. *DNA Repair (Amst)* (2020) 95:102945. doi: 10.1016/j.dnarep.2020.102945
21. Caglayan M, Horton JK, Dai DP, Stefanick DF, Wilson SH. Oxidized Nucleotide Insertion by Pol Beta Confounds Ligation During Base Excision Repair. *Nat Commun* (2017) 8:14045. doi: 10.1038/ncomms14045
22. Marteijn JA, Lans H, Vermeulen W, Hoeijmakers JH. Understanding Nucleotide Excision Repair and Its Roles in Cancer and Ageing. *Nat Rev Mol Cell Biol* (2014) 15(7):465–81. doi: 10.1038/nrm3822

23. Spivak G. Nucleotide Excision Repair in Humans. *DNA Repair (Amst)* (2015) 36:13–8. doi: 10.1016/j.dnarep.2015.09.003
24. Spivak G, Ganesan AK. The Complex Choreography of Transcription-Coupled Repair. *DNA Repair (Amst)* (2014) 19:64–70. doi: 10.1016/j.dnarep.2014.03.025
25. Kang TH. Circadian Rhythm of NER and ATR Pathways. *Biomolecules* (2021) 11(5):715. doi: 10.3390/biom11050715
26. Scharer OD. Nucleotide Excision Repair in Eukaryotes. *Cold Spring Harb Perspect Biol* (2013) 5(10):a012609. doi: 10.1101/cshperspect.a012609
27. Kolesnikova O, Radu L, Poterszman A. TFIIH: A Multi-Subunit Complex at the Cross-Roads of Transcription and DNA Repair. *Adv Protein Chem Struct Biol* (2019) 115:21–67. doi: 10.1016/bs.apcsb.2019.01.003
28. Moser J, Kool H, Giakzidis I, Caldecott K, Mullenders LH, Fousteri MI. Sealing of Chromosomal DNA Nicks During Nucleotide Excision Repair Requires XRCC1 and DNA Ligase III Alpha in a Cell-Cycle-Specific Manner. *Mol Cell* (2007) 27(2):311–23. doi: 10.1016/j.molcel.2007.06.014
29. Chang HHY, Pannunzio NR, Adachi N, Lieber MR. Non-Homologous DNA End Joining and Alternative Pathways to Double-Strand Break Repair. *Nat Rev Mol Cell Biol* (2017) 18(8):495–506. doi: 10.1038/nrm.2017.48
30. Aceytuno RD, Piett CG, Havali-Shahriari Z, Edwards RA, Rey M, Ye R, et al. Structural and Functional Characterization of the PNKP-XRCC4-LigIV DNA Repair Complex. *Nucleic Acids Res* (2017) 45(10):6238–51. doi: 10.1093/nar/gkx275
31. Jasin M, Rothstein R. Repair of Strand Breaks by Homologous Recombination. *Cold Spring Harb Perspect Biol* (2013) 5(11):a012740. doi: 10.1101/cshperspect.a012740
32. Nogueira A, Fernandes M, Catarino R, Medeiros R. RAD52 Functions in Homologous Recombination and Its Importance on Genomic Integrity Maintenance and Cancer Therapy. *Cancers (Basel)* (2019) 11(11):1622. doi: 10.3390/cancers11111622
33. Griffin WC, Trakselis MA. The MCM8/9 Complex: A Recent Recruit to the Roster of Helicases Involved in Genome Maintenance. *DNA Repair (Amst)* (2019) 76:1–10. doi: 10.1016/j.dnarep.2019.02.003
34. Ishikawa H, Barber GN. STING is an Endoplasmic Reticulum Adaptor That Facilitates Innate Immune Signalling. *Nature* (2008) 455(7213):674–8. doi: 10.1038/nature07317
35. Wang Y, Luo J, Alu A, Han X, Wei Y, Wei X. cGAS-STING Pathway in Cancer Biotherapy. *Mol Cancer* (2020) 19(1):136. doi: 10.1186/s12943-020-01247-w
36. Nicolai CJ, Wolf N, Chang IC, Kirn G, Marcus A, Ndubaku CO, et al. NK Cells Mediate Clearance of CD8(+) T Cell-Resistant Tumors in Response to STING Agonists. *Sci Immunol* (2020) 5(45):eaaz2738. doi: 10.1126/sciimmunol.aaz2738
37. Marcus A, Mao AJ, Lensink-Vasan M, Wang L, Vance RE, Raulet DH. Tumor-Derived cGAMP Triggers a STING-Mediated Interferon Response in Non-Tumor Cells to Activate the NK Cell Response. *Immunity* (2018) 49(4):754–63.e4. doi: 10.1016/j.immuni.2018.09.016
38. Dubensky TW Jr, Reed SG. Adjuvants for Cancer Vaccines. *Semin Immunol* (2010) 22(3):155–61. doi: 10.1016/j.smim.2010.04.007
39. Zitvogel L, Galluzzi L, Kepp O, Smyth MJ, Kroemer G. Type I Interferons in Anticancer Immunity. *Nat Rev Immunol* (2015) 15(7):405–14. doi: 10.1038/nri3845
40. Alsaab HO, Sau S, Alzhrani R, Tatiparti K, Bhise K, Kashaw SK, et al. PD-1 and PD-L1 Checkpoint Signaling Inhibition for Cancer Immunotherapy: Mechanism, Combinations, and Clinical Outcome. *Front Pharmacol* (2017) 8:561. doi: 10.3389/fphar.2017.00561
41. Maekawa N, Konnai S, Nishimura M, Kagawa Y, Takagi S, Hosoya K, et al. PD-L1 Immunohistochemistry for Canine Cancers and Clinical Benefit of Anti-PD-L1 Antibody in Dogs With Pulmonary Metastatic Oral Malignant Melanoma. *NPJ Precis Oncol* (2021) 5(1):10. doi: 10.1038/s41698-021-00147-6
42. Zhang X, Huang X, Xu J, Li E, Lao M, Tang T, et al. NEK2 Inhibition Triggers Anti-Pancreatic Cancer Immunity by Targeting PD-L1. *Nat Commun* (2021) 12(1):4536. doi: 10.1038/s41467-021-24769-3
43. Laumont CM, Wouters MCA, Smazynski J, Gierc NS, Chavez EA, Chong LC, et al. Single-Cell Profiles and Prognostic Impact of Tumor-Infiltrating Lymphocytes Coexpressing CD39, CD103, and PD-1 in Ovarian Cancer. *Clin Cancer Res* (2021) 27(14):4089–100. doi: 10.1158/1078-0432.CCR-20-4394
44. Simiczyjew A, Dratkiewicz E, Mazurkiewicz J, Zietek M, Matkowski R, Nowak D. The Influence of Tumor Microenvironment on Immune Escape of Melanoma. *Int J Mol Sci* (2020) 21(21):8359. doi: 10.3390/ijms21218359
45. Giavina-Bianchi MH, Giavina-Bianchi PFJ, Festa CN. Melanoma: Tumor Microenvironment and New Treatments. *Bras Dermatol* (2017) 92(2):156–66. doi: 10.1590/abd1806-4841.20176183
46. Patsoukis N, Wang Q, Strauss L, Boussiotis VA. Revisiting the PD-1 Pathway. *Sci Adv* (2020) 6(38):eabd2712. doi: 10.1126/sciadv.abd2712
47. Riley RS, June CH, Langer R, Mitchell MJ. Delivery Technologies for Cancer Immunotherapy. *Nat Rev Drug Discov* (2019) 18(3):175–96. doi: 10.1038/s41573-018-0006-z
48. Aldape K, Brindle KM, Chesler L, Chopra R, Gajjar A, Gilbert MR, et al. Challenges to Curing Primary Brain Tumours. *Nat Rev Clin Oncol* (2019) 16(8):509–20. doi: 10.1038/s41571-019-0177-5
49. Sundar SJ, Hsieh JK, Manjila S, Lathia JD, Sloan A. The Role of Cancer Stem Cells in Glioblastoma. *Neurosurg Focus* (2014) 37(6):E6. doi: 10.3171/2014.9.FOCUS14494
50. Li Y, Li A, Glas M, Lal B, Ying M, Sang Y, et al. C-Met Signaling Induces a Reprogramming Network and Supports the Glioblastoma Stem-Like Phenotype. *Proc Natl Acad Sci USA* (2011) 108(24):9951–6. doi: 10.1073/pnas.1016912108
51. Topalian SL, Drake CG, Pardoll DM. Immune Checkpoint Blockade: A Common Denominator Approach to Cancer Therapy. *Cancer Cell* (2015) 27(4):450–61. doi: 10.1016/j.ccell.2015.03.001
52. Ma T, Hu C, Lal B, Zhou W, Ma Y, Ying M, et al. Reprogramming Transcription Factors Oct4 and Sox2 Induce a BRD-Dependent Immunosuppressive Transcriptome in GBM-Propagating Cells. *Cancer Res* (2021) 81(9):2457–69. doi: 10.1158/0008-5472.CAN-20-2489
53. Zhai Y, Li G, Li R, Chang Y, Feng Y, Wang D, et al. Single-Cell RNA-Sequencing Shift in the Interaction Pattern Between Glioma Stem Cells and Immune Cells During Tumorigenesis. *Front Immunol* (2020) 11:581209. doi: 10.3389/fimmu.2020.581209
54. Li X, Liu M, Zhao J, Ren T, Yan X, Zhang L, et al. Research Progress About Glioma Stem Cells in the Immune Microenvironment of Glioma. *Front Pharmacol* (2021) 12:750857. doi: 10.3389/fphar.2021.750857
55. Khosravi N, Mokhtarzadeh A, Baghbanzadeh A, Hajiasgharzadeh K, Shahgoli VK, Hemmat N, et al. Immune Checkpoints in Tumor Microenvironment and Their Relevance to the Development of Cancer Stem Cells. *Life Sci* (2020) 256:118005. doi: 10.1016/j.lfs.2020.118005
56. Gangoso E, Southgate B, Bradley L, Rus S, Galvez-Cancino F, McGivern N, et al. Glioblastomas Acquire Myeloid-Affiliated Transcriptional Programs *via* Epigenetic Immunoediting to Elicit Immune Evasion. *Cell* (2021) 184(9):2454–70. doi: 10.1016/j.cell.2021.03.023
57. Zhou W, Ke SQ, Huang Z, Flavahan W, Fang X, Paul J, et al. Periostin Secreted by Glioblastoma Stem Cells Recruits M2 Tumour-Associated Macrophages and Promotes Malignant Growth. *Nat Cell Biol* (2015) 17(2):170–82. doi: 10.1038/ncb3090
58. Mi Y, Guo N, Luan J, Cheng J, Hu Z, Jiang P, et al. The Emerging Role of Myeloid-Derived Suppressor Cells in the Glioma Immune Suppressive Microenvironment. *Front Immunol* (2020) 11:737. doi: 10.3389/fimmu.2020.00737
59. Muik A, Stubbert LJ, Jahedi RZ, Geiβ Y, Kimpel J, Dold C, et al. Re-Engineering Vesicular Stomatitis Virus to Abrogate Neurotoxicity, Circumvent Humoral Immunity, and Enhance Oncolytic Potency. *Cancer Res* (2014) 74(13):3567–78. doi: 10.1158/0008-5472.CAN-13-3306
60. Fukuhara H, Ino Y, Todo T. Oncolytic Virus Therapy: A New Era of Cancer Treatment at Dawn. *Cancer Sci* (2016) 107(10):1373–9. doi: 10.1111/cas.13027
61. Zhu Z, Mesci P, Bernatchez JA, Gimple RC, Wang X, Schafer ST, et al. Zika Virus Targets Glioblastoma Stem Cells Through a SOX2-Integrin αvβ5 Axis. *Cell Stem Cell* (2020) 26(2):187–204.e10. doi: 10.1016/j.stem.2019.11.016
62. Nair S, Mazzoccoli L, Jash A, Govero J, Bais SS, Hu T, et al. Zika Virus Oncolytic Activity Requires CD8+ T Cells and is Boosted by Immune Checkpoint Blockade. *JCI Insight* (2021) 6(1):e144619. doi: 10.1172/jci.insight.144619
63. Lang FF, Conrad C, Gomez-Manzano C, Yung WKA, Sawaya R, Weinberg JS, et al. Phase I Study of DNX-2401 (Delta-24-RGD) Oncolytic Adenovirus: Replication and Immunotherapeutic Effects in Recurrent Malignant Glioma. *J Clin Oncol* (2018) 36(14):1419–27. doi: 10.1200/JCO.2017.75.8219
64. Ortensi B, Setti M, Osti D, Pelicci G. Cancer Stem Cell Contribution to Glioblastoma Invasiveness. *Stem Cell Res Ther* (2013) 4(1):18. doi: 10.1186/scrt166

65. Chen Z, Feng X, Herting CJ, Garcia VA, Nie K, Pong WW, et al. Cellular and Molecular Identity of Tumor-Associated Macrophages in Glioblastoma. *Cancer Res* (2017) 77(9):2266–78. doi: 10.1158/0008-5472.CAN-16-2310
66. Mitchem JB, Brennan DJ, Knolhoff BL, Belt BA, Zhu Y, Sanford DE, et al. Targeting Tumor-Infiltrating Macrophages Decreases Tumor-Initiating Cells, Relieves Immunosuppression, and Improves Chemotherapeutic Responses. *Cancer Res* (2013) 73(3):1128–41. doi: 10.1158/0008-5472.CAN-12-2731
67. Pathria P, Louis TL, Varner JA. Targeting Tumor-Associated Macrophages in Cancer. *Trends Immunol* (2019) 40(4):310–27. doi: 10.1016/j.it.2019.02.003
68. Azizi E, Carr AJ, Plitas G, Cornish AE, Konopacki C, Prabhakaran S, et al. Single-Cell Map of Diverse Immune Phenotypes in the Breast Tumor Microenvironment. *Cell* (2018) 174(5):1293–308.e36. doi: 10.1016/j.cell.2018.05.060
69. Cassetta L, Pollard JW. Targeting Macrophages: Therapeutic Approaches in Cancer. *Nat Rev Drug Discov* (2018) 17(12):887–904. doi: 10.1038/nrd.2018.169
70. Mosser DM, Edwards JP. Exploring the Full Spectrum of Macrophage Activation. *Nat Rev Immunol* (2008) 8(12):958–69. doi: 10.1038/nri2448
71. Qian M, Wang S, Guo X, Wang J, Zhang Z, Qiu W, et al. Hypoxic Glioma-Derived Exosomes Deliver microRNA-1246 to Induce M2 Macrophage Polarization by Targeting TERF2IP *via* the STAT3 and NF-kappaB Pathways. *Oncogene* (2020) 39(2):428–42. doi: 10.1038/s41388-019-0996-y
72. Park JE, Dutta B, Tse SW, Gupta N, Tan CF, Low JK, et al. Hypoxia-Induced Tumor Exosomes Promote M2-Like Macrophage Polarization of Infiltrating Myeloid Cells and microRNA-Mediated Metabolic Shift. *Oncogene* (2019) 38(26):5158–73. doi: 10.1038/s41388-019-0782-x
73. Wick W, Platten M, Weller M. Glioma Cell Invasion: Regulation of Metalloproteinase Activity by TGF-Beta. *J Neurooncol* (2001) 53(2):177–85. doi: 10.1023/a:1012209518843
74. Zhang L, Xu Y, Sun J, Chen W, Zhao L, Ma C, et al. M2-Like Tumor-Associated Macrophages Drive Vasculogenic Mimicry Through Amplification of IL-6 Expression in Glioma Cells. *Oncotarget* (2017) 8(1):819–32. doi: 10.18632/oncotarget.13661
75. Qi L, Yu H, Zhang Y, Zhao D, Lv P, Zhong Y, et al. IL-10 Secreted by M2 Macrophage Promoted Tumorigenesis Through Interaction With JAK2 in Glioma. *Oncotarget* (2016) 7(44):71673–85. doi: 10.18632/oncotarget.12317
76. Watters JJ, Schartner JM, Badie B. Microglia Function in Brain Tumors. *J Neurosci Res* (2005) 81(3):447–55. doi: 10.1002/jnr.20485
77. Mathivet T, Bouleti C, Van Woensel M, Stanchi F, Verschuere T, Phng LK, et al. Dynamic Stroma Reorganization Drives Blood Vessel Dysmorphia During Glioma Growth. *EMBO Mol Med* (2017) 9(12):1629–45. doi: 10.15252/emmm.201607445
78. Mazzone M, Bergers G. Regulation of Blood and Lymphatic Vessels by Immune Cells in Tumors and Metastasis. *Annu Rev Physiol* (2019) 81:535–60. doi: 10.1146/annurev-physiol-020518-114721
79. DeNardo DG, Ruffell B. Macrophages as Regulators of Tumour Immunity and Immunotherapy. *Nat Rev Immunol* (2019) 19(6):369–82. doi: 10.1038/s41577-019-0127-6
80. Jain RK. Antiangiogenesis Strategies Revisited: From Starving Tumors to Alleviating Hypoxia. *Cancer Cell* (2014) 26(5):605–22. doi: 10.1016/j.ccell.2014.10.006
81. Fukumura D, Kloepper J, Amoozgar Z, Duda DG, Jain RK. Enhancing Cancer Immunotherapy Using Antiangiogenics: Opportunities and Challenges. *Nat Rev Clin Oncol* (2018) 15(5):325–40. doi: 10.1038/nrclinonc.2018.29
82. Lee C, Lee J, Choi SA, Kim SK, Wang KC, Park SH, et al. M1 Macrophage Recruitment Correlates With Worse Outcome in SHH Medulloblastomas. *BMC Cancer* (2018) 18(1):535. doi: 10.1186/s12885-018-4457-8
83. Brockelmann PJ, de Jong MRW, Jachimowicz RD. Targeting DNA Repair, Cell Cycle, and Tumor Microenvironment in B Cell Lymphoma. *Cells* (2020) 9(10):2287. doi: 10.3390/cells9102287
84. Huang R, Zhou P-K. DNA Damage Repair: Historical Perspectives, Mechanistic Pathways and Clinical Translation for Targeted Cancer Therapy. *Signal Transduct Target Ther* (2021) 6(1):254. doi: 10.1038/s41392-021-00648-7
85. Wang L, Yang L, Wang C, Zhao W, Ju Z, Zhang W, et al. Inhibition of the ATM/Chk2 Axis Promotes cGAS/STING Signaling in ARID1A-Deficient Tumors. *J Clin Invest* (2020) 130(11):5951–66. doi: 10.1172/JCI130445
86. Sato H, Niimi A, Yasuhara T, Permata TBM, Hagiwara Y, Isono M, et al. DNA Double-Strand Break Repair Pathway Regulates PD-L1 Expression in Cancer Cells. *Nat Commun* (2017) 8(1):1751. doi: 10.1038/s41467-017-01883-9
87. Hu M, Zhou M, Bao X, Pan D, Jiao M, Liu X, et al. ATM Inhibition Enhances Cancer Immunotherapy by Promoting mtDNA Leakage and cGAS/STING Activation. *J Clin Invest* (2021) 131(3):e139333. doi: 10.1172/JCI139333
88. Zhang Q, Green MD, Lang X, Lazarus J, Parsels JD, Wei S, et al. Inhibition of ATM Increases Interferon Signaling and Sensitizes Pancreatic Cancer to Immune Checkpoint Blockade Therapy. *Cancer Res* (2019) 79(15):3940–51. doi: 10.1158/0008-5472.CAN-19-0761
89. Eich M, Roos WP, Nikolova T, Kaina B. Contribution of ATM and ATR to the Resistance of Glioblastoma and Malignant Melanoma Cells to the Methylating Anticancer Drug Temozolomide. *Mol Cancer Ther* (2013) 12(11):2529–40. doi: 10.1158/1535-7163.MCT-13-0136
90. Nakazawa M, Suzuki K, Takeshita M, Inamo J, Kamata H, Ishii M, et al. Distinct Expression of Coinhibitory Molecules on Alveolar T Cells in Patients With Rheumatoid Arthritis-Associated and Idiopathic Inflammatory Myopathy-Associated Interstitial Lung Disease. *Arthritis Rheumatol* (2021) 73(4):576–86. doi: 10.1002/art.41554
91. Walker LS, Sansom DM. Confusing Signals: Recent Progress in CTLA-4 Biology. *Trends Immunol* (2015) 36(2):63–70. doi: 10.1016/j.it.2014.12.001
92. Oyewole-Said D, Konduri V, Vazquez-Perez J, Weldon SA, Levitt JM, Decker WK. Beyond T-Cells: Functional Characterization of CTLA-4 Expression in Immune and Non-Immune Cell Types. *Front Immunol* (2020) 11:608024. doi: 10.3389/fimmu.2020.608024
93. Dovedi SJ, Elder MJ, Yang C, Sitnikova SI, Irving L, Hansen A, et al. Design and Efficacy of a Monovalent Bispecific PD-1/CTLA4 Antibody That Enhances CTLA4 Blockade on PD-1(+) Activated T Cells. *Cancer Discov* (2021) 11(5):1100–17. doi: 10.1158/2159-8290.CD-20-1445
94. Qureshi OS, Zheng Y, Nakamura K, Attridge K, Manzotti C, Schmidt EM, et al. Trans-Endocytosis of CD80 and CD86: A Molecular Basis for the Cell-Extrinsic Function of CTLA-4. *Science* (2011) 332(6029):600–3. doi: 10.1126/science.1202947
95. Kishore C, Bhadra P. Current Advancements and Future Perspectives of Immunotherapy in Colorectal Cancer Research. *Eur J Pharmacol* (2021) 893:173819. doi: 10.1016/j.ejphar.2020.173819
96. Sobhani N, Tardiel-Cyril DR, Davtyan A, Generali D, Roudi R, Li Y. CTLA-4 in Regulatory T Cells for Cancer Immunotherapy. *Cancers (Basel)* (2021) 13(6):1440. doi: 10.3390/cancers13061440
97. Tanaka A, Sakaguchi S. Regulatory T Cells in Cancer Immunotherapy. *Cell Res* (2017) 27(1):109–18. doi: 10.1038/cr.2016.151
98. Chen R, Wold MS. Replication Protein A: Single-Stranded DNA's First Responder: Dynamic DNA-Interactions Allow Replication Protein A to Direct Single-Strand DNA Intermediates Into Different Pathways for Synthesis or Repair. *Bioessays* (2014) 36(12):1156–61. doi: 10.1002/bies.201400107
99. Liu T, Huang J. RReplication Protein A and More: Single-Stranded DNA-Binding Proteins in Eukaryotic Cells. *Acta Biochim Biophys Sin (Shanghai)* (2016) 48(7):665–70. doi: 10.1093/abbs/gmw041
100. Choudhary SK, Li R. BRCA1 Modulates Ionizing Radiation-Induced Nuclear Focus Formation by the Replication Protein A P34 Subunit. *J Cell Biochem* (2002) 84(4):666–74. doi: 10.1002/jcb.10081
101. Wong JM, Ionescu D, Ingles CJ. Interaction Between BRCA2 and Replication Protein A Is Compromised by a Cancer-Predisposing Mutation in BRCA2. *Oncogene* (2003) 22(1):28–33. doi: 10.1038/sj.onc.1206071
102. Pedersen H, Anne Adanma Obara E, Elbæk KJ, Vitting-Serup K, Hamerlik P, Replication Protein A. (RPA) Mediates Radio-Resistance of Glioblastoma Cancer Stem-Like Cells. *Int J Mol Sci* (2020) 21(5):1588. doi: 10.3390/ijms21051588
103. Zhang J, Jiang H, Xu D, Wu WJ, Chen HD, He L. DNA-PKcs Mediates An Epithelial-Mesenchymal Transition Process Promoting Cutaneous Squamous Cell Carcinoma Invasion And Metastasis By Targeting The TGF-Beta1/Smad Signaling Pathway. *Onco Targets Ther* (2019) 12:9395–405. doi: 10.2147/OTT.S205017
104. Tan KT, Yeh CN, Chang YC, Cheng JH, Fang WL, Yeh YC, et al. PRKDC: New Biomarker and Drug Target for Checkpoint Blockade Immunotherapy. *J Immunother Cancer* (2020) 8(1):e000485. doi: 10.1136/jitc-2019-000485

105. Chen Y, Li Y, Guan Y, Huang Y, Lin J, Chen L, et al. Prevalence of PRKDC Mutations and Association With Response to Immune Checkpoint Inhibitors in Solid Tumors. *Mol Oncol* (2020) 14(9):2096–110. doi: 10.1002/1878-0261.12739
106. Yang H, Yao F, Marti TM, Schmid RA, Peng RW. Beyond DNA Repair: DNA-PKcs in Tumor Metastasis, Metabolism and Immunity. *Cancers (Basel)* (2020) 12(11):3389. doi: 10.3390/cancers12113389
107. Munster P, Mita M, Mahipal A, Nemunaitis J, Massard C, Mikkelsen T, et al. First-In-Human Phase I Study Of A Dual mTOR Kinase And DNA-PK Inhibitor (CC-115) In Advanced Malignancy. *Cancer Manag Res* (2019) 11:10463–76. doi: 10.2147/CMAR.S208720
108. Li S, Li L, Meng X, Jiang C, Cai J, Zhao Z, et al. DREAM: A Database of Experimentally Supported Protein-Coding RNAs and Drug Associations in Human Cancer. *Mol Cancer* (2021) 20(1):148. doi: 10.1186/s12943-021-01436-1
109. Peng L, Chen Z, Chen Y, Wang X, Tang N. MIR155HG is a Prognostic Biomarker and Associated With Immune Infiltration and Immune Checkpoint Molecules Expression in Multiple Cancers. *Cancer Med* (2019) 8(17):7161–73. doi: 10.1002/cam4.2583
110. Li Z, Meng X, Wu P, Zha C, Han B, Li L, et al. Glioblastoma Cell-Derived lncRNA-Containing Exosomes Induce Microglia to Produce Complement C5, Promoting Chemotherapy Resistance. *Cancer Immunol Res* (2021) 9 (12):1383–99. doi: 10.1158/2326-6066.CIR-21-0258
111. Li L, Wu P, Wang Z, Jiang C, Zhao Z, Cai J, et al. NoncoRNA: A Database of Experimentally Supported non-Coding RNAs and Drug Targets in Cancer. *J Hematol Oncol* (2020) 13(1):15. doi: 10.1186/s13045-020-00849-7
112. Meng X, Zhao Y, Han B, Jiang C, Liu Y, Cai J, et al. Dual Functionalized Brain-Targeting Nanoinhibitors Restrain Temozolomide-Resistant Glioma *via* Attenuating EGFR and MET Signaling Pathways. *Nat Commun* (2020) 11(1):594. doi: 10.1038/s41467-019-14036-x
113. Arrichiello G, Poliero L, Borrelli C, Paragliola F, Nacca V, Napolitano S, et al. Immunotherapy in Colorectal Cancer: Is the Long-Awaited Revolution Finally Happening? *Cancer Treat Res Commun* (2021) 28:100442. doi: 10.1016/j.ctarc.2021.100442
114. Colton M, Cheadle EJ, Honeychurch J, Illidge TM. Reprogramming the Tumour Microenvironment by Radiotherapy: Implications for Radiotherapy and Immunotherapy Combinations. *Radiat Oncol* (2020) 15(1):254. doi: 10.1186/s13014-020-01678-1
115. Vanpouille-Box C, Alard A, Aryankalayil MJ, Sarfraz Y, Diamond JM, Schneider RJ, et al. DNA Exonuclease Trex1 Regulates Radiotherapy-Induced Tumour Immunogenicity. *Nat Commun* (2017) 8:15618. doi: 10.1038/ncomms15618
116. Kroemer G, Galluzzi L, Kepp O, Zitvogel L. Immunogenic Cell Death in Cancer Therapy. *Annu Rev Immunol* (2013) 31:51–72. doi: 10.1146/annurev-immunol-032712-100008
117. Persa E, Szatmari T, Safrany G, Lumniczky K. *In Vivo* Irradiation of Mice Induces Activation of Dendritic Cells. *Int J Mol Sci* (2018) 19(8):2391. doi: 10.3390/ijms19082391
118. Grassberger C, Ellsworth SG, Wilks MQ, Keane FK, Loeffler JS. Assessing the Interactions Between Radiotherapy and Antitumour Immunity. *Nat Rev Clin Oncol* (2019) 16(12):729–45. doi: 10.1038/s41571-019-0238-9
119. Golden EB, Frances D, Pellicciotta I, Demaria S, Helen Barcellos-Hoff M, Formenti SC. Radiation Fosters Dose-Dependent and Chemotherapy-Induced Immunogenic Cell Death. *Oncoimmunology* (2014) 3:e28518. doi: 10.4161/onci.28518
120. Herrera FG, Irving M, Kandalaft LE, Coukos G. Rational Combinations of Immunotherapy With Radiotherapy in Ovarian Cancer. *Lancet Oncol* (2019) 20(8):e417–33. doi: 10.1016/S1470-2045(19)30401-2
121. Mouw KW, Goldberg MS, Konstantinopoulos PA, D'Andrea AD. DNA Damage and Repair Biomarkers of Immunotherapy Response. *Cancer Discov* (2017) 7(7):675–93. doi: 10.1158/2159-8290.CD-17-0226
122. McLaughlin M, Patin EC, Pedersen M, Wilkins A, Dillon MT, Milcher AA, et al. Inflammatory Microenvironment Remodelling by Tumour Cells After Radiotherapy. *Nat Rev Cancer* (2020) 20(4):203–17. doi: 10.1038/s41568-020-0246-1
123. Mackenzie KJ, Carroll P, Martin CA, Murina O, Fluteau A, Simpson DJ, et al. cGAS Surveillance of Micronuclei Links Genome Instability to Innate Immunity. *Nature* (2017) 548(7668):461–5. doi: 10.1038/nature23449
124. Min Y, Roche KC, Tian S, Eblan MJ, McKinnon KP, Caster JM, et al. Antigen-Capturing Nanoparticles Improve the Abscopal Effect and Cancer Immunotherapy. *Nat Nanotechnol* (2017) 12(9):877–82. doi: 10.1038/nnano.2017.113
125. Ma Y, Vassetzky Y, Dokudovskaya S. Mtorc1 Pathway in DNA Damage Response. *Biochim Biophys Acta Mol Cell Res* (2018) 1865(9):1293–311. doi: 10.1016/j.bbamcr.2018.06.011
126. Riegler J, Gill H, Ogasawara A, Hedehus M, Javinal V, Oeh J, et al. VCAM-1 Density and Tumor Perfusion Predict T-Cell Infiltration and Treatment Response in Preclinical Models. *Neoplasia* (2019) 21(10):1036–50. doi: 10.1016/j.neo.2019.08.003
127. Wu P, Geng B, Chen Q, Zhao E, Liu J, Sun C, et al. Tumor Cell-Derived TGFbeta1 Attenuates Antitumor Immune Activity of T Cells *via* Regulation of PD-1 mRNA. *Cancer Immunol Res* (2020) 8(12):1470–84. doi: 10.1158/2326-6066.CIR-20-0113
128. Liang H, Deng L, Hou Y, Meng X, Huang X, Rao E, et al. Host STING-Dependent MDSC Mobilization Drives Extrinsic Radiation Resistance. *Nat Commun* (2017) 8(1):1736. doi: 10.1038/s41467-017-01566-5
129. Choe EA, Cha YJ, Kim JH, Pyo KH, Hong MH, Park SY, et al. Dynamic Changes in PD-L1 Expression and CD8(+) T Cell Infiltration in Non-Small Cell Lung Cancer Following Chemoradiation Therapy. *Lung Cancer* (2019) 136:30–6. doi: 10.1016/j.lungcan.2019.07.027
130. Ribas A, Wolchok JD. Cancer Immunotherapy Using Checkpoint Blockade. *Science* (2018) 359(6382):1350–5. doi: 10.1126/science.aar4060
131. Kumar V, Patel S, Tcyganov E, Gabrilovich DI. The Nature of Myeloid-Derived Suppressor Cells in the Tumor Microenvironment. *Trends Immunol* (2016) 37(3):208–20. doi: 10.1016/j.it.2016.01.004
132. Togashi Y, Shitara K, Nishikawa H. Regulatory T Cells in Cancer Immunosuppression - Implications for Anticancer Therapy. *Nat Rev Clin Oncol* (2019) 16(6):356–71. doi: 10.1038/s41571-019-0175-7
133. Kachikwu EL, Iwamoto KS, Liao YP, DeMarco JJ, Agazaryan N, Economou JS, et al. Radiation Enhances Regulatory T Cell Representation. *Int J Radiat Oncol Biol Phys* (2011) 81(4):1128–35. doi: 10.1016/j.ijrobp.2010.09.034
134. Daro-Faye M, Kassouf W, Souhami L, Marcq G, Cury F, Niazi T, et al. Combined Radiotherapy and Immunotherapy in Urothelial Bladder Cancer: Harnessing the Full Potential of the Anti-Tumor Immune Response. *World J Urol* (2021) 39(5):1331–43. doi: 10.1007/s00345-020-03440-4
135. Zhu C, Anderson AC, Kuchroo VK. TIM-3 and its Regulatory Role in Immune Responses. *Curr Top Microbiol Immunol* (2011) 350:1–15. doi: 10.1007/82_2010_84
136. Han S, Feng S, Xu L, Shi W, Wang X, Wang H, et al. Tim-3 on Peripheral $CD4^+$ and $CD8^+$ T Cells Is Involved in the Development of Glioma. *DNA Cell Biol* (2014) 33(4):245–50. doi: 10.1089/dna.2013.2306
137. Van Praagh R. Etienne-Louis Arthur Fallot and His Tetralogy: A New Translation of Fallot's Summary and a Modern Reassessment of This Anomaly. *Eur J Cardiothorac Surg* (1989) 3(5):381–6. doi: 10.1016/1010-7940(89)90044-4
138. Kim JE, Patel MA, Mangraviti A, Kim ES, Theodros D, Velarde E, et al. Combination Therapy With Anti-PD-1, Anti-TIM-3, and Focal Radiation Results in Regression of Murine Gliomas. *Clin Cancer Res* (2017) 23(1):124–36. doi: 10.1158/1078-0432.CCR-15-1535
139. Fourcade J, Sun Z, Benallaoua M, Guillaume P, Luescher IF, Sander C, et al. Upregulation of Tim-3 and PD-1 Expression Is Associated With Tumor Antigen-Specific CD8+ T Cell Dysfunction in Melanoma Patients. *J Exp Med* (2010) 207(10):2175–86. doi: 10.1084/jem.20100637
140. Clausi MG, Stessin AM, Zhao Z, Tsirka SE, Ryu S. Neuroinflammatory Changes of the Normal Brain Tissue in Cured Mice Following Combined Radiation and Anti-PD-1 Blockade Therapy for Glioma. *Sci Rep* (2021) 11 (1):5057. doi: 10.1038/s41598-021-84600-3
141. Qiu B, Kline C, Mueller S. Radiation in Combination With Targeted Agents and Immunotherapies for Pediatric Central Nervous System Tumors - Progress, Opportunities, and Challenges. *Front Oncol* (2021) 11:674596. doi: 10.3389/fonc.2021.674596
142. Jordan M, Waxman DJ. CpG-1826 Immunotherapy Potentiates Chemotherapeutic and Anti-Tumor Immune Responses to Metronomic Cyclophosphamide in a Preclinical Glioma Model. *Cancer Lett* (2016) 373 (1):88–96. doi: 10.1016/j.canlet.2015.11.029
143. Krieg AM. CpG Still Rocks! Update on an Accidental Drug. *Nucleic Acid Ther* (2012) 22(2):77–89. doi: 10.1089/nat.2012.0340

144. Shirota Y, Shirota H, Klinman DM. Intratumoral Injection of CpG Oligonucleotides Induces the Differentiation and Reduces the Immunosuppressive Activity of Myeloid-Derived Suppressor Cells. *J Immunol* (2012) 188(4):1592–9. doi: 10.4049/jimmunol.1101304
145. Bezu L, Gomes-de-Silva LC, Dewitte H, Breckpot K, Fucikova J, Spisek R, et al. Combinatorial Strategies for the Induction of Immunogenic Cell Death. *Front Immunol* (2015) 6:187. doi: 10.3389/fimmu.2015.00187
146. Bracci L, Schiavoni G, Sistigu A, Belardelli F. Immune-Based Mechanisms of Cytotoxic Chemotherapy: Implications for the Design of Novel and Rationale-Based Combined Treatments Against Cancer. *Cell Death Differ* (2014) 21(1):15–25. doi: 10.1038/cdd.2013.67
147. Le DT, Jaffee EM. Regulatory T-Cell Modulation Using Cyclophosphamide in Vaccine Approaches: A Current Perspective. *Cancer Res* (2012) 72 (14):3439–44. doi: 10.1158/0008-5472.CAN-11-3912
148. Karachi A, Dastmalchi F, Mitchell DA, Rahman M. Temozolomide for Immunomodulation in the Treatment of Glioblastoma. *Neuro Oncol* (2018) 20(12):1566–72. doi: 10.1093/neuonc/noy072
149. Suryadevara CM, Desai R, Abel ML, Riccione KA, Batich KA, Shen SH, et al. Temozolomide Lymphodepletion Enhances CAR Abundance and Correlates With Antitumor Efficacy Against Established Glioblastoma. *Oncoimmunology* (2018) 7(6):e1434464. doi: 10.1080/2162402X.2018.1434464
150. Hasan MN, Luo L, Ding D, Song S, Bhuiyan MIH, Liu R, et al. Blocking NHE1 Stimulates Glioma Tumor Immunity by Restoring OXPHOS Function of Myeloid Cells. *Theranostics* (2021) 11(3):1295–309. doi: 10.7150/thno.50150
151. Zhang P, Su DM, Liang M, Fu J. Chemopreventive Agents Induce Programmed Death-1-Ligand 1 (PD-L1) Surface Expression in Breast Cancer Cells and Promote PD-L1-Mediated T Cell Apoptosis. *Mol Immunol* (2008) 45(5):1470–6. doi: 10.1016/j.molimm.2007.08.013
152. Mathios D, Kim JE, Mangraviti A, Phallen J, Park CK, Jackson CM, et al. Anti-PD-1 Antitumor Immunity is Enhanced by Local and Abrogated by Systemic Chemotherapy in GBM. *Sci Transl Med* (2016) 8(370):370ra180. doi: 10.1126/scitranslmed.aag2942
153. Coleman RL, Oza AM, Lorusso D, Aghajanian C, Oaknin A, Dean A, et al. Rucaparib Maintenance Treatment for Recurrent Ovarian Carcinoma After Response to Platinum Therapy (ARIEL3): A Randomised, Double-Blind, Placebo-Controlled, Phase 3 Trial. *Lancet* (2017) 390(10106):1949–61. doi: 10.1016/S0140-6736(17)32440-6
154. Gourley C, Balmana J, Ledermann JA, Serra V, Dent R, Loibl S, et al. Moving From Poly (ADP-Ribose) Polymerase Inhibition to Targeting DNA Repair and DNA Damage Response in Cancer Therapy. *J Clin Oncol* (2019) 37 (25):2257–69. doi: 10.1200/JCO.18.02050
155. Pujade-Lauraine E, Ledermann JA, Selle F, Gebski V, Penson RT, Oza AM, et al. Olaparib Tablets as Maintenance Therapy in Patients With Platinum-Sensitive, Relapsed Ovarian Cancer and a BRCA1/2 Mutation (SOLO2/ENGOT-Ov21): A Double-Blind, Randomised, Placebo-Controlled, Phase 3 Trial. *Lancet Oncol* (2017) 18(9):1274–84. doi: 10.1016/S1470-2045(17)30469-2
156. Scott CL, Swisher EM, Kaufmann SH. Poly (ADP-Ribose) Polymerase Inhibitors: Recent Advances and Future Development. *J Clin Oncol* (2015) 33(12):1397–406. doi: 10.1200/JCO.2014.58.8848
157. Lord CJ, Ashworth A. PARP Inhibitors: Synthetic Lethality in the Clinic. *Science* (2017) 355(6330):1152–8. doi: 10.1126/science.aam7344
158. Kim C, Wang XD, Yu Y. PARP1 Inhibitors Trigger Innate Immunity *via* PARP1 Trapping-Induced DNA Damage Response. *Elife* (2020) 9:e60637. doi: 10.7554/eLife.60637
159. Pantel K, Hille C, Scher HI. Circulating Tumor Cells in Prostate Cancer: From Discovery to Clinical Utility. *Clin Chem* (2019) 65(1):87–99. doi: 10.1373/clinchem.2018.287102
160. Gupta SK, Smith EJ, Mladek AC, Tian S, Decker PA, Kizilbash SH, et al. PARP Inhibitors for Sensitization of Alkylation Chemotherapy in Glioblastoma: Impact of Blood-Brain Barrier and Molecular Heterogeneity. *Front Oncol* (2019) 8:670. doi: 10.3389/fonc.2018.00670
161. Terkelsen T, Christensen LL, Fenton DC, Jensen UB, Sunde L, Thomassen C, et al. Population Frequencies of Pathogenic Alleles of BRCA1 and BRCA2: Analysis of 173 Danish Breast Cancer Pedigrees Using the BOADICEA Model. *Fam Cancer* (2019) 18(4):381–8. doi: 10.1007/s10689-019-00141-9
162. Murnyák B, Kouhsari MC, Hershkovitch R, Kálmán B, Marko-Varga G, Klekner Á, et al. PARP1 Expression and its Correlation With Survival is Tumour Molecular Subtype Dependent in Glioblastoma. *Oncotarget* (2017) 8 (28):46348–62. doi: 10.18632/oncotarget.18013
163. Xavier MA, Rezende F, Titze-de-Almeida R, Cornelissen B. BRCAness as a Biomarker of Susceptibility to PARP Inhibitors in Glioblastoma Multiforme. *Biomolecules* (2021) 11(8):1188. doi: 10.3390/biom11081188
164. O'Connor MJ. Targeting the DNA Damage Response in Cancer. *Mol Cell* (2015) 60(4):547–60. doi: 10.1016/j.molcel.2015.10.040
165. Shevtsov MA, Nikolaev BP, Ryzhov VA, Yakovleva LY, Marchenko YY, Parr MA, et al. Ionizing Radiation Improves Glioma-Specific Targeting of Superparamagnetic Iron Oxide Nanoparticles Conjugated With Cmhsp70.1 Monoclonal Antibodies (SPION-Cmhsp70.1). *Nanoscale* (2015) 7(48):20652–64. doi: 10.1039/c5nr06521f
166. Shevtsov M, Pitkin E, Ischenko A, Stangl S, Khachatryan W, Galibin O, et al. Ex Vivo Hsp70-Activated NK Cells in Combination With PD-1 Inhibition Significantly Increase Overall Survival in Preclinical Models of Glioblastoma and Lung Cancer. *Front Immunol* (2019) 10:454. doi: 10.3389/fimmu.2019.00454
167. Mullard A. Phosphatases Start Shedding Their Stigma of Undruggability. *Nat Rev Drug Discovery* (2018) 17(12):847–9. doi: 10.1038/nrd.2018.201
168. Zhou P, Shaffer DR, Alvarez Arias DA, Nakazaki Y, Pos W, Torres AJ, et al. *In Vivo* Discovery of Immunotherapy Targets in the Tumour Microenvironment. *Nature* (2014) 506(7486):52–7. doi: 10.1038/nature12988
169. Apostolidis SA, Rodríguez-Rodríguez N, Suárez-Fueyo A, Dioufa N, Ozcan E, Crispín JC, et al. Phosphatase PP2A is Requisite for the Function of Regulatory T Cells. *Nat Immunol* (2016) 17(5):556–64. doi: 10.1038/ni.3390
170. Maggio D, Ho WS, Breese R, Walbridge S, Wang H, Cui J, et al. Inhibition of Protein Phosphatase-2A With LB-100 Enhances Antitumor Immunity Against Glioblastoma. *J Neurooncol* (2020) 148(2):231–44. doi: 10.1007/s11060-020-03517-5
171. Lamas B, Vergnaud-Gauduchon J, Goncalves-Mendes N, Perche O, Rossary A, Vasson MP, et al. Altered Functions of Natural Killer Cells in Response to L-Arginine Availability. *Cell Immunol* (2012) 280(2):182–90. doi: 10.1016/j.cellimm.2012.11.018
172. Zhang J, Sarkar S, Cua R, Zhou Y, Hader W, Yong VW. A Dialog Between Glioma and Microglia That Promotes Tumor Invasiveness Through the CCL2/CCR2/interleukin-6 Axis. *Carcinogenesis* (2012) 33(2):312–9. doi: 10.1093/carcin/bgr289
173. Hirata A, Hashimoto H, Shibasaki C, Narumi K, Aoki K. Intratumoral IFN-α Gene Delivery Reduces Tumor-Infiltrating Regulatory T Cells Through the Downregulation of Tumor CCL17 Expression. *Cancer Gene Ther* (2019) 26 (9-10):334–43. doi: 10.1038/s41417-018-0059-5
174. Pilanc P, Wojnicki K, Roura AJ, Cyranowski S, Ellert-Miklaszewska A, Ochocka N, et al. A Novel Oral Arginase 1/2 Inhibitor Enhances the Antitumor Effect of PD-1 Inhibition in Murine Experimental Gliomas by Altering the Immunosuppressive Environment. *Front Oncol* (2021) 11:703465. doi: 10.3389/fonc.2021.703465

Conflict of Interest: The authors declare that the research was conducted in the absence of any commercial or financial relationships that could be construed as a potential conflict of interest.

Publisher's Note: All claims expressed in this article are solely those of the authors and do not necessarily represent those of their affiliated organizations, or those of the publisher, the editors and the reviewers. Any product that may be evaluated in this article, or claim that may be made by its manufacturer, is not guaranteed or endorsed by the publisher.

Copyright © 2022 Zhao, Xu, Ma, Chen, Jiang, Cai and Meng. This is an open-access article distributed under the terms of the Creative Commons Attribution License (CC BY). The use, distribution or reproduction in other forums is permitted, provided the original author(s) and the copyright owner(s) are credited and that the original publication in this journal is cited, in accordance with accepted academic practice. No use, distribution or reproduction is permitted which does not comply with these terms.

frontiers in Immunology

REVIEW
published: 14 January 2022
doi: 10.3389/fimmu.2021.813747

Current Understanding of Exosomal MicroRNAs in Glioma Immune Regulation and Therapeutic Responses

Jinwu Peng[1,2†], Qiuju Liang[3†], Zhijie Xu[1,2,4], Yuan Cai[1], Bi Peng[1], Jianbo Li[2], Wenqin Zhang[2], Fanhua Kang[2], Qianhui Hong[2], Yuanliang Yan[3,4] and Mingyu Zhang[5*]*

[1] Department of Pathology, Xiangya Hospital, Central South University, Changsha, China, [2] Department of Pathology, Xiangya Changde Hospital, Changde, China, [3] Department of Pharmacy, Xiangya Hospital, Central South University, Changsha, China, [4] National Clinical Research Center for Geriatric Disorders, Xiangya Hospital, Central South University, Changsha, China, [5] Department of Neurosurgery, Xiangya Hospital, Central South University, Changsha, China

OPEN ACCESS

Edited by:
Wen Cheng,
The First Affiliated Hospital of China Medical University, China

Reviewed by:
Hou-Qun Ying,
Second Affiliated Hospital of Nanchang University, China
Qiang Ju,
Qingdao University, China

***Correspondence:**
Yuanliang Yan
yanyuanliang@csu.edu.cn
Mingyu Zhang
hncszmy@163.com

[†]These authors have contributed equally to this work

Specialty section:
This article was submitted to Cancer Immunity and Immunotherapy, a section of the journal Frontiers in Immunology

Received: 12 November 2021
Accepted: 27 December 2021
Published: 14 January 2022

Citation:
Peng J, Liang Q, Xu Z, Cai Y, Peng B, Li J, Zhang W, Kang F, Hong Q, Yan Y and Zhang M (2022) Current Understanding of Exosomal MicroRNAs in Glioma Immune Regulation and Therapeutic Responses. Front. Immunol. 12:813747. doi: 10.3389/fimmu.2021.813747

Exosomes, the small extracellular vesicles, are released by multiple cell types, including tumor cells, and represent a novel avenue for intercellular communication *via* transferring diverse biomolecules. Recently, microRNAs (miRNAs) were demonstrated to be enclosed in exosomes and therefore was protected from degradation. Such exosomal miRNAs can be transmitted to recipient cells where they could regulate multiple cancer-associated biological processes. Accumulative evidence suggests that exosomal miRNAs serve essential roles in modifying the glioma immune microenvironment and potentially affecting the malignant behaviors and therapeutic responses. As exosomal miRNAs are detectable in almost all kinds of biofluids and correlated with clinicopathological characteristics of glioma, they might be served as promising biomarkers for gliomas. We reviewed the novel findings regarding the biological functions of exosomal miRNAs during glioma pathogenesis and immune regulation. Furthermore, we elaborated on their potential clinical applications as biomarkers in glioma diagnosis, prognosis and treatment response prediction. Finally, we summarized the accessible databases that can be employed for exosome-associated miRNAs identification and functional exploration of cancers, including glioma.

Keywords: exosomes, microRNAs, glioma, biomarker, therapeutic response

INTRODUCTION

Malignant gliomas, representing 80% of the whole primary brain tumors, are the most prevalent and fatal primary neoplasm of the central nervous system in adults (1). Clinicopathologically, glioma is categorized into grades I–IV based on the histologic criteria proposed by the World Health Organization (WHO), with grade IV, glioblastoma (GBM), as the most malignant (2–4). Despite the enhanced understanding of the molecular mechanism of gliomas and considerable progress in therapeutic approaches encompassing surgery, radiotherapy, chemotherapy and targeted therapy, recurrence is still observed in nearly all malignant gliomas, which generally causes death (5, 6).

Patients suffering from gliomas show an unsatisfactory prognosis, with a median survival time of approximately 12-15 months after diagnosis (7). Apart from the rapid proliferation, high aggressiveness, genetic heterogeneity and therapeutic recalcitrance of glioma, the poor survival of glioma patients also results from the insufficient understanding of the specific molecular mechanisms controlling disease progression and shortage of reliable tools for timely diagnosis and sensitive therapeutic monitoring (8). Hence, the molecular mechanisms correlated with glioma development and progression remain unclear, so do the non-invasive biomarkers with high sensitivity and specificity.

Extracellular vesicles (EVs), membrane-encased vesicles secreted by cells, deliver cytoplasmic or membrane contents to nearby cells and are detectable in biological fluids (9, 10). Although EVs were initially relegated as entities for cellular waste disposal, nowadays, they work as messengers in intercellular communication (11). EVs are either buds from the endosomal network (exosomes) or derived from the plasma membrane (microvesicles) (10). Exosomes are lipid bilayer-encapsulated vesicles with a diameter ranging from 30 to 120 nm and are shed by diverse cell populations containing neoplastic cells. With multiple biologically active cargoes, including proteins, lipids, mRNAs, and microRNAs (miRNAs), exosomes have emerged as important players in cell-to-cell communication (12). Exosomes are generated in endosomal compartments termed multivesicular bodies (MVBs) that are late endosomes encompassing various intraluminal vesicles (ILVs) formed by endosomal membrane invaginations. MVBs can subsequently integrate with plasma membranes, leading to the release of exosomes (13). Subsequently, exosomes are internalized into neighboring or distant cells and transport their components, thereby influencing the phenotype of target cells (14). Mounting evidence reveals that exosome-mediated intercellular communication also serves important roles in many respects of cancer progression, covering metastasis and drug resistance as well as interfering with the immune systems within the tumor microenvironment (15, 16). It was reported that tumor cells produce high levels of exosomes, where the components vary in distinct pathological and physiological conditions (17). Recent data confirmed that circulating exosomes appear as a promising means for biomarker discovery since they can be noninvasively collected, and their *in vivo* half-life is short, and their cargoes are protected from degradation (18).

MiRNAs is a kind of small non-coding RNAs, with 19-25 nucleotides that form base pairs with the 3'-untranslated regions (3'-UTR) of target mRNAs, which further cause either mRNA destabilization or translational repression (19, 20). MiRNAs function as irreplaceable intercellular communication tools, as they are transmitted between cells through exosomes and impact recipient cells' phenotype (21). Exosomal miRNAs have been connected with glioma progression *via* activation and/or suppression of certain signaling pathways (22). A better knowledge of the biological roles of exosomal miRNAs may facilitate the exploration and development of novel diagnoses and therapies for gliomas. In this review, we outlined the current findings regarding exosomal miRNAs involvement in tumor initiation and progression, emphasizing glioma cancer. Moreover, we summarized the available tools and platforms that help investigate the underlying regulatory mechanisms of exosomal miRNAs in gliomas. Finally, we highlighted the potential value of exosomal miRNAs in the future clinical application of gliomas.

PROPOSED ROLES OF EXOSOMAL miRNAs IN GLIOMA CANCER

Accumulative evidence reveals that exosomes mediate the initiation and progression of gliomas by transferring biomolecules between distinct cell populations (23). Among these molecules, exosomal miRNAs are the most intriguing due to their important role in multi-respect glioma biology, encompassing proliferation, migration and invasion, angiogenesis, immune suppression, and treatment resistance within the glioma microenvironment (**Table 1**, **Figure 1**). Notably, the effects of exosomal miRNAs on glioma are highly similar to non-exosomal-derived miRNAs.

Exosomal miRNAs and Proliferation of Glioma

Proliferation is an important part of cancer progression, characterized by the alteration of expression and/or activity of cell cycle-associated proteins. Cell growth is also stimulated by constitutively activated signal transduction pathways (50). Exosomes shuttle genetic messages between cells *via* exosomal miRNAs within the tumor environment, thus contributing to glioma cell proliferation. Exosomal miRNAs regulate the proliferation of glioma cells in the following ways. Glioma cells-derived exosomes are transmitted to glioma cancer cells, and exosomal miRNAs modulate the proliferation of recipient cells. For instance, Lan et al. observed the significantly enhanced levels of exosomal miR-301a in serum of glioma patients relative to healthy individuals. Moreover, miR-301a delivered by exosomes derived from GBM cells promoted proliferation and invasion of low-grade H4 glioma cells through directly targeting phosphatase and tensin homolog (PTEN) to enhance the AKT and FAK signaling pathways (24). Non-glioma-derived exosomes are transmitted to glioma cells and further modulate their proliferation. Figueroa et al. found that miR-1587 could be transferred by glioma related-mesenchymal stem cells (GA-hMSCs) to glioma stem-like cells (GSCs) *via* exosomes and increased GSC proliferation and clonogenicity to maintain a GSC-supportive niche *via* directly targeting the expression of nuclear receptor co-repressor-1 (NCOR1) (25). Li et al. also revealed that miR-7239-3p, released by M2 microglial exosomes, could enter glioma cells *via* endocytosis, resulting in the repression of brain and muscle ARNT-like protein-1 (Bmal1) expression and facilitating glioma cells proliferation and migration (26). In addition, the molecule mechanisms of exosomal miRNA in medulloblastoma (MB), another subtype

TABLE 1 | The biological roles of exosomal miRNAs in glioma biology.

Exosomal miRNAs	Donor cells/recipient cells	Targets	Biological functions	References
miR-301a	GBM[i] cells/low grade H4 glioma cells	PTEN	Promoting proliferation and invasion	(24)
miR-1587	GA-hMSCs[ii]/GSCs[iii]	NCOR1	Promoting proliferation	(25)
miR-7239-3p	M2 microglial/glioma cells	Bmal1	Promoting proliferation and invasion	(26)
miR-130b-3p	mono-macrophages/MB[iv] cells	SIK1	Suppressing proliferation, migration and invasion	(27)
miR-101-3p	mono-macrophages/MB cells	FOXP4 (common target)	Suppressing proliferation, migration and invasion	(28)
miR-423-5p		EZH2 (target gene of miR-101-3p)	Promoting apoptosis	
miR-148a	GBM cells /GBM cells	CADM1	Promoting proliferation and metastasis	(29)
miR-1246	hypoxic glioma cells/normoxic glioma cells	FRK	Promoting migration and invasion	(30)
miR-10b-5p		TFAP2A		
miR-181a-5p, miR-125b-5p, let-7b-5p	Group 3 MB cells/ SHH MB cells	ERK	Promoting invasion and migration	(31)
miR-15a	M2 macrophage/glioma	CCND1	Suppressing migration and invasion	(32)
miR-92a		RAP1B		
miR-1	GBM cells/HBMVEC[v]	ANXA2	Suppressing angiogenesis and invasion	(33)
miR-9	glioma cells / HUVECs[vi]	COL18A1, THBS2, PTCH1, PHD3	Promoting proliferation, migration, invasion and angiogenesis	(34)
miR-148a-3p	glioma cells/HUVECs	ERRFI1	Promoting angiogenesis and proliferation	(35)
miR-182-5p	GBM cells/HUVECs	KLF2 and KLF4	Promoting angiogenesis	(36)
miR-21	GSC/HBMVEC	VEGF	Promoting angiogenesis	(37)
miR-26a	GSCs/HBMECs	PTEN	Promoting proliferation, migration and angiogenesis	(38)
miR-944	GSCs/HUVECs	VEGFC	Suppressed proliferation, migration and angiogenesis	(39)
miR-1238	TMZ[vii]-resistant cells/TMZ-sensitive cells	CAV1	Promoting resistance to TMZ Enhancing anti-apoptosis	(40)
miR-151a	TMZ-resistant GBM cells/TMZ-sensitive GBM cells	XRCC4	Increasing chemosensitivity to TMZ	(41)
miR-221	glioma cells/glioma cells	DNM3	Promoting proliferation, migration and TMZ resistance	(42)
miR-301a	hypoxia glioma cells/normaxia-cultured glioma cells	TCEAL7	Promoting radiation resistance	(43)
miR-451	glioma cells/microglia or macrophages	c-Myc	Promoting proliferation and immunosuppression	(44)
miR-214-5p	GBM Cells/ microglia cells	CXCR5	Creating a tumor-supportive milieu	(45)
miR-1246	hypoxia glioma cells /macrophages	TERF2IP	Promoting immunosuppression Promoting proliferation and metastasis	(46)
miR-10a miR-21	hypoxic glioma cells/MDSC[viii]	Rora/IκBα/NF-κB, Pten/PI3K/AKT pathways	Promoting immunosuppression	(47)
miR-29a mir-92a	hypoxia glioma cells /MDSC	Hbp1 Prkar1a	Promoting immunosuppression and proliferation	(48)
miR-1246	(hypoxia) glioma cells/PBMCs[ix]	DUSP3	Promoting immunosuppression	(49)

[i]*Glioblastoma.*
[ii]*glioma related-mesenchymal stem cells.*
[iii]*glioma stem-like cells.*
[iv]*medulloblastoma.*
human brain microvascular endothelial cells.
[vi]*human umbilical vein endothelial cells.*
[vii]*Temozolomide.*
[viii]*myeloid-derived suppressor cells.*
[ix]*peripheral blood mononuclear cells.*

of glioma, have been recently investigated. Based on the finding of Huang's group, exosomal miR-130b-3p activated the p53 signaling pathway *via* silencing serine/threonine-protein kinase 1 (SIK1), thereby suppressing the proliferation, migration and invasion of MB cells (27). In line with this report, Xue et al. demonstrated that exosomes derived from MB patients' plasma could shuttle miR-101-3p and miR-423-5p to MB cells and suppress the proliferation, invasion and migration of MB cells. Mechanically, miR-101-3p and miR-423-5p exert their suppressive effect *via* a common target, forkhead box P4 (FOXP4), while miR-101-3p also binds to the 3'-UTR of enhancer of zeste homolog 2 (EZH2) to reinforce its inhibitory effects on tumors (28). In short, these studies indicated that selectively transferring miRNAs *via* exosomes between cells represents an essential means for intercellular communication, and for modulating the proliferation of gliomas.

Exosomal miRNAs and Invasion/Migration of Glioma

It is generally believed that the invasion of cancerous cells into surrounding vasculatures and tissues is the initial step for cancer metastasis, a leading cause of cancer-associated death (51).

Malignant gliomas have a unique invasion capacity: impeding the surgical removal of all glioma cells and making relapse inevitable (52, 53). Accumulative evidence suggests that exosomal cargos containing nucleic acids such as miRNAs play decisive roles in glioma migration and invasion. Cai et al. found that exosomal miR-148a expression was prominently elevated in the serum of GBM patients and was inversely related to the expression of cell adhesion molecule 1 (CADM1). MiR-148a delivered by glioma-derived exosomes could target CADM1 and then activate STAT3 pathway to facilitate the proliferation and metastasis of GBM cells (29). Numerous studies have illustrated that hypoxia leads to the epithelial-to-mesenchymal transition (EMT) (54), tumor invasion (55) and metastasis (56). Qian et al. found that the hypoxia microenvironment could stimulate miR-1246 in glioma. Besides, miR-10b-5p-enriched exosomes were then internalized by normoxia glioma cells to enhance the migration and invasion of glioma through suppressing fyn-related kinase (FPK) and Transcription factor AP-2 alpha

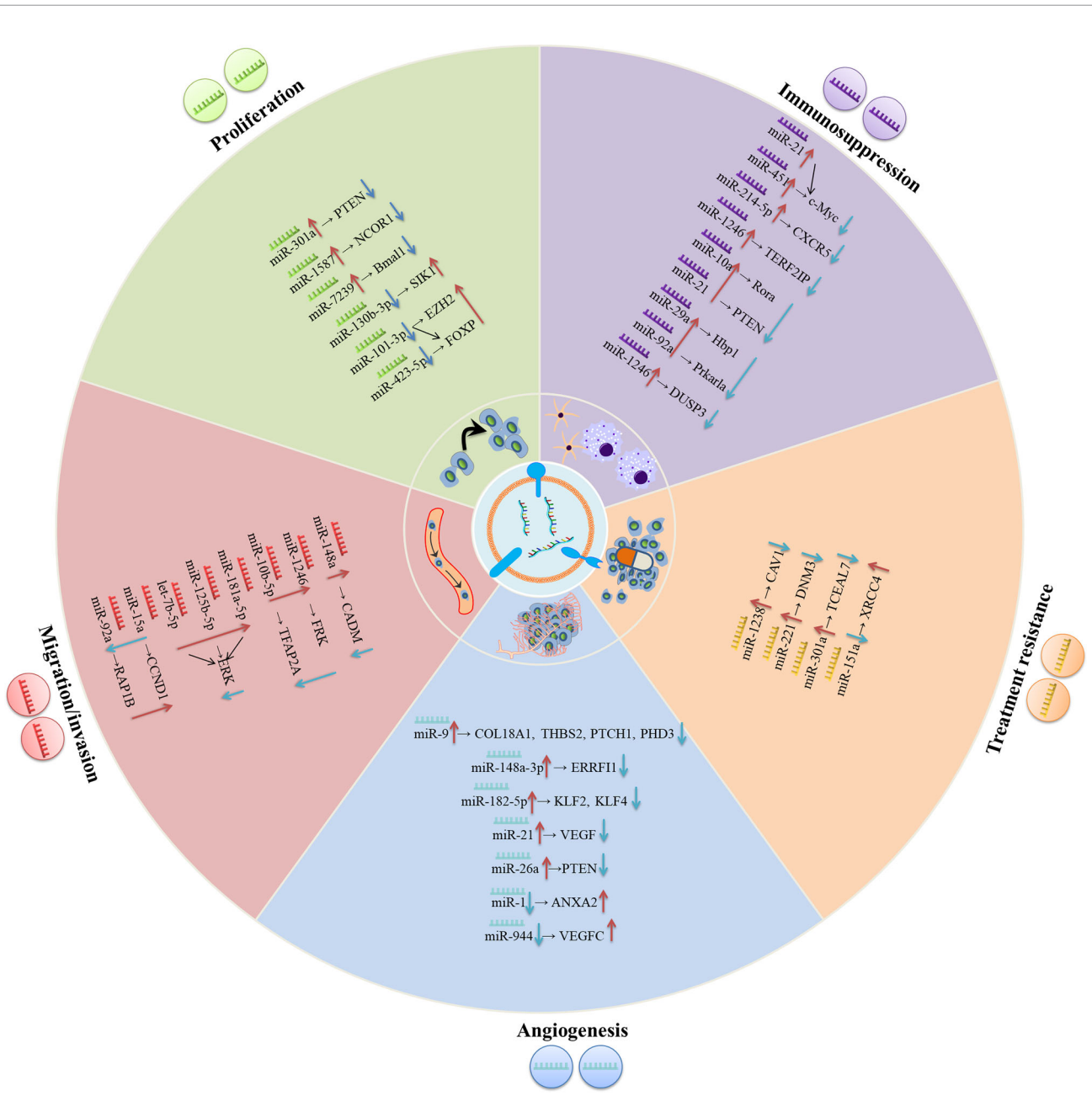

FIGURE 1 | The underlying molecular mechanisms of exosomal miRNAs in modulating the progression of gliomas. In the glioma environment, exosomal miRNAs are absorbed by recipient cells and subsequently exert their functions in varieties of biological processes including proliferation, migration/invasion, angiogenesis, treatment resistance, immunosuppression, etc.

(TFAP2A), respectively (30). Similarly, exosomal miRNAs could also drive the migration and invasion of MB cells. Transfer of Group 3 MB-derived exosomal miRNAs (miR-181a-5p/miR-125b-5p/let-7b-5p) could promote the invasion and migration of less invasive SHH MB cells by enhancing extracellular regulated kinases (ERK) activities in Ras/MAPK pathway (31). Finally, the exosomes released by cancer cells and the exosomes secreted from other cell types participated in glioma invasion and migration. MiR-15a and miR-92a were poorly expressed in M2 macrophages exosomes. It has been verified that M2 macrophages could secret miR-15a and miR-92a *via* exosomes, and subsequently, miR-15a and miR-92a separately repressed cyclin D1 (CCND1) and Ras-related protein Rap1b (Rap1b). Thus, the PI3K/AKT/mTOR signaling pathway was interfered, and glioma migration and invasion was suppressed (32).

Exosomal miRNAs and Angiogenesis in Glioma

As a pivotal hallmark of tumors, angiogenesis is a requisite for cancers to satisfy their needs for nutrients and oxygen (57). Aberrant angiogenesis could lead to malignant phenotypes and promote cancer metastasis (58). It is also established that angiogenesis relates to the progression of glioma (59). Nevertheless, the molecular mechanisms that regulate glioma angiogenesis are still unclear and will be the focus of current research. Since Folkman first discovered a theory about the correlation between angiogenesis and tumor growth, anti-angiogenic gene therapy has attracted the attention of many scientists with its apparent advantages (60). The development of angiogenesis inhibitors targeting pro-angiogenic signaling pathways regulated by vascular endothelial growth factor (VEGF) has exhibited clinical benefits in the treatment of varieties of cancers. While the resistance of patients to anti-VEGF therapy impeded cancer treatment (61). Therefore, a better understanding of the molecular mechanisms of tumor angiogenesis is necessary for a more effective anti-Angiogenic therapy.

The critical roles of miRNA in regulating tumor angiogenesis (62) were highlighted in studies. Exosomes that selectively packed miRNA and shed from tumor cells can be internalized by endothelial cells (ECs), thus facilitating the growth of new blood vessels (63, 64). Increasing evidence has revealed that exosomes regulate angiogenesis partially through delivering miRNAs in the glioma microenvironment. MiR-1 is a well-recognized tumor suppressor in several cancers (65). Loading miR-1 into GBM-derived EV could alleviate angiogenesis, invasion, and neurosphere formation of GBM cells through directly targeting and inhibiting annexin A2 (ANXA2). ANXA2 was evidenced to be an important oncogene whose expression was inversely correlated with miR-1 in GBM cells (33). In addition, miR-9 derived from glioma cells was internalized by vascular endothelial cells, which enhanced angiogenesis. Mechanically, miR-9 could target collagen type XVIII alpha 1 chain (COL18A1), thrombospondin 2 (THBS2), patched 1 (PTCH1), and egl-9 family hypoxia-inducible factor 3 (PHD3) to degrade these mRNA, contributing to initiating HIF-1α/VEGF signaling transduction (34). Besides, glioma-derived exosomal miR-148a-3p reinforced angiogenesis through activating the EGFR/MAPK signaling pathway with the ERBB receptor feedback inhibitor 1 (ERRFI1) (35).

Hypoxia is a universal manifestation of solid tumors. It is caused by the rapid tumor growth that runs out the supply of oxygen, and impairment of blood flow results from the aberrant blood vessels in the tumor (66). It can promote angiogenesis and tumor progression *via* altering the tumor microenvironment (TME) (67, 68). In a recent study by Li et al., hypoxic GBM-secreted miR-182-5p could be taken up by human umbilical vein ECs (HUVECs) *via* exosomes, which could promote angiogenesis by directly suppressing Kruppel-like Factor 2 and 4 (KLF2 and KLF4) and subsequently elevating VEGF receptors (VEGFR) expression (36).

Glioma stem cells (GSCs) are tumor cells that exist in primary GBM with stem-cell-like properties such as self-renew capacity and producing heterogeneous offspring (69). Moreover, GSCs have been elucidated to participate in tumor growth and angiogenesis (70, 71). GSCs trigger tumor angiogenesis by releasing factors that facilitate ECs proliferation and tube formation (72). Existing evidence demonstrated that GSCs secrete extracellular vesicles (containing exosomes) that include pro-angiogenic proteins, mRNA and miRNA, which are absorbed by human brain microvascular ECs (HBMVECs) (37–39, 73, 74). Sun et al. identified that overexpressed miR-21 in GSCs-derived exosomes could activate the angiogenic capacity of ECs by augmenting levels of VEGF, which further interplayed with VEGFR2 to trigger downstream PI3-kinase/Akt pathway (37). Furthermore, Wang et al. showed that GSCs-derived exosomes carrying miR-26a promoted the tube formation of HBMECs *in vitro* by targeting and suppressing PTEN, which activated the PI3K/Akt signaling pathway (38). Finally, a recently published report confirmed that exosome-mediated diffusion of miR-944 from GSCs to HUVECs decreased proliferation and angiogenesis by decreasing VEGFC expression and remarkably restraining Akt/ERK pathways (39). Thus, GSCs play a dual role in regulating angiogenesis in ECs, which depends on the exosomal miRNA.

Exosomal miRNAs and Treatment Resistance of Glioma

The mainstay treatments against glioma remain surgical resection, which is followed by chemotherapy and radiotherapy. Although these methods can remove the majority of the tumor masses, tumor recurrence remains inevitable, which raises great challenges to clinical management owing to treatment resistance (75). Evidence revealed that GSCs with intrinsic resistance to therapy cause the recurrence (76). Exosomes secreted by both tumor and stromal cells play an integral role in treating resistance because of their nature as mediators of intercellular communication (77). Moreover, it has been suggested that the key exosomal miRNA could target diverse signaling pathways or affect regulatory proteins and their corresponding genes, thereupon modulating GBM drug resistance (78). Exploring the machinery of treatment resistance is relevant for eliminating these aggressive tumors.

Temozolomide (TMZ), as a DNA alkylating agent, is the first-line treatment for GBM (79) and has been confirmed to exert its anti-tumor role through inducing DNA damage (80). TMZ treatment significantly prolongs the survival of GBM patients, while the existence of resistance limited the clinic efficacy (81). Relevant studies indicated that exosomes derived from TMZ-resistant glioma could confer TMZ chemoresistance to the recipient TMZ-sensitive cells *via* exosomes (40, 41). Thus, drug resistance increased with the secretion of exosomes (82). Yin et al. reported that bioactive miR-1238 could be incorporated into TMZ-resistant GBM cells-derived exosomes and absorbed by TMZ-sensitive cells, which disseminated TMZ resistance by directly targeting and suppressing caveolin-1 (CAV1) and subsequently activating EGFR-PI3K-Akt-mTOR pathway. The epidermal growth factor receptor (EGFR) played a pivotal role in TMZ resistance (40). Additionally, Zeng et al. demonstrated that miR-151a showed downregulated expression in TMZ-resistant GBM cells and recurrent specimens and was correlated with TMZ resistance. Further study revealed that TMZ-resistant GBM cells spread TMZ chemoresistance to TMZ-responsive GBM cells under an exosomal miR-151a loss-dependent condition. Mechanically, X-ray cross-complementing gene 4 (XRCC4) was directly targeted by miR-151a, and the repression of miR-151a elevated XRCC4 levels, activating DNA repair and increasing the resistance of glioma to TMZ (41). Finally, the level of serum exosomal miR-221 increased with the glioma grades, and gliomas with higher grades displayed a higher level of miR-221. Exosomal miR-221 was connected with decreased TMZ sensitivity by targeting dynamin-3 (DNM3) genes (42).

Exosomal miRNAs shed by glioma cells are also associated with the sensitivity to radiotherapy, which can impact treatment efficiency. According to recent data, exosomal miR-301a, which was specifically expressed and released by hypoxia GBM cells, could transfer to corresponding normoxia-cultured cells, where it repressed the expression of anti-oncogene transcription elongation factor A (SII)-like 7 (TCEAL7) and subsequently activated the Wnt/β-catenin Signaling pathway, thus decreasing radiation sensitivity (43).

Exosomal miRNAs and Immunosuppression in Glioma

Glioma-related immune cells, the substantial component in the glioma microenvironment, play an emerging role in the regulation of cancer progression and control of anti-tumor immunity (83–85). Macrophages/microglia (GAMs) and tumor-induced myeloid-derived suppressor cells (MDSCs), two prominent populations within the tumour stroma, can exert pro-tumorigenic effects and establish an immunosuppressive milieu (86, 87). M2 phenotypic conversion in glioma-associated GAMs and MDSCs expansion can help neoplastic cells evade immune system-mediate detection and destruction (88). Emerging studies suggest that exosomal miRNAs are carriers of information that have the potential to modulate macrophage fate of differentiation (46) and induce MDSCs accumulation and expansion (48), thereupon creating a favorable environment for glioma progression. Therefore, targeting these immune cells and relevant molecules appears as a novel and promising therapy for gliomas.

GAMs occupy the largest proportion in tumor-infiltrating cells for glioma and take up 30% of the whole glioma mass (89). The appearance and intensity of GAMs are closely related to gliomas progression, and conclusive evidence reveals the indispensable role of interplay between GAMs and gliomas in creating an immunosuppressive milieu, consequently favoring glioma growth and invasion (90). Nevertheless, the specific functioning mechanisms of tumor-infiltrated GAMs are yet to be addressed. Based on the report by Van der Vos, GBM-derived EVs were absorbed into microglia and monocyte/macrophage *via in vivo* combined with *in vivo* methods. That resulted in the transfer of miR-21 and miR-451, two abundant miRNAs within GBM-EVs with known oncogenic properties, into the latter cell types and decreased the level of c-Myc mRNA, a shared target of both miRNAs. The absorption of GBM-EVs was accompanied by alterations in microglia phenotype, covering enhanced proliferation and a shift in their cytokines profile towards immunosuppression (44). Furthermore, Yang and his colleagues demonstrated that the expression of miR-214-5p was aberrantly enhanced in GBM cells. It could be transferred into recipient microglia through exosomes, leading to the repression of C-X-C motif chemokine receptor 5 (CXCR5) and ameliorating the expression of pro-inflammatory cytokines such as interleukin 6 (IL-6), interleukin 8 (IL-8) and tumor necrosis factor-α (TNF-α) to regulate the inflammatory response of microglial cells, which helps create a tumor-supportive milieu (45). Besides, tumor-associated macrophages (TAM) are one of the main immune-related cells infiltrating the tumor microenvironment. They are generally categorized into two subtypes with distinct functions, namely classically activated (M1 macrophages) and alternatively activated (M2 macrophages), respectively. The former is characterized by anti-tumor activities, while the latter increases metastasis of tumors and angiogenesis and suppresses the anti-tumor immune response (91). Tumors provide a tumor-permissive milieu by exploiting macrophage polarization states and specifically skewing macrophages toward a pro-tumoral M2-like phenotype, thereby supporting cancer progression by immune suppression (92). What's more, emerging evidence indicates that exosomal miRNAs secreted by glioma cells can control the phenotypic plasticity of macrophages to facilitate tumor growth. For example, the recently published literature by Qian has determined that miR-1246 was upregulated in hypoxia glioma-derived exosomes (H-GDE) and GBM patients' cerebrospinal fluid (CSF), and delivery of H-GDE-derived miR-1246 contributed to inducing M2 macrophage polarization through targeting telomeric repeat binding factor 2 interacting protein (TERF2IP). Thus, the STAT3 signaling pathway was activated and NF-κB signaling pathway was repressed, promoting the development of the immunosuppressive microenvironment (46).

Myeloid-derived suppressor cells (MDSCs), as a heterogeneous population of cells expanding during cancer, can depress activation of T-cells and NK-cells to promote tumor growth, quicken formation of the pre-metastatic niche, and cause resistance to immunotherapy (93). Previous studies have evidenced that

tumor-derived exosomes drive MDSCs activation and expansion (94), and miRNAs play essential roles in regulating the expansion of functional MDSCs (95). However, the exact mechanisms where miRNA-containing exosomes derived from glioma cells can manipulate the differential of functional MDSCs remains to be defined. To the end, Guo et al. identified that hypoxia-stimulated glioma-derived exosomes (GDEs) could be taken up into MDSCs, exhibiting a stronger capacity to induce MDSCs compared with normoxia-stimulated GDEs. It was exactly the hypoxia-inducible enhanced expressed miR-10a and miR-21 within GDEs that reinforced MDSCs expansion and activation through targeting Rora/IκBα/NF-κB and Pten/PI3K/AKT pathways (47). Guo et al. also revealed that exosomal miR-29a and miR-92a, which were transferred from hypoxia-induced glioma cells to MDSCs could facilitate the formation of the immunosuppressive microenvironment by increasing the proliferation of functional MDSCs *via* silencing high-mobility group box transcription factor1 (Hbp1) and protein kinase cAMP-dependent type I regulatory subunit alpha (Prkar1a), separately (48). Additionally, they also demonstrated that miR-1246, which was abundant in GDEs, could also potentiate MDSCs with manifestations including repressing CD8+ cells proliferation and elevating the levels of interleukin 10 (IL-10) and transforming growth factor-beta (TGF-β) by activating the DUSP3/ERK pathway (49). The above-described studies indicate that glioma potently influences MDSCs differentiation and activation *via* exosomal miRNAs, thereupon impacting the entire tumor immune environment.

CLINICAL IMPLICATIONS OF EXOSOMAL miRNAs IN GLIOMA

Exosomal miRNAs as Biomarkers for Glioma

Precise diagnosis, and the timely/comprehensive monitoring of therapeutic response, remain the main challenges in glioma patients' care and treatment. Neuroimaging, magnetic resonance imaging (MRI) in particular, is regularly used for glioma diagnosis, staging, and monitoring therapeutic response. Although neuroimaging is suggestive of glioma diagnosis, there are still other brain lesions sharing radiological features, which makes differential diagnosis difficult (96). Additionally, the lowest resolution for the effective detection by MRI remains on the order of millimeters (97). Because of the dimension of a tumor cell, this disparity in scale translates into delayed diagnosis and treatment (98). Furthermore, MRI can exhibit the enhanced tumor volume following radiotherapy, generally, due to enhanced vascular permeability, an effect named pseudoprogression, and connected with the treatment (99). In the meantime, histopathologic examination of tumor specimens attained by surgery is currently recognized as the gold standard for glioma grading and typing. Nevertheless, this method bears high surgical risks, and repeated sampling of tumor specimens may be impractical (100). All these factors demonstrably highlight the urgent need for exploring minimally invasive biomarkers supportive for reliable and consistent diagnosis, prognostication, and treatment response prediction.

Although methods of early diagnosis and timely management of various cancer types have been established, such as detection of circulating tumor cells (CTCs) and cell-free nucleic acids (cfNAs) in the circulation, comparatively little progress has been made concerning clinical validation of intrinsic brain tumors. Broad sets of promising biomarkers have already been identified in the blood and CSF of patients afflicted with gliomas, but few were applied clinically (101).

In recent years, exosomes have become an emerging topic implicating multifaceted development and biological process through being secreted into nearly all human fluids, containing plasma, CSF, urine, breast milk, and saliva (102). Accumulative investigations have been centered on exosomes as they can be used as diagnostic, prognostic, and therapeutic markers (103). Previous studies have demonstrated that exosomes can cross the intact blood-brain barrier (BBB) (104). Besides, the bilayer-lipid membranes of exosomes protect the bioactive cargos they contain from enzymatic RNase degradation (105). MiRNAs within peripheral blood exosomes may be relevant biomarkers and therapeutic targets for glioma since they are tumor regulators possessing oncogene and suppressor gene roles (106). Exosomes are extractable from peripheral blood, and miRNAs can be detected by technologies. Exosomal miRNAs could be regarded as promising comprehensive biomarkers, as they possess the potential to present real-time information of disease and can predict progressive disease and assess the response of cancers to targeted therapies (106) (**Table 2**).

Some studies have reported the diagnostic implication of exosomal miRNAs derived from sera. Exosomal miRNAs are correlated with histopathologic grades of gliomas. For instance, RNU6-1, miR-320, and miR-574-3p were fast and reliable diagnostic markers of GBM patients as their circulating levels increased with the area under the curve (AUC) of 0.926 (107). This research opened up a novel avenue that exosomal miRNAs could be applied for GBM diagnosis. Ebrahimkhani characterized a set of exosomal miRNAs (miR-182-5p, miR-328-3p, miR-339-5p, miR-340-5p, miR-485-3p, miR-486-5p as well as miR-543) derived from human serum to distinguish GBM patients from healthy controls with a predictive accuracy of 91.7% (108). Moreover, Santangelo validated that the expression of miR-21/miR-222/miR-124-3p in serum exosomes of patients with high-grade gliomas (HGG) was remarkably higher than those with low-grade gliomas (LGG) and healthy individuals. The combination of miR-21+miR-222+miR-124-3p was more robust in discriminating HGG than healthy controls, but its accuracy markedly decreased after surgical resection of the tumors. Intriguingly, exosome-associated miR-21 expression alone appeared as the greatest predictor for differentiating patients with HGG from those with LGG, with an AUC of 0.83. Meanwhile, the results also revealed that high exosomal miR-21 together with low exosomal miR-222 and miR-124-3p expression could effectively help to distinguish brain tumors of glial origin from those without glial origin at initial neuroradiological assessment, which may be helpful for patients showing inconclusive biopsies or with masses in the essential and

TABLE 2 | Related studies about exosomal miRNAs from human fluids as diagnostic, prognostic and predictive biomarkers in glioma.

Exosomal miRNAs	Sample type	Expression status	Clinical value	Reference
miR-320 miR-574-3p RUN6-1	serum	↑	diagnostic biomarker for GBM[x]	(107)
miR-182-5p miR-328-3p miR-339-5p miR-340-5p miR-485-3p miR-486-5p miR-543	serum	↑ ↓ ↓ ↓ ↓ ↑ ↓	diagnostic biomarker for GBM	(108)
miR-21 miR-222 miR-124-3p	serum	↑	diagnostic biomarker for HGG[xi] diagnostic biomarke for grade prediction (HGG over LGG[xii], miR-21)	(109)
miR-766-5p	serum	↓ ↓	diagnostic biomarker for discriminating HGG over intracranial lymphoma	(110)
miR-301a	serum	↑	diagnostic biomarker for glioma prognostic biomarker for poor OS[xiii]	(24)
miR-454-3p	serum	↑	diagnostic biomarker for glioma prognostic biomarker for poor survival	(111)
miR-210	serum	↑	diagnostic biomarker for glioma and grade prediction (high grade over low grade) prognostic biomarker for recurrence and poor OS	(112)
miR-181b	serum	↓	prognostic biomarker for shorter post-surgical survival time	(113)
miR-182-5p miR-223-3p miR-34a-5p miR-497-5p	serum	↑ ↑ ↓ ↓	prognostic biomarker for LGG	(114)
miR-375	plasma	↑	diagnostic biomarker for glioma	(115)
miR-210 miR-449 miR-5194	Plasma	↑ ↓ ↓	diagnostic and prognostic biomarker showing association with histopathological grade (GBM over LGA[xiv])	(116)
miR-2276-5p	Plasma	↓	diagnostic biomarker for glioma and grade prediction (HGG over LGG) Prognostic biomarker for better OS	(117)
miR-21	CSF[xv]	↑	diagnostic biomarker for GBM	(118)
miR-21	CSF	↑	diagnostic biomarker for discriminating glioma patients over non-tumor brain disease diagnostic biomarker for grade prediction (GBM over grade II gliomas) prognostic biomarker for poor survival	(119)
miR-182-5p	Serum and CSF	↑	diagnostic biomarker for glioma and grade prediction (HGG over LGG) prognostic biomaker for glioma	(36)
miR-1246	CSF	↑	prognostic biomarker for recurrence	(49)
miR-9-5p	Serum and CSF	↑	prognostic biomaker for poor survival	(120)
miR-151a	CSF	↓	predictive biomarker for TMZ[xvi] response	(41)
miR-574-3p	serum	↑	predictive biomarker for the effect of radiotherapy for glioma patients	(121)
miR-21 miR-222 miR-124-3p	Serum	↑	predictive biomarker for therapy response in post-surgical following-up	(122)

[x] *glioblastoma multiforme.*
[xi] *high-grade glioma.*
[xii] *low-grade glioma.*
[xiii] *overall survival.*
[xiv] *low-grade astrocytoma.*
[xv] *cerebrospinal fluid.*
[xvi] *Temozolomide.*

intricate areas of the brain (109). Furthermore, according to the report from Wang's group, both miR-766-5p and miR-376-5p in serum exosomes were strikingly attenuated in intracranial lymphoma, and HGG patients relative to healthy controls, and the levels of exosomal miR-766-5p were lower in the intracranial lymphoma group than the HGG group. Exosomal miR-766-5p and miR-376-5p could effectively diagnose HGG with AUCs of 0.8883 and 0.7688, respectively. Besides, miR-766-5p could be used as an auxiliary indicator for the diagnosis of HGG of intracranial lymphoma, showing an AUC value of 0.7201 (110). Additionally, exosomal miR-301a was significantly upregulated in the serum of glioma patients, which was connected with ascending pathological grades and decreased Karnofsky performance status (KPS) scores. ROC curve analysis revealed that exosomal miR-301a exhibited a potential diagnostic value for discriminating gliomas patients from non-glioma patients (AUC=0.937) (24). Research by Shao et al.

revealed that miR-454-3p was markedly under-expressed in glioma tissues while over-expressed in exosomes, and exosomal miR-454-3p could function as a marker for glioma diagnosis with AUC value of 0.863. Levels of exosomal miR-454-3p in the postoperative serums were prominently lower relative to those in the preoperative serums (111). Finally, Lan et al. identified that exo-miR-210 whose expression was significantly reinforced in glioma patients and elevated with ascending pathological grades, could effectively identify glioma patients from healthy controls (AUC=0.856) (112).

The aforementioned dysregulations of exosomal miR-301a, miR-454-3p and miR-210 was also connected with the prognosis of glioma patients. Specifically, the expression of serum exosomal miR-301a was significantly diminished following the surgical removal of primary tumors and increased during GBM recurrence. Kaplan-Meier analysis suggested that malignant patients with an elevated exosomal miR-301a expression generally have a poorer survival (OS) (24). Similarly, enhanced expression of miR-454-3p (111) and miR-210 (112) in glioma serum exosomes were both related to poor prognosis. Another study also reported that augmented levels of exosomal miR-181b in GBM patients' serum could indicate a worse functional outcome and suggest a prominently shorter post-surgical survival time for GBM patients (113). Also, Caponnetto et al. analyzed and compared the miRNA profile of exosomes released by glioma-associated stem cells (GASC), and confirmed that abnormal expression levels of exosomal miRNAs probably contributed to the malignant progression phenotypes. These exosomal miRNAs from serum warrant further investigation for the improvement of LGG prognostic stratification (114).

In addition to sera, increasing research have focused on identifying promising biomarkers based on exosomal miRNAs attained from glioma patients' plasma. In a recent study by Xu et al, circulating exosomal miR-375 in the plasma of glioma patients was prominently reinforced and the extent of this upregulation was positively associated with tumor grades, indicating that miR-375-containing exosomes held great promise as a diagnostic marker (115). Similarly, Tabibkhooei et al. demonstrated that enhanced expression of miR-210 and declined expression of miR-5149 and miR-449 in plasma had a positive correlation with histopathological grade of glioma, which favored GBM detection and prognosis prediction. That implied that plasma exosomal miRNAs are expected to be novel biomarkers of GBM (116). Another study also confirmed that miR-2276-5p expression levels were declined in the plasma-derived exosomes of glioma patients compared with those of non-glioma controls and its expression was lower in HGG patients than in LGG patients. Exosomal miR-2276-5p could effectively diagnose glioma patients with an AUC of 0.8107. Furthermore, low levels of exosomal miR-2274-5p in glioma were linked to poorer survival rates (117).

Aberrant expression of exosomal miRNAs, a hallmark of glioma, can be detected in blood, and other body fluids, including CSF. For instance, Akers and colleagues proved that miR-21 expression levels were highly elevated in EVs derived from CSF of GBM patients relative to those from non-oncologic patients. CSF EV miR-21 could function as a feasible biomarker of GBM, with an AUC of 0.9 (118). Consistent with this finding, the data from Shi's group have highlighted that according to its reinforced expression in gliomas, CSF-derived exosomal miR-21 appeared as an excellent index to distinguish glioma and non-neoplastic brain diseases yielding an AUC of 0.927. Moreover, it had the potential to specifically separate GBM and grade II gliomas with an AUC value of 0.751. The authors also identified that a high abundance of miR-21 bore an inverse correlation with patients' survival (119). Both of the aforementioned studies suggest that expression levels of exosomal miR-21 in CSF could be a promising indicator applying for glioma diagnosis and prognosis. Another recently published paper has observed that glioma patients had enhanced expression of miR-182-5p from serum- and CSF-derived exosomes compared with healthy individuals, and high-grade patients, GBM patients, in particular, showcased higher exosomal miR-182-5p than LGG patients. Additionally, a dramatic drop in miR-182-5p expression was detected in the postoperative period. Exosome-mediated miR-182-5p, thereupon, could be a desirable diagnostic and prognostic biomarker of glioma (36). Moreover, CSF exosomal miR-1246 was associated with glioma and could potentially be applied for monitoring tumor recurrence after surgery (49). Finally, augmented expression of small EVs-derived miR-9-5p was linked to a decreased survival in IDH-mutated glioma patients, suggesting that miR-9-5p within the EVs from blood and CSF might be explored as a potential molecular biomarker (120).

Acquired drug resistance is emerging as a leading clinical limiting factor in the treatment of gliomas. Thereby, the identification of potential drug-resistant patients and exploration of alternative treatment timely are relevant to ameliorate prognosis. Exosomes can influence therapy resistance as delivery vehicles of miRNAs and can predict therapeutic responses as biomarkers. Zeng et al. identified that GBM patients with attenuated CSF exosomal miR-151a levels exhibited a worse prognosis, revealing a dismal response to TMZ (41). Additionally, miR-574-3p derived from serum exosomes was significantly diminished after radiotherapy, and it was proposed as an important candidate biomarker for evaluating the therapeutic effect of radiotherapy in glioma (121). Furthermore, reinforced expression levels of serum exosomal miR-21, miR-222 and miR-124-3p were associated with HGG progression. Specifically, after the chemo-radiotherapy, HGG patients with high levels of these miRNAs showed significantly shorter progression-free survival (PFS) and overall survival (OS) (122). Hence, the profiles of exosomal miRNAs could potentially predict the therapeutic response in glioma patients.

Exosomes contain not only miRNAs but also other noncoding RNAs (ncRNAs), including circular RNAs (circRNAs) or long non-coding RNAs (lncRNAs). Exosomal miRNA mediated glioma progression *via* interacting with circRNAs or lncRNAs. Accumulative studies have also focused on the expression of exosomal circRNAs/lncRNAs in serum of glioma patients. For example, exosomal circ_0072083 was reported to contribute to TMZ resistance in glioma *via* modulating exosomal miR-1252-5p-mediated nanog homeobox (NANOG) degradation. Moreover, exosomal circ_0072083 could serve as an independent diagnostic target for gliomas with an AUC of 0.85, and patients with high

expression of exosomal circ_0072083 displayed poorer OS (123). Also, Yin's team found that exosomal circMMP1 in serum facilitated the progression of glioma *via* functioning as a competitive endogenous RNA (ceRNA) of miR-433 (124). Furthermore, exosomal lncSBF2-AS1 transferred from TMZ-resistant GBM cells to chemoresponsive GBM cells could function as a ceRNAs for miR-151a-3p, contributing to the TMZ resistance (125). Consistently, based on the findings from Hao' group, lncRNA PTENP1 could be packaged into exosomes of human umbilical cord mesenchymal stem cells and transferred into U87 glioma cells, and subsequently impaired the cell growth *via* suppressing the expression of miR-10a-5p (126). All these studies have demonstrated that exosomal ncRNAs could be served as the promising diagnostic/prognostic markers and therapeutic targets.

To sum up, the multiple exosomal ncRNAs, miRNAs in particular, from serum, plasma, CSF and other body fluids will promote the broad application of exosome-based liquid biopsy strategies in the early diagnosis, prognosis and therapeutic response prediction of gliomas.

The Potential Application of Exosomal miRNAs in Anti-Glioma Treatment

Given the pivotal biological meanings of exosomal miRNAs in glioma, approaches that specifically target exosomes or exosomal cargoes including miRNAs, are emerging as promising therapies for gliomas. Among the potential therapeutic applications of exosomes, significant attention has been dedicated to applying these vesicles as nanocarriers to deliver small molecules, proteins and nucleic acids such as miRNAs (127). Despite the development of novel methods to engineer exosomal cargoes in producer cells, low yields of exosomes impede the widespread application of exosome-based therapies. Thereupon, some studies have been established to regulate exosomes production to treat cancer. For example, Li et al. confirmed that two intriguing compounds termed MOPIPP and vacuolin-1 could facilitate the vacuolization of endosomal compartments and disrupt the trafficking of late endosomes to lysosomes without exhibiting significant cytotoxicity. Thus exosomes production in GBM cells was enhanced, whereas selected miRNAs carried by the exosomes were identified to show qualitative similarity to those in untreated cells, suggesting that MOPIPP and vacuolin-1 could help develop exosome-based anti-cancer therapeutics (128). However, the potential action mechanism of these compounds should be further explored.

MiRNAs may be a novel antineoplastic agent as they can modulate the posttranscriptional expression of target genes (129–132). Restitution of several downregulated tumor-suppressor miRNAs could repress the growth of GBMs, indicating that certain miRNAs could be used for anti-glioma therapeutics (133). Currently, it seems unsuitable to use available vehicles to deliver miRNAs containing liposomes and viral vectors because of their low efficiency and safety (134). As nature miRNAs carriers, exosomes may be employed to provide tumor-suppressor miRNAs to mediate tumor growth suppression and realize personalized treatment (**Table 3**). For example, Fareh et al. engineered patients' derived GSCs to stably and continuously express the miR-302-367 cluster, and a large amount of tumor-suppressor miRNA was enclosed in exosomes which were absorbed by neighboring GSC. Thus, its targets containing Cyclin D1, Cyclin A, E2F transcription factor 1 (E2F1) and C-X-C motif chemokine receptor 4 (CXCR4) pathway were repressed, so did the proliferation and tumorigenicity of GSCs (135). Emerging studies have proved that decoy or sponge-like constructs could be employed for miRNA inhibition. They have potential therapeutic benefits by binding complementary miRNA(s) or seed sequences, which can impede the crosslink between miRNAs and their targets (147–149). Monfared and colleagues tried to down-regulated the expression of miR-21 in GBM cell lines, U87-MG and C6, through utilizing engineered exosomes packed with a miR-21-sponge construct. They found that cells treated with miR-21-sponge exosomes exhibited a decline in proliferation and an elevation in apoptotic rates (136). Thereupon, exosomes can be used as a promising therapeutic delivery vehicle in glioma treatment.

Recently, accumulative evidence has highlighted that mesenchymal stem cells (MSCs), as a novel approach, can overcome the demerits of previous therapies for gliomas (150, 151). MSCs can pass through the BBB and possess inherent tropism towards tumors and low immunogenicity (152). Additionally, MSCs may exert their therapeutic capacity *via* producing and secreting useful exosomes in glioma treatment (153). Several investigations have suggested the delivery of tumor-suppressive miRNAs to cancers through MSC-derived exosomes (154, 155). Studies on glioma have identified that exosomes displayed anti-glioma effects when tumor-suppressive miRNAs expression was elevated in the exosomes-donating MSCs, which revealed the considerable potential for the application of MSC-derived exosomes in treating gliomas. To the end, Lang and colleagues found that MSCs could be exploited as natural biofactories to produce exosomes carrying supraphysiological levels of miR-124a, an effective anti-glioma agent Exo-miR124a exosomes resulted in significantly repressing the viability and clonogenicity of GSCs. When systemically administered, the mice bearing intracranial GSCs xenografts were cured. Mechanistic studies proved that miR-124a acted through silencing Forkhead box (FOX)A2, contributing to abnormal intracellular lipid accumulation (137). Moreover, Yan and co-workers found that miR-512-5p was poorly expressed in GBM tissues and cells, and exosomes derived from miR-512-5p-transfected BMSCs were internalized by U87 cells, thus interfering with GBM cell proliferation and inducing cell cycle arrest through negatively regulating Jagged 1 (JAG1) (138). Furthermore, miR-29a-3p, a tumor suppressor in diverse malignant tumors, was demonstrated to directly target roundabout guidance receptor 1 (ROBO1), thus mitigating vasculogenic mimicry (VM) formation in gliomas. MSCs could be engineered to produce miR-29a-3p-overexpressing exosomes, and treatment with these exosomes restrained migration and VM formation, thereby suppressing the growth of glioma *in vitro* and *in vivo* (139). VM, a kind of alternative microvascular circulation bypassing the canonical VEGF-driven angiogenesis, shows resistance to anti-angiogenesis therapy (156). Tumor necrosis factor-related apoptosis-inducing ligand (TRAIL) has strong potential to kill cancerous cells by inducing apoptosis, with minimal effect on normal cells (157). Zhang et al. identified that miR-7 could sensitize GBM cells to TRAIL-induced apoptosis

TABLE 3 | Identification of exosomal miRNAs as potential anti-glioma therapeutics.

Exosomal miRNAs	Donor cells/recipient cells	Targets	Anti-glioma effects	References
miR-302-367	GSC[xvii]/GSC	Cyclin D1, CyclinA, E2F1, CXCR4 pathway	Suppressing proliferation	(135)
a miR-21-sponge construct	HEK-293T/U87-MG	PDCD4 and RECK	Suppressing proliferation Increasing apoptosis	(136)
miR-124a	MSCs[xviii]/ GSCs	(FOX)A2	Suppressing proliferation	(137)
miR-512-5p	BMSCs[xix]/GBM cells	JAG1	Suppressing proliferation Inducing cell cycle arrest	(138)
miR-29a-3p	MSC/glioma cells	ROBO1	Suppressing migration and VM	(139)
miR-7	MSCs/GBM[xx] cells	XIAP	Enhancing TRAIL sensitivity Increasing apoptosis and suppressing tumor growth	(140)
miR-146b	Marrow stromal cells/ glioma cells	EGFR, NF-κB and SMAD4	Suppressing growth, invasion and migration	(141)
miR-133b	MSC/glioma cells	EZH2	Suppressing proliferation, invasion and migration	(142)
miR-584-5p	MSC/glioma cells	CYP2J2 MMP-2 Bcl-2 and Bax	Suppressing proliferation and migration Suppressing metastasis Induce glioma cells apoptosis	(143)
miR-375	Marrow stromal cells/ glioma cells	SLC31A1	Suppressing proliferation, migration, invasion Increasing apoptosis	(144)
miR-199a	MSC/glioma cells	AGAP2	Suppressing proliferation, invasion and migration Enhancing chemosensitivity to TMZ	(145)
miR-124	WJ-MSC[xxi]/GBM cells	CDK6 IQGAP1, LAMC1, ITGB1 R-Ras and N-Ras	Suppressing proliferation Suppressing migration Increasing chemosensitivity to TMZ	(146)

[xvii]*glioma stem-like cells.*
[xviii]*mesenchymal stem cells.*
[xix]*bone mesenchymal stem cells.*
[xx]*glioblastoma.*
[xxi]*Wharton's jelly MSCs.*

and reinforced expression of miR-7 in TRAIL-overexpressed MSCs, increased apoptosis and repressed tumor growth in an exosomes-dependent fashion (140). Additionally, based on the report of Katakowsk's group, the delivery of exosomes derived from MSCs directly by intratumoral injections prominently decreased the growth of glioma xenograft in the rat brain with the inclusion of miR-146b. The anti-tumor effect of MSCs-derived exosomes was underpinned by concurrent inhibition of factors including EGFR, NF-kappaB and mothers against decapentaplegic homolog 4 (SMAD4) (141). It was also found that MSCs-derived exosomes transmitting miR-133b into glioma cells could inhibit EZH2 expression by disrupting the Wnt/β-catenin signaling pathway, thereupon repressing proliferation, invasion and migration of glioma cells (142). Moreover, transferring miR-584-5p through exosomes derived from MSCs could suppress the proliferation and migration of U87 cells *via* decreasing levels of cytochrome P450 family 2 subfamily J member 2 (CYP2J2). This move could also repress glioma metastasis through reducing expression of Matrix metalloproteinase-2 (MMP-2), and induce carcinoma cells apoptosis *via* decreasing levels of B-cell lymphoma-2 (BCL-2), an anti-apoptotic protein, and increasing expression levels of BCL-2 associated X (BAX), a pro-apoptotic protein (143). Exosomal miR-375 from human marrow stromal cells (hMSCs) resulted in suppressed cell proliferation, invasion and migration while promoted apoptosis through solute carrier family 31 member 1 (SLC31A1) inhibition (144). Similarly, miR-199a, when delivered by MSCs *via* the exosomes, could negatively regulate ArfGAP with GTPase domain, ankyrin repeat and PH domain 2 (AGAP2), thereby repressing the proliferation, invasion and migration of glioma cells *in vivo*, and ameliorating the chemosensitivity to TMZ and suppressing the tumor growth *in vivo* (145).

Until now, Studies of MSCs have focused primarily on BMSCs. However, the derivation of stem cells from Wharton's jelly (WJ) in the human umbilical cord also possesses various advantages. Compared to other sources of MSCs, Wharton's jelly MSCs (WJ-MSCs) display greater expansion capacity, a higher rate of proliferation, reinforced neurotrophic factors and a stronger potency to default neuronal lineage differentiation. Although these cells are characterized by exceptionally low immunogenicity, they have high neuroprotective potential and appear as a superior source for the application of MSCs without ethical limitations (158–160). Sharif et al. confirmed that WJ-MSCs could efficiently deliver exogenous miR-124 to U87 GBM cells *via* exosomes, ameliorating GBM cells' chemosensitivity to TMZ and decreasing proliferation and migration of GBM cells. Mechanically, mitigated expression of cyclin-dependent kinase 6 (CDK6) by the delivered miR-124 diminished the proliferation of GBM cells. Besides, the migration of GBM cells was attributed to the inhibition of IQ motif containing GTPase activating protein 1 ((IQGAP1), laminin c1 (LAMC1) and integrin b1 (ITGB1). At the same time, miR-124 also governed the chemosensitivity of GBM cells by targeting R-Ras and N-Ras (146). These studies suggest that MSCs could naturally package anti-tumor miRNAs into exosomes, illustrating their considerable potential for therapeutic applications. Nevertheless, many in-depth studies are required before these therapeutic strategies are available for clinical usage.

DATABASES ASSOCIATED WITH EXOSOMAL miRNAs

Exosomal miRNAs are key factors in causing various types of cancers, including gliomas. Therefore, it has attracted attention. In recent years, a series of databases linked to miRNAs have been developed, offering information concerning miRNAs and their targets. Deep base database can be used for the comprehensive annotation and mining of small RNAs containing miRNAs, lncRNAs and circRNAs sequencing from transcriptomic data. Thus, the expression of diverse non-coding RNAs and downloading data can be viewed (161). TargetScan (162) and PicTar (163) offer miRNA target predictions by relying on the complementarity between sequence and target sites, emphasizing the perfect base pairing within the seed region and sequence conservation. miRbase is a primary public repository where published miRNA sequences and annotation are archived, and a target gene prediction service is also provided (164). MiRDB, an online platform for miRNA target prediction and functional annotations, uses common features related to miRNA binding and target down-regulation, enabling the identification and prediction of miRNA targets with machine-learning methods (165). MicroRNA appears as a comprehensive resource of miRNA target predictions and expression profiles. It is implemented by miRanda algorithm, which combines current biological knowledge regarding target rules and the application of an up-to-date compendium of mammalian miRNAs (166). Hsu and colleagues developed an integrated resource, miRNAMap 2.0, which was helpful to elucidate the miRNA/target association, especially for humans, by employing three computational tools including Miranda, RNAhybrid and TargetScan to verify miRNA targets within 3'-UTR of the gene and known miRNA targets (167).

Moreover, some databases presented evidence for experimentally verifying miRNAs and their target genes. To this end, DIANA-TarBase, as a manually curated database, contains experimentally verified miRNA-target interactions, with detailed information concerning meta-data, experimental methodologies and conditions (168). MiRWalk offers predicted and validated information about miRNA-targe interaction and allows researchers to verify novel miRNA targets in the 3′-UTR and other regions of the known genes (169). Yang et al. introduced a novel database, namely starBase, which includes high-throughput sequencing data derived from 21 Argonaute CLIP-Seq and 10 Degradome-Seq experiments performed in 6 organisms. This database can contribute to the comprehensive investigation of miRNA-target interaction maps (170). miRecords, an integrated resource providing animal miRNA-target gene prediction, hosts a large and high-quality database of experimental tested miRNA-target interactions, which emphasizes the systematic and structured experimental documentation for each interaction (171).

CONCLUSION AND PERSPECTIVE

Exosomes, as a sub-group of EVs, serve as major conduits for cell-to-cell communication. Intercellular signal transduction *via* shuttling molecular cargo mediates the physiologic and pathophysiologic processes of diverse recipient cells. According to current findings, miRNAs can be selectively absorbed into exosomes and serve essential roles in the proliferation, invasion and migration, angiogenesis, therapeutic resistance and immune suppression of gliomas. Furthermore, the fact that exosomes carry many bioactive substances and can easily pass-through biological barriers, including BBB. Thus, they have great potential for clinical application, covering diagnosis, prognosis, and therapy.

Although the outlooks of exosomal miRNAs in the clinical application are broad, there are some challenges. For instance, standard technology is a must for the isolation and purification of exosomes. Exosomes in various body fluids often represent a heterogeneous group of vesicles, the origin of which is unknown. Consequently, the identification and isolation of the exosomes associated with specific tumors are extremely critical. However, this could be difficult to realize, as multiple approaches for isolation have their own merits and demerits. Additionally, the maximum use, normalization and quantitation of exosomes are still problems, as the number of genetic materials in biofluid exosomes is limited. More detailed investigations are required to broaden our current knowledge about exosome biogenesis, secretion and uptake, and specific sorting mechanisms of exosomal miRNAs. If we work out mechanisms underlying these complex processes, we may readily manipulate the exosomes, pack miRNAs, proteins or DNA of interest, and target exosomes to specific cell types or tissues, thus malignant glioma patients can be effectively treated. Finally, large-scale prospective studies are needed to obtain results with high reproducibility and substantiate the efficacy and safety of exosomal biomarkers management in patients. In conclusion, with the continuous understanding of these unknown substances, exosomes will exhibit increasing application value in clinical diagnosis, prognosis and therapy of cancers.

AUTHOR CONTRIBUTIONS

Conception and design: JP, QL, ZX, YY, and MZ. Writing, review, and/or revision of the manuscript: QL, YC, BP, JL, and WZ. Administrative, technical, or material support: FK, QH, and MZ. All authors approved final version of manuscript.

FUNDING

This study is supported by grants from the Science and Technology Innovation Program of Hunan Province (2021RC3029), the China Postdoctoral Science Foundation (2021T140754, 2020M672521), the Natural Science Foundation of Hunan Province (2020JJ5934), and the Postdoctoral Science Foundation of Central South University (248485).

ACKNOWLEDGMENTS

We thank the Language Editing Service of KetengEdit for assistance with the language editing.

REFERENCES

1. Chen X, Yan Y, Zhou J, Huo L, Qian L, Zeng S, et al. Clinical Prognostic Value of Isocitrate Dehydrogenase Mutation, O-6-Methylguanine-DNA Methyltransferase Promoter Methylation, and 1p19q Co-Deletion in Glioma Patients. *Ann Trans Med* (2019) 7(20):541. doi: 10.21037/atm.2019.09.126
2. Yan Y, Zeng S, Gong Z, Xu Z. Clinical Implication of Cellular Vaccine in Glioma: Current Advances and Future Prospects. *J Exp Clin Cancer Res CR* (2020) 39(1):257. doi: 10.1186/s13046-020-01778-6
3. Cheng Q, Huang C, Cao H, Lin J, Gong X, Li J, et al. A Novel Prognostic Signature of Transcription Factors for the Prediction in Patients With GBM. *Front Genet* (2019) 10:906. doi: 10.3389/fgene.2019.00906
4. Liu B, Liu J, Liao Y, Jin C, Zhang Z, Zhao J, et al. Identification of SEC61G as a Novel Prognostic Marker for Predicting Survival and Response to Therapies in Patients With Glioblastoma. *Med Sci Monit Int Med J Exp Clin Res* (2019) 25:3624–35. doi: 10.12659/msm.916648
5. Lapointe S, Perry A, Butowski NA. Primary Brain Tumours in Adults. *Lancet (Lond Engl)* (2018) 392(10145):432–46. doi: 10.1016/s0140-6736(18)30990-5
6. Wion D. Therapeutic Dormancy to Delay Postsurgical Glioma Recurrence: The Past, Present and Promise of Focal Hypothermia. *J Neurooncol* (2017) 133(3):447–54. doi: 10.1007/s11060-017-2471-3
7. Gurley SN, Abidi AH, Allison P, Guan P, Duntsch C, Robertson JH, et al. Mechanism of Anti-Glioma Activity and *In Vivo* Efficacy of the Cannabinoid Ligand KM-233. *J Neurooncol* (2012) 110(2):163–77. doi: 10.1007/s11060-012-0958-5
8. Alifieris C, Trafalis DT. Glioblastoma Multiforme: Pathogenesis and Treatment. *Pharmacol Ther* (2015) 152:63–82. doi: 10.1016/j.pharmthera.2015.05.005
9. Xu Z, Zeng S, Gong Z, Yan Y. Exosome-Based Immunotherapy: A Promising Approach for Cancer Treatment. *Mol Cancer* (2020) 19(1):160. doi: 10.1186/s12943-020-01278-3
10. Zhong Y, Li H, Li P, Chen Y, Zhang M, Yuan Z, et al. Exosomes: A New Pathway for Cancer Drug Resistance. *Front Oncol* (2021) 11:743556. doi: 10.3389/fonc.2021.743556
11. Kumar P, Becker JC, Gao K, Carney RP, Lankford L, Keller BA, et al. Neuroprotective Effect of Placenta-Derived Mesenchymal Stromal Cells: Role of Exosomes. *FASEB J Off Publ Fed Am Soc Exp Biol* (2019) 33(5):5836–49. doi: 10.1096/fj.201800972R
12. Phan J, Kumar P, Hao D, Gao K, Farmer D, Wang A. Engineering Mesenchymal Stem Cells to Improve Their Exosome Efficacy and Yield for Cell-Free Therapy. *J Extracell Vesicles* (2018) 7(1):1522236. doi: 10.1080/20013078.2018.1522236
13. Kowal J, Tkach M, Théry C. Biogenesis and Secretion of Exosomes. *Curr Opin Cell Biol* (2014) 29:116–25. doi: 10.1016/j.ceb.2014.05.004
14. Tkach M, Théry C. Communication by Extracellular Vesicles: Where We Are and Where We Need to Go. *Cell* (2016) 164(6):1226–32. doi: 10.1016/j.cell.2016.01.043
15. Milane L, Singh A, Mattheolabakis G, Suresh M, Amiji MM. Exosome Mediated Communication Within the Tumor Microenvironment. *J Cont Rel Off J Cont Release Soc* (2015) 219:278–94. doi: 10.1016/j.jconrel.2015.06.029
16. Liu Q, Peng F, Chen J. The Role of Exosomal MicroRNAs in the Tumor Microenvironment of Breast Cancer. *Int J Mol Sci* (2019) 20(16):3884. doi: 10.3390/ijms20163884
17. Logozzi M, Mizzoni D, Di Raimo R, Fais S. Exosomes: A Source for New and Old Biomarkers in Cancer. *Cancers* (2020) 12(9):2566. doi: 10.3390/cancers12092566
18. André-Grégoire G, Gavard J. Spitting Out the Demons: Extracellular Vesicles in Glioblastoma. *Cell Adhes Migr* (2017) 11(2):164–72. doi: 10.1080/19336918.2016.1247145
19. Bartel DP. MicroRNAs: Target Recognition and Regulatory Functions. *Cell* (2009) 136(2):215–33. doi: 10.1016/j.cell.2009.01.002
20. Lu TX, Rothenberg ME. MicroRNA. *J Allergy Clin Immunol* (2018) 141(4):1202–7. doi: 10.1016/j.jaci.2017.08.034
21. Kulkarni B, Kirave P, Gondaliya P, Jash K, Jain A, Tekade RK, et al. Exosomal miRNA in Chemoresistance, Immune Evasion, Metastasis and Progression of Cancer. *Drug Discov Today* (2019) 24(10):2058–67. doi: 10.1016/j.drudis.2019.06.010
22. Ghaemmaghami AB, Mahjoubin-Tehran M, Movahedpour A, Morshedi K, Sheida A, Taghavi SP, et al. Role of Exosomes in Malignant Glioma: microRNAs and Proteins in Pathogenesis and Diagnosis. *Cell Commun Signal CCS* (2020) 18(1):120. doi: 10.1186/s12964-020-00623-9
23. Saadatpour L, Fadaee E, Fadaei S, Nassiri Mansour R, Mohammadi M, Mousavi SM, et al. Glioblastoma: Exosome and microRNA as Novel Diagnosis Biomarkers. *Cancer Gene Ther* (2016) 23(12):415–8. doi: 10.1038/cgt.2016.48
24. Lan F, Qing Q, Pan Q, Hu M, Yu H, Yue X. Serum Exosomal miR-301a as a Potential Diagnostic and Prognostic Biomarker for Human Glioma. *Cell Oncol (Dordrecht)* (2018) 41(1):25–33. doi: 10.1007/s13402-017-0355-3
25. Figueroa J, Phillips LM, Shahar T, Hossain A, Gumin J, Kim H, et al. Exosomes From Glioma-Associated Mesenchymal Stem Cells Increase the Tumorigenicity of Glioma Stem-Like Cells *via* Transfer of miR-1587. *Cancer Res* (2017) 77(21):5808–19. doi: 10.1158/0008-5472.Can-16-2524
26. Li X, Guan J, Jiang Z, Cheng S, Hou W, Yao J, et al. Microglial Exosome miR-7239-3p Promotes Glioma Progression by Regulating Circadian Genes. *Neurosci Bull* (2021) 37(4):497–510. doi: 10.1007/s12264-020-00626-z
27. Huang S, Xue P, Han X, Zhang C, Yang L, Liu L, et al. Exosomal miR-130b-3p Targets SIK1 to Inhibit Medulloblastoma Tumorigenesis. *Cell Death Dis* (2020) 11(6):408. doi: 10.1038/s41419-020-2621-y
28. Xue P, Huang S, Han X, Zhang C, Yang L, Xiao W, et al. Exosomal miR-101-3p and miR-423-5p Inhibit Medulloblastoma Tumorigenesis Through Targeting FOXP4 and EZH2. *Cell Death Differ* (2021). doi: 10.1038/s41418-021-00838-4
29. Cai Q, Zhu A, Gong L. Exosomes of Glioma Cells Deliver miR-148a to Promote Proliferation and Metastasis of Glioblastoma via Targeting CADM1. *Bull Cancer* (2018) 105(7-8):643–51. doi: 10.1016/j.bulcan.2018.05.003
30. Qian M, Chen Z, Guo X, Wang S, Zhang Z, Qiu W, et al. Exosomes Derived From Hypoxic Glioma Deliver miR-1246 and miR-10b-5p to Normoxic Glioma Cells to Promote Migration and Invasion. *Lab Investig J Tech Methods Pathol* (2021) 101(5):612–24. doi: 10.1038/s41374-020-00522-0
31. Zhu LY, Wu XY, Liu XD, Zheng DF, Li HS, Yang B, et al. Aggressive Medulloblastoma-Derived Exosomal miRNAs Promote *In Vitro* Invasion and Migration of Tumor Cells *Via* Ras/MAPK Pathway. *J Neuropathol Exp Neurol* (2020) 79(7):734–45. doi: 10.1093/jnen/nlaa041
32. Yao J, Wang Z, Cheng Y, Ma C, Zhong Y, Xiao Y, et al. M2 Macrophage-Derived Exosomal microRNAs Inhibit Cell Migration and Invasion in Gliomas Through PI3K/AKT/mTOR Signaling Pathway. *J Trans Med* (2021) 19(1):99. doi: 10.1186/s12967-021-02766-w
33. Bronisz A, Wang Y, Nowicki MO, Peruzzi P, Ansari K, Ogawa D, et al. Extracellular Vesicles Modulate the Glioblastoma Microenvironment *via* a Tumor Suppression Signaling Network Directed by miR-1. *Cancer Res* (2014) 74(3):738–50. doi: 10.1158/0008-5472.Can-13-2650
34. Chen X, Yang F, Zhang T, Wang W, Xi W, Li Y, et al. MiR-9 Promotes Tumorigenesis and Angiogenesis and is Activated by MYC and OCT4 in Human Glioma. *J Exp Clin Cancer Res CR* (2019) 38(1):99. doi: 10.1186/s13046-019-1078-2
35. Wang M, Zhao Y, Yu ZY, Zhang RD, Li SA, Zhang P, et al. Glioma Exosomal microRNA-148a-3p Promotes Tumor Angiogenesis Through Activating the EGFR/MAPK Signaling Pathway *via* Inhibiting ERRFI1. *Cancer Cell Int* (2020) 20:518. doi: 10.1186/s12935-020-01566-4
36. Li J, Yuan H, Xu H, Zhao H, Xiong N. Hypoxic Cancer-Secreted Exosomal miR-182-5p Promotes Glioblastoma Angiogenesis by Targeting Kruppel-Like Factor 2 and 4. *Mol Cancer Res MCR* (2020) 18(8):1218–31. doi: 10.1158/1541-7786.Mcr-19-0725
37. Sun X, Ma X, Wang J, Zhao Y, Wang Y, Bihl JC, et al. Glioma Stem Cells-Derived Exosomes Promote the Angiogenic Ability of Endothelial Cells Through miR-21/VEGF Signal. *Oncotarget* (2017) 8(22):36137–48. doi: 10.18632/oncotarget.16661
38. Wang ZF, Liao F, Wu H, Dai J. Glioma Stem Cells-Derived Exosomal miR-26a Promotes Angiogenesis of Microvessel Endothelial Cells in Glioma. *J Exp Clin Cancer Res CR* (2019) 38(1):201. doi: 10.1186/s13046-019-1181-4
39. Jiang J, Lu J, Wang X, Sun B, Liu X, Ding Y, et al. Glioma Stem Cell-Derived Exosomal miR-944 Reduces Glioma Growth and Angiogenesis by Inhibiting

AKT/ERK Signaling. *Aging* (2021) 13(15):19243–59. doi: 10.18632/aging.203243
40. Yin J, Zeng A, Zhang Z, Shi Z, Yan W, You Y. Exosomal Transfer of miR-1238 Contributes to Temozolomide-Resistance in Glioblastoma. *EBioMedicine* (2019) 42:238–51. doi: 10.1016/j.ebiom.2019.03.016
41. Zeng A, Wei Z, Yan W, Yin J, Huang X, Zhou X, et al. Exosomal Transfer of miR-151a Enhances Chemosensitivity to Temozolomide in Drug-Resistant Glioblastoma. *Cancer Lett* (2018) 436:10–21. doi: 10.1016/j.canlet.2018.08.004
42. Yang JK, Yang JP, Tong J, Jing SY, Fan B, Wang F, et al. Exosomal miR-221 Targets DNM3 to Induce Tumor Progression and Temozolomide Resistance in Glioma. *J Neurooncol* (2017) 131(2):255–65. doi: 10.1007/s11060-016-2308-5
43. Yue X, Lan F, Xia T. Hypoxic Glioma Cell-Secreted Exosomal miR-301a Activates Wnt/β-Catenin Signaling and Promotes Radiation Resistance by Targeting Tceal7. *Mol Ther J Am Soc Gene Ther* (2019) 27(11):1939–49. doi: 10.1016/j.ymthe.2019.07.011
44. van der Vos KE, Abels ER, Zhang X, Lai C, Carrizosa E, Oakley D, et al. Directly Visualized Glioblastoma-Derived Extracellular Vesicles Transfer RNA to Microglia/Macrophages in the Brain. *Neuro-Oncology* (2016) 18(1):58–69. doi: 10.1093/neuonc/nov244
45. Yang JK, Liu HJ, Wang Y, Li C, Yang JP, Yang L, et al. Exosomal miR-214-5p Released From Glioblastoma Cells Modulates Inflammatory Response of Microglia After Lipopolysaccharide Stimulation Through Targeting Cxcr5. *CNS Neurol Disord Drug Targets* (2019) 18(1):78–87. doi: 10.2174/1871527317666181105112009
46. Qian M, Wang S, Guo X, Wang J, Zhang Z, Qiu W, et al. Hypoxic Glioma-Derived Exosomes Deliver microRNA-1246 to Induce M2 Macrophage Polarization by Targeting TERF2IP *via* the STAT3 and NF-κb Pathways. *Oncogene* (2020) 39(2):428–42. doi: 10.1038/s41388-019-0996-y
47. Guo X, Qiu W, Liu Q, Qian M, Wang S, Zhang Z, et al. Immunosuppressive Effects of Hypoxia-Induced Glioma Exosomes Through Myeloid-Derived Suppressor Cells *via* the miR-10a/Rora and miR-21/Pten Pathways. *Oncogene* (2018) 37(31):4239–59. doi: 10.1038/s41388-018-0261-9
48. Guo X, Qiu W, Wang J, Liu Q, Qian M, Wang S, et al. Glioma Exosomes Mediate the Expansion and Function of Myeloid-Derived Suppressor Cells Through microRNA-29a/Hbp1 and microRNA-92a/Prkar1a Pathways. *Int J Cancer* (2019) 144(12):3111–26. doi: 10.1002/ijc.32052
49. Qiu W, Guo X, Li B, Wang J, Qi Y, Chen Z, et al. Exosomal miR-1246 From Glioma Patient Body Fluids Drives the Differentiation and Activation of Myeloid-Derived Suppressor Cells. *Mol Ther J Am Soc Gene Ther* (2021) 29(12):3449–64. doi: 10.1016/j.ymthe.2021.06.023
50. Feitelson MA, Arzumanyan A, Kulathinal RJ, Blain SW, Holcombe RF, Mahajna J, et al. Sustained Proliferation in Cancer: Mechanisms and Novel Therapeutic Targets. *Semin Cancer Biol* (2015) 35 Suppl(Suppl):S25–54. doi: 10.1016/j.semcancer.2015.02.006
51. Duff D, Long A. Roles for RACK1 in Cancer Cell Migration and Invasion. *Cell Signal* (2017) 35:250–5. doi: 10.1016/j.cellsig.2017.03.005
52. Liu CA, Chang CY, Hsueh KW, Su HL, Chiou TW, Lin SZ, et al. Migration/Invasion of Malignant Gliomas and Implications for Therapeutic Treatment. *Int J Mol Sci* (2018) 19(4):1115. doi: 10.3390/ijms19041115
53. Vollmann-Zwerenz A, Leidgens V, Feliciello G, Klein CA, Hau P. Tumor Cell Invasion in Glioblastoma. *Int J Mol Sci* (2020) 21(6):1932. doi: 10.3390/ijms21061932
54. Lu X, Kang Y. Hypoxia and Hypoxia-Inducible Factors: Master Regulators of Metastasis. *Clin Cancer Res Off J Am Assoc Cancer Res* (2010) 16(24):5928–35. doi: 10.1158/1078-0432.Ccr-10-1360
55. Pennacchietti S, Michieli P, Galluzzo M, Mazzone M, Giordano S, Comoglio PM. Hypoxia Promotes Invasive Growth by Transcriptional Activation of the Met Protooncogene. *Cancer Cell* (2003) 3(4):347–61. doi: 10.1016/s1535-6108(03)00085-0
56. Chang Q, Jurisica I, Do T, Hedley DW. Hypoxia Predicts Aggressive Growth and Spontaneous Metastasis Formation From Orthotopically Grown Primary Xenografts of Human Pancreatic Cancer. *Cancer Res* (2011) 71(8):3110–20. doi: 10.1158/0008-5472.Can-10-4049
57. Saman H, Raza SS, Uddin S, Rasul K. Inducing Angiogenesis, a Key Step in Cancer Vascularization, and Treatment Approaches. *Cancers* (2020) 12(5):1172. doi: 10.3390/cancers12051172
58. Shanmugam MK, Warrier S, Kumar AP, Sethi G, Arfuso F. Potential Role of Natural Compounds as Anti-Angiogenic Agents in Cancer. *Curr Vasc Pharmacol* (2017) 15(6):503–19. doi: 10.2174/1570161115666170713094319
59. He Z, Ruan X, Liu X, Zheng J, Liu Y, Liu L, et al. FUS/circ_002136/miR-138-5p/SOX13 Feedback Loop Regulates Angiogenesis in Glioma. *J Exp Clin Cancer Res CR* (2019) 38(1):65. doi: 10.1186/s13046-019-1065-7
60. Li T, Kang G, Wang T, Huang H. Tumor Angiogenesis and Anti-Angiogenic Gene Therapy for Cancer. *Oncol Lett* (2018) 16(1):687–702. doi: 10.3892/ol.2018.8733
61. Itatani Y, Kawada K, Yamamoto T, Sakai Y. Resistance to Anti-Angiogenic Therapy in Cancer-Alterations to Anti-VEGF Pathway. *Int J Mol Sci* (2018) 19(4):1232. doi: 10.3390/ijms19041232
62. Wang Y, Wang L, Chen C, Chu X. New Insights Into the Regulatory Role of microRNA in Tumor Angiogenesis and Clinical Implications. *Mol Cancer* (2018) 17(1):22. doi: 10.1186/s12943-018-0766-4
63. Zhang G, Zhang Y, Cheng S, Wu Z, Liu F, Zhang J. CD133 Positive U87 Glioblastoma Cells-Derived Exosomal microRNAs in Hypoxia- Versus Normoxia-Microenviroment. *J Neurooncol* (2017) 135(1):37–46. doi: 10.1007/s11060-017-2566-x
64. Liu S, Sun J, Lan Q. Glioblastoma Microvesicles Promote Endothelial Cell Proliferation Through Akt/beta-Catenin Pathway. *Int J Clin Exp Pathol* (2014) 7(8):4857–66.
65. Nohata N, Hanazawa T, Enokida H, Seki N. microRNA-1/133a and microRNA-206/133b Clusters: Dysregulation and Functional Roles in Human Cancers. *Oncotarget* (2012) 3(1):9–21. doi: 10.18632/oncotarget.424
66. Emami Nejad A, Najafgholian S, Rostami A, Sistani A, Shojaeifar S, Esparvarinha M, et al. The Role of Hypoxia in the Tumor Microenvironment and Development of Cancer Stem Cell: A Novel Approach to Developing Treatment. *Cancer Cell Int* (2021) 21(1):62. doi: 10.1186/s12935-020-01719-5
67. Guo Z, Wang X, Yang Y, Chen W, Zhang K, Teng B, et al. Hypoxic Tumor-Derived Exosomal Long Noncoding RNA UCA1 Promotes Angiogenesis *via* miR-96-5p/AMOTL2 in Pancreatic Cancer. *Mol Ther Nucleic Acids* (2020) 22:179–95. doi: 10.1016/j.omtn.2020.08.021
68. Wang Y, Cen A, Yang Y, Ye H, Li J, Liu S, et al. miR-181a, Delivered by Hypoxic PTC-Secreted Exosomes, Inhibits DACT2 by Downregulating MLL3, Leading to YAP-VEGF-Mediated Angiogenesis. *Mol Ther Nucleic Acids* (2021) 24:610–21. doi: 10.1016/j.omtn.2021.02.027
69. Sampetrean O, Saya H. Characteristics of Glioma Stem Cells. *Brain Tumor Pathol* (2013) 30(4):209–14. doi: 10.1007/s10014-013-0141-5
70. Bao S, Wu Q, Sathornsumetee S, Hao Y, Li Z, Hjelmeland AB, et al. Stem Cell-Like Glioma Cells Promote Tumor Angiogenesis Through Vascular Endothelial Growth Factor. *Cancer Res* (2006) 66(16):7843–8. doi: 10.1158/0008-5472.Can-06-1010
71. Huang Z, Cheng L, Guryanova OA, Wu Q, Bao S. Cancer Stem Cells in Glioblastoma–Molecular Signaling and Therapeutic Targeting. *Protein Cell* (2010) 1(7):638–55. doi: 10.1007/s13238-010-0078-y
72. Folkins C, Shaked Y, Man S, Tang T, Lee CR, Zhu Z, et al. Glioma Tumor Stem-Like Cells Promote Tumor Angiogenesis and Vasculogenesis *via* Vascular Endothelial Growth Factor and Stromal-Derived Factor 1. *Cancer Res* (2009) 69(18):7243–51. doi: 10.1158/0008-5472.Can-09-0167
73. Treps L, Perret R, Edmond S, Ricard D, Gavard J. Glioblastoma Stem-Like Cells Secrete the Pro-Angiogenic VEGF-A Factor in Extracellular Vesicles. *J Extracell Vesicles* (2017) 6(1):1359479. doi: 10.1080/20013078.2017.1359479
74. Skog J, Würdinger T, van Rijn S, Meijer DH, Gainche L, Sena-Esteves M, et al. Glioblastoma Microvesicles Transport RNA and Proteins That Promote Tumour Growth and Provide Diagnostic Biomarkers. *Nat Cell Biol* (2008) 10(12):1470–6. doi: 10.1038/ncb1800
75. Daniel P, Sabri S, Chaddad A, Meehan B, Jean-Claude B, Rak J, et al. Temozolomide Induced Hypermutation in Glioma: Evolutionary Mechanisms and Therapeutic Opportunities. *Front Oncol* (2019) 9:41. doi: 10.3389/fonc.2019.00041
76. Chan XH, Nama S, Gopal F, Rizk P, Ramasamy S, Sundaram G, et al. Targeting Glioma Stem Cells by Functional Inhibition of a Prosurvival oncomiR-138 in Malignant Gliomas. *Cell Rep* (2012) 2(3):591–602. doi: 10.1016/j.celrep.2012.07.012

77. Li I, Nabet BY. Exosomes in the Tumor Microenvironment as Mediators of Cancer Therapy Resistance. *Mol Cancer* (2019) 18(1):32. doi: 10.1186/s12943-019-0975-5
78. Movahedpour A, Khatami SH, Khorsand M, Salehi M, Savardashtaki A, Mirmajidi SH, et al. Exosomal Noncoding RNAs: Key Players in Glioblastoma Drug Resistance. *Mol Cell Biochem* (2021) 476(11):4081–92. doi: 10.1007/s11010-021-04221-2
79. Yasaswi PS, Shetty K, Yadav KS. Temozolomide Nano Enabled Medicine: Promises Made by the Nanocarriers in Glioblastoma Therapy. *J Cont Rel Off J Cont Release Soc* (2021) 336:549–71. doi: 10.1016/j.jconrel.2021.07.003
80. Kondo N, Takahashi A, Mori E, Noda T, Zdzienicka MZ, Thompson LH, et al. FANCD1/BRCA2 Plays Predominant Role in the Repair of DNA Damage Induced by ACNU or TMZ. *PloS One* (2011) 6(5):e19659. doi: 10.1371/journal.pone.0019659
81. Jiapaer S, Furuta T, Tanaka S, Kitabayashi T, Nakada M. Potential Strategies Overcoming the Temozolomide Resistance for Glioblastoma. *Neurol Med Chir* (2018) 58(10):405–21. doi: 10.2176/nmc.ra.2018-0141
82. Yang C, Robbins PD. The Roles of Tumor-Derived Exosomes in Cancer Pathogenesis. *Clin Dev Immunol* (2011) 2011:842849. doi: 10.1155/2011/842849
83. Quail DF, Joyce JA. The Microenvironmental Landscape of Brain Tumors. *Cancer Cell* (2017) 31(3):326–41. doi: 10.1016/j.ccell.2017.02.009
84. Chen H, Li M, Guo Y, Zhong Y, He Z, Xu Y, et al. Immune Response in Glioma's Microenvironment. *Innov Surg Sci* (2020) 5(3-4):20190001. doi: 10.1515/iss-2019-0001
85. Zhang N, Dai Z, Wu W, Wang Z, Cao H, Zhang Y, et al. The Predictive Value of Monocytes in Immune Microenvironment and Prognosis of Glioma Patients Based on Machine Learning. *Front Immunol* (2021) 12:656541. doi: 10.3389/fimmu.2021.656541
86. De Leo A, Ugolini A, Veglia F. Myeloid Cells in Glioblastoma Microenvironment. *Cells* (2020) 10(1):18. doi: 10.3390/cells10010018
87. Locarno CV, Simonelli M, Carenza C, Capucetti A, Stanzani E, Lorenzi E, et al. Role of Myeloid Cells in the Immunosuppressive Microenvironment in Gliomas. *Immunobiology* (2020) 225(1):151853. doi: 10.1016/j.imbio.2019.10.002
88. Grabowski MM, Sankey EW, Ryan KJ, Chongsathidkiet P, Lorrey SJ, Wilkinson DS, et al. Immune Suppression in Gliomas. *J Neurooncol* (2021) 151(1):3–12. doi: 10.1007/s11060-020-03483-y
89. Lanza M, Casili G, Campolo M, Paterniti I, Colarossi C, Mare M, et al. Immunomodulatory Effect of Microglia-Released Cytokines in Gliomas. *Brain Sci* (2021) 11(4):466. doi: 10.3390/brainsci11040466
90. da Fonseca AC, Badie B. Microglia and Macrophages in Malignant Gliomas: Recent Discoveries and Implications for Promising Therapies. *Clin Dev Immunol* (2013) 2013:264124. doi: 10.1155/2013/264124
91. Pan Y, Yu Y, Wang X, Zhang T. Tumor-Associated Macrophages in Tumor Immunity. *Front Immunol* (2020) 11:583084. doi: 10.3389/fimmu.2020.583084
92. Ricketts TD, Prieto-Dominguez N, Gowda PS, Ubil E. Mechanisms of Macrophage Plasticity in the Tumor Environment: Manipulating Activation State to Improve Outcomes. *Front Immunol* (2021) 12:642285. doi: 10.3389/fimmu.2021.642285
93. Law AMK, Valdes-Mora F, Gallego-Ortega D. Myeloid-Derived Suppressor Cells as a Therapeutic Target for Cancer. *Cells* (2020) 9(3):561. doi: 10.3390/cells9030561
94. Xiang X, Poliakov A, Liu C, Liu Y, Deng ZB, Wang J, et al. Induction of Myeloid-Derived Suppressor Cells by Tumor Exosomes. *Int J Cancer* (2009) 124(11):2621–33. doi: 10.1002/ijc.24249
95. Li L, Zhang J, Diao W, Wang D, Wei Y, Zhang CY, et al. MicroRNA-155 and MicroRNA-21 Promote the Expansion of Functional Myeloid-Derived Suppressor Cells. *J Immunol (Baltimore Md 1950)* (2014) 192(3):1034–43. doi: 10.4049/jimmunol.1301309
96. Smirniotopoulos JG, Murphy FM, Rushing EJ, Rees JH, Schroeder JW. Patterns of Contrast Enhancement in the Brain and Meninges. *Radiographics Rev Publ Radiol Soc North Am Inc* (2007) 27(2):525–51. doi: 10.1148/rg.272065155
97. Sorensen AG, Batchelor TT, Wen PY, Zhang WT, Jain RK. Response Criteria for Glioma. *Nat Clin Pract Oncol* (2008) 5(11):634–44. doi: 10.1038/ncponc1204
98. Teodori L, Albertini MC, Uguccioni F, Falcieri E, Rocchi MB, Battistelli M, et al. Static Magnetic Fields Affect Cell Size, Shape, Orientation, and Membrane Surface of Human Glioblastoma Cells, as Demonstrated by Electron, Optic, and Atomic Force Microscopy. *Cytom Part A J Int Soc Anal Cytol* (2006) 69(2):75–85. doi: 10.1002/cyto.a.20208
99. Brandsma D, Stalpers L, Taal W, Sminia P, van den Bent MJ. Clinical Features, Mechanisms, and Management of Pseudoprogression in Malignant Gliomas. *Lancet Oncol* (2008) 9(5):453–61. doi: 10.1016/s1470-2045(08)70125-6
100. Weller M, Pfister SM, Wick W, Hegi ME, Reifenberger G, Stupp R. Molecular Neuro-Oncology in Clinical Practice: A New Horizon. *Lancet Oncol* (2013) 14(9):e370–9. doi: 10.1016/s1470-2045(13)70168-2
101. Westphal M, Lamszus K. Circulating Biomarkers for Gliomas. *Nat Rev Neurol* (2015) 11(10):556–66. doi: 10.1038/nrneurol.2015.171
102. Basu B, Ghosh MK. Extracellular Vesicles in Glioma: From Diagnosis to Therapy. *BioEssays News Rev Mol Cell Dev Biol* (2019) 41(7):e1800245. doi: 10.1002/bies.201800245
103. Han C, Sun X, Liu L, Jiang H, Shen Y, Xu X, et al. Exosomes and Their Therapeutic Potentials of Stem Cells. *Stem Cells Int* (2016) 2016:7653489. doi: 10.1155/2016/7653489
104. Dubois LG, Campanati L, Righy C, D'Andrea-Meira I, Spohr TC, Porto-Carreiro I, et al. Gliomas and the Vascular Fragility of the Blood Brain Barrier. *Front Cell Neurosci* (2014) 8:418. doi: 10.3389/fncel.2014.00418
105. Roma-Rodrigues C, Fernandes AR, Baptista PV. Exosome in Tumour Microenvironment: Overview of the Crosstalk Between Normal and Cancer Cells. *BioMed Res Int* (2014) 2014:179486. doi: 10.1155/2014/179486
106. Touat M, Duran-Peña A, Alentorn A, Lacroix L, Massard C, Idbaih A. Emerging Circulating Biomarkers in Glioblastoma: Promises and Challenges. *Expert Rev Mol Diagn* (2015) 15(10):1311–23. doi: 10.1586/14737159.2015.1087315
107. Manterola L, Guruceaga E, Gállego Pérez-Larraya J, González-Huarriz M, Jauregui P, Tejada S, et al. A Small Noncoding RNA Signature Found in Exosomes of GBM Patient Serum as a Diagnostic Tool. *Neuro-Oncology* (2014) 16(4):520–7. doi: 10.1093/neuonc/not218
108. Ebrahimkhani S, Vafaee F, Hallal S, Wei H, Lee MYT, Young PE, et al. Deep Sequencing of Circulating Exosomal microRNA Allows non-Invasive Glioblastoma Diagnosis. *NPJ Precis Oncol* (2018) 2:28. doi: 10.1038/s41698-018-0071-0
109. Santangelo A, Imbrucè P, Gardenghi B, Belli L, Agushi R, Tamanini A, et al. A microRNA Signature From Serum Exosomes of Patients With Glioma as Complementary Diagnostic Biomarker. *J Neurooncol* (2018) 136(1):51–62. doi: 10.1007/s11060-017-2639-x
110. Wang S, Xu Z, Zhang C, Yu R, Jiang J, Wang C, et al. High-Throughput Sequencing-Based Identification of Serum Exosomal Differential miRNAs in High-Grade Glioma and Intracranial Lymphoma. *BioMed Res Int* (2020) 2020:2102645. doi: 10.1155/2020/2102645
111. Shao N, Xue L, Wang R, Luo K, Zhi F, Lan Q. miR-454-3p Is an Exosomal Biomarker and Functions as a Tumor Suppressor in Glioma. *Mol Cancer Ther* (2019) 18(2):459–69. doi: 10.1158/1535-7163.Mct-18-0725
112. Lan F, Yue X, Xia T. Exosomal microRNA-210 Is a Potentially non-Invasive Biomarker for the Diagnosis and Prognosis of Glioma. *Oncol Lett* (2020) 19(3):1967–74. doi: 10.3892/ol.2020.11249
113. Hinman DD, Griffith BP, Wahlquist GI, Booss J. Monocyte-Mediated Immunosuppression in Chronic Multiple Sclerosis: Implications for Therapy. *Eur Neurol* (1987) 27(3):133–8. doi: 10.1159/000116145
114. Caponnetto F, Dalla E, Mangoni D, Piazza S, Radovic S, Ius T, et al. The miRNA Content of Exosomes Released From the Glioma Microenvironment Can Affect Malignant Progression. *Biomedicines* (2020) 8(12):564. doi: 10.3390/biomedicines8120564
115. Xu X, Liu Y, Li Y, Chen H, Zhang Y, Liu J, et al. Selective Exosome Exclusion of miR-375 by Glioma Cells Promotes Glioma Progression by Activating the CTGF-EGFR Pathway. *J Exp Clin Cancer Res CR* (2021) 40(1):16. doi: 10.1186/s13046-020-01810-9
116. Tabibkhooei A, Izadpanahi M, Arab A, Zare-Mirzaei A, Minaeian S, Rostami A, et al. Profiling of Novel Circulating microRNAs as a non-Invasive Biomarker in Diagnosis and Follow-Up of High and Low-Grade Gliomas. *Clin Neurol Neurosurg* (2020) 190:105652. doi: 10.1016/j.clineuro.2019.105652

117. Sun J, Sun Z, Gareev I, Yan T, Chen X, Ahmad A, et al. Exosomal miR-2276-5p in Plasma Is a Potential Diagnostic and Prognostic Biomarker in Glioma. *Front Cell Dev Biol* (2021) 9:671202. doi: 10.3389/fcell.2021.671202
118. Akers JC, Ramakrishnan V, Kim R, Skog J, Nakano I, Pingle S, et al. MiR-21 in the Extracellular Vesicles (EVs) of Cerebrospinal Fluid (CSF): A Platform for Glioblastoma Biomarker Development. *PloS One* (2013) 8(10):e78115. doi: 10.1371/journal.pone.0078115
119. Shi R, Wang PY, Li XY, Chen JX, Li Y, Zhang XZ, et al. Exosomal Levels of miRNA-21 From Cerebrospinal Fluids Associated With Poor Prognosis and Tumor Recurrence of Glioma Patients. *Oncotarget* (2015) 6(29):26971–81. doi: 10.18632/oncotarget.4699
120. Zottel A, Šamec N, Kump A, Raspor Dall'Olio LR, Dominkuš P, Romih R, et al. Analysis of miR-9-5p, miR-124-3p, miR-21-5p, miR-138-5p, and miR-1-3p in Glioblastoma Cell Lines and Extracellular Vesicles. *Int J Mol Sci* (2020) 21(22):8491. doi: 10.3390/ijms21228491
121. Li Z, Ye L, Wang L, Quan R, Zhou Y, Li X. Identification of miRNA Signatures in Serum Exosomes as a Potential Biomarker After Radiotherapy Treatment in Glioma Patients. *Ann Diagn Pathol* (2020) 44:151436. doi: 10.1016/j.anndiagpath.2019.151436
122. Olioso D, Caccese M, Santangelo A, Lippi G, Zagonel V, Cabrini G, et al. Serum Exosomal microRNA-21, 222 and 124-3p as Noninvasive Predictive Biomarkers in Newly Diagnosed High-Grade Gliomas: A Prospective Study. *Cancers* (2021) 13(12):3006. doi: 10.3390/cancers13123006
123. Ding C, Yi X, Chen X, Wu Z, You H, Chen X, et al. Warburg Effect-Promoted Exosomal Circ_0072083 Releasing Up-Regulates NANGO Expression Through Multiple Pathways and Enhances Temozolomide Resistance in Glioma. *J Exp Clin Cancer Res CR* (2021) 40(1):164. doi: 10.1186/s13046-021-01942-6
124. Yin K, Liu X. CircMMP1 Promotes the Progression of Glioma Through miR-433/HMGB3 Axis *In Vitro* and *In Vivo*. *IUBMB Life* (2020) 72(11):2508–24. doi: 10.1002/iub.2383
125. Zhang Z, Yin J, Lu C, Wei Y, Zeng A, You Y. Exosomal Transfer of Long non-Coding RNA SBF2-AS1 Enhances Chemoresistance to Temozolomide in Glioblastoma. *J Exp Clin Cancer Res CR* (2019) 38(1):166. doi: 10.1186/s13046-019-1139-6
126. Hao SC, Ma H, Niu ZF, Sun SY, Zou YR, Xia HC. hUC-MSCs Secreted Exosomes Inhibit the Glioma Cell Progression Through PTENP1/miR-10a-5p/PTEN Pathway. *Eur Rev Med Pharmacol Sci* (2019) 23(22):10013–23. doi: 10.26355/eurrev_201911_19568
127. Ha D, Yang N, Nadithe V. Exosomes as Therapeutic Drug Carriers and Delivery Vehicles Across Biological Membranes: Current Perspectives and Future Challenges. *Acta Pharm Sin B* (2016) 6(4):287–96. doi: 10.1016/j.apsb.2016.02.001
128. Li Z, Mbah NE, Maltese WA. Vacuole-Inducing Compounds That Disrupt Endolysosomal Trafficking Stimulate Production of Exosomes by Glioblastoma Cells. *Mol Cell Biochem* (2018) 439(1-2):1–9. doi: 10.1007/s11010-017-3130-x
129. Huntzinger E, Izaurralde E. Gene Silencing by microRNAs: Contributions of Translational Repression and mRNA Decay. *Nat Rev Genet* (2011) 12(2):99–110. doi: 10.1038/nrg2936
130. Wang TX, Tan WL, Huang JC, Cui ZF, Liang RD, Li QC, et al. Identification of Aberrantly Methylated Differentially Expressed Genes Targeted by Differentially Expressed miRNA in Osteosarcoma. *Ann Trans Med* (2020) 8(6):373. doi: 10.21037/atm.2020.02.74
131. Gu J, Zhang J, Huang W, Tao T, Huang Y, Yang L, et al. Activating miRNA-mRNA Network in Gemcitabine-Resistant Pancreatic Cancer Cell Associates With Alteration of Memory CD4(+) T Cells. *Ann Trans Med* (2020) 8(6):279. doi: 10.21037/atm.2020.03.53
132. Jin X, Yuan L, Liu B, Kuang Y, Li H, Li L, et al. Integrated Analysis of circRNA-miRNA-mRNA Network Reveals Potential Prognostic Biomarkers for Radiotherapies With X-Rays and Carbon Ions in non-Small Cell Lung Cancer. *Ann Trans Med* (2020) 8(21):1373. doi: 10.21037/atm-20-2002
133. Silber J, Lim DA, Petritsch C, Persson AI, Maunakea AK, Yu M, et al. miR-124 and miR-137 Inhibit Proliferation of Glioblastoma Multiforme Cells and Induce Differentiation of Brain Tumor Stem Cells. *BMC Med* (2008) 6:14. doi: 10.1186/1741-7015-6-14
134. Broderick JA, Zamore PD. MicroRNA Therapeutics. *Gene Ther* (2011) 18(12):1104–10. doi: 10.1038/gt.2011.50
135. Fareh M, Almairac F, Turchi L, Burel-Vandenbos F, Paquis P, Fontaine D, et al. Cell-Based Therapy Using miR-302-367 Expressing Cells Represses Glioblastoma Growth. *Cell Death Dis* (2017) 8(3):e2713. doi: 10.1038/cddis.2017.117
136. Monfared H, Jahangard Y, Nikkhah M, Mirnajafi-Zadeh J, Mowla SJ. Potential Therapeutic Effects of Exosomes Packed With a miR-21-Sponge Construct in a Rat Model of Glioblastoma. *Front Oncol* (2019) 9:782. doi: 10.3389/fonc.2019.00782
137. Lang FM, Hossain A, Gumin J, Momin EN, Shimizu Y, Ledbetter D, et al. Mesenchymal Stem Cells as Natural Biofactories for Exosomes Carrying miR-124a in the Treatment of Gliomas. *Neuro-Oncology* (2018) 20(3):380–90. doi: 10.1093/neuonc/nox152
138. Yan T, Wu M, Lv S, Hu Q, Xu W, Zeng A, et al. Exosomes Derived From microRNA-512-5p-Transfected Bone Mesenchymal Stem Cells Inhibit Glioblastoma Progression by Targeting JAG1. *Aging* (2021) 13(7):9911–26. doi: 10.18632/aging.202747
139. Zhang Z, Guo X, Guo X, Yu R, Qian M, Wang S, et al. MicroRNA-29a-3p Delivery *via* Exosomes Derived From Engineered Human Mesenchymal Stem Cells Exerts Tumour Suppressive Effects by Inhibiting Migration and Vasculogenic Mimicry in Glioma. *Aging* (2021) 13(4):5055–68. doi: 10.18632/aging.202424
140. Zhang X, Zhang X, Hu S, Zheng M, Zhang J, Zhao J, et al. Identification of miRNA-7 by Genome-Wide Analysis as a Critical Sensitizer for TRAIL-Induced Apoptosis in Glioblastoma Cells. *Nucleic Acids Res* (2017) 45(10):5930–44. doi: 10.1093/nar/gkx317
141. Katakowski M, Buller B, Zheng X, Lu Y, Rogers T, Osobamiro O, et al. Exosomes From Marrow Stromal Cells Expressing miR-146b Inhibit Glioma Growth. *Cancer Lett* (2013) 335(1):201–4. doi: 10.1016/j.canlet.2013.02.019
142. Xu H, Zhao G, Zhang Y, Jiang H, Wang W, Zhao D, et al. Mesenchymal Stem Cell-Derived Exosomal microRNA-133b Suppresses Glioma Progression *via* Wnt/β-Catenin Signaling Pathway by Targeting EZH2. *Stem Cell Res Ther* (2019) 10(1):381. doi: 10.1186/s13287-019-1446-z
143. Kim R, Lee S, Lee J, Kim M, Kim WJ, Lee HW, et al. Exosomes Derived From microRNA-584 Transfected Mesenchymal Stem Cells: Novel Alternative Therapeutic Vehicles for Cancer Therapy. *BMB Rep* (2018) 51(8):406–11. doi: 10.5483/bmbrep.2018.51.8.105
144. Deng SZ, Lai MF, Li YP, Xu CH, Zhang HR, Kuang JG. Human Marrow Stromal Cells Secrete microRNA-375-Containing Exosomes to Regulate Glioma Progression. *Cancer Gene Ther* (2020) 27(3-4):203–15. doi: 10.1038/s41417-019-0079-9
145. Yu L, Gui S, Liu Y, Qiu X, Zhang G, Zhang X, et al. Exosomes Derived From microRNA-199a-Overexpressing Mesenchymal Stem Cells Inhibit Glioma Progression by Down-Regulating AGAP2. *Aging* (2019) 11(15):5300–18. doi: 10.18632/aging.102092
146. Sharif S, Ghahremani MH, Soleimani M. Delivery of Exogenous miR-124 to Glioblastoma Multiform Cells by Wharton's Jelly Mesenchymal Stem Cells Decreases Cell Proliferation and Migration, and Confers Chemosensitivity. *Stem Cell Rev Rep* (2018) 14(2):236–46. doi: 10.1007/s12015-017-9788-3
147. Haraguchi T, Ozaki Y, Iba H. Vectors Expressing Efficient RNA Decoys Achieve the Long-Term Suppression of Specific microRNA Activity in Mammalian Cells. *Nucleic Acids Res* (2009) 37(6):e43. doi: 10.1093/nar/gkp040
148. Bak RO, Hollensen AK, Mikkelsen JG. Managing microRNAs With Vector-Encoded Decoy-Type Inhibitors. *Mol Ther J Am Soc Gene Ther* (2013) 21(8):1478–85. doi: 10.1038/mt.2013.113
149. Mullokandov G, Baccarini A, Ruzo A, Jayaprakash AD, Tung N, Israelow B, et al. High-Throughput Assessment of microRNA Activity and Function Using microRNA Sensor and Decoy Libraries. *Nat Methods* (2012) 9(8):840–6. doi: 10.1038/nmeth.2078
150. Ho IA, Toh HC, Ng WH, Teo YL, Guo CM, Hui KM, et al. Human Bone Marrow-Derived Mesenchymal Stem Cells Suppress Human Glioma Growth Through Inhibition of Angiogenesis. *Stem Cells (Dayton Ohio)* (2013) 31(1):146–55. doi: 10.1002/stem.1247
151. Yang C, Lei D, Ouyang W, Ren J, Li H, Hu J, et al. Conditioned Media From Human Adipose Tissue-Derived Mesenchymal Stem Cells and Umbilical Cord-Derived Mesenchymal Stem Cells Efficiently Induced the Apoptosis and Differentiation in Human Glioma Cell Lines *In Vitro*. *BioMed Res Int* (2014) 2014:109389. doi: 10.1155/2014/109389
152. Reagan MR, Kaplan DL. Concise Review: Mesenchymal Stem Cell Tumor-Homing: Detection Methods in Disease Model Systems. *Stem Cells (Dayton Ohio)* (2011) 29(6):920–7. doi: 10.1002/stem.645

153. Sharma A. Role of Stem Cell Derived Exosomes in Tumor Biology. *Int J Cancer* (2018) 142(6):1086–92. doi: 10.1002/ijc.31089
154. Lou G, Song X, Yang F, Wu S, Wang J, Chen Z, et al. Exosomes Derived From miR-122-Modified Adipose Tissue-Derived MSCs Increase Chemosensitivity of Hepatocellular Carcinoma. *J Hematol Oncol* (2015) 8:122. doi: 10.1186/s13045-015-0220-7
155. Wu H, Mu X, Liu L, Wu H, Hu X, Chen L, et al. Bone Marrow Mesenchymal Stem Cells-Derived Exosomal microRNA-193a Reduces Cisplatin Resistance of non-Small Cell Lung Cancer Cells *via* Targeting LRRC1. *Cell Death Dis* (2020) 11(9):801. doi: 10.1038/s41419-020-02962-4
156. Wu HB, Yang S, Weng HY, Chen Q, Zhao XL, Fu WJ, et al. Autophagy-Induced KDR/VEGFR-2 Activation Promotes the Formation of Vasculogenic Mimicry by Glioma Stem Cells. *Autophagy* (2017) 13 (9):1528–42. doi: 10.1080/15548627.2017.1336277
157. Stuckey DW, Shah K. TRAIL on Trial: Preclinical Advances in Cancer Therapy. *Trends Mol Med* (2013) 19(11):685–94. doi: 10.1016/j.molmed.2013.08.007
158. Drela K, Lech W, Figiel-Dabrowska A, Zychowicz M, Mikula M, Sarnowska A, et al. Enhanced Neuro-Therapeutic Potential of Wharton's Jelly-Derived Mesenchymal Stem Cells in Comparison With Bone Marrow Mesenchymal Stem Cells Culture. *Cytotherapy* (2016) 18(4):497–509. doi: 10.1016/j.jcyt.2016.01.006
159. Hsieh JY, Wang HW, Chang SJ, Liao KH, Lee IH, Lin WS, et al. Mesenchymal Stem Cells From Human Umbilical Cord Express Preferentially Secreted Factors Related to Neuroprotection, Neurogenesis, and Angiogenesis. *PloS One* (2013) 8 (8):e72604. doi: 10.1371/journal.pone.0072604
160. Wang HS, Hung SC, Peng ST, Huang CC, Wei HM, Guo YJ, et al. Mesenchymal Stem Cells in the Wharton's Jelly of the Human Umbilical Cord. *Stem Cells (Dayton Ohio)* (2004) 22(7):1330–7. doi: 10.1634/stemcells.2004-0013
161. Yang JH, Shao P, Zhou H, Chen YQ, Qu LH. Deepbase: A Database for Deeply Annotating and Mining Deep Sequencing Data. *Nucleic Acids Res* (2010) 38(Database issue):D123–30. doi: 10.1093/nar/gkp943
162. Lewis BP, Shih IH, Jones-Rhoades MW, Bartel DP, Burge CB. Prediction of Mammalian microRNA Targets. *Cell* (2003) 115(7):787–98. doi: 10.1016/s0092-8674(03)01018-3
163. Krek A, Grün D, Poy MN, Wolf R, Rosenberg L, Epstein EJ, et al. Combinatorial microRNA Target Predictions. *Nat Genet* (2005) 37 (5):495–500. doi: 10.1038/ng1536
164. Kozomara A, Birgaoanu M, Griffiths-Jones S. Mirbase: From microRNA Sequences to Function. *Nucleic Acids Res* (2019) 47(D1):D155–62. doi: 10.1093/nar/gky1141
165. Wong N, Wang X. miRDB: An Online Resource for microRNA Target Prediction and Functional Annotations. *Nucleic Acids Res* (2015) 43 (Database issue):D146–52. doi: 10.1093/nar/gku1104
166. Betel D, Wilson M, Gabow A, Marks DS, Sander C. The microRNA.Org Resource: Targets and Expression. *Nucleic Acids Res* (2008) 36(Database issue):D149–53. doi: 10.1093/nar/gkm995
167. Hsu SD, Chu CH, Tsou AP, Chen SJ, Chen HC, Hsu PW, et al. Mirnamap 2.0: Genomic Maps of microRNAs in Metazoan Genomes. *Nucleic Acids Res* (2008) 36(Database issue):D165–9. doi: 10.1093/nar/gkm1012
168. Vlachos IS, Paraskevopoulou MD, Karagkouni D, Georgakilas G, Vergoulis T, Kanellos I, et al. DIANA-TarBase V7.0: Indexing More Than Half a Million Experimentally Supported miRNA:mRNA Interactions. *Nucleic Acids Res* (2015) 43(Database issue):D153–9. doi: 10.1093/nar/gku1215
169. Dweep H, Sticht C, Pandey P, Gretz N. Mirwalk–Database: Prediction of Possible miRNA Binding Sites by "Walking" the Genes of Three Genomes. *J Biomed Inf* (2011) 44(5):839–47. doi: 10.1016/j.jbi.2011.05.002
170. Yang JH, Li JH, Shao P, Zhou H, Chen YQ, Qu LH. Starbase: A Database for Exploring microRNA-mRNA Interaction Maps From Argonaute CLIP-Seq and Degradome-Seq Data. *Nucleic Acids Res* (2011) 39(Database issue): D202–9. doi: 10.1093/nar/gkq1056
171. Xiao F, Zuo Z, Cai G, Kang S, Gao X, Li T. Mirecords: An Integrated Resource for microRNA-Target Interactions. *Nucleic Acids Res* (2009) 37 (Database issue):D105–10. doi: 10.1093/nar/gkn851

Conflict of Interest: The authors declare that the research was conducted in the absence of any commercial or financial relationships that could be construed as a potential conflict of interest.

Publisher's Note: All claims expressed in this article are solely those of the authors and do not necessarily represent those of their affiliated organizations, or those of the publisher, the editors and the reviewers. Any product that may be evaluated in this article, or claim that may be made by its manufacturer, is not guaranteed or endorsed by the publisher.

Copyright © 2022 Peng, Liang, Xu, Cai, Peng, Li, Zhang, Kang, Hong, Yan and Zhang. This is an open-access article distributed under the terms of the Creative Commons Attribution License (CC BY). The use, distribution or reproduction in other forums is permitted, provided the original author(s) and the copyright owner(s) are credited and that the original publication in this journal is cited, in accordance with accepted academic practice. No use, distribution or reproduction is permitted which does not comply with these terms.

frontiers in Immunology

ORIGINAL RESEARCH
published: 26 January 2022
doi: 10.3389/fimmu.2021.809808

The Non-N^6-Methyladenosine Epitranscriptome Patterns and Characteristics of Tumor Microenvironment Infiltration and Mesenchymal Transition in Glioblastoma

Jianye Xu[1,2†], Zijie Gao[1,2†], Kaining Liu[1,2], Yang Fan[1,2], Zongpu Zhang[1,2], Hao Xue[1,2], Xing Guo[1,2], Ping Zhang[1,2], Lin Deng[1,2], Shaobo Wang[1,2], Huizhi Wang[1,2], Qingtong Wang[1,2], Rongrong Zhao[1,2] and Gang Li[1,2]*

[1] Department of Neurosurgery, Qilu Hospital, Cheeloo College of Medicine and Institute of Brain and Brain-Inspired Science, Shandong University, Jinan, China, [2] Shandong Key Laboratory of Brain Function Remodeling, Jinan, China

Background: An increasing number of RNA modification types other than N^6-methyladenosine (m^{6}A) modification have been detected. Nonetheless, the probable functions of RNA modifications beyond m^{6}A in the tumor microenvironment (TME), mesenchymal (MES) transition, immunotherapy, and drug sensitivity remain unclear.

Methods: We analyzed the characteristics of 32 non-m^{6}A RNA modification regulators in 539 glioblastoma (GBM) patients and the TME cell infiltration and MES transition patterns. Using principal component analysis, a non-m^{6}A epitranscriptome regulator score (RM score) model was established. We estimated the association between RM score and clinical characteristics, TME status, GBM subtypes, and drug and immunotherapy response.

Results: Three definite non-m^{6}A RNA modification patterns associated with diverse biological pathways and clinical characteristics were identified. The high RM score group was characterized by a poor prognosis, enhanced immune infiltration, and MES subtype. Further analysis indicated that the high RM score group had a lower tumor mutation burden as well as a weaker response to immunotherapy. The higher RM score group may benefit more from drugs targeting the EGFR and WNT signaling pathways.

Conclusion: Our study exposed the potential relationship of non-m^{6}A RNA modification regulators with clinical features, TME status, and GBM subtype and clarified its therapeutic value.

Keywords: glioblastoma, non-m^{6}A RNA modification, tumor microenvironment, mesenchymal transition, immunotherapy

OPEN ACCESS

Edited by:
Quan Cheng,
Central South University, China

Reviewed by:
Hong Su,
Max Planck Institute for Biophysical Chemistry, Germany
Wei Hua,
Fudan University, China
Jianyang Du,
Shandong Provincial Hospital Affiliated to Shandong First Medical University, China

****Correspondence:***
Gang Li
dr.ligang@sdu.edu.cn

†These authors have contributed equally to this work

Specialty section:
This article was submitted to Cancer Immunity and Immunotherapy, a section of the journal Frontiers in Immunology

Received: *05 November 2021*
Accepted: *29 December 2021*
Published: *26 January 2022*

Citation:
Xu J, Gao Z, Liu K, Fan Y, Zhang Z, Xue H, Guo X, Zhang P, Deng L, Wang S, Wang H, Wang Q, Zhao R and Li G (2022) The Non-N^6-Methyladenosine Epitranscriptome Patterns and Characteristics of Tumor Microenvironment Infiltration and Mesenchymal Transition in Glioblastoma. Front. Immunol. 12:809808. doi: 10.3389/fimmu.2021.809808

INTRODUCTION

Glioblastoma (GBM) is the most ordinary malignant intracranial cancer (1). Patients with GBM have an approximately 14–16-month median survival time, and GBM is highly resistant to standard therapies because of its extraordinary immunosuppressive microenvironment and mesenchymal (MES) transition (2–4).

There are over 160 posttranscriptional RNA modifications (5). RNA modifications modulate the structure as well as functions of RNAs, which results in several diseases, including GBM (6, 7). In eukaryotic cells, the most common RNA modification is N^6-methyladenosine (m^{6}A) (8, 9). Intensive investigations have indicated that m^{6}A facilitates a broad range of critical functions, including embryogenesis, neurogenesis, hematopoiesis, and tumorigenesis (10–13). Indeed, an increasing number of RNA modifications beyond m^{6}A have been found and studied with the development of technology (14). We found that some RNA modifications have been recently reported to be widespread on mammalian RNA; these include pseudouridine (Ψ), N^6,2′-O-dimethyladenosine (m^{6}A$_m$), N^1-methyladenosine (m^{1}A), alternative polyadenylation (APA), N^7-methylguanosine (m^{7}G), 2′-O-methylated nucleotides (N$_m$), 5-methylcytidine (m^{5}C), N^4-acetylcytidine (ac^{4}C), adenosine-to-inosine RNA editing (I), and cytidine-to-uridine RNA editing (U) (14–16).

Ψ, the most abundant non-m^{6}A modification, is generated by uridine isomerization (17). Ψ "writers" include TRUB1, TRUB2, PUS1, PUS7, and DKC1 (18). Ψ is required for proper folding and translation of transfer RNA (tRNA), ribosomal RNA (rRNA) structure stabilization, small nuclear ribonucleoprotein (snRNP) biogenesis, and messenger RNA (mRNA) splicing (19–21).

Detected at an approximately 10-fold lower m^{6}A level, m^{1}A is involved in the methylation of the adenine base on the first nitrogen atom as well as carries positive electricity (22). The m^{1}A methylation process is mediated by methyltransferases (writers) consisting of TRMT61B, TRMT6, and TRMT61A, while the removal process is catalyzed *via* demethylases (erasers) containing ALKBH3, ALKBH1, and FTO (23–25). Various specific RNA-binding proteins (readers), including YTHDC1, YTHDF3, YTHDF2, and YTHDF1, can recognize the m^{1}A motif, thus affecting m^{1}A functions (26). m^{1}A is necessary for tRNA structure stabilization, proper rRNA biogenesis, and methylated mRNA translation (22, 27). If 2′-O-methyladenosine is the first ribotide behind the m^{7}G cap of mRNA, it could be methylated at the N^6 position to render m^{6}A$_m$, which is related to mRNA metabolism (28, 29). PCIF1 is the writer that creates the m^{6}A$_m$ modification, and FTO is the eraser of m^{6}A$_m$ (25, 30). APA cleaves mRNA at more than one site and adds poly (A) tails to generate different transcripts of the 3′-untranslated region (3′ UTR) or coding regions, which regulates the function, stability, and translation efficiency of RNAs (31). PABPN1, NUDT21, CLP1, PCF11, and CPSF6 can regulate the APA process (32).

At levels similar to those of m^{1}A, m^{7}G, a modification carrying a positive charge at the 5′ cap, is necessary for mRNA export, splicing, and translation (33). In addition, the METTL1-catalyzed m^{7}G tRNA methylome is important for the translation of mRNA (34). N$_m$ is relatively widespread in rRNA, tRNA, snRNA, and microRNA and can be installed by FBL (35, 36). In addition, N$_m$ is essential for adjusting the structure and function of ribosomes (37).

Appearing in both coding and non-coding regions, m^{5}C sites are chiefly CG-rich regions that accumulate in the UTRs of mRNA (38). The writer of m^{5}C is NSUN2, while the eraser is TET2 (14, 39, 40). In addition, YBX1 has been reported to be an m^{5}C reader (41). m^{5}C modification plays an essential role in mRNA export, tRNA structure stabilization, and rRNA translational fidelity (39, 42). Catalyzed by NAT10 and THUMPD1, ac^{4}C was subsequently discerned in serine and leucine 18S rRNA and tRNAs. ac^{4}C, the sole acetylation modification in eukaryotic RNA, regulates mRNA translation and ribosome biogenesis (43, 44).

RNA editing is a kind of programmed posttranscriptional mechanism altering nucleotides in selected transcripts (45). Catalyzed by ADAR, ADARB1, and ADARB2, RNA editing can transform the sequence as well as alter transcriptional procedures (46). Accumulating in 3′UTRs, U RNA editing alters the protein level (47). UPP1 can catalyze the phosphorolysis of uridine to uracil (48, 49).

To thoroughly comprehend the significance of RNA modifications beyond m^{6}A, investigation of the crosstalk among diverse patterns of RNA alterations is urgently needed. Ten kinds of non-m^{6}A RNA modification "regulators" may build a complex and significant regulatory network in GBM, which might help elucidate GBM tumorigenesis mechanisms.

Immune checkpoint blockade therapy (ICB therapy), also known as immunotherapy, has delivered promising clinical outcomes for various cancers; nevertheless, it commonly exhibits a poor response due to the tumor microenvironment (TME) (50, 51). Unfortunately, a large number of patients with GBM have not experienced outstanding survival benefits; that is, immunotherapy for GBM is far from reaching clinical expectations (52). Accordingly, to enhance the effect of immunotherapy for GBM, it is crucial to thoroughly investigate the immunosuppressive TME. Recent studies have revealed that m^{6}A plays a significant role in complex TME formation (53, 54). Estimating m^{6}A patterns of a type of tumor to characterize TME infiltration could guide more effective immunotherapy strategies (55, 56). Non-m^{6}A RNA modification as well as correlative regulators are highly related to the microenvironment of immune cells as well as tumor cells. TET2 deficiency in Treg cells results in T-cell activation (57). NAT10 regulates the function of CD4$^+$ T cells (58). However, few studies have systematically analyzed the non-m^{6}A RNA modification patterns of individual tumors, while these RNA modifications play a non-negligible role in tumorigenesis (16, 59).

Based on genetic transcription signatures, GBM can be categorized into three subtypes (MES; classical, CL; as well as proneural, PN) (3). MES transition promotes radiochemotherapy resistance in GBM (60, 61). The MES subtype is particularly aggressive among these three subtypes, while the PN subtype

yields the best prognosis (62, 63). In addition, the MES-subtype GBM promotes the formation of an immunosuppressive TME, while the TME advances the MES transition in GBM (62, 64). An increasing number of studies have demonstrated that non-m^{6}A RNA modification regulators are significantly correlated with MES transition. It has been reported that ADAR and YBX1 promote MES transition by regulating oncogenic microRNA maturation (65, 66). Nevertheless, research on RNA modifications beyond m^{6}A is still not as mature as that for m^{6}A for many reasons, including technology limitations. Accordingly, it is significant to investigate the non-m^{6}A epitranscriptome patterns and characteristics of TME infiltration and MES transition in GBM.

In this study, we explored somatic mutation data for 390 GBM cases from The Cancer Genome Atlas (TCGA, http://portal.gdc.cancer.gov/; http://xena.ucsc.edu/) and integrated gene expression data from 539 GBM samples from TCGA and Chinese Glioma Genome Atlas (CGGA, https://www.cgga.org.cn/) cohorts to evaluate the RNA modification patterns. We discovered that non-m^{6}A RNA modification patterns were associated with TME cell-infiltrating characteristics as well as MES transition. Next, according to differentially expressed genes (DEGs), we established a non-m^{6}A epitranscriptome "regulator" score (RM score) to evaluate the effect on the non-m^{6}A epitranscriptome in individual patients. Eventually, we verified the pertinence of the RM score in distinguishing the posttranscriptional and transcriptional events as well as evaluated its importance in predicting the response to targeted and ICB therapy.

MATERIALS AND METHODS

Data Collection and Processing

The study workflow chart is shown in **Figure S1A**. Genetic transcription data as well as clinical information on GBM patients were obtained from TCGA and the CGGA. Somatic mutation counts and copy number variation (CNV) were obtained from the TCGA database. In total, 539 GBM samples (CGGA_batch_1:139, CGGA_batch_2:249, TCGA:151) were gathered in this study for further analyses. We used sva package's "ComBat" algorithm to correct non-biotechnology deviations causing batch effects. R Bioconductor packages and R (version 4.10) were used to analyze the data.

Unsupervised Clustering for 32 Non-m^{6}A RNA Modification Regulators

We extracted 32 non-m^{6}A RNA modification regulators and their expression from the TCGA and CGGA databases. These non-m^{6}A RNA modification regulators included 10 RNA modification types, which are listed in **Table S1**. Using unsupervised cluster analysis, different non-m^{6}A RNA modification patterns concerning 32 non-m^{6}A RNA modification regulatory factors were identified, and the patients were classified into different clusters. We applied the Consensus Cluster Plus package to execute the steps above with1,000 repetitions to guarantee classification stability.

Gene Functional Annotation Based on Gene Set Variation Analysis

To analyze the differences in biological processes between non-m^{6}A RNA modification patterns, gene set variation analysis (GSVA) enrichment was performed *via* the "GSVA" R package. We downloaded the gene set "c5.go.bp.v7.4" as well as "c2.cp.kegg.v7.4" from the Molecular Signatures Database (MSigDB, https://www.gsea-msigdb.org/gsea/msigdb/index.jsp) for GSVA.

TME Cell Infiltration Estimation

First, single-sample gene set enrichment analysis (ssGSEA) was used to identify tumor immune-infiltrating cell abundance in GBM samples. The markers of 28 immune-related cells and types were obtained from the dataset of Bindea et al. (67). Using an unsupervised hierarchical clustering algorithm, 539 GBM samples were assigned to two groups based on immune infiltration. Next, ESTIMATE was used to calculate the immune score as well as stromal score (68). Then, we used CIBERSORT (http://cibersort.stanford.edu/) to measure the infiltration levels of 22 distinct immune cells among the GBM samples.

Estimation of the MES/PN Score

Verhaak et al. identified three prognostic subtypes by integrated genomic analysis (69). There are significant prognostic differences between different subtypes, and accurate identification of subtypes can also guide treatment strategies. We downloaded the gene sets "VERHAAK_GLIOBLASTOMA_MESENCHYMAL" and "VERHAAK_GLIOBLASTOMA_PRONEURAL" from the MSigDB database v7.4 and quantified the MES and PN scores of the GBM samples using the ssGSEA algorithm.

Identification of DEGs Among Non-m^{6}A RNA Modification Patterns

To identify non-m^{6}A RNA modification-related genes, DEGs among three different non-m^{6}A RNA modification characteristics were arranged *via* the limma R package. The significance criterion for DEGs was p-value <0.01. To evaluate the function of DEGs, Gene Ontology (GO) analysis was performed to calculate biological process (BP), molecular function (MF), and cellular component (CC) terms using DAVID (https://david.ncifcrf.gov/) with a p-value cutoff of <0.05.

Cell Lines and Cell Culture

U-118 MG (Chinese Academy of Sciences Cell Bank) and LN-229 (ATCC Cell Bank) cell lines were cultured in DMEM (Sigma, USA) supplemented with 10% FBS (Thermo Fisher Scientific, USA). THP-1 cells (Chinese Academy of Sciences Cell Bank) were cultured in RPMI-1640 (Sigma) supplemented with 10% FBS. The cell lines were incubated at 37°C with 5% CO_2. To induce their differentiation into macrophages, THP-1 cell lines were incubated with 100 ng/ml phorbol 12-myristate 13-acetate (PMA, Sigma) for 24 h.

Small Interfering RNA and Plasmid Transfection

Small interfering RNAs (siRNAs) targeting UPP1 and plasmid overexpression of FTO were synthesized (GenePharma, China). SiRNAs and plasmids were transfected with Lipofectamine™ 3000 reagent (Thermo Fisher Scientific) according to the protocol of the manufacturer.

Western Blotting

Protein was extracted from GBM cell lines. The blots were incubated with primary antibodies against UPP1 (Abcam, UK), FTO (Cell Signaling Technology, USA), and ACTIN (Cell Signaling Technology).

5-Ethynyl-2′-deoxyuridine Cell Proliferation Assay

A 5-ethynyl-2′-deoxyuridine (EdU) cell proliferation assay kit (RiboBio, #C10310-1; China) was used to evaluate the proliferative activity of GBM cells. The cell proliferation rate was assessed *via* the ratio of EdU-positive (red) cells to total Hoechst-positive (blue) cells.

Transwell Assay

To evaluate migratory ability, GBM cells were added to the top chamber in DMEM without FBS, and the bottom chamber was filled with 10% FBS DMEM. To measure the ability to recruit macrophages, macrophages were added to the top chamber in RPMI-1640 without FBS, and the bottom chamber was filled with 10% FBS RPMI-1640 and growth media of different groups of GBM cells. After 24 h of incubation, the membrane was fixed in 4% paraformaldehyde and stained with crystal violet.

Constructing the RM Scoring System to Evaluate Individual GBM Samples

First, overlapping DEGs distinguished from non-m^{6}A RNA modification clusters were chosen for analysis. Then, we analyzed the prognostic value for each overlapping DEG *via* a univariate Cox regression model, and significant prognostic genes were identified. Next, the PCA algorithms were used to generate the RM score. Both principal component 2 and principal component 1 were selected to describe the RM scoring system.

$$\text{RM score} = \sum PC2_i - PC1_i$$

where i is the DEG expression.

Immunofluorescence

Tumor tissues were obtained from 12 patients treated for GBM at Qilu Hospital. RNA quantity and quality were estimated *via* an Agilent 2100 bioanalyzer (Agilent Technologies) and a Nanodrop 2000 spectrophotometer (Thermo Fisher Scientific). The mRNA library was prepared by using the NEBNext® Ultra™ RNA Library Prep Kit (Beijing Novel Bioinformatics Co., Ltd.). The HiSeqX platform (Illumina) on the Illumina standard protocol was used for RNA sequencing. Next, we performed a PCA algorithm based on the expression of DEGs to calculate the RM scores of the 12 GBM patients. We selected three cases with the highest as well as three cases with the lowest scores and performed immunofluorescence (IF) staining. After blocking with 5% goat serum (Gibco, USA) for 30 min, samples were incubated with primary antibodies at 4°C overnight. The following primary antibodies were used: rabbit SOX2 antibody (3579, Cell Signaling Technology, 1:400, USA), mouse CD44 antibody (3570, Cell Signaling Technology, 1:400), mouse CD163 antibody (ab156769, Abcam, 1:100, UK), and rabbit FoxP3 antibody (12653, Cell Signaling Technology, 1:400). Next, the samples were incubated with fluorophore-conjugated secondary antibodies at 37°C for 1 h. Alexa Fluor 594 anti-rabbit antibody (A11037; Invitrogen; 1:400) and Alexa Fluor 488 anti-mouse antibody (A11029; Invitrogen; 1:400) were used. DAPI was used to stain the cell nuclei. All immunostained samples were analyzed using Leica Application Suite Software and a Leica TCS SP8 confocal system. ImageJ was used to analyze the fluorescence intensity.

Summary of Genomic and Clinical Information of the Immunotherapy Cohort

We analyzed gene expression-related clinical information of the immunotherapy cohort and identified two independent immunotherapy cohorts: advanced urothelial tumor with atezolizumab treatment (IMvigor210 cohort, http://research-pub.gene.com/IMvigor210CoreBiologies/packageVersions/) and metastatic melanoma with pembrolizumab treatment (GSE78220 cohort). We obtained the expression data and clinical annotations of the GSE78200 cohort from the Gene Expression Omnibus (GEO) database.

Association Analysis Between Drug Sensitivity and RM Score

Cancer Cell Line Encyclopedia (CCLE) RNA-seq data were obtained from https://portals.broadinstitute.org/ccle/. Cancer cell line drug responses, measured as area under the curves (AUCs) and drug pathways, were obtained from Genomics of Drug Sensitivity in Cancer (GDSC; https://www.cancerrxgene.org/downloads). Spearman correlation analysis was applied to estimate the association between drug sensitivity and RM score.

Comparison of the m^{6}A Score and the RM Score

The Bayesian information criterion (BIC) as well as Akaike information criterion (AIC) was applied to compare the two models. A model with lower BIC and AIC values was identified as a better model.

RM Score Among Clinical Traits in Pan-Cancer

Univariate Cox regression analysis was used to investigate the time-dependent prognostic value of RM score in Pan-cancer. Overall survival (OS) and progression-free survival (PFS) were selected to study the relationship between RM score and

prognosis. In addition, the correlation between RM score and 22 immune cell infiltration was calculated in 33 cancers, respectively.

Statistical Analysis

The statistical analyses were generated by R-4.0.1. Distance and Spearman correlation analyses were applied to calculate 32 RNA modification expression correlation coefficients. Kruskal–Wallis and one-way ANOVA tests were applied to appraise difference comparisons of more than three collections. To assess the relationship between patient survival and the RM score, the optimal cutoff point for survival information for each dataset was determined using the survminer package. The log-rank test and Kaplan–Meier analysis were applied to assess survival among different clusters as well as RM score groups. The hazard ratio (HR) of DEGs was calculated *via* a univariate Cox regression model. To evaluate whether the RM score serves as an independent predictor for survival, sex, age, and isocitrate dehydrogenase (IDH) status were considered variables in the multivariate Cox regression model analysis. Statistical analysis was two-sided, as well as $p < 0.05$ was regarded as statistically significant.

RESULTS

Landscape of Genetic Variations in Non-m^{6}A RNA Modification Regulators in GBM

A total of 32 non-m^{6}A RNA modification regulators (**Table S1**) were included in the current study. **Figure 1A** shows that these non-m^{6}A RNA modification regulators can dynamically and reversibly add, remove, and recognize non-m^{6}A RNA-modified sites and potentially change biological functions, such as splicing, stability, export, translation, and degradation of RNA. We first summarized the somatic mutation prevalence of 32 non-m^{6}A RNA modification regulators among GBM. Among 390 samples, 24 showed genetic alterations of non-m^{6}A RNA modification regulators, with a frequency of 6.67% (**Figure 1B**). These mutations were multifarious and included splicing-related mutations, missense mutations, and deletions (**Figure 1B**). The mutation frequency of ADARB2 was the highest, while PABPN1, TRUB1, TRUB2, NAT10, PUS1, and TRMT61A showed no mutations among the 390 GBM patients (**Figure 1B**). Further analyses revealed mutation co-occurrence relationships among YTHDF2, YTHDF1, TRMT61B, THUMPD1, METTL1, FTO, FBL, YTHDF3, and UPP1 (**Figure S1B**). Moreover, the investigation of 32 non-m^{6}A RNA modification regulators exhibited that CNV-related mutations were widespread. METTL1, CPSF6, PUS1, ADARB2, ADAR, and UPP1 showed widespread CNV amplification, while PABPN1, FBL, ALKBH1, and TRUB1 had CNV deletions (**Figure 1C**). The CNV alteration locations of 32 non-m^{6}A RNA modification regulators on chromosomes are presented in **Figure 1D**. To determine whether genetic variations affected non-m^{6}A RNA modification regulator expression among GBM cases, we analyzed the expression of these regulators between GBM and normal samples to determine whether CNV alterations could result in perturbations in non-m^{6}A RNA modification regulator expression. Non-m^{6}A RNA modification regulators with CNV amplification demonstrated substantially higher expression in GBM tissues than in normal brain tissues, while those with deletions exhibited the opposite trend (**Figures 1C, E**). Moreover, we determined that the regulator expression patterns significantly varied among the three subgroups (**Figure 1F**). O^6-methylguanine DNA methyltransferase (MGMT) methylation, isocitrate dehydrogenase 1 (IDH1) mutation, and chromosomal 1p/19q codeletion have been found to confer a favorable prognosis in GBM (70). The same phenotypes were investigated in groups classified based on molecular subtypes (**Figures S1D–F**). Based on the expression of 32 non-m^{6}A RNA modification regulators, we distinguished patients with GBM from normal controls (**Figure S1G**). The analyses revealed high genetic and transcriptomic landscape heterogeneity among non-m^{6}A regulators between GBM and normal cases, indicating that genetic variations and expression alterations among non-m^{6}A RNA modification genes play an essential role in GBM progression and occurrence.

Non-m^{6}A RNA Modification Patterns Mediated by 32 Regulators

To obtain an overall understanding of the expression pattern, 539 GBM cases from the TCGA and CGGA datasets that contained clinical information and OS data were enrolled. A univariate Cox regression model revealed that 10 of 32 non-m^{6}A regulators were associated with the survival of GBM patients (**Figure S1C**).

To investigate the relationships among regulators, we calculated pairwise correlations among the expression of the 32 regulators in the GBM cases (**Figure S2A**). We identified that the expression of DKC1, YBX1, TRMT6, and PUS7 was positively correlated with that of many other regulators, while the expression of UPP1 and ALKBH3 was negatively correlated with that of other regulators (**Figure S2A**). In addition, the protein–protein interactions between non-m^{6}A RNA modification regulators are shown in **Figure S1H**. The comprehensive landscape of the intricate associations between non-m^{6}A RNA modification regulators and the prognostic value for GBMs was visualized with the non-m^{6}A RNA modification regulator network (**Figure 2A**; **Figure S2A**). We identified significant correlations among 32 non-m^{6}A RNA modification regulators, which revealed that the crosstalk between the regulators of erasers, writers, and readers might participate in the formation of various non-m^{6}A RNA modification patterns.

Next, we used ConsensusClusterPlus to sort patients with three non-m^{6}A RNA modification patterns based on the expression profiles of 32 selected non-m^{6}A RNA modification regulators. After unsupervised clustering, 144 cases were termed Cluster_A, 227 cases were identified in Cluster_B, and the other 168 cases were termed Cluster_C (**Figures 2B**, **S2B**). The expression of the 32 regulators in different clusters is shown in **Figure 2C**. In the survival analysis of non-m^{6}A RNA modification patterns, a dominant survival disadvantage was found for the Cluster_B non-m^{6}A RNA modification pattern (**Figure 2D**). To identify the biological functions of the three non-m^{6}A RNA modification patterns, GSVA was performed. As exhibited in **Figure 2E**, Cluster_B was markedly enriched in pathways associated with

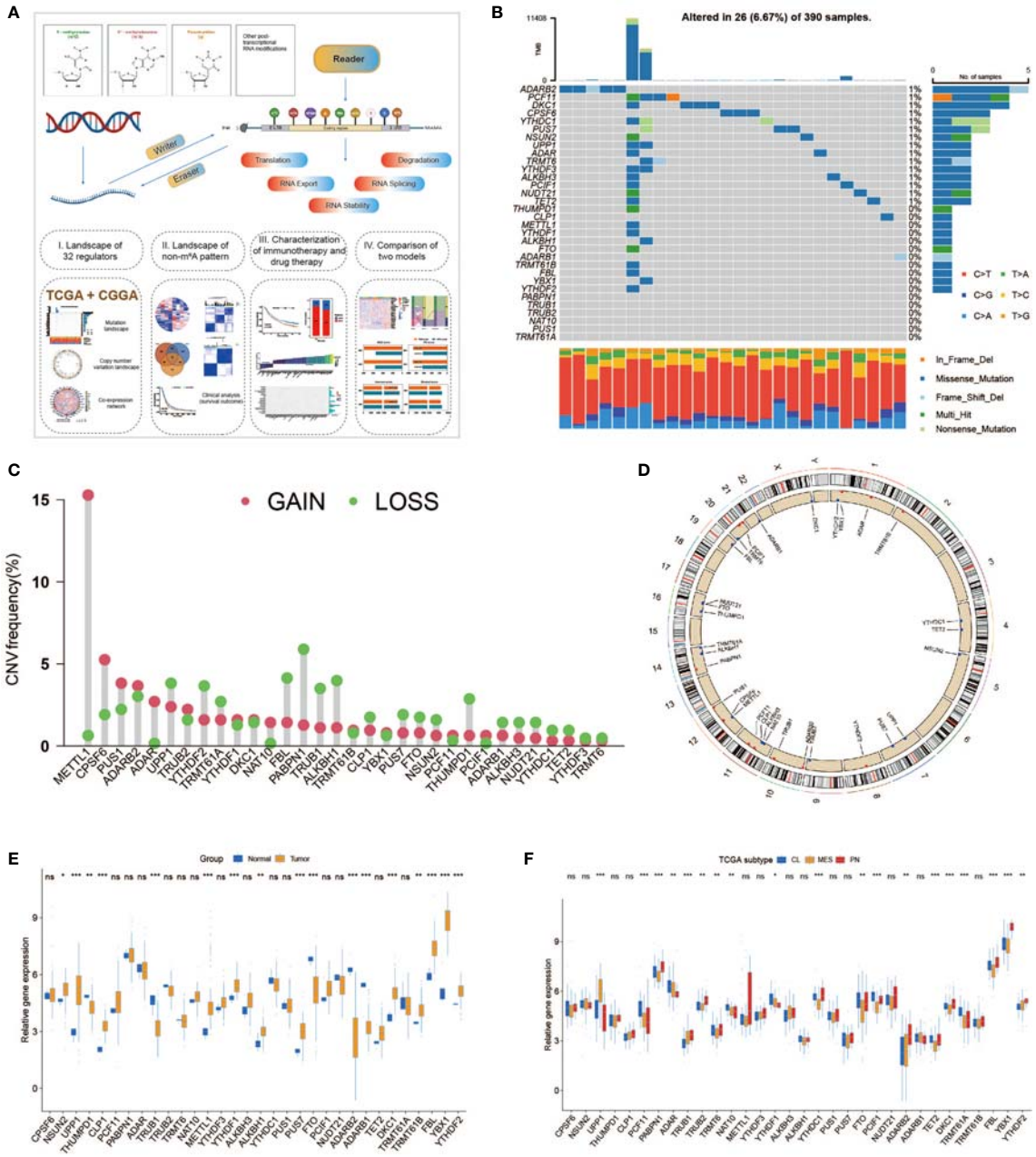

FIGURE 1 | Expression and mutational data landscape of 32 non-m^{6}A RNA-modified regulators in glioblastoma (GBM). **(A)** Landscape of this study workflow. **(B)** Mutation frequency of 32 non-m^{6}A RNA modification genes in 390 GBMs from The Cancer Genome Atlas (TCGA) database. **(C)** CNV variation frequency of non-m^{6}A RNA modification genes in TCGA-GBM. **(D)** The location of non-m^{6}A RNA modification genes on 23 chromosomes in TCGA-GBM. **(E)** Expression of 32 non-m^{6}A RNA modification genes between normal and GBM patients. **(F)** Expression of 32 non-m^{6}A RNA modification genes in different TCGA GBM subtypes. * means P<0.05; ** means P<0.01; *** means P<0.001; ns means P>0.05.

the formation of the immunosuppressive TME and MES transition, such as extracellular matrix (ECM) receptor interaction, TGF b, JAK STAT, WNT, and NOTCH signal paths. In addition, Cluster_A was prominently enriched in pathways regulating the cell cycle, cell aging, and DNA damage, while Cluster_C was markedly related to apoptosis processes (**Figure S2C**).

TME Cell Infiltration and MES Transition Characteristics in Distinct Non-m6A RNA Modification Patterns

SsGSEA was used to assess TME-infiltrating cells in GBM tissues. According to the abundance of infiltrating immune cells, we classified the GBM samples into high and low infiltration groups

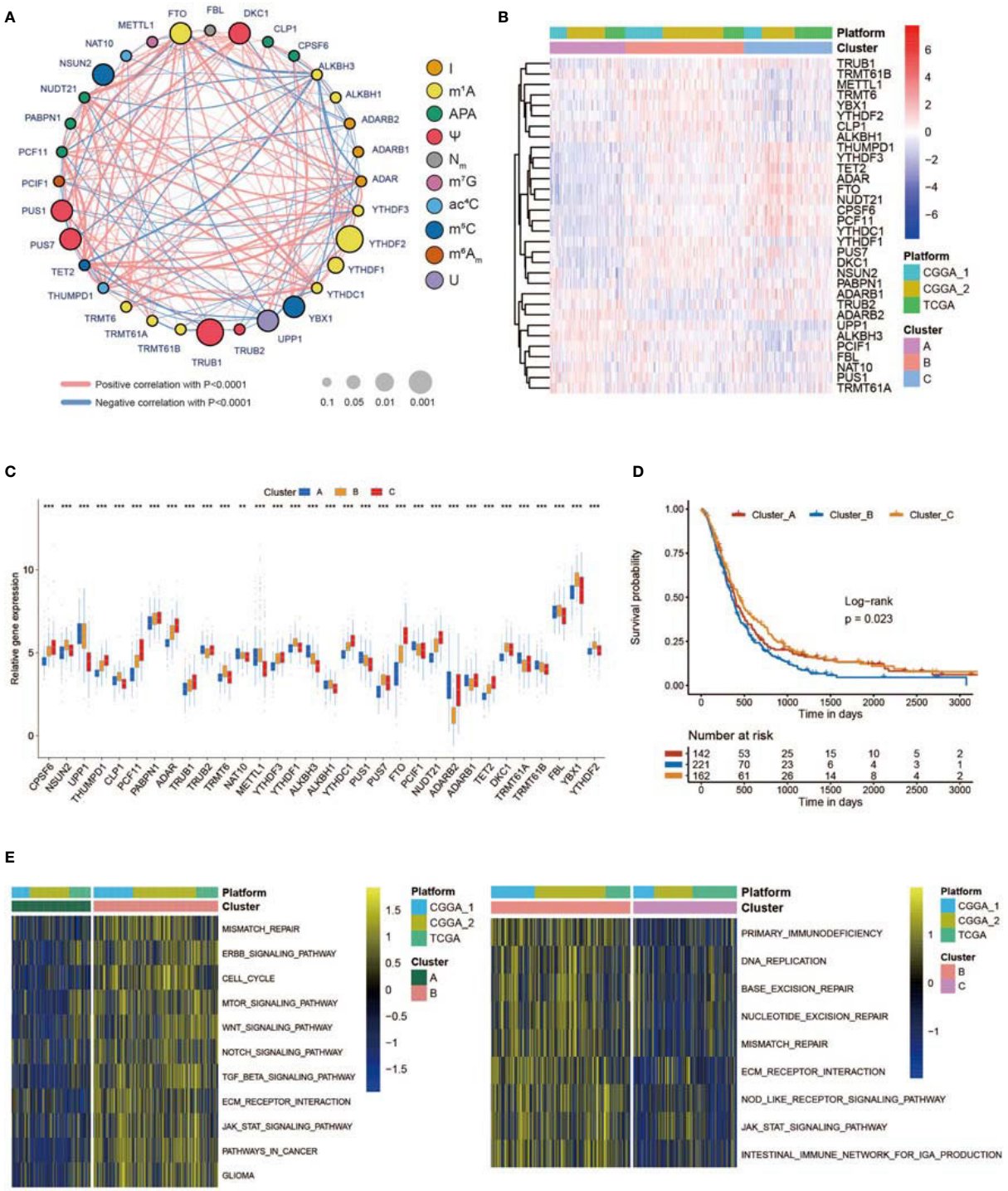

FIGURE 2 | Three RNA modification patterns of non-m^{6}A genes and relative biological functions. **(A)** Network plot showing the interaction between non-m^{6}A RNA modification genes in GBM. The size of the circle represents the *p*-value of each gene for the survival prognosis. Black dots represent hazard survival factors, and green dots represent favorable survival factors. The thickness of the lines represents the correlation value between genes. The red and blue lines represent positive and negative correlations, respectively. Ten RNA modification types are marked with different colors. **(B)** Heatmap showing the unsupervised clustering of 32 non-m^{6}A RNA modification regulators in 539 GBM patients. Each column represents a patient, and each row represents a non-m^{6}A RNA modification regulator. **(C)** Expression of 32 non-m^{6}A RNA modification genes between three non-m^{6}A RNA modification patterns. **(D)** Kaplan–Meier curves showing the survival information of three non-m^{6}A RNA modification patterns. **(E)** Heatmap showing the results of GSVA enrichment between different non-m^{6}A RNA modification patterns. * means P<0.05; *** means P<0.001.

(**Figure 3A**). Patients with 1p19q codeletion status or IDH mutation status were mainly enriched in the low infiltration group (**Figure 3A**). Analyses of TME cell infiltration *via* the CIBERSORT algorithm confirmed that Cluster_B was obviously enriched in innate immune cell infiltration, including the infiltration of mast cells, natural killer (NK) cells, macrophages, and dendritic cells (DCs) (**Figure 3B**; **Table S2**). In addition, abundant stromal elements in the TME are associated with immunosuppression (71). We uncovered that the stromal score of Cluster_B was the highest among the three clusters *via* the ESTIMATE algorithm (**Figure 3B**). When we investigated the MES and PN scores, we found that the MES score was the highest and the PN score was the lowest in Cluster_B (**Figure 3C**). The MES-subtype GBM tended to exhibit an immunosuppressive TME. Previous studies demonstrated that there were abundant immune cells in tumors with an immune-excluded group, and immune cells participated in the formation of an immunosuppressive TME (72, 73). We found that three non-m^{6}A patterns possessed definite TME infiltration characteristics. Cluster_B was termed an immune-excluded group, characterized by abundant innate immune cell infiltration, stromal activation, and a high MES score; Cluster_A was termed an immune-inflamed group, marked by abundant immune cell infiltration; and Cluster_C was termed an immune-desert phenotype, characterized by rare immune cell infiltration (**Figures 3A–C** and **S3A**). In addition, GBMs with an immune-excluded subtype had the worst prognosis (**Figure 2D**). Furthermore, to analyze the immune tolerance as well as activity condition of each pattern, we selected LGALS9, LAG3, ICOS, IL23A, LDHA, CTLA4, CD274, PTPRC, PDCD1, IL12A, ICOSLG, CD28, TNFRSF4, VTCN1, PDCD1LG2, TNFRSF18, TNFSF18, TNFSF4, CD80, CD86, CD8A, B2M, TNFSF9, YTHDF1, PVR, FGL1, CD40, SIGLEC15, LAMA3, CD40LG, HAVCR2, TNFRSF9, JAK2, JAK1, and LDHB as immune checkpoint-related molecules (74, 75). We uncovered that diverse immune checkpoint-related genes were significantly overexpressed in Cluster_B and Cluster_A (**Figure S3C**). In addition, we chose CD44, CHI3L1, FN1, SERPINE1, and TIMP1 as MES markers and OLIG2, DLL3, NCAM1, ASCL1, and SOX2 as PN markers (69, 76, 77). The expression of MES markers was high in Cluster_B, while the expression of PN markers was high in Cluster_C (**Figure S3D**). In addition, ssGSEA revealed that the immunosuppressive TME and MES transition pathways, such as the NF-κB and STAT3 signal paths, were obviously enriched in Cluster_B, whereas the monocyte and macrophage chemotaxis pathways were enriched in Cluster_A (**Figure 3D**). **Figure S3B** illustrates the proportion of GBM patients with the indicated clinical status and molecular traits in the three groups with different non-m^{6}A RNA modification patterns. Patients over 60 years old and those who were alive at the last follow-up were primarily in Cluster_C, while patients with IDH wild-type status and no MGMT methylation were mainly found in Cluster_B (**Figure S3B**).

We analyzed the specific relationship between the TME-infiltrating cell type as well as non-m^{6}A RNA modification regulators (**Figure S3E**). Patients were classified into low or high immune infiltration, MES, and PN score groups. Thirty-two non-m^{6}A RNA modification regulator expression levels in different groups are shown in **Figures S3F–H**. We focused on UPP1, a U regulator, which had a significant positive correlation with numerous TME-infiltrating immune cells (**Figure S3E**). Patients were classified into low and high UPP1 expression subgroups, and a beneficial prognosis was presented in patients with low UPP1 (**Figure S4A**). We used ESTIMATE to assess the overall levels of immune cell infiltration as well as the stromal score. The results showed that patients with a high expression of UPP1 exhibited high immune and stromal scores (**Figure S4B**). The specific difference in TME-infiltrating levels between patients with low and high UPP1 expression was explored. We observed that tumors with high UPP1 showed obviously increased infiltration of Treg T cells and M2 macrophages (**Figure S4B**). We uncovered that increased UPP1 resulted in the overexpression of immune checkpoint-related genes (**Figure S4C**). In addition, the expression of MES markers was higher, while that of PN markers was lower in patients with high UPP1 expression (**Figure S4D**). Subsequent pathway enrichment analyses showed that high UPP1 samples exhibited an obvious enhancement of the immunosuppressive TME and MES transition-related pathways, including the NF-κB, STAT3, and epithelial–mesenchymal transition (EMT) signal paths (**Figure S4E**). From the above results, we speculated that UPP1-mediated U may promote the formation of an immunosuppressive TME and facilitate MES transition. In addition, we investigated the characteristics of one m^{1}A and m^{6}A$_m$ eraser, FTO, which was negatively associated with various TME-infiltrating immune cells (**Figure S3E**). Patients with a high FTO exhibited a better prognosis (**Figure S5A**). We then found that a high expression of FTO was related to low immune and stromal scores (**Figure S5B**). We also discovered that a low FTO was related to the overexpression of a few immune checkpoint-related genes (**Figure S5C**). MES marker expression was higher, while PN marker expression was lower in patients with low FTO expression (**Figure S5D**). In addition, patients with low FTO expression showed prominent enrichment of the hypoxia pathway, STAT3 signaling pathway, and EMT signaling pathway (**Figure S5E**). Thus, FTO may inhibit the formation of an immunosuppressive TME and the process of MES transition.

To assess the role of UPP1 and FTO in diverse cellular processes of GBM cells, several experiments were performed. Downregulation of UPP1 or overexpression of FTO resulted in a significant decrease in the EdU-positive cell percentage (**Figures 4A, B**). In addition, the results of the Transwell assays revealed that UPP1 silencing and FTO overexpression reduced the number of GBM cells migrating to the membrane (**Figure 4C**). Interestingly, we found that UPP1 knockdown or FTO overexpression significantly inhibited the capability of conditioned medium from GBM cells to recruit THP1-differentiated macrophage (**Figure 4D**).

Non-m^{6}A RNA Modification Phenotype-Related DEGs in GBM

To characterize the potential biological behavior of the three non-m^{6}A patterns, we confirmed 243 RNA phenotype-related

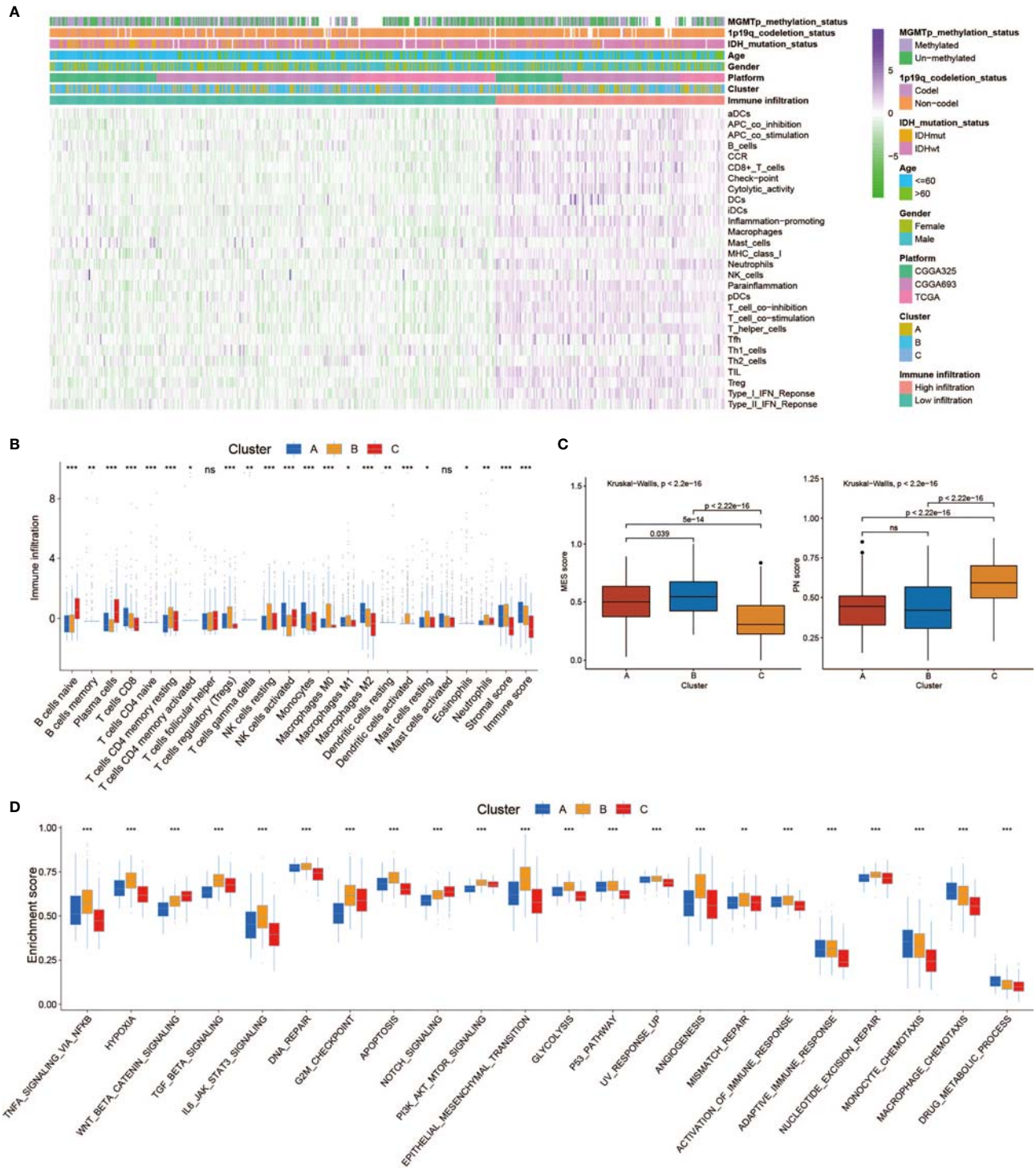

FIGURE 3 | Tumor microenvironment (TME), subtypes, and clinical information in three non-m^{6}A RNA modification clusters. **(A)** Unsupervised clustering of GBMs using ssGSEA scores from 28 immune-related gene sets. Two significant immune infiltration patterns are presented. The non-m^{6}A RNA modification patterns and other clinical characteristics were used as patient annotations. **(B)** The abundance of tumor-infiltrating immune cells, stromal scores, and immune scores in three non-m^{6}A RNA modification patterns. **(C)** Differences in mesenchymal/proneural (MES/PN) scores quantified by ssGSEA among the three non-m^{6}A RNA modification patterns. **(D)** Differences in the TME infiltration and MES transition pathways among three non-m^{6}A RNA modification patterns. * means P<0.05; ** means P<0.01; *** means P<0.001; ns means P>0.05.

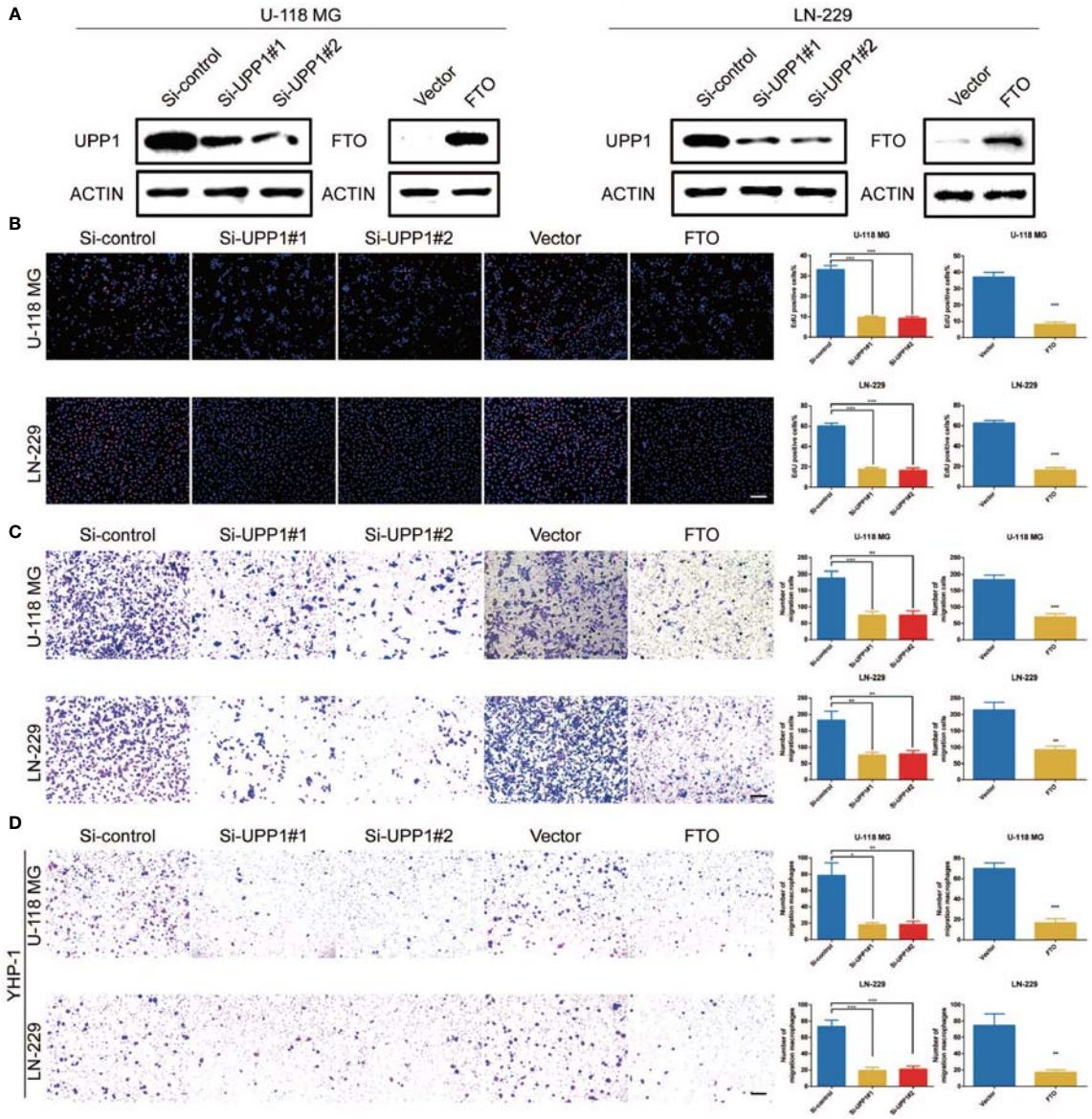

FIGURE 4 | UPP1 knockdown and FTO overexpression inhibit cell proliferation, migration, and macrophage recruitment. **(A)** Western blot analysis was performed to assess the expression levels of UPP1 and FTO. ACTIN was used as a loading control. **(B)** EdU was performed in U-118 MG and LN-229 transfected si-control, si-UPP1#1, si-UPP1#2, vector, and ov-FTO cells (scale bar = 100 μm). **(C)** Transwell assay performed in U-118 MG and LN-229 transfected si-control, si-UPP1#1, si-UPP1#2, vector, and ov-FTO cells (scale bar = 100 μm). **(D)** Transwell assays showed the ability of growth media of different GBM cells to recruit macrophages (scale bar = 100 μm). * means P<0.05; ** means P<0.01; *** means P<0.001.

DEGs (**Figure S6A**). Then, a univariate Cox regression model was applied to perform prognostic analysis for each DEG in the signature (**Table S3**). The DEGs with significant prognostic value were extracted for further analysis. To further corroborate this regulatory mechanism, unsupervised clustering methods were executed according to 150 DEGs (**Figure S6B**). The marked enriched biological functions of these DEGs are presented in **Figure S6C**. The unsupervised clustering algorithm sorted the cases into two subtypes: gene.cluster_1 and gene.cluster_2 (**Figure 5A**). The two patterns were identified in gene.cluster_1 and gene.cluster_2, marked by different signature genes (**Figure 5A**). Patients with 1p19q codeletion status or IDH mutation status were mainly concentrated in gene.cluster_2 (**Figure 5A**). In addition, in the two non-m^{6}A RNA modification DEG clusters, noticeable differences in non-m^{6}A RNA modification regulator expression were analyzed (**Figure 5B**). A total of 242 patients with GBM were termed gene.cluster_2, which was validated to be correlated with a favorable prognosis (**Figure 5C**). To our surprise, gene.cluster_1 was remarkably abundant in several immune

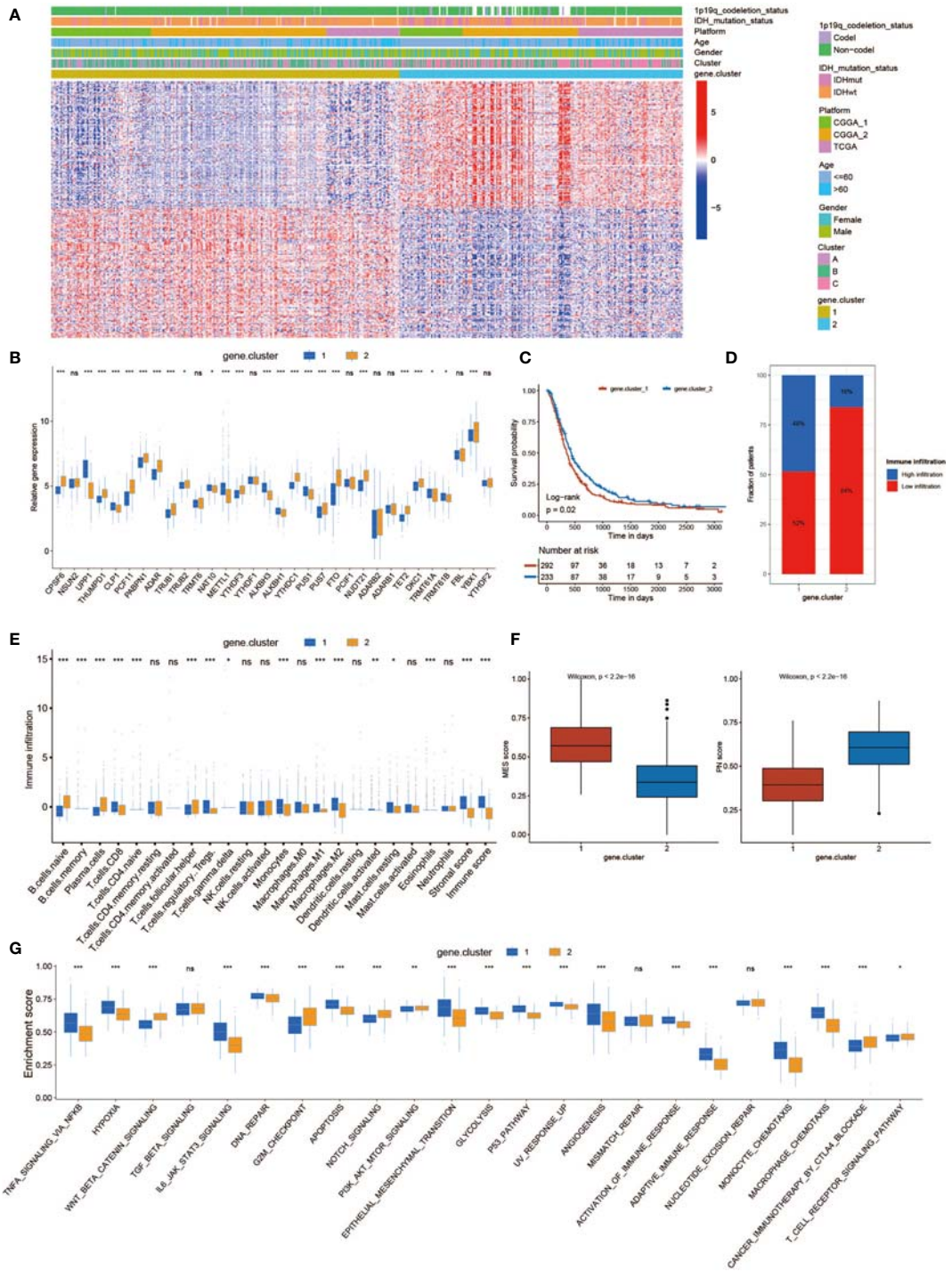

FIGURE 5 | Generation of a non-m^{6}A RNA modification-related gene set. **(A)** Unsupervised clustering of 150 DEGs dividing patients into two gene.clusters, named gene.cluster_1 and gene.cluster_2. Cluster, gender, age, platform, IDH status, and 1p19q status were applied for sample annotation. **(B)** The expression of 32 non-m^{6}A RNA modification regulators in two gene.clusters. **(C)** Survival analyses for the gene.cluster_1 (292 cases) and gene.cluster_2 (233 cases) cohorts (p = 0.02, log-rank test). **(D)** The proportion of immune infiltration in the two gene.clusters. **(E)** The abundance of each TME-infiltrating cell, stromal scores, and immune scores in the two gene.clusters. **(F)** Differences in MES/PN scores among the two gene.clusters. **(G)** Differences in the TME infiltration and MES transition pathways between the two gene.clusters. * means P<0.05; ** means P<0.01; *** means P<0.001; ns means P>0.05.

cell infiltrates (**Figures 5D, E**). In addition, the immune cell infiltration of gene.cluster_1 was stronger than that of gene.cluster_2 (**Figures 5D, E**). However, we found that the stromal score of gene.cluster_1 was higher than that of gene.cluster_2 (**Figure 5E**). In addition, gene.cluster_1 possessed a higher MES score and lower PN score than gene.cluster_2 (**Figure 5F**). These results indicate that patients in gene.cluster_1 had a highly immunosuppressive TME, which is related to a poor prognosis. Moreover, we determined that diverse immune checkpoint-related genes were significantly overexpressed in gene.cluster_1 (**Figure S6D**). In addition, the expression of MES markers was high in gene.cluster_1, while the expression of PN markers was high in gene.cluster_2 (**Figure S6E**). Moreover, ssGSEA revealed that the immunosuppressive TME and MES pathways were significantly enriched in gene.cluster_1, whereas T-cell receptor signaling pathways were enriched in gene.cluster_2 (**Figure 5G**).

Generation of the RM Score and Analysis of Clinical Traits

The above results showed that non-m^{6}A plays an essential role in shaping different TME landscapes as well as facilitating MES transition. However, these analyses only assessed the characteristics of the population and could not correctly evaluate the detailed information of non-m^{6}A RNA modification of each GBM case. Taking into account the complexity and individual heterogeneity of non-m^{6}A RNA modifications, we generated a scoring model to assess the non-m6A RNA modification patterns of individual GBM patients according to phenotype-related DEGs; this system was termed the RM score. The relationships among the non-m^{6}A RNA modification patterns, MES score, gene.cluster, and RM score were visualized in an alluvial diagram and in **Table S4** (**Figure 6A**). The Wilcoxon test revealed an obvious difference in the RM score between the gene.clusters. Gene.cluster_2 showed a lower median score than gene.cluster_1, which indicated that a high RM score could be closely linked to the immunosuppressive TME and MES transition signatures (**Figure 6B**). Moreover, Cluster_B showed a significantly increased RM score compared with Cluster_A and Cluster_C (**Figure 6B**). In addition, patients with stronger immune cell infiltration possessed higher RM scores (**Figure S7A**).

We investigated the value of the immune, MES, and PN scores in predicting patient prognosis. A high immune score, high MES score, or low PN score indicated a poor prognosis (**Figure S6F**). In addition, we observed a significantly negative relationship between the MES score and PN score (**Figure S6G**). Next, we evaluated the significance of the RM score in predicting GBM outcomes. With a cutoff value of −10.21, GBMs were classified into high or low RM score groups. GBMs with lower RM scores presented a significantly prolonged survival time (**Figure 6C**). To evaluate the stability of the RM scoring system, we used the RM score in other independent GBM databases to verify its prognostic significance, and the results indicated that a low RM score was correlated with better clinical benefit (**Figures S8A, B**). We analyzed whether the RM score could be regarded as an independent factor of survival for GBM. Multivariate Cox regression analysis was performed, confirming that the RM score was an independent and robust factor for predicting GBM patient outcomes [**Figure S8C**; HR (low RM score) = 0.53 (0.39–0.73)]. We also examined the survival prediction efficiency for the combination of RM score with immune score, RM score and MES score, and RM score and PN score. The results presented that the low RM and low immune score groups showed the best OS among the groups (**Figure S7B**). Furthermore, we observed that patients with low RM and MES scores or low RM scores and high PN scores had the most significant survival benefits (**Figures S8D, E**). We assessed the value of the RM scoring feature to evaluate the efficacy of radiotherapy or chemotherapy in GBMs. Among the patients who received adjuvant radiotherapy or chemotherapy at the same time, those with low RM scores exhibited the most significant therapeutic benefit (**Figure S7C**). Furthermore, patients over 60 years old, patients alive at the last follow-up, and patients with IDH mutations, 1p/19q codeletion, and MGMT methylation were mainly found in the low RM score group (**Figures S8F, G**).

Further analysis showed that the immune cell infiltration of patients with high RM scores was significantly higher than that of patients with low RM scores, while patients with high RM scores had higher stromal scores (**Figure S7D**). In addition, patients with high RM scores had higher MES scores and lower PN scores (**Figure S7E**). GBM patients with the MES subtype were characterized by higher TME levels, whereas GBM patients with the PN subtype were associated with lower TME levels. To exclude the influence of phenotypic and tumor immune infiltration correlations on the analysis results, we analyzed the correlation between RM scores and TME levels in patients with PN and MES subtypes (**Figure S9**). Moreover, to reveal the significance of the RM score in estimating the level of TME immune infiltration and MES transition, we studied the expression of immune checkpoint-related genes and MES/PN marker genes in different RM score groups. We found that most immune checkpoint-related genes were upregulated in the high RM score group (**Figure S7F**). In addition, the expression of MES markers was higher in high RM score patients, while the expression of PN markers was higher in low RM score patients (**Figure S7G**). We examined the relationship between the RM score and known biological signatures using Spearman analysis. A heatmap of the association matrix exhibited that the RM score was positively related to immunosuppressive TME and MES transition signatures (**Figure S7H**).

To verify the role of the RM score in evaluating the characteristics of TME infiltration and MES transition, IF staining was performed. The proportions of M2 macrophages (CD163$^+$) and FoxP3$^+$ Tregs infiltrated in tumors with high RM scores were higher than those in tumors with low RM scores (**Figure 6D**). Moreover, CD44 expression was also markedly increased in the high RM score group, while SOX2 expression was decreased (**Figure 6D**). These results further validated that tumors with high RM scores showed an immunosuppressive phenotype.

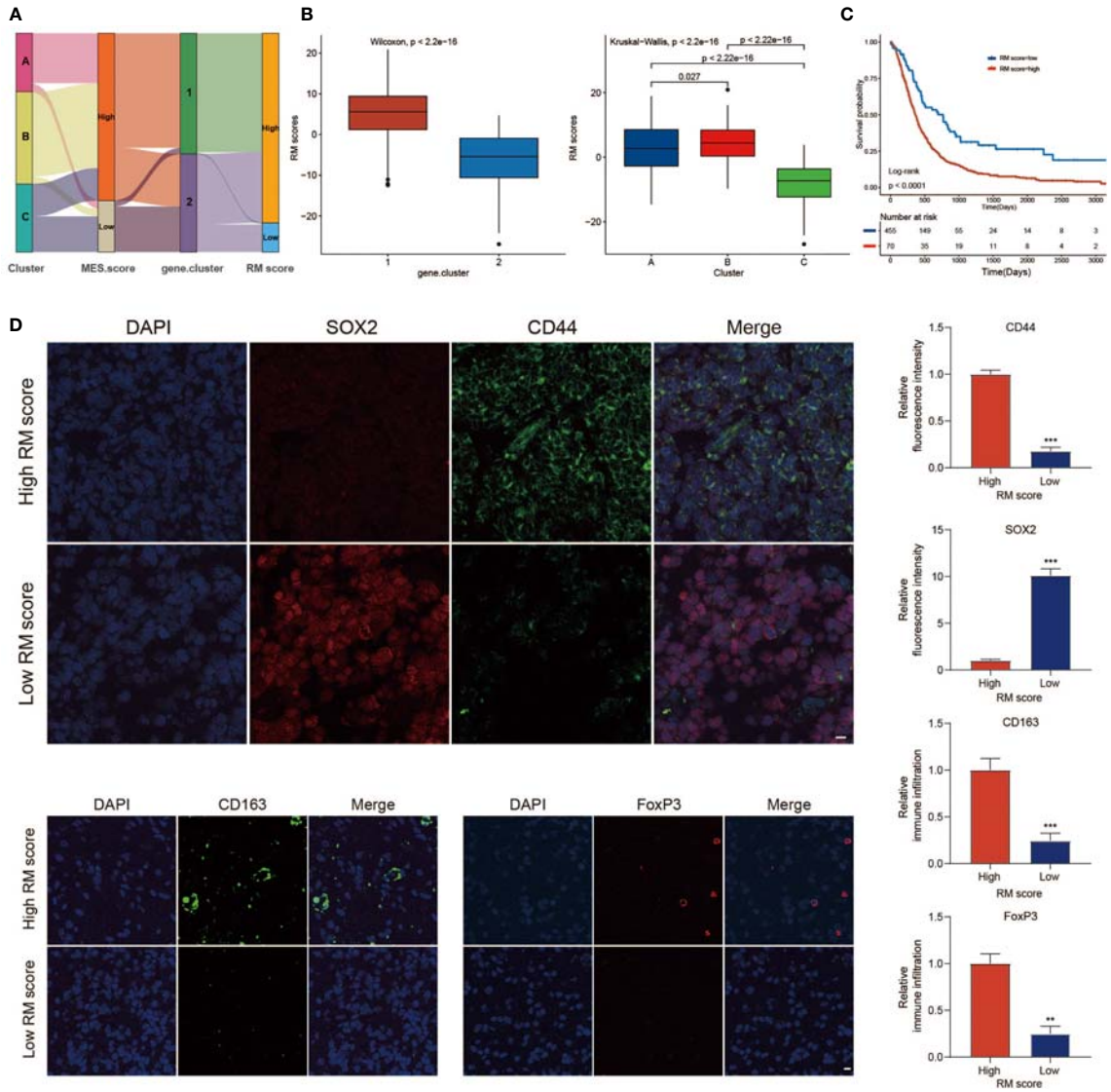

FIGURE 6 | Calculation of regulator score (RM) score. **(A)** Sankey plot showing the changes in non-m^{6}A RNA modification patterns, MES scores, gene.clusters, and RM scores. **(B)** Differences in RM scores among the two gene.clusters and three non-m^{6}A RNA modification patterns. **(C)** Survival analyses for the high RM score and low RM score patient groups. **(D)** IF staining in GBM tissues showed the expression of CD44, SOX2, CD163, and FoxP3. Histogram representing relative fluorescence intensity (scale bar = 15 μm). ** means P<0.01; *** means P<0.001.

The Correlation Between the RM Score and TMB

Increasing evidence has demonstrated a significant correlation between responsiveness to immunotherapy and tumor mutation burden (TMB) (78). Taking the clinical significance of TMB into account, we further analyzed the relationship between the RM score and the TMB. By comparing the TMB values for patients with high and low RM scores, we concluded that the RM score was negatively associated with the TMB value (**Figure 7A**). Patients with higher RM scores exhibited a lower TMB than patients with lower RM scores (**Figure 7B**). We divided the patients into different groups according to the immune setting of the TMB, as described previously (79). As shown in **Figure 7C**, we observed that patients with a high TMB had prolonged survival times compared with those with a low TMB. Considering the contrary survival significance of the TMB and RM score, we analyzed the cross-influence of these scores on the prognosis of patients with GBM. Stratified survival analyses revealed that patients with low RM scores together with high TMB scores had the most significant survival benefits (**Figure 7D**). Furthermore, we evaluated the somatic

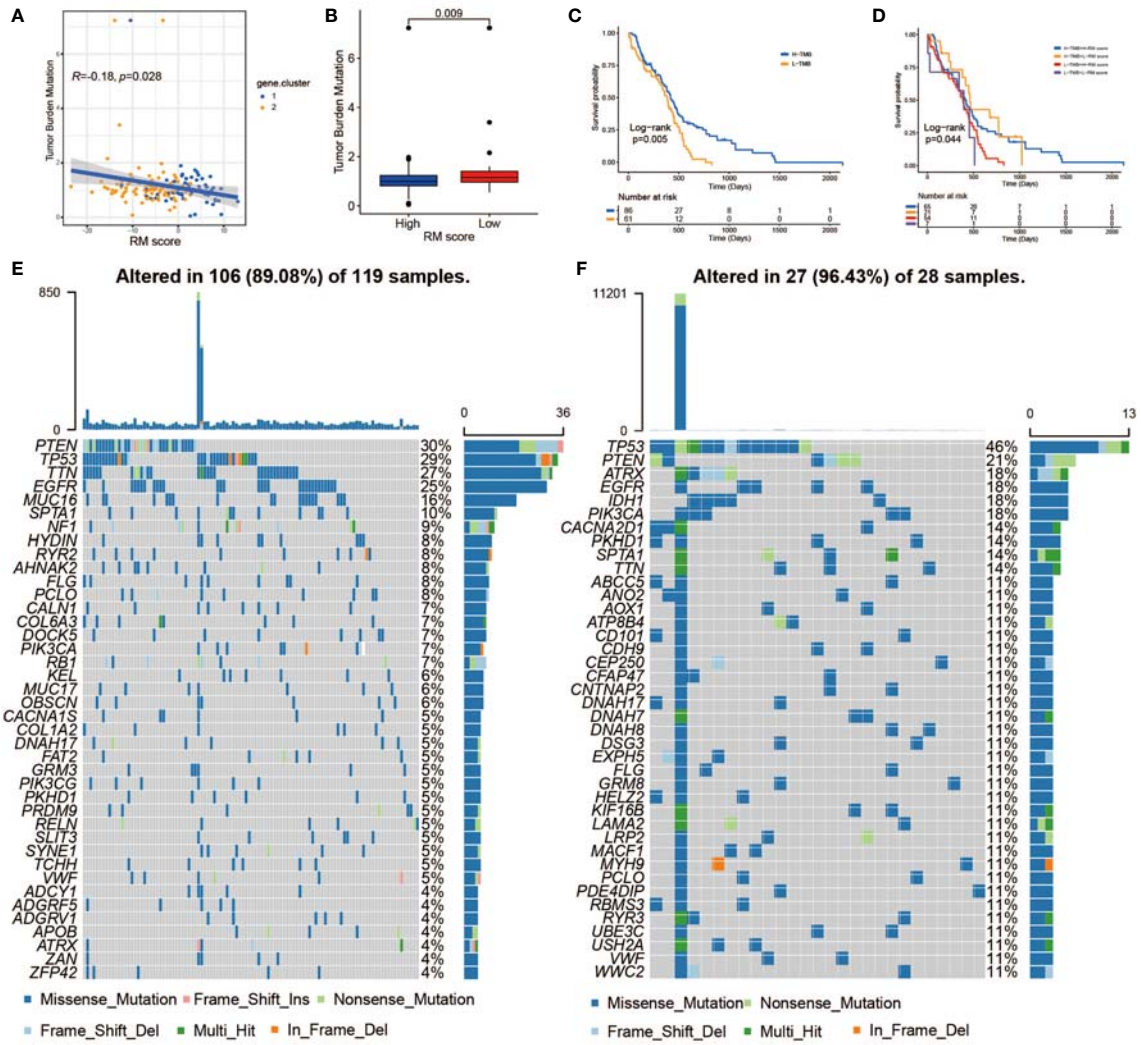

FIGURE 7 | The correlation between the RM score and TME infiltration, MES transition, and somatic variants. **(A)** Scatterplots indicating the negative relationship between RM score and TMB in TCGA-GBMs (r = –0.18, p < 0.028, Spearman correlation analysis). **(B)** TMB difference in the low and high RM score cohorts. **(C)** KM curves for the low and high TMB GBMs. H, high; L, low. **(D)** Survival analyses for subgroup GBMs stratified by RM score and TMB. **(E, F)** Waterfall plot showing tumor somatic mutations presented by those with high RM scores **(E)** and low RM scores **(F)**.

variant distribution of GBM driver genes among the high and low RM score groups using the maftools package. As shown in **Figures 7E, F**, the low RM score group presented more extensive TMB than the high RM score group. An increasing number of studies have shown that patients with a high TMB are more sensitive to anti-PD-1/PD-L1 immunotherapy (80). In addition, the alteration frequency of various genes was different between the low and high RM score groups (**Figures 7E, F**). In conclusion, the above findings corroborated that the difference in non-m^{6}A RNA modification patterns could be an important factor that predicted response efficiency to anti-PD-1/PD-L1 immunotherapy. These results might lead to novel strategies for exploring the mechanism of non-m^{6}A RNA modification composition and gene mutation in ICB therapy.

The Predictive Value of the RM Score in Predicting ICB Therapy Response

Significant efforts have been made to screen biomarkers that predict ICB treatment response; some previously studied biomarkers include the TMB as well as the PD-L1 expression level (81). Considering that the RM score is related to the TME, we examined the value of the RM score in predicting the response of GBMs to immunotherapy. The exploration was based on two independent immunotherapy studies (**Figures 8A–H**). We observed that patients who had lower RM scores exhibited obviously prolonged OS in the anti-PD-L1 research (IMvigor210; **Figure 8A**) and anti-PD-1 research (GSE78220; **Figure 8G**) (74, 82). The patients in the IMvigor210 cohort exhibited diverse degrees of response to anti-PD-L1

blockers, including partial response (PR), progressive disease (PD), complete response (CR), and stable disease (SD). We explored the differences in RM scores for patients with diverse responses to ICB therapy and concluded that the proportion of patients in the response groups (CR and PR) was significantly lower in the high RM score group than in the low RM score group, while the proportion of patients in the no/limited response groups (SD and PD) showed the opposite trend, indicating that the RM score could reveal the response of patients to ICB therapy (**Figure 8B**). The expression of PD-L1 on tumor cells (TCs) was substantially related to the RM score. The TC1 group exhibited the lowest RM score and was obviously different from the TC0 as well as TC2$^+$ groups (**Figure 8C**). Moreover, we observed that the PD-L1 level of immune cells (ICs) was positively related to the RM score, with IC0 exhibiting the lowest RM score and IC2 exhibiting the highest RM score (**Figure 8D**). By analyzing the relationship of the RM score with tumor neoantigen burden, we observed that patients with low RM scores together with a high neoantigen burden exhibited the most prolonged survival time (**Figure 8E**). In addition, patients with high RM scores showed significantly high levels of PD-L1 (**Figure 8F**). Finally, we confirmed the significant clinical response and therapeutic advantages of anti-PD-1 immunotherapy in patients with low RM scores versus those with high RM scores (**Figures 8H**, **S8H**). The RM score was also negatively correlated with the TMB in the GSE78220 cohort (**Figure S8I**).

Exploration of the Therapeutic Significance of the RM Score

To investigate the value of the RM score in predicting drug sensitivity, we calculated the correlation between the RM score and the AUC for drugs in multiple cancer cell lines. According to Spearman correlation analysis, we selected 68 drugs for which the RM score and drug sensitivity were significantly correlated in the GDSC database (**Figure 8I**) (83). The RM score was positively correlated with sensitivity to 12 drugs, including picolinic acid, chromatin histone methylation inhibitor EPZ5676, EGFR inhibitor AZD3759, gefitinib, erlotinib, and WNT inhibitors MN.64 and XAV939; the RM score was negatively correlated with drug sensitivity (and this positively correlated with drug resistance) for 56 drugs (**Figures 8I, J**). Furthermore, we explored the signal path targeted by the selected drugs. We observed that drugs whose sensitivity was positively related to the RM score targeted the EGFR and WNT signaling pathways. In contrast, drugs whose sensitivity was negatively related to the RM score targeted the cell cycle and apoptosis signal path (**Figure 8J**). In conclusion, these results revealed that the RM score model might serve as a potential factor for exploring proper therapy strategies.

Construction of the m^{6}A Score and Comparison of the m^{6}A and RM Scores

A total of 20 m^{6}A RNA modification regulators were enrolled in this study. Next, we classified patients into different m^{6}A RNA modification patterns according to the expression profiles of 20 selected m^{6}A RNA modification genes. After unsupervised clustering, 199 cases were termed m^{6}A Cluster_A, 197 cases were termed m^{6}A Cluster_B, and the other 143 cases were identified in m^{6}A Cluster_C (**Figure 9A**). In the survival analysis of m^{6}A RNA patterns, m^{6}A Cluster_B exhibited a particularly outstanding survival benefit (**Figure S10A**; p = 0.0018). In addition, we identified 295 DEGs using the limma package. Then, univariate Cox regression analysis was applied to determine the prognostic value for each DEG (**Table S5**), and the DEGs with significant prognostic value were extracted for further analysis. To further corroborate this regulatory information, an unsupervised clustering method was used according to the 172 DEGs. The patients were divided into two groups, m^{6}A gene.cluster_1 and m^{6}A gene.cluster_2, using the unsupervised clustering algorithm (**Figure 9B**). A total of 272 patients with GBM were termed m^{6}A gene.cluster_2, which was validated to be associated with a better prognosis (**Figure S10B**). Based on these DEGs, we generated a scoring system to assess the m^{6}A RNA modification pattern of each GBM patient. The relationships among m^{6}A RNA modification patterns, MES score, m^{6}A gene.cluster, and m^{6}A score were visualized in an alluvial diagram and in **Table S6** (**Figure 9C**). Patients with low m^{6}A scores demonstrated a prolonged survival time (**Figure 9D**). The Wilcoxon test revealed a significant difference in the m^{6}A score between the m^{6}A gene.clusters. M^{6}A gene.cluster_2 showed a lower median score than gene.cluster_1, which indicated that a high m^{6}A score could be closely linked to poor prognosis (**Figure S10C**). Moreover, compared with the other clusters, m^{6}A Cluster_B showed a significantly decreased m^{6}A score (**Figure S10D**). In addition, patients with high RM scores exhibited higher immune, stromal, and MES scores and lower PN scores (**Figures 9E, F**).

The value of the RM and m^{6}A scores in predicting patient outcomes and the TME was compared using the BIC and AIC values. With lower BIC and AIC values, the RM scoring model exhibited a better description of TME infiltration and MES transition than the m^{6}A scoring model (**Figure 9G**). There was no obvious difference between the RM and m^{6}A scores in predicting prognosis (**Figure S10E**).

RM Score Correlates With Immune Infiltration and Survival Prognosis in Pan-Cancer

According to the forest plots, a positive association was obvious between RM score and OS in KIRC, LGG, and LAML (**Figure S11A**). In addition, the PFS forest plot confirmed the role of RM score as a risk factor in KIRC and LGG (**Figure S11A**). As presented in **Figure S11B**, RM score is positively related to the TMB in BRCA, KIRC, LIHC, and THCA, whereas a negative association was observed in LAML and THYM. For microsatellite instability (MSI), a positive association in BRCA, DLBC, HNSC, PRAD, SKCM, and THCA, as well as a negative association in ACC, CESC, COAD, KUAD, LUSC, and UCEC, was identified (**Figure S11B**). In terms of immune cell infiltration, RM score was positively associated with regulatory T-cell content in BRCA, COAD, KIRC, KIRP, LGG, SKCM,

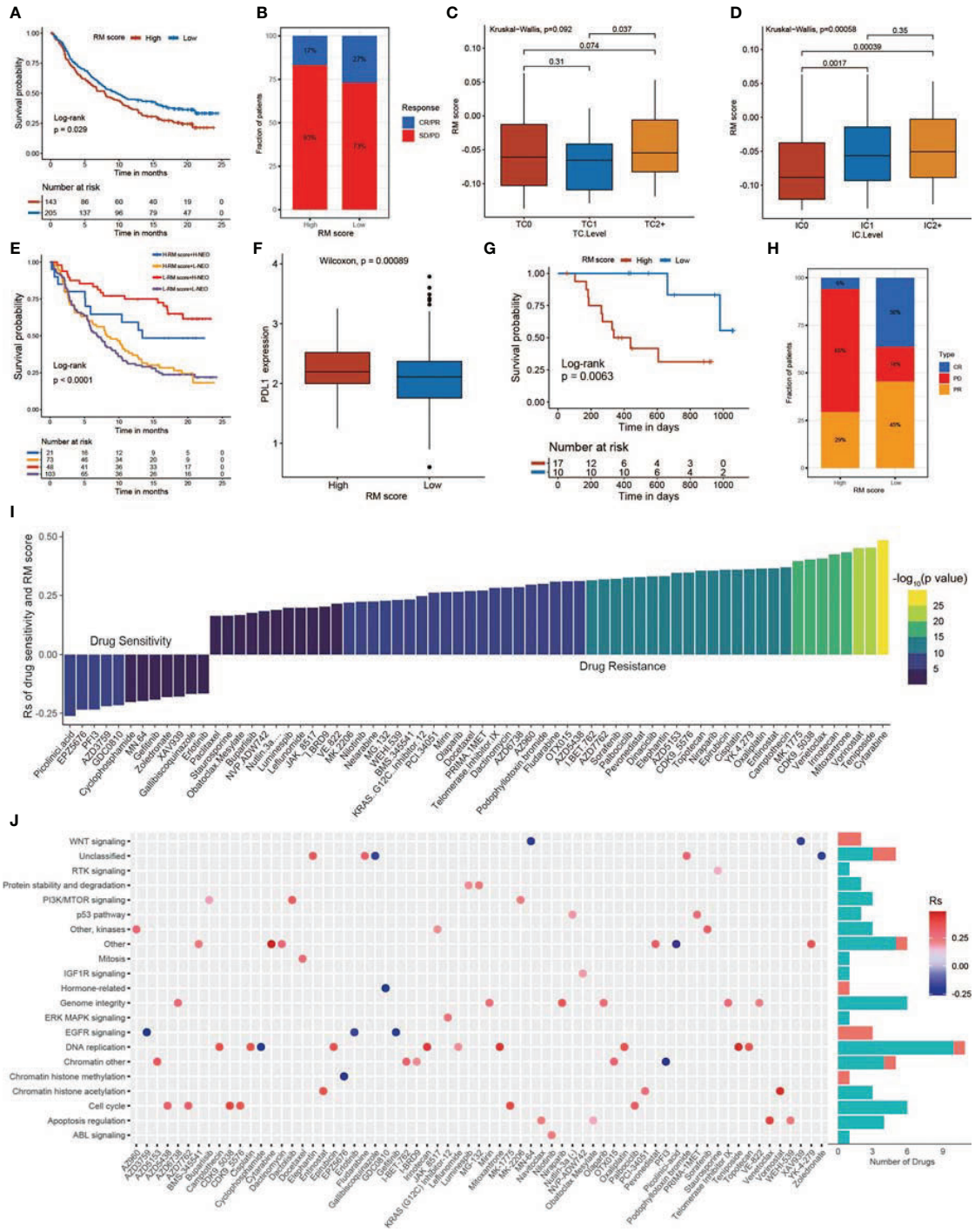

FIGURE 8 | The relationship between RM score and response to immunotherapy and drug sensitivity. **(A)** Survival analysis of the low and high RM score patient groups in an immune checkpoint blockade (ICB) therapy cohort. **(B)** The proportion of patients who responded to ICB therapy in the low or high RM score groups. **(C)** Differences in RM scores among the three tumor cell (TC) levels. (TC levels, level of IHC-assessed PD-L1 staining of tumor cells. TC0, <1%; TC1, ≥1% but <5%; TC2$^+$, ≥5% of tumor cells with staining for PD-L1, p = 0.092). **(D)** Differences in RM scores among the three immune cell (IC) levels. (IC levels, level of IHC-assessed PD-L1 staining of immune cells. IC0, <1%; IC1, ≥1% but <5%; IC2$^+$, ≥5% of immune cells staining for PD-L1, p = 0.00058). **(E)** Survival analyses of patients receiving ICB therapy stratified by RM score and TMB. **(F)** Differences in PD-L1 expression between the high and low RM score patients. **(G)** Survival analyses of the high and low RM score patient groups in another ICB therapy cohort (GSE78220). **(H)** Proportion of patients who responded to ICB therapy in the low or high RM score groups. **(I)** The relationship between RM score and drug AUC value. **(J)** Signal paths targeted by drugs whose AUC values are positive (red) or negative (blue) with RM score.

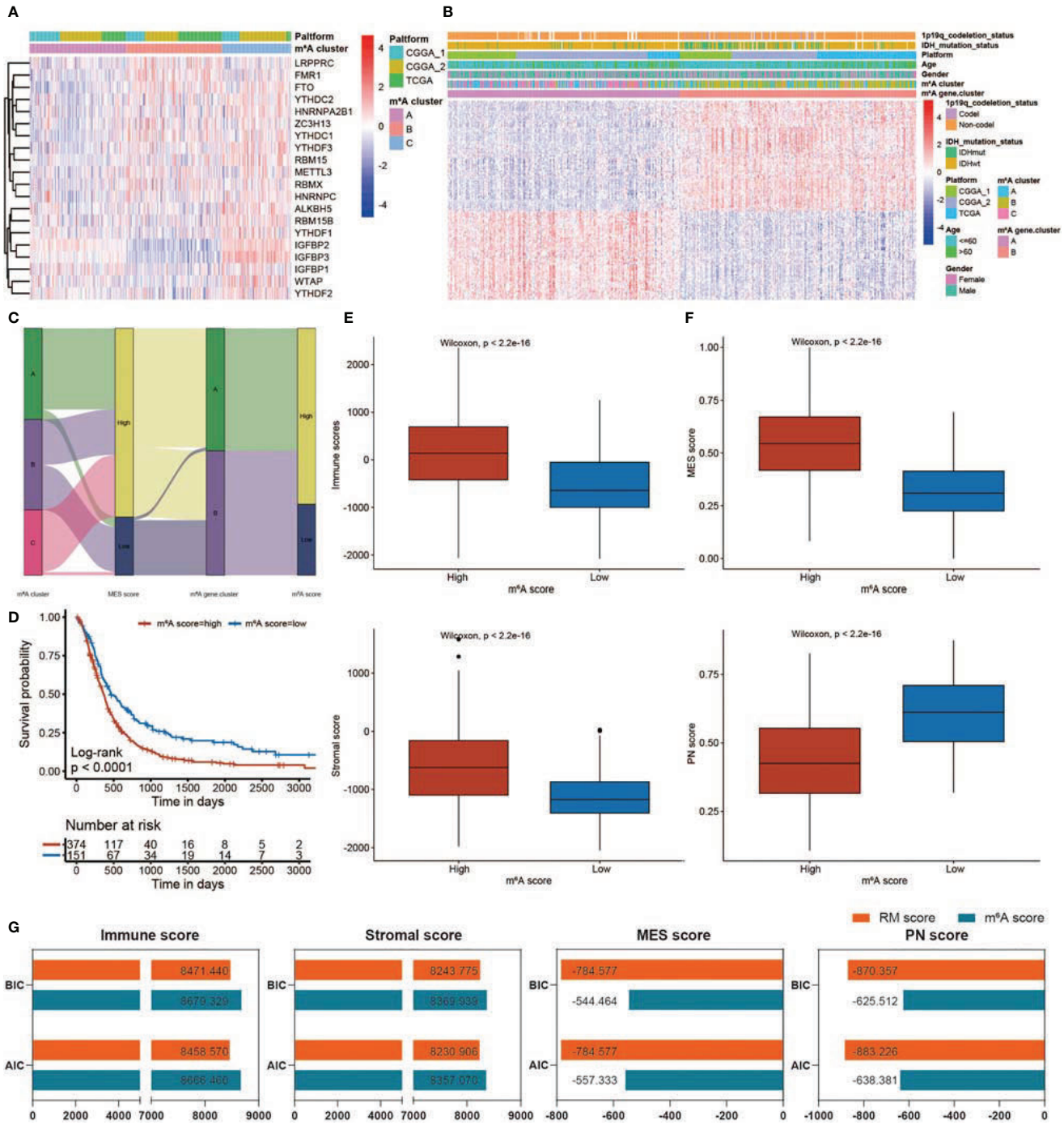

FIGURE 9 | Construction of the m^{6}A score and comparison of the m^{6}A and RM scores. **(A)** Heatmap showing unsupervised clustering for 20 m^{6}A RNA modification genes in 539 GBM patients. Each column represents patients, and each row represents an m^{6}A RNA modification regulator. **(B)** Unsupervised clustering of 172 DEGs dividing patients into two m^{6}A gene.clusters, termed m^{6}A gene.cluster_1 and m^{6}A gene.cluster_2. The m^{6}A gene.cluster, m^{6}A cluster, sex, age, platform, IDH status, and 1p19q status were applied for patient annotation. **(C)** Sankey diagram showing the distribution of m^{6}A RNA modification patterns, MES scores, m^{6}A gene.clusters, and m^{6}A scores. **(D)** KM curve showing survival analysis results of the high m^{6}A score and low m^{6}A score patient groups. **(E)** Differences in immune/stromal scores among GBMs with low m^{6}A scores and high m^{6}A scores. **(F)** Differences in MES/PN scores among GBMs with low m^{6}A scores and high m^{6}A scores. **(G)** Comparison of RM and m^{6}A scores using BIC and AIC values.

UCEC, and UCS (**Figure S11C**). In BLCA, CESC, KICH, LAML, and TGCT, RM score was positively associated with M2 macrophage infiltration (**Figure S11C**).

DISCUSSION

Increasing evidence has demonstrated that various RNA epigenetic modifications have an important effect on infection, the TME, and antitumor proliferation by interacting with several regulators. However, most studies have focused on a single regulator or a single kind of RNA modification, such as m^{6}A, and the mutual relationships and effects of regulators of various non-m^{6}A RNA modifications in cancer are not fully understood. Few studies have demonstrated that a given non-m^{6}A RNA modification influences tumorigenesis in GBM, probably because non-m^{6}A RNA modifications are not as abundant as m^{6}A modifications.

Here, we revealed global non-m^{6}A RNA alterations at the genetic as well as transcriptional levels and showed mutual correlations in GBMs. Surprisingly, there are complicated associations among 32 non-m^{6}A RNA alteration regulators. We constructed three non-m^{6}A RNA modification patterns based on 32 regulators. Cluster_A was characterized by abundant immune cell enrichment and classified as an immune-inflamed subtype; Cluster_B was characterized by the suppression of immune function as well as MES transition, corresponding to the immune-excluded subtype; and Cluster_C was marked by rare immune cell infiltration, corresponding to the immune-desert subtype. Although the immune-excluded subtype was related to abundant immune cell infiltration, the immune cells were inactive because of the distribution of effective immune cells in the tumor stroma. The stroma could permeate the tumor itself or might be confined to the tumor envelope, making immune cells appear to be inside the tumor (84). In addition, the MES score was the highest and the PN score was the lowest in Cluster_B. The immunosuppressive TME and MES transition pathways, such as the NF-κB and STAT3 signaling pathway, were markedly enriched in Cluster_B. The MES-subtype GBM tends to exhibit an immunosuppressive TME, while an immunosuppressive TME promotes GBM malignant progression *via* MES transition (62, 64). Our data demonstrated that there may be a positive feedback loop between the immunosuppressive TME and MES transition, resulting in a poor prognosis.

Furthermore, the mRNA expression differences among non-m^{6}A RNA modification patterns have been confirmed to be significantly related to RNA modification-, immune-, and MES-related biological signaling pathways. The DEGs were considered a non-m^{6}A RNA modification-related gene set. Similarly, two non-m^{6}A-related gene subtypes were identified based on the DEGs, which were obviously related to the immunosuppressive TME as well as MES transition signaling pathways. The MES subtype is particularly aggressive among these three subtypes, while the PN subtype has the best prognosis (85). This demonstrated again that the various non-m^{6}A RNA modifications were of great significance in the formation of TME patterns. In conclusion, a systematic evaluation of the non-m^{6}A RNA modification patterns will improve our understanding of TME cell infiltration and MES transition characterization.

Considering the heterogeneity of non-m^{6}A RNA modifications across individual tumors, a method for quantifying the non-m^{6}A RNA modification patterns of individual tumors is urgently needed. Accordingly, we developed a scoring model, the RM score, to evaluate the non-m^{6}A RNA modification pattern of individual GBMs. Patients with low RM scores demonstrated a prominent survival benefit. Patients in Cluster_B, characterized by an immune-excluded phenotype, exhibited a higher RM score. In addition, the RM score was significantly positively associated with immunosuppressive TME and MES transition signatures.

Immunotherapy is a developing field but is far from reaching clinical expectations in GBM patients because of the immunosuppressive TME. The MES transition not only promotes radiochemotherapy resistance but also shapes the immunosuppressive TME in GBM. Numerous studies have emphasized the non-negligible interaction between non-m^{6}A RNA regulators, the TME, and the MES transition. The RM scoring model could predict patient prognosis and sensitivity to radiochemotherapy as well as immunotherapy. Patients who were sensitive to radiochemotherapy and ICB therapy were mainly enriched in the low RM score group. In addition, the RM score was markedly positively correlated with immunosuppressive TME and MES transition signatures.

Our findings also revealed a significantly negative association between the RM score and TMB. Increasing evidence has demonstrated that patients with a high TMB present acceptable responses to immunotherapy. A high TMB status was correlated with a favorable prognosis. In addition, RM score could predict the response of a patient to anti-PD-1/L1 immunotherapy. Patients receiving ICB therapy in the IMvigor210 and GSE78220 cohorts were assessed, and we identified that the RM score was markedly decreased in patients responding to ICB, which validated the predictive significance of the RM score model. Overall, this study showed that patients with low RM scores had more obvious benefits from immunotherapy.

In addition, we investigated the possible treatment outcome of non-m^{6}A RNA modification regulators in GBMs. The RM score was positively correlated with the resistance of drugs that targeted the cell cycle and apoptosis signaling pathways and negatively correlated with the sensitivity of drugs that targeted the EGFR and WNT signaling pathways. These findings indicated that patients with higher RM scores might be more suitable for drugs targeting the EGFR and WNT signal paths instead of drugs targeting the cell cycle or apoptosis signaling pathways. Thus, non-m^{6}A RNA modification patterns could be used as a qualified predictor that can be used to predict the clinical outcome of targeted therapies or chemotherapy. Our findings reveal novel possibilities for improving the efficacy of ICB treatment, revealing different TME phenotypes as well as MES subtypes and suggesting the potential for personalized and precise immunotherapy for GBM.

Increasing evidence has demonstrated that the m^{6}A modification pattern is closely associated with the TME, prognosis, and other clinical characteristics. We constructed an

RM scoring system to evaluate the potential roles of RNA modifications beyond m^{6}A in the TME, MES transition, immunotherapy, and drug sensitivity. To further evaluate the superiority of the RM scoring model compared with the m^{6}A modification pattern, we constructed an m^{6}A scoring model and compared two models using the BIC and AIC algorithms. Finally, we confirmed that the RM scoring system is better than the m^{6}A scoring system in assessing TME and GBM subtypes.

In this study, we systematically assessed the non-m^{6}A RNA modification patterns of 539 GBMs on the basis of 32 regulator genes and associated these patterns with TME infiltration as well as MES transition characteristics. We constructed the RM score model to predict patient prognosis and the response to immunotherapy and targeted therapy. The systematic assessment of non-m^{6}A RNA modification patterns could not only improve our knowledge of the crosstalk of RNA modifications but also contribute to the development of more personalized and precise immunotherapy regimens.

DATA AVAILABILITY STATEMENT

Publicly available datasets and online tools were applied in this study. These resources could be found here: TCGA: https://portal.gdc.cancer.gov/; https://xena.ucsc.edu/; CGGA: http://www.cgga.org.cn/; GEO: https://www.ncbi.nlm.nih.gov/geo/query/acc.cgi?acc=GSE78220; GDSC: https://www.cancerrxgene.org/; CCLE: https://portals.broadinstitute.org/ccle/; IMvigor210: http://research-pub.gene.com/IMvigor210CoreBiologies/packageVersions.

ETHICS STATEMENT

The studies involving human participants were reviewed and approved by the Ethics Committee of the Qilu Hospital (Jinan, China) and performed in accordance with the relevant guidelines and regulations; the patient data were acquired from the publicly available datasets, and informed consent was given.

AUTHOR CONTRIBUTIONS

JX, ZG, and GL designed this work. JX, ZG, HX, and XG integrated and analyzed the data. JX, ZG, KL, ZZ, PZ, and LD wrote this manuscript. JX, ZG, YF, SW, HW, QW, and RZ edited and revised the manuscript. All authors contributed to the article and approved the submitted version.

FUNDING

This work was supported by grants from the National Natural Science Foundation of China (Nos. 81874083; 82072776; 82072775; 81702468; 81802966; 81902540, 81874082; 81472353), Natural Science Foundation of Shandong Province of China (Nos. ZR2019BH057; ZR2020QH174; ZR2021LSW025), the Jinan Science and Technology Bureau of Shandong Province (2021GXRC029), Key clinical Research project of Clinical Research Center of Shandong University (2020SDUCRCA011) and Taishan Pandeng Scholar Program of Shandong Province (No. tspd20210322).

SUPPLEMENTARY MATERIAL

The Supplementary Material for this article can be found online at: https://www.frontiersin.org/articles/10.3389/fimmu.2021.809808/full#supplementary-material

REFERENCES

1. Lapointe S, Perry A, Butowski NA. Primary Brain Tumours in Adults. *Lancet* (2018) 392(10145):432–46. doi: 10.1016/S0140-6736(18)30990-5
2. Yang F, He Z, Duan H, Zhang D, Li J, Yang H, et al. Synergistic Immunotherapy of Glioblastoma by Dual Targeting of IL-6 and CD40. *Nat Commun* (2021) 12(1):3424. doi: 10.1038/s41467-021-23832-3
3. Wang Q, Hu B, Hu X, Kim H, Squatrito M, Scarpace L, et al. Tumor Evolution of Glioma-Intrinsic Gene Expression Subtypes Associates With Immunological Changes in the Microenvironment. *Cancer Cell* (2017) 32 (1):42–56.e6. doi: 10.1016/j.ccell.2017.06.003
4. Zhang N, Zhang H, Wang Z, Dai Z, Zhang X, Cheng Q, et al. Immune Infiltrating Cells-Derived Risk Signature Based on Large-Scale Analysis Defines Immune Landscape and Predicts Immunotherapy Responses in Glioma Tumor Microenvironment. *Front Immunol* (2021) 12(3149). doi: 10.3389/fimmu.2021.691811
5. Boccaletto P, Machnicka MA, Purta E, Piatkowski P, Baginski B, Wirecki TK, et al. MODOMICS: A Database of RNA Modification Pathways. 2017 Update. *Nucleic Acids Res* (2018) 46(D1):D303–D7. doi: 10.1093/nar/gkx1030
6. Chen K, Song B, Tang Y, Wei Z, Xu Q, Su J, et al. Rmdisease: A Database of Genetic Variants That Affect RNA Modifications, With Implications for Epitranscriptome Pathogenesis. *Nucleic Acids Res* (2021) 49(D1):D1396–D404. doi: 10.1093/nar/gkaa790
7. Cheray M, Etcheverry A, Jacques C, Pacaud R, Bougras-Cartron G, Aubry M, et al. Cytosine Methylation of Mature Micrornas Inhibits Their Functions and Is Associated With Poor Prognosis in Glioblastoma Multiforme. *Mol Cancer* (2020) 19(1):36. doi: 10.1186/s12943-020-01155-z
8. Dominissini D, Moshitch-Moshkovitz S, Schwartz S, Salmon-Divon M, Ungar L, Osenberg S, et al. Topology of the Human and Mouse M6a RNA Methylomes Revealed by M6a-Seq. *Nature* (2012) 485(7397):201–6. doi: 10.1038/nature11112
9. Zhao BS, Roundtree IA, He C. Post-Transcriptional Gene Regulation by Mrna Modifications. *Nat Rev Mol Cell Biol* (2017) 18(1):31–42. doi: 10.1038/nrm.2016.132
10. Zhao BS, Wang X, Beadell AV, Lu Z, Shi H, Kuuspalu A, et al. M(6)a-Dependent Maternal Mrna Clearance Facilitates Zebrafish Maternal-to-Zygotic Transition. *Nature* (2017) 542(7642):475–8. doi: 10.1038/nature21355
11. Yoon KJ, Ringeling FR, Vissers C, Jacob F, Pokrass M, Jimenez-Cyrus D, et al. Temporal Control of Mammalian Cortical Neurogenesis by M(6)a Methylation. *Cell* (2017) 171(4):877–89.e17. doi: 10.1016/j.cell.2017.09.003
12. Zhang C, Chen Y, Sun B, Wang L, Yang Y, Ma D, et al. M(6)a Modulates Haematopoietic Stem and Progenitor Cell Specification. *Nature* (2017) 549 (7671):273–6. doi: 10.1038/nature23883

13. Barbieri I, Tzelepis K, Pandolfini L, Shi J, Millan-Zambrano G, Robson SC, et al. Promoter-Bound METTL3 Maintains Myeloid Leukaemia by M(6)a-Dependent Translation Control. *Nature* (2017) 552(7683):126–31. doi: 10.1038/nature24678
14. Wiener D, Schwartz S. The Epitranscriptome Beyond M(6)a. *Nat Rev Genet* (2021) 22(2):119–31. doi: 10.1038/s41576-020-00295-8
15. Shi H, Chai P, Jia R, Fan X. Novel Insight Into the Regulatory Roles of Diverse RNA Modifications: Re-Defining the Bridge Between Transcription and Translation. *Mol Cancer* (2020) 19(1):78. doi: 10.1186/s12943-020-01194-6
16. Zhao Z, Meng J, Su R, Zhang J, Chen J, Ma X, et al. Epitranscriptomics in Liver Disease: Basic Concepts and Therapeutic Potential. *J Hepatol* (2020) 73 (3):664–79. doi: 10.1016/j.jhep.2020.04.009
17. Li X, Zhu P, Ma S, Song J, Bai J, Sun F, et al. Chemical Pulldown Reveals Dynamic Pseudouridylation of the Mammalian Transcriptome. *Nat Chem Biol* (2015) 11(8):592–7. doi: 10.1038/nchembio.1836
18. Schwartz S, Bernstein DA, Mumbach MR, Jovanovic M, Herbst RH, Leon-Ricardo BX, et al. Transcriptome-Wide Mapping Reveals Widespread Dynamic-Regulated Pseudouridylation of Ncrna and Mrna. *Cell* (2014) 159 (1):148–62. doi: 10.1016/j.cell.2014.08.028
19. Jack K, Bellodi C, Landry DM, Niederer RO, Meskauskas A, Musalgaonkar S, et al. Rrna Pseudouridylation Defects Affect Ribosomal Ligand Binding and Translational Fidelity From Yeast to Human Cells. *Mol Cell* (2011) 44(4):660–6. doi: 10.1016/j.molcel.2011.09.017
20. Karijolich J, Yi C, Yu YT. Transcriptome-Wide Dynamics of RNA Pseudouridylation. *Nat Rev Mol Cell Biol* (2015) 16(10):581–5. doi: 10.1038/nrm4040
21. Li X, Ma S, Yi C. Pseudouridine: The Fifth RNA Nucleotide With Renewed Interests. *Curr Opin Chem Biol* (2016) 33:108–16. doi: 10.1016/j.cbpa.2016.06.014
22. Dominissini D, Nachtergaele S, Moshitch-Moshkovitz S, Peer E, Kol N, Ben-Haim MS, et al. The Dynamic N(1)-Methyladenosine Methylome in Eukaryotic Messenger RNA. *Nature* (2016) 530(7591):441–6. doi: 10.1038/nature16998
23. Li X, Xiong X, Wang K, Wang L, Shu X, Ma S, et al. Transcriptome-Wide Mapping Reveals Reversible and Dynamic N(1)-Methyladenosine Methylome. *Nat Chem Biol* (2016) 12(5):311–6. doi: 10.1038/nchembio.2040
24. Liu F, Clark W, Luo G, Wang X, Fu Y, Wei J, et al. ALKBH1-Mediated Trna Demethylation Regulates Translation. *Cell* (2016) 167(3):816–28.e16. doi: 10.1016/j.cell.2016.09.038
25. Wei J, Liu F, Lu Z, Fei Q, Ai Y, He PC, et al. Differential M(6)a, M(6)am, and M(1)a Demethylation Mediated by FTO in the Cell Nucleus and Cytoplasm. *Mol Cell* (2018) 71(6):973–85.e5. doi: 10.1016/j.molcel.2018.08.011
26. Dai X, Wang T, Gonzalez G, Wang Y. Identification of YTH Domain-Containing Proteins as the Readers for N1-Methyladenosine in RNA. *Anal Chem* (2018) 90(11):6380–4. doi: 10.1021/acs.analchem.8b01703
27. Hauenschild R, Tserovski L, Schmid K, Thuring K, Winz ML, Sharma S, et al. The Reverse Transcription Signature of N-1-Methyladenosine in RNA-Seq Is Sequence Dependent. *Nucleic Acids Res* (2015) 43(20):9950–64. doi: 10.1093/nar/gkv895
28. Boulias K, Toczydlowska-Socha D, Hawley BR, Liberman N, Takashima K, Zaccara S, et al. Identification of the M(6)am Methyltransferase PCIF1 Reveals the Location and Functions of M(6)am in the Transcriptome. *Mol Cell* (2019) 75(3):631–43 e8. doi: 10.1016/j.molcel.2019.06.006
29. Akichika S, Hirano S, Shichino Y, Suzuki T, Nishimasu H, Ishitani R, et al. Cap-Specific Terminal N (6)-Methylation of RNA by an RNA Polymerase II-Associated Methyltransferase. *Science* (2019) 363(6423). doi: 10.1126/science.aav0080
30. Sendinc E, Valle-Garcia D, Dhall A, Chen H, Henriques T, Navarrete-Perea J, et al. PCIF1 Catalyzes m6Am Mrna Methylation to Regulate Gene Expression. *Mol Cell* (2019) 75(3):620–30.e9. doi: 10.1016/j.molcel.2019.05.030
31. Elkon R, Ugalde A, Agami R. Alternative Cleavage and Polyadenylation: Extent, Regulation and Function. *Nat Rev Genet* (2013) 14(7):496–506. doi: 10.1038/nrg3482
32. Tian B, Manley JL. Alternative Polyadenylation of Mrna Precursors. *Nat Rev Mol Cell Biol* (2017) 18(1):18–30. doi: 10.1038/nrm.2016.116
33. Zhang LS, Liu C, Ma H, Dai Q, Sun HL, Luo G, et al. Transcriptome-Wide Mapping of Internal N(7)-Methylguanosine Methylome in Mammalian Mrna. *Mol Cell* (2019) 74(6):1304–16.e8. doi: 10.1016/j.molcel.2019.03.036
34. Lin S, Liu Q, Lelyveld VS, Choe J, Szostak JW, Gregory RI. Mettl1/Wdr4-Mediated M(7)G Trna Methylome Is Required for Normal Mrna Translation and Embryonic Stem Cell Self-Renewal and Differentiation. *Mol Cell* (2018) 71(2):244–55 e5. doi: 10.1016/j.molcel.2018.06.001
35. Dai Q, Moshitch-Moshkovitz S, Han D, Kol N, Amariglio N, Rechavi G, et al. Nm-Seq Maps 2'-O-Methylation Sites in Human Mrna With Base Precision. *Nat Methods* (2017) 14(7):695–8. doi: 10.1038/nmeth.4294
36. Grozhik AV, Jaffrey SR. Distinguishing RNA Modifications From Noise in Epitranscriptome Maps. *Nat Chem Biol* (2018) 14(3):215–25. doi: 10.1038/nchembio.2546
37. Wu S, Wang Y, Wang J, Li X, Li J, Ye K. Profiling of RNA Ribose Methylation in Arabidopsis Thaliana. *Nucleic Acids Res* (2021) 49(7):4104–19. doi: 10.1093/nar/gkab196
38. Squires JE, Patel HR, Nousch M, Sibbritt T, Humphreys DT, Parker BJ, et al. Widespread Occurrence of 5-Methylcytosine in Human Coding and Non-Coding RNA. *Nucleic Acids Res* (2012) 40(11):5023–33. doi: 10.1093/nar/gks144
39. Yang X, Yang Y, Sun BF, Chen YS, Xu JW, Lai WY, et al. 5-Methylcytosine Promotes Mrna Export - NSUN2 as the Methyltransferase and ALYREF as an M(5)C Reader. *Cell Res* (2017) 27(5):606–25. doi: 10.1038/cr.2017.55
40. Shen Q, Zhang Q, Shi Y, Shi Q, Jiang Y, Gu Y, et al. Tet2 Promotes Pathogen Infection-Induced Myelopoiesis Through Mrna Oxidation. *Nature* (2018) 554 (7690):123–7. doi: 10.1038/nature25434
41. Zou F, Tu R, Duan B, Yang Z, Ping Z, Song X, et al. Drosophila YBX1 Homolog YPS Promotes Ovarian Germ Line Stem Cell Development by Preferentially Recognizing 5-Methylcytosine Rnas. *Proc Natl Acad Sci USA* (2020) 117(7):3603–9. doi: 10.1073/pnas.1910862117
42. Li X, Xiong X, Yi C. Epitranscriptome Sequencing Technologies: Decoding RNA Modifications. *Nat Methods* (2016) 14(1):23–31. doi: 10.1038/nmeth.4110
43. Arango D, Sturgill D, Alhusaini N, Dillman AA, Sweet TJ, Hanson G, et al. Acetylation of Cytidine in Mrna Promotes Translation Efficiency. *Cell* (2018) 175(7):1872–86 e24. doi: 10.1016/j.cell.2018.10.030
44. Sharma S, Langhendries JL, Watzinger P, Kotter P, Entian KD, Lafontaine DL. Yeast Kre33 and Human NAT10 Are Conserved 18S Rrna Cytosine Acetyltransferases That Modify Trnas Assisted by the Adaptor Tan1/THUMPD1. *Nucleic Acids Res* (2015) 43(4):2242–58. doi: 10.1093/nar/gkv075
45. Licht K, Jantsch MF. Rapid and Dynamic Transcriptome Regulation by RNA Editing and RNA Modifications. *J Cell Biol* (2016) 213(1):15–22. doi: 10.1083/jcb.201511041
46. Nishikura K. A-to-I Editing of Coding and Non-Coding Rnas by Adars. *Nat Rev Mol Cell Biol* (2016) 17(2):83–96. doi: 10.1038/nrm.2015.4
47. Blanc V, Park E, Schaefer S, Miller M, Lin Y, Kennedy S, et al. Genome-Wide Identification and Functional Analysis of Apobec-1-Mediated C-to-U RNA Editing in Mouse Small Intestine and Liver. *Genome Biol* (2014) 15(6):R79. doi: 10.1186/gb-2014-15-6-r79
48. Cao D, Pizzorno G. Uridine Phosophorylase: An Important Enzyme in Pyrimidine Metabolism and Fluoropyrimidine Activation. *Drugs Today (Barcelona Spain: 1998)* (2004) 40(5):431–43. doi: 10.1358/dot.2004.40.5.850491
49. Cao D, Russell R, Zhang D, Leffert J, Pizzorno G. Uridine Phosphorylase (-/-) Murine Embryonic Stem Cells Clarify the Key Role of This Enzyme in the Regulation of the Pyrimidine Salvage Pathway and in the Activation of Fluoropyrimidines. *Cancer Res* (2002) 62(8):2313–7.
50. Brown C, Alizadeh D, Starr R, Weng L, Wagner J, Naranjo A, et al. Regression of Glioblastoma After Chimeric Antigen Receptor T-Cell Therapy. *N Engl J Med* (2016) 375(26):2561–9. doi: 10.1056/NEJMoa1610497
51. Scharping N, Menk A, Moreci R, Whetstone R, Dadey R, Watkins S, et al. The Tumor Microenvironment Represses T Cell Mitochondrial Biogenesis to Drive Intratumoral T Cell Metabolic Insufficiency and Dysfunction. *Immunity* (2016) 45(2):374–88. doi: 10.1016/j.immuni.2016.07.009
52. Xu S, Tang L, Li X, Fan F, Liu Z. Immunotherapy for Glioma: Current Management and Future Application. *Cancer Lett* (2020) 476:1–12. doi: 10.1016/j.canlet.2020.02.002
53. Niu Y, Lin Z, Wan A, Sun L, Yan S, Liang H, et al. Loss-of-Function Genetic Screening Identifies ALDOA as an Essential Driver for Liver Cancer Cell Growth Under Hypoxia. *Hepatol (Baltimore Md)* (2021) 74(3):1461–79. doi: 10.1002/hep.31846

54. Yin H, Zhang X, Yang P, Zhang X, Peng Y, Li D, et al. RNA M6a Methylation Orchestrates Cancer Growth and Metastasis *via* Macrophage Reprogramming. *Nat Commun* (2021) 12(1):1394. doi: 10.1038/s41467-021-21514-8
55. Zhang B, Wu Q, Li B, Wang D, Wang L, Zhou YL. M(6)a Regulator-Mediated Methylation Modification Patterns and Tumor Microenvironment Infiltration Characterization in Gastric Cancer. *Mol Cancer* (2020) 19(1):53. doi: 10.1186/s12943-020-01170-0
56. Du J, Ji H, Ma S, Jin J, Mi S, Hou K, et al. M6a Regulator-Mediated Methylation Modification Patterns and Characteristics of Immunity and Stemness in Low-Grade Glioma. *Briefings Bioinf* (2021) 22(5):bbab013. doi: 10.1093/bib/bbab013
57. Yue X, Lio CJ, Samaniego-Castruita D, Li X, Rao A. Loss of TET2 and TET3 in Regulatory T Cells Unleashes Effector Function. *Nat Commun* (2019) 10 (1):2011. doi: 10.1038/s41467-019-09541-y
58. Guo G, Shi X, Wang H, Ye L, Tong X, Yan K, et al. Epitranscriptomic N4-Acetylcytidine Profiling in CD4(+) T Cells of Systemic Lupus Erythematosus. *Front Cell Dev Biol* (2020) 8:842. doi: 10.3389/fcell.2020.00842
59. Nombela P, Miguel-Lopez B, Blanco S. The Role of M(6)a, M(5)C and Psi RNA Modifications in Cancer: Novel Therapeutic Opportunities. *Mol Cancer* (2021) 20(1):18. doi: 10.1186/s12943-020-01263-w
60. Bhat KPL, Balasubramaniyan V, Vaillant B, Ezhilarasan R, Hummelink K, Hollingsworth F, et al. Mesenchymal Differentiation Mediated by NF-Kappab Promotes Radiation Resistance in Glioblastoma. *Cancer Cell* (2013) 24 (3):331–46. doi: 10.1016/j.ccr.2013.08.001
61. Li H, Li J, Chen L, Qi S, Yu S, Weng Z, et al. HERC3-Mediated SMAD7 Ubiquitination Degradation Promotes Autophagy-Induced EMT and Chemoresistance in Glioblastoma. *Clin Cancer Res* (2019) 25(12):3602–16. doi: 10.1158/1078-0432.CCR-18-3791
62. Iwata R, Hyoung Lee J, Hayashi M, Dianzani U, Ofune K, Maruyama M, et al. ICOSLG-Mediated Regulatory T-Cell Expansion and IL-10 Production Promote Progression of Glioblastoma. *Neuro-Oncology* (2020) 22(3):333–44. doi: 10.1093/neuonc/noz204
63. Xu J, Zhang Z, Qian M, Wang S, Qiu W, Chen Z, et al. Cullin-7 (CUL7) Is Overexpressed in Glioma Cells and Promotes Tumorigenesis *via* NF-κb Activation. *J Exp Clin Cancer Res* (2020) 39(1):59. doi: 10.1186/s13046-020-01553-7
64. Zhang Z, Xu J, Chen Z, Wang H, Xue H, Yang C, et al. Transfer of Microrna *via* Macrophage-Derived Extracellular Vesicles Promotes Proneural-to-Mesenchymal Transition in Glioma Stem Cells. *Cancer Immunol Res* (2020) 8(7):966–81. doi: 10.1158/2326-6066.CIR-19-0759
65. Liu X, Fu Y, Huang J, Wu M, Zhang Z, Xu R, et al. ADAR1 Promotes the Epithelial-to-Mesenchymal Transition and Stem-Like Cell Phenotype of Oral Cancer by Facilitating Oncogenic Microrna Maturation. *J Exp Clin Cancer Res: CR* (2019) 38(1):315. doi: 10.1186/s13046-019-1300-2
66. Liu X, Chen D, Chen H, Wang W, Liu Y, Wang Y, et al. YB1 Regulates Mir-205/200b-ZEB1 Axis by Inhibiting Microrna Maturation in Hepatocellular Carcinoma. *Cancer Commun* (2021) 41(7):576–95. doi: 10.1002/cac2.12164
67. Bindea G, Mlecnik B, Tosolini M, Kirilovsky A, Waldner M, Obenauf A, et al. Spatiotemporal Dynamics of Intratumoral Immune Cells Reveal the Immune Landscape in Human Cancer. *Immunity* (2013) 39(4):782–95. doi: 10.1016/j.immuni.2013.10.003
68. Yoshihara K, Shahmoradgoli M, Martínez E, Vegesna R, Kim H, Torres-Garcia W, et al. Inferring Tumour Purity and Stromal and Immune Cell Admixture From Expression Data. *Nat Commun* (2013) 4:2612. doi: 10.1038/ncomms3612
69. Verhaak R, Hoadley K, Purdom E, Wang V, Qi Y, Wilkerson M, et al. Integrated Genomic Analysis Identifies Clinically Relevant Subtypes of Glioblastoma Characterized by Abnormalities in PDGFRA, IDH1, EGFR, and NF1. *Cancer Cell* (2010) 17(1):98–110. doi: 10.1016/j.ccr.2009.12.020
70. Jiang T, Nam DH, Ram Z, Poon WS, Wang J, Boldbaatar D, et al. Clinical Practice Guidelines for the Management of Adult Diffuse Gliomas. *Cancer Lett* (2021) 499:60–72. doi: 10.1016/j.canlet.2020.10.050
71. Chen DS, Mellman I. Elements of Cancer Immunity and the Cancer-Immune Set Point. *Nature* (2017) 541(7637):321–30. doi: 10.1038/nature21349
72. Qian M, Wang S, Guo X, Wang J, Zhang Z, Qiu W, et al. Hypoxic Glioma-Derived Exosomes Deliver Microrna-1246 to Induce M2 Macrophage Polarization by Targeting TERF2IP *via* the STAT3 and NF-κb Pathways. *Oncogene* (2020) 39(2):428–42. doi: 10.1038/s41388-019-0996-y
73. Xu J, Zhang J, Zhang Z, Gao Z, Qi Y, Qiu W, et al. Hypoxic Glioma-Derived Exosomes Promote M2-Like Macrophage Polarization by Enhancing Autophagy Induction. *Cell Death Dis* (2021) 12(4):373. doi: 10.1038/s41419-021-03664-1
74. Hugo W, Zaretsky JM, Sun L, Song C, Moreno BH, Hu-Lieskovan S, et al. Genomic and Transcriptomic Features of Response to Anti-PD-1 Therapy in Metastatic Melanoma. *Cell* (2016) 165(1):35–44. doi: 10.1016/j.cell.2016.02.065
75. Ayers M, Lunceford J, Nebozhyn M, Murphy E, Loboda A, Kaufman DR, et al. IFN-Gamma-Related Mrna Profile Predicts Clinical Response to PD-1 Blockade. *J Clin Invest* (2017) 127(8):2930–40. doi: 10.1172/JCI91190
76. Phillips HS, Kharbanda S, Chen R, Forrest WF, Soriano RH, Wu TD, et al. Molecular Subclasses of High-Grade Glioma Predict Prognosis, Delineate a Pattern of Disease Progression, and Resemble Stages in Neurogenesis. *Cancer Cell* (2006) 9(3):157–73. doi: 10.1016/j.ccr.2006.02.019
77. Behnan J, Finocchiaro G, Hanna G. The Landscape of the Mesenchymal Signature in Brain Tumours. *Brain* (2019) 142(4):847–66. doi: 10.1093/brain/awz044
78. McGranahan N, Furness AJS, Rosenthal R, Ramskov S, Lyngaa R, Saini SK, et al. Clonal Neoantigens Elicit T Cell Immunoreactivity and Sensitivity to Immune Checkpoint Blockade. *Science* (2016) 351(6280):1463. doi: 10.1126/science.aaf1490
79. Cristescu R, Mogg R, Ayers M, Albright A, Murphy E, Yearley J, et al. Pan-Tumor Genomic Biomarkers for PD-1 Checkpoint Blockade-Based Immunotherapy. *Science* (2018) 362(6411):eaar3593. doi: 10.1126/science.aar3593
80. Goodman AM, Kato S, Bazhenova L, Patel SP, Frampton GM, Miller V, et al. Tumor Mutational Burden as an Independent Predictor of Response to Immunotherapy in Diverse Cancers. *Mol Cancer Ther* (2017) 16(11):2598–608. doi: 10.1158/1535-7163.MCT-17-0386
81. Mariathasan S, Turley SJ, Nickles D, Castiglioni A, Yuen K, Wang Y, et al. Tgfbeta Attenuates Tumour Response to PD-L1 Blockade by Contributing to Exclusion of T Cells. *Nature* (2018) 554(7693):544–8. doi: 10.1038/nature25501
82. Balar AV, Galsky MD, Rosenberg JE, Powles T, Petrylak DP, Bellmunt J, et al. Atezolizumab as First-Line Treatment in Cisplatin-Ineligible Patients With Locally Advanced and Metastatic Urothelial Carcinoma: A Single-Arm, Multicentre, Phase 2 Trial. *Lancet* (2017) 389(10064):67–76. doi: 10.1016/S0140-6736(16)32455-2
83. Yang W, Soares J, Greninger P, Edelman EJ, Lightfoot H, Forbes S, et al. Genomics of Drug Sensitivity in Cancer (GDSC): A Resource for Therapeutic Biomarker Discovery in Cancer Cells. *Nucleic Acids Res* (2013) 41(Database issue):D955–61. doi: 10.1093/nar/gks1111
84. Joyce J, Fearon D. T Cell Exclusion, Immune Privilege, and the Tumor Microenvironment. *Science (New York NY)* (2015) 348(6230):74–80. doi: 10.1126/science.aaa6204
85. Wang Z, Zhang H, Xu S, Liu Z, Cheng Q. The Adaptive Transition of Glioblastoma Stem Cells and Its Implications on Treatments. *Signal Transduct Target Ther* (2021) 6(1):124. doi: 10.1038/s41392-021-00491-w

Conflict of Interest: The authors declare that the research was conducted in the absence of any commercial or financial relationships that could be construed as a potential conflict of interest.

Publisher's Note: All claims expressed in this article are solely those of the authors and do not necessarily represent those of their affiliated organizations, or those of the publisher, the editors and the reviewers. Any product that may be evaluated in this article, or claim that may be made by its manufacturer, is not guaranteed or endorsed by the publisher.

Copyright © 2022 Xu, Gao, Liu, Fan, Zhang, Xue, Guo, Zhang, Deng, Wang, Wang, Wang, Zhao and Li. This is an open-access article distributed under the terms of the Creative Commons Attribution License (CC BY). The use, distribution or reproduction in other forums is permitted, provided the original author(s) and the copyright owner(s) are credited and that the original publication in this journal is cited, in accordance with accepted academic practice. No use, distribution or reproduction is permitted which does not comply with these terms.

frontiers in Immunology

REVIEW
published: 17 February 2022
doi: 10.3389/fimmu.2022.829451

Tumor Immune Microenvironment and Immunotherapy in Brain Metastasis From Non-Small Cell Lung Cancer

Yuchang Wang[1,2,3,4†], *Rui Chen*[5†], *Yue Wa*[1,2,3,4], *Shikuan Ding*[1,2,3,4], *Yijian Yang*[1,2,3,4], *Junbo Liao*[1,2,3,4], *Lei Tong*[1,2,3,4] *and Gelei Xiao*[1,2,3,4*]

[1] Department of Neurosurgery, Xiangya Hospital, Central South University, Changsha, China, [2] Diagnosis and Treatment Center for Hydrocephalus, Xiangya Hospital, Central South University, Changsha, China, [3] Hunan International Scientific and Technological Cooperation Base of Brain Tumor Research, Xiangya Hospital, Central South University, Changsha, China, [4] National Clinical Research Center for Geriatric Disorders, Xiangya Hospital, Central South University, Changsha, China, [5] Department of Neurosurgery, Affiliated Nanhua Hospital, Hengyang Medical School, University of South China, Hengyang, China

OPEN ACCESS

Edited by:
Wen Cheng,
The First Affiliated Hospital of China Medical University, China

Reviewed by:
Gang Zhou,
Augusta University, United States
Xinwen Zhong,
East China Normal University, China

***Correspondence:**
Gelei Xiao
xiaogelei@csu.edu.cn

†These authors have contributed equally do this work

Specialty section:
This article was submitted to Cancer Immunity and Immunotherapy, a section of the journal Frontiers in Immunology

Received: *05 December 2021*
Accepted: *31 January 2022*
Published: *17 February 2022*

Citation:
Wang Y, Chen R, Wa Y, Ding S, Yang Y, Liao J, Tong L and Xiao G (2022) Tumor Immune Microenvironment and Immunotherapy in Brain Metastasis From Non-Small Cell Lung Cancer. Front. Immunol. 13:829451. doi: 10.3389/fimmu.2022.829451

Brain metastasis (BM), a devastating complication of advanced malignancy, has a high incidence in non-small cell lung cancer (NSCLC). As novel systemic treatment drugs and improved, more sensitive imaging investigations are performed, more patients will be diagnosed with BM. However, the main treatment methods face a high risk of complications at present. Therefore, based on immunotherapy of tumor immune microenvironment has been proposed. The development of NSCLC and its BM is closely related to the tumor microenvironment, the surrounding microenvironment where tumor cells live. In the event of BM, the metastatic tumor microenvironment in BM is composed of extracellular matrix, tissue-resident cells that change with tumor colonization and blood-derived immune cells. Immune-related cells and chemicals in the NSCLC brain metastasis microenvironment are targeted by BM immunotherapy, with immune checkpoint inhibition therapy being the most important. Blocking cancer immunosuppression by targeting immune checkpoints provides a suitable strategy for immunotherapy in patients with advanced cancers. In the past few years, several therapeutic advances in immunotherapy have changed the outlook for the treatment of BM from NSCLC. According to emerging evidence, immunotherapy plays an essential role in treating BM, with a more significant safety profile than others. This article discusses recent advances in the biology of BM from NSCLC, reviews novel mechanisms in diverse tumor metastatic stages, and emphasizes the role of the tumor immune microenvironment in metastasis. In addition, clinical advances in immunotherapy for this disease are mentioned.

Keywords: cancer, BM, immunotherapy, NSCLC, PD-1 inhibitor, PD-L1 inhibitor

Abbreviations: BM, brain metastasis; NSCLC, non-small cell lung cancer; BBB, blood-brain barrier; CNS, central nervous system; TME, tumor microenvironment; ECM, extracellular matrix; ICIs, immune checkpoint inhibitors; MMP, matrix metalloproteinases; CXCR, C-X-C chemokine receptor; EMT, epithelial-mesenchymal transition; CTCs, circulating tumor cells; MDK, midkine; PD-1, programmed cell death protein 1; CXCL, C-X-C motif chemokine ligand; Treg, regulatory T; CTLA-4, T-lymphocyte-associated protein-4; PD-L1, programmed cell death ligand 1; TILs, tumor infiltrate lymphocytes; TAM/M, tumor-associated macrophages and microglia; CAFs, cancer-associated fibroblasts.

INTRODUCTION

The rate of brain metastasis (BM) from solid tumors was about 7.3 persons/100,000 with most patients above 50 years (91.9%) who have a poorer prognosis. The most common primary lesions for BM are the lung (80%), melanoma (3.8%), breast (3.7%), and kidney/renal pelvis (3.0%) (1–3) (**Table 1**). Non-small cell lung cancer (NSCLC) accounts for almost half of all BM cases, and NSCLC is associated with a horrible prognosis (4, 5). Patients who do not receive therapy for BM from NSCLC have a median overall survival of only 1 to 2 months. Age, extracranial tumor activity, the number of BM, and the initial tumor type/molecular subtype are important factors determining patients' prognosis (6, 7). Previously, surgical resection was a high-risk procedure that placed strict limits on the number and location of the lesions in the brain (8). Whole-brain radiotherapy and stereotactic radiotherapy, both effective therapies and local controls for BM from NSCLC, are other options (9). However, radionecrosis may occur in more than 1/3 of patients, resulting in neurotoxicity (10). On the other hand, chemotherapeutic drugs are often incapable of crossing the blood-brain barrier (BBB) and reaching intracranial lesions. As a result, the use of chemotherapeutic drugs to slow the course of the central nervous system(CNS) is less meaningful (11).

The occurrence and BM of NSCLC are closely related to the tumor microenvironment (TME). TME is the surrounding microenvironment where tumor cells live. TME comprises cellular and non-cellular components such as blood vessels, fibroblasts, immune cells, bone marrow-derived inflammatory cells, signaling chemicals, and extracellular matrix (ECM) (12). Tumors and their surroundings are inextricably linked and constantly interact, with tumors influencing their microenvironment by releasing cellular signaling molecules that promote tumor angiogenesis and induce immune tolerance. So immune cells in the microenvironment influence cancer cells' growth and development. The microenvironment of the brain is different and bears little resemblance to other organs. Even when BM occurs, the microenvironment remains distinctly different from other organs (13).

Cancer immunotherapy has become a significant study issue in recent years, spawning new techniques to modulate the immune system. BM comprises complicated immunological microenvironment and signaling processes, with many potential treatment targets still to be discovered (11). Evasion of the host immune response is a hallmark of cancer progression. Blocking of cancer immunosuppression by targeting immune checkpoints provides a suitable strategy for immunotherapy in patients with advanced cancers such as NSCLC and melanoma (14). Immune checkpoint inhibitors (ICIs) target inhibitory immune checkpoints and boost the anti-tumor immune response. ICIs have shown excellent clinical success in advanced melanoma, metastatic kidney cancer, and NSCLC. Even pembrolizumab alone has been reported to eradicate stage IV BM from NSCLC (15). Because the immune response in the brain is so tightly controlled, researching immunomodulatory therapy for BM is challenging.

This article discusses the impact of TME on NSCLC and BM, focusing on the specificity of BM. The presence of barriers and specialized cells makes the TME of BM unusual and demonstrates differences from NSCLC in many aspects, especially in the immune. Features of BM suggests a lack of research about the brain and directs therapy in a new direction. The birth of immunotherapy is both dependent on the gradual refinement of the theory and inextricably linked to the remarkable efficacy in practice. The excellent role played in patients with BM from NSCLC has also led to combining traditional approaches and immunotherapy.

BBB

BBB is a selective barrier of CNS, which isolates the brain from the harmful substance from the systemic circulating blood, consisting of endothelial cells, pericytes, and the foot processes of astrocytes (16). BBB is the most important structure for the tumor cell to get through in BM. The key to the wholeness and selectivity of the BBB is the tight junction composed of claudins, occludins, zona occludens proteins, and junctional adhesion molecules (17).

The immunocytes are also involved in the destruction of BBB. T cell is founded as a helper of BBB crossing. In the research of Mustafa, Dana A M, et al., Guanylate-Binding Protein 1 is considered a vital T cell-induced protein, which promotes the tumor cells crossing the BBB. The patients who developed BM show Guanylate-Binding Protein 1 upregulate (18). In addition, as one of the most widely distributed cell types in the brain, astrocytes play an important part in the formation of BM, including BBB crossing. The astrocyte could secrete multiple matrix metalloproteinases (MMP), among which MMP2 and MMP9 are widely researched and considered a breaker of BBB (19). The research of Rempe et al. shows that MMP1 is strongly associated with BM by degrading Claudin and Occludin but not tight junction protein Zo-1 (20). Microglia is an immunocyte of the CNS, mediating apoptosis. However, when malignant tumors metastasize, they inhibit apoptosis and invade the BBB using tissue damage responses involving C-X-C chemokine receptor (CXCR)4 and *Wnt* signaling (21). According to the research of Qiao S et al. in melanoma, the microglia is found highly expressed MMP3, relating to the decrease of Zo-1, which may facilitate tumor invasion (22). The previous studies have mainly focused on breast cancer and melanoma, but the differences between tumor cell types are still unknown. Due to the importance of the BBB and its extensive interactions with surrounding cells and stroma, the study of the BBB is essential before further description of the development of BM. The role of BBB in the development of BM from NSCLC will be further described in the following section through the process of BM.

DEVELOPMENT OF BM FROM NSCLC

The development of BM from NSCLC is a complicated, interacting, and changing process that involves tumor cells (mutations, epigenetic variation), cytokines, interactions with other tumor cells, and normal cells in the surrounding area. Clinical identification of high-risk BM in individuals with NSCLC is critical. As a result, a thorough understanding of

TABLE 1 | Contrast of NSCLC BM, breast cancer BM, melanoma BM and primary brain cancer (Glioblastoma).

	NSCLC BM	breast cancer BM	melanoma BM	Glioblastoma
Median number of tumors per patient	3 (1-6)	3 (1-11)	2 (1-6)	1
Median single tumor volume in cc	0.06	0.01	0.12	43.20
Preference of distribution	the infratentorial area, frontal lobe	structures supplied by the posterior circulation areas	supratentorial area	supratentorial area (frontal, temporal, parietal and occipital lobes)
Common Mutations	EGFR, ALK, KRAS, RET, ROS-1	HER2, PR, ER	BRAF, NRAS	EGFR, PTEN, TP53, CDKN2A
Median OS in Months	5.0 、16	10.0-15.0	2.5-6.0	11.4-15
Median age of the patients (year)	62	48.8	60	64
Common biomarker in ICI	PD-L1	PD-L1	PD-L1, CTLA-4	None

NSCLC, non-small cell lung cancer; BM, brain metastasis; OS, overall survival; EGFR, epidermal growth factor receptor; ALK, anaplastic lymphoma kinase; KRAS, Kirsten rat sarcoma viral oncogene homolog; RET, rearranged during transfection; ROS-1, c-ros oncogene 1; HER2, Human epidermal growth factor receptor 2; PR, progesterone receptor; ER, estrogen receptor; BRAF, v-raf murine sarcoma viral oncogene homolog B1; NRAS, neuroblastoma RAS viral oncogene homolog; PTEN, phosphatase and tensin homolog; TP53, Tumor Protein P53; CDKN2A, Cyclin Dependent Kinase Inhibitor 2A.

NSCLC and BM is required. Since 1889, Paget introduced the "seed and soil" theory to explain BM (23), epithelial-mesenchymal transition (EMT), cancer stem cells, circulating tumor cells (CTCs), and other hypotheses have been proposed. Tumor metastasis mechanisms have steadily been added. The development of BM from NSCLC is closely related to the TME (11), which is involved in these mechanisms (**Figure 1**).

EMT is a fundamental notion in the development of metastasis. Most tumors originate from epithelial cells and spread into the surrounding connective tissue (cancerous mesenchymal cells). Mesenchymal cells, unlike epithelial cells, are rarely involved in intercellular interactions and lack cell polarity. Mesenchymal cells are more aggressive than epithelial cells because of these properties, and EMT is required to transform benign tumors into invasive carcinomas (24). The existence of EMT is demonstrated by abnormal expression of N-cadherin in tumor metastasis (25), and the transcription factor Snail, which regulates N-cadherin, is implicated in the migration and invasion of NSCLC cells mediated by Zinc transporter4. In the Snail-N-cadherin signaling axis, Zinc transporter4 plays a crucial regulatory role in encouraging NSCLC progression, and it may be a prognostic marker and treatment target for NSCLC (26). Hypoxia has also been identified as a critical cause of EMT in NSCLC. Hypoxia-inducible factor (HIF) is induced to activate in primary TME as the oxygen supply at the tumor's center decreases with tumor growth. HIF-1α, which elevates midkine (MDK) levels in NSCLC cells, is required for NSCLC cell proliferation in hypoxic environments. *Via* paracrine signaling, MDK stimulates endothelial cell migration and neointima formation. MDK produced by NSCLC cells also interacts with Notch2, activating *Notch* signaling, inducing EMT, upregulating NF-κB, and promoting cancer (27). MDK inhibitors could be a new treatment option for NSCLC patients. Angiogenesis and lymphangiogenesis are triggered by hypoxia, growth hormones, and receptors in the TME, which enhance cancer cell dispersion.

Circulating tumor cells, also known as CTCs, are injected into the local blood and lymph and survive the dissemination process. Tumor cells are first isolated from the primary tumors and spread throughout the surrounding tissues, capillaries, tiny veins, and lymphatic system. Tumor cells are vulnerable to physical and immunological damage once in circulation, making it harder for CTCs to launch a metastatic cascade response. To overcome the difficulties, tumor cells must boost the programming and intrinsic adaptation required for metastasis. Every CTC must get through the BBB to reach the brain. It is the first step to overcome the BBB for the CTCs to get to the brain and propagate. Several experiments have shown that the CTCs could traverse the BBB. However, the specific mechanism is not well understood yet (28). There are still some cells that succeed in overcoming the BBB. The tight junction of BBB makes it harder to pass than the other organs. Several cytokines, chemokines, and inflammatory agents can disrupt these interactions. Over 70% of BM shows varying degrees of BBB destruction, implying the CTCs might affect the tight junction (29).

The step CTCs crossing the BBB is like the leukocyte (rolling, adhesion, extravasation). Two possible pathways of extravasation have been described: the paracellular route and the transcellular route (30, 31). CD15 and CD15s interact with CD62E to promote lung cancer cell adherence to the brain endothelium, exhibiting features comparable to white blood cells but interfering with FUT4/CD15 and FUT7/CD15s can inhibit CTCs invasion (32–34). As reported, FUT4 has been linked to programmed cell death protein 1 (PD-1)-related immunosuppression, which leads to poorer prognosis in patients with operable lung cancer (35). CTCs could produce many factors to help destroy the BBB, including cyclooxygenase cyclooxygenase2, C-X-C motif chemokine ligand (CXCL)12/CXCR4, ST6GALNAC5, cathepsin S, MMP-1, α-crystallin, angiopoietin-like 4, and vascular endothelial growth factor (28, 36, 37). The link between CTCs and BBB is reciprocal, which frequently exhibits positive feedback. For example, when metastatic tumor cells and tumors penetrate brain tissue, the integrity of the BBB is destroyed, and the degradation of BBB integrity further promotes tumor BM.

TME AND IMMUNOTHERAPY OF BM FROM NSCLC

The TME of BM is not identical to that of primary NSCLC (13). In fact, in the physiological scenario, normal brain tissue differs from other tissues by a few key characteristics. The ECM composition and type of tissue-resident cells (including microglia, astrocytes, and neurons) in normal brain tissue are distinct. The brain is physically protected by the BBB, which plays an important role in the immune response (38). In the event of BM, the metastatic TME in BM is composed of ECM and tissue-resident cells that change with tumor colonization, as well as blood-derived immune cells. Even though the concept that the brain is an "immune privileged" organ was widely recognized, it is now widely believed that immune cells from the peripheral circulation can penetrate the skull (39). This change originates from the discovery of meningeal lymphatics and the hypothesis that BM might compromise the integrity of the BBB (40). The immune microenvironment of BM undergoes profound changes with the alteration of native immune cells in the brain and the entry of blood-derived immune cells, and these changes are often immunosuppressive (38) (**Table 2** and **Figure 2**).

T Cells and Regulatory T Cells

Regulatory T (Treg) cells are primarily CD4+ T cells that constitutively express CD25 molecules and specifically express foxp3 transcription factors. There is growing evidence for Treg cells' active involvement in the negative regulation of various physiological and pathological immune responses (41). Mature Treg cells are generated through two distinct developmental processes, CD25 + Treg cell progenitors and Foxp3lo Treg cell progenitors. In either developmental process, Treg cells are dependent on IL-2 for development and maintenance of activity (42). Different evidence exhibits different specialties of Treg from the two sources, with mature Treg cells from the former having a unique position in promoting immune tolerance and the latter having a unique role in preventing autoimmunity (43). When NSCLC occurs, T Cells and Treg cells keep the TME of BM in an immunosuppressed state. Many Treg cells infiltrating, especially a low CD8 + T cell to Treg cell ratio in tumor tissue, is significantly associated with poor prognosis (44). When BM occurs in NSCLC, the abundance and infiltration of CD8+ T cells, CD4+ T cells, and Treg cells in the microenvironment of BM are lower compared to the primary focus (45, 46). And this relatively low value does not involve changes in T cell sequences, with no statistically significant differences in T-cell receptor β sequence clonality in BM and

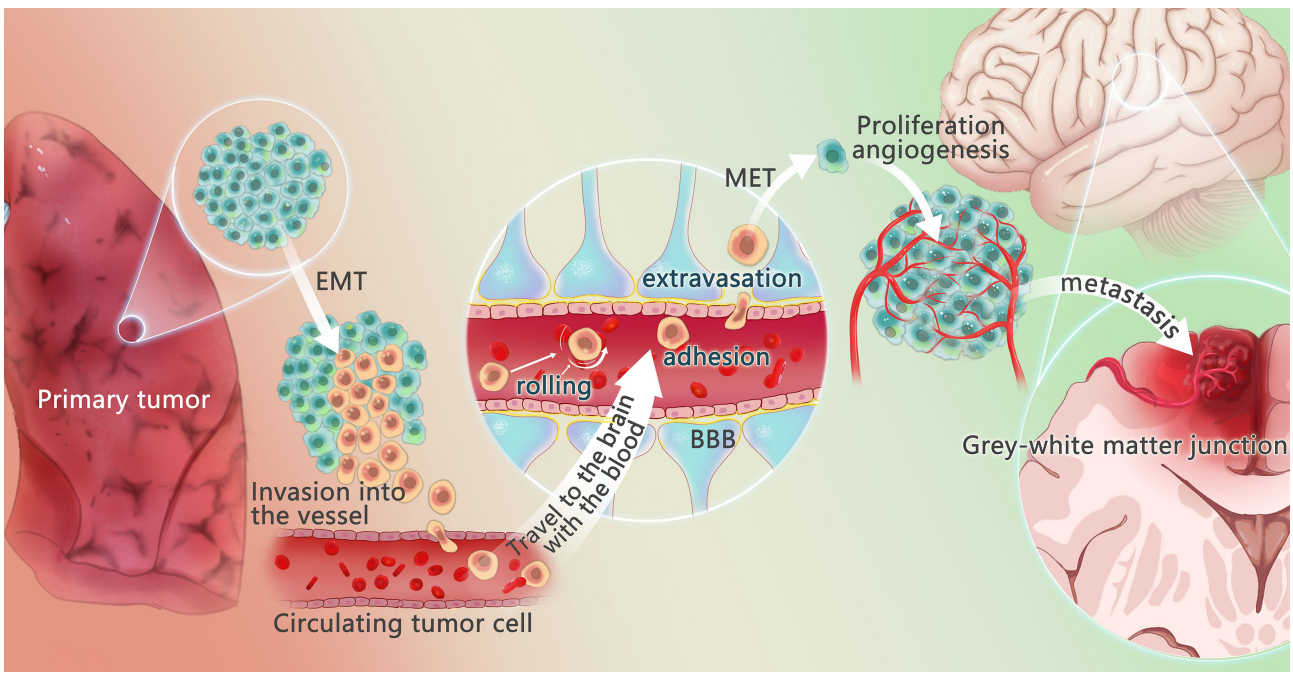

FIGURE 1 | Mechanism of lung cancer brain metastasis. The changes of tumor microenvironment may promote some tumor cells to undergo epithelial-mesenchymal transition (EMT) process, to get the potential of metastasis and avoid apoptosis. These tumor cells escape from the primary tumor in the lung, invade the vessels, and circulate through the vessels, called circulating tumor cells (CTCs). Under the action of chemokines, CTCs reach the brain, cross the blood-brain barrier through rolling, adhesion and extravasation under the effect of E-ligand and integrin, undergo mesenchymal-epithelial transformation (MET) to regain the characteristic of the primary tumor, recover the characteristics of the primary tumor, and produce and adapt to the new tumor microenvironment. Angiogenesis is required for the growth of metastases. When pure oxygen diffusion is not sufficient for the tumor, the tumor gradually develops a hypoxic microenvironment and overexpress angiogenesis-stimulating factors, promoting the angiogenesis. The brain metastasis often happens in the gray and white matter junction and vascular border zones, where there is a longer mean transit times (MTT)of blood flow, providing more chance to overcome the blood-brain barrier.

TABLE 2 | Feature of the TME of NSCLC brain metastasis comparing with primary tumor.

Microenvironment features		Significance
T cells	Fewer T cells in total (including Th1 cells or TILs) Lower abundance measurements of Th1 or CD8 T genes Inhibition of Th1 immune response	Form an immunosuppressed TME, providing a better chance for the tumor growth
Macrophage	Higher Gene expression levels of the macrophage (M2-like) marker arginase-I (ARG1) more anti-inflammatory TAMs Lower relative abundances of macrophage genes	Present an immunosuppressed TME
DC	Inhibition of DC maturation Lower relative abundances of DC genes	Suppress antigen presentation
VCAM1	Reduced expression of VCAM1	Suppress adhesion of leukocytes
Astrocytes	$pSTAT3^+$ reactive astrocytes	Inhibit $CD8^+$ T cell activation and increase expression of immuno-inhibitory protein PD-L1, promote brain metastasis
	EVs or gap junctions with tumor cell	Promote the survival of metastasis and increase the resistance of chemotherapy

TME, tumor microenvironment; NSCLC, non-small cell lung cancer; type 1 T helper; TILs, tumor Infiltrating Lymphocytes; TAMs, tumor associated macrophages; DC, dendritic cell; VCAM1, vascular cell adhesion molecule 1; pSTAT3, Phosphorylated transducer and activator of transcription-3; PD-L1, programmed death ligand 1; EVs, extracellular vesicles.

primary lung tumor and non-malignant lung parenchyma (47). More reduced T cell abundance and infiltration compared to NSCLC, along with suppression of antigen presentation (suppressed dendritic cells maturation), lymphocyte extravasation, and leukocyte adhesion (reduced vascular cell adhesion protein 1), together contribute to an immunosuppressive microenvironment in BM (47).

Tumor-infiltrating Treg cells expressed higher surface molecules related to T cell activation in CD25, T-lymphocyte-associated protein-4 (CTLA-4), PD-1, and TNF receptor superfamily members compared to Treg cells in lymphoid tissue, non-lymphoid tissue, or blood (48). CTLA-4 and PD-1 belong to the second signal, which comes after the initial signal to activate CTL in cancer immunity. In tumor immunity, the initial signal is T cell receptor recognition of the major histocompatibility complex accompanied by cancer-specific antigens. The second signal is often known as immunological checkpoints, including stimulatory and inhibitory molecules that keep the immune system active (49). Tumor cell invasion is suppressed after T cell activation. Cancer progression is characterized by the evasion of the host immune response. As a result, blocking cancer immunosuppression can occur throughout the entire process of immune activation, in which targeting immunological checkpoints is an effective immunotherapy method for BM. In BM from NSCLC, CTLA-4 has been less studied, while PD-1 has been more studied and related therapies have been developed. The primary physical role of PD-1 is to maintain peripheral tolerance and keep T cell responses within the appropriate physiological range (50). Because an immune response triggers the PD-1/programmed cell death ligand 1(PD-L1) regulatory mechanism, a negative feedback loop that reduces local T-cell reactions and tissue damage is created (51). When NSCLC occurs, tumor-derived IL-6 stimulates PD-L1(+) myeloid cells (52). When PD-1 binds to PD-L1, cytotoxic T cells that detect tumor cells become inactive, promoting immune escape (14).

As a result, the expression of PD-1/PD-L1 is one of the most critical indicators of tumor status (53). ICIs may be helpful in the treatment of individuals with NSCLC to prevent BM, as impaired peripheral immune function increases tumor spread. When BM occurs in NSCLC, activated T cells, monocytes, and dendritic cells are among the immune cells that express PD-1 (54). Meanwhile, tumor cells, as well as immune cells, such as T cells, B cells, macrophages, and dendritic cells, express PD-L1 (55). Due to differences in TME, there may be inconsistent responses to ICIs for NSCLC between primary tumor lesion and BM. On the one hand, PD-1 + tumor infiltrate lymphocytes (TILs) are less permeable in BM, which may significantly reduce the ICIs effect of anti-PD-1 (45). On the other hand, PD-L1 is generally higher at metastatic sites (56), which is also associated with the efficacy of ICIs. PD-1/PD-L1 expression in patients with BM from NSCLC taking immunotherapy may predict survival independently (57).

Based on the functional role of PD-1/PD-L1 expression and distribution, it is unavoidable to predict its illustrious future in treating BM from NSCLC. Both PD-1 and PD-L1 inhibitors were beneficial in patients with CNS diseases in the first trial focusing on a group of patients with BM from NSCLC and assessing the effects of immunotherapy (58). Despite this, the mechanism of action of PD-1/PD-L1 is not entirely clear (38), and drug development is underway, with more research as a goal in the future.

Tumor-Associated Macrophages and Microglia

Tumor-associated macrophages and microglia (TAM/M) are highly plastic and receptive to cytokine, chemokine, and growth factor signals. Their activation promotes cell invasion, angiogenesis, metastasis, and immunosuppression (59). TAM/M is the main non-tumor cell in glioma (60) and is second in density to BM lymphocytes (61). TAM/m activation types include a pro-inflammatory, anti-tumor M1-like phenotype and an anti-inflammatory, pro-tumor M2-like phenotype. M1 macrophages highly express inducible nitric oxide synthase and secrete IL-1, IL-12, NO, and TNF-α, which have tumor-killing effects. M1-type markers are TNF-α, CD80, CXCL9, and CXCL10 (62). In response to IFN-γ and lipopolysaccharide, M1 macrophages, which secrete high levels of IL-12, inhibit tumor development (63).M2-type macrophages secrete arginase, IL-10, lipopolysaccharide, IFN-γ, inhibit CD8+ T cell proliferation, and promote tumor cell growth.M2-type markers CD204 and CD206, CCL17 and CCL18, etc. (62). M2

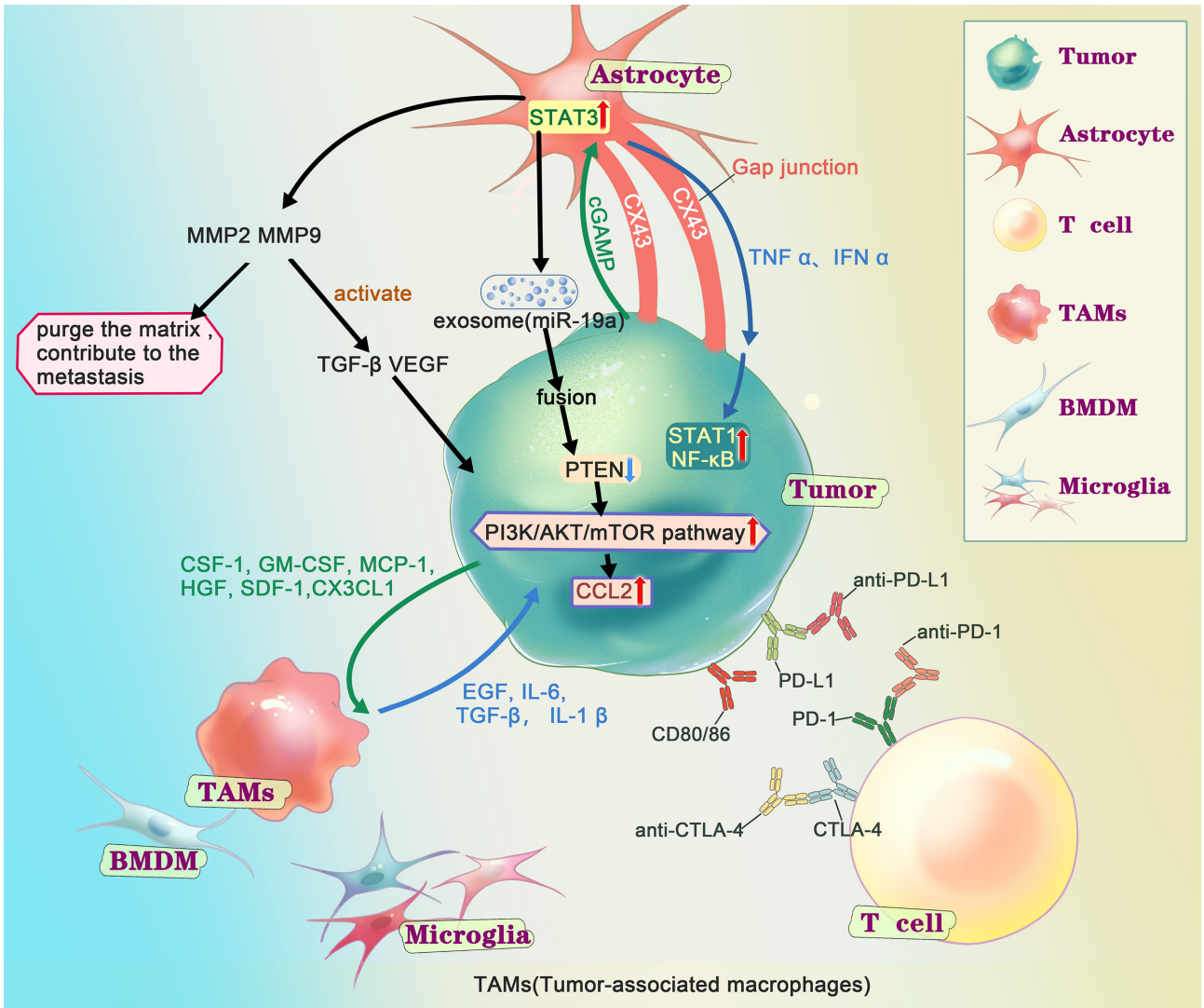

FIGURE 2 | Interactions of metastatic tumor cells with the brain microenvironment. After the tumor cells get into the CNS (central nervous system), according to the "seed and soil", series of interactions happened between the tumor cells and the microenvironment in brain. Extensive research has shown that astrocytes play an important role in metastasis through matrix metalloproteinase 2 (MMP2), MMP9, exosome and gap junction, generally supports the growth and invasion. MMP2、MMP9 are associated with tumor growth. On the one hand, it could degrade components of the extracellular matrix and basement membrane, on the other hand, it helps to activate TGF-β and VEGF. Several studies have shown that after fusion of AST-generating exosomes with tumor cells, miRNAs contained in the exosomes cause tumor cells to under-express PTEN and further activate the PI3K/AKT/mTOR pathway, leading to more chemokine ligand 2(CCL2), promoting the growth of tumor. There are gap junctions composed of connexin 43 (Cx43) between tumor cell and astrocyte. Through the gap junction, astrocyte release cytokines such as IFNα and TNFα, activating STAT1 and NF-κB pathways, supporting tumor growth. At the same time, tumor cell could transfer cGAMP to astrocytes, activate the STAT3 pathways. Tumor-associated macrophages and microglia (TAMs), including bone marrow-derived macrophages (BMDMs) and microglia (MG), secret growth factors (EGF, IL6, TGF-β, IL-1β), contribute to the colonization. And the tumor cells release chemokines and cytokines (CSF-1, GM-CSF, MCP-1, HGF, SDF-1, CX3CL) to recruit TAMs towards the tumor cells. There are immune checkpoints expressed on T-cells, such as PD-1 and CTLA-4, which tumor cells could bind and deactivate T-cells, suppressing anti-tumor immunity. Checkpoint immunotherapy use antibodies to inhibit immune checkpoint to prevent the T-cell from deactivation and control the tumor.

macrophages are exposed to IL-4 or IL-13 and produce immunosuppressive substances (IL-10 and TGF-β) that promote tumor growth by increasing STAT3 expression and inhibiting antigen presentation (63, 64).

In BM, the proportion of most immune cell subpopulations decreases, but with a few exceptions, such as M2-macrophages, whose ratio in the proportion is strongly associated with BM (65). Therefore, the change of TAM/m from M1 to M2 phenotype may be one of the reasons for the shift of TME from anti-tumor to pro-tumor (66). Recent in-depth studies of lung cancer BM have revealed that around 10% of TAM/m contain peripheral-derived macrophages in early metastases,

rising to 20% in massive metastases (67). In contrast to primary NSCLC, BM microenvironment macrophages infiltrate more and show elevated monocyte-derived macrophages (47). The phenomena may reflect the antitumor effect of TAM/m in the early stages of BM formation and the accumulation and activation of TAM/m in the later stages (66).

C-X3-C motif chemokine receptor 1/C-X3-C motif chemokine ligand 1 axis is a signaling pathway which regulates TAM/m (66). This pathway has been much studied in brain inflammation, and its activation regulates microglia activation in a quiescent state (68), thereby inhibiting the release of IL-6, TNF-α, etc. (69). The relationship between this pathway and BM is inconclusive and warrants investigation. Considering the complex involvement of C-X3-C motif chemokine receptor 1 in the metastatic cascade, its nonspecific inhibitors may not be an appropriate therapeutic option (66). In addition, colony-stimulating factor 1 receptor inhibitors acting on TAM have shown promise in melanoma and enhancing chemotherapy response and might be applied in BM (70). Overall, immunotherapy against TAM/m includes both modulation of TAM/M polarization and inhibition of the survival and function of TAM/M. Some of the mechanisms have been studied to some extent, but there is still a lack of clinical studies demonstrating the actual therapeutic effects of BM from NSCLC targeting these mechanisms.

Astrocytes

Astrocytes are one of the most abundant cell types specific to the CNS and play an essential role in mediating tissue-specific communication in the brain (39). Also, astrocytes are the most abundant glial cells in the TME of BM. After the injury, astrocytes alter their phenotype, inducing a transcriptional program known as reactive astrocyte proliferation (71). Reactive astrocytes, like microglia, have two faces. When in contact with tumor cells early enough, astrocytes maintain microenvironmental balance and trigger apoptosis, inhibiting metastatic colonization. However, with further interactions (72), the shift from a metastatic suppressive to a facilitative milieu due to the intricate interplay between astrocytes and microglia is created (39). The effects between tumor cells and reactive astrocytes are mutual. IL-8, macrophage movement inhibitory factor, and fibrinolytic enzyme activator inhibitor 1 secreted by metastatic lung cancer cells can activate astrocytes that produce growth factors (IL-6, IL-1, and TNF-α), encouraging tumor growth (72). Also, astrocytes express a significant variety of immunosuppressive molecules (IL-10, TGF-β, etc.) that influence innate and adaptive immune cells (39).

When infiltrating lung cancer cells are exposed to astrocytes, plasmin from the ECM is a defense against metastasis. Plasmin inhibits BM by converting astrocyte FasL into a paracrine death signal and inactivating the axon guidance molecule L1CAM. In contrast, plasminogen activator inhibitory serpins secreted by tumor cells are a barrier against plasmin (73). Once bound to the astrocyte gap junction network, CTCs use connexin 43 to transfer the second messenger cGAMP to astrocytes. Thus, the *STING* pathway is activated to produce inflammatory cytokines such as IFN-α and TNF-α (74), which act as paracrine signals to promote tumor growth. So, we know the principle that drugs working on gap links can treat established BM. In addition, astrocytes fight BM by exogenously secreting miRNA-142-3p, mediating the downregulation of transient receptor potential ankyrin-1. In BM from lung adenocarcinoma, the downregulation inhibits transient receptor potential ankyrin-1-mediated activation of fibroblast growth factor receptor 2 and impedes metastasis (75). In the BM of NSCLC, we suggest that reactive astrocytes contact with tumor cells after extravasation and produce plasmin as a defense against metastasis at first. In contrast, tumor cells build proteins, such as plasminogen activators, that allow them to survive despite the production of plasmin. At the same time, reactive astrocytes relax endothelial cell junctions by cytokine and regulate tumor cell gene expression by exosomes, thus influencing the progression of progressive BM around the lesion (76).

Cancer-Associated Fibroblast

The role of cancer-associated fibroblasts (CAFs) in the microenvironment of NSCLC BM remains to be explored. Evidence of fibroblastic entities and their presence in the brain is limited, though fibroblasts are linked to the progression and metastasis of many cancers (77) for their pro-angiogenic and immunosuppressive effects. CAFs are activated fibroblasts in TME that release a significant number of cytokines and chemokines that affect a variety of leukocytes, including CD8+ T cells, Treg cells, and macrophages (78), playing effects such as pro-angiogenesis and immune suppression. CAFs express fibroblast activation protein-α, whose immunosuppression is mediated by CXCL12. This chemokine attaches to cancer cells and rejects T cells *via* a process dependent on signaling by the CXCL12 receptor CXCR4 (79).

TME Difference Between BM From NSCLC and Other Brain Tumors

The TME in BM is different from the extracranial primary tumor. However, BM's molecular and genetic features often correlate with primary brain malignancies such as glioblastoma, some of which don't exist in the primary tumor (80). For example, EGFR-amplified BM from NSCLC shows similar oncogenic changes with EGFR-amplified classic glioblastoma and Her2+ breast cancer BM (81). The similarity may be an adaptive mechanism for BBB selectivity. At the same time, molecular features may regulate TME, which means the similarity in oncogenic changes also lead to the similarity in TME (82).

RECENT ADVANCEMENTS IN THE TREATMENT OF BM FROM NSCLC WITH IMMUNOTHERAPY

Because of the unique anatomical and physiological properties of the CNS, current therapeutic methods for BM from NSCLC are restricted, and the prognosis is poor. Therefore, immunotherapy has been increasingly popular in the treatment of NSCLC. Some

patients with NSCLC may benefit from ICIs (83). Intracranial and extracranial lesions may vary considerably in response to systemic immunotherapy due to genetic differences between BM and primary tumor, as well as TME variations (84) (**Table 3**).

The role of ICIs in BM has been studied in retrospective analysis, case series, and preliminary clinical trials. These discoveries and their quick translation into clinical practice are causing significant shifts in treating patients with BM from

TABLE 3 | Update of immunotherapy in NSCLC BM.

Study	Therapy tested	Control or comparator therapy	Number of patients	Median OS (months)	Median PFS (months)	Other outcomes
Marcus Skribek et al. (85)	ICI	None	51	5.7	1.9	iPFS=2.5months
Guowei Zhang et al. (86)	Nivolumab	None	With BM: 32;	14.8	2.8	ORR=20.0%; DCR=53.1%; DOR=9.8 months
			Without BM: 41	20.2	4.9	ORR=19.5%;DCR=56.1%;DOR=28.8 months;
Konstantinos Rounis et al. (87)	PD-1/PD-L1 inhibitors	None	24	6.77	Not reported	Median duration of intracranial response (months): 7.53 Intracranial TTP (months): 4,3
Kazushige Wakuda et al. (88)	Pembrolizumab	None	With BM: 23;	21.6	6.5	ORR: 57%
			Without BM: 64;	24.6	7.0	ORR: 42%
Sarah B Goldberg et al. (58)	Pembrolizumab	None	37	9.9	1.9	Median TTP=1.8 months; RR=29.7%;
Lucio Crinò et al. (89)	Nivolumab	None	409	8.6	3.0	ORR: 17%; DCR: 39%; One year PFS: 20%; One year OS: 43%;
Diego Cortinovis et al. (90)	Nivolumab	None	37	5.8	4.9	ORR: 19%; DCR: 49%; OS rate at 1 year: 35%; PFS rate at 1 year: 31%;
Clément Gauvain et al. (91)	Nivolumab	None	43	Not reached	3.9	Intracerebral DCR: 51%;
Anna Cho et al. (92)	GKRS + ICI	GKRS alone	GKRS alone: 286;	5.6	Not reported	none
			GKRS+ICI: 82	24.2		
Matthew J Shepard et al. (93)	ICI+SRS	SRS alone	ICI+SRS: 17	Not reached	Not reported	12-month CR: 84.9%; rate of peritumoral edema progression: 11.1%
			SRS alone: 34	15.9		12-month CR: 76.3% rate of peritumoral edema progression: 21.7%
Charu Singh et al. (94)	anti-PD-1 therapy + SRS (ICI group)	chemotherapy (CT) + SRS (CT group)	ICI group: 39	10	Not reported	Median times to initial response: 49; Median time to maximal response: 105
			CT group: 46	11.6		Median times to initial response:84; Median time to maximal response: 182
Linda Chen et al. (95)	SRS + non- concurrent ICI; SRS + Concurrent ICI;	SRS alone	SRS alone: 181 (NSCLC 79%);	12.9	3.7	Mean number of new metastases: 4
			SRS + non- concurrent ICI: 51 (NSCLC 69%);	14.5	2.3	Mean number of new metastases: 4
			SRS + Concurrent ICI: 28 (NSCLC 7%);	24.7	2.3	Mean number of new metastases: 2
Chenglong Sun et al. (96)	ICI + chemotherapy; ICI + anti-angiogenic therapy	ICI alone	ICI alone: 30	27.43	Not reported	Combination therapy produced better survivals than monotherapy
			ICI + chemotherapy: 29			
			ICI + anti-angiogenic therapy: 10			
Muhammad Zubair Afzal et al. (97)	carboplatin/pemetrexed plus pembrolizumab (Cohort B)	carboplatin/ pemetrexed (Cohort A)	Cohort A: 12	Not reported	4.1	ORR:58.3%; DCR: 75%; Median time to achieve response: 1.67 months;
			Cohort B: 5	Not reported	Not reached	ORR:80%; DCR: 80%; Median time to achieve response: 1.1 months;
Steven F Powell et al. (98)	Pembrolizumab + Platinum-Based Chemotherapy	Chemotherapy alone	Pembrolizumab + chemotherapy: 105	18.8	6.9	Incidences of treatment-related adverse events: 88.2%
			Chemotherapy alone: 66	7.6	4.1	Incidences of treatment-related adverse events: 82.8%

NSCLC, non-small cell lung cancer; BM, brain metastasis; OS, overall survival; PFS, progression-free survival; ICI, immune checkpoint inhibitor; iPFS, intracranial progression-free survival; ORR, objective response rate; DCR, disease control rate; DOR, duration of response; PD-1, programmed death 1; PD-L1, programmed cell death ligand 1; TTP, time to progression; RR, response rate; GKRS, gamma knife radiosurgery; SRS, stereotactic radiation surgery; CR, control rate; DBF, distant brain failure.

NSCLC (85). Multiple studies have consistently shown that ICIs improve overall survival in both primary tumors and BM, supporting the utility of ICIs in the treatment of BM (88). PD-1 and PD-L1 are the most clinically relevant immune checkpoints. Several medications have been approved for treatment in patients with lung cancer BM, including anti-PD-1 drugs such as pembrolizumab and nivolumab, and anti-PD-L1 drugs like atezolizumab (89).

Pembrolizumab has been demonstrated to generate CNS responses at rates comparable to extracranial malignancies, with the overall survival rate in NSCLC patients exceeding the historical rate of BM (87). Nivolumab is a complete human IgG4 ICI, which binds to PD-1 on activated immune cells, breaking the PD-L1 interaction and increasing the anti-tumor response (86). Studies have shown Nivolumab to have a potential therapeutic effect on BM (90, 91). Atezolizumab monoclonal antibody has also been proven to extend the life expectancy of individuals with BM.

ICIs have changed the way advanced cancer patients are treated. Despite the positive results of ICI therapy, only a tiny percentage of patients responded, severely limiting the growth of ICI therapy. As a result, immunotherapy for BM from NSCLC is being developed with other combination therapies, such as radiotherapy or chemotherapy (92–95). Recent research has discovered that cancer patients having radiotherapy and/or chemotherapy have varied immunogenicity patterns, which could improve the function of immunotherapy, promote efficiency, and reduce side effects (96–98). Because of their potential to influence innate and adaptive immunity, certain chemotherapeutic drugs, such as cyclophosphamide, may improve the anticancer efficacy of immunotherapy.

CONCLUSION

The significance and distinctiveness of BM compelled us to investigate it, and the TME is an essential research direction. NSCLC is the most prevalent tumor that causes BM, and while BM has a distinct TME, there are some similarities with original foci, such as the role of HIF. When BM occurs, the presence of BBB, as well as different types of ECM composition and tissue-resident cells, leads to the infiltration of blood-derived immune cells and the alteration of ECM and tissue-resident cells with tumor colonization, resulting in a distinct TME compared to primary NSCLC. Infiltration and phenotypic shifts of immune-related cells, in particular, cause alterations in signaling molecules that gradually transform the TME of BM from tumor rejection to growth. Because of these fundamental alterations, new ideas for treating BM from NSCLC emerged, and targeted immunotherapy was successfully implemented in practice. And the combination of conventional therapy and immunotherapy has begun. We feel that the importance of the TME is self-evident throughout the process, and it has facilitated the practice of immunotherapy. As a result of more in-depth research on the mechanism, treatment will be more comprehensive, and the prognosis of BM from NSCLC will be more encouraging.

AUTHOR CONTRIBUTIONS

YCW, YY, SD, and RC collected the related paper. LT, RC, YCW, SD, YW, and JL drafted and revised the manuscript. GX participated in the design of the review and helped to draft and revise the manuscript. All authors read and approved the final manuscript.

FUNDING

This work was supported by National Natural Science Foundation of China (No. 82171347), the Scientific Research Project of Hunan Provincial Health Commission of China (No. 202204040024), and the Students Innovations in Central South University of China (No. S2021105330599, No. 2021105330046, No. XCX2021035).

ACKNOWLEDGMENTS

I would like to express my gratitude to all those who helped us during the writing of this manuscript and thanks to all the peer reviewers for their opinions and suggestions.

REFERENCES

1. Singh R, Stoltzfus KC, Chen H, Louie AV, Lehrer EJ, Horn SR, et al. Epidemiology of Synchronous Brain Metastases. *Neuro-Oncol Adv* (2020) 2 (1):vdaa041. doi: 10.1093/noajnl/vdaa041
2. Fitzmaurice C, Abate D, Abbasi N, Abbastabar H, Abd-Allah F, Abdel-Rahman O, et al. Global, Regional, and National Cancer Incidence, Mortality, Years of Life Lost, Years Lived With Disability, and Disability-Adjusted Life-Years for 29 Cancer Groups, 1990 to 2017: A Systematic Analysis for the Global Burden of Disease Study. *JAMA Oncol* (2019) 5(12):1749–68. doi: 10.1001/jamaoncol.2019.2996
3. Lamba N, Kearney RB, Catalano PJ, Hassett MJ, Wen PY, Haas-Kogan DA, et al. Population-Based Estimates of Survival Among Elderly Patients With Brain Metastases. *Neuro-Oncology* (2020) 23(4):661–76. doi: 10.1093/neuonc/noaa233
4. Siegel RL, Miller KD, Fuchs HE, Jemal A. Cancer Statistics, 2021. *CA Cancer J Clin* (2021) 71(1):7–33. doi: 10.3322/caac.21654
5. Sosa E, D'Souza G, Akhtar A, Sur M, Love K, Duffels J, et al. Racial and Socioeconomic Disparities in Lung Cancer Screening in the United States: A Systematic Review. *CA Cancer J Clin* (2021) 71(4):299–314. doi: 10.3322/caac.21671
6. Sung H, Ferlay J, Siegel RL, Laversanne M, Soerjomataram I, Jemal A, et al. Global Cancer Statistics 2020: GLOBOCAN Estimates of Incidence and Mortality Worldwide for 36 Cancers in 185 Countries. *CA Cancer J Clin* (2021) 71(3):209–49. doi: 10.3322/caac.21660
7. Liu L, Bai H, Seery S, Li S, Wang C, Xue P, et al. Efficacy and Safety of Treatment Modalities Across EGFR Selected/Unselected Populations With Non-Small Cell Lung Cancer and Brain Metastases: A Systematic Review and Bayesian Network Meta-Analysis. *Lung Cancer (Amsterdam Netherlands)* (2021) 158:74–84. doi: 10.1016/j.lungcan.2021.02.031

8. Achrol AS, Rennert RC, Anders C, Soffietti R, Ahluwalia MS, Nayak L, et al. Brain Metastases. *Nat Rev Dis Primers* (2019) 5(1):5. doi: 10.1038/s41572-018-0055-y
9. Halasz LM, Weeks JC, Neville BA, Taback N, Punglia RS. Use of Stereotactic Radiosurgery for Brain Metastases From Non-Small Cell Lung Cancer in the United States. *Int J Radiat Oncol Biol Phys* (2013) 85(2):e109–16. doi: 10.1016/j.ijrobp.2012.08.007
10. Colaco RJ, Martin P, Kluger HM, Yu JB, Chiang VL. Does Immunotherapy Increase the Rate of Radiation Necrosis After Radiosurgical Treatment of Brain Metastases? *J Neurosurg* (2016) 125(1):17–23. doi: 10.3171/2015.6.Jns142763
11. Boire A, Brastianos PK, Garzia L, Valiente M. Brain Metastasis. *Nat Rev Cancer* (2020) 20(1):4–11. doi: 10.1038/s41568-019-0220-y
12. Spano D, Zollo M. Tumor Microenvironment: A Main Actor in the Metastasis Process. *Clin Exp Metastasis* (2012) 29(4):381–95. doi: 10.1007/s10585-012-9457-5
13. Vilariño N, Bruna J, Bosch-Barrera J, Valiente M, Nadal E. Immunotherapy in NSCLC Patients With Brain Metastases. Understanding Brain Tumor Microenvironment and Dissecting Outcomes From Immune Checkpoint Blockade in the Clinic. *Cancer Treat Rev* (2020) 89:102067. doi: 10.1016/j.ctrv.2020.102067
14. Gandhi L, Rodríguez-Abreu D, Gadgeel S, Esteban E, Felip E, De Angelis F, et al. Pembrolizumab Plus Chemotherapy in Metastatic Non–Small-Cell Lung Cancer. *New Engl J Med* (2018) 378(22):2078–92. doi: 10.1056/NEJMoa1801005
15. Marvin EA, Furrow KL, Kar A, Cuoco JA. Response of Pembrolizumab Alone for Non-Small Cell Lung Cancer With Brain Metastasis: A Case Report and Literature Review. *Front Oncol* (2020) 10:577159. doi: 10.3389/fonc.2020.577159
16. Arvanitis CD, Ferraro GB, Jain RK. The Blood-Brain Barrier and Blood-Tumour Barrier in Brain Tumours and Metastases. *Nat Rev Cancer* (2020) 20(1):26–41. doi: 10.1038/s41568-019-0205-x
17. Stamatovic SM, Keep RF, Andjelkovic AV. Brain Endothelial Cell-Cell Junctions: How to "Open" the Blood Brain Barrier. *Curr Neuropharmacol* (2008) 6(3):179–92. doi: 10.2174/157015908785777210
18. Mustafa DAM, Pedrosa R, Smid M, van der Weiden M, de Weerd V, Nigg AL, et al. T Lymphocytes Facilitate Brain Metastasis of Breast Cancer by Inducing Guanylate-Binding Protein 1 Expression. *Acta Neuropathol* (2018) 135(4):581–99. doi: 10.1007/s00401-018-1806-2
19. Rempe RG, Hartz AMS, Bauer B. Matrix Metalloproteinases in the Brain and Blood-Brain Barrier: Versatile Breakers and Makers. *J Cereb Blood Flow Metab* (2016) 36(9):1481–507. doi: 10.1177/0271678X16655551
20. Wu K, Fukuda K, Xing F, Zhang Y, Sharma S, Liu Y, et al. Roles of the Cyclooxygenase 2 Matrix Metalloproteinase 1 Pathway in Brain Metastasis of Breast Cancer. *J Biol Chem* (2015) 290(15):9842–54. doi: 10.1074/jbc.M114.602185
21. Chuang HN, van Rossum D, Sieger D, Siam L, Klemm F, Bleckmann A, et al. Carcinoma Cells Misuse the Host Tissue Damage Response to Invade the Brain. *Glia* (2013) 61(8):1331–46. doi: 10.1002/glia.22518
22. Qiao S, Qian Y, Xu G, Luo Q, Zhang Z. Long-Term Characterization of Activated Microglia/Macrophages Facilitating the Development of Experimental Brain Metastasis Through Intravital Microscopic Imaging. *J Neuroinflamm* (2019) 16(1):4. doi: 10.1186/s12974-018-1389-9
23. Coppes-Zantinga AR, Coppes MJ. Sir James Paget (1814-1889): A Great Academic Victorian. *J Am Coll Surg* (2000) 191(1):70–4. doi: 10.1016/S1072-7515(00)00250-7
24. Gavert N, Ben-Ze'ev A. Epithelial-Mesenchymal Transition and the Invasive Potential of Tumors. *Trends Mol Med* (2008) 14(5):199–209. doi: 10.1016/j.molmed.2008.03.004
25. Cao ZQ, Wang Z, Leng P. Aberrant N-Cadherin Expression in Cancer. *BioMed Pharmacother* (2019) 118:109320. doi: 10.1016/j.biopha.2019.109320
26. Jiang Y, Zhan H, Zhang Y, Yang J, Liu M, Xu C, et al. ZIP4 Promotes Non-Small Cell Lung Cancer Metastasis by Activating Snail-N-Cadherin Signaling Axis. *Cancer Lett* (2021) 521:71–81. doi: 10.1016/j.canlet.2021.08.025
27. Shin DH, Jo JY, Kim SH, Choi M, Han C, Choi BK, et al. Midkine Is a Potential Therapeutic Target of Tumorigenesis, Angiogenesis, and Metastasis in Non-Small Cell Lung Cancer. *Cancers* (2020) 12(9):2402. doi: 10.3390/cancers12092402
28. Stremitzer S, Berghoff AS, Volz NB, Zhang W, Yang D, Stintzing S, et al. Genetic Variants Associated With Colorectal Brain Metastases Susceptibility and Survival. *Pharmacogenom J* (2017) 17(1):29–35. doi: 10.1038/tpj.2015.86
29. Langley RR, Fidler IJ. The Biology of Brain Metastasis. *Clin Chem* (2013) 59(1):180–9. doi: 10.1373/clinchem.2012.193342
30. Herman H, Fazakas C, Hasko J, Molnar K, Meszaros A, Nyul-Toth A, et al. Paracellular and Transcellular Migration of Metastatic Cells Through the Cerebral Endothelium. *J Cell Mol Med* (2019) 23(4):2619–31. doi: 10.1111/jcmm.14156
31. Strilic B, Offermanns S. Intravascular Survival and Extravasation of Tumor Cells. *Cancer Cell* (2017) 32(3):282–93. doi: 10.1016/j.ccell.2017.07.001
32. Jassam SA, Maherally Z, Smith JR, Ashkan K, Roncaroli F, Fillmore HL, et al. CD15s/CD62E Interaction Mediates the Adhesion of Non-Small Cell Lung Cancer Cells on Brain Endothelial Cells: Implications for Cerebral Metastasis. *Int J Mol Sci* (2017) 18(7):1474. doi: 10.3390/ijms18071474
33. Jassam SA, Maherally Z, Smith JR, Ashkan K, Roncaroli F, Fillmore HL, et al. TNF-α Enhancement of CD62E Mediates Adhesion of Non-Small Cell Lung Cancer Cells to Brain Endothelium *via* CD15 in Lung-Brain Metastasis. *Neuro Oncol* (2016) 18(5):679–90. doi: 10.1093/neuonc/nov248
34. Jassam SA, Maherally Z, Ashkan K, Pilkington GJ, Fillmore HL. Fucosyltransferase 4 and 7 Mediates Adhesion of Non-Small Cell Lung Cancer Cells to Brain-Derived Endothelial Cells and Results in Modification of the Blood-Brain-Barrier: *In Vitro* Investigation of CD15 and CD15s in Lung-to-Brain Metastasis. *J Neurooncol* (2019) 143(3):405–15. doi: 10.1007/s11060-019-03188-x
35. Liu C, Li Z, Wang S, Fan Y, Zhang S, Yang X, et al. FUT4 is Involved in PD-1-Related Immunosuppression and Leads to Worse Survival in Patients With Operable Lung Adenocarcinoma. *J Cancer Res Clin Oncol* (2019) 145(1):65–76. doi: 10.1007/s00432-018-2761-y
36. Bos PD, Zhang XH, Nadal C, Shu W, Gomis RR, Nguyen DX, et al. Genes That Mediate Breast Cancer Metastasis to the Brain. *Nature* (2009) 459(7249):1005–9. doi: 10.1038/nature08021
37. Tominaga N, Kosaka N, Ono M, Katsuda T, Yoshioka Y, Tamura K, et al. Brain Metastatic Cancer Cells Release microRNA-181c-Containing Extracellular Vesicles Capable of Destructing Blood-Brain Barrier. *Nat Commun* (2015) 6:6716. doi: 10.1038/ncomms7716
38. Fares J, Ulasov I, Timashev P, Lesniak MS. Emerging Principles of Brain Immunology and Immune Checkpoint Blockade in Brain Metastases. *Brain* (2021) 144(4):1046–66. doi: 10.1093/brain/awab012
39. Quail DF, Joyce JA. The Microenvironmental Landscape of Brain Tumors. *Cancer Cell* (2017) 31(3):326–41. doi: 10.1016/j.ccell.2017.02.009
40. Louveau A, Smirnov I, Keyes TJ, Eccles JD, Rouhani SJ, Peske JD, et al. Structural and Functional Features of Central Nervous System Lymphatic Vessels. *Nature* (2015) 523(7560):337–41. doi: 10.1038/nature14432
41. Sakaguchi S. Naturally Arising Foxp3-Expressing CD25+CD4+ Regulatory T Cells in Immunological Tolerance to Self and Non-Self. *Nat Immunol* (2005) 6(4):345–52. doi: 10.1038/ni1178
42. Mahmud SA, Manlove LS, Schmitz HM, Xing Y, Wang Y, Owen DL, et al. Costimulation *via* the Tumor-Necrosis Factor Receptor Superfamily Couples TCR Signal Strength to the Thymic Differentiation of Regulatory T Cells. *Nat Immunol* (2014) 15(5):473–81. doi: 10.1038/ni.2849
43. Owen DL, Mahmud SA, Sjaastad LE, Williams JB, Spanier JA, Simeonov DR, et al. Thymic Regulatory T Cells Arise *via* Two Distinct Developmental Programs. *Nat Immunol* (2019) 20(2):195–205. doi: 10.1038/s41590-018-0289-6
44. Tanaka A, Sakaguchi S. Regulatory T Cells in Cancer Immunotherapy. *Cell Res* (2017) 27(1):109–18. doi: 10.1038/cr.2016.151
45. Kim R, Keam B, Kim S, Kim M, Kim SH, Kim JW, et al. Differences in Tumor Microenvironments Between Primary Lung Tumors and Brain Metastases in Lung Cancer Patients: Therapeutic Implications for Immune Checkpoint Inhibitors. *BMC Cancer* (2019) 19(1):19. doi: 10.1186/s12885-018-5214-8
46. Ikarashi D, Okimoto T, Shukuya T, Onagi H, Hayashi T, Sinicropi-Yao SL, et al. Comparison of Tumor Microenvironments Between Primary Tumors and Brain Metastases in Patients With NSCLC. *JTO Clin Res Rep* (2021) 2(10):100230. doi: 10.1016/j.jtocrr.2021.100230
47. Kudo Y, Haymaker C, Zhang J, Reuben A, Duose DY, Fujimoto J, et al. Suppressed Immune Microenvironment and Repertoire in Brain Metastases From Patients With Resected Non-Small-Cell Lung Cancer. *Ann Oncol* (2019) 30(9):1521–30. doi: 10.1093/annonc/mdz207

48. Tanaka A, Sakaguchi S. Targeting Treg Cells in Cancer Immunotherapy. *Eur J Immunol* (2019) 49(8):1140–6. doi: 10.1002/eji.201847659
49. Wei SC, Duffy CR, Allison JP. Fundamental Mechanisms of Immune Checkpoint Blockade Therapy. *Cancer Discov* (2018) 8(9):1069–86. doi: 10.1158/2159-8290.Cd-18-0367
50. Fehrenbacher L, Spira A, Ballinger M, Kowanetz M, Vansteenkiste J, Mazieres J, et al. Atezolizumab Versus Docetaxel for Patients With Previously Treated Non-Small-Cell Lung Cancer (POPLAR): A Multicentre, Open-Label, Phase 2 Randomised Controlled Trial. *Lancet* (2016) 387(10030):1837–46. doi: 10.1016/s0140-6736(16)00587-0
51. Boussiotis VA. Molecular and Biochemical Aspects of the PD-1 Checkpoint Pathway. *N Engl J Med* (2016) 375(18):1767–78. doi: 10.1056/NEJMra1514296
52. Li YD, Lamano JB, Lamano JB, Quaggin-Smith J, Veliceasa D, Kaur G, et al. Tumor-Induced Peripheral Immunosuppression Promotes Brain Metastasis in Patients With Non-Small Cell Lung Cancer. *Cancer Immunol Immunother* (2019) 68(9):1501–13. doi: 10.1007/s00262-019-02384-y
53. Lim JH, Um SW. The Risk Factors for Brain Metastases in Patients With Non-Small Cell Lung Cancer. *Ann Transl Med* (2018) 6(Suppl 1):S66. doi: 10.21037/atm.2018.10.27
54. Hargadon KM, Johnson CE, Williams CJ. Immune Checkpoint Blockade Therapy for Cancer: An Overview of FDA-Approved Immune Checkpoint Inhibitors. *Int Immunopharmacol* (2018) 62:29–39. doi: 10.1016/j.intimp.2018.06.001
55. Cha JH, Chan LC, Li CW, Hsu JL, Hung MC. Mechanisms Controlling PD-L1 Expression in Cancer. *Mol Cell* (2019) 76(3):359–70. doi: 10.1016/j.molcel.2019.09.030
56. Moutafi MK, Tao W, Huang R, Haberberger J, Alexander B, Ramkissoon S, et al. Comparison of Programmed Death-Ligand 1 Protein Expression Between Primary and Metastatic Lesions in Patients With Lung Cancer. *J Immunother Cancer* (2021) 9(4):e002230. doi: 10.1136/jitc-2020-002230
57. Hulsbergen AFC, Mammi M, Nagtegaal SHJ, Lak AM, Kavouridis V, Smith TR, et al. Programmed Death Receptor Ligand One Expression May Independently Predict Survival in Patients With Non-Small Cell Lung Carcinoma Brain Metastases Receiving Immunotherapy. *Int J Radiat Oncol Biol Phys* (2020) 108(1):258–67. doi: 10.1016/j.ijrobp.2020.04.018
58. Goldberg SB, Schalper KA, Gettinger SN, Mahajan A, Herbst RS, Chiang AC, et al. Pembrolizumab for Management of Patients With NSCLC and Brain Metastases: Long-Term Results and Biomarker Analysis From a Non-Randomised, Open-Label, Phase 2 Trial. *Lancet Oncol* (2020) 21(5):655–63. doi: 10.1016/s1470-2045(20)30111-x
59. Mantovani A, Marchesi F, Malesci A, Laghi L, Allavena P. Tumour-Associated Macrophages as Treatment Targets in Oncology. *Nat Rev Clin Oncol* (2017) 14(7):399–416. doi: 10.1038/nrclinonc.2016.217
60. Hambardzumyan D, Gutmann DH, Kettenmann H. The Role of Microglia and Macrophages in Glioma Maintenance and Progression. *Nat Neurosci* (2016) 19(1):20–7. doi: 10.1038/nn.4185
61. Klemm F, Maas RR, Bowman RL, Kornete M, Soukup K, Nassiri S, et al. Interrogation of the Microenvironmental Landscape in Brain Tumors Reveals Disease-Specific Alterations of Immune Cells. *Cell* (2020) 181(7):1643–60.e17. doi: 10.1016/j.cell.2020.05.007
62. Menga A, Serra M, Todisco S, Riera-Domingo C, Ammarah U, Ehling M, et al. Glufosinate Constrains Synchronous and Metachronous Metastasis by Promoting Anti-Tumor Macrophages. *EMBO Mol Med* (2020) 12(10):e11210. doi: 10.15252/emmm.201911210
63. Yang M, Li J, Gu P, Fan X. The Application of Nanoparticles in Cancer Immunotherapy: Targeting Tumor Microenvironment. *Bioact Mater* (2021) 6(7):1973–87. doi: 10.1016/j.bioactmat.2020.12.010
64. Mu X, Shi W, Xu Y, Xu C, Zhao T, Geng B, et al. Tumor-Derived Lactate Induces M2 Macrophage Polarization *via* the Activation of the ERK/STAT3 Signaling Pathway in Breast Cancer. *Cell Cycle* (2018) 17(4):428–38. doi: 10.1080/15384101.2018.1444305
65. Song SG, Kim S, Koh J, Yim J, Han B, Kim YA, et al. Comparative Analysis of the Tumor Immune-Microenvironment of Primary and Brain Metastases of Non-Small-Cell Lung Cancer Reveals Organ-Specific and EGFR Mutation-Dependent Unique Immune Landscape. *Cancer Immunol Immunother* (2021) 70(7):2035–48. doi: 10.1007/s00262-020-02840-0
66. Zhang W, Karschnia P, von Mücke-Heim IA, Mulazzani M, Zhou X, Blobner J, et al. *In Vivo* Two-Photon Characterization of Tumor-Associated Macrophages and Microglia (TAM/M) and CX3CR1 During Different Steps of Brain Metastasis Formation From Lung Cancer. *Neoplasia* (2021) 23(11):1089–100. doi: 10.1016/j.neo.2021.09.001
67. Schulz M, Michels B, Niesel K, Stein S, Farin H, Rödel F, et al. Cellular and Molecular Changes of Brain Metastases-Associated Myeloid Cells During Disease Progression and Therapeutic Response. *iScience* (2020) 23(6):101178. doi: 10.1016/j.isci.2020.101178
68. Ransohoff RM, Perry VH. Microglial Physiology: Unique Stimuli, Specialized Responses. *Annu Rev Immunol* (2009) 27:119–45. doi: 10.1146/annurev.immunol.021908.132528
69. Lyons A, Lynch AM, Downer EJ, Hanley R, O'Sullivan JB, Smith A, et al. Fractalkine-Induced Activation of the Phosphatidylinositol-3 Kinase Pathway Attentuates Microglial Activation *In Vivo* and *In Vitro*. *J Neurochem* (2009) 110(5):1547–56. doi: 10.1111/j.1471-4159.2009.06253.x
70. Poh AR, Ernst M. Targeting Macrophages in Cancer: From Bench to Bedside. *Front Oncol* (2018) 8:49. doi: 10.3389/fonc.2018.00049
71. Sofroniew MV, Vinters HV. Astrocytes: Biology and Pathology. *Acta Neuropathol* (2010) 119(1):7–35. doi: 10.1007/s00401-009-0619-8
72. Seike T, Fujita K, Yamakawa Y, Kido MA, Takiguchi S, Teramoto N, et al. Interaction Between Lung Cancer Cells and Astrocytes *via* Specific Inflammatory Cytokines in the Microenvironment of Brain Metastasis. *Clin Exp Metastasis* (2011) 28(1):13–25. doi: 10.1007/s10585-010-9354-8
73. Valiente M, Obenauf AC, Jin X, Chen Q, Zhang XH, Lee DJ, et al. Serpins Promote Cancer Cell Survival and Vascular Co-Option in Brain Metastasis. *Cell* (2014) 156(5):1002–16. doi: 10.1016/j.cell.2014.01.040
74. Chen Q, Boire A, Jin X, Valiente M, Er EE, Lopez-Soto A, et al. Carcinoma-Astrocyte Gap Junctions Promote Brain Metastasis by cGAMP Transfer. *Nature* (2016) 533(7604):493–8. doi: 10.1038/nature18268
75. Berrout J, Kyriakopoulou E, Moparthi L, Hogea AS, Berrout L, Ivan C, et al. TRPA1-FGFR2 Binding Event is a Regulatory Oncogenic Driver Modulated by miRNA-142-3p. *Nat Commun* (2017) 8(1):947. doi: 10.1038/s41467-017-00983-w
76. Zhang L, Zhang S, Yao J, Lowery FJ, Zhang Q, Huang WC, et al. Microenvironment-Induced PTEN Loss by Exosomal microRNA Primes Brain Metastasis Outgrowth. *Nature* (2015) 527(7576):100–4. doi: 10.1038/nature15376
77. Hu JL, Wang W, Lan XL, Zeng ZC, Liang YS, Yan YR, et al. CAFs Secreted Exosomes Promote Metastasis and Chemotherapy Resistance by Enhancing Cell Stemness and Epithelial-Mesenchymal Transition in Colorectal Cancer. *Mol Cancer* (2019) 18(1):91. doi: 10.1186/s12943-019-1019-x
78. Monteran L, Erez N. The Dark Side of Fibroblasts: Cancer-Associated Fibroblasts as Mediators of Immunosuppression in the Tumor Microenvironment. *Front Immunol* (2019) 10:1835. doi: 10.3389/fimmu.2019.01835
79. Fearon DT. The Carcinoma-Associated Fibroblast Expressing Fibroblast Activation Protein and Escape From Immune Surveillance. *Cancer Immunol Res* (2014) 2(3):187–93. doi: 10.1158/2326-6066.Cir-14-0002
80. Brastianos PK, Carter SL, Santagata S, Cahill DP, Taylor-Weiner A, Jones RT, et al. Genomic Characterization of Brain Metastases Reveals Branched Evolution and Potential Therapeutic Targets. *Cancer Discovery* (2015) 5(11):1164–77. doi: 10.1158/2159-8290.CD-15-0369
81. Verhaak RG, Hoadley KA, Purdom E, Wang V, Qi Y, Wilkerson MD, et al. Integrated Genomic Analysis Identifies Clinically Relevant Subtypes of Glioblastoma Characterized by Abnormalities in PDGFRA, IDH1, EGFR, and NF1. *Cancer Cell* (2010) 17(1):98–110. doi: 10.1016/j.ccr.2009.12.020
82. Zhang N, Zhang H, Wang Z, Dai Z, Zhang X, Cheng Q, et al. Immune Infiltrating Cells-Derived Risk Signature Based on Large-Scale Analysis Defines Immune Landscape and Predicts Immunotherapy Responses in Glioma Tumor Microenvironment. *Front Immunol* (2021) 12:691811. doi: 10.3389/fimmu.2021.691811
83. Amrane K, Geier M, Corre R, Léna H, Léveiller G, Gadby F, et al. First-Line Pembrolizumab for Non-Small Cell Lung Cancer Patients With PD-L1 ≥50% in a Multicenter Real-Life Cohort: The PEMBREIZH Study. *Cancer Med* (2020) 9(7):2309–16. doi: 10.1002/cam4.2806
84. Ma SC, Tang XR, Long LL, Bai X, Zhou JG, Duan ZJ, et al. Integrative Evaluation of Primary and Metastatic Lesion Spectrum to Guide Anti-PD-L1 Therapy of Non-Small Cell Lung Cancer: Results From Two Randomized Studies. *Oncoimmunology* (2021) 10(1):1909296. doi: 10.1080/2162402x.2021.1909296

85. Skribek M, Rounis K, Makrakis D, Agelaki S, Mavroudis D, De Petris L, et al. Outcome of Patients With NSCLC and Brain Metastases Treated With Immune Checkpoint Inhibitors in a 'Real-Life' Setting. *Cancers* (2020) 12 (12):3707. doi: 10.3390/cancers12123707
86. Zhang G, Cheng R, Wang H, Zhang Y, Yan X, Li P, et al. Comparable Outcomes of Nivolumab in Patients With Advanced NSCLC Presenting With or Without Brain Metastases: A Retrospective Cohort Study. *Cancer Immunol Immunother* (2020) 69(3):399–405. doi: 10.1007/s00262-019-02462-1
87. Rounis K, Skribek M, Makrakis D, De Petris L, Agelaki S, Ekman S, et al. Correlation of Clinical Parameters With Intracranial Outcome in Non-Small Cell Lung Cancer Patients With Brain Metastases Treated With Pd-1/Pd-L1 Inhibitors as Monotherapy. *Cancers* (2021) 13(7):1562. doi: 10.3390/cancers13071562
88. Wakuda K, Yabe M, Kodama H, Nishioka N, Miyawaki T, Miyawaki E, et al. Efficacy of Pembrolizumab in Patients With Brain Metastasis Caused by Previously Untreated Non-Small Cell Lung Cancer With High Tumor PD-L1 Expression. *Lung Cancer* (2021) 151:60–8. doi: 10.1016/j.lungcan.2020.11.009
89. Crinò L, Bronte G, Bidoli P, Cravero P, Minenza E, Cortesi E, et al. Nivolumab and Brain Metastases in Patients With Advanced non-Squamous non-Small Cell Lung Cancer. *Lung Cancer (Amsterdam Netherlands)* (2019) 129:35–40. doi: 10.1016/j.lungcan.2018.12.025
90. Cortinovis D, Chiari R, Catino A, Grossi F, DEM F, Sperandi F, et al. Italian Cohort of the Nivolumab EAP in Squamous NSCLC: Efficacy and Safety in Patients With CNS Metastases. *Anticancer Res* (2019) 39(8):4265–71. doi: 10.21873/anticanres.13590
91. Gauvain C, Vauléon E, Chouaid C, Le Rhun E, Jabot L, Scherpereel A, et al. Intracerebral Efficacy and Tolerance of Nivolumab in Non-Small-Cell Lung Cancer Patients With Brain Metastases. *Lung Cancer* (2018) 116:62–6. doi: 10.1016/j.lungcan.2017.12.008
92. Cho A, Untersteiner H, Hirschmann D, Shaltout A, Göbl P, Dorfer C, et al. Gamma Knife Radiosurgery for Brain Metastases in Non-Small Cell Lung Cancer Patients Treated With Immunotherapy or Targeted Therapy. *Cancers* (2020) 12(12):3668. doi: 10.3390/cancers12123668
93. Shepard MJ, Xu Z, Donahue J, Eluvathingal Muttikkal TJ, Cordeiro D, Hansen L, et al. Stereotactic Radiosurgery With and Without Checkpoint Inhibition for Patients With Metastatic Non-Small Cell Lung Cancer to the Brain: A Matched Cohort Study. *J Neurosurg* (2019) 133(3):1–8. doi: 10.3171/2019.4.Jns19822
94. Singh C, Qian JM, Yu JB, Chiang VL. Local Tumor Response and Survival Outcomes After Combined Stereotactic Radiosurgery and Immunotherapy in Non-Small Cell Lung Cancer With Brain Metastases. *J Neurosurg* (2019) 132 (2):512–7. doi: 10.3171/2018.10.Jns181371
95. Chen L, Douglass J, Kleinberg L, Ye X, Marciscano AE, Forde PM, et al. Concurrent Immune Checkpoint Inhibitors and Stereotactic Radiosurgery for Brain Metastases in Non-Small Cell Lung Cancer, Melanoma, and Renal Cell Carcinoma. *Int J Radiat Oncol Biol Phys* (2018) 100(4):916–25. doi: 10.1016/j.ijrobp.2017.11.041
96. Sun C, Zhou F, Li X, Zhao C, Li W, Li J, et al. PD-1/PD-L1 Inhibitor Combined With Chemotherapy Can Improve the Survival of Non-Small Cell Lung Cancer Patients With Brain Metastases. *Onco Targets Ther* (2020) 13:12777–86. doi: 10.2147/ott.S286600
97. Afzal MZ, Dragnev K, Shirai K. A Tertiary Care Cancer Center Experience With Carboplatin and Pemetrexed in Combination With Pembrolizumab in Comparison With Carboplatin and Pemetrexed Alone in Non-Squamous Non-Small Cell Lung Cancer. *J Thorac Dis* (2018) 10(6):3575–84. doi: 10.21037/jtd.2018.06.08
98. Powell SF, Rodríguez-Abreu D, Langer CJ, Tafreshi A, Paz-Ares L, Kopp HG, et al. Outcomes With Pembrolizumab Plus Platinum-Based Chemotherapy for Patients With Non-Small-Cell Lung Cancer and Stable Brain Metastases: Pooled Analysis of KEYNOTE-021, 189, and 407. *J Thorac Oncol: Off Publ Int Assoc Study Lung Cancer* (2021) S1556-0864:02287–5. doi: 10.1016/j.jtho.2021.06.020

Conflict of Interest: The authors declare that the research was conducted in the absence of any commercial or financial relationships that could be construed as a potential conflict of interest.

Publisher's Note: All claims expressed in this article are solely those of the authors and do not necessarily represent those of their affiliated organizations, or those of the publisher, the editors and the reviewers. Any product that may be evaluated in this article, or claim that may be made by its manufacturer, is not guaranteed or endorsed by the publisher.

Copyright © 2022 Wang, Chen, Wa, Ding, Yang, Liao, Tong and Xiao. This is an open-access article distributed under the terms of the Creative Commons Attribution License (CC BY). The use, distribution or reproduction in other forums is permitted, provided the original author(s) and the copyright owner(s) are credited and that the original publication in this journal is cited, in accordance with accepted academic practice. No use, distribution or reproduction is permitted which does not comply with these terms.

frontiers in Immunology

ORIGINAL RESEARCH
published: 21 February 2022
doi: 10.3389/fimmu.2022.841404

Diverse Macrophages Constituted the Glioma Microenvironment and Influenced by PTEN Status

Fengqi Zhou[1†], Qinyu Shi[1†], Xiao Fan[1†], Ruilei Yu[2†], Zhiqiang Wu[1], Binbin Wang[1], Wei Tian[1], Tianfu Yu[3], Minhong Pan[4], Yongping You[1*] and Yingyi Wang[1*]*

[1] Department of Neurosurgery, The First Affiliated Hospital of Nanjing Medical University, Nanjing, China, [2] Department of Radiology, The First Affiliated Hospital of Nanjing Medical University, Nanjing, China, [3] Department of Neurosurgery, The Affiliated Hospital of Nanjing University Medical School, Nanjing, China, [4] Department of Pathology, The First Affiliated Hospital of Nanjing Medical University, Nanjing, China

The glioma immune microenvironment (GIM), consisting of glioma cells, stromal cells, and immune cells, accelerates the initiation, development, immune evasion, chemoresistance, and radioresistance of glioblastoma (GBM), whereas the immunosuppressive mechanisms of GBM have not been thoroughly elucidated to date. The glioma data downloaded from The Cancer Genome Atlas (TCGA) and the Chinese Glioma Genome Atlas (CGGA) databases were used to evaluate the composition of tumor-infiltrating immune cells (TICs) by the CIBERSORT algorithm. RNA-seq datasets from the TCGA and CGGA were used to analyze the relationship between immune scores with patients' characteristics and TICs, which showed higher ratios of tumor-inhibiting/tumor-promoting signatures (M2/M1 macrophages) along with higher immune scores. The distribution of TICs among different glioma patients and the correlation with hazard ratio (HR) analysis suggested that M2 macrophages were abundant in malignant gliomas and indicated an unfavorable prognosis. We further analyzed TCGA cases with available mutation and copy-number alteration information, which showed that the status of PTEN could influence the immune microenvironment of glioma patients. Tissue microarrays of 39 GBM patients were carried out to confirm the clinical significance of PTEN and macrophage markers. We found that the high expression of PTEN was associated with a more extended survival period of glioma patients, positively correlated with M2 macrophages and negatively with M1 macrophages. Transwell and flow cytometry analyses demonstrated that PTEN status could prevent M1 to M2 polarization and M2

OPEN ACCESS

Edited by:
Quan Cheng,
Central South University, China

Reviewed by:
Xiaokuang Ma,
The University of Arizona College of Medicine – Phoenix, United States
Xi Yang,
Shanghai JiaoTong University, China

***Correspondence:**
Yingyi Wang
lindsay_wang3431@126.com
Yongping You
yypl9@njmu.edu.cn
Minhong Pan
panminhong@jsph.org.cn

[†]These authors have contributed equally to this work

Specialty section:
This article was submitted to Cancer Immunity and Immunotherapy, a section of the journal Frontiers in Immunology

Received: *22 December 2021*
Accepted: *31 January 2022*
Published: *21 February 2022*

Citation:
Zhou F, Shi Q, Fan X, Yu R, Wu Z, Wang B, Tian W, Yu T, Pan M, You Y and Wang Y (2022) Diverse Macrophages Constituted the Glioma Microenvironment and Influenced by PTEN Status. Front. Immunol. 13:841404. doi: 10.3389/fimmu.2022.841404

macrophage recruitment of gliomas *in vitro*. The newly discovered immunoregulatory activity of PTEN opens innovative avenues for investigations relevant to counteracting cancer development and progression.

Keywords: glioma, immune microenvironment, macrophages, PTEN, polarization

INTRODUCTION

Gliomas comprise nearly four-fifths of all common malignant central nervous system tumors, which include low-grade glioma (LGG) and glioblastoma (GBM) (1). LGG, according to the criteria established by the World Health Organization (WHO), defined as a lower grade (I–III), has a more favorable prognosis. Conversely, GBM classified as the highest grade (IV) has a more unfavorable prognosis (2, 3). Moreover, GBM is one of the most highly immunosuppressive and lethal tumors. Although standard therapies had improved, concluding surgical resection, radiotherapy, systemic therapy (chemotherapy, targeted therapy) (4), and supportive care, the median survival of GBM patients remains less than 16 months (5, 6), and treatment remains palliative.

Given that multiple components composed the glioma microenvironment, including blood vessels, parenchyma cells, extracellular matrix, soluble factors, and infiltrating immune cells (7, 8), tumor-associated macrophages (TAMs) are enriched in GBMs, serving as an essential element of the tumor microenvironment in GBM and playing crucial roles in supporting tumor growth (9, 10), suggesting that targeting TAMs may improve tumor outcome. It is well known that TAMs include two key populations: M2 macrophages serving as tumor supporters and M1 macrophages serving as tumor suppressors (11). In the tumor microenvironment, M2 macrophages play immune-suppressive roles *via* promoting tumor development (12). What is more, the majority of TAMs in GBMs have M2-like properties (13), which is verified in several studies that M2-polarized TAMs support the malignant growth of GBM (14–16). Although M2 macrophages have a remarkable effect on the development of GBMs, the mechanisms underlying the program and maintenance of M2 macrophages in the glioma microenvironment remain unknown.

Phosphatase and tensin homolog (PTEN) is an omnipresently expressed tumor suppressor, commonly inactivated in sporadic human cancers. In many tumors such as brain, prostate, and bladder, PTEN frequently showed genomic deletion (17, 18). Shortly after that, PTEN mutations were also found to increase the risks of cancer predisposition and neurological symptoms (19). PTEN is a central negative regulator of the phosphoinositide 3-kinase (PI3K)-Akt-mechanistic target of rapamycin (mTOR) signaling pathway, which plays a significant role in ruling a wide range of essential cellular processes such as cell proliferation, apoptosis, survival, and metabolism (20, 21).

In this study, we addressed glioma classification by identifying specific immune types based on The Cancer Genome Atlas (TCGA) and the Chinese Glioma Genome Atlas (CGGA) database. Glioma immune scores may provide novel insights into the glioma microenvironment, systematically investigating clinical, genomic, and biological conditions. M2 macrophages, existing more in the higher immune score patients, were influenced by PTEN status.

MATERIAL AND METHODS

Human Glioma Samples

Thirty-nine surgical resection specimens of glioma patients were obtained from the First Affiliated Hospital of Nanjing Medical University (Nanjing, China). All the specimens' histological features were identified by pathologists following the WHO criteria. This study protocol was approved by the Research Ethics Committee of Nanjing Medical University (Nanjing, Jiangsu, China).

Glioma Patient Databases

Databases from patients were downloaded from the TCGA database (n = 688) (http://cancergenome.nih.gov/) and CGGA database (n = 693) (http://www.cgga.org.cn). DNA copy number and mutation profiles were obtained from the TCGA website (http://cancergenome.nih.gov/).

Western Blot Analysis

Western blot analysis was performed as described previously (22). Immunoblot analysis used the following primary antibodies: anti-PTEN (#9188), Akt (#4685), phospho-Akt (#4060), CD163 (#93498), CD68 (#97778), CD206 (#24595), iNOS (#13120), and α-tubulin (#2144) were purchased from Cell Signaling Technology (MA, USA).

Flow Cytometry

Cells were incubated with fluorescence-conjugated antibodies for 30 min at 4°C, after being collected and washed. Cells were fixed and permeabilized with a fixation/permeabilization solution kit (BD Cytofix/Cytoperm) and 1% paraformaldehyde (PFA) for facilitating intracellular staining. The results were analyzed using the FlowJo 10.7 software program. This analysis used the following primary antibodies: Iba1 (#17198) and anti-rabbit IgG (H+L), F(ab′)2 fragment (PE conjugate) (#79408) were purchased from Cell Signaling Technology (MA, USA), and CD163-APC (130-100-612) was purchased from Miltenyi Biotec (Germany).

Polarization of Macrophages

For differentiating into an intermediate stage M0, THP-1 cells were stimulated by phorbol 12-myristate 13-acetate (PMA). After that, IFN-γ and LPS were used to stimulate the

polarization from M0 to M1 macrophages and then IL-4 and IL-13 for the polarization from M0 into M2 macrophages.

Cell Lines, Incubation, and Stable Cell Establishment

Three human GBM cell lines (U251, LN229, and U87) and the human monocyte cell line THP-1 cells were purchased from the Chinese Cell Repository (Shanghai, China). LN229 cells were infected with lentivirus containing PTEN-specific shRNA (shPTEN) or non-targeting control shRNA (shCONT). For establishing stably expressing shPTEN or shCONT, transfected LN229 cells were selected with additional 5 mg/ml puromycin for 3 to 4 weeks. The targeting sequence for PTEN-shRNA was 5′-GCTAGAACTTATCAAACCCTT-3′.

Macrophage Migration Assay

After differentiating THP-1 cells into M2 macrophages *in vitro*, the macrophage migration assay was performed. In a 24-well plate, U87, U251, $LN229^{shCONT}$, and $LN229^{shPTEN}$ cells were placed on the bottom of the lower chamber serving as a chemoattractant. Meanwhile, M2 macrophages were added in the upper transwell inserts (New York, USA, Cat: 09717050). After being incubated at 37°C and 5% CO_2 for 48 h, the remaining cells on the top of the membrane were wiped off with a cotton swab. Cells which migrated into the bottom of the membrane were fixed with 4% PFA and stained with crystal violet solution. After dipping into distilled water to remove excess staining, the results of migration were visualized under a microscope.

M1 Macrophage and Glioma Cell Transwell Co-Culture Assay

Cell culture inserts (3.0 μm) (New York, USA, Cat: 353492) were used to perform this indirect co-culture assay. In the presence of PMA, U87, U251, $LN229^{shCONT}$, and $LN229^{shPTEN}$ cells were seeded into the bottom wells. Meanwhile, the upper inserts were added with M1-polarized THP-1 cells. Macrophages were then collected and labeled with M2 macrophage marker CD163 and pan-macrophage marker Iba1 to identify the phenotypic changes using flow cytometry.

Estimation of TICs

After uploading the normalized gene expression data to the CIBERSORT web portal (https://cibersort.stanford.edu/), 100 permutations and the LM22 gene signature were used to determine the algorithm. The 22 immune cells mainly consisted of T cells, B cells, NK cells, and other myeloid subsets (23). TICs from tumor and normal samples were differentiated by principal component analysis (PCA). Cases with a CIBERSORT algorithm p-value <0.05 were filtered and selected for further analysis.

Immunohistochemistry

All immunohistochemistry experiments were performed according to the methods described in our previous study (24). Histochemistry score analyses were conducted by using the IHC profiler through ImageJ.

In-Vivo Tumorigenesis

Viable GBM cells were counted and engrafted intracranially into female Bagg albino (BALB)/c nude mice (4 weeks old). All the animal experiments were approved in accordance with the Animal Use Guidelines of the Chinese Ministry of Health (documentation 55,2001). Healthy female mice of Bagg albino (BALB)/c background, 4 weeks old, were randomly selected and used in this study for intracranial injection. Animals were maintained until neurological signs were apparent, at which point they were sacrificed. Brains were collected and fixed in 4% formaldehyde, cryopreserved in 30% sucrose, and then cryosectioned.

Immunofluorescent Analysis

Tumor sections were fixed with 4% paraformaldehyde, washed with PBS, permeabilized with 0.5% (vol/vol) Triton X-100 (California, USA, 1610407), and blocked with 3% (wt/vol) BSA (Saint Louis, USA, A7906) in PBS. Primary antibodies [anti-Iba1 (Cell Signaling Technology, #17198) and anti-CD163 (Boston, MA, USA, ab156769)] were added to the sections and incubated overnight at 4°C. After three washes with cold PBS, samples were incubated with secondary antibodies [Alex 488- or 568-labeled anti-rabbit or anti-mouse (Thermo Fisher Scientific)] for 1 h at room temperature, counterstained with 4,6-dianmino-2-phenylindole (DAPI) (Cell Signaling, 4083, 1:5,000), and sealed with mounting medium (Sigma-Aldrich, F4680).

Statistical Analysis

The differences in the variable groups were assessed by Student's t-test and one-way analysis of variance (one-way ANOVA). SPSS 24.0 (IBM, Chicago, USA), R3.3.1 (https://www.r-project.org/), and GraphPad Prism 8.0 programs were used for statistical analyses. The levels of infiltrating stromal and immune cells and tumor purity in the tumor samples were calculated by "Estimation of Stromal and Immune cells in Malignant Tumors using Expression data" (ESTIMATE) (25). The Gene Tree View software was used to generate heatmaps in this study. Kaplan–Meier curves and the log-rank test were used to conduct survival analysis with GraphPad Prism 8 software. Statistical values of p <0.05 were considered to be significant.

RESULTS

The Immune Cell Infiltration Landscape in Gliomas

RNA-seq datasets used in this study were downloaded from the TCGA and CGGA. Gliomas from the two datasets were arranged in order of increasing immune scores. The distribution of immune scores was evaluated among different groups and associated with other factors. We found a positive correlation between glioma immune scores and clinical or molecular characteristics, including age, grade, and histology. Moreover, patients who got lower immune scores have better overall survival (OS) than those who got higher immune scores. The mesenchymal subtype gliomas display higher immune scores

compared with the other three subtypes. Concerning genomic alterations, in glioma samples, the IDH mutation and 1p/19q codeletion indicated lower immune scores (**Figures 1A, B**). In addition, we evaluated the different enrichment levels of 22 immune cell types associated with the immune scores. Furthermore, the 22 tumor-infiltrating immune cell (TIC) cluster heatmaps are shown in **Figures 1A, B**. We noticed that B cells naive, B cells memory, plasma cells, T cells CD8, Tregs, NK cells resting, monocytes, macrophages M1, and neutrophils were negatively correlated with the immune score in the TCGA, while B cells naive, plasma cells, T cells CD4 (memory resting/activated), T cells (follicular helper/gamma delta), NK cells active, macrophages M1, dendritic cells activated, and neutrophils were negatively correlated with the immune score in the CGGA as well. According to the above findings, B cells naive, plasma cells, macrophages M1, and neutrophils were negatively correlated with the immune score in both the TCGA and the CGGA. We also observed that T cells (CD4 naive), macrophages M0 and M2, dendritic cells activated, and mast cells resting were positively correlated with the immune score in the TCGA, while B cells memory, T cells (CD4 naive), NK cells resting, and macrophages M2 were positively correlated with the immune score in the CGGA as well. It was quickly found that macrophages M2 and T cells (CD4 naive) were positively correlated with the immune scores in both the TCGA and the CGGA. Interestingly, we observed higher ratios of tumor-inhibiting/tumor-promoting signatures (M2/M1 macrophages) in higher immune scores than in immune scores–low gliomas.

Different Distribution of TICs Among Glioma Grades and Subtypes

Then we evaluated the distribution of the 22 TICs in different glioma groups, distinguished by immune scores, WHO grade, and TCGA subtypes using the TCGA (top) and CGGA datasets (bottom) (**Figure 2A**). In the TCGA, we found that the expression of tumor supporter M2 macrophages in the WHO IV group was the highest compared with the other two histology groups (WHO II and WHO III) and in the mesenchymal group compared with the other three subtypes (classical, neural, and proneural) (**Figures 2B, C**). In the CGGA, M2 macrophages' expression was higher in WHO IV than in WHO II (**Supplementary Figure 1A**) and the lowest in the neural subtypes (**Supplementary Figure 1B**). Total macrophages and M0 macrophages existed more in WHO IV compared with WHO III or II, both in the TCGA and CGGA (**Figure 2B** and **Supplementary Figure 1A**). The expression of total macrophages has no statistical difference among the four

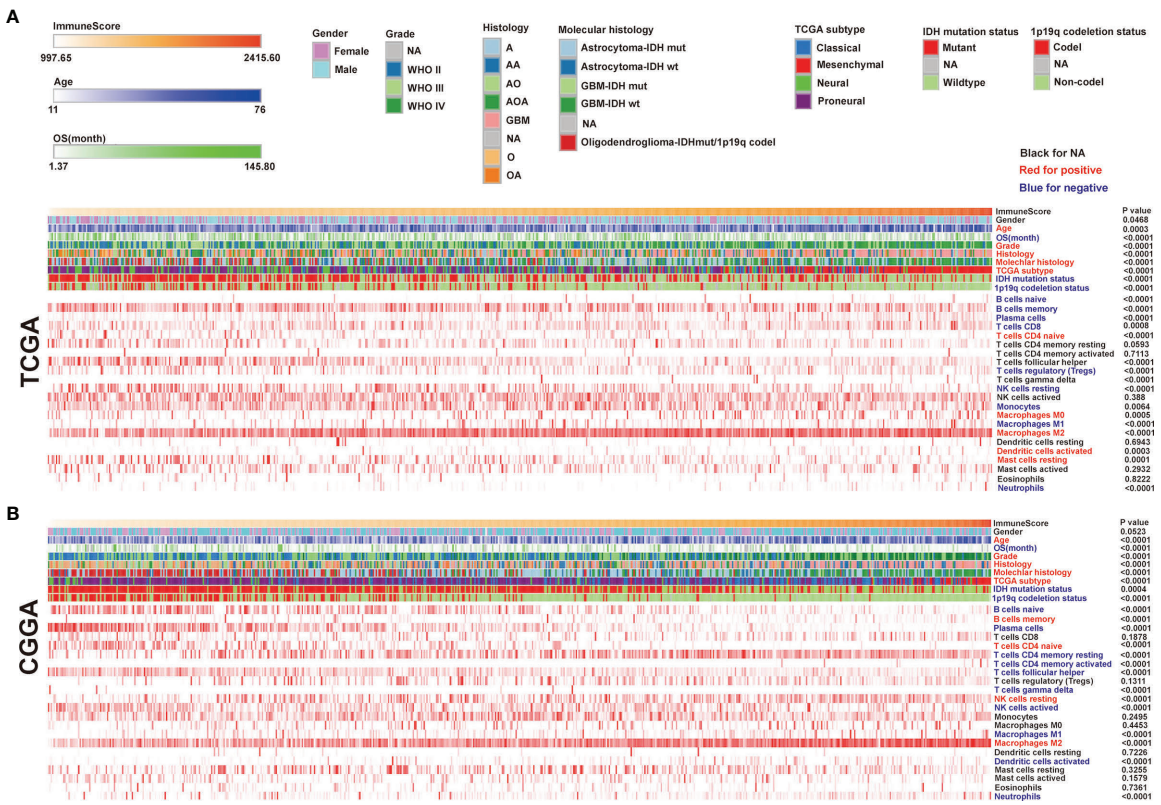

FIGURE 1 | The landscape of clinical and molecular characteristics in association with immune scores. The Cancer Genome Atlas (TCGA) **(A)** and the Chinese Glioma Genome Atlas (CGGA) **(B)** sets were arranged to increase immune scores. The relationship between immune scores and patients' characteristics was evaluated. Heatmaps of the enrichment levels of 22 immune cell types correlated with the immune scores in the TCGA and CGGA.

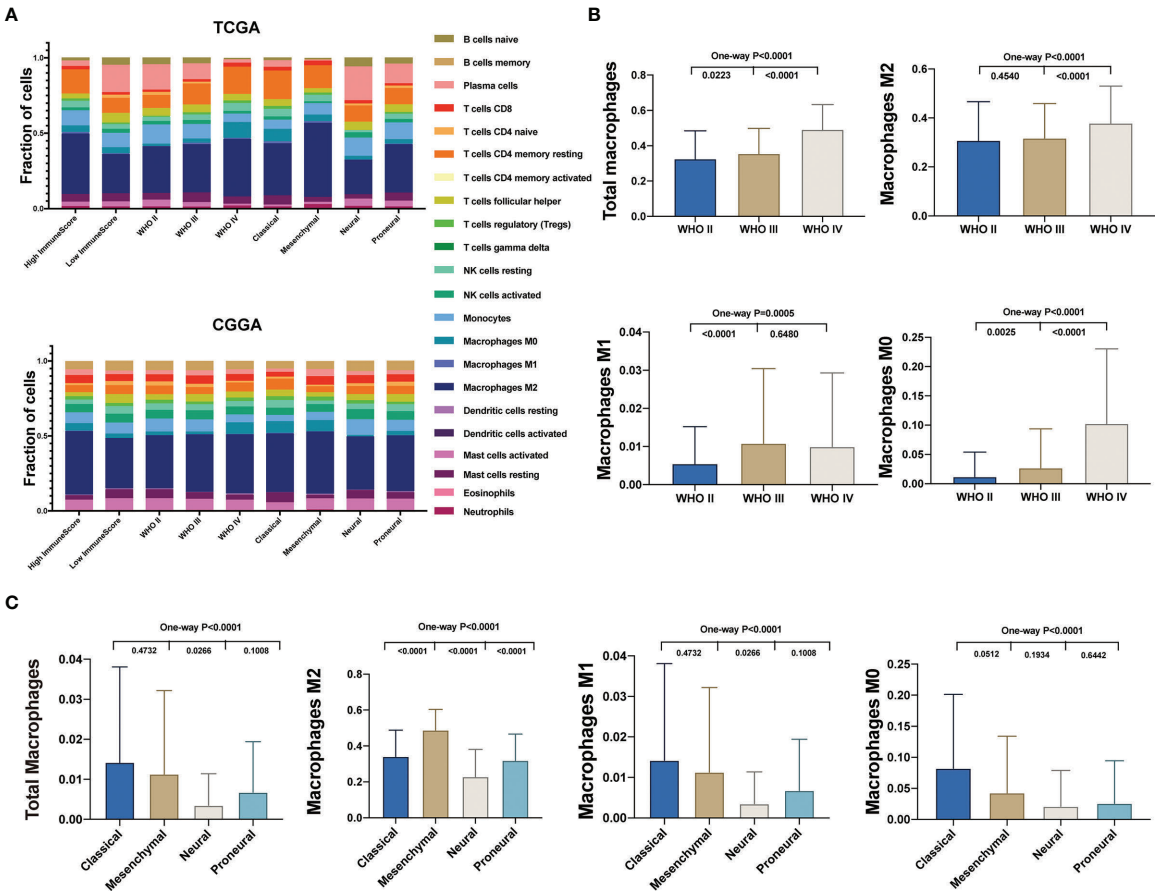

FIGURE 2 | Different distribution of TICs among glioma subtypes. **(A)** The fractions of 22 immune type cells in different glioma patients' characteristics in the TCGA (top) and CGGA (bottom). **(B)** Comparison of the total and different subtypes of macrophage expression between different WHO grade glioma specimens in the TCGA. **(C)** Comparison of the total and different subtypes of macrophage expression between TCGA subtypes in the TCGA.

subtypes, whereas M0 macrophages' expression showed in the neural subtype was the lowest (**Supplementary Figure 1B**). As for the expression of M1 macrophages, there was no statistical difference among WHO IV, III, and II or the four subtypes in the CGGA, although it was the lowest in WHO II or the highest in the classical subtype in TCGA (**Figures 2B, C** and **Supplementary Figures 1A, B**). In conclusion, we found that more malignant gliomas generally had a higher expression of M2 macrophages.

M2 Macrophages Indicated an Unfavorable Prognosis

The 22 immune cell types correlated with hazard ratio (HR) in the TCGA and CGGA were analyzed. We observed that monocytes were correlated with favorable outcomes both in the TCGA and CGGA. On the other hand, 10 of these 22 TICs were related to adverse outcomes, including M2 macrophages, which positively correlated with the immune score both in the TCGA and CGGA (**Figure 3A**). The dichotomization on median value was used to separate cases for depicting the survival curves. Parallel analyses were conducted in both the TCGA and CGGA datasets. We found that the high expression of total macrophages and M0 and M2 macrophages was associated with a shorter survival period in both the TCGA and CGGA datasets. On the contrary, there was no significantly different OS between higher and lower M1 macrophages in both the TCGA and CGGA datasets (**Figures 3B–E**). Taken together, these data suggested that M2 macrophages indicated an unfavorable prognosis.

Total macrophage enrichment is associated with distinct patterns of genomic alterations, and the glioma prognosis was correlated with the status of PTEN.

For uncovering the molecular mechanisms that influence tumor cell percentage within the glioma microenvironment, we analyzed TCGA cases with available mutation and copy-number alteration information. Based on the increasing total macrophages, cases were divided into four subgroups. Here, we showed the first quarter (low total macrophages) and fourth quarter (high total macrophages), frequent mutations in IDH1, 1p19q, PTEN, CIC, TTN, ATRX, and EGFR. Interestingly, PTEN mutations (including nonsense and missense mutations) almost happened in the high total macrophage group (**Figure 4A**). We also found that the expression of PTEN was negatively associated with the fraction of total macrophages and M2 macrophages

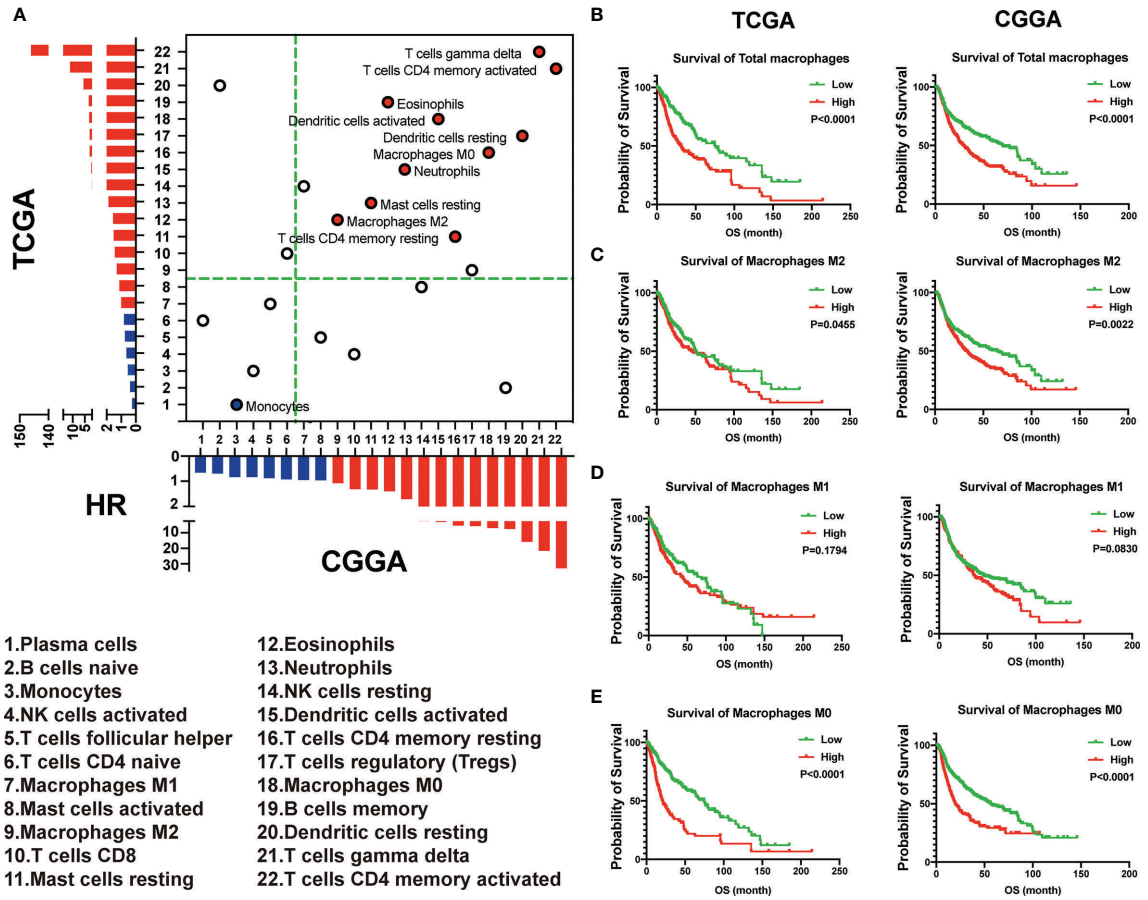

FIGURE 3 | M2 macrophages indicated an unfavorable prognosis. **(A)** The 22 immune cell types correlated with hazard ratio (HR) in the TCGA and CGGA. **(B–E)** The total and different subtypes of macrophages were associated with the prognosis in glioma patients in the TCGA (left) and CGGA (right), based on the results of the Kaplan–Meier survival analysis.

(**Figure 4B**). To assess our findings' clinical relevance, we have used tissue microarrays containing 39 GBM patients to carry out the immunohistochemical analysis of PTEN, CD68 (M1 macrophage marker), and CD163 (M2 macrophage marker). We further evaluated whether the expression of PTEN, CD163, and CD68 was associated with the prognosis of GBM patients. Kaplan–Meier survival analysis indicated that patients with low expression of PTEN exhibited much worse OS. On the contrary, increased expression of CD163 was associated with a more extended survival period (**Figure 4C**), and the expression of CD68 had no significant association with the OS of GBM patients (**Supplementary Figure 2A**). A highly significant positive correlation between PTEN and CD68 was found in these GBM specimens. In contrast, a negative correlation was found between PTEN and CD163 (**Figure 4D**). CD163 and CD68 expression levels also have an opposing correlation (**Supplementary Figure 2B**). Tumors with high total positive histochemistry scores (H-scores) (the summary of high positive, positive, and low positive H-scores) of PTEN expressed low CD163 and high CD68 levels (**Figures 4D, E**). Collectively, the status of PTEN was related not only to the polarization of macrophages in the glioma microenvironment but also to the prognosis of glioma patients.

PTEN impairs the macrophage polarization from M1 toward M2 and the recruitment of M2 macrophages.

To further examine the relationship between PTEN deletion/mutation and M2 macrophage infiltration *in vitro*, we chose U87 (PTEN deletion), U251 (PTEN mutation), and LN229 (PTEN wild type) cells for further study. Moreover, LN229 cells were transduced with a non-targeting control small hairpin RNA (shRNA) (shCONT) and shRNA targeting *PTEN* (shPTEN), respectively. We performed Western blot analyses of these glioma cell lines. The results revealed that PTEN was not expressed in U87 cells, and the PTEN expression was silenced with shPTEN in LN229^{shPTEN}. The levels of phosphorylated Akt (Ser 473) were significantly lower in LN229^{shCONT} compared with the other cell lines (U87, U251, and LN229^{shPTEN}) (**Figure 5A**). We established a co-culture system of glioma cells with M1 or M2 macrophages. After polarization of THP-1 cells into M2 macrophages, we subsequently collected M1 macrophages co-cultured with U87, U251, LN229^{shCONT}, and LN229^{shPTEN} cells, respectively, for Western blot and flow

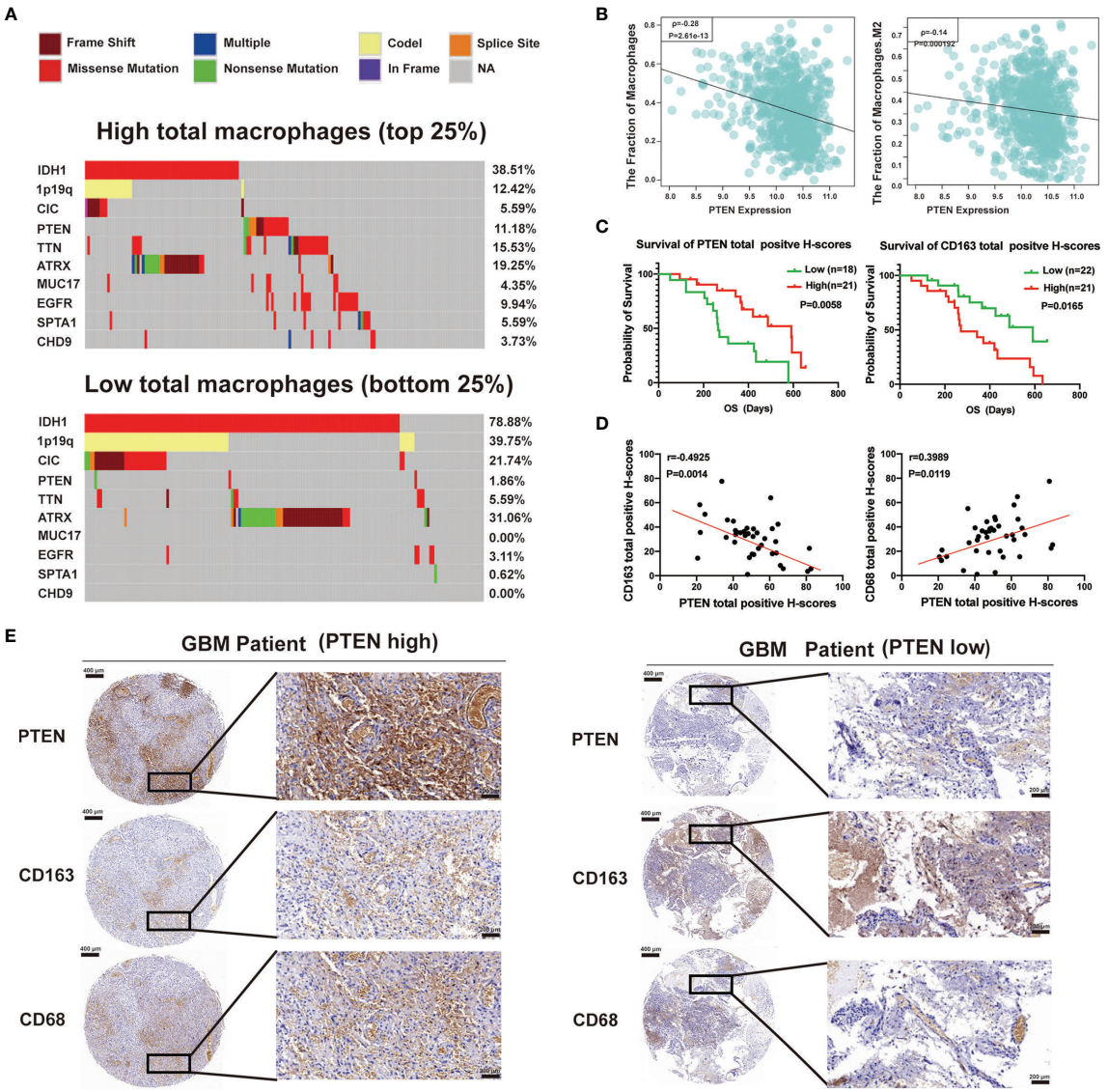

FIGURE 4 | Total macrophage enrichment is associated with distinct patterns of genomic alterations, and the glioma prognosis was correlated with the status of phosphatase and tensin homolog (PTEN). **(A)** Differential somatic mutations were detected by comparing gliomas with high and low total macrophages. **(B)** The relationship of total macrophages (left) or M2 macrophages (right) with the expression of PTEN in the TCGA database. **(C)** Kaplan–Meier curves of overall survival for patients with high or low total positive H-scores of PTEN (left) and CD163 (right). **(D)** Spearman correlation analysis between PTEN and CD163 (left) or CD68 (right) protein levels in GBM specimens. **(E)** Immunohistochemical staining of PTEN, CD163, and CD68 in human GBM tissues. Representative images of immunohistochemical staining from the same tumor samples (GBM patient PTEN high, left; GBM patient PTEN low, right) are shown. Scale bar: 400 μm (left), 200 μm (right).

cytometry analyses. Western blot analysis results showed that the expression levels of M2 macrophage markers CD206 and CD163 in these macrophages co-cultured with PTEN deletion, mutation, or silenced cells (U87, U251, and LN229^{shPTEN}) were significantly higher compared with those co-cultured with PTEN wild-type glioma cells (LN229^{shCONT}). On the contrary, the macrophages co-cultured with LN229^{shCONT} showed higher expression levels of M1 macrophage markers CD86 and iNOS (**Figure 5B**). The flow cytometry results revealed that the percentage of M2 macrophages (CD163^{+}/Iba1^{+}) was higher after being co-cultured with U87, U251, and LN229^{shPTEN} cells compared with LN229^{shCONT} cells (**Figure 5C**), and the statistical analysis of the percentage of M2 macrophages is shown in **Figure 5D**. To determine whether PTEN status could impact M2 macrophage migration, we subsequently co-cultured M2 macrophages, respectively, with U87, U251, LN229^{shCONT}, and LN229^{shPTEN} cells after polarizing THP-1 cells into M2 macrophages. The results revealed that the migration of M2 macrophages was remarkably decreased when co-cultured with LN229^{shCONT} cells (PTEN wild type) (**Figure 5E**), and the statistical analysis of the percentage of migrated M2 macrophage cells is shown in **Figure 5F**. To address

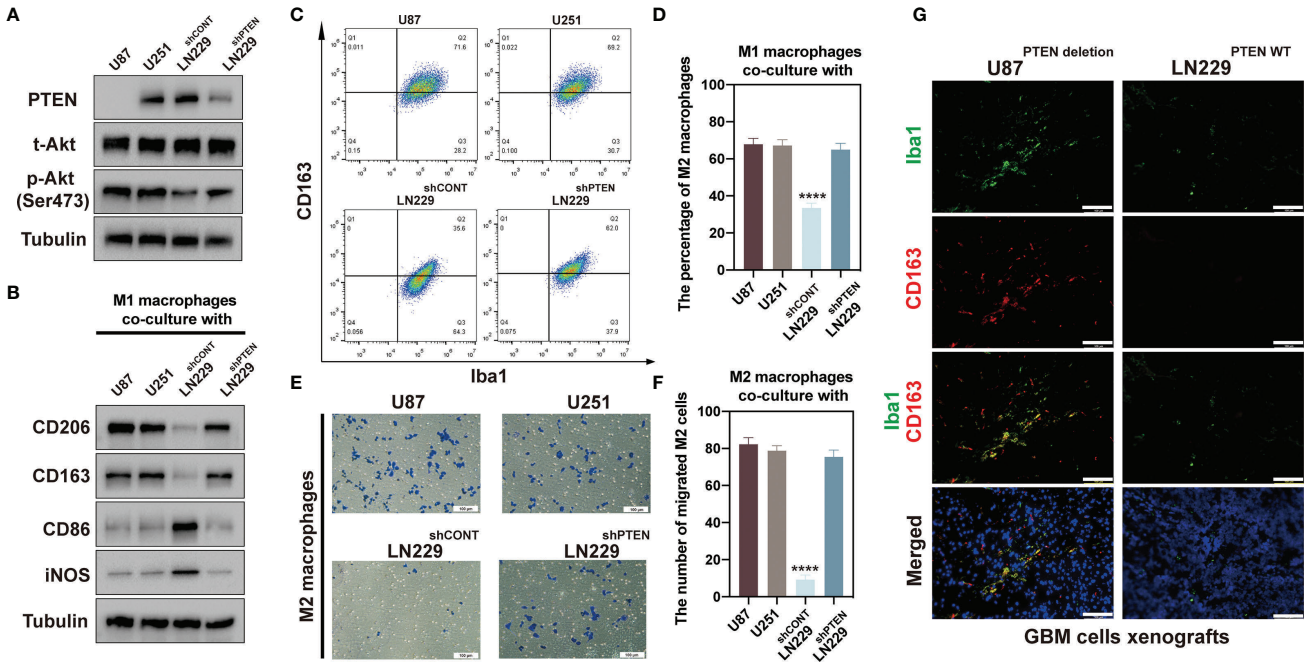

FIGURE 5 | PTEN deletion or mutation glioma cells promoted M1 macrophage differentiation toward M2 macrophage. **(A)** Immunoblot analyses of PTEN, total Akt, and phosphor-Akt (Ser473) expression in cell lysates of U87, U251, LN229^{shCONT}, and LN229^{shPTEN} cells. Tubulin served as the loading control. **(B)** Immunoblot analyses of CD206, CD163, CD86, and iNOS expression of macrophages after co-culture with U87, U251, LN229^{shCONT}, and LN229^{shPTEN} cells. Tubulin served as the loading control. **(C)** Flow cytometric analysis for pan-macrophage marker Iba1 and M2 macrophage marker CD163 expression in the collected macrophages after co-culture with U87, U251, LN229^{shCONT}, and LN229^{shPTEN} cells. **(D)** The percentage of M2 macrophages is summarized in the bar chart. **(E)** Representatives of M2 macrophage migration assays induced by U87, U251, LN229^{shCONT}, and LN229^{shPTEN} cells. Scale bar: 100 μm. **(F)** Statistical analysis of the percentage of the migrated M2 macrophage cells. The data were calculated as means ± standard error of the mean (SEM) of six independent experiments (right). **(G)** Immunofluorescent analysis of the pan macrophage marker Iba1 (green) and M2 marker CD163 (red) in GBM xenografts derived from U87 cells or LN229 cells. Frozen sections of these GBM xenografts were immunostained with antibodies against Iba1 and CD163 and counterstained with DAPI (blue). Marked reductions of CD163 and Iba1 signals were detected in the LN229-derived tumors. Scale bars: 100 μm (****$p < 0.0001$).

whether PTEN plays a role in TAM recruitment, we examined the effect of PTEN deletion or wild type on TAM density in GBM cell xenografts. We applied the M2-specific marker CD163 and the pan macrophage marker Iba1 to distinguish M2 TAMs in GBM cell-derived tumors. Frozen sections of these GBM xenografts derived from U87 (PETN deletion) cells or LN229 (PETN wild type) cells were immunostained with antibodies against Iba1 and CD163 and counterstained with DAPI (**Figure 5G**). As shown by the immunofluorescent analysis, marked reductions of CD163 and Iba1 signals were detected in the PTEN wild-type-derived tumors. These findings revealed that PTEN is an essential factor in preventing the polarization of M1 macrophages toward M2 macrophages and the migration of M2 macrophages *in vitro* and *in vivo*.

DISCUSSION

GBM is the most well-known primary brain malignancy in adults, characterized with extensively cellular heterogeneity and hierarchy. Diverse phenotypic tumor cells, prominent TAMs, other immune cells, and the extracellular matrix all together dispatch tumor progression and immune evasion (2, 26). The communication within those cells, including vascular cells, stromal cells, transformed cells, and infiltrating inflammatory cells in the tumor microenvironment, contributed to the poor prognosis of patients (10). Through the TCGA and CGGA databases, we evaluated the different enrichment levels of 22 immune cell types among glioma samples based on immune scores. We demonstrated that patients with lower immune scores had better OS. A potential explanation for this is that the progression and exacerbation of gliomas could be promoted by the inflammatory tumor microenvironment (27). Our results also confirmed that a macrophage-rich microenvironment could shape a mesenchymal glioma cell phenotype. Noticeably, most IDH1 and 1p/19q codeletion mutations occurred in the group with low immune scores, indicating that IDH mutations and 1p/19q codeletion negatively correlate with glioma immunity. These findings are consistent with the results of a previous study showing that IDH mutations were associated with low immune infiltration in gliomas (28, 29).

In recent years, several studies have investigated the immune landscape of glioma. For instance, Thorsson et al. revealed that the immunologically quiet subtype mainly was composed of LGG, containing the lowest level of lymphocyte infiltration (30).

Total macrophages-high included a significantly higher percentage of PTEN mutated than total macrophages-low, suggesting that PTEN mutations have a negative correlation with glioma immunity. To explore the impact of different PTEN statuses on the immunological classification of gliomas, glioma cells were separated into PTEN deletion, PTEN mutation, PTEN wild type, and PTEN wild type-shPTEN groups for *in-vitro* experiments. The subsequent experiments validated that the change or loss of PTEN wild-type status could promote tumor cells to reprogram macrophages from M1 to M2 and facilitate the migration of M2 macrophages.

PTEN status detection in glioma has tremendous potential to raise our understanding of this disease's pathology and identify efficient therapeutic approaches to improve clinical outcomes for glioma patients. As the most commonly lost tumor suppressor in primary glioma, PTEN loss, which served as one of the few prognostic biomarkers, is reproducibly associated with unfavorable prognosis in glioma patients. In conclusion, our results showed that the change of PTEN status could influence the immune response to tumor progression and has a key role in predicting which patients will respond to promising immunotherapies.

DATA AVAILABILITY STATEMENT

The original contributions presented in the study are included in the article/Supplementary Material. Further inquiries can be directed to the corresponding author.

ETHICS STATEMENT

The studies involving human participants were reviewed and approved by Research Ethics Committee of Nanjing Medical University (Nanjing, Jiangsu, China). The patients/participants provided their written informed consent to participate in this study.

AUTHOR CONTRIBUTIONS

YW, YY, and MP conceived and designed the experiments. FZ performed all the *in-vitro* experiments with the assistance of XF, BW, and RY. QS performed all the *in-vivo* experiments with the assistance of ZW, WT, and TY. FZ wrote the manuscript. All authors reviewed the paper. All authors contributed to the article and approved the submitted version.

FUNDING

This work was supported by grants from the National Natural Science Foundation of China (81772682) and the Priority Academic Program Development of Jiangsu Higher Education Institutions (PAPD).

ACKNOWLEDGMENTS

We would like to thank the Core Facility of the First Affiliated Hospital of Nanjing Medical University for the help in the detection of experimental samples.

SUPPLEMENTARY MATERIAL

The Supplementary Material for this article can be found online at: https://www.frontiersin.org/articles/10.3389/fimmu.2022.841404/full#supplementary-material

REFERENCES

1. Feng Q, Li L, Li M, Wang X. Immunological Classification of Gliomas Based on Immunogenomic Profiling. *J Neuroinflamm* (2020) 17(1):360. doi: 10.1186/s12974-020-02030-w
2. Ostrom QT, Bauchet L, Davis FG, Deltour I, Fisher JL, Langer CE, et al. The Epidemiology of Glioma in Adults: A "State of the Science" Review. *Neuro Oncol* (2014) 16(7):896–913. doi: 10.1093/neuonc/nou087
3. Louis DN, Perry A, Reifenberger G, von Deimling A, Figarella-Branger D, Cavenee WK, et al. The 2016 World Health Organization Classification of Tumors of the Central Nervous System: A Summary. *Acta Neuropathol* (2016) 131(6):803–20. doi: 10.1007/s00401-016-1545-1
4. Wen PY, Kesari S. Malignant Gliomas in Adults. *N Engl J Med* (2008) 359 (5):492–507. doi: 10.1056/NEJMra0708126
5. Furnari FB, Fenton T, Bachoo RM, Mukasa A, Stommel JM, Stegh A, et al. Malignant Astrocytic Glioma: Genetics, Biology, and Paths to Treatment. *Genes Dev* (2007) 21(21):2683–710. doi: 10.1101/gad.1596707
6. Stupp R, Hegi ME, Mason WP, van den Bent MJ, Taphoorn MJ, Janzer RC, et al. Effects of Radiotherapy With Concomitant and Adjuvant Temozolomide Versus Radiotherapy Alone on Survival in Glioblastoma in a Randomised Phase III Study: 5-Year Analysis of the EORTC-NCIC Trial. *Lancet Oncol* (2009) 10(5):459–66. doi: 10.1016/s1470-2045(09)70025-7
7. Lathia JD, Heddleston JM, Venere M, Rich JN. Deadly Teamwork: Neural Cancer Stem Cells and the Tumor Microenvironment. *Cell Stem Cell* (2011) 8 (5):482–5. doi: 10.1016/j.stem.2011.04.013
8. Rape A, Ananthanarayanan B, Kumar S. Engineering Strategies to Mimic the Glioblastoma Microenvironment. *Adv Drug Deliv Rev* (2014) 79-80:172–83. doi: 10.1016/j.addr.2014.08.012
9. Garris C, Pittet MJ. Therapeutically Reeducating Macrophages to Treat GBM. *Nat Med* (2013) 19(10):1207–8. doi: 10.1038/nm.3355
10. Hambardzumyan D, Gutmann DH, Kettenmann H. The Role of Microglia and Macrophages in Glioma Maintenance and Progression. *Nat Neurosci* (2016) 19(1):20–7. doi: 10.1038/nn.4185
11. Chanmee T, Ontong P, Konno K, Itano N. Tumor-Associated Macrophages as Major Players in the Tumor Microenvironment. *Cancers (Basel)* (2014) 6 (3):1670–90. doi: 10.3390/cancers6031670
12. Hao NB, Lü MH, Fan YH, Cao YL, Zhang ZR, Yang SM. Macrophages in Tumor Microenvironments and the Progression of Tumors. *Clin Dev Immunol* (2012) 2012:948098. doi: 10.1155/2012/948098
13. Komohara Y, Ohnishi K, Kuratsu J, Takeya M. Possible Involvement of the M2 Anti-Inflammatory Macrophage Phenotype in Growth of Human Gliomas. *J Pathol* (2008) 216(1):15–24. doi: 10.1002/path.2370
14. Pyonteck SM, Akkari L, Schuhmacher AJ, Bowman RL, Sevenich L, Quail DF, et al. CSF-1R Inhibition Alters Macrophage Polarization and Blocks Glioma Progression. *Nat Med* (2013) 19(10):1264–72. doi: 10.1038/nm.3337

15. Zhou W, Ke SQ, Huang Z, Flavahan W, Fang X, Paul J, et al. Periostin Secreted by Glioblastoma Stem Cells Recruits M2 Tumour-Associated Macrophages and Promotes Malignant Growth. *Nat Cell Biol* (2015) 17 (2):170–82. doi: 10.1038/ncb3090
16. Shi Y, Ping YF, Zhou W, He ZC, Chen C, Bian BS, et al. Tumour-Associated Macrophages Secrete Pleiotrophin to Promote PTPRZ1 Signalling in Glioblastoma Stem Cells for Tumour Growth. *Nat Commun* (2017) 8:15080. doi: 10.1038/ncomms15080
17. Li J, Yen C, Liaw D, Podsypanina K, Bose S, Wang SI, et al. PTEN, a Putative Protein Tyrosine Phosphatase Gene Mutated in Human Brain, Breast, and Prostate Cancer. *Science* (1997) 275(5308):1943–7. doi: 10.1126/science.275.5308.1943
18. Steck PA, Pershouse MA, Jasser SA, Yung WK, Lin H, Ligon AH, et al. Identification of a Candidate Tumour Suppressor Gene, MMAC1, at Chromosome 10q23.3 That Is Mutated in Multiple Advanced Cancers. *Nat Genet* (1997) 15(4):356–62. doi: 10.1038/ng0497-356
19. Álvarez-Garcia V, Tawil Y, Wise HM, Leslie NR. Mechanisms of PTEN Loss in Cancer: It's All About Diversity. *Semin Cancer Biol* (2019) 59:66–79. doi: 10.1016/j.semcancer.2019.02.001
20. Fruman DA, Rommel C. PI3K and Cancer: Lessons, Challenges and Opportunities. *Nat Rev Drug Discov* (2014) 13(2):140–56. doi: 10.1038/nrd4204
21. Pulido R. PTEN: A Yin-Yang Master Regulator Protein in Health and Disease. *Methods* (2015) 77-78:3–10. doi: 10.1016/j.ymeth.2015.02.009
22. Zhou F, Wang B, Wang H, Hu L, Zhang J, Yu T, et al. circMELK Promotes Glioblastoma Multiforme Cell Tumorigenesis Through the miR-593/EphB2 Axis. *Mol Ther Nucleic Acids* (2021) 25:25–36. doi: 10.1016/j.omtn.2021.05.002
23. Newman AM, Liu CL, Green MR, Gentles AJ, Feng W, Xu Y, et al. Robust Enumeration of Cell Subsets From Tissue Expression Profiles. *Nat Methods* (2015) 12(5):453–7. doi: 10.1038/nmeth.3337
24. Zhi T, Jiang K, Xu X, Yu T, Zhou F, Wang Y, et al. ECT2/PSMD14/PTTG1 Axis Promotes the Proliferation of Glioma Through Stabilizing E2F1. *Neuro Oncol* (2019) 21(4):462–73. doi: 10.1093/neuonc/noy207
25. Yoshihara K, Shahmoradgoli M, Martínez E, Vegesna R, Kim H, Torres-Garcia W, et al. Inferring Tumour Purity and Stromal and Immune Cell Admixture From Expression Data. *Nat Commun* (2013) 4:2612. doi: 10.1038/ncomms3612
26. Cai J, Zhang W, Yang P, Wang Y, Li M, Zhang C, et al. Identification of a 6-Cytokine Prognostic Signature in Patients With Primary Glioblastoma Harboring M2 Microglia/Macrophage Phenotype Relevance. *PloS One* (2015) 10(5):e0126022. doi: 10.1371/journal.pone.0126022
27. Pombo Antunes AR, Scheyltjens I, Duerinck J, Neyns B, Movahedi K, Van Ginderachter JA. Understanding the Glioblastoma Immune Microenvironment as Basis for the Development of New Immunotherapeutic Strategies. *Elife* (2020) 9:1–16. doi: 10.7554/eLife.52176
28. Amankulor NM, Kim Y, Arora S, Kargl J, Szulzewsky F, Hanke M, et al. Mutant IDH1 Regulates the Tumor-Associated Immune System in Gliomas. *Genes Dev* (2017) 31(8):774–86. doi: 10.1101/gad.294991.116
29. Berghoff AS, Kiesel B, Widhalm G, Wilhelm D, Rajky O, Kurscheid S, et al. Correlation of Immune Phenotype With IDH Mutation in Diffuse Glioma. *Neuro Oncol* (2017) 19(11):1460–8. doi: 10.1093/neuonc/nox054
30. Thorsson V, Gibbs DL, Brown SD, Wolf D, Bortone DS, Ou Yang TH, et al. The Immune Landscape of Cancer. *Immunity* (2018) 48(4):812–30.e814. doi: 10.1016/j.immuni.2018.03.023

Conflict of Interest: The authors declare that the research was conducted in the absence of any commercial or financial relationships that could be construed as a potential conflict of interest.

Publisher's Note: All claims expressed in this article are solely those of the authors and do not necessarily represent those of their affiliated organizations, or those of the publisher, the editors and the reviewers. Any product that may be evaluated in this article, or claim that may be made by its manufacturer, is not guaranteed or endorsed by the publisher.

Copyright © 2022 Zhou, Shi, Fan, Yu, Wu, Wang, Tian, Yu, Pan, You and Wang. This is an open-access article distributed under the terms of the Creative Commons Attribution License (CC BY). The use, distribution or reproduction in other forums is permitted, provided the original author(s) and the copyright owner(s) are credited and that the original publication in this journal is cited, in accordance with accepted academic practice. No use, distribution or reproduction is permitted which does not comply with these terms.

frontiers in Immunology

ORIGINAL RESEARCH
published: 24 February 2022
doi: 10.3389/fimmu.2022.834595

Matrix Remodeling-Associated Protein 8 as a Novel Indicator Contributing to Glioma Immune Response by Regulating Ferroptosis

Zhijie Xu[1†], Xi Chen[2,3†], Liying Song[4], Fang Yuan[5] and Yuanliang Yan[2,3]*

[1] Department of Pathology, Xiangya Hospital, Central South University, Changsha, China, [2] Department of Pharmacy, Xiangya Hospital, Central South University, Changsha, China, [3] National Clinical Research Center for Geriatric Disorders, Xiangya Hospital, Central South University, Changsha, China, [4] Department of Pharmacy, The Third Xiangya Hospital, Central South University, Changsha, China, [5] Department of Plastic Surgery, The Third Xiangya Hospital, Central South University, Changsha, China

OPEN ACCESS

Edited by:
Junxia Zhang,
Nanjing Medical University, China

Reviewed by:
Ying Zhao,
Zhejiang University, China
Zhiwang Song,
The First Affiliated Hospital of Nanchang University, China

***Correspondence:**
Yuanliang Yan
yanyuanliang@csu.edu.cn

[†]These authors have contributed equally to this work

Specialty section:
This article was submitted to Cancer Immunity and Immunotherapy, a section of the journal Frontiers in Immunology

Received: *13 December 2021*
Accepted: *31 January 2022*
Published: *24 February 2022*

Citation:
Xu Z, Chen X, Song L, Yuan F and Yan Y (2022) Matrix Remodeling-Associated Protein 8 as a Novel Indicator Contributing to Glioma Immune Response by Regulating Ferroptosis. Front. Immunol. 13:834595. doi: 10.3389/fimmu.2022.834595

Glioma is a highly malignant brain tumor with a poor survival rate. Novel biomarkers that act as prompt indicators of glioma are urgently needed. In this study, we identified and validated prognosis-related differentially expressed genes by datasets of glioma in the GEO and TCGA databases. Ferroptosis is a newly recognized process of cell death playing a vital role in cancer biology. Pearson correlation coefficient were used to discovery the prognosis-related genes which have the highest correlation with ferroptosis. Matrix remodeling-associated protein 8 (MXRA8) was identified as a novel prognosis indicator which may be involved in ferroptosis. The expression of MXRA8 was significantly higher in glioma compared with normal brain tissue, and increased expression of MXRA8 was associated with unfavorable survivals. Furthermore, *in vitro* analysis showed that knockdown of MXRA8 inhibited the cell viability in T98G and U251 cells and increased the sensitivity of glioma cells to temozolomide. We further observed that downregulation of MXRA8 elevated the levels of intracellular ferrous iron and lipid peroxidation, accompanied by upregulation of NCOA4 and suppression of FTH1. Moreover, co-expression analyses showed that GO term and KEGG pathways were mainly enriched in immunity-related pathways, such as neutrophil-related immunity, adaptive immune response, and cytokine binding. Through ssGSEA algorithm and TISIDB database, immunological analyses showed that MXRA8 was significantly correlated with various immune infiltration cells including NK cells, macrophages, and neutrophils. Meanwhile, MXRA8 was also associated with chemokines and multiple immunoinhibitory molecules, such as TGF-β1, IL-10, PD-L1, and CTLA4. We also found that MXRA8 was positively associated with immune infiltration score, and patients with higher immune score underwent worse overall survivals. Moreover, IHC staining indicated a highly positive correlation of MXRA8 with a macrophage marker CSF1R. The co-cultured models of glioma cells and M2 macrophages showed MXRA8 knockdown glioma cells alleviated the infiltration of M2 macrophage, while the reduced

M2 macrophage infiltration generated by MXRA8 could be rescued by Fer-1 treatment. These results suggest that MXRA8 promotes glioma progression and highlight the pivotal role of MXRA8 in ferroptosis and immune microenvironment of glioma. Therefore, MXRA8 may serve as a novel prognostic marker and therapeutic target for glioma.

Keywords: MXRA8, immune response, ferroptosis, glioma, prognosis

INTRODUCTION

Glioma is one of the most common primary brain tumor, with an annual incidence of 3–8 per 100,000 population (1). As the most malignant subtype of glioma, glioblastoma multiforme (GBM) have an around 14 months of median survival (2, 3). Despite the availability of conventional treatments, such as surgical resection, adjuvant radiotherapy, and chemotherapy, the effects of prolonged survivals in GBM patients were still limited (4). Hence, exploring novel prognostic biomarkers for glioma therapy is crucial.

Ferroptosis, a newly discovered form of regulated cell death, involves an iron-dependent accumulation of lethal lipid peroxidation (5). Dysregulation of iron metabolism were thought to be a hallmark for ferroptosis and triggers intracellular reactive oxygen species (ROS) production by the Fenton reaction (6). Furthermore, disruption of glutathione metabolism system could also cause overload of lipid peroxidation, leading to extremely harmful cell damages in the process of ferroptosis (7). Over the past years, the essential role of ferroptosis in regulation of diverse physiological conditions and pathological progression has been identified in humans, and it has been gradually recognized as an adaptive process to render cancer cells vulnerable to death (8). Some studies have shown that tumor suppressor gene, TP53, could repress the synthesis of glutathione leading to ferroptosis promotion (9). In glioma, it has been reported that p53-dependent inhibition of SLC7A11, a unit of the glutamate-cystine antiporter required for ferroptosis induction, could deplete glutathione and elevate the levels of intracellular ferrous iron (Fe^{2+}), H_2O_2, and lipid peroxidation (10). Furthermore, ferroptosis in glioma could be triggered by a battery of inducers, such as RSL3 and erastin, accompanied by suppression of proliferation and angiogenesis (11). Hence, induction of ferroptosis is emerging to be an effective strategy to eliminate glioma development, and the role of ferroptosis in glioma still needs to be further elucidated.

Emerging studies have established that immunotherapy could become an effective method by manipulating the immune system to recognize and attack cancer cells (12). Recently, the crosstalk between ferroptosis and antitumor immunity has been increasingly recognized. Study showed that ferroptosis could be integrated with immunotherapy through activated CD8+ T cells, by enhancing lipid peroxidation in cancers (13). Additionally, tumor cells treated by ferroptosis inhibit increased the resistance of a PD-L1 inhibitor (13). CD8+ T cell-derived IFN-γ cooperated with radiotherapy-activated ataxia-telangiectasia mutation (ATM) could induce ferroptosis in human fibrosarcoma cells and melanoma cells (14). These studies provoked a new insight of the relationship between ferroptosis activation and immune system regulation.

In the present study, we thus explored the differential expression of ferroptosis-related genes in glioma samples through the GEO datasets and TCGA database. We identified that Matrix remodeling-associated protein 8 (MXRA8) is highly expressed in glioma sample and is associated with poor prognosis of glioma. MXRA8 is reported to confer debilitating acute and chronic musculoskeletal disease, since it serves as an entry mediator for multiple arthritogenic alphaviruses (15). In terms of tumor progression, several studies have reported that high expressions of MXRA8 had poor overall survival (OS) in kidney renal clear cell carcinoma patients and is correlated with tumor microenvironment in esophageal squamous cell carcinoma (16). However, the underlying functions of MXRA8 in gliomas have not been elucidated. To further understand the role of MXRA8 in glioma, *in vitro* analysis is conducted and shows that knockdown of MXRA8 inhibited cell proliferations, increased the TMZ sensitivity, and induced ferroptosis in glioma. Further bioinformatics analysis revealed that MXRA8 function could be enriched in immune responses, and MXRA8 expression was positively associated with immunoinhibitory chemokines and checkpoints. Our data suggest that MXRA8 might act as a potential prognostic marker for glioma involving ferroptosis and immunity mediation.

MATERIALS AND METHODS

The DEGs in Glioma Screened From the GEO and TCGA Datasets

The GEO (http://www.ncbi.nlm.nih.gov/geo) is an open-source platform for the storage of gene expression, chips, and microarray data. Two expression profiling datasets (GSE147352 and GSE59612) were, respectively, downloaded from the GEO database. The GSE147352 dataset includes 103 glioma and 15 normal brain tissues. The GSE59612 dataset includes 39 glioma and 17 nonneoplastic brain tissues. According to the setting cutoff criteria (fold change ≥2, $p < 0.001$), the differentially expressed genes (DEGs) between glioma and normal brain were identified. LASSO Cox regression was applied to predict the prognosis-related genes in glioma. For LASSO analysis, RNA-seq data and the latest clinical follow-up information were downloaded from the TCGA using GDC API (https://portal.gdc.cancer.gov/repository), including 606 RNA-seq data samples. The gene expression profiles were normalized using the scale method provided in the R package "limma". To analyze the gene

signature that contains the most helpful biomarkers for prognosis, R package "glmnet" was used and then the risk score of each sample in all the datasets was calculated through the signature (17). For survival analysis, samples were divided into high- and low-risk groups relying on their own median risk score by using R package "survival." To verify the prognostic value of the MXRA8-based classifier, time-dependent (3-year, 5-year, and 10-year) receiver operating characteristics (ROC) were analyzed using the R package "timeROC" in the TCGA datasets (18).

Clinical Feature Analysis

GEPIA2.0 (http://gepia.cancer-pku.cn/) (19) and UALCAN (http://ualcan.path.uab.edu/analysis.html) (20) were used to access mRNA data of glioma and normal specimens from the TCGA database. Furthermore, the clinical and survival analyses were obtained from the CGGA database (http://www.cgga.org.cn). In total, 325 samples and 693 samples of RNA sequencing data from the CGGA database 2 (http://www.cgga.org) were used for subtype analysis of the grade, IDH type, methylation status, age, and survivals. Clinical specimens were collected from glioma patients admitted for operation in Beijing Tiantan Hospital (21). Xiantao tool (https://www.xiantao.love/products) is a comprehensive bioinformatics analysis portal which can perform differential expression, enrichment analysis, interaction network, and clinical significance across pan-cancer types (22). Univariate regression analysis was performed to analyze the demographic characteristics of MXRA8 expression in glioma using the Xiantao tool.

The GO and KEGG Pathway Analyses

LinkedOmics is an open-access portal that provides multiomics data across various cancer types with three analytical modules: LinkFinder, LinkInterpreter, and LinkCompare (23). The heatmaps of positively or negatively correlated genes with MXRA8 were analyzed with the LinkFinder module. Correlation analyses were performed using Spearman's correlation test. The LinkInterpreter module was used to analyze the Gene Ontology (GO) and Kyoto Encyclopedia of Genes and Genomes (KEGG) pathway.

Identification of the Association Between Prognostic and Ferroptosis-Related DEGs

To explore the relationship between ferroptosis and our prognostic genes, we first identified 60 ferroptosis-associated genes from the GeneCards (https://www.genecards.org/) (24), which contains up-to-date list of human ferroptosis-related genes. After merging samples, 142 glioma cases from the GEO database (GSE147352 and GSE59612) were qualified for subsequent analysis. Pearson's test was performed to examine the correlation between ferroptosis-related DEGs and our prognostic gene expression.

Immunological Analysis

Interactions between tumor and immune system were performed with the TISIDB database (25) and Xiantao tool (https://www.xiantao.love/products). We used the Xiantao tool to identify the demographic characteristics of MXRA8 expression and cancer immunology research in GBM, and then TISIDB was employed to cross-validate the roles of MXRA8 in immune-associated signaling pathways, such as tumor-infiltrating immune cells, and immunomodulators.

GEPIA2 is an interactive web server to analyze the RNA sequencing expression data of different cancer types and normal samples from the TCGA database and the GTEx projects, using a standard processing pipeline (26). Here, we computed the correlation between MXRA8 and immune monitoring sites in GBM and the corresponding normal tissues.

Cell Cultures, Reagents, siRNA Transfections, and Macrophage Polarization

T98G and U251 human glioma cell lines were obtained from the Cancer Research Institute, Central South University, China, as described in our previous study (27); glioma cells were incubated in DMEM (C11995500, HyClone, Logan, UT, USA) supplemented with 10% fetal bovine serum (04-001-1A, BI, Israel) and 1% penicillin and streptomycin (10378016, Gibco, Waltham, MA, USA) at 37°C with 5% CO_2. Temozolomide (TMZ) was purchased from Selleckchem (S1237, Berlin, Germany). Ras-selective lethal small molecule 3 (RSL3) and ferrostatin-1 (Fer-1) were purchased from APExBIO (B6095 for RSL3, A4371 for Fer-1, Houston, TX, USA). RSL3 and FER-1 were dissolved in DMSO under sterile conditions to storage concentration of 10 mM. Small interfering RNAs targeting MXRA8 and negative control siRNAs were synthesized by RiboBio (Guangzhou, China). As previously described (28), siRNAs were transfected into T98G and U251 cells for 48 h using Lipofectamine 3000 (L300015, Thermo Fisher Scientific, USA) according to the manufacturer's protocol. To polarize M0 macrophages to M1, THP-1 cells (2.5×10^5) were plated into 6-well plate and incubated with 320 nM phorbol 12-myristate 13-acetate (PMA; HY-18739, MedChemExpress, Monmouth Junction, NJ, USA) at 37°C for 6 h. To polarize M2 macrophages, cells were then treated with M2-polarizing reagents IL-4 (20 ng/ml; HY-P70445, MedChemExpress, USA) plus IL-13 (20 ng/ml; 200-13-10UG, Peprotech, USA) and incubated at 37°C for 72 h.

CCK-8 Assays and IC50

T98G and U251 cells were seeded in 96-well plates (2×10^3 cells/well) after transfection with siRNAs for 24 h. Various concentrations of TMZ (0, 0.39, 1.58, 6.25, 25, 100, and 400 μM) were added into the medium for 48 h. On the day of analysis, CCK-8 assays were conducted to examine cell viability following the manufacturer's protocols. In Brief, 10 μl CCK-8 test solution (B34304, Bimake, USA) was added into each well and incubated for 1 h. Optical density (OD) of the samples was detected at 450 nm using a VICTOR X2 microplate reader (PerkinElmer, USA). Variable slope was conducted to calculate IC50 values using the Graphpad Prism8.0 software [nonlinear regression; dose-response inhibition; log (inhibitor) vs. response-variable slope (4 parameters)].

Colony Formation Assay

The protocols used for the colony formation assay have been described previously (28). In brief, cells were transfected with siRNAs for 24 h and seeded in 6-well plates at a density of 1,000 cells per well. After incubating for 48 h, the cells were treated with different doses of TMZ. After incubation for approximately 14 days, colonies were stained with 0.3% w/v crystal violet/methanol for 20 min at room temperature.

Iron Assay

Ferrous iron concentration was analyzed in T98G and U251 cells using an iron colorimetric assay kit (ab83366, Abcam, Cambridge, MA, UUSA) according to the manufacturer's protocol. Briefly, cells were digested by trypsin without EDTA and were lysed in acid assay buffer at a density of 1×10^6 cells per 1.5 ml tube. The samples were centrifuged at 14,000×*g* for 15 min to remove insoluble material. Ferene S was added to react with Fe^{2+}, and a stable-colored complex was generated following the detection of absorbance at 593 nm by VICTOR X2 microplate reader (PerkinElmer, Waltham, MA, USA). The relative Fe^{2+} level was calculated as the ratio of concentration of all groups to concentration of siNC.

Malondialdehyde Determination

Malondialdehyde (MDA) lipid peroxidation assay (MAK085, Sigma, St. Louis, MO, USA) was used according to manufacturers' instructions. In brief, cells were collected by trypsin and lysed at a density of 1×10^6 cells per 1.5 ml tube. Furthermore, lysis solution was reacted with thiobarbituric acid. Colorimetric assays were used to measure the absorbance at 532 nm by VICTOR X2 microplate reader (PerkinElmer, USA). The relative MDA level was calculated as the ratio of concentration of all groups to concentration of siNC.

Western Blot Analysis

Cells were collected and lysed with RIPA lysis buffer with protease inhibitor cocktails (B14012, Bimake, Houston, TX, USA) at a ratio of 100:1 (v/v). The 50-μg protein extracts were equally loaded on 10% or 12% SDS-PAGE and then transferred to PVDF membranes (0.22 μm: ISEQ00010; 0.45 μm: IPVH00010). Following blocking with 5% skimmed milk for 1 h at room temperature, then membranes were incubated with primary antibodies diluted in 5% bovine serum albumin (D620272, Sangon Biotech, Shanghai, China) overnight at 4°C. Primary antibodies including MXRA8 antibody (1:1,000; ab185444, Abcam), NCOA4 antibody (1:1,000; ab86707, Abcam), FTH1 antibody (1:1,000; 4393, Cell Signaling Technology, Danvers, MA, USA), and GAPDH (1:10,000; 60004-1-Ig, Proteintech, Rosemont, IL, USA). For detection, the membranes were visualized by Immobilon Western chemiluminescent reagents (WBKLS0500, Millipore, Burlington, MA, USA).

M2 Macrophage Infiltration Assays

The M2 macrophage infiltration assays were performed as previous described (21). In brief, 2.5×10^5 M2 macrophage cells were seeded without serum for 12 h in the upper chamber of a Transwell plate (size 8 mm, Corning, Corning, NY, USA), while 2.5×10^5 T98G and U251 glioma cells were incubated with10% FBS in bottom plate. After coincubation at 37°C for 24 h, the cells in the upper chamber were fixed in 4% formalin and stained with 0.3% crystal violet. The infiltrated M2 macrophage cells were counted in three randomly selected fields from each membrane.

Immunohistochemistry

The glioma and normal brain tissues were obtained from the Department of Pathology, Xiangya Hospital. The tissues were paraffin embedded and the immunohistochemistry (IHC) was performed as previously described (29, 30). In brief, IHC was conducted using a Histomouse SP Kit (959551; Invitrogen, Waltham, MA, USA). Paraffin sections were immunostained through a streptavidin peroxidase procedure after microwave antigen retrieval. The signal was detected using a 3,3′-diaminobenzidine solution. The antibodies against MXRA8 (1:100, ab185444) and CSF1R (1:100, ab183316) were all purchased from Abcam. Images of the sections were independently examined and differentially quantified by two pathologists. IHC intensity score was scored as 0 (negative), 1 (weak brown), 2 (moderate brown), or 3 (strong brown). The extent of staining was scored as 0 (≤10%), 1 (11%–25%), 2 (26%–50%), 3 (51%–75%), or 4 (>75%). The final staining score was determined by multiplication of intensity scores and extent score and was classified as weakly positive (1–3), positive (4–6), and strongly positive (7–12). All paraffin-embedded specimens were collected following the ethical standards of the human experimental committee.

Statistical Analysis

All experiments were conducted and repeated at least three times and were reported as the means ± SD. The differences between which were analyzed for significance using Student's *t*-test for pairwise comparisons or ANOVA for multivariate analysis. Kaplan–Meier survival curves were estimated using the log-rank test to assess survival differences between groups. Data analysis was performed using GraphPad Prism 5 and SPSS 23.0. Differences were considered significant at $^*p < 0.05$, $^{**}p < 0.01$, and $^{***}p < 0.001$ for all tests.

RESULTS

Identification of Prognostic-Related Gene MXRA8

The present study's flow diagram is shown in **Figure 1A**. Two datasets from the GEO database (GSE147352 and GSE59612) were selected which have more than 50 samples. A total of 2,113 and 7,010 DEGs were identified between tumor and normal tissues, and 820 codifference genes were qualified for subsequent analysis (**Figure 1B**). Combined with the prognostic information, LASSON regression was then implemented to screen prognostic genes from the DEGs in the TCGA datasets. Finally, we found that 45 DEGs were significantly correlated with the OS of glioma patients (**Figure 1C**; **Supplemental Table S1**). Ferroptosis is an iron-dependent cell death with distinct

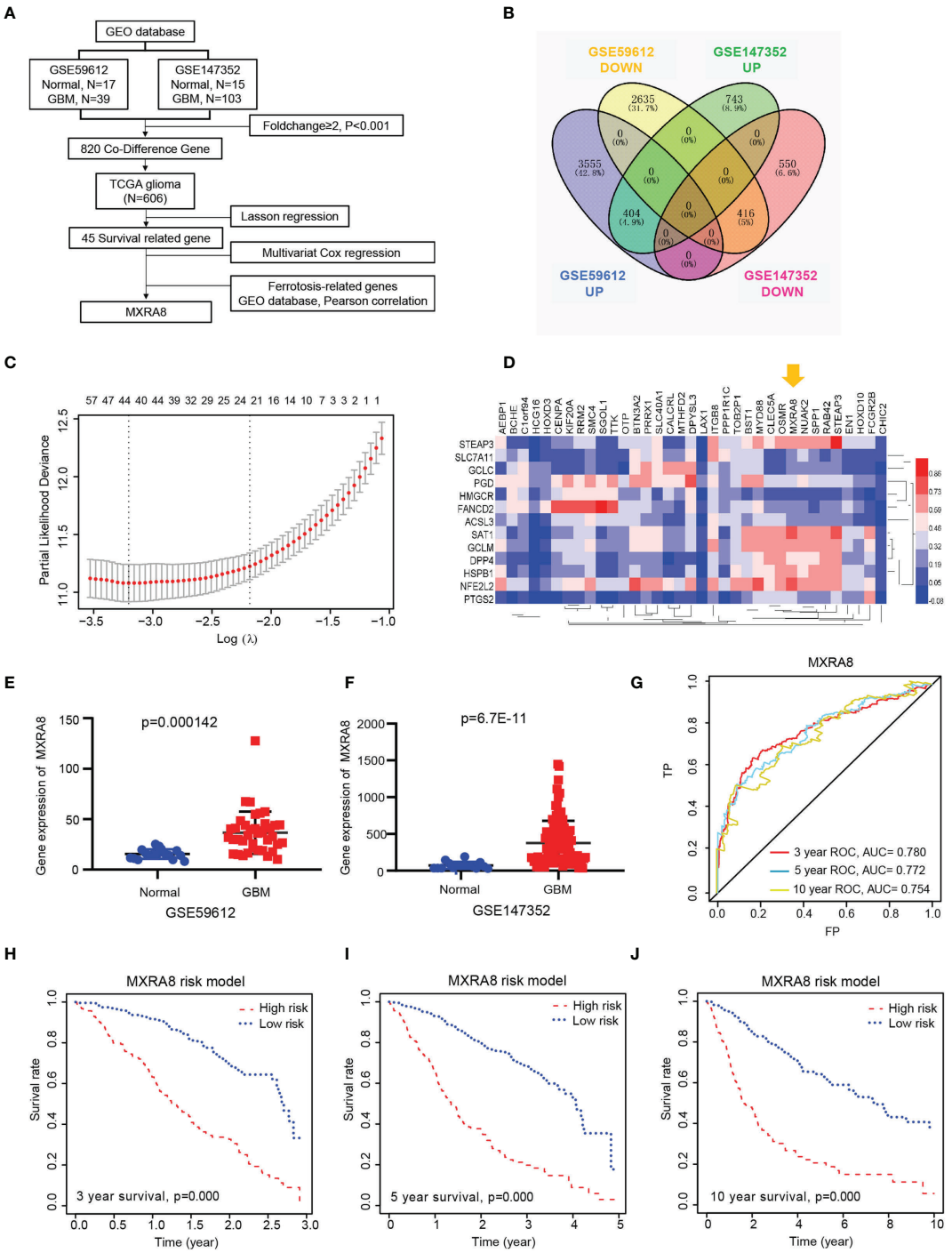

FIGURE 1 | MXRA8 was identified as a novel prognostic-related gene in glioma. **(A)** Flowchart presenting the process of identifying the gene and prognostic nomogram of glioma in this study. **(B)** Venn diagram to identify differentially expressed genes between glioma and normal brain tissue from the GEO database. The 404 overlapping genes were all upregulated in tumor tissue. The 416 overlapping genes were all downregulated in tumor tissue. **(C)** Prognostic genes were identified using the least absolute shrinkage and selection operator Cox regression model (LASSO). The generated coefficient distribution plots for the logarithmic (lambda) sequence for the selection of the best parameter (lambda). **(D)** Heatmap of the correlations between 35 upregulated prognostic genes and the 14 ferroptosis-related DEGs. **(E, F)** The expression of MXRA8 was compared between normal and GBM tissue in the GSE59612 **(E)** and GSE147352 **(F)** cohorts. **(G)** AUC of time-dependent ROC curves verified the prognostic performance of the risk score based on MARA8 in the TCGA cohort. Three-year survival **(H)**, 5-year survival **(I)**, and 10-year survival **(J)** curves for the OS of patients in the high-risk and low-risk groups in the TCGA cohort.

properties and recognizing functions involved in cancers (31). The correlations between the 45 prognostic genes and 14 ferroptosis-related DEGs in the GEO dataset were analyzed in **Figure 1D** and **Supplementary Figure S1**. Interestingly, a receptor for multiple arthritogenic alphaviruses, MXRA8, which showed the highest correlation with ferroptosis may be involved in glioma progression and prognosis. GSE59612 and GSE147352 datasets respectively showed that expression of MXRA8 was significantly higher in gliomas than those in normal tissues (**Figures 1E, F**). Furthermore, to determine the prognostic effect of MXRA8, time-dependent ROC was applied to determine the prognostic values of the MXRA8-based risk scores. The AUCs for 3-, 5-, and 10-year overall survival predictions for the risk scores were 0.780, 0.772, and 0.754, respectively (**Figure 1G**). Patients from the TCGA dataset were stratified into two (high-risk and low-risk) groups. The survival curves revealed significantly favorable overall survival in all groups with lower-risk scores (p = 0.000) both in 3, 5, and 10 years (**Figures 1H–J**) .

Validation of the Expression Level and Clinical Significance of MXRA8

To further validate the role of MXRA8 in the malignant progression of glioma, we analyzed its expression levels in the TCGA datasets from the GEPIA2.0 and UALCAN platform, respectively. As shown in **Figure 2A**, MXRA8 expression levels were higher in glioma than those in normal specimens. We also detected the expression of MXRA8 in different grades of glioma from two CGGA datasets (RNAseq_325 and RNAseq_693) and observed that MXRA8 was obviously elevated in high-grade glioma (**Figure 2B**). IDH mutation and 1p/19q codeletion are distinctive indicators in glioma, with a tendency of favorable prognosis (32). We then explored the association between MXRA8 expression and the status of IDH and 1p/19q. MXRA8 expression significantly increased in patients with wild-type IDH and noncodel 1p/19q (**Figures 2C, D**). Additionally, patients over 42 years old showed higher MXRA8 expression (**Figure 2E**). The lower expression of MXRA8 was correlated with better prognosis of gliomas (**Figure 2F**). Furthermore, the demographic characteristics of MXRA8 from the Xiantao tool were in satisfactory concordance with the above results (**Table 1**).

The Coexpression Network of MXRA8 in Glioma

In order to explore the biological functions of MXRA8 in glioma, we performed the coexpression pattern of MXRA8 screened from the TCGA-GBMLGG cohort by the LinkFinder module of LinkedOmics. **Figures 3A, B** shows the heatmaps of top 50 genes positively and negatively correlated with MXRA8, respectively. Additionally, we further performed GO and KEGG functional enrichment analyses to elaborate the potential biological roles of MXRA8 in GBM through the LinkInterpreter module. GO enrichment analysis mainly includes three parts: molecular function (MF), cellular component (CC), and biological process (BP). GO-MF enrichment analysis revealed that co-expression genes of MXRA8 mainly participated in extracellular matrix structural constituent, peptidase regulator activity, cytokine binding, antigen binding, immunoglobulin binding, etc. (**Figure 3C**). GO-CC analysis showed that these genes were significantly enriched in vesicle lumen, endoplasmic reticulum lumen, primary lysosome, ficolin-1-rich granule, vacuolar lumen, and so on (**Figure 3D**). GO-BP enrichment analysis suggested that these genes were significantly related to neutrophil-mediated immunity, granulocyte activation, interferon-gamma production, response to interferon-gamma, adaptive immune response, etc. (**Figure 3E**). KEGG pathway analysis indicated these genes were significantly related to inflammation and immune-associated signaling pathways, such as *Staphylococcus aureus* infection, autoimmune thyroid disease, leishmaniasis, intestinal immune network for IgA production, allograft rejection, etc. (**Figure 3F**). These findings suggested that MXRA8 might be involved in network of immunity-related functions in glioma.

Knockdown of MXRA8 Inhibits Proliferation and Enhances the Sensitivity of TMZ in Glioma

To further examine the biological effect of MXRA8 in glioma, we knocked down MXRA8 with two small interfering RNAs in T98G and U251 cell lines (**Figure 4A**). Cell growth was significantly decreased in siMXRA8 compared with siNC (**Figure 4B**). Likewise, in colony formation assays, cell proliferations were significantly inhibited after transfection of siMXRA8 in T98G and U251 cells (**Figure 4C**). Overcoming the resistance of TMZ has been a vital problem in glioma treatment (33). To confirm whether MXRA8 could influence TMZ sensitivity in glioma, T98G and U251 cells were transfected with MXRA8 siRNA or siNC, followed by temozolomide incubation. Upon knockdown of MXRA8, T98G and U251 cells both showed increased sensitivity to TMZ, which manifested as reduced cell proliferation rates and about a 6-fold inhibition in IC50 (**Figure 4D**). Similarly, MXRA8 reduction markedly decreased the colony formation rates of T98G and U251 cells after treatment of 200 and 100 μM TMZ, respectively (**Figure 4E**). Collectively, these results suggest that downregulation of MXRA8 improved the sensitivity of glioma to TMZ.

The Role of MXRA8 in Ferroptosis Regulation of Glioma

The correlations between the 45 prognostic genes and 14 ferroptosis-related DEGs in the GEO dataset are shown in **Figure 1D** and **Supplementary Figure S1**. Pearson's correlation coefficient indicated ferroptosis-related genes including DPP4, GCLM, HSPB1, NFE2L2, SAT1, STEAP3, and TFRC may be involved in MXRA8 function (Pearson's r >0.5). To elucidate the molecular mechanism of MXRA8, the correlation between MXRA8 expression and ferroptosis markers, NCOA4 and FTH1 were performed using the two CGGA datasets (mRNA_seq 323 and 693). The expression of MXRA8 was positively associated with levels of NCOA4 and was negatively related to levels of FTH1. Also, the protein expression

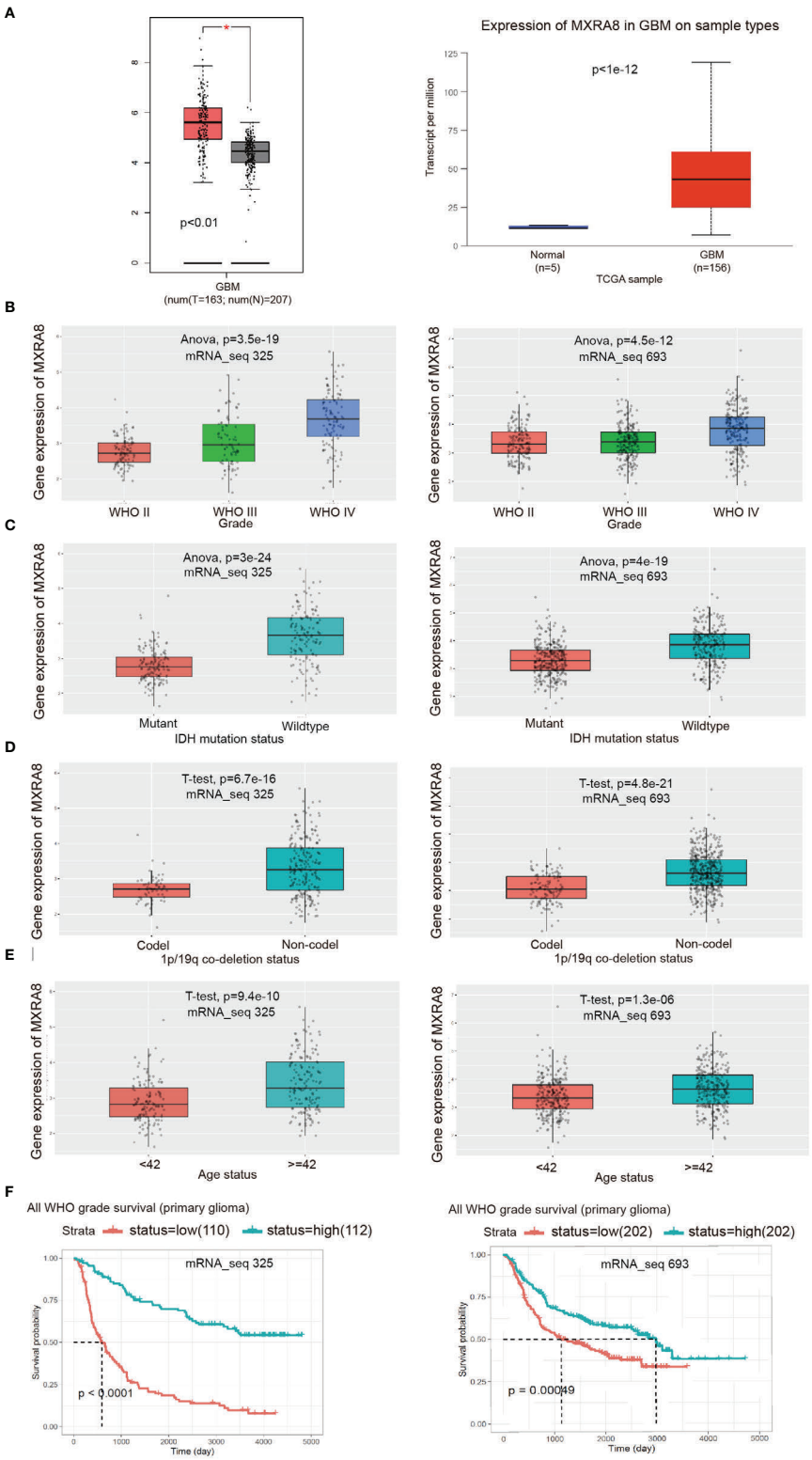

FIGURE 2 | Validation of the expression level and clinical significance of MXRA8. **(A)** Expression comparisons of MXRA8 between glioma and normal control from GEPIA2.0 and UALCAN platforms. The "asterisk" represents $p < 0.01$. **(B–F)** The correlation of MXRA8 expression level with WHO grade **(B)**, IDH status **(C)**, 1p/19q codeletion status **(D)**, ages **(E)**, and survivals **(F)** from the CGGA database.

TABLE 1 | The demographic characteristics of MXRA8 expression in glioma.

Characteristics	Total (*N*)	Odds ratio (OR)	*p*-value
WHO grade (G4 vs. G2 and G3)	635	10.482 (6.656–17.150)	<0.001
1p/19q codeletion (noncodel vs. codel)	689	4.732 (3.207–7.117)	<0.001
Primary therapy outcome (PD vs. CR and PR and SD)	462	1.682 (1.091–2.592)	0.018
IDH status (WT vs. Mut)	686	10.629 (7.273–15.836)	<0.001
Histological type (glioblastoma vs. astrocytoma and oligoastrocytoma and oligodendroglioma)	696	9.529 (6.084–15.516)	<0.001
Gender (male vs. female)	696	1.098 (0.813–1.484)	0.540
Age (>60 vs. ≤60)	696	3.237 (2.182–4.882)	<0.001
Race (White vs. Asian and Black or African American)	683	0.920 (0.502–1.676)	0.784

level of NCOA4 was increased in MXRA8 knockdown glioma cells, while FTH1 was reduced (**Figures 5A, B**). Ferroptosis is a process characterized by increased intracellular Fe^{2+} and lipid peroxidation, and the final product of lipid peroxidation is MDA. After MXRA8 knockdown, the intracellular Fe^{2+} and MDA levels were significantly increased by approximately 2-fold in T98G and U251 cells compared with controls (**Figures 5C, D**). To further understand the role of MXRA8 in cell proliferation and ferroptosis, Fer-1, a small molecule that serves as a ferroptosis inhibitor (34), was treated after MXRA8 knockdown. The results showed that Fer-1 could rescue the effects of cell growth inhibition induced by MXRA8 knockdown (**Figure 5E**). Moreover, Fer-1 reversed the increase of intracellular Fe^{2+} and MDA induced by downregulated MXRA8 (**Figures 5F, G**). Also, the protein expression of MXRA8 was reduced after treatment of ferroptosis agonist RSL3 (**Figure 5H**). Taken together, these data indicated that knockdown of MXRA8 could suppress cell survival and enable ferroptosis in glioma cells.

The Role of MXRA8 in Immune Mircoenviroment of Glioma

Increasing evidence has revealed the association between ferroptosis and immune microenvironment (35). Therefore, we further explored the role of MXRA8 in the immune microenvironment of glioma. The correlations between MXRA8 and various immune infiltration cells were analyzed by Xiantao tool using ssGSEA algorithm. Natural killer cells (NK), macrophages, and neutrophils were found to be positively correlated with MXRA8 in glioma (**Figures 6A–D**). Using TISIDB database, we further analyzed the associations between MXRA8 with immunoinhibitors. As shown in **Figures 6E, F**, indicated immunoinhibitors were found to have significant associations with the expression of MXRA8, while transforming growth factor beta 1 (TGFB1) showed the highest correlation coefficient. Moreover, **Figures G–O** shows the positive associations between MXRA8 expression levels and multiple immune checkpoint molecules, including PD-L1 and B7-H3. In addition, **Figures 6P–R** exhibits a positive correlation between MXRA8 and immune infiltration score in GSE59612, GSE147352, and TCGA glioma datasets. We further investigated the prognostic value of the immune infiltration score in the TCGA glioma dataset, and the results showed that patients with higher immune infiltration score had a poorer OS (**Figure 6S**). These results together indicated that MXRA8 might influence the prognosis of glioma patients through regulating the immune response.

The Effects of MXRA8 on M2 Macrophage Infiltration

The above results confirmed positive correlation between MXRA8 and macrophage infiltrations (**Figures 6A, B**) and cytokines (such as IL-10 and TGF-β1) that are involved in tumor-associated macrophage infiltration were highly consistent with expression of MXRA8. Through a correlation coefficient analysis performed in the GEO datasets (GSE59612 and GSE147352), we investigated the relationship between the expression of MXRA8 and the typical phenotype macrophage markers, including M (AIF1), M1 (IL12A, TNF, NOS2, PTGS2), and M2 (IL10, CCL163, TGFB1, CSF1R) (21) (**Figure 7A**; **Table 2**). The M2 macrophage markers CSF1R showed significantly positive correlation (cor_spearman >0.3, $p < 0.05$) with MXRA8 in both datasets. Using 10 paraffin-embedded specimens, IHC staining indicated the intensity of MXRA8 and CSF1R was stronger in GBM than normal. The staining intensity of macrophage M2 marker CSF1R was positively correlated with MXRA8 (Pearson's $r = 0.697$, $p = 0.025$) (**Figure 7B**). To further investigate MXRA8 effect in ferroptosis and macrophage infiltration, THP-1 cells were differentiated into M2 macrophage, and U251 and T98G cells were treated with Fer-1 after knockdown of MXRA8. The results showed that downregulation of MXRA8 decreased the infiltration of M2 macrophage, while the reduced M2 macrophage infiltration generated by MXRA8 knockdown was rescued by Fer-1 treatment (**Figure 7C**).

DISCUSSION

In this work, we aimed to investigate critical and novel indicators for prognosis of glioma. Through GEO datasets and TCGA database, 45 DEGs were screened, as these genes were strongly associated with OS of glioma patients. Intriguingly, among the 45 DEGs, MXRA8 was screened as an indicator of poor prognosis with malignancy clinical characteristics of malignancy including IDH wild type and 1p/19q noncodeletion. Furthermore, we demonstrated that knockdown of MXRA8 inhibited cell proliferations *in vitro* and contributed to increasing sensitivity of glioma cells to TMZ. These data firstly provide a novel perspective of MXRA8 which could serve as a prognostic indicator in glioma.

Emerging evidence showed that ferroptosis could be triggered by several signal pathways and/or small molecular compounds in glioma. For instance, dihydroartemisinin was identified to trigger ferroptosis accompanied with ROS generation and lipid

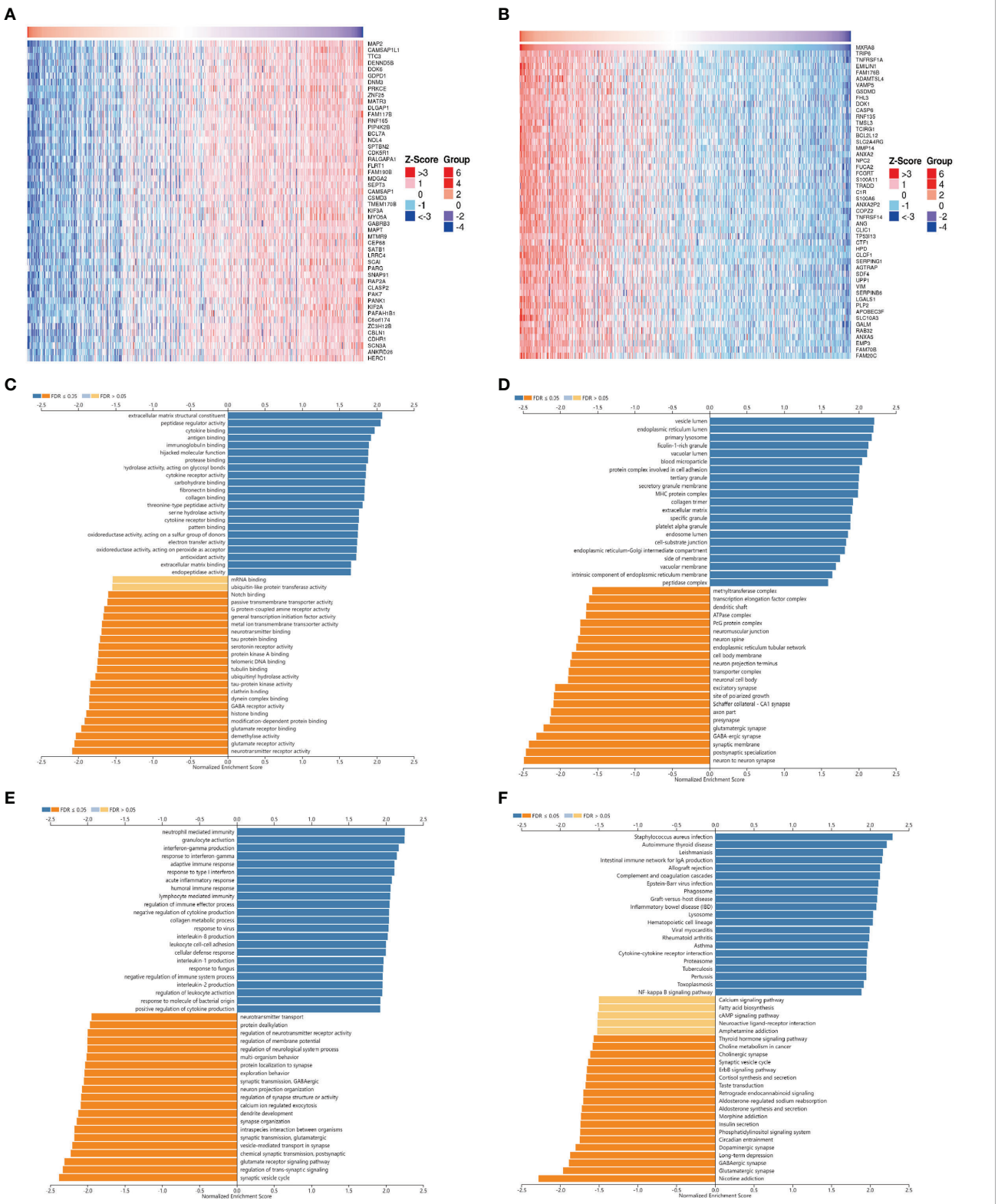

FIGURE 3 | The co-expression network of MXRA8 in glioma. **(A, B)** Heatmaps of top 50 genes positively and negatively related to MXRA8. Red represents positively linked genes and blue represents negatively linked genes. **(C–F)** GO terms for molecular functions, cellular component, biological process, and KEGG pathways of MXRA8 by GSEA analyses.

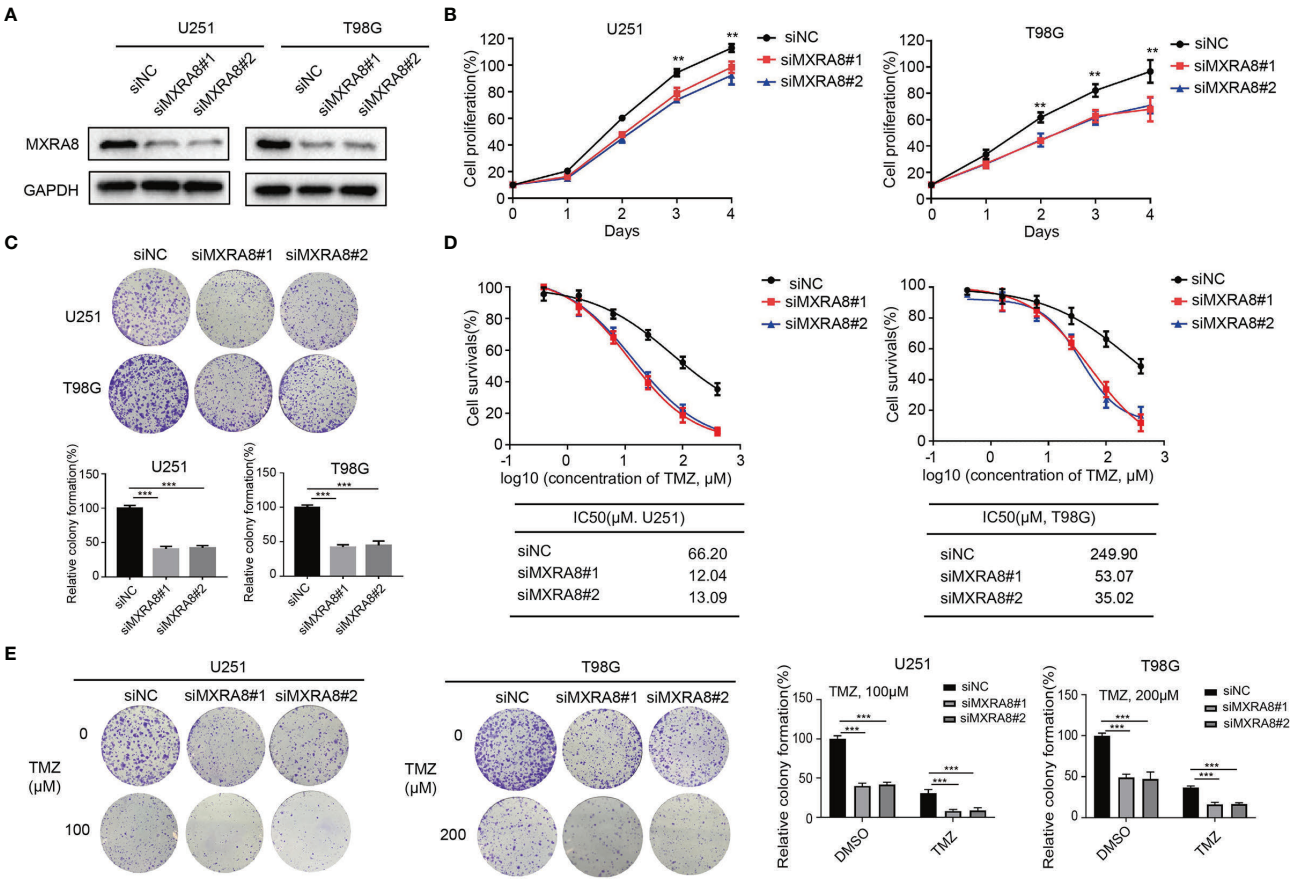

FIGURE 4 | Knockdown of MXRA8 inhibits proliferation and increased the sensitivity of TMZ of glioma. **(A)** After U251 and T98G cells were transfected with siMXRA8 or siNC for 48 h, the protein expression of MXRA8 was analyzed by Western blot assay. **(B)** T98G and U251 cell proliferation was examined after treating with siMXRA8 or siNC for 5 days. **(C)** The colony formation was analyzed in T98G and U251 cells after treating with siMXRA8 or siNC. **(D)** Cell viability assay was performed in U251 and T98G cells to evaluate cytotoxicity of TMZ after transfection of siMXRA8. **(E)** The colony formation assay was conducted to examine after incubation with TMZ in U251 and T98G cells transfected with siMXRA8 or siNC. $^{**}p < 0.01$; $^{***}p < 0.001$.

peroxidation (36). Furthermore, erastin could sensitize GBM cells to temozolomide by restraining SLC7A11 and cystathionine-γ-lyase function (37). This evidence suggests that targeting the pathway of ferroptosis could bring out the new strategies for glioma treatment. In our studies, we firstly found that downregulation of MXRA8 could induce ferroptosis by elevating the Fe^{2+} and MDA levels in glioma cells. Furthermore, we observed a significant correlation between MXRA8 expression and ferroptosis-related marker NCOA4 and FTH1 according to the CCGA datasets. NCOA4 is a selective cargo receptor for the selective autophagic turnover of ferritin in ferroptosis, while ferritin heavy polypeptide 1 (FTH1) is a subunit of ferritin. Since degradation of ferritin could elevate iron levels and generate cellular oxidative stress by the Fenton reaction (38), it has been proven that NCOA4 could bind up to FTH1 and thus deliver ferritin to the lysosome for degradation (39). In glioma, a study reported that NCOA4 caused degradation of ferritin and a subsequent increase in levels of $Fe^{2+}$and ultimately ferroptosis (40). Likewise, our study also demonstrated that inhibition of MXRA8 increased the protein expression of NCOA4 and decreased FTH1 protein levels in glioma cells. These above results could help us further understand the potential role of MXRA8 in mediating ferroptosis.

Multiple studies have revealed that immunosuppressive microenvironment was a nature of glioma, which further inhibits antitumor immune responses (41). An amount of immune cells, chemokines, and checkpoints were recognized as biomarkers of immune evasion and tumor progression. Glioma-associated macrophages could secrete cytokines such as IL-10 and TGF-β, which decrease the activities of immune cells and promote tumorigenesis (42, 43). Glioma-associated neutrophil infiltration which promoted tumor growth and resistance to antiangiogenic therapies was considered an indicator of poor prognosis (44, 45). Moreover, glioma cells express increased levels of immunosuppressive factors such as PD-L1, TIGIT, CD96, and CTLA-4, which negatively regulate presentation of antigens and T-cell responses (46–48). Especially, expression of PD-L1 could respond to the presence of T-cell-generating

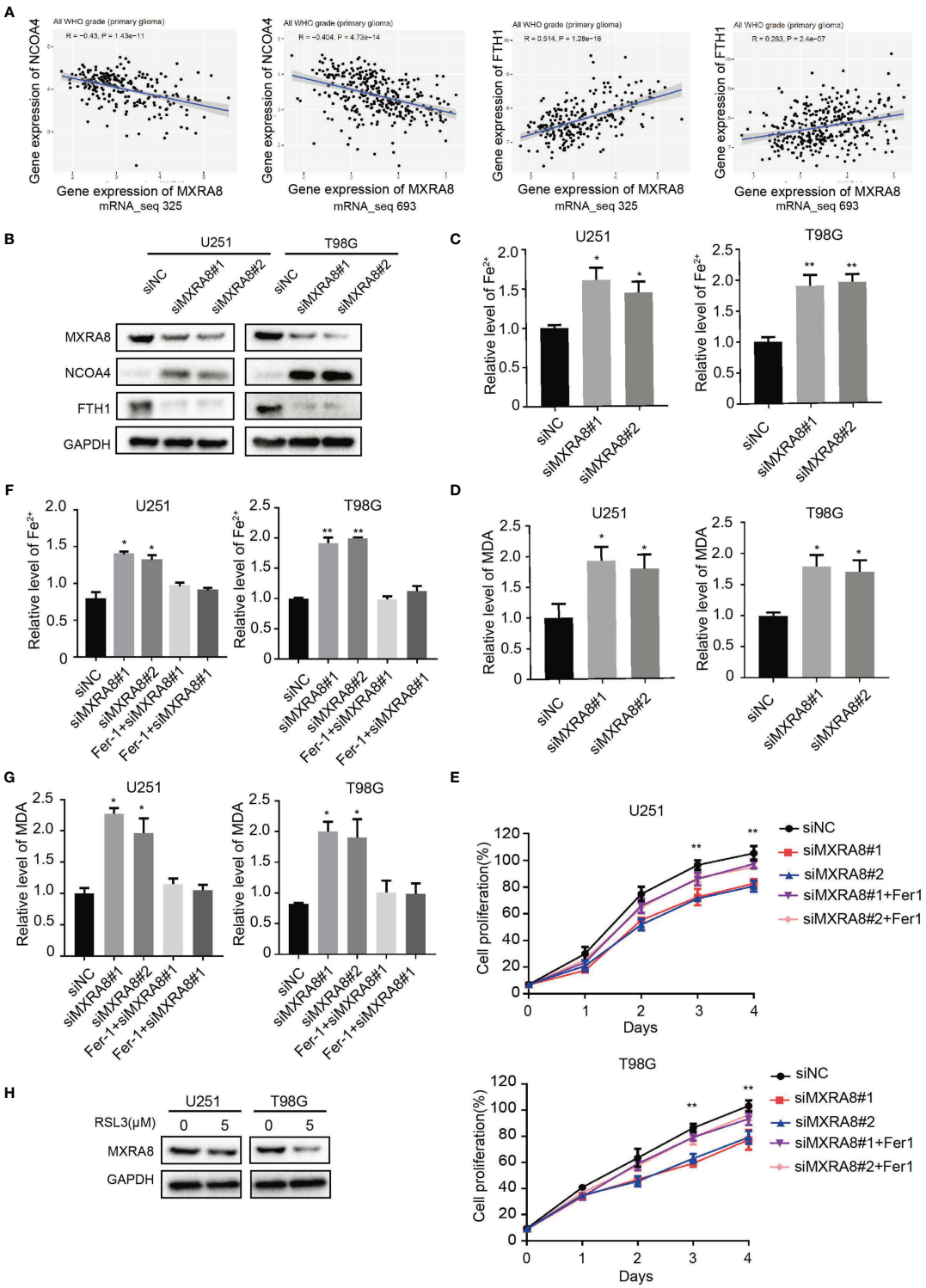

FIGURE 5 | MXRA8 regulates ferroptosis in glioma. **(A)** The correlation between expression of MXRA8 and ferroptosis-related proteins including NCOA4 and FTH1. **(B)** NCOA4 and FTH1 were examined by Western blot in U251 and T98G cells transfected with siNC or siMXRA8. **(C, D)** Fe^{2+} and MDA levels were detected in U251 and T98G cells transfected with siNC or siMXRA8. **(E)** Cell viability was measured in siNC- or siMXRA8-transfected cells after pretreatment with RSL3 (5 μM) and subsequent Fer-1 (20 μM). **(F, G)** Fe^{2+} and MDA levels detected in siNC- or siMXRA8-transfected cells pretreated with RSL3 (5 μM) and Fer-1 (20 μM) for 24 h, successively. **(H)** After treatment of 5 μM of RSL3 in U251 and T98G cells, Western blot assay were performed to examine the protein expression of MXRA8. $^{*}p < 0.05$; $^{**}p < 0.01$.

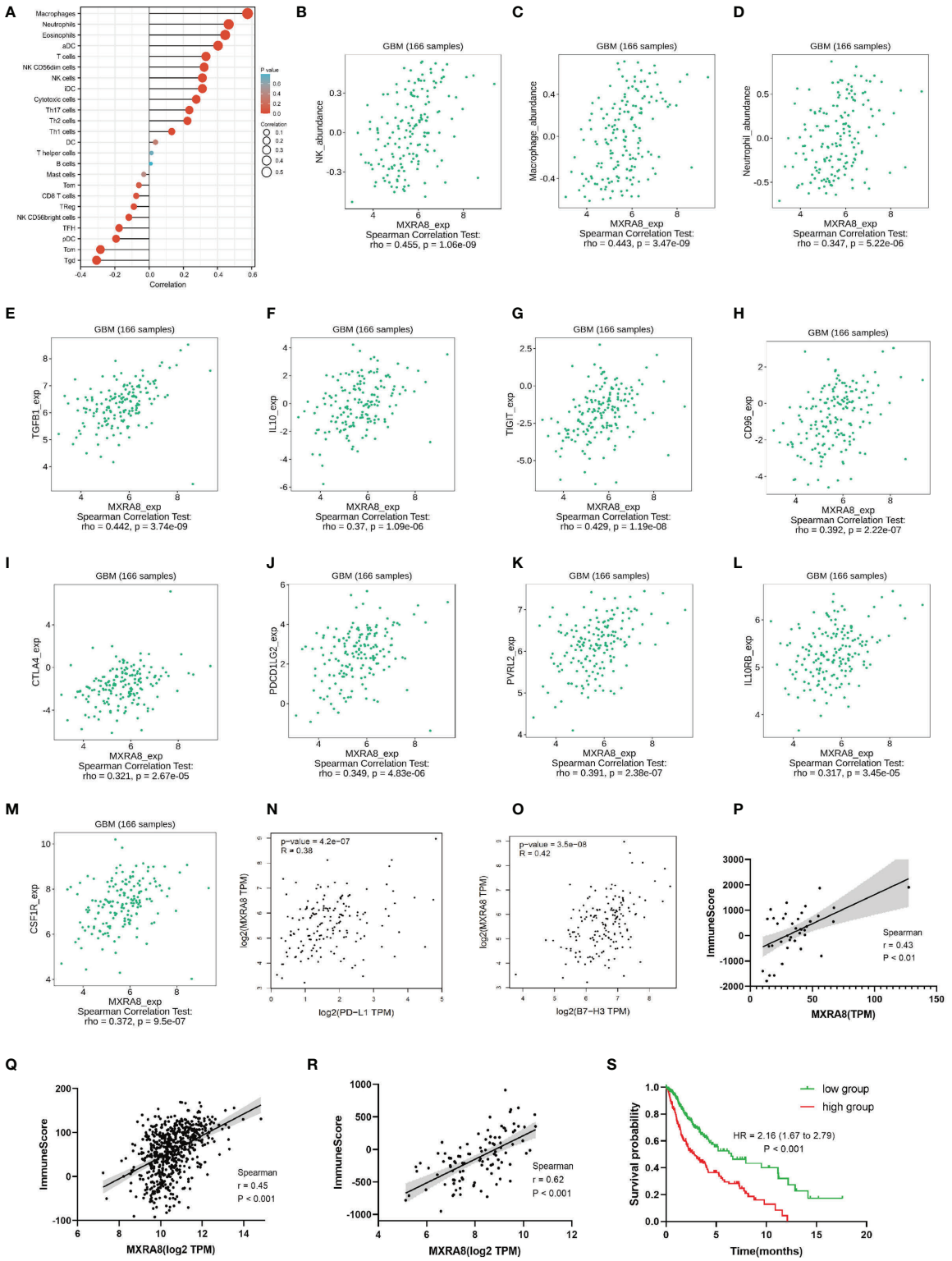

FIGURE 6 | The role of MXRA8 in immune microenvironment of glioma. **(A)** Immune infiltration cells associated with MXRA8 using ssGESA algorithm from the TCGA database. **(B–D)** Validations of NK cells, macrophages, and neutrophils by the TISIDB database. **(E–O)** Associations of the MXRA8 expression with chemokines **(E, F)** and multiple immunoinhibitory molecules **(G–O)** from the TISIDB database. **(P–R)** The association between MXRA8 with immune score calculated by ESTIMATE algorithm, based on GSE59612, GSE147352, and TCGA glioma datasets. **(S)** The Kaplan–Meier curve of immune score on overall survival of TCGA glioma datasets.

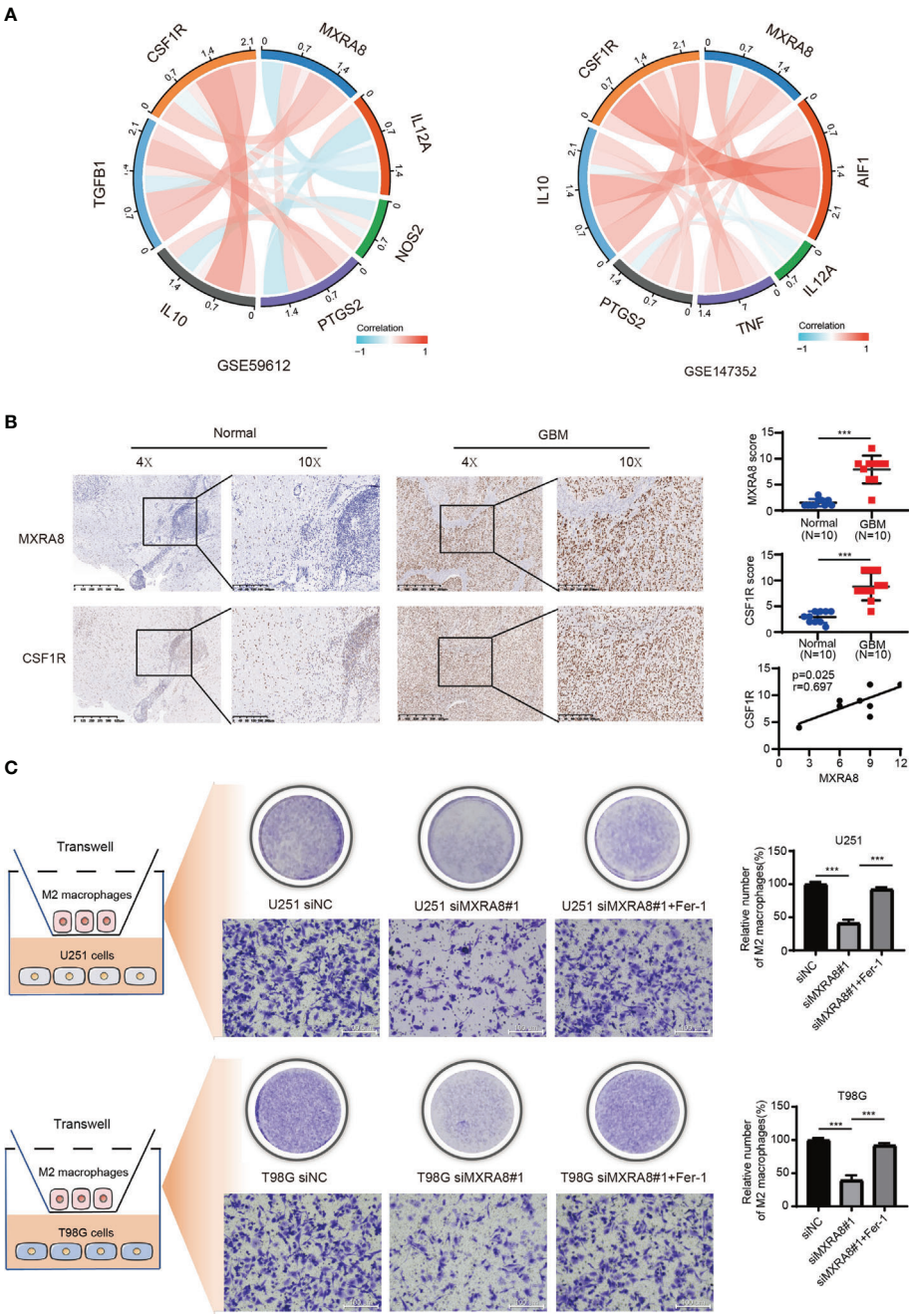

FIGURE 7 | The effects of MXRA8 on M2 macrophage infiltration *in vitro* by mediating ferroptosis. **(A)** The correlation coefficient between MXRA8 and classical phenotype markers of macrophages in the GEO datasets. **(B)** The expression level of MXRA8 and a M2 macrophage phenotype marker (CSF1R) in GBM and normal brain specimens determined by IHC analysis. **(C)** Infiltration of M2 macrophages in transfected siNC or siMXRA8 cells (U251 and T98G) after pretreatment with RSL3 (5 μM) and subsequent Fer-1 (20 μM). ***$p < 0.001$.

cytokine interferon gamma and trigger reduction of T-cell killing capacity, which further caused adaptive immune resistance (49, 50). In the present study, the results showed MXRA8 might participate in neutrophil-related immunity, adaptive immune response, and cytokine binding. Furthermore, our studies revealed that MXRA8 expression was positively associated with levels of these immunoinhibitory factors involved in microenvironment of glioma. Additionally, immune infiltration score in the TCGA glioma datasets showed that patients with high immune infiltration had a tendency with upregulation of MXRA8, which couples with worse OS. These results altogether imply that the expression of MXRA8 might be parallel to

TABLE 2 | The correlation coefficient analysis between MXRA8 and phenotype macrophage markers in the GEO datasets.

GSE147352				GSE147352			
Gene name	**Gene name**	**cor_spearman**	***p*-value**	**Gene name**	**Gene name**	**cor_spearman**	***p*-value**
MXRA8	IL12A	−0.422	0.007	MXRA8	IL12A	−0.190	0.002
	NOS2	−0.011	0.948		TNF	−0.041	<0.001
	IL10	0.163	0.007		CSF1R	0.331	0.025
	PTGS2	0.343	0.322		PTGS2	0.350	<0.001
	CSF1R	0.412	0.016		IL10	0.471	<0.001
	TGFB1	0.491	0.038		AIF1	0.557	<0.001

immunosuppression and developed as a therapeutic target of immunotherapy in glioma.

The role of macrophages in tumor growth was complex in dependence on various factors and might be polarized to antitumor (M1) or protumor (M2) phenotypes (51). Targeting M2 macrophages in the glioma microenvironment could become an alternative therapeutic strategy. CSF1R-regulated signaling is crucial for the differentiation of M2 macrophage polarization in various cancers, and blockade of CSF1R could convert macrophage polarization and inhibit glioma progression (52, 53). In our study, we found that CSF1R was positively correlated with MXRA8 expression in GBM, which suggested that functional activity of MXRA8 might be related to regulation of M2 macrophages. Furthermore, several studies have reported that ferroptosis-related gene signature promotes tumor progression by influencing macrophage infiltration in various cancers (54, 55), but the biological roles of ferroptosis in glioma-associated macrophages were still unclear. Our present study firstly demonstrated that knockdown of MXRA8 could inhibit M2 macrophage migration to glioma cells through regulation of ferroptosis. These findings indicate that targeting MXRA8-related ferroptosis might become a promising strategy for immunotherapy.

From now on, the integration between ferroptosis and immunity environment remains unclear, especially in glioma. Our study uncovers the essential roles of MXRA8 in glioma progression and highlights the importance of MXRA8 in regulating ferroptosis and immune microenvironments. We identified that MXRA8 supersession could enable ferroptosis activation, and a hint of MXRA8 in regulation of immune microenvironment was provided. Therefore, our findings suggest that MXRA8 could be a promising prognostic biomarker in patients with glioma.

DATA AVAILABILITY STATEMENT

The datasets presented in this study can be found in online repositories. The names of the repository/repositories and accession number(s) can be found in the article/**Supplementary Material**.

ETHICS STATEMENT

The studies involving human participants were reviewed and approved by the ethics committee of Xiangya Hospital, Central South University. Written informed consent for participation was not required for this study in accordance with the national legislation and the institutional requirements.

AUTHOR CONTRIBUTIONS

ZX and YY contributed to the conception and design of the study. YY and XC contributed to the writing, review, and/or revision of the manuscript. XC, YF, and LS provided administrative, technical, or material support. All authors contributed to the article and approved the submitted version.

FUNDING

This study is supported by grants from the China Postdoctoral Science Foundation (2021T140754, 2020M672521), the Science and Technology Innovation Program of Hunan Province (2021RC3029), the Natural Science Foundation of Hunan Province (2020JJ5934), and the Postdoctoral Science Foundation of Central South University (248485).

SUPPLEMENTARY MATERIAL

The Supplementary Material for this article can be found online at: https://www.frontiersin.org/articles/10.3389/fimmu.2022.834595/full#supplementary-material

Supplementary Table 1 | 45 DEGs were significantly correlated with the OS of glioma patients.

Supplementary Figure 1 | Heatmap of the correlations between 10 downregulated prognostic genes and the 14 ferroptosis related DEGs.

REFERENCES

1. Gusyatiner O, Hegi ME. Glioma Epigenetics: From Subclassification to Novel Treatment Options. *Semin Cancer Biol* (2018) 51:50–8. doi: 10.1016/j.semcancer.2017.11.010
2. Bai J, Varghese J, Jain R. Adult Glioma WHO Classification Update, Genomics, and Imaging: What the Radiologists Need to Know. *Top Magn Reson Imaging* (2020) 29(2):71–82. doi: 10.1097/RMR.0000000000000234
3. Chen X, Yan Y, Zhou J, Huo L, Qian L, Zeng S, et al. Clinical Prognostic Value of Isocitrate Dehydrogenase Mutation, O-6-Methylguanine-DNA

Methyltransferase Promoter Methylation, and 1p19q Co-Deletion in Glioma Patients. *Ann Transl Med* (2019) 7(20):541. doi: 10.21037/atm.2019.09.126
4. Jiapaer S, Furuta T, Tanaka S, Kitabayashi T, Nakada M. Potential Strategies Overcoming the Temozolomide Resistance for Glioblastoma. *Neurol Med Chir (Tokyo)* (2018) 58(10):405–21. doi: 10.2176/nmc.ra.2018-0141
5. Stockwell BR, Jiang X, Gu W. Emerging Mechanisms and Disease Relevance of Ferroptosis. *Trends Cell Biol* (2020) 30(6):478–90. doi: 10.1016/j.tcb.2020.02.009
6. Hirschhorn T, Stockwell BR. The Development of the Concept of Ferroptosis. *Free Radic Biol Med* (2019) 133:130–43. doi: 10.1016/j.freeradbiomed.2018.09.043
7. Zheng J, Conrad M. The Metabolic Underpinnings of Ferroptosis. *Cell Metab* (2020) 32(6):920–37. doi: 10.1016/j.cmet.2020.10.011
8. Liang C, Zhang X, Yang M, Dong X. Recent Progress in Ferroptosis Inducers for Cancer Therapy. *Adv Mater* (2019) 31(51):e1904197. doi: 10.1002/adma.201904197
9. Tarangelo A, Magtanong L, Bieging-Rolett KT, Li Y, Ye J, Attardi LD, et al. P53 Suppresses Metabolic Stress-Induced Ferroptosis in Cancer Cells. *Cell Rep* (2018) 22(3):569–75. doi: 10.1016/j.celrep.2017.12.077
10. Wang Z, Ding Y, Wang X, Lu S, Wang C, He C, et al. Pseudolaric Acid B Triggers Ferroptosis in Glioma Cells *via* Activation of Nox4 and Inhibition of xCT. *Cancer Lett* (2018) 428:21–33. doi: 10.1016/j.canlet.2018.04.021
11. Hu Z, Mi Y, Qian H, Guo N, Yan A, Zhang Y, et al. A Potential Mechanism of Temozolomide Resistance in Glioma-Ferroptosis. *Front Oncol* (2020) 10:897. doi: 10.3389/fonc.2020.00897
12. Xu S, Tang L, Li X, Fan F, Liu Z. Immunotherapy for Glioma: Current Management and Future Application. *Cancer Lett* (2020) 476:1–12. doi: 10.1016/j.canlet.2020.02.002
13. Wang W, Green M, Choi JE, Gijon M, Kennedy PD, Johnson JK, et al. CD8(+) T Cells Regulate Tumour Ferroptosis During Cancer Immunotherapy. *Nature* (2019) 569(7755):270–4. doi: 10.1038/s41586-019-1170-y
14. Lang X, Green MD, Wang W, Yu J, Choi JE, Jiang L, et al. Radiotherapy and Immunotherapy Promote Tumoral Lipid Oxidation and Ferroptosis *via* Synergistic Repression of SLC7A11. *Cancer Discov* (2019) 9(12):1673–85. doi: 10.1158/2159-8290.CD-19-0338
15. Zhang R, Kim AS, Fox JM, Nair S, Basore K, Klimstra WB, et al. Mxra8 Is a Receptor for Multiple Arthritogenic Alphaviruses. *Nature* (2018) 557 (7706):570–4. doi: 10.1038/s41586-018-0121-3
16. Zhang D, Qian C, Wei H, Qian X. Identification of the Prognostic Value of Tumor Microenvironment-Related Genes in Esophageal Squamous Cell Carcinoma. *Front Mol Biosci* (2020) 7:599475. doi: 10.3389/fmolb.2020.599475
17. Friedman J, Hastie T, Tibshirani R. Regularization Paths for Generalized Linear Models *via* Coordinate Descent. *J Stat Softw* (2010) 33(1):1–22. doi: 10.18637/jss.v033.i01
18. Blanche P, Dartigues JF, Jacqmin-Gadda H. Estimating and Comparing Time-Dependent Areas Under Receiver Operating Characteristic Curves for Censored Event Times With Competing Risks. *Stat Med* (2013) 32 (30):5381–97. doi: 10.1002/sim.5958
19. Wang F, Yuan C, Wu HZ, Liu B, Yang YF. Bioinformatics, Molecular Docking and Experiments *In Vitro* Analyze the Prognostic Value of CXC Chemokines in Breast Cancer. *Front Oncol* (2021) 11:665080. doi: 10.3389/fonc.2021.665080
20. Chandrashekar DS, Bashel B, Balasubramanya SAH, Creighton CJ, Ponce-Rodriguez I, Chakravarthi B, et al. UALCAN: A Portal for Facilitating Tumor Subgroup Gene Expression and Survival Analyses. *Neoplasia* (2017) 19 (8):649–58. doi: 10.1016/j.neo.2017.05.002
21. Ma W, Zhang K, Bao Z, Jiang T, Zhang Y. SAMD9 Is Relating With M2 Macrophage and Remarkable Malignancy Characters in Low-Grade Glioma. *Front Immunol* (2021) 12:659659. doi: 10.3389/fimmu.2021.659659
22. Zhang Z, Qiu X, Yan Y, Liang Q, Cai Y, Peng B, et al. Evaluation of Ferroptosis-Related Gene AKR1C1 as a Novel Biomarker Associated With the Immune Microenvironment and Prognosis in Breast Cancer. *Int J Gen Med* (2021) 14:6189–200. doi: 10.2147/IJGM.S329031
23. Vasaikar SV, Straub P, Wang J, Zhang B. LinkedOmics: Analyzing Multi-Omics Data Within and Across 32 Cancer Types. *Nucleic Acids Res* (2018) 46 (D1):D956–D63. doi: 10.1093/nar/gkx1090
24. Liang JY, Wang DS, Lin HC, Chen XX, Yang H, Zheng Y, et al. A Novel Ferroptosis-Related Gene Signature for Overall Survival Prediction in Patients With Hepatocellular Carcinoma. *Int J Biol Sci* (2020) 16(13):2430–41. doi: 10.7150/ijbs.45050
25. Ru B, Wong CN, Tong Y, Zhong JY, Zhong SSW, Wu WC, et al. TISIDB: An Integrated Repository Portal for Tumor-Immune System Interactions. *Bioinformatics* (2019) 35(20):4200–2. doi: 10.1093/bioinformatics/btz210
26. Tang Z, Li C, Kang B, Gao G, Li C, Zhang Z. GEPIA: A Web Server for Cancer and Normal Gene Expression Profiling and Interactive Analyses. *Nucleic Acids Res* (2017) 45(W1):W98–W102. doi: 10.1093/nar/gkx247
27. Dai S, Yan Y, Xu Z, Zeng S, Qian L, Huo L, et al. SCD1 Confers Temozolomide Resistance to Human Glioma Cells *via* the Akt/GSK3beta/beta-Catenin Signaling Axis. *Front Pharmacol* (2017) 8:960. doi: 10.3389/fphar.2017.00960
28. Chen X, Yan YL, Zeng SS, Gong ZC, Xu ZJ. Caveolin-1 Promotes Radioresistance *via* IRGM-Regulated Autophagy in Lung Cancer. *Ann Transl Med* (2021) 9(1):47. doi: 10.21037/atm-20-3293
29. Li J, Yao M, Zhu X, Li Q, He J, Chen L, et al. YAP-Induced Endothelial-Mesenchymal Transition in Oral Submucous Fibrosis. *J Dent Res* (2019) 98 (8):920–9. doi: 10.1177/0022034519851804
30. Yan Y, Xu Z, Qian L, Zeng S, Zhou Y, Chen X, et al. Identification of CAV1 and DCN as Potential Predictive Biomarkers for Lung Adenocarcinoma. *Am J Physiol Lung Cell Mol Physiol* (2019) 316(4):L630–L43. doi: 10.1152/ajplung.00364.2018
31. Mou Y, Wang J, Wu J, He D, Zhang C, Duan C, et al. Ferroptosis, a New Form of Cell Death: Opportunities and Challenges in Cancer. *J Hematol Oncol* (2019) 12(1):34. doi: 10.1186/s13045-019-0720-y
32. Ludwig K, Kornblum HI. Molecular Markers in Glioma. *J Neurooncol* (2017) 134(3):505–12. doi: 10.1007/s11060-017-2379-y
33. Yan Y, Xu Z, Chen X, Wang X, Zeng S, Zhao Z, et al. Novel Function of lncRNA ADAMTS9-AS2 in Promoting Temozolomide Resistance in Glioblastoma *via* Upregulating the FUS/MDM2 Ubiquitination Axis. *Front Cell Dev Biol* (2019) 7:217. doi: 10.3389/fcell.2019.00217
34. Miotto G, Rossetto M, Di Paolo ML, Orian L, Venerando R, Roveri A, et al. Insight Into the Mechanism of Ferroptosis Inhibition by Ferrostatin-1. *Redox Biol* (2020) 28:101328. doi: 10.1016/j.redox.2019.101328
35. Tang R, Xu J, Zhang B, Liu J, Liang C, Hua J, et al. Ferroptosis, Necroptosis, and Pyroptosis in Anticancer Immunity. *J Hematol Oncol* (2020) 13(1):110. doi: 10.1186/s13045-020-00946-7
36. Chen Y, Mi Y, Zhang X, Ma Q, Song Y, Zhang L, et al. Dihydroartemisinin-Induced Unfolded Protein Response Feedback Attenuates Ferroptosis *via* PERK/ATF4/HSPA5 Pathway in Glioma Cells. *J Exp Clin Cancer Res* (2019) 38(1):402. doi: 10.1186/s13046-019-1413-7
37. Chen L, Li X, Liu L, Yu B, Xue Y, Liu Y. Erastin Sensitizes Glioblastoma Cells to Temozolomide by Restraining xCT and Cystathionine-Gamma-Lyase Function. *Oncol Rep* (2015) 33(3):1465–74. doi: 10.3892/or.2015.3712
38. Santana-Codina N, Mancias JD. The Role of NCOA4-Mediated Ferritinophagy in Health and Disease. *Pharmaceuticals (Basel)* (2018) 11 (4):114. doi: 10.3390/ph11040114
39. Hou W, Xie Y, Song X, Sun X, Lotze MT, Zeh HJ3rd, et al. Autophagy Promotes Ferroptosis by Degradation of Ferritin. *Autophagy* (2016) 12 (8):1425–8. doi: 10.1080/15548627.2016.1187366
40. Zhang Y, Kong Y, Ma Y, Ni S, Wikerholmen T, Xi K, et al. Loss of COPZ1 Induces NCOA4 Mediated Autophagy and Ferroptosis in Glioblastoma Cell Lines. *Oncogene* (2021) 40(8):1425–39. doi: 10.1038/s41388-020-01622-3
41. Litak J, Mazurek M, Grochowski C, Kamieniak P, Rolinski J. PD-L1/PD-1 Axis in Glioblastoma Multiforme. *Int J Mol Sci* (2019) 20(21):5347. doi: 10.3390/ijms20215347
42. Qi L, Yu H, Zhang Y, Zhao D, Lv P, Zhong Y, et al. IL-10 Secreted by M2 Macrophage Promoted Tumorigenesis Through Interaction With JAK2 in Glioma. *Oncotarget* (2016) 7(44):71673–85. doi: 10.18632/oncotarget.12317
43. Cui X, Morales RT, Qian W, Wang H, Gagner JP, Dolgalev I, et al. Hacking Macrophage-Associated Immunosuppression for Regulating Glioblastoma Angiogenesis. *Biomaterials* (2018) 161:164–78. doi: 10.1016/j.biomaterials.2018.01.053
44. Lin YJ, Wei KC, Chen PY, Lim M, Hwang TL. Roles of Neutrophils in Glioma and Brain Metastases. *Front Immunol* (2021) 12:701383. doi: 10.3389/fimmu.2021.701383

45. Massara M, Persico P, Bonavita O, Mollica Poeta V, Locati M, Simonelli M, et al. Neutrophils in Gliomas. *Front Immunol* (2017) 8:1349. doi: 10.3389/fimmu.2017.01349
46. Qian J, Wang C, Wang B, Yang J, Wang Y, Luo F, et al. The IFN-Gamma/PD-L1 Axis Between T Cells and Tumor Microenvironment: Hints for Glioma Anti-PD-1/PD-L1 Therapy. *J Neuroinflamm* (2018) 15(1):290. doi: 10.1186/s12974-018-1330-2
47. Hung AL, Maxwell R, Theodros D, Belcaid Z, Mathios D, Luksik AS, et al. TIGIT and PD-1 Dual Checkpoint Blockade Enhances Antitumor Immunity and Survival in GBM. *Oncoimmunology* (2018) 7(8):e1466769. doi: 10.1080/2162402X.2018.1466769
48. Liu F, Huang J, Liu X, Cheng Q, Luo C, Liu Z. CTLA-4 Correlates With Immune and Clinical Characteristics of Glioma. *Cancer Cell Int* (2020) 20:7. doi: 10.1186/s12935-019-1085-6
49. Tumeh PC, Harview CL, Yearley JH, Shintaku IP, Taylor EJ, Robert L, et al. PD-1 Blockade Induces Responses by Inhibiting Adaptive Immune Resistance. *Nature* (2014) 515(7528):568–71. doi: 10.1038/nature13954
50. von Roemeling CA, Wang Y, Qie Y, Yuan H, Zhao H, Liu X, et al. Therapeutic Modulation of Phagocytosis in Glioblastoma can Activate Both Innate and Adaptive Antitumour Immunity. *Nat Commun* (2020) 11(1):1508. doi: 10.1038/s41467-020-15129-8
51. Yunna C, Mengru H, Lei W, Weidong C. Macrophage M1/M2 Polarization. *Eur J Pharmacol* (2020) 877:173090. doi: 10.1016/j.ejphar.2020.173090
52. Cannarile MA, Weisser M, Jacob W, Jegg AM, Ries CH, Ruttinger D. Colony-Stimulating Factor 1 Receptor (CSF1R) Inhibitors in Cancer Therapy. *J Immunother Cancer* (2017) 5(1):53. doi: 10.1186/s40425-017-0257-y
53. Przystal JM, Becker H, Canjuga D, Tsiami F, Anderle N, Keller AL, et al. Targeting CSF1R Alone or in Combination With PD1 in Experimental Glioma. *Cancers (Basel)* (2021) 13(10):2400. doi: 10.3390/cancers13102400
54. Yan Y, Cai J, Huang Z, Cao X, Tang P, Wang Z, et al. A Novel Ferroptosis-Related Prognostic Signature Reveals Macrophage Infiltration and EMT Status in Bladder Cancer. *Front Cell Dev Biol* (2021) 9:712230. doi: 10.3389/fcell.2021.712230
55. Qiu CJ, Wang XB, Zheng ZR, Yang CZ, Lin K, Zhang K, et al. Development and Validation of a Ferroptosis-Related Prognostic Model in Pancreatic Cancer. *Invest New Drugs* (2021) 39(6):1507–22. doi: 10.1007/s10637-021-01114-5

Conflict of Interest: The authors declare that the research was conducted in the absence of any commercial or financial relationships that could be construed as a potential conflict of interest.

Publisher's Note: All claims expressed in this article are solely those of the authors and do not necessarily represent those of their affiliated organizations, or those of the publisher, the editors and the reviewers. Any product that may be evaluated in this article, or claim that may be made by its manufacturer, is not guaranteed or endorsed by the publisher.

Copyright © 2022 Xu, Chen, Song, Yuan and Yan. This is an open-access article distributed under the terms of the Creative Commons Attribution License (CC BY). The use, distribution or reproduction in other forums is permitted, provided the original author(s) and the copyright owner(s) are credited and that the original publication in this journal is cited, in accordance with accepted academic practice. No use, distribution or reproduction is permitted which does not comply with these terms.

frontiers in Oncology

ORIGINAL RESEARCH
published: 10 March 2022
doi: 10.3389/fonc.2022.847821

The AlkB Family: Potential Prognostic Biomarkers and Therapeutic Targets in Glioblastoma

Songshan Feng[1], *Zhijie Xu*[2,3,4]*, *Jinwu Peng*[2,3,4] *and Mingyu Zhang*[1]*

[1] Department of Neurosurgery, Xiangya Hospital, Central South University, Changsha, China, [2] Department of Pathology, Xiangya Hospital, Central South University, Changsha, China, [3] Department of Pathology, Xiangya Changde Hospital, Changde, China, [4] National Clinical Research Center for Geriatric Disorders, Xiangya Hospital, Central South University, Changsha, China

The AlkB family of Fe (II) and α-ketoglutarate-dependent dioxygenases works by removing alkyl substituents from alkylation-damaged nucleic acid bases through oxidative dealkylation, subsequently affecting tumor progression and patient prognosis. However, the specific roles of the AlkB family in Glioblastoma remain to be elucidated. By taking advantage of the abundant bioinformatics databases, such as GEPIA2, cBioPortal and TIMER, we performed a comprehensive analysis of the AlkB family in GBM, and managed to identify the significant prognostic hallmarks and therapeutic targets within this family. We found that the expression levels of ALKBH2 and ALKBH8 were significantly up-regulated in GBM compared with normal tissues. Meanwhile, the patients with high levels of ALKBH2 and ALKBH8 possessed significant poor overall survival (OS). In addition, the results suggested that the biological function of the AlkB family was closely related to DNA damage repair, cell metabolism, cell proliferation and tumor immune infiltration in GBM. Furthermore, the high expression of ALKBH8 in GBM was verified by immunohistochemistry. Taken together, this study could provide meaningful information about the aberrant AlkB family associated with GBM initiation and progression, and help clinicians precisely predict patient survival and select alternative therapeutic drugs.

Keywords: glioblastoma, AlkB family, patient prognosis, DNA damage repair, immune infiltration

OPEN ACCESS

Edited by:
Wen Cheng,
The First Affiliated Hospital of China Medical University, China

Reviewed by:
Ming Li,
Fudan University, China
Yiqun Jiang,
Hunan Normal University, China

***Correspondence:**
Zhijie Xu
xzj1322007@csu.edu.cn
Mingyu Zhang
hncszmy@163.com

Specialty section:
This article was submitted to Cancer Immunity and Immunotherapy, a section of the journal Frontiers in Oncology

Received: *03 January 2022*
Accepted: *21 February 2022*
Published: *10 March 2022*

Citation:
Feng S, Xu Z, Peng J and Zhang M (2022) The AlkB Family: Potential Prognostic Biomarkers and Therapeutic Targets in Glioblastoma. Front. Oncol. 12:847821. doi: 10.3389/fonc.2022.847821

INTRODUCTION

Glioblastoma (GBM) is the most common malignant primary tumor of the central nervous system, accounting for about 14.5% of all primary brain tumors and 48% of all malignant primary brain tumors (1). It has the characteristics of easy recurrence, high malignancy and poor prognosis (2, 3). In the United States, the average age-adjusted incidence of GBM is 3.21 per 100,000 population (1). GBM patients have a poor prognosis with a 5-year survival rate of 7.2% and a median survival of 8 months (1). The standard approach for GBM is maximal safe surgical resection followed by radiotherapy with concomitant temozolomide (TMZ, an alkylating agent) and a further 6 cycles of temozolomide (4). Even after the most effective treatment, the average survival time of GBM patients is only 14.5-16.6 months (5). The illustration of the molecular profile of GBM confers great significance to understand the occurrence and development of the disease. It was reported that

patients with as isocitrate dehydrogenase 1 (IDH-1), IDH-2 mutation or MGMT methylation have relatively longer survival time (6, 7). However, we need to continue to depict the molecular features to combat this devastating disease.

The AlkB family of Fe (II) and α-ketoglutarate-dependent dioxygenases is a group of direct reversal DNA repair enzymes (8). The family of proteins works by removing alkyl substituents from alkylation-damaged nucleic acid bases through oxidative dealkylation (9, 10). So far, nine homologues (ALKBH1–8 and FTO) have been identified in human cells (11). The class of proteins possess a variety of biological functions, such as DNA repair, participating in the RNA metabolism, acting as demethylase or participating in fatty acid metabolism (12–14). And this family has been reported as prognostic biomarkers and therapeutic targets of different kinds of tumor, including head and neck cancer, ovarian serous carcinoma, lung adenocarcinoma, and colorectal cancer (15–18). In particular, ALKBH2 was discovered to play a significant role in TMZ and photodynamic therapy resistance in GBM (19, 20). However, the specific role of the AlkB family in GBM remains to be furtherly elucidated.

By taking advantage of the abundant bioinformatics databases (**Table 1**), we performed a comprehensive analysis of the AlkB family in GBM, and managed to identify the significant prognostic hallmarks and therapeutic targets within this family, which we believe could help clinicians precisely predict patient survival and select alternative therapeutic drugs.

MATERIALS AND METHODS

GEPIA2

GEPIA2 (Gene Expression Profiling Interactive Analysis, http://gepia2.cancer-pku.cn/#index) is a web resource based om tumor and normal samples from the TCGA and the GTEx databases, which provides differential gene expression profiling, correlation analysis, and patient survival analysis (21, 29). In this study, we utilized the "single gene analysis" module of GEPIA2 to compare mRNA expression differences between GBM and normal brain tissue. Student's t test was used to generate p values for mRNA expression, and $p < 0.05$ was considered statistically significant.

UALCAN

UALCAN (http://ualcan.path.uab.edu/index.html) is a convenient, interactive web-portal to perform analyses of TCGA gene expression data, which provides analyses of relative expression of genes across tumor and normal samples, estimation of the effect of gene expression level and clinicopathologic features on patient survival, and identification of the top up and down regulated genes in individual cancer types (22). In this research, the expression levels of the AlkB family were obtained through the "TCGA Gene analysis" module of the website. Differences in mRNA expression were calculated by Student's t test, and $p < 0.05$ was considered statistically significant.

The Human Protein Atlas

The Human Protein Atlas website (http://www.proteinatlas.org/) is an information database of protein expression patterns in normal human tissues and in cancer, which can identify clinically useful biomarkers by applying antibodies and protein expression data as tools (30). In this study, we obtained the protein expression profiles of the AlkB family members in normal brain and GBM tissues through this database.

PrognoScan

PrognoScan (http://dna00.bio.kyutech.ac.jp/PrognoScan/PrognoScan.html) is a database offering a tool for assessing the relationship between gene expression and tumor patient prognosis, which employs the minimum P-value approach for grouping patients so as to find the optimal cut point in continuous gene expression measurement (23). In our study, we utilized this useful database to evaluate the relationship between the AlkB family gene expression and GBM patient overall survival.

cBioPortal

The cBioPortal (cBio Cancer Genomics Portal, http://cbioportal.org) is a free resource for interactive exploration of multidimensional cancer genomics, through which we can get access to molecular profiles and clinical attributes from large-scale cancer genomics projects (24). In this study, we acquired the genetic alteration map of the AlkB family members in GBM tissues by searching this database.

STRING

The STRING (https://cn.string-db.org/) is an open-access database providing integration of all known and predicted protein-protein interactions (PPIs), including physical interactions and functional associations, by automated text mining of the scientific literature, databases of interaction

TABLE 1 | The online databases applied to evaluate the expression and biological functions of AlkB family in GBM.

Databases	Authors	Publication data	Samples	URL
GEPIA2	Tang et al. (21)	2019	Tissues	http://gepia2.cancer-pku.cn/#index
UALCAN	Chandrashekar et al. (22)	2017	Tissues	http://ualcan.path.uab.edu/index.html
PrognoScan	Mizuno et al. (23)	2009	–	http://dna00.bio.kyutech.ac.jp/PrognoScan/PrognoScan.html
cBioPortal	Cerami et al. (24)	2012	Tissues	http://cbioportal.org
STRING	Szklarczyk et al. (25)	2021	–	https://cn.string-db.org/
WebGestalt	Liao et al. (26)	2019	–	http://www.webgestalt.org/option.php
TIMER	Li et al. (27)	2017	Tissues	https://cistrome.shinyapps.io/timer/
LinkedOmics	Vasaikar et al. (28)	2018	Tissues	http://www.linkedomics.org/login.php

experiments, computational interaction predictions and systematic transfers of interaction evidence from one organism to another (25, 31). In our study, we utilized this database to analyze the interaction of altered proteins in tumor samples with mutation of at least one gene of AlkB family.

Cytoscape

Cytoscape is an open software which can visually integrate biomolecular interaction networks with high-throughput expression data and other molecular states into a unified conceptual framework (32). In the study, we performed functional integration of 38 altered proteins in tumor samples with mutation of at least one gene of AlkB family.

WebGestalt

WebGestalt (WEB-based Gene SeT AnaLysis Toolkit, http://www.webgestalt.org/option.php) is a functional enrichment analysis web tool, which supports three methods for enrichment analysis, including Over-Representation Analysis (ORA), Gene Set Enrichment Analysis (GSEA), and Network Topology-based Analysis (NTA) (26). In our study, we performed Gene ontology (GO) enrichment analysis by applying the WebGestalt website.

TIMER

TIMER web server (https://cistrome.shinyapps.io/timer/) is a comprehensive resource for systematical analysis of immune infiltrates across diverse cancer types (27, 33). In this study, we utilized "gene module" to explore the correlation between AlkB family gene expression and abundance of immune infiltrates. And the "survival module" was applied to assess the association of clinical outcome with immune cell infiltration and the AlkB family gene expression. The multivariable cox proportional hazard model was used as the statistical method.

LinkedOmics

LinkedOmics (http://www.linkedomics.org/login.php) is publicly available website which includes multi-omics data from all 32 TCGA Cancer types and 10 Clinical Proteomics Tumor Analysis Consortium (CPTAC) cancer cohorts (28). In our study, we applied the "LinkFinder" module to explore the correlated significant genes of AlkB family genes, and the "LinkInterpreter" module to perform the GO pathway enrichment analysis based on the association results.

Immunohistochemistry

5 cases of normal brain and 20 cases of GBM formalin-fixed, paraffin-embedded (FFPE) tumor tissue blocks were submitted for immunohistochemistry (IHC). IHC was performed following standard protocols. The slides were dewaxed, boiled in 0.01 M citrate buffer (pH 6.0) for 30 minutes, and then incubated with 3% hydrogen peroxide for 15 minutes. After washing with PBS, the slides were incubated with 5% normal bovine serum albumin (BSA) for 1 hour, followed by incubation with rabbit polyclonal antibody recognizing ALKBH8 (A7142, 1: 100, ABclonal Technology, Wuhan, China) overnight. After incubating with secondary antibody, the slides were then incubated with 3,3′ diaminobenzidine (DAB) (PV-6000D, ZSGB-BIO, Beijing, China) for staining. The slides were then counterstained with hematoxylin, dehydrated, cleared, and mounted. The study was approved by the Ethics Committee of Xiangya Hospital (Ethics approval No. 202201015).

Statistical Analyses

ALKBH8 expression profile difference between normal brain and GBM tissues was analyzed using Wilcoxon rank testing. P-value < 0.05 was considered to be statistically significant.

RESULTS

Aberrant Expression of AlkB Family Members in GBM Patients

We firstly searched the GEPIA2 database to explore the mRNA expression levels of the AlkB family (ALKBH1-8 and FTO) in GBM and normal brain tissue. The results revealed that the expression levels of ALKBH1/2/3/4/5/7/8/FTO were elevated, while the expression level of ALKBH6 was reduced compared with normal brain tissues (**Figure 1A**). We also utilized GEPIA2 to analyze the relative expression level of the AlkB family in GBM, and the result illustrated that ALKBH5/7/FTO had relatively higher expression levels among the family members (**Figure 1B**). Besides the GEPIA2 database, we applied UALCAN to explore the mRNA expression levels of the AlkB family in GBM and normal brain tissue. The results showed that the expression levels of ALKBH1/2/8 were significantly up-regulated and the expression levels of ALKBH5/6/FTO were significantly down-regulated in GBM compared with normal tissues (**Figure 2A**). After description of the mRNA expression levels of AlkB family, we applied the Human Protein Atlas to explore the protein expression levels of AlkB family in GBM. The results revealed that ALKBH2/4/7/8/FTO were highly or mediumly expressed, while ALKBH3/6 were lowly or not detected in GBM tissues (**Figure 2B**). Taken together, these results indicated the potential biological roles of up-regulated ALKBH2/8 in GBM pathogenesis.

Prognostic Value of AlkB Family mRNA Expression in GBM Patients

We next managed to investigate whether the mRNA expression levels of AlkB family genes were associated with GBM patients' survival. After searching the PrognoScan database, we found intriguingly that patients with higher transcription levels of ALKBH2 and ALKBH8 possessed significant shorter overall survival (OS) time based on the GEO GSE4271 dataset (34) (**Figure 3**). Conversely, patients with higher transcription level of FTO displayed significant longer OS time.

Genetic Alterations and Functional Analysis of the AlkB Family in GBM Patients

To furtherly explore the biological function of AlkB Family in GBM, we first evaluated the genetic alterations of the AlkB family genes by searching the cBioPortal database. The results presented

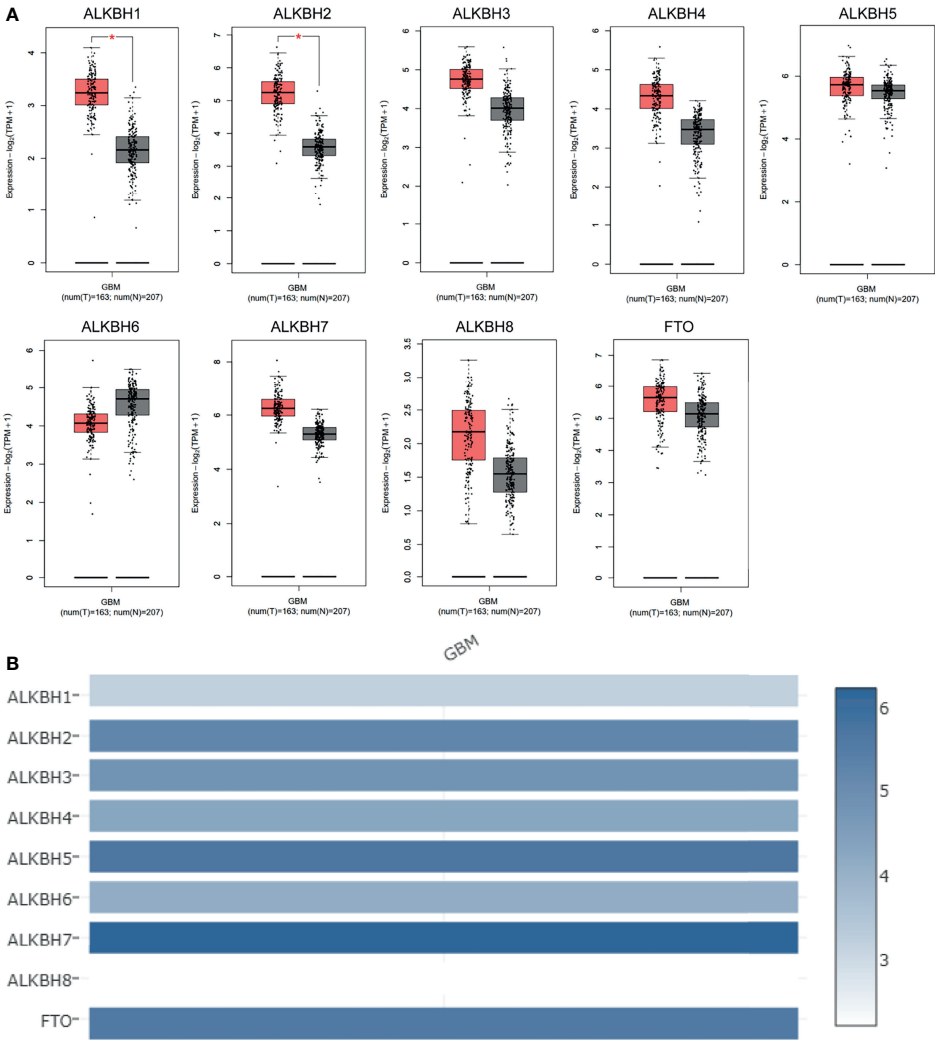

FIGURE 1 | mRNA expression levels of the AlkB family members in GBM. **(A)** mRNA expression levels of the AlkB family members in GBM and normal brain tissues based on the GEPIA2 database. T and N indicated the tumor and normal tissues, respectively. **(B)** The relative mRNA expression levels of the AlkB family in GBM based on the GEPIA2 database. *p < 0.05.

that the genetic alteration rates of ALKBH1-8/FTO in GBM tumor samples were 2.9%, 1.9%, 1.7%, 10%, 1.5%, 2.4%, 2.2%, 1% and 3%, respectively (**Figure 4A**). We also found that "mRNA high" was the most common alteration mode for most of the AlkB family members. After confirming the genetic alteration profiling of AlkB family in GBM, we explored the altered proteins and genes in GBM samples with mutation of at least one gene of AlkB family by utilizing the cBioPortal database, and identified 38 proteins (**Supplementary Table 1**) and 183 genes (**Supplementary Table 2**) most related to AlkB family genetic alterations. Then we conducted protein interaction analysis by applying the STRING website and Cytoscape software to depict the PPIs among these 38 altered proteins based on the corresponding nodes and combined scores (**Supplementary Table 3**). We found that a variety of proteins displayed the critical functions determining cell fate. Specifically, a series of DNA damage repair related proteins, including ATM, CHEK2 and MSH2, were closely associated with the functions of AlkB family in GBM. Moreover, we also identified other proteins playing pivotal roles in controlling metabolism and immunity (**Figure 4B**). After analyzing the altered proteins, we performed GO annotation and pathway enrichment analysis by applying the WebGestalt website based on the 183 altered genes. The GO annotation results suggested that the altered genes were mainly associated with biological regulation, response to stimulus and metabolic process. Regarding cellular components, the altered genes were mostly enriched in membrane and endomembrane system. In terms of molecular function categories, the altered genes were mostly related to protein binding, ion binding and nucleic acid binding (**Figure 5A**). The corresponding enriched GO pathways included leukocyte migration, extracellular structure organization and T cell activation (**Figure 5B**).

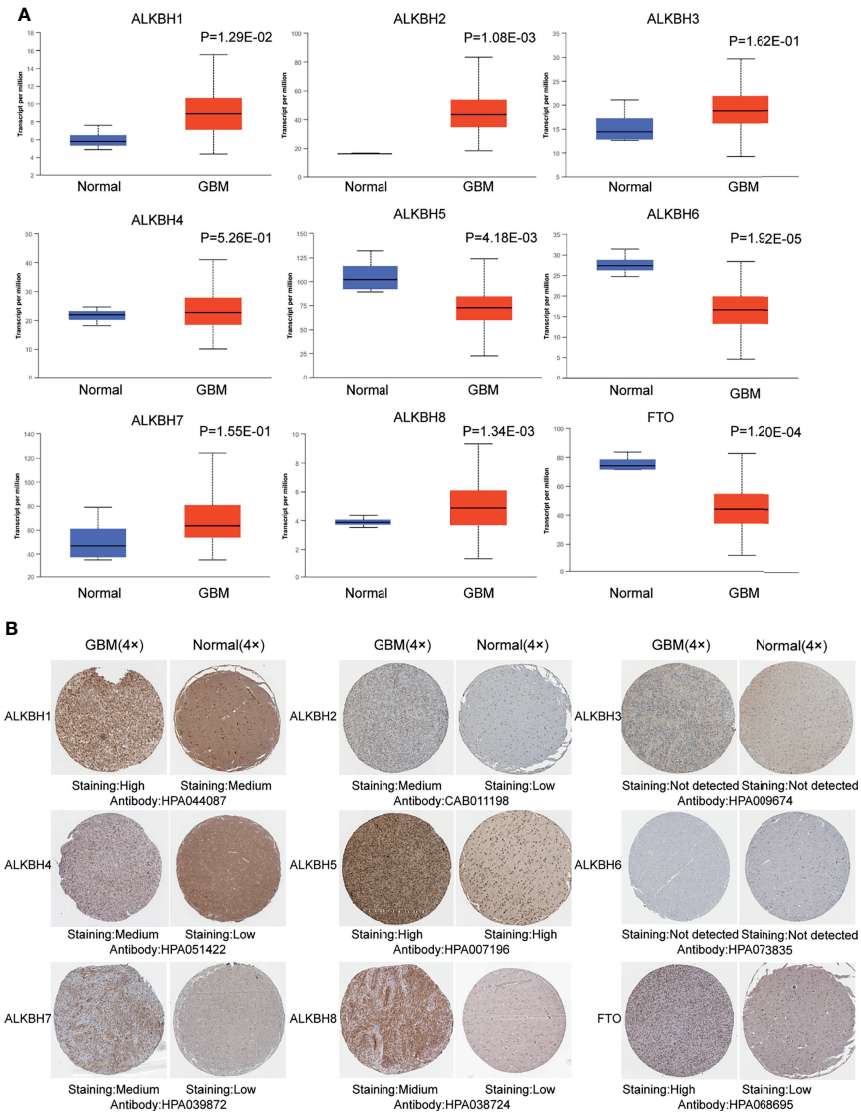

FIGURE 2 | mRNA and protein expression levels of the AlkB family members in GBM. **(A)** mRNA expression levels of the AlkB family members in GBM and normal brain tissues by searching the UALCAN website. **(B)** Representative immunohistochemical staining of the AlkB family members in GBM and normal brain tissues based on the Human Protein Atlas database.

Immune Cell Infiltration Based on the AlkB Family Gene Expression in GBM Patients

On account of the GO pathway enrichment results, we became interested in the correlation between AlkB family gene expression and abundance of immune infiltrates in GBM tissues. By searching the TIMER web server, we found that ALKBH1 expression level was positively correlated with CD8+ T cells, macrophages and neutrophils infiltration (**Figure 6A**). Regarding ALKBH2, its expression level was positively correlated with B cells and CD8+ T cells, and negatively correlated with CD4+ T cells, neutrophils and dendritic cells infiltration (**Figure 6B**). For ALKBH3, the only significant immune cells were macrophages, which was negatively correlated with the gene expression level (**Figure 6C**). Regarding ALKBH4, its expression level was positively correlated with CD8+ T cells, CD4+ T cells, macrophages and neutrophils (**Figure 6D**). For ALKBH5, its expression level was positively correlated with dendritic cells, and negatively correlated with B cells and CD8+ T cells infiltration (**Figure 6E**). Regarding ALKBH6, its expression level was not significantly tied to immune cell infiltration (**Figure 6F**). For ALKBH7, its expression level was positively correlated with B cells and CD8+ T cells, and negatively correlated with CD4+ T cells and dendritic cells infiltration (**Figure 6G**). Regarding ALKBH8, its expression level was not significantly related to immune cell infiltration (**Figure 6H**). For FTO, its expression level was positively

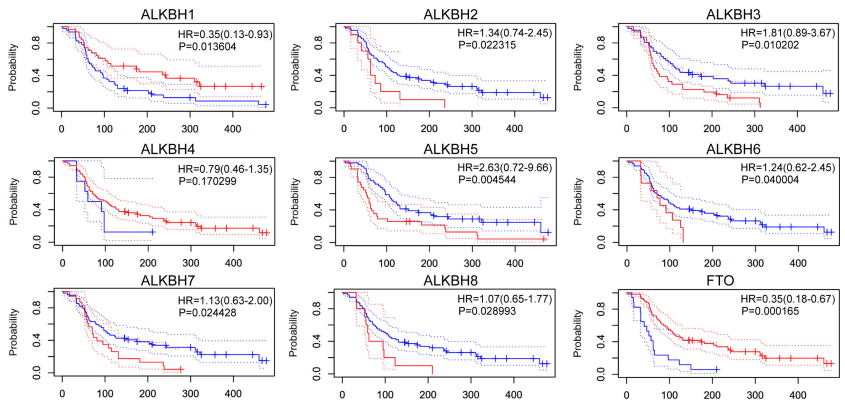

FIGURE 3 | Overall survival of GBM patients. The overall survival of GBM patients based on the AlkB family genes expression in GEO GSE4271 dataset.

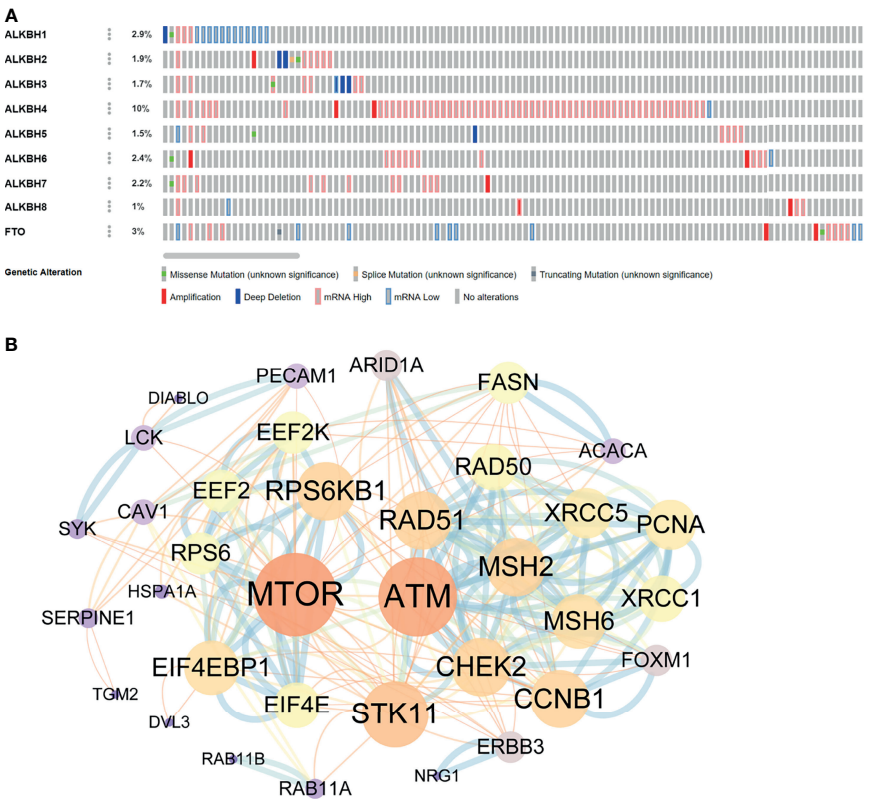

FIGURE 4 | Genetic alterations of the AlkB family genes and related PPIs. **(A)** The genetic alterations of the AlkB family genes in GBM by searching the cBioPortal database. **(B)** The PPIs among the altered proteins most related to AlkB family genetic alterations generated by applying the STRING website and Cytoscape software.

correlated with CD8+ T cells, CD4+ T cells, macrophages and neutrophils, which suggested active anti-tumor microenvironment and might explain patients with higher transcription level of FTO possessed significant longer OS time (**Figure 6I**). After analyzing the correlation between AlkB family gene expression and immune infiltrates in GBM tissues, we furtherly assessed the association of clinical outcome with immune cell infiltration and the AlkB family gene expression by applying the multivariable Cox proportional hazard model. The results revealed that CD4+ T cells, dendritic cells and ALKBH4/6/8 were significantly associated with patient survival (**Table 2**).

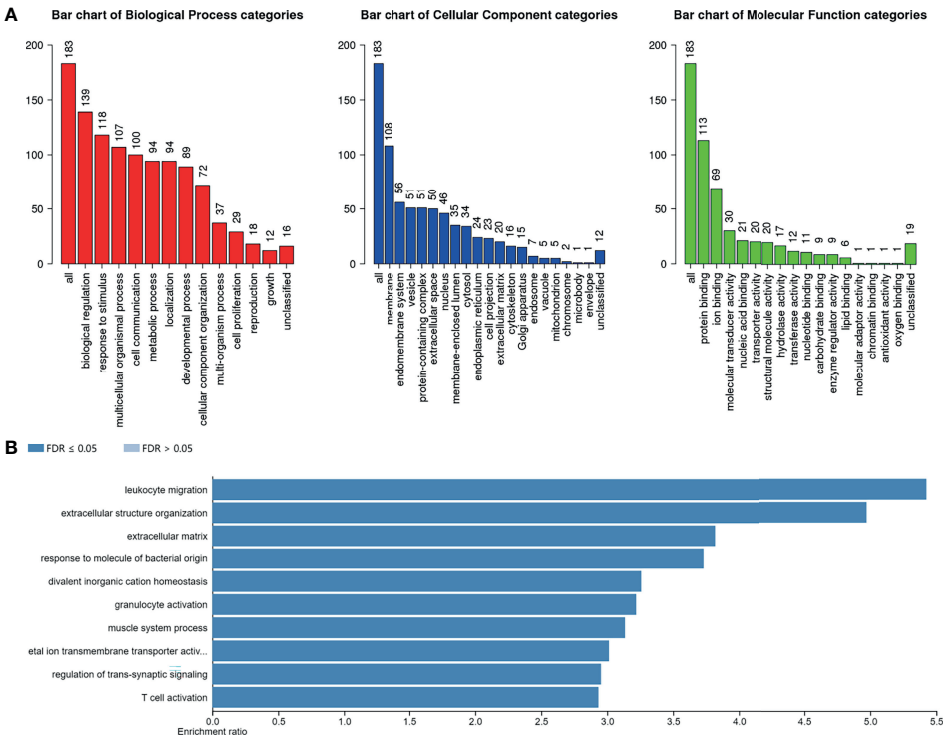

FIGURE 5 | GO annotation and pathway enrichment analysis of the altered genes. **(A)** GO annotation of altered genes related to the AlkB family genetic alterations including biological process, cellular component and molecular function categories by applying the WebGestalt website. **(B)** GO pathway enrichment analysis of the altered genes by applying the WebGestalt website.

Correlated Significant Genes and Corresponding Enriched GO Pathways of ALKBH2/8

After identifying ALKBH2/8/FTO as significant prognostic biomarkers based on the mRNA expression levels, we proceeded to explore the correlated significant genes of ALKBH2/8, and to perform the GO pathway enrichment analysis based on the association results by taking advantage of the LinkedOmics website. The positively and negatively correlated significant genes were exhibited in **Figures 7A, B**. We noticed that the correlated genes consisted of DNA damage repair related genes such as NTHL1, PCNA and ERCC8, and cell metabolism related genes such as MRPS26, EIF5A and EEF1G, which was consistent with the previous results. Concerning the GO pathway enrichment results, we found that mRNA processing was positively correlated with the expression level of both ALKBH2 and ALKBH8, and immune response was negatively correlated with ALKBH2/8 expression level, which might partly explain the worse survival of GBM patients with higher transcription levels of ALKBH2/8 (**Figures 8A, B**). The high expression of ALKBH8 in GBM was verified by IHC.

After analyzing the online databases, we performed the ALKBH8 staining in 5 normal brain tissues and 20 GBM tissues. The IHC results illustrated that ALKBH8 was highly expressed in GBM tissue compared with normal brain, which is consistent with the results obtained from the databases (**Figures 9A, B**).

DISCUSSION

The AlkB family members possess a variety of important biological functions and play significant roles in the development of tumor including GBM. By generating the genetic alteration analysis and associated altered proteins interaction interpretation, we identified a series of DNA damage repair related proteins such as ATM and CHEK2, suggesting the critical role of this family played in GBM. As a DNA repair enzyme, ALKBH2 functions through removing alkyl substituents from alkylation-damaged nucleic acid bases. It was reported that ALKBH2 was abundantly expressed in GBM cell lines and human GBM tissues, and enhanced resistance to the alkylating agents TMZ (20). Another study suggested ALKBH2 expression was implicated in resistance to photodynamic therapy in U87 GBM cells (19). Though the potential roles of this family members in cancer are rapidly uncovered, the comprehensive function of this particular family in GBM has not been elucidated yet.

Besides the DNA damage repair related proteins, we also found mTOR and its downstream effector molecules such as EIF4E and RPS6 were closely related to the AlkB family genetic alterations. In eukaryotes, mTOR signaling pathway integrates

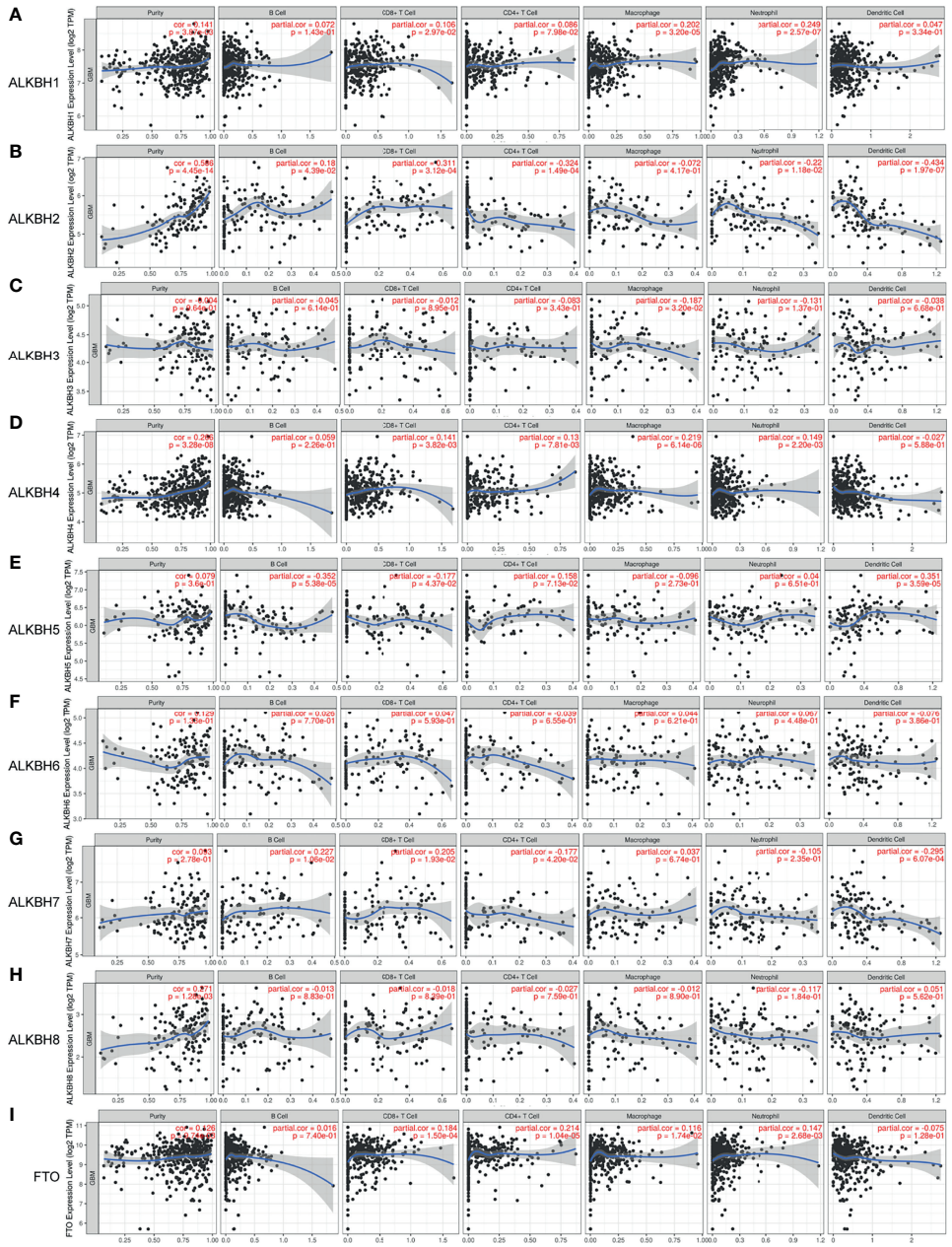

FIGURE 6 | Correlation between the AlkB family gene expression and abundance of immune infiltrates in GBM. **(A-I)** The effect of ALKBH1 **(A)**, ALKBH2 **(B)**, ALKBH3 **(C)**, ALKBH4 **(D)**, ALKBH5 **(E)**, ALKBH6 **(F)**, ALKBH7 **(G)**, ALKBH8 **(H)**, and FTO **(I)** on the tumor immune cell infiltration analyzed by the TIMER database.

both intracellular and extracellular signals and serves as a central regulator of cellular metabolism and survival (35, 36). Moreover, major DNA damage sensors such as ATM, ATR and DNA-PK communicate with the mTORC1 pathway to ensure an efficient response to the metabolic and genotoxic stresses (37). Beuvink et al. reported that mTOR inhibitor everolimus sensitizes tumor cells to DNA-damaged induced apoptosis (38). Another study suggested that m6A RNA modification catalyzed by enzymes including ALKBH5 and FTO had a fundamental role in the regulation of PI3K/Akt/mTOR signaling pathway in cancer (39). HT Zhu et al. revealed that ALKBH5 was upregulated and activated EGFR-PIK3CA-AKT-mTOR signaling pathway in epithelial ovarian cancer tissue (40). Yet, the crosstalk between AlkB family members and the metabolic pathways in GBM need to be furtherly elucidated.

Aberrant epigenetic landscapes largely affected tumor initiation and progression, and The AlkB family was continuingly studied within this aspect. DNA methylation is a critical epigenetic mark

TABLE 2 | The association of clinical outcome of GBM patients with immune cell infiltration and the AlkB family gene expression by applying the multivariable Cox proportional hazard model from the TIMER database.

	coef	HR	95%CI_l	95%CI_u	*P* value	sig
B cell	0.388	1.474	0.235	9.258	0.679	
CD8_Tcel	0.512	1.668	0.485	5.734	0.417	
CD4_Tcell	3.261	26.088	2.421	281.060	0.007	**
Macrophage	-1.035	0.355	0.026	4.917	0.440	
Neutrophil	-1.396	0.248	0.011	5.712	0.383	
Dendritic	2.075	7.967	2.265	28.029	0.001	**
ALKBH1	-0.008	0.992	0.485	2.032	0.983	
ALKBH2	-0.175	0.839	0.390	1.807	0.655	
ALKBH3	0.189	1.208	0.606	2.408	0.591	
ALKBH4	0.973	2.646	1.279	5.475	0.009	**
ALKBH5	0.147	1.158	0.585	2.293	0.674	
ALKBH6	0.821	2.272	1.211	4.260	0.011	*
ALKBH7	-0.115	0.891	0.444	1.789	0.746	
ALKBH8	-0.869	0.419	0.190	0.927	0.032	*
FTO	0.045	1.047	0.492	2.226	0.906	

*$p < 0.05$, **$p < 0.01$.

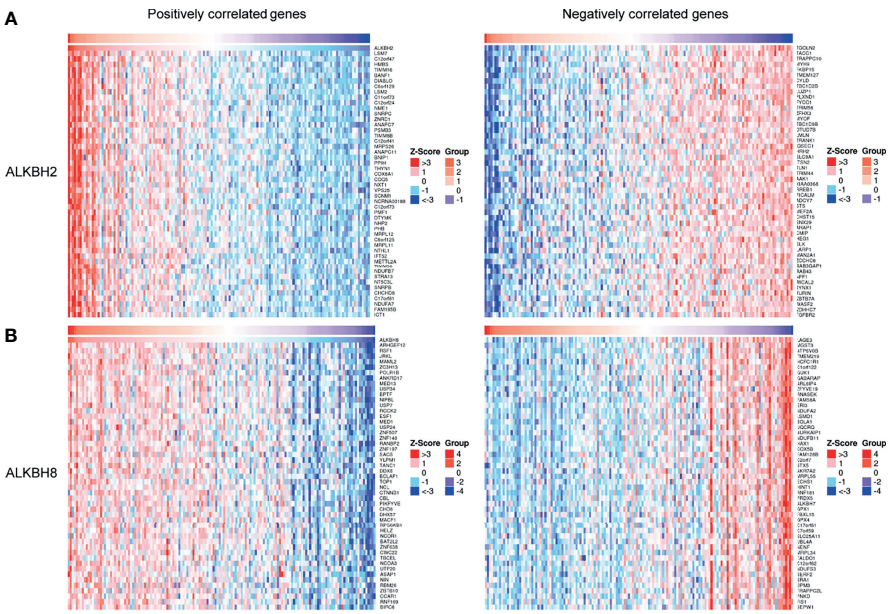

FIGURE 7 | Correlated significant genes of ALKBH2/8 in GBM. **(A, B)** The positively and negatively correlated significant genes of ALKBH2 **(A)** and ALKBH8 **(B)** by taking advantage of the LinkedOmics website.

which plays a fundamental role in cancer. Xie et al. demonstrated that ALKBH1 was a critical demethylase for DNA N6-mA and regulated specific genetic pathways in GBM. Depletion of ALKBH1 could cause transcriptional silencing of oncogenic pathways through decreasing chromatin accessibility and inhibit tumor cell proliferation (41). Besides DNA modifications, RNA processing also plays major roles in cells and tumors. N6-Methyladenosine (m6A) is the most prevalent internal chemical modification of mRNAs in eukaryotes, which can affect the stability and translation efficiency of mRNA (42–44). Our results suggested that mRNA processing was positively correlated with the expression level of both ALKBH2 and ALKBH8 based on the GO pathway enrichment analysis. Zhang et al. revealed that ALKBH5, a m6A demethylase, was highly expressed in glioblastoma stem-like cells (GSCs) and demethylated FOXM1 nascent transcripts leading to enhanced FOXM1 expression. Their work suggested ALKBH5-FOXM1 pathway was critical for GSC proliferation and tumorigenesis, and uncovered the critical function of ALKBH5 in GBM (45). FTO is another frequently studied RNA m6A demethylase. Rui Su et al. reported that R-2HG displayed anti-tumor activity in leukemia and glioma through targeting FTO, leading to MYC mRNA decay and downregulation of MYC/CEBPA-associated oncogenic pathways (46).

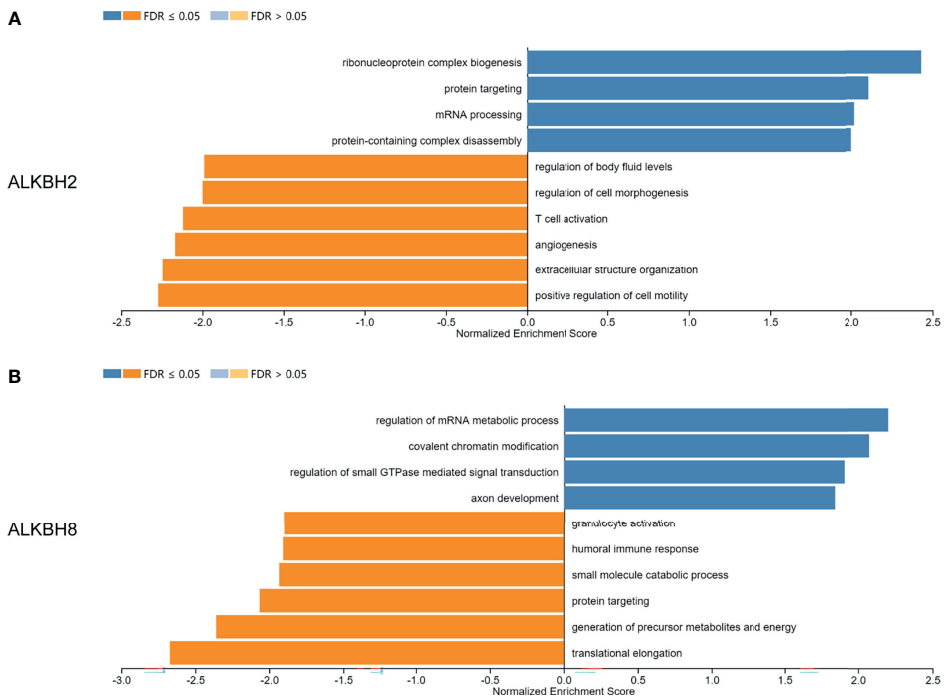

FIGURE 8 | GO pathway enrichment analysis based on the correlated genes of ALKBH2/8 in GBM. **(A, B)** The GO pathway enrichment results based on the correlated genes of ALKBH2 **(A)** and ALKBH8 **(B)** by taking advantage of the LinkedOmics website.

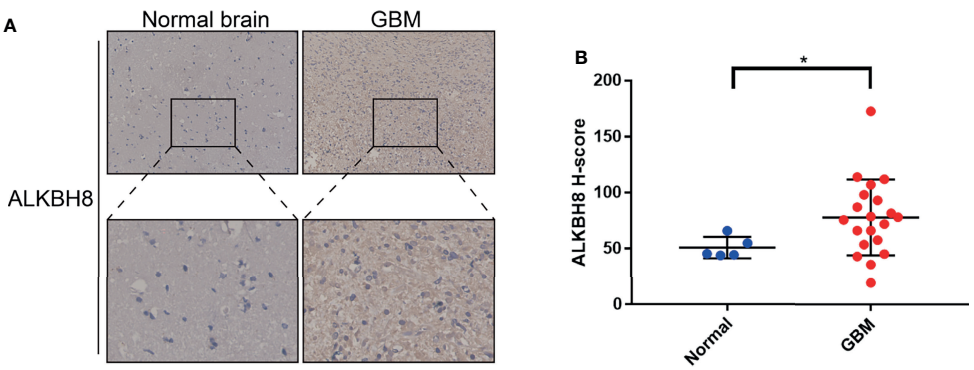

FIGURE 9 | Representative IHC images and H-score of ALKBH8 protein expression in GBM and normal brain tissues. **(A)** Immunohistochemical staining for ALKBH8 in human GBM and normal brain tissues. The specific ALKBH8 signal is shown in brown (DAB staining). **(B)** The difference of ALKBH8 protein expression between GBM and normal brain was assessed by Wilcoxon rank testing. *p < 0.05.

Accumulating evidence suggests that the tumor immune microenvironment plays a critical role in anti-cancer immunity, which may affect patient prognosis and the effect of immunotherapy (47, 48). Our results suggested significant correlation between AlkB family gene expression and abundance of immune infiltrates in GBM tissues based on the TIMER website, and the corresponding enriched GO pathways included leukocyte migration and T cell activation associated with the family genes genetic alterations. In addition to the significant roles of RNA m6A modifications in tumor-intrinsic oncogenic pathways, increasing evidence supports that RNA m6A metabolism also functions in tumor immune regulation (49, 50). Li and his colleague reported that ALKBH5 modulated Mct4/Slc16a3 expression and lactate content of the tumor microenvironment and promoted the composition of tumor-infiltrating Treg and myeloid-derived suppressor cells in melanoma and colorectal cancer, thus leading to resistance to immunotherapy. And deletion of ALKBH5 sensitized tumors to

cancer immunotherapy (51). Another study revealed that FTO expression level was increased in human melanoma and contributed to promoting melanoma tumorigenesis and anti-PD-1 resistance. Knockdown of FTO could sensitize melanoma cells to interferon gamma and anti-PD-1 treatment in mice (52). However, the relevance between AlkB family members and tumor immunity in GBM need to be furtherly explored.

We are aware of the limitations of this study. Firstly, the study mainly contains results from the public database, but is short of experimental verification. Though the expression of ALKBH8 in GBM was verified by IHC, more *in vitro* and *in vivo* experiments are needed to explore the biological function of this family in GBM. Secondly, the data sets used in different databases are inconsistent, and some contradictory data need to be further confirmed. Thirdly, we need further research to verify the therapeutic significance of AlkB family members in GBM patients.

In conclusion, by taking advantage of the abundant bioinformatics databases, we conducted this comprehensive analysis of the AlkB family in GBM for the first time, and managed to identify the value of evaluating patients' prognosis based on the mRNA expression levels of ALKBH2/8/FTO. In addition, we revealed that the biological function of the AlkB family was closely related to DNA damage repair, cell metabolism, cell proliferation and tumor immune infiltration in GBM, which needed to be furtherly explored in the future. We believe that the existing results could help researchers discover novel mechanisms associated with GBM initiation and progression, and help clinicians precisely predict patient survival and select alternative therapeutic drugs.

DATA AVAILABILITY STATEMENT

The original contributions presented in the study are included in the article/**Supplementary Material**. Further inquiries can be directed to the corresponding authors.

ETHICS STATEMENT

The studies involving human participants were reviewed and approved by Ethics Committee of Xiangya Hospital. Written informed consent for participation was not required for this study in accordance with the national legislation and the institutional requirements.

AUTHOR CONTRIBUTIONS

Acquisition of Data: SF and ZX. Analysis and Interpretation of Data: ZX and SF. Conception and Design: ZX and JP. Data Curation: SF. Development of Methodology: ZX. Performing the experiment: MZ. Writing the Manuscript: SF, JP, and MZ. All authors contributed to the article and approved the submitted version.

FUNDING

This study was supported by the National Natural Science Foundation of China (No. 82102848) and the Hunan Provincial Natural Science Foundation of China (No. 2020JJ8111).

ACKNOWLEDGMENTS

All authors thank TCGA and GEO databases for providing the worthy data and all the online-tools which are the free platforms for data analysis.

SUPPLEMENTARY MATERIAL

The Supplementary Material for this article can be found online at: https://www.frontiersin.org/articles/10.3389/fonc.2022.847821/full#supplementary-material

REFERENCES

1. Ostrom QT, Gittleman H, Truitt G, Boscia A, Kruchko C, Barnholtz-Sloan JS. CBTRUS Statistical Report: Primary Brain and Other Central Nervous System Tumors Diagnosed in the United States in 2011-2015. *Neuro Oncol* (2018) 20: iv1–iv86. doi: 10.1093/neuonc/noy131
2. Wen PY, Reardon DA. Neuro-Oncology in 2015: Progress in Glioma Diagnosis, Classification and Treatment. *Nat Rev Neurol* (2016) 12:69–70. doi: 10.1038/nrneurol.2015.242
3. Tan AC, Ashley DM, Lopez GY, Malinzak M, Friedman HS, Khasraw M. Management of Glioblastoma: State of the Art and Future Directions. *CA Cancer J Clin* (2020) 70:299–312. doi: 10.3322/caac.21613
4. Stupp R, Mason WP, Van Den Bent MJ, Weller M, Fisher B, Taphoorn MJ, et al. Radiotherapy Plus Concomitant and Adjuvant Temozolomide for Glioblastoma. *N Engl J Med* (2005) 352:987–96. doi: 10.1056/NEJMoa043330
5. Stupp R, Hegi ME, Mason WP, Van Den Bent MJ, Taphoorn MJ, Janzer RC, et al. Effects of Radiotherapy With Concomitant and Adjuvant Temozolomide Versus Radiotherapy Alone on Survival in Glioblastoma in a Randomised Phase III Study: 5-Year Analysis of the EORTC-NCIC Trial. *Lancet Oncol* (2009) 10:459–66. doi: 10.1016/S1470-2045(09)70025-7
6. Hegi ME, Diserens AC, Gorlia T, Hamou MF, De Tribolet N, Weller M, et al. MGMT Gene Silencing and Benefit From Temozolomide in Glioblastoma. *N Engl J Med* (2005) 352:997–1003. doi: 10.1056/NEJMoa043331
7. Eckel-Passow JE, Lachance DH, Molinaro AM, Walsh KM, Decker PA, Sicotte H, et al. Glioma Groups Based on 1p/19q, IDH, and TERT Promoter Mutations in Tumors. *N Engl J Med* (2015) 372:2499–508. doi: 10.1056/NEJMoa1407279
8. Fedeles BI, Singh V, Delaney JC, Li D, Essigmann JM. The AlkB Family of Fe (II)/alpha-Ketoglutarate-Dependent Dioxygenases: Repairing Nucleic Acid Alkylation Damage and Beyond. *J Biol Chem* (2015) 290:20734–42. doi: 10.1074/jbc.R115.656462
9. Sedgwick B, Bates PA, Paik J, Jacobs SC, Lindahl T. Repair of Alkylated DNA: Recent Advances. *DNA Repair (Amst)* (2007) 6:429–42. doi: 10.1016/j.dnarep.2006.10.005
10. Xie LJ, Liu L, Cheng L. Selective Inhibitors of AlkB Family of Nucleic Acid Demethylases. *Biochemistry* (2020) 59:230–9. doi: 10.1021/acs.biochem.9b00774
11. Aravind L, Koonin EV. The DNA-Repair Protein AlkB, EGL-9, and Leprecan Define New Families of 2-Oxoglutarate- and Iron-Dependent Dioxygenases. *Genome Biol* (2001) 2:RESEARCH0007. doi: 10.1186/gb-2001-2-3-research0007

12. Rajecka V, Skalicky T, Vanacova S. The Role of RNA Adenosine Demethylases in the Control of Gene Expression. *Biochim Biophys Acta Gene Regul Mech* (2019) 1862:343–55. doi: 10.1016/j.bbagrm.2018.12.001
13. Jia G, Fu Y, Zhao X, Dai Q, Zheng G, Yang Y, et al. N6-Methyladenosine in Nuclear RNA Is a Major Substrate of the Obesity-Associated FTO. *Nat Chem Biol* (2011) 7:885–7. doi: 10.1038/nchembio.687
14. Delaney JC, Essigmann JM. Mutagenesis, Genotoxicity, and Repair of 1-Methyladenine, 3-Alkylcytosines, 1-Methylguanine, and 3-Methylthymine in alkB Escherichia Coli. *Proc Natl Acad Sci USA* (2004) 101:14051–6. doi: 10.1073/pnas.0403489101
15. Pilzys T, Marcinkowski M, Kukwa W, Garbicz D, Dylewska M, Ferenc K, et al. ALKBH Overexpression in Head and Neck Cancer: Potential Target for Novel Anticancer Therapy. *Sci Rep* (2019) 9:13249. doi: 10.1038/s41598-019-49550-x
16. Cai Y, Wu G, Peng B, Li J, Zeng S, Yan Y, et al. Expression and Molecular Profiles of the AlkB Family in Ovarian Serous Carcinoma. *Aging (Albany NY)* (2021) 13:9679–92. doi: 10.18632/aging.202716
17. Wu G, Yan Y, Cai Y, Peng B, Li J, Huang J, et al. ALKBH1-8 and FTO: Potential Therapeutic Targets and Prognostic Biomarkers in Lung Adenocarcinoma Pathogenesis. *Front Cell Dev Biol* (2021) 9:633927. doi: 10.3389/fcell.2021.633927
18. Ke B, Ye K, Cheng S. ALKBH2 Inhibition Alleviates Malignancy in Colorectal Cancer by Regulating BMI1-Mediated Activation of NF-KappaB Pathway. *World J Surg Oncol* (2020) 18:328. doi: 10.1186/s12957-020-02106-0
19. Lee SY, Luk SK, Chuang CP, Yip SP, To SS, Yung YM. TP53 Regulates Human AlkB Homologue 2 Expression in Glioma Resistance to Photofrin-Mediated Photodynamic Therapy. *Br J Cancer* (2010) 103:362–9. doi: 10.1038/sj.bjc.6605797
20. Johannessen TC, Prestegarden L, Grudic A, Hegi ME, Tysnes BB, Bjerkvig R. The DNA Repair Protein ALKBH2 Mediates Temozolomide Resistance in Human Glioblastoma Cells. *Neuro Oncol* (2013) 15:269–78. doi: 10.1093/neuonc/nos301
21. Tang Z, Kang B, Li C, Chen T, Zhang Z. GEPIA2: An Enhanced Web Server for Large-Scale Expression Profiling and Interactive Analysis. *Nucleic Acids Res* (2019) 47:W556–60. doi: 10.1093/nar/gkz430
22. Chandrashekar DS, Bashel B, Balasubramanya SAH, Creighton CJ, Ponce-Rodriguez I, Chakravarthi B, et al. UALCAN: A Portal for Facilitating Tumor Subgroup Gene Expression and Survival Analyses. *Neoplasia* (2017) 19:649–58. doi: 10.1016/j.neo.2017.05.002
23. Mizuno H, Kitada K, Nakai K, Sarai A. PrognoScan: A New Database for Meta-Analysis of the Prognostic Value of Genes. *BMC Med Genomics* (2009) 2:18. doi: 10.1186/1755-8794-2-18
24. Cerami E, Gao J, Dogrusoz U, Gross BE, Sumer SO, Aksoy BA, et al. The Cbio Cancer Genomics Portal: An Open Platform for Exploring Multidimensional Cancer Genomics Data. *Cancer Discov* (2012) 2:401–4. doi: 10.1158/2159-8290.CD-12-0095
25. Szklarczyk D, Gable AL, Nastou KC, Lyon D, Kirsch R, Pyysalo S, et al. The STRING Database in 2021: Customizable Protein-Protein Networks, and Functional Characterization of User-Uploaded Gene/Measurement Sets. *Nucleic Acids Res* (2021) 49:D605–12. doi: 10.1093/nar/gkaa1074
26. Liao Y, Wang J, Jaehnig EJ, Shi Z, Zhang B. WebGestalt 2019: Gene Set Analysis Toolkit With Revamped UIs and APIs. *Nucleic Acids Res* (2019) 47:W199–205. doi: 10.1093/nar/gkz401
27. Li T, Fan J, Wang B, Traugh N, Chen Q, Liu JS, et al. TIMER: A Web Server for Comprehensive Analysis of Tumor-Infiltrating Immune Cells. *Cancer Res* (2017) 77:e108–10. doi: 10.1158/0008-5472.CAN-17-0307
28. Vasaikar SV, Straub P, Wang J, Zhang B. LinkedOmics: Analyzing Multi-Omics Data Within and Across 32 Cancer Types. *Nucleic Acids Res* (2018) 46:D956–63. doi: 10.1093/nar/gkx1090
29. Tang Z, Li C, Kang B, Gao G, Li C, Zhang Z. GEPIA: A Web Server for Cancer and Normal Gene Expression Profiling and Interactive Analyses. *Nucleic Acids Res* (2017) 45:W98–102. doi: 10.1093/nar/gkx247
30. Asplund A, Edqvist PH, Schwenk JM, Ponten F. Antibodies for Profiling the Human Proteome-The Human Protein Atlas as a Resource for Cancer Research. *Proteomics* (2012) 12:2067–77. doi: 10.1002/pmic.201100504
31. Snel B, Lehmann G, Bork P, Huynen MA. STRING: A Web-Server To Retrieve And Display The Repeatedly Occurring Neighbourhood Of A Gene. *Nucleic Acids Res* (2000) 28:3442–4. doi: 10.1093/nar/28.18.3442
32. Shannon P, Markiel A, Ozier O, Baliga NS, Wang JT, Ramage D, et al. Cytoscape: A Software Environment For Integrated Models Of Biomolecular Interaction Networks. *Genome Res* (2003) 13:2498–504. doi: 10.1101/gr.1239303
33. Li B, Severson E, Pignon JC, Zhao H, Li T, Novak J, et al. Comprehensive Analyses of Tumor Immunity: Implications for Cancer Immunotherapy. *Genome Biol* (2016) 17:174. doi: 10.1186/s13059-016-1028-7
34. Phillips HS, Kharbanda S, Chen R, Forrest WF, Soriano RH, Wu TD, et al. Molecular Subclasses of High-Grade Glioma Predict Prognosis, Delineate a Pattern of Disease Progression, and Resemble Stages in Neurogenesis. *Cancer Cell* (2006) 9:157–73. doi: 10.1016/j.ccr.2006.02.019
35. Sabatini DM. Twenty-Five Years of mTOR: Uncovering the Link From Nutrients to Growth. *Proc Natl Acad Sci USA* (2017) 114:11818–25. doi: 10.1073/pnas.1716173114
36. Xie X, Hu H, Tong X, Li L, Liu X, Chen M, et al. The mTOR-S6K Pathway Links Growth Signalling to DNA Damage Response by Targeting RNF168. *Nat Cell Biol* (2018) 20:320–31. doi: 10.1038/s41556-017-0033-8
37. Ma Y, Vassetzky Y, Dokudovskaya S. Mtorc1 Pathway in DNA Damage Response. *Biochim Biophys Acta Mol Cell Res* (2018) 1865:1293–311. doi: 10.1016/j.bbamcr.2018.06.011
38. Beuvink I, Boulay A, Fumagalli S, Zilbermann F, Ruetz S, O'reilly T, et al. The mTOR Inhibitor RAD001 Sensitizes Tumor Cells to DNA-Damaged Induced Apoptosis Through Inhibition of P21 Translation. *Cell* (2005) 120:747–59. doi: 10.1016/j.cell.2004.12.040
39. Zhao Q, Zhao Y, Hu W, Zhang Y, Wu X, Lu J, et al. M(6)A RNA Modification Modulates PI3K/Akt/mTOR Signal Pathway in Gastrointestinal Cancer. *Theranostics* (2020) 10:9528–43. doi: 10.7150/thno.42971
40. Zhu H, Gan X, Jiang X, Diao S, Wu H, Hu J. ALKBH5 Inhibited Autophagy of Epithelial Ovarian Cancer Through miR-7 and BCL-2. *J Exp Clin Cancer Res* (2019) 38:163. doi: 10.1186/s13046-019-1159-2
41. Xie Q, Wu TP, Gimple RC, Li Z, Prager BC, Wu Q, et al. N(6)-Methyladenine DNA Modification in Glioblastoma. *Cell* (2018) 175:1228–43.e20. doi: 10.1016/j.cell.2018.10.006
42. Wang X, Lu Z, Gomez A, Hon GC, Yue Y, Han D, et al. N6-Methyladenosine-Dependent Regulation of Messenger RNA Stability. *Nature* (2014) 505:117–20. doi: 10.1038/nature12730
43. Dominissini D, Moshitch-Moshkovitz S, Schwartz S, Salmon-Divon M, Ungar L, Osenberg S, et al. Topology of the Human and Mouse M6a RNA Methylomes Revealed by M6a-Seq. *Nature* (2012) 485:201–6. doi: 10.1038/nature11112
44. Wang X, Zhao BS, Roundtree IA, Lu Z, Han D, Ma H, et al. N(6)-Methyladenosine Modulates Messenger RNA Translation Efficiency. *Cell* (2015) 161:1388–99. doi: 10.1016/j.cell.2015.05.014
45. Zhang S, Zhao BS, Zhou A, Lin K, Zheng S, Lu Z, et al. M(6)A Demethylase ALKBH5 Maintains Tumorigenicity of Glioblastoma Stem-Like Cells by Sustaining FOXM1 Expression and Cell Proliferation Program. *Cancer Cell* (2017) 31:591–606.e6. doi: 10.1016/j.ccell.2017.02.013
46. Su R, Dong L, Li C, Nachtergaele S, Wunderlich M, Qing Y, et al. R-2hg Exhibits Anti-Tumor Activity by Targeting FTO/m(6)A/MYC/CEBPA Signaling. *Cell* (2018) 172:90–105.e23. doi: 10.1016/j.cell.2017.11.031
47. Binnewies M, Roberts EW, Kersten K, Chan V, Fearon DF, Merad M, et al. Understanding the Tumor Immune Microenvironment (TIME) for Effective Therapy. *Nat Med* (2018) 24:541–50. doi: 10.1038/s41591-018-0014-x
48. Tang T, Huang X, Zhang G, Hong Z, Bai X, Liang T. Advantages of Targeting the Tumor Immune Microenvironment Over Blocking Immune Checkpoint in Cancer Immunotherapy. *Signal Transduct Target Ther* (2021) 6:72. doi: 10.1038/s41392-020-00449-4
49. Han D, Liu J, Chen C, Dong L, Liu Y, Chang R, et al. Anti-Tumour Immunity Controlled Through mRNA M(6)A Methylation and YTHDF1 in Dendritic Cells. *Nature* (2019) 566:270–4. doi: 10.1038/s41586-019-0916-x
50. Yan G, An Y, Xu B, Wang N, Sun X, Sun M. Potential Impact of ALKBH5 and YTHDF1 on Tumor Immunity in Colon Adenocarcinoma. *Front Oncol* (2021) 11:670490. doi: 10.3389/fonc.2021.670490
51. Li N, Kang Y, Wang L, Huff S, Tang R, Hui H, et al. ALKBH5 Regulates Anti-PD-1 Therapy Response by Modulating Lactate and Suppressive Immune Cell Accumulation in Tumor Microenvironment. *Proc Natl Acad Sci USA* (2020) 117:20159–70. doi: 10.1073/pnas.1918986117

52. Yang S, Wei J, Cui YH, Park G, Shah P, Deng Y, et al. M(6)A mRNA Demethylase FTO Regulates Melanoma Tumorigenicity and Response to Anti-PD-1 Blockade. *Nat Commun* (2019) 10:2782. doi: 10.1038/s41467-019-10669-0

Conflict of Interest: The authors declare that the research was conducted in the absence of any commercial or financial relationships that could be construed as a potential conflict of interest.

Publisher's Note: All claims expressed in this article are solely those of the authors and do not necessarily represent those of their affiliated organizations, or those of the publisher, the editors and the reviewers. Any product that may be evaluated in this article, or claim that may be made by its manufacturer, is not guaranteed or endorsed by the publisher.

Copyright © 2022 Feng, Xu, Peng and Zhang. This is an open-access article distributed under the terms of the Creative Commons Attribution License (CC BY). The use, distribution or reproduction in other forums is permitted, provided the original author(s) and the copyright owner(s) are credited and that the original publication in this journal is cited, in accordance with accepted academic practice. No use, distribution or reproduction is permitted which does not comply with these terms.

frontiers in Oncology

ORIGINAL RESEARCH
published: 18 March 2022
doi: 10.3389/fonc.2022.844144

ITGA5 Is a Novel Oncogenic Biomarker and Correlates With Tumor Immune Microenvironment in Gliomas

Shuyu Li[1‡], Nan Zhang[2‡], Shiyang Liu[1], Hao Zhang[3], Jiajing Liu[4], Yiwei Qi[5], Qi Zhang[6*] and Xingrui Li[1*†]*

[1] Department of Thyroid and Breast Surgery, Tongji Hospital, Tongji Medical College, Huazhong University of Science and Technology, Wuhan, China, [2] One-Third Lab, College of Bioinformatics Science and Technology, Harbin Medical University, Harbin, China, [3] Department of Neurosurgery, Xiangya Hospital, Central South University, Changsha, China, [4] Department of Neurology, Affiliated People's Hospital, Fujian University of Traditional Chinese Medicine, Fuzhou, China, [5] Department of Neurosurgery, Tongji Hospital, Tongji Medical College of Huazhong University of Science and Technology, Wuhan, China, [6] Department of Plastic and Cosmetic Surgery, Tongji Hospital, Tongji Medical College of Huazhong University of Science and Technology, Wuhan, China

Gliomas are the most aggressive primary intracranial malignancies with poor overall survival. ITGA5 is one member of the integrin adhesion molecule family and is implicated in cancer metastasis and oncogenesis. However, few studies have explored the association between tumor immune microenvironment and ITGA5 expression level in gliomas. Firstly, we analyzed 3,047 glioma patient samples collected from the TCGA, the CGGA, and the GEO databases, proving that high ITGA5 expression positively related to aggressive clinicopathological features and poor survival in glioma patients. Then, based on the ITGA5 level, immunological characteristics and genomic alteration were explored through multiple algorithms. We observed that ITGA5 was involved in pivotal oncological pathways, immune-related processes, and distinct typical genomic alterations in gliomas. Notably, ITGA5 was found to engage in remolding glioma immune infiltration and immune microenvironment, manifested by higher immune cell infiltration when ITGA5 is highly expressed. We also demonstrated a strong correlation between ITGA5 and immune checkpoint molecules that may be beneficial from immune checkpoint blockade strategies. In addition, ITGA5 was found to be a robust and sensitive indicator for plenty of chemotherapy drugs through drug sensitivity prediction. Altogether, our comprehensive analyses deciphered the prognostic, immunological, and therapeutic value of ITGA5 in glioma, thus improving individual and precise therapy for combating gliomas.

Keywords: glioma, ITGA5, tumor microenvironment, immune cells (ICs), immune checkpoint

OPEN ACCESS

Edited by:
Wen Cheng,
The First Affiliated Hospital of China Medical University, China

Reviewed by:
Wancun Zhang,
Zhengzhou University, China
Zheng Zhang,
University of Pennsylvania, United States

***Correspondence:**
Xingrui Li
lixingrui@tjh.tjmu.edu.cn
Qi Zhang
zhangqi06172@163.com
Yiwei Qi
yiweiqi@tjh.tjmu.edu.cn

†ORCID:
Xingrui Li
orcid.org/0000-0002-6572-7740

‡These authors have contributed equally to this work and share first authorship

Specialty section:
This article was submitted to Cancer Immunity and Immunotherapy, a section of the journal Frontiers in Oncology

Received: *27 December 2021*
Accepted: *17 February 2022*
Published: *18 March 2022*

Citation:
Li S, Zhang N, Liu S, Zhang H, Liu J, Qi Y, Zhang Q and Li X (2022) ITGA5 Is a Novel Oncogenic Biomarker and Correlates With Tumor Immune Microenvironment in Gliomas. Front. Oncol. 12:844144. doi: 10.3389/fonc.2022.844144

INTRODUCTION

A glioma is the most frequent central nervous system malignancy with an annual incidence of about 7 cases per 100,000 people (1). Glioma patients usually present neurological symptoms such as headache, pain, weakness, mood change, seizures, and loss of physical function and cognitive function. Despite the vast advancements of surgery, standard chemoradiotherapy, and adjuvant therapies, glioma patients are still confronted with fatal prognoses (2). It is intensively acknowledged that glioma is a highly heterogeneous tumor entity accompanied by multiple molecule characteristics, which could significantly impact clinical outcomes. For example, the status of O-6-methylguanine-DNA methyltransferase (MGMT) promoter methylation is a prognostic biomarker in glioma patients treated by temozolomide, but showing a minimal benefit for elderly patients (3). Nowadays, there is an urgent need to identify novel and reliable prognostic biomarkers to improve the clinical outcomes of glioma.

Glioma is an immunosuppressive tumor that encompasses a complicated tumor microenvironment (TME) comprising various cellular components, namely, glioma cells, stromal cells, and immune cells. The most abundant immune cells are tumor-associated macrophages (TAMs), which play an essential role in helping glioma proliferation, invasion, chemoradiotherapy resistance (4). Generally speaking, a glioma is a specific tumor type in that the blood–brain barrier (BBB) establishes a naturally occurring "immunologically privileged" site (5). Vaccine-based immunotherapy and immune checkpoint targeted therapy may only be effective for some subpopulations expressing specific genes (6, 7). The immunosuppressive TME dramatically reduces the effectiveness of immunotherapy (8). Thus, a thorough understanding of the unique immunological status in heterogeneous glioma TME will be essential for the clinical application of glioma immunotherapy.

Integrin subunit alpha 5 (ITGA5) encodes a protein belonging to the integrin alpha chain family, which plays a vital function in cell surface adhesion and signaling. ITGA5 has a deep connection with tumor invasion, tumor progression, and chemotherapy resistance (9, 10). ITGA5 was shown to be of prognostic use in non-small cell lung cancer (11) and breast cancer bone metastasis (12). The ITGA5 monoclonal antibody M200 could effectively reduce bone metastasis and blunt cancer-associated bone destruction (12). ITGA5 was regulated in glioma cells and mediated glioma cell dispersion and invasion by cell–matrix and cell–cell interactions (13). Meanwhile, ITGA5 orchestrated the process of proliferation inhibition induced by tocopherols of glioma cells (14). Therefore, ITGA5 is an important gene modifier in oncogenesis and tumor development. More importantly, emerging evidence also certified that ITGA5 could function as a determinant of immune cell infiltration and promising prognostic biomarkers in gastrointestinal tumors (15). Liu et al. also constructed an ITGA5-comprising risk model based on eight genes, which was strongly related to the immune infiltration patterns in breast cancer (16). These results supported the possibility that ITGA5 modulated the immune infiltration characteristics and showed great prognostic value in tumor patients.

Overall, given the pivotal role of ITGA5 in malignancies, we hypothesized that a comprehensive elucidation of the ITGA5-related multi-omics landscape, especially TME contexture, may favor the deeper understanding of the gliomas pathogenesis and progression. In this study, we comprehensively investigated the ITGA5 expression patterns in gliomas based on genomic and transcriptional profiles with complete clinical annotations. To get more insights, immunological characteristics, functional annotation, chemotherapeutic response prediction, and overall survival (OS) were analyzed to interpret the correlation between ITGA5 and glioma tumor immune microenvironment. Collectively, our comprehensive analyses deciphered the prognostic, immunological, and therapeutic value of ITGA5 in glioma management, thus providing a target for individual and precise therapy for combating gliomas.

MATERIALS AND METHODS

Glioma Datasets and Preprocessing

The pan-cancer related data and the corresponding clinical information were downloaded and collected from The Cancer Genome Atlas (TCGA; https://xenabrowser.net/). Normal sample data were collected from the Genotype-Tissue Expression Project (GTEx; https://www.gtexportal.org). The glioma genomic information together with complete clinicopathological annotations was obtained from the TCGA, the Chinese Glioma Genome Atlas (CGGA; http://www.cgga.org.cn/), and the Gene Expression Omnibus (GEO; https://www.ncbi.nlm.nih.gov/geo/). In total, 9,807 pan-cancer patients containing 33 cancer types, and 8,295 normal samples containing 31 kinds of normal tissues, were involved. In addition, the transcriptional profiles of 3,047 glioma patients were acquired from 11 cohorts containing greater than 50 patients and samples with inadequate OS information were excluded. Specific information of the patients and the corresponding platforms are presented in **Table S1**.

Affymetrix and Agilent platforms were utilized for generating the raw data derived from the GEO database. The robust multichip average (RMA) algorithm was utilized to achieve background correction and normalization. The TCGA and the CGGA data portals provided the RNA-sequencing data. The fragments per kilobase million (FPKM) values were transformed into transcripts per kilobase million (TPM) values that possessed similar signal intensity with the RMA-processed values (17).

Genomic Alteration

The somatic mutations and somatic copy number variation (CNV) profiles were gathered from the TCGA datasets. The Genomic Identification of Significant Targets in Cancer (GISTIC) analysis was performed to evaluate the genomic features. The CNV landscape based on ITGA5 levels and the copy number gains or losses at the amplified or deleted peaks were assessed by GISTIC 2.0 analysis (https://gatk.broadinstitute.org) (18).

Evaluation of the Immunological Characteristics of the TME

The intratumoral immune cell abundance, stromal cell infiltration levels, and tumor purity were estimated by The Estimation of

Stromal and Immune cells in Malignant Tumor tissues using Expression (ESTIMATE) algorithm, and reflected by immune score, stromal score, and estimate score separately (19). The Tumor Immune Estimation Resource2.0 (TIMER2.0; http://timer.cistrome.org/) web server (20) was utilized for comprehensively analyzing the level of immune infiltrating cells in gliomas. The relative fraction of 10 types of immune cells in the tumor was estimated using the MCPcounter algorithm (21). The infiltration levels of 28 immune cells were presented by the enrichment scores based on corresponding signatures. The enrichment scores were calculated by the single sample gene set enrichment analysis (ssGSEA) implemented using the R gene set variation analysis (GSVA) package (22). The cancer immunity cycle reflected the anticancer immune response and comprises seven steps. The activities of these steps determined the fate of the tumor cells, which were evaluated the activities of these steps using the ssGSEA (23). The immune checkpoints, related to seven different immune processes, were retrieved from two prior literature (24, 25). The responses to immune checkpoint blockade immunotherapy in gliomas were extrapolated by the Tumor Immune Dysfunction and Exclusion (TIDE) algorithm (26). The responses to anti-PD1 and anti-CTLA4 therapies in gliomas were evaluated by the submap algorithm.

Functional Annotation

All gene sets derived from the Gene Ontology (GO) and the Kyoto Encyclopedia of Genes and Genomes (KEGG) were downloaded from the MSigDB database (27). Metabolism-relevant gene signatures were introduced previous study (28). Gene set enrichment analysis (GSEA) and GSVA based on ITGA5 transcriptional abundance were implemented by the clusterProfiler R package and GSVA R package (29).

Drug Response Prediction

The pharmacogenomic data sourced from the Genomics of Drug Sensitivity in Cancer (GDSC, https://www.cancerrxgene.org/) was used from predicting the drug susceptibility of included cases. The drug responses were performed as half-maximal inhibitory concentration (IC50) calculated by the pRRophetic R package.

Statistical Analysis

The survival of different groups was ascertained by Kaplan–Meier curves (KM curves) and compared using the log-rank test. We used the uni-Cox and multi-Cox regression analyses to test the independence of the prognostic factors and evaluate the hazard ratio. Pearson correlation and distance correlation analyses were used to calculate correlation coefficients. Contingency tables were analyzed by Fisher test. Based on the ITGA5 expression, patients were grouped as a high- or low-group. Most data visualizations were completed with the R ggplot2. OncoPrint delineating the mutation landscape was generated by the R maftools (30). All KM curves were implemented using the R survminer. Heatmaps were visualized based on complexHeatmap (31). All statistical analyses were conducted with R sv3.6.3 (https://www.r-project.org). $P < 0.05$ was considered statistically significant.

Multiple Immunofluorescence (IF)

The gliomas chip was baked at 60°C for 60 min for deparaffinization, then the antigen was retrieved by EDTA retrieval buffer and blocked in 3% BSA. Next, the samples were permeabilized with 0.1% Triton X-100. The gliomas tissue microarray was incubated with the primary antibodies of ITGA5 (10569-1-AP, Rabbit, 1:200, Proteintech, China), CD68 (GB113150, Rabbit, 1:3,000, Servicebio, China), and CD163 (16646-1-AP, Rabbit, 1:3,000, Proteintech, China) separately, then followed by the incubation with secondary antibodies (GB23301, GB23303, Servicebio, China) and tyramide signal amplification (TSA) [FITC-TSA, CY3-TSA, and CY5-TSA (Servicebio, China)]. The antigen repair was applied repeatedly between the intervals of each dye. Subsequently, the microarray was incubated with 4',6-Diamidino2-phenylindole dihydrochloride (DAPI). Microscopy detection was performed by the Pannoramic Scanner (3D HISTECH, Hungary).

RESULTS

ITGA5 Expression Was Positively Related to Aggressive Clinicopathological and Molecular Features in Gliomas

Based on the TCGA and the GTEx, we firstly examined the ITGA5 transcriptional abundance in 33 tumor types. The malignancy-related overexpressed patterns of ITGA5 were identified in cholangiocarcinoma (CHOL), head and neck squamous cell carcinoma (HNSC), kidney renal clear cell carcinoma (KIRC), acute myeloid leukemia (LAML), liver hepatocellular carcinoma (LIHC), pancreatic adenocarcinoma (PAAD), testicular germ cell tumors (TGCT), especially, brain lower-grade glioma (LGG) and glioblastoma multiforme (GBM) (**Figure 1A**). In gliomas, the ITGA5 transcriptional levels increased with more adverse clinicopathological characteristics, namely, greater age at diagnosis, 1p/19q non-codeletion, higher grade, wild-type isocitrate dehydrogenase (IDH) status, unmethylated MGMT status, and mesenchymal subtype (**Figure 1B**). Moreover, the ITGA5 amplification in gliomas with high-grade or invasive molecular signatures was validated both in the TCGA and the CGGA cohorts (**Figure 1C**). These results prompted that the ITGA5 expression was enhanced with the progression of glioma.

Elevated ITGA5 Levels Were Associated With Poor Survival of Glioma Patients

Next, we focused on the prognostic value of ITGA5 in a pan-cancer setting. The result of the Kaplan–Meier analysis demonstrated that ITGA5 was confirmed as a significant protective factor only in adrenocortical carcinoma (ACC). However, ITGA5 was identified as a mortality risk factor in a wide spectrum of cancer types, namely, bladder urothelial carcinoma (BLCA), breast invasive carcinoma (BRCA), cervical squamous cell carcinoma and endocervical adenocarcinoma (CESC), colon adenocarcinoma (COAD), HNSC, KIRC, kidney renal papillary cell carcinoma (KIRP), LIHC, lung adenocarcinoma (LUAD), lung squamous cell carcinoma (LUSC), mesothelioma (MESO), ovarian serous cystadenocarcinoma (OV), stomach adenocarcinoma (STAD), thyroid carcinoma (THCA), uterine corpus endometrial

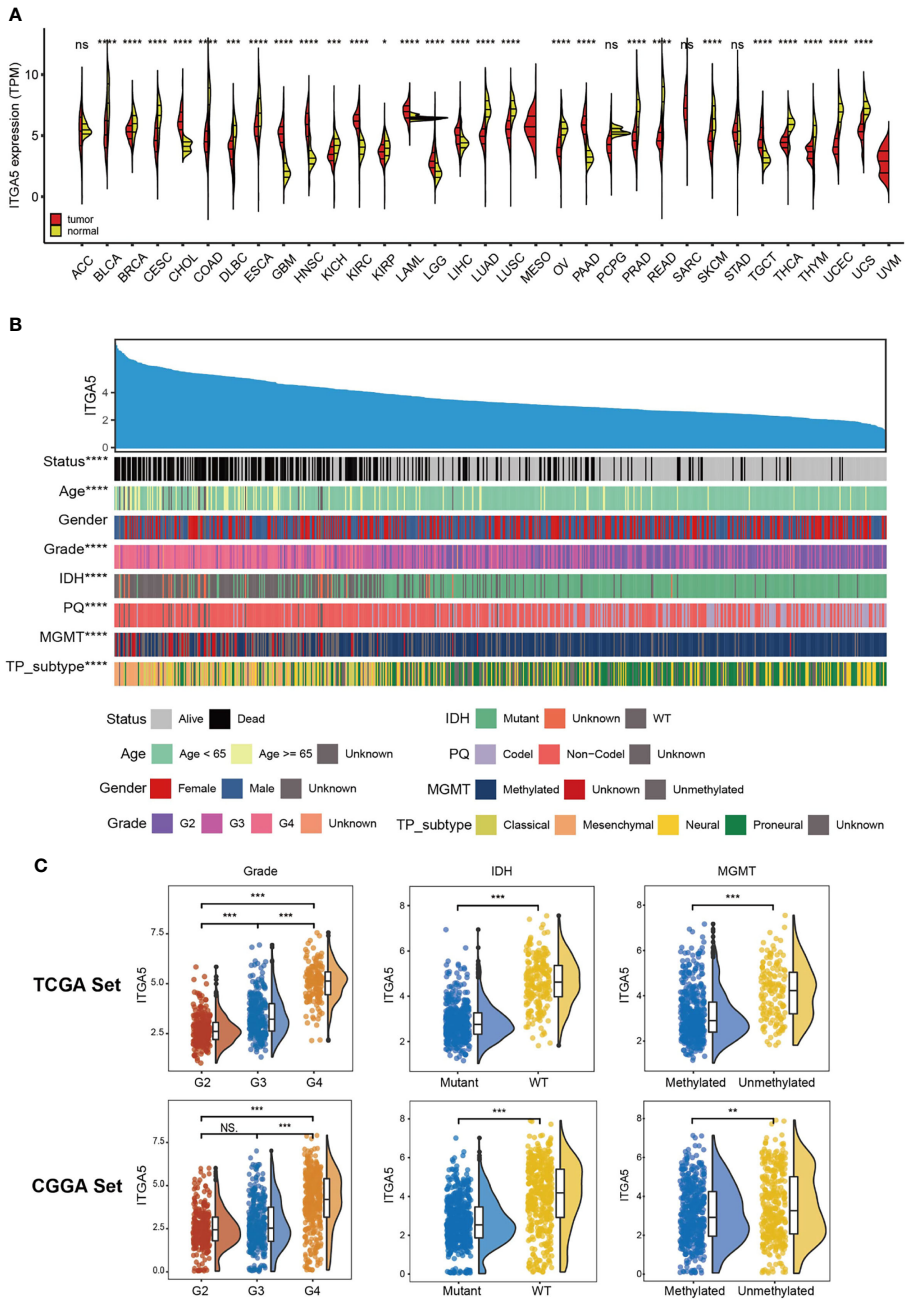

FIGURE 1 | The clinical and molecular characteristics in associations with ITGA5 expression. **(A)** ITGA5 levels among pan-cancer samples grouped by cancer and normal status from TCGA and GTEx. **(B)** An overview of the association between known clinical and molecular features in TCGA, namely, status, age, gender, grade, IDH mutation, 1p/19q codeletion, MGMT methylation, and TP subtype. **(C)** The expression levels of ITGA5 in different WHO grades, IDH states and MGMT methylational states from the TCGA and the CGGA datasets. NS, not statistically significant, *P < 0.05, **P < 0.01, ***P < 0.001, ****P < 0.0001.

carcinoma (UCEC), uveal melanoma (UVM), notably, LGG and GBM (**Figure 2A**). As expected, the adverse prognostic impacts of ITGA5 were obtained from 7 independent glioma sets from the GEO database (**Figure 2B**). Additionally, the uni-Cox and multi-Cox analyses indicated that ITGA5 was the independent indicator for the mortality in glioma patients (**Figure 2C**). Subsequently, the TCGA-based and the CGGA-based KM curves more firmly demonstrate the severe survival detriment in glioma patients with high ITGA5 expression (**Figures 2D, E**). The conspicuously impaired survival in high-ITGA5 groups was observed in 7 independent glioma sets from the GEO database as well (**Figure S1**). Moreover, the time-dependent receiver operating

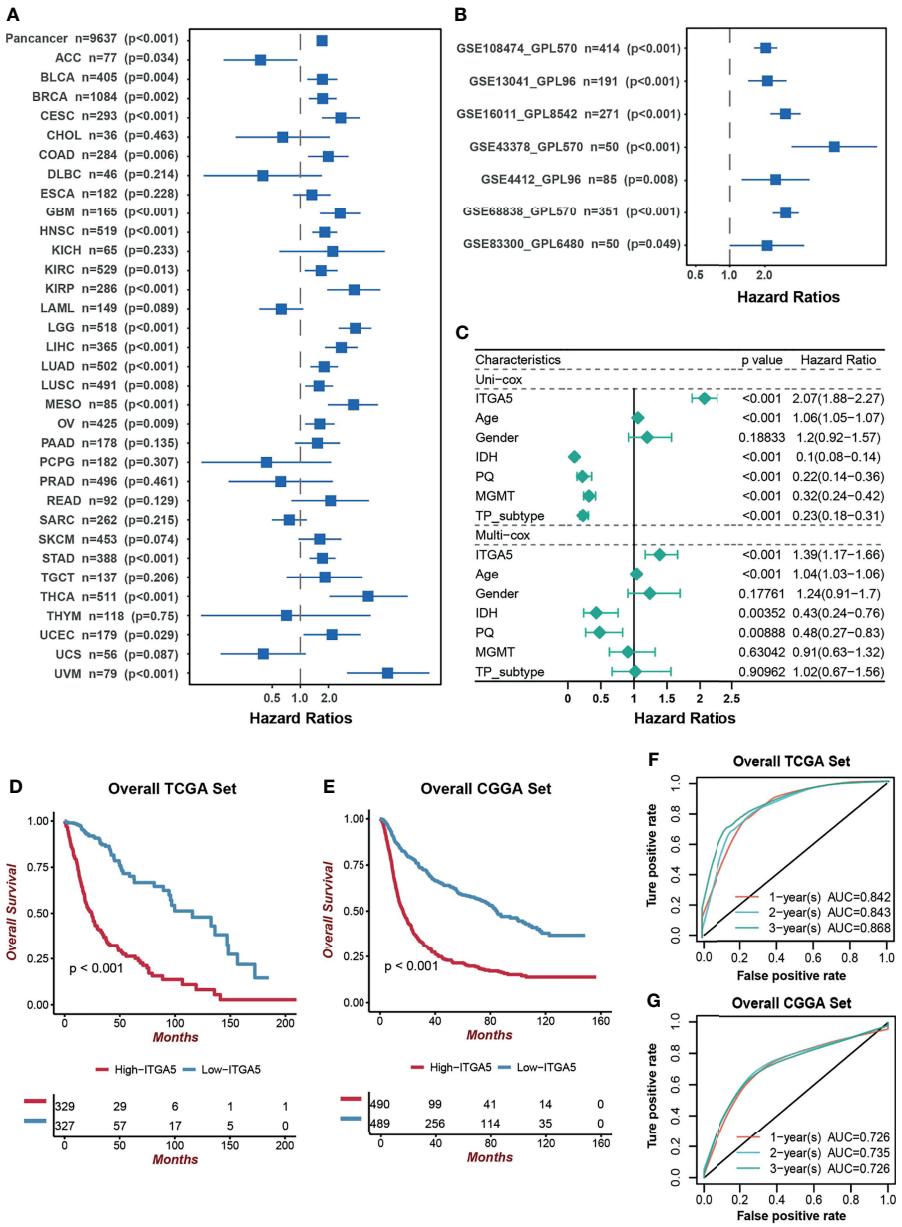

FIGURE 2 | The prognostic potential of ITGA5. **(A)** Univariate cox analysis of ITGA5 for overall survival of patients in the TCGA pan-cancer cohorts. **(B)** Univariate Cox analysis for overall survival of patients with gliomas based on the GEO datasets. **(C)** The forest plot of univariate and multivariate cox proportional hazard ratios for ITGA5 based on the TCGA dataset. **(D)** Kaplan–Meier curves for high and low ITGA5 level groups in the TCGA. **(E)** Kaplan–Meier curves for high and low ITGA5 level groups in the CGGA. **(F)** The time-dependent receiver operating characteristic curve of ITGA5 from the TCGA. **(G)** The time-dependent receiver operating characteristic curve of ITGA5 from the CGGA.

characteristic (ROC) curves of ITGA5 exhibited high sensitivity and specificity, which were demonstrated by the 1-, 2-, and 3-year all area under the curves (AUC) were greater than 0.842 in the TCGA gliomas dataset, and greater than 0.726 in the CGGA gliomas dataset, respectively **(Figures 2F, G)**. In conclusion, the higher ITGA5 abundance was closely associated with a higher mortality hazard in glioma patients. Therefore, ITGA5 could be exploited as a powerful indicator of clinical outcomes in gliomas.

ITGA5 Was Involved in the Oncogenic Process and Immune Regulation in Gliomas

To explore the potential pathological function of ITGA5, the GSVA analysis was performed in the TCGA gliomas cohort. The results revealed that ITGA5 contributed to the aberrant activities of several pivotal pro-oncogenic behaviors, such as focal adhesion, glycolysis gluconeogenesis, Janus kinase (JAK)/signal transducer, and activator

of transcription (STAT) signaling pathway, P53 signaling pathway, and the proteasome. Besides, the amplification of ITGA5 also potentiated a plethora of immune-related processes, namely, interleukin-4-(IL-4) mediated signaling pathway, macrophage fusion, negative regulation of macrophage apoptotic process, positive regulation of macrophage differentiation, and positive regulation of regulatory T cell differentiation (**Figure 3A**). It was worth emphasizing that the modulation of ITGA5 of these pathophysiological activities, especially focal adhesion, was highly prevalent across multiple cancers (**Figure 3B**). The GSEA analysis reaffirmed the crucial role of ITGA5 in carcinogenesis and shaping tumor immune microenvironment, nicely exemplified by priming the regulation of T cell proliferation, regulation of macrophage chemotaxis, response to interferon-beta, apoptosis, antigen processing and presentation, natural killer cell-mediated cytotoxicity (**Figure 3C**). Overall, the high expression of ITGA5 supplied a fertile niche favoring glioma progression by activating oncological signaling pathways and immune reprogramming.

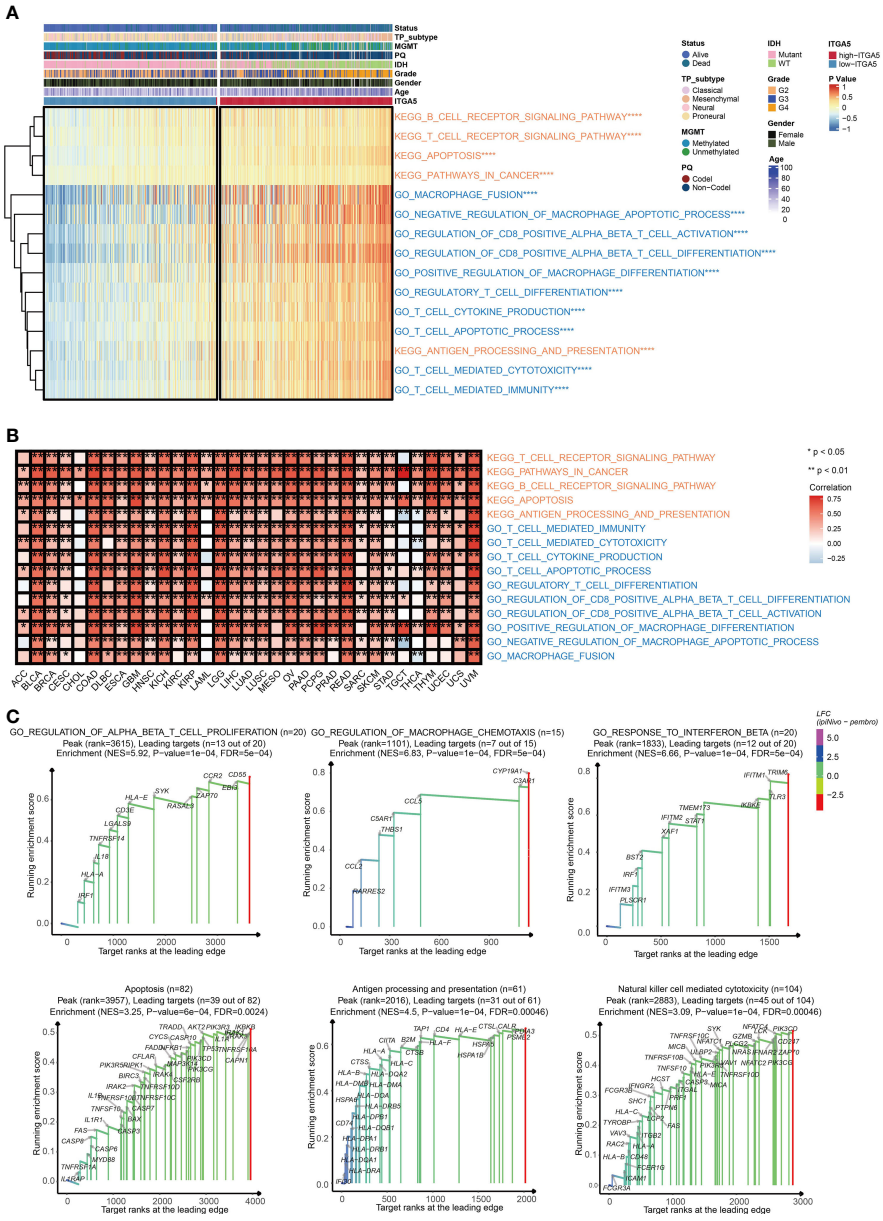

FIGURE 3 | The functional annotation based on ITGA5 expression. **(A)** The heatmap for gene set variation analysis of the ITGA5 from the TCGA. *P < 0.05, **P < 0.01, ***P < 0.001, ****P < 0.0001. **(B)** The heatmap showing the relationship between the above pathways and ITGA5 in the TCGA pan-cancer cohorts. **(C)** GSEA plots for several signaling pathways positively regulated by ITGA5.

ITGA5 Expression Was Relevant to Distinct Genomic Alterations

Genomic instability contributes to multiple steps of the gliomas progressive trajectory. To explore the underlying genetic regulation role of ITAG5, the CNV and somatic mutation analyses were taken in the TCGA glioma dataset to present the ITGA5-based genomic landscapes. The global CNV profile revealed that the amplification in the high-ITGA5 group was concentrated on chr 7 and chr 12, specifically, 7p11.2 and 12q14.1, and the deletion concentrated on chr9, specifically, 9p21.2 and 9p21.3. In the low-ITGA5 group, it was indicated that chr 12 gain, chr 2 loss, chr 10 loss, and chr 11 loss, and the amplification was mainly found on 12p13.32, the deletion was mainly focused on 2q37.1, 2q37.3,10q26.3, and 11p15.5 (**Figure 4A**, **Figure S2A**). The detailed amplificated or deleted CNV oncoplots are presented in **Figure S2B**. The global views of mutational distribution showed that cellular tumor antigen p53 (TP53) mutation was enriched in both the high-ITGA5 group and the low-ITGA5 group (38 and 47%, respectively) (**Figure 4B**). Besides, isocitrate dehydrogenase [NADP] cytoplasmic (IDH1) mutation was generally presented in the low-ITGA5 group as 88% and was partially observed in the high-ITGA5 groups as 32%. The three followed most frequently mutated genes were titin (TTN) (22%), epidermal growth factor receptor (EGFR) (20%), and phosphatase and tensin homolog (PTEN) (20%) in the high-ITGA5 group, and was

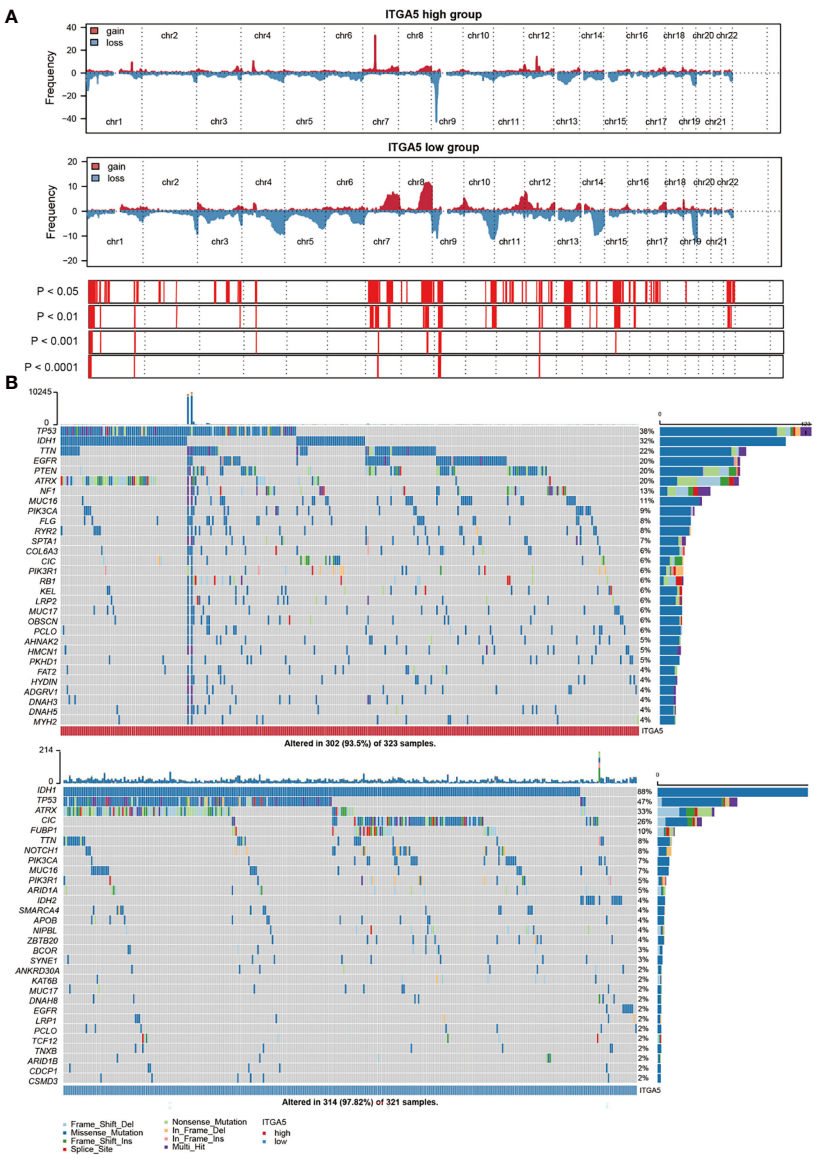

FIGURE 4 | ITGA5-associated genomic alterations in gliomas samples. **(A)** Main copy-number changes in gliomas with high and low ITGA5 expression. **(B)** Somatic mutations detected in gliomas with high and low ITGA5 expression.

alpha-thalassemia/mental retardation syndrome x-linked chromatin remodeler (ATRX) (33%), capicua transcriptional repressor (CIC) (26%) and far upstream element binding protein (FUBP1) (10%) in the low-ITGA5 group (**Figure 4B**).

Furthermore, the ratio of mutation frequencies between high-ITGA5 and low-ITGA5 groups was performed by Fisher's exact test and ranked by increasing p-value. The high-ITGA5 group beard extremely lower IDH1 and CIC mutation load, higher PTEN, EGFR, and NF1 mutation load than the low-ITGA5 group (**Figure S3A**). Additionally, the co-concurrent or mutually exclusive mutations of the 25 most frequently mutated genes are shown in **Figure S3B**. The high-ITGA5 groups showed markedly more numerous co-concurrent genetic alterations than the low-ITGA5 group. The EGFR mutation frequently cooccurred with collagen type VI alpha 3 chain (COL6A3) mutation in the high-ITGA5 group. Other intimate mutation sites included obscurin (OBSCN) and COL6A3, IDH1 and TP53, ATRX, and TP53. In the low-ITGA5 group, the common co-mutation included NOTCH1 and CIC, IDH1 and ATRX, and so on. Meanwhile, some intensive mutually exclusive pairs of gene alteration were identified, such as IDH1-PTEN and TP53-EGFR in the high-ITGA5 group, and IDH1-EGFR and IDH1-IDH2 in the low-ITGA5 group (**Figure S3B**).

ITGA5 Was Correlated With Tumor Immune Microenvironment in Gliomas

Metabolism has been well-established as a determinant in the viability and efficacy of immune cells (32). Then, the physiopathological impact of ITGA5 in the metabolic programming and cancer immunity cycle progressions was evaluated by GSVA analysis. Based on the TCGA dataset, ITGA5 was positively correlated with glycogen biosynthesis, cyclooxygenase arachidonic acid metabolism, and drug metabolism by other enzymes (**Figure 5A**). Another noteworthy observation was that ITGA5 exerted a pleiotropic effect in most steps of the immune cascade (**Figure 5A**). Considering that immune cells were the essential constituents of the TME, the immune infiltration characteristics were identified by the ESTIMATE, the MCP counter, the ssGSEA, and the TIMER algorithms of the TCGA datasets (**Figure 5B**). Notably, the ITGA5 expression showed a particularly positive correlation with the stromal score, immune score, ESTIMATE score, and tumor purity. Besides, ITGA5 expression was associated with the high intratumoral infiltration of various immune cells, namely, macrophages, natural killer cells, $CD8^+$ T cells, and regulatory T cells (Tregs). Then, we further explored the relationship between macrophage infiltration and ITGA5 from the ssGSEA and the TIMER (**Figures 5C, D**).

High-ITGA5 Group in Gliomas Exhibited Greater M2 Macrophage Infiltration

To confirm the positive correlations between ITGA5 and macrophages identified from transcriptomic analyses, the multiple IF was performed on the human glioma tissue microassay. Staining for CD68 (the pan-macrophage marker) revealed that there was more diffuse intra-tumoral macrophage infiltration in the high-ITGA5 group than in the low-ITGA5 group (**Figure 6**). Of more concern was that the high-ITGA5 group displayed a higher M2-macrophage abundance, which was prompted by CD163 (the M2-macrophage marker) fluorescence distribution (**Figure 6**).

The Potential Immunotherapeutic and Chemotherapeutic Targets in Glioma Patients With High ITGA5 Expression

Given that immune checkpoints are the underpinnings of immune therapy, the global views of immune-checkpoints expressions would be of great clinical interest. Then the correlation analysis was performed between ITGA5 and multiple putative immune checkpoint molecules involving antigen presentation, cell adhesion, co-inhibition or co-stimulation, and ligand-receptor interaction. The results exhibited an intimate connection between ITGA5 and most immune checkpoint molecules in gliomas, especially in programmed cell death 1 (PD-1), programmed cell death 1 ligand 1 (PD-L1), and cytotoxic T-lymphocyte associated protein 4 (CTLA-4) (**Figure 7A**). Besides, additional validation of the intimate connection of ITGA5 and immune checkpoints was performed in the pan-cancer set (**Figure S4**). These data collectively suggested that ITGA5 inhibition may work synergistically with existing immunotherapy strategies and enhance anti-glioma activity. We further explored the relationship between ITGA5 and some immune checkpoints, such as PDCD1 (PD-1), CD274 (PD-L1), and PDCD1LG2 (PD-L2) in gliomas based on the TCGA dataset (**Figure S5C**).

To further evaluate the sensitivity of ITGA5 to immunotherapy, we applied the TIDE and the submap algorithms to glioma patients in the TCGA. By TIDE, we found that patients with high ITGA5 showed better immunotherapy response compared to patients with low ITGA5 (**Figure S5A**). The results of the submap showed that the high- and low-ITGA5 groups had different responses to immunotherapy in that the high-ITGA5 group had a significant response to anti-PD-1 immunotherapy in gliomas based on the TCGA (**Figure S5B**).

There has been a regrettable case that conventional chemotherapy with temozolomide provides modest benefit for the survival of gliomas patients, which may impute to the impaired drug permeability owing to the BBB, the particular immune contexture in the central nervous system, or the extreme heterogeneity of gliomas. Thus, the GDSC database was adopted to assess the drug response of high-ITGA5 and low-ITGA5 glioma groups, and the predictive accuracy was measured by 10-fold cross-validation. The results demonstrated that high-ITGA5 groups exhibited significantly lower IC50 of Bexarotene, Bicalutamide, Bortezomib, Bryostatin-1, Cytarabine, Luminespib, Midostaurin, Selumetinib than the low-ITGA5 group (**Figure 7B**). The therapeutic efficacy of the above-nominated pharmacological methods deserved further investigation.

DISCUSSION

Glioma has a lethal ending with limited treatment methods, the highest grade of which has an OS of about 15 months (33). The

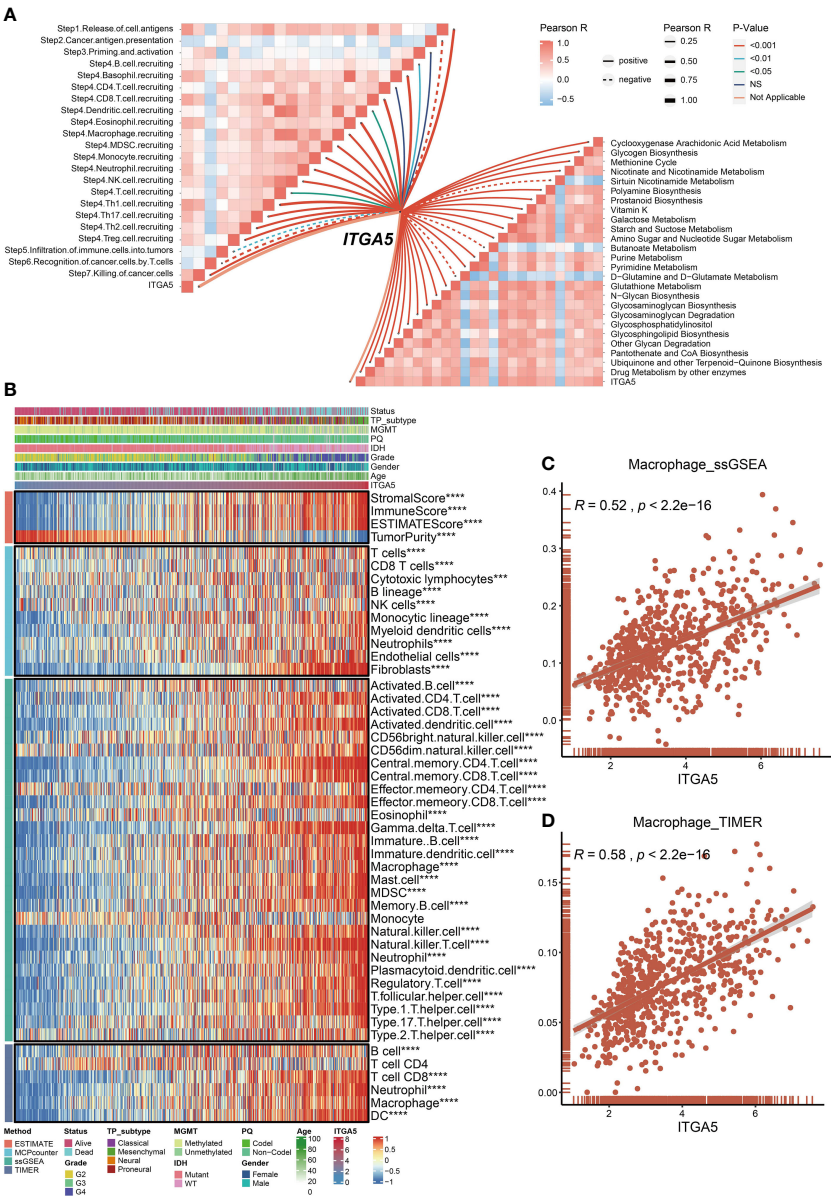

FIGURE 5 | Roles of ITGA5 in immune and metabolism phenotypes in the TCGA cohort. **(A)** Correlations between ITGA5 and enrichment scores of metabolism-relevant pathways together with the steps of the cancer immune cascades. **(B)** Heatmap visualized the abundance of infiltrating immune cell populations with different ITGA5 levels, based on the ESTIMATE, the MCPcounter, the ssGSEA, and the TIMER algorithms. *P < 0.05, **P < 0.01, ***P < 0.001, ****P < 0.0001. **(C)** The corrplot of the correlation between ITGA5 expression and macrophage cell level of the ssGSEA. **(D)** The corrplot of the correlation between ITGA5 expression and macrophage cell level of the TIMER.

heterogeneity and complicated immunosuppressive TME are the main obstacles for glioma patients with optimal outcomes. The systematical application of novel excavated biomarkers will be conductive to glioma management in combination with conventional diagnostic and therapeutic strategies. In the present study, by comprehensive bioinformatic analysis, we identified that ITGA5 was positively related to aggressive clinicopathological and molecular features in gliomas. Elevated ITGA5 level was tightly linked to the survival detriment of gliomas patients. Moreover, ITGA5 was relevant to distinct genomic alterations and tumor immune microenvironment in gliomas. ITGA5 could be a therapeutic indicator of checkpoint inhibitors as well. Finally, the glioma patients with higher expression of ITGA5 may present better outcomes of chemotherapy treatment, namely, bexarotene, bicalutamide, and bortezomib, which provided more therapeutic choices in the future.

ITGA5 is also known as interferon α5 belonging to the integrin alpha chain family, which plays a pivotal role in cell

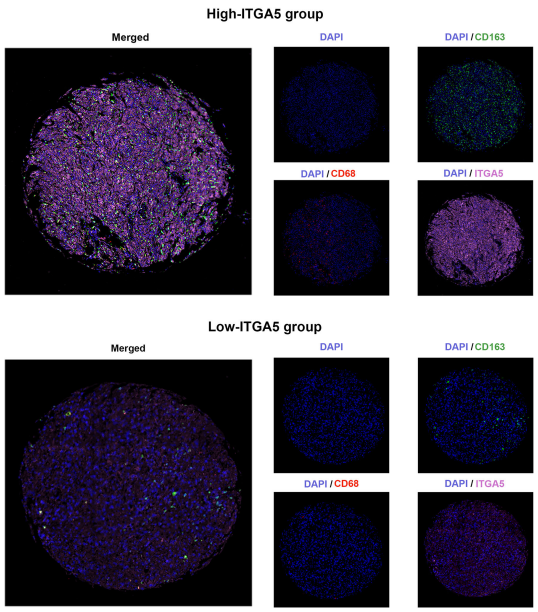

FIGURE 6 | The multiple immunofluorescence staining of ITGA5, CD68, and CD163 in gliomas.

surface adhesion. Biologically, interferon α subunits have a small cytoplasmic tail, a relatively large extracellular domain, and a transmembrane domain. In pathological settings, integrin demonstrated a remarkable oncogenic potency in tumor progression. The extracellular domain acts as the cell receptor for growth factors and adhesion proteins from the TME (34). The cytoplasmic tail is a link to the cell cytoskeleton and cellular signaling cascade like focal adhesion kinase (FAK)-Src signaling (34). The FAK-Src signaling regulated by integrin allows downstream activation of several signaling pathways, namely, the Mitogen-Activated Protein Kinase (MAPK)/Extracellular Regulated Kinase (Erk) signaling pathway, phosphatidylinositol 3-kinase (PI3-K)/Protein kinase B (Akt) signaling pathway, Stress-Activated MAP Kinases (SAPKs) signaling, and c-Jun N-terminal kinase (JNK) activation (35). The activation of PI3K/Akt is the key regulator of induction of tumor metastasis through the engagement of extracellular matrix ligand (36). MAPK/Erk pathways are highly related to tumor progression, survival, and proliferation (37). In our results, ITGA5 was found to mediate lots of different oncological and immune pathways such as glycolysis gluconeogenesis, JAK/STAT signaling pathway, P53 signaling pathway, antigen processing pathway, and immune cell activation pathway. The dysregulated metabolism of the tumor and immune cells in TME is recognized as a key contributor to tumor progression. Our results prompted that ITGA5 may perturb the biochemical homeostasis in TME by not only oncogenic pathway but also immune and metabolic reprogramming, which was partially consistent with the previous oncological studies.

Genomic alteration is one of the fundamental factors for diagnosis, classification, treatment, and prognosis in gliomas. The typical biomarkers of genomic alteration are routinely tested in clinical practice, namely, IDH mutant, MGMT promoter methylation, PTEN mutation, ATRX mutation, and TERT promoter mutation (38). Surprisingly, although patients underwent the systematic diagnosis and treatment depending on the WHO classification, the prognosis varies differently, strongly implying that the current diagnosis system is not fully appropriate for the survival predictions or the reflection of glioma heterogeneity. Chen reported a phenomenon that the ITGA5 downregulation could inhibit the glioma proliferation, which could be rescued by circPTN (39). Moreover, Kita also confirmed that ITGA5, which was upregulated by Ets-1, could be secreted by glioma cells to boost tumor migration and invasion, finally contributing to glioma malignancy (40). Consistently, our results also revealed that ITGA5 might be an oncogenic factor, presuming that the high ITGA5 expression possibly indicated a low survival rate in glioma patients. In the other aspect, our genomic alterations analysis results showed that ITGA5 was associated with poor mutation, namely, P53 mutation, ATRX mutation, and PTEN mutation. Especially, the high expression of ITGA5 had relatively lower IDH mutations. IDH mutation is a classic prognostic indicator in judging glioma, and there is a certain negative correlation between ITGA5 expression level and IDH mutation level.

A glioma has a different immunosuppressive "cold" tumor environment affecting the effectiveness of immunotherapy (41). TAMs are the most abundant infiltration immune cells in brain cancer validated from high-dimensional single-cell profiling and other methods (42). TAMs contribute to tumor immunosuppressive environments and potentially mediate tumor-induced polarization states, promoting tumor malignancy, and therapeutic resistance to irradiation (43). In our results, from the ssGSEA and the TIMER analyses, ITGA5 was positively correlated with TAMs, possibly resulting in a worse survival rate. Furthermore, it also found that upregulated ITGA5 significantly increased the quantities of multiple immune cells, namely, dendritic cells, natural killer cells, $CD8^+$ T cells, neutrophils, activated $CD4^+$ T cells, central memory T cells, Tregs, and myeloid-derived suppressor cells. Among these cells, immunosuppressive cells such as Tregs and myeloid-derived suppressor cells were increased more significantly with the increase of ITGA5 expression, suggesting that ITGA5 was essential in the formation of glioma immunosuppressive microenvironment (44). It is well-documented that the immune checkpoint targeted therapy in glioma patients remains challenging because of the immunosuppressive state (6). Besides, we also proved that high-ITGA5 gliomas were accompanied by high immunotherapy biomarker expression, namely, PD-1, PD-L1, CTLA-4, and VEGF, thus showing an ITGA5-targeted therapeutic potential to be synergistic with immunotherapy. Therefore, our results presented that the high ITGA5 expression patients seem to have a relative "hot" immune environment that might be beneficial to immune therapy.

Up to now, there are emerging studies devoted to developing novel and effective strategies to address the deficiencies of anti-glioma treatment. EGFR has been the target of treatment in glioma patients (45) both in a highly selective pan-human EGFR inhibitor or immunotherapies (46). Interestingly, ITGA5 depletion delayed gefitinib-mediated EGFR endocytosis, which makes EGFR target

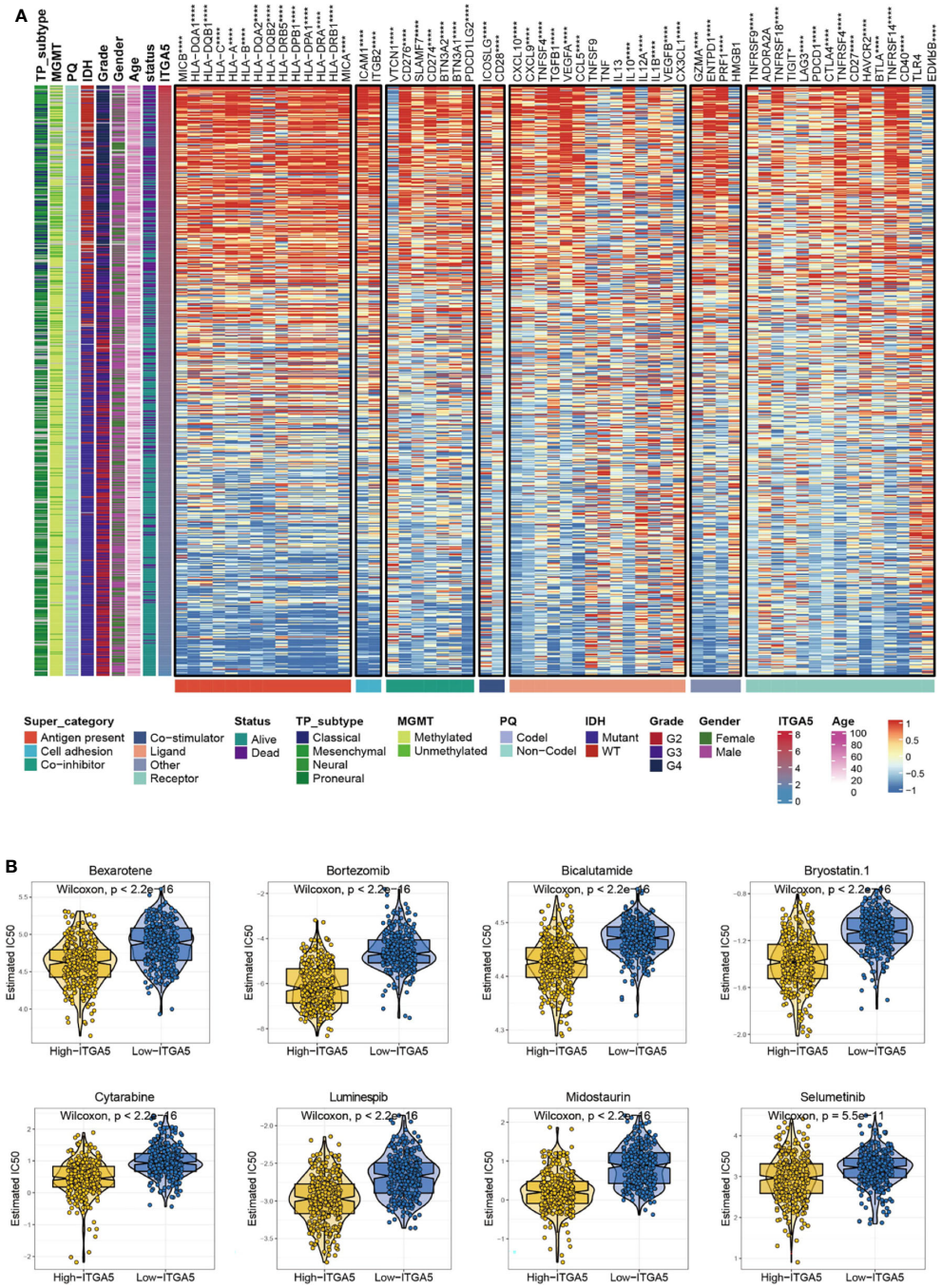

FIGURE 7 | The potential ITGA5-involved immune checkpoints treatment and chemotherapeutic targets in gliomas. **(A)** Correlations between ITGA5 and seven types of immune checkpoints levels in gliomas. *P <0.05, **P <0.01, ***P <0.001, ****P <0.0001. **(B)** The box plots of the estimated IC50 for several chemotherapeutic drugs among high-ITGA5 and low-ITGA5 groups.

therapy more sensitive (47). In addition, the inhibitor of ITGA5 attenuates glioma growth (48) and cell dispersion (13). In our results, we found that patients with high expression of ITGA5 had low IC50 of Bexarotene, Bicalutamide, Bortezomib, Bryostatin-1, Cytarabine, Luminespib, Midostaurin, and Selumetinib. This result emphasized that the high ITGA5 expression was a robust and reliable indicator for the therapeutic sensitivity of these potential molecular drugs. The biosafety and biocompatibility of these drugs in clinical trials have been successfully experimentally validated. Among them, it was noted that some drugs, represented by Bexarotene, Bryostatin-1, Cytarabine, and Pazopanib, possess the excellent capability of crossing BBB to locally exert a targeted

effect. This might provide a pivotal clue for guiding glioma drug treatment.

However, there are still some limitations. In the first place, since this study data analysis are mainly from the open-access online databases, additional external verification of clinical datasets would be beneficial. Secondly, because this is a retrospective study, and prospective clinical studies in large-cohorts should be applied to verify in the future. Thirdly, there is a relatively poor investigation of the mechanism of ITGA5 and its role in interfering with the immune system. Thus more comprehensive studies are needed to further interpret the role of ITGA5 in gliomas immunology.

CONCLUSION

In summary, our findings demonstrated that ITGA5 is upregulated in glioma and differs in multiple molecular phenotypic gliomas, acting as a potential biomarker for predicting glioma prognosis. It is particularly noteworthy that ITGA5 is involved in remolding glioma immune infiltration and TME that is closely related to immunotherapy. High expression of ITGA5 may benefit immune checkpoint targeted therapy and chemotherapy. Further studies exploring the role and mechanism of ITGA5 will endow great potential for the development of diagnostic and anti-glioma therapeutic strategies.

DATA AVAILABILITY STATEMENT

The datasets presented in this study can be found in online repositories. The names of the repository/repositories and accession number(s) can be found in the article/**Supplementary Material**.

ETHICS STATEMENT

All procedures performed in studies involving human participants were in accordance with the ethical standards of the institutional and/or national research committee and with the 1964 Helsinki declaration and its later amendments or comparable ethical standards.

AUTHOR CONTRIBUTIONS

Shu-YL and NZ contributed equally as co-first authors. Shu-YL and NZ conceived and designed the study. Shi-YL and HZ. drafted the manuscript. J-JL. did the statistical analysis, supervised by Y-WQ, QZ, and X-RL. All authors listed have made a substantial, direct, and intellectual contribution to the work and approved it for publication.

FUNDING

This work was supported by the National Natural Science Foundation of China [Grant Nos. 81802676] and the Wuhan Youth Cadre Project (2017zqnlxr01 and 2017zqnlxr02).

SUPPLEMENTARY MATERIAL

The Supplementary Material for this article can be found online at: https://www.frontiersin.org/articles/10.3389/fonc.2022.844144/full#supplementary-material

Supplementary Figure 1 | The Kaplan–Meier curves of ITGA5 in 7 independent GEO datasets.

Supplementary Figure 2 | The genomic alterations in high-ITGA5 and low-ITGA5 groups. **(A)** Amplification and deletions in gliomas with high and low ITGA5 expression. **(B)** The detailed amplification and deletion of chromosome copy number variation in gliomas with high and low ITGA5 expression.

Supplementary Figure 3 | The somatic mutations in high-ITGA5 and low-ITGA5 groups. **(A)** The forest plot illustrates the difference in mutation patterns between high-ITGA5 and low-ITGA5 groups. **(B)** The heatmap presents the somatic interaction in gliomas with high and low ITGA5 levels.

Supplementary Figure 4 | The correlation between ITGA5 expression and recognized immune checkpoints in pan-cancer.

Supplementary Figure 5 | The evaluation of the sensitivity of ITGA5 to immunotherapy. **(A)** TIDE predicting the immunotherapy responses related to ITGA5 in gliomas. **(B)** Submap analysis of ITGA5 expression levels in gliomas. **(C)** The corrplot of the correlation between ITGA5 expression and immune checkpoints.

Supplementary Table 1 | Specific information of the patients and the corresponding platforms.

REFERENCES

1. Ostrom QT, Patil N, Cioffi G, Waite K, Kruchko C, Barnholtz-Sloan JS. CBTRUS Statistical Report: Primary Brain and Other Central Nervous System Tumors Diagnosed in the United States in 2013-2017. *Neuro Oncol* (2020) 22 (12 Suppl 2):iv1–iv96. doi: 10.1093/neuonc/noaa200
2. Delgado-Martin B, Medina MA. Advances in the Knowledge of the Molecular Biology of Glioblastoma and Its Impact in Patient Diagnosis, Stratification, and Treatment. *Adv Sci (Weinh)* (2020) 7(9):1902971. doi: 10.1002/advs.201902971
3. Wick W, Weller M, van den Bent M, Sanson M, Weiler M, von Deimling A, et al. MGMT Testing–the Challenges for Biomarker-Based Glioma Treatment. *Nat Rev Neurol* (2014) 10(7):372–85. doi: 10.1038/nrneurol.2014.100
4. Buonfiglioli A, Hambardzumyan D. Macrophages and Microglia: The Cerberus of Glioblastoma. *Acta Neuropathol Commun* (2021) 9(1):54. doi: 10.1186/s40478-021-01156-z
5. Lah TT, Novak M, Breznik B. Brain Malignancies: Glioblastoma and Brain Metastases. *Semin Cancer Biol* (2020) 60:262–73. doi: 10.1016/j.semcancer.2019.10.010
6. Qi Y, Liu B, Sun Q, Xiong X, Chen Q. Immune Checkpoint Targeted Therapy in Glioma: Status and Hopes. *Front Immunol* (2020) 11:578877. doi: 10.3389/fimmu.2020.578877
7. Weller M, Roth P, Preusser M, Wick W, Reardon DA, Platten M, et al. Vaccine-Based Immunotherapeutic Approaches to Gliomas and Beyond. *Nat Rev Neurol* (2017) 13(6):363–74. doi: 10.1038/nrneurol.2017.64
8. Prager BC, Bhargava S, Mahadev V, Hubert CG, Rich JN. Glioblastoma Stem Cells: Driving Resilience Through Chaos. *Trends Cancer* (2020) 6(3):223–35. doi: 10.1016/j.trecan.2020.01.009

9. Kuninty PR, Bansal R, De Geus SWL, Mardhian DF, Schnittert J, van Baarlen J, et al. ITGA5 Inhibition in Pancreatic Stellate Cells Attenuates Desmoplasia and Potentiates Efficacy of Chemotherapy in Pancreatic Cancer. *Sci Adv* (2019) 5(9):eaax2770. doi: 10.1126/sciadv.aax2770
10. Wang X, Che X, Yu Y, Cheng Y, Bai M, Yang Z, et al. Hypoxia-Autophagy Axis Induces VEGFA by Peritoneal Mesothelial Cells to Promote Gastric Cancer Peritoneal Metastasis Through an Integrin Alpha5-Fibronectin Pathway. *J Exp Clin Cancer Res* (2020) 39(1):221. doi: 10.1186/s13046-020-01703-x
11. Dingemans AM, van den Boogaart V, Vosse BA, van Suylen RJ, Griffioen AW, Thijssen VL. Integrin Expression Profiling Identifies Integrin Alpha5 and Beta1 as Prognostic Factors in Early Stage Non-Small Cell Lung Cancer. *Mol Cancer* (2010) 9:152. doi: 10.1186/1476-4598-9-152
12. Pantano F, Croset M, Driouch K, Bednarz-Knoll N, Iuliani M, Ribelli G, et al. Integrin Alpha5 in Human Breast Cancer is a Mediator of Bone Metastasis and a Therapeutic Target for the Treatment of Osteolytic Lesions. *Oncogene* (2021) 40(7):1284–99. doi: 10.1038/s41388-020-01603-6
13. Blandin AF, Noulet F, Renner G, Mercier MC, Choulier L, Vauchelles R, et al. Glioma Cell Dispersion is Driven by Alpha5 Integrin-Mediated Cell-Matrix and Cell-Cell Interactions. *Cancer Lett* (2016) 376(2):328–38. doi: 10.1016/j.canlet.2016.04.007
14. Samandari E, Visarius T, Zingg JM, Azzi A. The Effect of Gamma-Tocopherol on Proliferation, Integrin Expression, Adhesion, and Migration of Human Glioma Cells. *Biochem Biophys Res Commun* (2006) 342(4):1329–33. doi: 10.1016/j.bbrc.2006.02.110
15. Zhu H, Wang G, Zhu H, Xu A. ITGA5 is a Prognostic Biomarker and Correlated With Immune Infiltration in Gastrointestinal Tumors. *BMC Cancer* (2021) 21(1):269. doi: 10.1186/s12885-021-07996-1
16. Liu S, Song A, Wu Y, Yao S, Wang M, Niu T, et al. Analysis of Genomics and Immune Infiltration Patterns of Epithelial-Mesenchymal Transition Related to Metastatic Breast Cancer to Bone. *Transl Oncol* (2021) 14(2):100993. doi: 10.1016/j.tranon.2020.100993
17. Liu Z, Meng Q, Bartek J Jr, Poiret T, Persson O, Rane L, et al. Tumor-Infiltrating Lymphocytes (TILs) From Patients With Glioma. *Oncoimmunology* (2017) 6(2):e1252894. doi: 10.1080/2162402X.2016.1252894
18. Mermel CH, Schumacher SE, Hill B, Meyerson ML, Beroukhim R, Getz G. GISTIC2.0 Facilitates Sensitive and Confident Localization of the Targets of Focal Somatic Copy-Number Alteration in Human Cancers. *Genome Biol* (2011) 12(4):R41. doi: 10.1186/gb-2011-12-4-r41
19. Yoshihara K, Shahmoradgoli M, Martinez E, Vegesna R, Kim H, Torres-Garcia W, et al. Inferring Tumour Purity and Stromal and Immune Cell Admixture From Expression Data. *Nat Commun* (2013) 4:2612. doi: 10.1038/ncomms3612
20. Li T, Fu J, Zeng Z, Cohen D, Li J, Chen Q, et al. TIMER2.0 for Analysis of Tumor-Infiltrating Immune Cells. *Nucleic Acids Res* (2020) 48(W1):W509–W14. doi: 10.1093/nar/gkaa407
21. Becht E, Giraldo NA, Lacroix L, Buttard B, Elarouci N, Petitprez F, et al. Erratum to: Estimating the Population Abundance of Tissue-Infiltrating Immune and Stromal Cell Populations Using Gene Expression. *Genome Biol* (2016) 17(1):249. doi: 10.1186/s13059-016-1113-y
22. Hanzelmann S, Castelo R, Guinney J. GSVA: Gene Set Variation Analysis for Microarray and RNA-Seq Data. *BMC Bioinf* (2013) 14:7. doi: 10.1186/1471-2105-14-7
23. Xu L, Deng C, Pang B, Zhang X, Liu W, Liao G, et al. TIP: A Web Server for Resolving Tumor Immunophenotype Profiling. *Cancer Res* (2018) 78 (23):6575–80. doi: 10.1158/0008-5472.Can-18-0689
24. Schreiber RD, Old LJ, Smyth MJ. Cancer Immunoediting: Integrating Immunity's Roles in Cancer Suppression and Promotion. *Science* (2011) 331(6024):1565–70. doi: 10.1126/science.1203486
25. Zhang M, Wang X, Chen X, Zhang Q, Hong J. Novel Immune-Related Gene Signature for Risk Stratification and Prognosis of Survival in Lower-Grade Glioma. *Front Genet* (2020) 11:363. doi: 10.3389/fgene.2020.00363
26. Jiang P, Gu S, Pan D, Fu J, Sahu A, Hu X, et al. Signatures of T Cell Dysfunction and Exclusion Predict Cancer Immunotherapy Response. *Nat Med* (2018) 24(10):1550–8. doi: 10.1038/s41591-018-0136-1
27. Liberzon A, Birger C, Thorvaldsdottir H, Ghandi M, Mesirov JP, Tamayo P. The Molecular Signatures Database (MSigDB) Hallmark Gene Set Collection. *Cell Syst* (2015) 1(6):417–25. doi: 10.1016/j.cels.2015.12.004
28. Rosario SR, Long MD, Affronti HC, Rowsam AM, Eng KH, Smiraglia DJ. Pan-Cancer Analysis of Transcriptional Metabolic Dysregulation Using The Cancer Genome Atlas. *Nat Commun* (2018) 9(1):5330. doi: 10.1038/s41467-018-07232-8
29. Yu G, Wang LG, Han Y, He QY. Clusterprofiler: An R Package for Comparing Biological Themes Among Gene Clusters. *OMICS* (2012) 16(5):284–7. doi: 10.1089/omi.2011.0118
30. Mayakonda A, Lin DC, Assenov Y, Plass C, Koeffler HP. Maftools: Efficient and Comprehensive Analysis of Somatic Variants in Cancer. *Genome Res* (2018) 28(11):1747–56. doi: 10.1101/gr.239244.118
31. Gu Z, Eils R, Schlesner M. Complex Heatmaps Reveal Patterns and Correlations in Multidimensional Genomic Data. *Bioinformatics* (2016) 32 (18):2847–9. doi: 10.1093/bioinformatics/btw313
32. Pearce EL, Pearce EJ. Metabolic Pathways in Immune Cell Activation and Quiescence. *Immunity* (2013) 38(4):633–43. doi: 10.1016/j.immuni.2013.04.005
33. Stupp R, Mason WP, van den Bent MJ, Weller M, Fisher B, Taphoorn MJ, et al. Radiotherapy Plus Concomitant and Adjuvant Temozolomide for Glioblastoma. *N Engl J Med* (2005) 352(10):987–96. doi: 10.1056/NEJMoa043330
34. Huang R, Rofstad EK. Integrins as Therapeutic Targets in the Organ-Specific Metastasis of Human Malignant Melanoma. *J Exp Clin Cancer Res* (2018) 37 (1):92. doi: 10.1186/s13046-018-0763-x
35. Aksorn N, Chanvorachote P. Integrin as a Molecular Target for Anti-Cancer Approaches in Lung Cancer. *Anticancer Res* (2019) 39(2):541–8. doi: 10.21873/anticanres.13146
36. Li M, Wang Y, Li M, Wu X, Setrerrahmane S, Xu H. Integrins as Attractive Targets for Cancer Therapeutics. *Acta Pharm Sin B* (2021) 11(9):2726–37. doi: 10.1016/j.apsb.2021.01.004
37. Asl ER, Amini M, Najafi S, Mansoori B, Mokhtarzadeh A, Mohammadi A, et al. Interplay Between MAPK/ERK Signaling Pathway and MicroRNAs: A Crucial Mechanism Regulating Cancer Cell Metabolism and Tumor Progression. *Life Sci* (2021) 278:119499. doi: 10.1016/j.lfs.2021.119499
38. Cohen AL, Colman H. Glioma Biology and Molecular Markers. *Cancer Treat Res* (2015) 163:15–30. doi: 10.1007/978-3-319-12048-5_2
39. Chen J, Chen T, Zhu Y, Li Y, Zhang Y, Wang Y, et al. circPTN Sponges miR-145-5p/miR-330-5p to Promote Proliferation and Stemness in Glioma. *J Exp Clin Cancer Res* (2019) 38(1):398. doi: 10.1186/s13046-019-1376-8
40. Kita D, Takino T, Nakada M, Takahashi T, Yamashita J, Sato H. Expression of Dominant-Negative Form of Ets-1 Suppresses Fibronectin-Stimulated Cell Adhesion and Migration Through Down-Regulation of Integrin Alpha5 Expression in U251 Glioma Cell Line. *Cancer Res* (2001) 61(21):7985–91.
41. Sampson JH, Gunn MD, Fecci PE, Ashley DM. Brain Immunology and Immunotherapy in Brain Tumours. *Nat Rev Cancer* (2020) 20(1):12–25. doi: 10.1038/s41568-019-0224-7
42. Friebel E, Kapolou K, Unger S, Nunez NG, Utz S, Rushing EJ, et al. Single-Cell Mapping of Human Brain Cancer Reveals Tumor-Specific Instruction of Tissue-Invading Leukocytes. *Cell* (2020) 181(7):1626–42 e20. doi: 10.1016/j.cell.2020.04.055
43. Sa JK, Chang N, Lee HW, Cho HJ, Ceccarelli M, Cerulo L, et al. Transcriptional Regulatory Networks of Tumor-Associated Macrophages That Drive Malignancy in Mesenchymal Glioblastoma. *Genome Biol* (2020) 21(1):216. doi: 10.1186/s13059-020-02140-x
44. Pombo Antunes AR, Scheyltjens I, Duerinck J, Neyns B, Movahedi K, Van Ginderachter JA. Understanding the Glioblastoma Immune Microenvironment as Basis for the Development of New Immunotherapeutic Strategies. *Elife* (2020) 9. doi: 10.7554/eLife.52176
45. Sepulveda-Sanchez JM, Vaz MA, Balana C, Gil-Gil M, Reynes G, Gallego O, et al. Phase II Trial of Dacomitinib, a Pan-Human EGFR Tyrosine Kinase Inhibitor, in Recurrent Glioblastoma Patients With EGFR Amplification. *Neuro Oncol* (2017) 19(11):1522–31. doi: 10.1093/neuonc/nox105
46. Reardon DA, Desjardins A, Vredenburgh JJ, O'Rourke DM, Tran DD, Fink KL, et al. Rindopepimut With Bevacizumab for Patients With Relapsed EGFRvIII-Expressing Glioblastoma (ReACT): Results of a Double-Blind Randomized Phase II Trial. *Clin Cancer Res* (2020) 26(7):1586–94. doi: 10.1158/1078-0432.CCR-18-1140
47. Blandin AF, Cruz Da Silva E, Mercier MC, Glushonkov O, Didier P, Dedieu S, et al. Gefitinib Induces EGFR and Alpha5beta1 Integrin Co-Endocytosis in

Glioblastoma Cells. *Cell Mol Life Sci* (2021) 78(6):2949–62. doi: 10.1007/s00018-020-03686-6

48. Farber K, Synowitz M, Zahn G, Vossmeyer D, Stragies R, van Rooijen N, et al. An Alpha5beta1 Integrin Inhibitor Attenuates Glioma Growth. *Mol Cell Neurosci* (2008) 39(4):579–85. doi: 10.1016/j.mcn.2008.08.005

Conflict of Interest: The authors declare that the research was conducted in the absence of any commercial or financial relationships that could be construed as a potential conflict of interest.

Publisher's Note: All claims expressed in this article are solely those of the authors and do not necessarily represent those of their affiliated organizations, or those of the publisher, the editors and the reviewers. Any product that may be evaluated in this article, or claim that may be made by its manufacturer, is not guaranteed or endorsed by the publisher.

Copyright © 2022 Li, Zhang, Liu, Zhang, Liu, Qi, Zhang and Li. This is an open-access article distributed under the terms of the Creative Commons Attribution License (CC BY). The use, distribution or reproduction in other forums is permitted, provided the original author(s) and the copyright owner(s) are credited and that the original publication in this journal is cited, in accordance with accepted academic practice. No use, distribution or reproduction is permitted which does not comply with these terms.

GLOSSARY

MGMT	O-6-methylguanine-DNA methyltransferase
TME	tumor microenvironment
TAMs	tumor-associated macrophages
BBB	blood–brain barrier
ITGA5	integrin subunit alpha 5
TCGA	The Cancer Genome Atlas
GTEx	Genotype-Tissue Expression Project
CGGA	Chinese Glioma Genome Atlas
GEO	Gene Expression Omnibus
RMA	robust multichip average
FPKM	fragments per kilobase million
TPM	transcripts per kilobase million
OS	Overall survival
IF	Immunofluorescence
DAPI	4',6-Diamidino2-phenylindole dihydrochloride
CNV	copy number variation
GISTIC	Genomic Identification of Significant Targets in Cance
ESTIMATE	Estimation of Stromal and Immune cells in Malignant Tumor tissues using Expression
TIMER	Tumor Immune Estimation Resource
GSVA	gene set variation analysis
ssGSEA	single sample gene set enrichment analysis
GO	Gene Ontology
KEGG	Kyoto Encyclopedia of Genes and Genomes
GSEA	Gene set enrichment analysis
GDSC	Genomics of Drug Sensitivity in Cancer
IC50	half-maximal inhibitory concentration
CHOL	cholangiocarcinoma
HNSC	head and neck squamous cell carcinoma
KIRC	kidney renal clear cell carcinoma
LAML	acute myeloid leukemia
LIHC	liver hepatocellular carcinoma
PAAD	pancreatic adenocarcinoma
TGCT	testicular germ cell tumors
LGG	lower-grade glioma
GBM	glioblastoma multiforme
IDH	isocitrate dehydrogenase

(Continued)

Continued

ACC	adrenocortical carcinoma
BLCA	bladder urothelial carcinoma
BRCA	breast invasive carcinoma
CESC	cervical squamous cell carcinoma and endocervical adenocarcinoma
COAD	colon adenocarcinoma
KIRP	kidney renal papillary cell carcinoma
LUAD	lung adenocarcinoma
LUSC	lung squamous cell carcinoma
MESO	mesothelioma
OV	ovarian serous cystadenocarcinoma
STAD	stomach adenocarcinoma
THCA	thyroid carcinoma
UCEC	uterine corpus endometrial carcinoma
UVM	uveal melanoma
JAK	Janus kinase
STAT	signal transducer and activator of transcription
IL-4	interleukin-4
TTN	titin
EGFR	epidermal growth factor receptor
PTEN	phosphatase and tensin homolog
ATRX	alpha-thalassemia/mental retardation syndrome x-linked chromatin remodeler
CIC	capicua transcriptional repressor
FUBP1	far upstream element binding protein 1
COL6A3	collagen type VI alpha 3 chain
PD-1	programmed cell death 1
PD-L1	Programmed cell death 1 ligand 1
CTLA-4	cytotoxic T-lymphocyte associated protein 4
FAK	focal adhesion kinase
MAPK	Mitogen-Activated Protein Kinase
Erk	Extracellular Regulated Kinase
PI3-K	phosphatidylinositol 3-kinase
Akt	protein kinase B
SAPK	stress-activated MAP kinases
JNK	c-Jun N-terminal kinase
ROC	receiver operating characteristic
AUC	area under the curves
IDH1	isocitrate dehydrogenase [NADP] cytoplasmic
OBSCN	obscurin
Tregs	regulatory T cells
TIDE	Tumor Immune Dysfunction and Exclusion

frontiers in Oncology

ORIGINAL RESEARCH
published: 18 March 2022
doi: 10.3389/fonc.2022.814742

The Role of m5C-Related lncRNAs in Predicting Overall Prognosis and Regulating the Lower Grade Glioma Microenvironment

Hongshu Zhou[1], *Ming Meng*[1], *Zeyu Wang*[1], *Hao Zhang*[1], *Liting Yang*[1,2,3,4], *Chuntao Li*[1,2,3,4]* *and Liyang Zhang*[1,2,3,4]*

[1] Department of Neurosurgery, Xiangya Hospital, Central South University, Changsha, China, [2] Hypothalamic Pituitary Research Center, Xiangya Hospital, Central South University, Changsha, China, [3] Brain Tumor Center, Xiangya Hospital, Central South University, Changsha, China, [4] National Clinical Research Center for Geriatric Disorders, Xiangya Hospital, Central South University, Changsha, China

OPEN ACCESS

Edited by:
Wen Cheng,
The First Affiliated Hospital of China Medical University, China

Reviewed by:
Pan Chen,
Hunan Cancer Hospital, China
Xiaoping Liu,
Guangzhou Medical University, China

***Correspondence:**
Liyang Zhang
zhangliyang@csu.edu.cn
Chuntao Li
chuntao.li@csu.edu.cn

Specialty section:
This article was submitted to Cancer Immunity and Immunotherapy, a section of the journal Frontiers in Oncology

Received: 14 November 2021
Accepted: 17 February 2022
Published: 18 March 2022

Citation:
Zhou H, Meng M, Wang Z, Zhang H, Yang L, Li C and Zhang L (2022) The Role of m5C-Related lncRNAs in Predicting Overall Prognosis and Regulating the Lower Grade Glioma Microenvironment. Front. Oncol. 12:814742. doi: 10.3389/fonc.2022.814742

Glioma is the most lethal primary brain tumor with a poor prognosis and high recurrence rate. Enormous efforts have been made to find therapeutic targets for gliomas. In the current study, we identified m5C-related lncRNAs through Pearson correlation analysis by the criteria |R| >0.5 and p<0.001 in TCGA LGG and CGGA325 datasets. We then established an eight-lncRNA m5C-related prognostic signature (m5C LPS) through lasso cox regression analysis and multivariate analysis. The performance of the signature was confirmed in the CGGA325 dataset and evaluated in differential subgroups divided by relevant clinicopathological characteristics. Patients were then divided into high and low risk groups using risk scores calculated with the signature. Next, we performed GO, KEGG and gene set enrichment analysis (GSEA) and identified the m5C LPS to be related with glioma microenvironment, immune response, EMT, cell cycle, and hypoxia. Correlation of the risk groups with immune cell infiltration, somatic mutation, and CNVs was then explored. Responses to immuno- and chemotherapies in different risk groups were evaluated using submap and pRRophetic R packages respectively. The high-risk group was more sensitive to anti-CTLA4 therapy and to compounds including Temozolomide, Bleomycin, Cisplatin, Cyclopamine, A.443654 (Akt inhibitor), AZD6482 (PI3K inhibitor), GDC0941(PI3K inhibitor), and metformin. We present for the first time a m5C-related lncRNA signature for lower grade glioma patient prognosis and therapy response prediction with validated performance, providing a promising target for future research.

Keywords: lower grade glioma, 5-methylcytosine, lncRNA, tumor microenvironment, prognosis

INTRODUCTION

Glioma is the most common type of primary malignant tumor in the central nervous system with a poor prognosis and a high recurrence rate. Lower grade glioma (LGG) refers to a subtype of glioma with WHO grade II or III that presents a less invasive nature and generally better prognosis. Even with surgical resection, chemotherapy and radiotherapy, a large portion of this heterogeneous group of

tumors will evolve into high grade glioblastomas. Efforts have been made in developing novel treatment strategies and effective biomarkers for individualized glioma therapy (1). Current biomarkers for disease stratification and individualized treatment include IDH1 mutation, 1p/19q codeletion, MGMT promoter methylation, TP53 and TERT promoter mutation.

RNA modifications regulate multiple cellular processes under biological and pathological conditions. 5-methylcytosine (m5C) is one of the modes of RNA modification mainly accumulating in the vicinity of the 3'UTR, 5'UTR, and near the binding site of Argonaute (2). It confers conserved, tissue-specific and dynamic transcriptional regulation effects including structural stability and metabolism of RNA, tRNA recognition, and stress response (3). m5C modifications are catalyzed by the NSUN family proteins including NSUN1-7 and DNA methyltransferase homologue DNMT2 (4), DNMT1, DNMT3A, and DNMT3B. The m5C RNA methyltransferases display different cellular functions. NSUN1 and NSUN5 modify cytoplasmic ribosomal RNAs; NSUN2, NSUN6 and DNMT2 methylate cytoplasmic transfer RNAs; NSUN3 and NSUN4 install m5C in mitochondrial RNAs (5). Aly/REF export factor ALYREF is reported to be a m5C binding protein facilitating the export of m5C modified mRNAs (6). Depletion of this 'reader' protein leads to retention of m5C methylated mRNAs. Another reader of m5C modifications is YBX1 which maintains the stability of target mRNA (7). Aberrant m5C RNA modification is implicated in multiple diseases including cancer (8). Bioinformatics analyses have implicated m5C regulators in prognosis for lung adenocarcinoma (9), hepatocellular carcinoma (10), glioma (7), and others.

Long non-coding RNAs (lncRNAs) are a subgroup of RNAs with over 200 nucleotides that exert non-coding functions. LncRNAs are ideal potential biomarkers for their specificity of expression in different tissues. Furthermore, lncRNAs exert tumorigenic or metastatic effects through different mechanisms including epigenetic modification, post-transcriptional modification, RNA decay or scaffold, and cis-regulation (11). Dysregulation of lncRNAs has been reported to play important roles in glioma genesis. The expression of lncRNAs such as H19, HOXA11-AS, MALAT1, and CRNDE are positively correlated with glioma. MEG3 is highly expressed in normal brain tissue while downregulated in glioma (12). HOXA11-AS is a cell cycle-related lncRNA and a biomarker for glioma prognosis. MALAT1 is reported to be glioma suppressive through attenuating ERK/MAPK-mediated growth and MMP2 mediated invasiveness (13). An NSUN2 methylated lncRNA, NMR, is highly expressed in esophageal squamous cell carcinoma and promotes tumor cell migration and invasion (14). NSUN2 is also reported to target lncRNA H19 and increase its stability through m5C modification. The m5C-modified lncRNA H19 can then be bound to an oncoprotein leading to Myc accumulation, thus exerting oncogenic effects (15). However, there are few studies on the relationship of m5C-related lncRNAs and glioma.

In the current study, we identified eight m5C-related lncRNAs using Pearson correlation analysis and established a m5C related lncRNA prognostic signature (m5C LPS). Performance of the m5C LPS was confirmed in the CGGA325 dataset and evaluated in subgroups divided by several clinicopathological characteristics. Patients were then divided into high and low risk groups using risk scores calculated with the signature. We performed GO, KEGG and gene set enrichment analysis (GSEA) and found that m5C related lncRNAs were related with glioma microenvironment, immune response, EMT, cell cycle, and hypoxia. Correlations of the risk groups with immune cell infiltration, somatic mutation, and copy number variations (CNV) were then explored. Deletions on Chr 9p, 10, 13q and 14q and amplifications on Chr 7, 19, 20 were observed mainly in the high-risk group. CDKN2B, PTEN, EGFR, and IGF2R showed higher CNV rates in the high-risk group. Responses to immunological therapies and chemotherapeutics in different risk groups were evaluated. The high-risk group was found to be more responsive to anti-CTLA4 therapy and to Temozolomide, Bleomycin, Cisplatin, Cyclopamine, A.443654 (Akt inhibitor), AZD6482 (PI3K inhibitor), GDC0941(PI3K inhibitor), and metformin.

MATERIALS AND METHODS

Data Acquisition and Preparation

Transcriptome profiling data of LGG were downloaded from UCSC Xena website (http://xena.ucsc.edu) as a training set. Corresponding clinical data were also retrieved. CGGA325 expression and clinical information data were downloaded from the CGGA website (http://www.cgga.org.cn). Somatic mutation and copy number variations (CNVs) data were obtained from the TCGA website (https://portal.gdc.cancer.gov/). Somatic mutation data was analyzed using the 'maftools' R package. Significant copy number variations were detected with GISTIC 2.0 from GenePattern website (https://www.genepattern.org/). Inclusion criteria: TCGA-LGG cases with complete clinical information, corresponding somatic mutation and CNV data were included in the study. CGGA325 data of WHO grade II and III glioma patients with complete clinical information were filtered for use.

Identification of m5C-Related lncRNAs

LGG transcription data was annotated using Genome Reference Consortium Human Build 38 (GRCh38) to identify lncRNAs and protein coding genes in the TCGA LGG dataset. Regulators of m5C were acquired in previous literature which included NSUN1-7, DNMT1, DNMT2, TRDMT1, DNMT3A, DNMT3B, TET1, TET2, TET3, ALYREF, and YBX1. Next, we performed pearson correlation analysis in the TCGA LGG dataset to identify m5c related lncRNAs by the criteria $|R|>0.5$ and $p<0.001$. Univariate cox regression analysis was then performed to acquire m5c-related lncRNAs significantly related to patient prognosis ($p<0.05$). An identical procedure was performed in LGG samples of CGGA325 dataset and m5C related lncRNAs in the CGGA325 dataset were acquired. Finally prognostic m5C-related lncRNAs were obtained through intersecting results acquired from the TCGA and CGGA datasets.

Construction of the Prognostic Signature

Lasso regression analysis and multivariate cox regression analysis were utilized to construct a risk score signature in the TCGA dataset

following the formula: *Risk score* = $\Sigma_{i=1}^{n}$ ($coef_i * exp_i$) with $coef_i$ and exp_i representing survival correlation regression coefficient and expression value of each lncRNA, respectively. Risk score was then calculated for each patient in the training set. The median value of risk scores was set as the cutoff to divide the training set into high and low risk groups. Survival analysis was performed and time dependent receiver operating characteristic (ROC) curves were plotted to evaluate the prognostic ability of the signature. Identical analyses were performed in the validation set to verify the signature prognostic value.

Multivariate Cox regression was then performed to establish a nomogram with the m5C-related lncRNAs risk score and clinical features including age, sex, and WHO grade. A calibration plot and concordance index (C-index) were utilized to examine the predictive accuracy of the nomogram using R package 'rms'. ROC curves and the area under curve (AUC) were also evaluated with R package 'timeROC' to review the prognostic ability of the nomogram.

Functional Analyses

In order to explore differential gene pathways between the high and low risk groups defined by the m5C LPS, Gene Ontology (GO) and Kyoto Encyclopedia of Genes and Genomes (KEGG) pathway enrichment analyses were performed using the 'clusterProfiler' R package with BH adjusted p value <0.01. Gene set enrichment analysis was performed with 1000 permutations, p value < 0.05 and false discovery rate < 0.25 using the GSEA 4.1.0 software downloaded from the Broad Institute website (http://software.broadinstitute.org/gsea/).

Estimation of Immune Infiltration, Somatic Mutation, CNVs and Prediction of Therapy Response

CIBERSORTx was used to estimate the abundance of 22 types of immune cells in the tumor mass (16). CNVs of the high and low risk groups were analyzed with the GISTIC 2.0 module on GenePattern website. The SubMap module on GenePattern website was utilized to evaluate response to immune checkpoint inhibitors of the two risk groups in the TCGA LGG dataset (17, 18) with default parameters.

Sample Collection

We collected 27 LGG samples from the Department of Neurosurgery, Xiangya Hospital, Central South University. The current study was approved by the Ethics Committee of Xiangya Hospital (No. 201703478). All participants provided informed consent and approval.

RNA Extraction and rt-qPCR Analysis

Total RNA was extracted using TRIzol Reagent according to manufacturer's instructions. RevertAid First Strand cDNA Synthesis Kit (ThermoFisher)was used in reverse transcription reaction. ChamQ Universal SYBR qPCR Master Mix (Vazyme, China) and StepOne Real-time PCR systems (Applied Biosystems) were used for rt-qPCR reaction. The experimental condition was set as: 95°C 60s, 95°C 15s, and 60°C 30s for 40 cycles. Reactions were repeated in triplicate for each sample. Expression levels were calculated using $2^{-\Delta\Delta Ct}$ method. Primer sequences are listed in **Supplementary Table S1**.

Statistical Analysis

Statistical analysis was performed using R software (version 4.0.0). Univariate and multivariate Cox proportional hazards models and lasso regression were used to determine significant prognostic lncRNAs. The Kaplan–Meier curve was used for comparison of overall survival of different subgroups. ROC curve was used to evaluate the predictive efficiency of the m5C-LPS. GSEA 4.1.0 software was used for functional annotation. The rt- qPCR results were analyzed with Student's t-test. A $p < 0.05$ was considered statistically significant.

RESULTS

Construction of m5c-Related lncRNAs Signature in LGG Patients

A study flowchart is shown in **Figure 1A**. Gene expression data of 504 LGG samples with complete clinical information was retrieved from TCGA database. We performed Pearson correlation analysis by the criteria $|R|>0.5$ and $p<0.001$ acquiring 1121 m5C-related lncRNAs. We then utilized univariate regression analysis ($p<0.05$) and acquired 607 prognostic m5c-related lncRNAs. Gene expression and clinical data of 172 LGG samples was retrieved from the CGGA325 dataset (**Table 1**). Pearson correlation analysis ($|R|>0.5$, $p<0.001$) and univariate regression analysis ($p<0.05$) yielded 271 prognostic m5C-related lncRNAs. Examining the results from analyses of TCGA and CGGA datasets, 138 common m5C-related prognostic lncRNAs were retrieved. We utilized LASSO Cox regression analysis to filter out prognostic m5C-related lncRNAs yielding 18 lncRNAs (**Figures 1B, C**). We applied multivariate regression analysis to the 18 m5C-related prognostic lncRNAs and constructed a m5C-related LPS consisted of eight lncRNAs (**Table 2**). A heatmap of the correlations between the eight lncRNAs and m5C regulators was plotted (**Figure 1D**).

Evaluation and Validation of the m5C-Related lncRNAs Prognostic Signature

Risk scores of patients in the TCGA dataset were calculated according to the m5C LPS. Patients were divided into high and low risk groups by the median of risk scores. Survival analysis using Kaplan-Meier curves revealed longer overall survival time in the low-risk group (**Figure 2A**). Distribution of risk scores and survival status was plotted in **Figure 2B**, indicating poorer survival in high-risk patients. We then utilized ROC curves to evaluate the prognostic ability of the m5C LPS. One-, three-, and five-year AUC was 0.873, 0.865, and 0.772, respectively (**Figure 2C**), indicating a promising prognostic ability for m5C LPS.

Validation of the m5C LPS was conducted in CGGA325 dataset from which we extracted data of 172 LGG patients. We calculated risk scores with the m5C LPS and divided patients into high and low risk groups in the aforementioned manner.

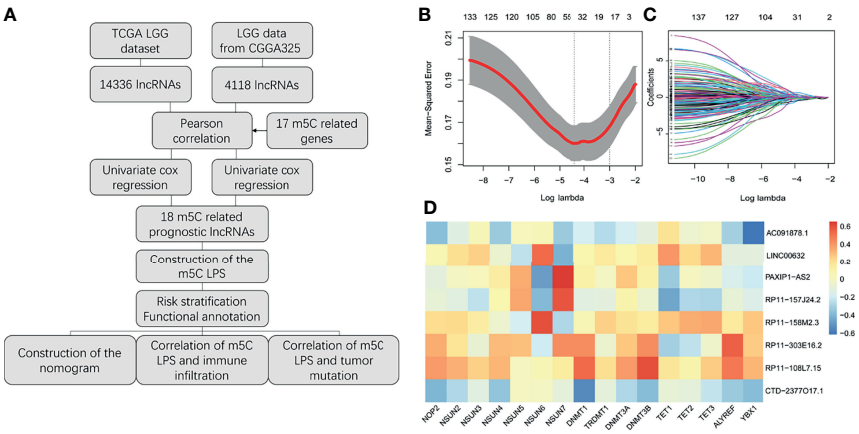

FIGURE 1 | Construction of the m5C related lncRNAs prognostic signature. **(A)** Study flow chart. **(B, C)** Lasso regression analysis for m5C LPS construction. **(D)** Heatmap of the correlations of m5C-related lncRNAs and m5C regulators.

Consistently, survival analysis showed significantly longer OS in the low-risk group than the high-risk group (**Figures 2D, E**). Moreover, one-, three-, and five-year AUC being 0.781, 0.825, 0.782 respectively proved the m5C LPS had a robust prognostic ability in the CGGA dataset (**Figure 2F**). We further validated expressions of the eight lncRNAs in 27 LGG samples collected from the Department of Neurosurgery, Xiangya Hospital of Central South University (**Supplementary Figure 2**). LncRNAs AC091878.1 and RP11-108L7.15 identified as protective factors in the m5C LPS were found to be significantly higher in WHO Grade II tumors while LINC00632 and PAXIP.AS1 presented significantly higher expression in WHO Grade III gliomas.

Correlation of m5C-Related lncRNAs and Clinicopathological Features

We sought to explore correlation of the m5C LPS with clinicopathological features. MGMT methylation, 1p/19q codeletion, IDH status, and WHO grade were significantly different between the high and low risk groups (**Figure 3A**). Correlation of OS with expression of each lncRNA in the m5C LPS was also investigated through Kaplan-Meier curves (**Figure 3B**). Patients were divided into high and low expression groups according to the expression of each lncRNA. Overall survival was significantly longer in the low expression group for lncRNAs PAXIP1-AS2, RP11-303E16.2, RP11-157J24.2, RP11-108L7.15, while with lncRNAs AC091878.1, LNC00632, RP11-158M2.3, and CTD-2377O17.1 the overall survival was significantly longer in the high expression group, indicating their protective roles in glioma. We then investigated the differential expression of each lncRNA in subgroups divided by WHO grade, IDH mutation, 1p19q codeletion, and MGMT methylation status (**Figure 3C**). Expression of RP11-108L7.15 was only significantly different between WHO grade II and III with no significant difference

TABLE 1 | Clinical characteristics of cases in TCGA, CGGA and collected glioma samples.

		TCGA LGG (n = 504)		LGG cases in CGGA325 (n = 172)		Clinical samples (n = 27)	
		Cases	Percentage	Cases	Percentage	Cases	Percentage
Age	≥40	267	53.0%	84	48.8%	19	70.4%
	<40	237	47.0%	88	51.2	8	29.6%
Gender	Female	280	55.6%	66	38.4%	12	44.4%
	Male	224	54.4%	106	61.6%	15	55.6%
WHO	II	245	48.6%	98	57.0%	13	48.1%
Grade	III	259	51.4%	74	43.0%	14	51.9%
IDH mutation	Mutant	407	80.8%	127	73.8%	7	25.9%
	Wildtype	97	19.2%	44	25.6%	6	22.2%
	NA			1		14	
1p19q codeletion	Codeletion	163	32.3%	55	32.0%	–	–
	Non-codeletion	341	67.7%	115	66.9%		
	NA			2			
MGMT-nip methylation	Methylated	416	82.5%	85	49.4%	9	33.3%
	Non-methylated	88	17.5%	71	41.3%	4	14.8%
	NA			6		15	

TABLE 2 | The eight prognostic m5C-related lncRNAs.

	coef	exp(coef)	se(coef)	z	p
AC091878.1	-1.3674	0.2548	0.3093	-4.421	9.84e-06
LINC00632	0.5022	1.6523	0.2221	2.261	0.02377
PAXIP1-AS2	0.7085	2.0310	0.1832	3.866	0.00011
RP11-157J24.2	0.3221	1.3801	0.1211	2.660	0.00782
RP11-158M2.3	-0.4040	0.6676	0.1013	-3.988	6.67e-05
RP11-303E16.2	0.7230	2.0605	0.1684	4.294	1.76e-05
RP11-108L7.15	-0.8362	0.4334	0.3211	-2.604	0.00922
CTD-2377O17.1	-0.6980	0.4976	0.2523	-2.767	0.00566

between IDH, 1p/19q codeletion or MGMT methylation subgroups. Expression of RP11-158M2.3 was significantly different between WHO grade, IDH and MGMT methylation subgroups. Significant differences were also observed in the expression of CTD-2377O17.1 between WHO grade, IDH and 1p19q codeletion subgroups. The other lncRNAs from the m5C LPS all showed significant differences in subgroups of WHO grade, IDH, 1p19q codeletion and MGMT methylation, indicating their differential roles in gliomas.

We also investigated the distribution of m5C LPS risk scores between different clinicopathological subgroups (**Figures 4A–F**). Risk score was significantly higher in the following subgroups namely, IDH wild type, WHO grade III, 1p19q non-codeletion, MGMT promoter unmethylated, and age > 40. Survival analysis was also performed in each subgroup *via* KM curve and proved the m5C LPS had robust prognostic ability in each subgroup of different clinicopathological characteristics (**Figures 4G–L**).

Construction of the Nomogram

Univariate and multivariate analyses were used to investigate the prognostic value of the m5C LPS (**Figure 5A**). In univariate analysis, a hazard ratio (HR) of 1.12 (CI: 1.1-1.15) with p value <0.01 indicated that the m5C LPS risk score is a prognostic indicator. In multivariate analysis, the risk score presented an HR of 1.07 (CI: 1.05-1.1) with a p value <0.01 indicating the risk score to be a prognostic indicator independent of age, grade and MGMT status. An ROC curve was implemented to evaluate the specificity and sensitivity of prognostic indicators and manifested a higher AUC for the risk score than other clinicopathological features (**Figure 5B**). We then constructed a nomogram with the m5C LPS risk score and other clinicopathological features (**Figure 5D**). A C-index of 0.823 and conformity in nomogram-predicted and actual 1, 3, 5-year OS of patients (**Figure 5C**) indicated a promising prognostic ability.

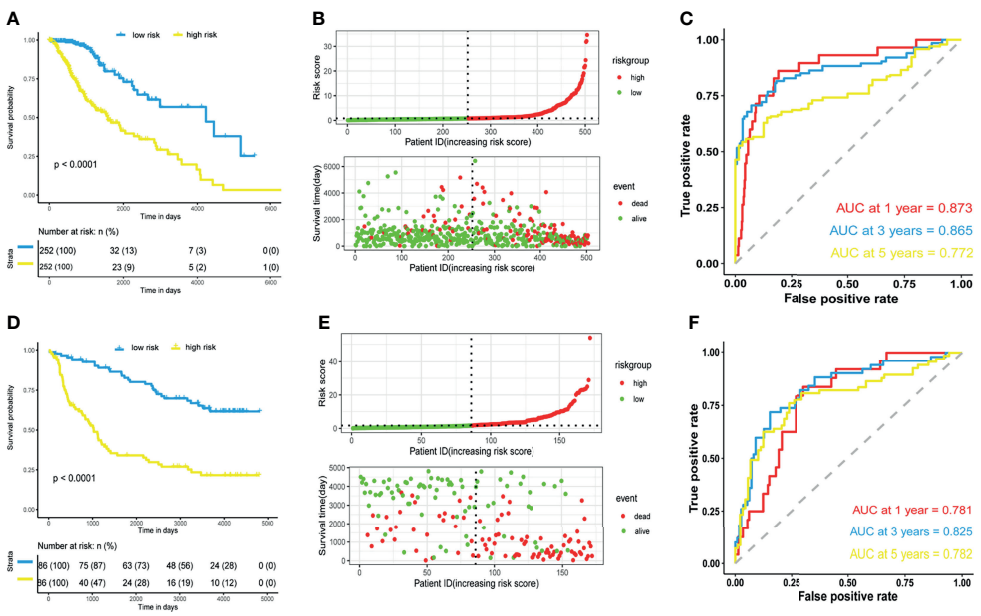

FIGURE 2 | Prognostic performance of the m5C-related lncRNAs signature. **(A, D)** Kaplan-Meier curve showing a better overall survival in low-risk group than the high-risk group in the TCGA and CGGA datasets. **(B, E)** Risk score distribution of patients based on m5C-related lncRNAs signature and survival status in the TCGA and CGGA datasets. **(C, F)** Receiver operating characteristic (ROC) curves showing performance of the signature in predicting 1/3/5-year overall survival in the TCGA and CGGA datasets.

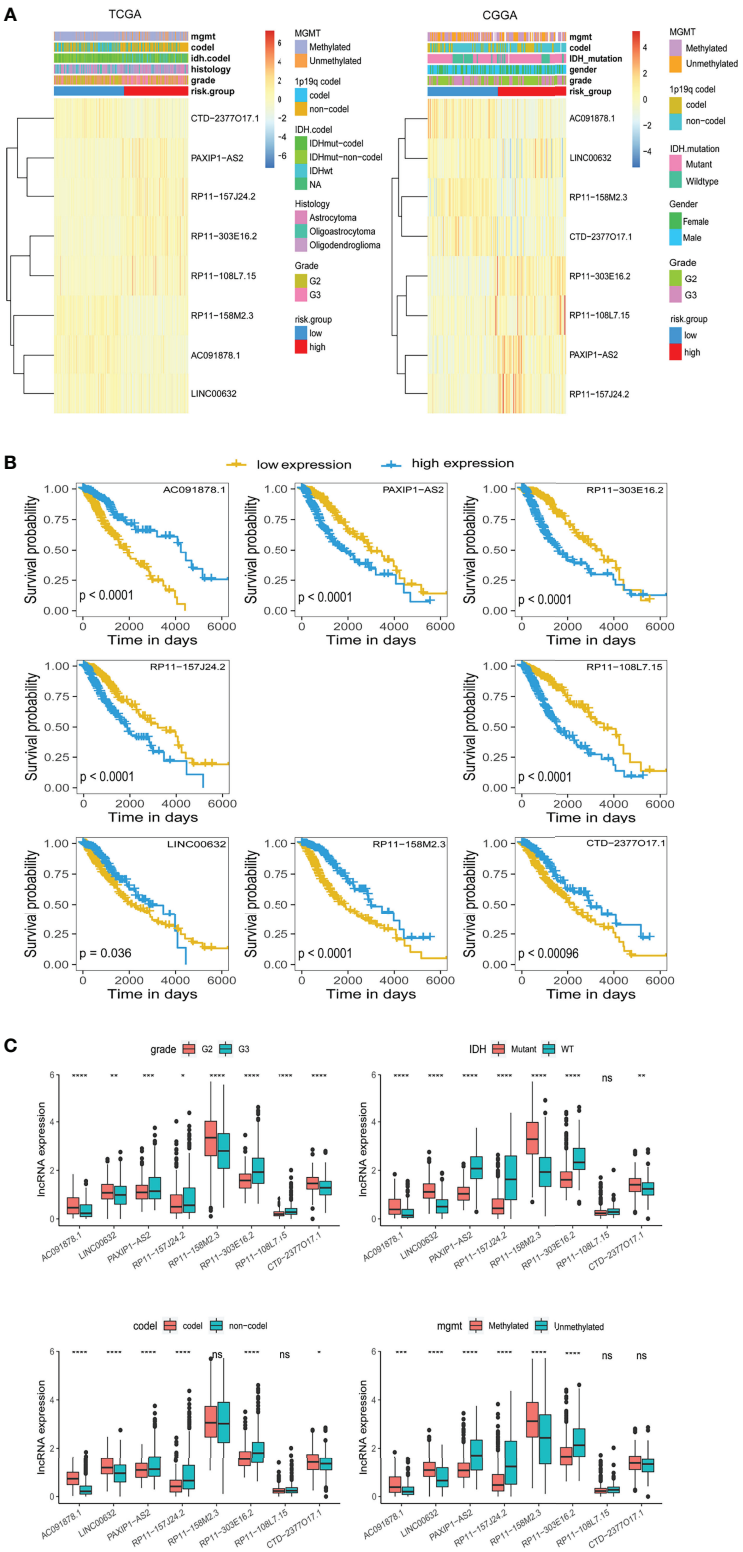

FIGURE 3 | Differential expression of lncRNAs constituting the m5C LPS. **(A)** Heatmaps showing m5C-related lncRNAs expression and clinicopathological features in the TCGA and CGGA datasets. **(B)** Kaplan-Meier curves showing the overall survival of patients grouped by expression of each m5C-related lncRNA in the TCGA dataset. **(C)** Differential expression of the eight m5C-related lncRNAs in WHO grade, IDH, 1p/19q codeletion, and MGMT promoter methylation subgroups. *p<0.5, **p<0.01, ***p<0.001, ****p<0.0001, ns, no significance.

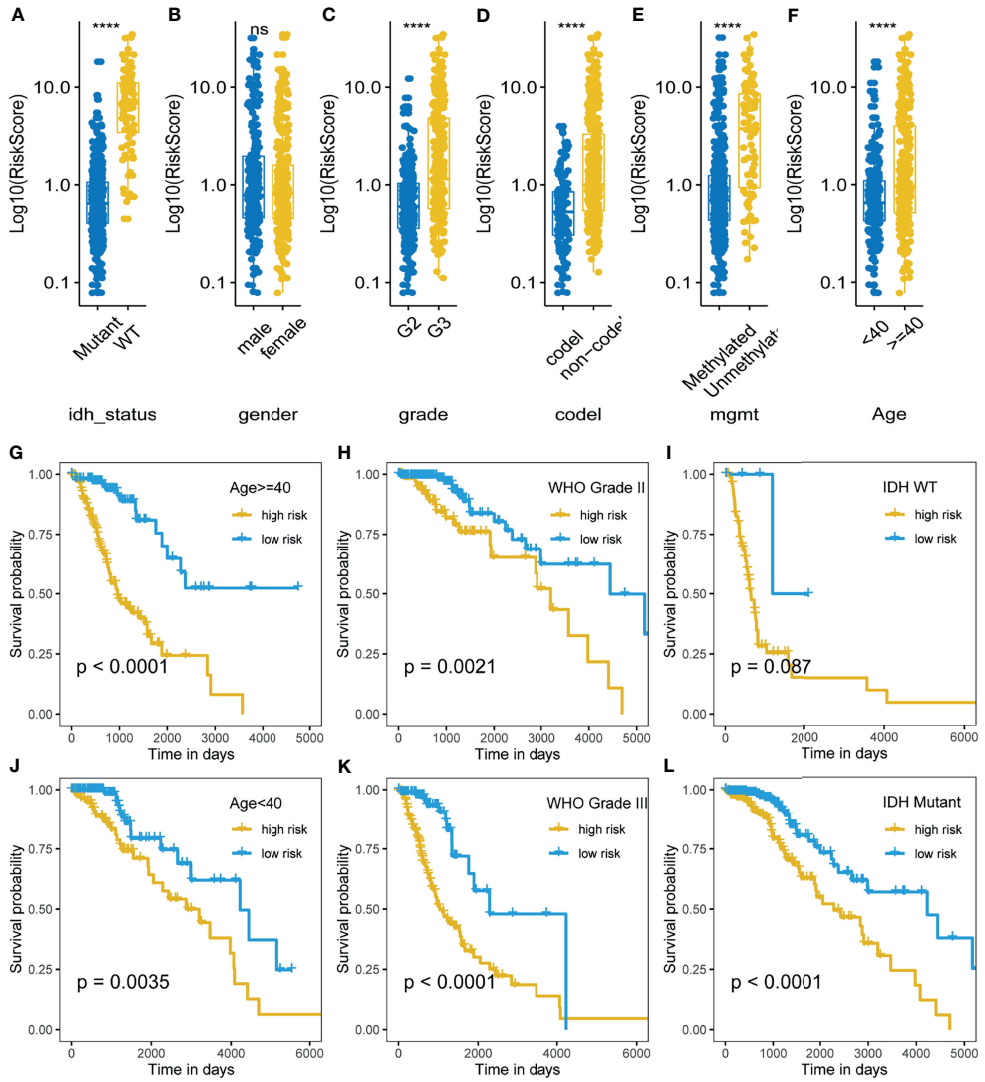

FIGURE 4 | Correlation and prognostic performance of the m5C LPS. **(A–F)** Different risk scores between patients grouped by clinicopathological features including IDH mutation status, 1p/19q codeletion status, MGMT methylation status, WHO grade, age and gender. **(G–L)** Kaplan-Meier curves showing stable performance of the signature in differential subgroups of LGG patients including age, WHO grade, and IDH status. ****p<0.0001, ns, no significance.

Functional Annotation of Low and High-Risk Groups

We performed GO, KEGG and GSEA analyses to identify pathways activated in the high-risk group. Th1, Th2 and Th17 cell differentiation, ECM-receptor interaction pathways were enriched in the high-risk group. GO showed extracellular matrix organization, epithelial to mesenchymal transition (EMT), and interferon gamma mediated signaling pathway were enriched in the high-risk group. GSEA analysis identified glycolysis, epithelial to mesenchymal transition (EMT), inflammatory response, interferon gamma response, PI3K-AKT-mTOR signaling, IL6-JAK-STAT3 signaling, IL2-STAT3 signaling, E2F targets, interferon alpha response, G2M checkpoint, and hypoxia were positively correlated with high-risk group (**Figures 6A–C**). The analyses indicated m5C related lncRNAs were possibly related with the glioma tumor microenvironment, immune response, EMT, cell cycle, and hypoxia.

Correlation of m5C-Related lncRNAs With the Glioma Tumor Microenvironment and Response to Immunotherapies

We next investigated the correlation of m5C related lncRNAs with glioma immune infiltration using CIBERSORTx. An overall high proportion of M2 macrophages, monocytes, CD4 memory T cells, activated and resting mast cells in LGG is shown in **Figure 7A**. Monocytes, memory B cells, activated mast cells and naïve CD4 T cells presented a significantly higher proportion in

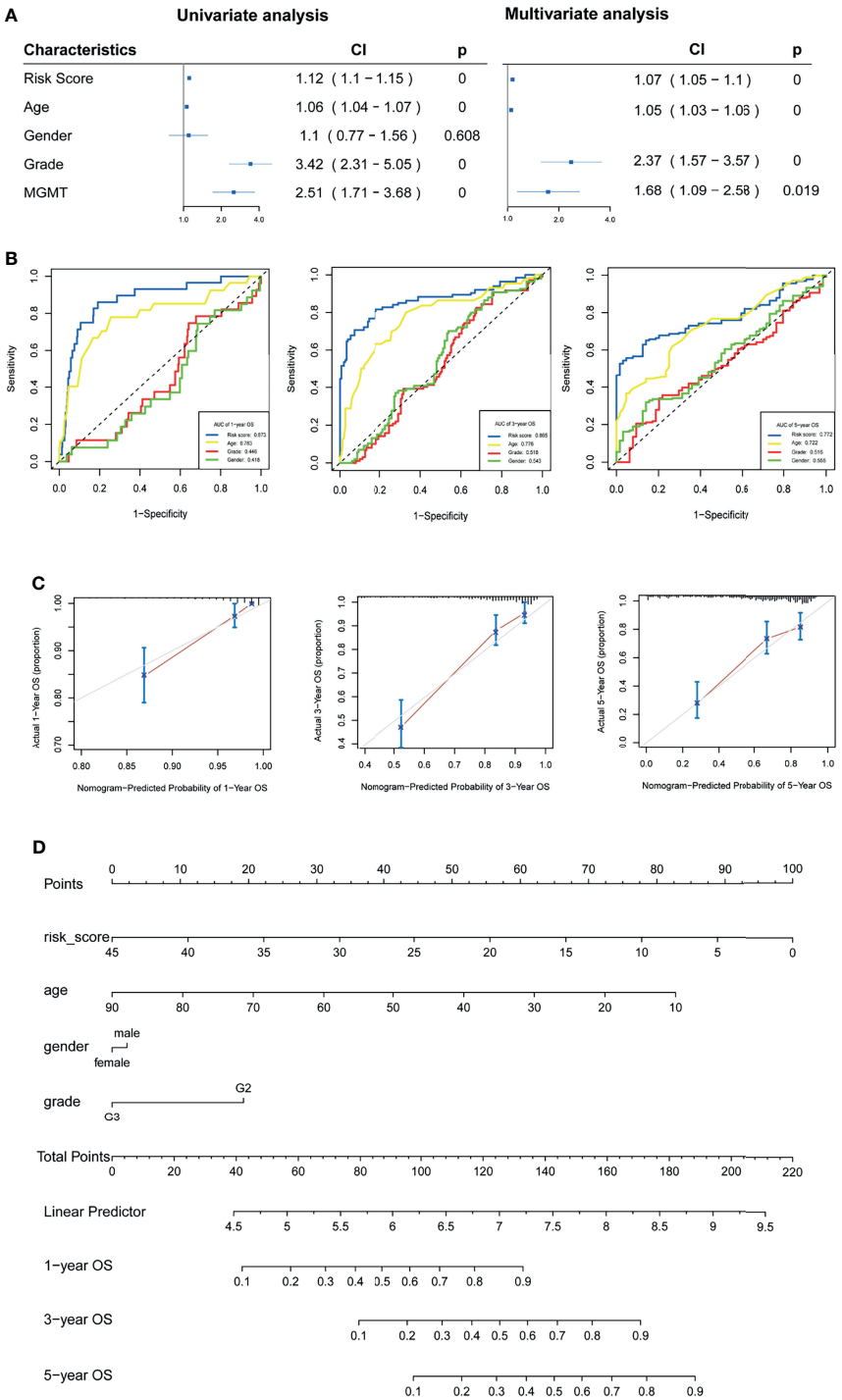

FIGURE 5 | Verification of the m5C LPS and construction of the nomogram. **(A)** Forest plots showing the results of univariate and multivariate Cox regression analyses on the prognostic performance of the risk score and clinicopathological features. **(B)** ROC curves showing prediction performance of the risk score and clinicopathological features. **(C)** Calibration curve of the nomogram for 1,3,5-year OS. **(D)** Construction of the nomogram using risk score and clinicopathological features.

the low-risk group ($p<0.05$) while M1 macrophages, CD8 T cells, resting mast cells, activated and resting CD4 memory T cells manifested a higher infiltration in the high-risk group ($p<0.05$). A positive correlation with the risk score was found in infiltration of M1 macrophages, CD8 T cells, and resting CD4 T cells, while a negative correlation was identified in infiltration of CD4 naïve T cells, monocytes, and activated mast cells (**Figure 7B**). HLA family proteins were also found to be significantly higher in the

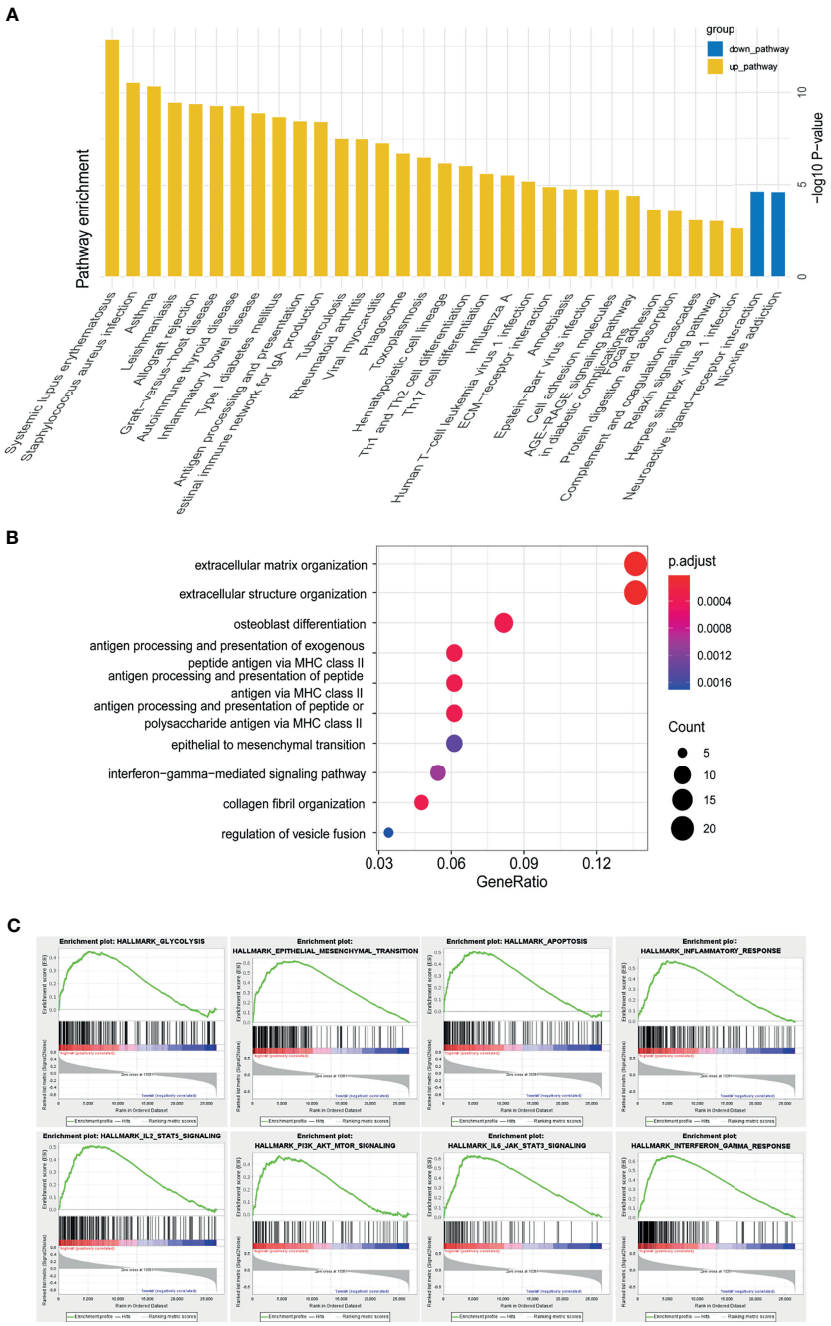

FIGURE 6 | Functional annotation of risk groups identified through the m5C LPS. **(A)** KEGG pathway enrichment analysis between high and low risk groups. **(B)** Dotplot of GO biological processes. **(C)** GSEA analysis showing pathways enriched in the high-risk group.

high-risk group (**Figure 7C**). Immune checkpoint proteins including LAG3, CTLA4, HAVCR2, PDCD1, and CD274 also showed significantly higher expression in the high-risk group than in low-risk group (**Figure 7D**).

Research indicates therapeutic effects for anti-PD1 and anti-CTLA4 therapies in glioma (19). We therefore explored possible correlations of the m5C LPS with anti-PD1 and anti-CTLA4 therapies using a subclass mapping algorithm (20). We compared the expression matrix of high and low risk groups to that of a melanoma dataset in which patients underwent anti-PD1 and anti-CTLA4 therapies (17). High risk group patients were generally more responsive to anti-CTLA4 (nominal p value = 0.012) and anti-PD1 therapies (nominal p value = 0.14) (**Figure 7E**).

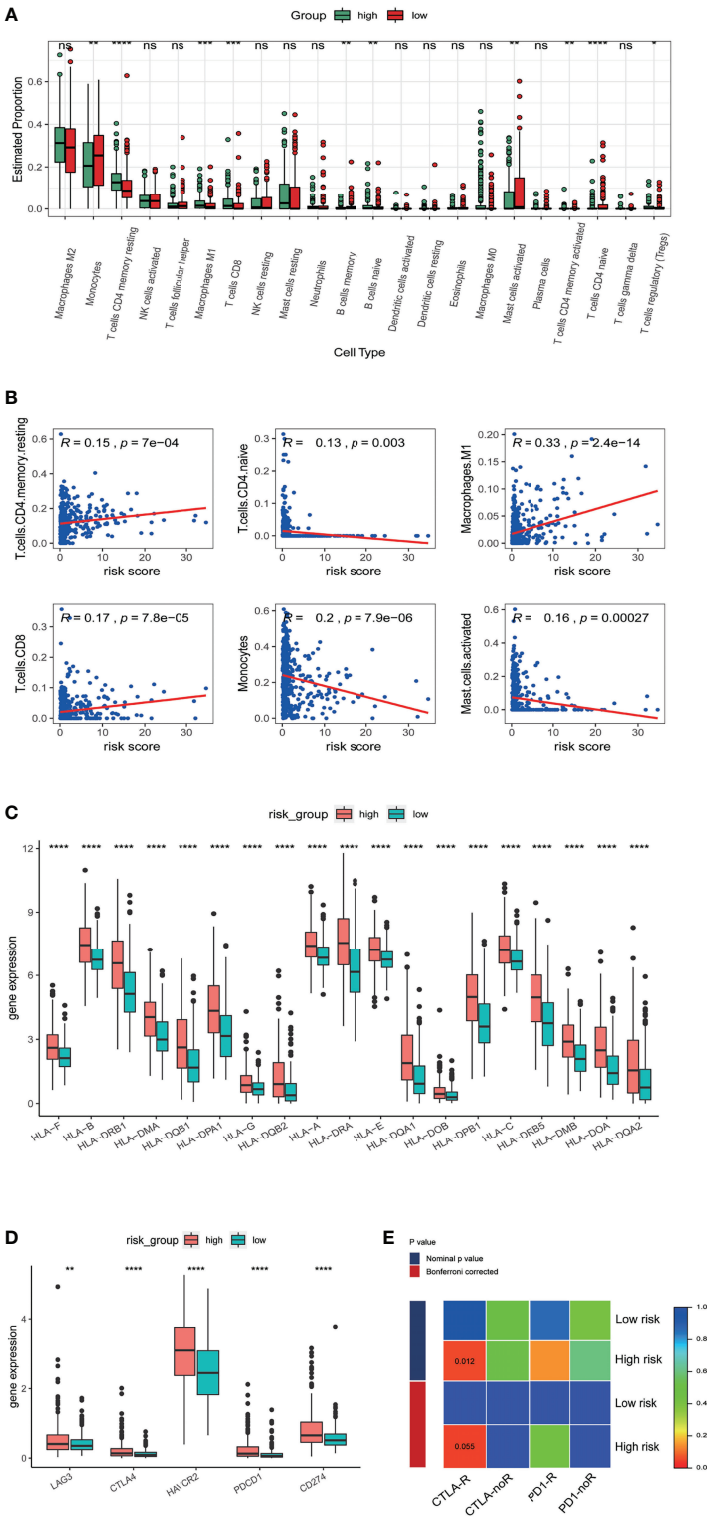

FIGURE 7 | Correlation of the risk score with immune cell infiltration and prediction of responses to immune checkpoint inhibitors. **(A)** Estimated proportion of 22 tumor infiltrating immune cells in high and low risk groups. **(B)** Correlation of risk score with proportion of six tumor-infiltrating immune cell types. **(C)** The expression levels of HLA family genes in low- and high-risk groups in TCGA database. **(D)** The expression levels of CD274 (PD-L1), CTLA4, HAVCR2, LAG3, and PDCD1 (PD1) in low- and high-risk groups in TCGA database. **(E)** Sensibility of patient responses to PD1 and CTLA4 inhibitors in different risk groups. *p<0.5, **p<0.01, ***p<0.001, ****p<0.0001, ns, no significance.

Differential Somatic Mutations and Copy Number Variations in Different Risk Groups

The 2016 WHO classification of CNS tumors incorporated molecular characteristics including somatic mutations and copy number variations (CNVs) with histological features for a summed-up diagnosis. We analyzed the somatic mutations and CNVs in the current study and explored their relationship with the m5C LPS risk groups. We compared the top differentially mutated genes in the high and low risk groups. IDH1, CIC, and FUBP1 had higher mutation rates in the low-risk group while EGFR, NF1 and PTEN showed higher mutation rates in the high-risk group (**Figures 8A, B**). We also investigated cooccurrence and mutually exclusive genes in the risk groups. EGFR, PTEN and NF1 showed mutual exclusivity with IDH1, TP53 and ATRX in the high-risk group. Cooccurrence was observed in CIC with IDH1, PTEN with EGFR and NF1, and FUBP1 with NF1 and CIC in the high-risk group (**Figure 8C**). We also performed GISTIC2 to identify driver CNVs in different risk groups (18). The high-risk group presented an overall higher rate of copy number amplification and deletion with the exception that deletion on 1p and 19q was observed predominantly in the low-risk group. Deletions on Chr 9p, 10, 13q and 14q and amplifications on Chr 7, 19, 20 were observed mainly in the high-risk group (**Figure 8D**). Distribution of CNVs in different genes between the two risk groups were also analyzed (**Figure 8E**). CDKN2B, PTEN, CDK6, EGFR, PRKCH, and IGF2R showed higher CNV rates in the high-risk group while CDKN2C and PDGFC showed higher CNV rates in the low-risk group.

m5C-Related LPS in Prediction of Chemotherapeutics Response

Temozolomide has been the first line treatment after surgery for gliomas for some time (21). However, with vast differences in response to temozolomide in patients, researchers have been investigating novel chemotherapeutics for glioma (22, 23). In light of the aforementioned findings in enriched pathways and CNVs in the m5C LPS high risk group, we used the 'pRRophetic' package to predict response of patients to chemotherapeutics in different risk groups. We selected Temozolomide, Bleomycin, Cisplatin, Cyclopamine, A.443654 (Akt inhibitor), AZD6482 (PI3K inhibitor), GDC0941(PI3K inhibitor), and metformin to analyze levels of response in different risk groups. Results revealed a lower estimated IC50 in the high-risk group for the chosen drugs (**Figure 9**).

DISCUSSION

Unlike the neurons that are terminally differentiated cells, astrocytes still retain the ability to self-renew and proliferate, which can potentially transform to cancer cells under pathological conditions. This may be attributed to the different effects of abnormal activation of intracellular pathways in neurons and glial cells in the brain (24). Previous studies indicated that the most common histological type of primary CNS tumor is glioma, which is derived from glial cells of astrocytic, oligodendroglia and ependymal origin, with an annual incidence of 5-6/100,000 individuals worldwide (25, 26). Our previous study presented a novel integrated system for glioma individualized therapeutics modeling and screening (27). Studies have also reported predictive models of tumor prognosis and therapeutics using bioinformatics methods (9, 22).

In the current study we identified the m5C-related LPS containing eight lncRNAs, two of which have been reported in the literature. LINC00632 was reported to be associated with several tumors including multiple myeloma cell drug resistance (28), and melanoma invasion and metastasis (29). PAXIP1-AS2 is involved in endometrial cancer development (30). Univariate and multivariate Cox regression analyses with other clinicopathological factors confirmed the risk score to be an independent prognostic factor for LGG patients. The robust predictive performance of the m5C LPS was also confirmed *via* ROC curves in differential clinicopathological subgroups. Many studies have implicated plasma/serum lncRNAs with tumor initiation and diagnosis (31, 32). The current study is the first to construct a m5C-related lncRNA signature in lower grade glioma. The m5C LPS presented a good prognostic ability with one-, three-, and five- year AUC being 0.873, 0.865, and 0.772 respectively compared to existing signatures with AUC ranging from 0.741 to 0.901 (**Supplementary Table 2**) (33–36). The m5C LPS also correlated significantly with immune cell infiltration, tumor mutation, and copy number variation. The m5C LPS could be utilized in diagnosis, drug response and prognosis prediction of lower grade glioma.

LncRNAs have been reported to participate in tumor initiation and progression through reprogramming tumor microenvironment. LINC00665 was reported to affect the infiltration of macrophages and DCs, suppress Tregs, and prevent T cell exhaustion. LncRNA TCL6 is related to tumor infiltrating lymphocytes and immune checkpoint molecules including PD1, PDL1 and CTLA4. Multiple lncRNAs are reported to regulate macrophage polarization and their protein secretion (37). The current study identified T cell differentiation, interferon gamma and alpha signaling pathways to be enriched in the high-risk group. M1 macrophages, CD8 T cells, resting mast cells, activated and resting CD4 memory T cells were found to be highly infiltrated in the high-risk group. Infiltration of M1 macrophages, CD8 T cells and resting CD4 T cells was found to be positively correlated with the risk score while infiltration of CD4 naïve T cells, monocytes and activated mast cells was negatively correlated with the risk score. Differential infiltration of various immune cells in the two risk groups may be the result of the overall difference between m5C LPS high and low risk groups or the direct effect of m5C lncRNAs differential expression. HLA proteins play important roles in antitumor immunity through maintaining CTL antigen presentation and modulating NK cell function. We thus evaluated the expression

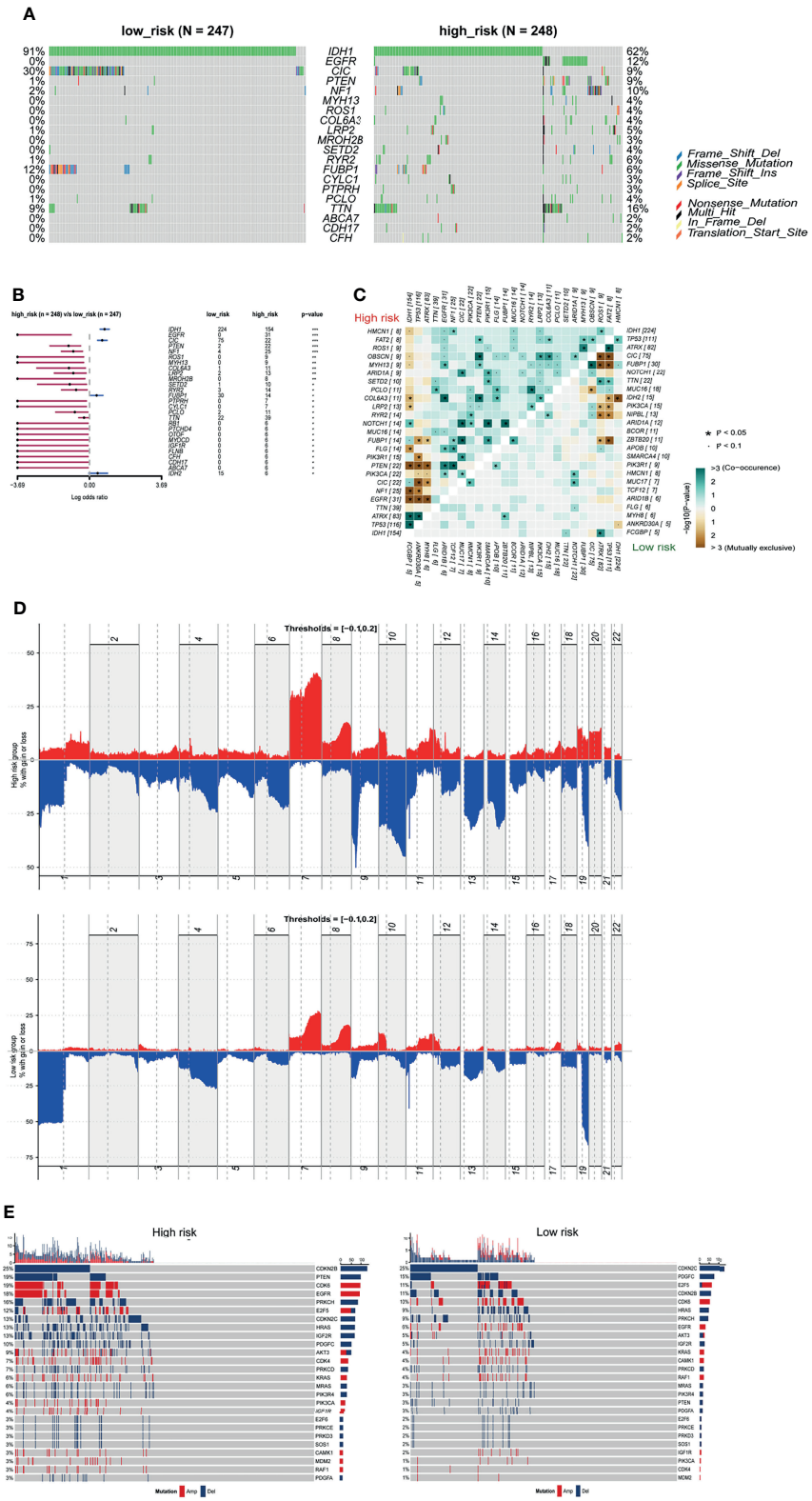

FIGURE 8 | Somatic mutation and CNVs in different risk groups. **(A)** Seven significantly different mutated driver genes between high and low risk groups. **(B)** Forest plot of differentially mutated genes between high and low risk groups. **(C)** Heatmap of mutually exclusive and co-occurrent mutated genes in high and low risk groups. **(D)** Distribution of copy number variations in high and low risk groups. **(E)** Differential CNVs of genes in high and low risk groups.

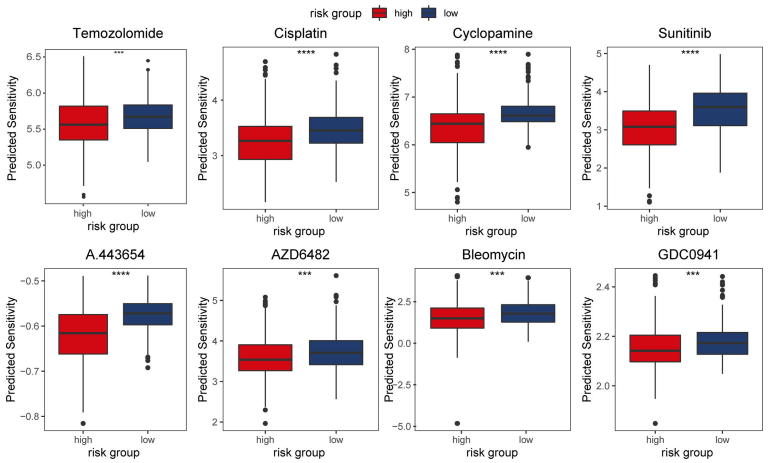

FIGURE 9 | Predicted response of patients in TCGA dataset to chemotherapeutic agents in different risk groups.

of HLA proteins in different risk groups. Expression of HLA and immune checkpoint proteins was significantly higher in the high-risk group. Response to immune checkpoint inhibitors in both risk groups was explored using a subclass mapping algorithm. The high-risk group was found to be more responsive to anti-CTLA4 therapy. The mechanism of correlation between m5C lncRNAs and immune infiltration/response are to be further explored.

We also evaluated somatic mutation, CNVs, and response to chemotherapeutic agents in different risk groups. IDH1, CIC, NIPBL, and FUBP1 showed significantly higher mutation rates in the low-risk group while EGFR, NF1, and PTEN showed higher mutation rates in the high-risk group. Deletion on 1p and 19q was observed predominantly in the low-risk group. These results conform to reports of better prognosis in patients with IDH1 mutation or 1p19q codeletion. In predicting chemotherapeutics response, we investigated agents including Akt inhibitor A.443654, PI3K inhibitor AZD6482 and GDC0941 targeting pathways indicated in GSEA analysis. Results showed that cases in the high-risk group were more responsive to the drugs. Mechanism of the correlation between m5C LPS and therapeutics response needs further research. Still, *in vitro* validation of drug response experiments is needed to confirm the predictions.

In summary, we report a lncRNA signature that may contribute to stratification of LGG patients in their prognosis and response to immune- and chemotherapies. There are limitations to the current study including a restricted number of cases in the validation set, lack of further *in vitro* and *in vivo* studies into the correlations of m5C related lncRNAs with tumor immune microenvironment, somatic mutation and CNVs. However, the m5C-related lncRNA prognostic signature should stimulate further laboratory research into the specific lncRNAs from which it is composed, as well as potential biomarker research using patient-derived tumor or serum samples.

DATA AVAILABILITY STATEMENT

The datasets presented in this study can be found in online repositories. The names of the repository/repositories and accession number(s) can be found in the article/**Supplementary Material**.

ETHICS STATEMENT

The studies involving human participants were reviewed and approved by the ethics committee of Xiangya Hospital, Central South University. The patients/participants provided their written informed consent to participate in this study.

AUTHOR CONTRIBUTIONS

CL and LZ conceived and designed the study. HSZ, MM, ZW, and HZ performed the data mining and statistical analyses. HSZ drafted the initial manuscript. LZ, CL, and LY made critical comments and revision for the initial manuscript. All authors reviewed and approved the final manuscript.

SUPPLEMENTARY MATERIAL

The Supplementary Material for this article can be found online at: https://www.frontiersin.org/articles/10.3389/fonc.2022.814742/full#supplementary-material

Supplementary Figure 1 | Realtime-qPCR validation of relative expression of the eight lncRNAs of m5C-related LPS in 27 LGG samples.

Supplementary Figure 2 | Relative expression of m5C LPS lncRNAs in IDH wild type and IDH mutant samples.

Supplementary Figure 3 | Relative expression of m5C LPS lncRNAs in MGMT promoter methylated and unmethylated samples.

REFERENCES

1. Xu S, Tang L, Li X, Fan F, Liu Z. Immunotherapy for Glioma: Current Management and Future Application. *Cancer Lett* (2020) 476:1–12. doi: 10.1016/j.canlet.2020.02.002
2. Squires JE, Patel HR, Nousch M, Sibbritt T, Humphreys DT, Parker BJ, et al. Widespread Occurrence of 5-Methylcytosine in Human Coding and Non-Coding RNA. *Nucleic Acids Res* (2012) 40(11):5023–33. doi: 10.1093/nar/gks144
3. Zhao BS, Roundtree IA, He C. Post-Transcriptional Gene Regulation by mRNA Modifications. *Nat Rev Mol Cell Biol* (2017) 18(1):31–42. doi: 10.1038/nrm.2016.132
4. Shi H, Chai P, Jia R, Fan X. Novel Insight Into the Regulatory Roles of Diverse RNA Modifications: Re-Defining the Bridge Between Transcription and Translation. *Mol Cancer* (2020) 19(1):78. doi: 10.1186/s12943-020-01194-6
5. Bohnsack KE, Hobartner C, Bohnsack MT. Eukaryotic 5-Methylcytosine (M (5)C) RNA Methyltransferases: Mechanisms, Cellular Functions, and Links to Disease. *Genes (Basel)* (2019) 10(2):102. doi: 10.3390/genes10020102
6. Yang X, Yang Y, Sun BF, Chen TS, Xu JW, Lai WY, et al. 5-Methylcytosine Promotes mRNA Export - NSUN2 as the Methyltransferase and ALYREF as an M(5)C Reader. *Cell Res* (2017) 27(5):606–25. doi: 10.1038/cr.2017.55
7. Wang P, Wu M, Tu Z, Tao C, Hu Q, Li K. Identification of RNA: 5-Methylcytosine Methyltransferases-Related Signature for Predicting Prognosis in Glioma. *Front Oncol* (2020) 10:1119. doi: 10.3389/fonc.2020.01119
8. Chen X, Li A, Sun BF, Yang Y, Han YN, Yuan X, et al. 5-Methylcytosine Promotes Pathogenesis of Bladder Cancer Through Stabilizing mRNAs. *Nat Cell Biol* (2019) 21(8):978–90. doi: 10.1038/s41556-019-0361-y
9. Pan J, Huang Z, Xu Y. M5c-Related lncRNAs Predict Overall Survival of Patients and Regulate the Tumor Immune Microenvironment in Lung Adenocarcinoma. *Front Cell Dev Biol* (2021) 9:671821. doi: 10.3389/fcell.2021.671821
10. He Y, Yu X, Li J, Zhang Q, Zheng Q, Guo W. Role of M5c-Related Regulatory Genes in the Diagnosis and Prognosis of Hepatocellular Carcinoma. *Am J Transl Res* (2020) 12(3):912–22.
11. Rinn JL. lncRNAs: Linking RNA to Chromatin. *Cold Spring Harb Perspect Biol* (2014) 6(8):a018614. doi: 10.1101/cshperspect.a018614
12. Bhan A, Soleimani M, Mandal SS. Long Noncoding RNA and Cancer: A New Paradigm. *Cancer Res* (2017) 77(15):3965–81. doi: 10.1158/0008-5472.CAN-16-2634
13. Han Y, Wu Z, Wu T, Huang Y, Cheng Z, Li X, et al. Tumor-Suppressive Function of Long Noncoding RNA MALAT1 in Glioma Cells by Downregulation of MMP2 and Inactivation of ERK/MAPK Signaling. *Cell Death Dis* (2016) 7:e2123. doi: 10.1038/cddis.2015.407
14. Li Y, Li J, Luo M, Zhou C, Shi X, Yang W, et al. Novel Long Noncoding RNA NMR Promotes Tumor Progression via NSUN2 and BPTF in Esophageal Squamous Cell Carcinoma. *Cancer Lett* (2018) 430:57–66. doi: 10.1016/j.canlet.2018.05.013
15. Sun Z, Xue S, Zhang M, Xu H, Hu X, Chen S, et al. Aberrant NSUN2-Mediated M(5)C Modification of H19 lncRNA Is Associated With Poor Differentiation of Hepatocellular Carcinoma. *Oncogene* (2020) 39(45):6906–19. doi: 10.1038/s41388-020-01475-w
16. Newman AM, Steen CB, Liu CL, Gentles AJ, Chaudhuri AA, Scherer F, et al. Determining Cell Type Abundance and Expression From Bulk Tissues With Digital Cytometry. *Nat Biotechnol* (2019) 37(7):773–82. doi: 10.1038/s41587-019-0114-2
17. Roh W, Chen P-L, Reuben A, Spencer CN, Prieto PA, Miller JP, et al. Integrated Molecular Analysis of Tumor Biopsies on Sequential CTLA-4 and PD-1 Blockade Reveals Markers of Response and Resistance. *Sci Trans Med* (2017) 9(379): eaah3560. doi: 10.1126/scitranslmed.aah3560
18. Mermel CH, Schumacher SE, Hill B, Meyerson ML, Beroukhim R, Getz G. GISTIC2.0 Facilitates Sensitive and Confident Localization of the Targets of Focal Somatic Copy-Number Alteration in Human Cancers. *Genome Biol* (2011) 12(41):R41. doi: 10.1186/gb-2011-12-4-r41
19. Reardon DA, Gokhale PC, Klein SR, Ligon KL, Rodig SJ, Ramkissoon SH, et al. Glioblastoma Eradication Following Immune Checkpoint Blockade in an Orthotopic, Immunocompetent Model. *Cancer Immunol Res* (2016) 4(2):124–35. doi: 10.1158/2326-6066.CIR-15-0151
20. Hoshida Y, Brunet JP, Tamayo P, Golub TR, Mesirov JP. Subclass Mapping: Identifying Common Subtypes in Independent Disease Data Sets. *PloS One* (2007) 2(11):e1195. doi: 10.1371/journal.pone.0001195
21. Omuro A, DeAngelis LM. Glioblastoma and Other Malignant Gliomas: A Clinical Review. *JAMA* (2013) 310(17):1842–50. doi: 10.1001/jama.2013.280319
22. Tian R, Li Y, Liu Q, Shu M. Identification and Validation of an Immune-Associated RNA-Binding Proteins Signature to Predict Clinical Outcomes and Therapeutic Responses in Glioma Patients. *Cancers (Basel)* (2021) 13(7):1730. doi: 10.3390/cancers13071730
23. Zhang XN, Yang KD, Chen C, He ZC, Wang QH, Feng H, et al. Pericytes Augment Glioblastoma Cell Resistance to Temozolomide Through CCL5-CCR5 Paracrine Signaling. *Cell Res* (2021) 31(10):1072–87. doi: 10.1038/s41422-021-00528-3
24. Morris LG, Veeriah S, Chan TA. Genetic Determinants at the Interface of Cancer and Neurodegenerative Disease. *Oncogene* (2010) 29(24):3453–64. doi: 10.1038/onc.2010.127
25. Jiang T, Nam DH, Ram Z, Poon WS, Wang J, Boldbaatar D, et al. Clinical Practice Guidelines for the Management of Adult Diffuse Gliomas. *Cancer Lett* (2021) 499:60–72. doi: 10.1016/j.canlet.2020.10.050
26. Luo C, Xu S, Dai G, Xiao Z, Chen L, Liu Z, et al. Tumor Treating Fields for High-Grade Gliomas. *BioMed Pharmacother* (2020) 127:110193. doi: 10.1016/j.biopha.2020.110193
27. Zhang L, Liu F, Weygant N, Zhang J, Hu P, Qin Z, et al. A Novel Integrated System Using Patient-Derived Glioma Cerebral Organoids and Xenografts for Disease Modeling and Drug Screening. *Cancer Lett* (2021) 500:87–97. doi: 10.1016/j.canlet.2020.12.013
28. Jakobsen T, Dahl M, Dimopoulos K, Grønbæk K, Kjems J, Kristensen LS. Genome-Wide Circular RNA Expression Patterns Reflect Resistance to Immunomodulatory Drugs in Multiple Myeloma Cells. *Cancers (Basel)* (2021) 13(3):365. doi: 10.3390/cancers13030365
29. Hanniford D, Ulloa-Morales A, Karz A, Berzoti-Coelho MG, Moubarak RS, Sánchez-Sendra B, et al. Epigenetic Silencing of CDR1as Drives IGF2BP3-Mediated Melanoma Invasion and Metastasis. *Cancer Cell* (2020) 37(1):55–70 e15. doi: 10.1016/j.ccell.2019.12.007
30. Swain U, Friedlander G, Sehrawat U, Sarusi-Portuguez A, Rotkopf R, Ebert C, et al. TENT4A Non-Canonical Poly(A) Polymerase Regulates DNA-Damage Tolerance via Multiple Pathways That Are Mutated in Endometrial Cancer. *Int J Mol Sci* (2021) 22(13):6957. doi: 10.3390/ijms22136957
31. Hu W, Liu C, Bi ZY, Zhou Q, Zhang H, Li LL, et al. Comprehensive Landscape of Extracellular Vesicle-Derived RNAs in Cancer Initiation, Progression, Metastasis and Cancer Immunology. *Mol Cancer* (2020) 19(1):102. doi: 10.1186/s12943-020-01199-1
32. Liao Y, Zhang B, Zhang T, Zhang Y, Wang F. LncRNA GATA6-AS Promotes Cancer Cell Proliferation and Inhibits Apoptosis in Glioma by Downregulating lncRNA Tug1. *Cancer Biother Radiopharm* (2019) 34 (10):660–5. doi: 10.1089/cbr.2019.2830
33. Wang C, Qiu J, Chen S, Li Y, Hu H, Cai Y, et al. Prognostic Model and Nomogram Construction Based on Autophagy Signatures in Lower Grade Glioma. *J Cell Physiol* (2021) 236(1):235–48. doi: 10.1002/jcp.29837
34. Lin W, Wu S, Chen X, Ye Y, Weng Y, Pan Y, et al. Characterization of Hypoxia Signature to Evaluate the Tumor Immune Microenvironment and Predict Prognosis in Glioma Groups. *Front Oncol* (2020) 10:796. doi: 10.3389/fonc.2020.00796
35. Xu J, Liu F, Li Y, Shen L. A 1p/19q Codeletion-Associated Immune Signature for Predicting Lower Grade Glioma Prognosis. *Cell Mol Neurobiol* (2020). doi: 10.1007/s10571-020-00959-3
36. Yu H, Zhang D, Lian M. Identification of an Epigenetic Prognostic Signature for Patients With Lower-Grade Gliomas. *CNS Neurosci Ther* (2021) 27 (4):470–83. doi: 10.1111/cns.13587
37. Zhang Y, Liu Q, Liao Q. Long Noncoding RNA: A Dazzling Dancer in Tumor Immune Microenvironment. *J Exp Clin Cancer Res* (2020) 39(1):231. doi: 10.1186/s13046-020-01727-3

Conflict of Interest: The authors declare that the research was conducted in the absence of any commercial or financial relationships that could be construed as a potential conflict of interest.

Publisher's Note: All claims expressed in this article are solely those of the authors and do not necessarily represent those of their affiliated organizations, or those of the publisher, the editors and the reviewers. Any product that may be evaluated in

this article, or claim that may be made by its manufacturer, is not guaranteed or endorsed by the publisher.

Copyright © 2022 Zhou, Meng, Wang, Zhang, Yang, Li and Zhang. This is an open-access article distributed under the terms of the Creative Commons Attribution License (CC BY). The use, distribution or reproduction in other forums is permitted, provided the original author(s) and the copyright owner(s) are credited and that the original publication in this journal is cited, in accordance with accepted academic practice. No use, distribution or reproduction is permitted which does not comply with these terms.

frontiers | Frontiers in Immunology

ORIGINAL RESEARCH
published: 04 April 2022
doi: 10.3389/fimmu.2022.849592

Pan-Cancer Analysis Shows That ALKBH5 Is a Potential Prognostic and Immunotherapeutic Biomarker for Multiple Cancer Types Including Gliomas

Cheng Wei[1†], Bo Wang[1†], Dazhao Peng[1†], Xiaoyang Zhang[1], Zesheng Li[1], Lin Luo[2], Yingjie He[3], Hao Liang[1], Xuezhi Du[3], Shenghui Li[1], Shu Zhang[1], Zhenyu Zhang[2], Lei Han[1*] and Jianning Zhang[1*]*

[1] Tianjin Neurological Institute, Key Laboratory of Post-Neuroinjury Neuro-repair and Regeneration in Central Nervous System, Ministry of Education and Tianjin City, Tianjin Medical University General Hospital, Tianjin, China, [2] Department of Neurosurgery, The First Affiliated Hospital of Zhengzhou University, Zhengzhou, China, [3] Department of Hepatopancreatobiliary Surgery, The Second Hospital of Tianjin Medical University, Tianjin, China

OPEN ACCESS

Edited by:
Quan Cheng,
Central South University, China

Reviewed by:
Jun Ma,
University of Minnesota Twin Cities, United States
Shengyan Xiang,
Moffitt Cancer Center, United States
Hua Yang,
University of South Florida, United States

***Correspondence:**
Jianning Zhang
jianningzhang2021@163.com
Lei Han
superhanlei@tmu.edu.cn
Zhenyu Zhang
fcczhangzy1@zzu.edu.cn

[†]These authors have contributed equally to this work

Specialty section:
This article was submitted to Cancer Immunity and Immunotherapy, a section of the journal Frontiers in Immunology

Received: 06 January 2022
Accepted: 11 March 2022
Published: 04 April 2022

Citation:
Wei C, Wang B, Peng D, Zhang X, Li Z, Luo L, He Y, Liang H, Du X, Li S, Zhang S, Zhang Z, Han L and Zhang J (2022) Pan-Cancer Analysis Shows That ALKBH5 Is a Potential Prognostic and Immunotherapeutic Biomarker for Multiple Cancer Types Including Gliomas. Front. Immunol. 13:849592. doi: 10.3389/fimmu.2022.849592

Background: AlkB homolog 5 (ALKBH5) is a N^6-methyladenosine (m^6A) demethylase associated with the development, growth, and progression of multiple cancer types. However, the biological role of ALKBH5 has not been investigated in pan-cancer datasets. Therefore, in this study, comprehensive bioinformatics analysis of pan-cancer datasets was performed to determine the mechanisms through which ALKBH5 regulates tumorigenesis.

Methods: Online websites and databases such as NCBI, UCSC, CCLE, HPA, TIMER2, GEPIA2, cBioPortal, UALCAN, STRING, SangerBox, ImmuCellAI, xCell, and GenePattern were used to extract data of ALKBH5 in multiple cancers. The pan-cancer patient datasets were analyzed to determine the relationship between ALKBH5 expression, genetic alterations, methylation status, and tumor immunity. Targetscan, miRWalk, miRDB, miRabel, LncBase databases and Cytoscape tool were used to identify microRNAs (miRNAs) and long non-coding RNAs (lncRNAs) that regulate expression of ALKBH5 and construct the lncRNA-miRNA-ALKBH5 network. *In vitro* CCK-8, wound healing, Transwell and M2 macrophage infiltration assays as well as *in vivo* xenograft animal experiments were performed to determine the biological functions of ALKBH5 in glioma cells.

Results: The pan-cancer analysis showed that ALKBH5 was upregulated in several solid tumors. ALKBH5 expression significantly correlated with the prognosis of cancer patients. Genetic alterations including duplications and deep mutations of the *ALKBH5* gene were identified in several cancer types. Alterations in the *ALKBH5* gene correlated with tumor prognosis. GO and KEGG enrichment analyses showed that ALKBH5-related genes were enriched in the inflammatory, metabolic, and immune signaling pathways in glioma. ALKBH5 expression correlated with the expression of immune checkpoint (ICP) genes,

and influenced sensitivity to immunotherapy. We constructed a lncRNA-miRNA network that regulates ALKBH5 expression in tumor development and progression. *In vitro* and *in vivo* experiments showed that ALKBH5 promoted proliferation, migration, and invasion of glioma cells and recruited the M2 macrophage to glioma cells.

Conclusions: ALKBH5 was overexpressed in multiple cancer types and promoted the development and progression of cancers through several mechanisms including regulation of the tumor-infiltration of immune cells. Our study shows that ALKBH5 is a promising prognostic and immunotherapeutic biomarker in some malignant tumors.

Keywords: ALKBH5, pan-cancer, prognosis, immune, glioma, lncRNA-miRNA-ALKBH5 network

INTRODUCTION

Nucleoside modifications affect the biological functions and stability of the RNA molecules. According to MODOMICS, the database of RNA modifications, 163 different nucleoside modifications have been reported for RNA molecules in all organisms (1). The most abundant RNA modification is N^6-methyladenosine (m^6A), which involves methylation of the 6^{th} nitrogen atom of the adenine (A) molecule in either messenger RNAs (mRNAs) or non-coding RNAs (ncRNAs) (2, 3). The m^6A modification is catalyzed by the m^6A methylation writer complex consisting of several proteins including METTL3 and METTL14, and is reversed by demethylase erasers such as FTO and ALKBH5 (4). The m^6A modification is recognized by m^6A reader proteins belonging to the YTHDF and YTHDC protein families, and modulates translation, localization, mRNA splicing, or stability of the modified mRNA or ncRNA (5). Several studies have shown that aberrant regulation of m^6A RNA modifications is associated with the development and progression of various cancers (6–8).

AlkB homolog 5 (ALKBH5) is a widely reported m^6A RNA demethylase that belongs to the AlkB family of DNA and RNA demethylases, which mediates the repair of N-alkylated nucleobases by oxidative demethylation and consists of 9 mammalian homologs (9). The full-length ALKBH5 has 394 amino acids and ALKBH5 mainly locates on nuclear speckles that facilitate the assembly of mRNA-processing factors, which sustains the view that nuclear nascent RNAs are the main substrates of ALKBH5. ALKBH5 plays a significant role in several biological processes such as cell proliferation, osteogenesis, spermatogenesis, and ossification (10–13). ALKBH5 also plays an oncogenic or tumor suppressive role in different kinds of cancers, such as breast cancer, glioblastoma, ovarian cancer, lung cancer, liver cancer, pancreatic cancer, gastrointestinal cancer, acute myeloid leukemia (AML) and osteosarcoma (14–20). On the one hand, breast cancer stem cell (BCSC) phenotype could be induced by hypoxia through HIF-dependent and ALKBH5-mediated regulation of NANOG mRNA (14). And ALKBH5 was highly expressed in glioblastoma stem-like cells (GSCs) and maintained tumorigenic activity of GSCs *via* maintaining FOXM1 expression and cell proliferation program (15). Hu et al. found that ALKBH5 promoted epithelial ovarian cancer cell proliferation and invasion by inhibiting autophagy through miR-7 and Bcl-2 (16). Chen et al. discovered that ALKBH5 was essential for the development and maintenance of AML and the self-renewal of leukemia stem/initiating cells (LSCs/LICs), and ALKBH5 played a tumorigenic role in AML through post-transcriptional regulation of its key targets, such as TACC3 (21). On the other hand, ALKBH5 inhibited tumor growth and metastasis *via* decreasing YTHDFs-mediated YAP expression and suppressing miR-107/LATS2-mediated YAP activity (17). Zheng et al. found that ALKBH5-mediated m6A demethylation led to post-transcriptional inhibition of LY6/PLAUR Domain Containing 1 (LYPD1), which inhibited malignant progression of hepatocellular carcinoma (22). In osteosarcoma, ALKBH5 could inhibit tumor progression through epigenetic silencing of m6A-dependent pre-miR-181B-1/YAP signaling pathway (20). Furthermore, Tariq M Rana revealed that ALKBH5 regulated the response of anti-PD-1 therapy by regulating lactate in tumor microenvironment and inhibiting immune cell recruitment (23). These results indicate that altered ALKBH5 expression could both promote and suppress carcinogenesis based on cancer type and ALKBH5 acts as a significant role in tumor immune microenvironment. At present, there are few systematic studies on ALKBH5 in pan-cancer, especially in glioma.

In this study, we performed systematic bioinformatics analysis to determine the biological functions and prognostic significance of ALKBH5 in several cancers using the patient data in multiple databases. The functional significance of altered expression levels of ALKBH5 was comprehensively investigated in various cancers in regard to prognosis, genetic alterations, expression levels of ALKBH5-related genes, tumor immunity, and the lncRNA-miRNA network regulating ALKBH5 expression. We also specifically analyzed the relationship between ALKBH5 expression and the growth and progression of gliomas using both *in vitro* and *in vivo* models.

MATERIALS AND METHODS

Analysis of ALKBH5 Gene and Protein Expression

The Human Protein Atlas (HPA) online website (https://www.proteinatlas.org/) was used to analyze ALKBH5 in "Tissue Atlas". The expression data of ALKBH5 gene in different human normal tissues were obtained (24). The row data source was TMM

normalized. Normalized eXpression (NX), the resulting transcript expression values, were calculated for each gene in every sample. Online website (https://www.proteinatlas.org/about/assays+annotation) showed the detailed information. NX ≥ 1 was regarded as "Low specificity" in at least one tissue, but not increased in other tissue. Then, the Cancer Genome Atlas (TCGA) cohort was used to analyze ALKBH5 expression in 33 tumors, including adrenocortical carcinoma (ACC), bladder urothelial carcinoma (BLCA), breast invasive carcinoma (BRCA), cervical squamous cell carcinoma and endocervical adenocarcinoma (CESC), cholangiocarcinoma (CHOL), colon adenocarcinoma (COAD), lymphoid neoplasm diffuse large B-cell lymphoma (DLBC), esophageal carcinoma (ESCA), glioblastoma multiforme (GBM), head and neck cancer (HNSC), kidney chromophobe (KICH), kidney renal clear cell carcinoma (KIRC), kidney renal papillary cell carcinoma (KIRP), acute myeloid leukemia (LAML), brain lower grade glioma (LGG), liver hepatocellular carcinoma (LIHC), lung adenocarcinoma (LUAD), lung squamous cell carcinoma (LUSC), Mesothelioma (MESO), ovarian serous cystadenocarcinoma (OV), pancreatic adenocarcinoma (PAAD), pheochromocytoma and paraganglioma (PCPG), prostate adenocarcinoma (PRAD), rectum adenocarcinoma (READ), sarcoma (SARC), skin cutaneous melanoma (SKCM), stomach adenocarcinoma (STAD), testicular germ cell tumors (TGCT), thyroid carcinoma (THCA), thymoma (THYM), uterine corpus endometrial carcinoma (UCEC), uterine carcinosarcoma (UCS) and uveal melanoma (UVM) *via* Gene Expression Profiling Interactive Analysis 2.0 (GEPIA2) (http://gepia2.cancer-pku.cn/#index) (25). All abbreviations showed in **Supplementary Table 1**. Using TCGA combined with Genotype Tissue Expression (GTEx) cohort, ALKBH5 expression was analyzed between tumors and corresponding normal tissues in 27 tumors *via* SangerBox (http://SangerBox.com/Tool) (26). ALKBH5 mRNA expression data of glioma with different gardes, subtypes and new types (oligodendroglioma, astrocytoma and glioblastoma) were obtained from the Chinese Glioma Genome Atlas (CGGA) (http://www.cgga.org.cn; dataset ID: mRNAseq_325 and mRNAseq_693) and TCGA databases.

Moreover, RNA-Seq data (lllumina HiSeq X Ten, Novogene) and corresponding pathological and clinical data of external 100 glioma samples were obtained to further validate the correlation between ALKBH5 mRNA expression and glioma grades or prognosis. All human glioma samples were taken from patients undergoing surgery at the First Affiliated Hospital of Zhengzhou University. Tissue samples were graded by neuropathologists according to World Health Organization (WHO) standards and stored in liquid nitrogen. Glioma specimens were divided into grade II (30 cases), grade III (20 cases) and grade IV (50 cases). Histological and clinical data of glioma specimens are shown in **Supplementary Table 2**. This study was approved by the institutional review boards of the hospital and obtained written informed consent from all patients.

In addition, the ALKBH5 protein expression data for 44 tissues under physiological conditions were obtained in HPA portal. The subcellular localization information of ALKBH5 was obtained using the Cell Atlas module. The conserved functional domains of ALKBH5 proteins were analyzed in different species using "HomoloGene" function of NCBI database. The expression levels of ALKBH5 protein were also analyzed in Clinical Proteomic Tumor Analysis Consortium (CPTAC) module *via* UALCAN portal (http://ualcan.path.uab.edu/index.html) (27). The CPTAC database normalized the expression values in each proteome data to the standard deviation of the median. The total ALKBH5 protein expression level was compared between tumors and normal tissues *via* retrieving "ALKBH5". Five available data sets for tumors were selected, including OV, breast cancer, clear cell RCC (ccRCC), lung adenocarcinoma and UCEC.

Survival Prognosis Analysis

The overall survival (OS) and disease-free survival (DFS) survival map data for ALKBH5 in various tumor types in TCGA database were obtained *via* GEPIA2 online website. The high-expression and low-expression cohorts of ALKBH5 was obtained through the expression threshold of the cutoff-high (50%) and cutoff-low (50%) values. The "Survival Analysis" module of GEPIA2 was used to analyze special survival plots with log-rank P-values.

Then, the COX_OS (overall survival) and COX_DSS (disease specific survival) analysis data of ALKBH5 for different tumors was analyzed on SangerBox portal. In Kaplan-Meier Plotter website (https://kmplot.com/analysis/), the relationship between ALKBH5 expression and prognosis of tumor patients, such as OS, progression free survival (PFS), first progression (FP), post progression survival (PPS) and relapse free survival (RFS), was analyzed (28). The Kaplan-Meier survival plots of ovarian, lung, gastric and liver cancer cases were generated in the "mRNA gene chip" and "mRNA RNA-seq" modules. The log-rank P-value, hazard ratio (HR) and 95% confidence intervals were computed. Through CGGA mRNAseq_325 (CGGA_325), CGGA mRNAseq_693 (CGGA_693) and TCGA mRNAseq databases, the relationship between ALKBH5 and overall survival of glioma patients in primary glioma, recurrent glioma, LGG (WHO I-III) and GBM (WHO IV) was analyzed. Through these three databases, the relationship between ALKBH5 expression and prognosis in IDH mut+1p/19q codeletion, IDH mut+1p/19q noncodeletion and IDH wild groups was analyzed in glioma. The relationship between ALKBH5 expression and prognosis in IDH status, 1p/19q codeletion status and MGMT promoter status was also analyzed in glioma *via* CGGA_325 and CGGA _693 datasets. Cox regression analysis of CGGA_325 combined with CGGA _693 and TCGA datasets in glioma was performed *via* SPSS and nomogram was used to visualize the results *via* SangerBox.

Genetic Alteration Analysis

Firstly, the genetic mutation ratios of *ALKBH5* in various tumors was explored *via* the "Gene_Mutation" module of the Tumor Immune Estimation Resource 2.0 (TIMER2) website (http://timer.cistrome.org/) (29). The row data represented the percentages of *ALKBH5* mutation in tumors.

Then, the characteristics of *ALKBH5* genetic alterations were explored by the online cBioPortal database (https://www.cbioportal.org/) (30). TCGA Pan Cancer Atlas Studies in the

"Quick select" section was selected for query. The mutation type, alteration frequency, and copy number alteration (CNA) data were observed across TCGA tumor datasets in the "Cancer Types Summary" module.

Databases of somatic mutations and somatic copy number alternations (CNAs) were obtained from TCGA datasets. CNAs correlated with ALKBH5 expression, and the threshold copy number at alteration peaks were analyzed by GISTIC 2.0 (https://cloud.genepattern.org/) (31). The patients were divided into the first 25% ALKBH5^{high} (n=166) and the last 25% ALKBH5^{low} (n=166) groups according to the expression value of ALKBH5. The maftools package was also used in R software (https://www.r-project.org/) to download and visualize the somatic mutations of patients with 25% ALKBH5^{high} and 25% ALKBH5^{low} glioma across TCGA databases (32).

ALKBH5-Related Gene Enrichment Analysis

Through searching the STRING website (https://string-db.org/), "ALKBH5" was queried in the "protein name" module and "*Homo sapiens*" in the organism module (33). The following main parameters was set: meaning of network edges ("evidence"), minimum required interaction score ["low confidence (0.150)"], active interaction sources ("experiments" and "database") and maximum number of interactors to show ("no more than 50 interactors" in the 1st shell). The available ALKBH5-binding proteins was analyzed. Then, the top 10 ALKBH5-associated targeting genes in TCGA tumors were generated by the "Similar Gene Detection" module of GEPIA2. The "correlation analysis" module of GEPIA2 was used to explore the correlation between ALKBH5 and these 10 ALKBH5-associated targeting genes. The P-value and the correlation coefficient (R) were generated. The correlation scatter plot of 10 genes was generated *via* the $\log_2$ TPM. We obtained a heatmap of these top 9 targeting genes *via* the "Gene_Corr" function of TIMER2.

Analyses of ALKBH5 related genes in CGGA_325, CGGA_693 and TCGA databases were performed using R package. The first 100 genes positively or negatively correlated with ALKBH5 expression were screened in CGGA_325, CGGA_693 and TCGA databases, and a total of 200 genes were used for subsequent analysis. SangerBox portal was used to analyze and map the results of GO-BP analysis of ALKBH5 related genes in glioma. Then, GSE93054 database (https://www.ncbi.nlm.nih.gov/geo/query/acc.cgi?acc=GSE93054) was used to analyze the biological functions of ALKBH5 related genes in glioma stem cells (GSCs). In GSC11 and GSC17 cells, 3032 and 5158 differentially expressed genes were found after knockdown ALKBH5, respectively. Among them, 1150 differentially expressed genes were intersected within GSC11 and GSC17 cell lines. GO-BP and KEGG enrichment analyses of ALKBH5 related genes was analyzed and mapped in glioma by SangerBox portal.

Analysis of Immune Cell Infiltration

The relationships between ALKBH5 expression and ESTIMATE score and tumor infiltration immune cells (TIICs) in multiple tumors were explored *via* the SangerBox website, including CD4+ T cells, CD8+ T cells, B cells, neutrophils, macrophages, etc. XCell (https://xcell.ucsf.edu/) and ImmuCellAI (http://bioinfo.life.hust.edu.cn/ImmuCellAI#!/) portals were used to analyze the relationship between ALKBH5 expression and immune-related cells in glioma *via* CGGA_325, CGGA_693 and TCGA datasets (34, 35).

Metagene analysis was performed with gene set variation analysis (GSVA) using the R package GSVA. Metagenes included HCK, IgG, Interferon, LCK, MHC-I, MHC-II and STAT1 clusters (**Supplementary Table 3**). The relationships between ALKBH5 expression and microsatellite instability (MSI), tumor mutation burden (TMB), Neoantigens and immune checkpoint (ICP) in different tumors from TCGA cohorts were investigated *via* the SangerBox website. These checkpoint genes included ADORA2A, BTLA, BTNL2, CD160, CD200, CTLA4, HHLA2, ICOS, IDO1, LAG3, PDCD1, TNFRSF14, VTCN1, etc. Spearman's rank correlation test was performed, and the partial correlation (cor) and P-value were generated. Details of immune checkpoint receptor and ligand genes shown in **Supplementary Table 4**.

LncRNA-miRNA-ALKBH5 Regulatory Network Analysis

Upstream binding miRNAs of ALKBH5 were predicted by several target gene prediction programs, consisting of miRWalk (http://mirwalk.umm.uni-heidelberg.de/), miRDB (http://mirdb.org/), miRabel and TargetScan (http://www.targetscan.org/vert_72/) (36–39). Only the 49 predicted miRNAs that appeared in these four programs were included for subsequent analyses. Then, top 10 miRNAs ranked in TargetScan program were regarded as candidate miRNAs of ALKBH5, including miR-4732-5p, miR-193a-3p, miR-362-3p, miR-193b-3p, miR-589-5p, miR-4736, miR-6840-3p, miR-329-3p, miR-5008-5p and miR-6132. The CGGA microRNA_array_198 cohort was used to analyze the clinical features of the top 10 miRNAs. In addition, upstream target lncRNAs by miRNA screened were predicted and analyzed in "Experimental module" and "Prediction module" *via* LncBase database (http://carolina.imis.athena-innovation.gr/diana_tools/web/index.php?r=lncba sev2%2Findex) (40). Subsequently, Cytoscape software was applied to visualize the lncRNA-miRNA-ALKBH5 regulatory network.

Cell Lines and Culture

Human astrocytes (HA) and human glioma cell lines (U87, LN229, U251, A172 and B19) were obtained from ATCC (American Type Culture Collection, Manassas, VA, USA). Human THP-1 cells were purchased from the Shanghai Cell Bank of the Chinese Academy of Sciences (Shanghai, China). All cell line authentication service was applied and mycoplasma was also routinely tested. Astrocyte medium (AM) (Cat. #1801, ScienCell, USA) was used to culture human astrocytes, supplemented with 10 mL of fetal bovine serum (FBS) (Cat. #0010, ScienCell, USA), 5 mL of penicillin/streptomycin solution (P/S) (Cat. #0503, ScienCell, USA) and 5 mL of Astrocyte Growth Supplement (AGS) (Cat. #1852, ScienCell, USA). The glioma cell lines were cultured in DMEM Medium (Dulbecco's Modified

Eagle Medium, Gibco, USA) and THP-1 cells were cultured in RPMI 1640 medium with 10% FBS (FBS, BI serum, Israel) and cultured in a 37°C constant temperature incubator containing 5% CO_2.

SiRNAs or Plasmids Delivery, Total RNA Isolation, Reverse Transcription and Quantitative Real-Time Polymerase Chain Reaction

The ALKBH5 siRNAs were purchased from Shanghai GenePharma Co., Ltd. SiRNAs were applied to knockdown the expression of ALKBH5 in U87 and U251 cell lines and transfected *via* Lipofectamine ™ RNAiMax (13778150, Thermo Fisher Scientific, USA) reagent. The ALKBH5 overexpression plasmids (pEGFP-C1B-ALKBH5) were kindly supplied by professor Xudong Wu (Tianjin Medical University, China) and transfected into cell lines *via* Lipofectamine 3000. RT-qPCR was applied to detect the efficiency of ALKBH5 knockdown or overexpression. Glioma cells were planted in 6-well plates, 5μL Lipofectamine ™ RNAiMAX and 40 pmol siRNA were mixed in each well for 5 min. Then, mixture was added into the cells for transfection. After transfection, the cells were replaced with full medium at 24h. The cells were collected after 48h. The total RNA was extracted with TRIzol reagent (Thermo Fisher Scientific, Inc.). The GoScript reverse transcription system (Promega Corporation) was used to synthesize cDNA. The mRNA expression status was detected *via* GoTaq®qPCR Master Mix (Promega Corporation) on ABI QuantStudio 3. GAPDH was applied as an internal control. The oligonucleotide primers used for quantitative PCR were as follows: ALKBH5, 5'- GGACCCCATCCACATCTTCG-3' forward and 5'-GGCCGTATG CAGTGAGTGAT-3' reverse; GAPDH, 5'-GGTGGTCTCCTCTGACTTCAACA-3' forward and 5'-GTTGCTGTAGCCAAA TTCGTTGT-3' reverse. The following PCR program was used: 95°C for 10 min, 40 cycles of amplification (15 sec at 95°C, 40 sec at 60°C and 1 min at 72°C) and a final extension step (72°C for 2 min). All PCR experiments were performed in triplicate. The siRNA sequences were shown below: siALKBH5#1, 5'-CUGCGCAACAAGUA CUUCUTT-3'sense and 5'-AGAAGUACUUGUUG CGCA GTT-3' antisense; siALKBH5#2, 5'-CCUCAGGAAGACAA GAUUATT-3'sense and 5'-UAAUCUUGUCUUCC UGAGGTT-3' antisense; negative control (NC), 5'-UUCUC CGAACGUG UCACGUTT-3'sense and 5'-ACGUGACACGU UCGGAGAATT-3' antisense.

CCK-8 Experiment

The CCK-8 reagent was purchased from APExBIO (USA). The 2×10^3 cells were seeded into 96-well plates in advance. The test was started 24 hours later and lasted for 6 consecutive days (0, 1, 2, 3, 4, 5, 6 days). The medium was absorbed and discarded, and CCK-8 reagent was mixed with serum-free medium in a 5ml eppendorf tube (CCK8 reagent: Serum-free medium =10 μL: 90 μL per well) and added into 96-well plates with 100 μL per well. OD value at 450 wavelength was detected on a microplate after incubation at 37°C for 1h.

Wound Healing and Transwell Experiments

Wound healing assay: According to the density of 2.5×10^5 cells per well, U87, U251 and LN229 cells were inoculated in the 6-well plate. Then, siALKBH5#1, siALKBH5#2 or ALKBH5 plasmids were transfected into the 6-well plate. After 24 h, 200 μL pipetting head was used to scratch the cells in the plate and the serum-free medium was replaced to collect images under an inverted microscope (IX81, Olympus Company, Japan) at 0 h, 12h and 24 h.

Transwell assay: The upper chamber of Transwell assay was coated with a layer of Matrigel matrix glue (Corning Company, USA) (matrix glue: Serum-free medium=1:4). Then, the cells were resuspended and counted using serum-free medium. The cells were seeded into the upper chamber at a density of 5×10^4, and the lower chamber was added 500 μL full medium. After 24h, the cells were fixated with 4% paraformaldehyde for 10 min, 1% crystal violet was used to staining cells for 10 s. The remaining cells in the upper chamber were slightly wiped off, and images were collected under a positive microscope (BX53, Olympus Company, Japan). In addition, the number of cells passing through the chamber was counted in four random fields under the microscope.

M2 Macrophage Infiltration Assay

THP-1 cells were differentiated into macrophages induced by 150 nM phorbol 12-myristate 13-acetate (PMA; Sigma, USA) with 24 h. Then, macrophage M2 polarization was obtained by incubation with 20 ng/ml of interleukin 4 (R&D Systems, #204-IL) and 20 ng/ml of interleukin 13 (R&D Systems, #213-ILB) for 48 h. M2 macrophage infiltration assays were applied through seeding 1.0×10^5 M2 macrophage cells (300μl) without serum in the upper chamber of a Transwell plate for 48 h (size 5mm, Corning, NY, USA). In bottom plate, U87 and U251 glioma cells (1.0×10^5) were cultured with10% FBS in DMEM (700μl). After incubation for 48 h, the cells in the upper chamber were fixed with 4% paraformaldehyde for 10 min and stained with 0.1% crystal violet for 10s. The infiltrated M2 macrophage cells were counted in three randomly selected fields from each membrane.

Subcutaneous Xenograft Experiment

All mouse experiments were conducted in accordance with protocols approved by the Tianjin medical university animal care and use committee and followed guidelines for animal welfare. Four-week-old BALB/c female nude mice were purchased from Beijing HFK Bioscience Co.,LTD. The tumor masses were subcutaneously embedded in nude mice and the nude mice were randomly divided into two groups (n=5) when the tumor masses grew to 4 to 5mm in diameter. These two groups were control group and siALKBH5 group. After that, tumor volumes were measured every 2 days and ALKBH5 siRNA were injected into the siALKBH5 group at a dose of 10 μL of siRNA versus 10 μL of Lipofectamine ™ 3000 per nude mouse. After 21 days, mice were euthanatized, subcutaneous tumors were removed and images were collected. The tumor volume was calculated with the formula Volume= (length × width^2)/2.

Statistical Analysis

Through the online databases mentioned above, the statistical analysis was automatically computed in this study. These results were considered as statistically significant at $^{*}P<0.05$, $^{**}P<0.01$, $^{***}P<0.001$ and $^{****}P<0.0001$.

RESULTS

ALKBH5 Expression Is Upregulated in Multiple Tumors Including Gliomas

The flowchart of this study is shown in **Supplementary Figure 1**. The normalized expression (NX) levels of ALKBH5 were analyzed in various tumor tissues and their corresponding adjacent normal tissues as well as various tumor cells and the corresponding non-tumor cells in The Human Protein Atlas (THPA) database. ALKBH5 mRNA expression levels were higher in the normal human skeletal muscle, heart muscle, and tongue tissues (NX>50; **Figure 1A**). In most other normal human tissues, ALKBH5 mRNA expression level was detectable (NX>10) but low (NX<50) (**Figure 1A**). Moreover, TCGA database analyses of tumor tissues from 33 cancer types showed that ALKBH5 mRNA expression levels were tumor-specific and had the highest expression in Sarcoma (**Figure 1B**). TCGA and GTEx database analyses showed that the ALKBH5 mRNA levels were upregulated in the adrenocortical carcinoma (ACC), breast invasive carcinoma (BRCA), cervical squamous cell carcinoma and endocervical adenocarcinoma (CESC), cholangiocarcinoma (CHOL), colon adenocarcinoma (COAD), esophageal carcinoma (ESCA), glioblastoma multiforme (GBM), head and neck cancer (HNSC), kidney renal clear cell carcinoma (KIRC), acute myeloid leukemia (LAML), brain lower grade glioma (LGG), liver hepatocellular carcinoma (LIHC), lung adenocarcinoma (LUAD), lung squamous cell carcinoma (LUSC), ovarian serous cystadenocarcinoma (OV), pancreatic adenocarcinoma (PAAD), prostate adenocarcinoma (PRAD), skin cutaneous melanoma (SKCM), stomach adenocarcinoma (STAD), testicular germ cell tumors (TGCT), thyroid carcinoma (THCA) and uterine carcinosarcoma (UCS) tumor tissues compared to the corresponding normal tissues, while decreased in kidney renal papillary cell carcinoma (KIRP), rectum adenocarcinoma (READ) and uterine corpus endometrial carcinoma (UCEC) (All abbreviations showed in **Supplementary Table 1**) (**Figure 1C**).

Next, we analyzed ALKBH5 mRNA expression levels in different WHO grades, subtypes, and new types of gliomas. Glioblastoma is classified into four subtypes (classical, mesenchymal, neural, and proneural) based on the molecular signatures (41). The gliomas are classified into the following three types according to the fifth edition of the World Health Organization (WHO) classification of tumors of the Central Nervous System (CNS) (WHO CNS5): IDH-mutant and 1p/19q-codeleted (mut+codel) oligodendroglioma, IDH-mutant (mut+non-codel) astrocytoma, and IDH-wildtype (IDH-wild) glioblastoma (42). CGGA and TCGA database analyses showed that ALKBH5 expression levels were positively associated with glioma grades (**Figure 2A**). Moreover, the expression levels of ALKBH5 mRNA correlated with the WHO CNS5 types and glioma subtypes (**Figures 2B, C**). Analysis of 100 glioma cases collected also showed that ALKBH5 expression level was positively correlated with glioma grade, which was consistent with our analysis results in CGGA and TCGA databases (**Figure 2D**). Isocitrate dehydrogenase (IDH) mutations and chromosomal 1p/19q codeletions are associated with better survival outcomes of glioma patients (43). Furthermore, promoter methylation status of the O6-methylguanine DNA methyltransferase (MGMT) is a prognostic indicator of the clinical response to treatment of glioblastoma patients with temozolomide (TMZ) (44). Then, we explored the relationship between ALKBH5 mRNA expression and the status of *IDH* gene mutations, 1p/19q codeletion, and MGMT promoter methylation. Analysis of the TCGA database and the CGGA_325, CGGA_693 datasets showed significantly higher ALKBH5 mRNA levels in the glioma patients with wild-type IDH and chromosomal 1p/19q non-codeletion, and significantly reduced in the glioma patients with MGMT promoter methylation (**Supplementary Figures 2A–C**).

Finally, we then investigated the expression characteristics of the ALKBH5 protein in 43 different normal tissues and various cancers using the THPA database, respectively. ALKBH5 protein expression was higher in most normal tissues and lower in soft tissues (**Supplementary Figure 3A**). ALKBH5 protein was localized in the nucleoplasm, cytosol, and golgi apparatus (**Supplementary Figure 3B**). NCBI database analysis showed that ALKBH5 protein was conserved in multiple species (**Supplementary Figure 3C**). CPTAC database analysis showed that ALKBH5 protein levels were significantly increased in the ovarian cancer, breast cancer, clear cell renal cell carcinoma (ccRCC), and lung adenocarcinoma tissues, and significantly reduced in the uterine corpus endometrial carcinoma (UCEC) tissues compared with the corresponding normal tissues (**Supplementary Figure 3D**).

In summary, our results showed that ALKBH5 mRNA and protein levels were upregulated in several tumors. Furthermore, ALKBH5 expression levels correlated with the grades, subtypes, and clinical features of gliomas.

ALKBH5 Expression Is Associated With the Prognosis of Various Tumors Including Gliomas

The prognostic value of ALKBH5 expression levels in multiple cancers was analyzed by comparing the rates of overall survival (OS), progression free survival (PFS), disease free survival (DFS), post progression survival (PPS), first progression (FP), and relapse free survival (RFS) in the cancer patients with high or low ALKBH5 expression levels.

GEPIA2 database analysis of the pan-cancer cohorts showed that OS was significantly reduced in BLCA (HR=1.5), LAML (HR=2.0), LGG (HR=1.6), and UVM (HR=4.9) patients with high ALKBH5 mRNA expression levels and significantly increased in CESC (HR=0.62) patients with high ALKBH5 mRNA expression levels (**Figure 2F**). The results showed that patients with high ALKBH5 mRNA expression level had a worse

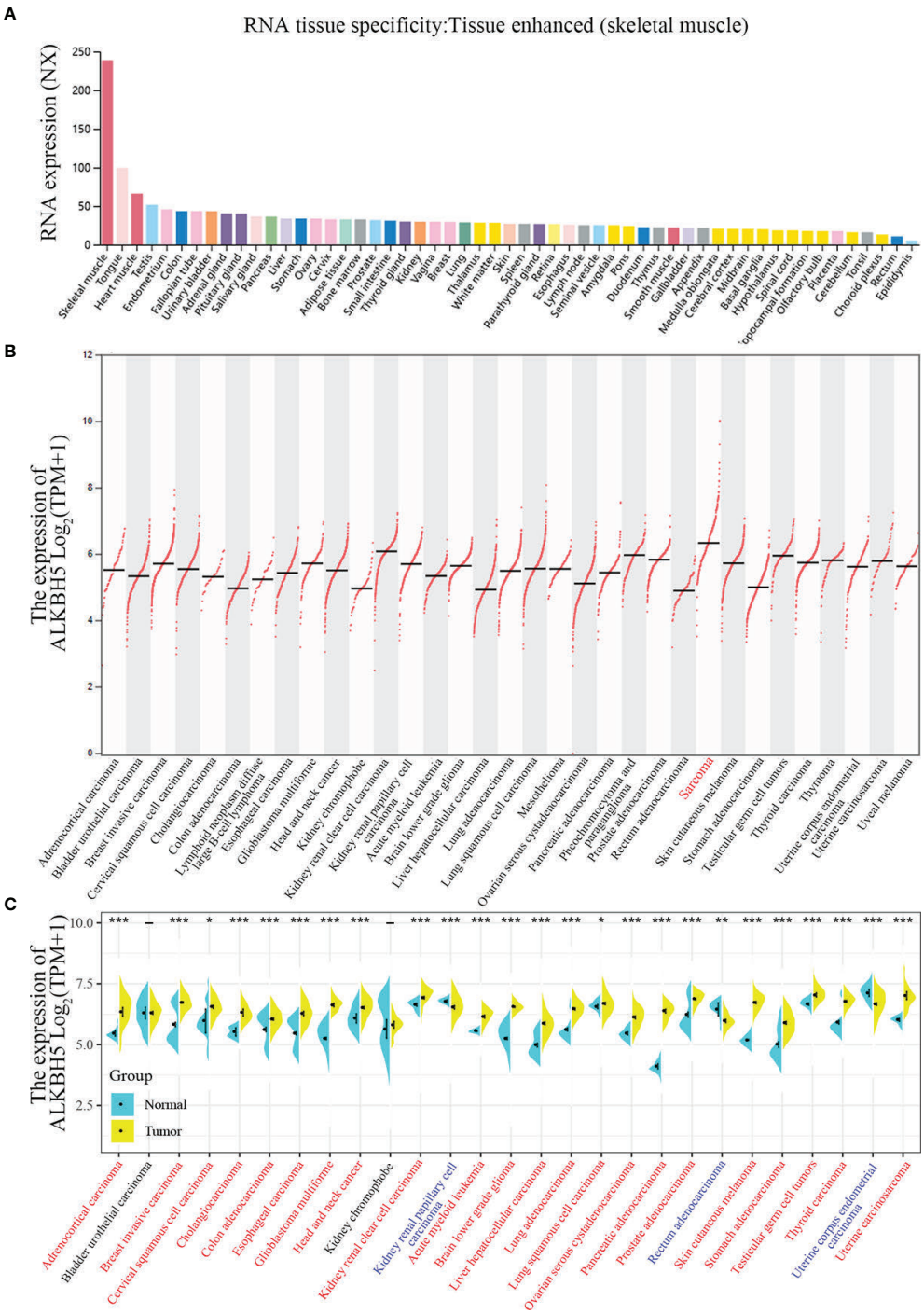

FIGURE 1 | ALKBH5 expression levels in normal tissues and cancers. **(A)** ALKBH5 consensus Normalized eXpression (NX) levels for 54 normal tissue types and 7 blood cell types, generated by the three transcriptomics datasets (GTEx, HPA and FANTOM5); **(B)** ALKBH5 mRNA expression levels in 33 different tumor types from TCGA database *via* GEPIA2 portal (Sarcoma with the highest expression is shown in red label); **(C)** ALKBH5 mRNA expression levels in different tumors and corresponding normal tissues from TCGA and GTEx database by SangerBox. Red label tumors represented up-regulation of ALKBH5 compared with corresponding normal tissues, blue label tumors represented down-regulation of ALKBH5 compared with corresponding normal tissues, and black label tumors represented no significant difference of ALKBH5 between tumor tissues and corresponding normal tissues or absence of normal samples. *P<0.05, **P<0.01, ***P<0.001.

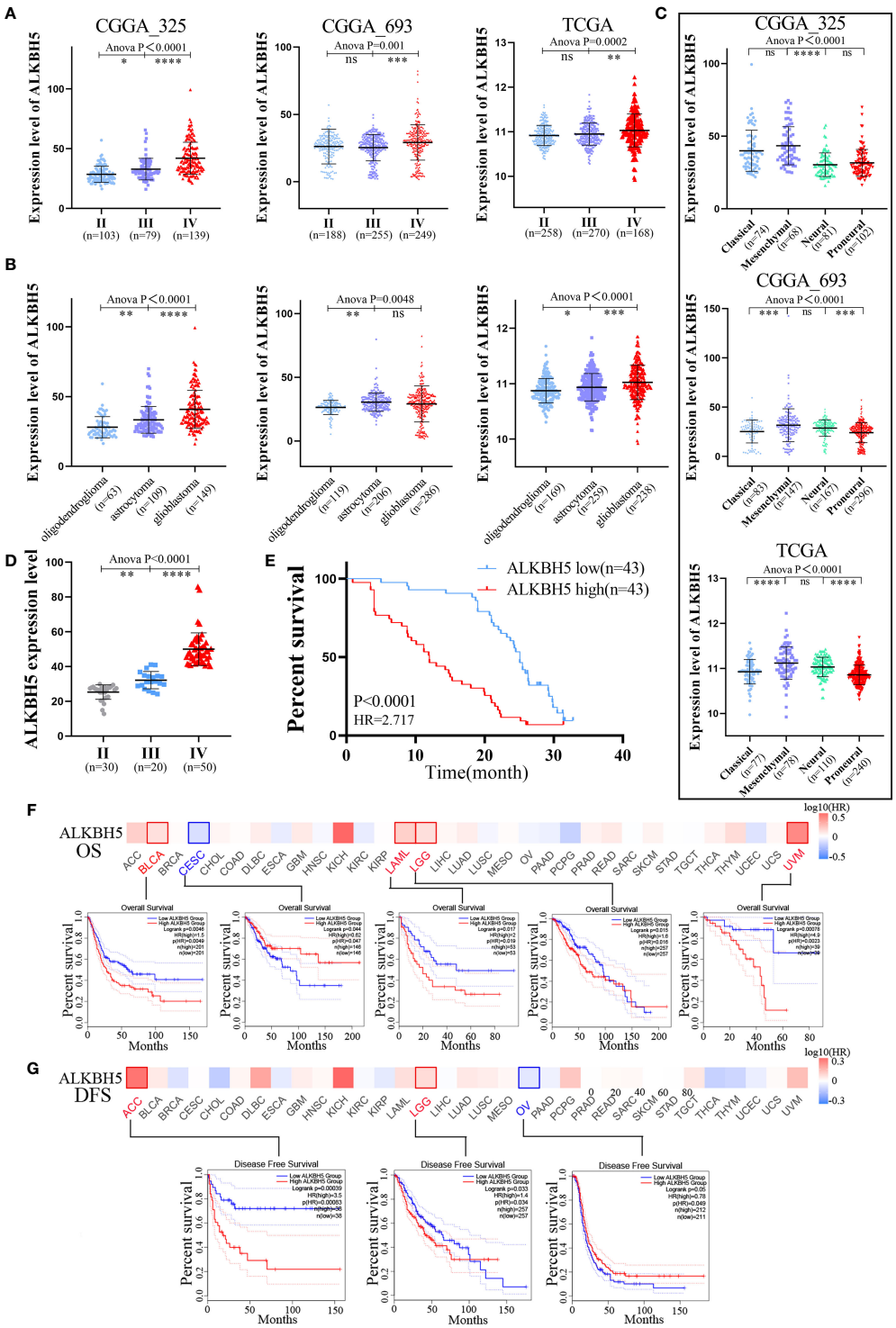

FIGURE 2 | Clinical and molecular characteristics of ALKBH5 in pan-cancer, including gliomas. **(A)** The correlation between ALKBH5 expression and glioma WHO grade (II, II and IV) in CGGA_325, CGGA_693 and TCGA datasets; **(B)** The correlation between ALKBH5 expression and glioma three types (oligodendroglioma, astrocytoma and glioblastoma) in CGGA_325, CGGA_693 and TCGA datasets; **(C)** The relationship between ALKBH5 expression and glioma subtypes (classical, mesenchymal, neural, and proneural) in CGGA_325, CGGA_693 and TCGA datasets; **(D)** The correlation between ALKBH5 expression and grades in 100 glioma samples, including grade II (n=30), grade III(n=20) and grade IV (n=50) samples; **(E)** Overall survival (OS) of different ALKBH5 expression level in 100 glioma samples. The GEPIA2 tool was used to perform OS **(F)** and disease-free survival (DFS) **(G)** analyses of different tumors in TCGA by ALKBH5 expression. Red label indicated positively correlated, blue label indicated negatively correlated. *P<0.05, **P<0.01, ***P<0.001, ****P<0.0001.

prognosis (OS) than those with low ALKBH5 mRNA expression in BLCA, LAML, LGG and UVM. Furthermore, DFS was significantly reduced in the ACC (HR=3.5) and LGG (1.4) patients with high ALKBH5 mRNA expression levels and significantly increased in the OV (HR=0.78) patients with high ALKBH5 mRNA expression levels (**Figure 2G**). The results suggested that patients with high ALKBH5 mRNA expression level had a worse prognosis (DFS) than those with low ALKBH5 mRNA expression in ACC and LGG. Cox regression analysis of the SangerBox database showed that ALKBH5 mRNA expression levels were associated with OS and disease specific survival (DSS) of patients with multiple cancers. The results showed that the high mRNA expression of ALKBH5 was associated with shorter OS in KICH (HR=7.29), LGG (HR=3.42), LAML (HR=2.11), GBM (HR=1.60) and BLCA (HR=1.40) and shorter DSS in KICH (HR=10.50), LGG (HR=3.23), GBM (HR=1.56) and BLCA (HR=1.42) (**Supplementary Figures 4A, B**). Furthermore, integrated analysis of GEO, EGA, and TCGA databases in the Kaplan-Meier Plotter website showed that ALKBH5 mRNA expression was negatively associated with the OS and PFS rates of ovarian cancer patients, OS, FP and PPS rates of gastric cancer patients, and OS and PPS rates of lung cancer patients (**Supplementary Figures 4C–E**). ALKBH5 mRNA expression showed positive association with OS, PFS, and RFS rates of liver cancer patients (**Supplementary Figure 4F**).

The correlation between ALKBH5 mRNA expression levels and the prognosis of patients with primary glioma, recurrent glioma, low grade glioma (LGG) or glioblastoma (GBM) was investigated using the CGGA and TCGA datasets. In the CGGA_325, CGGA_693, and TCGA datasets, high ALKBH5 expression levels were associated with shorter OS in primary glioma and LGG patients (**Supplementary Figures 5A–C**). Analysis of 100 glioma cases also showed that glioma patients with high ALKBH5 mRNA expression levels had shorter OS compared with patients with low ALKBH5 expression level (**Figure 2E**). Then, Cox regression analyses demonstrated that tumor grade, chemotherapy, IDH mutation status, 1p/19q codeletion, and ALKBH5 mRNA expression levels were independent prognostic predictors based on the CGGA_325 combined with CGGA_693 dataset (**Supplementary Figure 6A**). In TCGA database, tumor grade, age of patients, IDH mutation status and 1p/19q codeletion were independent prognostic predictors (**Supplementary Figure 6B**). The nomograms were constructed by combining all the independent prognostic markers, namely, tumor grades, ALKBH5 mRNA expression levels, IDH mutation status, 1p/19q codeletion status and MGMT promoter status, based on the results of the Cox regression analysis (**Supplementary Figures 6C, D**).

The prognostic efficacy of the factors included in the nomogram were analyzed in the glioma patients from the CGGA_325 and CGGA_693 datasets. The results showed that ALKBH5 mRNA expression levels significantly correlated with the prognosis of glioma patients with different IDH mutations, 1p/19q codeletion, and MGMT promoter status; the high mRNA expression of ALKBH5 negatively correlated with the prognosis of glioma patients in the CGGA_325 and CGGA_693 datasets (**Supplementary Figures 7A–C**). ALKBH5 mRNA expression was associated with the prognosis of the glioma patients in the CGGA_325 and CGGA_693 datasets, but was independent of chemotherapy and/or radiotherapy (**Supplementary Figures 7D, E**).

Overall, the results demonstrated that the ALKBH5 mRNA and protein expression levels were associated with the prognosis of multiple cancers. Moreover, higher ALKBH5 mRNA and protein expression was associated with poorer prognosis of glioma patients.

Alterations in the *ALKBH5* Gene Are Associated With Development and Progression of Multiple Tumors Including Gliomas

Genetic alterations such as the mutations, deletions, or amplifications of oncogenes or tumor suppressor genes are associated with growth and progression of several tumors (45). Therefore, we first analyzed different types of alterations including mutations, structural variations, amplifications, and deep deletions in the *ALKBH5* gene in using the TCGA cancer datasets with the cBioPortal portal. The most common genetic alteration in the *ALKBH5* gene were amplifications in the sarcomas (>8%), uterine carcinosarcomas, liver hepatocellular carcinoma and pancreatic adenocarcinomas; mutations (1.3%) in the bladder urothelial carcinomas; and deep deletions (>2%) in the diffuse large B-cell lymphomas (**Figure 3A**). TIMER database analysis showed that BLCA (6/411), BRCA-Her2 (1/79), and UCEC (6/531) were the top 3 cancers with the highest *ALKBH5* gene mutation rates (**Figure 3B**). cBioPortal database analysis showed that missense mutations were the main type of *ALKBH5* gene mutations in cancers (**Figure 3C**).

Next, the relationship between ALKBH5 expression and specific genomic characteristics such as somatic mutations and copy number variations (CNVs) was analyzed in the TCGA glioma dataset. The $ALKBH5^{high}$ group (n = 166) showed high frequency of somatic mutations in the *TP53* (37%), *TTN* (31%), *PTEN* (30%), and *EGFR* (24%) genes and the $ALKBH5^{low}$ group (n = 166) showed high frequency of mutations in the *IDH1* (66%), *TP53* (46%), *ATRX* (32%), and *CIC* (24%) genes (**Figures 3D, E**). The comparison of the CNV profiles in the $ALKBH5^{low}$ (n = 166) and $ALKBH5^{high}$ (n = 166) samples is shown in **Figure 3F**. In the $ALKBH5^{high}$ samples, we observed amplification peaks in the 1q32.1, 3q26.33, 4q12, 7p11.2, 8q24.22, and 12q15 chromosomal regions, and deletions in the 1p36.23, 4q34.3, 9p21.2, 13q14.2 and 13q22.1 chromosomal locations. In the $ALKBH5^{low}$ samples, we observed amplification peaks in the 4q12, 7p11.2, 12q13.3 and 19p13.3 chromosomal locations and frequent deletions in the 4q35.1 and 9p21.3 chromosomal regions (**Figure 3G**).

Overall, these results showed ALKBH5 gene mutations, amplifications, and deletions in multiple tumors. Missense mutations were the most frequent type of ALKBH5 gene mutations in various tumors. Moreover, the glioma tissues

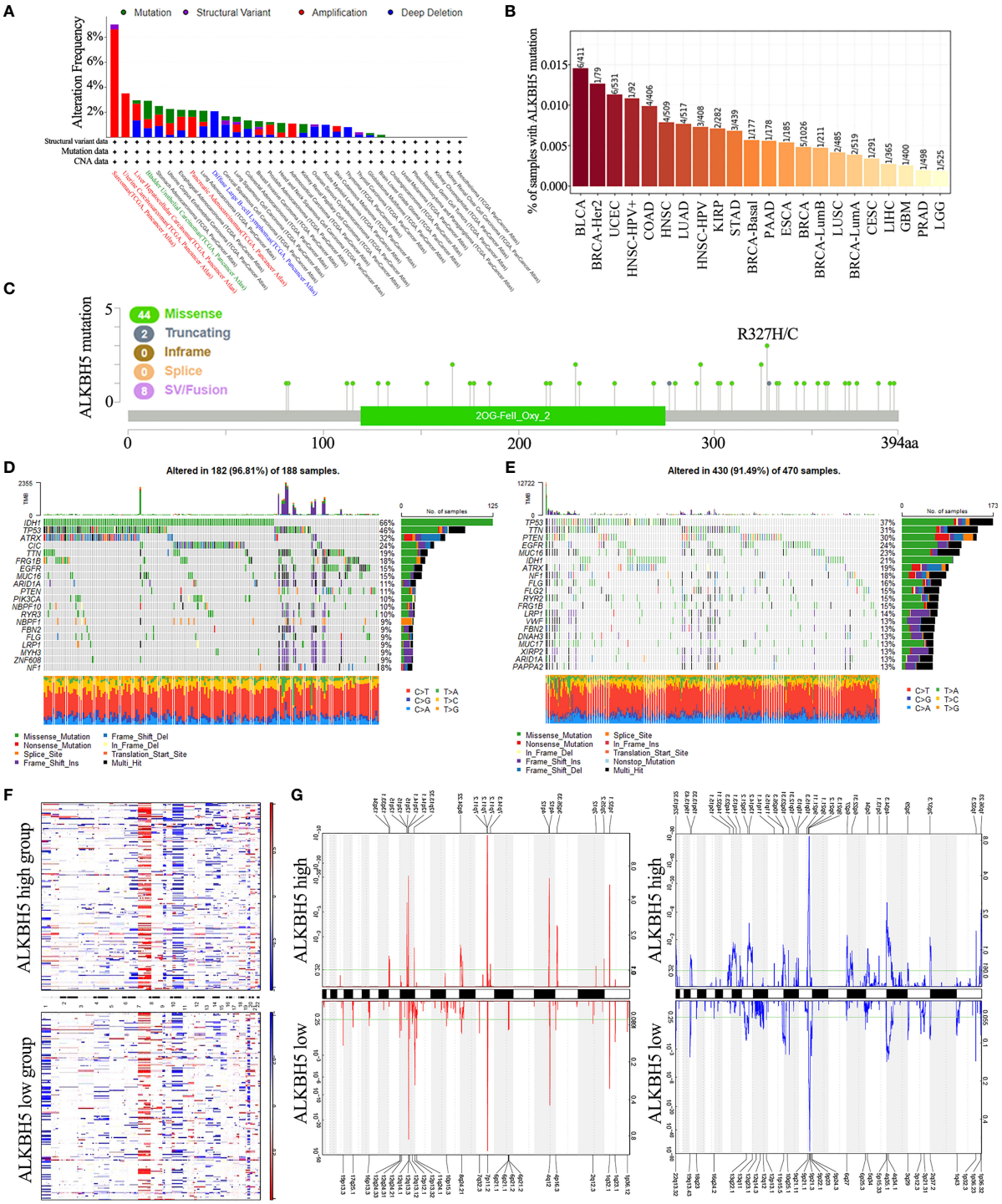

FIGURE 3 | Distinct genomic profiles associated with ALKBH5 expression and integrative analysis of complex cancer genomics and clinical profiles. **(A)** Genetic alteration features (Mutation, Structural Variant, Amplification and Deep Deletion) of ALKBH5 in 32 different tumors were analyzed in TCGA database by the cBioPortal tool. The red label represented the tumors with the top 3 levels of amplification. The green label represented the tumor with the highest mutation level and the blue label represented the tumor with the highest deep deletion level; **(B)** Mutation rates of ALKBH5 gene in various tumors via TIMER portal; **(C)** The mutation sites of ALKBH5 in multiple tumors by the cBioPortal tool. Detection of differential somatic mutations in gliomas, including 25% ALKBH5^{low} group **(D)** and 25% ALKBH5^{high} group **(E)**. Only the top 20 genes with the highest mutation rates were shown; **(F)** The CNAs profile analysis about 25% ALKBH5^{low} group and 25% ALKBH5^{high} group in TCGA dataset via GISTIC2.0; **(G)** Frequency of amplifications and deletions in gliomas with low and high ALKBH5 expression (Blue, deletion; red, amplification).

showed distinct somatic mutations and CNVs based on the expression levels of ALKBH5. This suggested that alterations in the ALKBH5 gene may regulate the initiation, growth and progression of various tumors, especially gliomas.

ALKBH5 and Related Genes Regulate Immunity, Immune Signaling, and Metabolism in Gliomas and Other Cancer Types

STRING database analysis identified ten ALKBH5-binding proteins, namely, FTO, METTL3, METTL14, ALKBH1, YTHDC1, YTHDF1, JMJD4, YTHDF2, DDX3X and WTAP as shown in the protein-protein interaction (PPI) network (**Figure 4A**). GEPIA2 database analysis of 33 cancer types showed the following top 10 ALKBH5-related genes: GID4 (R=0.71), TOP3A (R=0.67), MAPK7 (R=0.66), NT5M (R=0.61), FLII (R=0.59), ZNF18 (R=0.57), DRG2 (R=0.57), COPS3 (R=0.56), MED9 (R=0.56) and PRPSAP2 (R=0.56) (all $P<0.0001$; **Figure 4B**). TIMER2 database was then used to confirm the association between ALKBH5 and the top 9 ALKBH5-related genes (GID4 was not annotated in TIMER2 portal) in 40 cancer types (**Figure 4C**).

Next, in order to further exploring the biological functions of ALKBH5 in glioma. GO-BP and KEGG enrichment analyses of ALKBH5-related genes in glioma was performed. **Figures 5A–C** showed the enrichment patterns of the top 200 genes positively (100 genes) or negatively (100 genes) correlated with ALKBH5 expression in glioma from the CGGA_325, CGGA_693 and TCGA databases. In CGGA_325 and CGGA_693 databases, GO-BP analyses showed wnt signaling pathway, stimulatory C-type lectin receptors signaling pathway, innate immune response activating cell surface receptor signaling pathway, cell-cell signaling by wnt, interleukin-1-mediated signaling pathway and NIK/NF-kappaB signaling (**Figures 5D, E**). In TCGA database, GO-BP analysis showed response to hypoxia and response to oxygen levels (**Figure 5F**). These results showed that ALKBH5 could regulate immunity and metabolism correlated signaling pathways in glioma. In addition, GSE93054 dataset was used to further exploring the correlation between ALKBH5 and immunity and metabolism. **Figure 5G** showed the 1150 intersectional genes of differentially expressed genes in GSC11 (3032 differentially expressed genes) and GSC17 (5158 differentially expressed genes) cell lines after ALKBH5 knockdown in GSE93054 dataset. The GO-BP analysis of these

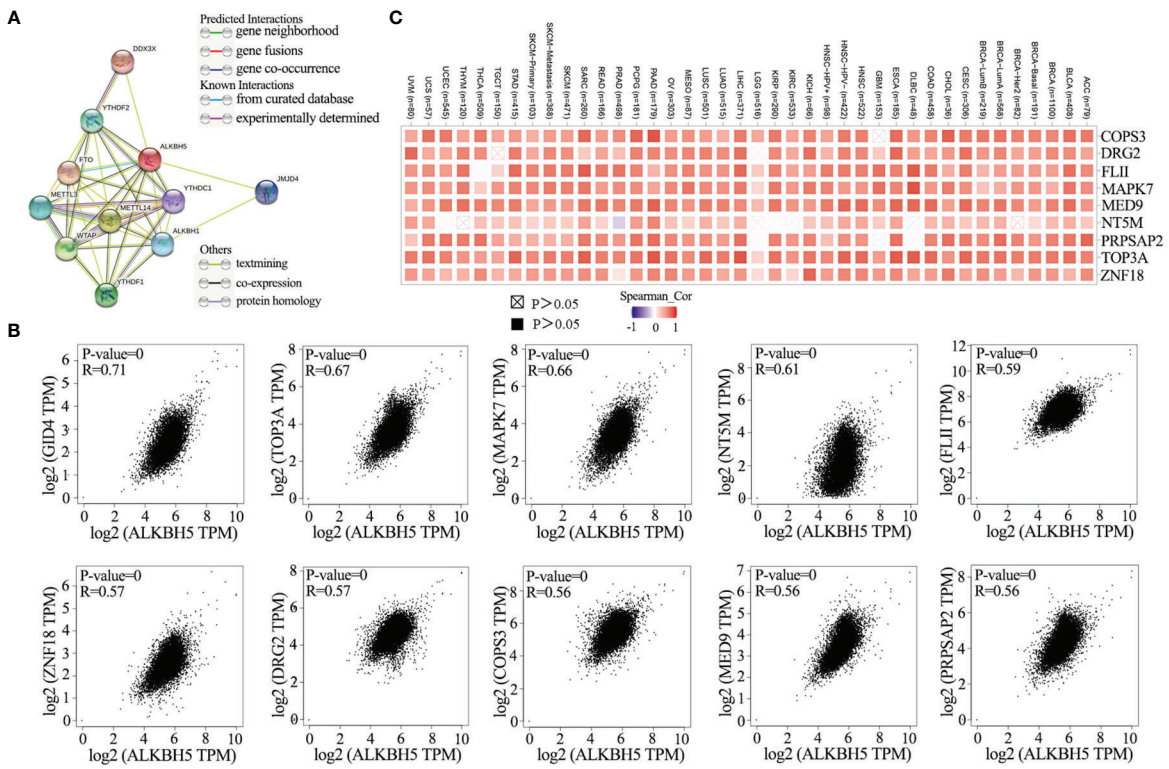

FIGURE 4 | ALKBH5-related genes enrichment analysis in pan-cancers. **(A)** ALKBH5-binding proteins were displayed using the STRING tool (DDX3X, YTHDC1, YTHDF1, YTHDF2, FTO, METTL3, METTL14, WTAP, JMJD4, ALKBH1); **(B)** The top 10 ALKBH5-correlated genes was displayed in various tumors and the correlations between ALKBH5 expression and selected targeting genes were analyzed *via* the GEPIA2 website. These top 10 genes included GID4 (R=0.71), TOP3A (R=0.67), MAPK7 (R=0.66), NT5M (R=0.61), FLII (R=0.59), ZNF18 (R=0.57), DRG2 (R=0.57), COPS3 (R=0.56), MED9 (R=0.56) and PRPSAP2 (R=0.56). The P-value and partial correlation (R) were generated *via* the purity-adjusted Spearman's rank correlation test; **(C)** The corresponding heatmap data of ALKBH5 and its positively correlated genes in various tumors *via* TIMER2.0.

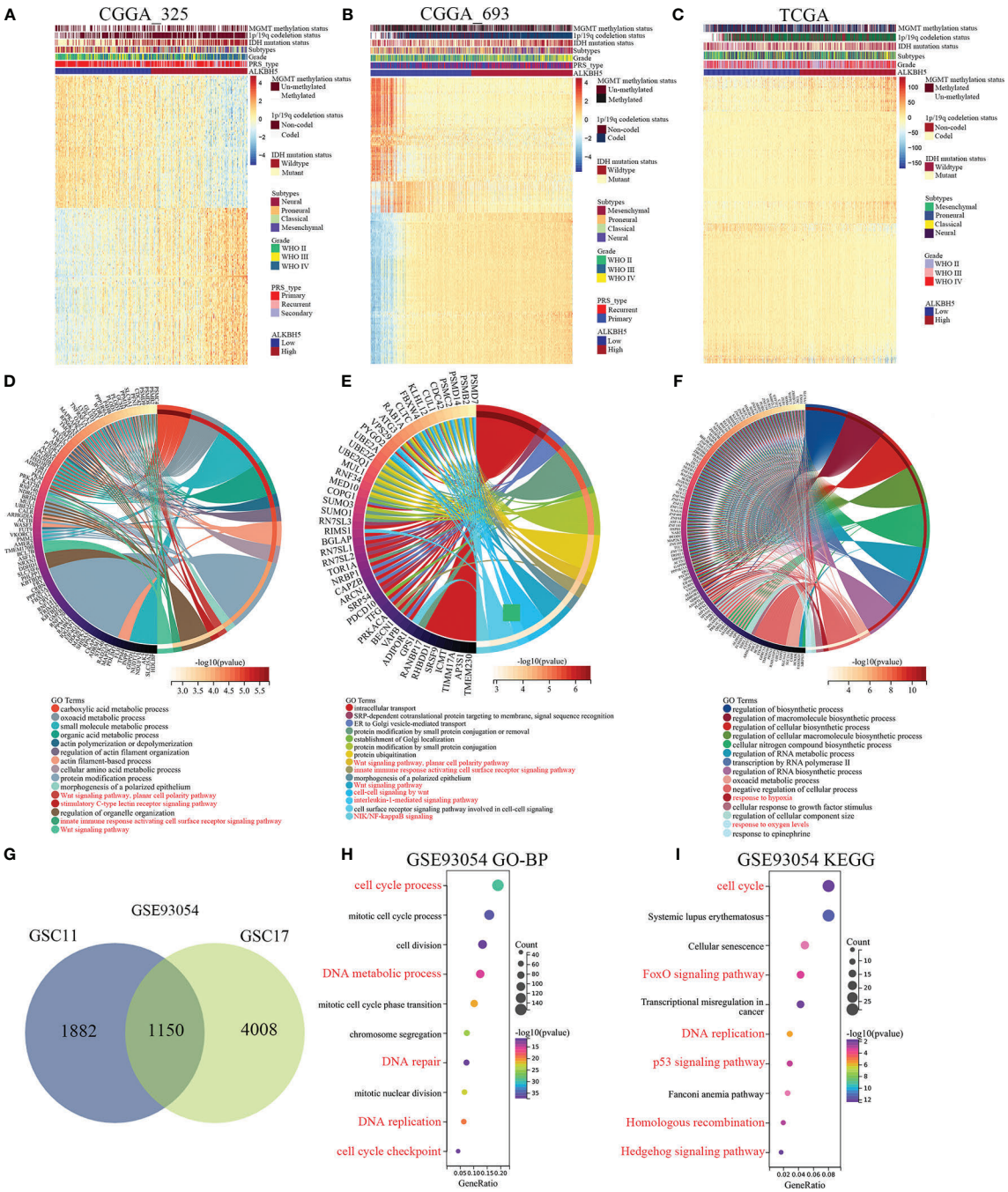

FIGURE 5 | ALKBH5-related genes enrichment analysis in glioma by CGGA_325, CGGA_693 and TCGA datasets. **(A-C)** Heatmap showing the enrichment patterns of the top 200 genes positively (100) or negatively (100) correlated with ALKBH5 expression of glioma in the CGGA_325, CGGA_693 and TCGA databases. **(D-F)** Alterations in different classifications of biological functions in gliomas samples with ALKBH5 expression in the CGGA_325, CGGA_693 and TCGA databases. **(G)** Venn diagram showing the 1150 intersectional genes of differentially expressed genes in GSC11 (3032 differentially expressed genes) and GSC17 (5158 differentially expressed genes) cell lines after ALKBH5 knockdown in GSE93054 dataset. The GO-BP **(H)** and KEGG **(I)** pathway enrichment analyses were applied with the 1150 intersectional genes of differentially expressed genes in GSE93054 dataset. Red label indicated that these GO-BP or KEGG analysis was associated with cell cycle, DNA damage repair, metabolism, or immunity.

1150 genes showed the enrichment processes, including cell cycle process, DNA metabolic process, DNA repair, DNA replication and cell cycle checkpoint in **Figure 5H**. And the KEGG enrichment analysis showed that these 1150 genes enriched in the cell cycle, FoxO signaling pathway, DNA repair, p53 signaling pathway, Homologous recombination, Hedgehog signaling pathway and so on (**Figure 5I**).

These results indicated that ALKBH5 expression was associated with cell cycle, DNA damage repair, metabolism, or immunity. Therefore, we then studied the relationship between ALKBH5 and immune in a variety of tumors.

ALKBH5 Regulates Tumor Infiltration of Immune Cells in Multiple Human Cancers

The above results suggested that ALKBH5 may regulate the tumor immune microenvironment (TIM) in multiple cancer types, we studied the relationship between ALKBH5 expression levels and the composition of tumor infiltrating immune cells (TIICs) in various tumors. Several studies have shown that TIICs are important components of the tumor microenvironment and regulate tumor initiation, progression, and metastasis (46, 47). Firstly, we evaluated the correlation between ESTIMATE scores (ESTIMATE, immune, and stromal scores) and ALKBH5 expression levels in pan-cancers. Immune score reflects the proportion of infiltrated immune cells in the tumor tissues; stromal score reflects the proportion of stromal cells in the tumor tissues. ESTIMATE score is the sum of immune and stromal scores, and reflects the status of the tumor immune microenvironment and tumor purity. Our results demonstrated negative correlation between ALKBH5 expression and the ESTIMATE, immune, and stromal scores in LUAD, LUSC, UCEC, LIHC, CESC, SARC, BRCA and THCA (**Figure 6A**). This suggested that high ALKBH5 expression was associated with decreased infiltration of immune and stromal cells in several tumors, thereby resulting in high tumor purity. Conversely, ALKBH5 expression showed positive correlation with ESTIMATE, immune, and stromal scores in COAD, LGG, and UVM (**Figure 6A**). **Supplementary Figure 8** showed the positive correlations between ALKBH5 mRNA expression level and ESTIMATE score, Immune score and Stromal score in glioma.

Then, we investigated the relationship between ALKBH5 expression and TIIC levels in various tumors using the Sangerbox database. ALKBH5 expression showed negative correlation with multiple immune cell types in LUAD, LUSC, UCEC, CESC, SARC, BRCA, and THCA, and positive correlation with immune cell types in COAD, LGG and UVM (**Figure 6B**). The immune cell types included activated CD4+ and CD8+ T cells, activated dendritic cells, central memory CD4+ and CD8+ T cells, effector memory CD4+ and CD8+ T cells, gamma delta T cells, immature B cells, macrophages, MDSCs, memory B cells, natural killer cells, natural killer T cells, and regulatory T cells (**Figure 6B**).

ALKBH5 Regulates Interferon Signaling, Lymphocyte Activation, and Activation of Antigen-Presenting Cells in Glioma

Since ALKBH5 expression shows positive correlation with tumor infiltration of immune cells in LGG, we further analyzed the relationship between ALKBH5 and tumor infiltrating immune cells in glioma using the ImmuCellAI and xCell databases. ALKBH5 expression levels showed positive correlation with various TIICs in the CGGA_325, CGGA_693, and TCGA glioma datasets; moreover, ALKBH5 expression correlated with the proportions of immune and stromal cells in the gliomas (**Figure 7** and **Supplementary Figure 9**). This suggested that ALKBH5 expression modulated the recruitment of immune cells into the glioma and may affect the sensitivity of glioma patients to immunotherapy.

We then further investigated the effects of ALKBH5 expression on the tumor immune microenvironment (TIM) of glioma by screening seven metagenes, namely, *HCK, IgG, Interferon, LCK, MHC-I, MHC-II*, and *STAT1*, which reflect the status of inflammation and immune responses (48, 49). Our results showed higher enrichment scores for the lymphocyte-specific kinase (*LCK*), major histocompatibility complex I (*MHC-I*), major histocompatibility complex II (*MHC-II*) and signal transducer and activator of transcription 1 (*STAT1*) metagenes in glioma patients with high ALKBH5 expression levels from the CGGA_325, CGGA_693, and TCGA datasets (**Supplementary Figure 10**). This suggested that ALKBH5 expression regulated interferon signaling, lymphocyte activation, and activation of antigen-presenting cells in the gliomas.

ALKBH5 Correlates With Immune Checkpoint Blockade Proteins and Is a Potential Biomarker of Tumor Immunotherapeutic Response in Multiple Tumors

Antitumor immunity is a strong predictor of the efficacy of tumor immunotherapy and correlates with microsatellite instability (MSI), tumor mutation burden (TMB), and neoantigens in the tumor microenvironment (50). Tumors with high MSI (MSI-H) and TMB respond favorably to immune checkpoint inhibition therapies (51). Neoantigens are mutated antigens that are specifically expressed by the tumor tissues and are potential targets for T cell-based tumor immunotherapy (52). Therefore, we investigated the relationship between ALKBH5 expression levels and MSI, TMB or neoantigens to determine if ALKBH5 was a predictor of immunotherapeutic responses in multiple cancer types. ALKBH5 expression showed positive correlation with MSI in LUAD (P=0.038), UCEC (P=3.6e-06), CESC (P=0.027), COAD (P=1e-19) and READ (P=0.017), and negative association with MSI in PRAD (P=0.0071), THCA (P=0.0036), DLBC (P=0.026) and KICH (P=0.023) (**Figure 6C**). Furthermore, ALKBH5 expression showed positive relationship with TMB in UCEC (P=2.3e-10), CESC (P=0.0036), COAD (P=1.7e-12), STAD (P=0.026), READ (P=2.3E-07) and KICH (P=0.014), and negative association with TMB in LUAD (P=0.047) and THCA (P=0.014) (**Figure 6D**). ALKBH5 expression also showed positive correlation with neoantigens in UCEC (P=0.0015), COAD (P=0.0072), READ (P=0.0069) and LGG (P=0.012), and negative association with neoantigens in BRCA (P=0.003) and THCA (P=0.0086) (**Figure 6E**).

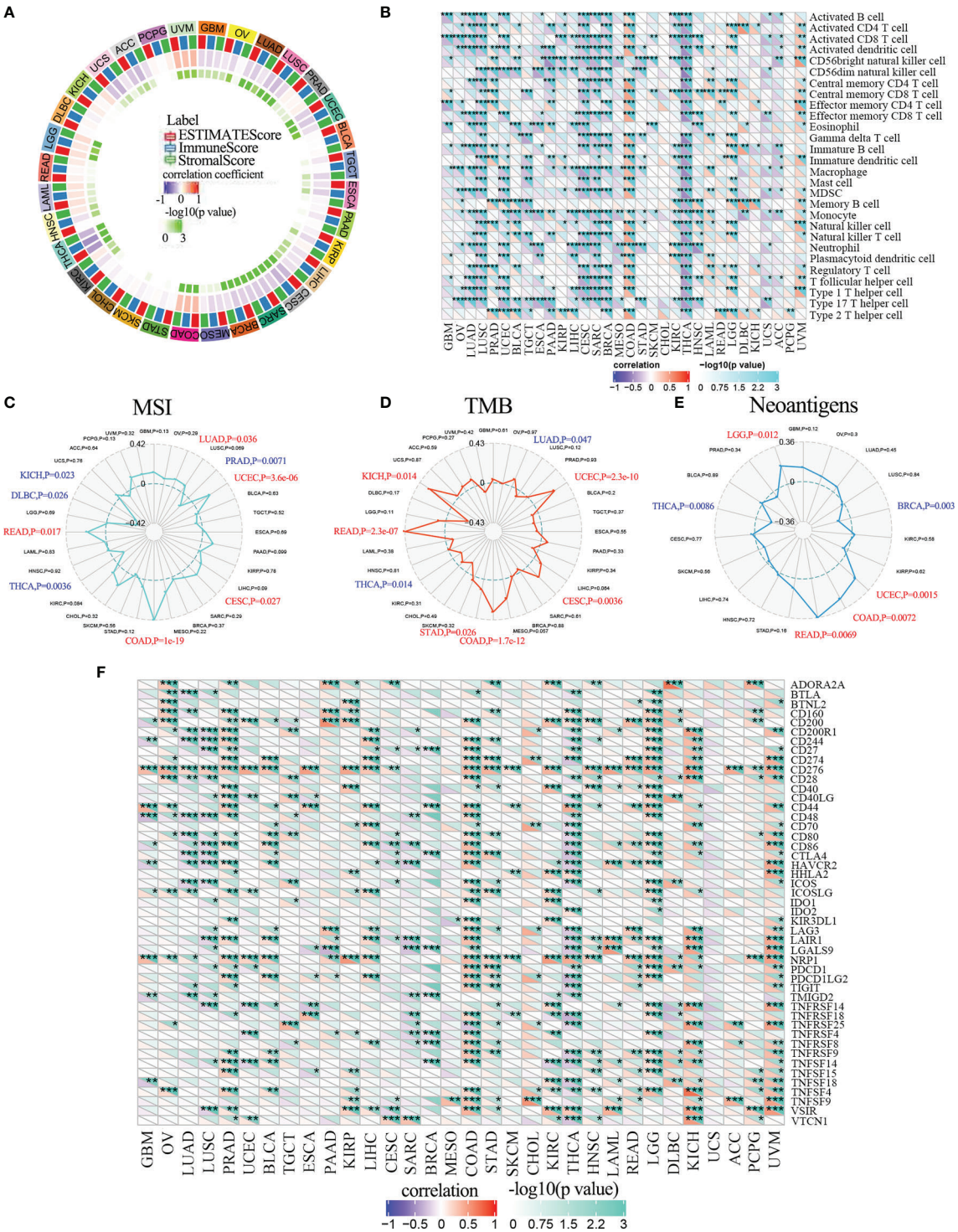

FIGURE 6 | ALKBH5 mRNA expression and immune infiltration. **(A)** The correlations between ESTIMATE scores (ESTIMATE Score, Immune Score, and Stromal Score) and ALKBH5 expression were analyzed in various tumors by Sangerbox portal. **(B)** The relationship between ALKBH5 expression and immune cell infiltration level was analyzed in various tumors by Sangerbox online website. The relationship between ALKBH5 mRNA expression and MSI **(C)**, TMB **(D)**, neoantigen **(E)** and ICP-gene **(F)** in multiple cancers. Red label indicated positive correlation with ALKBH5 expression and blue label indicated negative correlation with ALKBH5 expression. **P*<0.05, ***P*<0.01, ****P*<0.001, *****P*<0.0001.

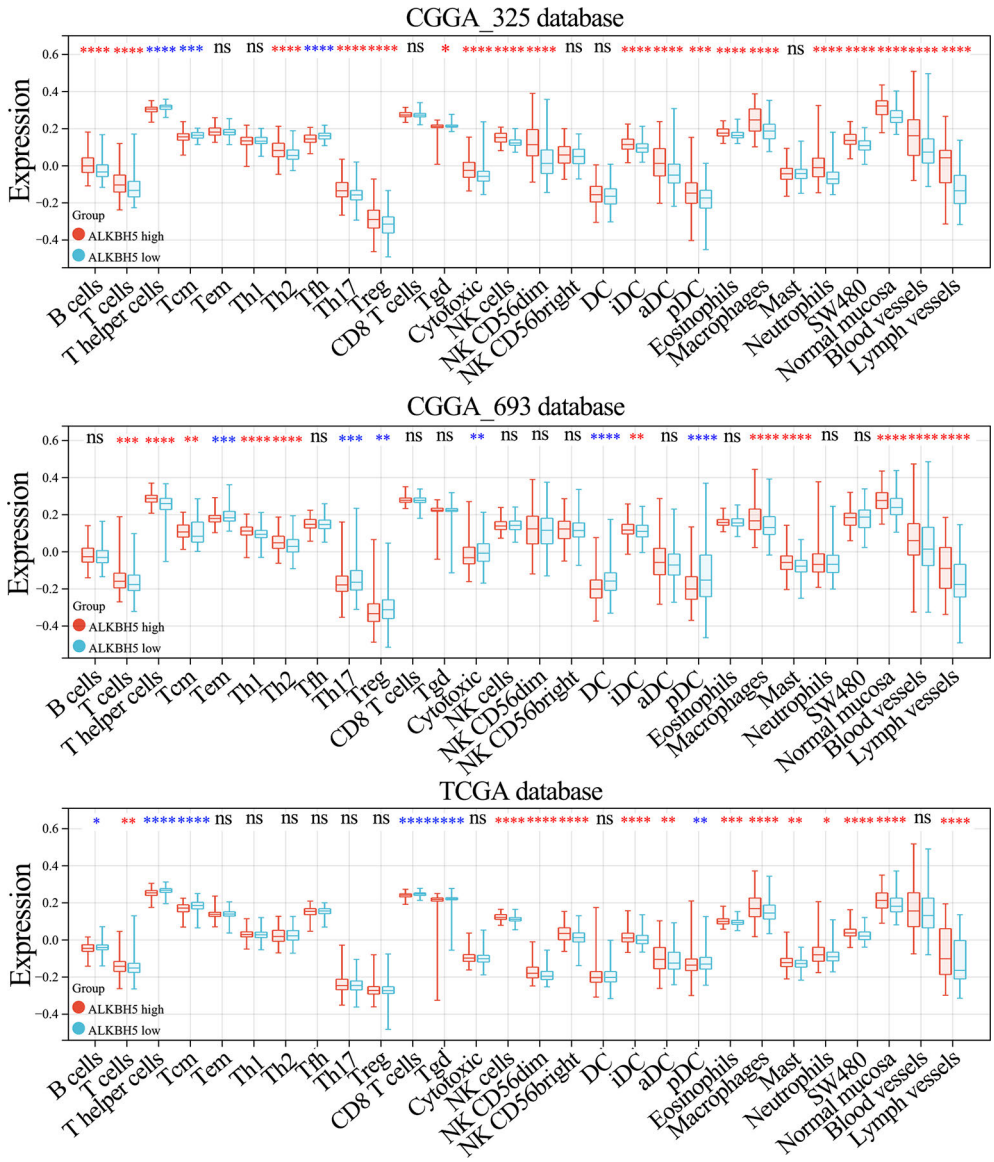

FIGURE 7 | Correlation between ALKBH5 mRNA expression and tumor immune-related cells in glioma. The correlation between ALKBH5 mRNA expression and immune cells types in glioma calculated by xCell algorithm in CGGA_325, CGGA_693 and TCGA datasets. ns (nonsense), *P<0.05, **P<0.01, ***P<0.001, ****P<0.0001.

The immune checkpoint (ICP) blockade proteins are the most promising targets of cancer immunotherapeutic treatments because they regulate the infiltration of immune cells into the tumor microenvironment (48). Therefore, we analyzed the relationship between expression levels of ICP genes and ALKBH5 in multiple cancer types. ALKBH5 expression showed a positive correlation with ICP genes in UVM, KICH, LGG and COAD (**Figure 6F**). ALKBH5 expression showed positive correlation with 34 out of 47 ICP genes in COAD and 32 out of 47 ICP genes in UVM (**Figure 6F**). These results suggested that ALKBH5 affected the sensitivity of UVM, KICH, LGG and COAD to the immune checkpoint inhibitor therapies. In THCA, ALKBH5 expression showed negative correlation with the ICP genes (**Figure 6F**). This suggested that THCA patients with high ALKBH5 expression may respond poorly to immunotherapies targeting ICP genes. Next, we analyzed the correlation between ALKBH5 and various ICP receptors and ligands in glioma patients from the CGGA_325, CGGA_693, and TCGA datasets (49). ALKBH5 expression showed positive association with ICP receptors such as TNFRSF14, CD40, CD96 and CD200R1, and ICP ligands such as PDCD1LG2, CD70, TNFSF14, ICOSLG and CD274 in glioma tissues (**Supplementary Figure 11**). Therefore, we hypothesized that high ALKBH5 expression altered the immune microenvironment in the glioma tissues by modulating the expression levels of ICP receptors and ligands such as TNFRSF14, CD40, CD96, PDCD1LG2, CD70 and TNFSF14.

This suggested that ALKBH5 mediated the activation of ICP genes and was an ideal target for immunotherapy of glioma patients.

Overall, our results suggested that ALKHB5 expression levels modulated the sensitivity of several tumors to immunotherapy. Therefore, ALKBH5 is a potential immunotherapy biomarker and predictor of tumor immunotherapeutic response.

Construction of the Upstream lncRNA-miRNA Regulatory Network That Regulates ALKBH5 Expression Levels in Gliomas and Other Tumors

In recent years, several studies have shown that long non-coding RNAs (lncRNAs) play a significant role in tumorigenesis by regulating the expression of the downstream mRNAs through sequestering of their target miRNAs (53, 54). Therefore, we investigated the lncRNA-miRNA network that may regulate ALKBH5 expression in various tumors. First, we screened the miRWalk, miRDB, Targetscan, and miRabel databases and identified 49 miRNAs that potentially target the ALKBH5 mRNAs (**Figure 8A**). The top 10 ALKBH5 mRNA-targeting miRNAs were hsa-miR-4732-5p, hsa-miR-193a-3p, hsa-miR-362-3p, hsa-miR-193b-3p, hsa-miR-589-5p, hsa-miR-4736, hsa-miR-6840-3p, hsa-miR-329-3p, hsa-miR-5008-5p and hsa-miR-6132 (**Figure 8B**).

Among these 10 ALKBH5 mRNA-targeting miRNAs, 5 miRNAs (hsa-miR-193a-3p, hsa-miR-362-3p, hsa-miR-193b-3p, hsa-miR-589-5p and hsa-miR-329-3p) were found in the CGGA database (**Figures 8C, D** and **Supplementary Figure 12**). Bioinformatics analysis showed that the expression levels of hsa-miR-193a-3p (**Supplementary Figure 12A**), hsa-miR-362-3p (**Supplementary Figure 12C**), and hsa-miR-193b-3p (**Supplementary Figure 12E**) were positively associated with glioma grades, whereas, the expression levels of hsa-miR-589-5p (**Figure 8C**) and hsa-miR-329-3p (**Supplementary Figure 12G**) showed negative correlation with glioma grades. Kaplan-Meier survival curve analysis of glioma patients in the CGGA database showed that hsa-miR-589-5p was associated with the prognosis of primary glioma patients (**Figure 8D**). The expression levels of hsa-miR-329-3p were not associated with the prognosis of glioma patients (**Supplementary Figure 12H**). These results suggested that hsa-miR-589-5p potentially targeted ALKBH5 expression in the gliomas.

Next, we identified 769 predicted lncRNAs and 73 validated lncRNAs that may target hsa-miR-589-5p using the LncBase database. The top 20 predicted lncRNAs and top 20 validated lncRNAs were used to construct a lncRNA-miRNA-ALKBH5 regulatory network using the cytoscape software (**Figure 8E**). These results demonstrated the upstream lncRNA-miRNA regulatory network that may regulate the aberrant expression of ALKBH5 in the gliomas.

ALKBH5 Promotes *In Vitro* and *In Vivo* Proliferation, Migration, and Invasion of Glioma Cells and Affect the Recruitment of M2 Macrophages

Next, we analyzed ALKBH5 expression levels in various glioma cell lines by qRT-PCR. ALKBH5 mRNA levels were significantly higher in the U87-MG and U251-MG cell lines compared to the other glioma cell lines and were consistent with the results from the CCLE database (**Figure 9A** and **Supplementary Figure 13**). We then used specific ALKBH5-targeting siRNAs to knockdown the expression levels of ALKBH5 in the U87-MG and U251-MG cells (**Figure 9B**). And ALKBH5 was overexpressed by using the ALKBH5 overexpression plasmid (**Supplementary Figure 14A**). CCK-8 assay, Wound healing assay and Transwell assay results showed that ALKBH5 knockdown suppressed the cell proliferation, migration and invasion of U87-MG and U251-MG and ALKBH5 overexpression promoted the cell proliferation, migration and invasion of LN229 *in vitro* (**Figures 9C-G** and **Supplementary Figures 14B–D**). Moreover, THP-1 cells were differentiated into M2 macrophage on the basis of classical inducing methods (**Supplementary Figure 15**) (55–57). Silencing of ALKBH5 in U87 and U251 cells significantly reduced the infiltration of M2 macrophages (**Figure 9H**), consisting with the results of our previous analysis (**Figure 7** and **Supplementary Figure 9**). Furthermore, tumor xenograft experiments showed that ALKBH5 knockdown suppressed the *in vivo* growth of glioma cells (**Figures 9I–K**). These results showed that ALKBH5 promoted *in vitro* and *in vivo* proliferation, migration, and invasion of glioma cells.

DISCUSSION

N^6-methyladenosine (m^6A) modification is the most common chemical modification in messenger RNAs (mRNAs), and non-coding RNAs (ncRNAs) (58). The reversible N6-methylation of adenosine is a dynamic post-transcriptional modification process involving three protein complexes, namely, m^6A readers, m^6A writers, and m^6A erasers (59). Several studies have shown that aberrant m^6A modification regulates the development, growth, and progression of various tumors (1).

ALKBH5 is a m^6A demethylase that is associated with the development and progression of multiple cancer types (60), such as glioblastoma, ovarian cancer, lung cancer, liver cancer, pancreatic cancer and osteosarcoma. However, pan-cancer analysis of ALKBH5 has not been investigated. Therefore, we investigated the functional role of ALKBH5 in multiple tumors, especially gliomas. The analysis included the effects of ALKBH5 RNA expression levels on prognosis, as well as the genetic alterations in the *ALKBH5* gene, GO and KEGG analyses of ALKBH5-related genes, and tumor immunity. We also investigated the upstream lncRNA-miRNA network that regulates ALKBH5 expression in gliomas and its effects on glioma progression.

In this study, we first performed comprehensive bioinformatics analysis to determine the functional role of ALKBH5 in multiple cancers using the patient data from various databases. The results showed that ALKBH5 mRNA and protein levels were upregulated compared to the corresponding normal tissues in multiple cancers including glioma. Our analysis was confirmed by the previous studies. ALKBH5 mRNA was increased in epithelial ovarian cancer tissue as compared to the normal ovarian tissues and ALKBH5

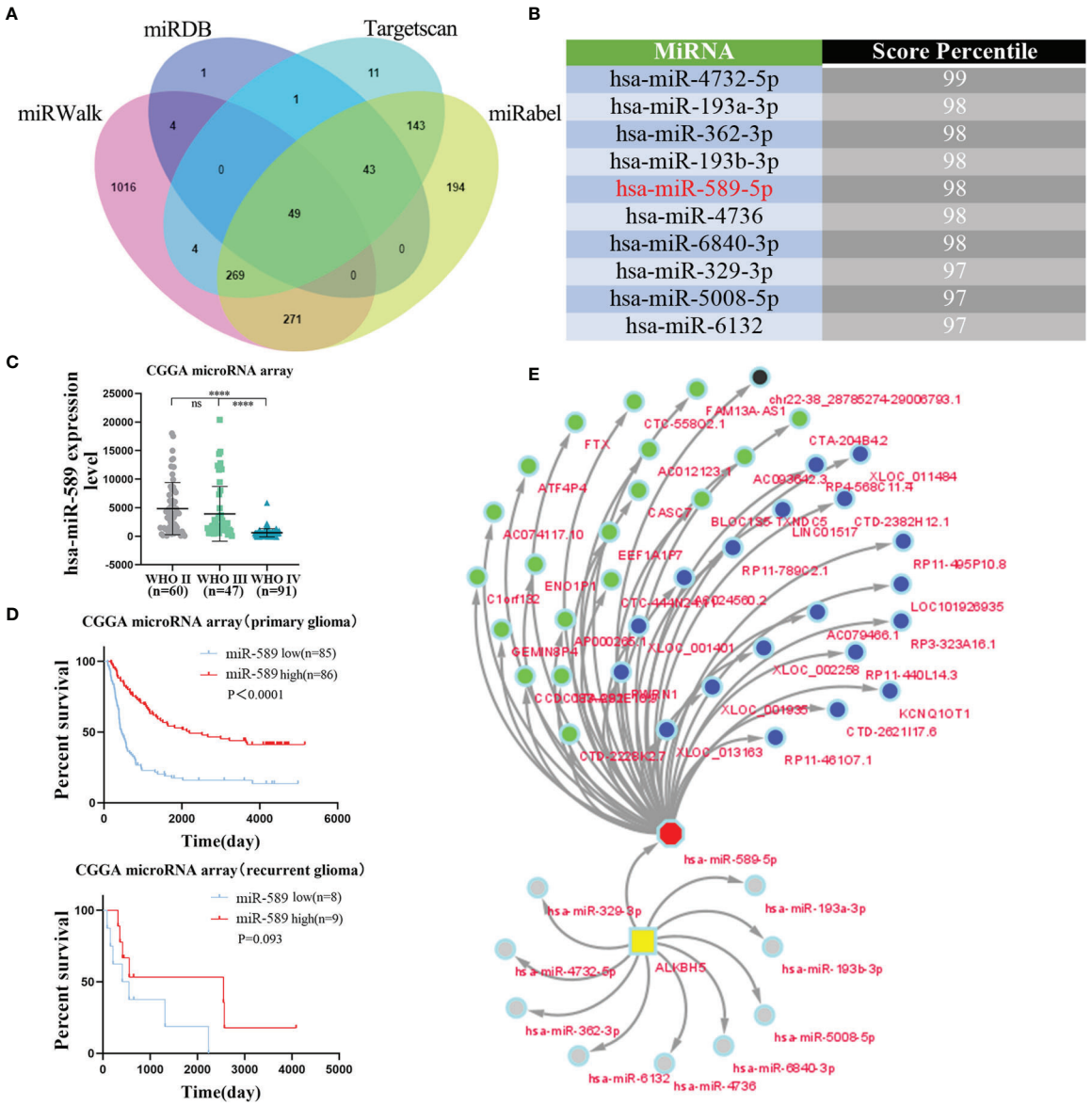

FIGURE 8 | The lncRNA-miRNA-ALKBH5 regulatory network constructed. **(A)** The upstream miRNAs of ALKBH5 were predicted by miRWalk, miRDB, Targetscan and miRabel databases and the intersection was taken (49 intersection miRNAs). **(B)** The top 10 miRNAs targeting ALKBH5 were displayed in Targetscan database. **(C)**The relationship between hsa-miR-589 expression and grade in glioma from CGGA microRNA array dataset. **(D)** The relationship between hsa-miR-589 expression and prognosis in glioma patients from CGGA microRNA array dataset. **(E)**The lncRNA-miRNA-ALKBH5 regulatory network was constructed by Cytoscape. ns (nonsense), ****P<0.0001.

silencing could inhibit the proliferation and invasion of epithelial ovarian cancer cells (16). Xu et al. found that ALKBH5 protein expression was increased in colon cancer and could promote colon cancer progression by decreasing methylation of the lncRNA NEAT1 (61). Gu et al. discovered that the mRNA and protein expressions of ALKBH5 were overexpressed in endometrial cancer cells and promoted proliferation and invasion of endometrial cancer *via* erasing IGF1R m^6A-modifications (62). For glioma, Ji et al. found that the mRNA and protein expressions of ALKBH5 were upregulated in glioma and promoted the glioma cells proliferation by increasing the mRNA stability of G6PD (63). ALKBH5 expression was associated with tumor grades, subtypes, and new WHO tumor types (IDH mut+codel, IDH mut+non-codel and IDH wild) in glioma. The pan-cancer analysis showed correlation between ALKBH5 mRNA expression and the prognosis of cancer patients. Analysis of 100 glioma cases discovered that glioma patients with high ALKBH5 expression levels had shorter OS compared with patients with low ALKBH5 expression level. IDH mutations, considered as truncal events, are occurred in the vast

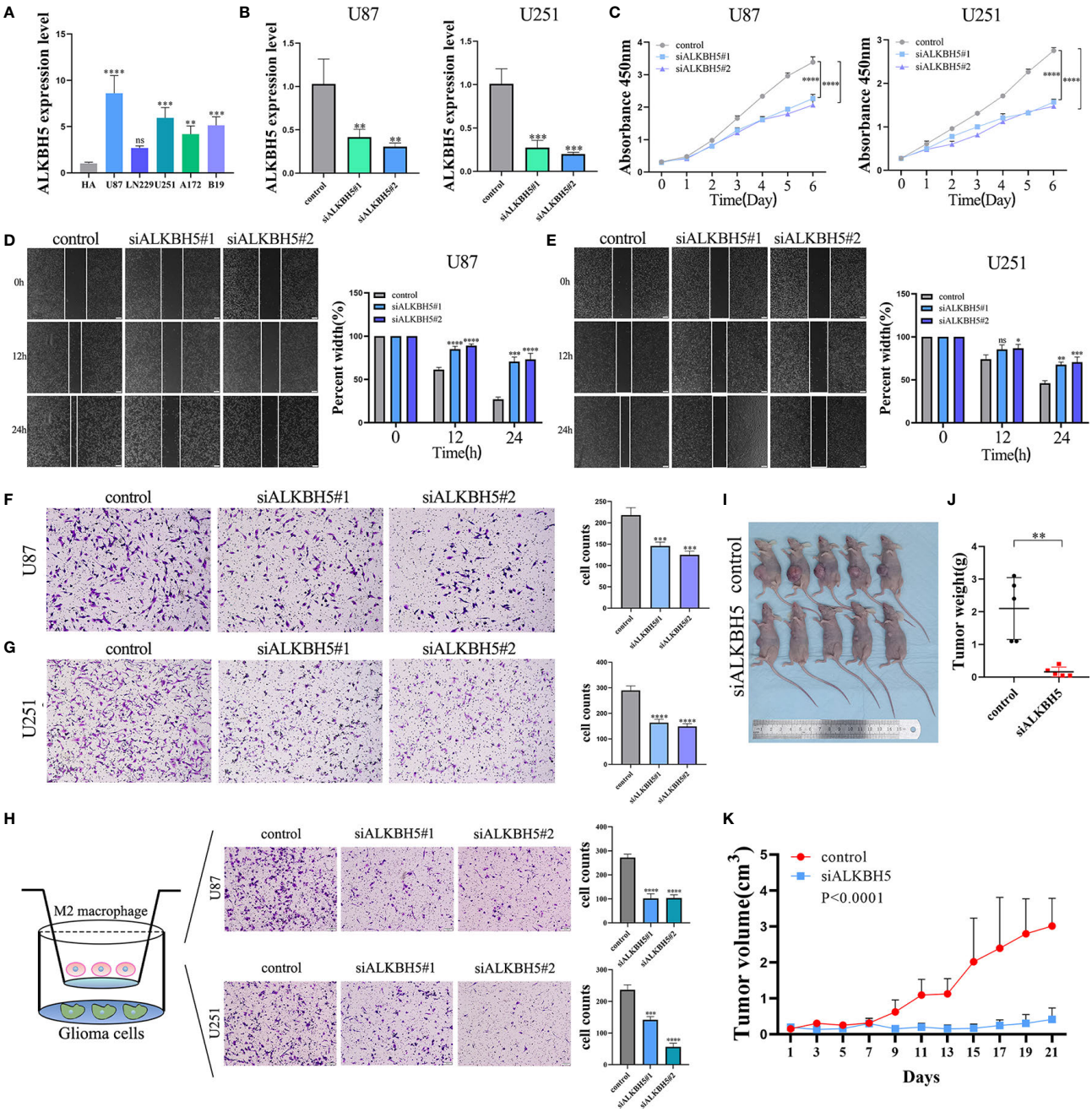

FIGURE 9 | The biological functions of ALKBH5 in glioma. **(A)** The expression levels of ALKBH5 were verified in multi-cell lines, including human astrocyte (HA), U87, LN229, U251, A172 and B19 cell lines. **(B)** Verification of knockdown efficiency of ALKBH5 in U87 and U251 cell lines. The biological functions of ALKBH5 on glioma cell lines were verified by CCK-8 **(C)**, wound healing **(D, E)** and Transwell **(F, G)** experiments. Xenograft mouse models were generated by subcutaneous injection of U87 cells into nude mice. Seven days after implanted, mice were treated with control siRNA (n=8) or ALKBH5 siRNA (n=8). **(H)** Infiltration of M2 macrophage in control (left), siALKBH5#1 (middle), siALKBH5#2 (right) of U87 and U251 cells. Representative image of subcutaneous tumors **(I)**, tumor weight **(J)** and tumor growth curve **(K)**, in si-ALKBH5 treated or control siRNA treated xenograft models with U87 cells. ns (nonsense), **P*<0.05, ***P*<0.01, ****P*<0.001, *****P*<0.0001.

majority of low-grade gliomas (LGG) and secondary GBM (64). The 2016 WHO Classification of CNS tumors included several tumor-specific molecular alterations in the classification and diagnosis of gliomas. The 1p/19q co-deletion status were included in the oligodendroglioma stratification. Multiple studies have shown that 1p/19q co-deletion had significant prognostic value in the WHO oligodendrocytoma subgroup (49). In our studies, high ALKBH5 expression was associated

with clinical features such as IDH wildtype status, 1p/19q non-codeleted status, and demethylation of MGMT, all of which were related to poor prognosis in the glioma patients. Cox regression analysis showed that ALKBH5 was an independent prognostic predictor in glioma patients. Recent research showed that ALKBH5 mRNA and protein expression were upregulated in glioblastoma stem-like cells (GSCs) and ALKBH5 could maintain the tumorigenicity of GSCs by maintaining FOXM1 expression (15). And Guo et al. found that lncRNA SOX2OT could enhance SOX2 expression through ALKBH5-mediated epigenetic regulation in glioblastoma, thereby promoting temozolomide resistance (65). Moreover, Catherine Seva et al. reported that ALKBH5 promoted radio-resistance and invasion capability of glioblastoma stem cells (GBMSCs) (66). These findings demonstrated that high ALKBH5 expression was associated with unfavorable survival outcomes in gliomas. Overall, our analysis showed that ALKBH5 was a potential prognostic biomarker in various cancers, especially in glioma.

Somatic mutations in critical genes transform normal cells into cancer cells (67). Moreover, somatic mutations in the cancer cells contribute significantly to immune evasion and poor responses to therapies (68). We identified amplifications, mutations, and deep deletions as the most frequent alterations in the *ALKBH5* gene in several cancer types. In this study, gliomas with low ALKBH5 expression showed higher proportion (66%) of IDH1 mutations compared to those with high ALKBH5 expression (21%). Previous reports showed that IDH mutations were more abundant in LGG, and the survival rate of LGG patients was higher than those with HGG (69). The low ALKBH5 expressing glioma patients (46%) also showed increased frequency of mutations in *TP53* compared to the high ALKBH5 expressing group (37%). TP53 is a well-known tumor suppressor gene that inhibits GBM progression. The high ALKBH5-expressing glioma patients showed higher EGFR mutational rate compared to those with low ALKBH5 expression (24% vs. 15%). Previous studies showed that EGFR activation in patients with GBM was associated with worse survival outcomes (70). Therefore, ALKBH5 is a potential prognostic biomarker for patients with glioma and multiple cancer types.

In order to explore the biological functions of ALKBH5, we applied GO and KEGG analysis of ALKBH5 related genes. GO and KEGG pathway enrichment analysis showed that high ALKBH5 expression correlated with the activation of metabolic and immune signaling pathways in various tumors. In glioma, ALKBH5 could affect immunity, metabolism, cell cycle, DNA damage repair *via* CGGA_325, CGGA_693, TCGA and GSE93054 datasets. We focused on the effect of ALKBH5 on immunity, for the significant role of immune system in preventing and fighting tumors. In recent years, cancer immunotherapy, restoring the immune system's ability to recognize and destroy tumor cells, has shown significant clinical results, but only for a small number of tumors (64). And the tumor-infiltrating immune cells play a significant role in the tumor microenvironment (TME), which provides a favorable microenvironment for the survival of cancer cells, and is associated with regulation of tumor immunosurveillance and therapeutic response of tumors (71, 72). ESTIMATE analysis showed that high expression of ALKBH5 correlated significantly with the infiltration of immune cells and stromal cells in multiple cancers. These results suggested that ALKBH5 inhibited the infiltration of immune cells into tumors, thereby enabling the tumor cells to evade the immune system. Tariq M Rana et al. found that ALKBH5 could regulate the expression of Mct4/Slc16a3 and lactate content in tumor microenvironment, as well as the composition of tumor infiltrating Treg and bone marrow derived inhibitory cells, thereby inhibiting immune cells accumulation in tumor microenvironment in some tumors, which was consistent with our analysis (23).

In recent years, immunotherapy has been widely applied in tumors, but many solid tumors showed poor immunotherapy effect due to their special immunosuppressive microenvironment (49). As an immunologically "cold tumor", glioma is considered to be highly resistant to immunotherapy. However, our research found that ALKBH5 expression was positively correlated with the infiltration of immune cells into the tumors in glioma and may affect the sensitivity of glioma patients to immunotherapy. Wu et al. found that ALKBH5 promoted the generation of immunosuppressive tumor microenvironment *via* hypoxia-induced paraspeckle assembly and IL8 secretion (73). These results suggested that ALKBH5 could be acted as a potential therapeutic target for glioma and as a novel marker to predict prognosis of glioma patients (74). In addition, analysis of the seven inflammation and immune related clusters suggested that high ALKBH5 expression activated the antigen-presenting cells and lymphocytes, and enhanced interferon signaling in the glioma tissues. Overall, these data suggested that glioma patients with high ALKBH5 expression may benefit from immunotherapy. This study provides theoretical basis for the application of immunotherapy in patients with glioma (49).

Recent studies have shown that tumors with high MSI (MSI-H), TMB or neoantigens show better response to immunotherapy (75). ICP proteins play a significant role in the tumor-infiltration of immune cells and immunotherapy (76). Therefore, ICP gene expression is used to select tumor patients that may benefit from immune checkpoint blockage (ICB) therapy (77). Our results showed that the expression of ALKBH5 was closely related to MSI, TMB, and neoantigens in various tumors. ALKBH5 expression correlated with the expression of multiple ICP genes in multiple cancers. This suggested that ALKBH5 regulated tumor immunity in several cancer types. Therefore, ALKBH5 may be a potential predictive biomarker of immunotherapeutic responses in patients with malignant tumors. Finally, we used Targetscan, miWalk, miRDB, miRabel and other websites to identify ALKBH5-targeting miRNAs and lncRNAs and constructed a lncRNA-miRNA-ALKBH5 regulatory network that regulates the abnormal expression of ALKBH5 in various cancers. Furthermore, *in vivo* and *in vitro* experiments with glioma cells showed that ALKBH5 acted as an oncogene and promoted the growth, migration, and invasiveness of the glioma cells. And ALKBH5 knockdown could reduce the infiltration of M2 macrophage in U87 and U251 cells.

In summary, our results suggested that ALKBH5 was aberrantly expressed in various cancers and significantly correlated with the prognosis of cancer patients. *ALKBH5* gene alterations including mutations, duplications, and amplifications were identified in a wide variety of cancer types. ALKBH5 expression showed significant association with the infiltration of immune cells into the tumor microenvironment and immunotherapeutic response in multiple cancers. Therefore, ALKBH5 is a potential immunotherapeutic biomarker for selecting tumor patients that may benefit from immune checkpoint blockade (ICB) therapy in glioma and other cancers. *In vitro* and *in vivo* experiments confirmed that ALKBH5 functioned as an oncogene in gliomas. Our study suggested that ALKBH5 was a promising prognostic biomarker as well as a potential predictor of sensitivity to immunotherapy in several malignant tumors and glioma.

LIST OF ABBREVIATIONS

The information is shown in **Supplementary Table 1**.

DATA AVAILABILITY STATEMENT

The original contributions presented in the study are included in the article/**Supplementary Material**. Further inquiries can be directed to the corresponding authors.

ETHICS STATEMENT

The animal study was reviewed and approved by Ethics Committee of the Tianjin Neurological Institute and Hospital (Tianjin Medical University General Hospital).

AUTHOR CONTRIBUTIONS

CW, BW and DP contributed equally to this study and made substantial contributions to conception and design, acquisition of data, and analysis and interpretation of data. LL and ZZ supplied the RNA-seq data and clinical information of 100 glioma patients. XZ, LL, ZL, YH and XD performed the experiments and were involved in drafting the article. HL, SL and SZ were mainly responsible for editing the data and revised the article critically for important intellectual content. LH, ZZ and JZ had given final approval of the version to be published. All authors read and approved the final manuscript.

FUNDING

The project was supported by the grants (Nos. 81773187, 81702465) from National Nature Science Foundation of China and by Tianjin high school program for young and middle-aged talents backbone and Tianjin young medical talents program.

ACKNOWLEDGMENTS

We thank professor Xudong Wu (Department of Cell Biology, State Key Laboratory of Experimental Hematology, The Province and Ministry Co-sponsored Collaborative Innovation Center for Medical Epigenetics, Key Laboratory of Immune Microenvironment and Disease, Tianjin Medical University, Tianjin, China.) for providing the ALKBH5 overexpression plasmids.

SUPPLEMENTARY MATERIAL

The Supplementary Material for this article can be found online at: https://www.frontiersin.org/articles/10.3389/fimmu.2022.849592/full#supplementary-material

Supplementary Figure 1 | Flow chart of bioinformatics analyses.

Supplementary Figure 2 | ALKBH5 expression in different IDH status, 1p/19q status and MGMT promotor status in glioma. The expression level of ALKBH5 in different IDH status **(A)**, 1p/19q status **(B)** and MGMT promotor status **(C)** of gliomas in CGGA_325, CGGA_693 and TCGA databases. *P<0.05, **P<0.01, ***P<0.001, ****P<0.0001.

Supplementary Figure 3 | ALKBH5 protein expression, location and conservation. **(A)** ALKBH5 protein expression in 44 normal tissues via THPA portal; **(B)** Localization of ALKBH5 protein in cells was displayed via THPA portal; **(C)** Conservation of ALKBH5 protein among different species through NCBI; **(D)** ALKBH5 protein expression in multiple tumors compared with adjacent normal tissues in TCGA database, including ovarian cancer (P=0.0178), breast cancer (P<0.0001), clear cell RCC (P<0.0001), lung adenocarcinoma (P<0.0001) and UCEC (P=0.0126).

Supplementary Figure 4 | Correlation between ALKBH5 mRNA expression and prognosis of tumor patients. The relationships between ALKBH5 expression level and OS **(A)** and DSS **(B)** of various cancers by SangerBox (P<0.05). The Kaplan-Meier plotter was applied to survival analysis by ALKBH5 mRNA expression level in ovarian cancer **(C)**, gastric cancer **(D)**, lung cancer **(E)** and liver cancer **(F)**, including overall survival (OS), progression free survival (PFS), first progression (FP), post progression survival (PPS) and relapse free survival (RFS).

Supplementary Figure 5 | The relationships between ALKBH5 expression and prognosis of glioma patients. Kaplan-Meier analysis of ALKBH5 expression in the overall survival of patients with primary gliomas **(A)**, recurrent glioma, low grade glioma (LGG), and glioblastoma (GBM) in CGGA_325 **(A)**, CGGA_693 **(B)** and TCGA **(C)** databases.

Supplementary Figure 6 | Univariate and multivariate Cox analyses of ALKBH5 and clinical features in glioma. Univariate and multivariate Cox analyses of ALKBH5 and clinical features of glioma in CGGA_325 combined with CGGA_693 **(A)** and TCGA **(B)** databases. The nomogram model of ALKBH5 and clinical features in CGGA_325 combined with CGGA_693 **(C)** and TCGA datasets **(D)**. *P<0.05, **P<0.01, ***P<0.001, ****P<0.0001.

Supplementary Figure 7 | Prognosis analyses of glioma patients. Kaplan-Meier analyses of overall survival among four patient groups stratified by the ALKBH5 mRNA level and IDH status **(A)**, 1p/19q status **(B)**, MGMT promotor status **(C)**, radiotherapy **(D)**, and chemotherapy **(E)** in CGGA_325 and CGGA_693 datasets. *P<0.05, **P<0.01, ***P<0.001, ****P<0.0001.

Supplementary Figure 8 | Correlation between ALKBH5 mRNA expression and ESTIMATE Score in glioma. The correlations between ALKBH5 mRNA expression level and ESTIMATE Score (P=5.5e-3, R=0.13) (A), Immune Score (P=0.02, R=0.09) (B) and Stromal Score (P=9.0e-4, R=0.13) (C) of glioma in TCGA dataset.

Supplementary Figure 9 | Relationship between ALKBH5 expression and immune cell infiltration in glioma. Comparison of immune cell infiltration between ALKBH5 high expression and ALKBH5 low expression groups in glioma by CGGA_325 **(A)**, CGGA_693 **(B)** and TCGA **(C)** datasets via ImmuCellAI algorithm. Red asterisk represents the positive correlation between ALKBH5 expression and the level of immune cell infiltration, blue asterisk represents the negative correlation between ALKBH5 expression and the level of immune cell infiltration. *P<0.05, **P<0.01, ***P<0.001, ****P<0.0001.

Supplementary Figure 10 | Correlation analysis between ALKBH5 and immune and inflammatory-related metagenes in glioma. Enrichment scores of seven immune and inflammatory-related metagenes in glioma patients with different ALKBH5 mRNA expression level status in CGGA_325 **(A)**, CGGA_693 **(B)** and TCGA **(C)** datasets. *P<0.05, **P<0.01, ***P<0.001, ****P<0.0001.

Supplementary Figure 11 | Correlation between ALKBH5 and immune checkpoint (ICP) genes in glioma. The correlation between ALKBH5 expression and ICP genes (receptors and ligands) of glioma in CGGA_325 **(A)**, CGGA_693 **(B)** and TCGA **(C)** datasets. The red dots represent the positive correlation between ALKBH5 and ICP genes, while the green dots represent the negative correlation between ALKBH5 and ICP genes.

Supplementary Figure 12 | The relationships between the expressions of miRNAs and grade and prognosis in glioma. The relationships between the expressions of has-miR-193a-3p **(A, B)**, has-miR-362-3p **(C, D)**, has-miR-193b **(E, F)** and miR-329 **(G, H)** and grades or prognosis of primary and recurrent glioma in CGGA microRNA array database. *P<0.05, **P<0.01, ***P<0.001, ****P<0.0001.

Supplementary Figure 13 | The abundance of ALKBH5 mRNA expression in a variety of glioma cell lines by CCLE database. Cell lines labeled in red (U87-MG, U251-MG, A172 and LN229) were used to detect the relative expression level of ALKBH5 in this study *via* qPCR.

Supplementary Figure 14 | The biological functions of ALKBH5 in glioma. **(A)** Verification of overexpression efficiency of ALKBH5 via RT-qPCR in LN229 cell lines. The biological functions of ALKBH5 on LN229 cell lines were verified by CCK-8 **(B)**, wound healing **(C)** and Transwell **(D)** experiments. *P<0.05, **P<0.01, ***P<0.001, ****P<0.0001.

Supplementary Figure 15 | Morphological changes of THP1 cells induced by PMA, IL-4 and IL-13. Morphological changes of THP1 cells were observed 24 h after PMA induction and 24h/48 h after IL-4 and IL-13 induction.

REFERENCES

1. Chen XY, Zhang J, Zhu JS. The Role of M(6)A RNA Methylation in Human Cancer. *Mol Cancer* (2019) 18:103. doi: 10.1186/s12943-019-1033-z
2. Deng X, Su R, Weng H, Huang H, Li Z, Chen J. RNA N(6)-Methyladenosine Modification in Cancers: Current Status and Perspectives. *Cell Res* (2018) 28:507–17. doi: 10.1038/s41422-018-0034-6
3. Wang T, Kong S, Tao M, Ju S. The Potential Role of RNA N6-Methyladenosine in Cancer Progression. *Mol Cancer* (2020) 19:88. doi: 10.1186/s12943-020-01204-7
4. Dixit D, Prager BC, Gimple RC, Poh HX, Wang Y, Wu Q, et al. The RNA M6a Reader YTHDF2 Maintains Oncogene Expression and Is a Targetable Dependency in Glioblastoma Stem Cells. *Cancer Discov* (2021) 11:480–99. doi: 10.1158/2159-8290.CD-20-0331
5. Kan L, Ott S, Joseph B, Park ES, Dai W, Kleiner RE, et al. A Neural M(6)A/Ythdf Pathway is Required for Learning and Memory in Drosophila. *Nat Commun* (2021) 12:1458. doi: 10.1038/s41467-021-21537-1
6. Zhang L, Wan Y, Zhang Z, Jiang Y, Gu Z, Ma X, et al. IGF2BP1 Overexpression Stabilizes PEG10 mRNA in an M6a-Dependent Manner and Promotes Endometrial Cancer Progression. *Theranostics* (2021) 11:1100–14. doi: 10.7150/thno.49345
7. Nombela P, Miguel-Lopez B, Blanco S. The Role of M(6)A, M(5)C and Psi RNA Modifications in Cancer: Novel Therapeutic Opportunities. *Mol Cancer* (2021) 20:18. doi: 10.1186/s12943-020-01263-w
8. Chen H, Gao S, Liu W, Wong CC, Wu J, Wu J, et al. RNA N(6)-Methyladenosine Methyltransferase METTL3 Facilitates Colorectal Cancer by Activating the M(6)A-GLUT1-Mtorc1 Axis and Is a Therapeutic Target. *Gastroenterology* (2021) 160:1284–300. doi: 10.1053/j.gastro.2020.11.013
9. Purslow JA, Nguyen TT, Egner TK, Dotas RR, Khatiwada B, Venditti V. Active Site Breathing of Human Alkbh5 Revealed by Solution NMR and Accelerated Molecular Dynamics. *Biophys J* (2018) 115:1895–905. doi: 10.1016/j.bpj.2018.10.004
10. Han Z, Wang X, Xu Z, Cao Y, Gong R, Yu Y, et al. ALKBH5 Regulates Cardiomyocyte Proliferation and Heart Regeneration by Demethylating the mRNA of YTHDF1. *Theranostics* (2021) 11:3000–16. doi: 10.7150/thno.47354
11. Li Z, Wang P, Li J, Xie Z, Cen S, Li M, et al. The N(6)-Methyladenosine Demethylase ALKBH5 Negatively Regulates the Osteogenic Differentiation of Mesenchymal Stem Cells Through PRMT6. *Cell Death Dis* (2021) 12:578. doi: 10.1038/s41419-021-03869-4
12. Aik W, Scotti JS, Choi H, Gong L, Demetriades M, Schofield CJ, et al. Structure of Human RNA N(6)-Methyladenine Demethylase ALKBH5 Provides Insights Into its Mechanisms of Nucleic Acid Recognition and Demethylation. *Nucleic Acids Res* (2014) 42:4741–54. doi: 10.1093/nar/gku085
13. Wang HF, Kuang MJ, Han SJ, Wang AB, Qiu J, Wang F, et al. BMP2 Modified by the M(6)A Demethylation Enzyme ALKBH5 in the Ossification of the Ligamentum Flavum Through the AKT Signaling Pathway. *Calcif Tissue Int* (2020) 106:486–93. doi: 10.1007/s00223-019-00654-6
14. Zhang C, Samanta D, Lu H, Bullen JW, Zhang H, Chen I, et al. Hypoxia Induces the Breast Cancer Stem Cell Phenotype by HIF-Dependent and ALKBH5-Mediated M(6)A-Demethylation of NANOG mRNA. *Proc Natl Acad Sci USA* (2016) 113:E2047–56. doi: 10.1073/pnas.1602883113
15. Zhang S, Zhao BS, Zhou A, Lin K, Zheng S, Lu Z, et al. M(6)A Demethylase ALKBH5 Maintains Tumorigenicity of Glioblastoma Stem-Like Cells by Sustaining FOXM1 Expression and Cell Proliferation Program. *Cancer Cell* (2017) 31:591–606. doi: 10.1016/j.ccell.2017.02.013
16. Zhu H, Gan X, Jiang X, Diao S, Wu H, Hu J. ALKBH5 Inhibited Autophagy of Epithelial Ovarian Cancer Through miR-7 and BCL-2. *J Exp Clin Cancer Res* (2019) 38:163. doi: 10.1186/s13046-019-1159-2
17. Jin D, Guo J, Wu Y, Yang L, Wang X, Du J, et al. M(6)A Demethylase ALKBH5 Inhibits Tumor Growth and Metastasis by Reducing YTHDFs-Mediated YAP Expression and Inhibiting miR-107/LATS2-Mediated YAP Activity in NSCLC. *Mol Cancer* (2020) 19:40. doi: 10.1186/s12943-020-01161-1
18. Tang B, Yang Y, Kang M, Wang Y, Wang Y, Bi Y, et al. M(6)A Demethylase ALKBH5 Inhibits Pancreatic Cancer Tumorigenesis by Decreasing WIF-1 RNA Methylation and Mediating Wnt Signaling. *Mol Cancer* (2020) 19:3. doi: 10.1186/s12943-019-1128-6
19. Hu BB, Wang XY, Gu XY, Zou C, Gao ZJ, Zhang H, et al. N(6)-Methyladenosine (M(6)A) RNA Modification in Gastrointestinal Tract Cancers: Roles, Mechanisms, and Applications. *Mol Cancer* (2019) 18:178. doi: 10.1186/s12943-019-1099-7
20. Yuan Y, Yan G, He M, Lei H, Li L, Wang Y, et al. ALKBH5 Suppresses Tumor Progression *via* an M(6)A-Dependent Epigenetic Silencing of pre-miR-181b-1/YAP Signaling Axis in Osteosarcoma. *Cell Death Dis* (2021) 12:60. doi: 10.1038/s41419-020-03315-x
21. Shen C, Sheng Y, Zhu AC, Robinson S, Jiang X, Dong L, et al. RNA Demethylase ALKBH5 Selectively Promotes Tumorigenesis and Cancer Stem Cell Self-Renewal in Acute Myeloid Leukemia. *Cell Stem Cell* (2020) 27:64–80. doi: 10.1016/j.stem.2020.04.009
22. Chen Y, Zhao Y, Chen J, Peng C, Zhang Y, Tong R, et al. ALKBH5 Suppresses Malignancy of Hepatocellular Carcinoma *via* M(6)A-Guided Epigenetic Inhibition of LYPD1. *Mol Cancer* (2020) 19:123. doi: 10.1186/s12943-020-01239-w

23. Li N, Kang Y, Wang L, Huff S, Tang R, Hui H, et al. ALKBH5 Regulates Anti-PD-1 Therapy Response by Modulating Lactate and Suppressive Immune Cell Accumulation in Tumor Microenvironment. *Proc Natl Acad Sci USA* (2020) 117:20159–70. doi: 10.1073/pnas.1918986117
24. Peng D, Wei C, Zhang X, Li S, Liang H, Zheng X, et al. Pan-Cancer Analysis Combined With Experiments Predicts CTHRC1 as a Therapeutic Target for Human Cancers. *Cancer Cell Int* (2021) 21:566. doi: 10.1186/s12935-021-02266-3
25. Tang Z, Kang B, Li C, Chen T, Zhang Z. GEPIA2: An Enhanced Web Server for Large-Scale Expression Profiling and Interactive Analysis. *Nucleic Acids Res* (2019) 47:W556–60. doi: 10.1093/nar/gkz430
26. Hu J, Qiu D, Yu A, Hu J, Deng H, Li H, et al. YTHDF1 Is a Potential Pan-Cancer Biomarker for Prognosis and Immunotherapy. *Front Oncol* (2021) 11:607224:607224. doi: 10.3389/fonc.2021.607224
27. Chandrashekar DS, Bashel B, Balasubramanya S, Creighton CJ, Ponce-Rodriguez I, Chakravarthi B, et al. UALCAN: A Portal for Facilitating Tumor Subgroup Gene Expression and Survival Analyses. *Neoplasia* (2017) 19:649–58. doi: 10.1016/j.neo.2017.05.002
28. Sun CC, Li SJ, Hu W, Zhang J, Zhou Q, Liu C, et al. Comprehensive Analysis of the Expression and Prognosis for E2Fs in Human Breast Cancer. *Mol Ther* (2019) 27:1153–65. doi: 10.1016/j.ymthe.2019.03.019
29. Li T, Fu J, Zeng Z, Cohen D, Li J, Chen Q, et al. TIMER2.0 for Analysis of Tumor-Infiltrating Immune Cells. *Nucleic Acids Res* (2020) 48:W509–14. doi: 10.1093/nar/gkaa407
30. Cerami E, Gao J, Dogrusoz U, Gross BE, Sumer SO, Aksoy BA, et al. The Cbio Cancer Genomics Portal: An Open Platform for Exploring Multidimensional Cancer Genomics Data. *Cancer Discov* (2012) 2:401–4. doi: 10.1158/2159-8290.CD-12-0095
31. Xu D, Wang Y, Liu X, Zhou K, Wu J, Chen J, et al. Development and Clinical Validation of a Novel 9-Gene Prognostic Model Based on Multi-Omics in Pancreatic Adenocarcinoma. *Pharmacol Res* (2021) 164:105370. doi: 10.1016/j.phrs.2020.105370
32. Mayakonda A, Lin DC, Assenov Y, Plass C, Koeffler HP. Maftools: Efficient and Comprehensive Analysis of Somatic Variants in Cancer. *Genome Res* (2018) 28:1747–56. doi: 10.1101/gr.239244.118
33. Szklarczyk D, Gable AL, Nastou KC, Lyon D, Kirsch R, Pyysalo S, et al. The STRING Database in 2021: Customizable Protein-Protein Networks, and Functional Characterization of User-Uploaded Gene/Measurement Sets. *Nucleic Acids Res* (2021) 49:D605–12. doi: 10.1093/nar/gkaa1074
34. Aran D, Hu Z, Butte AJ. Xcell: Digitally Portraying the Tissue Cellular Heterogeneity Landscape. *Genome Biol* (2017) 18:220. doi: 10.1186/s13059-017-1349-1
35. Miao YR, Zhang Q, Lei Q, Luo M, Xie GY, Wang H, et al. ImmuCellAI: A Unique Method for Comprehensive T-Cell Subsets Abundance Prediction and its Application in Cancer Immunotherapy. *Adv Sci (Weinh)* (2020) 7:1902880. doi: 10.1002/advs.201902880
36. Sticht C, de la Torre C, Parveen A, Gretz N. Mirwalk: An Online Resource for Prediction of microRNA Binding Sites. *PloS One* (2018) 13:e206239. doi: 10.1371/journal.pone.0206239
37. Chen Y, Wang X. miRDB: An Online Database for Prediction of Functional microRNA Targets. *Nucleic Acids Res* (2020) 48:D127–31. doi: 10.1093/nar/gkz757
38. Crepet A, Papadopoulos A, Elegbede CF, Ait-Dahmane S, Loynet C, Millet G, et al. Mirabel: An Integrated Project for Risk and Cost/Benefit Analysis of Peanut Allergy. *Regul Toxicol Pharmacol* (2015) 71:178–83. doi: 10.1016/j.yrtph.2014.12.006
39. Kern F, Krammes L, Danz K, Diener C, Kehl T, Kuchler O, et al. Validation of Human microRNA Target Pathways Enables Evaluation of Target Prediction Tools. *Nucleic Acids Res* (2021) 49:127–44. doi: 10.1093/nar/gkaa1161
40. Karagkouni D, Paraskevopoulou MD, Tastsoglou S, Skoufos G, Karavangeli A, Pierros V, et al. DIANA-LncBase V3: Indexing Experimentally Supported miRNA Targets on Non-Coding Transcripts. *Nucleic Acids Res* (2020) 48:D101–10. doi: 10.1093/nar/gkz1036
41. Verhaak RG, Hoadley KA, Purdom E, Wang V, Qi Y, Wilkerson MD, et al. Integrated Genomic Analysis Identifies Clinically Relevant Subtypes of Glioblastoma Characterized by Abnormalities in PDGFRA, IDH1, EGFR, and NF1. *Cancer Cell* (2010) 17:98–110. doi: 10.1016/j.ccr.2009.12.020
42. Louis DN, Perry A, Wesseling P, Brat DJ, Cree IA, Figarella-Branger D, et al. The 2021 WHO Classification of Tumors of the Central Nervous System: A Summary. *Neuro Oncol* (2021) 23:1231–51. doi: 10.1093/neuonc/noab106
43. Eckel-Passow JE, Lachance DH, Molinaro AM, Walsh KM, Decker PA, Sicotte H, et al. Glioma Groups Based on 1p/19q, IDH, and TERT Promoter Mutations in Tumors. *N Engl J Med* (2015) 372:2499–508. doi: 10.1056/NEJMoa1407279
44. Chen X, Zhang M, Gan H, Wang H, Lee JH, Fang D, et al. A Novel Enhancer Regulates MGMT Expression and Promotes Temozolomide Resistance in Glioblastoma. *Nat Commun* (2018) 9:2949. doi: 10.1038/s41467-018-05373-4
45. Martincorena I, Raine KM, Gerstung M, Dawson KJ, Haase K, Van Loo P, et al. Universal Patterns of Selection in Cancer and Somatic Tissues. *Cell* (2017) 171:1029–41. doi: 10.1016/j.cell.2017.09.042
46. Mikami S, Mizuno R, Kondo T, Shinohara N, Nonomura N, Ozono S, et al. Clinical Significance of Programmed Death-1 and Programmed Death-Ligand 1 Expression in the Tumor Microenvironment of Clear Cell Renal Cell Carcinoma. *Cancer Sci* (2019) 110:1820–8. doi: 10.1111/cas.14019
47. Sui S, An X, Xu C, Li Z, Hua Y, Huang G, et al. An Immune Cell Infiltration-Based Immune Score Model Predicts Prognosis and Chemotherapy Effects in Breast Cancer. *Theranostics* (2020) 10:11938–49. doi: 10.7150/thno.49451
48. Schizas D, Charalampakis N, Kole C, Economopoulou P, Koustas E, Gkotsis E, et al. Immunotherapy for Pancreatic Cancer: A 2020 Update. *Cancer Treat Rev* (2020) 86:102016. doi: 10.1016/j.ctrv.2020.102016
49. Li G, Huang R, Fan W, Wang D, Wu F, Zeng F, et al. Galectin-9/TIM-3 as a Key Regulator of Immune Response in Gliomas With Chromosome 1p/19q Codeletion. *Front Immunol* (2021) 12:800928:800928. doi: 10.3389/fimmu.2021.800928
50. Picard E, Verschoor CP, Ma GW, Pawelec G. Relationships Between Immune Landscapes, Genetic Subtypes and Responses to Immunotherapy in Colorectal Cancer. *Front Immunol* (2020) 11:369:369. doi: 10.3389/fimmu.2020.00369
51. Goodman AM, Sokol ES, Frampton GM, Lippman SM, Kurzrock R. Microsatellite-Stable Tumors With High Mutational Burden Benefit From Immunotherapy. *Cancer Immunol Res* (2019) 7:1570–3. doi: 10.1158/2326-6066.CIR-19-0149
52. Li L, Goedegebuure SP, Gillanders WE. Preclinical and Clinical Development of Neoantigen Vaccines. *Ann Oncol* (2017) 28:i11–7. doi: 10.1093/annonc/mdx681
53. Han TS, Hur K, Cho HS, Ban HS. Epigenetic Associations Between lncRNA/circRNA and miRNA in Hepatocellular Carcinoma. *Cancers (Basel)* (2020) 12(9):2622. doi: 10.3390/cancers12092622
54. Thomson DW, Dinger ME. Endogenous microRNA Sponges: Evidence and Controversy. *Nat Rev Genet* (2016) 17:272–83. doi: 10.1038/nrg.2016.20
55. Genin M, Clement F, Fattaccioli A, Raes M, Michiels C. M1 and M2 Macrophages Derived From THP-1 Cells Differentially Modulate the Response of Cancer Cells to Etoposide. *BMC Cancer* (2015) 15:577. doi: 10.1186/s12885-015-1546-9
56. Wang D, Yang L, Yue D, Cao L, Li L, Wang D, et al. Macrophage-Derived CCL22 Promotes an Immunosuppressive Tumor Microenvironment *via* IL-8 in Malignant Pleural Effusion. *Cancer Lett* (2019) 452:244–53. doi: 10.1016/j.canlet.2019.03.040
57. Ma W, Zhang K, Bao Z, Jiang T, Zhang Y. SAMD9 Is Relating With M2 Macrophage and Remarkable Malignancy Characters in Low-Grade Glioma. *Front Immunol* (2021) 12:659659:659659. doi: 10.3389/fimmu.2021.659659
58. Yi YC, Chen XY, Zhang J, Zhu JS. Novel Insights Into the Interplay Between M(6)A Modification and Noncoding RNAs in Cancer. *Mol Cancer* (2020) 19:121. doi: 10.1186/s12943-020-01233-2
59. He L, Li H, Wu A, Peng Y, Shu G, Yin G. Functions of N6-Methyladenosine and its Role in Cancer. *Mol Cancer* (2019) 18:176. doi: 10.1186/s12943-019-1109-9
60. Wang J, Wang J, Gu Q, Ma Y, Yang Y, Zhu J, et al. The Biological Function of M6a Demethylase ALKBH5 and its Role in Human Disease. *Cancer Cell Int* (2020) 20:347. doi: 10.1186/s12935-020-01450-1
61. Guo T, Liu DF, Peng SH, Xu AM. ALKBH5 Promotes Colon Cancer Progression by Decreasing Methylation of the lncRNA Neat1. *Am J Transl Res* (2020) 12:4542–9.
62. Pu X, Gu Z, Gu Z. ALKBH5 Regulates IGF1R Expression to Promote the Proliferation and Tumorigenicity of Endometrial Cancer. *J Cancer* (2020) 11:5612–22. doi: 10.7150/jca.46097

63. Liu Z, Chen Y, Wang L, Ji S. ALKBH5 Promotes the Proliferation of Glioma Cells *via* Enhancing the mRNA Stability of G6PD. *Neurochem Res* (2021) 46:3003–11. doi: 10.1007/s11064-021-03408-9
64. Wang ZL, Wang Z, Li GZ, Wang QW, Bao ZS, Zhang CB, et al. Immune Cytolytic Activity Is Associated With Genetic and Clinical Properties of Glioma. *Front Immunol* (2019) 10:1756:1756. doi: 10.3389/fimmu.2019.01756
65. Liu B, Zhou J, Wang C, Chi Y, Wei Q, Fu Z, et al. LncRNA SOX2OT Promotes Temozolomide Resistance by Elevating SOX2 Expression *via* ALKBH5-Mediated Epigenetic Regulation in Glioblastoma. *Cell Death Dis* (2020) 11:384. doi: 10.1038/s41419-020-2540-y
66. Kowalski-Chauvel A, Lacore MG, Arnauduc F, Delmas C, Toulas C, Cohen-Jonathan-Moyal E, et al. The M6a RNA Demethylase ALKBH5 Promotes Radioresistance and Invasion Capability of Glioma Stem Cells. *Cancers (Basel)* (2020) 13(1):40. doi: 10.3390/cancers13010040
67. Martincorena I, Campbell PJ. Somatic Mutation in Cancer and Normal Cells. *Science* (2015) 349:1483–9. doi: 10.1126/science.aab4082
68. Zacharakis N, Chinnasamy H, Black M, Xu H, Lu YC, Zheng Z, et al. Immune Recognition of Somatic Mutations Leading to Complete Durable Regression in Metastatic Breast Cancer. *Nat Med* (2018) 24:724–30. doi: 10.1038/s41591-018-0040-8
69. Zhang H, Wang Z, Dai Z, Wu W, Cao H, Li S, et al. Novel Immune Infiltrating Cell Signature Based on Cell Pair Algorithm Is a Prognostic Marker in Cancer. *Front Immunol* (2021) 12:694490:694490. doi: 10.3389/fimmu.2021.694490
70. Chen R, Wang X, Dai Z, Wang Z, Wu W, Hu Z, et al. TNFSF13 Is a Novel Onco-Inflammatory Marker and Correlates With Immune Infiltration in Gliomas. *Front Immunol* (2021) 12:713757:713757. doi: 10.3389/fimmu.2021.713757
71. Zeng D, Li M, Zhou R, Zhang J, Sun H, Shi M, et al. Tumor Microenvironment Characterization in Gastric Cancer Identifies Prognostic and Immunotherapeutically Relevant Gene Signatures. *Cancer Immunol Res* (2019) 7:737–50. doi: 10.1158/2326-6066.CIR-18-0436
72. Bader JE, Voss K, Rathmell JC. Targeting Metabolism to Improve the Tumor Microenvironment for Cancer Immunotherapy. *Mol Cell* (2020) 78:1019–33. doi: 10.1016/j.molcel.2020.05.034
73. Dong F, Qin X, Wang B, Li Q, Hu J, Cheng X, et al. ALKBH5 Facilitates Hypoxia-Induced Paraspeckle Assembly and IL8 Secretion to Generate an Immunosuppressive Tumor Microenvironment. *Cancer Res* (2021) 81:5876–88. doi: 10.1158/0008-5472.CAN-21-1456
74. Xu S, Li X, Tang L, Liu Z, Yang K, Cheng Q. CD74 Correlated With Malignancies and Immune Microenvironment in Gliomas. *Front Mol Biosci* (2021) 8:706949:706949. doi: 10.3389/fmolb.2021.706949
75. Filipovic A, Miller G, Bolen J. Progress Toward Identifying Exact Proxies for Predicting Response to Immunotherapies. *Front Cell Dev Biol* (2020) 8:155:155. doi: 10.3389/fcell.2020.00155
76. Bonaventura P, Shekarian T, Alcazer V, Valladeau-Guilemond J, Valsesia-Wittmann S, Amigorena S, et al. Cold Tumors: A Therapeutic Challenge for Immunotherapy. *Front Immunol* (2019) 10:168:168. doi: 10.3389/fimmu.2019.00168
77. Jia Q, Chiu L, Wu S, Bai J, Peng L, Zheng L, et al. Tracking Neoantigens by Personalized Circulating Tumor DNA Sequencing During Checkpoint Blockade Immunotherapy in Non-Small Cell Lung Cancer. *Adv Sci (Weinh)* (2020) 7:1903410. doi: 10.1002/advs.201903410

Conflict of Interest: The authors declare that the research was conducted in the absence of any commercial or financial relationships that could be construed as a potential conflict of interest.

Publisher's Note: All claims expressed in this article are solely those of the authors and do not necessarily represent those of their affiliated organizations, or those of the publisher, the editors and the reviewers. Any product that may be evaluated in this article, or claim that may be made by its manufacturer, is not guaranteed or endorsed by the publisher.

Copyright © 2022 Wei, Wang, Peng, Zhang, Li, Luo, He, Liang, Du, Li, Zhang, Zhang, Han and Zhang. This is an open-access article distributed under the terms of the Creative Commons Attribution License (CC BY). The use, distribution or reproduction in other forums is permitted, provided the original author(s) and the copyright owner(s) are credited and that the original publication in this journal is cited, in accordance with accepted academic practice. No use, distribution or reproduction is permitted which does not comply with these terms.

frontiers | Frontiers in Immunology

ORIGINAL RESEARCH
published: 06 April 2022
doi: 10.3389/fimmu.2022.850226

Characterising Distinct Migratory Profiles of Infiltrating T-Cell Subsets in Human Glioblastoma

Paris M. Kollis[1,2], Lisa M. Ebert[1,2,3], John Toubia[4], Cameron R. Bastow[5], Rebecca J. Ormsby[6], Santosh I. Poonnoose[6,7], Sakthi Lenin[8], Melinda N. Tea[8], Stuart M. Pitson[2,8], Guillermo A. Gomez[9], Michael P. Brown[1,2,3†] and Tessa Gargett[1,2,3†]*

[1] Translational Oncology Laboratory, Centre for Cancer Biology, SA Pathology and University of South Australia, Adelaide, SA, Australia, [2] Adelaide Medical School, Faculty of Health and Medical Sciences, University of Adelaide, Adelaide, SA, Australia, [3] Cancer Clinical Trials Unit, Royal Adelaide Hospital, Adelaide, SA, Australia, [4] Australian Cancer Research Foundation (ACRF) Cancer Genomics Facility, Centre for Cancer Biology, SA Pathology and University of South Australia, Adelaide, SA, Australia, [5] Chemokine Biology Laboratory, Molecular Life Sciences, University of Adelaide, Adelaide, SA, Australia, [6] Flinders Health and Medical Research Institute, College of Medicine and Public Health, Flinders University, Adelaide, SA, Australia, [7] Department of Neurosurgery, Flinders Medical Centre, Adelaide, SA, Australia, [8] Molecular Therapeutics Laboratory, Centre for Cancer Biology, SA Pathology and University of South Australia, Adelaide, SA, Australia, [9] Tissue Architecture and Organ Function Laboratory, Centre for Cancer Biology, SA Pathology and University of South Australia, Adelaide, SA, Australia

OPEN ACCESS

Edited by:
Hamid Reza Mirzaei, Tehran University of Medical Sciences, Iran

Reviewed by:
Ann Ager, Cardiff University, United Kingdom
Stephen Gottschalk, St. Jude Children's Research Hospital, United States

***Correspondence:**
Tessa Gargett
tessa.gargett@sa.gov.au

[†]These authors share senior authorship

Specialty section:
This article was submitted to Cancer Immunity and Immunotherapy, a section of the journal Frontiers in Immunology

Received: *07 January 2022*
Accepted: *15 March 2022*
Published: *06 April 2022*

Citation:
Kollis PM, Ebert LM, Toubia J, Bastow CR, Ormsby RJ, Poonnoose SI, Lenin S, Tea MN, Pitson SM, Gomez GA, Brown MP and Gargett T (2022) Characterising Distinct Migratory Profiles of Infiltrating T-Cell Subsets in Human Glioblastoma. Front. Immunol. 13:850226. doi: 10.3389/fimmu.2022.850226

Glioblastoma is the most common and aggressive form of primary brain cancer, with no improvements in the 5-year survival rate of 4.6% over the past three decades. T-cell-based immunotherapies such as immune-checkpoint inhibitors and chimeric antigen receptor T-cell therapy have prolonged the survival of patients with other cancers and have undergone early-phase clinical evaluation in glioblastoma patients. However, a major challenge for T-cell-based immunotherapy of glioblastoma and other solid cancers is T-cell infiltration into tumours. This process is mediated by chemokine-chemokine receptor and integrin-adhesion molecule interactions, yet the specific nature of the molecules that may facilitate T-cell homing into glioblastoma are unknown. Here, we have characterised chemokine receptor and integrin expression profiles of endogenous glioblastoma-infiltrating T cells, and the chemokine expression profile of glioblastoma-associated cells, by single-cell RNA-sequencing. Subsequently, chemokine receptors and integrins were validated at the protein level to reveal enrichment of receptors CCR2, CCR5, CXCR3, CXCR4, CXCR6, CD49a, and CD49d in glioblastoma-infiltrating T-cell populations relative to T cells in matched patient peripheral blood. Complementary chemokine ligand expression was then validated in glioblastoma biopsies and glioblastoma-derived primary cell cultures. Together, enriched expression of homing receptor-ligand pairs identified in this study implicate a potential role in mediating T-cell infiltration into glioblastoma. Importantly, our data characterising the migratory receptors on endogenous tumour-infiltrating T cells could be exploited to enhance the tumour-homing properties of future T-cell immunotherapies for glioblastoma.

Keywords: T cells, chemokine receptors, integrins, chemokines, glioblastoma, migration, scRNA-seq

INTRODUCTION

Glioblastoma is the most common and aggressive form of primary brain cancer in adults (1). Despite standard treatment employing surgery, radiotherapy and chemotherapy, glioblastoma consistently recurs within 6-9 months of initial treatment, illustrating its treatment-resistant nature. Therefore, it is not surprising that the abysmal survival rate of 4.6% at 5 years has not improved over the past three decades (2). With no new or improved survival-prolonging treatment strategies developed in the last 15 years (3), patients and their carers are in desperate need of new therapeutics.

Despite the dramatic success of T-cell-based immunotherapies such as chimeric antigen receptor (CAR) T cells and immune checkpoint inhibitors (ICIs) in patients with other cancers (4, 5), early clinical data indicate that ICIs are only effective in a minority of glioblastoma patients, while CAR T-cell therapy appears promising and safe (6, 7). Among other challenges including immunosuppression and a lack of tumour neoantigens, success of these therapies is limited partly because of restricted T-cell infiltration into glioblastoma (8). The sustained anti-tumour effect of ICIs like anti-PD-1 requires reactivation of endogenous infiltrating anti-tumour T cells (6). Similarly, CAR T cells must be capable of infiltrating tumours to exert their tumour-killing functions (8). In both instances, T cells require the correct migratory receptor repertoire to migrate to and infiltrate the tumour site. Therefore, by enhancing the migratory capabilities of endogenous T cells and CAR T cells alike, T-cell-based immunotherapies could be improved to treat glioblastoma patients.

Despite apparent challenges, such as the blood-brain barrier (BBB) composed of tight-junction endothelial cells (ECs) and astrocyte endfeet (9), some endogenous T cells are nevertheless capable of infiltrating glioblastoma (10). The passage of T cells from the bloodstream into tissues such as tumours is a tightly regulated, multi-step process. This initially involves the tethering and rolling of T cells along the vessel wall, followed by firm adhesion to the endothelium, and finally transmigration through the vessel wall (11). The firm adhesion step is facilitated by chemokine-chemokine receptor axes and integrin-adhesion molecule interactions, whereby chemokines facilitate firm adhesion of T cells to endothelial cells (ECs) *via* integrin activation and binding, then direct the migration of T cells within the tissue parenchyma (12). Only T cells expressing the correct combination of these chemokine and adhesion receptors are expected to effectively infiltrate glioblastoma.

T-cell subsets that participate in anti-tumour immunity, including $CD4^+$ and $CD8^+$ memory subsets and T regulatory cells (Tregs), have been identified in glioblastoma (10, 13, 14). Based on previous antigen experience, T cells are characterised as naïve, T-central memory (Tcm), T-effector memory (Tem), and T-effector memory re-expressing CD45RA (Temra) populations. Tcm, Tem and Temra differ in their immediate effector function upon antigen exposure and circulation. Tcm cells rapidly respond to secondary antigen exposure and differentiate into effector T-cell populations in secondary lymphoid organs or the site of the response (15). Conversely, Tem and Temra populations recognise antigen directly in tissues and mount immediate effector responses (16). Antigen exposure also gives rise to T-resident memory (Trm) cells, which do not recirculate but reside in peripheral tissues to provide immediate protection against secondary local infections and cancer (17). Recently, Trm cells have been identified in the healthy brain (18) and have been shown to express homing receptors important for tissue retention (19). However, Trm cells have yet to be identified in glioblastoma and the migratory profile of Trm cells in these tumours has not been characterised. The activation- and exhaustion-specific markers of Tregs and activated $CD4^+$ and $CD8^+$ T cells have been investigated in glioblastoma (14, 20, 21) but the migratory receptors required by these subsets for glioblastoma-homing remain unknown. While T-cell infiltration of glioblastoma is a prerequisite for the efficacy of immunotherapy, a thorough characterisation of the migratory phenotypes on T cells in glioblastoma has not been performed.

Here, using single-cell RNA-sequencing (scRNA-seq) and flow cytometry on glioblastoma patient biopsies, we characterise for the first time the chemokine receptor and integrin expression profiles of endogenous glioblastoma-infiltrating T cells. We identify that T-cell subsets expressing CCR2, CCR5, CXCR3, CXCR4, CXCR6, CD49a, and CD49d are enriched in glioblastoma tumours compared to matched peripheral blood samples. Additionally, validation of complementary chemokines implicates specific chemokine-chemokine receptor axes in T-cell homing and infiltration of glioblastoma tumours. Importantly, these findings identify migratory receptors that could be exploited to improve T-cell-based immunotherapy for glioblastoma and possibly other solid tumours.

MATERIALS AND METHODS

Human Samples

Clinical samples (tumour tissue and blood) from patients with histologically confirmed glioblastoma multiforme were obtained through the South Australian Neurological Tumour Bank (SANTB) and use of the tissues was approved by the Central Adelaide Local Health Network Human Research Ethics Committee (CALHN HREC; approval number R20160727). All human specimens were used in accordance with the Declaration of Helsinki, and participants provided written consent.

Single Cell Transcriptomics

To interrogate genes related to glioblastoma T-cell homing, we used our previously published scRNA-seq dataset based on a total of 13,903 cells from three primary glioblastoma specimens (22). Refer to Ebert et al. (2020) for detailed methods on tumour specimen processing for single-cell sequencing, as well as single-cell library processing (22). Briefly, using R version 3.6.3 and Seurat version 3.1.5, cells with (i) fewer than 200 genes, (ii) gene numbers outside ±2 standard deviations from the mean, or (iii) a mitochondrial gene fraction greater than 10% were excluded. Remaining cells were log normalised by total expression and scaled to 10,000 transcripts/cell with the NormalizeData function

in Seurat. Using the FindIntegrationAnchors (dims = 1:30, k.filter = 200) and IntegrateData (dims = 1:30) functions, cells from different libraries were combined by assessing the pairwise correspondence between a set of representative genes (anchors). The FindVariableGenes function was used to identify variable genes returning 2000 features using vst as the selection method. The data were then scaled and principal component analysis applied using the ScaleData and RunPCA functions respectively. Cells were clustered based on gene expression profiles using the FindNeighbors and FindClusters functions with resolution set to 0.5. UMAP plots were generated using the first 20 principal components, and clusters annotated based on expression of reported cell-lineage markers (23).

To identify different subsets of lymphocytes, the lymphocyte clusters were first isolated from non-lymphocyte clusters. Subsequently, the isolated lymphocyte cells were re-clustered as described above. UMAP plots were generated using the first 11 principal components, and clusters annotated based on expression of cell-lineage markers. *EBF1* and *CD19* delineated B cells and *CD14* and *CD68* identified contaminating macrophages. *CD3D* and *NCR1* identified T-cell and NK-cell-clusters respectively. $CD4^+$, $CD8^+$ T cells and Tregs were visualised using *CD4*, *CD8* and *FOXP3* respectively. T cells expressing high levels of *TCF7*, *SELL*, *CCR7*, *IL7R*, *PTGER2*, and *KLRG1* were considered Tcm-like. *GZMB*, *PDCD1*, *HLA-DRA*, and *KLRC1* were used to classify effectors or recently activated T cells. Additionally, *ITGA1*, *ITGAE*, and *CXCR6* were used to identify Trm cells (13).

To screen for chemokine receptor, integrin, chemokine, and adhesion molecule gene expression, the frequency of cells positive for genes of interest were obtained using the FetchData function from the merged and normalised libraries of the BT20, BT23 and BT26 scRNA-seq dataset. Cells were considered positive for a gene of interest if at least one unique molecular identifier (UMI) corresponding to the gene was detected in the cell. Cell populations were identified as previously described (22).

Sample Preparation and Storage

Glioblastoma samples were obtained as pieces of resected tumour tissue, or as tumour fragments recovered from aspirates following Cavitron Ultrasonic Surgical Aspirator (CUSA) ablation, and dissociated as described previously (22). For tumour biopsies, a portion of the sample was embedded in optimal cutting temperature (OCT) medium, flash-frozen using supercooled isopentane, and stored at -80°C. Remaining tumour biopsy was rinsed to remove blood and dissociated to generate single-cell suspensions using Accutase (Thermo Fisher Scientific) or the Human Tumor Dissociation kit in combination with the gentleMACS Octo Dissociator (Miltenyi Biotec) according to the manufacturer's recommendations. Tissue fragments in CUSA aspirates were first sedimented by slow centrifugation at 70g for 1 min and the supernatant was discarded. The remaining tissue fragments were dissociated using Accutase or the Human Tumor Dissociation kit as described above. Following digestion, dissociated samples were centrifuged at 300g for 5 min to pellet cells, and supernatants for chemokine analyses harvested and stored at -80°C. Dissociated cells were resuspended and filtered through a 70μm strainer. For cryopreservation, a portion of the cells were resuspended in 90% foetal bovine serum (FBS) + 10% dimethyl sulphoxide (DMSO), frozen in a Mr Frosty freezing chamber (Thermo Fisher Scientific) at -80°C overnight, then stored in liquid nitrogen for flow cytometry analyses. The remaining cells were used to generate glioma neural stem (GNS) cell cultures as previously described (22, 24). GNS cell-line supernatants were harvested when the cells were 75-95% confluent and stored at -80°C for chemokine analyses.

Peripheral blood mononuclear cells (PBMC) were harvested from patient blood *via* density centrifugation (Lymphoprep), resuspended in 90% FBS + 10% DMSO, then frozen in a Mr Frosty freezing chamber (Thermo Fisher Scientific) at -80°C overnight and stored in liquid nitrogen for flow cytometry analyses.

Immunofluorescence Staining of Cryosections

Sections cut from OCT-embedded fresh tissues (5-12μm thickness) were fixed for 20 minutes in Cytofix/Cytoperm (BD) at room temperature (RT), washed in PBS and blocked using 10% human plasma, 10% normal donkey serum and 10% normal goat serum in PBS containing 1% bovine serum albumin (BSA) for 30 minutes at RT. 5μg/mL purified mouse anti-CD3 (UCHT1; BioLegend) and 0.67μg/mL rabbit anti-CD31 (polyclonal; Bethyl Labs #IHC-00055) antibodies were incubated with tissue sections for 12 hours at 4°C. Following washing, tissue sections were incubated with goat anti-mouse IgG-AF488 (Abcam) and donkey anti-rabbit IgG-AF555 (Abcam) detection antibodies at a dilution of 1:500 for 1 hour at RT. Following washing, tissue sections were blocked using 10% normal mouse serum in PBS containing 1% BSA for 30 minutes at RT. Sections were then incubated with mouse anti-GD2-AF647 (14.G2A; BD) at a dilution of 1:100 for 2 hours at RT. After washing, sections were mounted using ProLong Gold anti-fade mounting medium with DAPI (Life Technologies), cured overnight, and sealed with nail varnish before viewing.

Microscopy and Imaging

Confocal imaging was performed on a Zeiss LSM 800 confocal microscope equipped with 405nm, 488nm, 561nm and 640nm lasers, using 20x objective and Zen 2.6 system software. Fluorescence overlays were created by combining Z-stacks, merging channels, and applying false colour using ImageJ (National Institutes of Health).

Flow Cytometry

For flow cytometry analysis, cryopreserved, dissociated tumour specimens were rapidly thawed at 37°C, washed, and incubated in pre-warmed Roswell Park Memorial Institute (RPMI) media and 20U/mL DNase I (Sigma) for 15 minutes at 37°C. Cells were then washed and resuspended in a 30% isotonic Percoll (Sigma)/RPMI solution with 2mM EDTA. Using a syringe and needle, 70% isotonic Percoll/RPMI with 2mM EDTA was underlaid beneath the cell suspension, then centrifuged at 500g for 30 mins without

the brake at RT. Lymphocytes were harvested from the interphase and washed with complete RPMI media to remove excess Percoll. Isolated lymphocytes were resuspended in PBS and plated at a density of $3x10^5$ cells/well in 96-well V-bottom plates. Cryopreserved patient PBMC were rapidly thawed at 37°C, washed, and resuspended in PBS to be plated at a density of $5x10^5$ cells/well. Five flow cytometry panels were designed to simultaneously analyse chemokine receptor and/or integrin expression while identifying T-cell subsets. A core combination of antibodies to identify T-cell subsets including: anti-CD3-PerCP-Cy5.5 (UCHT1; BD), anti-CD4-BV510 (SK3; BD), anti-CD8-BV786 (RPA-T8; BD), anti-CD25-BB515 (2A3; BD), anti-CD69-PE-Cy7 (FN50; BD), anti-CD45RO-BUV395 (UCHL1; BD), anti-CCR7-APC (2-L1-A; BD) or anti-CCR7-BV421 (G043H7; BD), anti-CD127-PE (A019D5; Biolegend), and anti-CD103-BV605 (Ber-ACT8; Biolegend) were used in each panel with an additional 2-3 antibodies to detect different chemokine receptors and/or integrins. Patient samples were randomly allocated to the different flow panels with larger biopsies that provided a greater yield of T cells used in multiple flow panels. Patient tumour samples digested with Accutase were allocated to the flow cytometry panel containing CXCR3 and CCR6 antibodies as the standard dissociation protocol with GentleMACS reagents (Miltenyi) significantly reduced the detection of these receptors. Cells were pelleted *via* centrifugation at 400g for 3 minutes, resuspended in PBS with 1:1000 Fixable viability stain 780 (BD) and incubated for 20 minutes at RT. Cells were washed with FACS buffer (PBS, 1% BSA) and Fc receptors blocked with human Fc block (BD) for 5 minutes on ice. For chemokine receptor analyses, the following antibodies were used: anti-CCR2-BUV737 (LS132.1D9, BD), anti-CCR4-BV421 (1G1; BD), anti-CCR5-PE-CF594 (2D7; BD), anti-CCR6-BUV737 (11A9; BD), anti-CCR7-APC, anti-CCR7-BV421, anti-CXCR3-APC (G025H7; Biolegend), anti-CXCR4-BV421 (12G5; BD), anti-CXCR6-BV421 (13B 1E5; BD), and anti-CX3CR1-PE-CF594 (2A9-1; BD). For panels with anti-CCR5, chemokine receptor staining was staggered as previously recommended (25). First, cells were incubated with chemokine receptor antibodies, except anti-CCR5, in Brilliant Staining Buffer Plus (BSB+; BD) for 10 mins at RT. Anti-CCR5-PE-CF594 was then added and cells were incubated for a further 10 minutes at RT. For panels without anti-CCR5, cells were incubated with chemokine receptor antibodies in BSB+ for 20 mins at RT. To the above suspensions, our core T-cell antibody cocktail diluted in BSB+ (BD) was added and incubated for a further 20 minutes on ice. For integrin panels, cells were incubated with anti-CCR7 at RT for 20 minutes, then incubated for a further 20-minutes on ice with the above T-cell cocktail supplemented with anti-CD11a-BV421 (HI111; BD) and anti-CD49d-BUV737 (9F10; BD), or anti-CD51-APC (NKI-M9; Biolegend) and anti-CD49a-BUV737 (SR84; BD). Stained cells were washed with PBS and fixed with Cytofix/Cytoperm (BD) for 20 minutes on ice. Lastly, cells were washed with PBS, resuspended in FACS buffer, and stored at 4°C protected from light until acquisition. Samples were acquired on a BD LSR Fortessa Special Order Research Product using FACS Diva Software version 8.0. Analysis was performed using FlowJo™ version 10.8.1 (BD).

Enzyme-Linked Immunosorbent Assay (ELISA)

To detect CXCL16 and CCL20 in supernatants harvested from GNS cell-lines and dissociated glioblastoma and CUSA samples, the DuoSet ELISA Human CXCL16 kit (DY1164; R&D Systems) and DuoSet ELISA Human CCL20 kit (DY36005; R&D Systems) were used according to the manufacturer's recommendations. Samples were analysed at 450 nm (FLUOstar Omega microplate reader), and concentrations of chemokines calculated from standard curves generated with GraphPad Prism version 8.4.3.

Cytometric Bead-Based Immunoassay

To detect the chemokines CCL2, CCL3, CCL4, CCL5, CXCL9, CXCL10, CXCL11, CXCL12 and CX3CL1 in supernatants harvested from GNS cell-lines and dissociated glioblastoma and CUSA samples, a LEGENDplex Custom Human Chemokine Panel kit (Biolegend) was used according to the manufacturer's recommendations. Standards and samples were acquired on a BD LSR Fortessa Special Order Research Product and chemokine concentrations determined using the LEGENDplex data analysis software version 2021-07-01 (Biolegend).

Statistical Analyses

Statistical analysis and graphing were performed in GraphPad Prism version 8.4.3. Pairwise comparisons were performed using two-tailed paired Student's t test. For all tests, p values under 0.05 were considered significant. Significance was represented as: *p<0.05, **p<0.01, ***p<0.001, ****p<0.0001.

RESULTS

Endogenous T Cells Infiltrate Glioblastoma

To identify glioblastoma tissues with infiltrating T cells, frozen sections were prepared from patients' biopsies (n=6) for confocal microscopy. Sections were stained for CD3 (green) to identify glioblastoma-infiltrating T cells, GD2 (magenta) to visualise tumour cells, and CD31 (white) to identify ECs (**Figure 1A**). In all instances, T cells were visualised near $CD31^+$ blood ECs and among $GD2^+$ glioblastoma cells (**Figure 1A**), but not within blood vessels. Importantly, this confirmed that glioblastoma tissues contained endogenous T cells that had infiltrated the glioblastoma parenchyma and were not restricted to the blood vessel lumen.

Three of these glioblastoma biopsies, all of which contained tumour-infiltrating T cells, (BT20, BT23, BT26; refer to **Table 1**), were matched to our previously published scRNA-seq dataset (22). This dataset was generated by dissociating three primary glioblastoma patient specimens (**Table 1**) to single-cell suspensions and subjecting them to scRNA-seq using the 10X Chromium platform. Detailed methods and data analysis pipelines are described in the materials and methods section and our recent publication (22). Upon clustering of cells based on their transcriptome, expression of reported lineage-markers was used to identify the cell-type of each cluster. Subsequently,

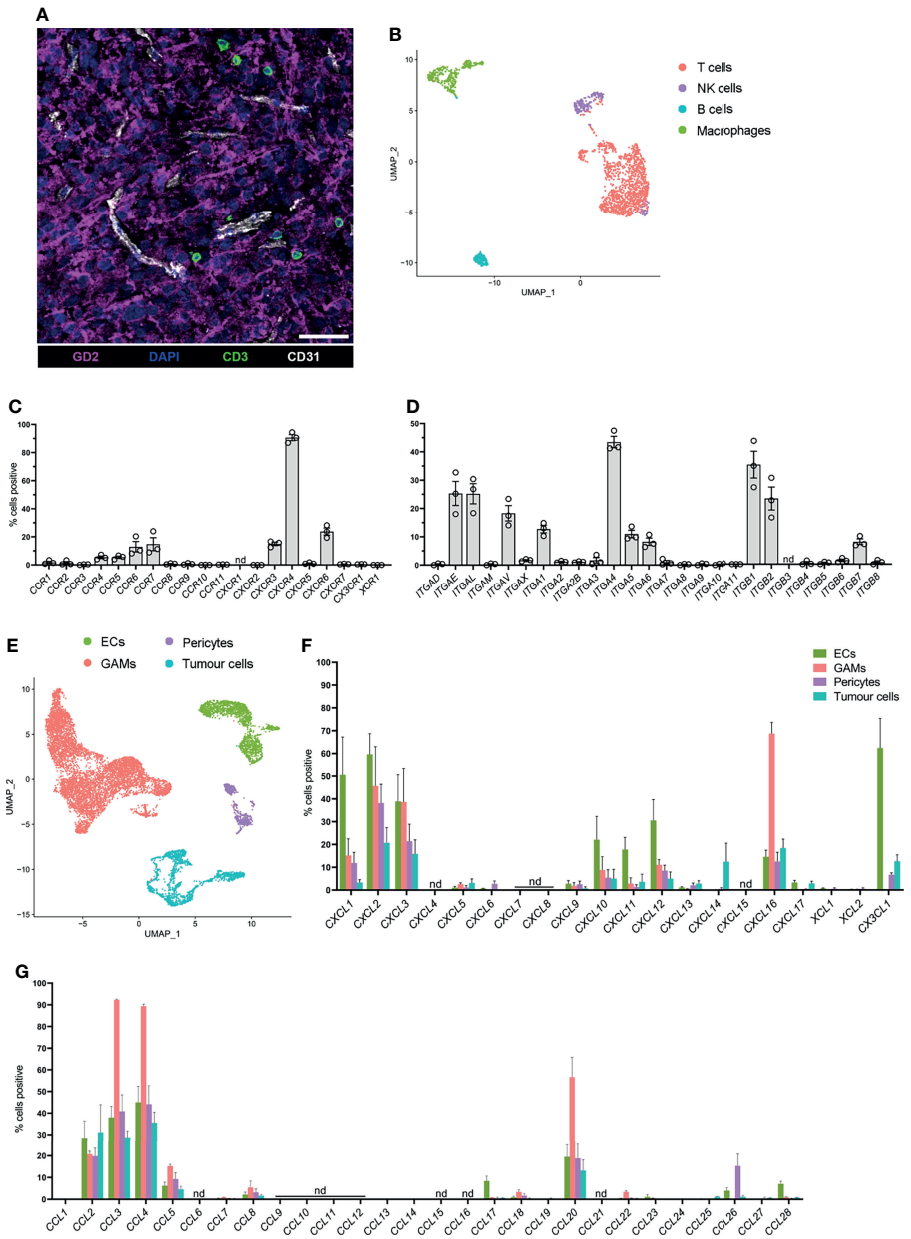

FIGURE 1 | Endogenous T cells that infiltrate glioblastoma express distinct homing marker genes, and complementary chemokine genes are detected in other glioblastoma-associated cell clusters. **(A)** Representative 7µm glioblastoma tissue section identifying endogenous CD3$^+$ T cells (green) localised adjacent to tumour-associated CD31$^+$ blood endothelial cells (white) and infiltrating GD2$^+$ tumour parenchyma (magenta). DAPI was used as a nuclear stain, scale bar: 50µm, representative of n=6 patient samples. **(B)** UMAP plot of T cells, NK cells, B cells, and macrophages identified within the lymphocyte cluster from pooled scRNA-seq analysis of n=3 patient glioblastoma biopsies. Cell clusters were identified according to differentially expressed genes (see **Supplementary Figure 1**). **(C, D)** Frequency of T cells within the lymphocyte cluster positive for **(C)** chemokine receptor and **(D)** integrin genes. Each dot represents one patient, bars represent mean ± SEM. nd=not detected. **(E)** UMAP plot of non-lymphocyte glioblastoma-associated cell clusters from pooled scRNA-seq analysis of n=3 patient glioblastoma biopsies. Endothelial cells (ECs), glioblastoma-associated macrophages and microglia (GAMs), pericytes and tumour cells were clustered and identified according to differentially expressed genes. **(F, G)** Frequency of ECs, GAMs, pericytes and tumour cells positive for **(F)** *CXCL*-, *XCL*- and *CX3CL1*, and **(G)** *CCL*-chemokine genes. Bars represent mean ± SEM, nd, not detected.

clusters were identified as ECs, glioblastoma-associated macrophages/microglia (GAMs), pericytes, and lymphocytes (**Supplementary Figure 1A**). Clustered cells expressing a range of genes associated with glial and neural cell types but lacking stromal lineage-markers were annotated as tumour cells (**Supplementary Figure 1A**). Utilising this existing dataset, expression of chemokine receptors and integrins was interrogated in glioblastoma-infiltrating T cells for this study.

TABLE 1 | Glioblastoma patient demographics and their samples used in this study.

Patient ID	Sex	Age	Diagnosis	IDH mutation status	Samples available	Use in study
BT4	Female	59	Primary glioblastoma	Not reported in patient notes	Tumour biopsy	Flow cytometry
					Blood	Flow cytometry
BT8	Female	49	Recurrent glioblastoma	Not reported in patient notes	CUSA	Flow cytometry
					Blood	Flow cytometry
BT15	Male	74	Recurrent glioblastoma	Not reported in patient notes	Tumour biopsy	Flow cytometry
					Blood	Flow cytometry
BT16	Female	58	Glioblastoma	IDH WT	CUSA	Flow cytometry
					Blood	Flow cytometry
BT18	Female	33	Recurrent glioblastoma	Not reported in patient notes	CUSA	Flow cytometry
					Blood	Flow cytometry
BT20	Male	55	Primary glioblastoma	Not reported in patient notes	Tumour biopsy	scRNA-seq
						IF
						Flow cytometry
					CUSA	Flow cytometry
					Blood	Flow cytometry
					GNS cell-line	ELISA
BT23	Male	78	Primary glioblastoma	Not reported in patient notes	Tumour biopsy	IF
					CUSA	scRNA-seq
						Flow cytometry
					Blood	Flow cytometry
BT26	Male	69	Primary glioblastoma	Not reported in patient notes	Tumour biopsy	IF
					CUSA	scRNA-seq
						Flow cytometry
					Blood	Flow cytometry
					GNS cell-line	Chemokine quantification
BT29	Male	66	Glioblastoma	IDH WT	GNS cell-line	Chemokine quantification
BT38	Male	78	Glioblastoma	Not reported in patient notes	Tumour biopsy	Flow cytometry
					Blood	Flow cytometry
					GNS cell-line	Chemokine quantification
BT39	Male	65	Glioblastoma	IDH WT	GNS cell-line	Chemokine quantification
BT41	Male	67	Glioblastoma	IDH WT	GNS cell-line	Chemokine quantification
BT43	Male	45	Glioblastoma	IDH WT	Tumour biopsy	Flow cytometry
					Blood	Flow cytometry
BT45	Male	49	Glioblastoma	Not reported in patient notes	Tumour biopsy	Flow cytometry
					Blood	Flow cytometry
BT48	Male	68	Glioblastoma	Not reported in patient notes	Tumour biopsy	Flow cytometry
					Blood	Flow cytometry
BT49	Female	50	Glioblastoma	Not reported in patient notes	Tumour biopsy	Flow cytometry
						IF
					Blood	Flow cytometry
BT50	Female	67	Glioblastoma	Not reported in patient notes	Tumour biopsy	Chemokine quantification
						Flow cytometry
						IF
					Blood	Flow cytometry
BT52	Female	63	Glioblastoma	IDH1 WT	Tumour biopsy	Flow cytometry
					Blood	Flow cytometry

(Continued)

TABLE 1 | Continued

Patient ID	Sex	Age	Diagnosis	IDH mutation status	Samples available	Use in study
BT53	Male	67	Glioblastoma	Not reported in patient notes	Tumour biopsy	Flow cytometry
					Blood	Flow cytometry
					GNS cell-line	Chemokine quantification
BT55	Female	78	Glioblastoma	IDH WT	GNS cell-line	Chemokine quantification
BT57	Female	68	Glioblastoma	IDH WT	Tumour biopsy	Chemokine quantification
						Flow cytometry
					Blood	Flow cytometry
BT58	Male	69	Primary glioblastoma	IDH WT	Tumour biopsy	Chemokine quantification
						Flow cytometry
					CUSA	Chemokine quantification
					Blood	Flow cytometry
					GNS cell-line	Chemokine quantification
BT59	Male	62	Glioblastoma	Not reported in patient notes	Tumour biopsy	Chemokine quantification
						Flow cytometry
					CUSA tumour	Chemokine quantification
					Blood	Flow cytometry
					GNS cell-line	Chemokine quantification
BT61	Female	42	Secondary glioblastoma arising from pre-existing grade 2 astrocytoma	Not reported in patient notes	Tumour biopsy	Chemokine quantification
BT62	Female	53	Likely glioblastoma but may be anaplastic oligodendroglioma	IDH1 R132H negative	Tumour biopsy	Chemokine quantification
					CUSA	Chemokine quantification
BT63	Female	36	Recurrent glioblastoma	Not reported in patient notes	Tumour biopsy	Chemokine quantification
					GNS cell-line	Chemokine quantification
BT64	Female	64	Glioblastoma	IDH WT	Tumour biopsy	Chemokine quantification
						Flow cytometry
					CUSA	Chemokine quantification
					Blood	Flow cytometry
BT66	Male	32	Glioblastoma	Not reported in patient notes	Tumour biopsy	Flow cytometry
					Blood	Flow cytometry
					GNS cell-line	Chemokine quantification
BT67	Female	64	Recurrent glioblastoma	Not reported in patient notes	Tumour biopsy	Chemokine quantification
BT68	Female	68	Glioblastoma	IDH WT	Tumour biopsy	Chemokine quantification

CUSA, Cavitron Ultrasonic Surgical Aspirator; GNS, glioma neural stem; IDH, isocitrate dehydrogenase; IF, immunofluorescence; scRNA-seq, single-cell RNA-sequencing; WT, wild-type.

Glioblastoma-Associated T Cells Express Chemokine Receptor and Integrin Genes

To screen for chemokine receptor and integrin genes expressed by glioblastoma-infiltrating T cells, the lymphocyte cluster was isolated and re-clustered with the bioinformatics pipeline described (see above and Materials and Methods) to further separate lymphocyte populations according to differentially expressed genes (**Figure 1B**). B cells were identified *via EBF1* and *CD19* expression, contaminating macrophages *via CD14* and *CD68* expression, T cells *via CD3D* expression and NK cells *via NCR1* expression (**Figure 1B** and **Supplementary Figures 1B, C**). Frequencies of T cells positive for chemokine receptor (**Figure 1C**) and integrin genes (**Figure 1D**) in each patient were determined. Within glioblastoma-infiltrating T cells, a large

proportion of cells were positive for *CXCR4* and the proportion of cells positive for chemokine receptors *CCR4*, *CCR5*, *CCR6*, *CCR7*, *CXCR3*, and *CXCR6* ranged between 5-25% (**Figure 1C**). Additionally, integrin genes *ITGAE*, *ITGAL*, *ITGAV*, *ITGA1*, *ITGA4*, *ITGA5*, *ITGA6*, *ITGB1*, *ITGB2*, and *ITGB7* were detected in a moderate proportion of T cells (**Figure 1D**). All other receptors investigated were either undetectable or were expressed in low frequencies of T cells. Remaining cells in the lymphocyte cluster were also screened for chemokine receptor and integrin gene expression. B cells, NK cells and contaminating macrophages also expressed chemokine receptor and integrin genes with some overlap in the expression of receptors with T cells (**Supplementary Figures 2A, B**). Together, these data identify infiltrating T cells in glioblastoma biopsies and define a putative expression profile of glioblastoma-homing markers.

Glioblastoma-Associated Cell Populations Express Complementary Chemokine Genes

Chemokine receptor-mediated T-cell recruitment is directed by complementary chemokine ligands expressed in the glioblastoma microenvironment; thus, the expression of chemokines was screened in non-lymphocyte clusters (**Figure 1E**). There were varying proportions of cells positive for chemokines *CCL2*, *CCL3*, *CCL4*, *CCL5*, *CCL20*, *CXCL1*, *CXCL2*, *CXCL3*, *CXCL10*, *CXCL11*, *CXCL12*, *CXCL16*, and *CX3CL1* (**Figures 1F, G**), among non-lymphocyte cell populations. Subsequently, chemokine receptors identified in glioblastoma-infiltrating T cells were selected for further investigation based on expression of the receptor at the gene level within T-cell clusters, and/or expression of the cognate ligand(s) identified within non-lymphocyte clusters. Thus, the chemokine receptors CCR2, CCR4, CCR5, CCR6, CXCR3, CXCR4, CXCR6, and CX3CR1 were selected for further validation by flow cytometry. Similarly, integrins CD49a (*ITGA1*), CD49d (*ITGA4*), CD51 (*ITGAV*), and CD11a (*ITGAL*) were selected for further validation based on elevated gene expression in glioblastoma-infiltrating T cells.

Analysis of T-Cell Subsets in Glioblastoma Biopsies and Matched Blood Samples

Previous studies have identified that memory T cells, including Tcm, Tem and Temra, and $CD4^+$ Tregs can infiltrate glioblastoma (10, 13, 14, 20). Additionally, Trm cells have been characterised in the healthy brain (18). In keeping with this, our scRNA-seq data revealed heterogenous expression of genes associated with a Tcm-like signature (*TCF7*, *SELL*, *CCR7*, *IL7R*, *PTGER2*, and *KLRG1*), and effector-like genes (*GZMB*, *PDCD1*, *HLA-DRA*, and *KLRC1*) (**Supplementary Figure 1C**) (13). Additionally, our scRNA-seq dataset revealed *FOXP3* expression in a small proportion of glioblastoma Tregs, and expression of *ITGA1*, *ITGAE*, and *CXCR6* which are associated with a Trm signature (**Supplementary Figure 1C**) (13). Considering these subsets play distinct roles in tumour immunity (10, 17, 26), a multicolour flow cytometry panel was designed to simultaneously identify these populations and interrogate chemokine receptor and integrin expression (**Figures 2A, B**). Paired blood (**Figure 2A**) and dissociated glioblastoma samples (**Figure 2B**) were analysed to identify homing receptors enriched on glioblastoma-infiltrating T-cell subsets compared to paired blood samples as a means of identifying migratory axes that may be of biological importance. Tregs were identified as $CD4^+CD25^+CD127^{low}$ (27), and $CD4^+$ or $CD8^+$ Trm cells as $CD69^+CD103^+$ (18). Trm cells were not detected in the peripheral blood samples and only identified within glioblastoma. Within the $CD103^-$ population, CCR7 and CD45RO expression patterns distinguished naïve ($CCR7^+CD45RO^-$), Tcm ($CCR7^+CD45RO^+$), Tem ($CCR7^-CD45RO^+$), and Temra ($CCR7^-CD45RO^-$) populations for both $CD4^+$ and $CD8^+$ T cells (10, 16). Following identification of T-cell subsets, frequencies of these subsets were compared between matched patient blood and glioblastoma biopsies (**Figure 2C**). Of note, significantly fewer naïve $CD4^+$ and $CD8^+$ T cells were detected in glioblastoma biopsies compared to paired blood samples, indicating limited blood contamination of these resected glioblastoma biopsies obtained at surgery. In contrast, there was a significant enrichment of $CD4^+$ and $CD8^+$ Tcm, Tem, and Trm populations in glioblastoma biopsies, with $CD4^+$ Tcm and $CD8^+$ Tem and Trm populations most abundant overall. There was also a significant decrease in the proportion of $CD8^+$ Temra cells in glioblastoma compared to blood samples, while the proportions of $CD4^+$ Temra cells in blood and glioblastoma were negligible. Proportions of Tregs between the blood and tumour samples were similar.

$CCR2^+$, $CCR5^+$, $CXCR3^+$ and $CXCR6^+$ $CD4^+$ T-Cell Subsets Are Enriched in Glioblastoma

Following identification of T-cell subsets (**Figure 2**), expression of CCR2, CCR4, CCR5, CCR6, CXCR3, CXCR4, CXCR6, and CX3CR1 was investigated on glioblastoma and blood $CD4^+$ (**Figure 3**) and $CD8^+$ (**Figure 4**) T-cell subsets. Here, naïve blood T cells served as an internal negative control for chemokine receptor staining as this population lacks the expression of inflammatory chemokine receptors, except for CXCR3 and CXCR4, where naïve T cells and live $CD3^-$ cells containing distinct negative and positive populations were used to set gates for these receptors respectively (**Supplementary Figure 3**).

Our standard process for dissociation of tumour tissue specimens using gentleMACS reagents was found to significantly diminish CXCR3 and CCR6 staining (data not shown). Hence, other patient samples digested with Accutase were used to interrogate these receptors. Representative histograms for $CD4^+$ T-cell subsets illustrate the typical chemokine receptor expression patterns observed, and demonstrate that staining for CCR2, CCR5, CXCR3 and CXCR6 was robust in glioblastoma-infiltrating T-cell populations compared to matched blood naïve $CD4^+$ T cells (**Figure 3A** and **Supplementary Figure 4**). Quantitative analysis of chemokine receptor expression revealed a significant increase in the proportion of $CCR2^+CD4^+$ Tcm and Treg cells in glioblastoma compared to blood samples from the same patients (**Figure 3B**). CCR4 expression was most abundant in Tregs, however there was no difference in the proportion of $CCR4^+$ Tregs in glioblastoma

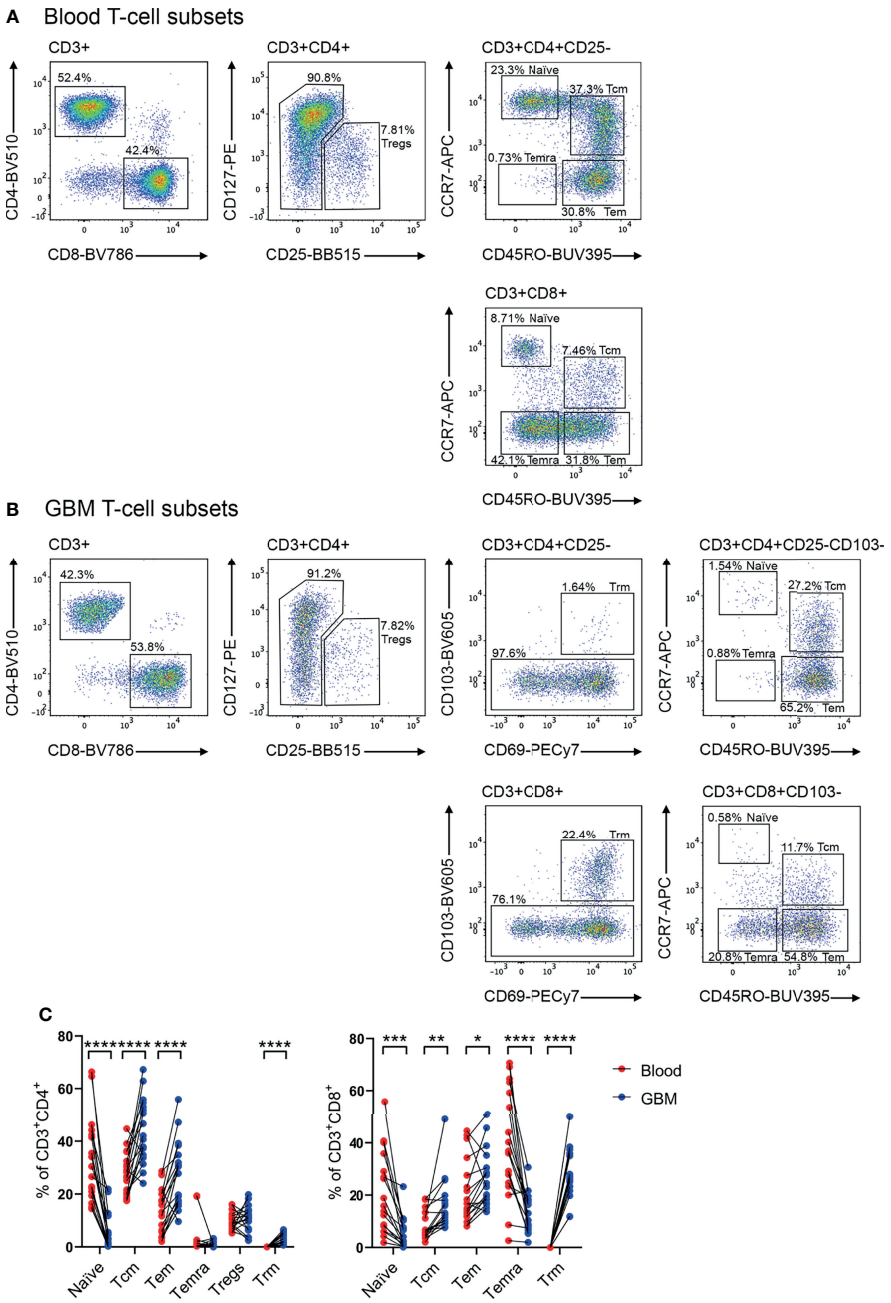

FIGURE 2 | Identification of T-cell subsets in glioblastoma-patient blood and tumour biopsies. Representative flow cytometry gating strategy for **(A)** blood- and **(B)** glioblastoma (GBM)- associated T cells. Staining of lineage-specific surface markers identifies T regulatory cells (Tregs: $CD3^+CD4^+CD25^+CD127^{low}$), and $CD4^+$ and $CD8^+$ naïve T cells ($CD103^-CD45RO^-CCR7^+$), T central memory (Tcm: $CD103^-CD45RO^+CCR7^+$), T effector memory (Tem: $CD103^-CD45RO^+CCR7^-$), T effector memory re-expressing CD45RA (Temra: $CD103^-CD45RO^-CCR7^-$), and T resident memory (Trm: $CD103^+CD69^+$) populations. Plots are representative of matched patient blood and GBM samples n=18 each. **(C)** Proportions of naïve, Tcm, Tem, Temra, Tregs and Trm cell subsets in GBM patient blood and dissociated tumour biopsies. Proportions are presented as frequency of $CD3^+CD4^+$ and $CD3^+CD8^+$ T-cell populations, respectively. Each dot represents one patient, lines represent paired patient samples. Two-tailed paired Student's t test, *p < 0.05, **p < 0.01, ***p < 0.001, ****p < 0.0001.

compared to peripheral blood (**Figure 3C**). Strikingly, all glioblastoma $CD4^+$ T-cell subsets highly expressed CCR5, and CCR5 expression was significantly enriched in glioblastoma T cells compared to blood (**Figure 3D**). CCR6 expression was relatively low in $CD4^+$ T-cell subsets compared to other chemokine receptors analysed, and no significant differences in CCR6 expression were observed between T-cell subsets in glioblastoma and blood (**Figure 3E**). $CXCR3^+$ cells were abundant in all $CD4^+$ T-cell subsets, however enrichment was only statistically significant in $CD4^+$ Tem and Tregs in glioblastoma biopsies

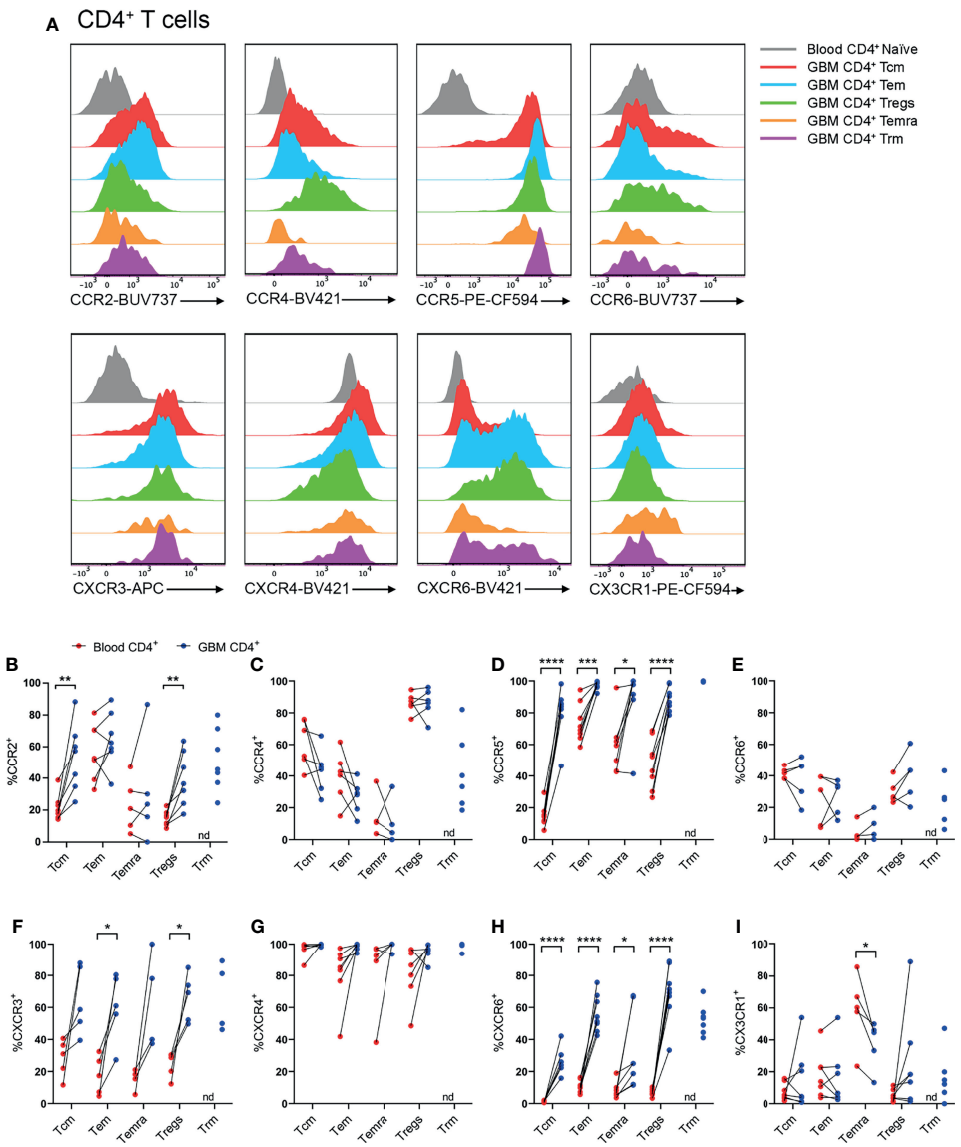

FIGURE 3 | CCR2$^+$, CCR5$^+$, CXCR3$^+$ and CXCR6$^+$ CD4$^+$ T-cell populations are significantly enriched in patient glioblastoma compared to peripheral blood. **(A)** Representative histograms showing chemokine receptor expression within CD4$^+$ T-cell subsets in glioblastoma (GBM) (coloured) and naïve CD4$^+$ T cells in matched blood samples (grey). Also see **Supplementary Figure 4** for additional blood CD4$^+$ T-cell subsets. Representative of matched blood and GBM samples n=5-8 each. **(B–I)** Proportions of CD4$^+$ T-cell subsets in blood and matched GBM biopsies expressing **(B)** CCR2, **(C)** CCR4, **(D)** CCR5, **(E)** CCR6, **(F)** CXCR3, **(G)** CXCR4, **(H)** CXCR6 and **(I)** CX3CR1. Each dot represents one patient, lines represent paired patient sample. Two-tailed paired Student's t test, *p < 0.05, **p < 0.01, ***p < 0.001, ****p < 0.0001, nd=not detected.

compared to paired blood samples (**Figure 3F**). Equally high proportions of CD4$^+$ T-cell subsets in both blood and glioblastoma expressed CXCR4, hence no enrichment of this receptor was observed in glioblastoma (**Figure 3G**). As high proportions of both blood and glioblastoma-associated CD4$^+$ T-cell subsets expressed CXCR4, the geometric mean fluorescence intensity (gMFI) was compared to determine whether CXCR4 abundance on T-cell subsets differed between glioblastoma and blood samples. Strikingly, there was a significant increase in the abundance of CXCR4 on all CD4$^+$ T-cell subsets in glioblastoma compared to blood samples (**Supplementary Figure 5A**). CXCR6, an established marker of CD69$^+$CD103$^+$ Trm cells, was expressed on CD4$^+$ Trm cells as anticipated, but also enriched in all other CD4$^+$ T-cell subsets in glioblastoma compared to blood (**Figure 3H**). Lastly, CX3CR1 expression was low among all CD4$^+$ T-cell subsets except CD4$^+$ Temra cells, where CX3CR1 expression was enriched in the blood and significantly lower in glioblastoma (**Figure 3I**). Together, our flow cytometry analysis demonstrates that CCR5 and CXCR6 are expressed by large proportions of all glioblastoma-infiltrating CD4$^+$ T-cell subsets,

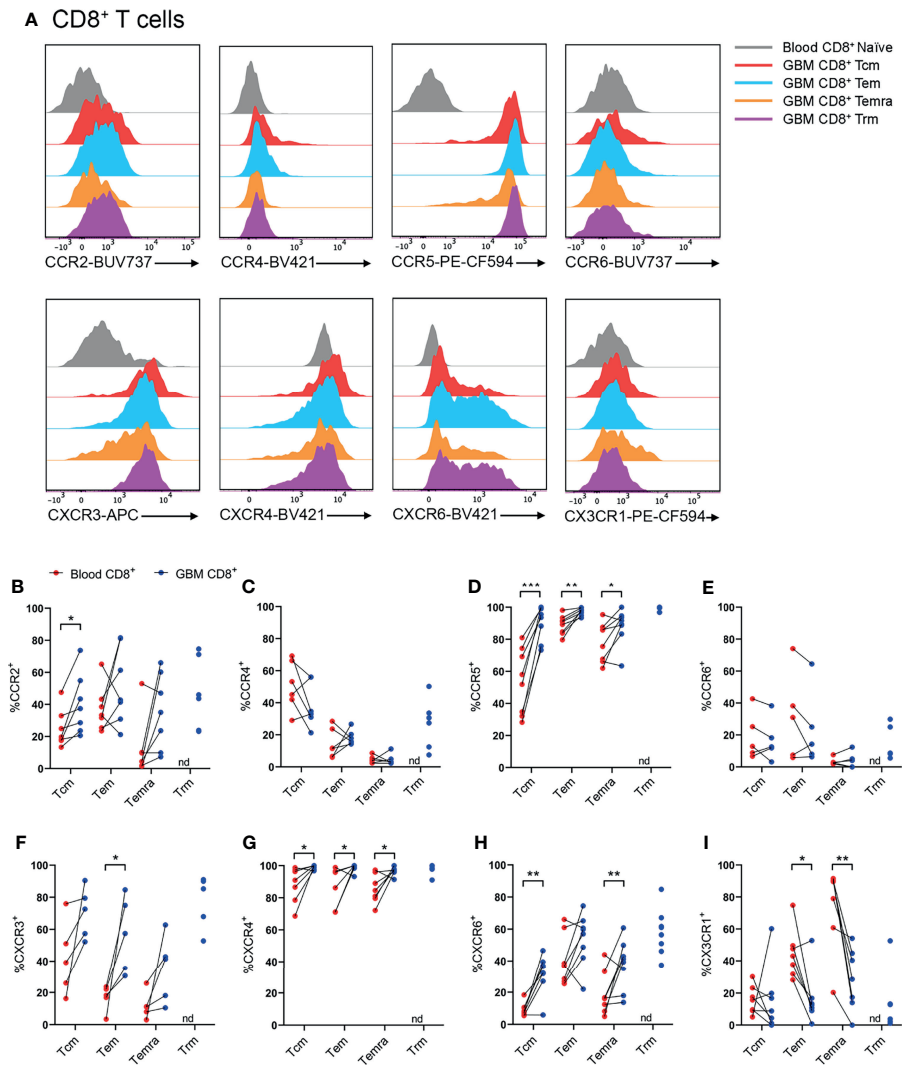

FIGURE 4 | CCR2$^+$, CCR5$^+$, CXCR3$^+$, CXCR4$^+$ and CXCR6$^+$ CD8$^+$ T-cell populations are significantly enriched in patient glioblastoma compared to peripheral blood. **(A)** Representative histograms showing chemokine receptor expression within CD8$^+$ T-cell subsets in glioblastoma (GBM) (coloured) and naïve CD8$^+$ T cells in matched blood samples (grey). Also see **Supplementary Figure 6** for additional blood CD8$^+$ T-cell subsets Representative of n=5-8 matched blood and GBM samples. **(B–I)** Proportions of CD8$^+$ T-cell subsets in blood and matched GBM biopsies expressing **(B)** CCR2, **(C)** CCR4, **(D)** CCR5, **(E)** CCR6, **(F)** CXCR3, **(G)** CXCR4, **(H)** CXCR6 and **(I)** CX3CR1. Each dot represents one patient, lines represent paired patient sample. Two-tailed paired Student's t test, *p < 0.05, **p < 0.01, ***p < 0.001, nd, not detected.

whereas CCR2 and CXCR3 enrichment was only observed in glioblastoma-infiltrating CD4$^+$ Tcm and Tregs, and Tem and Tregs respectively.

CCR2$^+$, CCR5$^+$, CXCR3$^+$, CXCR4$^+$ and CXCR6$^+$ CD8$^+$ T-Cell Subsets Are Enriched in Glioblastoma

Within CD8$^+$ T-cell subsets, representative histograms highlighted robust expression of CCR5, CXCR3, and CXCR6 compared to naïve peripheral blood CD8$^+$ T cells (**Figure 4A** and **Supplementary Figure 6**). Similar to CD4$^+$ T cells, there was enrichment of CCR2$^+$CD8$^+$ Tcm cells in glioblastoma compared to paired blood samples, and approximately 50% of CD8$^+$ glioblastoma Trms expressed CCR2 (**Figure 4B**). CCR4$^+$ cells were most abundant within the CD8$^+$ Tcm population, but expression of this receptor in glioblastoma samples was not enriched for any CD8$^+$ T-cell subsets compared to matched blood samples (**Figure 4C**). Like CD4$^+$ T-cell subsets, CCR5 was expressed by a high proportion of all CD8$^+$ T-cell subsets and was significantly enriched for all CD8$^+$ T-cell subsets in glioblastoma (**Figure 4D**). CCR6 was expressed at similar proportions between blood and glioblastoma specimens for all CD8$^+$ T-cell subsets (**Figure 4E**). Like CD4$^+$ glioblastoma T cells, CXCR3 was expressed moderately by all CD8$^+$ T-cell subsets, and there was a significantly greater proportion of CXCR3$^+$CD8$^+$ Tem cells in glioblastoma biopsies compared to paired blood samples

(**Figure 4F**). CXCR4 expression was uniformly high for all CD8$^+$ T-cell subsets and significantly enriched in glioblastoma compared to peripheral blood (**Figure 4G**). Additionally, CXCR4 gMFI was significantly increased for all CD8$^+$ T-cell subsets in glioblastoma (**Supplementary Figure 5B**). Although all CD8$^+$ glioblastoma T-cell subsets expressed modest levels of CXCR6, expression was only enriched within glioblastoma compared to blood for Tcm and Temra cells (**Figure 4H**). Lastly, CX3CR1 expression was greatest in the blood for CD8$^+$ Tem and Temra populations with a significant reduction in the frequency of CX3CR1$^+$CD8$^+$ Tem and Temra cells in glioblastoma samples. Overall, CCR5 and CXCR4 show the most prominent expression on CD8$^+$ T-cell subsets in glioblastoma tissues, with CCR2, CXCR3 and CXCR6 displaying subset-specific glioblastoma enrichment in Tcm, Tem, and Tcm and Temra populations respectively.

CD11a$^+$, CD49a$^+$ and CD49d$^+$ T Cells Are Abundant and/or Enriched in Glioblastoma

Utilising the same core panel for identification of T-cell subsets as **Figures 3**, **4**, integrins identified by scRNA-seq were investigated by flow cytometry. Subsequently, proportions of T cells expressing integrins were compared between paired blood and glioblastoma samples (**Figure 5**). All T-cell subsets in blood and glioblastoma biopsies uniformly expressed high levels of CD11a (integrin αL; **Figures 5A, B** and **Supplementary Figures 4**, **6**). Positive gates for CD49a and CD51 expression on glioblastoma T-cell subsets were set based on paired blood naïve T cells, which were uniformly CD49a$^-$ and CD51$^-$ (**Figures 5A, B** and **Supplementary Figure 3**). Live CD3$^-$ cells containing distinct populations of CD49d$^+$ and CD49d$^-$ cells were used to set positive gates for CD49d$^+$ T cells (**Supplementary Figure 3**). Despite high proportions of T cells

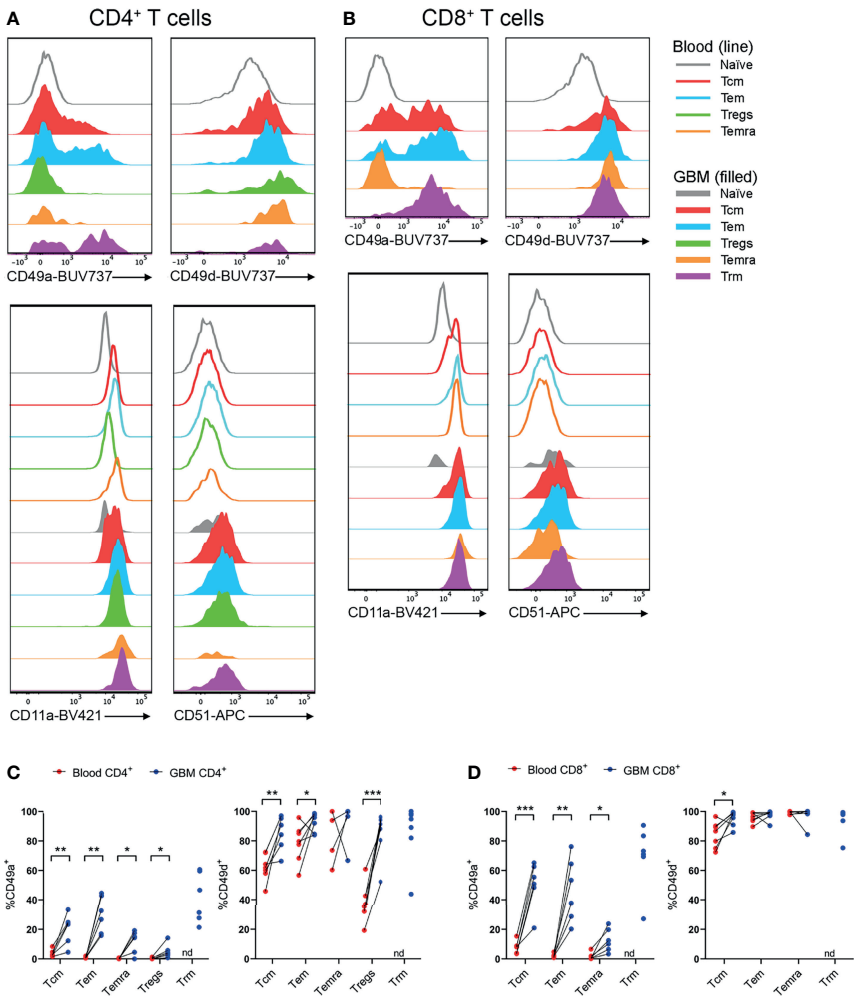

FIGURE 5 | CD49a$^+$ and CD49d$^+$ T cells are enriched in glioblastoma biopsies compared to peripheral blood. **(A, B)** Representative histograms showing CD49a, CD49d, CD11a and CD51 expression within **(A)** CD4$^+$ and **(B)** CD8$^+$ T-cell subsets in glioblastoma (GBM) biopsies (filled) and T cells in matched blood samples (line). Also see **Supplementary Figures 4**, **6** for additional blood T-cell subsets Representative of matched blood and GBM samples n=6-7 each. **(C, D)** Proportions of CD49a- and CD49d-expressing **(C)** CD4$^+$ and **(D)** CD8$^+$ T-cell subsets in blood and matched GBM biopsies. Each dot represents one patient, lines represent paired patient samples. Two-tailed paired Student's t test, *p < 0.05, **p < 0.01, ***p < 0.001, nd, not detected.

positive for *ITGAV*, we did not detect CD51 protein in any T-cell subsets in glioblastoma biopsies or paired blood samples (**Figures 5A, B**). Importantly, we demonstrated efficacy of this CD51 antibody clone with the Malme-3M human melanoma cell-line (data not shown). In contrast, CD49a (integrin α1) expression was significantly enriched within $CD4^+$ Tcm, Tem, Temra and Tregs, and $CD8^+$ Tcm, Tem and Temra subsets in glioblastoma infiltrates compared to blood, and both $CD4^+$ and $CD8^+$ Trm cells expressed this integrin (**Figures 5C, D**). Additionally, $CD4^+$ Tcm, Tem and Tregs expressing CD49d (integrin α4) were enriched in glioblastoma (**Figure 5D**). High proportions of $CD8^+$ T-cell subsets expressed CD49d, and enrichment for CD49d expression in glioblastoma was significant for the $CD8^+$ Tcm population (**Figure 5D**). Given large proportions of T cells in blood and glioblastoma expressed CD11a and CD49d, the abundance of these integrins on T cells, as measured by gMFI, was compared between blood and glioblastoma samples (**Supplementary Figure 5**). We observed no differences in the abundance of CD11a for $CD4^+$ T-cell subsets, while there was an increase in the abundance of CD11a on the $CD8^+$ Temra population (**Supplementary Figures 5A, B**). There was a significant decrease in the abundance of CD49d on the $CD4^+$ Tem population in glioblastoma compared to blood samples, and a significant increase in CD49d gMFI on $CD4^+$ Tregs in glioblastoma (**Supplementary Figure 5A**). However, there was no difference in the abundance of CD49d on $CD8^+$ T-cell subsets between glioblastoma and paired blood samples (**Supplementary Figure 5B**). Physiological T-cell surveillance of the brain includes migration across post-capillary blood-vessels into perivascular spaces adjacent to the brain parenchyma (12). This pathway requires adherence of T cells, which occurs *via* the integrins CD11a and CD49d interacting with adhesion molecules ICAM-1 and VCAM-1, respectively, on BBB ECs. Indeed, we identified expression of ICAM-1 and VCAM-1 at the gene level within glioblastoma-associated clusters *via* scRNA-seq (**Supplementary Figure 7A**). Together, these data suggest that CD11a-ICAM-1, CD49a and CD49d-VCAM-1 contribute to the infiltration of subsets of T cells into glioblastoma.

Complementary Chemokines Are Detected in Glioblastoma Biopsies, CUSA Samples and Primary Glioblastoma Cell-Lines

Having identified that $CCR2^+$, $CCR5^+$, $CXCR3^+$, $CXCR4^+$, and $CXCR6^+$ T-cell subsets were enriched in glioblastoma, we subsequently validated the expression of complementary chemokines in dissociated glioblastoma biopsies and patient-derived glioblastoma cell-lines (**Figure 6**). We also tested for the complementary chemokines to CCR6 and CX3CR1 because these receptors have been implicated in brain-homing in other studies (28, 29). The CCR4 chemokines were not selected for further analysis as we observed low proportions of non-lymphocyte cell populations expressing the complementary chemokines CCL17 and CCL22 *via* scRNA-seq (**Figure 1G**) and observed no enrichment of $CCR4^+$ T cells in glioblastoma (**Figures 3C, 4C**). To measure chemokines present within tumour tissue, the supernatant fraction from dissociated glioblastoma biopsies and CUSA aspirates, expected to contain soluble factors released from extracellular tissue spaces, was retained for analysis. In addition, we also collected supernatants from short-term cultures of tumour cells cultured under defined GNS cell conditions (24) to measure active secretion of chemokines by tumour cells. Chemokines were detected in both sample types *via* ELISA or cytometric bead-based assay. Notably, this approach favours the detection of soluble chemokines, as chemokines sequestered intracellularly or tethered to the cell surface *via* transmembrane domains or glycosaminoglycans (GAGs) are likely to remain in the cellular fraction. Of all chemokines assayed, the CCR2/CCR4 ligand CCL2 was the most abundant chemokine detected in tumour biopsy, CUSA and cultured GNS cell supernatants, and was present above the limit of detection in all samples analysed (**Figure 6A**). Interestingly, CCR5 ligands: CCL3, CCL4 and CCL5 were detected in the majority of supernatants harvested from dissociated tumour biopsy and CUSA, but little was detected in GNS cell supernatants (**Figures 6B–D**). Of the CXCR3 ligands, CXCL9 was detected in the majority of dissociated tumour specimens but was below the level of detection in all GNS cell cultures analysed (**Figure 6E**), CXCL10 was largely absent from dissociated tumour specimens, but highly expressed by few GNS cell samples (**Figure 6F**), and CXCL11 was below the lower limit of detection in all samples (**Figure 6G**). This was in contrast to expression of these ligands detected *via* scRNA seq (**Figure 1F**), but may reflect the high affinity of CXCL10 and CXCL11 for GAGs (30, 31). CXCL12, the sole chemokine ligand for CXCR4, was abundant in 6 out of 12 supernatants from the GNS cell cultures, however it was undetectable in all dissociated tumour biopsy and CUSA samples analysed (**Figure 6H**). CXCL16, the chemokine ligand of CXCR6, was detected in supernatants from the majority of dissociated tumour and GNS cell samples (**Figure 6I**). CX3CL1 was below the lower limit of detection in supernatants from all dissociated glioblastoma tumour biopsy, CUSA and GNS cell samples analysed (**Figure 6J**). However, measures here for both CXCL16 and CX3CL1 may underestimate their abundance as they are expressed as transmembrane chemokines and CXCL16 exhibits selective GAG binding (32–34). CCL20, the chemokine ligand of CCR6, was not detected in either dissociated tumour or GNS cell supernatants (**Figure 6K**). Comparing chemokine abundance between dissociated tumour and cultured GNS cell supernatants, CCL3, CCL4, CCL5 and CXCL9 were abundant in dissociated tumour samples, with little detected in supernatants from cultured tumour cells, suggesting non-tumour-cell populations were the source of these chemokines in glioblastoma. In contrast, glioblastoma tumour cells may be the main source of CCL2, CXCL10 and CXCL12 production in the tumour microenvironment given the elevated CCL2 detected in GNS cell culture supernatants and the minimal levels of CXCL10 and CXCL12 detected in dissociated tumour supernatants. Considered together with the analyses of receptor expression on glioblastoma T cells, these data implicate the CCR2-CCL2, CCR5-CCL3/4/5, CXCR3-CXCL9, CXCR4-CXCL12 and

CXCR6-CXCL16 chemokine axes in T-cell infiltration and/or retention in glioblastoma.

DISCUSSION

Chemokine receptors and integrins play critical roles in chemotaxis, adhesion, and extravasation of T cells into tumours. It is widely reported that integrins expressed on T cells undergo conformational changes upon chemokine-chemokine receptor binding to facilitate greater adhesion to blood ECs (11, 35). Our work has identified potential chemokine-chemokine receptor axes and integrins that may direct T cells to glioblastoma. In our study, scRNA-seq analysis and protein validation implicate the CCR2-CCL2, CCR5-CCL3/4/5, CXCR3-CXCL9, CXCR4-CXCL12, and CXCR6-CXCL16 chemokine axes, and CD49a, CD49d, and CD11a integrins in glioblastoma infiltration. Few studies have investigated homing of T cells in glioblastoma, and our study is the first to systematically identify chemokine ligand and receptor pairs in primary tumour material from newly diagnosed glioblastoma patients. The brain is considered an immune-privileged site and migration of T cells to this tissue is normally tightly regulated. Whilst the BBB is compromised in glioblastoma, extravasation of T cells across the BBB is still a rate-limiting factor in successful CAR T-cell therapies (36). Therefore, understanding the factors that regulate entry of T cells into glioblastoma is important to tailor therapeutic approaches.

Our study is also the first to identify CXCR6$^+$ T-cell subsets as being enriched in glioblastoma, as well as demonstrating CXCL16 expression in dissociated tumour biopsies and glioblastoma cell-lines. We identified CXCR6$^+$ T cells enriched in CD4$^+$ Tcm, Tem, Temra, and Tregs, and CD8$^+$ Tcm and Temra populations. CXCR6, a marker of Trm cells, was indeed expressed by a high proportion of both CD4$^+$ and CD8$^+$ Trm cells in glioblastoma. The CXCR6-CXCL16 axis may regulate

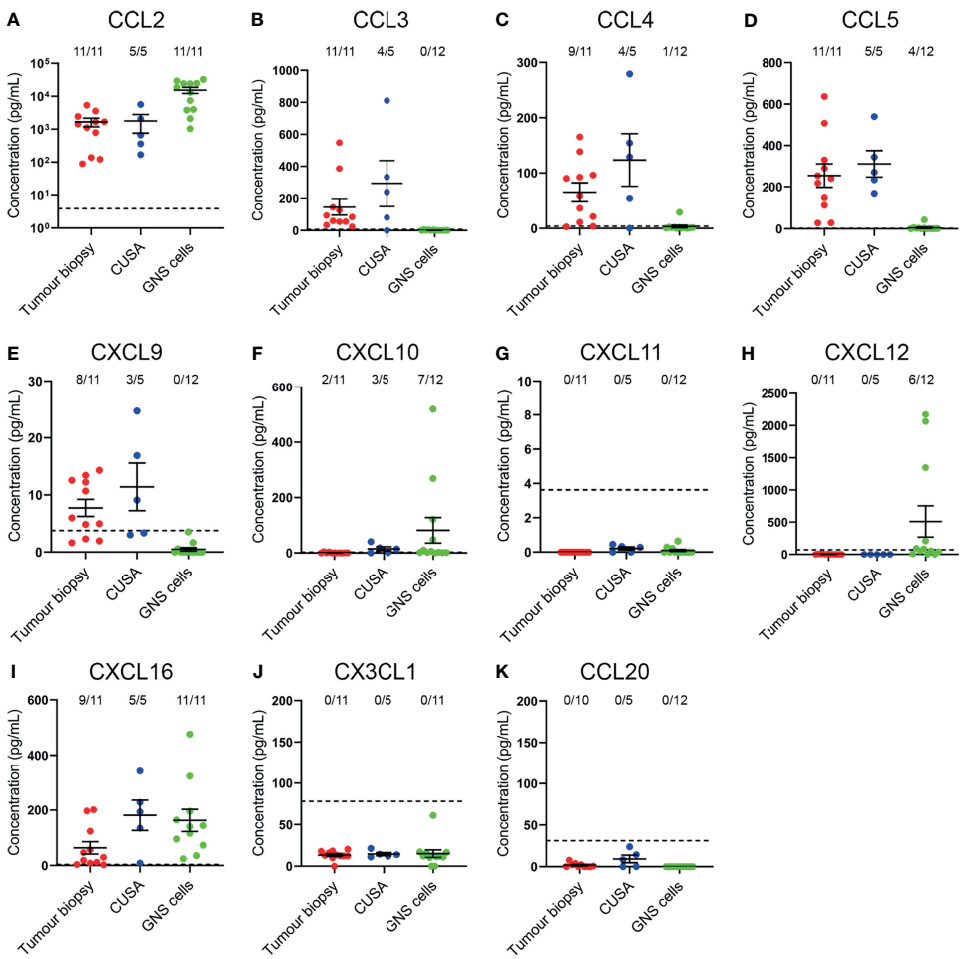

FIGURE 6 | Complementary chemokines are detected in glioblastoma biopsies and CUSA samples, and supernatants from cultured GNS cells. **(A–K)** Chemokine abundance in supernatants from dissociated tumour biopsy, dissociated tumour fragments recovered from CUSA samples, and cultured GNS cells. Each dot represents one sample, bars represent mean ± SEM. Dotted line represents lower limit of detection. The number of samples above this threshold for each chemokine is displayed.

migration, retention or survival in glioblastoma. Indeed, this axis has been shown to be important for $CD8^+$ T-cell anti-tumour responses or retention in tumours (19, 37) and critical for T-cell survival within murine melanoma tumours by positioning T cells with intratumoral dendritic cells (DCs) secreting pro-survival cytokines (38). Ultimately, the CXCR6-CXCL16 axis has been demonstrated to be essential in $CD8^+$ T-cell responses to ICI therapy and mediating cancer regression in mouse models of colorectal cancer and melanoma (39). Thus, CAR T cells engineered to express CXCR6 exerted superior anti-tumour activity in pre-clinical models of pancreatic cancer compared to CAR T cells without this genetic modification (40). Whether CXCR6 drives T-cell migration, retention or survival in glioblastoma remains an important question given its requirement in CAR T-cell and ICI therapy in other tumour models.

Importantly, we have shown that $CCR5^+$ cells are significantly enriched in all glioblastoma-infiltrating T-cell subsets, and CCR5 ligands were detected in supernatants from dissociated glioblastoma biopsies, implicating a key role for this axis in the infiltration and/or retention of T cells in glioblastoma. Enrichment of $CCR5^+$ T cells has been observed in other cancer types, suggesting a potential role for migration to these tumours (41). However, whether CCR5 mediates migration to the brain and glioblastoma remains unclear. Higher proportions of $CCR5^+$ T cells have been identified in human cerebrospinal fluid (CSF) compared to peripheral blood (42) and effector $CCR5^+CD8^+$ T cells were found to be enriched in human glioblastoma (43). Therefore, the importance of the CCR5 chemokine receptor axis in glioblastoma infiltration should be explored further.

The CXCR4-CXCL12 axis has known roles in T-cell surveillance and infiltration of the brain parenchyma during homeostasis and central nervous system (CNS) pathologies (44, 45). Here, we observed high proportions of both patient blood and glioblastoma T-cell subsets expressing CXCR4, and significantly greater abundance of CXCR4, by measure of gMFI, on glioblastoma T-cell subsets. However, in contrast to enrichment of $CXCR4^+$ T cells in glioblastoma, the greater abundance of CXCR4 on these cells may reflect redundancy of this axis in tumour infiltration as ligation of CXCR4 by CXCL12 results in receptor internalisation and desensitisation (46). We were unable to detect CXCL12 in supernatants from dissociated glioblastoma tumour biopsy and CUSA samples. This may be attributed to the intracellular or membrane-bound localisation of CXCL12 observed in tumour-associated ECs (47). Interestingly, in mouse models of multiple sclerosis, T cells that have passed BBB-associated ECs are restricted to the perivascular niche by CXCL12 localised to the basolateral surface of these ECs (45). Thus in multiple sclerosis, CXCR4 restricts T cells migrating across astrocyte endfeet and entering the brain. Whether similar brain infiltration mechanisms are employed in glioblastoma remain unknown. However, CXCR4-blockade in combination with anti-PD-1 has been shown to have a synergistic effect in increasing the proportion of $IFN\gamma^+$ and $TNF\alpha^+$ producing $CD4^+$ and $CD8^+$ T cells in the brains of mice with glioblastoma (48).

The CCR2/CCR4-CCL2 axis has been identified in previous *in vitro* glioblastoma studies. High abundance of CCL2 has been detected in glioma tumour tissue and cell-line supernatants by ELISA, and glioblastoma-patient peripheral blood Tregs could be recruited to glioblastoma-conditioned medium in a CCL2-dependent manner (49, 50). We also observed high levels of CCL2 in supernatants from dissociated glioblastoma biopsies and GNS cells, inferring that CCL2 could recruit T cells through CCR2 or CCR4 to glioblastoma. However, here we show that T cells are more likely to be recruited *via* CCR2 than CCR4 given that both $CCR2^+$ Tregs, and $CCR2^+$ Tcm cells were enriched in glioblastoma tissues, and we found no enrichment of $CCR4^+$ T cells in glioblastoma. Indeed, pathogenic Th17 cells have been shown to migrate to the inflamed CNS in murine models of multiple sclerosis *via* CCR2 (51). Thus, our findings now suggest that high CCL2 abundance identified by multiple glioblastoma studies may mediate trafficking to glioblastoma through CCR2 rather than CCR4. This remains an important question for future studies.

CXCR3 is widely expressed by activated T cells and was highly enriched on glioblastoma-infiltrating T-cell subsets. Studies investigating brain viral infection have demonstrated that CXCR3 mediates T-cell entry from the CSF into the brain parenchyma (52, 53). Additionally, T cells in human CSF are enriched for $CXCR3^+$ and $CCR5^+$ compared to peripheral blood (42). A study investigating the role of CXCR3 signalling in glioblastoma observed that CXCR3-KO mice had a reduced survival compared to WT mice (54). However, glioblastoma-infiltrating T-cell numbers were not significantly different between groups, suggesting that CXCR3 did not mediate infiltration of T cells in this model. In keeping with this, recent studies in subcutaneous mouse tumour models have shown that CXCR3 is not required for tumour infiltration but is important for positioning T cells to receive anti-tumour activation signals from intratumoral DCs when paired with anti-PD-1 therapy (55). Therefore, these discrepancies highlight the need for future studies using immunocompetent mouse glioblastoma models as it is unclear whether CXCR3 mediates infiltration or positioning of T cells within glioblastoma. Identifying the function of CXCR3 will better instruct the use of immunotherapies to treat glioblastoma *via* augmenting CXCR3 expression on CAR T cells infused *via* the CSF to improve entry to the brain, or improve T cell-DC interactions to enhance anti-tumour responses when paired with ICI therapy.

Despite high proportions of T cells and non-lymphocyte populations identified as positive for *CCR6* and *CCL20 via* scRNA-seq respectively, $CCR6^+$ T cells were not enriched in glioblastoma and we were unable to detect CCL20 in supernatants *via* ELISA. A prior study has identified CCL20 expression by immunohistochemistry within human glioblastoma tissues, and this has correlated with increased T-cell infiltration (56). Notably however, CCL20 was limited to the cytoplasm of tumour cells, with little secreted in the glioblastoma microenvironment. This may explain why we did not detect CCL20 by ELISA in supernatants from dissociated glioblastoma specimens or GNS cells. Additional work is necessary to

determine whether the high proportion of cells expressing *CCL20* has any biological significance given our data showed a lack of enrichment of $CCR6^+$ T-cell subsets and no detection of CCL20 protein by ELISA.

CX3CL1 is constitutively expressed in the healthy brain by neurons and astrocytes, and exists in transmembrane and soluble forms (32, 57). Considering that only the soluble form would be present in supernatants, this may explain why CX3CL1 protein was below the limit of detection for all glioblastoma biopsies and GNS cell-lines analysed despite varying proportions of cells expressing *CX3CL1* identified by scRNA-seq analysis. Regardless, a study using a murine model of glioma found no expression of *Cx3cr1* in glioma-infiltrating T cells, nor a role for this receptor in T-cell recruitment to glioma (58). Similarly, we observed a decrease in the proportion of $CX3CR1^+CD4^+$ Temra and $CX3CR1^+CD8^+$ Tem and Temra subsets in glioblastoma compared to paired blood samples, suggesting little requirement for CX3CR1 in glioblastoma infiltration.

We found high expression of $CD11a^+$, and enrichment of $CD49a^+$ and $CD49d^+$ T cells in glioblastoma. We also identified expression of ICAM-1 and VCAM-1, the cognate receptors for the CD11a and CD49d integrins respectively, at the gene level within glioblastoma-associated clusters *via* scRNA-seq. CD11a and CD49d have been implicated in T-cell glioblastoma-infiltration in a previous study *in vitro*, where transmigration of T-cells across glioblastoma-isolated ECs occurred in a ICAM-1 and VCAM-1-dependent manner (59). Furthermore, neutralising CD49d *in vivo* abrogates homing of cytotoxic T cells to intracranial tumours (60). In line with this, we found high frequencies of all T-cell subsets expressing CD49d in glioblastoma tissues and uniformly high expression of CD11a. Unlike CD11a and CD49d, a role for CD49a in glioblastoma has not been investigated. CD49a is a type IV collagen receptor, a marker of T-cell tissue residency, and $CD49a^+$ Trm cells have been observed to populate the human brain (18). Accordingly, the greatest frequency of $CD49a^+$ cells identified here were the Trm populations, yet moderate proportions of multiple $CD4^+$ and $CD8^+$ T-cell subsets expressed CD49a and were enriched in glioblastoma. Early studies in other tumour models have demonstrated CD49a expression is critical for $CD8^+$ T cell anti-tumour responses at mucosal sites (61). Importantly, a recent study investigating the functionality of CD49a in melanoma tumour models has shown that CD49a is upregulated on tumour-infiltrating T cells by the tumour microenvironment and enhances T-cell motility (62). Given the likely function of CD49a in tumour retention, its role in glioblastoma should be investigated further.

A limitation of our study is that enrichment of migratory receptors within tumours does not demonstrate their functional requirement. Here, enrichment of migratory receptors within glioblastoma suggests that they may be important in the processes underlying tumour infiltration, or receptor expression may be induced in T cells by the tumour environment following infiltration. Alternatively, the enrichment of chemokine receptors might be a bystander effect of memory or effector T cells concentrating at the tumour site, and not as a result of their requirement for tumour infiltration. Furthermore, additional modifications and downstream signalling molecules will also affect chemokine receptor responsiveness and activity (63). However, having identified key receptors amongst all known homing receptors, further functional studies with orthotopic xenograft glioblastoma tumour models and syngeneic immunocompetent models can identify receptor-dependent roles in glioblastoma-homing. These models would directly address the requirement of these receptors in glioblastoma infiltration and identify receptors with non-chemotactic or redundant functions in anti-tumour responses. Importantly, investigating the endogenous intratumoral T-cell migratory profile is an approach that can be leveraged to identify unique migratory receptors important for T-cell infiltration in other solid tumours and guide subsequent functional assays. In turn, by enhancing the expression of appropriate migratory receptors, T-cell-based therapies could be improved and implemented in clinical trials for glioblastoma and possibly other solid tumours.

DATA AVAILABILITY STATEMENT

The raw sequencing datasets presented in this article are not readily available due to patient confidentiality, as required by our Human Research Ethics Committee. The processed gene expression matrix with raw mRNA counts for all cells in the T cell cluster has been made publicly available. This data can be found on figshare: 10.6084/m9.figshare.19119698. Other original datasets presented in the study are either contained in the article or will be made available by the authors, *via* the corresponding author (TG, tessa.gargett@sa.gov.au).

ETHICS STATEMENT

The studies involving human participants were reviewed and approved by Central Adelaide Local Health Network Human Research Ethics. The patients/participants provided their written informed consent to participate in this study.

AUTHOR CONTRIBUTIONS

PK: Conceptualisation, data curation, formal analysis, investigation, methodology, writing – original draft, writing – review & editing. LE:Conceptualisation, data curation, investigation, funding acquisition, methodology, resources, supervision, writing – review & editing. JT: Data curation, formal analysis, methodology, writing – review & editing. CB: Conceptualisation, data curation, methodology, writing – review & editing. RO: Resources. SIP: Resources. SL:Resources. MT: Resources. SMP: Funding acquisition, resources. GG: Funding acquisition, resources, writing – review & editing. MB: Conceptualisation, funding acquisition, resources, supervision, writing – review & editing. TG: Conceptualisation, funding acquisition, methodology, resources,

supervision, writing – review & editing. All authors contributed to the article and approved the submitted version.

FUNDING

This work was supported by the Neurosurgical Research Foundation, The Hospital Research Foundation Group, a Tour de Cure Senior Research Grant, the Cancer Council SA Beat Cancer Project, the Royal Adelaide Hospital Research Fund, and the Health Services Charitable Gifts Board (Adelaide). scRNA-seq experiments were funded by a Cure Brain Cancer Foundation Infrastructure Grant to SMP, GG, and MB. SMP was supported by the National Health and Medical Research Council of Australia (1156693). GG was supported by the Australian Research Council (FT16010036). PK was supported by a University of Adelaide Honours Scholarship.

ACKNOWLEDGMENTS

The authors would like to thank Mariana Oksdath Mansilla, Sally Perrin and Kaitlin Scheer (Centre for Cancer Biology) for their assistance in the initial analysis of the scRNA-seq data, Nga Truong and Kristyna Sedivakova (Centre for Cancer Biology) for the isolation of peripheral blood mononuclear cells from glioblastoma patient blood samples, and Erica Yeo (Centre for Cancer Biology) for GNS cell-line culture and supernatant harvesting. Additionally, we thank A/Prof Philip Gregory (Centre for Cancer Biology) for providing human melanoma cell-lines for flow cytometry experiments, Dr Kerrie Foyle (University of Adelaide) for reagents, and A/Prof Craig Wallington-Gates (Flinders Medical Centre) for offering statistical advice. We also acknowledge the support and generosity of the patients and medical and technical staff from SA Pathology and the SA Neurological Tumour Bank (supported by Flinders University, Flinders Foundation and The Neurosurgical Research Foundation), who made collection of tissue specimens possible. scRNA-seq experiments were performed at the Australian Cancer Research Foundation (ACRF) Cancer Genomics and Cancer Discovery Accelerator facilities, established with the generous support of the Australian Cancer Research Foundation.

SUPPLEMENTARY MATERIAL

The Supplementary Material for this article can be found online at: https://www.frontiersin.org/articles/10.3389/fimmu.2022.850226/full#supplementary-material

REFERENCES

1. Tamimi AF, Juweid M. Epidemiology and Outcome of Glioblastoma. In: S De Vleeschouwer, editor. *Glioblastoma*. Brisbane: Codon Publications (2017). p. 143–53.
2. Brown MP, Ebert LM, Gargett T. Clinical Chimeric Antigen Receptor-T Cell Therapy: A New and Promising Treatment Modality for Glioblastoma. *Clin Transl Immunol* (2019) 8(5):e1050. doi: 10.1002/cti2.1050
3. Poon MTC, Sudlow CLM, Figueroa JD, Brennan PM. Longer-Term (≥ 2 Years) Survival in Patients With Glioblastoma in Population-Based Studies Pre- and Post-2005: A Systematic Review and Meta-Analysis. *Sci Rep* (2020) 10(1). doi: 10.1038/s41598-020-68011-4
4. Porter DL, Levine BL, Kalos M, Bagg A, June CH. Chimeric Antigen Receptor–Modified T Cells in Chronic Lymphoid Leukemia. *N Engl J Med* (2011) 365(8):725–33. doi: 10.1056/NEJMoa1103849
5. Long GV, Atkinson V, Lo S, Sandhu S, Guminski AD, Brown MP, et al. Combination Nivolumab and Ipilimumab or Nivolumab Alone in Melanoma Brain Metastases: A Multicentre Randomised Phase 2 Study. *Lancet Oncol* (2018) 19(5):672–81. doi: 10.1016/S1470-2045(18)30139-6
6. Sanders S, Debinski W. Challenges to Successful Implementation of the Immune Checkpoint Inhibitors for Treatment of Glioblastoma. *IJMS* (2020) 21(8):2759. doi: 10.3390/ijms21082759
7. Brown CE, Alizadeh D, Starr R, Weng L, Wagner JR, Naranjo A, et al. Regression of Glioblastoma After Chimeric Antigen Receptor T-Cell Therapy. *New Engl J Med* (2016) 375(26):2561–9. doi: 10.1056/NEJMoa1610497
8. Chuntova P, Chow F, Watchmaker PB, Galvez M, Heimberger AB, Newell EW, et al. Unique Challenges for Glioblastoma Immunotherapy—Discussions Across Neuro-Oncology and Non-Neuro-Oncology Experts in Cancer Immunology. Meeting Report From the 2019 SNO Immuno-Oncology Think Tank. *Neuro-Oncology* (2021) 23(3):356–75. doi: 10.1093/neuonc/noaa277
9. Engelhardt B, Ransohoff RM. Capture, Crawl, Cross: The T Cell Code to Breach the Blood–Brain Barriers. *Trends Immunol* (2012) 33(12):579–89. doi: 10.1016/j.it.2012.07.004
10. Mohme M, Schliffke S, Maire CL, Rünger A, Glau L, Mende KC, et al. Immunophenotyping of Newly Diagnosed and Recurrent Glioblastoma Defines Distinct Immune Exhaustion Profiles in Peripheral and Tumor-Infiltrating Lymphocytes. *Clin Cancer Res* (2018) 24(17):4187–200. doi: 10.1158/1078-0432.CCR-17-2617
11. Slaney CY, Kershaw MH, Darcy PK. Trafficking of T Cells Into Tumors. *Cancer Res* (2014) 74(24):7168–74. doi: 10.1158/0008-5472.CAN-14-2458
12. Ratnam NM, Gilbert MR, Giles AJ. Immunotherapy in CNS Cancers: The Role of Immune Cell Trafficking. *Neuro-Oncology* (2019) 21(1):37–46. doi: 10.1093/neuonc/noy084
13. Mathewson ND, Ashenberg O, Tirosh I, Gritsch S, Perez EM, Marx S, et al. Inhibitory CD161 Receptor Identified in Glioma-Infiltrating T cells by Single-Cell Analysis. *Cell* (2021) 184(5):1281–98e26. doi: 10.1016/j.cell.2021.01.022
14. Friebel E, Kapolou K, Unger S, Nunez NG, Utz S, Rushing EJ, et al. Single-Cell Mapping of Human Brain Cancer Reveals Tumor-Specific Instruction of Tissue-Invading Leukocytes. *Cell* (2020) 181(7):1626–42e20. doi: 10.1016/j.cell.2020.04.055
15. Osborn JF, Hobbs SJ, Mooster JL, Khan TN, Kilgore AM, Harbour JC, et al. Central Memory CD8+ T Cells Become CD69+ Tissue-Residents During Viral Skin Infection Independent of CD62L-Mediated Lymph Node Surveillance. *PloS Pathog* (2019) 15(3):e1007633. doi: 10.1371/journal.ppat.1007633
16. Mahnke YD, Brodie TM, Sallusto F, Roederer M, Lugli E. The Who's Who of T-Cell Differentiation: Human Memory T-Cell Subsets. *Eur J Immunol* (2013) 43(11):2797–809. doi: 10.1002/eji.201343751
17. Gebhardt T, Palendira U, Tscharke DC, Bedoui S. Tissue-Resident Memory T Cells in Tissue Homeostasis, Persistent Infection, and Cancer Surveillance. *Immunol Rev* (2018) 283(1):54–76. doi: 10.1111/imr.12650
18. Smolders J, Heutinck KM, Fransen NL, Remmerswaal EBM, Hombrink P, ten Berge IJM, et al. Tissue-Resident Memory T Cells Populate the Human Brain. *Nat Commun* (2018) 9(1):4593. doi: 10.1038/s41467-018-07053-9
19. Muthuswamy R, McGray AR, Battaglia S, He W, Miliotto A, Eppolito C, et al. CXCR6 by Increasing Retention of Memory CD8+ T Cells in the Ovarian Tumor Microenvironment Promotes Immunosurveillance and Control of Ovarian Cancer. *J ImmunoTher Cancer* (2021) 9(10):e003329. doi: 10.1136/jitc-2021-003329
20. Fu W, Wang W, Li H, Jiao Y, Huo R, Yan Z, et al. Single-Cell Atlas Reveals Complexity of the Immunosuppressive Microenvironment of Initial and Recurrent Glioblastoma. *Front Immunol* (2020) 11. doi: 10.3389/fimmu.2020.00835

21. Woroniecka K, Chongsathidkiet P, Rhodin K, Kemeny H, Dechant C, Farber SH, et al. T-Cell Exhaustion Signatures Vary With Tumor Type and Are Severe in Glioblastoma. *Clin Cancer Res* (2018) 24(17):4175–86. doi: 10.1158/1078-0432.CCR-17-1846
22. Ebert LM, Yu W, Gargett T, Toubia J, Kollis PM, Tea MN, et al. Endothelial, Pericyte and Tumor Cell Expression in Glioblastoma Identifies Fibroblast Activation Protein (FAP) as an Excellent Target for Immunotherapy. *Clin Transl Immunol* (2020) 9(10). doi: 10.1002/cti2.1191
23. Neftel C, Laffy J, Filbin MG, Hara T, Shore ME, Rahme GJ, et al. An Integrative Model of Cellular States, Plasticity, and Genetics for Glioblastoma. *Cell* (2019) 178(4):835–49e21. doi: 10.1016/j.cell.2019.06.024
24. Pollard SM, Yoshikawa K, Clarke ID, Danovi D, Stricker S, Russell R, et al. Glioma Stem Cell Lines Expanded in Adherent Culture Have Tumor-Specific Phenotypes and Are Suitable for Chemical and Genetic Screens. *Cell Stem Cell* (2009) 4(6):568–80. doi: 10.1016/j.stem.2009.03.014
25. Jalbert E, Shikuma CM, Ndhlovu LC, Barbour JD. Sequential Staining Improves Detection of CCR2 and CX3CR1 on Monocytes When Simultaneously Evaluating CCR5 by Multicolor Flow Cytometry. *Cytometry Part A* (2013) 83A(3):280–6. doi: 10.1002/cyto.a.22257
26. Reiser J, Banerjee A. Effector, Memory, and Dysfunctional $CD8^+$ T Cell Fates in the Antitumor Immune Response. *J Immunol Res* (2016) 2016:8941260. doi: 10.1155/2016/8941260
27. Klein S, Kretz CC, Krammer PH, Kuhn A. CD127low/- and FoxP3+ Expression Levels Characterize Different Regulatory T-Cell Populations in Human Peripheral Blood. *J Invest Dermatol* (2010) 130(2):492–9. doi: 10.1038/jid.2009.313
28. Reboldi A, Coisne C, Baumjohann D, Benvenuto F, Bottinelli D, Lira S, et al. C-C Chemokine Receptor 6–Regulated Entry of TH-17 Cells Into the CNS Through the Choroid Plexus is Required for the Initiation of EAE. *Nat Immunol* (2009) 10(5):514–23. doi: 10.1038/ni.1716
29. Broux B, Pannemans K, Zhang X, Markovic-Plese S, Broekmans T, Eijnde BO, et al. CX_3CR1 Drives Cytotoxic $CD4^+CD28^-$ T Cells Into the Brain of Multiple Sclerosis Patients. *J Autoimmun* (2012) 38:10–9. doi: 10.1016/j.jaut.2011.11.006
30. Campanella GSV, Lee EMJ, Sun J, Luster AD. CXCR3 and Heparin Binding Sites of the Chemokine IP-10 (CXCL10). *J Biol Chem* (2003) 278(19):17066–74. doi: 10.1074/jbc.M212077200
31. Dyer DP, Salanga CL, Volkman BF, Kawamura T, Handel TM. The Dependence of Chemokine–Glycosaminoglycan Interactions on Chemokine Oligomerization. *Glycobiology* (2015) 26(3):312–26. doi: 10.1093/glycob/cwv100
32. Bazan JF, Bacon KB, Hardiman G, Wang W, Soo K, Rossi D, et al. A New Class of Membrane-Bound Chemokine With a CX3C Motif. *Nature* (1997) 385(6617):640–4. doi: 10.1038/385640a0
33. Matloubian M, David A, Engel S, Ryan JE, Cyster JG. A Transmembrane CXC Chemokine Is a Ligand for HIV-Coreceptor Bonzo. *Nat Immunol* (2000) 1 (4):298–304. doi: 10.1038/79738
34. De Paz JL, Moseman EA, Noti C, Polito L, Von Andrian UH, Seeberger PH. Profiling Heparin–Chemokine Interactions Using Synthetic Tools. *ACS Chem Biol* (2007) 2(11):735–44. doi: 10.1021/cb700159m
35. Bertoni A, Alabiso O, Galetto A, Baldanzi G. Integrins in T Cell Physiology. *IJMS* (2018) 19(2):485. doi: 10.3390/ijms19020485
36. Arvanitis CD, Ferraro GB, Jain RK. The Blood–Brain Barrier and Blood–Tumour Barrier in Brain Tumours and Metastases. *Nat Rev Cancer* (2020) 20 (1):26–41. doi: 10.1038/s41568-019-0205-x
37. Matsumura S, Wang B, Kawashima N, Braunstein S, Badura M, Cameron TO, et al. Radiation-Induced CXCL16 Release by Breast Cancer Cells Attracts Effector T Cells. *J Immunol* (2008) 181(5):3099–107. doi: 10.4049/jimmunol.181.5.3099
38. Di Pilato M, Kfuri-Rubens R, Pruessmann JN, Ozga AJ, Messemaker M, Cadilha BL, et al. CXCR6 Positions Cytotoxic T cells to Receive Critical Survival Signals in the Tumor Microenvironment. *Cell* (2021) 184(17):4512–30e22. doi: 10.1016/j.cell.2021.07.015
39. Wang B, Wang Y, Sun X, Deng G, Huang W, Wu X, et al. CXCR6 Is Required for Antitumor Efficacy of Intratumoral CD8+ T Cell. *J ImmunoTher Cancer* (2021) 9(8):e003100. doi: 10.1136/jitc-2021-003100
40. Lesch S, Blumenberg V, Stoiber S, Gottschlich A, Ogonek J, Cadilha BL, et al. T Cells Armed With C-X-C Chemokine Receptor Type 6 Enhance Adoptive Cell Therapy for Pancreatic Tumours. *Nat Biomed Eng* (2021) 5(11):1246–60. doi: 10.1038/s41551-021-00737-6
41. Parsonage G, Machado LR, Hui JW-Y, McLarnon A, Schmaler T, Balasothy M, et al. CXCR6 and CCR5 Localize T Lymphocyte Subsets in Nasopharyngeal Carcinoma. *Am J Pathol* (2012) 180(3):1215–22. doi: 10.1016/j.ajpath.2011.11.032
42. Kivisäkk P, Trebst C, Liu Z, Tucky BH, Sørensen TL, Rudick RA, et al. T-Cells in the Cerebrospinal Fluid Express a Similar Repertoire of Inflammatory Chemokine Receptors in the Absence or Presence of CNS Inflammation: Implications for CNS Trafficking. *Clin Exp Immunol* (2002) 129(3):510–8. doi: 10.1046/j.1365-2249.2002.01947.x
43. Chen P-Y, Wu CY-J, Fang J-H, Chen H-C, Feng L-Y, Huang C-Y, et al. Functional Change of Effector Tumor-Infiltrating CCR5+CD38+HLA-DR+CD8+ T Cells in Glioma Microenvironment. *Front Immunol* (2019) 10. doi: 10.3389/fimmu.2019.02395
44. Takamura S. Niches for the Long-Term Maintenance of Tissue-Resident Memory T Cells. *Front Immunol* (2018) 9(1214). doi: 10.3389/fimmu.2018.01214
45. McCandless EE, Wang Q, Woerner BM, Harper JM, Klein RS. CXCL12 Limits Inflammation by Localizing Mononuclear Infiltrates to the Perivascular Space During Experimental Autoimmune Encephalomyelitis. *J Immunol* (2006) 177 (11):8053–64. doi: 10.4049/jimmunol.177.11.8053
46. Orsini MJ, Parent J-L, Mundell SJ, Benovic JL. Trafficking of the HIV Coreceptor Cxcr4. *J Biol Chem* (1999) 274(43):31076–86. doi: 10.1074/jbc.274.43.31076
47. Rao S, Sengupta R, Choe EJ, Woerner BM, Jackson E, Sun T, et al. CXCL12 Mediates Trophic Interactions Between Endothelial and Tumor Cells in Glioblastoma. *PloS One* (2012) 7(3):e33005. doi: 10.1371/journal.pone.0033005
48. Wu A, Maxwell R, Xia Y, Cardarelli P, Oyasu M, Belcaid Z, et al. Combination Anti-CXCR4 and Anti-PD-1 Immunotherapy Provides Survival Benefit in Glioblastoma Through Immune Cell Modulation of Tumor Microenvironment. *J Neurooncol* (2019) 143(2):241–9. doi: 10.1007/s11060-019-03172-5
49. Jordan JT, Sun W, Hussain SF, Deangulo G, Prabhu SS, Heimberger AB. Preferential Migration of Regulatory T Cells Mediated by Glioma-Secreted Chemokines can be Blocked With Chemotherapy. *Cancer Immunol Immunother* (2008) 57(1):123–31. doi: 10.1007/s00262-007-0336-x
50. Vasco C, Canazza A, Rizzo A, Mossa A, Corsini E, Silvani A, et al. Circulating T Regulatory Cells Migration and Phenotype in Glioblastoma Patients: An *In Vitro* Study. *J Neurooncol* (2013) 115(3):353–63. doi: 10.1007/s11060-013-1236-x
51. Kara EE, McKenzie DR, Bastow CR, Gregor CE, Fenix KA, Ogunniyi AD, et al. CCR2 Defines *In Vivo* Development and Homing of IL-23-Driven GM-CSF-Producing Th17 Cells. *Nat Commun* (2015) 6(1):8644. doi: 10.1038/ncomms9644
52. Christensen JE. Efficient T-Cell Surveillance of the CNS Requires Expression of the CXC Chemokine Receptor 3. *J Neurosci* (2004) 24(20):4849–58. doi: 10.1523/JNEUROSCI.0123-04.2004
53. Klein RS, Lin E, Zhang B, Luster AD, Tollett J, Samuel MA, et al. Neuronal CXCL10 Directs CD8 + T-Cell Recruitment and Control of West Nile Virus Encephalitis. *J Virol* (2005) 79(17):11457–66. doi: 10.1128/JVI.79.17.11457-11466.2005
54. Liu C, Luo D, Reynolds BA, Meher G, Katritzky AR, Lu B, et al. Chemokine Receptor CXCR3 Promotes Growth of Glioma. *Carcinogenesis* (2011) 32 (2):129–37. doi: 10.1093/carcin/bgq224
55. Chow MT, Ozga AJ, Servis RL, Frederick DT, Lo JA, Fisher DE, et al. Intratumoral Activity of the CXCR3 Chemokine System Is Required for the Efficacy of Anti-PD-1 Therapy. *Immunity* (2019) 50(6):1498–512e5. doi: 10.1016/j.immuni.2019.04.010
56. Kimura T, Takeshima H, Nomiyama N, Nishi T, Kino T, Kochi M, et al. Expression of Lymphocyte-Specific Chemokines in Human Malignant Glioma: Essential Role of LARC in Cellular Immunity of Malignant Glioma. *Int J Oncol* (2002) 21:707–15. doi: 10.3892/ijo.21.4.707
57. Schwaeble WJ, Stover CM, Schall TJ, Dairaghi DJ, Trinder PKE, Linington C, et al. Neuronal Expression of Fractalkine in the Presence and Absence of Inflammation. *FEBS Lett* (1998) 439(3):203–7. doi: 10.1016/S0014-5793(98)01384-2
58. Liu C, Luo D, Streit WJ, Harrison JK. CX3CL1 and CX3CR1 in the GL261 Murine Model of Glioma: CX3CR1 Deficiency Does Not Impact Tumor

Growth or Infiltration of Microglia and Lymphocytes. *J Neuroimmunol* (2008) 198(1-2):98–105. doi: 10.1016/j.jneuroim.2008.04.016
59. Lohr J, Ratliff T, Huppertz A, Ge Y, Dictus C, Ahmadi R, et al. Effector T-Cell Infiltration Positively Impacts Survival of Glioblastoma Patients and Is Impaired by Tumor-Derived TGF-β. *Clin Cancer Res* (2011) 17(13):4296–308. doi: 10.1158/1078-0432.CCR-10-2557
60. Sasaki K, Zhu X, Vasquez C, Nishimura F, Dusak JE, Huang J, et al. Preferential Expression of Very Late Antigen-4 on Type 1 CTL Cells Plays a Critical Role in Trafficking Into Central Nervous System Tumors. *Cancer Res* (2007) 67(13):6451–8. doi: 10.1158/0008-5472.CAN-06-3280
61. Sandoval F, Terme M, Nizard M, Badoual C, Bureau MF, Freyburger L, et al. Mucosal Imprinting of Vaccine-Induced CD8+ T Cells Is Crucial to Inhibit the Growth of Mucosal Tumors. *Sci Transl Med* (2013) 5(172):172ra20. doi: 10.1126/scitranslmed.3004888
62. Melssen MM, Lindsay RS, Stasiak K, Rodriguez AB, Briegel AM, Cyranowski S, et al. Differential Expression of CD49a and CD49b Determines Localization and Function of Tumor-Infiltrating CD8+ T Cells. *Cancer Immunol Res* (2021) 9(5):583–97. doi: 10.1158/2326-6066.CIR-20-0427
63. Hauser MA, Kindinger I, Laufer JM, Späte A-K, Bucher D, Vanes SL, et al. Distinct CCR7 Glycosylation Pattern Shapes Receptor Signaling and Endocytosis to Modulate Chemotactic Responses. *J Leukoc Biol* (2016) 99 (6):993–1007. doi: 10.1189/jlb.2VMA0915-432RR

Conflict of Interest: The authors declare that the research was conducted in the absence of any commercial or financial relationships that could be construed as a potential conflict of interest.

Publisher's Note: All claims expressed in this article are solely those of the authors and do not necessarily represent those of their affiliated organizations, or those of the publisher, the editors and the reviewers. Any product that may be evaluated in this article, or claim that may be made by its manufacturer, is not guaranteed or endorsed by the publisher.

Copyright © 2022 Kollis, Ebert, Toubia, Bastow, Ormsby, Poonnoose, Lenin, Tea, Pitson, Gomez, Brown and Gargett. This is an open-access article distributed under the terms of the Creative Commons Attribution License (CC BY). The use, distribution or reproduction in other forums is permitted, provided the original author(s) and the copyright owner(s) are credited and that the original publication in this journal is cited, in accordance with accepted academic practice. No use, distribution or reproduction is permitted which does not comply with these terms.

frontiers | Frontiers in Immunology

ORIGINAL RESEARCH
published: 14 April 2022
doi: 10.3389/fimmu.2022.823910

Immune Gene Signatures and Immunotypes in Immune Microenvironment Are Associated With Glioma Prognose

Xiang-Xu Wang[1†], Haiyan Cao[2†], Yulong Zhai[2†], Shi-Zhou Deng[1], Min Chao[2], Yaqin Hu[2,3], Yueyang Mou[2,3], Shaochun Guo[2], Wenjian Zhao[2], Chen Li[2], Yang Jiao[2], Guolian Xue[2,3], Liying Han[2], Hong-Mei Zhang[1] and Liang Wang[2*]*

[1] Department of Clinical Oncology, Xijing Hospital, Fourth Military Medical University, Xi'an, China, [2] Department of Neurosurgery, Tangdu Hospital, Fourth Military Medical University, Xi'an, China, [3] College of Life Sciences, Northwest University, Xi'an, China

OPEN ACCESS

Edited by:
Quan Cheng,
Central South University, China

Reviewed by:
Ke Sai,
Sun Yat-sen University Cancer Center (SYSUCC), China
Mingzhu Zheng,
Southeast University, China

***Correspondence:**
Liang Wang
Drwangliang@126.com
Hong-Mei Zhang
zhm@fmmu.edu.cn

[†]These authors have contributed equally to this work

Specialty section:
This article was submitted to Cancer Immunity and Immunotherapy, a section of the journal Frontiers in Immunology

Received: *28 November 2021*
Accepted: *07 March 2022*
Published: *14 April 2022*

Citation:
Wang X-X, Cao H, Zhai Y, Deng S-Z, Chao M, Hu Y, Mou Y, Guo S, Zhao W, Li C, Jiao Y, Xue G, Han L, Zhang H-M and Wang L (2022) Immune Gene Signatures and Immunotypes in Immune Microenvironment Are Associated With Glioma Prognose. Front. Immunol. 13:823910. doi: 10.3389/fimmu.2022.823910

Glioma is the most common primary malignant brain tumor in adults with very poor prognosis. The limited new therapeutic strategies for glioma patients can be partially attributed to the complex tumor microenvironment. However, knowledge about the glioma immune microenvironment and the associated regulatory mechanisms is still lacking. In this study, we found that, different immune subtypes have a significant impact on patient survival. Glioma patients with a high immune response subtype had a shorter survival compared with patients with a low immune response subtype. Moreover, the number of B cell, T cell, NK cell, and in particular, the macrophage in the immune microenvironment of patients with a high immune response subtype were significantly enhanced. In addition, 132 genes were found to be related to glioma immunity. The functional analysis and verification of seven core genes showed that their expression levels were significantly correlated with the prognosis of glioma patients, and the results were consistent at tissue levels. These findings indicated that the glioma immune microenvironment was significantly correlated with the prognosis of glioma patients and multiple genes were involved in regulating the progression of glioma. The identified genes could be used to stratify glioma patients based on immune subgroup analysis, which may guide their clinical treatment regimen.

Keywords: glioma, immunotype, immune microenvironment, macrophages, immunotherapy

INTRODUCTION

Glioma is the most common malignant tumor of the central nervous system, belonging to the neuroepithelial group of tumors (1). According to the WHO classification guidelines for central nervous system tumors (2021 edition), gliomas are classified by IDH1/2 mutation and 1p/19q codeletion (2). At present, the treatment modes for glioma mainly include craniotomy and comprehensive therapeutics based on radiotherapy and chemotherapy. Even with such aggressive therapeutic strategy, the prognosis of gliomas remains unsatisfactory (3, 4). The dismal outcome

may be attributed to the complex heterogeneity of gliomas, their invasive growth, and the difficulties associated with complete resection for protecting important neurological functions. In addition, The presence of the blood-brain barrier, making it difficult for macromolecular drugs to pass through (5, 6). At present, immunotherapy has shown significant therapeutic advantages in treatment for several cancer types. However, recent results of the phase 3 clinical trial CheckMate-143 were disappointing. There was no significant difference in median overall survival between nivolumab *vs.* bevacizumab administration in patients with recurrent GBM (7–9).

It has been reported that the infiltration abundance and functional state of immune cells in the glioma immune microenvironment are special, which may be significantly related to the distinct prognosis of glioma patients (10). Janet V Cross etc. (11) showed that a highly inhibitory tumor immune microenvironment can promote tumor growth. However, a systematic and comprehensive classification for different immune types to guide the evaluation of prognosis and treatment response remains lacking. The immune microenvironment of glioma contains several different types of immune cells, including macrophages, microglial, myeloid suppressors, dendritic, B cells, T cells, and NK cells (12, 13). A subtype of tumor-associated macrophages in the tumor microenvironment can promote tumor metastasis and resistance to chemotherapy (14). The interaction between various immune cells and their effects on tumor cells constitute a complex functional system. The complexity of the glioma immune microenvironment is induced by both the microenvironment of the central nervous system and by tumor cells. Elucidating the immune characteristics of the glioma immune microenvironment would help design targeted strategies. In addition, studying the composition of the glioma immune microenvironment and identifying specific immune-related genes and immune cell types in the microenvironment associated with glioma prognosis would contribute to our understanding of the molecular mechanisms underlying glioma immunosuppression (15).

Here, by exploring transcriptome data in The Chinese Glioma Genome Atlas (CGGA) (http://cgga.org.cn) and The Cancer Genome Atlas (TCGA) (http://cancergenome.nih.gov) database, we discovered that the glioma subtype with a high immune response had a shorter survival time compared with patients with a low immune response subtype. We further analyzed the genes associated with immune typing, seven genes related to patient prognosis and their corresponding characteristics were investigated accordingly. We constructed a prognostic prediction model for glioma immunotherapy and the findings may provide valuable information for developing targeted immunotherapy for glioma patients. The differences in tumor immune microenvironment and related differential gene expression may provide new options for designing individualized treatment regimens and identifying new targets for immunotherapy for glioma patients.

MATERIALS AND METHODS

Glioma Datasets

Gene expression data and clinical information were retrospectively obtained from publicly available datasets in the CGGA (http://www.cgga.org.cn/) and TCGA databases (https://cancergenome.nih.gov/). A total of 1438 samples were enrolled in this analysis, including both the CGGA cohort (n=749) (**Table 1**) and TCGA cohort (n=689).

Immune-Subgroup Identification and Verification

To estimate the immune status of each sample, a total of 25 immune-related gene sets were manually selected from previously

TABLE 1 | Differences in clinical features among immune subtypes of glioma.

Variables	Overall n = 749	High n = 374	Low n = 375	p
Age [mean (SD)]	43.26 (12.23)	45.71 (13.84	40.81 (9.81)	<0.001
Risk_score [mean (SD)]	1.47 (1.30)	2.44 (1.20)	0.49 (0.19)	<0.001
OS_time [mean (SD)]	3.22 (2.88)	1.80 (1.88)	4.64 (3.00)	<0.001
Gender (%)				0.678
Male	442 (59.0)	224 (59.9)	218 (58.1)	
Female	307 (41.0)	150 (40.1)	157 (41.9)	
Grade (%)				<0.001
Grade II	218 (29.1)	38 (10.2)	180 (48.0)	
Grade III	240 (32.0)	90 (24.1)	150 (40.0)	
Grade IV	291 (38.9)	246 (65.8)	45 (12.0)	
IDH (%)				<0.001
Wildtype	339 (45.3)	282 (75.4)	57 (15.2)	
Mutation	410 (54.7)	92 (24.6)	318 (84.8)	
PRS_type (%)				<0.001
Primary	502 (67.0)	220 (58.8)	282 (75.2)	
Recurrent	222 (29.6)	134 (35.8)	88 (23.5)	
Secondary	25 (3.3)	20 (5.3)	5 (1.3)	
OS_status(%)				<0.001
Dead	456 (60.9)	314 (84.0)	142 (37.9)	
Alive	293 (39.1)	60 (16.0)	233 (62.1)	

published literature (16). We performed unsupervised clustering of glioma samples based on the ssGSEA scores for the 25 immune-related gene sets and identified three distinct immune subgroups. The ssGSEA score was calculated using the "GSVA" package in R. The "ConsensusClusterPlus" package was used to determine the number of stable clusters (17). The ESTIMATE algorithm [doi: 10.1038/ncomms3612] was used to analyze the Immune Score, Stromal Score, ESTIMATE Score, and tumor purity.

Gene Set Variation Analysis (GSVA) for KEGG Enrichment and Hallmark Pathways

Gene set variation analysis (GSVA) algorithm was used to investigate the variations in pathways among the different immune-subgroups using the 'GSVA' package (18). The "c2.cp.kegg.v6.2.symbols" and "h.all.v7.2.symbols" gene sets from Molecular Signatures Database (MSigDB) (http://www.gsea-msigdb.org) were downloaded and used for the GSVA analysis.

Comparisons of Fractions of Immune Cell Infiltrations

The deconvolution approach based on CIBERSORT (19) was used to estimate the abundances of 22 immune cell types based on their gene expression profiles and significant samples with an empirical CIBERSORT $P<0.05$ were selected for further comparison. We compared the fractions of 22 immune cell types among the three immune-subgroups using the Mann–Whitney U test.

Selection of Immune-Subgroup Related Genes (IRGs)

CGGA data were correspondingly divided into the immune-H, immune-M, and immune-L clusters. According to the set values of $P<0.05$ and $|\log2FC|>1$, we used the "limma" package to identify the differentially expressed genes (DEGs). The Venn diagram was drawn to identify overlapping IRGs from the above analyses. The DEGs among the IRGs in all three immune-subgroups were selected using the Venn diagram.

Construction of a Prognostic Model Based on the IRGs

We used lasso and multivariate analyses to select the significant prognostic IRGs. We calculated the regression coefficients and hazard ratios (HRs) for each gene. Finally, the relevant mRNAs were identified. The prognostic risk score model for glioma patients was a weighted sum of each optimal prognosis mRNA expression and the relative regression coefficient calculated using the multivariate model. The risk score formula was as follows:

$$Risk\ Score = \sum i\ \ Coef\ \ (mRNAi)\ \ *\ \ Exp(mRNAi)$$

All patients were divided into high- and low-risk groups based on the median risk score. The Kaplan–Meier survival curves of the two groups were plotted. ROC curves were plotted to evaluate the specificity and sensitivity of the model.

Western Blotting (WB)

We selected eight pairs of glioma tissues including the carcinoma and peritumoral tissues for WB. Tissues were lysed with the RIPA buffer (Pierce, Rockford). The protein concentration was measured using a BCA protein assay kit (Pierce, Rockford). Equal amounts of total protein were loaded on SDS-PAGE gel, transferred onto poly vinylidene fluoride (PVDF) membranes (Millipore, Bedford) and then immunoblotted with the primary antibodies (Listed in **Table 2**) for 24h at 4°C. After washing with TBST buffer, PVDF membranes were incubated with secondary horseradish peroxidase-conjugated goat anti-mouse or anti-rabbit antibody (TDY BIOTEC, Beijing, China) and detected using an enhanced chemiluminescence system (Thermo Scientific, Rockford, IL), according to the manufacturer's instructions. The expression of Actin was used as internal control.

Immunohistochemistry (IHC)

We selected 154 glioma chip tissues for IHC staining. The expressions of seven core genes and their relationships with patient survival were analyzed. For IHC, the experiments were performed as described previously (20). Antibodies used in the IHC staining are listed in **Table 2**. The IHC score of target proteins was independently evaluated by two pathologists according to the proportion and intensity of positive cells within five microscopic visual fields per slide (200-fold magnification) (21). A proportion score represented the estimated proportion of positively stained tumor cells and the intensity score represented the average intensity of the positive tumor cells. The proportion and intensity scores were then multiplied to obtain a total score, which ranged from 0 to 16. A total score of 0-2, 3-7, 8-12, 13-16 was defined as being negative (-), weak positive (+), moderate positive (++), and strong positive (+++), respectively (21).

TABLE 2 | Primary antibodies used for western blot and immunohistochemistry.

Antibody	Company (Cat. No.)	Working Dilutions
SVOP	HUAAN (ER65055)	WB: 1/1000 IHC: 1/400
TNR	proteintech (19730-1-AP)	WB: 1/1000 IHC: 1/400
VAMP5	proteintech (11822-1-AP)	WB: 1/1000 IHC: 1/400
IGFBP2	BIOSS (bs-1108R)	WB: 1/1000 IHC: 1/400
TAGLN2	Santa (sc-373928)	WB: 1/1000 IHC: 1/400
METTL7B	Abclonal (A7200)	WB: 1/1000 IHC: 1/400
VIM	BIOSS (bs-8533R)	WB: 1/1000 IHC: 1/400

Flow Cytometry

We selected fresh tissues from glioma patients with grade II, III and IV. The tissues were cleaned with PBS and were cut into pieces with ophthalmic scissors. Then the tissues were collected into a 15ml centrifuge tube with 7ml PBS, then 1ml collagenase I was added into the centrifuge tube. Single cell suspension was collected with 700 mesh cell sieves. After washing by PBS, fluorescent antibodies CD3, CD4, CD8, CD11, CD16 and CD22 (listed in **Table 3**, purchased from Thermo Fisher Scientific) were added to cell suspension at a ratio of 1:20. After incubation at 4°C for 1h, they were cleaned by PBS for 3 times. The cell precipitates were resected with 500ul PBS and detected by flow cytometry.

RESULTS

Identification of Three Immune-Subgroups Based on 25 Immune-Related Gene Sets

Using the CGGA cohort, first, we performed an unsupervised clustering analysis and identified three distinct immune-subgroup patterns based on the ssGSEA scores of 25 immune-related gene sets (**Figures 1A**, **S1A–E**). The three immune-subgroups were correspondingly termed as the immune-H (high) (n = 226), immune-M (media) (n = 185), and immune-L (low) (n=338). The immune-H subgroup had the highest values of ESTIMATE Score, Immune Score, and Stromal Score; it was also associated with the lowest tumor purity (**Figures 1B–E**). Notably, these results indicated that the immune-H subgroup consisted of the highest number of immune cells and stromal cells, while the immune-L subgroup consisted of the highest number of tumor cells; these values in the immune-M subgroup were between in those for the immune-H and immune-L subgroups. Moreover, the 3D-PCA plot showed that the immune subtypes were also distinctly divided into three clusters, namely the immune-H, immune-M, and immune-L, which suggested that our method could well distinguish among the three immune-subgroups (**Figure 1F**). Patients in the immune-L subgroup showed better overall survival, while those in the immune-H subgroup exhibited the worst prognosis (**Figure 1G**) (log-rank test, $P < 0.001$).

Association Analysis and Risk Score Comparison of Clinical Features of Glioma

To explore the correlation between immune subtypes and clinical characteristics, we drew an alluvial diagram for immune-subgroups with different risk-subgroups, IDH status, grade stages, PRS types, and survival status (**Figure 2A**). The results indicated that the immune-H subgroup with the higher risk score was most likely related to IDH wild type, higher grades, recurrence status, and death. Whereas the immune-L subgroup exhibited a lower risk score, IDH mutation, lower grade, primary status, and better survival status. The correlation results are specifically shown in **Figures S2A–F** and **S3A–F**. Statistical analysis of the clinical data showed that higher risk scores were more likely associated with older age, higher recurrence, IDH wild type, higher immune subtype, and poorer prognosis ($P<0.001$), while there were no significant differences between gender (**Figures 2B–G**). At the same time, we divided gliomas into low grade and high grade groups to analyze the relationship between different immune subtypes and patient prognosis. We found that high immune subtypes were significantly correlated with poor prognosis of patients with low grade (Left) and high grade (Right) glioma patients (**Figure S2G**).

TABLE 3 | Primary antibodies used for Flow cytometry.

Antibody	Company (Cat. No.)	Working Dilutions
CD3-FITC	eBioscience (11-0037-42)	FCM: 1/20
CD4-PE	eBioscience (12-0049-42)	FCM: 1/20
CD8-PE	eBioscience (12-0088-42)	FCM: 1/20
CD11-PE	eBioscience (CD11B04-4)	FCM: 1/20
CD16-FITC	eBioscience (11-0168-42)	FCM: 1/20
CD22-PE	eBioscience (12-0029-41)	FCM: 1/20

Enriched Molecular Pathways and Immune Cell Infiltration Among Three Immune-Subgroups of Glioma

To examine the molecular mechanisms of action in different subtypes, we performed the gene set variation analysis (GSVA) to evaluate the enriched pathways in the KEGG and hallmark gene sets. **Figures 3A, B** shows the differentially enriched pathways from the KEGG database and hallmark gene sets between the immune-H and immune-L subgroups. Enriched pathways in the immune-H subgroup mainly comprised immune-related pathways, including systemic lupus erythematosus, inflammation, and antigen processing and presentation. Similar results were obtained in immune-H vs immune-M and immune-M vs immune-L subgroup analyses (**Figures S4A–D**).

Moreover, we investigated whether the three immune-subgroups of glioma had different tumor immune microenvironments (TIME) (**Figure 3C**). Indeed, the immune-H subgroup had high infiltration levels of regulatory T cells (Tregs), M2 macrophages, and neutrophils, while the immune-L subgroup had remarkable enrichment of resting mast cells. Furthermore, we found a significant increase of CD3, CD4, CD8, CD16, CD11, CD22 positive immune cell infiltrates in grade IV glioma tissues compared with grade II and III (**Figures 4A, B**). These results indicated that the gliomas in the immune-H subgroup and grade IV glioma group were dominated by infiltration of suppressive immune cell types.

To test the expression of immune-related genes in each group, we examined the expression of HLA and the immune checkpoint genes in the three immune subgroups. Notably, the expressions of all the HLA genes were highest in the immune-H subgroup, while lowest in the immune-L subgroup (ANOVA test, $P < 0.001$) (**Figure S5A**). Further analysis of immune checkpoints showed that multiple inhibitory checkpoints (CD274, CTLA4, HAVCR2, LAG3, PDCD1LG2, TIGIT) were significantly overexpressed in high immune subtypes (**Figure S5B**). These results showed that the immune-subgroups were significantly associated with the expressions of immune-related genes.

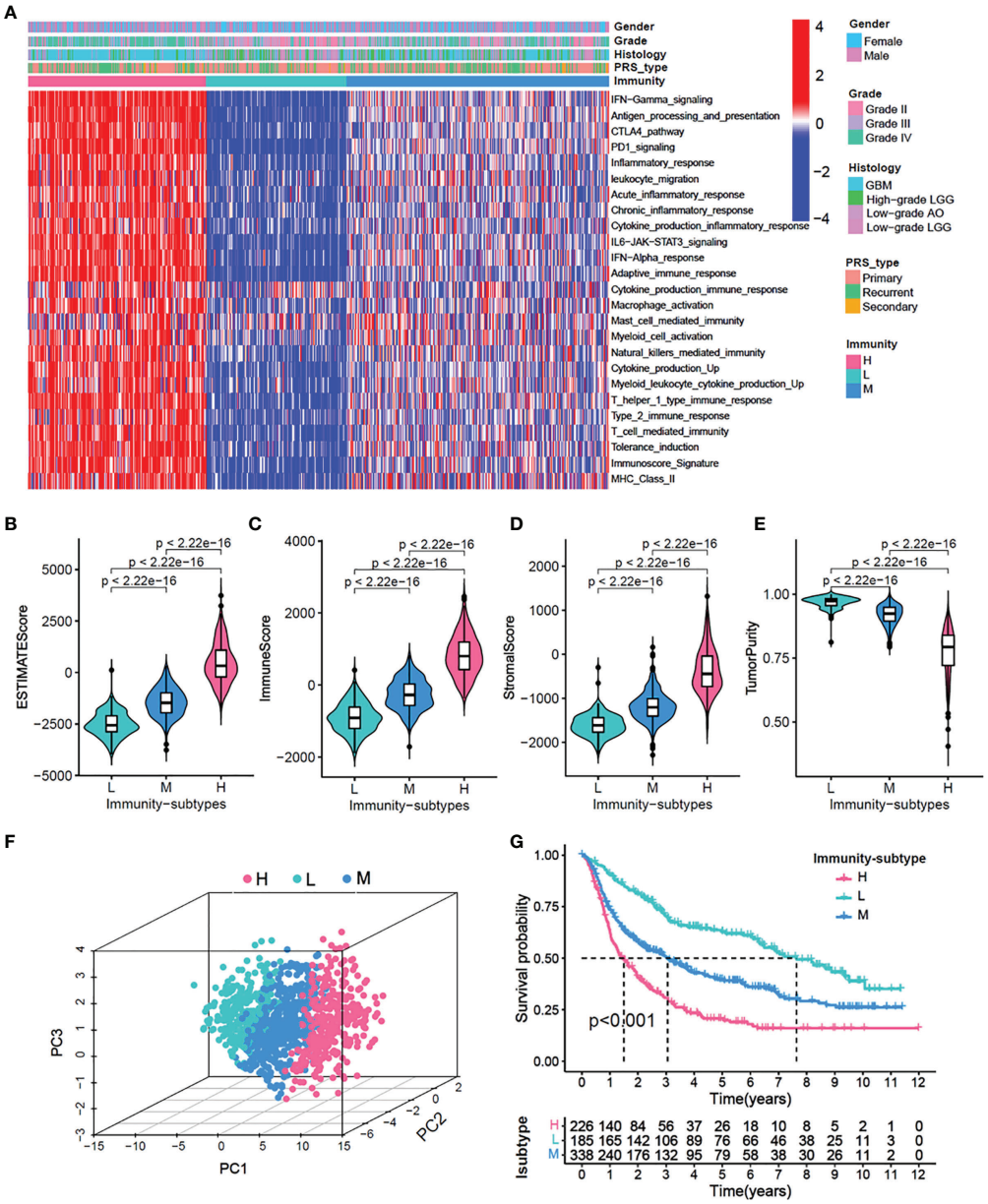

FIGURE 1 | Identification of three immunity-subgroups base on 25 immunity-related gene sets. **(A)** The heatmap showing the glioma samples divided into three distinct sub-group based on the GSVA enrichment scores of 25 immunity-related gene sets. Three subgroups defined as immunity-H, immunity-M and immunity-L. Color bars at the top of the graph labels, the gender, grade, histology, PRS type. **(B–E)** Comparison of stromal scores **(B)**, immune scores **(C)**, estimated scores **(D)**, tumor purity **(E)** among three immunity-subgroups. **(F)** PCA analyses for three immunity-subgroups depicted by the dot in different colors. immunity-H, pink, immunity-M, blue; immunity-L, aquamarine. **(G)** OS Kaplan-Meier survival analysis among three immunity-subgroups (Log-rank test).

Differential Gene Expression Analysis Among Three Immune-Subgroups

We identified a total of 1937 DEGs ($|\log_2 FC| > 1$ and FDR < 0.05) between the immune-H and immune-L subgroups and the volcano plot was used to show the distribution of the DEGs between the two subgroups (**Figure 5A**). Specifically, 1262 DEGs in immune-H vs immune-L, 532 DEGs in immune-H vs immune-M, 11 DEGs in immune-M vs immune-L, and 132 DEGs in immune-H vs immune-M vs immune-L were obtained (**Figure 5B**). As shown in **Figure 5C**, the heatmap displays 132 DEGs among the three groups. The GSEA for GO enrichment showed that the immune-H subgroup was highly enriched in genes associated with the immune-related pathways (**Figure 5D**), including immunoglobulin complex, immunoglobulin receptor binding, complement activation, T cell receptor complex, and immune response-regulating cell surface receptor signaling

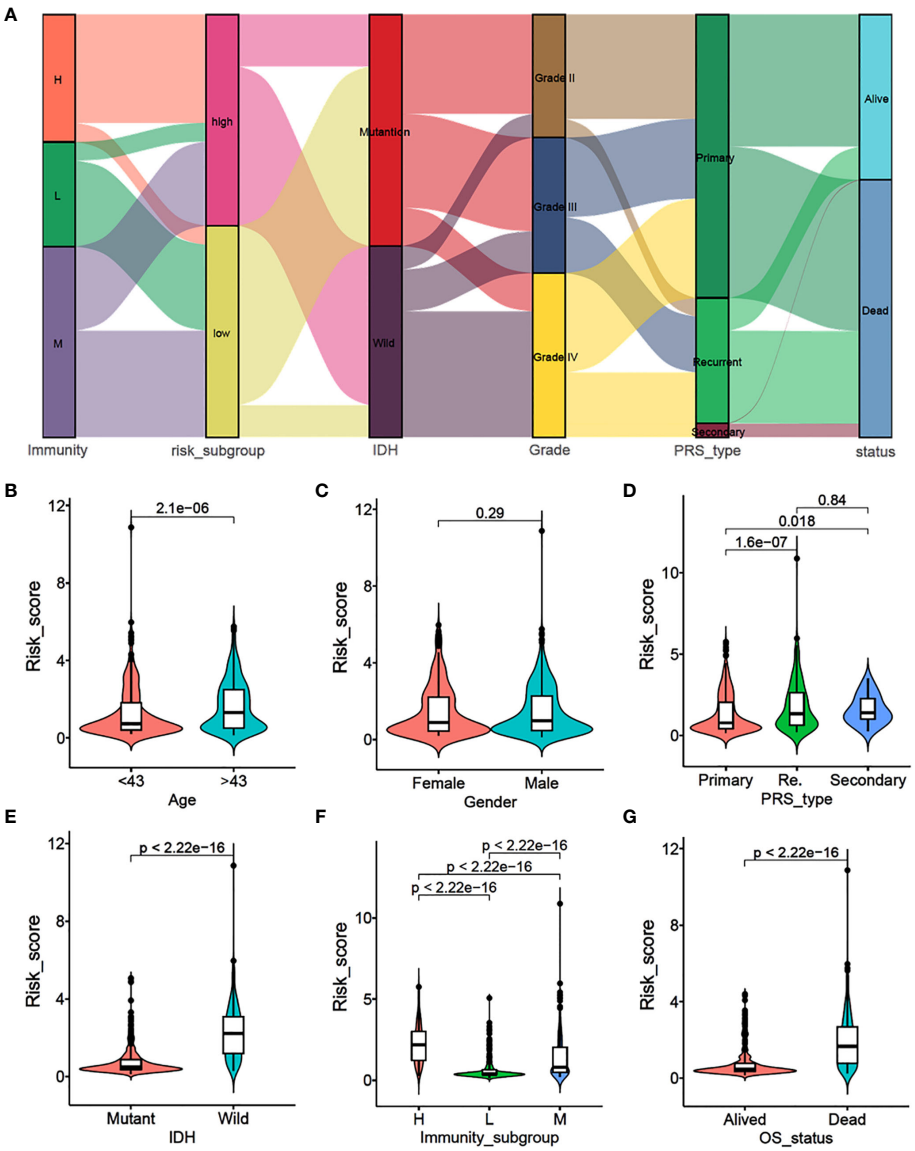

FIGURE 2 | Association analysis and risk score comparison of clinical features of glioma. **(A)** Alluvial diagram of immunity-sub-groups with different risk-subgroups, IDH status, grade stages, PRS types and survival status. **(B–G)** The risk score comparison between different clinical features. **(B)** Age, **(C)** Gender, **(D)** PRS type, **(E)** IDH status, **(F)** immunity-subgroup and **(G)** survival status.

pathway involved in phagocytosis. This result was in line with elevated immune activity in the immune-H group.

Construction of the Prognostic Model Based on Glioma Immunophenotyping

In the CGGA cohort, 14 of 132 DEGs were identified and selected through the lasso-Cox regression algorithm (**Figures 6A, B**). Finally, a total of seven prognostic-related hub genes were identified by multivariate Cox regression analysis, and the risk scores were calculated to predict the prognostic risk of glioma (**Figures 6C–F**). The multivariate Cox forest plot showed the hazard ratios of SVOP, TNR, VAMP5, IGFBP2, METTL7B, VIM, and TAGLN2. The risk score was calculated using the following formula: risk score $= \sum_i^n coef_i * mRNA_i$, where i, represents the expressions of the seven hub genes. The risk score, survival status, and the expressions of the seven hub genes were calculated using the prognostic model and the process is illustrated in **Figures 6D–F**. Samples were classified into low- and high-risk subgroups according to the median risk score. Survival analysis indicated that patients in the low-risk subgroup had significantly longer overall survival time as compared to that of the high-risk patients (**Figure 6G**, $P < 0.001$, log-rank test). ROC curve analysis showed that the

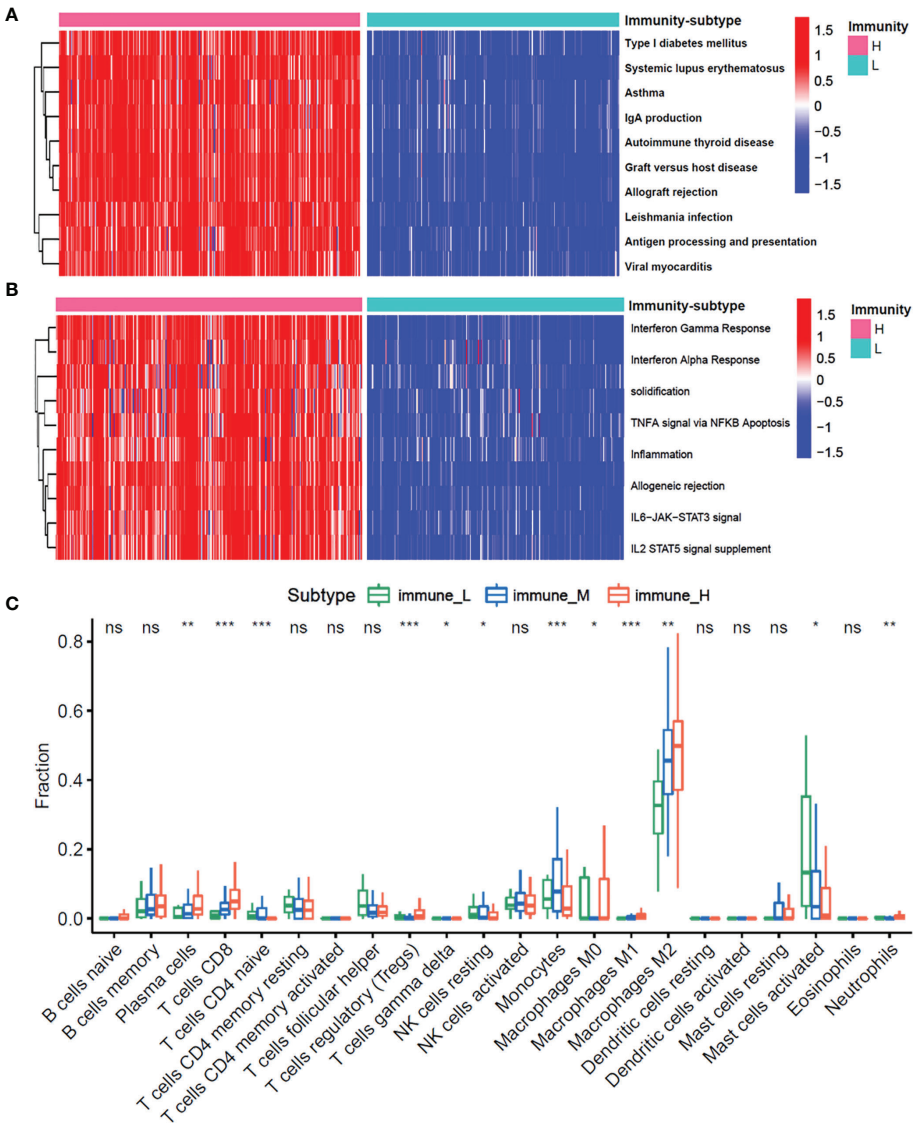

FIGURE 3 | The enrichment molecular pathways and immune cells infiltration among three immunity-subgroups of glioma. **(A, B)** Heatmap shows the GSVA score of top 10 KEGG pathways **(A)** and 50 hallmarks pathways **(B)** curated from MSigDB between immunity-H and immunity-L subtypes. **(C)** The abundance of each 22 types of infiltrating cell in three immunity-subtypes. *P≤0.05, **P≤0.01, ***P≤0.001. ns, no significance.

specificity and sensitivity were highest when the risk scores were 0.782, 0.843, 0.852, and 0.857 according to the 1-, 2-, 3-, and 5-year survival-based area under the receiver operating characteristic curve (AUC) values, respectively (**Figure 6H**).

Univariate Cox and K-M Survival Analysis of the Seven Hub Genes in CGGA and TCGA Cohorts

The results of univariate Cox regression analysis of the seven prognostic-related genes are shown in **Figure 7A** in CGGA cohort. Among them, SVOP and TNR were determined as the protective factors with HR values<1, whereas the remaining five genes, VAMP5, IGFBP2, METTL7B, VIM, and TAGLN2 were determined as the risk factors with hazard ratio (HR) values >1. According to the optimal cutoff value, a total of 749 samples were divided into two groups according to the expression levels of the seven genes. Survival analysis indicated that patients with high expression of SVOP or TNR had significantly longer overall survival than those with low expression of SVOP/TNR (**Figures 7B, C**), while the results of VAMP5, IGFBP2, METTL7B, VIM, and TAGLN2 showed opposite trends (**Figures 7D–H**). Similar results were obtained in TCGA cohort (**Figures S4A–H**).

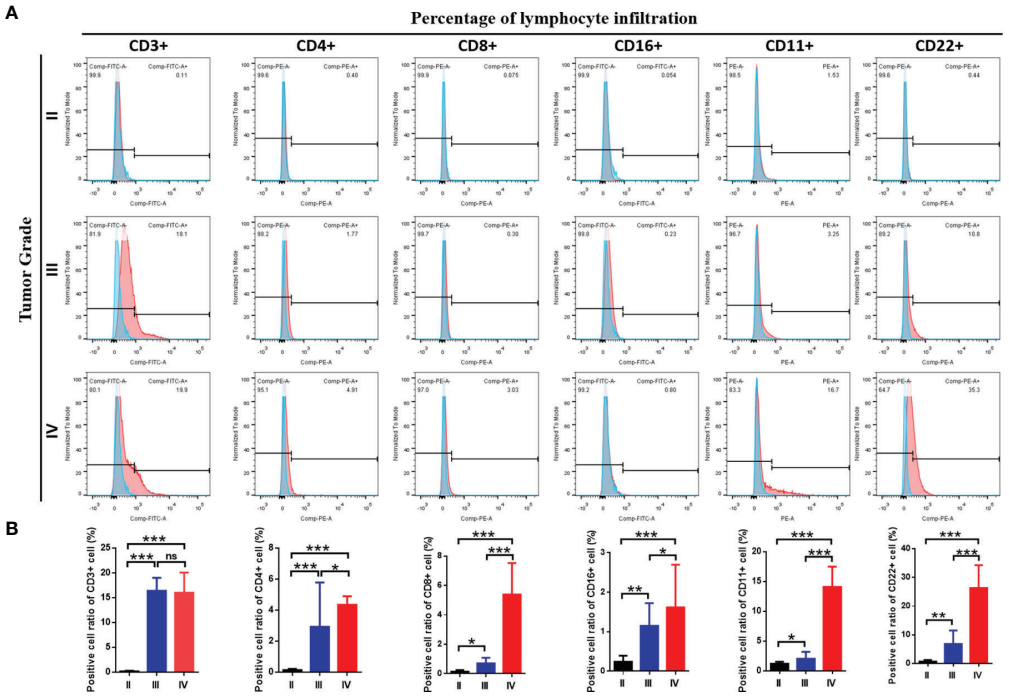

FIGURE 4 | The immune cells infiltration among three grades of glioma. **(A)** Flow cytometry results showed the abundance of each 6 types of infiltrating cell in three grades and **(B)** the results of statistical analysis showed the proportion of cell infiltration.*P≤0.05, **P≤0.01, ***P≤0.001. ns, no significance.

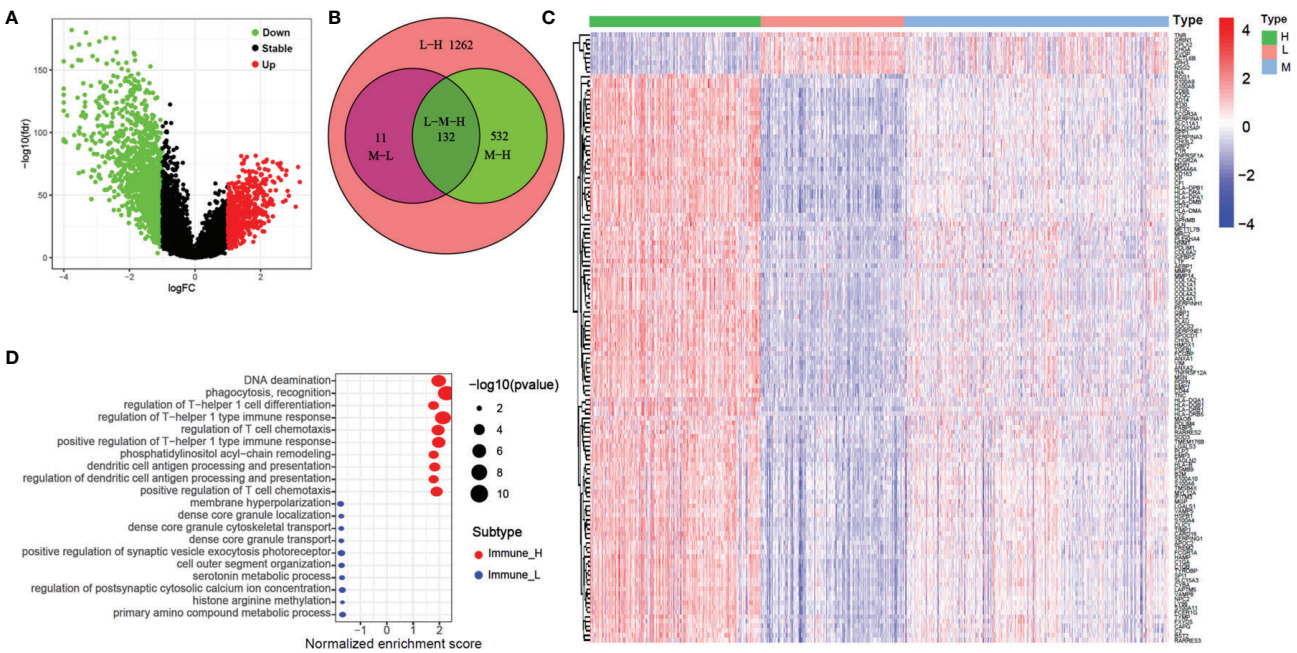

FIGURE 5 | Volcano plot, heatmap and GO enrichment analysis of differential gene among three glioma immune subtype. **(A)** The volcano plot of different genes between immunity-H and immunity-L subtype. **(B)** The Venn plot showed the different genes among three glioma immune subtype. **(C)** The heatmap shown that the different genes among three glioma immune subtype. **(D)** GO enrichment analysis of differential gene among between immunity-H and immunity-L subtypes.

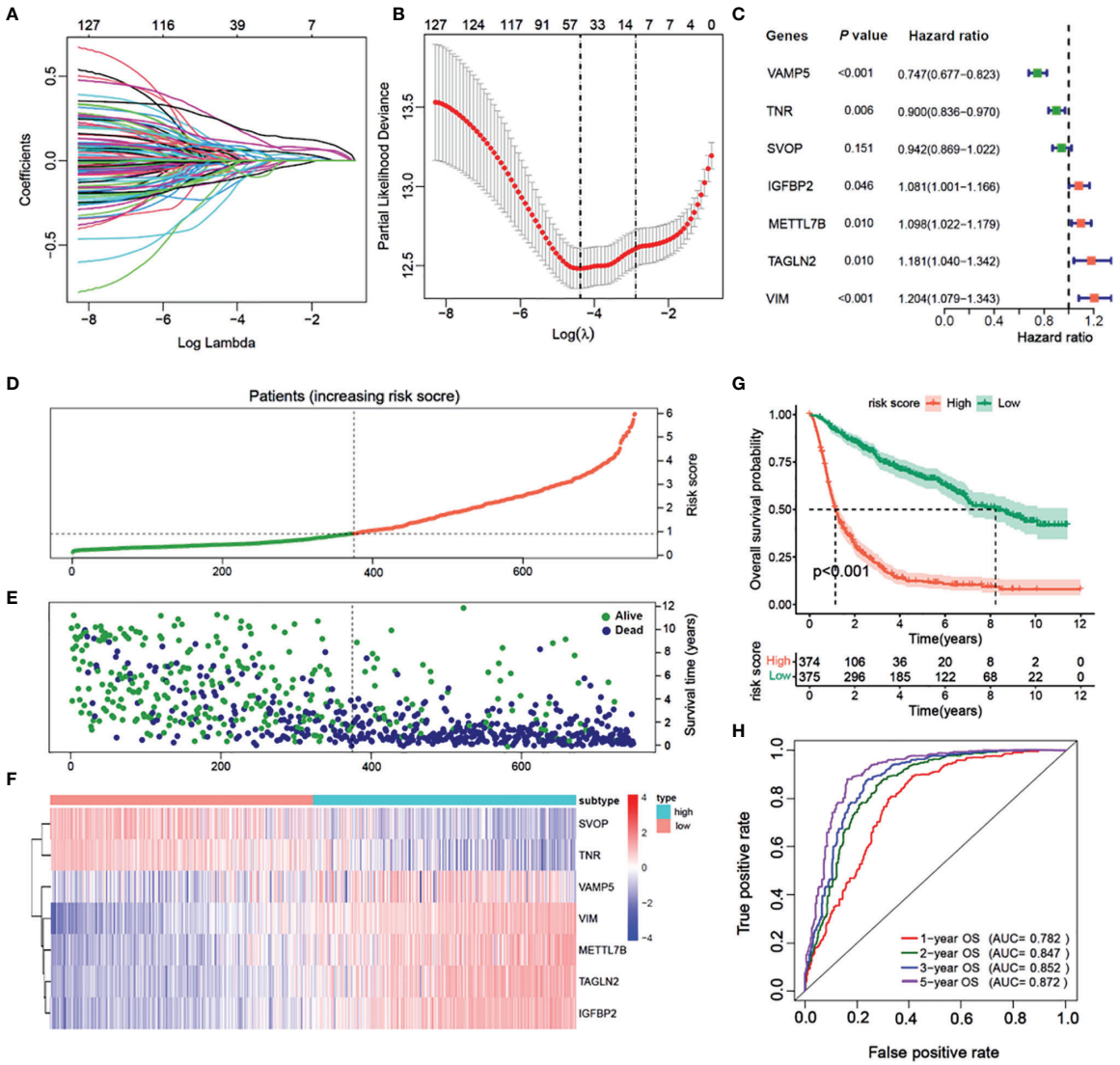

FIGURE 6 | Construction of a prognostic model based on differential genes of immune subtypes. **(A)** The LASSO coefficients profile of the 132 significate genes selected for overall survival against the log lambda sequence. **(B)** Ten-fold cross-validated error (first vertical line equals the minimum error, whereas the second vertical line shows the cross-validated error within 1 standard error of the minimum). **(C)** Forest plot of 7 immunity-subtype-related genes identified by multivariate Cox regression. **(D)** Glioma patients are sorted by risk score, red is high risk, green is low risk. **(E)** The survival status of Glioma patients, dark blue is dead, light green is alive. **(F)** The heatmap of the 7-hub gene expression. **(G)** Kaplan–Meier curve survival analysis between high risk and low risk, red line means high risk group, blue line means low risk group; **(H)** Time–ROC curve analysis of the 7 hub genes signature, red line means 1-year OS, green line means 2-year OS, blue line means 3-year DFS, purple line means 3-year DFS.

Furthermore, we compared the expressions of the seven hub genes among GBM, LGG, and normal tissues. The expression of SVOP was upregulated in the normal tissue than in the GBM (GBM < LGG < normal tissues) (**Figures S7A**). The expressions of VAMP5, IGFBP2, METTL7B, VIM, and TAGLN2 were lower in normal tissue than in GBM (GBM > LGG > normal tissues) (**Figures S7C–G**), while the expressions of TNR in LGG was the highest as compared to both the groups (**Figures S7B**). Subsequently, the glioma patients were divided into low grade and high grade in CCGA and TCGA databases respectively, and the relationships between seven core genes and prognosis of patients were analyzed (**Figures S8A–D**). The results were basically consistent with **Figures 6** and **S7**.

The Seven Hub Genes Are Significantly Related to Immune Cell Infiltration and T-Cell Inflammation-Associated GEP

To examine the correlation between the seven prognostic-related genes and immune cell infiltrations, the relative abundances of 22 types of infiltrating immune cells in

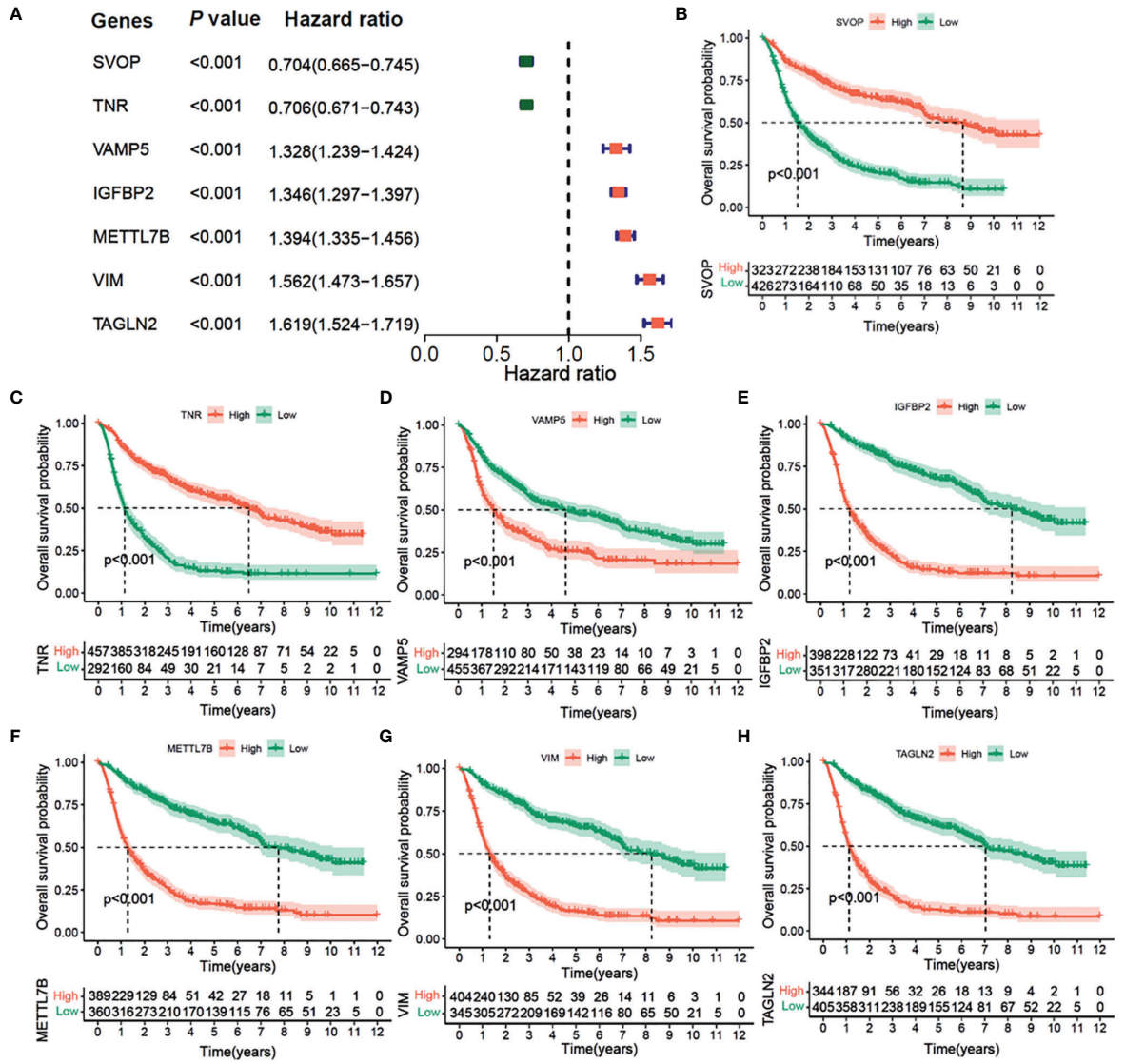

FIGURE 7 | Univariate Cox Forest plot and Kaplan–Meier survival analysis of 7 hub genes in CGGA cohort. **(A)** Univariate Cox Forest plot of 7 immunity-subtype-related genes. **(B)** Kaplan–Meier curve survival analysis of 7 hub genes, **(B)** SVOP, **(C)** TNR, **(D)** VAMP5, **(E)** IGFBP2, **(F)** METTL7N, **(G)** VIM, **(H)** TAGLN2.

gliomas were quantified using CIBERSORT (**Figure 8A**). The SVOP and TNR expression had a negative correlation with regulatory T cells (Tregs), M2 macrophages, and neutrophils, while the risk scores based on VAMP5, IGFBP2, METTL7B, VIM, TAGLN2 were significantly positively correlated with these immunosuppressive cell types.

Furthermore, we explored the correlation between the seven hub genes and T-cell inflammation-associated gene expression profile (GEP) (16). The results showed that the SVOP and TNR expressions were negatively associated with T-cell inflammation GEP, while VAMP5, IGFBP2, METTL7B, VIM, TAGLN2 were significantly positively associated with T-cell inflammation-related GEP (**Figure 8B**). These results confirmed that the seven hub genes were significantly related to the immune response and may be potential markers for predicting immunotherapeutic responses.

Functional Validation of the Seven Hub Genes in Clinical Specimens

We verified the expression of seven core molecules at the tissue levels, and the results showed that the expression of five molecules (VAMP, SVOP, Transgelin2, VIM, METTL7B) in glioma tissues was significantly higher than that in adjacent tissues, while the expression of TNR was on the contrary, and IGFBP2 had no significant significance (**Figure 9A**).

We further validated the protein expression levels of these genes in clinical specimens. A total of 154 glioma samples were divided into high-expression (n=77) and low-expression (n=77) groups according

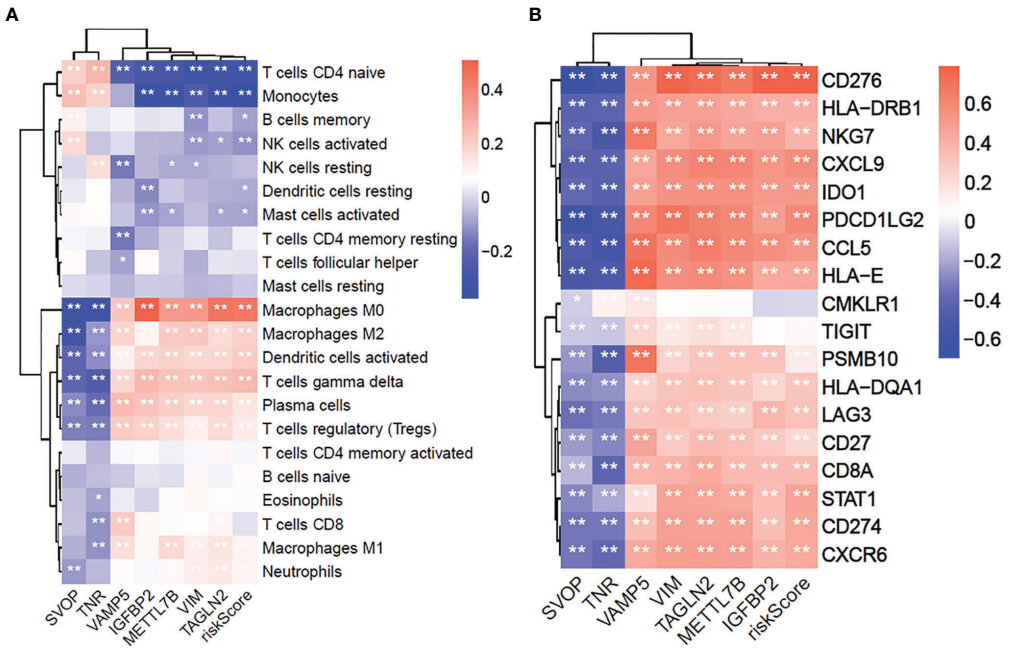

FIGURE 8 | The 7 core prognostic genes of glioma are significantly related to immune cells infiltration and GEP genes. **(A)** The correlation between 7 prognostic hub genes and 22 immune cells infiltration. **(B)** The correlation between 7 prognostic hub genes and 18 GEP expression. *P≤0.05, **P≤0.01.

to the IHC scores for the seven genes. Five of these seven genes were significantly related to the survival of glioma patients and one among them did not show statistical significance (**Figures 9B–H**). However, the expression and prognosis of SVOP were contrary to the results from the database analysis. Further investigation of the function and mechanism of these molecules is needed.

DISCUSSION

The WHO classification guidelines for central nervous system tumors (2021 Edition) classify several tumors with specific molecular changes into unique subgroups. This is of great significance to obtain different prognostic results and can guide the formulation of individualized treatment strategies (2). With the deepened understanding of the immune system, several immunotherapeutic agents have been tested in clinical trials, but most of them ended in failure. One of the underlying reasons is that these clinical trials did not fully consider the characteristics of the patients' tumor immune microenvironment and failed to distinguish and identify suitable enrolled patients (8). The tumor immune microenvironment is extremely complex, which not only includes a large number of highly heterogeneous tumor cells, but also different types of immune cells and states such as exhaustion and decrepit, thereby leading to mixed effects in immunotherapeutic responses. The current understanding of the glioma immune microenvironment is insufficient to guide clinical practice.

Immunotherapy has revolutionized tumor therapy. In this therapeutic strategy, the drugs can penetrate the blood-brain barrier for the treatment of glioma (22). However, many clinical trials for immunotherapy have not shown favorable results (8, 9). The main reason may be attributed to the complex tumor immune microenvironment, leading to significant heterogeneity in the tumor microenvironment of different patients; thus, the individualized treatment was not easy to achieve (23, 24). Given this, we screened the genetic data in CGGA and TCGA databases and explored the data in the perspective of glioma immune microenvironment classification. A total of seven immune genes related to glioma prognosis were identified and protein expression verification based on pathological tissue samples was performed. In this study, we divided the glioma patients in CGGA and TCGA cohort into three immune subtypes according to their GSVA enrichment scores. The immune-H subtype was significantly correlated with the poor prognosis in all glioma patients. This suggested that our immune-typing may have direct significance for immunotherapy of glioma patients.

Although glioma immunotherapy has been unfavorable, studies on the glioma immune microenvironment have attracted great attention. Previous studies based on single-cell sequencing show significant heterogeneity in tumors (25, 26). This is also one of the possible reasons for the complexity of the tumor immune microenvironment. Therefore, it is important to examine the underlying molecular mechanisms for different immune subtypes in different tumor types. In this study, we queried the KEGG and hallmarks pathways and found that differentially enriched pathways showing significant differences between the immune-H and immune-L subtypes were mainly related to the regulation of the immune microenvironment in

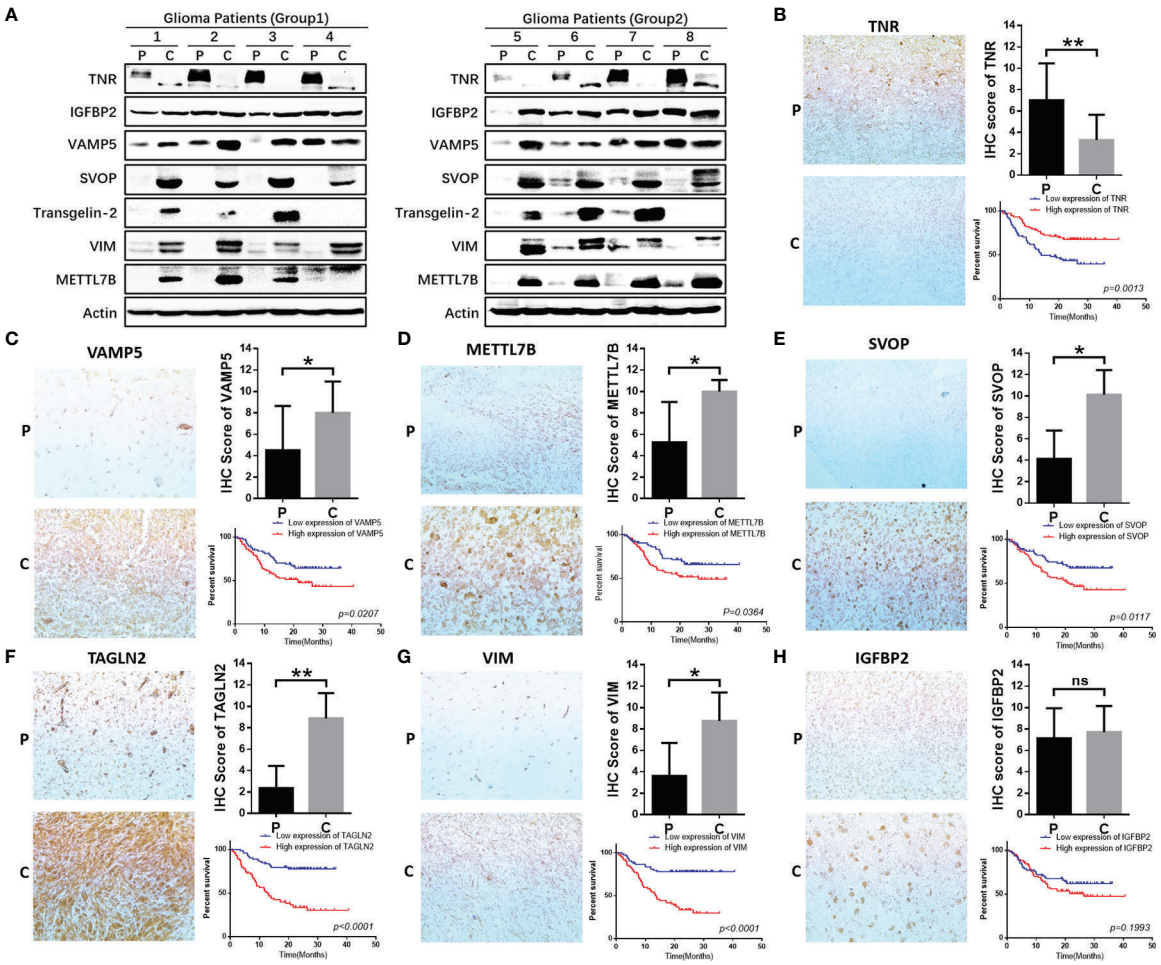

FIGURE 9 | Functional validation of 7 hub genes in clinical specimens. **(A)** WB assay was used to detect the expression differences of 7 core genes in glioma tissues and adjacent tissues. **(B–H)** Immunohistochemical staining and statistical analysis of tumor and adjacent tissues in patients with glioma, and Kaplan-Meier curve analysis of overall survival in glioma patients by the expression of 7 core genes. Death/total number of patients in each subgroup were presented. (P, paracancerous; C, cancer). *P≤0.05, **P≤0.01, ***P≤0.001. ns, no significance.

glioma. In the immune-H subtype, the immune cells showed higher infiltration than those in the immune-M and immune-L subtypes. Furthermore, 132 genes with significant differential expression were screened by GO enrichment and were found to be mainly enriched in immune-related pathways. Seven immune-related core genes were further screened by LASSO regression analysis and the correlation with the prognostic risk of patients was found to be significant. Through prognostic analysis, these seven genes were found to be significantly correlated with the prognosis of glioma patients and the high-risk score subgroup was significantly correlated with the poor prognosis of these patients. Thus, these identified genes may be potential new targets for immunotherapy for glioma patients and may be of great importance for screening and identifying patients who could benefit from immunotherapy.

Search for new immunotherapeutic strategies is critical to overcoming the obstacles in glioma immunotherapy, however, the molecular markers identified in many previous studies couldn't be transformed for clinical applicability (27). At present, there were few reports on the 7 molecules we screened, the mechanism involved with tumor immune microenvironment is not clear. Bo-Ra Na have shown that TAGLN 2 is the only molecule in TAGLN family that is related to immune cells and participated in the regulation of immune cell activity (28). Hye-Ran Kim have shown that TAGLN2 could participate in lipopolysaccharide induced macrophage activation through NF KB pathway (29). Through database analysis, some scholars found that mettl7b was highly expressed in gliomas and were associated with poor prognosis, but its specific molecular mechanism was not clear (30). Ting Li have pointed out that IGFBP2 can regulate PD-L1 expression by activating EGFR-STAT3 signaling pathway in melanoma and participate in tumor immunotherapy resistance, but its specific mechanism needs to be further studied (31). However, the mechanism of other molecules in the regulation of tumor immune microenvironment have not been reported.

In our study, the expression of seven core genes in tumor and para tumor tissues was verified by immunohistochemistry and western blotting. The results showed that the expressions of five genes (TNR, VAMP5, METTL7B, TAGLN2, VIM) were high and consistent with the findings from the CGGA and TCGA databases. However, the expression and prognostic prediction for SVOP were contrary to the database findings and there were no significant differences in the expression and prognosis of IGFBP2.

Through analyzing the TCGA-GBM and CGGA-GBM data, the results of SVOP molecules in different databases are quite opposite, and our validation data correlated with that in TCGA database. We believe that the possible reasons include that there are still defects in the current understanding of molecular typing of glioma patients, and the possible effects of IDH, P53, 1P/19Q, PTEN, TERT promoter methylation status and MGMT promoter methylation status on the prognosis of patients are not fully considered in the analysis. According to the report of Prof. Zhao et al. (32), in TCGA database, SVOP is related to hypermethylation status and prognosis in patients with GBM, which may be one of the reasons for inconsistent conclusions, but the internal mechanism has not been reported. SVOP and IGFBP2 may play different functions in different grades of gliomas and follow-up studies in these contexts are in progress.

In conclusion, we analyzed the CGGA and TCGA databases for immune functions, grouped glioma patients, and investigated the specificity and complexity of the glioma immune microenvironment. The identified seven core genes may provide potential targets for glioma immunotherapy and were significantly related to the prognosis of glioma patients. These results emphasize the importance of tumor immunotyping in the development of glioma. Therefore, targeting the related molecules for immunoassay is expected to become a feasible treatment strategy in combined immunotherapy.

DATA AVAILABILITY STATEMENT

Publicly available datasets were analyzed in this study. This data can be found here: CGGA databases: http://www.cgga.org.cn/; TCGA databases: https://cancergenome.nih.gov/.

ETHICS STATEMENT

The studies involving human participants were reviewed and approved by IEC of Institution for National Drug Clinical Trials, Tangdu Hospital, Fourth Military Medical University. Written informed consent to participate in this study was provided by the participants' legal guardian/next of kin.

AUTHOR CONTRIBUTIONS

X-XW, HC, and YZ designed research, analyzed and interpreted data, and wrote the manuscript. S-ZD, MC, YH, YM, and SG performed research and collected, analyzed, and interpreted data. WZ, CL, and YJ collected data, performed IHC, data analysis and manuscript preparation. X-XW performed bioinformatics, data analysis and manuscript preparation. GX and LH performed research. H-MZ and LW designed research, guided experiment and wrote the manuscript. Author order reflects the relative size and importance of the contributions to the project and manuscript. All authors contributed to the article and approved the submitted version.

FUNDING

This work was supported by the National Natural Science Foundation of China (nos. 81802772, 81772661), the Natural Science Foundation of Shaanxi Province (nos. 2020JZ-30, 2021JZ-35), Clinical Study of Toripalimab with Anlotinib for Patients with Recurrent Glioblastoma (nos. ChiCTR2000039175), Talent Project of Tangdu Hospital, The Fourth Military Medical University (nos. 2021ZTXM016, 2021ZTXM007, 2021SHRC021, 2021SHRC020, 2021SHRC033, 2021SHRC001).

SUPPLEMENTARY MATERIAL

The Supplementary Material for this article can be found online at: https://www.frontiersin.org/articles/10.3389/fimmu.2022.823910/full#supplementary-material

REFERENCES

1. Ilkhanizadeh S, Lau J, Huang M, Foster DJ, Wong R, Frantz A, et al. Glial Progenitors as Targets for Transformation in Glioma. *Adv Cancer Res* (2014) 121:1–65. doi: 10.1016/B978-0-12-800249-0.00001-9
2. Yuan L, Shen J, Chen Z. Catalytic Ozonation of P-Chloronitrobenzene Over Pumice-Supported Zinc Oxyhydroxide. *Water Sci Technol* (2013) 68 (8):1895–900. doi: 10.2166/wst.2013.449
3. Stupp R, Brada M, van den Bent MJ, Tonn JC, Pentheroudakis G. High-Grade Glioma: ESMO Clinical Practice Guidelines for Diagnosis, Treatment and Follow-Up. *Ann Oncol* (2014) 25(Suppl 3):iii93–101. doi: 10.1093/annonc/mdu050
4. Tan AC, Ashley DM, Lopez GY, Malinzak M, Friedman HS, Khasraw M. Management of Glioblastoma: State of the Art and Future Directions. *CA Cancer J Clin* (2020) 70(4):299–312. doi: 10.3322/caac.21613
5. Tong N, He Z, Ma Y, Wang Z, Huang Z, Cao H, et al. Tumor Associated Macrophages, as the Dominant Immune Cells, Are an Indispensable Target for Immunologically Cold Tumor-Glioma Therapy? *Front Cell Dev Biol* (2021) 9:706286. doi: 10.3389/fcell.2021.706286
6. Xie Y, He L, Lugano R, Zhang Y, Cao H, He Q, et al. Key Molecular Alterations in Endothelial Cells in Human Glioblastoma Uncovered Through Single-Cell RNA Sequencing. *JCI Insight* (2021) 6(15):150861. doi: 10.1172/jci.insight.150861
7. Reardon DA, Brandes AA, Omuro A, Mulholland P, Lim M, Wick A, et al. Effect of Nivolumab vs Bevacizumab in Patients With Recurrent Glioblastoma: The CheckMate 143 Phase 3 Randomized Clinical Trial. *JAMA Oncol* (2020) 6(7):1003–10. doi: 10.1001/jamaoncol.2020.1024
8. Buerki RA, Chheda ZS, Okada H. Immunotherapy of Primary Brain Tumors: Facts and Hopes. *Clin Cancer Res* (2018) 24(21):5198–205. doi: 10.1158/1078-0432.CCR-17-2769
9. Mangani D, Weller M, Roth P. The Network of Immunosuppressive Pathways in Glioblastoma. *Biochem Pharmacol* (2017) 130:1–9. doi: 10.1016/j.bcp.2016.12.011
10. Martinez-Lage M, Lynch TM, Bi Y, Cocito C, Way GP, Pal S, et al. Immune Landscapes Associated With Different Glioblastoma Molecular Subtypes. *Acta Neuropathol Commun* (2019) 7(1):203. doi: 10.1186/s40478-019-0803-6
11. Simpson KD, Templeton DJ, Cross JV. Macrophage Migration Inhibitory Factor Promotes Tumor Growth and Metastasis by Inducing Myeloid-

Derived Suppressor Cells in the Tumor Microenvironment. *J Immunol* (2012) 189(12):5533–40. doi: 10.4049/jimmunol.1201161
12. Gieryng A, Pszczolkowska D, Walentynowicz KA, Rajan WD, Kaminska B. Immune Microenvironment of Gliomas. *Lab Invest* (2017) 97(5):498–518. doi: 10.1038/labinvest.2017.19
13. Quail DF, Joyce JA. Microenvironmental Regulation of Tumor Progression and Metastasis. *Nat Med* (2013) 19(11):1423–37. doi: 10.1038/nm.3394
14. Shi Y, Ping YF, Zhou W, He ZC, Chen C, Bian BS, et al. Tumour-Associated Macrophages Secrete Pleiotrophin to Promote PTPRZ1 Signalling in Glioblastoma Stem Cells for Tumour Growth. *Nat Commun* (2017) 8:15080. doi: 10.1038/ncomms15080
15. Friebel E, Kapolou K, Unger S, Nunez NG, Utz S, Rushing EJ, et al. Single-Cell Mapping of Human Brain Cancer Reveals Tumor-Specific Instruction of Tissue-Invading Leukocytes. *Cell* (2020) 181(7):1626–42.e20. doi: 10.1016/j.cell.2020.04.055
16. Cristescu R, Mogg R, Ayers M, Albright A, Murphy E, Yearley J, et al. Pan-Tumor Genomic Biomarkers for PD-1 Checkpoint Blockade-Based Immunotherapy. *Science* (2018) 362(6411):3593. doi: 10.1126/science.aar3593
17. Wilkerson MD, Hayes DN. ConsensusClusterPlus: A Class Discovery Tool With Confidence Assessments and Item Tracking. *Bioinformatics* (2010) 26 (12):1572–3. doi: 10.1093/bioinformatics/btq170
18. Hanzelmann S, Castelo R, Guinney J. GSVA: Gene Set Variation Analysis for Microarray and RNA-Seq Data. *BMC Bioinf* (2013) 14:7. doi: 10.1186/1471-2105-14-7
19. Chen B, Khodadoust MS, Liu CL, Newman AM, Alizadeh AA. Profiling Tumor Infiltrating Immune Cells With CIBERSORT. *Methods Mol Biol* (2018) 1711:243–59. doi: 10.1007/978-1-4939-7493-1_12
20. Huang Q, Zhan L, Cao H, Li J, Lyu Y, Guo X, et al. Increased Mitochondrial Fission Promotes Autophagy and Hepatocellular Carcinoma Cell Survival Through the ROS-Modulated Coordinated Regulation of the NFKB and TP53 Pathways. *Autophagy* (2016) 12(6):999–1014. doi: 10.1080/15548627.2016.1166318
21. Li J, Huang Q, Long X, Zhang J, Huang X, Aa J, et al. CD147 Reprograms Fatty Acid Metabolism in Hepatocellular Carcinoma Cells Through Akt/mTOR/SREBP1c and P38/PPARalpha Pathways. *J Hepatol* (2015) 63(6):1378–89. doi: 10.1016/j.jhep.2015.07.039
22. Zeng J, See AP, Phallen J, Jackson CM, Belcaid Z, Ruzevick J, et al. Anti-PD-1 Blockade and Stereotactic Radiation Produce Long-Term Survival in Mice With Intracranial Gliomas. *Int J Radiat Oncol Biol Phys* (2013) 86(2):343–9. doi: 10.1016/j.ijrobp.2012.12.025
23. Chen Z, Hambardzumyan D. Immune Microenvironment in Glioblastoma Subtypes. *Front Immunol* (2018) 9:1004. doi: 10.3389/fimmu.2018.01004
24. Xu S, Tang L, Li X, Fan F, Liu Z. Immunotherapy for Glioma: Current Management and Future Application. *Cancer Lett* (2020) 476:1–12. doi: 10.1016/j.canlet.2020.02.002
25. Patel AP, Tirosh I, Trombetta JJ, Shalek AK, Gillespie SM, Wakimoto H, et al. Single-Cell RNA-Seq Highlights Intratumoral Heterogeneity in Primary Glioblastoma. *Science* (2014) 344(6190):1396–401. doi: 10.1126/science.1254257
26. Sottoriva A, Spiteri I, Piccirillo SG, Touloumis A, Collins VP, Marioni JC, et al. Intratumor Heterogeneity in Human Glioblastoma Reflects Cancer Evolutionary Dynamics. *Proc Natl Acad Sci USA* (2013) 110(10):4009–14. doi: 10.1073/pnas.1219747110
27. Griveau A, Seano G, Shelton SJ, Kupp R, Jahangiri A, Obernier K, et al. A Glial Signature and Wnt7 Signaling Regulate Glioma-Vascular Interactions and Tumor Microenvironment. *Cancer Cell* (2018) 33(5):874–89.e7. doi: 10.1016/j.ccell.2018.03.020
28. Na BR, Kim HR, Piragyte I, Oh HM, Kwon MS, Akber U, et al. TAGLN2 Regulates T Cell Activation by Stabilizing the Actin Cytoskeleton at the Immunological Synapse. *J Cell Biol* (2015) 209(1):143–62. doi: 10.1083/jcb.201407130
29. Kim HR, Lee HS, Lee KS, Jung ID, Kwon MS, Kim CH, et al. An Essential Role for TAGLN2 in Phagocytosis of Lipopolysaccharide-Activated Macrophages. *Sci Rep* (2017) 7(1):8731. doi: 10.1038/s41598-017-09144-x
30. Xiong Y, Li M, Bai J, Sheng Y, Zhang Y. High Level of METTL7B Indicates Poor Prognosis of Patients and Is Related to Immunity in Glioma. *Front Oncol* (2021) 11:650534. doi: 10.3389/fonc.2021.650534
31. Li T, Zhang C, Zhao G, Zhang X, Hao M, Hassan S, et al. IGFBP2 Regulates PD-L1 Expression by Activating the EGFR-STAT3 Signaling Pathway in Malignant Melanoma. *Cancer Lett* (2020) 477:19–30. doi: 10.1016/j.canlet.2020.02.036
32. Zhao J, Wang L, Kong D, Hu G, Wei B. Construction of Novel DNA Methylation-Based Prognostic Model to Predict Survival in Glioblastoma. *J Comput Biol* (2020) 27(5):718–28. doi: 10.1089/cmb.2019.0125

Conflict of Interest: The authors declare that the research was conducted in the absence of any commercial or financial relationships that could be construed as a potential conflict of interest.

Publisher's Note: All claims expressed in this article are solely those of the authors and do not necessarily represent those of their affiliated organizations, or those of the publisher, the editors and the reviewers. Any product that may be evaluated in this article, or claim that may be made by its manufacturer, is not guaranteed or endorsed by the publisher.

Copyright © 2022 Wang, Cao, Zhai, Deng, Chao, Hu, Mou, Guo, Zhao, Li, Jiao, Xue, Han, Zhang and Wang. This is an open-access article distributed under the terms of the Creative Commons Attribution License (CC BY). The use, distribution or reproduction in other forums is permitted, provided the original author(s) and the copyright owner(s) are credited and that the original publication in this journal is cited, in accordance with accepted academic practice. No use, distribution or reproduction is permitted which does not comply with these terms.

frontiers | Frontiers in Immunology

ORIGINAL RESEARCH
published: 26 April 2022
doi: 10.3389/fimmu.2022.798583

Roles of the m^{6}A Modification of RNA in the Glioblastoma Microenvironment as Revealed by Single-Cell Analyses

Feng Yuan[1†], Xiangming Cai[2†], Zixiang Cong[1], Yingshuai Wang[3], Yuanming Geng[4], Yiliyaer Aili[4], Chaonan Du[1], Junhao Zhu[1], Jin Yang[5], Chao Tang[5], Aifeng Zhang[2,6], Sheng Zhao[2,7,8] and Chiyuan Ma[1,2,4,5,9]*

[1] Department of Neurosurgery, Affiliated Jinling Hospital, Medical School of Nanjing University, Nanjing, China, [2] School of Medicine, Southeast University, Nanjing, China, [3] Department of Internal Medicine III, University Hospital Munich, Ludwig Maximilians-University Munich, Munich, Germany, [4] Department of Neurosurgery, The Affiliated Jinling Hospital of Nanjing Medical University, Nanjing, China, [5] Department of Neurosurgery, Jinling Hospital, Nanjing, China, [6] Department of Pathology, School of Medicine, Southeast University, Nanjing, China, [7] Department of Biochemistry and Molecular Biology, School of Medicine, Southeast University, Nanjing, China, [8] The Key Laboratory of Developmental Genes and Human Disease, Institute of Life Sciences, Southeast University, Nanjing, China, [9] Department of Neurosurgery, Jinling Hospital, The First School of Clinical Medicine, Southern Medical University, Nanjing, China

Purpose: Glioblastoma multiforme (GBM) is a common and aggressive form of brain tumor. The N^6-methyladenosine (m^{6}A) mRNA modification plays multiple roles in many biological processes and disease states. However, the relationship between m^{6}A modifications and the tumor microenvironment in GBM remains unclear, especially at the single-cell level.

Experimental Design: Single-cell and bulk RNA-sequencing data were acquired from the GEO and TCGA databases, respectively. We used bioinformatics and statistical tools to analyze associations between m^{6}A regulators and multiple factors.

Results: *HNRNPA2B1* and *HNRNPC* were extensively expressed in the GBM microenvironment. m^{6}A regulators promoted the stemness state in GBM cancer cells. Immune-related BP terms were enriched in modules of m^{6}A-related genes. Cell communication analysis identified genes in the GALECTIN signaling network in GBM samples, and expression of these genes (*LGALS9*, *CD44*, *CD45*, and *HAVCR2*) correlated with that of m^{6}A regulators. Validation experiments revealed that *MDK* in MK signaling network promoted migration and immunosuppressive polarization of macrophage. Expression of m^{6}A regulators correlated with ICPs in GBM cancer cells, M2 macrophages and T/NK cells. Bulk RNA-seq analysis identified two expression patterns (low m^{6}A/high ICP and high m^{6}A/low ICP) with different predicted immune infiltration and responses to ICP inhibitors. A predictive nomogram model to distinguish these 2 clusters was constructed and validated with excellent performance.

OPEN ACCESS

Edited by:
Wen Cheng,
The First Affiliated Hospital of China Medical University, China

Reviewed by:
Wenzhi Guo,
First Affiliated Hospital of Zhengzhou University, China
Xuejun Yang,
Tianjin Medical University, China
Ailiang Zeng,
University of Texas MD Anderson Cancer Center, United States

***Correspondence:**
Chiyuan Ma
machiyuan_nju@126.com

†These authors have contributed equally to this work and share first authorship

Specialty section:
This article was submitted to Cancer Immunity and Immunotherapy, a section of the journal Frontiers in Immunology

Received: *20 October 2021*
Accepted: *28 March 2022*
Published: *26 April 2022*

Citation:
Yuan F, Cai X, Cong Z, Wang Y, Geng Y, Aili Y, Du C, Zhu J, Yang J, Tang C, Zhang A, Zhao S and Ma C (2022) Roles of the m^{6}A Modification of RNA in the Glioblastoma Microenvironment as Revealed by Single-Cell Analyses. Front. Immunol. 13:798583. doi: 10.3389/fimmu.2022.798583

Conclusion: At the single-cell level, m^{6}A modification facilitates the stemness state in GBM cancer cells and promotes an immunosuppressive microenvironment through ICPs and the GALECTIN signaling pathway network. And we also identified two m^{6}A-ICP expression patterns. These findings could lead to novel treatment strategies for GBM patients.

Keywords: glioblastoma, immune microenvironment, m^{6}A, single-cell analysis, cell communication

INTRODUCTION

Glioblastoma multiforme (GBM) is the most common primary tumor of the central nervous system, and it is extremely aggressive (1). Standard treatment for GBM is surgical resection followed by chemoradiotherapy, with a 5-year survival of 7.2% (1, 2). Immunotherapy has achieved growing success across systemic cancers, and has become a prominent player in the treatment of GBM (3). Nonetheless, the high degree of genetic heterogeneity and immunosuppressive microenvironment that characterize GBM represent important challenges to the application of immunotherapy to this disease (1). Advancements in knowledge of the immune cells in the GBM microenvironment, particularly glioma-associated microglia, macrophages and T cells, might lead to novel strategies to strengthen anti-tumor immunity (3).

An important aspect of the behavior of these key immune cells involves the N^6-methyladenosine (m^{6}A) modification, which has emerged as the most abundant chemical modification of protein-coding and noncoding RNAs (4, 5). To date, regulators of the m^{6}A modification have been reported to be involved in cancer biology, including cancer progression and other processes (4). Notably, the roles of m^{6}A regulators in mediating immunotherapy resistance have been highlighted in recent studies. For instance, expression of *METTL3* in macrophages was suggested to synergize with PD-1-based therapy in B16 melanoma (6), and *METTL3* and *METTL14* have been shown to regulate immune response to anti-PD-1 treatment in melanoma and colorectal carcinoma (7). Together, these findings indicate a role for m^{6}A regulators as potential therapeutic targets in anticancer immunotherapy.

Several m^{6}A regulators have been reported to be upregulated and to play vital roles in GBM, including enhancing cell self-renewal and proliferation in glioblastoma stem cells (GSCs) (8). However, some opposing findings have shown lower expression levels of some m^{6}A writers in GBM and have detected anticancer properties of m^{6}A regulators (8, 9). This conflict suggests a complex role of m^{6}A-related methylation in the occurrence and development of GBM. Notably, though, *FTO*, *YTHDF2*, and *RBM15* were found to have prognosis predictive value in GBM (8, 10). In addition, patients with higher m^{6}A related risk scores were more sensitive to temozolomide treatment and showed lower drug resistance overall (10).

These findings suggested critical and complex roles of m^{6}A modification in GBM, and more research opportunities and challenges have emerged. Recent development of single-cell analysis methods provides more comprehensive approaches to explore the potential mechanism of action of m^{6}A modifications in GBM at the cellular level. Herein, for the first time, we used scRNA-seq data to thoroughly analyze (**Figure 1**) the roles of m^{6}A modifications in the GBM microenvironment, especially its relationship with functional states, cell communication and immune checkpoints (ICPs).

MATERIALS AND METHODS

Datasets

Five publicly available human GBM scRNA-seq datasets (11–15) were obtained from the Gene Expression Omnibus (GEO) database (http://www.ncbi.nlm.nih.gov/geo/). Bulk RNA-seq datasets and DNA methylation profiles were obtained from the Cancer Genome Atlas (TCGA, https://portal.gdc.cancer.gov/) and the Repository of Molecular Brain Neoplasia Data (REMBRANDT) (16) datasets. These bulk datasets were

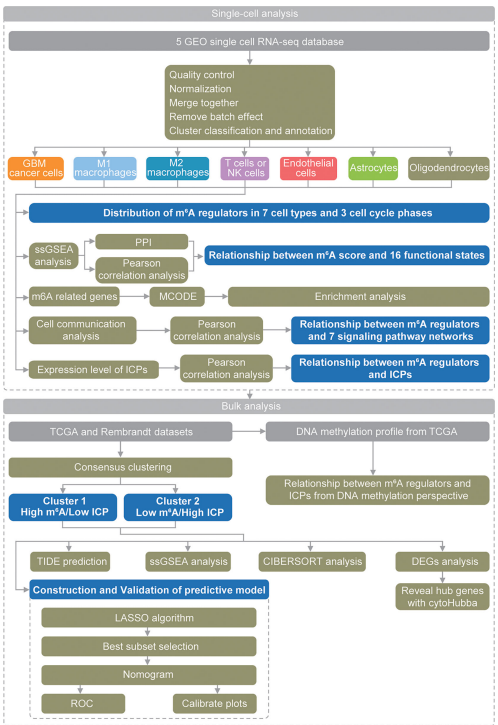

FIGURE 1 | Schematic diagram of the study design.

downloaded *via* the University of California, Santa Cruz (UCSC) Xena browser (https://xenabrowser.net/) and Chinese Glioma Genome Atlas (CGGA, http://www.cgga.org.cn/) websites. A summary description of included scRNA-seq datasets is provided in **Supplementary Table S2**.

Single-Cell RNA-seq Analysis

The "Seurat" R package (version 4.0.2) (17) was used to perform single-cell RNA-seq analyses. We only included in this study samples with at least 10 000 detected genes. Quality control (QC) was based on following standards: 1) genes detected in fewer than 3 cells were excluded; 2) cells with fewer than 200 total detected genes were excluded; 3) cells with at least 5% (for GSE141383, GSE84465, GSE103224, GSE89567) or 10% (for GSE138794) of mitochondrial genes were excluded; 4) cells with at most 3% (for GSE141383, GSE138794, GSE103224, GSE89567) or 1% (for GSE84465) of ribosomal genes were excluded; 5) cells with at least 0.1% of hemoglobin genes were excluded and 6) cells with total gene expression between first quartile − 1.5 × interquartile range (IQR) and third quartile + 1.5 × IQR were retained to exclude cellular doublets.

Unnormalized datasets were normalized with the "NormalizeData" function in R. Then, these five datasets were merged together, and the zero imputation method was applied to investigate missing data relating to significant markers (**Supplementary Table S3**). The batch effect was removed *via* the "fastMNN" algorithm from the "SeuratWrappers" R package (version 0.3.0).

Principal component analysis (PCA) was performed, and the top 20 PCs were used for cluster classification. The initial 20 PCs were also utilized in the further visualization process through the t-distributed stochastic neighbor embedding (t-SNE) algorithm. After cluster classification, different cell clusters were identified and annotated manually within the CellMarker database (http://biocc.hrbmu.edu.cn/CellMarker/) (18). The cell cycle score was calculated with the "CellCycleScoring" function. Cell communication network analysis was conducted with the "CellChat" R package (version 1.1.1). Gene Expression Profiling Interactive Analysis (GEPIA) (http://gepia.cancer-pku.cn/) was used to compare the expression levels of m^6A regulators between GBM and normal samples with bulk RNA-seq datasets.

Single-Sample Gene Set Enrichment Analysis

The ssGSEA algorithm was conducted with the "GSVA" R package (version 1.34.0) to calculate enrichment scores for several gene signatures. The gene set for m^6A included 13 m^6A readers (*YTHDC1*, *YTHDC2*, *IGF2BP1*, *IGF2BP2*, *IGF2BP3*, *YTHDF1*, *YTHDF2*, *YTHDF3*, *HNRNPA2B1*, *HNRNPC*, *ELAVL1*, *LRPPRC* and *FMR1*), 8 m^6A writers (*METTL3*, *METTL14*, *WTAP*, *KIAA1429*, *RBM15*, *RBM15B*, *ZC3H13* and *CBLL1*) and 2 m^6A erasers (*FTO* and *ALKBH5*). The gene lists (**Supplementary Table S1**) for other biological states were from CancerSEA (http://biocc.hrbmu.edu.cn/CancerSEA).

m^6A Related Genes

Analyses of Pearson correlations between m^6A scores and gene expression were conducted to filter m^6A related genes under the following criteria: (1) R value greater than 0.3 or less than -0.3 and (2) $P < 0.05$. In M2 macrophages, we strengthened the criteria for m^6A related genes to R value greater than 0.5 or less than -0.5. The Molecular Complex Detection (MCODE) plugin from Cytoscape software (version 3.8.1) was applied to identify core gene modules with scores greater than 10.

Functional Annotation

Enrichment analyses of biological processes (BP) Gene Ontology (GO) annotations and Kyoto Encyclopedia of Genes and Genomes (KEGG) pathway analyses were performed based on the "clusterProfiler" R package (version 3.14.3) with adjusted $P < 0.05$ as the cutoff criterion.

Protein-Protein Interaction Network Analysis

The PPI network was constructed with Search Tool for the Retrieval of Interacting Genes (STRING) (https://string-db.org/) and visualized with Cytoscape.

Bulk RNA-seq Analysis

To better understand the interaction between m^6A regulators and immune checkpoints (ICPs), the "ConsensusClusterPlus" R package (version 1.50.0) was applied to identify distinct clusters of bulk RNA-seq samples with correlated expression levels of m^6A regulators and ICPs. The Tumor Immune Dysfunction and Exclusion (TIDE) algorithm was utilized to predict potential therapeutic responses of ICP inhibitors. Morpheus (https://software.broadinstitute.org/morpheus) was used to identify differentially expressed genes (DEGs) between clusters. The cutoff criteria for DEGs were: $P < 0.05$ and $|\log2 \text{ fold-change}| \geq 1$. An enrichment analysis of DEGs was conducted and hub genes in DEGs were visualized in a PPI network. The ssGSEA for various gene signatures was performed for each sample. We also conducted the Cell Type Identification by Estimating Relative Subsets of RNA Transcripts (CIBERSORT) analysis of the abundance scores of immune cells in GBM samples. A Pearson correlation analysis among the methylation levels and expression levels of m^6A regulators and ICPs was performed and visualized with Cytoscape software.

Construction of Predictive Model

To sort GBM patients into 2 clusters, the TCGA and REMBRANDT datasets were used as a training dataset and validation dataset separately. A least absolute shrinkage and selection operator (LASSO) regression analysis was used to identify all genes with $P < 0.05$. Then, best subset selection was performed to determine the final multivariate logistic regression model. A nomogram was constructed to show the predictive model. The evaluation of the nomogram model was performed with receiver operating characteristic (ROC) curve analysis and calibration curve analysis. "glmnet" (version 4.1), "rms" (version 6.1.0), and "timeROC" (version 0.4) R packages were used for the construction of predictive model.

Sample Source

Tumor tissues were surgically harvested at Jinling Hospital in accordance with institution-approved protocols. The tissues were collected from 2 glioma patients (without preoperative radiotherapy or chemotherapy), confirmed pathologically as specimens of grade IV gliomas, and fixed in formalin before paraffin-embedded. Tissues from two nontumoral cases were also collected as control. Written informed consent had been obtained from participants.

Cell Lines and Culture

The human GBM cell line U87MG were purchased from cell bank of Shanghai Institute of Biochemistry and Cell Biology and grown in Dulbecco's Modified Eagle's medium (DMEM) containing 10% fetal bovine serum (FBS, Gibco, USA). THP-1 was kindly provided by Wentao Liu laboratory, Nanjing Medical University and cultured in 1640 medium with 10% FBS. Cells were cultured at 37°C in a humidified atmosphere with 5% CO2.

Proteins and Reagents

Antibodies against *MDK* (11009-1-AP) and *CD206* (60143-1-lg) was purchased from proteintech, and that against *LRP1* (ab92544) was from Abcam. The β-Actin polyclonal antibody (AP0060) and goat anti-rabbit IgG-HRP (BS13278) were purchased from Bioworld. Midkine protein (abs00930) was from Absin Bioscience Inc. The jetPRIME transfection reagent (101000046) was from Polyplus. Anti-CD206 APC (17–2069–41) and its isotype control (17–4714–81) were purchased from eBioscience. And anti-CD11b FITC (101205), its isotype control (400633), and cell staining buffer (420201) was purchased from BioLegend.

Transfections With siRNA

The MDK small interfering RNA (siMDK; forward, 5'-GACCA AAGCA AAGGC CAAATT-3'; reverse, 5'-UUUGG CCUUU GCUUU GGUCTT-3') and negative control siRNA (siCon; forward, 5'-UUCUC CGAAC GUGUC ACGUTT-3'; reverse, 5'-ACGUG ACACG UUCGG AGAATT-3') were synthesized by GenePharma (Shanghai, China). U87MG was transfected with 100ul/L MDK siRNA and negative control siRNA respectively, using jetPRIME transfection reagent. Cells were transfected with siRNAs for 48 h prior to the following experiments.

Western Blot Assay

Total proteins of cells were extracted, quantified using BCA kit (23235, Thermo), separated by 10% SDS-PAGE, and transferred onto polyvinylidene difluoride membrane. The membrane was blocked with 5% defatted milk powder for 1.5 h, and was incubated overnight in primary antibody (anti-β-Actin at 1:10000; anti-MDK at 1:1000) at 4°C. On the following day, the membrane was incubated in secondary antibody (goat anti-rabbit IgG-HRP 1:20000) for 1 h at room temperature. After adding ECL chromogenic substrate (Millipore, US), the membrane was imaged using a gel imaging system.

qPCR

RNA was extracted using Ultrapure RNA Kit (CW0597, CWBIO). cDNA was synthesized using a reverse transcription kit (AE311, TransGern) following the instructions in the manual. The endogenous levels of MDK mRNA were determined using the SYBRGreen PCR Kit (AQ131, TransGern). PCR conditions were: denaturation at 94°C for 30 s, followed by 40 cycles of denaturation at 94°C for 5 s, annealing at 61°C for 35 s, followed by elongation at 95°C for 10 s. GAPDH was used as reference gene for MDK. The following primers were used: MDK-F (5'-AAGGATTGCGGCGTGGGTTTC-3'), MDK-R (5'-TGGCGGACTTTGGTGCCTGTG-3'), GAPDH-F (5'-AATCCCATCACCATCTTCCA-3'), and GAPDH-R (5'-AAATGAGCCCCAGCCTTCT-3'). Relative expression level of MDK was calculated using 2-ΔΔCt approach.

Transwell Assay for Cell Migration

THP-1 was primed with 185 ng/ml PMA for 24 hours, and then added to the top chamber of Transwell unit at a density of 3×10^5 cells/unit. Next, U87MG cell suspension was added into the lower chamber. The transwell chamber was cultured at 37°C for 24 h in a cell incubator. The cells were fixed with methanol for 15 min, and stained with 0.1% crystal violet solution for 5 min. Then, cells on the upper surface of the chamber bottom were removed gently with a cotton swab. Finally, observe the invaded cells on the lower surface under an inverted microscope. Three separate membranes were analyzed for each condition.

Flow Cytometry

Staining for cell surface markers was done by re-suspending each sample in 100 μl cell staining buffer containing the antibody cocktail. Three groups were set here. Isotype controls were added into group 1. Anti-CD206 APC and anti-CD11b FITC were added into group 2 (siCon) and 3 (siMDK). Cells were incubated at 4°C for 30 minutes and then washed with cell staining buffer. Cells with $CD11b^+/CD206^+$ phenotype were identified as M2 macrophages. Data were immediately acquired using CytoFLEX (Beckman Coulter) and analyzed with FlowJo software (version 10.5.3).

Immunohistochemistry

Paraffin-embedded clinical tissue specimens were sectioned, dewaxed, and dehydrated. Antigen retrieval was conducted using a pressure cooker for 3 min. Then, sections were washed with 3% methanol H2O2. Subsequently, the sections were incubated overnight at 4°C using primary antibodies against *MDK* (11009-1-AP, 1:500) and *LRP1* (ab92544, 1:300), and treated with biotin-free EnVision detection kit (Dako) for secondary antibody. The labeled antigens were visualized by 3,3'-diaminobenzidine tetrahydrochloride as a chromogen. Finally, the sections were counterstained with hematoxylin. ImageJ software and IHC Profiler plugin were applied for qualitative assessment of IHC slides. Five random fields were observed under microscope.

Sections were scored using Histochemistry score (H-SCORE) method. Staining proportion was scored from 0 to 3, with 0 if

negative, 1 if < 25% of cells stained positively, 2 if 26–50% of cells stained positively, and 3 if > 50% of cells stained positively. In addition, the staining intensity was scored as 0, no staining; 1, weak; 2, moderate; and 3, strong. These two scores were multiplied by each other to calculate the expression score of *MDK* and *LRP1*, with 0-3 represents low expression, and 4–9 represents high expression.

Immunofluorescence Staining

Segments of samples were dehydrated with 15% and 30% sucrose solution sequentially, embedded in OCT compound, and cryosectioned into 8 μm sections. Fixation was conducted with 4% paraformaldehyde for 15 min. After washing with PBS at room temperature, samples were incubated with 0.1% Triton X-100 for 5-15 min, were followed by washing with PBS. Sections were blocked with 10% goat serum for 1 h at room temperature. Primary antibody was added for overnight incubation at 4°C.

On the following day, primary antibody was removed by rinsing with PBS, and TRITC/FITC -labelled secondary antibody (1:100) was added and incubated at room temperature for 30 min and subsequently stained with DAPI (1:400) for 1-2 min. Coverslips were mounted. Images were obtained under a laser scanning confocal microscope.

Statistical Analysis

All statistical analyses were performed in R software (version 3.6.0 and 4.0.2). Student's t-test and chi-square test or Fisher's exact test were used for comparisons of continuous variables and categorical variables. Bar charts were drawn to display the comparisons using the "ggplot" R package (version 3.3.3). The Kaplan–Meier approach was performed to estimate survival, and the overall survival (OS) was compared with log-rank tests. We also applied Pearson correlation analyses to evaluate two continuous variables, after calculating the mean value of these variables in each sample. To avoid the influence of missing data, we excluded samples with missing data in correlation analyses, and only conducted the correlation analysis when there were more than 3 samples. The correlation analysis results were visualized with "corrgram" (version 1.13) and "ggplot" R packages. $P < 0.05$ values were set as indicating statistical significance.

RESULTS

Analysis of scRNA-seq Data Identifies 7 Types of Cells in GBM

We obtained scRNA-seq profiles of 52 851 single cells from 22 GBM samples (**Supplementary Table S2**). Following the application of a QC standard, 47 978 single cells were retained (**Supplementary Figure 1**; **Supplementary Table S2**). To visualize the distribution of the scRNA-seq profile, we employed a t-distributed stochastic neighbor embedding (t-SNE) algorithm to reduce the dimensionality of these datasets (**Figure 2A**). After appropriate elimination of the batch effect within these datasets with the "fastMNN" algorithm, the data was well integrated (**Figure 2B**). With unsupervised classification, cells were successfully classified into 17 clusters (**Figure 2C**). Based on the expression patterns of markers from CellMarker, we manually annotated these clusters as the following 7 cell types: 1) GBM cancer cells (expressing *SOX2*, *PARP1*, and *CCND2*); 2) M1 macrophages (*CD68*, *CD74*, *TSPO*, and *CD86*); 3) M2 macrophages (*CD68*, *CD74*, and *CD163*); 4) T cells or natural killer (NK) cells (*CXCR4* and *S100A4*); 5) endothelial cells (*A2M* and *APOLD1*); 6) astrocytes (*GFAP* and *SOX9*); 7) oligodendrocytes (*CNP*, *MBP*, and *PLP1*) (**Figure 2D–F, H**). We also detected heterogeneous cell compositions among these included samples (**Figure 2I**). DEGs for cell types were identified (**Figure 2G**; **Supplementary Table S4**), and enrichment analyses for these DEGs were conducted to show related BP and pathways of each cell type (**Supplementary Tables S4**).

HNRNPA2B1 and *HNRNPC* Show Extensive Expression in the GBM Microenvironment

First, we obtained the expression levels from the bulk transcriptome of 23 m^6A regulators in GBM and normal samples from GEPIA, and found that most m^6A regulators have relatively higher expression levels in GBM compared with that in normal samples. Especially notable were *HNRNPA2B1*, *HNRNPC*, and *WTAP* (**Supplementary Figure 2J**). Then, to explore the expression patterns of m^6A regulators in GBM samples at the single-cell level, we drew t-SNE plots of these m^6A regulators. In general, all 23 m^6A regulators were expressed in all 7 cell types, but not in all cells (**Figure 3**; **Supplementary Figures 2A–I**).

Notably, *HNRNPA2B1* and *HNRNPC* showed extensive expression pattern in all cell types, but the expression of these m^6A regulators was higher in M1 macrophages, GBM cancer cells, and T/NK cells. We further explored the expression levels of these m^6A regulators in different cell cycle phases (**Figure 3P**). Heterogeneity of cell cycle distribution was observed in these included samples (**Supplementary Figure 3H**). The GBM cancer cells exhibited the most and largest proportion of cells at S and G_2M phases. Interestingly, other types of cells, except M1 macrophages, had about 30% to 50% cells in the S and G_2M phases. In general, cells at G_1 phase showed higher expression of m^6A regulators than did cells at S and G_2M phases (**Figure 3R**). For cells at S phase, *HNRNPC* had highest expression level relative to other m^6A regulators. A higher expression level of *HNRNPA2B1* was observed in cells at G_2M phase. For cells at G_1 phase, m^6A regulators with higher expression levels were *HNRNPA2B1*, *HNRNPC*, *WTAP*, and *YTHDC1*.

Similar results were observed in all 7 types of cells, except for M2 macrophages (**Supplementary Figures 3A–G**). For M2 macrophages at S phase, *HNRNPA2B1* was more highly expressed than was *HNRNPC*. These results indicated intratumor heterogeneity of m^6A regulators and intertumor heterogeneity of cell types and cell cycle phases in different samples. The following analyses of expression of m^6A modification factors in GBM were based on subsets of the noted cell types.

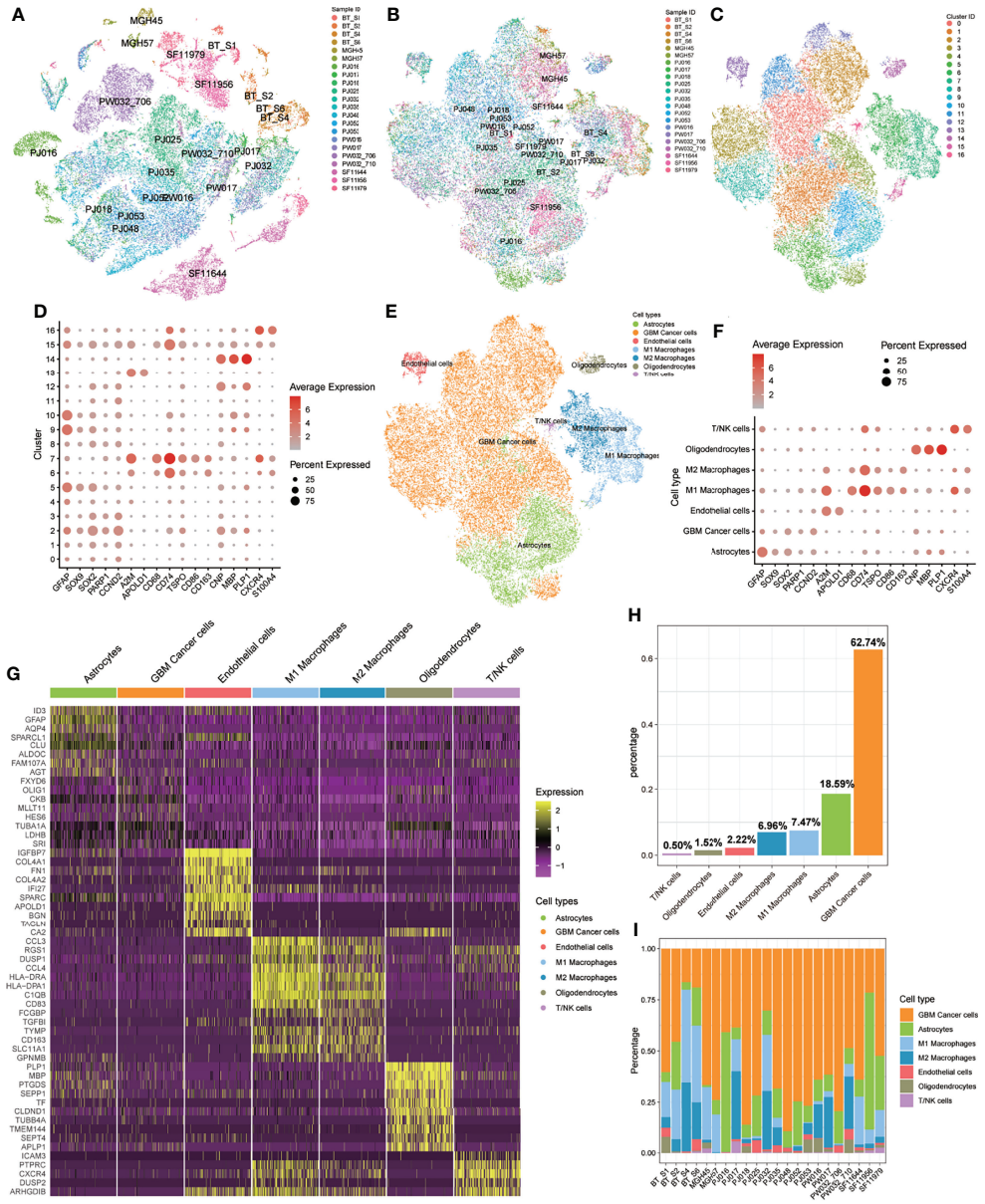

FIGURE 2 | Identification of 17 cell clusters and 7 types of cells in GBM tumors. **(A, B)** tSNE plot of GBM cells before **(A)** and after **(B)** batch effect elimination. **(C)** Unsupervised classification successfully identified 17 cell clusters. **(D)** All 17 clusters were annotated by CellMarker according to the composition of the marker genes. **(E)** tSNE plot of 7 cell types. **(F)** Expression levels of marker genes in the 7 cell types. **(G)** Heatmap of differentially expressed features in each cell type. **(H)** Distribution of 7 cell types for all included cells. **(I)** Distribution of 7 cell types in each included sample.

m^{6}A Regulators Associate With Functional States

To assess the potential relationship between m^{6}A score and scores representing 16 functional states, we conducted a series of Pearson correlation analyses in all 7 cell types (**Figures 4A, B**). Specifically, we found that in GBM cancer cells, the m^{6}A score was significantly correlated with the stemness score ($R = 0.49$, $P < 0.05$). To further explore the relationship between m^{6}A regulators and stemness-related genes, we calculated the mean expression levels of genes in each sample, conducted Pearson correlation and PPI analyses between these two sets of genes (**Figures 4C, D**), and visualized these results into an m^{6}A regulation network (**Figure 4E**). These results displayed extensive positive correlations between m^{6}A regulators and stemness-related genes. Notably, *SOX2*, which can reprogram differentiated glioma cells to glioma stem-like cells (GSCs), has been identified as a *bona fide* m^{6}A target of *METTL3* (19), but the downstream m^{6}A reader of *SOX2* in GBM remains unknown. In colorectal carcinoma, *IGF2BP2* has been proven to be a downstream m^{6}A reader of *SOX2* (20). Our regulation network

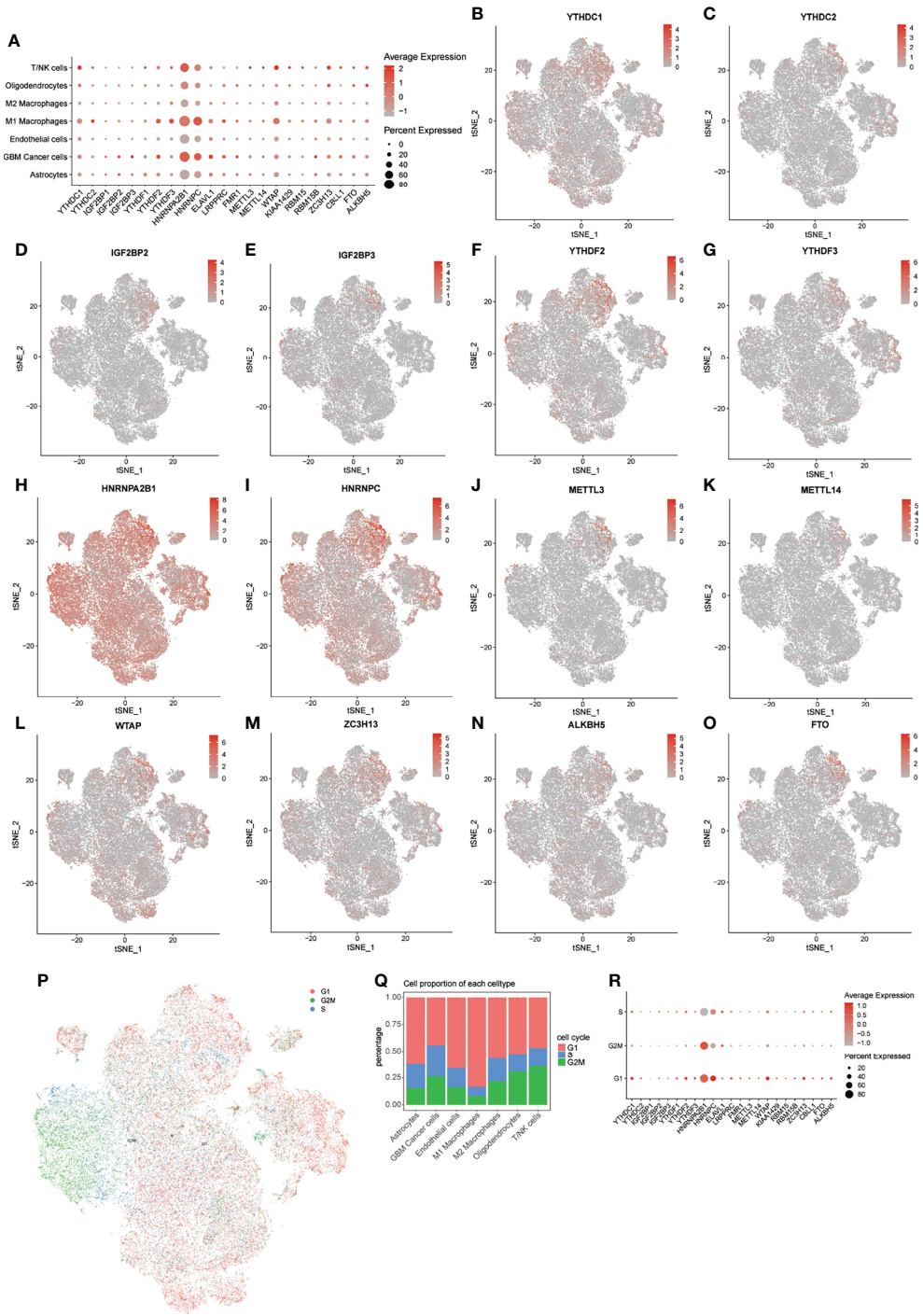

FIGURE 3 | Distribution of m^{6}A regulators in GBM microenvironment. **(A)** Expression levels of m^{6}A regulators in the 7 cell types. **(B–O)** tSNE plots of 14 m^{6}A regulators. **(P)** tSNE plot of cells in 3 cell cycles. **(Q)** Distribution of cells in 3 stages of the cell cycle in 7 cell types. **(R)** Expression levels of m^{6}A regulators in 3 stages of the cell cycle.

suggested that both *IGF2BP2* and *ELAVL1* were potential downstream m^{6}A readers of *SOX2* in GBM (**Figure 4E**).

Beside the stemness score in GBM cancer cells, we also found that differentiation score in GBM cancer cells; apoptosis, ferroptosis, and pyroptosis scores in M1 macrophages; epithelial-mesenchymal transition (EMT), invasion, and metastasis scores in M2 macrophages; apoptosis, DNA damage, and pyroptosis scores in T/NK cells; and angiogenesis, invasion, and pyroptosis scores in

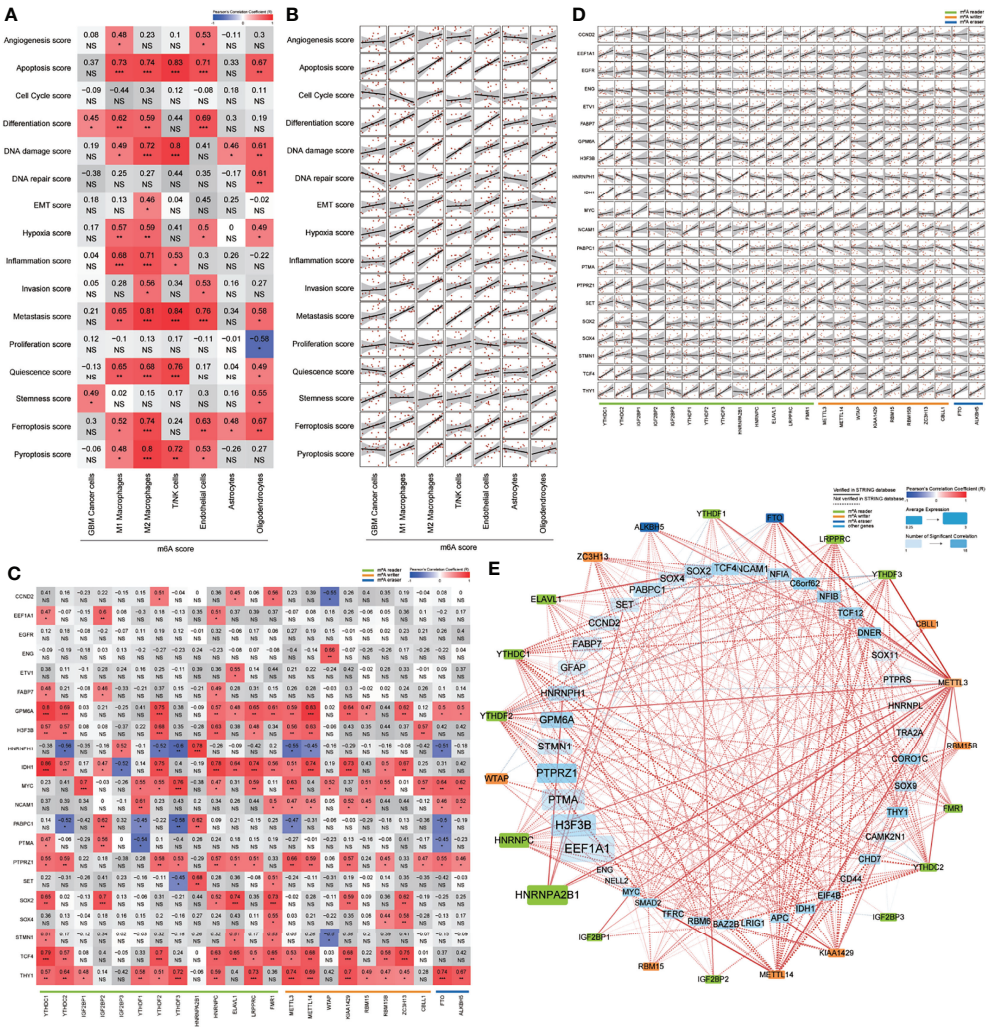

FIGURE 4 | Relationship between m^{6}A modification and 16 functional states. **(A, B)** Correlation heatmap **(A)** and correlation analysis **(B)** of m^{6}A score and 16 functional state scores in 7 cell types. **(C, D)** Correlation heatmap **(C)** and correlation analysis **(D)** of m^{6}A regulators and partial stemness related genes in GBM cancer cells. **(E)** Correlation network of m^{6}A regulators and stemness related genes in GBM cancer cells. NS: $P > 0.05$, $^*P \leq 0.05$, $^{**}P \leq 0.01$, $^{***}P \leq 0.001$.

endothelial cells were all significantly correlated with m^{6}A score. We further conducted Pearson correlation analyses between these gene sets and m^{6}A regulators. By combining of these correlation analyses with PPI analyses, we constructed 13 m^{6}A regulation networks (**Supplementary Figure 4**). These networks provided valuable information about potential regulatory mechanisms of m^{6}A regulators in the GBM microenvironment, which will be explored and verified in further studies.

Modules of m^{6}A Related Genes Associate With Immune-Related Terms

By conducting the Pearson correlation analysis between m^{6}A score and all genes in all 7 cell types, we filtered m^{6}A related genes for each cell type under the $P < 0.05$ criterion. With PPI analysis and the MCODE plugin from Cytoscape software (Degree cutoff = 2; Node score cutoff = 0.2; K-core = 2 and Max depth = 100), we identified functional modules of m^{6}A related genes in a PPI network (**Supplementary Figure 5**; **Supplementary Table S5**). Enrichment analysis was applied for each cluster to explore potential related BP and pathways (**Supplementary Table S5**). As expected, all cell types had clusters related to mRNA modification. Also, we found energy conversion and cell cycle related terms in clusters of most cell types. Specifically, terms related to antigen processing and presentation process were enriched in cluster 2 of GBM cancer cells and cluster 1 of endothelial cells (**Supplementary Table S5**). In KEGG analyses, terms relating to "PD-L1 expression and PD-1 checkpoint pathway in cancer" were enriched in cluster 2 of M2 macrophages and cluster 1 and 2 of endothelial cells (**Supplementary Table S5**).

m^{6}A Regulators Promote Immunosuppressive Activities Through the GALECTIN Signaling Network

We performed cell communication analysis in all samples and each sample separately to explore robust signal pathways in the GBM cancer microenvironment. Through subgroup analysis for each included sample, we discovered that genes from the GALECTIN (*LGALS9*, *CD44*, *CD45*, and *HAVCR2*), GRN (*GRN* and *SORT1*), MK (*MDK*, *PTPRZ1*, *NCL*, *ITGA6*, *ITGB1*, *LRP1*, and *SDC4*), PTN (*PTN*, *PTPRZ1*, *NCL*, *SDC3*, and *SDC4*), SPP1 (*SPP1*, *CD44*, *ITGAV*, and *ITGB1*), ANNEXIN (*ANXA1* and *FPR1*), and VISFATIN (*NAMPT* and *INSR*) signaling pathway networks were detected in most samples with consistent network patterns (**Supplementary Figures 6M, N**; **Supplementary Figure 6**; **Supplementary Table S6**). Specifically, M1 and M2 macrophages targeted other cells in the GALECTIN, GRN and SPP1 signaling pathway networks (**Supplementary Figures 6C, D, G, H**), and GBM cancer cells regulated other cells in the MK and PTN signaling pathway network (**Supplementary Figures 6M, N**; **Supplementary Figures 6E, F**).

Next, we conducted a Pearson correlation analysis to investigate whether m^{6}A regulators were involved in the regulation of these signaling pathway networks (**Supplementary Figures 7**-**10**). The GALECTIN signaling network plays an important role increasing induced regulatory T (iTreg) cell stability and suppressing T-cell proliferation (21). The expression level of genes in the GALECTIN signaling pathway network were higher in M1 macrophages, M2 macrophages, and T/NK cells (**Supplementary Figure 10C**). Our Pearson correlation analysis showed that in M2 macrophages, expression levels of *YTHDC1*, *YTHDC2*, *IGF2BP2*, *IGF2BP2*, *HNRNPC*, *ELAVL1*, *LRPPRC*, *ZC3H13*, and *ALKBH5* were positively correlated with expression of *LGALS9*, the gene encoding galectin-9 (**Supplementary Figures 8A, B**). In T/NK cells, *CD44* expression was positively correlated with that of *YTHDF2* and *HNRNPA2B1* and negatively correlated with *FTO* and *ALKBH5*. In T/NK cells, expression of *HAVCR2*, which encodes TIM-3, was positively correlated with that of *YTHDF2*. These results suggested that m^{6}A modification may promote immunosuppressive activities through the GALECTIN signaling pathway network in the GBM immune microenvironment.

MDK Induces Macrophage Migration and M2 Polarization

Research reported that *LRP1* attenuates proinflammatory macrophage activation as receptor for *MDK* (22). And our prementioned cell communication analysis found MK signaling pathway network (*MDK*, *PTPRZ1*, *NCL*, *ITGA6*, *ITGB1*, *LRP1*, and *SDC4*) in GBM samples. We assumed that the MK network (*MDK*/*LRP1*) played a significant role regulating macrophage activation in GBM. First, we collected four samples (Normal = 2; GBM = 2). IHC analysis showed a trend that the expression of *MDK* and *LRP1* was higher in GBM patients (**Figure 5A**). To further validate our hypothesis, we first knockdown the expression of MDK in U87MG cell line with siRNA (**Figure 5B**), and coculture its supernate with induced THP-1. Tanswell assay revealed that compared with negative control (siCon), the knockdown of MDK (siMDK) significantly deceased the migration of macrophages (**Figure 5C**). Then, we induced THP-1 (human monocyte line) into macrophages in the upper chamber of transwell unit, and added recombinant protein MDK into the lower chamber of it. Interestingly, the addition of MDK protein showed significant effect on macrophages migration as well (**Figure 5D**). To assess the effect of MDK on the polarization of macrophages, we cocultured induced THP-1 with supernate from GBM in siMDK and siCon groups respectively. Flow cytometry showed less M2 polarization ($CD11b^+/CD206^+$) in the siMDK group, compared with siCon group (**Figure 5E**). The results suggested that *MDK* significantly induces an immunosuppressive macrophage differentiation. Finally, we conducted immunofluorescence staining to explore the co-localization of MDK and CD206 (marker of M2 macrophages). Results revealed more co-localization of *MDK* and *CD206* in GBM tissues compared with that in normal brain tissues (**Figure 5F**).

m^{6}A Regulators Correlate With ICPs in Immune Microenvironment

Having demonstrated that m^{6}A regulators were associated with immune related process, we next addressed whether m^{6}A regulators were correlated with ICPs in the GBM microenvironment (**Supplementary Figure 11**). Our results revealed that in GBM cancer cells, expression of *CD274* (PD-L1), *PDCD1LG2* (PD-L2), *LGALS9* (Galectin-9), and *PVR* (CD155) were positively correlated with the expression of multiple m^{6}A regulators, especially *YTHDF2*, *YTHDF3*, *LRPPRC*, *METTL3*, *RBM15B*, *FTO*, and *ALKBH5* (**Supplementary Figures 11A, B**). In M2 macrophages, *LGALS9*, *CD86*, and *PVR* showed positive correlations with *YTHDC1*, *YTHDC2*, *YTHDF2*, *YTHDF3*, *ELAVL1*, *LRPPRC*, *METTL3*, *METTL14*, *ZC3H13*, and *ALKBH5* (**Supplementary Figures 11E, F**). Also, we found positive correlations between *HAVCR2* (TIM-3) and *YTHDF2* (**Supplementary Figures 11G, H**) in T/NK cells. These results indicated that m^{6}A modification may upregulate these suppressive immune check points and further promote the immunosuppressive microenvironment.

Bulk RNA-seq Analysis Identifies Two m^{6}A-ICP Expression Patterns

As we have determined that ICPs in the GBM microenvironment were correlated with m^{6}A regulators, we next explored the m^{6}A-ICP expression pattern in bulk RNA-seq profiles. According to the similarities of expression of 23 m^{6}A regulators and 13 ICPs, we performed consensus clustering, an unsupervised clustering algorithm, in TCGA, CGGA and REMBRANDT datasets, respectively. The optimal clustering stability was obtained when K = 2 (**Supplementary Figures 12A–F**; **Supplementary Figures 15A–C**), and samples were clustered into two subgroups with different distinct features. Cluster 1 showed a low m^{6}A/high ICP expression pattern in the heatmap of expression levels. A high m^{6}A/low ICP expression pattern was observed for cluster 2

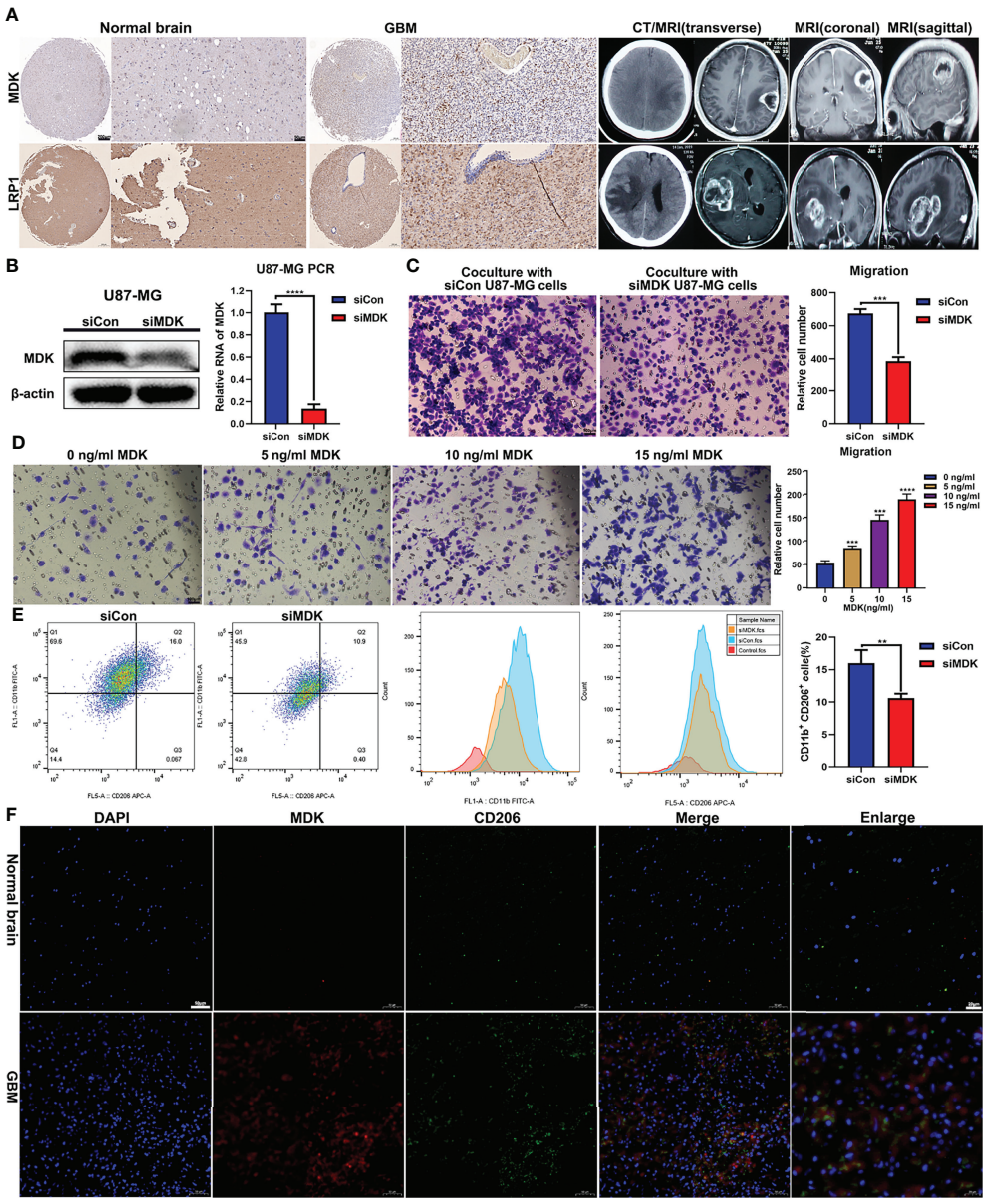

FIGURE 5 | *MDK* promotes migration and immunosuppressive polarization of macrophage. **(A)** The expression of *MDK* and *LRP1* in GBM tissues (n = 2) and normal tissues (n = 2) determined using IHC (scale bar = 50 μm). And the CT and MRI images of GBM patients. **(B)** The siRNA knockdown effect confirmed with western blot and qPCR experiments. **(C)** THP-1 was treated with 185 ng/ml PMA for 24 h in the upper chamber of transwell unit. And then, coculture it with supernate from U87MG medium in the lower chamber for 24 h. The image showed the macrophages migrate through the membrane of chamber (scale bar = 100 μm). **(D)** THP-1 was treated with 185 ng/ml PMA for 24 h in the upper chamber of transwell unit. And then, coculture it with MDK protein at various concentration gradients in the lower chamber for 24 h. The image showed the macrophages migrate through the membrane of chamber (scale bar = 100 μm). **(E)** THP-1 was treated with 185 ng/ml PMA for 24 h. And then, coculture it with supernate from U87MG medium for 72 h The flow cytometry showed the expression levels of CD11b and CD206 in these cells. Bar plot showed the proportion of M2 macrophages ($CD11b^+/CD206^+$). $^{**}p < 0.01$, $^{***}p < 0.001$, $^{****}p < 0.0001$.
(F) Immunofluorescence staining showed the expression levels and co-localization of MDK and CD206 in normal brain tissues and GBM tissues.

(**Figures 6A, B**; **Supplementary Figure 15D**). PCA for expression levels of m^6A regulators and ICPs revealed prominent differences between these 2 subgroups (**Figures 6C, E**; **Supplementary Figure 15E**). Notably, the predicted potential therapeutic response of ICP inhibitors, conducted with the TIDE algorithm, was significantly different between these 2 subgroups in TCGA and REMBRANDT datasets (**Figures 6D, F**; $P < 0.001$). Patients in cluster 1 were more likely to response to ICP inhibitor therapy (> 50% were predicted responders), but fewer than 25% patients in cluster 2 were predicted to response to this

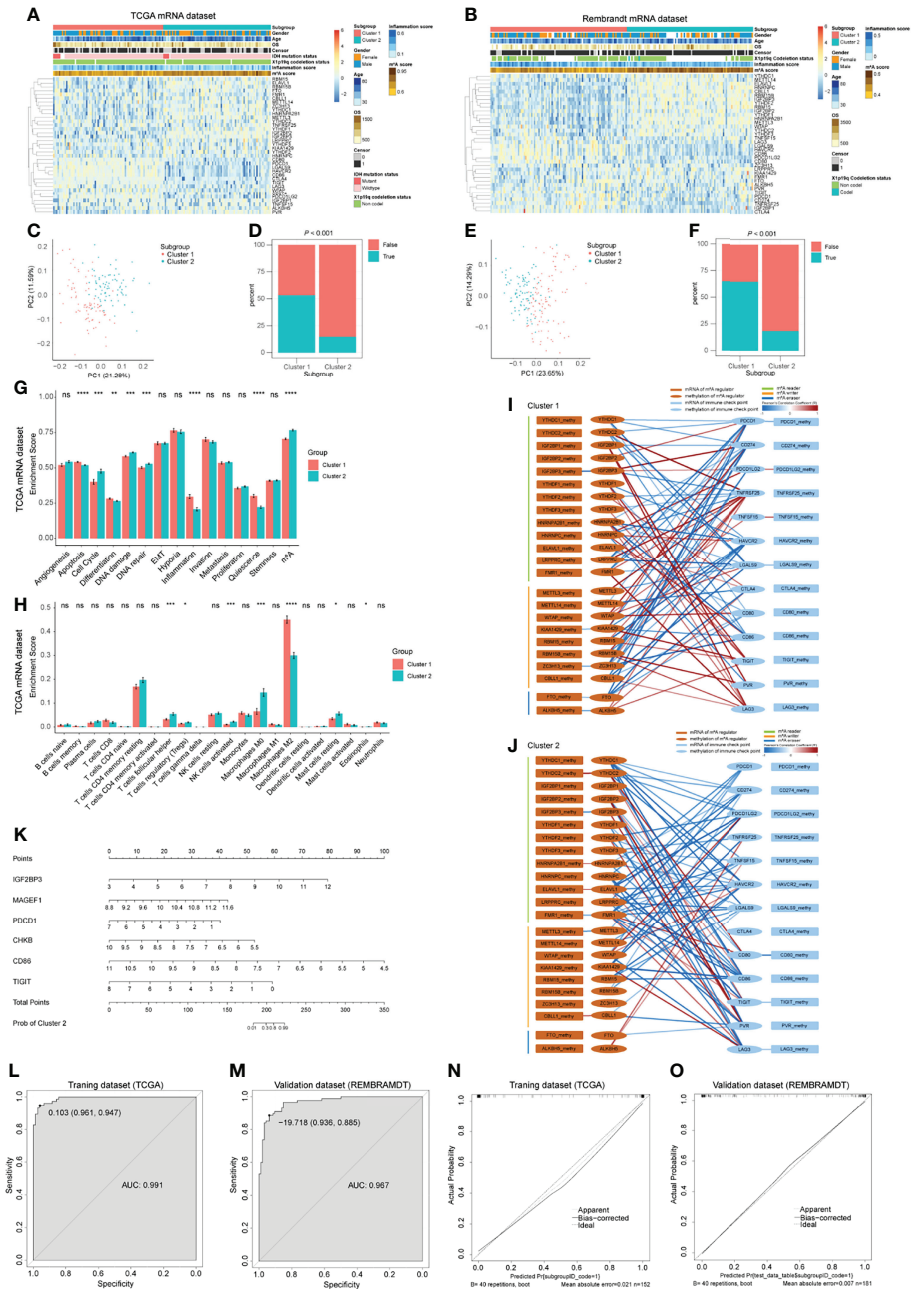

FIGURE 6 | Bulk RNA-seq analysis for GBM patients and predictive model construction and validation. **(A, B)** Heatmap of m^{6}A regulators and immune checkpoints (ICPs) revealed the different m^{6}A-ICP expression patterns for 2 clusters identified by consensus clustering (for TCGA **(A)** and REMBRANDT **(B)** datasets separately). **(C, E)** Principal component analysis of 2 identified clusters (for TCGA **(C)** and REMBRANDT **(E)** datasets separately). **(D, F)** Predicted potential therapeutic response of ICP inhibitors of 2 identified clusters (for TCGA **(D)** and REMBRANDT **(F)** datasets separately). **(G)** Bar charts illustrating the differences of functional state scores between 2 identified clusters for TCGA dataset. **(H)** Bar charts illustrating the differences of CIBERSORT scores between 2 identified clusters for TCGA dataset. ns: $P > 0.05$, $^*P \leq 0.05$, $^{**}P \leq 0.01$, $^{***}P \leq 0.001$, $^{****}P \leq 0.0001$. **(I, J)** Correlation network of the expression levels and methylation levels of m^{6}A regulators and ICPs in 2 identified clusters. **(K)** The nomogram for distinguishing 2 identified clusters. **(L, M)** ROC curves of the nomogram distinguishing 2 identified clusters (L for training dataset and G for validation dataset). **(N, O)** Calibrate plots of the nomogram distinguishing 2 identified clusters (N for training dataset and O for validation dataset).

immunotherapy. In the CGGA datasets, although no statistical significance was observed between these two clusters, cluster 1 showed a trend with higher response proportion to ICP inhibitor therapy (**Supplementary Figure 15F**). However, the overall survival and clinical characteristics, including age, gender, IDH mutation status, and X1p19q codeletion status, were similar between these two clusters (**Supplementary Figures 12G–J**).We further assessed the potential difference of functional

states between these 2 clusters. An ssGSEA analysis detected consistent trends between TCGA and REMBRAMDT datasets with statistical significance in the following functional states: apoptosis, cell cycle, DNA damage, DNA repair, inflammation, quiescence and m^{6}A modification (**Figure 6G**; **Supplementary Figures 13A**). In order to explore the immune infiltration of these 2 clusters, we utilized the CIBERSORT algorithm and compared the enrichment scores of 22 types of immune cells between these 2 clusters. Interestingly, in both TCGA and REMBRAMDT datasets, the proportion of follicular helper T cells in cluster 1 was lower than that in cluster 2, and there were more M2 macrophages in cluster 1 compared with cluster 2 (**Figure 6H**; **Supplementary Figure 13B**).

In revealing differences between the two clusters at the gene level, we detected 224 up-regulated DEGs and 33 down-regulated DEGs in cluster 1 compared with cluster 2 in TCGA dataset (**Supplementary Figure 13E**). However, no DEGs were found in the REMBRAMDT dataset. Enrichment analyses of these 224 up-regulated DEGs uncovered immune-related BP terms (**Supplementary Figure 13F**). KEGG analysis on the up-regulated DEGs was also conducted (**Supplementary Figure 13G**). We further performed PPI network analyses for all DEGs, and the "cytoHubba" plugin from Cytoscape software was used to reveal hub genes. *CASR*, *CCL19*, *CCR8*, *CCL13*, *RLN3*, *TAS2R42*, *SSTR4*, *MTNR1A*, and *RXFP3* were detected as hub genes (**Supplementary Figure 13H**).

In order to address the potential regulatory mechanism between m^{6}A regulators and ICPs at the multiomics level, samples with mRNA-seq profiles and DNA methylation profiles from TCGA were extracted for Pearson correlation analysis. Complex correlation networks of the expression levels and methylation levels of m^{6}A regulators and ICPs for all samples and two clusters, respectively, were constructed (**Supplementary Figure 14A**; **Figures 6I, J**). Extensive correlation between expression levels of m^{6}A regulators and ICPs were observed, and significant negative correlations between expression levels and DNA methylation levels were detected in *IGF2BP3*, *METTLE3*, *ALKBH5*, *CTLA4*, and *TIGIT* (**Supplementary Figure 14A**). In the subnetworks of these 2 clusters, more positive correlations between expression levels of m^{6}A regulators and ICPs were found in cluster 1. For *IGF2BP3*, a negative correlation between expression levels and DNA methylation levels were consistent in these two clusters. However, other statistically significant negative correlations between expression levels and DNA methylation levels were different between cluster 1 and 2 (**Figures 6I, J**). These results suggested different underlying mechanisms of the expression and DNA methylation of m^{6}A regulators and ICPs between cluster 1 and 2 GBM patients.

Construction and Validation of Predictive Model

Having demonstrated that these 2 clusters had distinct features, we next constructed and validated a predictive nomogram model to distinguish these 2 clusters. The LASSO algorithm identified 32 genes, with the optimal λ being 0.02800602 (**Supplementary Figures 14B, C**). Then, a best subset selection analysis was performed to determine the final model. Because of the limitations of the computing power of our device, we only analyzed models with up to 16 variables. The final model contains the following 6 variables: *IGF2BP3*, *MAGEF1*, *PDCD1*, *CHKB*, *CD86*, and *TIGIT*. The final multivariable logistic regression model was visualized as a nomogram (**Figure 6K**). The nomogram showed excellent discrimination performance in TCGA (training cohort, area under curve (AUC) = 0.991), REMBRANDT (validation cohort, AUC = 0.967) and CGGA (validation cohort, AUC = 0.721) datasets (**Figures 6L, M**; **Supplementary Figure 15G**). Calibration plots were drawn, and the calibration was as expected in both training and validation cohorts (**Figure 6N, O**; **Supplementary Figure 15H**). These evaluations proved that the nomogram model performed well in distinguishing these 2 GBM clusters.

DISCUSSION

Treatment, especially immunotherapy, for GBM remains a challenge (1, 2). The role of m^{6}A modification has been shown to be involved in cancer biology (4) and mediating immunotherapy resistance (6, 7). Therefore, there is an urgent need to apply new technologies, including single-cell analysis, to explore potential mechanisms of m^{6}A modification in the GBM microenvironment. However, to date, no study has provided an m^{6}A modification landscape for GBM microenvironment at the single-cell level. In this study, we retrieved single-cell RNA-seq datasets and used them to identify 7 types of cells in the GBM microenvironment and evaluated the associations between m^{6}A regulators and functional states, potential BP, cell communication, and ICPs for these cell types. We discovered that m^{6}A modification facilitates the stemness state in GBM cancer cells and promotes an immunosuppressive microenvironment through ICPs and the GALECTIN signaling pathway network. With bulk RNA-seq datasets, we further identified 2 clusters of patients with distinct m^{6}A-ICP expression patterns (low m^{6}A/high ICP and high m^{6}A/low ICP) and predicted the responses to ICP inhibitors. A well performing nomogram model was constructed to distinguish these 2 GBM clusters.

The high inter-tumor heterogeneity of GBM immune microenvironment has reached a broad consensus. In the current research, we observed high inter-tumor heterogeneity of M1 and M2 macrophage proportions (**Figure 2A**). In around half of included samples, the infiltration proportions of M2 macrophage were higher than that of M1 macrophages. And higher proportions of M1 macrophages were found in the other samples (**Figure 2I**). Sørensen et al. (23) reported interesting phenomenon that on average 44% and 8% of the tumor associated macrophages (TAM) expressed the marker HLA-DR and TNF-α for M1 macrophages, respectively, while 10% and 3% of TAMs expressed IL10 and TGF-β1, which were markers for M2 macrophages. Also, these proportions varied greatly among

different samples. These results indicated that the proportions of M1 and M2 macrophages in GBM have high inter-tumor heterogeneity.

There has been limited discussion about the distribution of expression of m^{6}A regulators in different cell types and throughout cell cycle phases. The bulk RNA-seq dataset revealed that most m^{6}A regulators have relatively high expression levels in GBM compared with levels in normal samples. This finding was especially apparent for *HNRNPA2B1*, *HNRNPC* and *WTAP* (**Supplementary Figure 2J**). A previous study has shown increased expression of *METTL3* and decreased expression levels of *METTL14* and *ALKBH5* and no significantly changes to the expression of *FTO* in GSCs (8). Another research detected elevated *ALKBH5* in GSCs (24). The present study detected the expression levels of 23 m^{6}A regulators in 7 types of cells and 3 cell cycle phases. We found that expression levels of m^{6}A regulators were higher in M1 macrophages, GBM cancer cells, and T/NK cells than in other types of cells (**Figure 3A**), and cells at G_1 phase showed higher expression levels of m^{6}A regulators relative to that of cells at S and G_2M phases (**Figure 3R**). *HNRNPA2B1* and *HNRNPC* had obviously higher expression levels than other m^{6}A regulators in all 7 types of cells and 3 cell cycle phases. Thus, besides the intratumor heterogeneity of m^{6}A regulators, we also detected obvious intertumor heterogeneity of cell types and cell cycle phases in different samples (**Figure 3Q**; **Supplementary Figure 3H**). These results suggested that the roles of m^{6}A modification in GBM may be different in different types of cells, and further investigations of m^{6}A modifications in GBM should take cell type into consideration.

Multiple studies have analyzed the mechanisms by which m^{6}A modification maintains stemness of GSCs. For example, *ALKBH5* promotes stemness of GSCs by sustaining *FOXM1* expression (24, 25) and *METTL3* (19), *HNRNPA2B1* and *HNRNPC* (26) maintain stemness of GSCs by targeting *SOX2*. The product of the *SOX2* gene is an oncogenic transcription factor in many cancers; accordingly, in the current research, we found significant positive correlations between *SOX2* and *YTHDC1*, *IGF2BP2*, *HNRNPC*, *ELAVL1*, *FMR1*, *KIAA1429*, and *ZC3H13* in GBM cancer cells (**Figure 4D, E**). Among these m^{6}A regulators, IGF2BP2 had been proven to be a downstream m^{6}A reader of *SOX2* in colorectal carcinoma (20). Our results suggested that *YTHDC1*, *IGF2BP2*, *HNRNPC*, *ELAVL1*, *FMR1*, *KIAA1429*, and *ZC3H13* may have potential interactions with *SOX2* and further promote stemness of GBM cancer cells. The research of Su et al. demonstrated that *FTO* plays a carcinogenic role maintaining the self-renewal ability of GSCs *via* *FTO*/m^{6}A/*MYC*/*CEBPA* signaling (27). Importantly, *MYC* is a commonly activated oncogene in human cancer. Our correlation analysis uncovered positive correlations between *MYC* and *IGF2BP1*, *YTHDF1*, *YTHDF2*, *YTHDF3*, *HNRNPC*, *LRPPRC*, *METTL3*, *WTAP*, *KIAA1429*, *RBM15*, *RBM15B*, *CBLL1*, *FTO*, and *ALKBH5* (**Figure 4D, E**). The *IGF2BP1* protein has been proposed to protect *MYC* mRNA from endonucleolytic attack (28). These results indicated a more extensive potential stemness regulation network between MYC and these m^{6}A regulators in GBM cancer cells.

The m^{6}A modification was reported to play a role in programmed cell death, including apoptosis (9, 29–32), ferroptosis (33, 34) and pyroptosis (35, 36). These studies mainly focused on cancer cells, and none of them have discussed the immune cells in the tumor microenvironment. In our research, we found that the m^{6}A score was significantly correlated with apoptosis, ferroptosis and pyroptosis in M1 macrophages and apoptosis and pyroptosis in T/NK cells in GBM microenvironment (**Figures 4A, B**). Further correlation analysis of m^{6}A regulators and these programmed cell death-related gene sets were visualized as regulation networks (**Supplementary Figures 4B–D, H, J**). These results indicated a potentially complex mechanism of m^{6}A modification-mediated programmed cell death in M1 macrophages and T/NK cells. It remains unknown whether programmed cell death in these immune cells could lead to the immunosuppressive microenvironment in GBM or not. And the regulatory role of m^{6}A regulators in these processes is still unclear. Further research is needed in order to verify these findings and to analyze its impact on the GBM microenvironment.

The GALECTIN signaling pathway network includes 3 ligand-receptor pairs (*LGALS9-CD44*, *LGALS9-CD45*, *LGALS9-HAVCR2*; **Supplementary Table S6**). *LGALS9* (Galectin-9) and *HAVCR2* (TIM-3) are known as immune check points. *CD45* (PTPRC) was an essential regulator of T cell activation (37), and *CD44* is involved in diverse cellular processes including proliferation, apoptosis, and angiogenesis (38). Limited studies have discussed the role of m^{6}A modification in the GALECTIN network. Wang et al. reported that *IGF2BP1* stabilizes mRNA transcripts of *CD44* and further promotes proliferation and invasion of GBM (39). A study from Lin et al. found positive correlations between expression of *YTHDF2* and *HAVCR2* in lower-grade glioma (40). In the current research, we observed robust occurrence of the GALECTIN network in included samples (**Supplementary Figures 6A, B**), which indicated that the GALECTIN network plays an important role in the GBM microenvironment. The network mainly started from M1 and M2 macrophages and was targeted at other types of cells in the GBM microenvironment. Relatively high expression levels of genes in the GALECTIN network were detected in M1 macrophages, M2 macrophages, and T/NK cells (**Supplementary Figure 10C**). Further correlation analysis found extensive significant correlations between m^{6}A regulators and genes in the GALECTIN network (**Supplementary Figures 7C, D**; **Supplementary Figure 8**). These results indicated that the m^{6}A modification was involved in the potential regulatory mechanism of the GALECTIN network. However, the detailed regulatory pathways between m^{6}A modification and the GALECTIN network is still known. And whether inhibiting the GALECTIN network by regulation of m^{6}A modification could lead to better prognosis of GBM patients remains to be further verified.

We conducted a series of *in vitro* experiments to validate the regulation role of *MDK* in GBM microenvironment (**Figure 5**). Based on our results, *MDK*, which was secreted by GBM cancer cells, induced the migration and immunosuppressive

polarization of macrophages. Our results were consistent with the role of MDK identified by Zhang et al. in 2021 (41). In their gallbladder cancer research, *MDK* interacts with its receptor *LRP1*, which is expressed by tumor-infiltrating macrophages, and further promotes immunosuppressive macrophage differentiation. We assume that MDK could be a treatment target for GBM, further *in vivo* validation and translational research are expected to develop a novel therapy for GBM.

Rapid progress in cancer immunotherapy, especially in the development of ICP inhibitors, has revolutionized the treatment of many solid tumors and driven the study of immunotherapy in glioma. However, the effect of ICP blockades in GBM has not been satisfactory (42). Some studies have found that m^6A modification was correlated with immune infiltration in glioma (43–47). However, to date, no research has analyzed the relationship between m^6A modification and ICPs in GBM. In the current study, we revealed extensive correlations between m^6A regulators and ICPs in GBM cancer cells, M2 macrophages, and T/NK cells (**Supplementary Figure 11**). Notably, in GBM cancer cells, *CD274* (PD-L1), *PDCD1LG2* (PD-L2), *LGALS9* (Galectin-9), and *PVR* (CD155) were correlated with m^6A regulators. In the bulk RNA-seq analysis, we identified 2 clusters of patients. Cluster 1 patients (low m^6A/high ICP) showed higher predicted response rates to ICP inhibitors, and cluster 2 patients (high m^6A/low ICP) had lower predicted response rates (**Figures 6A, B, D, F**). Although these 2 clusters showed different m^6A-ICP expression patterns, they had similar overall survival times (**Supplementary Figures 12I, J**). These results indicated that these 2 clusters may have different mechanisms for immune escape and require different treatment strategies.

In the current research, the LASSO analysis and best subset selection analysis filtered 6 genes, which could distinguish these 2 clusters. Among them, IGF2BP3 was a m^6A reader. PDCD1, CD86, and TIGIT were significant ICPs. MAGEF1 (melanoma antigen family F1) is a member of MAGE family and belongs to type 2 MAGE (T2M) category (48). Arora et al. 's research found that in glioma downregulation of T2Ms was associated with immune infiltration and poor overall survival (48). Weon et al. reported that MAGEF1 alters DNA repair enzymes *via* the cytosolic iron-sulfur cluster assembly (CIA) pathway (49). And MAGEF1 was highly amplified in multiple human cancer types and related with increased mutational burden (49). Based on these findings, MAGEF1 might related with ICPs *via* m6A modification or CIA pathways, which needed to be further explored. CHKB (choline kinase beta) played a key role maintaining the normal phosphatidylcholine level (50). The relationship between CHKB and glioma haven't been explored. Our results showed that lower expression level of CHKB suggested higher possibility of cluster 2 (high m^6A/low ICP; **Figure 6K**). However, the potential mechanisms need to be further analyzed.

Based on the correlations between m^6A regulators and ICPs found in the current study, we suggest that by targeting these related m^6A regulators, researchers may downregulate the expression of these immune suppressive ICPs and further enhance the efficacies of ICP inhibitors for cluster 2 patients. Further research is needed to verify these findings and to specify how it influences strategies directing the use of ICP inhibitors for GBM.

Research have found that tumors with extensive infiltration of immunosuppressive macrophages are refractory to ICP inhibitor therapy (51, 52). However, contrary results were observed in our research. TIDE algorithm predicted that cluster 1 was more responsive to ICP inhibitors (**Figures 6D, F**), and CIBERSORT algorithm showed higher M2 macrophage infiltration in cluster 1 (**Figure 6H**; **Supplementary Figure 13B**). These results may reflect the inner complexity of GBM. Further high-quality research of ICP inhibitors in GBM are expected.

The current research revealed the m^6A regulators expression landscape of GBM at single-cell level. Our research suggested that by altering the m^6A modification in GBM, researchers may be able to influence the stemness status and immunosuppressive microenvironment of GBM. Combined with immunotherapy, these regulations have potential to advance the treatment effect of immunotherapy.

Some limitations in the current study should be acknowledged. First, as a retrospective study, these analyses were conducted using published datasets, and the results about potential mechanisms of action of m^6A modifications in the GBM microenvironment need further experimental validation. Second, we were not able to identify clusters of GSCs and to separate the T/NK cluster into more detailed clusters. Here, the problem may be due to limited cell numbers for these cell types. Third, missing data was observed after merging the 5 single-cell datasets. However, the data of m^6A regulators was almost complete, and only a few datasets partially lacked genes for some ICPs (**Supplementary Table S3**). Also, the information regarding the rest of the genes is complete. To avoid the influence of the missing data in the analysis, we excluded samples with missing data in the analyses of correlations between m^6A regulators and ICPs (**Supplementary Figure 11**).

CONCLUSION

Through analyses at the single-cell level, for the first time, we discovered that m^6A modification facilitates stemness state in GBM cancer cells and promotes the immunosuppressive microenvironment through ICPs and the GALECTIN signaling pathway network in the GBM microenvironment. We further identified 2 clusters of patients with distinct m^6A-ICP expression patterns (low m^6A/high ICP and high m^6A/low ICP) and predicted the response of ICP inhibitors in bulk RNA-seq analysis. A well performing nomogram model was constructed to distinguish these 2 GBM clusters. We hope the novel understanding of the roles of m^6A modification in the GBM microenvironment may assist the development of immunotherapy and precision treatment in GBM.

DATA AVAILABILITY STATEMENT

Publicly available datasets were analyzed in this study. This data can be found here: The data analyzed in this study were obtained from Gene Expression Omnibus (GEO) at GSE141383, GSE138794, GSE84465, GSE103224, GSE89567, GSE124731 and GSE108474 (REMBRANDT), and from the Cancer Genome Atlas (TCGA, https://portal.gdc.cancer.gov/) and Chinese Glioma Genome Atlas (CGGA, http://www.cgga.org.cn/).

ETHICS STATEMENT

The studies involving human participants were reviewed and approved by Jinling Hospital research ethics board. The patients/participants provided their written informed consent to participate in this study.

AUTHOR CONTRIBUTIONS

CM, XC and SZ were involved in conception and design of the study. FY, XC, YG, YA, CD, JZ, JY, CT, and ZC were involved in development of methodology, acquisition of data, analysis and interpretation of data. XC was involved in writing of the manuscript. YW and AZ contributed to the interpretation of the experimental results. CM oversaw the conception and design of the study, interpretation of data and writing of the manuscript. All authors contributed to the article and approved the submitted version.

ACKNOWLEDGMENTS

We thank the authors of datasets (GSE141383, GSE138794, GSE84465, GSE103224, GSE89567, GSE124731, REMBRANDT, and TCGA) for sharing these valuable data. We thank Department of Neurosurgery, Jinling Hospital for help during the research. Special thanks to Wenjing Gou, Guodong Yuan, Hucheng Qin, Fengqi Zhou, Haining Lv, Huheng Fu, Xuan Wang, Shirong Ruan, Ting Tang, Peng Xu and Yanling Han for their help in the validation experiments.

SUPPLEMENTARY MATERIAL

The Supplementary Material for this article can be found online at: https://www.frontiersin.org/articles/10.3389/fimmu.2022.798583/full#supplementary-material

Supplementary Figure 1 | Quality control of samples from **(A)** GSE141383, **(B)** GSE138794, **(C)** GSE84465, **(D)** GSE103224, and **(E)** GSE89567 datasets.

Supplementary Figure 2 | Distribution of m^6A regulators in GBM microenvironment. **(A–I)** tSNE plots of 9 m^6A regulators. **(J)** Expression levels of 23 m^6A regulators in GBM and normal samples from bulk RNA-seq dataset in GEPIA website.

Supplementary Figure 3 | Expression levels of m^6A regulators in 3 cell cycles. **(A-G)** Expression levels of m^6A regulators in 3 stages of the cell cycle from GBM cancer cells **(A)**, oligodendrocytes **(B)**, astrocytes **(C)**, M1 macrophages **(D)**, M2 macrophages **(E)**, T/NK cells **(F)**, and endothelial cells **(G)**. **(H)** Distribution of 3 stages of the cell cycle in each included sample.

Supplementary Figure 4 | correlation network of m^6A regulators and functional states. **(A)** correlation network of m^6A regulators and differentiation related genes in GBM cancer cells. **(B-D)** correlation network of m^6A regulators and apoptosis **(B)**, ferroptosis **(C)**, and pyroptosis **(D)** related genes in M1 macrophages. **(E-G)** correlation network of m^6A regulators and EMT **(E)**, invasion **(F)**, and metastasis **(G)** related genes in M2 macrophages. **(H–J)** correlation network of m^6A regulators and apoptosis **(H)**, DNA damage **(I)**, and pyroptosis **(J)** related genes in T/NK cells. **(K-M)** correlation network of m^6A regulators and angiogenesis **(K)**, invasion **(L)**, and metastasis **(M)** related genes in endothelial cells.

Supplementary Figure 5 | m^6A related gene clusters and functional annotation. **(A-C)** PPI networks of cluster 1 **(A)**, cluster 2 **(B)**, and cluster 3 **(C)** of m^6A related genes in GBM cancer cells. **(D–F)** PPI networks of cluster 1 **(D)**, cluster 2 **(E)**, and cluster 3 **(F)** of m^6A related genes in M1 macrophages. **(G-I)** PPI networks of cluster 1 **(G)**, cluster 2 **(H)**, and cluster 3 **(I)** of m^6A related genes in M2 macrophages. **(J, K)** PPI networks of cluster 1 **(J)**, and cluster 2 **(K)** of m^6A related genes in T/NK cells. **(L-N)** PPI networks of cluster 1 **(L)**, cluster 2 **(M)**, and cluster 3 **(N)** of m^6A related genes in endothelial cells. **(O-Q)** PPI network and enriched biological process terms of cluster 1 **(O)**, cluster 2 **(P)**, and cluster 3 **(Q)** of m^6A related genes in oligodendrocytes.

Supplementary Figure 6 | Cell communication analysis reveals robust signal pathways in the GBM cancer microenvironment. **(A, B)** The GALECTIN signaling pathway network as detected in cell communication analyses for all samples **(A)** and each sample **(B)**. **(C, D)** The GRN signaling pathway network as detected in cell communication analyses for all samples **(C)** and each sample **(D)**. **(E, F)** The PTN signaling pathway network as detected in cell communication analyses for all samples **(E)** and each sample **(F)**. **(G, H)** The SPP1 signaling pathway network as detected in cell communication analyses for all samples **(G)** and each sample **(H)**. **(I, J)** The ANNEXIN signaling pathway network as detected in cell communication analyses for all samples **(I)** and each sample **(J)**. **(K, L)** The VISFATIN signaling pathway network as detected in cell communication analyses for all samples **(K)** and each sample **(L)**. **(M, N)** The MK signaling pathway network as detected in cell communication analyses for all samples **(M)** and each sample **(N)**.

Supplementary Figure 7 | Correlation analysis of m^6A regulators and genes in signaling pathway networks in GBM cancer cells and M1 macrophages. **(A, B)** Correlation heatmap **(A)** and correlation analysis **(B)** of m^6A regulators and genes in signaling pathway networks in GBM cancer cells. **(C, D)** Correlation heatmap **(C)** and correlation analysis **(D)** of m^6A regulators and genes in signaling pathway networks in M1 macrophages. NS: $P > 0.05$, $^*P \le 0.05$, $^{**}P \le 0.01$, $^{***}P \le 0.001$.

Supplementary Figure 8 | Correlation analysis of m^6A regulators and genes in signaling pathway networks in M2 macrophages and T/NK cells. **(A, B)** Correlation heatmap **(A)** and correlation analysis **(B)** of m^6A regulators and genes in signaling pathway networks in M2 macrophages. **(C, D)** Correlation heatmap **(C)** and correlation analysis **(D)** of m^6A regulators and genes in signaling pathway networks in T/NK cells. NS: $P > 0.05$, $^*P \le 0.05$, $^{**}P \le 0.01$, $^{***}P \le 0.001$.

Supplementary Figure 9 | Correlation analysis of m^6A regulators and genes in signaling pathway networks in endothelial cells and astrocytes. **(A, B)** Correlation heatmap **(A)** and correlation analysis **(B)** of m^6A regulators and genes in signaling pathway networks in endothelial cells. **(C, D)** Correlation heatmap **(C)** and correlation analysis **(D)** of m^6A regulators and genes in signaling pathway networks in astrocytes. NS: $P > 0.05$, $^*P \le 0.05$, $^{**}P \le 0.01$, $^{***}P \le 0.001$.

Supplementary Figure 10 | Correlation analysis of m^6A regulators and genes in signaling pathway networks in oligodendrocytes. **(A, B)** Correlation heatmap **(A)** and correlation analysis **(B)** of m^6A regulators and genes in signaling pathway networks in oligodendrocytes. **(C)** Expression levels of genes in signaling pathway networks in 7 cell types. NS: $P > 0.05$, $^*P \le 0.05$, $^{**}P \le 0.01$, $^{***}P \le 0.001$.

Supplementary Figure 11 | Correlation analysis of m^6A regulators and immune checkpoints (ICPs). **(A, B)** Correlation heatmap **(A)** and correlation analysis **(B)** of m^6A regulators and ICPs in GBM cancer cells. **(C, D)** Correlation heatmap **(C)** and correlation analysis **(D)** of m^6A regulators and ICPs in M1 macrophages. **(E, F)** Correlation heatmap **(E)** and correlation analysis **(F)** of m^6A regulators and ICPs in M2 macrophages. **(G, H)** Correlation heatmap **(G)** and correlation analysis (H) of m^6A regulators and ICPs in T/NK cells. **(I, J)** Correlation heatmap **(I)** and correlation analysis (J) of m^6A regulators and ICPs in endothelial cells. **(K, L)** Correlation heatmap (K) and correlation analysis (L) of m^6A regulators and ICPs in astrocytes. **(M, N)** Correlation heatmap (M) and correlation analysis (N) of m^6A regulators and ICPs in oligodendrocytes. NS: $P > 0.05$, $^*P \le 0.05$, $^{**}P \le 0.01$, $^{***}P \le 0.001$.

Supplementary Figure 12 | Identification and validation of 2 clusters of GBM patients in bulk RNA-seq analysis. **(A, D)** Consensus clustering matrix for k = 2, which was the optimal cluster number in the TCGA dataset **(A)** and REMBRANDT dataset **(D)**. **(B, E)** CDF curves of the consensus score (k = 2-6) in the TCGA dataset **(B)** and REMBRANDT dataset **(E)**. **(C, F)** Relative change in the area under the CDF curve (k = 2-6) in the TCGA dataset **(C)** and REMBRANDT dataset **(F)**. **(G, H)** Clinical features of 2 identified clusters in the TCGA dataset **(G)** and REMBRANDT dataset **(H)**. **(I, J)** Kaplan-Meier survival analyses of 2 identified clusters in the TCGA dataset **(I)** and REMBRANDT dataset **(J)**

Supplementary Figure 13 | comparison of 2 identified clusters of GBM patients in bulk RNA-seq analysis. **(A)** Bar charts illustrating the differences of functional state scores between 2 identified clusters for REMBRANDT dataset. **(B)** Bar charts illustrating the differences of functional state scores between 2 identified clusters for REMBRANDT dataset. **(C, D)** Bar charts illustrating the differences of expression levels of m^6A regulators, immune checkpoints, and genes in detected cell communication signaling pathway networks between 2 identified clusters for TCGA **(C)** and REMBRANDT **(D)** dataset. **(E)** Volcano plot of differentially expressed genes (DEGs) between 2 identified clusters in TCGA dataset. **(F, G)** GO **(F)** and KEGG **(G)** analyses of up-regulated DEGs in TCGA dataset. **(H)** PPI network showing hub genes of up-regulated DEGs in TCGA dataset. ns: $P > 0.05$, $^*P \le 0.05$, $^{**}P \le 0.01$, $^{***}P \le 0.001$, $^{****}P \le 0.0001$.

Supplementary Figure 14 | Multiomic analysis and LASSO analysis. **(A)** Correlation network of the expression levels and methylation levels of m^6A regulators and ICPs in all GBM samples from TCGA dataset. **(B, C)** LASSO regression analysis of training dataset (TCGA).

Supplementary Figure 15 | Bulk RNA-seq analysis with CGGA dataset. **(A),** Consensus clustering matrix for k = 2, which was the optimal cluster number in the CGGA dataset. **(B)** CDF curves of the consensus score (k = 2-6) in the CGGA dataset. **(C)** Relative change in the area under the CDF curve (k = 2-6) in the CGGA dataset. **(D)** Heatmap of m^6A regulators and immune checkpoints (ICPs) revealed the different m^6A-ICP expression patterns for 2 clusters identified by consensus clustering for CGGA dataset. **(E)** Principal component analysis of 2 identified clusters for CGGA dataset. **(F)** Predicted potential therapeutic response of ICP inhibitors of 2 identified clusters for CGGA dataset. **(G)** ROC curve of the nomogram distinguishing 2 identified clusters for validation dataset (CGGA). **(H)** Calibrate plot of the nomogram distinguishing 2 identified clusters for validation dataset (CGGA).

REFERENCES

1. Wu W, Klockow JL, Zhang M, Lafortune F, Chang E, Jin L, et al. Glioblastoma Multiforme (GBM): An Overview of Current Therapies and Mechanisms of Resistance. *Pharmacol Res* (2021) 171:105780. doi: 10.1016/j.phrs.2021.105780
2. Ostrom QT, Cioffi G, Gittleman H, Patil N, Waite K, Kruchko C, et al. CBTRUS Statistical Report: Primary Brain and Other Central Nervous System Tumors Diagnosed in the United States in 2012-2016. *Neuro Oncol* (2019) 2:1: v1–v100. doi: 10.1093/neuonc/noz150
3. Ott M, Prins RM, Heimberger AB. The Immune Landscape of Common CNS Malignancies: Implications for Immunotherapy. *Nat Rev Clin Oncol* (2021) 18:794–44. doi: 10.1038/s41571-021-00518-9
4. Zaccara S, Ries RJ, Jaffrey SR. Reading, Writing and Erasing mRNA Methylation. *Nat Rev Mol Cell Biol* (2019) 20:608–24. doi: 10.1038/s41580-019-0168-5
5. Huang W, Chen TQ, Fang K, Zeng ZC, Ye H, Chen YQ. N6-Methyladenosine Methyltransferases: Functions, Regulation, and Clinical Potential. *J Hematol Oncol* (2021) 14:117. doi: 10.1186/s13045-021-01129-8
6. Yin H, Zhang X, Yang P, Zhang X, Peng Y, Li D, et al. RNA M6a Methylation Orchestrates Cancer Growth and Metastasis *via* Macrophage Reprogramming. *Nat Commun* (2021) 12:1394. doi: 10.1038/s41467-021-21514-8
7. Wang L, Hui H, Agrawal K, Kang Y, Li N, Tang R, et al. M(6) A RNA Methyltransferases METTL3/14 Regulate Immune Responses to Anti-PD-1 Therapy. *EMBO J* (2020) 39:e104514. doi: 10.15252/embj.2020104514
8. Zhang Y, Geng X, Li Q, Xu J, Tan Y, Xiao M, et al. M6a Modification in RNA: Biogenesis, Functions and Roles in Gliomas. *J Exp Clin Cancer Res* (2020) 39:192. doi: 10.1186/s13046-020-01706-8
9. Li F, Zhang C, Zhang G. M6a RNA Methylation Controls Proliferation of Human Glioma Cells by Influencing Cell Apoptosis. *Cytogenet Genome Res* (2019) 159:119–25. doi: 10.1159/000499062
10. Chai RC, Wu F, Wang QX, Zhang S, Zhang KN, Liu YQ, et al. M(6)A RNA Methylation Regulators Contribute to Malignant Progression and Have Clinical Prognostic Impact in Gliomas. *Aging (Albany NY)* (2019) 11:1204–25. doi: 10.18632/aging.101829
11. Yuan J, Levitin HM, Frattini V, Bush EC, Boyett DM, Samanamud J, et al. Single-Cell Transcriptome Analysis of Lineage Diversity in High-Grade Glioma. *Genome Med* (2018) 10:57. doi: 10.1186/s13073-018-0567-9
12. Darmanis S, Sloan SA, Croote D, Mignardi M, Chernikova S, Samghababi P, et al. Single-Cell RNA-Seq Analysis of Infiltrating Neoplastic Cells at the Migrating Front of Human Glioblastoma. *Cell Rep* (2017) 21:1399–410. doi: 10.1016/j.celrep.2017.10.030
13. Chen AX, Gartrell RD, Zhao J, Upadhyayula PS, Zhao W, Yuan J, et al. Single-Cell Characterization of Macrophages in Glioblastoma Reveals MARCO as a Mesenchymal Pro-Tumor Marker. *Genome Med* (2021) 13:88. doi: 10.1186/s13073-021-00906-x
14. Wang L, Babikir H, Müller S, Yagnik G, Shamardani K, Catalan F, et al. The Phenotypes of Proliferating Glioblastoma Cells Reside on a Single Axis of Variation. *Cancer Discov* (2019) 9:1708–19. doi: 10.1158/2159-8290.Cd-19-0329
15. Venteicher AS, Tirosh I, Hebert C, Yizhak K, Neftel C, Filbin MG, et al. Decoupling Genetics, Lineages, and Microenvironment in IDH-Mutant Gliomas by Single-Cell RNA-Seq. *Science* (2017) 355:eaai8478. doi: 10.1126/science.aai8478
16. Gusev Y, Bhuvaneshwar K, Song L, Zenklusen JC, Fine H, Madhavan S. The REMBRANDT Study, a Large Collection of Genomic Data From Brain Cancer Patients. *Sci Data* (2018) 5:180158. doi: 10.1038/sdata.2018.158
17. Hao Y, Hao S, Andersen-Nissen E, Mauck WM 3rd, Zheng S, Butler A, et al. Integrated Analysis of Multimodal Single-Cell Data. *Cell* (2021) 184:3573–87.e29. doi: 10.1016/j.cell.2021.04.048
18. Zhang X, Lan Y, Xu J, Quan F, Zhao E, Deng C, et al. CellMarker: A Manually Curated Resource of Cell Markers in Human and Mouse. *Nucleic Acids Res* (2019) 47:D721–d8. doi: 10.1093/nar/gky900
19. Visvanathan A, Patil V, Arora A, Hegde AS, Arivazhagan A, Santosh V, et al. Essential Role of METTL3-Mediated M(6)A Modification in Glioma Stem-Like Cells Maintenance and Radioresistance. *Oncogene* (2018) 37:522–33. doi: 10.1038/onc.2017.351
20. Li T, Hu PS, Zuo Z, Lin JF, Li X, Wu QN, et al. METTL3 Facilitates Tumor Progression *via* an M(6)A-IGF2BP2-Dependent Mechanism in Colorectal Carcinoma. *Mol Cancer* (2019) 18:112. doi: 10.1186/s12943-019-1038-7
21. Gieseke F, Kruchen A, Tzaribachev N, Bentzien F, Dominici M, Müller I. Proinflammatory Stimuli Induce Galectin-9 in Human Mesenchymal Stromal Cells to Suppress T-Cell Proliferation. *Eur J Immunol* (2013) 43:2741–9. doi: 10.1002/eji.201343335
22. Mantuano E, Brifault C, Lam MS, Azmoon P, Gilder AS, Gonias SL. LDL Receptor-Related Protein-1 Regulates Nfκb and microRNA-155 in Macrophages to Control the Inflammatory Response. *Proc Natl Acad Sci USA* (2016) 113:1369–74. doi: 10.1073/pnas.1515480113
23. Sørensen MD, Dahlrot RH, Boldt HB, Hansen S, Kristensen BW. Tumour-Associated Microglia/Macrophages Predict Poor Prognosis in High-Grade

Gliomas and Correlate With an Aggressive Tumour Subtype. *Neuropathol Appl Neurobiol* (2018) 44:185–206. doi: 10.1111/nan.12428
24. Cui Q, Shi H, Ye P, Li L, Qu Q, Sun G, et al. M(6)A RNA Methylation Regulates the Self-Renewal and Tumorigenesis of Glioblastoma Stem Cells. *Cell Rep* (2017) 18:2622–34. doi: 10.1016/j.celrep.2017.02.059
25. Zhang S, Zhao BS, Zhou A, Lin K, Zheng S, Lu Z, et al. M(6)A Demethylase ALKBH5 Maintains Tumorigenicity of Glioblastoma Stem-Like Cells by Sustaining FOXM1 Expression and Cell Proliferation Program. *Cancer Cell* (2017) 31:591–606.e6. doi: 10.1016/j.ccell.2017.02.013
26. Fang X, Yoon JG, Li L, Tsai YS, Zheng S, Hood L, et al. Landscape of the SOX2 Protein-Protein Interactome. *Proteomics* (2011) 11:921–34. doi: 10.1002/pmic.201000419
27. Su R, Dong L, Li C, Nachtergaele S, Wunderlich M, Qing Y, et al. R-2hg Exhibits Anti-Tumor Activity by Targeting FTO/m(6)A/MYC/CEBPA Signaling. *Cell* (2018) 172:90–105.e23. doi: 10.1016/j.cell.2017.11.031
28. Bell JL, Wächter K, Mühleck B, Pazaitis N, Köhn M, Lederer M, et al. Insulin-Like Growth Factor 2 mRNA-Binding Proteins (IGF2BPs): Post-Transcriptional Drivers of Cancer Progression? *Cell Mol Life Sci* (2013) 70:2657–75. doi: 10.1007/s00018-012-1186-z
29. Xi Z, Wang P, Xue Y, Shang C, Liu X, Ma J, et al. Overexpression of miR-29a Reduces the Oncogenic Properties of Glioblastoma Stem Cells by Downregulating Quaking Gene Isoform 6. *Oncotarget* (2017) 8:24949–63. doi: 10.18632/oncotarget.15327
30. Vu LP, Pickering BF, Cheng Y, Zaccara S, Nguyen D, Minuesa G, et al. The N (6)-Methyladenosine (M(6)A)-Forming Enzyme METTL3 Controls Myeloid Differentiation of Normal Hematopoietic and Leukemia Cells. *Nat Med* (2017) 23:1369–76. doi: 10.1038/nm.4416
31. Park YM, Hwang SJ, Masuda K, Choi KM, Jeong MR, Nam DH, et al. Heterogeneous Nuclear Ribonucleoprotein C1/C2 Controls the Metastatic Potential of Glioblastoma by Regulating PDCD4. *Mol Cell Biol* (2012) 32:4237–44. doi: 10.1128/mcb.00443-12
32. Deng J, Chen S, Wang F, Zhao H, Xie Z, Xu Z, et al. Effects of hnRNP A2/B1 Knockdown on Inhibition of Glioblastoma Cell Invasion, Growth and Survival. *Mol Neurobiol* (2016) 53:1132–44. doi: 10.1007/s12035-014-9080-3
33. Ma L, Zhang X, Yu K, Xu X, Chen T, Shi Y, et al. Targeting SLC3A2 Subunit of System X(C)(-) is Essential for M(6)A Reader YTHDC2 to be an Endogenous Ferroptosis Inducer in Lung Adenocarcinoma. *Free Radic Biol Med* (2021) 168:25–43. doi: 10.1016/j.freeradbiomed.2021.03.023
34. Song Z, Jia G, Ma P, Cang S. Exosomal miR-4443 Promotes Cisplatin Resistance in Non-Small Cell Lung Carcinoma by Regulating FSP1 M6a Modification-Mediated Ferroptosis. *Life Sci* (2021) 276:119399. doi: 10.1016/j.lfs.2021.119399
35. Guo M, Yan R, Ji Q, Yao H, Sun M, Duan L, et al. IFN Regulatory Factor-1 Induced Macrophage Pyroptosis by Modulating M6a Modification of Circ_0029589 in Patients With Acute Coronary Syndrome. *Int Immunopharmacol* (2020) 86:106800. doi: 10.1016/j.intimp.2020.106800
36. Diao MY, Zhu Y, Yang J, Xi SS, Wen X, Gu Q, et al. Hypothermia Protects Neurons Against Ischemia/Reperfusion-Induced Pyroptosis *via* M6a-Mediated Activation of PTEN and the PI3K/Akt/GSK-3β Signaling Pathway. *Brain Res Bull* (2020) 159:25–31. doi: 10.1016/j.brainresbull.2020.03.011
37. Al Barashdi MA, Ali A, McMullin MF, Mills K. Protein Tyrosine Phosphatase Receptor Type C (PTPRC or CD45). *J Clin Pathol* (2021) 74:548–52. doi: 10.1136/jclinpath-2020-206927
38. Mooney KL, Choy W, Sidhu S, Pelargos P, Bui TT, Voth B, et al. The Role of CD44 in Glioblastoma Multiforme. *J Clin Neurosci* (2016) 34:1–5. doi: 10.1016/j.jocn.2016.05.012
39. Wang RJ, Li JW, Bao BH, Wu HC, Du ZH, Su JL, et al. MicroRNA-873 (miRNA-873) Inhibits Glioblastoma Tumorigenesis and Metastasis by Suppressing the Expression of IGF2BP1. *J Biol Chem* (2015) 290:8938–48. doi: 10.1074/jbc.M114.624700
40. Lin X, Wang Z, Yang G, Wen G, Zhang H. YTHDF2 Correlates With Tumor Immune Infiltrates in Lower-Grade Glioma. *Aging (Albany NY)* (2020) 12:18476–500. doi: 10.18632/aging.103812
41. Zhang Y, Zuo C, Liu L, Hu Y, Yang B, Qiu S, et al. Single-Cell RNA-Sequencing Atlas Reveals an MDK-Dependent Immunosuppressive Environment in ErbB Pathway-Mutated Gallbladder Cancer. *J Hepatol* (2021) 75:1128–41. doi: 10.1016/j.jhep.2021.06.023
42. Ho RLY, Ho IAW. Recent Advances in Glioma Therapy: Combining Vascular Normalization and Immune Checkpoint Blockade. *Cancers (Basel)* (2021) 13:3686. doi: 10.3390/cancers13153686
43. Xu S, Tang L, Dai G, Luo C, Liu Z. Expression of M6a Regulators Correlated With Immune Microenvironment Predicts Therapeutic Efficacy and Prognosis in Gliomas. *Front Cell Dev Biol* (2020) 8:594112. doi: 10.3389/fcell.2020.594112
44. Lin S, Xu H, Zhang A, Ni Y, Xu Y, Meng T, et al. Prognosis Analysis and Validation of M(6)A Signature and Tumor Immune Microenvironment in Glioma. *Front Oncol* (2020) 10:541401. doi: 10.3389/fonc.2020.541401
45. Pan Y, Xiao K, Li Y, Li Y, Liu Q. RNA N6-Methyladenosine Regulator-Mediated Methylation Modifications Pattern and Immune Infiltration Features in Glioblastoma. *Front Oncol* (2021) 11:632934. doi: 10.3389/fonc.2021.632934
46. Du J, Ji H, Ma S, Jin J, Mi S, Hou K, et al. M6a Regulator-Mediated Methylation Modification Patterns and Characteristics of Immunity and Stemness in Low-Grade Glioma. *Brief Bioinform* (2021) 22:bbab013. doi: 10.1093/bib/bbab013
47. Zheng J, Wang X, Qiu Y, Wang M, Yu H, Zhou Z, et al. Identification of Critical M(6)A RNA Methylation Regulators With Prognostic Value in Lower-Grade Glioma. *BioMed Res Int* (2021) 2021:9959212. doi: 10.1155/2021/9959212
48. Arora M, Kumari S, Singh J, Chopra A, Chauhan SS. Downregulation of Brain Enriched Type 2 MAGEs Is Associated With Immune Infiltration and Poor Prognosis in Glioma. *Front Oncol* (2020) 10:573378. doi: 10.3389/fonc.2020.573378
49. Weon JL, Yang SW, Potts PR. Cytosolic Iron-Sulfur Assembly Is Evolutionarily Tuned by a Cancer-Amplified Ubiquitin Ligase. *Mol Cell* (2018) 69:113–25.e6. doi: 10.1016/j.molcel.2017.11.010
50. Bardhan M, Polavarapu K, Bevinahalli NN, Veeramani PK, Anjanappa RM, Arunachal G, et al. Megaconial Congenital Muscular Dystrophy Secondary to Novel CHKB Mutations Resemble Atypical Rett Syndrome. *J Hum Genet* (2021) 66:813–23. doi: 10.1038/s10038-021-00913-1
51. Kawashima S, Inozume T, Kawazu M, Ueno T, Nagasaki J, Tanji E, et al. TIGIT/CD155 Axis Mediates Resistance to Immunotherapy in Patients With Melanoma With the Inflamed Tumor Microenvironment. *J Immunother Cancer* (2021) 9:e003134. doi: 10.1136/jitc-2021-003134
52. Yang F, He Z, Duan H, Zhang D, Li J, Yang H, et al. Synergistic Immunotherapy of Glioblastoma by Dual Targeting of IL-6 and CD40. *Nat Commun* (2021) 12:3424. doi: 10.1038/s41467-021-23832-3

Conflict of Interest: The authors declare that the research was conducted in the absence of any commercial or financial relationships that could be construed as a potential conflict of interest.

Publisher's Note: All claims expressed in this article are solely those of the authors and do not necessarily represent those of their affiliated organizations, or those of the publisher, the editors and the reviewers. Any product that may be evaluated in this article, or claim that may be made by its manufacturer, is not guaranteed or endorsed by the publisher.

Copyright © 2022 Yuan, Cai, Cong, Wang, Geng, Aili, Du, Zhu, Yang, Tang, Zhang, Zhao and Ma. This is an open-access article distributed under the terms of the Creative Commons Attribution License (CC BY). The use, distribution or reproduction in other forums is permitted, provided the original author(s) and the copyright owner(s) are credited and that the original publication in this journal is cited, in accordance with accepted academic practice. No use, distribution or reproduction is permitted which does not comply with these terms.

frontiers | Frontiers in Immunology

ORIGINAL RESEARCH
published: 23 May 2022
doi: 10.3389/fimmu.2022.899710

Recurrence- and Malignant Progression-Associated Biomarkers in Low-Grade Gliomas and Their Roles in Immunotherapy

Chubei Teng[1,2,3], *Yongwei Zhu*[1,2], *Yueshuo Li*[2], *Luohuan Dai*[1,2], *Zhouyang Pan*[1,2], *Siyi Wanggou*[1,2*] and *Xuejun Li*[1,2*]

[1] Department of Neurosurgery, Xiangya Hospital, Central South University, Changsha, China, [2] Hunan International Scientific and Technological Cooperation Base of Brain Tumor Research, Xiangya Hospital, Central South University, Changsha, China, [3] Department of Neurosurgery, The First Affiliated Hospital, University of South China, Hengyang, China

OPEN ACCESS

Edited by:
Wen Cheng,
The First Affiliated Hospital of China Medical University, China

Reviewed by:
Shimin Shuai,
Southern University of Science and Technology, China
Jie Xiong,
Changsha University, China

***Correspondence:**
Xuejun Li
lxjneuro@csu.edu.cn
Siyi Wanggou
zokygwong@gmail.com

Specialty section:
This article was submitted to Cancer Immunity and Immunotherapy, a section of the journal Frontiers in Immunology

Received: 19 March 2022
Accepted: 12 April 2022
Published: 23 May 2022

Citation:
Teng C, Zhu Y, Li Y, Dai L, Pan Z, Wanggou S and Li X (2022) Recurrence- and Malignant Progression-Associated Biomarkers in Low-Grade Gliomas and Their Roles in Immunotherapy. Front. Immunol. 13:899710. doi: 10.3389/fimmu.2022.899710

Despite a generally better prognosis than high-grade glioma (HGG), recurrence and malignant progression are the main causes for the poor prognosis and difficulties in the treatment of low-grade glioma (LGG). It is of great importance to learn about the risk factors and underlying mechanisms of LGG recurrence and progression. In this study, the transcriptome characteristics of four groups, namely, normal brain tissue and recurrent LGG (rLGG), normal brain tissue and secondary glioblastoma (sGBM), primary LGG (pLGG) and rLGG, and pLGG and sGBM, were compared using Chinese Glioma Genome Atlas (CGGA) and Genotype-Tissue Expression Project (GTEx) databases. In this study, 296 downregulated and 396 upregulated differentially expressed genes (DEGs) with high consensus were screened out. Univariate Cox regression analysis of data from The Cancer Genome Atlas (TCGA) yielded 86 prognostically relevant DEGs; a prognostic prediction model based on five key genes (HOXA1, KIF18A, FAM133A, HGF, and MN1) was established using the least absolute shrinkage and selection operator (LASSO) regression dimensionality reduction and multivariate Cox regression analysis. LGG was divided into high- and low-risk groups using this prediction model. Gene Set Enrichment Analysis (GSEA) revealed that signaling pathway differences in the high- and low-risk groups were mainly seen in tumor immune regulation and DNA damage-related cell cycle checkpoints. Furthermore, the infiltration of immune cells in the high- and low-risk groups was analyzed, which indicated a stronger infiltration of immune cells in the high-risk group than that in the low-risk group, suggesting that an immune microenvironment more conducive to tumor growth emerged due to the interaction between tumor and immune cells. The tumor mutational burden and tumor methylation burden in the high- and low-risk groups were also analyzed, which indicated higher gene mutation burden and lower DNA methylation level in the high-risk group, suggesting that with the accumulation of genomic mutations and epigenetic changes, tumor cells continued to evolve and led to the

progression of LGG to HGG. Finally, the value of potential therapeutic targets for the five key genes was analyzed, and findings demonstrated that KIF18A was the gene most likely to be a potential therapeutic target. In conclusion, the prediction model based on these five key genes can better identify the high- and low-risk groups of LGG and lay a solid foundation for evaluating the risk of LGG recurrence and malignant progression.

Keywords: low-grade glioma (LGG), recurrence, malignant progression, cell cycle checkpoint, immune microenvironment, nomogram

INTRODUCTION

Low-grade gliomas (LGGs) make up about 7.6% of all brain tumors and 31.8% of gliomas. Occurring at all ages, LGGs have an incidence rate of 2.31/100,000 in the 0–14 years age group, 1.43/10,000 for 15–39 years of age, and 1.57/100,000 in the age group of 40 years and older. Besides, LGG incidence is higher in men (5.51/10,000) than in women (3.65/100,000) (1). Surgical resection remains the mainstay of treatment for LGGs, and adjuvant treatment with chemoradiotherapy is administered if needed. Reportedly, LGG patients have a 5-year survival rate of 70%–97% and a 10-year survival rate of 49%–76% (2, 3). About 52%–62% of patients have a recurrence within 5 years (4–6). In these recurrent cases, some have LGGs, while 17%–32% progress to high-grade gliomas (HGGs) (7–10). Worse prognosis of recurrent LGGs is predominantly a resultant of their malignant transformation. It is currently believed that the transition of LGGs to more aggressive HGGs is induced by the intrinsic diversity and heterogeneity of tumor cells that evolve to overt malignancy and develop resistance to therapy during tumor growth, eventually leading to a worse prognosis (11).

In the studies on the recurrence and evolution of gliomas by (12, 13) exome sequencing and DNA methylation data were derived from 23 and 19 patients before and after recurrence, respectively, for comparative analysis, from which the researchers discovered intratumoral heterogeneity during initial growth and subclones sharing epigenetic [glioma CpG island methylator phenotype (G-CIMP)] alterations, TP53 and ATRX mutations, and copy number alterations (12, 13). Although LGGs may come back without malignant progression after subtotal resection, some distinct subclones may give rise to HGGs spontaneously or following the use of temozolomide (TMZ). Particularly, spontaneous evolution is associated with alterations in cell cycle genes caused by gene mutations and promoter hypomethylation. Treatment-associated progression to HGGs involves downregulation of RB gene expression, activation of AKT-Mammalian Target Of Rapamycin (AKT-mTOR) pathway, genetic defects in the DNA mismatch repair (MMR) pathway, and hypermethylation of O^6-methylguanine-DNA methyltransferase (MGMT) (13, 14). By comparing the DNA and RNA sequencing data of LGG patients with those with recurrent LGGs evolving to secondary glioblastoma (sGBM), Jiang et al. discovered that sGBM was significantly enriched with TP53 mutation, somatic hypermutation, MET-exon-14 (METex14) skipping, PTPRZ1-MET (ZM) fusion, and MET amplification; from their point of view, METex14 suppresses MET degradation and activates the Signal Transducer and Activator of Transcription 3 (STAT3) signaling pathway to promote tumor growth and angiogenesis and result in a significantly worse prognosis (15). Therefore, mutations in key genes and accumulation of mutations are the driving forces for the evolution and malignant progression of LGG.

Ample evidence has demonstrated the immunosuppressive nature of gliomas in the antitumor immune response. Antigen presentation was limited by the elevated expression of immunosuppressive factors in glioma cells such as programmed cell death ligand 1 (PD-L1) and indolamine 2,3-dioxygenase (IDO) (16). Glioma-associated microglia and macrophages (GAMs) inhibit immune cell activity by producing interleukin-10 (IL-10), chemokine C-C ligand 20 (CCL20), CCL22, and prostaglandin E2.5 (17). Moreover, regulatory T cells (Tregs) mediate immunosuppressive activities through phagocytosis of cytotoxic T lymphocytes in the glioma microenvironment (18). These immunosuppressive activities may induce tumor immune escape, promote the evolution of tumor cells, and eventually lead to recurrence and malignant progression of gliomas.

As sequencing technology advances, numerous large-scale tumor sequencing databases have been established to support tumor research with a sufficiently large sample size and abundant gene data resources. Additionally, the emergence of single-cell sequencing helps form the basis for studying the genetic characteristics of tumor subclones and deepening our knowledge regarding the characteristics of immune cell infiltration and the immune microenvironment. In this study, The Cancer Genome Atlas (TCGA) and Chinese Glioma Genome Atlas (CGGA) databases were applied to establish a transcriptomics-based gene prediction model that helps assess the risk of recurrence and malignant progression of LGGs for accurate and efficient prognosis prediction. On this basis, immune cell infiltration and the immune microenvironment in LGGs at varying risks of recurrence and malignant progression were characterized to evaluate potential immunotherapies.

MATERIALS AND METHODS

Data Source

A total of 530 patients' mRNA expressions sequenced by Illumina HiSeq were downloaded from TCGA-LGG from UCSC Xena database (https://xenabrowser.net/datapages/), and corresponding clinical information was also downloaded. After filtering based on overall survival status (OS) and overall survival days (OS.time), there remained 465 samples without any Not Available (NA)

values (19). The CGGA sequence datasets (CGGA.mRNAseq_325 and CGGA.mRNAseq_693) were collected from CGGA database (http://www.cgga.org.cn) (20). The mRNA expression of normal brain tissue was collected from Genotype-Tissue Expression Project (GTEx, https://www.gtexportal.org) (21). To remove batch effects between GTEx and CGGA_325 datasets, we used the ComBat function in sva package to integrate both datasets.

Differential Expression Analysis

The limma package of R was used to compare differences in gene expression in two defined groups, and the genes with significance cutoff criteria p value <0.05 (adjusted) and absolute fold change more than 2 were identified as the differentially expressed genes (DEGs).

Prognosis Analysis

Univariate Cox regression analysis was used to identify the relationship between single signature and prognosis of patients. A single signature can be the mRNA expression value of a gene or a clinical feature. Multivariate Cox regression analysis was used to identify the relationship between multiple signatures and prognosis of patients. Univariate Cox and multivariate Cox regression analyses were performed by the coxph function of survival package of R.

Dimension Reduction and Risk Score Modeling

The least absolute shrinkage and selection operator (LASSO) method was used to further reduce the less important features. The multivariate Cox regression with a stepwise procedure was used to filter the redundant variables and formed the final risk score model to predict the prognosis of the patients. The Beta values in multivariate Cox analysis were retracted as the gene coefficient. The surv_cutpoint function in the Survminer package was used to determine the optimal cutting point of the risk score, so that the samples in the dataset could be divided into high- and low-risk groups. The calculation of risk score is show:

Risk score = $\sum$ coef (i)*log 2 (counts (i)+1), where i represents the corresponding gene.

Bio Function Analysis

The Gene Ontology (GO) enrichment analysis was performed based on DEGs by clusterprofile package of R (22). Based on Gene Set Enrichment Analysis (GSEA) and Gene Set Variation Analysis (GSVA) methods, we collected three gene sets (1,615 REACTOME gene sets, 186 Kyoto Encyclopedia of Genes and Genomes (KEGG) gene sets, 50 hallmark gene sets) from the Molecular Signatures Database (MSigDB v7.5.1) to explore enrichment signaling pathways between clusters or groups (23).

Immune-Related Analysis

The abundance of six immune cell types, B cell, CD4 T cell, CD8 T cell, neutrophil, macrophage, and dendritic cell, in the tumor microenvironment is estimated using TIMER based on mRNA expression (24). The two other tools, CIBERSORT and xCell, were also used to estimate the abundance of member cell types in a mixed-cell population (25, 26). Several immune infiltration-related signatures from the study by Mariathasan et al. (27) were used to analyze their association with risk score.

Correlation Analysis of Risk Score With Tumor Mutational Burden and Tumor Methylation Burden

Tumor mutational burden (TMB) is broadly defined as the number of somatic mutations per megabase of interrogated genomic sequence. The somatic mutation file *.maf of TCGA-LGG was downloaded from the GDC Data Portal (https://portal.gdc.cancer.gov) to calculate the TMB values. TCGA-LGG DNA methylation (HumanMethylation450) profile was downloaded from the UCSC Xena database (https://xenabrowser.net/datapages). Probes with a beta value greater than 0.8 were identified as sites of complete methylation, and the number of complete methylated probes was used to evaluate the tumor methylation burden. We used the abbreviations TMB.mut and TMB.met for tumor mutational burden and tumor methylation burden, respectively. The Pearson correlation was calculated by cor.test package of R.

Nomogram Analysis of Risk Score With Clinicopathological and Molecular Characteristics

Univariate and multivariate Cox analyses were used to assess the independent prognostic factors of risk score compared with clinical features. Then, we used a nomogram to integrate risk score and clinical features to improve prognosis prediction accuracy. The performance of the nomogram model was tested using receiver operating characteristic (ROC) and decision curve analysis (DCA) curves of 1, 3, and 5 years.

Cancer Cell Line Encyclopedia

Chronos, an algorithm for inferring gene knockout fitness effects based on an explicit model of cell proliferation dynamics after CRISPR gene knockout, was used to evaluate the effect of genes (28).

Cell Culturing and Processing

The two glioma cell lines used in this study were U87 and U251, both from Xiangya Hospital. The cells were cultured in Dulbecco's Modified Eagle Medium (DMEM) containing 10% bovine serum in a 37°C, 5% CO_2 incubator. Cells were inoculated on a six-well plate, and the experimental group was treated with BTB-1, a specific and reversible inhibitor of KIF18A. BTB-1 was dissolved with dimethylsulfoxide (DMSO) and diluted to a working concentration of 30 μM/L. Cells were treated for 24 h, and the control group was added with the same amount of DMSO (29). Finally, the two glioma cell lines were divided into four groups (U87 with DMSO, U87 with BTB-1, U251 with DMSO, and U251 with BTB-1).

Evaluation of the Effect of BTB-1 on the Transcription Level of KIF18A in Glioma Cells

We used QRT-PCR to detect KIF18A mRNA levels in the four glioma cell lines, adding RNeasy Mini Kit (Qiagen, Hilden, NRW, Germany) to each group to extract total RNA. RNA was reversely

transcribed into cDNA using Uni RT&qPCR Kit (TransGen Biotech, Beijing, China). Quantitative polymerase chain reaction was performed on Applied Biosystems QuantStudio 1 real-time fluorescent quantitative PCR system (Thermo Fisher Scientific, Waltham, MA, USA). Cycle conditions for qPCR were as follows: an initial denaturation step at 95°C for 15 min, followed by 40 cycles of amplification at 95°C, and annealing/extension at 56°C for 32 s. glyceraldehyde-phosphate dehydrogenase (GAPDH) was used as the internal control. Each experiment was carried out in triplicate. The primers were synthesized by Sangon Biotech, Shanghai, China. Their sequences are as follows: KIF18A, forward 5′-AAAAAGTGGTAGTTTGGGCTGA-3′ and reverse 5′-CTT TCAAGGGAGATGGCATTAG-3′; GAPDH, forward 5′-CATGAGAAGTATGACAACAGCCT-3′ and reverse 5′-AGTCCTTCCACGATACCAAAG-3′.

Evaluation of the Effect of BTB-1 on Glioma Cell Proliferation

Cell Counting Kit-8 (CCK-8) was used to detect cell proliferation ability. Four groups of glioma cells were inoculated into 96-well plates with 5 wells in each group, and about 3,000 cells in each well were cultured in 100-μl medium for 0, 12, 24, and 36 h, respectively. Here, 10 μl CCK-8 solution was added to each well and incubated for 1.5 h. Absorbance was detected at 450-nm wavelength using absorbance Microplate reader (Spectra Max, ABS Plus), and Optical Density (OD) value was measured. The average OD values of each group were taken.

Evaluation of the Effect of BTB-1 on Glioma Cell Cycle

Flow cytometry was used to detect cell cycle distribution to evaluate the effect of BTB-1 on glioma cell cycle. U87 and U251 cells with different processes were collected and washed twice with Phosphate Buffer Saline (PBS), then fixed with 70% ethanol at 4°C for 12 h, and then incubated with Prodium Iodide (PI)/RNase buffer. Flow cytometry (CYTEK Athena, USA) used red fluorescence and scattered light at 488 nm. The percentages of each cell cycle were analyzed.

Gene Expression Data With Immunotherapy

For further immunotherapy research, the IMvigor210 dataset was downloaded to evaluate the predictive power of the risk score for immunotherapy [programmed cell death protein-1 (PD-1)] response, and it was available from http://research-pub.gene.com/IMvigor210CoreBiologies with completed information about the response to PD-L1 blockade (30).

Statistical Analysis

The difference between two groups was compared by Wilcoxon test. Kaplan–Meier analysis with log-rank tests was used to perform survival curves. The ROC curve and corresponding Area Under the Curve (AUC) were generated by using the R package "timeROC." * p-value <0.05, ** p-value <0.01, *** p-value <0.001, and p-value <0.05 are statistically significant. All analyses were performed using R 4.1.0 (https://cran.r-project.org).

RESULTS

Identification of Recurrence Factors in Low-Grade Glioma

Based on data acquired from CGGA and GTEx databases, a comprehensive analysis was carried out on the DEGs between normal brain tissue and recurrent LGG (rLGG), normal brain tissue and secondary GBM (sGBM), primary LGG (pLGG) and rLGG, as well as pLGG and sGBM (**Figure 1A**). A total of 4 DEG datasets were obtained, and DEGs with high consensus were defined as those with consistent differential expression trends in at least three datasets (**Supplementary Table S1**), and a Venn diagram was established to present the DEG datasets with upregulated and downregulated expressions (**Figures 1B, C**). Eventually, 296 downregulated and 396 upregulated DEGs were screened through the above processes. Gene Ontology (GO) analysis was then used to annotate the functions of downregulated and upregulated DEGs. The biological process (BP) category of downregulated DEGs was mainly enriched in the regulation of membrane potential, modulation of chemical synaptic transmission, regulation of trans-synaptic signaling, etc. While for the cellular component (CC) category, the downregulated DEGs were associated with presynapse, transporter complex, transmembrane transporter complex, etc. In the molecular function (MF) category, the downregulated DEGs primarily participated in channel activity, passive transmembrane transporter activity, ion channel activity, etc. (**Figure 1D**). While the BP category of the upregulated DEGs was enriched mostly in the nuclear division, organelle fission, chromosome segregation, etc. In the CC category, the upregulated DEGs mainly showed associations with the chromosomal region, spindle, collagen-containing, etc. As for the MF category, the upregulated DEGs were involved primarily in antigen binding, microtubule binding, tubulin binding, etc. (**Figure 1E**).

Identification of Main Contributors of Recurrence and Malignant Progression Factors and Construction of a Gene Signature Model

Recurrence and malignant progression of LGG constitute the primary factors affecting its prognosis. Therefore, in order to determine the main contribution factors, the data of LGG patients were extracted from TCGA database for univariate Cox regression analysis on the identified highly consistent DEGs. The False Discovery Rate (FDR) values of the training set and test set are used for filtering. It was found that 24 downregulated and 62 upregulated DEGs were associated with the prognosis of LGG ($p < 0.05$) (**Supplementary Table S2**). The top 39 DEGs with statistically significant differences are shown in **Figure 2A**. Subsequently, LASSO regression, one of the techniques in machine learning, was adopted to dispose of dimension reduction of the 86 DEGs with prognostic significance (**Figures 2B, C**). Multivariate Cox regression was then used to establish the prognosis prediction model to identify

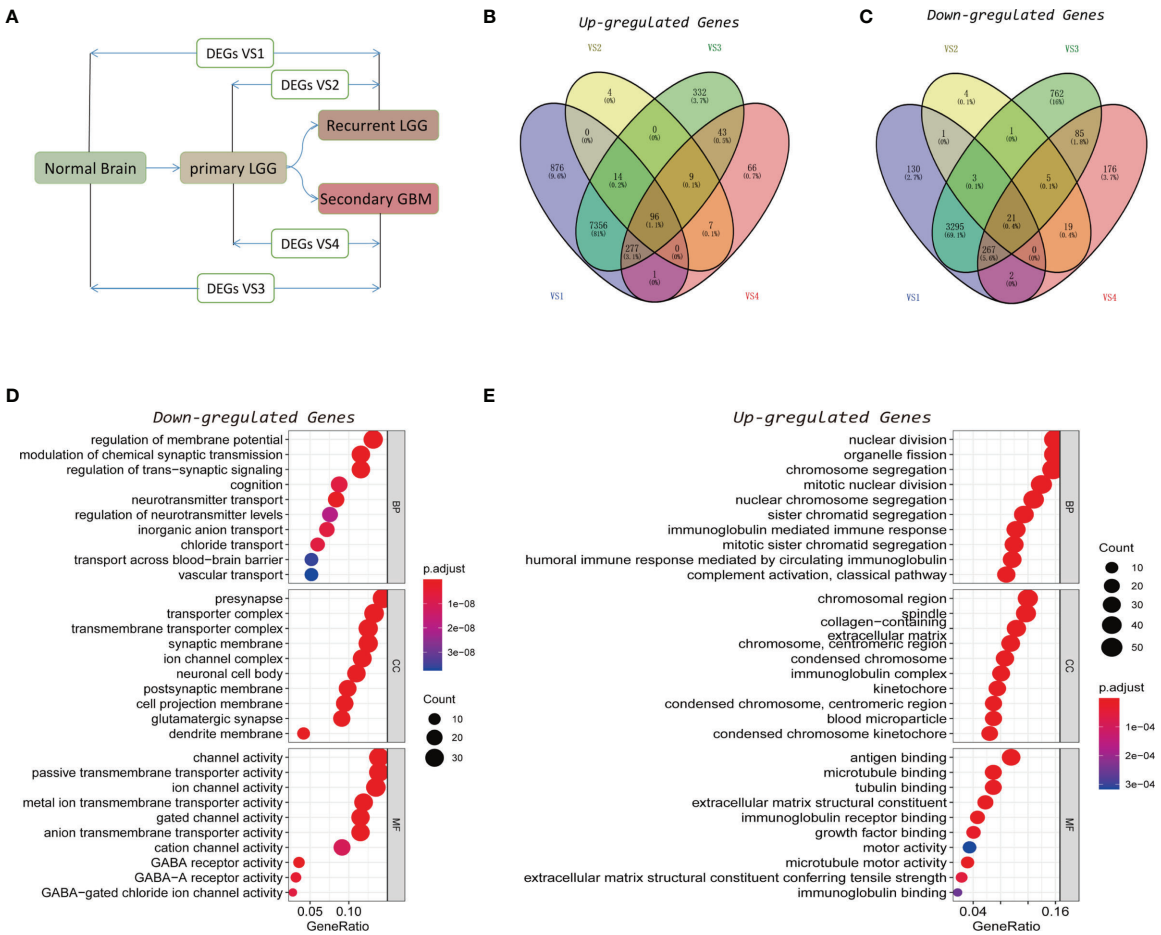

FIGURE 1 | Identification of recurrence factors in low-grade gliomas. **(A)** Analysis design diagram of differentially expressed genes (DEGs). **(B, C)** Venn diagram was used to display the upregulated **(B)** and downregulated **(C)** genes in the four sets of DEGs. **(D, E)** Gene Ontology (GO) analysis of the consistent upregulated **(D)** and downregulated **(E)** genes in the four sets of DEGs.

the main contributors. Corresponding results revealed that HOXA1, KIF18A, FAM133A, hepatocyte growth factor (HGF), and MN1 were the primary contributors ($p < 0.05$) (**Figure 2D**). Finally, the patients in the training dataset were stratified according to the risk scores obtained in the 5-gene signature model (**Figure 2E**). It was found that the established model could well predict the prognosis of TCGA-LGG patients, showing good stability at the same time (Area Under the Curve (AUC) of 1-, 3-, and 5-year ROC: 0.8776, 0.8749, and 0.7682, respectively) (**Figures 2F, G**).

Validation of Risk Signature in the Test Dataset and Validation Dataset

Two sub-datasets of CGGA (CGGA325 and CGGA693) were collected to verify the effectiveness and stability of the 5-gene signature prediction model. In the CGGA325 dataset, the model could well stratify the high-risk and low-risk LGG groups. Survival analysis showed that the prognosis of the high-risk group was significantly worse than that of the low-risk group ($p < 0.05$) (**Figures 3A–D**). Furthermore, in the CGGA693 dataset, the model could still better stratify the risk of LGG patients, and the prognosis of the high-risk group was also obviously worse than that of the low-risk group, as indicated by survival analysis ($p < 0.05$) (**Figures 3E–H**).

The Gene Set Enrichment Analysis of the High- and Low-Risk Groups

In order to clarify the mechanism of LGG recurrence or malignant progression, the differences in signaling pathways between high-risk and low-risk groups were analyzed based on TCGA-LGG dataset. Meanwhile, GSVA and GSEA were performed to analyze the signaling pathway differences between high-risk and low-risk groups based on REACTOME gene set, KEGG gene set, and hallmark gene set. In the REACTOME gene set, several signaling pathways were significantly activated in the high-risk group compared with the low-risk group, including cell cycle G2/M

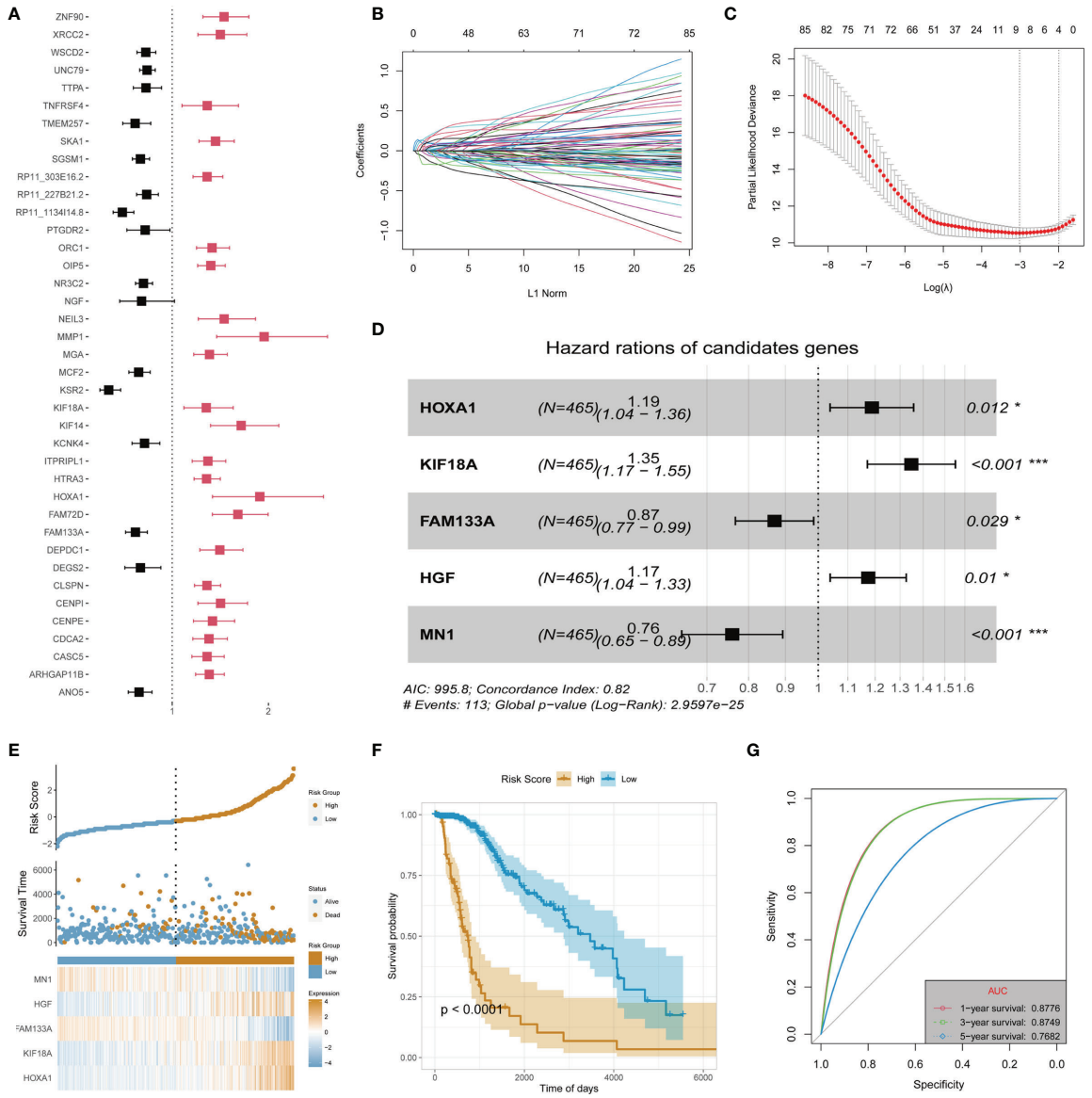

FIGURE 2 | Identification of main contributors of recurrence and malignant progression factors and construction of risk signature in TCGA-LGG cohort. **(A)** Univariate Cox analysis of all recurrence factors. **(B)** Cross-validation for tuning the coefficient selection in the least absolute shrinkage and selection operator (LASSO) regression. **(C)** LASSO regression of the 86 OS-associated genes. **(D)** Multivariate Cox regression analysis for the 5 genes. **(E)** Allocation of patients in the training set on the basis of the risk score. **(F)** Kaplan–Meier curves display the diversity in OS between the high-risk and low-risk groups in the training set. **(G)** Area Under the Curve (AUC) of time-dependent receiver operating characteristic (ROC) curves examined the prognostic performance of the risk score in the training set. "*" means 0.01<p<0.05, "***"means p<0.001.

checkpoint, RB tumor suppressor/checkpoint signaling in response to DNA damage, Gap-filling DNA repair synthesis and ligation in TC-NER, Toll-like receptor 3 (TLR3) cascade (**Figure 4A**). KEGG gene set-based analysis revealed that signaling pathways such as cell cycle, extracellular matrix (ECM)–receptor interaction, Janus kinase/signal transducers and activators of transcription (JAK-STAT) signaling pathway, complement and coagulation cascades, and cytokine receptor interaction were obviously activated in the high-risk group, while calcium signaling pathway, long-term potentiation, neuroactive ligand–receptor interaction, etc., were inactivated in the high-risk group (**Figures 4B, C**). At the same time, similar results can be obtained by the CGGA database based on KEGG GSEA (**Figures 4E, F**). In the tumor-specific gene set of hallmark, there existed activation in cell cycle G2/M checkpoint and tumor immune-related signaling pathways (**Figure 4D**). Collectively, these signals are mainly related to tumor immune regulation and DNA damage-related cell cycle checkpoints, indicating that these mechanisms may be significantly involved in LGG recurrence and malignant progression.

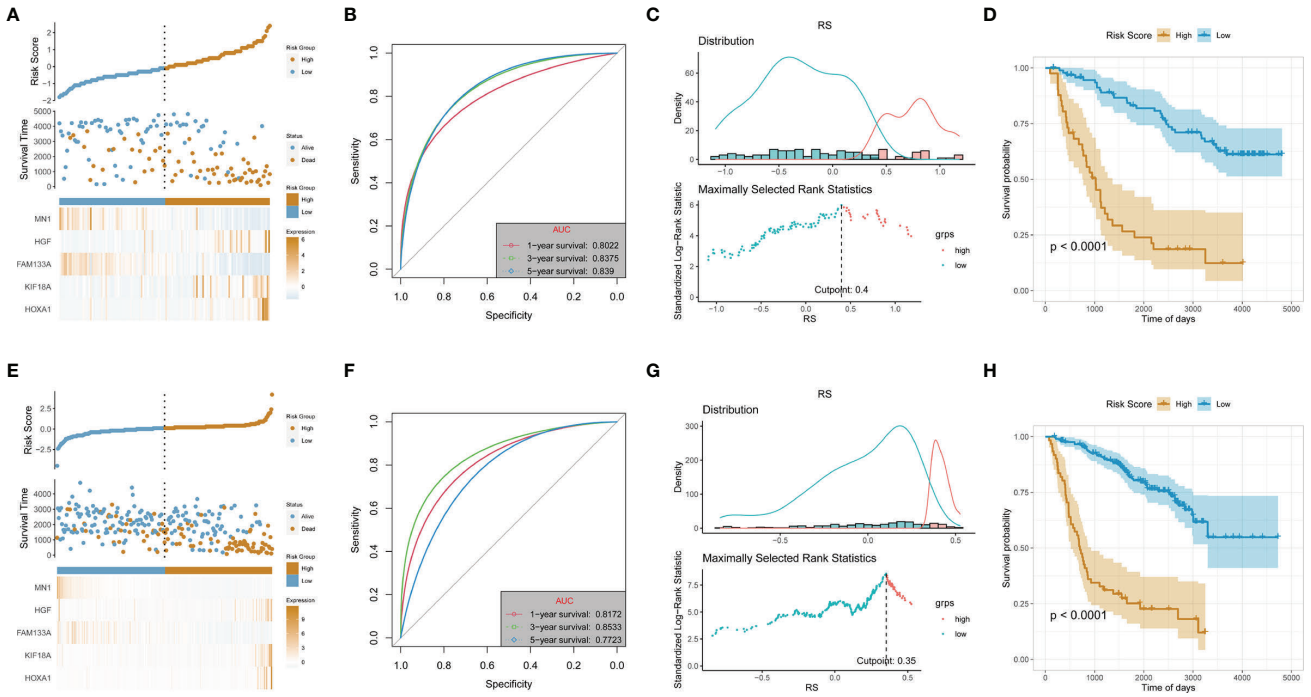

FIGURE 3 | Validation of risk signature in the test dataset (CGGA_325 cohort) and validation dataset (CGGA_693). **(A, E)** Allocation of patients in the training set on the basis of the risk score in the test and validation dataset. **(B, F)** Area Under the Curve (AUC) of 1-, 3-, and 5-year receiver operating characteristic (ROC) curves examined the prognostic performance of the risk score in the test and validation dataset. **(C, G)** Determine the optimal cut point for risk score in the test and validation dataset. **(D, H)** Kaplan–Meier curves display the diversity in OS between the low- and high-risk score groups in the test and validation dataset.

Infiltrated Immune Cells in High- and Low-Risk Score Groups From the Training and Validation Cohorts

Based on the above exploration, multiple tumor immune-related pathways were discovered to be activated in the high-risk group of TCGA-LGG, suggesting an intimate association of the tumor immune microenvironment with LGG recurrence and malignant progression. Accordingly, the infiltration of immune cells was further evaluated in the high- and low-risk score groups of TCGA-LGG. The abundance of immune cells in the tumor microenvironment was evaluated by the TIMER algorithm according to mRNA expressions. The results showed that the infiltration of B cells, CD4 T cells, CD8 T cells, neutrophils, macrophages, and dendritic cells in the high-risk score group was stronger than that in the low-risk score group of LGG (**Figure 5A**). Further analyses were continued by using CIBERSORT and the xCell algorithm. Analysis based on CIBERSORT revealed that the infiltration of anti-inflammatory immune cells such as CD8 T cells, CD4 memory resting T cells, and M2 macrophages was stronger in the high-risk score group than that in the low-risk score group (**Figure 5B**). xCell-based analysis also indicated that the infiltration of most immune cells increased in the high-risk score group (**Figure 5C**). Collectively, these data suggest that the high-risk score group of LGG has stronger immune cell infiltration than that of the low-risk score group. In addition, using CGGA database (CGGA325 and CGGA693) as validation sets, we also found that immune cell infiltration in the LGG high-risk group was stronger than that in the low-risk group by ssGSEA algorithm (**Figures 5D, E**).

Genomic and Methylation Characteristics in the High- and Low-Risk Score Groups From TCGA-LGG Cohort

As mentioned above, DNA damage-related cell cycle checkpoint pathways were activated in the high-risk score group of LGG, suggesting that there may be more frequent gene mutations in this group. For an in-depth understanding of gene mutations in the high- and low-risk score groups of LGG, further grouping was performed based on TMB (TMB.mut), including high and low TMB.mut groups of LGG (**Figure 6A**). Survival analysis between high and low TMB.mut groups showed that the prognosis of high TMB.mut was significantly poorer than that in the low TMB.mut group ($p < 0.001$) (**Figure 6B**). Correlation analysis revealed a good positive correlation between risk factor stratification and TMB.mut stratification ($R = 0.34$, $p < 0.05$), that was, the mutation burden of the high-risk score group was significantly higher than that of the low-risk score group of LGG (**Figures 6C-E**). Simultaneous exploration was performed on the level of methylation in the high- and low-risk score groups of LGG. Similarly, two groups of high and low TMB.met were divided based on tumor methylation burden (TMB.met) (**Figure 6F**). Survival analysis indicated a significantly poorer

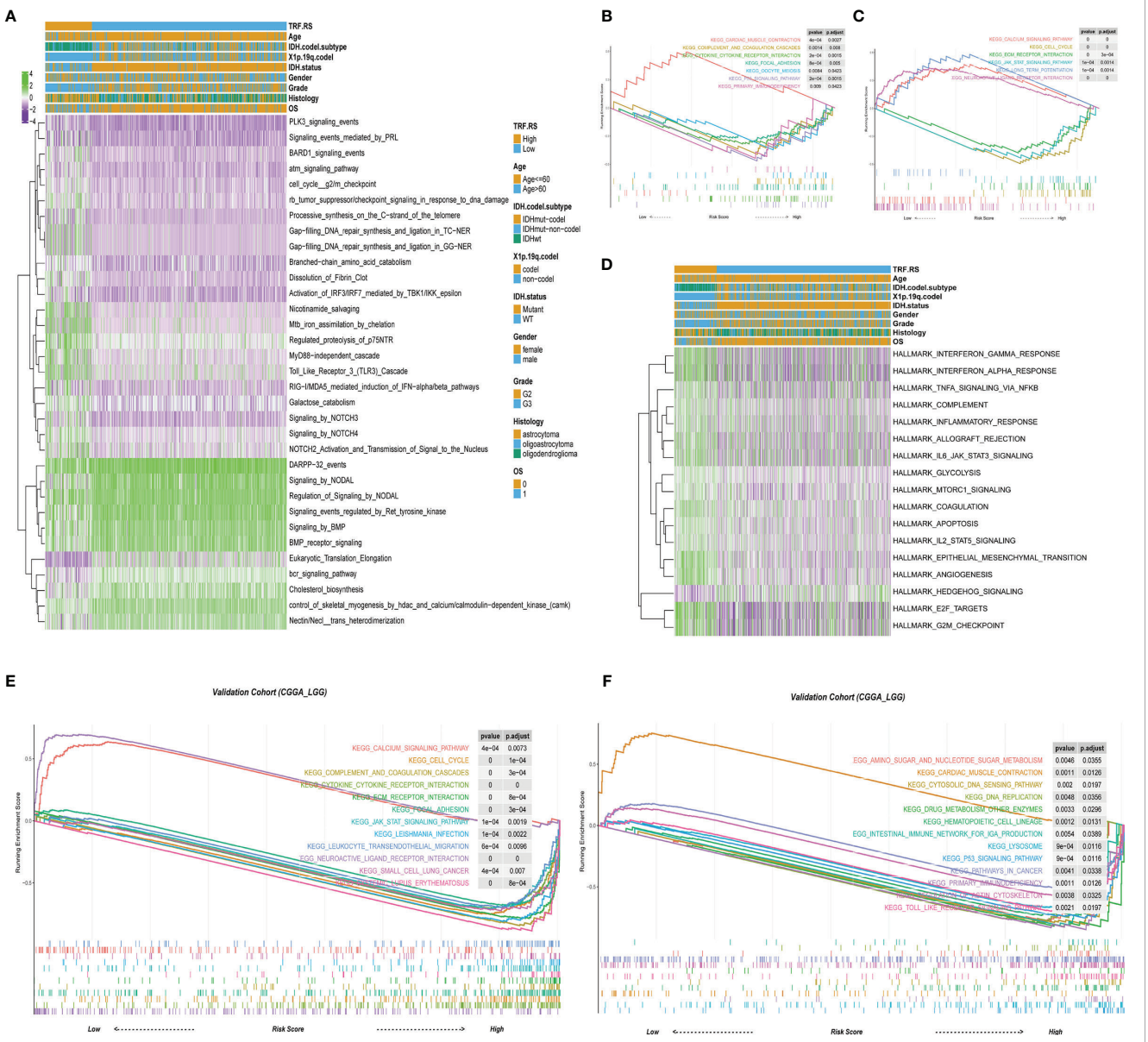

FIGURE 4 | The biology function enrichment analysis between the low- and high-risk score groups. **(A)** Gene Set Variation Analysis (GSVA) results based on the REACTOME gene sets. **(B, C)** Gene Set Enrichment Analysis (GSEA) results based on the Kyoto Encyclopedia of Genes and Genomes (KEGG) gene sets. **(D)** GSVA results based on the hallmark gene sets. **(E, F)** GSEA results based on the KEGG gene sets in the validation cohort (CGGA-LGG).

prognosis in the low TMB.met group than that in the high TMB.met group ($p < 0.001$) (**Figure 6G**); moreover, the correlation analysis presented a negative correlation between risk factor stratification and TMB.met stratification ($R = -0.39$, $p < 0.05$), suggesting that the DNA methylation level of the LGG high-risk score group was remarkably lower than that of the low-risk score group (**Figures 6H–J**). We further analyzed the mutation of major driver genes in the high- and low-risk groups, and the driver genes with a high mutation frequency in the high-risk group were TP53, EGFR, IDH1, etc. (**Figure 6K**). The driver genes with a high mutation frequency in the low-risk group were IDH1, TP53, ATRX, etc. (**Figure 6L**). TP53 mutation had a strong coexisting relationship with the high-risk group, and IDH1 mutation had a strong coexisting relationship with the low-risk group (**Figure 6L**).

Independent Prognostic Value of the Tumor Recurrence Factor (TRF) Risk Score

Subsequent analyses were conducted to integrate the 5-gene signature prediction model established based on its expression characteristics with other clinical features and promote its

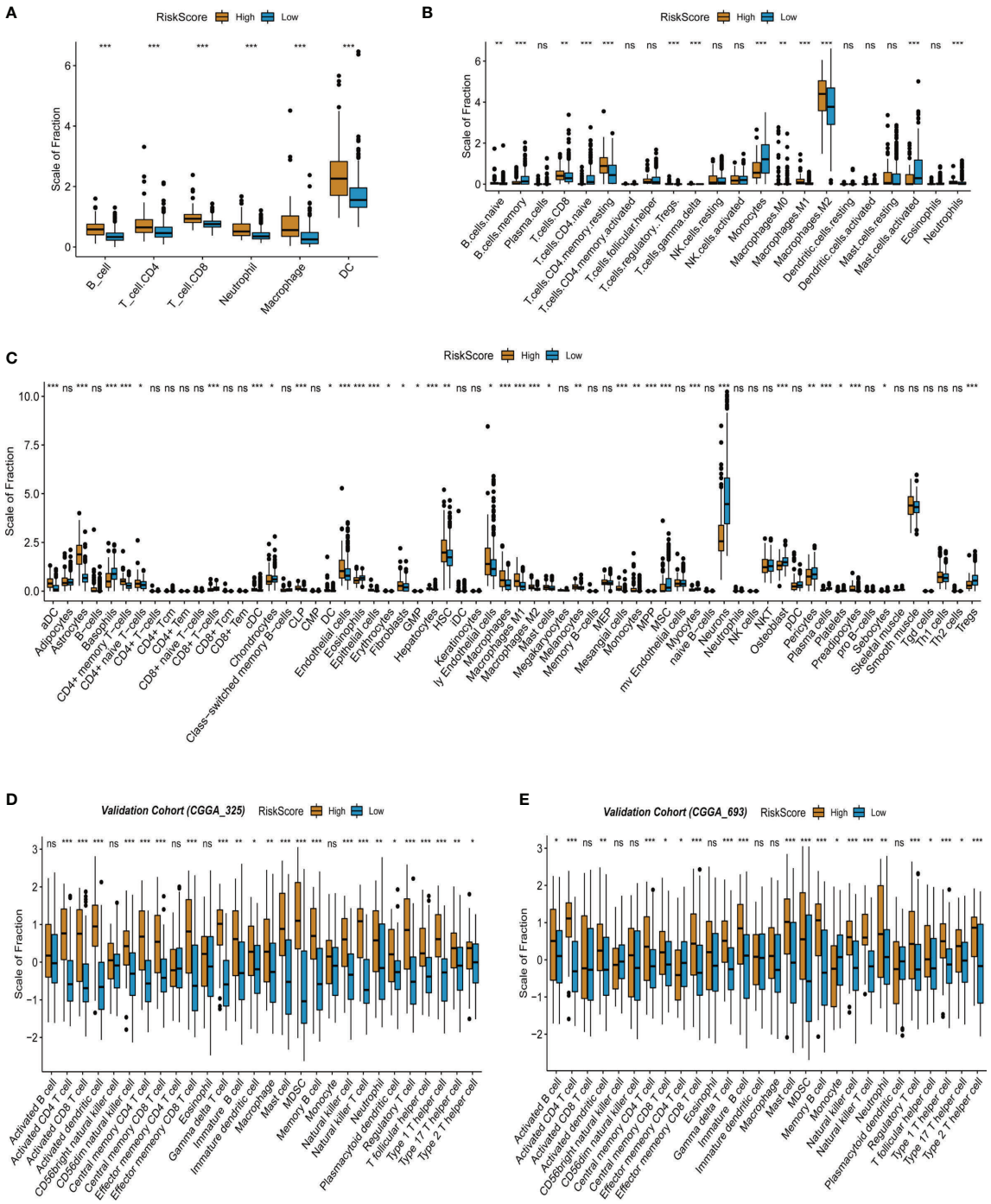

FIGURE 5 | Infiltrated immune cells in the high- and low-risk score group from the training and validation cohorts. **(A)** Immune infiltrates in the two groups based on the TIMER algorithm from TCGA-LGG cohort. **(B)** Immune infiltrates in the two groups based on the CIBERSORT algorithm from TCGA-LGG cohort. **(C)** Immune infiltrates in the two groups based on the xCell algorithm from TCGA-LGG cohort. **(D)** Immune infiltrates in the two groups based on the ssGSEA algorithm from the validation cohort (CGGA 325). **(E)** Immune infiltrates in the two groups based on the ssGSEA algorithm from the validation cohort (CGGA 693). "*" means 0.01<p<0.05, "**"means 0.001<p<0.01, "****"means p<0.001, "ns"means no significance.

application in prognosis judgment. Firstly, multivariate Cox regression analysis was performed for determining the independent prognostic factors of Histology, Grade, IDH.status, X1p.19q.codel, Age, and Tumor Recurrence Factor (TRF) risk score (**Figure 7A**). The Tumor Recurrence Factor risk score and Age were found to be relatively significant independent prognostic factors ($p < 0.001$), followed by IDH.status ($p = 0.055$) (**Figure 7D**). After that, a nomogram was constructed based on

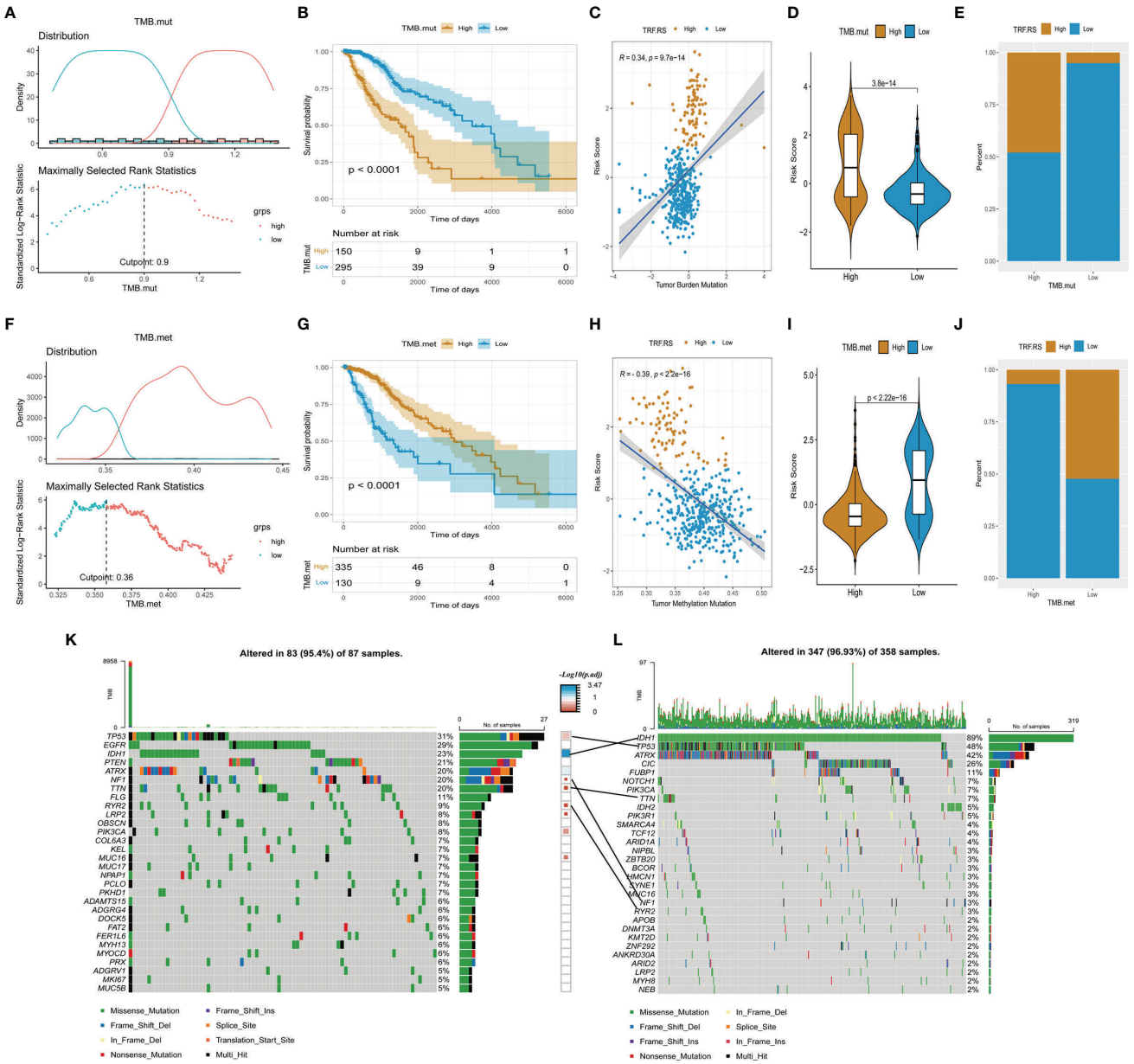

FIGURE 6 | Genomic and methylation characteristics in the high- and low-risk score group from TCGA-LGG cohort. **(A, F)** Determine the optimal cut point for TMB.mut and TMB.met. **(B, G)** Comparison of overall survival between the low and high group of TMB.mut and TMB.met. **(C, H)** Scatter distribution of the risk score with TMB.mut and TMB.met. **(D, I)** Comparison of the risk score between the low and high group of TMB.mut and TMB.met. **(E, J)** Comparison of the proportion of risk score type between the low and high group of TMB.mut and TMB.met. **(K, L)** Oncoplot of the high and low group of risk score.

IDH.status, Age, and Tumor Recurrence Factor risk score to predict the prognosis of TCGA-LGG patients. Using the Calibration diagram to verify the prediction efficacy of the constructed nomogram, it could be found that its 1-, 3-, and 5-year prognostic prediction efficacy had high accuracy and stability (**Figure 7C**). Furthermore, the ROC curve was then drawn to compare the prediction efficacy of IDH.status, Age, Tumor Recurrence Factor risk score, and nomogram model. It could be noticed that the 1-, 3-, and 5-year prognostic prediction efficacy of the nomogram was higher than that of other features in 1, 3, and 5 years. Among them, the Area Under the Curve (AUC) of 1-year ROC was 0.8591 (IDH.status), 0.8176 (Age), 0.8777 (Tumor Recurrence Factor risk score), and 0.9396 (nomogram) (**Figure 7E**); that of 3-year ROC was 0.8172 (IDH.status), 0.7594 (Age), 0.0.8674 (Tumor Recurrence Factor risk score), and 0.9433 (nomogram) (**Figure 7F**); and that of 5-year ROC was 0.6918 (IDH.status), 0.6976 (Age), 0.7501 (Tumor Recurrence Factor risk score), and 0.8595 (nomogram)

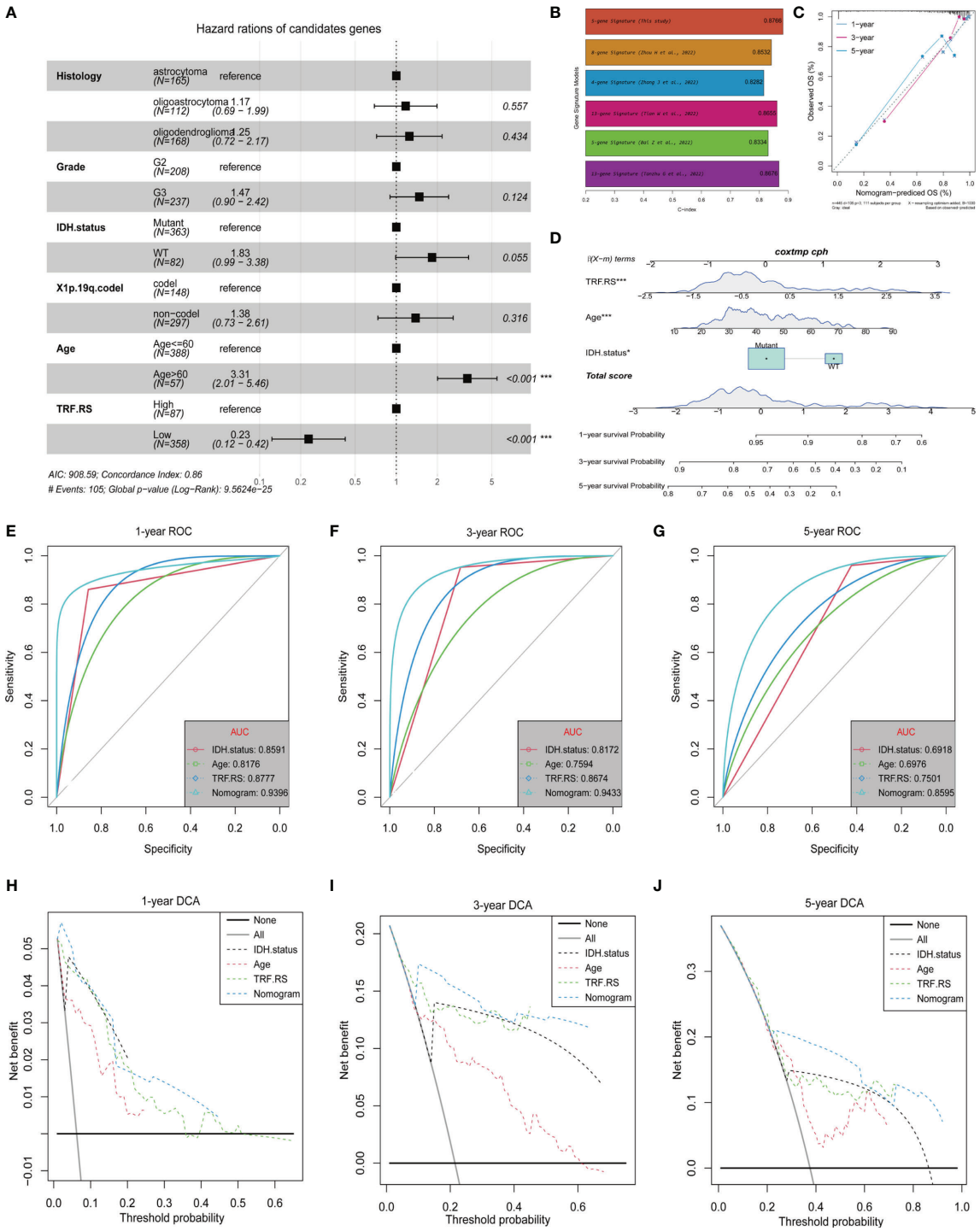

FIGURE 7 | Independent prognostic value of the Tumor Recurrence Factor risk score. **(A)** Forest plot of multivariate Cox analysis between the Tumor Recurrence Factor risk score and clinical traits. **(B)** Comparison of the prediction power between this study and other studies. **(C)** Calibration plot was used to predict the 1-, 3-, and 5-year survival in TCGA-LGG cohorts. **(D)** Nomogram of TCGA-LGG cohorts was used to predict overall survival. **(E–G)** Receiver operating characteristic (ROC) curves showed the 1-, 3-, and 5-year predictive efficiency of risk score, age, IDH mutation status, and nomogram model. **(H–J)** Decision curve analysis (DCA) curves showed the 1-, 3-, and 5-year predictive efficiency of risk score, age, IDH mutation status, and nomogram model. "*" means 0.01<p<0.05, "***"means p<0.001.

(**Figure 7G**). Furthermore, the DCA curve was generated to examine the prediction efficacy of IDH.status, Age, Tumor Recurrence Factor risk score, and nomogram model. Similar results were observed as described above, which support the strong stability of the prediction efficacy of the constructed nomogram (**Figures 7H–J**). Moreover, we selected some relevant literature to compare the predictive power of the prognostic models. Compared with other models, our prediction model has better predictive power (**Figure 7B**) (31–35).

Evaluation of Potential Therapeutic Targets of Risk Signature Genes Based on the CCLE Database

In order to further explore whether the genes of the main contributors were potential therapeutic targets, the responses of the five genes to different tumor cell lines after inhibition were evaluated based on the CCLE database. KIF18A and MN1 were discovered to be potential therapeutic targets. Specifically, KIF18A, as a risk factor, could significantly reduce the proliferation of most tumor cell lines (including brain tumor cell lines) (**Figures 8B, G**), while MN1, as a protective factor, could enhance the proliferation of most tumor cell lines (including brain tumor cell lines) (**Figures 8E, J**). However, the other 3 genes could not induce corresponding changes in tumor cell lines after being inhibited (**Figures 8A, C, D, F, H, I**), suggesting no potential therapeutic target value.

Evaluation of the Effect of KIF18A Inhibitor BTB-1 on the Function of Glioma Cell Lines

As mentioned above, KIF18A was found to be a potential therapeutic target. Therefore, to evaluate its potential therapeutic value, we treated glioma cells with BTB-1, a specific small-molecule inhibitor of KIF18A, to evaluate its effect on glioma cell function. KIF18A mRNA expression in U87 and U251 cells decreased ($p < 0.05$) (**Figure 9A**). It suggested that BTB-1 could inhibit the expression of KIF18A. As a further study on the effect of BTB-1 on cell proliferation, CCK-8 test showed that in U87 and U251 cell lines, the cell proliferation rate of the BTB-1 treatment group was lower than that of the control group. It was suggested that BTB-1 could inhibit cell proliferation (**Figure 9B**). The results of flow cytometry were shown in **Figure 9C**. The G2/M phase ratios of U87 and U251 cells treated with BTB-1 were 31.4% and 31.1%, and those of the control group were 22.6% and 22.2%, respectively, with statistically significant differences ($p < 0.05$). In conclusion, the cell cycle of BTB-1-treated glioma cells stagnated in G2/M phase, and the proportion of cells in the G2/M phase increased. These results suggest that BTB-1 inhibits

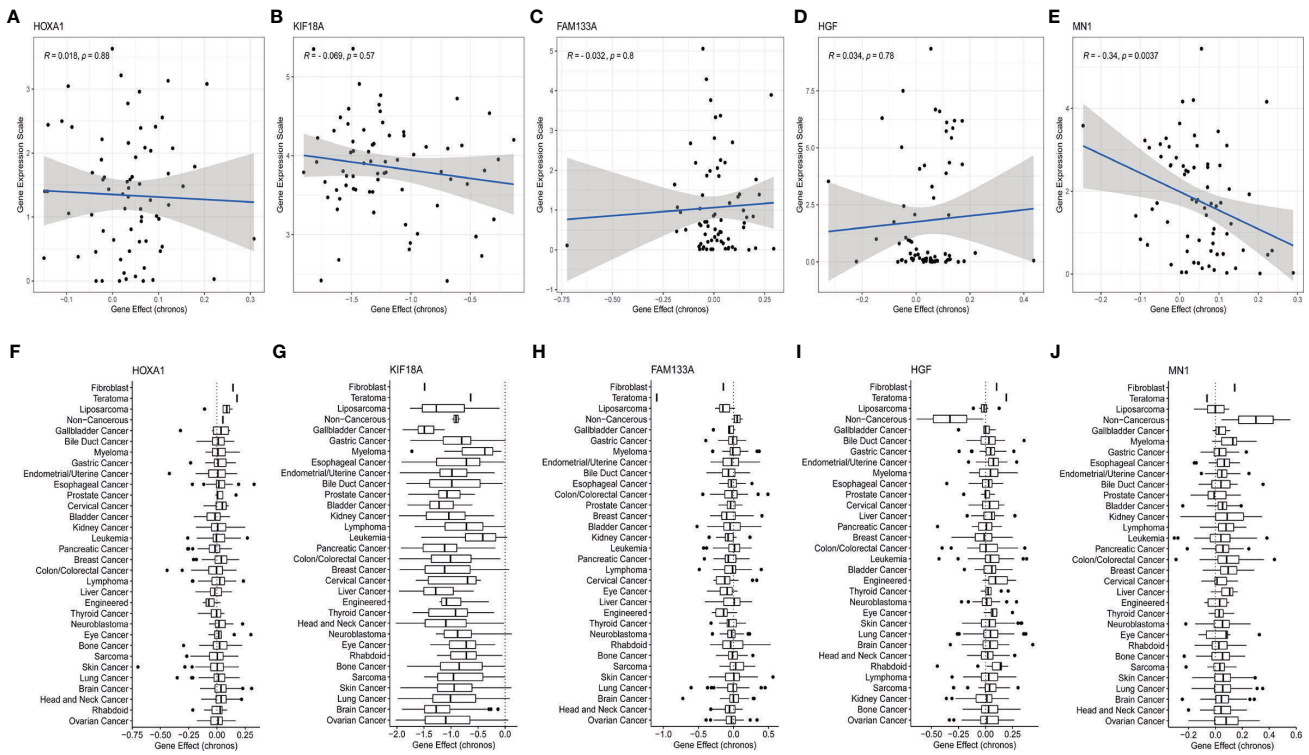

FIGURE 8 | Evaluation of the potential therapeutic targets of risk signature genes based on the CCLE database. **(A–E)** Scatter distribution of gene expression and gene effect of the 5 genes, including HOXA1, KIF18A, FAM133A, HGF, and MN1, in brain cancer cell lines. **(F–J)** Distribution of gene effects of the 5 genes, including HOXA1, KIF18A, FAM133A, HGF, and MN1, in various cancer cell lines.

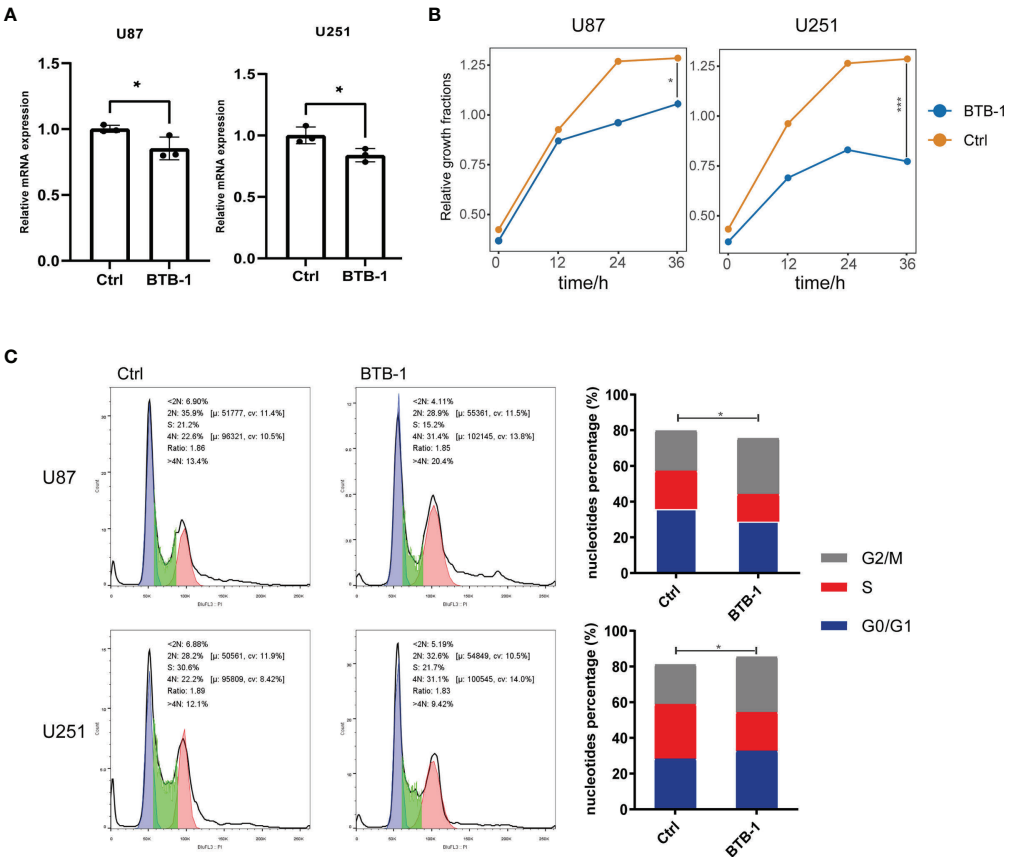

FIGURE 9 | Evaluation of the effect of KIF18A inhibitor BTB-1 on the function of glioma cell lines. **(A)** Evaluation of the effect of BTB-1 on the transcription level of KIF18A in glioma cells. **(B)** Evaluation of the effect of BTB-1 on glioma cell proliferation. **(C)** Evaluation of the effect of BTB-1 on glioma cell cycle. "*" means 0.01<p<0.05, "***"means p<0.001.

the proliferation of tumor cells mainly by inhibiting KIF18A and arresting glioma cells in the G2/M phase.

Evaluation of Response to Immunotherapy Based on the Tumor Recurrence Factor Risk Score

To test whether this predictive model can predict the immunotherapy response of LGG, we first assessed the differences in key factors in the immune response process between the high- and low-risk groups and found that the expression of these factors was higher in the high-risk group than that in the low-risk group (**Figure 10A**). Further analysis of the association between the Tumor Recurrence Factor risk score and common immune checkpoints of tumors showed that the Tumor Recurrence Factor risk score was correlated with CD47, CTLA7, HAVCR2, LAG3, PDCD1, and other immune checkpoints (**Figure 10B**). Independent analysis of the association between the 5 genes and immune checkpoints showed that all of the 5 genes were closely related to immune checkpoints (**Figure 10C**). Finally, the IMvigor210 dataset model (a database of bladder cancer) was selected and patients with bladder cancer in the database were divided into the high- and low-risk score groups (**Figure 10D**). Meanwhile, survival analysis showed that the model had a significant difference in prognosis between the high- and low-risk score groups of bladder cancer (**Figure 10E**), with relatively good stability in predicting the prognosis (**Figure 10F**). Analysis of the data of immunotherapy effect in the database revealed that the low-risk score group had a better response to immunotherapy than that in the high-risk score group (**Figure 10G**). With respect to the above, the constructed gene signature model not only has good universality and stability in predicting tumor prognosis but also provides a potential reference for predicting tumor response to immunotherapy.

DISCUSSION

LGG has a better prognosis than that of HGG, which, however, shows a deterioration in its prognosis primarily owing to the risk of recurrence and malignant progression, becoming a critical concern in the treatment of LGG. Based on transcriptome analysis, a new prediction model was established in our study, which can effectively evaluate the risk of LGG and predict the

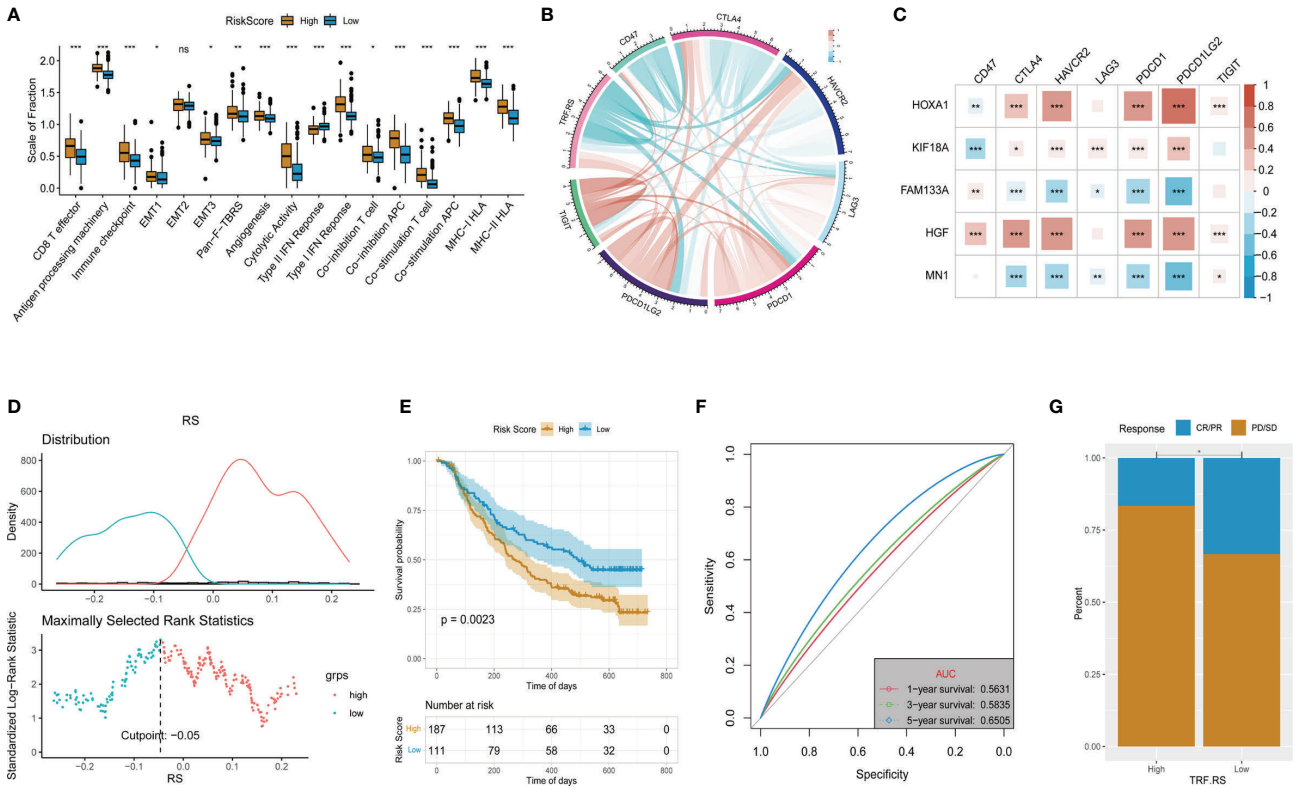

FIGURE 10 | Evaluation of the response to immunotherapy. **(A)** Comparation of the immune response signature between the high- and low-risk groups. **(B)** Corelationships between the Tumor Recurrence Factor risk score and common immune checkpoints. **(C)** Corelationships between the 5 key genes and common immune checkpoints. **(D)** Determine the optimal cut point for the Tumor Recurrence Factor risk score. **(E)** Comparison of the overall survival between the low and high Tumor Recurrence Factor risk score. **(F)** Receiver operating characteristic (ROC) curves showed the 1-, 3-, and 5-year predictive efficiency of the Tumor Recurrence Factor risk score. **(G)** Comparison of the proportion of response to treatment between the low and high Tumor Recurrence Factor risk score. "*" means 0.01<p<0.05, "**"means 0.001<p<0.01, "***"means p<0.001,"ns"means no significance

risk of recurrence and malignant progression. Finally, a total of 5 genes related to the recurrence and malignant progression of LGG were screened in our study, including three risk factors (HOXA1, HGF, and KIF18A) and two protective factors (FAM133A and MN1).

HOXA1 is highly expressed in breast cancer, ovarian cancer, gastric cancer, and various other cancers, which has regulatory roles on cell differentiation, apoptosis, and migration (36–38). For instance, in glioblastoma, long non-coding RNA (lncRNA) HOTAIRM1 has been documented to upregulate the expression of HOXA1 by blocking the binding of G9a and EZH2 to histones H3K9 and H3K27, resulting in the inability of methyltransferase to methylate the promoter of HOXA1 (39). At present, there is no relevant research on its downstream pathway in glioma. HOXA1 was found to upregulate the expression of BCL2 in breast cancer, which could also enhance cell proliferation and promote malignant transformation of cancer cells by activating STAT5a/b and MAPK signaling pathways (40). Furthermore, HGF is mainly produced by stromal cells, and its receptor is the mesenchymal–epithelial transition (MET) factor (41). HGF can bind to MET to activate various pathways such as Ras/MAPK, PI3K/Akt, and STAT, thereby regulating cell growth, movement, and morphogenesis (42–45). It has been reported that HGF and MET were highly expressed in glioma to promote tumor growth and angiogenesis, which could also boost tumor evolution and malignant progression to HGG by activating AKT and MAPK pathways (46, 47). Meanwhile, KIF18A belongs to the kinesin 9 family. It has a significantly upregulated expression in G2/M phase, which can contribute to the arrangement of chromosomes on the equatorial plate by adjusting the length of microtubules (Mts), ensuring the normal separation of sister chromosomes and normal progression of mitosis (48–51). High expression of KIF18A has been confirmed in multiple cancers such as breast cancer, lung cancer, and colorectal cancer (52–54). Prior cell function experiments showed that overexpression of KIF18A in the HeLa cell line could significantly increase the number of cells with multipolar mitotic spindles (50). At the same time, KIF18A can combine with microtubules (Mts), move along Mts, and has microtubule depolymerizing activity, both of which require the participation of ATP as a major substrate to supply energy (55, 56). Accordingly, considering the ATPase activity of KIF18A, Catarinella et al. (29) developed a small-molecule drug BTB-1, which can inhibit KIF18A in an ATP-competitive and Mt-uncompetitive manner; and tumor cells after BTB-1 treatment

showed abnormal spindle formation and chromosome division, resulting in tumor cell apoptosis. In our study, analysis of data acquired from the CCLE database revealed the potential therapeutic target significance of KIF18A, that was, inhibiting its expression or function could inhibit tumor growth. Further *in vitro* experiments on glioma cell lines (U87 and U251) confirmed that KIF18A's specific inhibitor BTB-1 inhibited the proliferation of glioma cells significantly, and the cell cycle stagnated in G2/M phase. Therefore, the mechanism of treating glioma with KIF18A as a target is worthy of further study.

FAM133A is a type of Cancer-Testis Antigen (CTA), a class of proteins that is highly expressed in immune privilege sites such as the brain and testis (57). High expression of FAM133A in cervical cancer and pancreatic cancer has been reported to be associated with the malignant degree of tumors (58, 59). While in glioma, FAM133A is the downstream target of miR-155. The low expression of miR-155 in IDH1-mutant glioma can upregulate the expression of FAM133A, which may further reduce the invasiveness and proliferation of IDH1-mutant glioma by targeting Matrix metalloproteinase-14 (MMP14) (60). Therefore, consistent with previous reports, this study indicated that LGG patients with a high expression of FAM133A had a better prognosis. Furthermore, MN1 was initially found to cause gene rearrangement by chromosomal balanced translocation, which plays an important role in the pathogenesis of meningioma and myeloproliferative diseases (61, 62). The loss-of-function mutation of MN1 may induce CEBALID syndrome, which is manifested as neurodevelopmental impairments and facial deformities (63). According to current research, the genomic changes of MN1 are predominated by rearrangement (64–67), with the report of the deletion and increase of adjacent loci as well (67). Moreover, in astroblastoma or neuroepithelial tumors, patients with MN1 rearrangement were reported to have longer survival and better prognosis (65, 68). However, some researchers considered no significant superiority in the clinical progression and prognosis of these patients (69). So far, it is unknown with respect to the relationship between the expression of MN1 at the transcriptome level and the prognosis of glioma. In the present study, the prognosis of LGG patients was poorer in the case of low expression of MN1, accompanied by a higher risk of progression to HGG. Further analysis of data acquired from the CCLE database revealed stronger cell proliferation and invasion abilities in cell lines of brain tumors with the silencing of MN1 expression. Consequently, it is believed that MN1 may be related to the normal development and differentiation of the nervous system. Its low expression may increase the stemness of glioma cells to boost the malignant progression of glioma. Its role and mechanism in the malignant progression of glioma need to be further studied.

Furthermore, in our study, the abnormality of DNA damage-related cell cycle checkpoints showed an intimate association with the recurrence and malignant progression of LGG. The cell cycle consists of four phases: G1, S, G2 and M. Cells have a strict cell cycle checkpoint mechanism to ensure the correct transmission of genetic materials to the next generation of cells. Dysfunction in checkpoints can lead to abnormal proliferation of cells and tumorigenesis (70). Under normal circumstances, in the case of DNA damage, the ATR-CHK1-CDC25 pathway may be activated to inhibit cyclinA/B-CDK1 complex and hence block the cell replication arresting at G2 phase (71). While the CDK1 gene is overexpressed in glioma, which may promote the G2 phase transition of cells with DNA damage. It has been documented that the expression of CDK1 is positively correlated with the grade of glioma, which may also increase with malignant progression after recurrence (72–74). In addition, Rb is a tumor suppressor, and its inactivation by mutation can activate E2F protein to overexpress cyclinE/A. The cyclinE/A-CDK2 is an important complex of cell cycle checkpoints. The overexpressed cyclinE/A plays a critical promoting role in G1/S cell transition of cells with DNA damage (75). Deletion or downregulation of Rb gene is common in gliomas (76), and its downregulation is more common in HGG (77, 78). Moreover, van Thuijl et al. (14) believed that patients with LGG treated with TMZ can induce Rb gene mutation, resulting in tumor recurrence and progression to HGG. Collectively, in our opinion, there may be a regulation disorder in the cell cycle checkpoints related to DNA damage through various mechanisms during the progression of LGG to induce continuous accumulation of genomic mutations, leading to tumor evolution and further progression to HGG.

Immune cell infiltration in the tumor, as an indicator of the tumor microenvironment, plays a critical role in the recurrence and progression of glioma. The proposed impact is double-edged generally. To be specific, while immune cells play a role in discouraging tumor progression, due to the "immune escape" mechanism, besides avoiding attack by the immune system, tumor cells can even "tame" immune cells by regulating the phenotype and function of immune cells (e.g., secreting cytokines, chemokines, etc.) and hence contribute to a microenvironment conducive to tumor progression (79–81). On the other hand, the "tamed" immune cells can also secrete cytokines to regulate the DNA methylation of tumor cells, thereby promoting the evolution of tumors (17). In this study, the degree of immune cell infiltration was significantly higher in the LGG high-risk group than that in the low-risk group. GSEA and GSVA also found that immunosuppressive and anti-inflammatory pathways were significantly activated in the high-risk group. It is suggested that LGG in the high-risk group can create an immunosuppressive microenvironment more conducive to tumor growth and evolution through tumor–immune cell interaction under stronger immune cell infiltration. Moreover, an immune barrier is developed in the tumor marginal microenvironment by immune cells at the periphery of tumors, which may facilitate the development of LGG chemoradiotherapy resistance and boost the recurrence and malignant progression of LGG (82).

CONCLUSIONS

We obtained 5 genes (HOXA1, HGF, KIF18A, FAM133A, MN1) associated with LGG recurrence and malignant progression through differential expression gene analysis and established a stable and efficient prognostic model based on these. Among the

five genes, KIF18A is considered to be the most significant potential therapeutic target. Its specific inhibitor BTB-1 can block the cell cycle of glioma cells in G2/M phase to inhibit the proliferation of glioma cells. We also found that abnormal DNA damage-related cell cycle checkpoints and changes in the tumor immune microenvironment may be important mechanisms leading to tumor cell evolution and LGG progression to HGG.

DATA AVAILABILITY STATEMENT

No new data were generated in this study, and all data used in this study are publicly available online. All the codes in this study are available on GitHub, linked to: https://github.com/Richard-Li-lab-team/LGG_TRF.

AUTHOR CONTRIBUTIONS

CT conceived and designed the experiments, authored and reviewed drafts of the paper, and approved the final draft. YZ analyzed the data, prepared figures and tables, and approved the final draft. YL helped to complete validation experiments. LD prepared figures and tables, collected literature, and approved the final draft. ZP collected literature and approved the final draft. SW conceived and designed the experiments, reviewed drafts of the paper, and approved the final draft. XL conceived and designed the experiments, reviewed drafts of the paper, and approved the final draft.

ACKNOWLEDGMENTS

The authors thank TCGA, CGGA, GTEx, CCLE, and IMvigor210 datasets that made the data available, and all data obtained from these datasets kept to the rules for their usage and publication.

SUPPLEMENTARY MATERIAL

The Supplementary Material for this article can be found online at: https://www.frontiersin.org/articles/10.3389/fimmu.2022.899710/full#supplementary-material

REFERENCES

1. Ostrom QT, Cioffi G, Waite K, Kruchko C, Barnholtz-Sloan JS. CBTRUS Statistical Report: Primary Brain and Other Central Nervous System Tumors Diagnosed in the United States in 2014-2018. *Neuro Oncol* (2021) 23(12 Suppl 2):iii1–iii105. doi: 10.1093/neuonc/noab200
2. McGirt MJ, Chaichana KL, Attenello FJ, Weingart JD, Than K, Burger PC, et al. Extent of Surgical Resection is Independently Associated With Survival in Patients With Hemispheric Infiltrating Low-Grade Gliomas. *Neurosurgery* (2008) 63(4):700–7. doi: 10.1227/01.Neu.0000325729.41085.73
3. Smith JS, Chang EF, Lamborn KR, Chang SM, Prados MD, Cha S, et al. Role of Extent of Resection in the Long-Term Outcome of Low-Grade Hemispheric Gliomas. *J Clin Oncol* (2008) 26(8):1338–45. doi: 10.1200/jco.2007.13.9337
4. Fukuya Y, Ikuta S, Maruyama T, Nitta M, Saito T, Tsuzuki S, et al. Tumor Recurrence Patterns After Surgical Resection of Intracranial Low-Grade Gliomas. *J Neurooncol* (2019) 144(3):519–28. doi: 10.1007/s11060-019-03250-8
5. Shaw EG, Berkey B, Coons SW, Bullard D, Brachman D, Buckner JC, et al. Recurrence Following Neurosurgeon-Determined Gross-Total Resection of Adult Supratentorial Low-Grade Glioma: Results of a Prospective Clinical Trial. *J Neurosurg* (2008) 109(5):835–41. doi: 10.3171/jns/2008/109/11/0835
6. Sanai N, Chang S, Berger MS. Low-Grade Gliomas in Adults. *J Neurosurg* (2011) 115(5):948–65. doi: 10.3171/2011.7.Jns101238
7. Murphy ES, Leyrer CM, Parsons M, Suh JH, Chao ST, Yu JS, et al. Risk Factors for Malignant Transformation of Low-Grade Glioma. *Int J Radiat Oncol Biol Phys* (2018) 100(4):965–71. doi: 10.1016/j.ijrobp.2017.12.258
8. Delgado-López PD, Corrales-García EM, Martino J, Lastra-Aras E, Dueñas-Polo MT. Diffuse Low-Grade Glioma: A Review on the New Molecular Classification, Natural History and Current Management Strategies. *Clin Transl Oncol* (2017) 19(8):931–44. doi: 10.1007/s12094-017-1631-4
9. Westphal M, Lamszus K. The Neurobiology of Gliomas: From Cell Biology to the Development of Therapeutic Approaches. *Nat Rev Neurosci* (2011) 12 (9):495–508. doi: 10.1038/nrn3060
10. Jansen E, Hamisch C, Ruess D, Heiland DH, Goldbrunner R, Ruge MI, et al. Observation After Surgery for Low Grade Glioma: Long-Term Outcome in the Light of the 2016 WHO Classification. *J Neurooncol* (2019) 145(3):501–7. doi: 10.1007/s11060-019-03316-7
11. Amirouchene-Angelozzi N, Swanton C, Bardelli A. Tumor Evolution as a Therapeutic Target. *Cancer Discovery* (2017) 7(8):805–17. doi: 10.1158/2159-8290.Cd-17-0343
12. Mazor T, Pankov A, Johnson BE, Hong C, Hamilton EG, Bell RJA, et al. DNA Methylation and Somatic Mutations Converge on the Cell Cycle and Define Similar Evolutionary Histories in Brain Tumors. *Cancer Cell* (2015) 28 (3):307–17. doi: 10.1016/j.ccell.2015.07.012
13. Johnson BE, Mazor T, Hong C, Barnes M, Aihara K, McLean CY, et al. Mutational Analysis Reveals the Origin and Therapy-Driven Evolution of Recurrent Glioma. *Science* (2014) 343(6167):189–93. doi: 10.1126/science.1239947
14. van Thuijl HF, Mazor T, Johnson BE, Fouse SD, Aihara K, Hong C, et al. Evolution of DNA Repair Defects During Malignant Progression of Low-Grade Gliomas After Temozolomide Treatment. *Acta Neuropathol* (2015) 129 (4):597–607. doi: 10.1007/s00401-015-1403-6
15. Hu H, Mu Q, Bao Z, Chen Y, Liu Y, Chen J, et al. Mutational Landscape of Secondary Glioblastoma Guides MET-Targeted Trial in Brain Tumor. *Cell* (2018) 175(6):1665–78.e18. doi: 10.1016/j.cell.2018.09.038
16. Wainwright DA, Balyasnikova IV, Chang AL, Ahmed AU, Moon KS, Auffinger B, et al. IDO Expression in Brain Tumors Increases the Recruitment of Regulatory T Cells and Negatively Impacts Survival. *Clin Cancer Res* (2012) 18(22):6110–21. doi: 10.1158/1078-0432.Ccr-12-2130
17. Zhu C, Mustafa D, Zheng PP, van der Weiden M, Sacchetti A, Brandt M, et al. Activation of CECR1 in M2-Like TAMs Promotes Paracrine Stimulation-Mediated Glial Tumor Progression. *Neuro Oncol* (2017) 19(5):648–59. doi: 10.1093/neuonc/now251
18. Colombo MP, Piconese S. Regulatory-T-Cell Inhibition Versus Depletion: The Right Choice in Cancer Immunotherapy. *Nat Rev Cancer* (2007) 7 (11):880–7. doi: 10.1038/nrc2250
19. Ceccarelli M, Barthel FP, Malta TM, Sabedot TS, Salama SR, Murray BA, et al. Molecular Profiling Reveals Biologically Discrete Subsets and Pathways of Progression in Diffuse Glioma. *Cell* (2016) 164(3):550–63. doi: 10.1016/j.cell.2015.12.028
20. Zhao Z, Zhang KN, Wang Q, Li G, Zeng F, Zhang Y, et al. Chinese Glioma Genome Atlas (CGGA): A Comprehensive Resource With Functional Genomic Data From Chinese Glioma Patients. *Genomics Proteomics Bioinf* (2021) 19(1):1–12. doi: 10.1016/j.gpb.2020.10.005
21. Carithers LJ, Moore HM. The Genotype-Tissue Expression (GTEx) Project. *Biopres Biobank* (2015) 13(5):307–8. doi: 10.1089/bio.2015.29031.hmm
22. Wu T, Hu E, Xu S, Chen M, Guo P, Dai Z, et al. Clusterprofiler 4.0: A Universal Enrichment Tool for Interpreting Omics Data. *Innovation (N.Y)* (2021) 2(3):100141. doi: 10.1016/j.xinn.2021.100141

23. Liberzon A, Birger C, Thorvaldsdóttir H, Ghandi M, Mesirov JP, Tamayo P. The Molecular Signatures Database (MSigDB) Hallmark Gene Set Collection. *Cell Syst* (2015) 1(6):417–25. doi: 10.1016/j.cels.2015.12.004
24. Li T, Fu J, Zeng Z, Cohen D, Li J, Chen Q, et al. TIMER2.0 for Analysis of Tumor-Infiltrating Immune Cells. *Nucleic Acids Res* (2020) 48(W1):W509–w14. doi: 10.1093/nar/gkaa407
25. Chen B, Khodadoust MS, Liu CL, Newman AM, Alizadeh AA. Profiling Tumor Infiltrating Immune Cells With CIBERSORT. *Methods Mol Biol* (2018) 1711:243–59. doi: 10.1007/978-1-4939-7493-1_12
26. Aran D, Hu Z, Butte AJ. Xcell: Digitally Portraying the Tissue Cellular Heterogeneity Landscape. *Genome Biol* (2017) 18(1):220. doi: 10.1186/s13059-017-1349-1
27. Mariathasan S, Turley SJ, Nickles D, Castiglioni A, Yuen K, Wang Y, et al. Tgfβ Attenuates Tumour Response to PD-L1 Blockade by Contributing to Exclusion of T Cells. *Nature* (2018) 554(7693):544–8. doi: 10.1038/nature25501
28. Dempster JM, Boyle I, Vazquez F, Root DE, Boehm JS, Hahn WC, et al. Chronos: A Cell Population Dynamics Model of CRISPR Experiments That Improves Inference of Gene Fitness Effects. *Genome Biol* (2021) 22(1):343. doi: 10.1186/s13059-021-02540-7
29. Catarinella M, Grüner T, Strittmatter T, Marx A, Mayer TU. BTB-1: A Small Molecule Inhibitor of the Mitotic Motor Protein Kif18A. *Angew Chem Int Ed Engl* (2009) 48(48):9072–6. doi: 10.1002/anie.200904510
30. Vander Velde N, Guerin A, Ionescu-Ittu R, Shi S, Wu EQ, Lin SW, et al. Comparative Effectiveness of Non-Cisplatin First-Line Therapies for Metastatic Urothelial Carcinoma: Phase 2 IMvigor210 Study Versus US Patients Treated in the Veterans Health Administration. *Eur Urol Oncol* (2019) 2(1):12–20. doi: 10.1016/j.euo.2018.07.003
31. Zhou H, Meng M, Wang Z, Zhang H, Yang L, Li C, et al. The Role of M5c-Related lncRNAs in Predicting Overall Prognosis and Regulating the Lower Grade Glioma Microenvironment. *Front Oncol* (2022) 12:814742. doi: 10.3389/fonc.2022.814742
32. Zhang J, Wang N, Wu J, Gao X, Zhao H, Liu Z, et al. 5-Methylcytosine Related LncRNAs Reveal Immune Characteristics, Predict Prognosis and Oncology Treatment Outcome in Lower-Grade Gliomas. *Front Immunol* (2022) 13:844778. doi: 10.3389/fimmu.2022.844778
33. Tian W, Yan G, Chen K, Han X, Zhang W, Sun L, et al. Development and Validation of a Novel Prognostic Model for Lower-Grade Glioma Based on Enhancer RNA-Regulated Prognostic Genes. *Front Oncol* (2022) 12:714338. doi: 10.3389/fonc.2022.714338
34. Bai Z, Wang X, Zhang Z. Establishment and Validation of a 5 M6a RNA Methylation Regulatory Gene Prognostic Model in Low-Grade Glioma. *Front Genet* (2022) 13:655169. doi: 10.3389/fgene.2022.655169
35. Tanzhu G, Li N, Li Z, Zhou R, Shen L. Molecular Subtypes and Prognostic Signature of Pyroptosis-Related lncRNAs in Glioma Patients. *Front Oncol* (2022) 12:779168. doi: 10.3389/fonc.2022.779168
36. Belpaire M, Ewbank B, Taminiau A, Bridoux L, Deneyer N, Marchese D, et al. HOXA1 Is an Antagonist of Erα in Breast Cancer. *Front Oncol* (2021) 11:609521. doi: 10.3389/fonc.2021.609521
37. Shah N, Sukumar S. The Hox Genes and Their Roles in Oncogenesis. *Nat Rev Cancer* (2010) 10(5):361–71. doi: 10.1038/nrc2826
38. Yuan C, Zhu X, Han Y, Song C, Liu C, Lu S, et al. Elevated HOXA1 Expression Correlates With Accelerated Tumor Cell Proliferation and Poor Prognosis in Gastric Cancer Partly *via* Cyclin D1. *J Exp Clin Cancer Res* (2016) 35:15. doi: 10.1186/s13046-016-0294-2
39. Li Q, Dong C, Cui J, Wang Y, Hong X. Over-Expressed lncRNA HOTAIRM1 Promotes Tumor Growth and Invasion Through Up-Regulating HOXA1 and Sequestering G9a/EZH2/Dnmts Away From the HOXA1 Gene in Glioblastoma Multiforme. *J Exp Clin Cancer Res* (2018) 37(1):265. doi: 10.1186/s13046-018-0941-x
40. Hou L, Xu B, Mohankumar KM, Goffin V, Perry JK, Lobie PE, et al. The Prolactin Receptor Mediates HOXA1-Stimulated Oncogenicity in Mammary Carcinoma Cells. *Int J Oncol* (2012) 41(6):2285–95. doi: 10.3892/ijo.2012.1660
41. Nakamura T, Sakai K, Nakamura T, Matsumoto K. Hepatocyte Growth Factor Twenty Years on: Much More Than a Growth Factor. *J Gastroenterol Hepatol* (2011) 26 (Suppl 1):188–202. doi: 10.1111/j.1440-1746.2010.06549.x
42. Ebens A, Brose K, Leonardo ED, Hanson MGJr., Bladt F, Birchmeier C, et al. Hepatocyte Growth Factor/Scatter Factor Is an Axonal Chemoattractant and a Neurotrophic Factor for Spinal Motor Neurons. *Neuron* (1996) 17(6):1157–72. doi: 10.1016/s0896-6273(00)80247-0
43. Maina F, Klein R. Hepatocyte Growth Factor, A Versatile Signal for Developing Neurons. *Nat Neurosci* (1999) 2(3):213–7. doi: 10.1038/6310
44. Lock LS, Royal I, Naujokas MA, Park M. Identification of an Atypical Grb2 Carboxyl-Terminal SH3 Domain Binding Site in Gab Docking Proteins Reveals Grb2-Dependent and -Independent Recruitment of Gab1 to Receptor Tyrosine Kinases. *J Biol Chem* (2000) 275(40):31536–45. doi: 10.1074/jbc.M003597200
45. Awad AJ, Burns TC, Zhang Y, Abounader R. Targeting MET for Glioma Therapy. *Neurosurg Focus* (2014) 37(6):E10. doi: 10.3171/2014.9.Focus14520
46. Mulcahy EQX, Colón RR, Abounader R. HGF/MET Signaling in Malignant Brain Tumors. *Int J Mol Sci* (2020) 21(20):7546. doi: 10.3390/ijms21207546
47. Gürsel DB, Connell-Albert YS, Tuskan RG, Anastassiadis T, Walrath JC, Hawes JJ, et al. Control of Proliferation in Astrocytoma Cells by the Receptor Tyrosine Kinase/PI3K/AKT Signaling Axis and the Use of Prodium Iodide-103 and TCN as Potential Anti-Astrocytoma Therapies. *Neuro Oncol* (2011) 13(6):610–21. doi: 10.1093/neuonc/nor035
48. Mayr MI, Hümmer S, Bormann J, Grüner T, Adio S, Woehlke G, et al. The Human Kinesin Kif18A Is a Motile Microtubule Depolymerase Essential for Chromosome Congression. *Curr Biol* (2007) 17(6):488–98. doi: 10.1016/j.cub.2007.02.036
49. Stumpff J, von Dassow G, Wagenbach M, Asbury C, Wordeman L. The Kinesin-8 Motor Kif18A Suppresses Kinetochore Movements to Control Mitotic Chromosome Alignment. *Dev Cell* (2008) 14(2):252–62. doi: 10.1016/j.devcel.2007.11.014
50. Du Y, English CA, Ohi R. The Kinesin-8 Kif18A Dampens Microtubule Plus-End Dynamics. *Curr Biol* (2010) 20(4):374–80. doi: 10.1016/j.cub.2009.12.049
51. Tang F, Pan MH, Wan X, Lu Y, Zhang Y, Sun SC. Kif18a Regulates Sirt2-Mediated Tubulin Acetylation for Spindle Organization During Mouse Oocyte Meiosis. *Cell Div* (2018) 13:9. doi: 10.1186/s13008-018-0042-4
52. Marquis C, Fonseca CL, Queen KA, Wood L, Vandal SE, Malaby HLH, et al. Chromosomally Unstable Tumor Cells Specifically Require KIF18A for Proliferation. *Nat Commun* (2021) 12(1):1213. doi: 10.1038/s41467-021-21447-2
53. Zhong Y, Jiang L, Lin H, Li X, Long X, Zhou Y, et al. Overexpression of KIF18A Promotes Cell Proliferation, Inhibits Apoptosis, and Independently Predicts Unfavorable Prognosis in Lung Adenocarcinoma. *IUBMB Life* (2019) 71(7):942–55. doi: 10.1002/iub.2030
54. Nagahara M, Nishida N, Iwatsuki M, Ishimaru S, Mimori K, Tanaka F, et al. Kinesin 18A Expression: Clinical Relevance to Colorectal Cancer Progression. *Int J Cancer* (2011) 129(11):2543–52. doi: 10.1002/ijc.25916
55. Gupta MLJr., Carvalho P, Roof DM, Pellman D. Plus End-Specific Depolymerase Activity of Kip3, a Kinesin-8 Protein, Explains its Role in Positioning the Yeast Mitotic Spindle. *Nat Cell Biol* (2006) 8(9):913–23. doi: 10.1038/ncb1457
56. Varga V, Helenius J, Tanaka K, Hyman AA, Tanaka TU, Howard J. Yeast Kinesin-8 Depolymerizes Microtubules in a Length-Dependent Manner. *Nat Cell Biol* (2006) 8(9):957–62. doi: 10.1038/ncb1462
57. Whitehurst AW. Cause and Consequence of Cancer/Testis Antigen Activation in Cancer. *Annu Rev Pharmacol Toxicol* (2014) 54:251–72. doi: 10.1146/annurev-pharmtox-011112-140326
58. Xu F, Shen J, Xu S. Multi-Omics Data Analyses Construct a Six Immune-Related Genes Prognostic Model for Cervical Cancer in Tumor Microenvironment. *Front Genet* (2021) 12:663617. doi: 10.3389/fgene.2021.663617
59. Bai K, Zhao T, Li Y, Li X, Zhang Z, Du Z, et al. Integrating Genetic and Transcriptomic Data to Reveal Pathogenesis and Prognostic Markers of Pancreatic Adenocarcinoma. *Front Genet* (2021) 12:747270. doi: 10.3389/fgene.2021.747270
60. Huang GH, Du L, Li N, Zhang Y, Xiang Y, Tang JH, et al. Methylation-Mediated miR-155-FAM133A Axis Contributes to the Attenuated Invasion and Migration of IDH Mutant Gliomas. *Cancer Lett* (2018) 432:93–102. doi: 10.1016/j.canlet.2018.06.007
61. Buijs A, Sherr S, van Baal S, van Bezouw S, van der Plas D, Geurts van Kessel A, et al. Translocation (12;22) (P13;Q11) in Myeloproliferative Disorders Results in Fusion of the ETS-Like TEL Gene on 12p13 to the MN1 Gene on 22q11. *Oncogene* (1995) 10(8):1511–9.

62. Lekanne Deprez RH, Riegman PH, Groen NA, Warringa UL, van Biezen NA, Molijn AC, et al. Cloning and Characterization of MN1, A Gene From Chromosome 22q11, Which Is Disrupted by a Balanced Translocation in a Meningioma. *Oncogene* (1995) 10(8):1521–8.
63. Mak CCY, Doherty D, Lin AE, Vegas N, Cho MT, Viot G, et al. MN1 C-Terminal Truncation Syndrome Is a Novel Neurodevelopmental and Craniofacial Disorder With Partial Rhombencephalosynapsis. *Brain* (2020) 143(1):55–68. doi: 10.1093/brain/awz379
64. Sturm D, Orr BA, Toprak UH, Hovestadt V, Jones DTW, Capper D, et al. New Brain Tumor Entities Emerge From Molecular Classification of CNS-PNETs. *Cell* (2016) 164(5):1060–72. doi: 10.1016/j.cell.2016.01.015
65. Lehman NL, Usubalieva A, Lin T, Allen SJ, Tran QT, Mobley BC, et al. Genomic Analysis Demonstrates That Histologically-Defined Astroblastomas Are Molecularly Heterogeneous and That Tumors With MN1 Rearrangement Exhibit the Most Favorable Prognosis. *Acta Neuropathol Commun* (2019) 7 (1):42. doi: 10.1186/s40478-019-0689-3
66. Mhatre R, Sugur HS, Nandeesh BN, Chickabasaviah Y, Saini J, Santosh V. MN1 Rearrangement in Astroblastoma: Study of Eight Cases and Review of Literature. *Brain Tumor Pathol* (2019) 36(3):112–20. doi: 10.1007/s10014-019-00346-x
67. Hirose T, Nobusawa S, Sugiyama K, Amatya VJ, Fujimoto N, Sasaki A, et al. Astroblastoma: A Distinct Tumor Entity Characterized by Alterations of the X Chromosome and MN1 Rearrangement. *Brain Pathol* (2018) 28(5):684–94. doi: 10.1111/bpa.12565
68. Łastowska M, Trubicka J, Sobocińska A, Wojtas B, Niemira M, Szałkowska A, et al. Molecular Identification of CNS NB-FOXR2, CNS EFT-CIC, CNS HGNET-MN1 and CNS HGNET-BCOR Pediatric Brain Tumors Using Tumor-Specific Signature Genes. *Acta Neuropathol Commun* (2020) 8 (1):105. doi: 10.1186/s40478-020-00984-9
69. Baroni LV, Rugilo C, Lubieniecki F, Sampor C, Freytes C, Nobre L, et al. Treatment Response of CNS High-Grade Neuroepithelial Tumors With MN1 Alteration. *Pediatr Blood Cancer* (2020) 67(12):e28627. doi: 10.1002/pbc.28627
70. Houtgraaf JH, Versmissen J, van der Giessen WJ. A Concise Review of DNA Damage Checkpoints and Repair in Mammalian Cells. *Cardiovasc Revasc Med* (2006) 7(3):165–72. doi: 10.1016/j.carrev.2006.02.002
71. Fernet M, Mégnin-Chanet F, Hall J, Favaudon V. Control of the G2/M Checkpoints After Exposure to Low Doses of Ionising Radiation: Implications for Hyper-Radiosensitivity. *DNA Repair (Amst)* (2010) 9(1):48–57. doi: 10.1016/j.dnarep.2009.10.006
72. Mitra J, Enders GH. Cyclin A/Cdk2 Complexes Regulate Activation of Cdk1 and Cdc25 Phosphatases in Human Cells. *Oncogene* (2004) 23(19):3361–7. doi: 10.1038/sj.onc.1207446
73. Huang Q, Dong J, Wang AD, Shao NY, Sun JY, Li XN, et al. [Establishment of Malignant Progression Associated Gene Expression Profiles in Human Brain Glioma]. *Zhonghua Zhong Liu Za Zhi* (2003) 25(5):437–40.
74. Chen H, Huang Q, Zhai DZ, Dong J, Wang AD, Lan Q. [CDK1 Expression and Effects of CDK1 Silencing on the Malignant Phenotype of Glioma Cells]. *Zhonghua Zhong Liu Za Zhi* (2007) 29(7):484–8.
75. Giacinti C, Giordano A. RB and Cell Cycle Progression. *Oncogene* (2006) 25 (38):5220–7. doi: 10.1038/sj.onc.1209615
76. Chkheidze R, Raisanen J, Gagan J, Richardson TE, Pinho MC, Raj K, et al. Alterations in the RB Pathway With Inactivation of RB1 Characterize Glioblastomas With a Primitive Neuronal Component. *J Neuropathol Exp Neurol* (2021) 80(12):1092–8. doi: 10.1093/jnen/nlab109
77. Kheirollahi M, Mehr-Azin M, Kamalian N, Mehdipour P. Expression of Cyclin D2, P53, Rb and ATM Cell Cycle Genes in Brain Tumors. *Med Oncol* (2011) 28(1):7–14. doi: 10.1007/s12032-009-9412-8
78. Ferreira WA, Araújo MD, Anselmo NP, de Oliveira EH, Brito JR, Burbano RR, et al. Expression Analysis of Genes Involved in the RB/E2F Pathway in Astrocytic Tumors. *PloS One* (2015) 10(8):e0137259. doi: 10.1371/journal.pone.0137259
79. Shiao SL, Ganesan AP, Rugo HS, Coussens LM. Immune Microenvironments in Solid Tumors: New Targets for Therapy. *Genes Dev* (2011) 25(24):2559–72. doi: 10.1101/gad.169029.111
80. Domingues P, González-Tablas M, Otero Á, Pascual D, Miranda D, Ruiz L, et al. Tumor Infiltrating Immune Cells in Gliomas and Meningiomas. *Brain Behav Immun* (2016) 53:1–15. doi: 10.1016/j.bbi.2015.07.019
81. Mantovani A, Romero P, Palucka AK, Marincola FM. Tumour Immunity: Effector Response to Tumour and Role of the Microenvironment. *Lancet* (2008) 371(9614):771–83. doi: 10.1016/s0140-6736(08)60241-x
82. Hide T, Shibahara I, Kumabe T. Novel Concept of the Border Niche: Glioblastoma Cells Use Oligodendrocytes Progenitor Cells (GAOs) and Microglia to Acquire Stem Cell-Like Features. *Brain Tumor Pathol* (2019) 36(2):63–73. doi: 10.1007/s10014-019-00341-2

Conflict of Interest: The authors declare that the research was conducted in the absence of any commercial or financial relationships that could be construed as a potential conflict of interest.

Publisher's Note: All claims expressed in this article are solely those of the authors and do not necessarily represent those of their affiliated organizations, or those of the publisher, the editors and the reviewers. Any product that may be evaluated in this article, or claim that may be made by its manufacturer, is not guaranteed or endorsed by the publisher.

Copyright © 2022 Teng, Zhu, Li, Dai, Pan, Wanggou and Li. This is an open-access article distributed under the terms of the Creative Commons Attribution License (CC BY). The use, distribution or reproduction in other forums is permitted, provided the original author(s) and the copyright owner(s) are credited and that the original publication in this journal is cited, in accordance with accepted academic practice. No use, distribution or reproduction is permitted which does not comply with these terms.

frontiers | Frontiers in Oncology

ORIGINAL RESEARCH
published: 02 June 2022
doi: 10.3389/fonc.2022.899443

The Identification of Necroptosis-Related Subtypes, the Construction of a Prognostic Model, and the Characterization of the Tumor Microenvironment in Gliomas

Yueyang Ba[1†], Jiahao Su[2†], Shuangqi Gao[1†], Zhi Liao[1], Zhimin Wu[1], Chengan Cao[1], Chaofeng Liang[1], Jin Gong[1*] and Ying Guo[1*]*

[1] Department of Neurosurgery, The Third Affiliated Hospital, Sun Yat-sen University, Guangzhou, China,
[2] Department of Neurosurgery, Zhongshan City People's Hospital, Zhongshan, China

Necroptosis is a recently discovered form of cell death that plays a vital role in the progression of cancer, the spread of metastases, and the immunologic response to tumors. Due to the dual role of necrotic apoptotic processes in tumor pathogenesis and the heterogeneity of gliomas, the function of necroptosis in the glioma microenvironment is still poorly understood. We characterized the expression of necroptosis-related genes (NRGs) within glioma samples at both the genetic and transcriptional levels, identifying three distinct subtypes. Additionally, we constructed a risk score, which is capable of accurately predicting patient prognosis, correlates with tumor mutation burden (TMB), tumor stem cell index (CSC), immune checkpoints, and predicts tumor drug sensitivity. To facilitate its application in the clinic, we developed a nomogram and demonstrated that it predicts the prognosis of glioma patients with good accuracy and reliability using multiple datasets. We examined the function of necroptosis in the tumor microenvironment (TME) and the prognosis of gliomas, which may be useful for guiding individualized treatment plans for gliomas targeting necroptosis.

Keywords: necroptosis, glioma, nomogram, tumor microenvironment, TMB

OPEN ACCESS

Edited by:
Quan Cheng,
Central South University, China

Reviewed by:
Zixiang Cong,
Nanjing University, China
Xinwei Han,
Zhengzhou University, China
Weimin Zhong,
Xiamen Fifth Hospital, China

***Correspondence:**
Chaofeng Liang
lcfjeff@163.com
Jin Gong
chinaclinic2000@126.com
Ying Guo
guoy@mail.sysu.edu.cn

†These authors have contributed equally to this work and share first authorship

Specialty section:
This article was submitted to Cancer Immunity and Immunotherapy, a section of the journal Frontiers in Oncology

Received: *18 March 2022*
Accepted: *06 May 2022*
Published: *02 June 2022*

Citation:
Ba Y, Su J, Gao S, Liao Z, Wu Z, Cao C, Liang C, Gong J and Guo Y (2022) The Identification of Necroptosis-Related Subtypes, the Construction of a Prognostic Model, and the Characterization of the Tumor Microenvironment in Gliomas. Front. Oncol. 12:899443. doi: 10.3389/fonc.2022.899443

INTRODUCTION

Among the many malignant tumors in the central nervous system, glioma is the most common, characterized by ease of recurrence and a high mortality rate (1). Diffuse gliomas are classified into 3 grades (WHO II, WHO III, WHO IV), and the higher the grade, the worse the prognosis (2).

Although the survival time of glioma patients has improved by using various treatments including surgery, radiotherapy, and chemotherapy, it is still far from expected (3, 4). With the development of molecular pathology, several molecular markers have been found to be relevant to the occurrence, progression, and prognosis of gliomas. These markers include methylation of the MGMT promoter, IDH mutations, and co-deletion of chromosome 1p/19q (5, 6). However, due to the high heterogeneity of gliomas, these markers are currently not fully adequate for predicting

prognosis and guiding individualized therapy. Thus, it is imperative to construct reliable new prognostic models to predict the microenvironment of the tumor and to guide individualized therapies.

Necroptosis, a cystathionine-independent programmed death, is regulated mainly by receptor-interacting protein [RIP] kinase 3 (RIPK3), RIPK1, and mixed-lineage kinase structural domain-like pseudokinase (MLKL) (7, 8). As a new form of necrotic cell death, necrotrophic apoptosis is indispensable for the biological processes of cancer development, progression, metastasis and prognosis, and immune surveillance (9–14). In tumors, it has dual functions; its key mediators promote tumorigenesis and progression (15, 16); and it also prevents tumor development when apoptosis is compromised (17, 18). Targeting necrotic apoptosis is a promising immunotherapeutic approach for eliminating tumor cells when tumors become apoptosis-resistant. A variety of drugs and chemotherapeutic agents that have been approved for clinical trials are selective necroptosis inducers for specific tumors (11). Due to the high heterogeneity of gliomas, the impact of necroptosis on their prognosis and immunotherapy is not well elucidated. Because of technical limitations, most research has focused on individual drug or mediator targets, whereas immunotherapy and prognosis are the results of all relevant genes working in concert. Therefore, there is an urgent need to comprehensively understand the impact of necroptosis markers on the TME, immunotherapy response, and prognosis of glioma. However, the role played by necroptosis-related genes in the development and prognosis of glioma has not been effectively elucidated by current studies.

In this research, we comprehensively assessed the immune landscape of necroptosis-related genes (NRGs) in glioma patients. We explored the effect of NRGs on the TME and immunotherapy of gliomas. We then constructed a risk score capable of accurately predicting tumor immune status, prognosis, and sensitivity to chemotherapy. The final risk score was combined with clinical data to construct a nomogram that provides guidance for the clinical application.

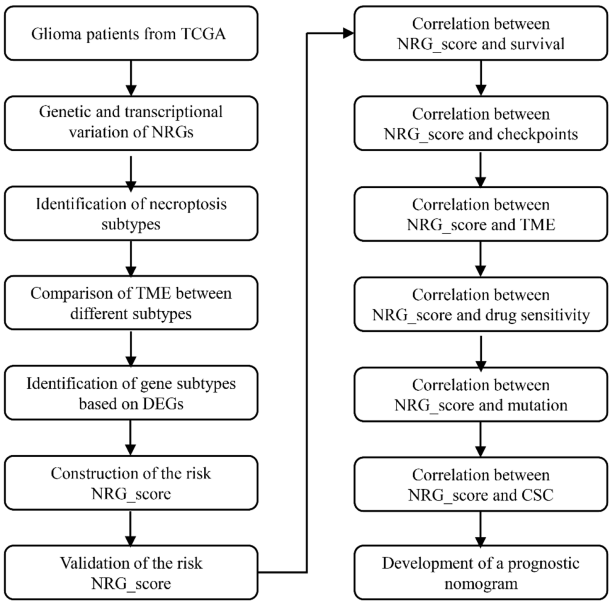

FIGURE 1 | The entire analytical process of the study.

MATERIALS AND METHODS

Datasets

In **Figure 1**, we present an overview of the analysis of this research. The Cancer Genome Atlas (TCGA) database was searched on January 1, 2022, to obtain the RNA transcriptomic datasets (HTSeq- per kilobase million (FPKM) and HTSeq-Counts) and associated clinical information for the patient's 5 normal brain tissue samples and 698 glioma samples. RNA transcriptome data (FPKM and counts data) from normal brains were obtained from the GTEx database (http://xena.ucsc.edu/) on January 1, 2022. RNA transcriptome data and corresponding clinical data were collected from the Chinese Glioma Genome Atlas (CCGA) database for 693 and 325 patients with glioma (12).

The GTEx and TCGA datasets were merged to remove batch effects by the "Combat" algorithm, and the CGGA dataset was merged in the same way. Fragments We converted the values as transcripts per kilobase million (TPM) from FPKM. The Counts value matrix was used only to identify differential expression, while the TPM matrix was used for other analysis. Patients with missing overall survival values and duplicate samples were excluded when constructing models for prognostic analysis. The TCGA set was randomly assigned to the training and test groups by Perl and caret R packages in a ratio of 2:1. For validation of the prognostic model, the Rembrandt and CGGA datasets were utilized as the external validation datasets. The clinical data of these datasets are available in **Supplementary Tables 1, 2**. Since TCGA, Rembrandt, and CGGA databases are open access data and publicly available, this research did not need ethical approval. The copy number variation (CNV) and somatic datasets of glioma were also collected from the Xena and TCGA, respectively. Data analysis was performed using Perl (5.34.0) and R (version 4.1.0).

Copy Number, Mutation Analysis, and Differential Expression Analysis of NRGs

From the necroptosis gene set M24779.gmt of the MSigDB (http://www.broad.mit.edu/gsea/msigdb/) and previous reports on necroptosis (19), we ended up with 67 necroptosis-associated genes (**Supplementary Table 3**). The Perl and R software were applied for CNV analysis, the 'RCircos' package was applied to show the distribution of NRGs alterations in chromosomes, and the 'maftools' were used to map the oncoplot of gene mutation. The 'limma' and 'reshape2' packages were used to identify differences in NRGs expression in normal brain tissue and gliomas. We further performed protein-protein interaction (PPI) networks for 67 NRGs using the STRING (https://cn.string-db.org/) and the interaction score was set to the highest confidence (0.9). The top 50 differentially expressed NRGs

among them were visualized using ggplot2 for correlation analysis.

Consensus Clustering Analysis of NRGs

Prognostic risk network plots were drawn using the 'RColorBrewer', 'psych', 'igraph', and 'reshape2' packages. Based on the expression levels of NRGs, patients with glioma were classified into distinct NRGclusters using the R package "ConsensusClusterPlus".

Clinical Features and Prognosis of Glioma Based on Molecular Subtypes

A correlation analysis was applied among the differences in molecular subtypes, as determined by consistent clustering, and different clinicopathological characteristics and prognosis. Clinical and pathological characteristics of the patients included survival time, survival status, gender, age, WHO grade, the status of radiation therapy or chemotherapy, the presence of mutations for IDH, 1p/19q codeletion, and MGMT promoter phosphorylation. Using the "survminer" and "survival" R packages, we examined prognostic differences of different subtypes based on Kaplan-Meier curves.

TME, PD-L1, and PD-1 in Different Molecular Subtypes

Our evaluation of each patient's immune and stromal component was performed utilizing the ESTIMATE. To evaluate the proportions of distinct immune cell types, the CIBERSORT algorithm was applied (20). By using "ssGSEA" in the R package "GSVA" (21), we quantified the levels of cellular infiltration of the immune system. Further analysis was conducted on the expression of PD-1 and PD-L1 among the subtypes.

Identification and Functional Enrichment of DEGs

Functional enrichment analysis of DEGs between distinct subtypes was conducted with the "clusterprofiler" package (adjusted p-value < 0.05). The clusterprofiler is a popular machine learning algorithm, which was extensively utilized in medical studies (22–27).

Construction of the NRG_Score

NRG_score was constructed to evaluate the necroptosis of tumors. A univariate Cox regression analysis was applied on these prognostic DEGs among NRGclusters. Following this, patients were classified into four geneClusters using the consensus clustering analysis. The consensus clustering is a popular bioinformatics algorithm, which was extensively utilized in cancer-related studies (28–32).

Patients with missing overall survival values and duplicate samples were excluded. Patients with glioma from TCGA datasets were randomly classified into the training and test groups by the Perl and Caret R packages in a ratio of 2:1. For the training set, the NRG_score was figured out using Lasso Cox and multivariate Cox regression analysis. In calculating the NRG_score, the following formula was used:

$$NRG_score = \sum(Expi * Coefi)$$

Expi and Coefi of this equation correspond to the expression and risk coefficients, respectively. A median risk score was used for dividing patients into high-risk (NRG_score > median) and low-risk groups (NRG_score < median). The data was presented in a graphical format after principal component analysis (PCA) was conducted utilizing the package "ggplot2".

Acquisition of Clinical Specimens, RNA Isolation, and Quantitative Real-Time Polymerase Chain Reaction PCR (RT-qPCR)

Six pairs of gliomas and non-tumor tissues adjacent to the tumors were collected from glioma patients at Zhongshan City People's Hospital. The removed samples were immediately stored at -80°C until use. Informed consent was obtained from all patients with glioma participating in this research. The ethics committee of Zhongshan City People's Hospital reviewed and approved the study.

Total RNA was extracted from glioma tissue using TRIzol reagent (Thermo Fisher Scientific, USA). RNA was reverse transcribed to Complementary DNA using HIScriptIIIRT SuperMix (Vazyme, Nanjing, China). The qRT-PCR analysis was performed using SYBR Green qPCR Master Mix (Vazyme, Nanjing, China) on ABI QuantStudioTM 5 (Agilent Technologies, USA). In all PCR experiments, data were quantified using the 2-ΔΔCt method and normalized by GAPDH. Primers for specific target genes (**Supplementary Table 4**) were synthesized by Genepharma Biotech (Shanghai, China).

To further assess the changes in protein levels of these genes, typical immunohistochemical results were obtained from the Human Protein Atlas (HPA) and analyzed for histochemistry score (H-SCORE). The staining intensity was divided into 4 grades: negative, grade 0; weakly positive, grade 1; positive, grade 2; strong positive, grade 3. Score H-SCORE according to the percentage of positive staining, H-SCORE = ∑ (Pixi) = (weakly positive Pi × 1) + (positive Pi × 2) + (strong positive Pi × 3) (where Pi represents the percentage of positive cells in the number of all cells in the section, and i represents the staining intensity; the total score range is 0 ~ 300).

Survival, TMB, CSC, Mutation, Drug Sensitivity Analysis in High and Low-Risk Groups

We compared the difference of NRG_score in two groups. PCA analysis was applied to verify the differentiation of patients among the two groups. The receiver operating characteristic (ROC) and Kaplan-Meier survival analysis were applied for the prognostic prediction of patients. To assess the immune cells infiltrating the glioma, CIBERSORT was conducted. In addition, we evaluated the correlation of the 11 NRGs in the model with the infiltrating immune cells. The ESTIMATE package was applied to compare the TME between the two risk groups. We

also evaluated the differences between TMB, gene mutations, PD-L1, PD-1, and CSC between the two risk groups. Using the "pRRophetic" package, semi-inhibitory concentrations (IC50) were calculated to assess the sensitivity of gliomas to common chemotherapy agents.

The Development and Validation of a Nomogram

Using the 'RMS' package, we compiled the risk scores with the patient's clinicopathological information and developed a predictive nomogram. In this nomogram, every variable corresponds to a score, and the total score is calculated by averaging all variables for one patient. The prediction power of the nomogram was assessed using time-dependent ROC curves for each dataset. To describe the accordance between the predicted and observed survival outcomes for 1-, 3-, and 5-years, calibration plots of the nomogram were analyzed. We also compared the accuracy of the WHO grade and the nomogram in predicting 1-, 3-, and 5-year survivals using time-dependent ROC curves.

Statistical Analyses

The statistical analysis was conducted using R (4.1.0). A p-value or adjusted p-value of 0.05 is used as the level of statistical significance.

RESULTS

The Landscape of Genetic and Transcriptional Variation of NRGs in Glioma

The overview of the analysis of this research was presented in **Figure 1**. This study involved 67 NRGs in total. We first summarized the frequency of somatic mutations in these NRGs in glioma patients and found that LGG patients had a relatively high frequency of mutations (**Figure 2A**). As shown in **Figure 2A**, mutations occurred in 451 (89.13%) of 506 LGG samples, with missense mutations being the most common mutation classification. Among them, IDH1 had the highest mutation rate (77%), followed by ATRX (37%), EGFR (6%), and IDH2 (4%). As shown in **Figure 2B**, out of 365 samples of GBM patients without IDH1 mutation, 144 (32.60%) patients had mutations in NRGs, with EGFR having the highest mutation rate (20%), followed by ATRX (4%), FLT3 (2%) and BRAF (2%). Next, we explored the impact of mutations in these NRGs on the prognosis of glioma patients. As shown in **Figure 2C**, patients with a high tumor mutation burden (TMB) had significantly lower survival rates than those with lower TMB. Furthermore, the mutation frequency of NRGs gradually increased with increasing glioma grade (**Figure 2D**).

These NRGs were examined for the frequency of somatic copy number variation (CNV) in glioma from the TCGA cohort, and we found that CNV was frequent across all NRGs. The incidence of NRG deletion in glioma samples was mostly greater than the incidence of acquisition. Among them, CDKN2A, TARDBP, TNFRSF1B, BNIP3, SIRT3, and TLR3 had a higher incidence of loss, while EGFR, MYC, BRAF, TNFRSF1A, DIABLO, GATA3, and TNFSF10 had a higher incidence of CNV gain (**Figure 2E**). The location of these NRGs on chromosomes with altered CNVs is depicted in **Figure 2F**.

Comparing the differential expression of 67 NRGs in 1153 normal brain tissues (GTEx 1148, TCGA 5) with 698 glioma tissues (TCGA), we found 63 DEGs (all FDR <0.05, **Figure 2G**). As shown in **Figure 3A** and **Supplementary Table 5**, NRGs were categorized as highly expressed, lowly expressed, or not differentially expressed (|FoldChange| <1.2) in gliomas. Among them, 35 genes, including EGFR, MYC, CDKN2A, TERT, IDH1, GATA3, PLK1, ID1, and TLR3, were up-regulated; 16 genes, including TSC1, HDAC9, USP22, STUB1, ATRX, MAPK8, ALK, HSP90AA1, and BNIP3, were down-regulated; and the expression of 16 genes, including MLKL, AXL, BACH2, SQSTM1, IPMK, MAP3K7, CFLAR, and BCL2, was not significantly changed. To further explore the interactions between these NRGs, a PPI network was constructed. The result revealed that ZBP1, CASP8, CD40, CFLAR, CYLD, FAS, FADD, RIPK1, and RIPK3 were the hub genes (all combined score > 0.9) (**Figure 3B**). The relevant heatmap of the top 50 NRGs in TCGA was shown in **Figure 3C**. Our analysis revealed significant differences in genetic profiles and expression levels of NRGs between normal brain tissue and glioma, suggesting a potential role of NRGs in glioma.

Identification of NRGclusters in Glioma

To explore the important role played by NRGs in glioma patients, a comprehensive analysis was performed. Univariate regression analysis (**Supplementary Table 6**) showed that 50 of these NRGs had prognostic value (P<0.05). As shown in **Figure 4A** and **Supplementary Table 7**, NRGs interacted, co-expressed, and had a combined effect on the prognosis of glioma patients. Most of NRGs were positively correlated with each other and were risk factors.

Further investigating the role played by the NRGs in gliomas, we utilized a consensus clustering algorithm to examine subtypes of glioma patients according to the expression of NRGs (**Supplementary Figure 1A-F**). It appears that k = 3 is the best choice for classifying the dataset into NRGcluster A, B, and C (**Figure 4B**). In this scenario, the different subtypes are strongly correlated within groups and weakly correlated between groups.

Using ssGSEA to assess immune activity among glioma patients of different subtypes, we explored the role of necroptosis in glioma immunity. It was found that the infiltrating immune cells differed significantly between NRGclusters (**Figure 4C** and **Supplementary Table 8**). The infiltration level of immune cells was commonly high in NRGcluster C compared to the other two subtypes, especially activated CD8 T cells, activated dendritic cells, activated CD4 T cells, gamma delta T cells, MDSCs, immature B cells, natural killer cells, macrophages, and neutrophilia, etc.

Following this, we analyzed the immune checkpoints of these subtypes and found that both PD-1 and PD-L1 expression was higher in NRGcluster C than those in the other two subtypes (**Figures 4D, E**). TME scores of these NRGclusters were assessed

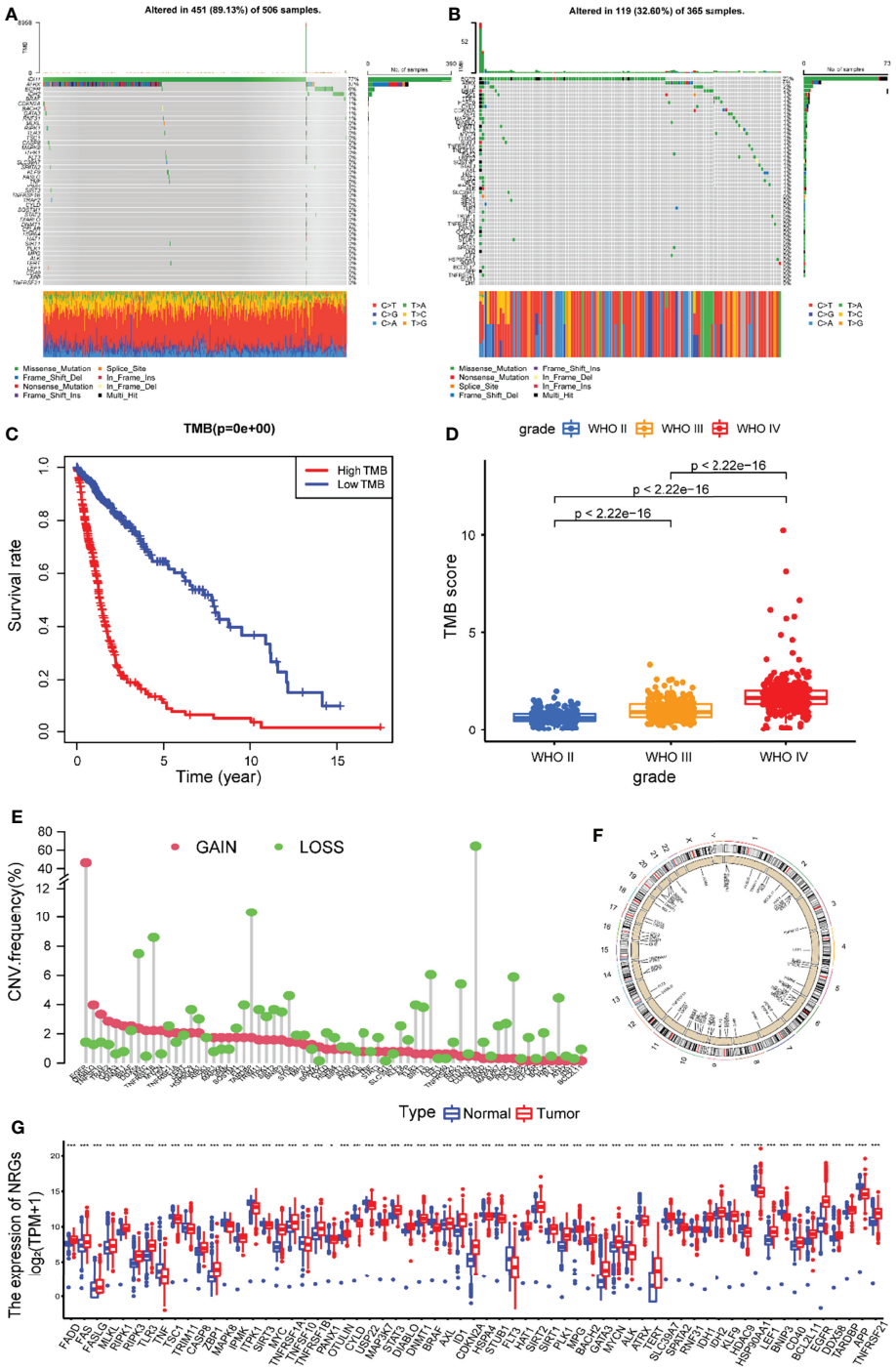

FIGURE 2 | The landscape of genetic and transcriptional variation of NRG in glioma. Mutation frequencies of 67 NRGs in 506 patients with LGG **(A)** and 365 GBM patients without IDH1 mutation **(B)** from the TCGA dataset. **(C)** Kaplan-Meier survival analysis of the high TMB and low TMB groups. **(D)** Comparison of TMB score in gliomas of different grades. **(E)** The CNV variation frequencies of 67 NRGs in the patients with LGG or GBM from the TCGA dataset. **(F)** Locations of CNV alterations of 67 NRGs on 23 chromosomes. **(G)** The differential expression of 67 NRGs between gliomas and normal brain tissue. NRGs, necroptosis-related genes; LGG, low grade gliomas; GBM, glioblastoma; TCGA, The Cancer Genome Atlas; CNV, copy number variant; ***P<0.001, **P<0.01, *P<0.05.

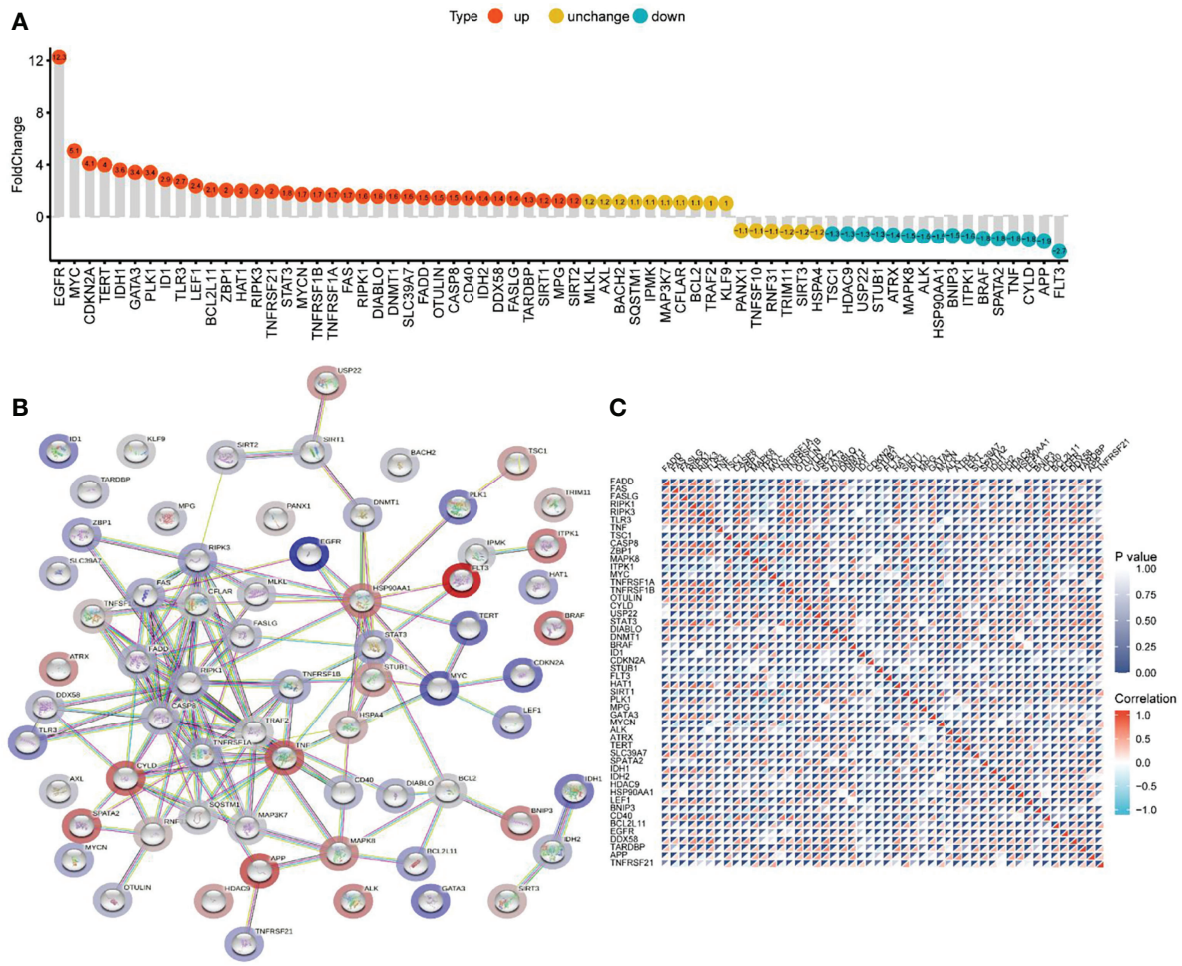

FIGURE 3 | The differential expression, PPI network, and expression correlation of NRGs. **(A)** Differential expression of NRGs in normal brain tissue and glioma. **(B)** The PPI network of NRGs. **(C)** The correlation of expression of NRGs.

utilizing the ESTIMATE, and similar to previous results, they were higher in NRGcluster C than those in the other two subtypes (**Figure 4F**).

Identification of geneClusters Based on DEGs

To further investigate the biological mechanisms underlying the differences in several NRGclusters, we applied the "limma" package to find DEGs of three subtypes and obtained 2012 DEGs by taking intersections (**Figure 5A**). The GO functional enrichment analysis of these DEGs revealed that they were enriched in biological processes related to immunity (**Figure 5B** and **Supplementary Table 9**). The KEGG analysis revealed that DEGs were enriched in pathways related to immune and inflammatory responses (**Figure 5C** and **Supplementary Table 9**). The previous results suggest that NRGs may be critical in tumor immunity. To further investigate the underlying regulatory mechanisms of NRGs, we initially conducted the univariate Cox regression analysis on 2012 DEGs and found that 1,866 of them were associated with prognosis (**Supplementary Table 10**). Then, based on these prognosis-related DEGs, a cluster analysis of samples was performed (**Supplementary Figure 2A–F**), and it was found that the samples of glioma patients in TCGA could be divided into geneClusters A-D 4 subtypes optimally (**Figure 5D**).

To verify the differences in prognosis across geneClusters, we performed survival analysis. According to the Kaplan-Meier curve, the prognosis of glioma patients in geneCluster A was worse than those in the other two subtypes ($P < 0.001$, **Figure 5E**). Subsequently, we compared the clinicopathological data and DEGs in patients of the 4 geneClusters. We found that poor prognosis in the geneCluster A group was associated with age > 40 years, WHO class IV, unmutated IDH, and unphosphorylated MGMT promoter (**Figure 5F**). In addition, the expression of NRGs was also generally significantly different between geneClusters(**Figure 5G**).

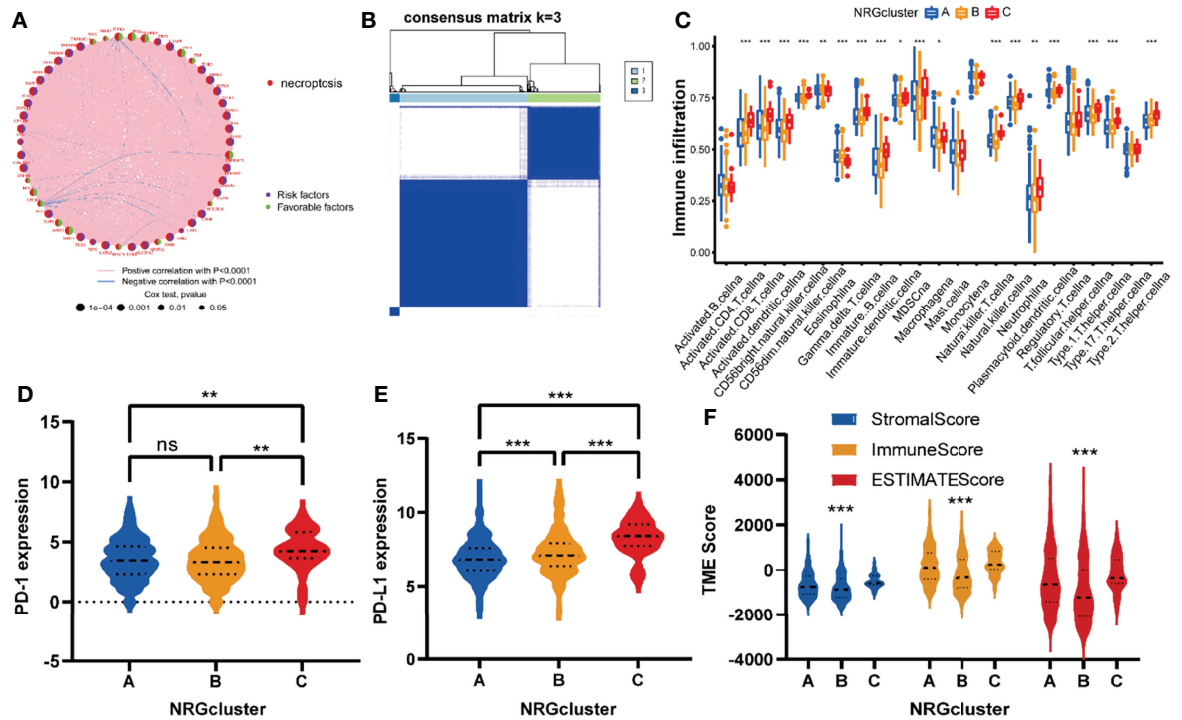

FIGURE 4 | NRGclusters of gliomas divided by consensus clustering algorithm and clinicopathological characteristics of distinct subtypes. **(A)** Interactions of NRGs in glioma. The thickness of the line that connects a pair of NRGs indicates the strength of their association. Positive correlations are indicated in red and negative correlations in blue. **(B)** Heatmap of the consensus clustering matrix (k = 3) dividing glioma patients into the three NRGclusters. **(C)** The comparison of infiltration levels of immune cells in three NRGclusters. **(D, E)** Expression of PD-1 and PD-L1 in three NRG clusters. **(F)** Correlation between three NRGclusters and TME scores. TME, tumor microenvironment; ***P<0.001, **P<0.01, *P<0.05, ns P > 0.05.

Development and Validation of the Risk NRG_Score

NRG_score was constructed based on the prognosis-related DEGs of different subtypes. We divided the TCGA glioma patients into training (n = 444) and validation sets (n = 218) in the ratio of 2:1, utilizing the package "caret". We then applied Lasso regression analysis to screen out the optimum 23 prognostic genes among the DEGs (**Figures 6A, B**). The Subsequent multivariate Cox regression analysis was conducted on them, and we finally got 11 genes, including 5 low-risk genes (SEMA4G, NRG3, IDI1, ARHGAP12, CALN1) and 6 high-risk genes (SCYL2, PTDSS1, H2AX, PHF11, FAM171A1, PPM1M) (**Figure 6C**). According to the multivariate cox regression results, the formula of NRG_score was constructed as follows: risk score = (0.0268*expression of SCYL2) + (0.0176*expression of PTDSS1) + (-0.0540*expression of SEMA4G) + (-0.0235*expression of NRG3) +(-0.0079*expression of IDI1) +(0.0017*expression of H2AX) + (0.0367*expression of PHF11) + (-0.0129*expression of ARHGAP12) + (0.0046*expression of FAM171A1) + (0.0214*expression of PPM1M) + (-0.0225*expression of CALN1).

The glioma patients of TCGA were assigned to high-risk (NRG_score > median, n = 222) and low-risk (NRG_score < median, n = 222) groups. The expression of most NRGs is significantly different between the high and low risk groups (**Figure 6D**). The PCA analysis (**Figure 7A**) showed that NRG_score was able to discriminate patients well.

We explored the distribution of NRG_score among different subtypes. The NRG_scores of patients in three NRGclusters are statistically significantly different (P<0.01) (**Figure 7B**). Similarly, the NRG_score also differed significantly among several geneClusters (**Figure 7C**), with geneCluster A patients having the highest risk score, geneCluster C having the lowest risk score, and geneClusters B and D in the middle. Next, we examined the distribution of patients within the NRGcluster groups, the geneCluster groups, and the NRG_score risk groups (**Figure 7D**).

Based on the previous results, we found that the higher the NRG_score, the lower the survival rate of glioma patients. Further validating the result, we ranked all patients according to the NRG_score. According to the NRG risk distribution plot, the number of patients who died increased with increasing risk scores, and most of these deaths were attributed to patients with high-risk scores (**Figures 7E, F**). We present the expression level of the genes involved in the risk model (**Figure 7G**). In the high-risk group, glioma patients had a lower survival rate than that in the low-risk group (P < 0.001; **Figure 7H**). In addition, the NRG risk score had high prognostic predictive performance, with AUC values of 0.887, 0.930, and 0.893 for 1-, 3- and 5-year survival, respectively (**Figure 7I**).

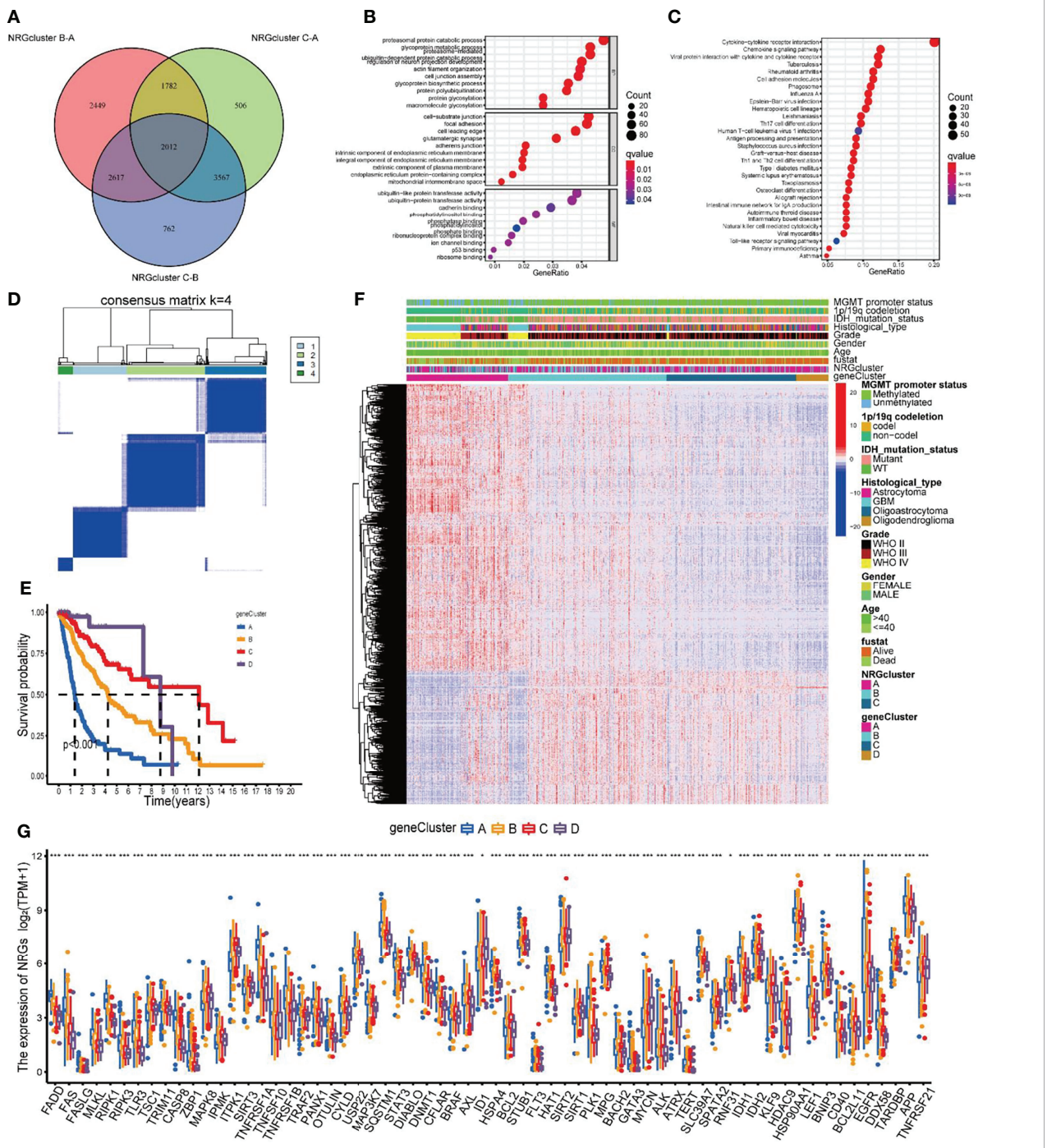

FIGURE 5 | Identification of gene subtypes based on DEGs. **(A)** The Venn diagrams for the three NRGclusters. **(B, C)** Functional enrichment analysis of GO and KEGG for DEGs among three NRGclusters. **(D)** Heatmap of the consensus clustering matrix (k = 4) dividing glioma patients into four geneClusters. **(E)** Kaplan-Meier survival analysis of the four geneClusters. **(F)** The clinicopathologic features of the four geneClusters. **(G)** The differential expression of 67 NRGs among the geneClusters. DEGs differentially expressed genes; GO, Gene Ontology; KEGG, Kyoto Encyclopedia of Genes and Genomes; NRGs, necroptosis-related genes. ***P<0.001, **P<0.01, *P<0.05.

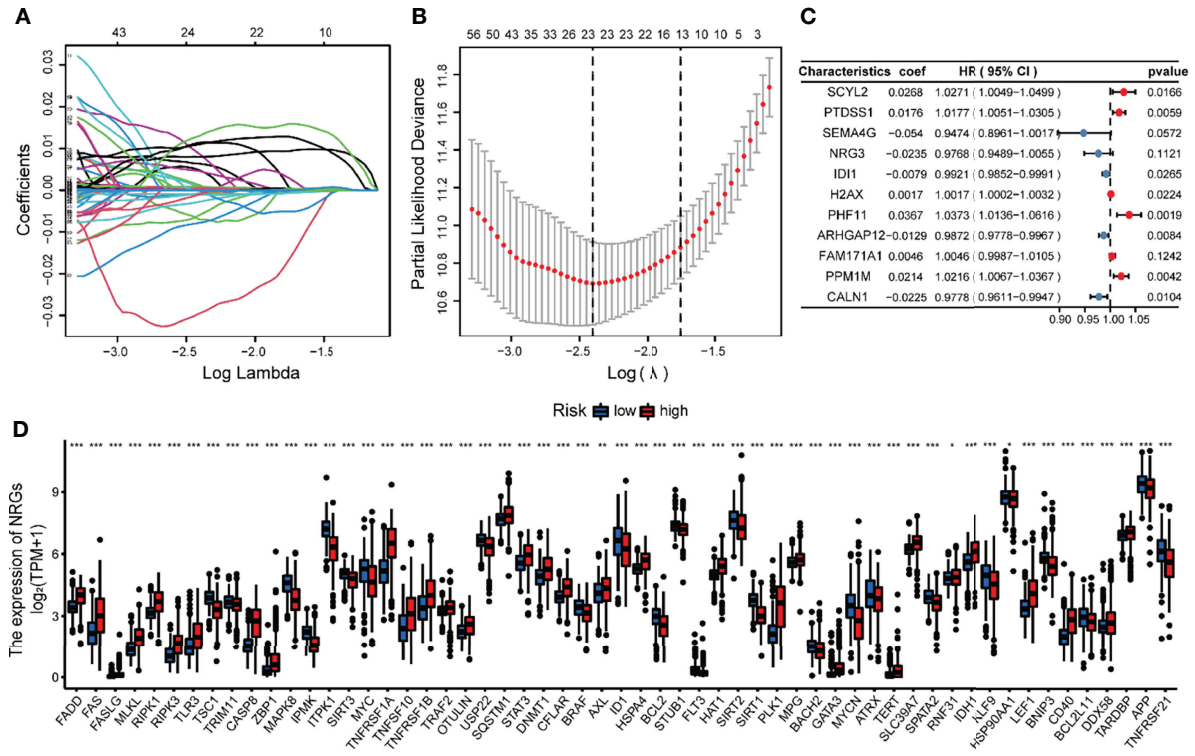

FIGURE 6 | Identification of representative candidate prognostic genes and differential expression of NRGs between the high and low-risk groups. **(A)** The LASSO regression analysis of the candidate prognostic genes. **(B)** The partial likelihood of deviance of the prognostic genes. **(C)** Forest plot of the multivariate Cox regression analysis for candidate genes. **(D)** The differential expression of NRGs between the high and low-risk groups. ***P<0.001, **P<0.01, *P<0.05.

To further validate the excellent prognostic predictive performance of NRG_score, we utilized the same formula to calculate the risk scores of patients in the internal test dataset and two external validation sets of CGGA and Rembrandt, and we divided the patients into two risk groups. We found that the number of patients who died increased significantly with increasing NRG_score in the internal test group (**Supplementary Figure 3A**), the two external validation sets of the CGGA (**Supplementary Figure 3B**), and Rembrandt (**Supplementary Figure 3C**). According to the survival analysis of the three validation sets (**Supplementary Figures 3D–F**), the survival rate of glioma patients was higher in the low-risk group than that in the high-risk group (P<0.001). The analysis of the predictive prognostic performance of NRG risk score (**Supplementary Figures 3G–I**) found that the AUC values of 1-, 3-, and 5-year survival remained high for the three validation sets, and the apparent NRG risk scores had excellent predicting prognostic power.

Validation of Expression Levels of 11 Genes in the Prognostic Model

To further evaluate the expression levels of genes in the model in clinical samples, we subjected 6 pairs of gliomas and their adjacent normal tissues to RT-qPCR analysis. As shown in **Figure 8**, 11 genes were significantly differentially expressed in glioma and adjacent normal brain tissues. In glioma tissues, most genes were upregulated in expression levels, while CALN1 expression was downregulated.

To further assess the changes in protein levels of these genes, typical immunohistochemical results obtained from the Human Protein Atlas (HPA) were presented. Among them, NRG3 and PHF11 protein expression data were not available in HPA. As shown in **Figure 9**, the differential trends in protein expression levels of the other nine genes were approximately the same as those in the mRNA expression levels. The above results verified the expression changes of 11 genes in the model at mRNA and protein levels and laterally confirmed the reliability of the genes included in the model.

Comparison of TME and Checkpoints Between the Two Risk Groups

To assess the correlation between NRG scores and TME, we utilized the CIBERSORT algorithm to assess the level of immune cells infiltration. The NRG_score was positively correlated with CD8 + T cells, M1 macrophages, M0 macrophages, M2 macrophages, activated NK cells, follicular helper T cells, and neutrophils, and negatively correlated with CD4 memory resting T cells, Eosinophils, activated mast cells, and monocytes (**Figure 10A**). We also found that the high-risk group had significantly higher TME Scores, reflecting a higher level of immune cells infiltration (**Figure 10B**).

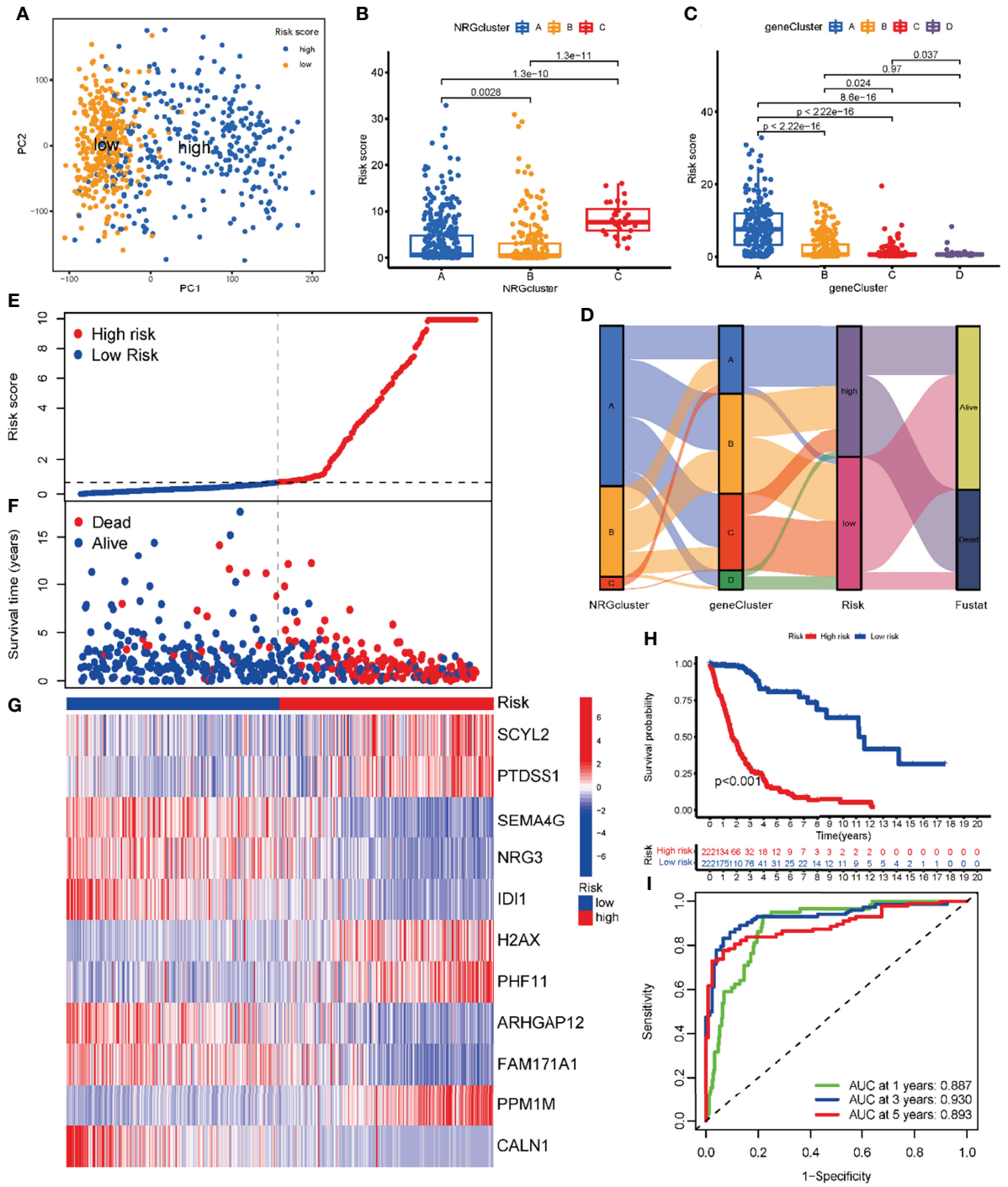

FIGURE 7 | Development of the risk NRG_score in the training dataset. **(A)** PCA analysis based on the NRG_score. The blue and yellow dots represent the high- and low-risk groups, respectively. **(B)** Comparison of NRG_score in different NRGclusters. **(C)** Comparison of NRG_score in different geneClusters. **(D)** Alluvial diagram of the distribution of subtypes with different NRG_score and survival outcomes. **(E)** The ranked dot of the distribution of the NRG_score. **(F)** Scatter plots of the distribution of the survival status in patients from high- and low-risk groups. **(G)** The expression of genes in the NRG_score model in patients from two risk groups. **(H)** Kaplan-Meier survival analysis of the two risk groups. **(I)** ROC curves of the NRG_score model for predicting the sensitivity and specificity of 1-, 3-, 5-year survival in patients with glioma.

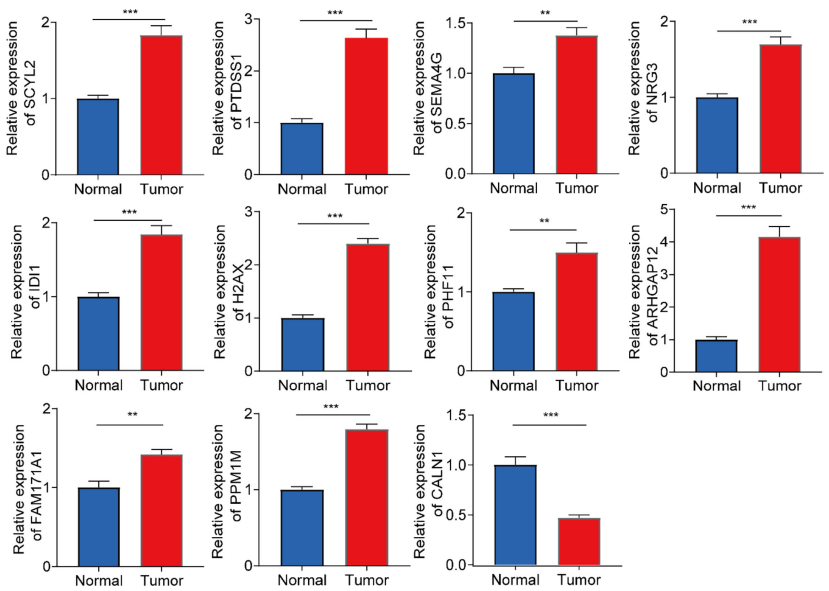

FIGURE 8 | RT-qPCR analysis on the expression levels of 11 genes in the prognostic model in 6 pairs of gliomas and their adjacent normal tissues. ***P<0.001, **P<0.01.

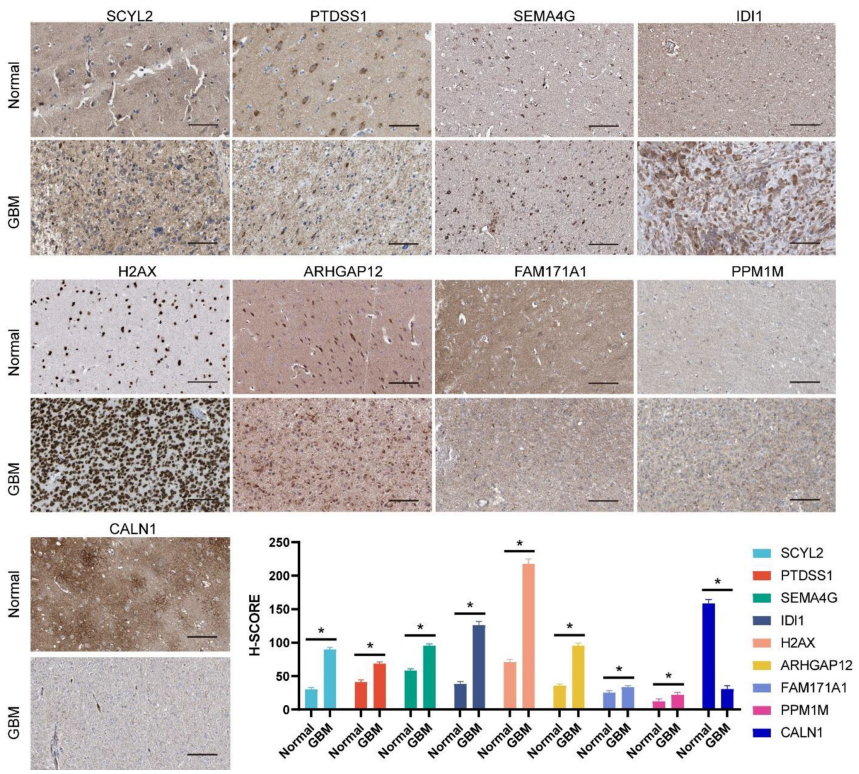

FIGURE 9 | Protein expression levels of genes incorporated in the prognostic model between normal brain and glioma tissue as demonstrated by immunohistochemical analysis and the H-SCORE analysis. Bar = 100μm. *p < 0.05.

In addition, we evaluated the correlation between the expression of 11 genes in the risk model and the abundance of immune cells. There was a significant correlation between the expression of 11 genes and immune cells (**Figure 10C**). In addition, 33 immune checkpoints including PD-L1, PD-1, and CTLA-4 were differentially expressed in the two groups (**Figure 10D**).

Correlation Between NRG_Score and Mutation, CSC, and Drug Sensitivity

To further evaluate whether glioma patients could benefit from immunotherapy, we conducted a tumor mutation analysis. According to the results, a significantly higher TMB was observed in the high-risk group than that in the low-risk group (**Figure 11A**), indicating that immunotherapy was more likely to

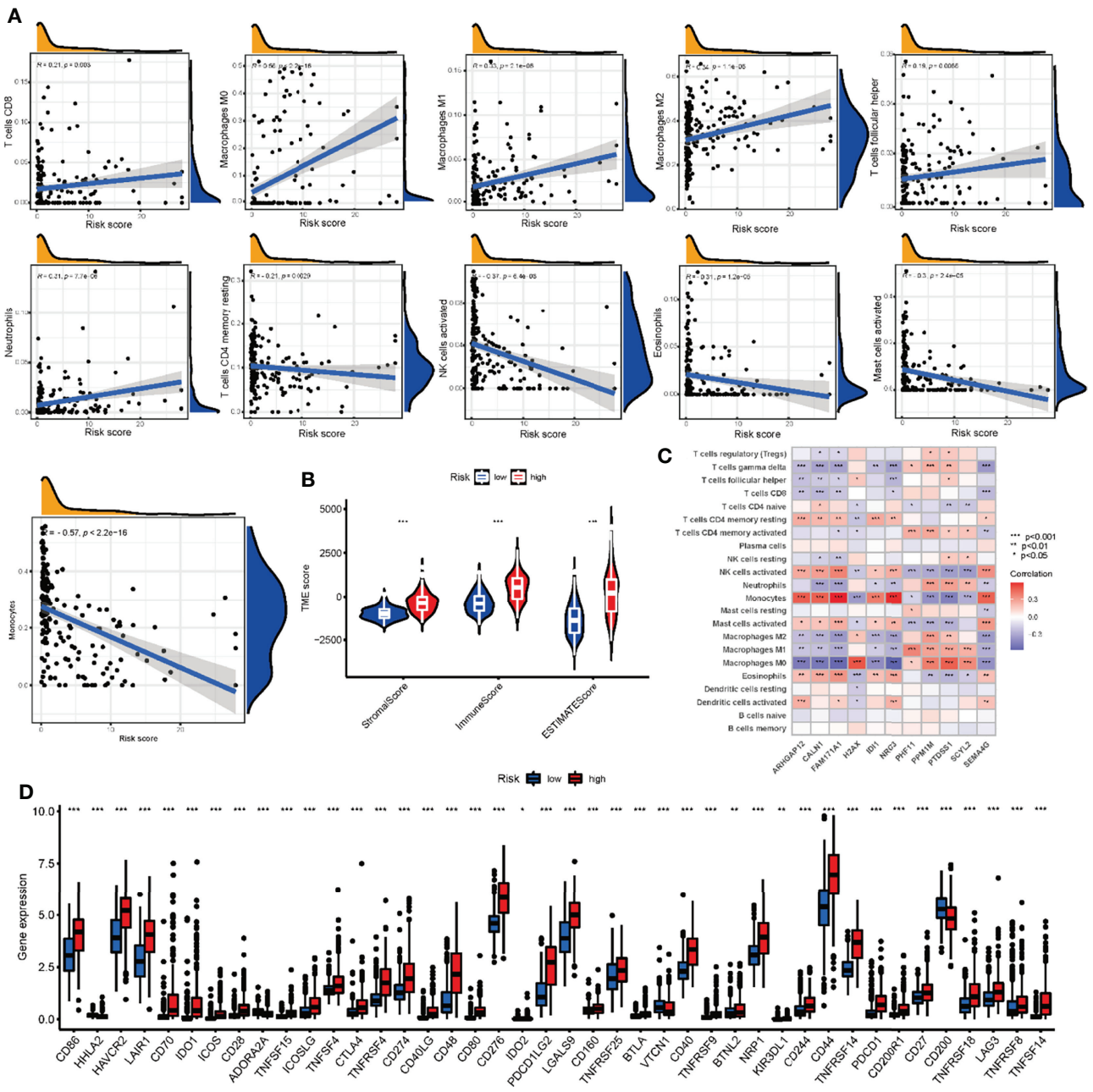

FIGURE 10 | Comparison of TME and checkpoints between the high- and low-risk groups. **(A)** Correlations between infiltrating immune cells and NRG_score. **(B)** Correlations between TME scores and NRG_score. **(C)** Correlations between the abundance of infiltrating immune cells and expression of NRGs in risk score model. **(D)** Expression of immune checkpoints between the two risk groups. TME, tumor microenvironment; NRGs, necroptosis-related genes. ***P<0.001, ** P<0.01, *P<0.05.

be effective in patients in the high-risk group. According to Spearman correlation analysis, TMB correlated positively with NRG_score (R=0.59, p<0.001, **Figure 11B**). Following this, we examined the correlation between CSC and NRG_score, and found it to be negative (R=-0.51, p<0.001, **Figure 11C**), suggesting low tumor stem cell characteristics and high differentiation in patients with high NRG_score. Furthermore, we examined the distribution of somatic mutations between two risk groups. We found that IDH1, CIC, FUBP1, and ATRX mutation frequencies were significantly higher in patients of the low-risk group than those in patients of the high-risk group, while PTEN, TTN, EGFR, and MUC16 genes were mutated more frequently in patients of the high-risk group (**Figures 11D, E**).

We then evaluated the predictive value of NRG_score on patients' chemotherapeutic drug sensitivity. We found that the IC50s for angiogenesis inhibitors such as sunitinib, and sorafenib were lower in patients of the high-risk group than those in patients of the low-risk group (**Figure 11F** and **Supplementary Figure 4A**). For the commonly used EGFR tyrosine kinase inhibitors, the sensitivity differed between the risk groups. Compared to the low-risk group, patients in the high-risk group had lower IC50 values for Erlotinib (**Supplementary**

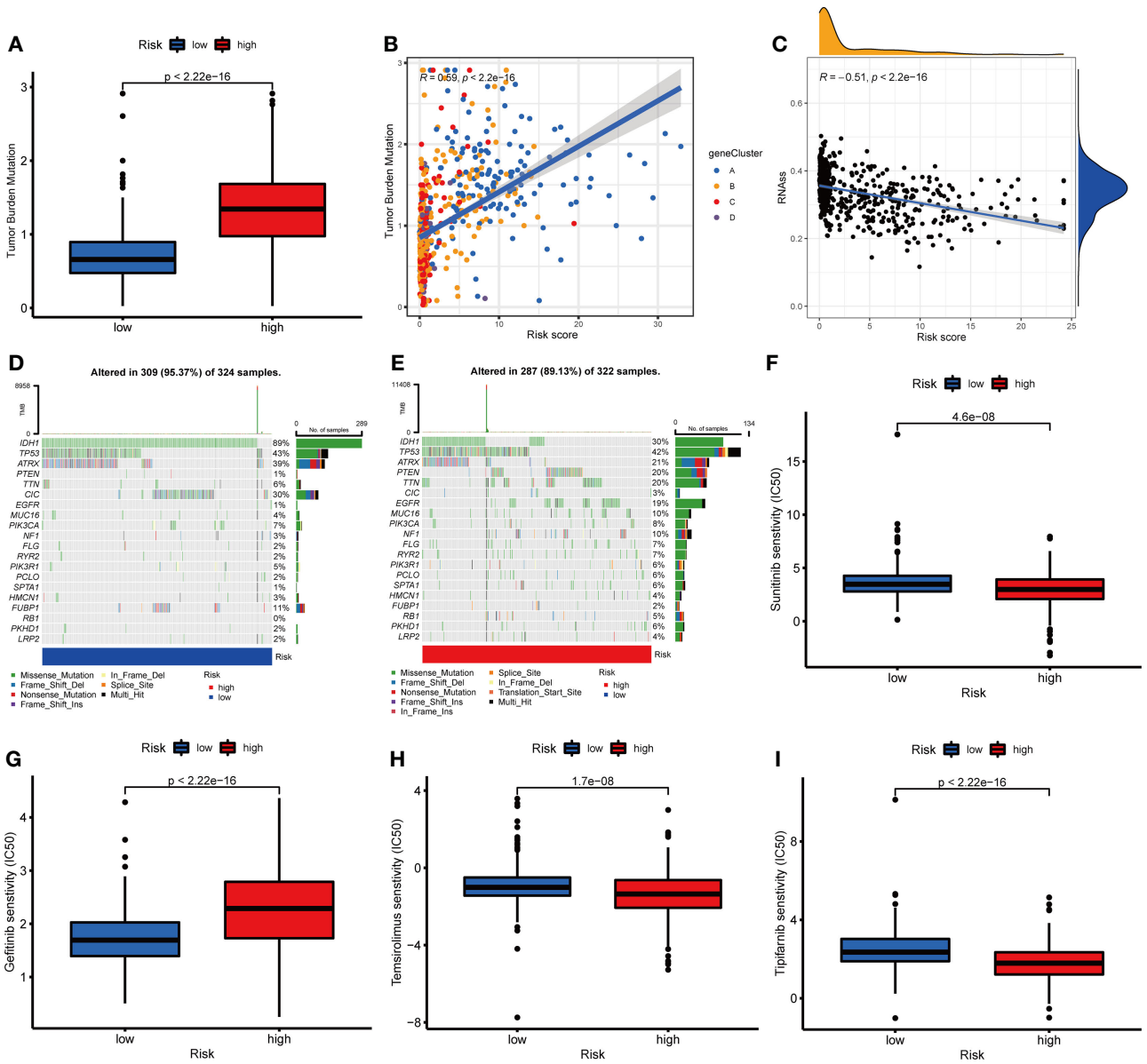

FIGURE 11 | Correlation between NRG_score and mutation, CSC index, and drug sensitivity. **(A)** Comparison of TMB in two risk groups. **(B)** Spearman correlation analysis between TMB and the NRG_score. **(C)** Spearman correlation analysis between CSC index and the NRG_score. **(D, E)** The waterfall plot of somatic mutation features in the low- **(D)** and high-risk **(E)** groups. **(F–I)** Comparison of chemotherapy sensitivity in glioma between two risk groups.

Figure 4B) and higher IC50 values for Gefitinib and Nilotinib (**Figure 11G** and **Supplementary Figure 4C**). In addition, the IC50 values of Temsirolimus (**Figure 11H**), Tipifarnib (**Figure 11I**), Bicalutamide (**Supplementary Figure 4D**), Gemcitabine (**Supplementary Figure 4E**), Parthenolide (**Supplementary Figure 4F**), Salubrinal (**Supplementary Figure 4G**), and vinblastine (**Supplementary Figure 4I**) were lower in the patients of the high-risk group than those of the low-risk group, while IC50 value of shikonin (**Supplementary Figure 4H**) was higher in patients of the high-risk group than that in the low-risk group. It appears that the NRG_score may be used to predict patients' drug sensitivity, even in the sense of guiding the selection of different classes of drugs in the same category.

Development and Validation of a Nomogram to Predict Survival

To make the NRG_score easier to apply clinically, we combined it with the clinicopathology of glioma patients to develop a nomogram for predicting patients' prognosis (**Figure 12A** ands **Supplementary Table 11**). The AUC values of the nomogram for predicting the 1-year, 3-year, and 5-year survival rates of the training set were 0.908, 0.927, and 0.896, respectively (**Figure 12B**), and the calibration curves also suggested high accordance between the predicted probabilities and the observed probabilities, indicating the high reliability of the nomogram (**Figure 12C**). Similarly, we also demonstrated high accuracy of nomogram in predicting 1-, 3-, and 5-year survival with high reliability in an internal validation set (**Figure 12D**), and two external validation sets (CGGA (**Figure 12E**), and Rembrandt (**Figure 12F–I**).

Subsequently, we compared the predictive accuracy of our nomogram with that of the WHO-grade in the training and validation datasets. We found that the AUC values of 1,3,5-year survival (**Supplementary Figures 5A, E, I**) were higher than those predicted by WHO grade in the training dataset. The same results were obtained in the internal validation dataset (**Supplementary Figures 5B, F, J**), the CGGA external validation set (**Supplementary Figures 5C, G, K**), and the Rembrandt external validation set (**Supplementary Figures 5D, H, L**), indicating that the nomogram has better predictive performance than that of the WHO grade.

DISCUSSION

Targeting necroptosis has also emerged as a promising therapeutic approach to bypass apoptosis resistance and support anti-tumor immunity. However, the role played by necroptosis-related genes in the development and prognosis of glioma has not been effectively elucidated by current studies. Ferroptosis-related genes (33), pyroptosis-related genes (34), and autophagy-related genes (35) have been reported in the literature for predicting survival in patients with glioma. However, the effect of necroptosis-related genes (NRGs) on predicting the survival of patients with gliomas and on the tumor microenvironment in gliomas has not been reported. Therefore, our study still has some theoretical and clinical significance.

In this study, we first analyzed the overall variation of 67 NRGs at the genetic and transcriptional levels in glioma patients. Based on candidate NRGs, we divided patients into 3 NRGclusters and 4 geneClusters. To further investigate the potential role of NRGs in regulating immunity in patients with glioma, we found that the level of immune cells infiltration and TME scores were generally higher in geneCluster C than those in the other subtypes. Immune checkpoint comparison also revealed that PD-L1 and PD-1 were higher in geneCluster C than those in the other subtypes.

To further investigate the biological behavior behind the differences in several NRGclusters, we screened the differential genes and performed GO, KEGG functional enrichment analysis, and found that DEGs were enriched in immune and inflammation-related pathways, indicating that NRGs are indispensable for these processes.

As well, we conducted the univariate Cox regression, Lasso regression, and multivariate Cox regression analysis on the DEGs to screen out prognosis-related genes, and four geneClusters were identified based on the consensus clustering analysis. A survival analysis revealed significant differences in prognosis among the four subtypes. The patients were randomly assigned to training and validation groups. And by lasso regression and multivariate cox regression analysis, we finally screened for 11 genes to construct a risk score model. It was found that the model had excellent predictive performance when it came to predicting the prognosis of patients in these datasets.

Moreover, the risk score correlated and predicted well for treatments such as TMB, immune checkpoint, immune cell infiltration, and CSC. Furthermore, the risk score can be used as a guide in predicting the sensitivity to chemotherapy drugs. To facilitate more clinical application, we combined the NRG_score with clinical information and developed a nomogram to predict the prognosis of patients with glioma in datasets. ROC curves and calibration plots demonstrated that the nomogram was highly predictive and reliable. Moreover, the predictive powers of the nomogram were more accurate than those of the WHO grade. As such, the nomogram may be applied to predict the prognosis of patients suffering from gliomas. The study makes it clear that NRGs are indispensable to glioma progression, immunomodulation, and treatment, and that they can provide a guide for sensitive drug screening during chemotherapy, which could provide new ideas for individually targeted therapies.

We screened for DEGs between a normal brain and glioma tissue from 67 NRGs and constructed PPI networks to explore hub genes. It was found that ZBP1, CASP8, CD40, CFLAR, CYLD, FAS, FADD, RIPK1, and RIPK3 were the hub genes. Yang et al. (36) reported that the DNA-dependent activator of IFN regulatory factors (ZBP1) plays an important role in IFN signaling during anti-necrotic apoptosis. ZBP1 is involved in regulating RIPK1/RIPK3-FADD-caspase-8 cell death complex assembly, along with their important regulatory role in

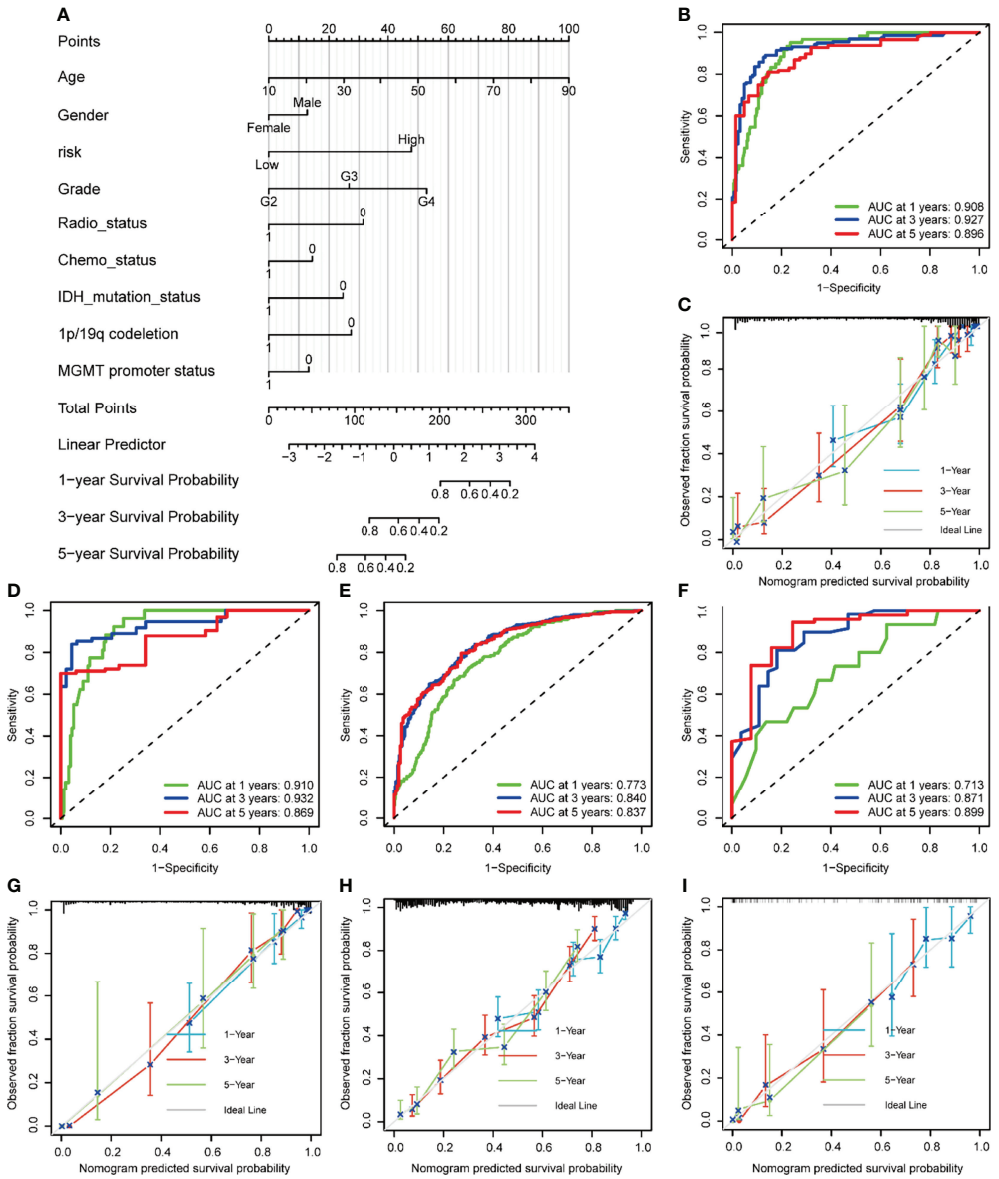

FIGURE 12 | Construction and validation of a nomogram to predict survival of patients with glioma. **(A)** Nomogram for predicting the 1-, 3-, 5-year survival of glioma patients in the training set. **(B)** ROC curves of the nomogram for predicting the sensitivity and specificity of 1-, 3-, 5-year survival in glioma patients in the training dataset. **(C)** Calibration curves of the nomogram for predicting 1-, 3-, and 5-year survival in glioma patients in the training dataset. **(D-F)** ROC curves of the nomogram for predicting the sensitivity and specificity of 1-, 3-, 5-year survival in glioma patients in the TCGA testing dataset(D), CGGA **(E)**, and Rembrandt **(F)**. **(G-I)** Calibration curves of the nomogram for predicting 1-, 3-, 5-year survival in glioma patients in the TCGA testing dataset **(G)**, CGGA **(H)**, Rembrandt **(I)**.

necroptosis (37, 38). Osborn et al. (39) reported that the Fas-associated death domain (FADD), a negative regulator of necroptosis, plays a vital role in T cell receptor-mediated necroptosis.

By inhibiting necroptosis, caspase-8 also contributes to survival (40–42). And it has been reported (43) that inhibition of caspase-8 leads to CYLD-dependent necroptosis. He et al. (44) reported that the anti-apoptotic protein CFLAR (CASP8 and FADD-like apoptosis regulator) plays a key role in necroptosis in T lymphocytes. A large body of literature reports that RIPK acts as an important sensor, receiving stimuli from both inside and outside the cell, and is involved in several biological processes such as immune response, inflammation, and cell death; RIPK1 and RIPK3 are essential for necroptosis (7, 13, 14, 45).

Correlation analysis showed that the expression of numerous NRGs was positively correlated and most of them were risk factors, suggesting a common role in regulating necroptosis. In contrast to previous studies focusing on a single gene, it is equally

important to investigate the role played by the gene set as a whole. Based on the consensus clustering analysis, glioma patients were divided into three subtypes (43, 44).

We performed two layers of clustering, the first layer is NRGcluster, and the second layer is geneCluster. The main purpose of NRGcluster is to find the number of clusters with the strongest intra-group correlation and the weakest inter-group correlation. The second layer of clustering builds on the first layer of clustering to find the differentially expressed genes among different NRGclusters for a deeper geneCluster. For a deeper understanding of the differences among these NRGclusters, we performed enrichment analyses of DEGs within each subtype. GO and KEGG results also revealed substantial enrichment in immune and inflammation-related biological pathways, which suggested that NRG may be indispensable for the regulation of tumor immunity.

The consensus clustering analysis was conducted on prognosis-related DEGs, and several geneClusters were finally derived. The prognosis and expression of NRGs differed significantly among the geneClusters. To facilitate generalized application, we developed an NRG_score risk prediction model and confirmed the high predictive efficacy and reliability of the model in all datasets. NRG_score was used to categorize patients into high- and low-risk groups. By comparing the expression of NRGs in two risk groups, we found that the expression of NRGs such as ZBP1, RIPK1, RIPK3, FADD, FAS, and MLKL was widely lower in the low-risk group than those in the high-risk group, suggesting that the risk score can well reflect the incidence of necroptosis.

To investigate the mechanisms of immune modulation by NRGs, we performed a comparative analysis of the infiltration of immune cells, immune checkpoints, TMB, and CSC in the two risk groups. High-grade gliomas have a poor prognosis, and although some patients respond better to radiotherapy treatment, tumor heterogeneity is high. This highlights the critical role of TME in glioma development and progression. Targeting the heterogeneity of glioma TME provides new ideas for the treatment of glioma (46). There is a combination of immune cells, stromal cells, fibroblasts, endothelial cells, cellular stroma, and blood vessels surrounding the TME, which are responsible for the heterogeneity of the tumor as well as for its development and prognosis (47). It was found that our NRG_score was significantly related to the infiltration of immune cells. A positive correlation was found between NRG_score and CD8 + T cells, M1 macrophages, follicular helper T cells, M2 macrophages, and neutrophils, M0 macrophages, and a negative correlation was found with activated NK cells, Eosinophils, activated mast cells, CD4 memory resting T cells, and Monocytes.

Monocytes perform a crucial role in immune surveillance and immunological response regulation (48, 49). We found that necrotizing apoptosis was negatively correlated with monocyte expression. This may be because monocytes migrate to the tumor region during pathological situations, such as necroptosis in glioma, and then differentiate into immunological cells, such as macrophages. It has been reported (46) that monocyte-derived macrophages are essential in the regulation of the microenvironment of brain tumors, which supports our findings. Macrophages (Mφs) generally regulate immune responses and ultimately maintain immune homeostasis through biological processes such as pathogen phagocytosis and antigen presentation (50). Mφs can be simplified as inflammatory M1 or immunosuppressive M2 Mφs (51), and the M1, and M2 of Mφ are convertible between them and exist continuously and uniformly (52). Our study found that the infiltration of several subtypes of macrophages was elevated in the high-risk group of gliomas. Moreover, the pro-inflammatory and immunosuppressive functions of each macrophage were again uniformly present, which laterally reflects part of the source of glioma tumor heterogeneity. Follicular helper T cells are a class of CD4+ T cell subpopulations (53), whose main function is to assist B cells in humoral immunity and enhance the immune response (54). High CD8+ T cells infiltration is also a sign of high immune response. We found a higher incidence of necroptosis and a higher immune response in the high-risk group than those in the low-risk group. There is also evidence (8) suggesting that exposure to necrotizing apoptotic cells within the TME is associated with an increased number of tumor-specific CD8+ T cells within the tumor tissue. This is in accordance with our results. NK cells, as innate immune cells, can target tumor cells and perform a crucial role in tumor detection, elimination of malignant cells, and limiting tumor metastasis (55, 56). The negative association of activated NK cells with risk scores found in our study is consistent with previous studies. Consistent with the results of increased immune cell infiltration, the TME scores were higher in the high-risk group than those in the low-risk group, and the expression of genes in the model was most significantly correlated with immune cell expression. It is suggested that the immune microenvironment can be scored and predicted by the correlation between NRG_score and immune cell infiltration in the risk model.

With the development of immunology and molecular biology for tumors, immune checkpoint-based immunotherapy provides a new idea for tumor treatment. The PD-L1 and PD-1 perform a vital role in tumorigenesis and progression and could be a target for tumor immunotherapy. It has been reported that PD-1 and PD-L1 exert a vital role in the progression and immunotherapy of glioma (57). According to Baral et al., The expression of PD-L1 correlates with the WHO grade in gliomas. The expression of PD-L1 is common in GBM but is mostly restricted to a small subpopulation of infiltrating T cells, forming a "molecular barrier" that contributes to tumor immune escape and promotes tumor malignancy (58). A high PD-L1 expression is related to prognosis, and therefore screening out the Tipifarnibpatients with high PD-L1 expression is important for predicting good immunotherapy outcomes. Consistent with previous findings, we also found that patients with glioma had higher PD-1, PD-L1, and worse prognosis in the high-risk group than those in the low-risk group. Our risk score model can also assist in predicting PD-L1 expression, which is valuable as a guide to screening out patients with good responses to PD-1 immunotherapy.

TMB could be utilized to predict the survival of patients after treatment with immune checkpoint inhibitors (ICIs) in a variety of cancers. Most patients with tumors with a higher TMB, except for gliomas, will likely benefit from ICI therapy and have a better prognosis. Generally, patients with higher TBM gliomas often have a worse prognosis (59). These patients' poor prognosis is

most likely due to their own high WHO grade. A higher TMB in these patients may be the result of their previous exposure to temozolomide, which may lead to the development of less immunogenic subclonal mutations (60). In addition, we found that patients in the high-risk group had higher TBM values and that the TMB and the NRG_score were positively related. Additionally, the NRG_score and CSC showed a negative correlation. These studies suggest that patients with high-risk scores have malignantly differentiated tumor cells with inherently high heterogeneity, which may also result in different responses to antitumor immunotherapy and low dependence on TMB. Therefore, the response of patients to PD-1 and TMB may not always be consistent.

We further investigated the tumor mutations in two risk groups. We found a lower frequency of IDH1 and CIC mutations and a higher frequency of PTEN, EGFR, and TTN mutations in patients from the high-risk group than those from the low-risk group. Zhang et al. (61) reported that IDH and CIC mutations occurred primarily in low-grade gliomas and that they were associated with a significantly higher survival rate. In contrast, EGFR, PTEN, and TTN were related to worse survival. This is in accordance with our findings.

From the above results, we speculated that patients screened from the high-risk group may be easier to benefit from multiple drugs such as immunotherapy than patients in the low-risk group. Thus, we assessed the patients' sensitivity to currently used chemotherapy and immunotherapy drugs. For angiogenesis inhibitors, the patients in the high-risk group were more likely to benefit from sunitinib and sorafenib than from other similar drugs. And among PI3K-Akt-mTOR pathway inhibitors, Temsirolimus was preferred over Everolimus for patients with high-risk glioma. Tipifarnib and Lonafarnib are a class of Farnesyl transferase inhibitors that induce death in radiotherapy-insensitive gliomas (62–64). We also found that patients in the high-risk group were more sensitive to Tipifamib than Lonafarnib. Interestingly, for the commonly used epidermal growth factor receptor tyrosine kinase inhibitors, patients in the high-risk group were more sensitive to Erlotinib, while the low-risk group should prefer the highly sensitive Gefitinib and Nilotinib. In addition, Bicalutamide, Gemcitabine, Parthenolide, Salubrinal, vinblastine, and Shikonin have also been reported for the treatment of glioma (65–69). Patients in the high-risk group may benefit more from Bicalutamide, Gemcitabine, Parthenolide, Salubrinal, and vinblastine; While in the low-risk group, the patients were more sensitive to shikonin. The results revealed that NRG_score can be used to predict the drug sensitivity of patients and even provide guidance in the selection of different drugs in the same class.

To facilitate clinical application, we combined NRG_score with clinical data to develop a nomogram for predicting the prognosis of patients. In the training set, the internal validation set, and both external validation sets of CGGA and Rembrandt, the model proved to have excellent predictive efficacy and high reliability.

Our study has several limitations. First, there are not many studies on necroptosis, especially its study in glioma is even less. The selected NRGs may only be the tip of the iceberg, and more basic studies are needed to confirm more necroptosis molecules. Secondly, we chose all public data from public databases; it would be more convincing to use prospective own data.

CONCLUSIONS

We integrated the broad impact of NRGs on tumor immunity, TME, and prognosis at genetic and transcriptional levels. We constructed risk scores and a nomogram for the survival prediction of patients with glioma. The findings of this research provide new insights into personalized targeted therapies for gliomas.

DATA AVAILABILITY STATEMENT

The datasets presented in this study can be found in online repositories. The names of the repository/repositories and accession number(s) can be found in the article/**Supplementary Material**.

ETHICS STATEMENT

The identification of necroptosis-related subtypes, the construction of a prognostic model, and the characterization of the tumor microenvironment in gliomas were reviewed and approved by Zhongshan City People's Hospital. The patients/participants provided their written informed consent to participate in this study.

AUTHOR CONTRIBUTIONS

CL, JG, and YG conceived the project. YB, JS, and SG contributed to data analysis and interpretation, and manuscript writing and revision. ZL, ZW, and CC contributed to data acquisition and conducted the experiments. All authors read and approved the submitted manuscript.

FUNDING

Funding for this research was provided by the Science and Technology Program of Guangzhou, China under Grant to YG (Grant No. 201604020080); by the Guangdong Basic and Applied Basic Research Foundation under Grant to YG (Grant No. 2018B0303110014 and No. 2020B090924004), and by the Natural Science Foundation of Guangdong under Grant to Jin Gong (Grant NO. 2021A1515010464).

ACKNOWLEDGMENTS

We thank contributions from the TCGA network. We thank Prof. Jiang Tao's team at Beijing Tiantan Hospital of Capital

Medical University for their great contribution to the construction of the Chinese Glioma Genome Atlas (CGGA) database for basic and clinical medical research on glioma in China.

SUPPLEMENTARY MATERIAL

The Supplementary Material for this article can be found online at: https://www.frontiersin.org/articles/10.3389/fonc.2022.899443/full#supplementary-material

REFERENCES

1. Ostrom QT, Patil N, Cioffi G, Waite K, Kruchko C, Barnholtz-Sloan JS. Cbtrus Statistical Report: Primary Brain and Other Central Nervous System Tumors Diagnosed in the United States in 2013-2017. *Neuro Oncol* (2020) 22: iv1–iv96. doi: 10.1093/neuonc/noaa200
2. Louis DN, Perry A, Wesseling P, Brat DJ, Cree IA, Figarella-Branger D, et al. The 2021 Who Classification of Tumors of the Central Nervous System: A Summary. *Neuro-Oncology* (2021) 23:1231–51. doi: 10.1093/neuonc/noab106
3. Ho VK, Reijneveld JC, Enting RH, Bienfait HP, Robe P, Baumert BG, et al. Changing Incidence and Improved Survival of Gliomas. *Eur J Cancer* (2014) 50:2309–18. doi: 10.1016/j.ejca.2014.05.019
4. Li D, Lu J, Li H, Qi S, Yu L. Identification of a Long Noncoding Rna Signature to Predict Outcomes of Glioblastoma. *Mol Med Rep* (2019) 19:5406–16. doi: 10.3892/mmr.2019.10184
5. Killela PJ, Pirozzi CJ, Healy P, Reitman ZJ, Lipp E, Rasheed BA, et al. Mutations in Idh1, Idh2, and in the Tert Promoter Define Clinically Distinct Subgroups of Adult Malignant Gliomas. *Oncotarget* (2014) 5:1515–25. doi: 10.18632/oncotarget.1765
6. Yan H, Parsons DW, Jin G, McLendon R, Rasheed BA, Yuan W, et al. Idh1 and Idh2 Mutations in Gliomas. *N Engl J Med* (2009) 360:765–73. doi: 10.1056/NEJMoa0808710
7. Della Torre L, Nebbioso A, Stunnenberg HG, Martens JHA, Carafa V, Altucci L. The Role of Necroptosis: Biological Relevance and Its Involvement in Cancer. *Cancers (Basel)* (2021) 13:684. doi: 10.3390/cancers13040684
8. Snyder AG, Hubbard NW, Messmer MN, Kofman SB, Hagan CE, Orozco SL, et al. Intratumoral Activation of the Necroptotic Pathway Components Ripk1 and Ripk3 Potentiates Antitumor Immunity. *Sci Immunol* (2019) 4:eaaw2004. doi: 10.1126/sciimmunol.aaw2004
9. Seehawer M, Heinzmann F, D'Artista L, Harbig J, Roux PF, Hoenicke L, et al. Necroptosis Microenvironment Directs Lineage Commitment in Liver Cancer. *Nature* (2018) 562:69–75. doi: 10.1038/s41586-018-0519-y
10. Stoll G, Ma Y, Yang H, Kepp O, Zitvogel L, Kroemer G. Pro-Necrotic Molecules Impact Local Immunosurveillance in Human Breast Cancer. *Oncoimmunology* (2017) 6:e1299302. doi: 10.1080/2162402x.2017.1299302
11. Gong Y, Fan Z, Luo G, Yang C, Huang Q, Fan K, et al. The Role of Necroptosis in Cancer Biology and Therapy. *Mol Cancer* (2019) 18:100. doi: 10.1186/s12943-019-1029-8
12. Zhao Z, Zhang KN, Wang Q, Li G, Zeng F, Zhang Y, et al. Chinese Glioma Genome Atlas (Cgga): A Comprehensive Resource With Functional Genomic Data From Chinese Glioma Patients. *Genomics Proteomics Bioinf* (2021) 19:1–12. doi: 10.1016/j.gpb.2020.10.005
13. Feng Y, Wang W, Zhang Y, Fu X, Ping K, Zhao J, et al. Synthesis and Biological Evaluation of Celastrol Derivatives as Potential Anti-Glioma Agents by Activating Rip1/Rip3/Mlkl Pathway to Induce Necroptosis. *Eur J Med Chem* (2022) 229:114070. doi: 10.1016/j.ejmech.2021.114070
14. Vergara GA, Eugenio GC, Malheiros SMF, Victor EDS, Weinlich R. Ripk3 Is a Novel Prognostic Marker for Lower Grade Glioma and Further Enriches Idh Mutational Status Subgrouping. *J Neurooncol* (2020) 147:587–94. doi: 10.1007/s11060-020-03473-0
15. McCormick KD, Ghosh A, Trivedi S, Wang L, Coyne CB, Ferris RL, et al. Innate Immune Signaling Through Differential Ripk1 Expression Promote Tumor Progression in Head and Neck Squamous Cell Carcinoma. *Carcinogenesis* (2016) 37:522–9. doi: 10.1093/carcin/bgw032
16. Park S, Hatanpaa KJ, Xie Y, Mickey BE, Madden CJ, Raisanen JM, et al. The Receptor Interacting Protein 1 Inhibits P53 Induction Through Nf-Kappab Activation and Confers a Worse Prognosis in Glioblastoma. *Cancer Res* (2009) 69:2809–16. doi: 10.1158/0008-5472.Can-08-4079
17. Höckendorf U, Yabal M, Herold T, Munkhbaatar E, Rott S, Jilg S, et al. Ripk3 Restricts Myeloid Leukemogenesis by Promoting Cell Death and Differentiation of Leukemia Initiating Cells. *Cancer Cell* (2016) 30:75–91. doi: 10.1016/j.ccell.2016.06.002
18. Feng X, Song Q, Yu A, Tang H, Peng Z, Wang X. Receptor-Interacting Protein Kinase 3 Is A Predictor of Survival and Plays A Tumor Suppressive Role in Colorectal Cancer. *Neoplasma* (2015) 62:592–601. doi: 10.4149/neo_2015_071
19. Zhao Z, Liu H, Zhou X, Fang D, Ou X, Ye J, et al. Necroptosis-Related Lncrnas: Predicting Prognosis and the Distinction Between the Cold and Hot Tumors in Gastric Cancer. *J Oncol* (2021) 2021:6718443. doi: 10.1155/2021/6718443
20. Newman AM, Liu CL, Green MR, Gentles AJ, Feng W, Xu Y, et al. Robust Enumeration of Cell Subsets From Tissue Expression Profiles. *Nat Methods* (2015) 12:453–7. doi: 10.1038/nmeth.3337
21. Subramanian A, Tamayo P, Mootha VK, Mukherjee S, Ebert BL, Gillette MA, et al. Gene Set Enrichment Analysis: A Knowledge-Based Approach for Interpreting Genome-Wide Expression Profiles. *Proc Natl Acad Sci U S A* (2005) 102:15545–50. doi: 10.1073/pnas.0506580102
22. Yu G, Wang LG, Han Y, He QY. Clusterprofiler: An R Package for Comparing Biological Themes Among Gene Clusters. *Omics* (2012) 16:284–7. doi: 10.1089/omi.2011.0118
23. Wu T, Hu E, Xu S, Chen M, Guo P, Dai Z, et al. Clusterprofiler 4.0: A Universal Enrichment Tool for Interpreting Omics Data. *Innovation (N Y)* (2021) 2:100141. doi: 10.1016/j.xinn.2021.100141
24. Xie T, Guo X, Wu D, Li S, Lu Y, Wang X, et al. Pafah1b3 Expression Is Correlated With Gastric Cancer Cell Proliferation and Immune Infiltration. *Front Oncol* (2021) 11:591545. doi: 10.3389/fonc.2021.591545
25. Qiu H, Tian W, He Y, Li J, He C, Li Y, et al. Integrated Analysis Reveals Prognostic Value and Immune Correlates of Cd86 Expression in Lower Grade Glioma. *Front Oncol* (2021) 11:654350. doi: 10.3389/fonc.2021.654350
26. Li CY, Cai JH, Tsai JJP, Wang CCN. Identification of Hub Genes Associated With Development of Head and Neck Squamous Cell Carcinoma by Integrated Bioinformatics Analysis. *Front Oncol* (2020) 10:681. doi: 10.3389/fonc.2020.00681
27. Chen Q, Lu X, Xie J, Ma N, Xu W, Zhang Z, et al. Analysis of L Antigen Family Member 3 as a Potential Biomarker and Therapeutic Target Associated With the Progression of Hepatocellular Carcinoma. *Front Oncol* (2022) 12:813275. doi: 10.3389/fonc.2022.813275
28. Liu Z, Xu H, Weng S, Ren Y, Han X. Stemness Refines the Classification of Colorectal Cancer With Stratified Prognosis, Multi-Omics Landscape, Potential Mechanisms, and Treatment Options. *Front Immunol* (2022) 13:828330. doi: 10.3389/fimmu.2022.828330
29. Liu Z, Weng S, Xu H, Wang L, Liu L, Zhang Y, et al. Computational Recognition and Clinical Verification of Tgf-B-Derived Mirna Signature With Potential Implications in Prognosis and Immunotherapy of Intrahepatic Cholangiocarcinoma. *Front Oncol* (2021) 11:757919. doi: 10.3389/fonc.2021.757919
30. Liu Z, Lu T, Wang L, Liu L, Li L, Han X. Comprehensive Molecular Analyses of a Novel Mutational Signature Classification System With Regard to Prognosis, Genomic Alterations, and Immune Landscape in Glioma. *Front Mol Biosci* (2021) 8:682084. doi: 10.3389/fmolb.2021.682084
31. Liu Z, Liu L, Weng S, Guo C, Dang Q, Xu H, et al. Machine Learning-Based Integration Develops an Immune-Derived Lncrna Signature for Improving Outcomes in Colorectal Cancer. *Nat Commun* (2022) 13:816. doi: 10.1038/s41467-022-28421-6
32. Liu Z, Guo Y, Yang X, Chen C, Fan D, Wu X, et al. Immune Landscape Refines the Classification of Colorectal Cancer With Heterogeneous Prognosis, Tumor Microenvironment and Distinct Sensitivity to Frontline Therapies. *Front Cell Dev Biol* (2021) 9:784199. doi: 10.3389/fcell.2021.784199
33. Wan RJ, Peng W, Xia QX, Zhou HH, Mao XY. Ferroptosis-Related Gene Signature Predicts Prognosis and Immunotherapy in Glioma. *CNS Neurosci Ther* (2021) 27:973–86. doi: 10.1111/cns.13654

34. Chao B, Jiang F, Bai H, Meng P, Wang L, Wang F. Predicting the Prognosis of Glioma by Pyroptosis-Related Signature. *J Cell Mol Med* (2022) 26:133–43. doi: 10.1111/jcmm.17061
35. Feng S, Liu H, Dong X, Du P, Guo H, Pang Q. Identification and Validation of an Autophagy-Related Signature for Predicting Survival in Lower-Grade Glioma. *Bioengineered* (2021) 12:9692–708. doi: 10.1080/21655979.2021.1985818
36. Yang D, Liang Y, Zhao S, Ding Y, Zhuang Q, Shi Q, et al. Zbp1 Mediates Interferon-Induced Necroptosis. *Cell Mol Immunol* (2020) 17:356–68. doi: 10.1038/s41423-019-0237-x
37. Baik JY, Liu Z, Jiao D, Kwon HJ, Yan J, Kadigamuwa C, et al. Zbp1 Not Ripk1 Mediates Tumor Necroptosis in Breast Cancer. *Nat Commun* (2021) 12:2666. doi: 10.1038/s41467-021-23004-3
38. Malireddi RKS, Kesavardhana S, Kanneganti TD. Zbp1 and Tak1: Master Regulators of Nlrp3 Inflammasome/Pyroptosis, Apoptosis, and Necroptosis (Pan-Optosis). *Front Cell Infect Microbiol* (2019) 9:406. doi: 10.3389/fcimb.2019.00406
39. Osborn SL, Diehl G, Han SJ, Xue L, Kurd N, Hsieh K, et al. Fas-Associated Death Domain (Fadd) Is a Negative Regulator of T-Cell Receptor-Mediated Necroptosis. *Proc Natl Acad Sci U S A* (2010) 107:13034–9. doi: 10.1073/pnas.1005997107
40. Someda M, Kuroki S, Miyachi H, Tachibana M, Yonehara S. Caspase-8, Receptor-Interacting Protein Kinase 1 (Ripk1), and Ripk3 Regulate Retinoic Acid-Induced Cell Differentiation and Necroptosis. *Cell Death Differ* (2020) 27:1539–53. doi: 10.1038/s41418-019-0434-2
41. Fritsch M, Günther SD, Schwarzer R, Albert MC, Schorn F, Werthenbach JP, et al. Caspase-8 Is the Molecular Switch for Apoptosis, Necroptosis and Pyroptosis. *Nature* (2019) 575:683–7. doi: 10.1038/s41586-019-1770-6
42. Mandal R, Barrón JC, Kostova I, Becker S, Strebhardt K. Caspase-8: The Double-Edged Sword. *Biochim Biophys Acta Rev Cancer* (2020) 1873:188357. doi: 10.1016/j.bbcan.2020.188357
43. Legarda D, Justus SJ, Ang RL, Rikhi N, Li W, Moran TM, et al. Cyld Proteolysis Protects Macrophages From Tnf-Mediated Auto-Necroptosis Induced by Lps and Licensed by Type I Ifn. *Cell Rep* (2016) 15:2449–61. doi: 10.1016/j.celrep.2016.05.032
44. He MX, He YW. Cflar/C-Flipl: A Star in the Autophagy, Apoptosis and Necroptosis Alliance. *Autophagy* (2013) 9:791–3. doi: 10.4161/auto.23785
45. Shan B, Pan H, Najafov A, Yuan J. Necroptosis in Development and Diseases. *Genes Dev* (2018) 32:327–40. doi: 10.1101/gad.312561.118
46. Klemm F, Maas RR, Bowman RL, Kornete M, Soukup K, Nassiri S, et al. Interrogation of the Microenvironmental Landscape in Brain Tumors Reveals Disease-Specific Alterations of Immune Cells. *Cell* (2020) 181:1643–60.e17. doi: 10.1016/j.cell.2020.05.007
47. Hinshaw DC, Shevde LA. The Tumor Microenvironment Innately Modulates Cancer Progression. *Cancer Res* (2019) 79:4557–66. doi: 10.1158/0008-5472.Can-18-3962
48. Guilliams M, Mildner A, Yona S. Developmental and Functional Heterogeneity of Monocytes. *Immunity* (2018) 49:595–613. doi: 10.1016/j.immuni.2018.10.005
49. Ginhoux F, Jung S. Monocytes and Macrophages: Developmental Pathways and Tissue Homeostasis. *Nat Rev Immunol* (2014) 14:392–404. doi: 10.1038/nri3671
50. Chen H, Shi R, Luo B, Yang X, Qiu L, Xiong J, et al. Macrophage Peroxisome Proliferator-Activated Receptor Γ Deficiency Delays Skin Wound Healing Through Impairing Apoptotic Cell Clearance in Mice. *Cell Death Dis* (2015) 6:e1597. doi: 10.1038/cddis.2014.544
51. Yang L, Zhang Y. Tumor-Associated Macrophages: From Basic Research to Clinical Application. *J Hematol Oncol* (2017) 10:58. doi: 10.1186/s13045-017-0430-2
52. Kim J, Bae JS. Tumor-Associated Macrophages and Neutrophils in Tumor Microenvironment. *Mediators Inflammation* (2016) 2016:6058147. doi: 10.1155/2016/6058147
53. Crotty S. T Follicular Helper Cell Differentiation, Function, and Roles in Disease. *Immunity* (2014) 41:529–42. doi: 10.1016/j.immuni.2014.10.004
54. Crotty S. Follicular Helper Cd4 T Cells (Tfh). *Annu Rev Immunol* (2011) 29:621–63. doi: 10.1146/annurev-immunol-031210-101400
55. Glasner A, Levi A, Enk J, Isaacson B, Viukov S, Orlanski S, et al. Nkp46 Receptor-Mediated Interferon-Γ Production by Natural Killer Cells Increases Fibronectin 1 to Alter Tumor Architecture and Control Metastasis. *Immunity* (2018) 48:107–19.e4. doi: 10.1016/j.immuni.2017.12.007
56. Langers I, Renoux VM, Thiry M, Delvenne P, Jacobs N. Natural Killer Cells: Role in Local Tumor Growth and Metastasis. *Biologics* (2012) 6:73–82. doi: 10.2147/btt.S23976
57. Xue S, Hu M, Iyer V, Yu J. Blocking the Pd-1/Pd-L1 Pathway in Glioma: A Potential New Treatment Strategy. *J Hematol Oncol* (2017) 10:81. doi: 10.1186/s13045-017-0455-6
58. Baral A, Ye HX, Jiang PC, Yao Y, Mao Y. B7-H3 and B7-H1 Expression in Cerebral Spinal Fluid and Tumor Tissue Correlates With the Malignancy Grade of Glioma Patients. *Oncol Lett* (2014) 8:1195–201. doi: 10.3892/ol.2014.2268
59. Samstein RM, Lee CH, Shoushtari AN, Hellmann MD, Shen R, Janjigian YY, et al. Tumor Mutational Load Predicts Survival After Immunotherapy Across Multiple Cancer Types. *Nat Genet* (2019) 51:202–6. doi: 10.1038/s41588-018-0312-8
60. McGranahan N, Furness AJ, Rosenthal R, Ramskov S, Lyngaa R, Saini SK, et al. Clonal Neoantigens Elicit T Cell Immunoreactivity and Sensitivity to Immune Checkpoint Blockade. *Science* (2016) 351:1463–9. doi: 10.1126/science.aaf1490
61. Zhang L, Giuste F, Vizcarra JC, Li X, Gutman D. Radiomics Features Predict Cic Mutation Status in Lower Grade Glioma. *Front Oncol* (2020) 10:937. doi: 10.3389/fonc.2020.00937
62. Haas-Kogan DA, Banerjee A, Poussaint TY, Kocak M, Prados MD, Geyer JR, et al. Phase Ii Trial of Tipifarnib and Radiation in Children With Newly Diagnosed Diffuse Intrinsic Pontine Gliomas. *Neuro Oncol* (2011) 13:298–306. doi: 10.1093/neuonc/noq202
63. Cloughesy TF, Wen PY, Robins HI, Chang SM, Groves MD, Fink KL, et al. Phase Ii Trial of Tipifarnib in Patients With Recurrent Malignant Glioma Either Receiving or Not Receiving Enzyme-Inducing Antiepileptic Drugs: A North American Brain Tumor Consortium Study. *J Clin Oncol* (2006) 24:3651–6. doi: 10.1200/jco.2006.06.2323
64. Yust-Katz S, Liu D, Yuan Y, Liu V, Kang S, Groves M, et al. Phase 1/1b Study of Lonafarnib and Temozolomide in Patients With Recurrent or Temozolomide Refractory Glioblastoma. *Cancer* (2013) 119:2747–53. doi: 10.1002/cncr.28031
65. Huang C, Luo Y, Zhao J, Yang F, Zhao H, Fan W, et al. Shikonin Kills Glioma Cells Through Necroptosis Mediated by Rip-1. *PLoS One* (2013) 8:e66326. doi: 10.1371/journal.pone.0066326
66. He Y, Meng H, Xu H, Fan L, Zhou Z, Xu B, et al. Regulation of Integrated Stress Response Sensitizes U87mg Glioblastoma Cells to Temozolomide Through the Mitochondrial Apoptosis Pathway. *Anat Rec (Hoboken)* (2018) 301:1390–7. doi: 10.1002/ar.23839
67. Bastiancich C, Bastiat G, Lagarce F. Gemcitabine and Glioblastoma: Challenges and Current Perspectives. *Drug Discovery Today* (2018) 23:416–23. doi: 10.1016/j.drudis.2017.10.010
68. Hou Y, Sun B, Liu W, Yu B, Shi Q, Luo F, et al. Targeting of Glioma Stem-Like Cells With a Parthenolide Derivative Act001 Through Inhibition of Aebp1/Pi3k/Akt Signaling. *Theranostics* (2021) 11:555–66. doi: 10.7150/thno.49250
69. Lassaletta A, Scheinemann K, Zelcer SM, Hukin J, Wilson BA, Jabado N, et al. Phase Ii Weekly Vinblastine for Chemotherapy-Naïve Children With Progressive Low-Grade Glioma: A Canadian Pediatric Brain Tumor Consortium Study. *J Clin Oncol* (2016) 34:3537–43. doi: 10.1200/jco.2016.68.1585

Conflict of Interest: The authors declare that the research was conducted in the absence of any commercial or financial relationships that could be construed as a potential conflict of interest.

Publisher's Note: All claims expressed in this article are solely those of the authors and do not necessarily represent those of their affiliated organizations, or those of the publisher, the editors and the reviewers. Any product that may be evaluated in this article, or claim that may be made by its manufacturer, is not guaranteed or endorsed by the publisher.

Copyright © 2022 Ba, Su, Gao, Liao, Wu, Cao, Liang, Gong and Guo. This is an open-access article distributed under the terms of the Creative Commons Attribution License (CC BY). The use, distribution or reproduction in other forums is permitted, provided the original author(s) and the copyright owner(s) are credited and that the original publication in this journal is cited, in accordance with accepted academic practice. No use, distribution or reproduction is permitted which does not comply with these terms.

frontiers | Frontiers in Oncology

ORIGINAL RESEARCH
published: 08 June 2022
doi: 10.3389/fonc.2022.860640

PD-L2 Serves as a Potential Prognostic Biomarker That Correlates With Immune Infiltration and May Predict Therapeutic Sensitivity in Lower-Grade Gliomas

Qijun Xie[†], *Xianlong Huang*[†], *Wu Huang*[†] *and Fang Liu*[*]

Department of Neurosurgery, The affiliated Changzhou No.2 People's Hospital of Nanjing Medical University, Changzhou, China

Although patients with lower-grade gliomas (LGGs; grades II and III) have a relatively favorable prognosis, patients frequently relapse and tend to progress to higher-grade gliomas, leading to treatment resistance, poor survival, and ultimately treatment failure. However, until now, thorough research has not yet been reported on the relationship between PD-L2 and immune infiltration and therapeutic sensitivity to immunotherapy and TMZ-based chemotherapy of LGGs. In this study, we found that the expression of PD-L2 is upregulated in glioma, with high PD-L2 expression predicting a worse prognosis. Univariate and multivariate Cox regression analysis both indicated that PD-L2 represented an independent prognostic factor with high accuracy in survival prediction for LGGs. A nomogram comprising of age, grade, IDH mutation, and PD-L2 was established for predicting OS. Additionally, PD-L2 was found to be remarkably correlated with immune infiltration and some anti-tumor immune functions. The degree of PD-L2 expression was also found to be strongly related to the prediction of therapeutic sensitivity to immunotherapy and TMZ-based chemotherapy. Furthermore, immunohistochemistry demonstrated that PD-L2 and the macrophage biomarker CD68 were both increased in glioma, with PD-L2 expression having a strong positive connection with CD68 expression. Taken together, PD-L2 is a prognostic biomarker for LGGs patients that may provide novel insights into glioma individualized therapeutic strategies and guide effective immunotherapy and chemotherapy.

Keywords: lower-grade gliomas (LGGs), PD-L2, tumor immune microenvironment, immune infiltration, prognosis, therapeutic sensitivity

Abbreviations: CGGA, Chinese Glioma Genome Atlas; GBM, Glioblastoma; GO, Gene Ontology; GSVA, Gene Set Variation Analysis; ICIs, Immune checkpoint inhibitors; IC50, half-maximal inhibitory concentration; IHC, Immunohistochemical; IPS, Immunophenoscore; KEGG, Kyoto Encyclopedia of Genes and Genomes; LGGs, lower-grade gliomas; OS, Overall survival; ssGSEA, Single Sample Gene Set Enrichment Analysis; TCGA, The Cancer Genome Atlas; TCIA, The Cancer Immunome Atlas; TIME, Tumor immune microenvironment; TMZ, Temozolomide; TIICs, Tumor-infiltrating immune cells; TAMs, tumor-associated macrophages.

OPEN ACCESS

Edited by:
Wen Cheng,
The First Affiliated Hospital of China Medical University, China

Reviewed by:
Alexander David Barrow,
The University of Melbourne, Australia
Edjah K Nduom,
National Institutes of Health (NIH), United States
Zhe Wang,
City of Hope National Medical Center, United States
Yumeng Huang,
Shanghai Jiao Tong University, China

***Correspondence:**
Fang Liu
czdoctorliu@hotmail.com

[†]*These authors have contributed equally to this work and share first authorship*

Specialty section:
This article was submitted to Cancer Immunity and Immunotherapy, a section of the journal Frontiers in Oncology

Received: *23 January 2022*
Accepted: *13 May 2022*
Published: *08 June 2022*

Citation:
Xie Q, Huang X, Huang W and Liu F (2022) PD-L2 Serves as a Potential Prognostic Biomarker That Correlates With Immune Infiltration and May Predict Therapeutic Sensitivity in Lower-Grade Gliomas. Front. Oncol. 12:860640. doi: 10.3389/fonc.2022.860640

INTRODUCTION

Gliomas are the most prevalent and fatal primary malignant intracranial tumors of the central nervous system (CNS), with a poor prognosis and fast progression (1, 2). According to the World Health Organization (WHO) classification criterion, gliomas can be classified as grade I-IV based on histopathological characteristics and biological behaviors (3). Lower-grade gliomas (LGGs) are classified as WHO grades II and III, while glioblastoma multiforme is classified as WHO grade IV (GBM) (4, 5). Despite the recent multimodal therapeutic strategies that have yielded some recent advances, including surgical resection, radio-chemotherapy, and immunotherapy, the survival and prognosis of glioma patients are still dismal with a 5-year survival rate of 20-30% (6–8). Studies have shown that the median survival time of LGGs is highly variable, and its biological behavior shows great intrinsic heterogeneity, which can rapidly develop into high-grade glioblastoma (GBM) (9, 10). Novel and effective prognostic biomarkers for early diagnosis, prognosis evaluation, and treatment response prediction of LGGs patients are urgently needed due to the lack of accurate and effective approaches to predict the prognosis of LGGs patients.

PD-L2 is the second ligand for PD-1, with a two- to six-fold affinity for PD-1 compared to PD-L1, and it can be produced by stromal, immune, or tumor cells (11).PD-L2 is a less studied PD-1 ligand, which plays an important role in cancer progression and immune regulation. Recent studies have linked PD-L2 expression to a poor prognosis in a variety of malignancies, such as lung adenocarcinoma (12), esophageal cancer (13), renal cell carcinoma (14), gastric cancer (15), colorectal cancer (16). Multiple recent studies have revealed that the tumor immune microenvironment (TIME) works as an immunosuppressive therapeutic barrier and is increasingly recognized as a crucial regulator of tumorigenesis, progression, maintenance, and therapy resistance (17–20). Tumor-infiltrating immune cells (TIICs), such as tumor-associated macrophages (TAMs), may be able to predict cancer prognosis and the efficacy of chemotherapy and immunotherapy in the TIME, which might be a viable target for anti-cancer therapy (21, 22). Quantifying tumor-infiltrating immune cells and revealing the significance of tumor immune microenvironment components and signatures may thus aid in better understanding their role in tumor immune escape, predicting patient prognosis, and guiding the development of innovative therapeutic strategies (23). A growing body of research suggests that transcriptional signatures could well evaluate the tumor immune microenvironment and predict clinical prognosis in glioma (24, 25). Nevertheless, until now, the literature lacks a comprehensive analysis of the association between PD-L2 and infiltrating immune cells in the LGGs TME, as well as the relationship between PD-L2 and therapeutic sensitivity to immunotherapy and chemotherapy.

In this study, we comprehensively analyzed the expression pattern and prognostic value of PD-L2 in glioma with RNA-seq data and corresponding clinical data from The Cancer Genome Atlas (TCGA) (n = 529) and the Chinese Glioma Genome Atlas (CGGA) (n = 443) datasets. Furthermore, an accurate nomogram integrating PD-L2, age, grade, and IDH mutation status was constructed to predict the 1-, 3- and 5-year OS of patients with LGGs, which revealed a high efficacy for prognosis prediction. The relationship between PD-L2 and tumor-infiltrating immune cells (TIICs) infiltration in the tumor immune microenvironment (TIME) was then investigated. Subsequently, we further explored the potential biological processes and pathways of PD-L2 involvement in the pathogenesis of LGGs. Furthermore, the predictive value of PD-L2 in the efficacy of therapeutic sensitivity to immunotherapy and chemotherapy was also investigated. Our findings could shed light on the critical role of PD-L2 as a novel biomarker and potential therapeutic target in LGGs, as well as provide an underlying mechanism between PD-L2 and tumor-immune interactions.

MATERIALS AND METHODS

Ethics Statement

The experiments were undertaken with the understanding and written consent of each subject. The study was approved by the Ethical Review Boards of the Affiliated Changzhou No. 2 People's Hospital of Nanjing Medical University and conformed to the standards set by the Declaration of Helsinki.

Gene Expression Data Acquisition and Analysis

Glioma tissues (WHO grade II and grade III, n=20) and normal brain tissue (n=2) embedded in paraffin were collected from patients undergoing surgery in the Department of Neurosurgery, The Affiliated Changzhou No. 2 People's Hospital of Nanjing Medical University. The RNA-seq data and corresponding clinical data of LGG patients were downloaded from The Cancer Genome Atlas (TCGA; http://cancergenome.nih.gov/) and the Chinese Glioma Genome Atlas (CGGA, http://www.cgga.org.cn). The collected clinical data included age, gender, grade, IDH mutation status, 1p/19q codeletion status, and histological types.

Evaluation of the Independent Prognostic Factor and Survival Analysis

Correlations between PD-L2 expression and the clinicopathological and molecular features were analyzed by the "ComplexHeatmap", "ggalluvial", and "ggpubr" R package. Univariate and multivariate Cox regression analyses were used to determine whether PD-L2 could be used as an independent prognostic factor in patients with LGGs, regardless of clinical and molecular characteristics such as age, gender, grade, IDH mutation status, 1p/19q codeletion status, and histological types. According to the median expression level of PD-L2, glioma patients were divided into high-expression and low-expression groups. The Kaplan–Meier survival analysis was performed to evaluate overall survival (OS) using the 'survival' R package.

Development and Validation of the Nomogram Model

The nomogram including age, grade, IDH mutation status, and PD-L2 for prediction of 1-, 3-, and 5-years survival probability was conducted and verified in the TCGA cohort as well as CGGA cohort. The concordance index (C-index) and a calibration curve plot were then used to evaluate the nomogram's predictive accuracy and discriminative ability.

Infiltration Patterns in the Tumor Microenvironment

The ESTIMATE algorithm (Estimation of Stromal and Immune cells in Malignant Tumors using Expression data) was applied to calculate the immune score, stromal score, estimate score, and tumor purity based on the transcriptome profile of TCGA and CGGA LGG cohorts (26). Single-sample gene set enrichment analysis (ssGSEA) is an algorithm performed to quantify immune cell infiltration in a single sample according to the expression levels of immune cell-specific markers in the tumor microenvironment using the "limma", "GSEABase", and "GSVA" packages (27–29). To identify TME infiltrating immune cells, the list of immune cell-specific markers gene sets was collected from a previous study (30). The correlation between PD-L2 expression and tumor-infiltrating immune cells (TIICs) infiltration in the tumor immune microenvironment was analyzed by the ssGSEA analysis (31). To validate the accuracy of the ssGSEA, we analyzed the correlation of PD-L2 expression with the abundances of six types of immune cells (B cells, $CD4^+$ T cells, $CD8^+$ T cells, neutrophils, macrophages, and dendritic cells) from the online TIMER (https://cistrome.shinyapps.io/timer/) database (32). Currently acknowledged methods including TIMER, QUANTISEQ, CIBERSORT–ABS, CIBERSORT were performed to calculate the relationship between the expression of PD-L2 and the abundance of infiltrating immune cells among the LGGs samples from the TCGA dataset. The "GSVA" R package was used to compare the ssGSEA scores of immune cell infiltration and immune-related functions or pathways between high-PD-L2 and low-PD-L2 expression groups. Subsequently, the KEGG, GOBP, and hallmark pathways were used to identify the potential biological functions and pathways associated with PD-L2 expression level using the "GSVA" R package. Among them, Hallmark (h.all.v7.4.symbols.gmt), KEGG (c2.cp.kegg.v7.4.symbols.gmt), and GOBP (c5.go.bp.v7.4.symbols.gmt) gene sets were downloaded from Molecular Signatures Database (http://www.gsea-msigdb.org/). Statistical significance was determined for functional categories with an adjusted P-value < 0.05 or a false discovery rate (FDR) < 0.05.

Therapeutic Sensitivity Prediction

Next, we further predict the therapeutic sensitivity of LGGs patients to anti-PD-1 and anti-CTLA-4 immunotherapy and chemosensitivity of temozolomide (TMZ). To better predict the therapeutic sensitivity of immune checkpoint inhibitors (ICIs), we downloaded the immune cell and immunophenotype data from The Cancer Immunome Atlas (TCIA) (https://tcia.at/home). The immunophenogram was used to predict anti-PD1/PD-L1 therapy responses in LGGs. The immunophenogram was used to calculate the immunophenoscore (IPS) among four types (CTLA4 positive + PD-1 positive, CTLA4 negative + PD-1 negative, CTLA4 positive + PD-1 negative, CTLA4 negative + PD-1 positive, CTLA4 negative + PD-1 positive) from the TCGA-GBM database. The IPS scale ranged from 0 to 10.A high PD-1 positive IPS predicts a good response to anti-PD-1/PD-L1 therapy. Furthermore, we used the R package "pRRophetic" to predict the chemosensitivity of temozolomide (TMZ) based on half-maximal inhibitory concentration (IC50) in different groups (33, 34).

Immunohistochemistry

In formalin-fixed, paraffin-embedded surgical specimens of normal brains and different grades (WHO grade II-III) of human gliomas, immunohistochemical (IHC) staining was used to detect PD-L2 and CD68 expression. First, all paraffin specimens were cut into 4 μm thick slices, dewaxed in xylene (10 min x 2) and rehydrated with graded ethanol (100%, 95%, and 75% for 2 min, respectively), and then washed with phosphate-buffered saline (PBS; 3 times for 3 min). After antigen retrieval in 10 mM sodium citrate buffer (pH 6.0) and blocking endogenous peroxidase activity with 3% H2O2 (five minutes), the slides were incubated with 10% normal goat serum for 30 minutes at 37°C. Then the sections were incubated overnight with rabbit polyclonal anti-PD-L2 (Invitrogen, PA5-82484, 1:300), anti-CD68 (ZSGB-BIO, ZM-0464, ready-to-use) at 4°C, followed by incubation with biotinylated goat anti-rabbit immunoglobulin G (IgG) secondary antibody (ZSGB-BIO, ZDR5306, ready-to-use). The sections were then stained with DAB (3,3-diaminobenzidine), counterstained with hematoxylin, dehydrated, dried, and mounted. Three experienced pathologists were invited to evaluate all immunostained slides for IHC scores. The numbers of positively stained PD-L2 cells and CD68 cells were counted under the high-magnification lens (400×) in six randomly selected visual fields (35). The immunoreactive score (IRS) was calculated by multiplying the intensity of the staining by the percentage of positive cells. The staining intensity was scored as follows: 0 (negative), 1 (weak staining), 2 (moderate staining), and 3 (strong staining). The percentage of cells that were positive was scored as follows: 0 score (0% positive cells), 1 score (1%–25% positive cells), 2 score (26%–50% positive cells), 3 score (51%–75% positive cells), and 4 score (76%–100% positive cells) (36).

Statistical Analysis

R (version 4.1.0) and publicly available packages were used for all statistical studies. P value<0.05 was considered statistically significant. (*P<0.05, **P<0.01, and ***P<0.001).

RESULTS

PD-L2 Expression Was Upregulated in Glioma and Associated With Clinical and Molecular Characteristics

The PD-L2 expression level was significantly increased with an increasing grade of glioma in the TCGA cohort (**Figures 1A, B**).

We then performed to investigate the relationship between the expression of PD-L2 and clinicopathological characteristics of LGGs patients in the TCGA and CGGA databases (**Table 1**). The results showed that PD-L2 was significantly higher expressed in IDH wildtype than that in the IDH mutation (p< 0.001), and in 1p19q non-codeletion than 1p19q codeletion (p<0.001). Furthermore, PD-L2 expression was significantly higher in LGGs patients with a dead status than in those with an alive status(p<0.05). The expression level of PD-L2 was also found to be highly correlated with histological types (p < 0.05, **Table 1** and **Figure 1**). Consistent with the above findings, we found substantial differences between the high- and low-PD-L2 expression groups in terms of survival, grade, IDH mutation status, 1p/19q codeletion status, and histological types in the CGGA cohort (**P < 0.05, Supplementary Figure 1** and **Supplementary Figure 2**).

The major clinicopathological characteristics of the 20 patients with LGGs are summarized in **Supplementary Table 1**. The average age of patients was 50 (range, 13–73 years), 15 males and 5 females. As for grade, 45% patients were in grade II.

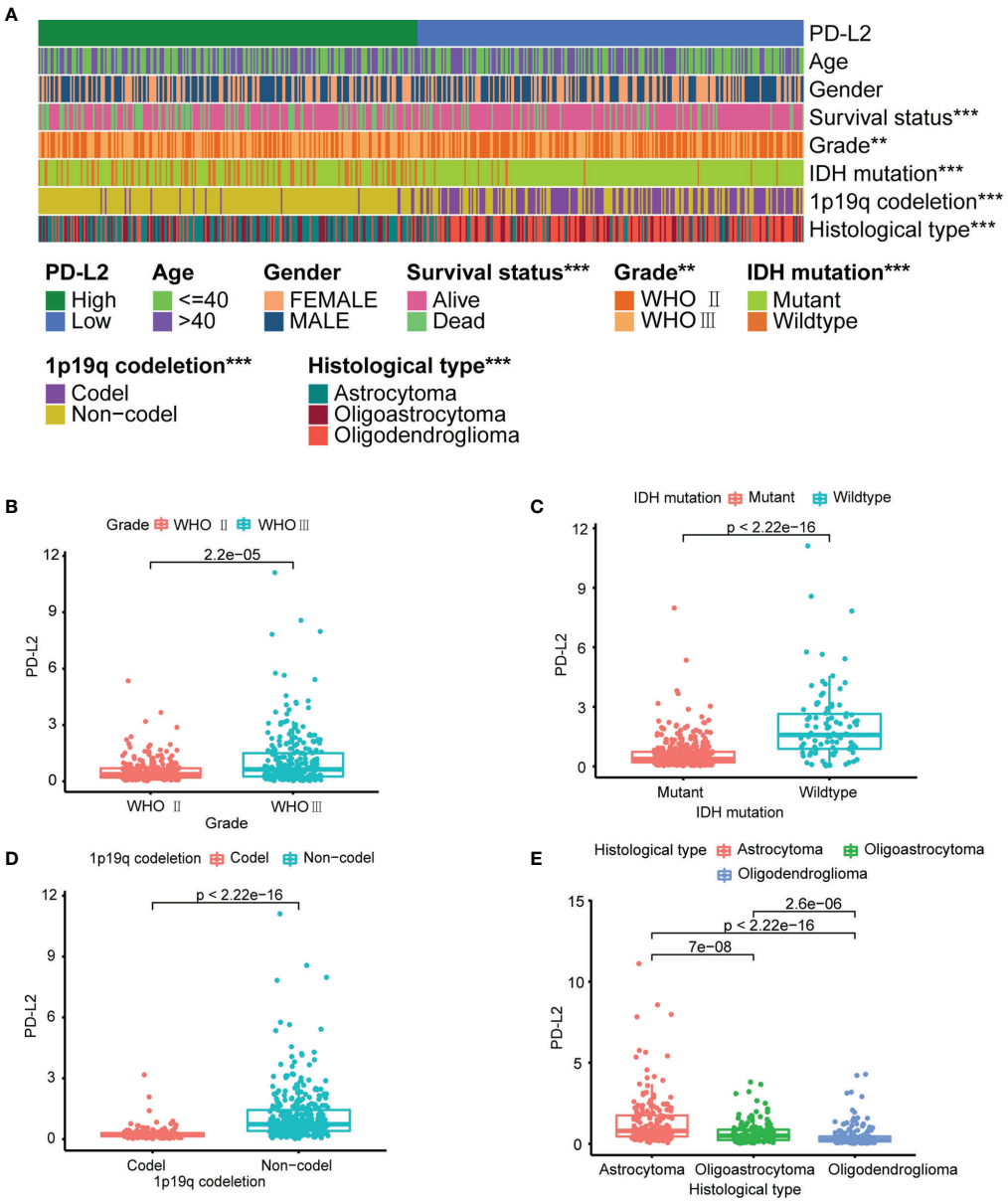

FIGURE 1 | PD-L2 expression is associated with clinicopathological features in the TCGA dataset. **(A)** The heatmap showing the correlation between the expression levels of PD-L2 and the clinicopathological features including age, gender, survival status, grade, IDH mutation status, 1p/19q codeletion status, and histological types. **(B–E)** The scatter diagram showed that grade, IDH mutation status, 1p/19q codeletion status and histological types were significantly associated with PD-L2 expression (***P<0.001; **P<0.01).

TABLE 1 | Correlation between PD-L2 expression and clinicopathologic characteristics of patients with LGGs in TCGA and CGGA cohorts.

Variables	TCGA				CGGA			
	Total	PD-L2^{High}	PD-L2^{Low}	P-Value	Total	PD-L2^{High}	PD-L2^{Low}	P-Value
Age								
<=40	248	121 (48.4%)	127 (49.8%)	0.752	189	98 (51.9%)	77 (50.7%)	0.826
>40	257	129 (51.6%)	128 (50.2%)		152	91 (48.1%)	75 (49.3)	
Gender								
Female	226	111 (44.4%)	115 (45.1%)	0.875	150	77 (40.7%)	73 (48.0%)	0.178
Male	279	139 (55.6%)	140 (54.9%)		191	112 (59.3%)	79 (52%)	
Survival status								
Alive	382	170 (68.0%)	212 (83.1%)	<0.001	173	82 (43.4%)	91 (59.9%)	0.002
Dead	123	80 (32.0%)	43 (16.9%)		168	107 (56.6%)	61 (40.1%)	
Grade								
WHOII	245	104 (41.6%)	141 (55.3%)	0.002	140	78 (41.3%)	62 (40.8%)	0.929
WHOIII	260	146 (58.4%)	114 (44.7%)		201	111 (58.7%)	90 (59.2%)	
IDH mutation								
Mutant	411	168 (67.2%)	243 (95.3%)	<0.001	261	131 (69.3%)	130 (85.5%)	<0.001
Wildtype	94	82 (32.8%)	12 (4.7%)		80	58 (30.7%)	22 (14.5%)	
1p19q codeletion								
Codel	167	15 (6.0%)	152 (59.6%)	<0.001	105	24 (12.7%)	81 (53.3%)	<0.001
Non-codel	338	235 (94.0%)	103 (40.4%)		236	165 (87.3%)	71 (46.7%)	
Histological type								
Astrocytoma	190	139 (55.6%)	51 (20.0%)	<0.001	227	152 (80.4%)	75 (49.3%)	<0.001
Oligoastrocytoma	127	65 (26.0%)	62 (24.3%)		66	19 (10.1%)	47 (30.9%)	
Oligodendroglioma	188	46 (18.4%)	142 (55.7%)		48	18 (9.5%)	30 (19.7%)	

Astrocytoma was the main histological type (n = 11), followed by oligodendroglioma (n = 7) and oligoastrocytoma (n = 2). Other clinical and molecular characteristics of these patients are presented in **Supplementary Table 1**. Subsequently, the protein levels of PD-L2 were further validated *via* IHC staining in the normal brain tissue and gliomas samples from the Affiliated Changzhou No. 2 People's Hospital of Nanjing Medical University (n=20). IHC staining of PD-L2 in tissue samples from primary gliomas WHO grade II-III patients (n = 20) and normal brain (n = 2) demonstrated that PD-L2 protein levels were more often increased in LGGs (WHO grade II-III) samples, while expression was low/undetectable in normal brain tissues **(Figure 2).** Taken together, these results indicated that PD-L2 levels were considerably higher in glioma tissue than in normal brain tissue.

PD-L2 Was an Independent Prognostic Factor in LGGs

We investigated the impact of PD-L2 expression on overall survival (OS). Patients were divided into a high expression group and a low expression group based on the median PD-L2 expression level. The Kaplan-Meier survival analysis revealed

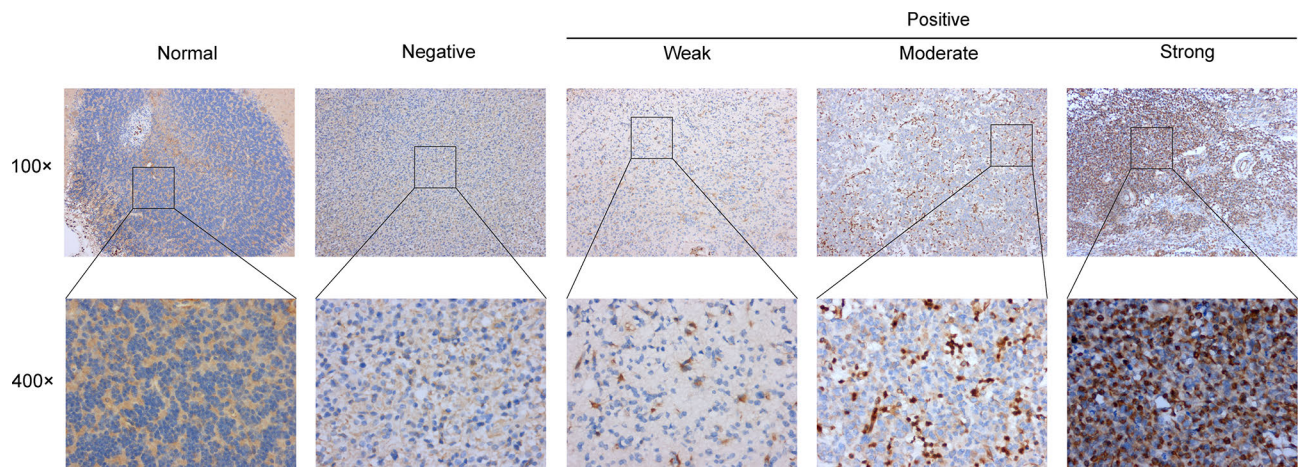

FIGURE 2 | Representative images of immunohistochemical (IHC) staining of PD-L2 protein in glioma tissues and normal brain tissue (×100 and ×400).

that patients with higher levels of PD-L2 expression had a worse prognosis than those with lower levels of PD-L2 expression in the TCGA and CGGA cohorts (P < 0.001, **Figures 3A, B**).

Next, to assess the independent prognostic value of PD-L2 and other clinical-pathological factors in LGGs, Univariate and multivariate Cox regression analysis indicated that PD-L2 expression remained an independent prognostic factor of OS for patients with LGGs (HR: 1.939; 95% confidence interval [CI]: 1.355-2.775) after adjusting for the six clinicopathological factors (age, gender, grade, IDH mutation status, 1p/19q codeletion status, and histological types) (**Table 2**).We developed a nomogram model based on independent prognostic factors (age, grade, IDH mutation status, and PD-L2 expression) to quantitatively evaluate the 1-, 3-, and 5-year OS of patients with LGGs (**Figure 4A**). The C-index of the nomogram was calculated to be 0.826, and the calibration curves for the 1-, 3- and 5-year OS had an excellent predictive effect (**Figures 4B–D**). Additionally, external validation was done by the CGGA samples. The C-index was 0.701 and the calibration curves for probabilities for 1-, 3- and 5-year OS revealed good agreement between the predicted nomogram and actual survival (**Figures 4E-G**). Conclusively, this nomogram model based on PD-L2 expression may be a promising prognostic model for evaluating the clinical prognosis of LGGs.

PD-L2 Expression Correlated With Immune Cell Infiltration and Tumor Immune Microenvironment

Then, using the ESTIMATE algorithm, we investigated the potential relationship between PD-L2 expression and immune infiltration and discovered that PD-L2 expression was positively correlated with the stroma score, immune score, and ESTIMATE score, as well as negatively correlated with tumor purity in the TCGA cohort (**Figure 5A**). To further explore the immune infiltration difference of 23 immune cells and the immune status betweenthehigh-PD-L2 and low-PD-L2 expression groups in the TIME, we quantified the infiltrating scores of diverse immune cell subpopulations and the activity of immune-related functions or pathways with ssGSEA. The difference and correlation analyses revealed that the high-PD-L2 expression group was associated with more tumor-infiltrating immune cells, including CD8+ T cells, CD4+ T cells, B cells, macrophages, neutrophils, dendritic cells, regulatory T cells (Tregs), MDSCs, and natural killer T cells (NKT) (**Figures 5B, C** and **Supplementary Figure 3**). Additionally, the analysis by the TIMER database showed that PD-L2 expression was negatively correlated with tumor purity and positively associated with the infiltrating levels of B cells, $CD8^+$T cells, $CD4^+$ T cells, macrophages, neutrophils, and dendritic cells (**Supplementary Figure 4**). Furthermore, immune-related functions or pathways such as antigen-presenting cell (APC) co-inhibition, APC co-stimulation, chemokine receptor (CCR), Check-point, cytolytic activity, human leukocyte antigen (HLA), inflammation-promoting, MHC class I, para-inflammation, T-cell co-inhibition, T-cell co-stimulation, and type I and II interferon responses were associated with significantly higher ssGSEA scores in the high-PD-L2 expression group (P < 0.05, **Figure 5D**). Notably, we got similar results in the validation set, the results from the CGGA cohort also indicated that PD-L2 played a major role in immune cell infiltration in the tumor immune microenvironment of gliomas (**Supplementary Figures 5**, **6**).

Our results have demonstrated that PD-L2 expression was found to be positively associated with macrophages in patients with LGGs in the TCGA (r = 0.59, P < 0.05) and CGGA cohorts (r = 0.69, P < 0.05) (**Supplementary Figures 3**, **6**) and the TIMER database's correlation analysis showed that PD-L2 was substantially associated with macrophage (r = 0.753, P < 0.05) (**Supplementary Figure 4**). In consistence with the findings described above, PD-L2 was more positively correlated with macrophages (**Supplementary Figure 7**). Therefore, we detected the expression of CD68 in glioma and normal brain tissues using IHC staining to further explore the relationship between PD-L2 and CD68. IHC staining results showed that the CD68 expression was observed in normal brain tissues with weak staining, while moderate or strong CD68 staining was detected in

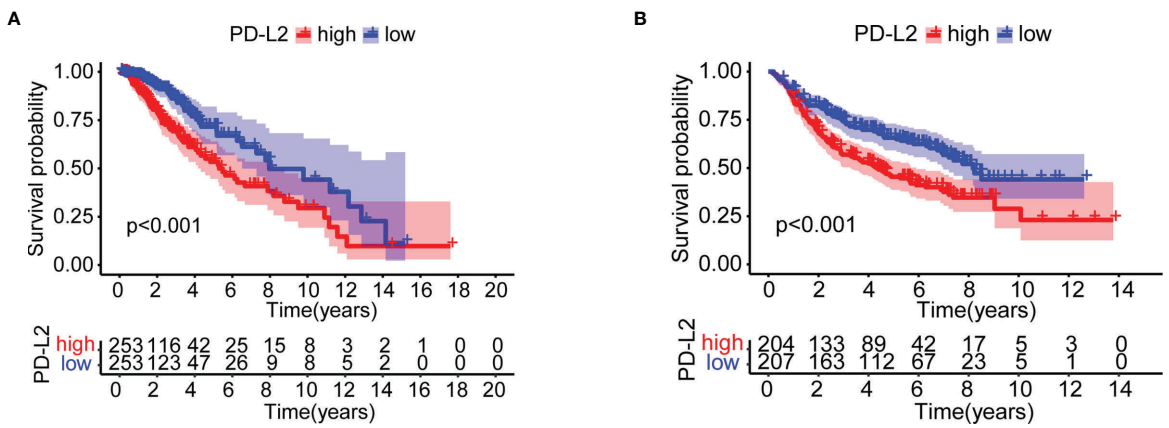

FIGURE 3 | Kaplan–Meier overall survival (OS) curves for patients in the TCGA **(A)** and CGGA **(B)** datasets assigned to high- and low-expression groups.

TABLE 2 | Univariate and multivariate analysis of association of PD-L2 and prognostic factors with overall survival in LGGs based on the TCGA and CGGA databases.

Predictor	TCGA				CGGA			
	Univariate analysis		Multivariate analysis		Univariate analysis		Multivariateanalysis	
	HR (95%CI)	P-value	HR (95% CI)	P-value	HR (95% CI)	P-value	HR (95% CI)	P-value
Age (>40)	2.889 (2.009-4.155)	<0.001	2.942 (1.890-4.580)	<0.001	1.150 (0.849-1.556)	0.367		
Gender (Male)	1.124 (0.800-1.580)	0.499			1.276 (0.936-1.739)	0.123		
WHO grade (III vs II)	3.059 (2.046-4.573)	<0.001	1.992 (1.277-3.107)	0.002	3.041 (2.128-4.347)	<0.001	3.159 (2.191-4.555)	<0.001
IDH mutation (Wildtype)	5.385 (3.777-7.679)	<0.001	2.965 (1.813-4.848)	<0.001	2.078 (1.493-2.892)	<0.001	1.573 (1.091-4.555)	0.015
1p/19q codeletion	0.401 (0.256-0.629)	<0.001	0.816 (0.431-1.546)	0.533	0.377 (0.256-0.555)	<0.001	0.595 (0.324-1.093)	0.094
Histological type	0.577 (0.392-0.848)	0.005	1.092 (0.642-1.856)	0.745	0.511 (0.394-0.662)	<0.001	0.820 (0.535-1.259)	0.365
PD-L2	2.794 (2.163-3.610)	<0.001	1.939 (1.355-2.775)	<0.001	1.738 (1.420-2.128)	<0.001	1.384 (1.097-1.747)	0.006

LGGs tissues (WHO II and WHO III) in almost all cases (**Figure 6A**). Furthermore, correlation analysis revealed a positive connection between PD-L2 and CD68 (r = 0.59, P 0.05) in glioma specimens (**Figure 6B**), which was comparable with the results of correlation analysis in the TCGA and CGGA cohorts (**Figures 6C, D**). Taken together, our findings confirmed the positive correlation between PD-L2 levels and the abundance of macrophage infiltration in LGGs.

Functional Annotation and Pathway Enrichment of PD-L2

To further investigate the underlying immune-related biological processes and tumor-related pathways associated with the expression of PD-L2, we performed the KEGG, GOBP, and hallmark pathways enrichment analysis in the TCGA cohort. The findings revealed that the high-PD-L2 expression group was considerably enriched in several biological processes, including that for cytokine-cytokine receptor interaction, response to interferon−gamma, inflammatory response, angiogenesis, chemokine production, apoptosis, hypoxia, interleukin (IL)-6, and IL-8 production. Moreover, tumor-related pathways such as JAK/STAT signaling pathway, Toll-like receptor signaling pathway, PI3K/AKT/mTOR signaling, TGF-beta signaling, IL-2-STAT5 signaling pathway, IL-6-JAK-STAT3 signaling pathway, P53 pathway signaling, TNFA signaling *via* NFKB were found to be enriched in the high-PD-L2 expression group (**Figures 7A-C**).

Prediction of Therapeutic Sensitivity to Immunotherapy and TMZ-Based Chemotherapy

Subsequently, to predict the potential chemosensitivity of temozolomide (TMZ) in LGGs, the relationship between PD-L2 expression and TMZ-based chemotherapy was explored and the results revealed a substantial positive correlation between PD-L2 expression and TMZ-based chemotherapy (r = 0.54, P < 0.05) (**Figure 8A**). Additionally, patients in the low-expression group showed a more sensitive response to TMZ-based chemotherapy based on the estimated IC50 (**P < 0.05, Figure 8B**). In consideration of the importance of ICIs in immunotherapy, the immunophenogram was then used to predict the response to anti-PD-1/PD-L1 therapy. We discovered that the high-PD-L2 expression group had significantly higher IPS than the low-PD-L2 expression group in the CTLA4 positive + PD-1 positive, CTLA4 positive + PD-1 negative, and CTLA4 negative + PD-1 positive types (P< 0.05) (**Figure 8C**). These findings suggested that patients with high levels of PD-L2 expression were more likely to respond well to anti-PD-1/PD-L1 therapy or a combination of anti-PD-1/PD-L1 and anti-CTLA-4 therapy, suggesting that PD-L2 had good potential in predicting ICIs response and may benefit from immunotherapies. Conclusively, PD-L2 could contribute to the selection of optimal immunotherapy and chemotherapy strategy in glioma patients.

DISCUSSION

Patients with LGGs have a more favorable prognosis than those with GBM, but many advances to higher-grade gliomas, resulting in recurrence and poor survival, posing a therapeutic challenge to physicians (37–39).Despite standard treatment of maximally safe surgical resection followed by radiotherapy and adjuvant chemotherapy with temozolomide, the prognosis of glioma, particularly glioblastoma, remains poor and almost all patients relapse inevitably (40, 41). Identifying new prognostic markers of LGGs at an early stage of the tumor, thus, can successfully predict and enhance the clinical prognosis of glioma patients. A previous study showed that PD-L2 was found to be able to predict the poor prognosis of glioma patients (42, 43). However, the specific role of PD-L2 in LGGs and their therapeutic sensitivity to immunotherapy and TMZ-based chemotherapy have not been

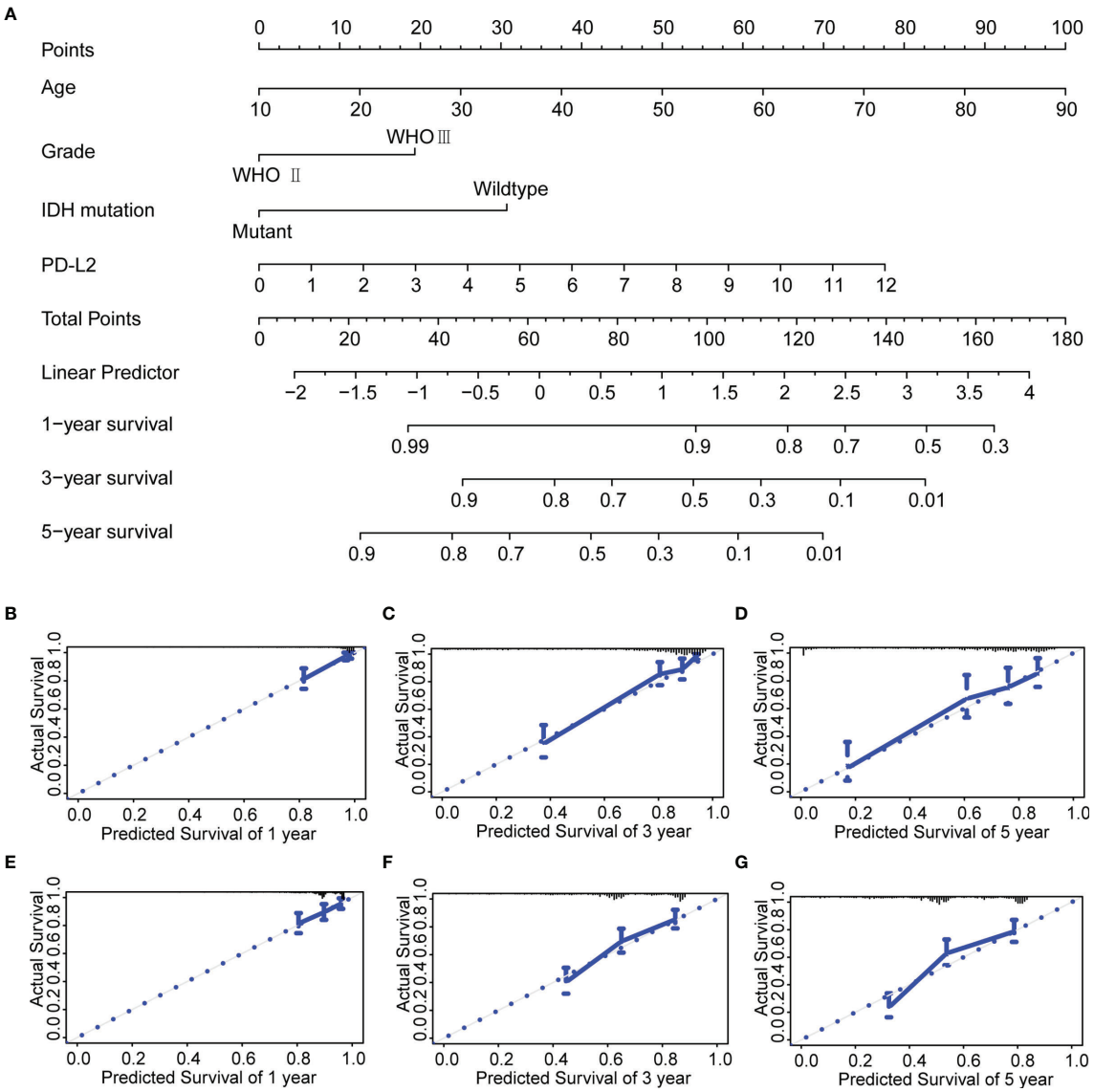

FIGURE 4 | Construction and evaluation of a prognostic nomogram. **(A)** The prognostic nomogram predicts the probability of the 1-, 3-, and 5-year OS. **(B–D)** The calibration curve of the nomogram for predicting the 1-, 3-, and 5-year OS in the TCGA database. **(E–G)** The calibration curve of the nomogram for predicting the 1-, 3-, and 5-year OS in the CGGA database.

reported, and few studies have been performed to explore the relationship between PD-L2 and TIICs in the LGGs tumor immune microenvironment (TIME). In this study, we discovered that PD-L2 is elevated in LGGs samples and is substantially associated with a poor prognosis in glioma patients in the CGGA and TCGA cohorts. Univariate and multivariate Cox regression analysis confirmed that high PD-L2 expression was found to be an independent prognostic factor of patients with LGGs. Additionally, we established a nomogram that integrates PD-L2 with clinicopathological factors (age, grade, and IDH mutation status) and discovered that it performs exceptionally well in predicting 1-, 3-, and 5-year OS in glioma patients.

The role of tumor immune microenvironment in the occurrence, development, invasion, and drug-resistance of gliomas is becoming increasingly recognized (44, 45), with numerous published studies demonstrating that tumor-infiltrating immune cells (TIICs) play a critical role in the tumorigenesis, invasion, metastasis, diagnosis, treatment, and prognosis of gliomas (46–48). In our study, PD-L2 expression was found to positively correlate with the immune score, stromal score, and ESTIMATE score, as well as negatively correlate with tumor purity, indicating that high PD-L2 expression was positively correlated with immune infiltration in LGGs. Numerous studies have previously described that the role of

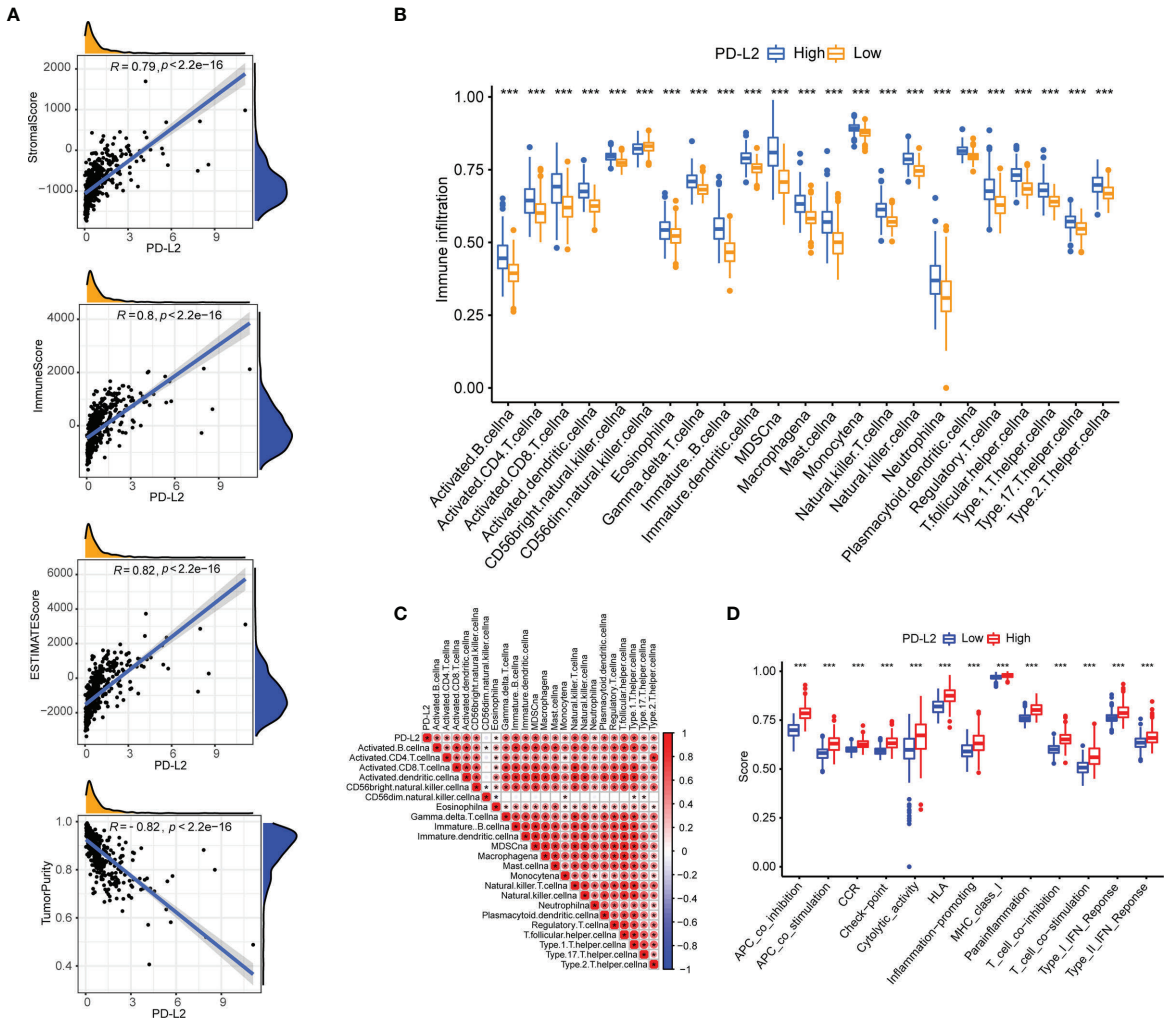

FIGURE 5 | The association of PD-L2 with the tumor immune microenvironment and immune status in the TCGA cohort. **(A)** PD-L2 was positively correlated with the stroma score, immune score, and ESTIMATE score, as well as negatively correlated with tumor purity in the TCGA cohort. **(B)** The abundance of tumor-infiltrating immune cells in the high-PD-L2 and low-PD-L2 expression groups. **(C)** Pearson correlation analysis ofPD-L2 expression and immune cell infiltration. **(D)** The immune pathway functions between the high- and low- expression patients. ***P<0.001.

tumor-infiltrating immune cells in various cancers is increasingly being viewed as a critical factor driving or mediating tumor progression and influencing therapeutic outcomes and patient prognosis (49, 50).Unlike a previous study (42), we further investigate the correlation between PD-L2 and TIICs *via* GSVA analysis and the online website TIMER. Notably, our results revealed that PD-L2 is closely associated with TIICs infiltration in LGGs, especially macrophages, which can be validated by the analysis of the online website TIMER.

Tumor-associated macrophages (TAMs), which play a significant role in carcinogenesis, progression, metastasis, invasion, immunosuppression, angiogenesis, and the immune response to cancer, have been linked to treatment failure and poor prognosis in LGGs patients in several recent studies. Multiple recent studies have shown that TAMs, which play an important role in tumorigenesis, progression, metastasis, invasion, immunosuppression, angiogenesis, and immune response to cancer, are linked to treatment failure and poor prognosis in LGGs patients (51, 52). Our immune cell correlation analysis revealed that PD-L2 was positively associated with macrophages in the TCGA and CGGA cohorts (r = 0.59, r = 0.69, respectively, P < 0.05). Our immunohistochemistry results are in accordance with a previous study that CD68 expression in lower-grade glioma tissues (LGGs, WHO II and WHO III) was significantly higher than the expression in normal brain tissues. Further analysis demonstrated PD-L2 expression was significantly positively correlated with macrophage infiltration in our glioma samples (r = 0.59, P < 0.05). Additionally, several lines of evidence indicate that a high TAMs infiltration, especially M2 macrophages, are closely associated with poor clinical outcomes in a wide variety of

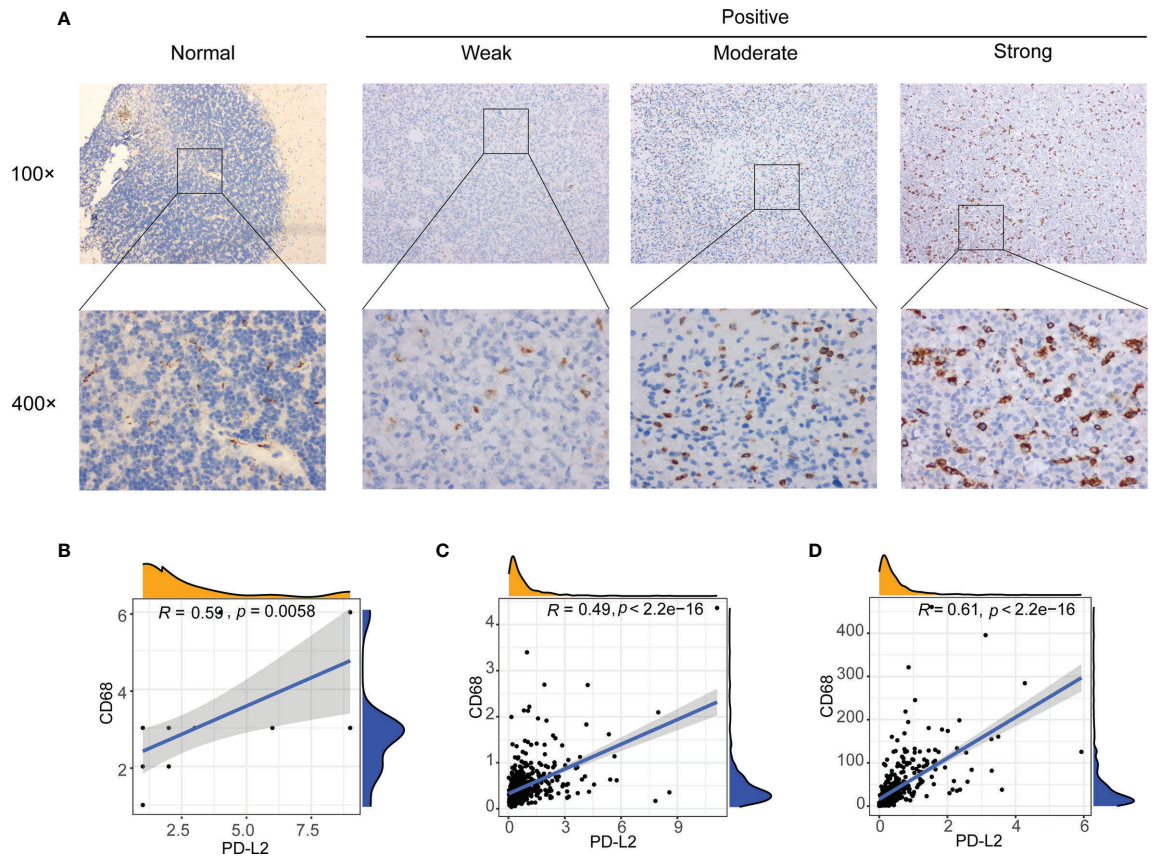

FIGURE 6 | Correlation between PD-L2 expression and macrophages marker (CD68 expression) in gliomas. **(A)** Representative images of immunohistochemical (IHC) staining of CD68 protein in glioma tissues and normal brain tissue (×100 and ×400). **(B–D)** PD-L2 expression was significantly associated with macrophages marker (CD68 expression) in glioma specimens **(B)**, TCGA database **(C)**, and CGGA database **(D)**.

tumors and are now being recognized as potential biomarkers for diagnosis and prognosis of malignant tumors, as well as an attractive therapeutic target in cancer therapy (53–56). Chanmee et al. have reported that achieving TAMs-targeting cancer therapy by changing its polarization from M2 macrophages to M1 macrophages, inhibiting macrophage recruitment, and inhibiting the survival of TAMs, can enhance the response to treatment (57, 58).Therefore, targeting the tumor immune checkpoints and macrophages targeting may be a novel strategy for effective cancer treatments.

Immunotherapy is thought to be one of the most promising glioma treatments (59). Emerging evidence has indicated that immune checkpoint blockade (ICB) therapies such as anti-programmed death 1 (PD-1), ant-programmed cell death-ligand 1 (PD-L1) and anti-cytotoxic T lymphocyte-associated protein 4 (CTLA-4) have emerged as a promising approach as anti-cancer immunotherapy, dramatically changing treatment in solid tumors (60–62). However, the majority of patients still showed adaptive resistance with a low response rate in most cancers, especially for tumors with a low mutational burden (63–65). As a result, to improve the clinical prognosis of cancer patients, we must investigate new targets and predict the therapeutic sensitivity of immune checkpoint inhibitors (ICIs). Here, our study indicated that patients with high expression of PD-L2 are associated with a high response rate to treatment by ICIs, suggesting that PD-L2 had good potential in predicting ICIs response and high expression of PD-L2 may more likely to yield considerable clinical benefit from immunotherapy. So far, temozolomide (TMZ), a DNA alkylating agent, has become the first-line chemotherapy for the treatment of glioma, and resistance to it posed a major challenge (66–68). Therefore, it is crucial to investigate promising and reliable biomarkers for glioma therapy that can predict potential the chemosensitivity of TMZ-based chemotherapy. We discovered that patients with a low-PD-L2 expression group exhibited a more sensitive response to TMZ-based chemotherapy based on the estimated IC50, suggesting that patients with low PD-L2 were more likely to benefit from TMZ-based chemotherapy in LGGs. Combining the therapeutic sensitivity to immunotherapy and TMZ-based chemotherapy, patients with high PD-L2 may benefit from immunotherapy, whereas patients with low PD-L2 may benefit from TMZ-based chemotherapy, which implies the possible

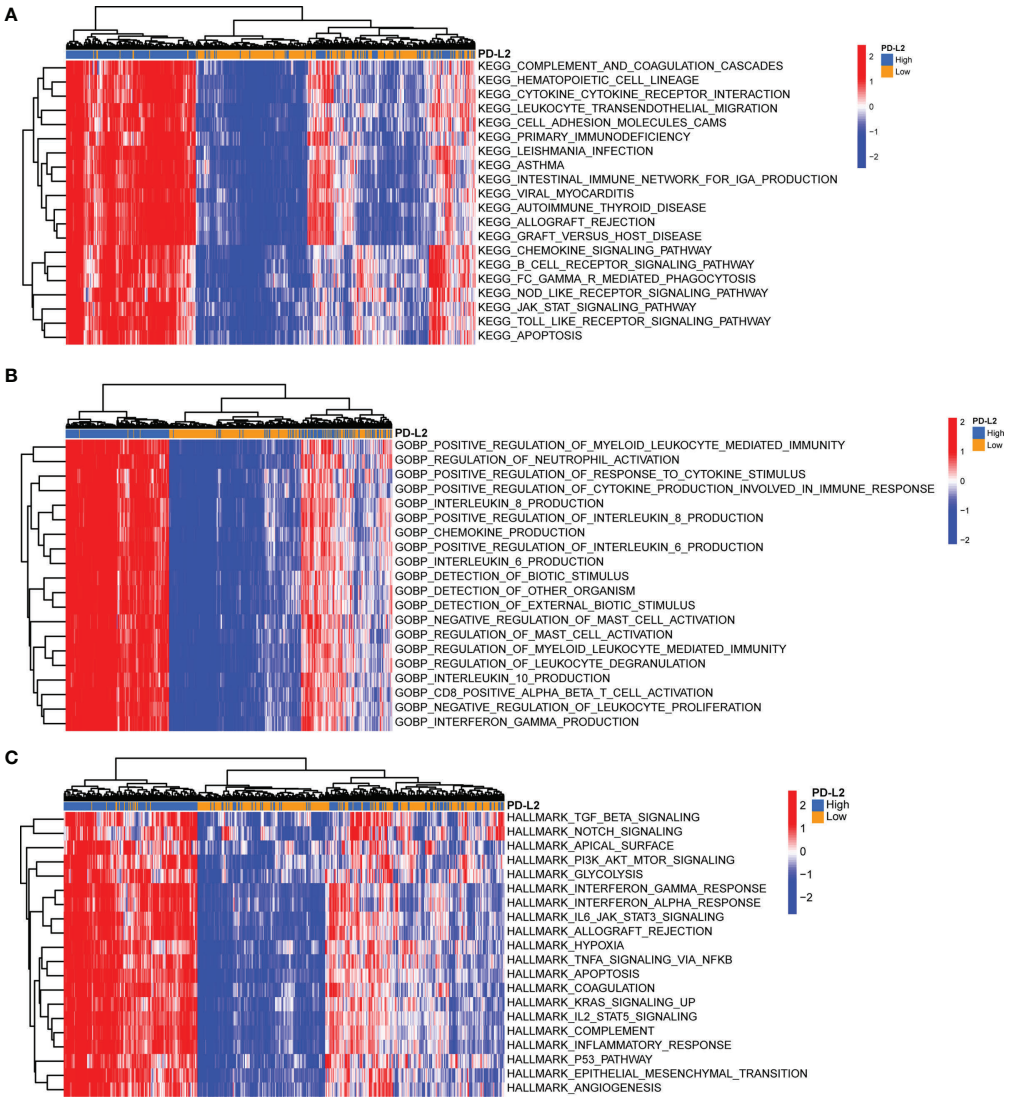

FIGURE 7 | Gene Set Variation Analysis (GSVA) of biological processes and tumor-related pathways associated with the expression of PD-L2 in the TCGA cohort. Top 20 significant Kyoto Encyclopedia of Genes and Genomes (KEGG) pathways **(A)**, Gene Ontology (GO) biological processes **(B)**, and hallmark pathways **(C)** identified by GSVA analysis. GSVA, Gene Set Variation Analysis; GO, Gene Ontology; KEGG, Kyoto Encyclopedia of Genes and Genomes.

values of PD-L2 for selecting an optimal therapeutic strategy. These findings, however, will need to be further verified in the future.

Nevertheless, there are still some limitations to the present study. Firstly, we should consider the effect of tissue heterogeneity on prognostic assessments. Secondly, although we found that PD-L2 was associated with macrophage infiltration in the IHC analysis, the potential biological mechanism and pathway of PD-L2 promoting macrophage infiltration in the glioma immune microenvironment needed to be further validated using *in-vivo* or *in-vitro* experiments. Thus, we will expand the sample size and collect more complete clinical samples for further verification in our future study. Thirdly, the present findings may be the basis for further studies to validate the outcomes, such as we can further explore the development of single-cell sequencing in glioma to provide a stronger predictive value to a large extent.

CONCLUSION

In conclusion, our study demonstrates that PD-L2 is overexpressed in glioma tissues and is associated with a poor prognosis. Moreover, PD-L2 overexpression correlates with immune cell infiltration, especially macrophages. The relationship between PD-L2 and the tumor immune

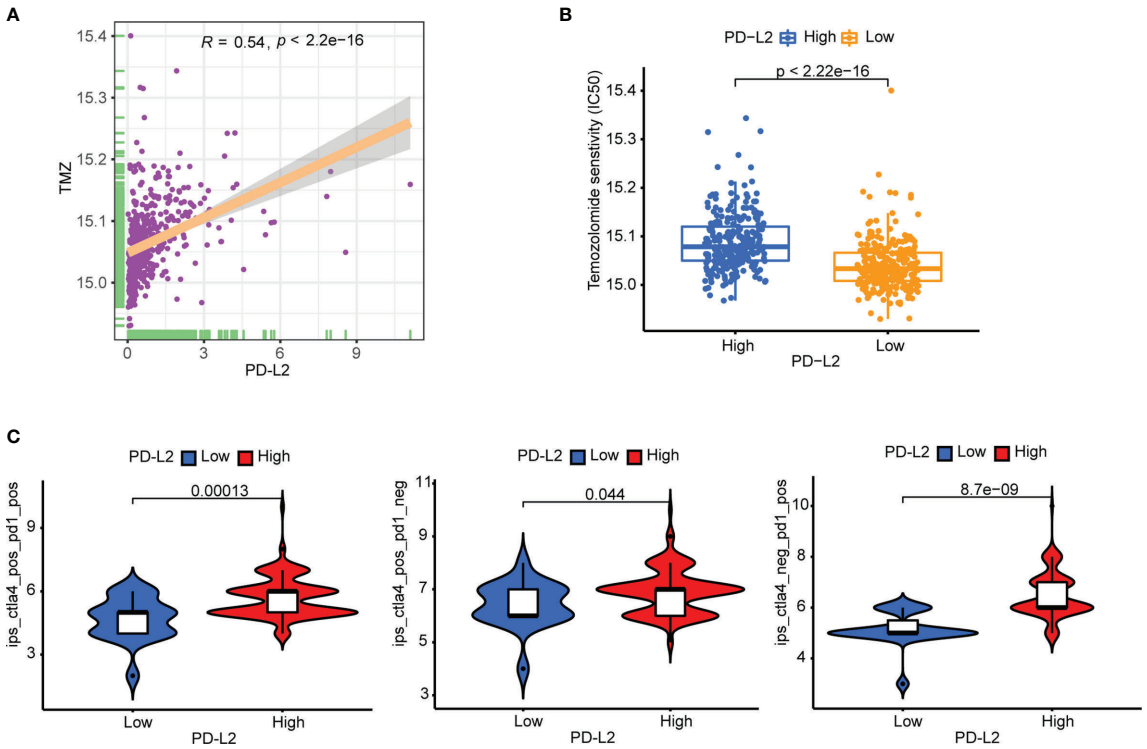

FIGURE 8 | Therapeutic sensitivity prediction to immunotherapy and TMZ-based chemotherapy in the TCGA cohort. **(A)** PD-L2 was significantly positively correlated with the TMZ-based chemotherapy. **(B)** The low-PD-L2 expression patients showed a more sensitive response to TMZ-based chemotherapy based on the estimated IC50. **(C)** Patients with high PD-L2 expression had higher immunophenoscores (IPS) in three subgroups: CTLA-4 positive PD-1 positive, CTLA-4 negative PD-1 positive, and CTLA-4 positive PD-1 negative. TMZ, temozolomide; IC50, half-maximal inhibitory concentration; IPS, immunophenoscore.

microenvironment, as well as therapeutic sensitivity to immunotherapy and TMZ-based chemotherapy in LGGs, has never been investigated before. More importantly, PD-L2 may be a promising predictive biomarker that contributes to the selection of optimal individualized therapeutic strategy by predicting therapeutic sensitivity to immunotherapy and TMZ-based chemotherapy for future studies of patients with LGGs.

DATA AVAILABILITY STATEMENT

The original contributions presented in the study are included in the article/**Supplementary Material**. Further inquiries can be directed to the corresponding author.

ETHICS STATEMENT

The studies involving human participants were reviewed and approved by The affiliated Changzhou No.2 People's Hospital of Nanjing Medical University. The patients/participants provided their written informed consent to participate in this study.

AUTHOR CONTRIBUTIONS

QX contributed to the study conceptualization, methodology, software, investigation, writing - original draft. XH contributed to the study writing - review & editing, data curation. WH contributed to the study supervision, material preparation, data collection, formal analysis, visualization. FL writing - review & editing, supervision, conceptualization writing - review & editing, language revision, funding acquisition. All authors contributed to the article and approved the submitted version.

FUNDING

Sponsored by Key Research and Development Program of Jiangsu Province (No.BE2019652), Changzhou international cooperation program (CZ20200039) and Development Program of Changzhou City (CE20205024).

SUPPLEMENTARY MATERIAL

The Supplementary Material for this article can be found online at: https://www.frontiersin.org/articles/10.3389/fonc.2022.860640/full#supplementary-material

REFERENCES

1. Siegel RL, Miller KD, Fuchs HE, Jemal A. Cancer Statistics, 2021. *CA Cancer J Clin* (2021) 71(1):7–33. doi: 10.3322/caac.21654
2. Lapointe S, Perry A, Butowski NA. Primary Brain Tumours in Adults. *Lancet* (2018) 392(10145):432–46. doi: 10.1016/s0140-6736(18)30990-5
3. Louis DN, Perry A, Reifenberger G, von Deimling A, Figarella-Branger D, Cavenee WK, et al. The 2016 World Health Organization Classification of Tumors of the Central Nervous System: A Summary. *Acta Neuropathol* (2016) 131(6):803–20. doi: 10.1007/s00401-016-1545-1
4. Gusyatiner O, Hegi ME. Glioma Epigenetics: From Subclassification to Novel Treatment Options. *Semin Cancer Biol* (2018) 51:50–8. doi: 10.1016/j.semcancer.2017.11.010
5. Gittleman H, Sloan AE, Barnholtz-Sloan JS. An Independently Validated Survival Nomogram for Lower-Grade Glioma. *Neuro Oncol* (2020) 22 (5):665–74. doi: 10.1093/neuonc/noz191
6. Stupp R, Mason WP, van den Bent MJ, Weller M, Fisher B, Taphoorn MJ, et al. Radiotherapy Plus Concomitant and Adjuvant Temozolomide for Glioblastoma. *N Engl J Med* (2005) 352(10):987–96. doi: 10.1056/NEJMoa043330
7. Omuro A, DeAngelis LM. Glioblastoma and Other Malignant Gliomas: A Clinical Review. *Jama* (2013) 310(17):1842–50. doi: 10.1001/jama.2013.280319
8. Lim M, Xia Y, Bettegowda C, Weller M. Current State of Immunotherapy for Glioblastoma. *Nat Rev Clin Oncol* (2018) 15(7):422–42. doi: 10.1038/s41571-018-0003-5
9. Zhang M, Wang X, Chen X, Zhang Q, Hong J. Novel Immune-Related Gene Signature for Risk Stratification and Prognosis of Survival in Lower-Grade Glioma. *Front Genet* (2020) 11:363. doi: 10.3389/fgene.2020.00363
10. Yu H, Zhang D, Lian M. Identification of an Epigenetic Prognostic Signature for Patients With Lower-Grade Gliomas. *CNS Neurosci Ther* (2021) 27 (4):470–83. doi: 10.1111/cns.13587
11. Solinas C, Aiello M, Rozali E, Lambertini M, Willard-Gallo K, Migliori E. Programmed Cell Death-Ligand 2: A Neglected But Important Target in the Immune Response to Cancer? *Transl Oncol* (2020) 13(10):100811. doi: 10.1016/j.tranon.2020.100811
12. Takamori S, Takada K, Azuma K, Jogo T, Shimokawa M, Toyokawa G, et al. Prognostic Impact of Programmed Death-Ligand 2 Expression in Primary Lung Adenocarcinoma Patients. *Ann Surg Oncol* (2019) 26(6):1916–24. doi: 10.1245/s10434-019-07231-z
13. Okadome K, Baba Y, Nomoto D, Yagi T, Kalikawe R, Harada K, et al. Prognostic and Clinical Impact of PD-L2 and PD-L1 Expression in a Cohort of 437 Oesophageal Cancers. *Br J Cancer* (2020) 122(10):1535–43. doi: 10.1038/s41416-020-0811-0
14. Erlmeier F, Weichert W, Autenrieth M, Wiedemann M, Schrader AJ, Hartmann A, et al. PD-L2: A Prognostic Marker in Chromophobe Renal Cell Carcinoma? *Med Oncol* (2017) 34(5):71. doi: 10.1007/s12032-017-0926-1
15. Nakayama Y, Mimura K, Kua LF, Okayama H, Min AKT, Saito K, et al. Immune Suppression Caused by PD-L2 Expression on Tumor Cells in Gastric Cancer. *Gastric Cancer* (2020) 23(6):961–73. doi: 10.1007/s10120-020-01079-z
16. Wang H, Yao H, Li C, Liang L, Zhang Y, Shi H, et al. PD-L2 Expression in Colorectal Cancer: Independent Prognostic Effect and Targetability by Deglycosylation. *Oncoimmunology* (2017) 6(7):e1327494. doi: 10.1080/2162402x.2017.1327494
17. Bornhorst M. New Insights Into Low Grade Glioma Tumor Microenvironment for Improved Patient Management. *Neuro Oncol* (2021) 24(1):27–8. doi: 10.1093/neuonc/noab224
18. Deep G, Agarwal R. Targeting Tumor Microenvironment With Silibinin: Promise and Potential for a Translational Cancer Chemopreventive Strategy. *Curr Cancer Drug Targets* (2013) 13(5):486–99. doi: 10.2174/15680096113139990041
19. Relation T, Dominici M, Horwitz EM. Concise Review: An (Im)Penetrable Shield: How the Tumor Microenvironment Protects Cancer Stem Cells. *Stem Cells* (2017) 35(5):1123–30. doi: 10.1002/stem.2596
20. Hanahan D, Weinberg RA. Hallmarks of Cancer: The Next Generation. *Cell* (2011) 144(5):646–74. doi: 10.1016/j.cell.2011.02.013
21. Sica A, Schioppa T, Mantovani A, Allavena P. Tumour-Associated Macrophages are a Distinct M2 Polarised Population Promoting Tumour Progression: Potential Targets of Anti-Cancer Therapy. *Eur J Cancer* (2006) 42(6):717–27. doi: 10.1016/j.ejca.2006.01.003
22. Waniczek D, Lorenc Z, Śnietura M, Wesecki M, Kopec A, Muc-Wierzgoń M. Tumor-Associated Macrophages and Regulatory T Cells Infiltration and the Clinical Outcome in Colorectal Cancer. *Arch Immunol Ther Exp (Warsz)* (2017) 65(5):445–54. doi: 10.1007/s00005-017-0463-9
23. Finotello F, Trajanoski Z. Quantifying Tumor-Infiltrating Immune Cells From Transcriptomics Data. *Cancer Immunol Immunother* (2018) 67 (7):1031–40. doi: 10.1007/s00262-018-2150-z
24. Lin W, Wu S, Chen X, Ye Y, Weng Y, Pan Y, et al. Characterization of Hypoxia Signature to Evaluate the Tumor Immune Microenvironment and Predict Prognosis in Glioma Groups. *Front Oncol* (2020) 10:796. doi: 10.3389/fonc.2020.00796
25. Zheng J, Zhou Z, Qiu Y, Wang M, Yu H, Wu Z, et al. A Pyroptosis-Related Gene Prognostic Index Correlated With Survival and Immune Microenvironment in Glioma. *J Inflamm Res* (2022) 15:17–32. doi: 10.2147/jir.S341774
26. Yoshihara K, Shahmoradgoli M, Martínez E, Vegesna R, Kim H, Torres-Garcia W, et al. Inferring Tumour Purity and Stromal and Immune Cell Admixture From Expression Data. *Nat Commun* (2013) 4:2612. doi: 10.1038/ncomms3612
27. Li H, Wang G, Wang W, Pan J, Zhou H, Han X, et al. A Focal Adhesion-Related Gene Signature Predicts Prognosis in Glioma and Correlates With Radiation Response and Immune Microenvironment. *Front Oncol* (2021) 11:698278. doi: 10.3389/fonc.2021.698278
28. Zhao B, Wang Y, Wang Y, Dai C, Wang Y, Ma W, et al. Investigation of Genetic Determinants of Glioma Immune Phenotype by Integrative Immunogenomic Scale Analysis. *Front Immunol* (2021) 12:557994. doi: 10.3389/fimmu.2021.557994
29. Hänzelmann S, Castelo R, Guinney J. GSVA: Gene Set Variation Analysis for Microarray and RNA-Seq Data. *BMC Bioinform* (2013) 14:7. doi: 10.1186/1471-2105-14-7
30. Charoentong P, Finotello F, Angelova M, Mayer C, Efremova M, Rieder D, et al. Pan-Cancer Immunogenomic Analyses Reveal Genotype-Immunophenotype Relationships and Predictors of Response to Checkpoint Blockade. *Cell Rep* (2017) 18(1):248–62. doi: 10.1016/j.celrep.2016.12.019
31. Gentles AJ, Newman AM, Liu CL, Bratman SV, Feng W, Kim D, et al. The Prognostic Landscape of Genes and Infiltrating Immune Cells Across Human Cancers. *Nat Med* (2015) 21(8):938–45. doi: 10.1038/nm.3909
32. Li T, Fan J, Wang B, Traugh N, Chen Q, Liu JS, et al. TIMER: A Web Server for Comprehensive Analysis of Tumor-Infiltrating Immune Cells. *Cancer Res* (2017) 77(21):e108–10. doi: 10.1158/0008-5472.Can-17-0307
33. Geeleher P, Cox NJ, Huang RS. Clinical Drug Response can be Predicted Using Baseline Gene Expression Levels and *In Vitro* Drug Sensitivity in Cell Lines. *Genome Biol* (2014) 15(3):R47. doi: 10.1186/gb-2014-15-3-r47
34. Geeleher P, Cox N, Huang RS. Prrophetic: An R Package for Prediction of Clinical Chemotherapeutic Response From Tumor Gene Expression Levels. *PLoS One* (2014) 9(9):e107468. doi: 10.1371/journal.pone.0107468
35. Roongrotwattanasiri K, Pawankar R, Kimura S, Mori S, Nonaka M, Yagi T. Decreased Expression of FOXP3 in Nasal Polyposis. *Allergy Asthma Immunol Res* (2012) 4(1):24–30. doi: 10.4168/aair.2012.4.1.24
36. Zhang GC, Yu XN, Sun JL, Xiong J, Yang YJ, Jiang XM, et al. UBE2M Promotes Cell Proliferation *via* the β-Catenin/Cyclin D1 Signaling in Hepatocellular Carcinoma. *Aging (Albany NY)* (2020) 12(3):2373–92. doi: 10.18632/aging.102749
37. Chaichana KL, McGirt MJ, Laterra J, Olivi A, Quiñones-Hinojosa A. Recurrence and Malignant Degeneration After Resection of Adult Hemispheric Low-Grade Gliomas. *J Neurosurg* (2010) 112(1):10–7. doi: 10.3171/2008.10.Jns08608
38. Brat DJ, Verhaak RG, Aldape KD, Yung WK, Salama SR, Cooper LA, et al. Comprehensive, Integrative Genomic Analysis of Diffuse Lower-Grade Gliomas. *N Engl J Med* (2015) 372(26):2481–98. doi: 10.1056/NEJMoa1402121
39. Suzuki H, Aoki K, Chiba K, Sato Y, Shiozawa Y, Shiraishi Y, et al. Mutational Landscape and Clonal Architecture in Grade II and III Gliomas. *Nat Genet* (2015) 47(5):458–68. doi: 10.1038/ng.3273

40. Khasraw M, Lassman AB. Advances in the Treatment of Malignant Gliomas. *Curr Oncol Rep* (2010) 12(1):26–33. doi: 10.1007/s11912-009-0077-4
41. Li T, Yang W, Li M, Zhang S, Zhou X, Zuo M, et al. Engrailed 2 (EN2) Acts as a Glioma Suppressor by Inhibiting Tumor Proliferation/Invasion and Enhancing Sensitivity to Temozolomide. *Cancer Cell Int* (2020) 20:65. doi: 10.1186/s12935-020-1145-y
42. Wang ZL, Li GZ, Wang QW, Bao ZS, Wang Z, Zhang CB, et al. PD-L2 Expression is Correlated With the Molecular and Clinical Features of Glioma, and Acts as an Unfavorable Prognostic Factor. *Oncoimmunology* (2019) 8(2): e1541535. doi: 10.1080/2162402x.2018.1541535
43. Fu Y, Liu CJ, Kobayashi DK, Johanns TM, Bowman-Kirigin JA, Schaettler MO, et al. GATA2 Regulates Constitutive PD-L1 and PD-L2 Expression in Brain Tumors. *Sci Rep* (2020) 10(1):9027. doi: 10.1038/s41598-020-65915-z
44. Barthel L, Hadamitzky M, Dammann P, Schedlowski M, Sure U, Thakur BK, et al. Glioma: Molecular Signature and Crossroads With Tumor Microenvironment. *Cancer Metastasis Rev* (2021) 41(1):53–75. doi: 10.1007/s10555-021-09997-9
45. Li G, Qin Z, Chen Z, Xie L, Wang R, Zhao H. Tumor Microenvironment in Treatment of Glioma. *Open Med (Wars)* (2017) 12:247–51. doi: 10.1515/med-2017-0035
46. Kim AR, Choi KS, Kim MS, Kim KM, Kang H, Kim S, et al. Absolute Quantification of Tumor-Infiltrating Immune Cells in High-Grade Glioma Identifies Prognostic and Radiomics Values. *Cancer Immunol Immunother* (2021) 70(7):1995–2008. doi: 10.1007/s00262-020-02836-w
47. Gieryng A, Pszczolkowska D, Walentynowicz KA, Rajan WD, Kaminska B. Immune Microenvironment of Gliomas. *Lab Invest* (2017) 97(5):498–518. doi: 10.1038/labinvest.2017.19
48. Gajewski TF, Schreiber H, Fu YX. Innate and Adaptive Immune Cells in the Tumor Microenvironment. *Nat Immunol* (2013) 14(10):1014–22. doi: 10.1038/ni.2703
49. Roxburgh CS, McMillan DC. The Role of the *in Situ* Local Inflammatory Response in Predicting Recurrence and Survival in Patients With Primary Operable Colorectal Cancer. *Cancer Treat Rev* (2012) 38(5):451–66. doi: 10.1016/j.ctrv.2011.09.001
50. Bykov Y, Kim SH, Zamarin D. Preparation of Single Cells From Tumors for Single-Cell RNA Sequencing. *Methods Enzymol* (2020) 632:295–308. doi: 10.1016/bs.mie.2019.05.057
51. Tong N, He Z, Ma Y, Wang Z, Huang Z, Cao H, et al. Tumor Associated Macrophages, as the Dominant Immune Cells, Are an Indispensable Target for Immunologically Cold Tumor-Glioma Therapy? *Front Cell Dev Biol* (2021) 9:706286. doi: 10.3389/fcell.2021.706286
52. Zhu C, Kros JM, Cheng C, Mustafa D. The Contribution of Tumor-Associated Macrophages in Glioma Neo-Angiogenesis and Implications for Anti-Angiogenic Strategies. *Neuro Oncol* (2017) 19(11):1435–46. doi: 10.1093/neuonc/nox081
53. Xiang X, Wang J, Lu D, Xu X. Targeting Tumor-Associated Macrophages to Synergize Tumor Immunotherapy. *Signal Transduct Target Ther* (2021) 6 (1):75. doi: 10.1038/s41392-021-00484-9
54. Ngambenjawong C, Gustafson HH, Pun SH. Progress in Tumor-Associated Macrophage (TAM)-Targeted Therapeutics. *Adv Drug Deliv Rev* (2017) 114:206–21. doi: 10.1016/j.addr.2017.04.010
55. Yang L, Zhang Y. Tumor-Associated Macrophages: From Basic Research to Clinical Application. *J Hematol Oncol* (2017) 10(1):58. doi: 10.1186/s13045-017-0430-2
56. Komohara Y, Fujiwara Y, Ohnishi K, Takeya M. Tumor-Associated Macrophages: Potential Therapeutic Targets for Anti-Cancer Therapy. *Adv Drug Deliv Rev* (2016) 99(Pt B):180–5. doi: 10.1016/j.addr.2015.11.009
57. Brown JM, Recht L, Strober S. The Promise of Targeting Macrophages in Cancer Therapy. *Clin Cancer Res* (2017) 23(13):3241–50. doi: 10.1158/1078-0432.Ccr-16-3122
58. Chanmee T, Ontong P, Konno K, Itano N. Tumor-Associated Macrophages as Major Players in the Tumor Microenvironment. *Cancers (Basel)* (2014) 6 (3):1670–90. doi: 10.3390/cancers6031670
59. Chen Z, Wu H, Yang H, Fan Y, Zhao S, Zhang M. Identification and Validation of RNA-Binding Protein-Related Gene Signature Revealed Potential Associations With Immunosuppression and Drug Sensitivity in Glioma. *Cancer Med* (2021) 10(20):7418–39. doi: 10.1002/cam4.4248
60. Pardoll DM. The Blockade of Immune Checkpoints in Cancer Immunotherapy. *Nat Rev Cancer* (2012) 12(4):252–64. doi: 10.1038/nrc3239
61. He X, Xu C. Immune Checkpoint Signaling and Cancer Immunotherapy. *Cell Res* (2020) 30(8):660–9. doi: 10.1038/s41422-020-0343-4
62. Ribas A, Wolchok J. Cancer Immunotherapy Using Checkpoint Blockade. *Science* (2018) 359(6382):1350–5. doi: 10.1126/science.aar4060
63. Qin S, Xu L, Yi M, Yu S, Wu K, Luo S. Novel Immune Checkpoint Targets: Moving Beyond PD-1 and CTLA-4. *Mol Cancer* (2019) 18(1):155. doi: 10.1186/s12943-019-1091-2
64. Marin-Acevedo J, Kimbrough E, Lou Y. Next Generation of Immune Checkpoint Inhibitors and Beyond. *J Hematol Oncol* (2021) 14(1):45. doi: 10.1186/s13045-021-01056-8
65. Pérez-Ruiz E, Melero I, Kopecka J, Sarmento-Ribeiro A, García-Aranda M, De Las Rivas J. Cancer Immunotherapy Resistance Based on Immune Checkpoints Inhibitors: Targets, Biomarkers, and Remedies. *Drug Resist Updat* (2020) 53:100718. doi: 10.1016/j.drup.2020.100718
66. Choi S, Yu Y, Grimmer MR, Wahl M, Chang SM, Costello JF. Temozolomide-Associated Hypermutation in Gliomas. *Neuro Oncol* (2018) 20(10):1300–9. doi: 10.1093/neuonc/noy016
67. Chang L, Su J, Jia X, Ren H. Treating Malignant Glioma in Chinese Patients: Update on Temozolomide. *Onco Targets Ther* (2014) 7:235–44. doi: 10.2147/ott.S41336
68. Hu YH, Jiao BH, Wang CY, Wu JL. Regulation of Temozolomide Resistance in Glioma Cells *via* the RIP2/NF-κb/MGMT Pathway. *CNS Neurosci Ther* (2021) 27(5):552–63. doi: 10.1111/cns.13591

Conflict of Interest: The authors declare that the research was conducted in the absence of any commercial or financial relationships that could be construed as a potential conflict of interest.

Publisher's Note: All claims expressed in this article are solely those of the authors and do not necessarily represent those of their affiliated organizations, or those of the publisher, the editors and the reviewers. Any product that may be evaluated in this article, or claim that may be made by its manufacturer, is not guaranteed or endorsed by the publisher.

Copyright © 2022 Xie, Huang, Huang and Liu. This is an open-access article distributed under the terms of the Creative Commons Attribution License (CC BY). The use, distribution or reproduction in other forums is permitted, provided the original author(s) and the copyright owner(s) are credited and that the original publication in this journal is cited, in accordance with accepted academic practice. No use, distribution or reproduction is permitted which does not comply with these terms.

frontiers | Frontiers in Immunology

ORIGINAL RESEARCH
published: 12 July 2022
doi: 10.3389/fimmu.2022.902143

Characterization of Fatty Acid Metabolism-Related Genes Landscape for Predicting Prognosis and Aiding Immunotherapy in Glioma Patients

Feng Jiang[1†], Fei Luo[1†], Ni Zeng[2], Yan Mao[3], Xinfang Tang[4], Jimei Wang[1], Yifang Hu[5*] and Chuyan Wu[6*]*

[1] Department of Neonatology, Obstetrics and Gynecology Hospital of Fudan University, Shanghai, China, [2] Department of Dermatology, Affiliated Hospital of Zunyi Medical University, Zunyi, China, [3] Department of Pediatrics, The First Affiliated Hospital of Nanjing Medical University, Nanjing, China, [4] Department of Nephrology, The Affiliated Lianyungang Oriental Hospital of Xuzhou Medical University, The Affiliated Lianyungang Oriental Hospital of Kangda College of Nanjing Medical University, The Affiliated Lianyungang Oriental Hospital of Bengbu Medical College, Lianyungang, China, [5] Department of Geriatric Endocrinology, The First Affiliated Hospital of Nanjing Medical University, Nanjing, China, [6] Department of Rehabilitation Medicine, The First Affiliated Hospital of Nanjing Medical University, Nanjing, China

Glioma is a highly malignant brain tumor with a poor survival rate. The involvement of fatty acid metabolism in glioma was examined to find viable treatment options. The information was gathered from the Cancer Genome Atlas (TCGA) and the Chinese Glioma Genome Atlas (CGGA) databases. A prognostic signature containing fatty acid metabolism-dependent genes (FAMDs) was developed to predict glioma outcome by multivariate and most minor absolute shrinkage and selection operator (LASSO) regression analyses. In the TCGA cohort, individuals with a good score had a worse prognosis than those with a poor score, validated in the CGGA cohort. According to further research by "pRRophetic" R package, higher-risk individuals were more susceptible to crizotinib. According to a complete study of the connection between the predictive risk rating model and tumor microenvironment (TME) features, high-risk individuals were eligible for activating the immune cell-associated receptor pathway. We also discovered that anti-PD-1/PD-L1 and anti-CTLA4 immunotherapy are more effective in high-risk individuals. Furthermore, we demonstrated that CCNA2 promotes glioma proliferation, migration, and invasion and regulates macrophage polarization. Therefore, examining the fatty acid metabolism pathway aids our understanding of TME invasion properties, allowing us to develop more effective immunotherapies for glioma.

Keywords: fatty acid metabolism, tumor microenvironment, prognosis, signature, glioma

OPEN ACCESS

Edited by:
Quan Cheng,
Central South University, China

Reviewed by:
Mingyue Tan,
Shanghai University of Traditional Chinese Medicine, China
Kai Huang,
Nanchang University, China
Jiang Li,
Sun Yat-sen University, China

***Correspondence:**
Chuyan Wu
chuyan_w@hotmail.com
Yifang Hu
973682801@qq.com
Jimei Wang
wjm821920@163.com

†These authors have contributed equally to this work

Specialty section:
This article was submitted to Cancer Immunity and Immunotherapy, a section of the journal Frontiers in Immunology

Received: *22 March 2022*
Accepted: *01 June 2022*
Published: *12 July 2022*

Citation:
Jiang F, Luo F, Zeng N, Mao Y, Tang X, Wang J, Hu Y and Wu C (2022) Characterization of Fatty Acid Metabolism-Related Genes Landscape for Predicting Prognosis and Aiding Immunotherapy in Glioma Patients. Front. Immunol. 13:902143. doi: 10.3389/fimmu.2022.902143

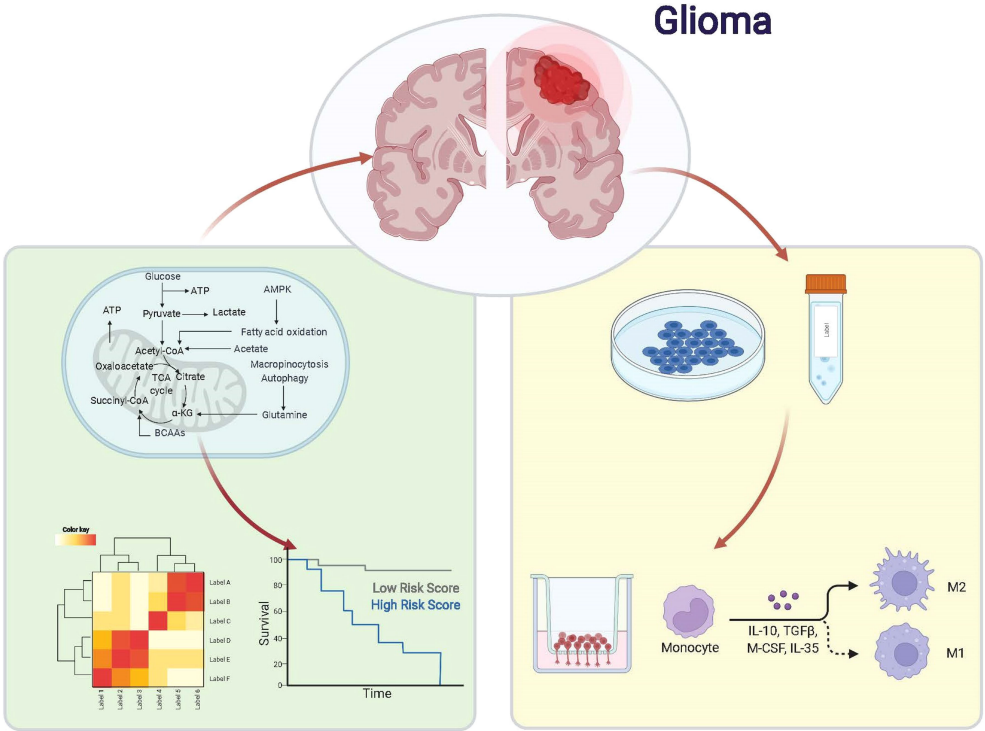

GRAPHICAL ABSTRACT |

INTRODUCTION

Glioma is the most prevalent type of primary brain tumor and accounts for almost 80% of the central nervous system (CNS) malignancies (1). Although there are mounting options for treating glioma, mainly comprising surgery, chemotherapy, and immunotherapy, the prognosis is still not ideal, with a median survival of 8 months for glioma patients by CBTRUS data (2). At present, glioma patients' treatment options mainly depend on WHO classification (WHO I-IV) (3, 4), as well as molecular subtypes, like IDH mutations, 1p19q deletion status, and MGMT methylation (5–7). Nevertheless, there are still significant differences in drug resistance, recurrence rates, and survival times for glioma patients with the same subtype. Available biomarkers cannot provide glioma patients a personalized treatment and optimal survival time. Therefore, identifying novel targets for the glioma therapy approach and prognostic assessment is warranted.

Different from normal cells, cancer cells have distinct metabolic features. When the carcinogenic signal is inhibited, they cope with unfavorable microenvironments by changing their metabolism to preserve cancer cell proliferation and survival (8–10). With a deep understanding of tumor biology and the complexity of tumor metabolism, modern metabolic reprogramming is a sign of a malignant tumor. Cancer cells and tumors have a lot of metabolic variabilities compared to normal tissues, but essentially little metabolic activity is unique to tumors. And there is metabolic heterogeneity between different tumors (11, 12), which leads to the difference in the efficacy of metabolic drugs in other tumors. Metabolic characterization and metabolic reliance change as cancer progress from premalignant lesions to regional invasion and metastasis (13, 14). In recent years, the link between fatty acid metabolism and tumor development has been a popular topic. Fatty acid metabolism is critical for tumor cell proliferation and spread. In terms of synthesis, fatty acids can participate in the structural synthesis of phospholipids on the cancer cell membrane and the transduction of necessary signals (such as PI3K/Akt/mTOR) (15, 16). In terms of decomposition, cancer cells mainly use fatty acids β-ATP produced by oxidation to maintain the required energy, and nicotinamide adenine dinucleotide phosphate (NADPH) is used to maintain the redox balance in the body (17). Increased lipolysis and fatty acid production induced by the activated nuclear factors-B (NF-B) signal has been demonstrated to cause lymph node metastases in cervical cancer patients (18). Through remodeling, active fatty acid oxidation may help AML cells survive and bone marrow adipocytes lipolyze (19). Furthermore, the expression pattern of genes involved in fatty acid metabolism is linked to the degree of malignancy, prognosis, and immunophenotype of glioma (20). The function of fatty acid metabolic features in the therapeutic therapy of gliomas, on the other hand, has not been well investigated.

The genetic information of glioma samples was analyzed using two databases to thoroughly estimate the fatty acid metabolism model and create the dependent predictive risk score model. And the survival result of glioma patients was independently predicted

using the constructed scoring model. The relationship between the TME cell infiltration characteristics and the prediction risk rating model was also looked into. The predictive risk score approach correctly identifies glioma patients who are immunotherapy candidates, indicating that maybe fatty acid metabolism would be an essential individual TME feature for glioma development. These findings bring up new research pathways into the metabolic process of glioma and its treatment (Graphic Abstract, **Figure 1** Flowchart).

MATERIALS AND METHODS

Downloading and Analyzing Data

TCGA database (https://portal.gdc.cancer.gov/) was applied to retrieve raw RNA sequencing (RNA-seq) data profiles for 701 glioma tissue samples. The TCGA database also yielded clinical information on 668 glioma samples, including age, gender, grade, and prognostic factors. CGGA database (http://www.cgga.org.cn/index.jsp) was used to retrieve the mRNA sequencing data of 1018 glioma samples. Since glioma has no normal tissue data in TCGA, to analyze differential gene expression, we combined 1152 cases of normal brain tissue in the GTEx (https://xenabrowser.net/datapages/) database. Using the annotation platform, the Ensembl Gene IDs were transformed into matching gene symbols. The mean value was used if more than one probe targeted the same Entrez Gene ID. In addition, clinical data for each CGGA sample was retrieved from the CGGA database (21). The GTEx and TCGA databases were transformed into log2 (FPKM+1), and the CGGA database was transformed into log2 (RNA-seq+1). Previous research found 309 genes involved in fatty acid metabolism (22–24). In TCGA cohorts, 191 candidate genes were chosen among these genes.

Enrichment Analysis of DEGs

Fatty acid metabolism-dependent DEGs in normal and tumor tissues were used to evaluate the R package "limma". Statistical significance was assigned to genes with an FDR of less than 0.05. To validate the key biological properties and cellular functional pathways connected to fatty acids, "cluster profile" software was used to conduct a GO and KEGG enrichment analysis of differential genes. $P < 0.05$ is considered as statistical significance. To show the enrichment analysis findings, we utilized the R software packages "enrich plot" and "ggplot2".

Construction of Risk Prediction Model of Fatty Acid Related Genes

We firstly classified the TCGA dataset into a training group and a testing group according to 2:1, while CGGA was used as another validation set. To begin, the expression levels of DEGs associated with fatty acid metabolism were compared to the prognosis findings for each sample. The genes associated with prognosis were selected from the DEGs linked to fatty acid metabolism using univariate and multivariate cox regression methods in the TCGA cohort. Genes having a P value of less than 0.001 were chosen. The mutation and gene association in tumor samples from the training set were analyzed using the R software package "maftools". The prognosis-related genes were further processed utilizing the "glmnet" R software package, and the prognosis risk score model of glioma OS was constructed using LASSO. The penalty parameter (λ) of the model was determined by ten cross verifications. The risk score for every sample is generated by the method below.

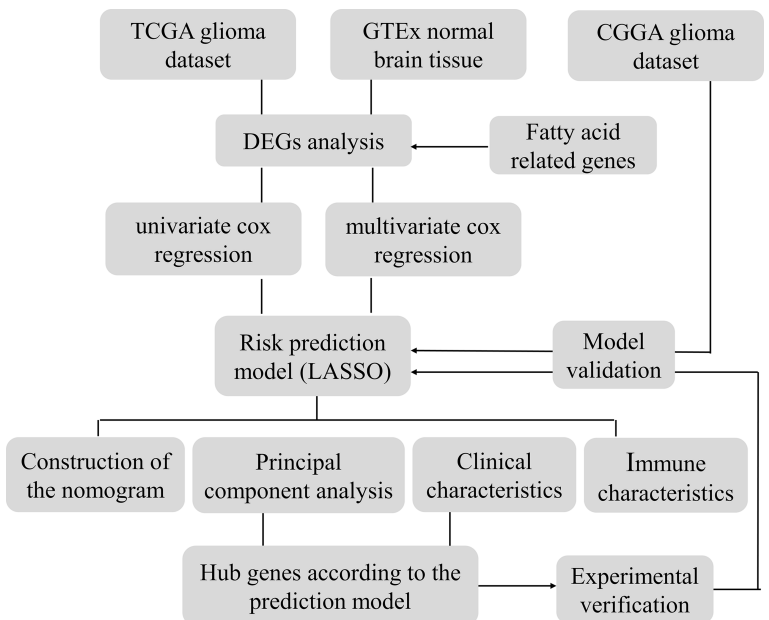

FIGURE 1 | Flowchart.

$$Risk\ \ Score = \sum_1^i (Coefi * ExpGenei)$$

"ExpGene" is the transcriptomic value from the predictive risk score model, and "Coef" is the non-zero regression coefficient obtained utilizing LASSO. All samples were separated into two subgroups based on the median value of risk scores: low- and high-risk groups. To examine OS variations between high- and low-score subgroups, Kaplan-Meier (K-M) and the log-rank procedure were performed. The ROC curve was drawn using the R software package "survivalROC" to analyze the predictive risk score model's prediction accuracy. Finally, we checked the test set to see whether the predictive risk score model was reliable.

PCA of Risk Score Model

We used the limma software package for principal component analysis (PCA) of gene expression to understand the significant differences between the two groups. We first analyzed the face of all DEGs related to fatty acid metabolism by PCA. After that, the gene expression in the predictive risk rating model was analyzed by principal component analysis. Finally, the PCA results are presented on the two-dimensional graph using the "ggplot2" software package.

The Link Between Risk Ratings and Clinical Characteristics

According to the sample ID, the value of every sample was blended with the associated clinical features. Limma R software tool was adopted to investigate the association between risk scores and clinical data. The TCGA database was also employed to collect the expression levels of immunological checkpoints (symbolized by PD-1/PD-L1 and CTLA4). Immunological checkpoint levels in the two subgroups were then investigated. Simultaneously, clinical data on glioma in the CGGA cohort was gathered to establish the association between clinical factors and risk scores. According to clinical characteristics, the data were separated into two subgroups, and the differences in risk scores were examined. To assess the two groups, the Kruskal Wallis (K-W) method was utilized. A p value of < 0.05 was defined as statistical significance.

Assessment of Immune Characteristics Between Two Subgroups

Gsva is an unsupervised, nonparametric approach for evaluating route modifications or biological processes using expression matrix samples. The "gsva" R program was employed to assess the differences in biological processes between the lower and higher subgroups. As a reference gene set, we used the "C2. Cp. kegg. V7.4. Symbol" gene set from the molecular feature database (https://www.gsea-msigdb.org/gsea/msigdb). A statistically meaningful enrichment route is one with an FDR of less than 0.05. To calculate the IC50 of temozolomide within every sample, the pRRophetic R program was utilized. The IC50 value represents a substance's ability to block certain biological or metabolic activities. To estimate the degree of immune-related infiltration in each patient in the TCGA set, ssGSEA was calculated by "GSEABase" and GSVA R packages (25). The data sets were gathered for the prior study's assessment of immune-related aspects in TME (**Table S1**). The ssGSEA algorithm's enrichment index reflected the degree to which each immune-related trait was expressed in each sample. The differences in enrichment scores between the lower and higher subgroups were analyzed. The relationship between prognosis-related genes and immune cells was indeed investigated. Finally, in the two risk score subgroups, TIDE was utilized to predict immune checkpoint reaction inhibitors of PD-1 and CTLA-4 (26).

Construct Nomogram

Nomogram of gender, age, grade, histological type, IDH1 mutation status, pq status, MGMT status, and predictive risk score model was built according to the TCGA cohort, utilizing the "RMS" software package in R to predict the OS of the glioma. To forecast the nomogram's accuracy, a time-dependent calibration curve was created. Furthermore, a multivariate Cox regression analysis was done to see if a predictive model can be employed as an independent predictor of OS in glioma patients. The AUC was then determined using a ROC curve to confirm the nomogram's predictive value.

Analysis of Survival-Related Hub Genes According to the Prediction Model

First, the limma R software program was used to compare the data of two subgroups to identify DEGs, which were defined as genes with an adjusted p-value < 0.05. Based on the string database (https://string-db.org/; version: 11.0), data from the PPI network with interaction scores > 0.40 (median confidence) were produced (**Table S2**). Then, to further analyze and show PPI network data, utilize Cytoscape software (version 3.9.1). Cytohubba is a Cytoscape plug-in that uses a topological technique to find the center gene among all DEGs. Then, the deferentially expressed genes were gathered in normal brain tissue and glioma tissue. The clusterprofiler software tool was employed to do a Go and KEGG enrichment analysis of genes. Finally, a gene from the hub gene was chosen for model validation, and all samples were separated into two subgroups according to this gene's expression: low expression and high expression. To see whether there was a variation in survival between the two subgroups, Kaplan Meier analysis was utilized. This gene was then investigated for immune cell infiltration.

Cell Culture and Transfection

The glioma cells (LN229, T98G, U251, U87, and U118) and the normal control cell NHA were cultured in DMEM with 10% FBS at 37°C in a 5% CO2 incubator. The logarithmic phase cells were chosen for the following functional studies. For CCNA2 knockdown or overexpression, glioma cells were transfected with plasmid si-CCNA2 or CCNA2-cDNA utilizing Lipofectamine® 3000 transfection reagent, following the manufacturer's manual.

Macrophage Polarization and Co-Culture

To obtain M0 macrophages, THP-1 cells were firstly induced by 320 NM PMA for 24h; To polarize M0 to M2 macrophages, cells were then treated with 20ng/ml IL-4 and 20ng/ml IL-13 for 48h. M0 macrophages were put into upper wells for cell co-culture, and U251-NC and U251-shCCNA2 cells were seeded into the bottom

well. Macrophages were then collected and labeled with M1- and M2-like markers to identify the polarization features.

qRT-PCR

Total RNA was extracted from cells utilizing Trizol reagent (Invitrogen, America), then cDNAs were created using the HiScript Synthesis kit (Vazyme, China). Subsequently, the PCR mixture consisted of cDNA, ddH2O, primer, and SYBR Green Master Mix. Finally, qRT-PCR amplification was measured on the StepOnePlus Real-Time PCR system (Applied Biosystems, US). Primers were as follows: CCNA2, forward-5'- TGG AAA GCA AAC AGT AAA CAG CC-3', reverse-5'- GGG CAT CTT CAC GCT CTA TTT-3'; iNOS, forward-5'- TCA TCC GCT ATG CTG GCT AC-3', reverse-5'- CCC GAA ACC ACT CGT ATT TGG-3', TNF-α, forward-5'-GAG GCC AAG CCC TGG TAT G-3', reverse-5'-CGG GCC GAT TGA TCT CAG C-3'; IL-1β, forward-5'- GAA ATG CCA CCT TTT GAC AGT G-3', reverse-5'-TGG ATG CTC TCA TCA GGA CAG-3', CD206, forward-5'- CTA CAA GGG ATC GGG TTT ATG GA-3', reverse-5'-TTG GCA TTG CCT AGT AGC GTA-3', Arg1, forward-5'- TTG GGT GGA TGC TCA CAC TG-3', reverse-5'-GTA CAC GAT GTC TTT GGC AGA-3'; YM1/2, forward-5'-TCA GCA GGT TCC CTA CGC A-3', reverse-5'-GCA GGA TTT GCC AGT GAA GTC-3'.

Western Blot

The western blot procedure was conducted as described previously (27). Primary antibodies in this study included iNOS (1:1000, Proteintech), CD206 (1:1000, Proteintech), β-Actin (1:1000, Bioss).

Flow Cytometry

To examine the polarization of macrophages, M0 macrophages were collected, fixed, then incubated with F4/80-FITC, iNOS-APC, and CD206-PE for 30 min at four °C, based on the manufacturer's instructions. Cells were determined using a flow cytometer (Cytoflex, USA), and the data were analyzed using FlowJoTM software (Version 10.7.1).

CCK-8 and Clone Assay

CCK-8 and plate colony assays were utilized to examine the glioma cells' proliferation capacity. The CCK8 kit (Beyotime, China) was used to quantify cell growth at 0h, 24h, 48h, 72h, and 96h by the manufacturer's protocol. Absorbance at 450 nm was determined on enzyme labeling (Thermo, USA). For the cloning test, about 500 cells from various groups were placed in each well of a six-well plate. Once colonies appeared, 4% paraformaldehyde and crystal violet were employed to stain and fix cells.

Transwell Invasion Assay

After si-CCNA2 and CCNA2-cDNA transfection, 5×104 glioma cells were placed into the upper chambers of Transwell in an empty DMEM medium, which was pre-coated with Matrigel (Biosciences, USA), while the lower chamber was filled with DMEM containing 10% FBS. For macrophage migration assay, M2 macrophage was placed on upper chambers, and glioma cells were added to the lower chamber. After 24 hours, the invasive cells were fixed with 4% formalin, then stained with 0.1% crystal violet. The stained cells were visualized and counted in an inverted microscope.

Subcutaneous Xenograft Assay

Nanjing medical university animal care and use committee and followed guidelines for animal welfare. Four-week-old BALB/c male nude mice were used to construct the xenograft model, which randomly classified into two groups. The glioma cells infected with siCCNA2 or control were subcutaneously embedded in nude mice, respectively. Tumor volumes were measured every one week. After one month, mice were euthanized, and subcutaneous tumors were removed. Tumor weight and pictures were finally recorded.

Statistical Analysis

To assess the differences between poor and good score subgroups, the Wilcoxon rank sum test was utilized. The variation in OS between the good and poor subgroups was determined using Kaplan Meier analysis. The independent determinants of OS in glioma were determined using the Cox regression procedure. The predictive efficacy of the nomogram, clinical factors, and predictive risk score model was evaluated using a ROC curve. R 4.0.4 was used to conduct all statistical analyses ($P < 0.05$).

RESULTS

Differential Expression Analysis Between Normal and Glioma Samples

We analyzed the transcriptional activity of FAMDs in tumor and normal samples and identified 191 genes in TCGA datasets with an FDR < 0.05. It comprises 95 down-regulated genes and 96 genes that have been up-regulated (**Figure S1A**). Then, to double-check, we performed KEGG and GO enrichment analysis. Fatty acid metabolism, catabolism, and other activities have been discovered to be substantially abundant in biological processes (**Figure S1B**). KEGG terms for fatty acid breakdown, metabolism, and biosynthesis are abundant (**Figure S1C**).

Establishment of the Prognostic Model in the Training Set

Glioma patients in the TCGA database were randomly divided into a training cohort and a testing cohort at a 2:1 ratio, we used the training set to construct a prognostic model. On 191 FAMDs, a Univariate Cox regression analysis was conducted. With a p value of 0.001, a total of 133 genes associated with prognosis were discovered (**Table S3**). The somatic mutation profile of the 18 genes involved in fatty acid metabolism that have been linked to prognosis was first summarized. As indicated in **Figure 2A**, a total of 477 of 984 glioma samples had mutations in FAMDs, with a prevalence of 48.48 percent. IDH1 has the most mutations. Further research revealed that ACACB and TBXAS1 had a mutation co-occurrence association (**Figures 2B–D**). The number of genes was then reduced using the LASSO Cox regression analysis. Finally, ten genes were employed to create a predictive risk score model

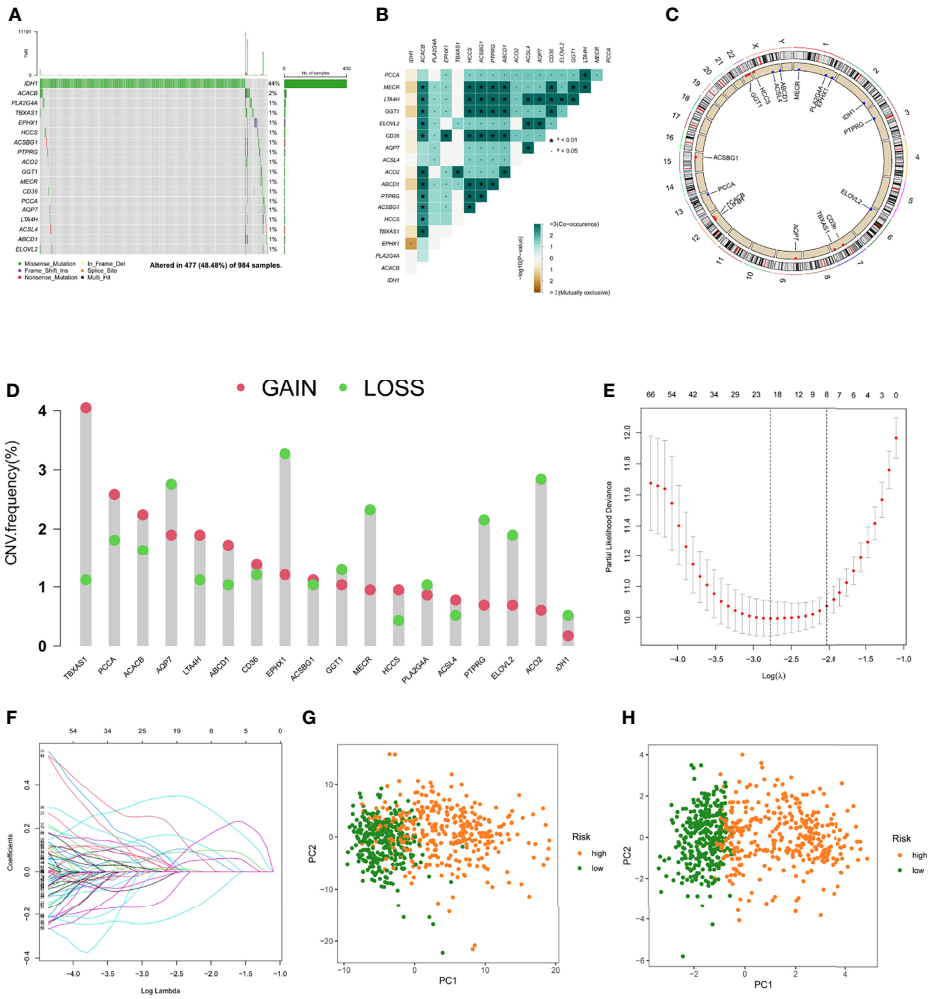

FIGURE 2 | Predictive risk score model development. **(A)** The frequency of mutations in 18 FAMDs in 984 glioma patients from the TCGA cohort. **(B)** Mutation co-occurrence and selection analysis for 18 genes involved in fatty acid metabolism. Green denotes co-occurrence; purple denotes exclusion. **(C)** Locations of CNV alterations in FAMDs on 23 chromosomes. **(D)** Frequencies of CNV gain, loss, and non-CNV among FAMDs. **(E)** LASSO coefficients for the FAMDs involved in fatty acid metabolism. **(F)** Gene discovery for the construction of a predictive risk score model. **(G)** Principal component analysis of FAMDs in glioma. **(H)** In the TCGA cohort, principal component analysis was used to identify cancers from standard samples using a fatty acid metabolism vulnerability index. High-risk patients were represented by the red group, whereas the blue group represented low-risk patients. *P<0.01, •P<0.05.

(ACO2, PTGR1, GPD1, HCCS, ABCD1, RETSAT, SMS, CA2, ELOVL5, and SCD) (**Figures 2E, 2F**). The following formula was used to compute every sample's score: risk score = (-0.362) × ACO2 + (0.246) × PTGR1 + (0.127) × GPD1 + (0.411) ×HCCS + (0.241) × ABCD1 + (0.326) × RETSAT + (0.338) × SMS + (0.202) × CA2 + (0.256) × ELOVL5 + (-0.429) × SCD. **Table S4** shows how this was accomplished. To fully differentiate glioma samples, the risk score model was applied (**Figures 2G, 2H**)

In the training set, patients were classified into the high- and low-risk group according to the median value. K-M curves showed that the high-risk group had a poor prognosis compared to low-risk patients ($p < 0.05$) (**Figure 3A**). The highest AUC value reached 0.898 for 1-year OS, and 0.932 for 3-year OS (**Figure 3E**). To better discern the survival differences between these two groups, we ranked all patients based on their risk scores, then plotted to scatter maps to describe each patient's survival time and status (**Figures 3B–D**).

Validation of the Prognostic Model in the Testing Set, Entire TCGA and CGGA Set

To verify the robustness of this risk model, the predictive performance was determined in the testing set, entire TCGA and CGGA set. Similarly, patients in these cohorts were categorized into high- and low-risk groups, according to the cut-off value achieved in the training cohort. There were 116 high-risk patients, 84 low-risk patients in the testing set, and 350 high-risk patients, 318 low-risk patients in the entire TCGA set, and 615 high-risk patients, 313 low-risk patients in the CGGA set.

K-M curves indicated that high-risk individuals in these cohorts had a shorter OS than the low-risk group ($p < 0.05$)

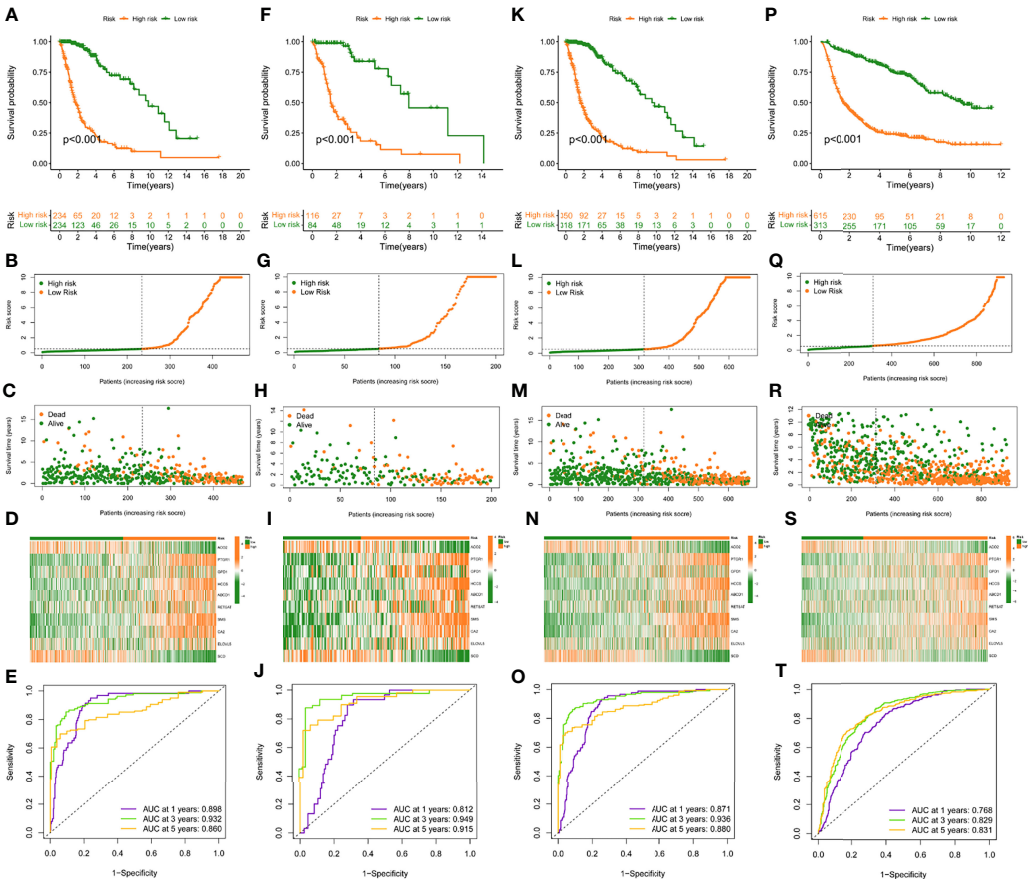

FIGURE 3 | Construction and validation of risk model in TCGA training, testing, entire cohort, and CGGA cohort. **(A, F, K, P)**, **(K–M)** curves of subgroups for OS in TCGA training, testing, entire cohort, and CGGA cohort. The distribution plots of risk score **(B**, **G**, **L**, **Q)**, survival status **(C**, **H**, **M**, **R)**, and 10 selected FAMDs **(D**, **I**, **N**, **S)** in TCGA training, testing, entire cohort, and CGGA cohort. **(E**, **J**, **O**, **T)** ROC curve analysis of risk score in predicting 1-, 3-, and 5-year OS in TCGA training, testing, entire cohort, and CGGA cohort.

(**Figures 3F, K, P**). The AUC for predictive OS was 0.812 at 1 year, 0.949 at 3 years in the testing cohort, 0.871 at 1 year, 0.936 at 3 years in the entire TCGA cohort, 0.768 at 1 year, 0.829 at 3 years in the CGGA cohort (**Figures 3J, O, T**). Also, we graded respectively different populations in these cohorts based on their risk score. The high-risk group exhibited a poor prognosis compared to low-risk patients, which was consistent with the findings in the training set (**Figures 3G–I, L–N, Q–S**).

The Connection Between the Risk Model and Clinical Information

To investigate the relationship between the risk model and clinical features, we determined the risk scores of related samples in terms of age, gender, grade, IDH1 mutation status, pq status, and MGMT status. Although there was no significant difference in risk score by gender, significant variations in risk score by age, grade, IDH1 mutation status, pq status, and MGMT status ($p<0.05$; **Figures 4A–F**). Higher scores were linked to being older, having higher grades, wild type IDH1 mutations, unmethylated MGMT status, and non-codel pq status. The accuracy of the prognostic risk model was validated by plotting a time-dependent ROC at 5 years (**Figure 4G**). Age, grade, IDH status, pq status, and risk score were predictive factors of OS in multivariate analysis among characteristics linked with OS in univariate analysis (**Figure 4H**).

Construction of Survival-Prediction Nomogram

A nomogram comprising gender, age, grade, IDH1 mutation, MGMT status, pq status, and risk score was created to predict OS in glioma tissues (**Figure 5A**). **Figure 5B** shows calibration curves for patients with gliomas at 1, 3, and 5 years, demonstrating that nomograms may reliably predict OS in these patients. The nomogram (AUC = 0.774) has a stronger predictive value than a single indicator such age (AUC = 0.684), grade (AUC = 0.660), or the prognostic risk scoring model (AUC = 0.767; **Figure 5C**). The predictive risk score model and grade were shown to be independent prognostic factors in multivariate and univariate Cox regression analysis (**Figures 5D, E**).

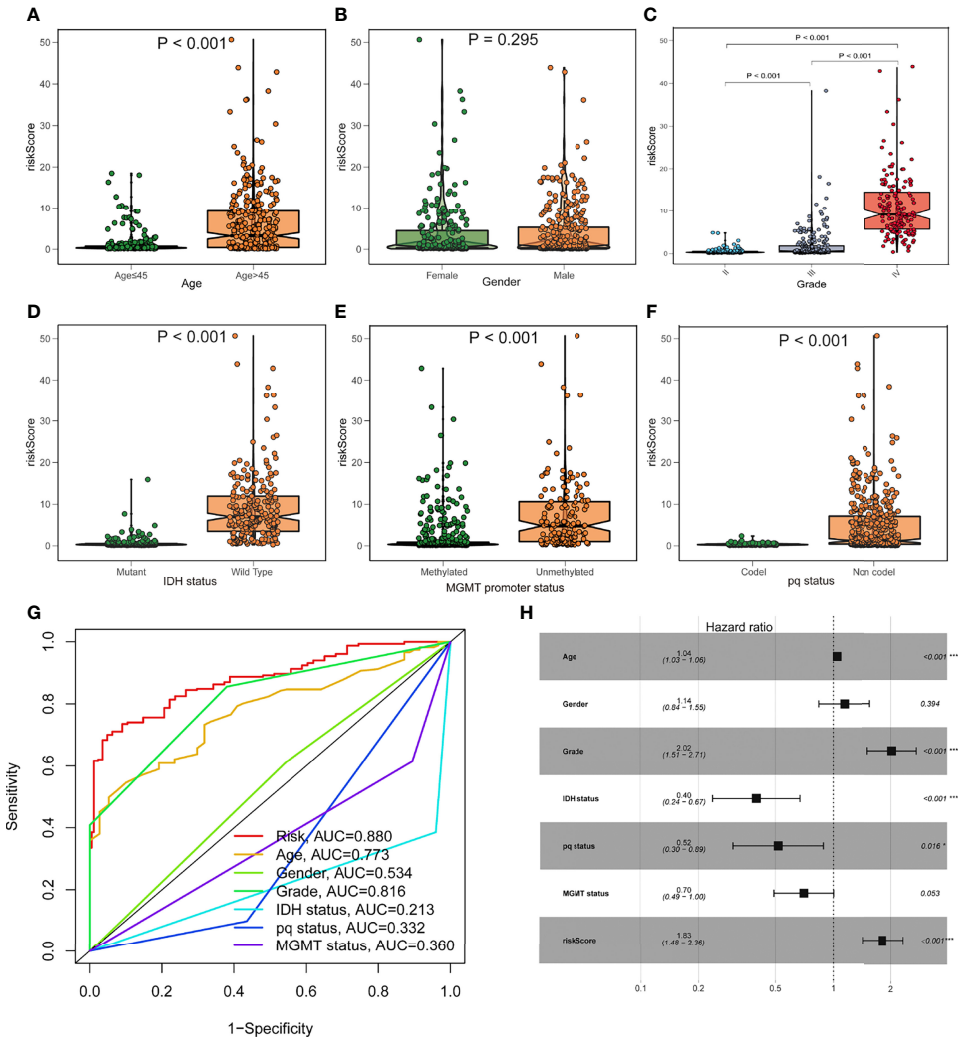

FIGURE 4 | Prognostic value of the fatty acid metabolism score model in glioma patient survival. **(A–F)** The association between risk score and clinicopathological variables such as age **(A)**, gender **(B)**, grade **(C)**, IDH1 status **(D)**, MGMT promoter status **(E)**, and pq status **(F)**. **(G)** ROC curves are used to assess the predictive power of clinical characteristics. **(H)** The forest plot of the TCGA cohort's multivariate Cox regression analysis. *p < 0.05; ***p < 0.001.

Response of Two Groups to Crizotinib

The association between risk level and medication resistance was examined since risk score is linked to poor prognosis. The "pRRophic" R package has been used to estimate the therapeutic efficacy of crizotinib in the TCGA cohort using the half maximal inhibitory concentration (IC50). For the management of glioma, samples with a low-risk score were more susceptible to crizotinib (**Figures 6A, B**). In TCGA data, there was a high association between chemotherapy drugs sensitivity and risk score at 3 years, according to PFS (progression-free survival) (**Figure 6C**). The elevated score was significantly closely linked with the intensive activation of matrix pathways, including epithelial mesenchymal transformation 1 (EMT1), angiogenesis, and Wnt targets, according to an analysis of the activity of matrix-related pathways leading to chemotherapy resistance (**Figure 6D**).

GSVA

Gsva enrichment analysis showed that most metabolic pathways, including the biosynthetic metabolic pathway of unsaturated fatty acids, increased in the low-risk score. Genetic abdominal muscle analysis of high scoring population showed that it was related to immunity, such as primary immunodeficiency, natural killer cell mediated cytotoxicity, etc. (**Figure 7A**). The risk score was negatively connected with the fatty acid metabolism score, which was generated using ssGSEA, which examined the expression of fat metabolism-related genes in glioma patients and was consistent with GSVA (**Figures S2A–C**). Although the fat metabolic score could reliably predict the survival in patients at 5 years using a time-dependent ROC, the predictive value (AUC = 0.385) was poorer than the risk rating model (AUC = 0.880) (**Figures S2D–E**). In addition, we compared several

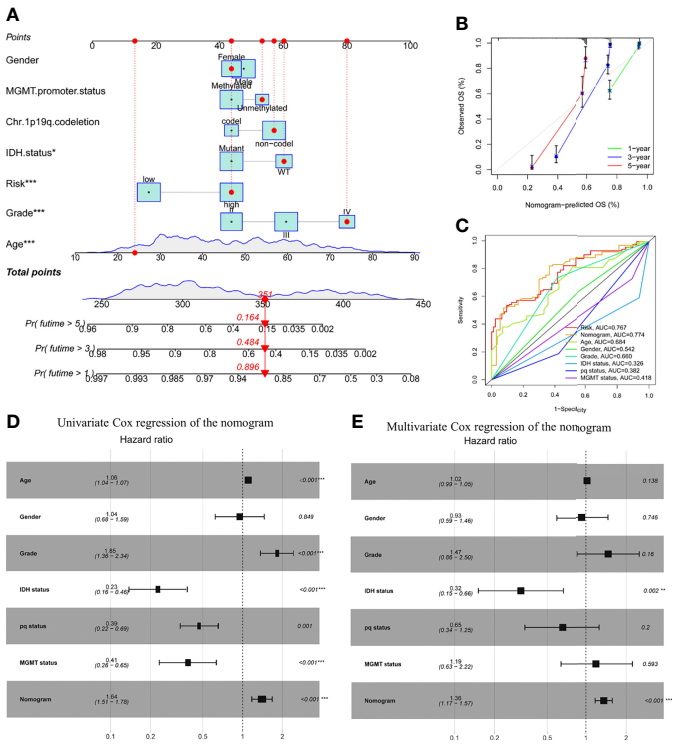

FIGURE 5 | Prognostic efficacy of risk score in OS of patients from the TCGA cohort when combined with clinical-pathological features. **(A)** Nomogram indicates OS in the TCGA cohort of patients. **(B)** The nomogram's calibration plots. The y-axis represents actual survival, whereas the x-axis represents nomogram-predicted survival. **(C)** Receiver operating characteristic charts for risk score and clinical features. **(D, E)** The nomogram's univariate and multivariate Cox regression analyses. *p < 0.05; **p < 0.01; ***p < 0.001..

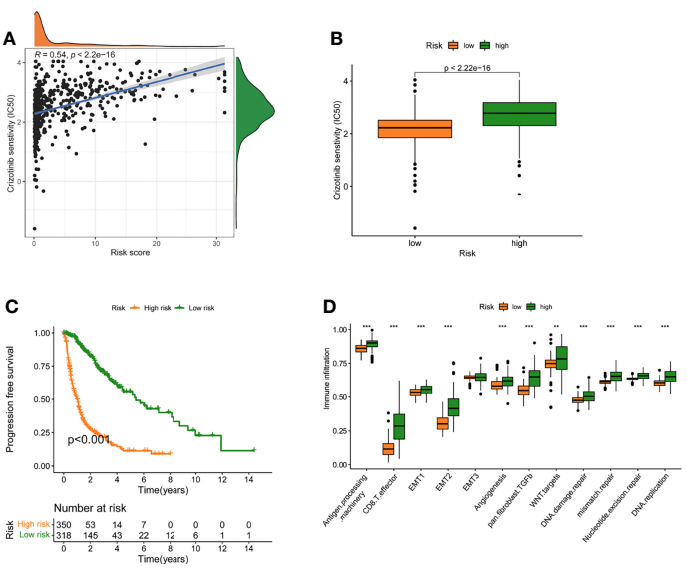

FIGURE 6 | A model of fatty acid metabolism in the context of chemotherapy. **(A)** The relationship between patient risk ratings and crizotinib's projected IC50 value. **(B)**The disparities in crizotinib response between groups with poor and good risk scores. **(C)** The TCGA cohort's progression-free survival (PFS) was compared between low- and high-risk score groups. **(D)** Variation in stroma-activated networks between groups with low and high-risk scores (**p < 0.01; ***p < 0.001).

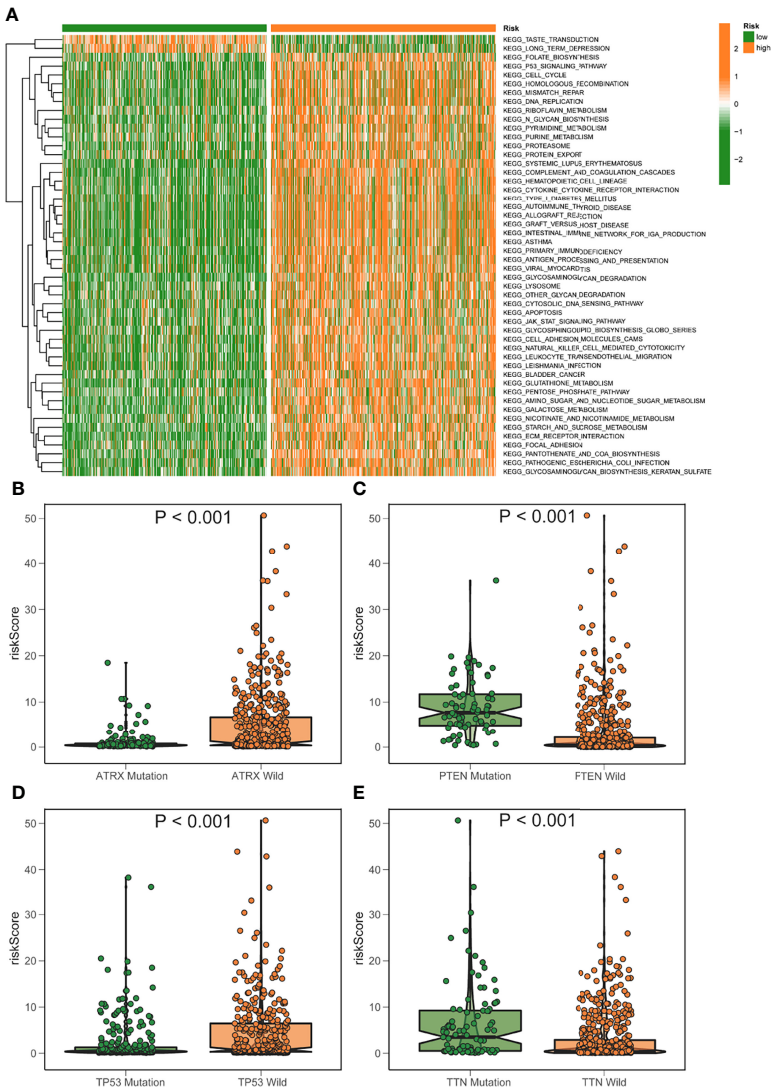

FIGURE 7 | GSVA analysis of elevated/low score groups diagram. **(A)** GSVA enrichment heatmap for excellent and poor score groups. **(B–E)** Varied mutant genes, namely ATRX mutation **(B)** PTEN mutation **(C)** TP53 mutation **(D)** and TTN mutation **(E)** have different fatty metabolism scores.

mutant genes with high mutation frequency in glioma, TP53, ATRX, PTEN, and TTN. Patients with TP53 and ATRX mutations had higher risk scores and statistically significant differences (**Figures 7B–E**).

Characteristics of the Immune System in the High- and Low-Risk Groups

The high score group demonstrated an increasing trend in T cells CD8, macrophage M1, and macrophage M2 compared to the low score group, consistent with the high score group's reduced survival rate. The group with the lowest ranking had a higher increase in monocytes and mast cells activated (**Figure 8A**). Furthermore, the high-risk group's type I IFN response, type II IFN response, checkpoint, HLA, T cell co-inhibition, T cell co-stimulation, etc., were all activated, suggesting that patients with immune suppression in the high-risk group would react to immunotherapy (**Figure 8B**). The TCGA samples were additionally immunotype, and the elevated/low score groups had substantial variations in C3, C4, and C5 (**Figures 8C, D**). CTLA4 and PD-1 inhibition are two examples of immunotherapy that have achieved significant advances in cancer treatment. As a result, we looked at the predictive risk score model's capacity to distinguish between individuals who react to immune checkpoint inhibitor treatment in various ways. The findings revealed that the projected risk score was highly connected with immune checkpoint gene expression (PD-1, PD-L1, and CTLA4) and that the expression was considerably higher in the high-risk group. This shows that our risk ratings for fatty acid metabolism might be relevant in determining immunotherapy prognosis (**Figures 8E–J**).

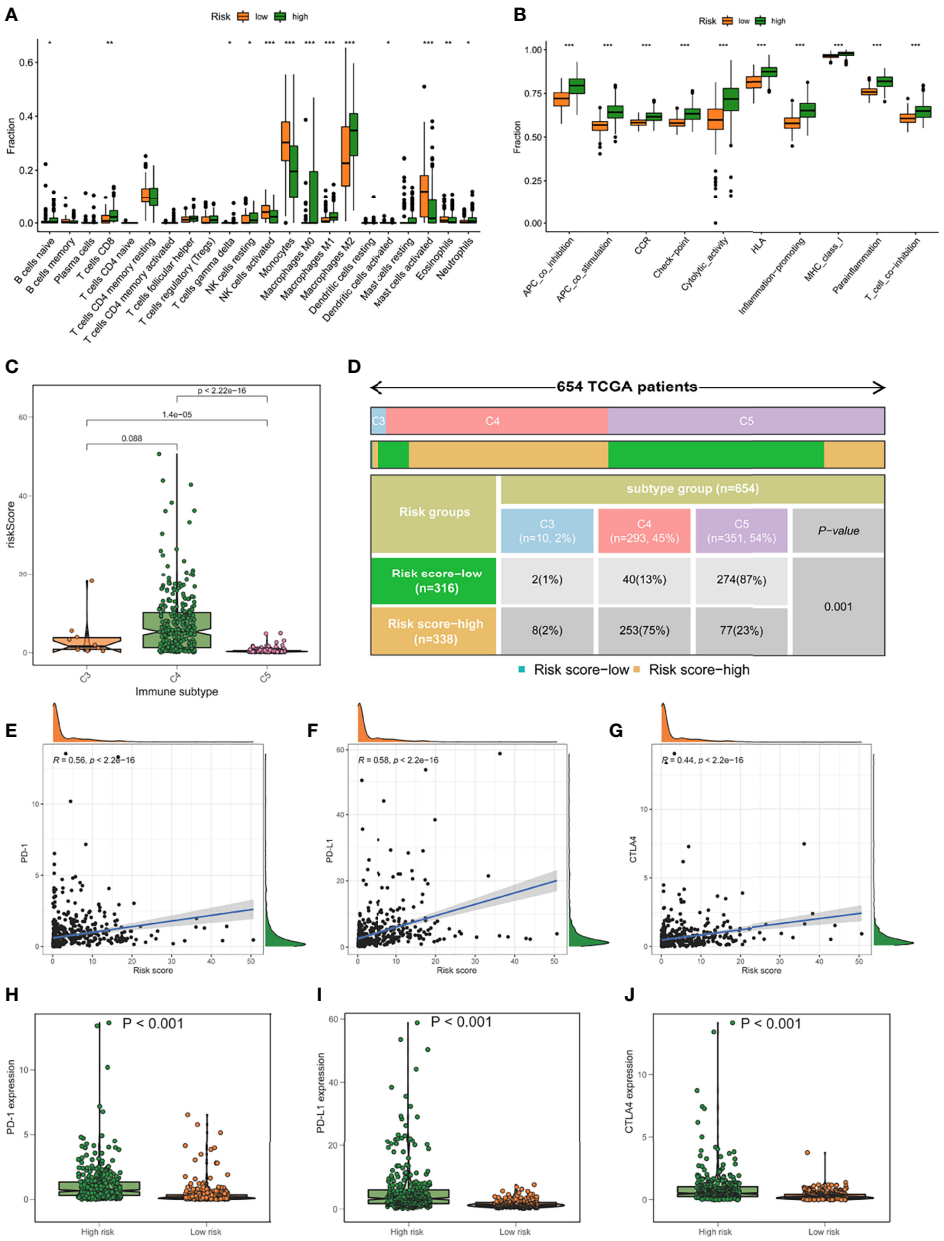

FIGURE 8 | Model of fatty acid metabolism in immunotherapy. **(A)** The difference in immune infiltration between high-risk and low-risk scores. **(B)** The difference between subjects with a high score and those with a poor rating in terms of the known function related to immune modulation. **(C, D)** The distribution of immunological subtypes (C3, C4, and C5) across risk groupings are shown in a heatmap and table. **(E–G)** Immune checkpoint transcriptional activation and hazard score, PD-L1**(E)**, PD1**(F)**, and CTLA3 correlation analysis **(G)**. **(H–J)** The disparities between the low-risk and high-risk groups in terms of identified Immune checkpoint genes. *P<0.05, **P<0.01, ***P<0.001.

Verification of Prediction Model by the Hub Gene in DEGs of High- and Low-Risk Groups

The expression patterns of DEGs in the low- and high-risk groups were analyzed using the string online database. As illustrated in **Figure S3**, a protein interaction diagram of DEGs was created. PPI network data is processed and shown using the Cytoscape program. **Figure 9A** depicts the DEG interaction, with red indicating up-regulated transcripts in the excellent score group and green indicating up-regulated genes in the poor score group. Cytohubba is a Cytoscape plug-in that helps you find the core gene among DEGs. As seen in **Figure 9B**, we chose 10 genes from the network. To further understand the roles of DEGs, researchers used the R software tool "goplot" to conduct a Go

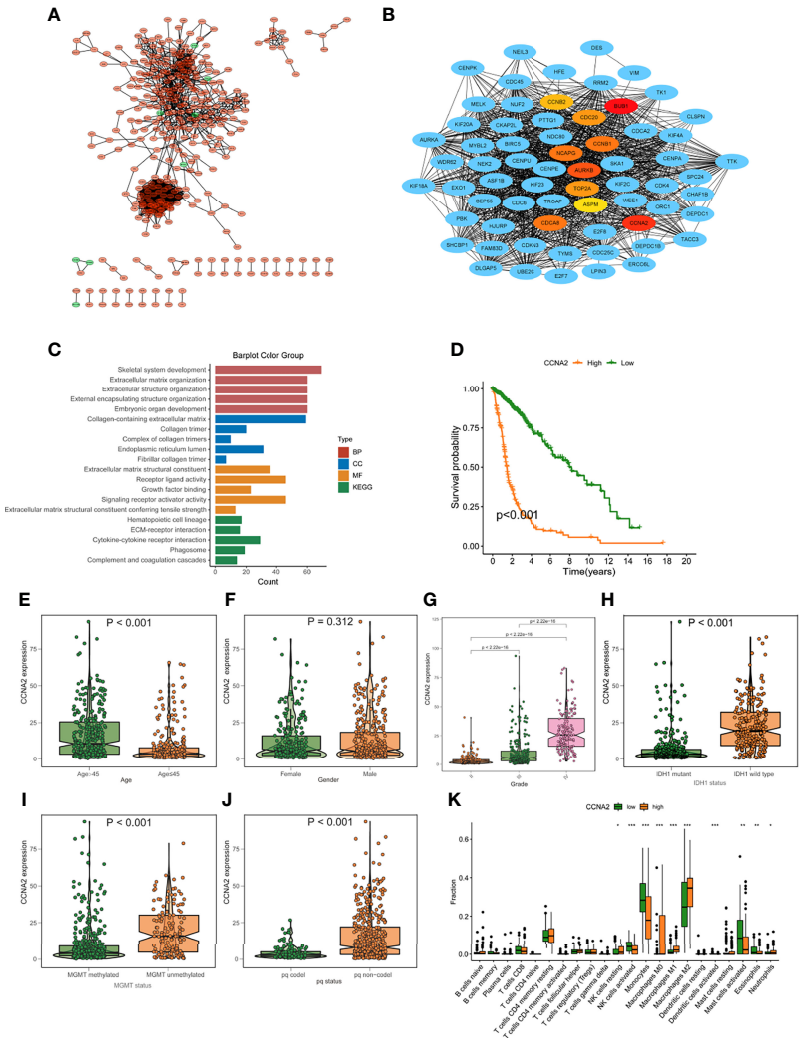

FIGURE 9 | Protein-protein interaction (PPI) graph. **(A)** PPI network generated by Cytoscape (red): DEGs that exhibited strongly in the excellent score category; green: DEGs that showed highly in the low-risk score group. **(B)** The top ten hub genes were chosen by cytoHubba. **(C)** The findings of GO and KEGG enrichment analysis on DEGs. **(D)** Mortality analysis for patients divided into subgroups based on CCNA2 mRNA expression. **(E-J)** The difference in CCNA2 mRNA expression between various clinical characteristics, such as age **(E)**, gender **(F)**, grade **(G)**, IDH1 mutation **(H)**, MGMT promoter status **(I)**, and pq status **(J, K)** In subjects with elevated/low CCNB1 mRNA expression, the number of TME-infiltrating cells. *p < 0.05; **p < 0.01; ***p < 0.001.

and KEGG study. The genes are engaged in skeletal system development, extracellular matrix organization, extracellular structure organization, etc., according to GO findings. These genes were shown to be abundant in hematopoietic cell lineage, ECM-receptor interaction, cytokine-cytokine receptor interaction, etc., according to KEGG findings (**Figure 9C**). For verification, we used CCNA2 in the hub gene. The expression levels of CCNA2 were shown to be substantially linked with the mortality of glioma patients in a survival study (**Figure 9D**). Furthermore, CCNA2 expression increased with age and grade. However, in the IDH1 mutation, pq codel, MGMT methylated group, CCNA2 expression was dramatically reduced (**Figures 9E–J**). To see whether there is a difference in TME immune infiltration between individuals with high- and low– CCNA2 expression. Compared to patients with low transcription, tumors with high CCNA2 expression showed considerably higher macrophages M2 and M1 (**Figure 9K**).

CCNA2 Promoted Malignant Glioma Progression *In Vitro*, and *Vivo*

To further validate the role of CCNA2 in glioma, we assessed if changes in CCNA2 expression affect glioma cell proliferation and malignant abilities. We first detected the expression of CCNA2 in different cells by qRT-PCR and found that CCNA2 mRNA levels were significantly high in LN229, T98G, U251, U87, and U118 cells compared to NHA (**Figure 10A**). We chose U251 for si-CCNA2 and U87 for CCNA2 cDNA transfections. The results indicated that CCNA2 shRNA reduced CCNA2

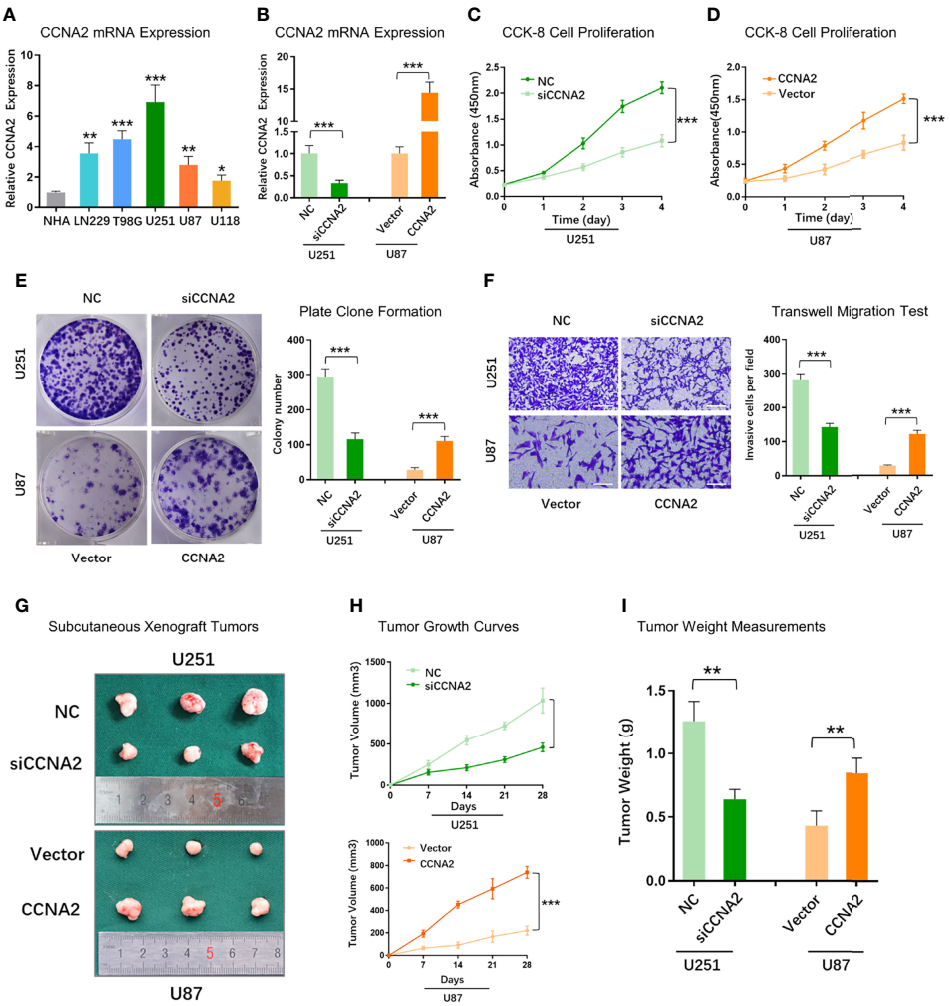

FIGURE 10 | CCNA2 promoted glioma cell proliferation and migration. **(A)** qRT-PCR of CCNA2 mRNA expression in NHA and glioma cells. **(B)** qRT-PCR of CCNA2 levels in U251 and U87 cells transfected with si-CCNA2 and CCNA2-cDNA. **(C, D)** CCK-8 of the cell growth curve in transfected U251 and U87 cells. **(E)** Colony assay in transfected U251 and U87 cells. **(F)** Transwell invasion test in transfected U251 and U87 cells. **(G)** Representative images of subcutaneous xenograft tumors implanted with U251-siCCNA2 and U87-CCNA2 cells. **(H, I)** Tumor volume and tumor weight of indicated xenograft models. $^{*}P < 0.05$, $^{**}P < 0.01$, $^{***}P < 0.001$.

expression in U251 cells, whereas CCNA2 cDNA up-regulated CCNA2 expression in U87 cells (**Figure 10B**). The CCK-8 (**Figures 10C, D**) and colony formation (**Figure 10E**) results demonstrated that down-regulation of CCNA2 expression inhibited U251 cell proliferation, whereas up-regulation of CCNA2 expression promoted tumor U87 cell proliferation. In transwell assay, suppressing CCNA2 expression significantly resulted in a reduction of invaded U251 cells, whilst upregulating CCNA2 expression significantly expanded the amount of invaded U87 cells (**Figure 10F**). Moreover, the animal experiment suggested that CCNA2 knockdown suppressed glioma growth *in vivo*, while CCNA2 overexpression promoted tumor growth (**Figures 10G–I**). These results indicated that CCNA2 facilitated *in vitro* and *in vivo* proliferation, migration, and invasion of glioma cells.

CCNA2 Regulated Macrophages Polarization

To further examine the relationship between CCNA2 and macrophage polarization *in vitro*, we chose U251 cells for further study. U251 cells were transfected with shCtrl and shCCNA2, then co-cultured with macrophages. The result of qRT-PCR showed that the macrophages co-cultured with U251-siCCNA2 had higher M1-like markers iNOS, TNF-α, and IL-1β (**Figure 11A**), while having lower M2-like markers CD206, Arg1 and YM1/2 compared with controls (**Figure 11B**). Western blot and flow cytometry showed that knockdown of CCNA2 significantly inhibited the shift to M2 macrophages compared with the NC group (**Figures 11C–F**). IHC staining indicated that CCNA2 expression and M2 macrophage marker CD206 were stronger in GBM than usual (**Figure 11G**). Transwell assay

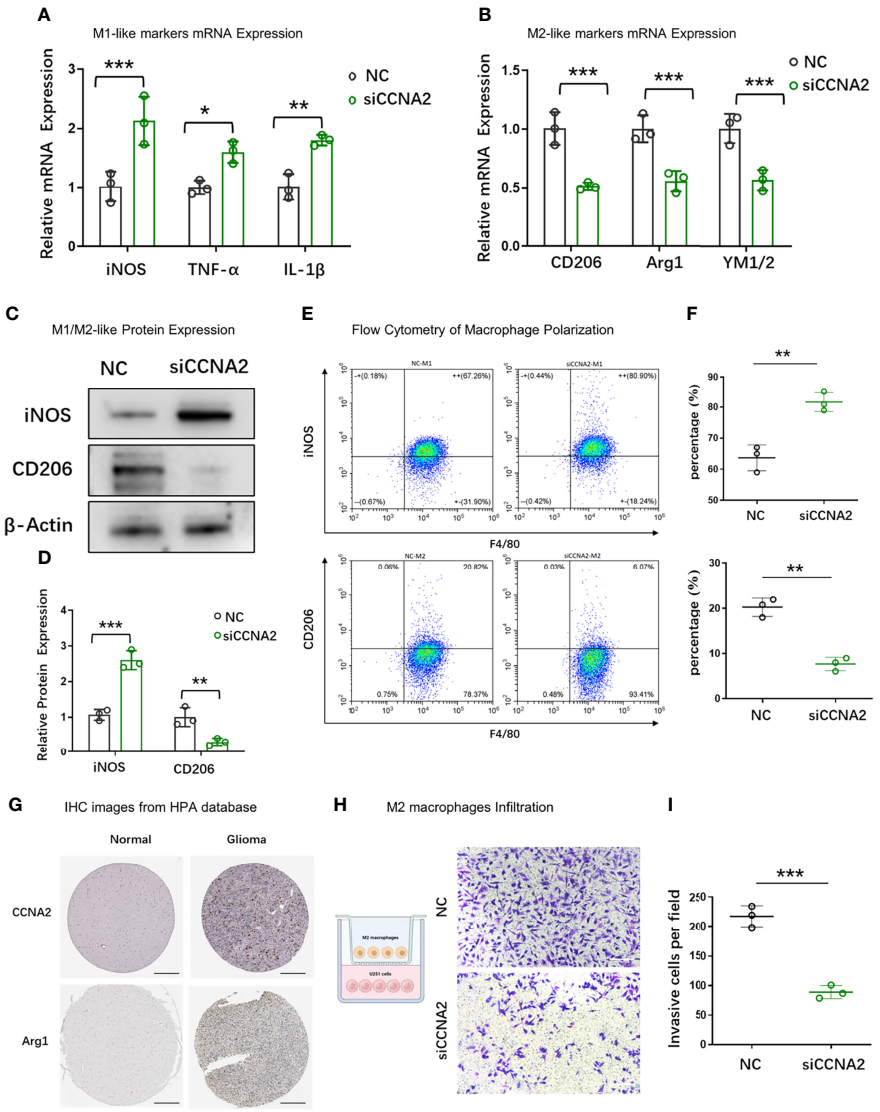

FIGURE 11 | Effect of CCNA2 on macrophage polarization. **(A, B)** mRNA expression levels of M1-like and M2-like markers of macrophages after co-cultured with U251-siCCNA2 cells and controls. **(C, D)** Protein levels of iNOS and CD206 of macrophages after co-cultured with transfected cells. **(E, F)** Flow cytometry analysis of iNOS and CD206 expression in indicated groups. **(G)** Representative IHC images of CCNA2 and M2-like marker Arg1 in normal brain and glioma tissues from the HPA database. **(H, I)** M2 macrophage infiltration after co-cultured with indicated cells. $^{*}P < 0.05$, $^{**}P < 0.01$, $^{***}P < 0.001$.

showed that silencing CCNA2 in U251 cells significantly decreased the M2 macrophage infiltration (**Figures 11H, I**). The results showed that CCNA2 regulated the polarization of macrophages.

DISCUSSION

For a long time, people have been considering the metabolic conversion of cancer cells from the perspective of how and why cancer cells give priority to the use of glucose through aerobic glycolysis (the so-called Warburg effect). In the past few years, we have made great progress in understanding the newly connected metabolic networks intertwined with carcinogenic signals of cancer cells. Among these metabolic reprogramming theories, the deregulation of lipid metabolism is considered one of the primary metabolic markers of tumor cells (28). Aside from aberrant glucose metabolism, cancer cells' lipid, nucleic acid, and amino acid metabolism will vary (29). It has been discovered that lipid initiating changes plays a crucial role in membrane synthesis, signal transduction, and energy production of cancer cells (30). Most research now concentrates on the involvement of a single gene in glioma, and the full impact of numerous fatty acid metabolism genes is unknown. Understanding the significance of distinct fatty acid metabolism processes in glioma and their association with immunotherapy may suggest

appropriate treatment methods by increasing the knowledge of fatty acid metabolism in tumor progression.

There are many successfully constructed prognostic models for glioma, such as the methylation-related or immune-related models in glioma (31–35) and other tumors (36, 37). But research focused on fatty acid metabolism. The connection between FAMDs and glioma was investigated. Univariate Cox regression assessment and lasso cox regression analysis were employed to assess prognostic risk. In the TCGA training cohort, a scoring model was developed for 191 expression levels associated with metabolism in normal and tumor brain tissue. In patients with glioma, the predictive risk score approach was utilized to predict OS. And we validate the model in the TCGA testing cohort, TCGA entire cohort, and CGGA cohort. We used a clinical correlation study to better know about the importance of these genes in glioma. The poor score subgroup and the good score subgroup had different survival rates. The testing cohort yielded the same findings, showing that the predictive risk score model may identify patients with low-risk viability. The predicted risk score model was developed using a multivariate analysis of prognostic data. Furthermore, by combining nomograms with specific clinicopathological variables, we may improve the prediction power of our prognostic risk score model.

Because gliomas need to be treated with a combination of chemotherapy drugs in the later stage. As a result, to better understand the relevance of the predictive risk model in glioma, we evaluated the medication treatment responses of patients in the good and poor score groups. The risk score was positively correlated with crizotinib resistance, which was consistent with previous studies (38). Our personalized PFG score for patients with glioma can be used for the prognosis of glioma. Individuals with elevated ratings had considerable matrix activation, suggesting the existence of chemoresistance, which was similar to previous findings. Chemoresistance is common in individuals with high hazard scores, hence immunotherapy is usually avoided. Most individuals with poor glioma are not candidates for immunotherapy (Immunologic checkpoint, inhibiting [PD-1/L1 and CTLA4]). As a result, distinguishing people who are candidates for immunotherapy is critical in clinical practice. Patients with high-level scores are rich in inhibitory immune cells and immune inflammatory cells. In addition, patients with better scores have the functions of activating type I and II IFN responses which can promote inflammation. All of this suggests that individuals with good scores are candidates for immunotherapy, which is consistent with cancer immune dysfunction and resistance being predicted.

Because the high- and low-score subgroups varied significantly, the distinct genes in the 2 categories were investigated further. CCNA2 was discovered to be necessary. Not only was CCNA2 mRNA expression linked to the clinical stage, but it was also linked to a worse prognosis. The CCNA2 knockdown has also been shown to suppress cell growth by impairing cell cycle progression and inducing cell apoptosis (39). Rui et al. reported that the ability of cancer cell proliferation, invasion, and metastasis was decreased after down-regulated expression of CCNA2 in prostate cancer cell lines (40). However, no research on CCNA2 in glioma has been published, and the process in glioma has to be investigated further.

In conclusion, the fatty acid predictive risk score model may be utilized to assess the fatty acid metabolism network completely. The calculated risk score may be used to classify a patient's clinicopathological characteristics, such as clinical stages. Furthermore, the risk score is linked to the prognosis of patients and may predict immunotherapy. As a result, the clinical practice may be successfully guided by relative risk and clinical-stage to produce a more tailored clinical follow-up approach. These results present a unique, efficient, and accurate predictive and immunotherapy response prediction methodology, paving the way for tailored cancer immunotherapy in the future.

DATA AVAILABILITY STATEMENT

Public data in this study could be found as follows: TCGA (https://portal.gdc.cancer.gov/) and CGGA database (http://www.cgga.org.cn/index.jsp), normal brain tissue from GTEx database (https://xenabrowser.net/datapages/).

ETHICS STATEMENT

The animal study was reviewed and approved by Ethics Committee of the Nanjing Medical University (No. IACUC-2012013).

AUTHOR CONTRIBUTIONS

FJ and YH conceived the manuscript. NZ, YM, and XT wrote the manuscript. JW, FL, and CW conducted the statistical analysis. All authors reviewed the paper and approved the submission.

FUNDING

This study was funded by the National Natural Science Foundation of China (NO.8172539) and the Nanjing Municipal Science and Technology Bureau (Grant number 2019060002). The funding bodies had no role in the study design, data collection, analysis, and interpretation of data.

ACKNOWLEDGMENTS

We would like to thank the Core Facility of the First Affiliated Hospital of Nanjing Medical University for its help in the experiment.

SUPPLEMENTARY MATERIAL

The Supplementary Material for this article can be found online at: https://www.frontiersin.org/articles/10.3389/fimmu.2022.902143/full#supplementary-material

Supplementary Figure 1 | Differential expression analysis between normal and glioma samples.

Supplementary Figure 2 | Fatty acid metabolism score.

Supplementary Figure 3 | The protein interaction diagram.

Supplementary Table 1 | The gene collections were gathered for the prior study's assessment of immune-related aspects in TME.

Supplementary Table 2 | PPI network data.

Supplementary Table 3 | 133 genes associated with prognosis after univariate cox analysis.

Supplementary Table 4 | 10 genes were utilized to create a predictive risk score model.

REFERENCES

1. Nicholson JG, Fine HA. Diffuse Glioma Heterogeneity and Its Therapeutic Implications. *Cancer Discovery* (2021) 11:575–90. doi: 10.1158/2159-8290.CD-20-1474
2. Ostrom QT, Patil N, Cioffi G, Waite K, Kruchko C, Barnholtz-Sloan JS. CBTRUS Statistical Report: Primary Brain and Other Central Nervous System Tumors Diagnosed in the United States in 2013-2017. *Neuro Oncol* (2020) 22: v1–v96. doi: 10.1093/neuonc/noaa200
3. Louis DN, Perry A, Wesseling P, Brat DJ, Cree IA, Figarella-Branger D, et al. The 2021 WHO Classification of Tumors of the Central Nervous System: A Summary. *Neuro Oncol* (2021) 23:1231–51. doi: 10.1093/neuonc/noab106
4. Wen PY, Huse JT. 2016 World Health Organization Classification of Central Nervous System Tumors. *Continuum (Minneap Minn)* (2017) 23:1531–47. doi: 10.1212/CON.0000000000000536
5. Yan H, Parsons DW, Jin G, McLendon R, Rasheed BA, Yuan W, et al. IDH1 and IDH2 Mutations in Gliomas. *N Engl J Med* (2009) 360:765–73. doi: 10.1056/NEJMoa0808710
6. Rasheed BK, Wiltshire RN, Bigner SH, Bigner DD. Molecular Pathogenesis of Malignant Gliomas. *Curr Opin Oncol* (1999) 11:162–7. doi: 10.1097/00001622-199905000-00004
7. Costello JF, Futscher BW, Tano K, Graunke DM, Pieper RO. Graded Methylation in the Promoter and Body of the O6-Methylguanine DNA Methyltransferase (MGMT) Gene Correlates With MGMT Expression in Human Glioma Cells. *J Biol Chem* (1994) 269:17228–37. doi: 10.1016/S0021-9258(17)32544-9
8. Faubert B, Solmonson A, DeBerardinis RJ. Metabolic Reprogramming and Cancer Progression. *SCIENCE* (2020) 368(6487):eaaw5473. doi: 10.1126/science.aaw5473
9. Vaupel P, Schmidberger H, Mayer A. The Warburg Effect: Essential Part of Metabolic Reprogramming and Central Contributor to Cancer Progression. *Int J Radiat Biol* (2019) 95:912–9. doi: 10.1080/09553002.2019.1589653
10. Sun L, Zhang H, Gao P. Metabolic Reprogramming and Epigenetic Modifications on the Path to Cancer. *Protein Cell* (2021). doi: 10.1007/s13238-021-00846-7
11. Tasdogan A, Faubert B, Ramesh V, Ubellacker JM, Shen B, Solmonson A, et al. Metabolic Heterogeneity Confers Differences in Melanoma Metastatic Potential. *NATURE* (2020) 577:115–20. doi: 10.1038/s41586-019-1847-2
12. Kim J, DeBerardinis RJ. Mechanisms and Implications of Metabolic Heterogeneity in Cancer. *Cell Metab* (2019) 30:434–46. doi: 10.1016/j.cmet.2019.08.013
13. Yu TJ, Ma D, Liu YY, Xiao Y, Gong Y, Jiang YZ, et al. Bulk and Single-Cell Transcriptome Profiling Reveal the Metabolic Heterogeneity in Human Breast Cancers. *Mol Ther* (2021) 29:2350–65. doi: 10.1016/j.ymthe.2021.03.003
14. Sengupta D, Pratx G. Imaging Metabolic Heterogeneity in Cancer. *Mol Cancer* (2016) 15:4. doi: 10.1186/s12943-015-0481-3
15. Hopkins BD, Goncalves MD, Cantley LC. Insulin-PI3K Signalling: An Evolutionarily Insulated Metabolic Driver of Cancer. *Nat Rev Endocrinol* (2020) 16:276–83. doi: 10.1038/s41574-020-0329-9
16. Cheng SC, Quintin J, Cramer RA, Shepardson KM, Saeed S, Kumar V, et al. mTOR- and HIF-1alpha-Mediated Aerobic Glycolysis as Metabolic Basis for Trained Immunity. *SCIENCE* (2014) 345:1250684. doi: 10.1126/science.1250684
17. Pramono AA, Rather GM, Herman H, Lestari K, Bertino JR. NAD- and NADPH-Contributing Enzymes as Therapeutic Targets in Cancer: An Overview. *Biomolecules* (2020) 10(3):358. doi: 10.3390/biom10030358
18. Zhang C, Liao Y, Liu P, Du Q, Liang Y, Ooi S, et al. FABP5 Promotes Lymph Node Metastasis in Cervical Cancer by Reprogramming Fatty Acid Metabolism. *THERANOSTICS* (2020) 10:6561–80. doi: 10.7150/thno.44868
19. Tabe Y, Konopleva M, Andreeff M. Fatty Acid Metabolism, Bone Marrow Adipocytes, and AML. *Front Oncol* (2020) 10:155. doi: 10.3389/fonc.2020.00155
20. Qi Y, Chen D, Lu Q, Yao Y, Ji C. Bioinformatic Profiling Identifies a Fatty Acid Metabolism-Related Gene Risk Signature for Malignancy, Prognosis, and Immune Phenotype of Glioma. *Dis Markers* (2019) 2019:3917040. doi: 10.1155/2019/3917040
21. Zhao Z, Zhang KN, Wang Q, Li G, Zeng F, Zhang Y, et al. Chinese Glioma Genome Atlas (CGGA): A Comprehensive Resource With Functional Genomic Data From Chinese Glioma Patients. *Genomics Proteomics Bioinf* (2021) 19:1–12. doi: 10.1016/j.gpb.2020.10.005
22. Zhang S, Chang W, Wu H, Wang YH, Gong YW, Zhao YL, et al. Pan-Cancer Analysis of Iron Metabolic Landscape Across the Cancer Genome Atlas. *J Cell Physiol* (2020) 235:1013–24. doi: 10.1002/jcp.29017
23. Peng Y, Xu C, Wen J, Zhang Y, Wang M, Liu X, et al. Fatty Acid Metabolism-Related lncRNAs Are Potential Biomarkers for Predicting the Overall Survival of Patients With Colorectal Cancer. *Front Oncol* (2021) 11:704038. doi: 10.3389/fonc.2021.704038
24. Peng Y, Xu C, Wen J, Zhang Y, Wang M, Liu X, et al. Corrigendum: Fatty Acid Metabolism-Related lncRNAs Are Potential Biomarkers for Predicting the Overall Survival of Patients With Colorectal Cancer. *Front Oncol* (2021) 11:831864. doi: 10.3389/fonc.2021.704038
25. Yi M, Nissley DV, McCormick F, Stephens RM. ssGSEA Score-Based Ras Dependency Indexes Derived From Gene Expression Data Reveal Potential Ras Addiction Mechanisms With Possible Clinical Implications. *Sci Rep* (2020) 10:10258. doi: 10.1038/s41598-020-66986-8
26. Dheeraj A, Agarwal C, Schlaepfer IR, Raben D, Singh R, Agarwal R, et al. A Novel Approach to Target Hypoxic Cancer Cells *via* Combining Beta-Oxidation Inhibitor Etomoxir With Radiation. *Hypoxia (Auckl)* (2018) 6:23–33. doi: 10.2147/HP.S163115
27. Odagiri S, Shimazu A, Shimokawaji M, Ishikura Y, Yoshimatsu H. Use of a New Stapling Instrument for Permanent Occlusion of the Aorta in the Surgical Procedure for Thromboexclusion. *Ann Thorac Surg* (1989) 47:466–9. doi: 10.1016/0003-4975(89)90399-8
28. Cheng C, Geng F, Cheng X, Guo D. Lipid Metabolism Reprogramming and its Potential Targets in Cancer. *Cancer Commun (Lond)* (2018) 38:27. doi: 10.1186/s40880-018-0301-4
29. Broadfield LA, Pane AA, Talebi A, Swinnen JV, Fendt SM. Lipid Metabolism in Cancer: New Perspectives and Emerging Mechanisms. *Dev Cell* (2021) 56:1363–93. doi: 10.1016/j.devcel.2021.04.013
30. Liu Q, Luo Q, Halim A, Song G. Targeting Lipid Metabolism of Cancer Cells: A Promising Therapeutic Strategy for Cancer. *Cancer Lett* (2017) 401:39–45. doi: 10.1016/j.canlet.2017.05.002
31. Lu L, Hu Y, Wang C, Jiang F, Wu C. Methylation and Expression of the Exercise-Related TLR1 Gene Is Associated With Low Grade Glioma Prognosis and Outcome. *Front Mol Biosci* (2021) 8:747933. doi: 10.3389/fmolb.2021.747933
32. Zhang H, Luo YB, Wu W, Zhang L, Wang Z, Dai Z, et al. The Molecular Feature of Macrophages in Tumor Immune Microenvironment of Glioma Patients. *Comput Struct Biotechnol J* (2021) 19:4603–18. doi: 10.1016/j.csbj.2021.08.019
33. Wang Z, Su G, Dai Z, Meng M, Zhang H, Fan F, et al. Circadian Clock Genes Promote Glioma Progression by Affecting Tumour Immune Infiltration and Tumour Cell Proliferation. *Cell Prolif* (2021) 54:e12988. doi: 10.1111/cpr.12988
34. Zhang N, Dai Z, Wu W, Wang Z, Cao H, Zhang Y, et al. The Predictive Value of Monocytes in Immune Microenvironment and Prognosis of Glioma Patients Based on Machine Learning. *Front Immunol* (2021) 12:656541. doi: 10.3389/fimmu.2021.656541
35. Zhang N, Zhang H, Wang Z, Dai Z, Zhang X, Cheng Q, et al. Immune Infiltrating Cells-Derived Risk Signature Based on Large-Scale Analysis Defines Immune Landscape and Predicts Immunotherapy Responses in Glioma Tumor Microenvironment. *Front Immunol* (2021) 12:691811. doi: 10.3389/fimmu.2021.691811
36. Jiang F, Wu C, Wang M, Wei K, Zhou G, Wang J. Multi-Omics Analysis of Tumor Mutation Burden Combined With Immune Infiltrates in Melanoma. *Clin Chim Acta* (2020) 511:306–18. doi: 10.1016/j.cca.2020.10.030
37. Jiang F, Miao XL, Zhang XT, Yan F, Mao Y, Wu CY, et al. A Hypoxia Gene-Based Signature to Predict the Survival and Affect the Tumor Immune Microenvironment of Osteosarcoma in Children. *J Immunol Res* (2021) 2021:5523832. doi: 10.1155/2021/5523832

38. Junca A, Villalva C, Tachon G, Rivet P, Cortes U, Guilloteau K, et al. Crizotinib Targets in Glioblastoma Stem Cells. *Cancer Med* (2017) 6:2625–34. doi: 10.1002/cam4.1167
39. Gan Y, Li Y, Li T, Shu G, Yin G. CCNA2 Acts as a Novel Biomarker in Regulating the Growth and Apoptosis of Colorectal Cancer. *Cancer Manag Res* (2018) 10:5113–24. doi: 10.2147/CMAR.S176833
40. Yang R, Du Y, Wang L, Chen Z, Liu X. Weighted Gene Co-Expression Network Analysis Identifies CCNA2 as a Treatment Target of Prostate Cancer Through Inhibiting Cell Cycle. *J Cancer* (2020) 11:1203–11. doi: 10.7150/jca.38173

Conflict of Interest: The authors declare that the research was conducted in the absence of any commercial or financial relationships that could be construed as a potential conflict of interest.

Publisher's Note: All claims expressed in this article are solely those of the authors and do not necessarily represent those of their affiliated organizations, or those of the publisher, the editors and the reviewers. Any product that may be evaluated in this article, or claim that may be made by its manufacturer, is not guaranteed or endorsed by the publisher.

Copyright © 2022 Jiang, Luo, Zeng, Mao, Tang, Wang, Hu and Wu. This is an open-access article distributed under the terms of the Creative Commons Attribution License (CC BY). The use, distribution or reproduction in other forums is permitted, provided the original author(s) and the copyright owner(s) are credited and that the original publication in this journal is cited, in accordance with accepted academic practice. No use, distribution or reproduction is permitted which does not comply with these terms.

frontiers | Frontiers in Oncology

TYPE Original Research
PUBLISHED 12 August 2022
DOI 10.3389/fonc.2022.889351

Check for updates

OPEN ACCESS

EDITED BY
Wen Cheng,
The First Affiliated Hospital of China Medical University, China

REVIEWED BY
Xin Wu,
Zhejiang Chinese Medical University, China
Kai Shu,
Huazhong University of Science and Technology, China

*CORRESPONDENCE
Siyi Wanggou
zokygwong@gmail.com
Xuejun Li
lxjneuro@csu.edu.cn

†These authors have contributed equally to this work

SPECIALTY SECTION
This article was submitted to Neuro-Oncology and Neurosurgical Oncology, a section of the journal Frontiers in Oncology

RECEIVED 04 March 2022
ACCEPTED 19 July 2022
PUBLISHED 12 August 2022

CITATION
Chen L, Xiong Z, Zhao H, Teng C, Liu H, Huang Q, Wanggou S and Li X (2022) Identification of the novel prognostic biomarker, MLLT11, reveals its relationship with immune checkpoint markers in glioma. *Front. Oncol.* 12:889351. doi: 10.3389/fonc.2022.889351

COPYRIGHT
© 2022 Chen, Xiong, Zhao, Teng, Liu, Huang, Wanggou and Li. This is an open-access article distributed under the terms of the Creative Commons Attribution License (CC BY). The use, distribution or reproduction in other forums is permitted, provided the original author(s) and the copyright owner(s) are credited and that the original publication in this journal is cited, in accordance with accepted academic practice. No use, distribution or reproduction is permitted which does not comply with these terms.

Identification of the novel prognostic biomarker, MLLT11, reveals its relationship with immune checkpoint markers in glioma

Long Chen[1,2,3†], Zujian Xiong[1,2,3†], Hongyu Zhao[1,2,3], Chubei Teng[1,2,3], Hongwei Liu[1,2,3], Qi Huang[1,2,3], Siyi Wanggou[1,3*] and Xuejun Li[1,3*]

[1]Department of Neurosurgery, Xiangya Hospital, Central South University, Changsha, China, [2]Xiangya School of Medicine, Central South University, Changsha, China, [3]Hunan International Scientific and Technological Cooperation Base of Brain Tumor Research, Xiangya Hospital, Central South University, Changsha, China

Aim: This study aimed to explore the expression pattern of *MLLT11* under different pathological features, evaluate its prognostic value for glioma patients, reveal the relationship between *MLLT11* mRNA expression and immune cell infiltration in the tumor microenvironment (TME), and provide more evidence for the molecular diagnosis of glioma and immunotherapy.

Methods: Using large-scale bioinformatic approach and RNA sequencing (RNA-seq) data from public databases The Cancer Genome Atlas (TCGA), Chinese Glioma Genome Atlas (CGGA), and The Gene Expression Omnibus (GEO)), we investigated the relationship between *MLLT11* mRNA levels and pathologic characteristics. The distribution in the different subtypes was observed based on Verhaak bulk and Neftel single-cell classification. Then, Gene Ontology (GO) and Kyoto Encyclopedia of Genes and Genomes (KEGG) enrichment analysis were used for bioinformatic analysis. Kaplan–Meier survival analysis and Cox regression analysis were used for survival analysis. Correlation analyses were performed between *MLLT11* expression and 22 immune cells and immune checkpoints in the TME.

Results: We found that *MLLT11* expression is decreased in high-grade glioma tissues; we further verified this result by RTPCR, Western blotting, and immunohistochemistry using our clinical samples. According to the Verhaak classification, high *MLLT11* expression is mostly clustered in pro-neutral (PN) and neutral (NE) subtypes, while in the Neftel classification, *MLLT11* mainly clustered in neural progenitor-like (NPC-like) neoplastic cells. Survival analysis revealed that low levels of *MLLT11* expression are associated with a poorer prognosis; *MLLT11* was identified as an independent prognostic factor in multivariate Cox regression analyses. Functional enrichment analyses of *MLLT11* with correlated expression indicated that low *MLLT11* expression is

associated with the biological process related to the extracellular matrix, and the high expression group is related to the synaptic structure. Correlation analyses suggest that declined *MLLT11* expression is associated with increased macrophage infiltration in glioma, especially M2 macrophage, and verified by RTPCR, Western blotting, and immunohistochemistry using our clinical glioma samples. *MLLT11* had a highly negative correlation with immune checkpoint inhibitor (ICI) genes including *PDCD1*, *PD-L1*, *TIM3(HAVCR2)*, and *PD-L2 (PDCD1LG2)*.

Conclusion: *MLLT11* plays a crucial role in the progression of glioma and has the potential to be a new prognostic marker for glioma.

KEYWORDS

glioma, bioinformatics, single-cell RNA sequencing, tumoral heterogeneity, immune infiltration

Introduction

Glioma, divided into lower-grade glioma (WHO grades 2 and 3) and high-grade glioma (WHO grade 4), is one of the most common intracranial malignant tumors, and its annual incidence rate is about 3–6.4/100,000. Among them, glioblastoma (GBM) contributes to the worst prognosis, with a median survival time of approximately 12–15 months even after standard treatment of surgery, radiotherapy, and chemotherapy (1, 2). Nowadays, glioma molecular characteristics, such as the status of isocitrate dehydrogenase (IDH) mutation, methylation of O6-methylguanine-DNA methyltransferase (MGMT), and 1p/19q codeletion status, complement traditional therapy, and tumor-treating fields (TTFs) have been identified as important indicators for glioma classification and outcome prediction (1, 3). New therapies such as molecular targeting treatment and immunotherapy are enrolled in the treatment strategy, but only a few are actually able to improve clinical outcomes. The potential reason is that glioma tends to be a multi-gene and multi-step genetic heterogeneous disease, and tumor heterogeneity may probably be the root of treatment failure (4, 5). Recently, it has been found that GBM can be further divided into four different subtypes, pro-neural (TCGA-PN), neural (TCGA-NE), classical (TCGA-CL), and mesenchymal (TCGA-MES) (6, 7), based on their molecular feature. Neftel et al. (8) confirmed the existence of four different cell subtypes in GBM at the single-cell level, including neural progenitor-like (NPC-like), oligodendrocyte progenitor-like (OPC-like), astrocyte-like (AC-like), and mesenchymal-like (MES-like) states, and relate them to the corresponding bulk subtypes. In addition, the tumor immune microenvironment plays a pivotal role in tumor aggression. The tumor and its microenvironment influence each other during the tumor growth through cellular signaling of molecular or infiltrated immune cells. GBM can induce the activation of a variety of immune cell types, such as tumor-infiltrating macrophages, which produce a large number of cytokines, growth factors, and interleukin, so as to produce a suitable tumor microenvironment (TME) and promote the growth and proliferation of glioma cells (9). Thus, an in-depth understanding of the key molecules and mechanisms is of great significance for the diagnosis and treatment of glioma.

The *MLLT11* gene, located on chromosome 1q21, encodes a protein with a molecular weight of ~9 kDa and consists of 270 amino acids (10). Regarding the function of *MLLT11* as an "oncogene" signature in hematologic diseases (11), studies are currently mainly focused on hematologic disorders. The expression of *MLLT11* markedly increased in several hematologic disorders, including lymphocytic leukemia, lymphoma, and myelodysplastic syndrome (12, 13). Although the specific function of *MLLT11* is not well defined, it exhibits proapoptotic functions in some solid tumors, such as ovarian and liver cancer (10, 14, 15).

At present, it has been shown that there is a correlation between the level of *MLLT11* expression and the degree of cell differentiation (16–18). In the central nervous system (CNS), *MLLT11* expression is gradually upregulated as neural stem cells (NSCs) differentiate into neurons, and its high expression promotes neuronal differentiation and maturation (16, 19). Moreover, *MLLT11* also plays an important role in tumor cell and immune cell interaction in the TME (20). Considering the *MLLT11* function in various tumors and to reveal its function in glioma, we explored its expression pattern and clinicopathological significance that can offer new insights for glioma treatment.

In this study, we analyzed the expression profile of *MLLT11* in gliomas. Large-scale bioinformatic analysis, enrolling both bulk and

single-cell data, was performed by downloading gene expression data from known databases. Then, *MLLT11* expression in tumor samples and normal brain tissues was confirmed by real-time quantitative polymerase chain reaction (qPCR), Western blotting, and immunohistochemistry (IHC) in our institute. Moreover, we evaluated the prognostic value of *MLLT11* in the treatment for gliomas systematically and comprehensively. We found that among gliomas, there were distinct differences in *MLLT11* expression among different grades of gliomas, and there was also a clear propensity for *MLLT11* expression among the different subtypes. In addition, we explored the relationship between *MLLT11* and immune infiltration and found that, with increasing malignancy, the expression level of *MLLT11* showed a decreasing trend, and *MLLT11* expression was negatively correlated with M2-type macrophages in the TME. Furthermore, by qPCR, Western blotting, and IHC, we found that both mRNA and protein levels of M2-type macrophage-specific markers were obviously increased with higher glioma pathological grade. These results suggest that in high-grade gliomas, along with downregulated *MLLT11* expression, more M2-type macrophages are recruited into the TME to promote tumor growth. Based on these data, we conclude that *MLLT11* is a potential prognostic biological marker and may probably be a clinical therapeutic target for glioma patients.

Materials and methods

Dataset and data processing

We collected expression data and corresponding metadata from lower-grade glioma (LGG) and GBM samples in TCGA, CGGA, and GEO databases. A total of 697 samples from TCGA were downloaded from The University of California Santa Cruz (UCSC) Xena (https://xenabrowser.net/), including LGG and GBM. In addition, 1,319 samples were downloaded from the CGGA website (http://www.cgga.org.cn/). CGGA samples included mRNAseq_693, mRNAseq_325, and CGGA_array datasets. Furthermore, 444 bulk samples were collected from GEO datasets, including GSE43378, GSE16011, GSE74187, and GSE83300. A total of 3,589 cells from four primary GBM patients' single-cell RNA sequencing (scRNA-seq) data according to Smart-seq2 protocol, GSE84465, were normalized following Seurat (v3.1.1) pipeline (21, 22). In this study, 105 normal brain cortex samples from GTEx databases were used for comparisons (http://commonfund.nih.gov/GTEx/). All bulk RNA-seq count data were normalized into transcripts per kilobase million (TPM). In addition, we also collected posttraumatic normal brain tissue (n = 9) and glioma samples (n = 27) from the Department of Neurosurgery in Xiangya Hospital, Central South University, including nine cases of grade 2, 3, and 4 gliomas, respectively. This study was approved by the medical ethics committee of Xiangya Hospital, Central South University.

Group division and survival analysis

The patients were divided into $MLLT11^{high}$ and $MLLT11^{low}$ groups according to *MLLT11* expression and the survival data by the cutoff calculated by the maximally selected rank statistics. The Kaplan–Meier survival curve was depicted to estimate survival distribution by R packages named *survival* and *survminer*. The log-rank test was used to assess statistical significance between groups. The coxph function in R package survival was used for Cox regression analysis. The receiver operating characteristic (ROC) curve was generated to assess the accuracy of the model with the R package *pROC* (23).

Differential gene identification and enrichment analysis

The differentially expressed genes (DEGs) were identified in each dataset through using the R package *limma* for normalized data false discovery rate (FDR) <0.05 and |log2 [fold change (FC)]|>1.5). Then, with the R package *clusterProfiler* (24), the pathway enrichment analysis was performed for the up-expressed and the down-expressed DEGs. The functional and pathway enrichment analysis includes Gene Ontology (GO) and Kyoto Encyclopedia of Genes and Genomes (KEGG) pathway. The KEGG gene signatures were obtained from the Molecular Signatures Database v6.2 version (MSigDB, https://www.gsea-msigdb.org/gsea/msigdb). The pathway was scored using the single-sample gene set enrichment analysis (ssGSEA) (25), as implemented in the *GSVA* R package (26). Then, principal component analysis (PCA) was used for dimensionality reduction of the pathway score matrix.

Immune infiltration analysis

CIBERSORT deconvolution algorithm was introduced, referring to the LM22 set (27) and the normalized signature matrices (28), to analyze the relative abundance of infiltrating immune cells. The association analysis and plots were conducted with the utilization of the R package *ggstatsplot*.

qPCR

Total RNA of the collected glioma tissues and normal tissue samples was extracted by TRIzol kit (Accurate Biology, China, AG21101) and RNA purification kit (Thermo Scientific, K0731), reverse transcribed to cDNA by RT-qPCR kit (Thermo Scientific, K16225). Amplification was performed according to the SYBR green (Bio-Rad, #1725274) method with three replicate wells per sample in a total reaction system of 20 µl.

PCR reaction conditions (ABI 7300 Real-Time System) were as follows: 95°C for 15 min, 40 cycles of amplification at 95°C for 15 s, 60°C for 1 min. β-Actin was used as an internal reference and $2^{-\Delta\Delta Ct}$ formula was used to calculate the relative expression of the targeted gene. Targeted gene primer sequences were as follows: *MLLT11*: (forward) 5'-GTAGCCAGTACAG TTCCTTTCT-3', (reverse) 5'-AAGTTGAAGGTGCTGTA CTCAA-3'; *ARG1*: (forward) 5'-GGACCTGCCCTTTGCTGA CATC-3', (reverse) 5'-TCTTCTTGACTTCTGCCACCTTGC-3'; *CD206*: (forward) 5'-TCCGACCCTTCCTTGACTAA TCCTC-3', (reverse) 5'-AGTATGTCTCCGCTTCATGC CATTG-3'; *IL-10*: (forward) 5'-GTTGTTAAAGGAGTCCTTG CTG-3', (reverse) 5'-TTCACAGGGAAGAAATCGATGA-3'; *CD163*: (forward) 5'-ATCAACCCTGCATCTTTAGACA-3', (reverse) 5'-CTTGTTGTCACATGTGATCCAG-3'; *CD115*: (forward) 5'-GTCCTGAAGGTGGCTGTGAAGATG-3', (reverse) 5'-GCTCCCAGAAGGTTGACGATGTTC-3'; PDGFβ: (forward) 5'-TCTCTGCTGCTACCTGCGTCTG-3', (reverse) 5'-AAGGAGCGGATCGAGTGGTCAC-3'.

Western blotting

Clinical glioma samples and normal brain tissue samples were collected, and total protein was extracted. The concentration of protein was determined by the bicinchoninic acid (BCA) method and calculating the loading capacity. Boiled at 100°C for 5 min and stored at -80°C for further use. The protein sample (100 ng) was separated by 15%, 10% sodium dodecyl sulfate polyacrylamide gel electrophoresis (SDS-PAGE), and the separated protein bands were transferred onto the polyvinylidene fluoride (PVDF) membrane. The membrane was blocked in 5% nonfat milk for 2 h at room temperature and washed for 10 min with phosphate buffer solution with 0.05% Tween 20 (PBST) (three times), then incubated overnight at 4°C with *MLLT11* I antibody solution (1:2,000, Abcam, ab109016) and arginase-1 (*ARG1*) antibody (1:1,000, Proteintech, 16001-1-AP) that had been diluted in PBST and then washed with PBS for 10 min (three times). The membrane was incubated in the antibody II solution (Goat Anti-Rabbit IgG, 1:5,000, Proteintech) for 1 h at room temperature and washed with PBST for 10 min (three times). The protein bands stained by the antibody were visualized using enhanced chemiluminescence (WesternBright Sirius, Advansta, 200425-03), and β-actin was used as an internal reference followed by exposure to X–ray films (Bio-Rad). Relative protein expressions were analyzed from band intensities using ImageJ software.

Immunohistochemistry

Glioma specimens of different grades and normal brain tissue were fixed with formalin, embedded in paraffin, and then made into 4-μm sections. Sections were dewaxed and rehydrated pretreated for antigen retrieval in citrate buffer and quenched for endogenous peroxidase with 3% hydrogen peroxide (H_2O_2). Nonspecific antigenic sites were blocked with 10% normal goat serum, and sections were incubated overnight with *MLLT11* I antibody (1:100, Abcam, ab109016) and *CD163* I antibody (1:500, CST, #93498) at 4°C. These were then incubated with secondary antibody (goat anti-rabbit IgG, 1:5,000, Proteintech) and stained with diaminobenzidine tetrahydrochloride (DAB) and hematoxylin. IHC images were acquired, and the score of *MLLT11* and *CD163* protein expression was calculated by image processing software ImageJ.

Statistical analysis

All bioinformatic statistical analyses in this study were performed using R version 4.1.0 (The R Foundation for Statistical Computing, http://www.rproject.org/). The Wilcoxon rank-sum test was used to determine the expression levels of *MLLT11* with regard to pathological characteristics. The survival probability was determined using Kaplan–Meier survival curves by log-rank test. The Pearson correlation was applied to evaluate the relationship between *MLLT11* expression and immune cell infiltration and immune checkpoints. The heatmap was drawn with the R package *pheatmap*. All statistical tests were two-sided. The $p < 0.05$ was considered statistically significant.

Results

Clinical and molecular characteristics of *MLLT11* in gliomas

We first compared the *MLLT11* expression among LGG, GBM, and normal brain cortex in TCGA and GTEX dataset and found no significant difference between normal brain and WHO grade 2 and WHO grade 3 gliomas, but the expression of *MLLT11* in GBM is the lowest among the four histological groups. Then, the exploration of *MLLT11* expression in glioma histology revealed that GBM showed the lowest expression, followed by astrocytoma, and no difference between normal brain, oligoastrocytoma, and oligodendroglioma (Figures 1A, B). According to median age, patients were divided into high and low age subgroups, and there were significant differences in the expression of *MLLT11* between the high age subgroup and the low age subgroup in TCGA datasets (Figure 1C). Meanwhile, no significant *MLLT11* expression difference was found in LGG between the young and old groups except for GBM (Figure 1D). The same result is also seen in CGGA dataset (Supplementary Figures 1A, B). Furthermore, the *MLLT11* expression difference can also be analyzed in different WHO pathological grades in the high

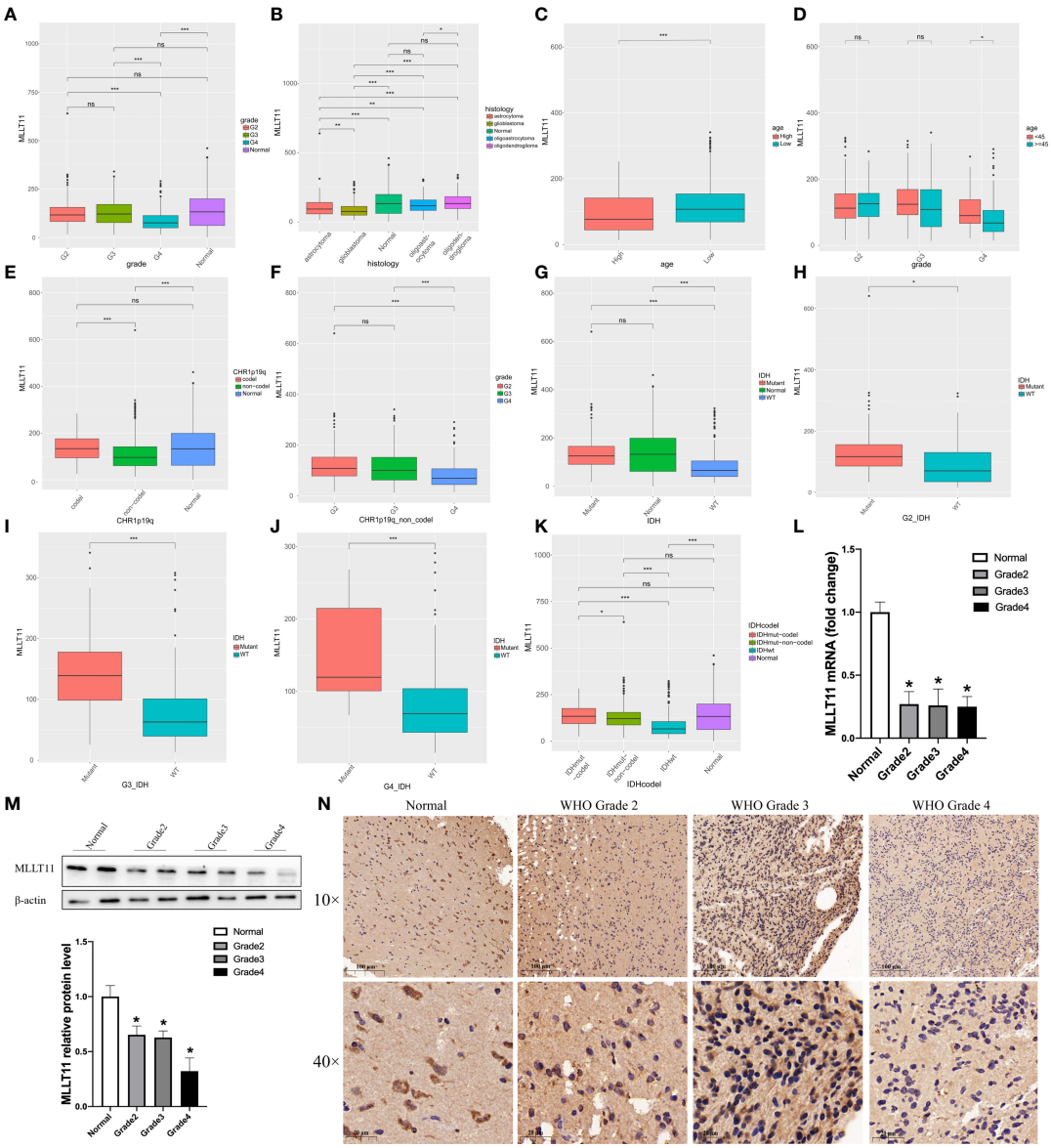

FIGURE 1
Clinical and molecular characteristics of MLLT11 in gliomas. **(A, B)** The expression of MLLT11 in different WHO pathological grades. **(C, D)** The expression of MLLT11 stratified by age and WHO pathological grades. **(E, F)** The expression of MLLT11 in 1p19q codeletion and non-codeletion glioma. **(G–J)** The expression of MLLT11 in IDH mutant and wild type and stratified by age and different WHO pathological grades. **(K)** The expression of MLLT11 in IDH mutation combined with 1p/19q codeletion and IDH mutation combined with 1p/19q non-codeletion. **(L, M)** Representative images of qPCR and Western blotting for MLLT11 in normal brain tissue and different tumor grades. **(N)** Representative images of IHC staining for MLLT11 in normal brain tissue and different WHO pathological grades of glioma. *p < 0.05, **p < 0.01, ***p < 0.001; ns, no statistics. G2, Grade 2; G3, Grade 3; G4, Grade 4; IDH, isocitrate dehydrogenase; WT, wildtype.

age subgroup and the low age subgroup. The result shows that in both high-age and low-age groups, the expression level of *MLLT11* has a significant downward trend with the increase of tumor grade (Supplementary Figures 1C, D). Of note, in the CGGA dataset and TCGA dataset, no significant difference was found between men and women for *MLLT11* expression in different WHO pathological grades (Supplementary Figures 1E–G).

In recent years, with the rapid development of the molecular pathology of glioma, a series of molecular markers, such as IDH mutation, 1p/19q codeletion, and MGMT methylation status,

have been considered to be related to the malignancy of glioma and patient prognosis. Therefore, these clinical-related molecular biomarkers were also explored in this study. We found that there was a significant difference in the expression of *MLLT11* between 1p19q codeletion and non-codeletion status in TCGA datasets. Compared with 1p19q non-codeletion, the expression of *MLLT11* in 1p19q codeletion was higher (Figure 1E), and the same result was found in LGG (Supplementary Figures 1H, I). In patients with non-codeletion, the expression of *MLLT11* gradually decreased with the increase of tumor grade (Figure 1F). Furthermore, the expression level of *MLLT11* was significantly different between IDH mutation and non-mutation, which was validated in CGGA and TCGA datasets. The expression of *MLLT11* in the IDH mutant subtype, similar to the normal brain, was significantly higher than that of IDH wild-type glioma, and the difference was more obvious in GBM (Figures 1G–J). A similar result was found in CGGA_325, CGGA_693, and CGGA_array datasets (Supplementary Figures 1J–O). In addition, we also found that compared with IDH mutation or 1p/19q codeletion alone, the expression of *MLLT11* with IDH mutation combined with 1p/19q codeletion was the highest (Figure 1K), suggesting that the prognostic value of *MLLT11* expression is consistent with the known IDH mutation combined with 1p/19q codeletion.

qPCR, Western blotting, and IHC staining were used to detect the mRNA transcription level and protein expression of *MLLT11* in glioma samples of different grades (n = 27) and normal brain tissues (n = 9) from our institution. The clinical characteristics and molecular pathology of these patients are shown in Supplementary Table 1. qPCR results showed that the expression level of *MLLT11* in tumor tissues was significantly lower than that in normal brain tissues ($p < 0.05$), but no significant difference was found between different grades of glioma (Figure 1L). Furthermore, Western blotting and IHC results confirmed that the expression of *MLLT11* was higher in normal brain tissues and LGG when compared with that of GBM tissues (Figures 1M, N). Moreover, glioma patients with higher *MLLT11* expression level experienced favorable outcomes among the glioma patients in the above analysis. Based on the above information, we infer that *MLLT11* decreased significantly in GBM and may play an important role in invasive processes of gliomas.

MLLT11 expression level shows a subtype preference in glioblastoma

Currently, during clinical diagnosis and treatment, molecular subclasses in glioma provide new insights into predicting patient prognosis (6), and studies based on bulk expression in TCGA suggest that GBM can be classified into four subtypes, namely, classical (TCGA-CL), mesenchymal (TCGA-ME), pro-neural (TCGA-PN), and neural (TCGA-NE), of which the PN subtype has a relatively good prognosis, but the CL and ME subtypes are more aggressive and have a poor prognosis (7, 29). In this study, we detected *MLLT11* expression in LGG, GBM samples, and normal tissues from TCGA and GTEx datasets and found that increased *MLLT11* expression was associated with the NE and PN subtypes in TCGA and CGGA datasets (Figures 2A–D).

To clarify the role of *MLLT11* in glioma, we further analyzed *MLLT11* expression in gliomas from single-cell dimension. Seven clusters of cells were identified from four glioma samples, mainly including astrocytes, oligodendrocytes, oligodendrocyte precursor cells (OPCs), neoplastic cells, neurons, vascular endothelial cells, and immune cells (Figure 2E). The expression of *MLLT11* was mainly concentrated in neoplastic cells, immune cells, and OPCs (Figure 2F). In addition, scRNA-seq clustering was carried out according to the four types proposed in GBM by Neftel et al. (8) in 2019, mainly including four cell clusters, AC-like, NPC-like, OPC-like, and MES-like, in which TCGA-PN subtype corresponds to NPC-like cellular state (8). Our results showed that *MLLT11* was mainly expressed in NPC-like cells, which was significantly different from the other three clusters of cell subtypes (Figures 2G–I). This is consistent with the expression of bulk tumor sequencing, that is, *MLLT11* is mainly upregulated in TCGA-NE and TCGA-PN. It is suggested that *MLLT11* can be used as a marker of GBM subtype.

The expression level of *MLLT11* refers to the prognosis of the glioma patient

From the above bioinformatic analysis result, we conclude that the expression of *MLLT11* has significant correlation with glioma malignancy, i.e., in gliomas, *MLLT11* expression tends to decrease with increasing tumor malignancy. To further test and verify the reliability of this result, we evaluated the prognostic value of *MLLT11* in eight datasets from TCGA, CGGA, and GEO. In these datasets, patients were divided into low-expression subgroup and high-expression subgroup, and survival analysis was performed using log-rank test analysis. The results revealed that, in TCGA ($p < 0.0001$), CGGA_array ($p < 0.001$), and CGGA_RNAseq_325 datasets ($p < 0.01$), patients (LGG and GBM) with a higher expression of *MLLT11* showed significantly better prognosis than that of the low-expression subgroup (Figures 3A–C). In the GSE43378 dataset, although no obvious statistical significance in the survival analysis was found between the *MLLT11* high- and low-expression groups, there was still a similar trend between them ($p = 0.16$) (Figure 3D). Also, among GBM patients, we also find that patients with a high expression of *MLLT11* show better prognosis in CGGA_RNAseq_693 dataset ($p < 0.05$), GSE16011 dataset ($p < 0.01$), GSE74187 dataset ($p < 0.001$), and GSE83300 dataset ($p < 0.01$) (Figures 3E–H).

To explore the influence on the survival of glioma patients, we evaluated the prognostic value of *MLLT11* in TCGA dataset

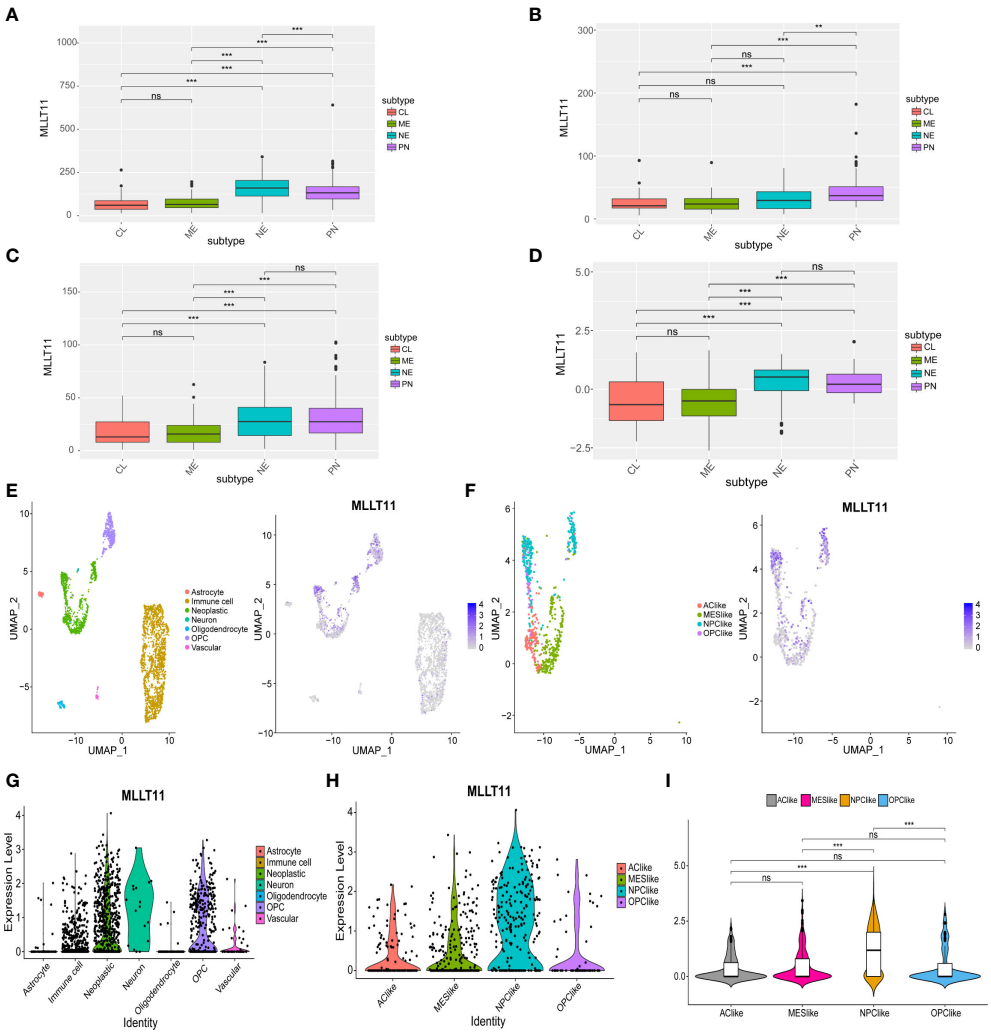

FIGURE 2
The expression of MLLT11 in different glioma subtypes. **(A–D)** MLLT11 expression level in different molecular subtypes in TCGA, CGGA_325, CGGA_691, and CGGA_array datasets based on bulk expression. **(E–I)** ScRNA-seq results for MLLT11 expression in GBM. **(E)** The cells were categorized into eight clusters (left). Blue scatter plots represent MLLT11 expression distribution in eight clusters (right). **(F)** Tumor cells were extracted and categorized into four different cell clusters based on the scRNA expression level (left), and MLLT11 expression is shown in blue scatter spots (right). **(G, H)** The expression levels of MLLT11 in the eight cell clusters and four molecular subtypes were shown by violin plot. **(I)** MLLT11 was mainly expressed in NPC-like subtypes compared with the other three subtypes. **p < 0.01, ***p < 0.001; ns, no statistics.

cohorts. We applied the multivariate Cox regression analysis to investigate the prognostic power of the signature, and the result revealed that the expression of *MLLT11* hazard ratios (HR) = 0.47, p < 0.026) is an independent prognostic biomarker for glioma patients after adjusting for age, gender, IDH, MGMT promoter, Telomerase reverse transcriptase (TERT) promoter, and 1p19q codeletion status (Figure 3I). Moreover, ROC curve analysis in TCGA dataset was used to comprehensively assess the sensitivity and specificity of the model. The area under the curve (AUC) of *MLLT11* was 68% in the pan-glioma cohort (Figure 3J).

Differentially expressed genes and functional enrichment analysis between the *MLLT11* high- and low-expression groups

We analyzed DEGs between the groups with low and high *MLLT11* expression in TCGA. By using the criteria |log FC| >1.5 and FDR <0.05, we obtained 301 DEGs (230 upregulated and 71 downregulated) (Figure 4A). The KEGG enrichment analysis indicated that the *MLLT11* upregulated DEGs were involved in pathways related to neuroactive ligand–receptor

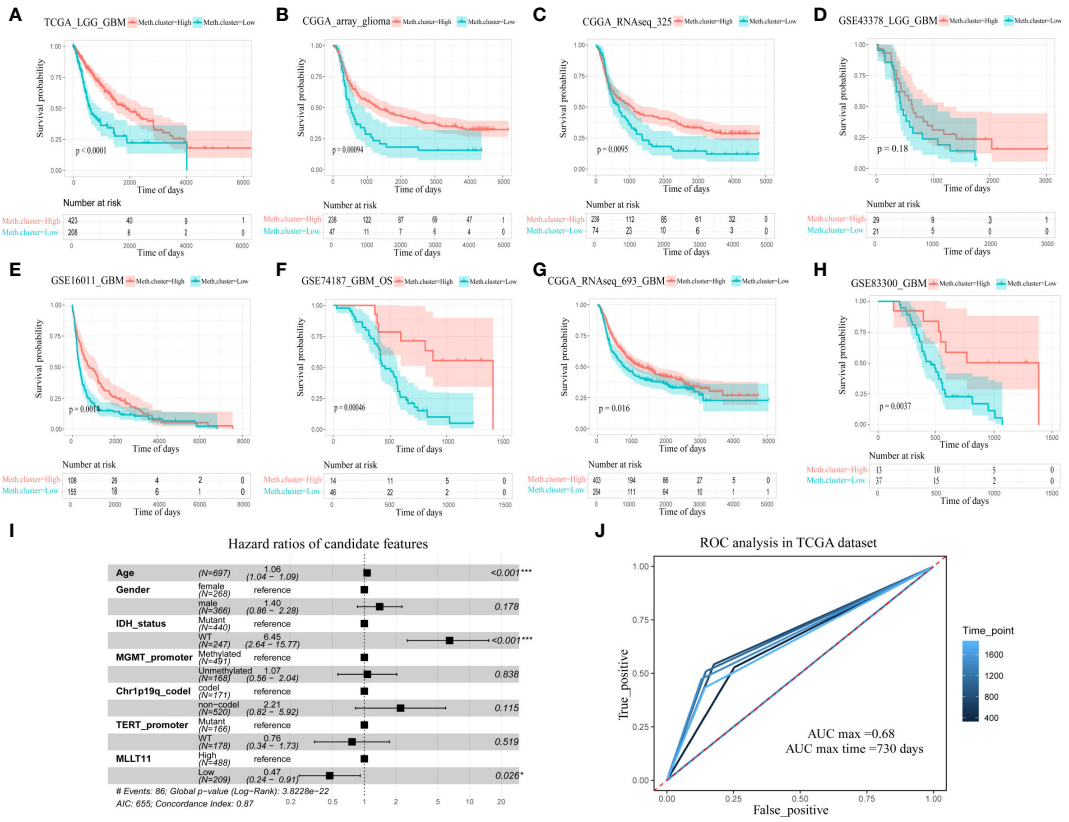

FIGURE 3
The relationship between MLLT11 expression and survival for glioma. **(A–H)** Kaplan–Meier plots of MLLT11 in TCGA and CGGA datasets, **(A)** TCGA_LGG_GBM, **(B)** CGGA_array, **(C)** CGGA_325, **(D)** GSE43378, **(E)** GSE16011, **(F)** GSE74187, **(G)** CGGA_693, and **(H)** GSE82009. **(I)** The forest diagram represents the multifactor Cox regression analysis in which the variables include MLLT11, gender, age, IDH mutation status, 1p19q deletion status, MGMT methylation, and TERT promoter status. **(J)** ROC curve analysis of the model in pan-glioma cohort in TCGA dataset. *p < 0.05, **p < ***p < 0.001.

interaction, synaptic vesicle cycle, cAMP signaling pathway, glutamatergic synapse, and GABAergic synapse (Figure 4B), while the *MLLT11* downregulated DEGs were involved in pathways related to complement and coagulation cascades and arachidonic acid metabolism (Figure 4C). Similarly, in the CGGA_325 dataset and CGGA_array dataset, the *MLLT11* upregulated genes are also mainly enriched in GABAergic synapse, retrograde endocannabinoid signaling, synaptic vesicle cycle, and glutamatergic synapse (Supplementary Figures S2B, S3B). The *MLLT11* downregulated genes were mainly enriched in the pathway of extracellular matrix (ECM)–receptor interaction, protein digestion and absorption, and complement and coagulation cascades (Supplementary Figure 2C). In the biological process category, in TCGA dataset, *MLLT11* upregulated DEG-enriched GO terms were identified, mainly involved in the pathway of the development and regulation of the synapse structure, regulation of membrane potential, and postsynaptic membrane potential (Figure 4D). MLLT11 downregulated DEGs were mainly enriched in the pathway of ECM and extracellular structure organization and regulation of response to wounding and regulation of wound healing (Figure 4E). The same results were also found in CGGA datasets (Supplementary Figures 2D, E, 3C, D). Based on these analyses, *MLLT11* may influence the glioma microenvironment *via* ECM organization and might promote the synapse information to influence the progression of glioma.

Principal component analysis and *MLLT11*-related biological process

Based on the results of clinicopathological characteristics and survival analysis, we deduced that *MLLT11* might play an essential biological function in glioma initiation and progression. To further investigate the biological process

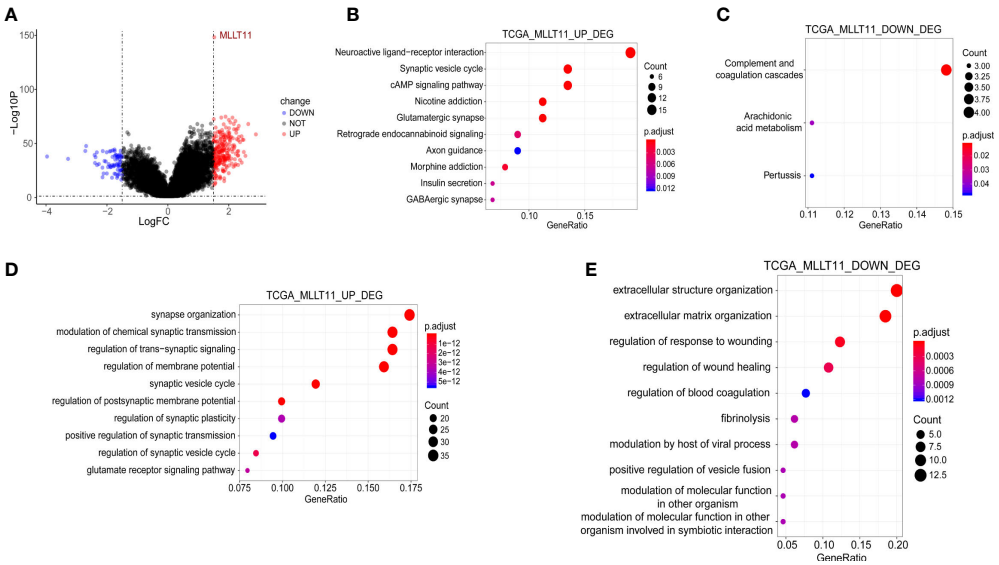

FIGURE 4
Functional enrichment analysis between the MLLT11 high- and low-expression groups in gliomas. **(A)** Differential expression genes (DEGs). **(B, C)** KEGG enrichment analysis of the upregulated genes in the high MLLT11 subgroup and the downregulated genes in the high MLLT11 subgroup. **(D, E)** GO analysis of the upregulated genes in the high MLLT11 subgroup and the downregulated genes in the high MLLT11 subgroup.

associated with *MLLT11* expression, we performed PCA to investigate differences in metabolism status between the low-expression subgroup and high-expression subgroup based on the expression of *MLLT11*. PCA results showed that the contribution of PCA1(Dim1) and PCA2(Dim2) to the total variance accounted for 55.5% and 15.1%, respectively, in TCGA dataset (Figure 5A). Similarly, in the CGGA dataset, Dim1 and Dim2 account for 66.4% and 7% to the total variance, respectively (Figure 5B). Furthermore, we performed KEGG enrichment analyses of the DEGs to explore the difference of metabolism status between the *MLLT11* low-expression and high-expression subgroups in TCGA and CGGA. We found that, in the low-expression subgroup, the DEGs were significantly involved in multiple tumor- and immune-related pathways, such as leukocyte trans-endothelial migration, cytokine–cytokine receptor interaction, intestinal immune network for IgA production, graft-versus-host disease, primary immunodeficiency, autoimmune thyroid disease, glycosaminoglycan degradation, lysosome, ECM–receptor interaction, and glutathione metabolism (Figures 5C, D). However, in the *MLLT11* low-expression subgroup, ubiquitin-mediated proteolysis, taurine and hypotaurine metabolism, WNT signaling pathway, mammalian/mechanistic target of rapamycin (mTOR) signaling pathway, including erb-B1 (EGFR, HER1),erb-B2(HER2)、erb-B3(HER3) and erb-B4 (HER4) (ERBB) signaling pathway, and phosphatidylinositol signaling system were enriched. These results have occurred similarly in other datasets in the CGGA (Supplementary Figures 4A–D). These suggest that the aggressiveness of glioma is associated with an abnormal immune status.

Relationships between *MLLT11* expression and immune cells and immune checkpoint markers

To investigate the mechanism by which high expression of *MLLT11* contributes to a better prognosis, we explored the correlation between *MLLT11* expression and immune infiltrating levels of 22 immune cells by CIBERSORT algorithm, including B cells, T cells, Natural killer (NK) cells, monocytes, macrophages, dendritic cells, mast cells, eosinophils, and neutrophils. Pearson correlation analysis was used to identify immune cells that strongly associated with *MLLT11* expression ($|r| > 0.4$, $p < 0.05$) in the CGGA and TCGA sequencing datasets. Results in TCGA dataset show that the expression of *MLLT11* was positively correlated with the infiltration level of naive $CD4^+$ T cells and $CD8^+$ T cells and negatively correlated with the infiltration level of macrophages, especially M2 macrophages (Figures 6A, B). Similar results were found in CGGA array and CGGA 325 dataset (Supplementary Figures 5A, B). Furthermore, by qPCR, IHC, and Western blotting, in different pathological grades of glioma tissues, we found a significant increase in the expression levels of M2-type macrophage-specific markers with increasing tumor grade, including *CD206*, *CD163*, *ARG1*, *CD115*, and *IL-10* (Figure 7).

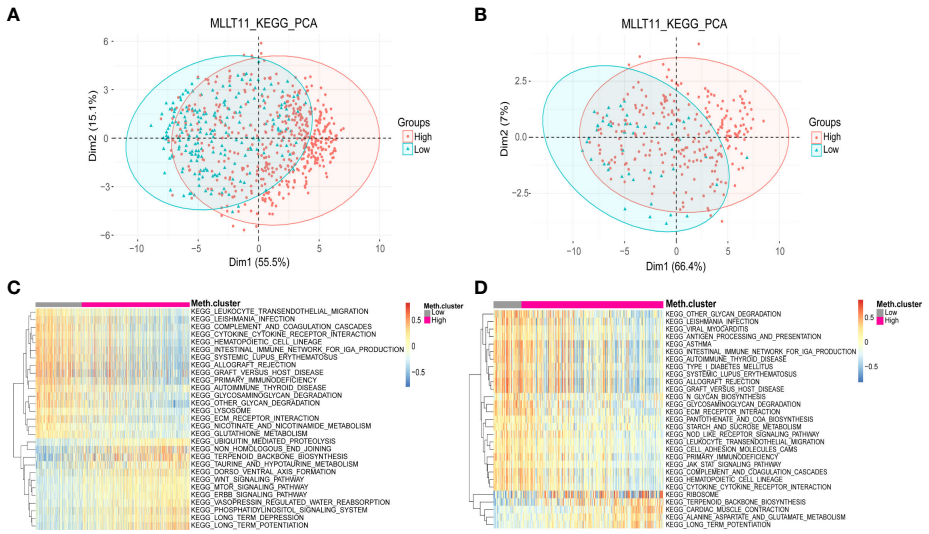

FIGURE 5
Distinct metabolism status in patients with MLLT11 low expression and high expression in glioma. **(A, B)** PCA between the low-expression and high-expression groups based on total DEGs in TCGA and CGGA dataset. **(C, D)** KEGG pathway enrichment analyses of DEGs in MLLT11 low-expression and high-expression groups in TCGA and CGGA dataset.

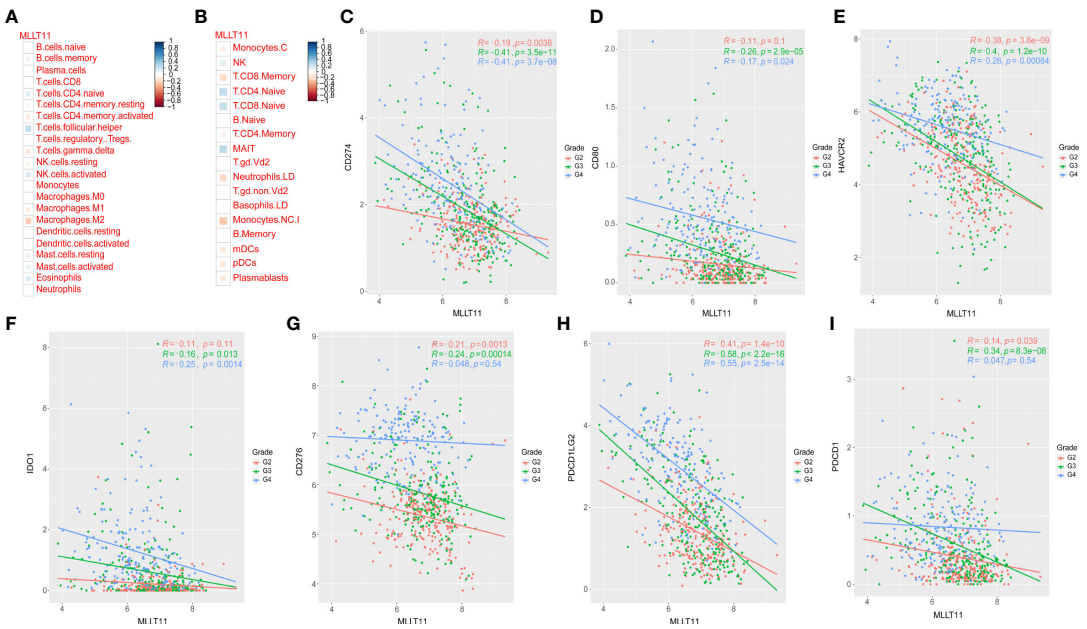

FIGURE 6
Relationships between MLLT11 expression and immune cells and immune checkpoint markers. **(A, B)** Correlation analysis of MLLT11 with 22 immune cells in TCGA dataset. **(C–I)** Correlation between MLLT11 and seven immune checkpoints in TCGA dataset. **(C)** CD274, **(D)** CD80, **(E)** HAVCR2, **(F)** IDO1, **(G)** CD276, **(H)** PDCD1LG2, **(I)** PDCD1.

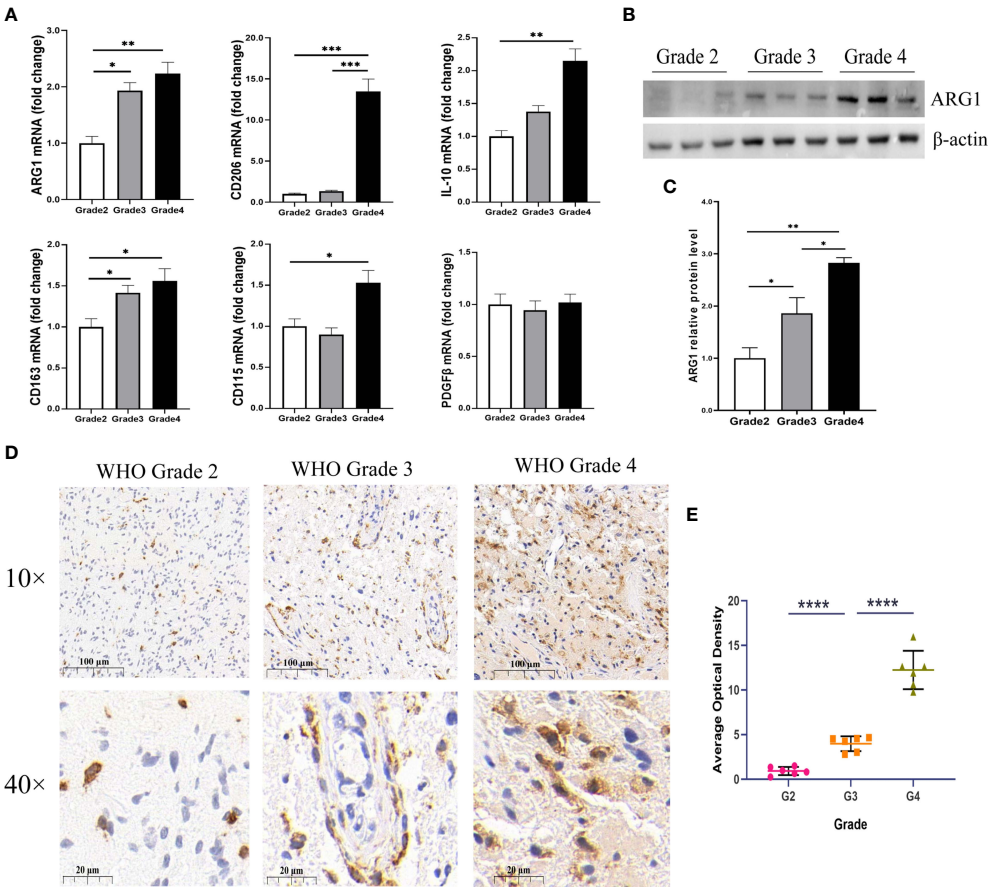

FIGURE 7
Expression of M2 macrophage markers in different WHO pathological grades of glioma. **(A)** The mRNA expression levels of M2-type macrophage-specific markers, including ARG1, CD206, IL-10, CD163, CD115, and PDGFβ in different grades of glioma samples (n = 24). **(B)** Representative Western blotting images of ARG1 and **(C)** bar charts of normalized protein expression levels of ARG1 in different grades of gliomas samples (n = 18). **(D)** Representative images of immunohistochemical (IHC) staining for CD163 in different grades of gliomas (n = 18). **(E)** Quantification of CD163 IHC staining in different pathological grades of gliomas (n = 18). *p < 0.05, **p < 0.01, ***p < 0.001, and ****p < 0.0001.

This may be that in the process of tumor progression, with the decrease of *MLLT11* expression level and the increase of immune infiltration level, the generated M2 immune cells might promote the aggressive process.

Recently, immunotherapy has dramatically advanced in the treatment of cancer. Considering the importance of immune checkpoint molecules for the immune response and immunotherapy, several common immune checkpoint members were enrolled in our analysis and assessed the correlation between *MLLT11* and these immune checkpoints, such as HAVCR2 (TIM-3), CD274 (*PD-L1*), *CD276 (B7-H3)*, *CD80*, *PDCD1*LG2 (PD-L2), *PDCD1* (PD-1), and IDO1. Pearson correlation analysis was performed to explore the relationship between the *MLLT11* expression level and seven immune checkpoints in CGGA dataset and TCGA dataset. In TCGA datasets, among WHO grade 3 glioma, *MLLT11* showed a highly negative correlation with PD-1 ($r = -0.34$, $p = 8.3 \times 10^{-28}$), *PD-L1* ($r = -0.41$, $p = 3.5 \times 10^{-11}$), *TIM3(HAVCR2)* ($r = -0.4$, $p = 1.2 \times 10^{-11}$), and PD-L2 (*PDCD1*LG2) ($r = -0.58$, $p < 2.2 \times 10^{-16}$) (Figure 6). Similarly, a strong negative correlation was found between *MLLT11* and *PD-L1* ($r = -0.41$, $p = 3.7 \times 10^{-8}$), *TIM3 (HAVCR2)* ($r = -0.26$ $p = 8.4 \times 10^{-4}$), and PD-L2(*PDCD1*LG2) ($r = -0.55$, $p = 2.5 \times 10^{-14}$) in GBM (Figure 6). A similar trend can be seen in the CGGA_325 and CGGA_array datasets (Supplementary Figures 6A–G, 7A–G). These findings indicate that *MLLT11* may have a critical role in the immune response; especially when *MLLT11* expression is low, immunotherapy may be more effective.

Discussion

Gliomas account for 80% of all malignant brain tumors, and GBMs occupy about 50% of gliomas. Due to the existence of inter- and intra-glioma heterogeneity, despite the standard treatment of precision surgery, combination of radiotherapy and chemotherapy, and even TTFs, the 5-year survival rate for GBM remains unsatisfactory. Thus, novel therapeutic approaches are needed urgently. However, the origin and progression of glioma are extremely complex processes with multiple steps, and multiple regulators have been confirmed to be involved in the regulation of this process; therefore, exploring and identifying suitable regulators are feasible approaches for the treatment of glioma.

The *MLLT11* gene is primarily responsible for encoding a 9-kDa transmembrane protein and highly expressed in some cancer cell lines and normal hematopoietic tissues (30, 31). Elevated *MLLT11* expression was associated with poor prognosis in several human cancers, such as pediatric acute myeloid leukemia, ovarian cancer, and gastrointestinal malignancy (32, 33). However, in the nervous system, the opposite is true. During embryonic development, studies have shown that *MLLT11* plays an important role in neuronal differentiation and maintenance. Lin et al. (19) found that during the differentiation of neural stem/precursor cells into neurons, the expression of *MLLT11* was significantly upregulated. This indicates that *MLLT11* may play an essential role in neuronal differentiation during CNS development. Our results found that *MLLT11* is highly expressed in normal brain tissues and decreased with the increase of tumor grade. Based on these pieces of evidence, in the CNS, we infer that *MLLT11* is at least involved in promoting differentiation and inhibiting cancer development.

In analyzing the age effect, we found a significant statistical difference in the expression of *MLLT11* between the young and old subgroups. In the old subgroup, the expression of *MLLT11* was low, and *vice versa*. Further analysis stratified by tumor grade indicated that there was no statistical difference in the expression of *MLLT11* between the young and old subgroups in LGG, but in GBM, *MLLT11* expression in the old subgroup was significantly lower than that in the young subgroup. Based on these pieces of evidence, considering that the incidence of GBM is often in elderly patients, we speculated that *MLLT11* may be a gene promoting differentiation and a tumor-suppressive effect, and *MLLT11* may play a key role in the progression of glioma. In addition, 1p19q codeletion and IDH mutation status are of great significance in predicting the prognosis of glioma. Moreover, 1p19q codeletion and IDH mutation suggest a better prognosis. In our analysis, compared with patients with 1p19q codeletion and IDH mutation alone, *MLLT11* expression is higher in the combination of the two, indicating that the expression pattern of *MLLT11* has a similar role in predicting the prognosis of glioma patients as that of 1p19q deletion and IDH mutation.

We further analyzed the expression of *MLLT11* in the RNA-seq data from TCGA and CGGA. It was firmly established that the expression of *MLLT11* was obviously upregulated in TCGA-PN phenotype compared with TCGA-MES. Furthermore, from an scRNA-seq perspective, we deeply analyzed *MLLT11* expression differences in different cell clusters, and the results demonstrated that *MLLT11* was mainly expressed in neoplastic cells, immune cells, and OPC clusters. The *MLLT11* expression in tumor cells was further analyzed to explore the expression distribution in four subtypes of GBM based on single-cell sequencing proposed by Neftel et al. (8). The scRNA-seq analysis suggested that the *MLLT11* expression level in NPC-like subtypes was significantly higher than that of the other three subtypes, AC-like, OPC-like, and MES-like. The bulk PN subtype corresponded to the NPC-like cell subtype, with both subtypes referring to better prognosis in their own classification. Thus, the expression distribution of *MLLT11* in the bulk sample was consistent with that at single-cell sequencing level. Furthermore, survival analysis based on independent datasets from TCGA and CGGA datasets found that high levels of *MLLT11* expression tend to predict better outcomes. These results lead us to believe that *MLLT11* has an important predictive value for glioma prognosis.

In order to further explain the clinical prognostic role of *MLLT11*, we performed KEGG and GO enrichment analysis on the DEGs. The upregulated DEGs of *MLLT11* were mainly enriched in neuroactive ligand–receptor interaction, synapse organization, synaptic vesicle cycle, and the regulation of synapse-related signals, as well as glutamatergic synapse-related signaling pathway. As we all know, epilepsy is a common symptom in patients with glioma and the combination of antiepileptic drugs plays an important role in the treatment of glioma (34, 35). Venkataramani et al. (36) revealed a direct link between neurons and glioma cells through different glioma disease models and clinical tumor specimens and finally confirmed that functional chemical synapses exist between presynaptic neurons and postsynaptic glioma cells. Also known as neuron–glioma synapses (NGSs), these synaptic-like structures play a "bidirectional switch" role in gliomas. For example, alpha-amino-3-hydroxy-5-methyl-4-isoxazole propionic acid (AMAP)-induced currents promote postsynaptic glioma cell proliferation, which in turn triggers electrical activity in presynaptic neurons through NGSs, and this abnormal electrical activity often manifests as seizures in glioma patients (37, 38). Glioma cells and elevated levels of the excitatory neurotransmitter glutamate could disrupt cerebral cortical networks and provoke tumor-associated epileptic conditions (39, 40). Similarly, in this study, we also found that *MLLT11* upregulated DEGs may be related to the pathogenesis of seizures in glioma-related epilepsy (GRE) patients. Moreover, the *MLLT11* downregulated DEGs mainly clustered in ECM-related pathways, suggesting that the progression of tumor is

related to the ECM. The role of the ECM in various cancers has also been proven. For example, the ECM-related pathway is activated and involved in cancer initiation and progression in prostate cancer (41). In gastric cancer, the ECM pathway also plays a pivotal role during tumor invasion and metastasis (42). Also, in colorectal cancer, the ECM participates in the process of epithelial–mesenchymal transition (EMT) and finally leads to tumor malignant progression (43).

In addition, KEGG enrichment analysis was performed on metabolism-related pathways, and the downregulated DEGs were mainly related to leukocyte trans-endothelial migration, complement and coagulation cascades, lysosome, cytokine–cytokine receptor interaction, and ECM–receptor interaction. These pathways are closely related to glioma malignancy. For example, the complement system is considered to be an important system for immune monitoring and homeostasis. It plays an important role in the immune system of organisms. If it is not controlled properly, the immune system can also take action against healthy cells (44, 45). Because glioma patients are often accompanied by lower immunity, we have reason to believe that it is closely related to the complement system. Cytokines are recognized to be key factors in the TME, possessing an immunosuppressive function and inflammatory activity and participating in the progression of GBM (46). Moreover, the ECM–receptor interaction pathways play a role in tumor invasion and metastasis, and the interaction between ECM and the glioma microenvironment is an important contributor to the malignant progression of glioma (47).

Macrophages are the most important immune cells in tumor-related inflammation and play an important role in tumor-related inflammation. At present, macrophages can be divided into two types based on their polarization status: M1-subtype and M2-subtype tumor-associated macrophages (TAMs) (48). M1-subtype TAMs participate in Th1 immune response and have an antitumor effect, while M2 macrophages participate in Th2 immune response and promote tumor growth (49, 50). Previous studies have found that there were a large number of TAMs in GBM. There is a correlation between TAM density and glioma grade, indicating that TAMs support tumor development (51, 52). Interestingly, negative correlations were found in this study between *MLLT11* expression and M2 macrophages, as well as M1 macrophages. It is suggested that, during the progression from low-grade to high-grade glioma, the downregulated *MLLT11* may contribute to recruiting macrophages, which probably mediates the polarization of macrophages to M2, so as to promote tumor progression. In conclusion, our results demonstrate that the expression of *MLLT11* is related to immune cell infiltration and may contribute to the poor prognosis of glioma patients. Further scientific research is needed to explore how glioma cells recruit M2 macrophages during the downregulation of *MLLT11*.

In recent years, immune checkpoint inhibitors (ICI) have brought significant survival benefits to patients in many tumor species. Similarly, preclinical studies have shown that ICIs have great prospects in the treatment of GBM. Therefore, in this study, we also investigated the correlation between *MLLT11* expression and several common immune checkpoint members. Results refer that *MLLT11* had a highly negative correlation with *PDCD1*, *PD-L1*, *TIM3(HAVCR2)*, and PD-L2 (*PDCD1*LG2) in grade 3 glioma analysis. In GBM, *MLLT11* was strongly negatively correlated with *PD-L1*, *TIM3(HAVCR2)*, and PD-L2(*PDCD1*LG2). Based on the above confirmed relationship between *MLLT11* and immune checkpoint, we conclude that *MLLT11* has great potential in tumor immunotherapy, and targeting *MLLT11* and other immune checkpoint molecules is likely to be a novel approach for glioma treatment.

In summary, based on the above bioinformatic analysis and experimental validation in glioma, we systematically explored the expression pattern of *MLLT11* according to the clinicopathologic features, molecular subclasses, and prognosis of glioma. Meanwhile, we also analyzed the relationship between *MLLT11* and immune cells in the TME. These results initially illuminate a critical role for *MLLT11* in the progression of glioma. Further studies are needed to explore *MLLT11* as a novel biomarker or therapeutic mediator in glioma, and relevant pharmaceutical studies targeting *MLLT11* will have great potential.

Data availability statement

Publicly available datasets were analyzed in this study. This data can be found here: UCSC Xena (https://xenabrowser.net/), CGGA website (http://www.cgga.org.cn/), GEO datasets (GSE43378, GSE16011, GSE74187, GSE83300), GTEx databases(http://commonfund.nih.gov/GTEx/).

Ethics statement

This study was reviewed and approved by Ethic Committee of the Xiangya Hospital of Central South University. Written informed consent for participation was not required for this study in accordance with the national legislation and the institutional requirements.

Author contributions

LC and ZX were responsible for project design, experiment implementation, data analysis and manuscript drafting. SW and XL were responsible for the revision of manuscript and supervision of the project, also contributed to the discussion. HZ participant experimental design and provided some technical guidance. CT, HL and QH were responsible for collecting clinical samples, assisting in the implementation of

the experiment and revising the paper. All authors contributed to the article and approved the submitted version.

Funding

This work was supported by the National Natural Science Foundation of China (Grant No. 81770781, 81472594) and Natural Science Foundation of Hunan Province, China (Grant No. 2019JJ50978).

Conflict of interest

The authors declare that the research was conducted in the absence of any commercial or financial relationships that could be construed as a potential conflict of interest.

Publisher's note

All claims expressed in this article are solely those of the authors and do not necessarily represent those of their affiliated organizations, or those of the publisher, the editors and the reviewers. Any product that may be evaluated in this article, or claim that may be made by its manufacturer, is not guaranteed or endorsed by the publisher.

Supplementary material

The Supplementary Material for this article can be found online at: https://www.frontiersin.org/articles/10.3389/fonc.2022.889351/full#supplementary-material

SUPPLEMENTARY FIGURE 1
Clinical and molecular characteristics of MLLT11 for gliomas in TCGA and CGGA datasets. **(A, B)** The relationship between age and MLLT11 expression for different WHO pathological grades in CGGA_array and CGGA_693 datasets. **(C-E)** The expression of MLLT11 between female and male in different WHO pathological grades and normal brain tissues. **(C)** TCGA, **(D)** CGGA_325, **(E)** CGGA_693. **(F, G)** Expression of MLLT11 between 1p19q co deletion and non co deletion for grade 2 and 3 gliomas in TCGA dataset. **(H–M)** Expression of MLLT11 between IDH mutant and wild type. MLLT11 expression levels between IDH mutant and wild-type at different WHO pathological grades. **(H, I)** CGGA_325, **(J, K)** CGGA_693, **(L, M)** CGGA_array.

SUPPLEMENTARY FIGURE 2
Functional enrichment analysis between the MLLT11 high- and low-expression groups for gliomas in CGGA_325 dataset. **(A)** Differential expression genes (DEGs). **(B, C)** KEGG enrichment analysis of the up-regulated gene in the high MLLT11 subgroup and the down-regulated gene in the high MLLT11 subgroup. **(D, E)** GO analysis of the up-regulated gene in the high MLLT11 subgroup and the down-regulated gene in the high MLLT11 subgroup.

SUPPLEMENTARY FIGURE 3
Functional enrichment analysis between the MLLT11 high- and low-expression groups for gliomas in CGGA_array dataset. **(A)** Differential expression genes (DEGs). **(B)** KEGG enrichment analysis of the up-regulated gene in the high MLLT11 subgroup in the high MLLT11 subgroup. **(C, D)** GO analysis of the up-regulated gene in the high MLLT11 subgroup and the down-regulated gene in the high MLLT11 subgroup.

SUPPLEMENTARY FIGURE 4
Distinct metabolism status in patients with MLLT11 low-expression and high-expression in glioma. **(A)** PCA between the low-expression and high-expression groups based on total DEG in CGGA_325 dataset. **(B)** KEGG pathway enrichment analyses of DEGs in MLLT11 low-expression and high-expression groups in CGGA_325 dataset. **(C)** PCA between the low-expression and high-expression groups based on total DEG in CGGA_693 dataset. **(D)** KEGG pathway enrichment analyses of DEGs in MLLT11 low-expression and high-expression groups in CGGA_693 dataset.

SUPPLEMENTARY FIGURE 5
Correlation analysis of MLLT11 with 22 immune cells in CGGA_array **(A)** and CGGA_325 datasets **(B)**.

SUPPLEMENTARY FIGURE 6
Correlation between MLLT11 and seven immune checkpoints in CGGA_325 dataset. **(A)** CD80, **(B)** CD274, **(C)** CD276, **(D)** HAVCR2, **(E)** IDO1, **(F)** PDCD1, **(G)** PDCD1LG2

SUPPLEMENTARY FIGURE 7
Correlation between MLLT11 and seven immune checkpoints in CGGA_array dataset. **(A)** CD80, **(B)** CD274, **(C)** CD276, **(D)** HAVCR2, **(E)** IDO1, **(F)** PDCD1, **(G)** PDCD1LG2

References

1. Louis DN, Perry A, Wesseling P, Brat DJ, Cree IA, Figarella-Branger D, et al. The 2021 WHO classification of tumors of the central nervous system: a summary. *Neuro Oncol* (2021) 23(8):1231–51. doi: 10.1093/neuonc/noab106

2. Zhang H, Wang R, Yu Y, Liu J, Luo T, Fan F. Glioblastoma treatment modalities besides surgery. *J Cancer* (2019) 10(20):4793–806. doi: 10.7150/jca.32475

3. Cancer Genome Atlas Research N, Brat DJ, Verhaak RG, Aldape KD, Yung WK, Salama SR, et al. Comprehensive, integrative genomic analysis of diffuse lower-grade gliomas. *N Engl J Med* (2015) 372(26):2481–98. doi: 10.1056/NEJMoa1402121

4. Jiang T, Mao Y, Ma W, Mao Q, You Y, Yang X, et al. CGCG clinical practice guidelines for the management of adult diffuse gliomas. *Cancer Lett* (2016) 375(2):263–73. doi: 10.1016/j.canlet.2016.01.024

5. Jiang T, Nam DH, Ram Z, Poon WS, Wang J, Boldbaatar D, et al. Clinical practice guidelines for the management of adult diffuse gliomas. *Cancer Lett* (2021) 499:60–72. doi: 10.1016/j.canlet.2020.10.050

6. Verhaak RG, Hoadley KA, Purdom E, Wang V, Qi Y, Wilkerson MD, et al. Integrated genomic analysis identifies clinically relevant subtypes of glioblastoma characterized by abnormalities in PDGFRA, IDH1, EGFR, and NF1. *Cancer Cell* (2010) 17(1):98–110. doi: 10.1016/j.ccr.2009.12.020

7. Wang Q, Hu B, Hu X, Kim H, Squatrito M, Scarpace L, et al. Tumor evolution of glioma-intrinsic gene expression subtypes associates with immunological changes in the microenvironment. *Cancer Cell* (2017) 32(1):42–56.e6. doi: 10.1016/j.ccell.2017.06.003

8. Neftel C, Laffy J, Filbin MG, Hara T, Shore ME, Rahme GJ, et al. An integrative model of cellular states, plasticity, and genetics for glioblastoma. *Cell* (2019) 178(4):835–49.e21. doi: 10.1016/j.cell.2019.06.024

9. Gieryng A, Pszczolkowska D, Walentynowicz KA, Rajan WD, Kaminska B. Immune microenvironment of gliomas. *Lab Invest* (2017) 97(5):498–518. doi: 10.1038/labinvest.2017.19

10. Tiberio P, Cavadini E, Callari M, Daidone MG, Appierto V. AF1q: a novel mediator of basal and 4-HPR-induced apoptosis in ovarian cancer cells. *PloS One* (2012) 7(6):e39968. doi: 10.1371/journal.pone.0039968

11. Tse W, Zhu W, Chen HS, Cohen A. A novel gene, AF1q, fused to MLL in t (1,11) (q21;q23), is specifically expressed in leukemic and immature hematopoietic cells. *Blood* (1995) 85(3):650–6. doi: 10.1182/blood.V85.3.650.bloodjournal853650

12. Xiong Y, Li Z, Ji M, Tan AC, Bemis J, Tse JV, et al. MIR29B regulates expression of MLLT11 (AF1Q), an MLL fusion partner, and low MIR29B expression associates with adverse cytogenetics and poor overall survival in AML. *Br J Haematol* (2011) 153(6):753–7. doi: 10.1111/j.1365-2141.2011.08662.x

13. Strunk CJ, Platzbecker U, Thiede C, Schaich M, Illmer T, Kang Z, et al. Elevated AF1q expression is a poor prognostic marker for adult acute myeloid leukemia patients with normal cytogenetics. *Am J Hematol* (2009) 84(5):308–9. doi: 10.1002/ajh.21396

14. Co NN, Tsang WP, Tsang TY, Yeung CL, Yau PL, Kong SK, et al. AF1q enhancement of gamma irradiation-induced apoptosis by up-regulation of BAD expression *via* NF-kappaB in human squamous carcinoma A431 cells. *Oncol Rep* (2010) 24(2):547–54. doi: 10.3892/OR_00000891

15. Liao J, Chen H, Qi M, Wang J, Wang M. MLLT11-TRIL complex promotes the progression of endometrial cancer through PI3K/AKT/mTOR signaling pathway. *Cancer Biol Ther* (2022) 23(1):211–24. doi: 10.1080/15384047.2022.2046450

16. Stanton-Turcotte D, Hsu K, Moore SA, Yamada M, Fawcett JP, Iulianella A. Mllt11 regulates migration and neurite outgrowth of cortical projection neurons during development. *J Neurosci* (2022) 42(19):3931–48. doi: 10.1523/JNEUROSCI.0124-22.2022

17. Parcelier A, Maharzi N, Delord M, Robledo-Sarmiento M, Nelson E, Belakhdar-Mekid H, et al. AF1q/MLLT11 regulates the emergence of human prothymocytes through cooperative interaction with the notch signaling pathway. *Blood* (2011) 118(7):1784–96. doi: 10.1182/blood-2011-01-333179

18. Tse W, Deeg HJ, Stirewalt D, Appelbaum FR, Radich J, Gooley T. Increased AF1q gene expression in high-risk myelodysplastic syndrome. *Br J Haematol* (2005) 128(2):218–20. doi: 10.1111/j.1365-2141.2004.05306.x

19. Lin HJ, Shaffer KM, Sun Z, Jay G, He WW, Ma W. AF1q, a differentially expressed gene during neuronal differentiation, transforms HEK cells into neuron-like cells. *Brain Res Mol Brain Res* (2004) 131(1-2):126–30. doi: 10.1016/j.molbrainres.2004.07.022

20. Park J, Hwang JY, Thore A, Kim S, Togano T, Hagiwara S, et al. AF1q inhibited T cell attachment to breast cancer cell by attenuating intracellular adhesion molecule-1 expression. *J Cancer Metastasis Treat* (2019) 5:17. doi: 10.20517/2394-4722.2018.84

21. Patel AP, Tirosh I, Trombetta JJ, Shalek AK, Gillespie SM, Wakimoto H, et al. Single-cell RNA-seq highlights intratumoral heterogeneity in primary glioblastoma. *Science* (2014) 344(6190):1396–401. doi: 10.1126/science.1254257

22. Darmanis S, Sloan SA, Croote D, Mignardi M, Chernikova S, Samghababi P, et al. Single-cell RNA-seq analysis of infiltrating neoplastic cells at the migrating front of human glioblastoma. *Cell Rep* (2017) 21(5):1399–410. doi: 10.1016/j.celrep.2017.10.030

23. Robin X, Turck N, Hainard A, Tiberti N, Lisacek F, Sanchez JC, et al. pROC: an open-source package for r and s+ to analyze and compare ROC curves. *BMC Bioinf* (2011) 12:77. doi: 10.1186/1471-2105-12-77

24. Yu G, Wang LG, Han Y, He QY. clusterProfiler: an r package for comparing biological themes among gene clusters. *OMICS* (2012) 16(5):284–7. doi: 10.1089/omi.2011.0118

25. Barbie DA, Tamayo P, Boehm JS, Kim SY, Moody SE, Dunn IF, et al. Systematic RNA interference reveals that oncogenic KRAS-driven cancers require TBK1. *Nature* (2009) 462(7269):108–12. doi: 10.1038/nature08460

26. Hanzelmann S, Castelo R, Guinney J. GSVA: gene set variation analysis for microarray and RNA-seq data. *BMC Bioinf* (2013) 14:7. doi: 10.1186/1471-2105-14-7

27. Gentles AJ, Newman AM, Liu CL, Bratman SV, Feng W, Kim D, et al. The prognostic landscape of genes and infiltrating immune cells across human cancers. *Nat Med* (2015) 21(8):938–45. doi: 10.1038/nm.3909

28. Monaco G, Lee B, Xu W, Mustafah S, Hwang YY, Carre C, et al. RNA-Seq signatures normalized by mRNA abundance allow absolute deconvolution of human immune cell types. *Cell Rep* (2019) 26(6):1627–40.e7. doi: 10.1016/j.celrep.2019.01.041

29. Phillips HS, Kharbanda S, Chen R, Forrest WF, Soriano RH, Wu TD, et al. Molecular subclasses of high-grade glioma predict prognosis, delineate a pattern of disease progression, and resemble stages in neurogenesis. *Cancer Cell* (2006) 9 (3):157–73. doi: 10.1016/j.ccr.2006.02.019

30. Busson-Le Coniat M, Salomon-Nguyen F, Hillion J, Bernard OA, Berger R. MLL-AF1q fusion resulting from t(1;11) in acute leukemia. *Leukemia* (1999) 13 (2):302–6. doi: 10.1038/sj.leu.2401299

31. Zhang HP, Chen QK, Xu JF. LPAR5 stimulates the malignant progression of non-small-cell lung carcinoma by upregulating MLLT11. *Eur Rev Med Pharmacol Sci* (2020) 24(17):8902–10. doi: 10.26355/eurrev_202009_22831

32. Tse W, Meshinchi S, Alonzo TA, Stirewalt DL, Gerbing RB, Woods WG, et al. Elevated expression of the AF1q gene, an MLL fusion partner, is an independent adverse prognostic factor in pediatric acute myeloid leukemia. *Blood* (2004) 104(10):3058–63. doi: 10.1182/blood-2003-12-4347

33. Tiberio P, Lozneanu L, Angeloni V, Cavadini E, Pinciroli P, Callari M, et al. Involvement of AF1q/MLLT11 in the progression of ovarian cancer. *Oncotarget* (2017) 8(14):23246–64. doi: 10.18632/oncotarget.15574

34. van Breemen MS, Rijsman RM, Taphoorn MJ, Walchenbach R, Zwinkels H, Vecht CJ. Efficacy of anti-epileptic drugs in patients with gliomas and seizures. *J Neurol* (2009) 256(9):1519–26. doi: 10.1007/s00415-009-5156-9

35. Goldstein ED, Feyissa AM. Brain tumor related-epilepsy. *Neurol Neurochir Pol* (2018) 52(4):436–47. doi: 10.1016/j.pjnns.2018.06.001

36. Venkataramani V, Tanev DI, Strahle C, Studier-Fischer A, Fankhauser L, Kessler T, et al. Glutamatergic synaptic input to glioma cells drives brain tumour progression. *Nature* (2019) 573(7775):532–8. doi: 10.1038/s41586-019-1564-x

37. Labrakakis C, Patt S, Hartmann J, Kettenmann H. Glutamate receptor activation can trigger electrical activity in human glioma cells. *Eur J Neurosci* (1998) 10(6):2153–62. doi: 10.1046/j.1460-9568.1998.00226.x

38. Osswald M, Jung E, Sahm F, Solecki G, Venkataramani V, Blaes J, et al. Brain tumour cells interconnect to a functional and resistant network. *Nature* (2015) 528(7580):93–8. doi: 10.1038/nature16071

39. Campbell SL, Buckingham SC, Sontheimer H. Human glioma cells induce hyperexcitability in cortical networks. *Epilepsia* (2012) 53(8):1360–70. doi: 10.1111/j.1528-1167.2012.03557.x

40. Ruda R, Trevisan E, Soffietti R. Epilepsy and brain tumors. *Curr Opin Oncol* (2010) 22(6):611–20. doi: 10.1097/CCO.0b013e32833de99d

41. Andersen MK, Rise K, Giskeodegard GF, Richardsen E, Bertilsson H, Storkersen O, et al. Integrative metabolic and transcriptomic profiling of prostate cancer tissue containing reactive stroma. *Sci Rep* (2018) 8(1):14269. doi: 10.1038/s41598-018-32549-1

42. Yan P, He Y, Xie K, Kong S, Zhao W. In silico analyses for potential key genes associated with gastric cancer. *PeerJ* (2018) 6:e6092. doi: 10.7717/peerj.6092

43. Rahbari NN, Kedrin D, Incio J, Liu H, Ho WW, Nia HT, et al. Anti-VEGF therapy induces ECM remodeling and mechanical barriers to therapy in colorectal cancer liver metastases. *Sci Transl Med* (2016) 8(360):360ra135. doi: 10.1126/scitranslmed.aaf5219

44. Schmidt CQ, Verschoor A. Complement and coagulation: so close, yet so far. *Blood* (2017) 130(24):2581–2. doi: 10.1182/blood-2017-10-811943

45. Ricklin D, Hajishengallis G, Yang K, Lambris JD. Complement: a key system for immune surveillance and homeostasis. *Nat Immunol* (2010) 11(9):785–97. doi: 10.1038/ni.1923

46. Albulescu R, Codrici E, Popescu ID, Mihai S, Necula LG, Petrescu D, et al. Cytokine patterns in brain tumour progression. *Mediators Inflamm* (2013) 2013:979748. doi: 10.1155/2013/979748

47. Cui X, Morales RT, Qian W, Wang H, Gagner JP, Dolgalev I, et al. Hacking macrophage-associated immunosuppression for regulating glioblastoma angiogenesis. *Biomaterials.* (2018) 161:164–78. doi: 10.1016/j.biomaterials.2018.01.053

48. Sielska M, Przanowski P, Wylot B, Gabrusiewicz K, Maleszewska M, Kijewska M, et al. Distinct roles of CSF family cytokines in macrophage infiltration and activation in glioma progression and injury response. *J Pathol* (2013) 230(3):310–21. doi: 10.1002/path.4192

49. Staudt ND, Jo M, Hu J, Bristow JM, Pizzo DP, Gaultier A, et al. Myeloid cell receptor LRP1/CD91 regulates monocyte recruitment and angiogenesis in tumors. *Cancer Res* (2013) 73(13):3902–12. doi: 10.1158/0008-5472.CAN-12-4233

50. Cao X, Lai SWT, Chen S, Wang S, Feng M. Targeting tumor-associated macrophages for cancer immunotherapy. *Int Rev Cell Mol Biol* (2022) 368:61–108. doi: 10.1016/bs.ircmb.2022.02.002

51. Yin W, Ping YF, Li F, Lv SQ, Zhang XN, Li XG, et al. A map of the spatial distribution and tumour-associated macrophage states in glioblastoma and grade-4 IDH-mutant astrocytoma. *J Pathol* (2022). doi: 10.1002/path.5984

52. Andersen JK, Miletic H, Hossain JA. Tumor-associated macrophages in gliomas-basic insights and treatment opportunities. *Cancers (Basel)* (2022) 14 (5):1319. doi: 10.3390/cancers14051319

frontiers | Frontiers in Immunology

TYPE Original Research
PUBLISHED 21 December 2022
DOI 10.3389/fimmu.2022.842524

Check for updates

OPEN ACCESS

EDITED BY
Wen Cheng,
The First Affiliated Hospital of China Medical University, China

REVIEWED BY
Mian Guo,
The Second Affiliated Hospital of Harbin Medical University, China
Jianxiong Ji,
Zhejiang University, China

*CORRESPONDENCE
Yu Long
yu.long@hrbmu.edu.cn
Ruohan Sun
ruohan.sun@hrbmu.edu.cn

†These authors have contributed equally to this work and share first authorship

SPECIALTY SECTION
This article was submitted to Cancer Immunity and Immunotherapy, a section of the journal Frontiers in Immunology

RECEIVED 23 December 2021
ACCEPTED 28 November 2022
PUBLISHED 21 December 2022

CITATION
Mu L, Han Z, Yu S, Wang A, Chen D, Kong S, Gu Y, Xu L, Liu A, Sun R and Long Y (2022) Pan-cancer analysis of ASB3 and the potential clinical implications for immune microenvironment of glioblastoma multiforme. *Front. Immunol.* 13:842524. doi: 10.3389/fimmu.2022.842524

COPYRIGHT
© 2022 Mu, Han, Yu, Wang, Chen, Kong, Gu, Xu, Liu, Sun and Long. This is an open-access article distributed under the terms of the Creative Commons Attribution License (CC BY). The use, distribution or reproduction in other forums is permitted, provided the original author(s) and the copyright owner(s) are credited and that the original publication in this journal is cited, in accordance with accepted academic practice. No use, distribution or reproduction is permitted which does not comply with these terms.

Pan-cancer analysis of ASB3 and the potential clinical implications for immune microenvironment of glioblastoma multiforme

Long Mu[1†], Zhibin Han[1†], Shengkun Yu[1†], Aowen Wang[1†], Dongjiang Chen[2], Sijia Kong[3], Yifei Gu[1], Lin Xu[1], Axiang Liu[1], Ruohan Sun[4*] and Yu Long[1*]

[1]Department of Neurosurgery, The First Affiliated Hospital of Harbin Medical University, Harbin, China, [2]Division of Neuro-Oncology and Preston A. Wells, Jr. Center for Brain Tumor Therapy, Lillian S. Wells Department of Neurosurgery, University of Florida, Gainesville, FL, United States, [3]Obstetrics and Gynecology Department, Peking University Shenzhen Hospital, Shenzhen, China, [4]Department of Neurology, The First Affiliated Hospital of Harbin Medical University, Harbin, China

Background: Ankyrin repeat and SOCS Box containing 3 (ASB3) is an E3 ubiquitin ligase. It has been reported to regulate the progression of some cancers, but no systematic pan-cancer analysis has been conducted to explore its function in prognosis and immune microenvironment.

Method: In this study, mRNA expression data were downloaded from TCGA and GTEx database. Next generation sequencing data from 14 glioblastoma multiforme (GBM) samples by neurosurgical resection were used as validation dataset. Multiple bioinformatics methods (ssGSEA, Kaplan-Meier, Cox regression analysis, GSEA and online tools) were applied to explore ASB3 expression, gene activity, prognosis of patients in various cancers, and its correlation with clinical information, immune microenvironment and pertinent signal pathways in GBM. The biological function of ASB3 in tumor-infiltrating lymphocytes (TILs) was verified using an animal model.

Results: We found that ASB3 was aberrant expressed in a variety of tumors, especially in GBM, and significantly correlated with the prognosis of cancer patients. The level of ASB3 was related to the TMB, MSI and immune cell infiltration in some cancer types. ASB3 had a negative association with immune infiltration and TME, including regulatory T cells (Tregs), cancer-associated fibroblasts, immunosuppressors and related signaling pathways in GBM. ASB3 overexpression reduced the proportion of Tregs in TILs. GSEA and PPI analysis also showed negative correlation between ASB3 expression and oncogenetic signaling pathways in GBM.

Conclusion: A comprehensive pan-cancer analysis of ASB3 showed its potential function as a biomarker of cancer prognosis and effective prediction of immunotherapy response. This study not only enriches the understanding of the biological function of ASB3 in pan-cancer, especially in GBM immunity, but also provides a new reference for the personalized immunotherapy of GBM.

KEYWORDS

glioblastoma multiforme, E3 ubiquitin ligases, ASB3, tumor microenvironment, Tregs

Introduction

Cancer is the leading cause of death in every country in the world and an important obstacle to improving life expectancy, there is no absolute cure for cancer today (1, 2). Glioblastoma multiforme (GBM) is the most common malignant primary brain tumor with 49.1% of malignant brain tumors (3). Although the comprehensive treatment of GBM has made progress including surgery, radiotherapy and chemotherapy, the overall prognosis is still poor and the long-term survival rate remains low (4).

In recent years, cancer immunotherapy has become a prominent cancer treatment, especially immune checkpoint inhibitors (ICIs) therapy (5). Previous studies have shown that the disturbance of tumor microenvironment (TME), especially the tumor immune microenvironment (TIME), is one of the main causes of tumor malignant progression (6). However, many cancer patients do not achieve a persistent response to currently available antigens (7). The immune system in the brain follows different principles from the immune system elsewhere, not only is the access to the tumor restricted by the blood-brain barrier (BBB), but the host is subjected to considerable endogenous and therapeutically induced immunosuppression (8). Hence, exploring novel immunotherapeutic biomarkers, especially from GBM, can help cancer patients to formulate precise immunotherapy strategies and achieve more durable immune responses.

The ubiquitin-proteasome system (UPS) is one of the most important ways to regulate protein levels and a series of physiological and pathological processes in various organisms, controlling most proteins *via* ubiquitination and deubiquitination of substrates (9). The ankyrin repeat and suppressor of cytokine signaling (SOCS) box containing (ASB) family is comprised of 18 proteins and belongs to the SOCS box protein superfamily, they interact with Cul5-Rbx2 to form E3 ubiquitin ligases (E3s) and play important roles through ubiquitination-mediated pathway (10). The ASB3 gene from the ASB family is located on chromosome 2p16.2, which has 3 transcriptional variants encoding 2 isoforms. The ASB3 protein contains 518 amino acid residues, constituting 11 linked ankyrin repeats, followed by a SOCS box domain at the C-terminal of the peptide chain (11). ASB3 has been reported to play important roles in a variety of biological processes. In hepatocellular carcinoma (HCC), ASB3 knockdown promotes mitochondrial apoptosis by activating the interdependent cleavage of Beclin1 and caspase-8 (12). The mutations and down-regulated expression of ASB3 gene promote the growth and metastasis of colorectal cancer (CRC) cells (13). Furthermore, ASB3 mediates ubiquitination and degradation of tumor necrosis factor receptor II (TNFR2) (14). At present, there are few systematic studies on ASB3 in pan-cancer, especially in GBM.

In this study, we applied multiple bioinformatics methods to explore the expression level and gene activity of ASB3 in pan-cancer. Meanwhile, the relationship between ASB3 and GBM TME and its related signaling pathways was comprehensively analyzed in combination with public databases and sequencing data of patients in our institution. The role of ASB3 expression in the TIME was biologically validated using an animal model. The results indicate that ASB3 may be a potential target for future cancer immunotherapy development.

Materials and methods

Clinical samples collection

During the period from 2019 to 2021, surgically resected samples from glioma patients were collected, and postoperative pathology showed GBM. With the consent of the patients or their families, partial samples were collected and stored in a -80° C refrigerator. This study has been approved by the Ethics Committee of the First Affiliated Hospital of Harbin Medical University, and all patients or their families consented. Samples were sent to Novogene (https://novogene.com/) for quality inspection and sequencing. The raw data has been deposited in NCBI's Sequence Read Archive (SRA, PRJNA786896).

Data source

The gene expression RNA-seq mRNA profiles of GTEx (Genotype-Tissue Expression) cohorts of brain and GDC TCGA (The Cancer Genome Atlas) cohorts of 33 cancer types, and their relevant clinical information were downloaded from UCSC Xena (https://xena.ucsc.edu/). The gene list of E3s and deubiquitinating enzymes (DUBs) were downloaded from iUUCD (The Integrated Annotations for Ubiquitin and Ubiquitin-like Conjugation Database, http://iuucd.biocuckoo.org/) (15, 16).

Pan-cancer analysis

After removing 8 cancer types without normal tissues, the mRNA expression data from 25 cancer types (BRCA, BLCA, COAD, CESC, CHOL, ESCA, GBM, HNSC, KIRP, KICH, KIRC, LGG, LIHC, LUSC, LUAD, PRAD, PAAD, PCPG, READ, SARC, SKCM, STAD, THYM, THCA and UCEC) were used to analyze ASB3 expression in normal and tumor tissues by Limma with a cutoff ($P < 0.05$). The ssGSEA (single-sample Gene Set Enrichment Analysis) was used to explore the gene activity of ASB3 by the R package "GSVA". Patients were divided into ASB3 high expression group and low expression group according to the median value of ASB3 expression. Kaplan-Meier (KM) curves and Cox regression were used for evaluating the effect of ASB3 mRNA expression on the survival time and prognosis of patients with cancer. The correlation between ASB3 expression and tumor mutational burden (TMB) or microsatellite instability (MSI) were calculated utilizing the Spearman's rank correlation coefficient by the R package "fmsb".

TME and TIME analysis

Estimation of STromal and Immune cells in MAlignant Tumours using Expression data (ESTIMATE) is an evaluation method to infer immune cells, stromal cells, and tumor purity in tumor samples according to gene expression characteristics (17). We used the R package "estimate" to obtain the infiltration levels of immune cells and stromal cells from the expression profile of GBM, and applied the Spearman's rank correlation coefficient to evaluate their correlation with the mRNA expression level of ASB3. TISIDB (http://cis.hku.hk/TISIDB/) is an online website tool integrating a variety of data types and public databases, which provides multiple interactive information between tumor and the immune system (18). Tumor Immune Estimation Resource (TIMER) is a comprehensive tool for analyzing immune infiltrates of various cancers in a systematic way (19). TISIDB and TIMER were used to investigate the connection between ASB3 and multiple cancer immune microenvironments in the aspects of immune cell infiltration and immunosuppressor.

Gene set enrichment analysis (GSEA)

GSEA is a widely-used computational method, which can extract effective biological insights from a large number of gene expression data (20, 21). It was applied to explore the biological pathways related to the ASB3 by using mRNA expression data from TCGA and clinical samples from neurosurgical resection of GBM patients.

Functional enrichment analysis and PPI network construction

To explore the potential function of ASB3 in GBM, GSEA and Gene Ontology (GO) or Kyoto Encyclopedia of Genes and Genomes (KEGG) analyses were applied to identify signaling pathways most correlated with ASB3 by using mRNA expression data from TCGA. The protein-protein interaction (PPI) network was established by Metascape using genes negatively associated with ASB3. Cytoscape is a network visualization software program, and the plug-in Molecular COmplex DEtection (MCODE) can identify the most critical modules.

Murine glioma lines

Mice glioma cell line (GL261) was gifted from Dr. Anhua Wu (The First Hospital of China Medical University, Shenyang, China). Cells were incubated at 37°C in an incubator with a gas environment of 5% CO_2, and the medium used was Dulbecco's modified eagle medium (DMEM) (C11995500BT, Gibco) containing 10% fetal bovine serum (FB15015, Clark) and a 1% penicillin-streptomycin mixture (15140-122, Gibco). The ASB3 overexpression sequence (NM_023906.3) was constructed by Comate Bioscience Co. Ltd. The recombinant lentivirus was prepared by transfecting pLVX-IRES-ZsGreen1 Vector (PT4064-5, ClonTech), pSPAX2 and pMD2.G (Hunan Fenghui Biotechnology) into 293T cells. After the lentiviral transfection, GL261 cells were cultured in a single clone by limiting dilution.

Real-time quantitative reverse transcription-PCR

Total RNA was isolated from GL261 cells using E.Z.N.A.® Total RNA Kit I (R6834, Omega). Then, the RNA concentration was determined using a NanoDrop One Spectrophotometer (Thermo Fisher Scientific), and reverse transcription was performed to obtain cDNA (RR047A, Takara). Finally, the expression level of ASB3 was determined through RT-qPCR using the Applied Biosystems StepOne machine (Applied

Biosystems) and SYBR Green (4913914001, Roche). Primers for β-actin and ASB3 were purchased from Comate Bioscience Co. Ltd., with the following sequences: β-actin-F:5'-GTGACGTTGACATCCGTAAAGA-3'; β-actin-R:5'-GCCGGACTCATCGTACTCC-3'; ASB3-F:5'-TTGAAGTATGGAGCCCAGTTA-3'; ASB3-R:5'-CCAGCAAGCAGGAGATGTG-3'. Relative quantification of the gene expression was carried out *via* the double delta Ct analysis.

Western blotting

GL261 cells were lysed in RIPA buffer (P0013E, Beyotime) containing protease inhibitor (BL612A, Biosharp) and phosphatase inhibitor (AR1183, Boster) cocktail. Protein concentration was measured using a BCA assay (P0010S, Beyotime). Anti-ASB3 (AP16752a, Abcepta) was used as the primary antibody, anti-GAPDH (10494-1-AP, Proteintech) was used as the control, and IRDye® 800CW Goat anti-Rabbit IgG (D10629-12, LI-COR) was used as the secondary antibody. Western blotting was detected automatically using the Odyssey Infrared Imaging System (LI-COR).

Brain tumor mice models

All *in vivo* experiments were conducted in accordance with protocols approved by the Animal Experimental Center of First Affiliated Hospital of Harbin Medical University and followed guidelines for animal welfare. Female C57BL/6 mice (6- to 8-week-old) were purchased from Liaoning Changsheng biotechnology co., Ltd. Mice were anesthetized and 1×10^5 GL261 or ASB3 overexpression GL261 tumor cells in a 5μL volume were intracranially injected at 2.0mm lateral to the bregma at a depth of 3.0mm below the dura mater with a sterile Hamilton syringe fitted with a 26-gauge needle. Humanitarian endpoints were reached when animals exhibited the following deficits: (i) reluctant to move, (ii) weight loss >20% body weight, (iii) hunched posture, and (iv) lethargy.

Flow cytometry analysis

Tumor-infiltrating lymphocytes (TILs) were collected from 37%, and 70% of the interface of Percoll (17-0891-09, GE Pharmacia) gradient, centrifuged at 500 × g for 30 minutes and washed once. Flow cytometry was performed using NovoCyte 2070R (Agilent Technologies). The viability of TILs was determined using the Zombie Red™ Fixable Viability Kit (423109, BioLegend). Cell surface staining antibodies, anti-CD3 (145-2C11), anti-CD4 (GK1.5), anti-CD8 (53-6.7), anti-PD-1 (RMP1-30), were purchased from BioLegend. The level of FOXP3 (Forkhead Box P3) were determined by intracellular staining using the True-Nuclear™ Transcription Factor Buffer Set (BioLegend) and anti-FOXP3 (FJK-16s, eBioscience). Appropriate isotype controls were used. All FCS data were analyzed using FlowJo 10.3 software.

Immunohistochemistry

Paraffin sections with a thickness of 4μm were dewaxed and hydration in xylene and concentration gradient ethanol. Antigen repair was performed in EDTA buffer and heated under microwave for 18 minutes. Blocking was done using 5% BSA to reduce nonspecific staining. ASB3 (bs-7736R, Bioss) primary antibody working solution was added dropwise to the slides and placed in a wet box overnight at 4°C. The following day, after treatment according to the instructions of SABC-AP kit (SA1052, Boster), the exposed ASB3 protein was labeled with 0.01% DAB chromogenic solution and the nuclei were stained with hematoxylin. The staining results were observed under a light microscope.

Statistical analysis

R software (v4.0.5) was used to analyze statistics. Identification of differentially expressed genes was assessed by Limma package with Wilcox Test (P filter = 0.05, $\log_2$FC filter = 2). The relation between various clinical characteristics of GBM patients and ASB3 expression was detected using Wilcoxon or Kruskal-Wallis tests. $P < 0.05$ represented significance in statistics. Experimental data are presented as mean ± SEM. Mann-Whitney tests were used to determine significant differences between two groups. Statistical analyses were performed using GraphPad Prism 9 software. P values of less than 0.05 were considered significant (*, $P < 0.05$; **, $P < 0.01$; ***, $P < 0.001$).

Results

Pan-cancer analysis of ASB3 expression

Through the conjoint analysis of transcriptome data of normal brain tissues from GTEx and GBM samples from TCGA, we identified 1923 differentially expressed mRNAs and 149 mRNAs related to the survival of GBM patients. ASB3 was chosen to do the next analysis (Figure 1). In comparison with normal tissues, ASB3 mRNA expression was markedly upregulated in 10 types of tumors (BLCA, COAD, CHOL, ESCA, HNSC, KIRC, LUAD, LIHC, LUSC and STAD), and was notably downregulated in 5 cancer types (LGG, GBM, KICH, PRAD and UCEC, Figure 2A). We sorted the tumor types according to the gene expression levels of ASB3

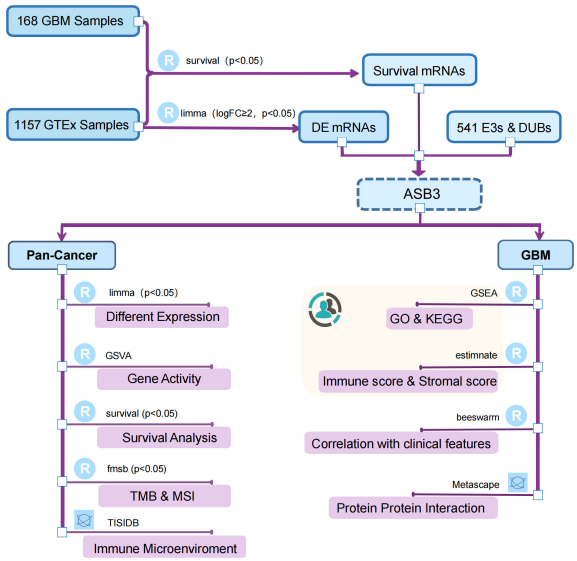

FIGURE 1
Flow chart of this study. The canary yellow background indicates an independent dataset validation from GBM patients of our institution.

(Figure 2B). Box plots demonstrated the significant different expression distribution of ASB3 across tumor and normal samples in 15 cancer types (Figure 2C). ASB3 was dysregulated in many kinds of cancers, particularly in GBM, illustrating ASB3 might have certain functions in GBM and other cancers.

Pan-cancer analysis of ASB3 activity

We calculated the ASB3 gene activity of each sample by the ssGSEA algorithm and compared the ASB3 gene activity between normal and tumor groups. The results indicated that ASB3 gene activity was decreased in 4 cancer types including BRCA, GBM, THCA and UCEC, and was increased in 9 cancer types involving COAD, LGG, CHOL, LIHC, KIRP, KICH, KIRC, HNSC and PCPG compared with normal group (Figure 3A). According to the ranking of ASB3 gene activity in 33 cancer types, LGG and GBM were found to have the highest gene activity (Figure 3B). Box plots showed the significant different activity distribution of ASB3 across normal and tumor samples in 13 cancer types (Figure 3C). Based on the above results, we could infer that ASB3 plays a crucial role in GBM.

Pan-cancer survival analysis of ASB3 expression

To assess the prognostic value of ASB3, survival analysis was conducted in pan-cancer. We found that high-expressed ASB3 led to a worse prognosis in ACC, LIHC, KIRC and KICH. On the contrary, patients with high-expressed ASB3 had a better survival time in GBM, LUAD, SKCM and THYM (Figure 4). ASB3 may has diverse prognostic value in different cancers.

Correlation of ASB3 and TMB or MSI in pan-cancer

By analyzing the relationship between ASB3 expression and TMB or MSI, we found that ASB3 was positively correlation with TMB in ACC, SKCM, MESO, LUSC and BLCA, conversely with TMB in THYM, PRAD and ESCA (Figure S1A). ASB3 was positively related with MSI in UCEC, THCA, SKCM, READ, LUSC, HNSC and COAD, negatively related with MSI in TGCT, KIRP, KIRC, GBM and CESC (Figure S1B). Thus, ASB3 may be used as the judgment index of TMB and MSI.

Correlation of ASB3 expression with clinical characteristics of GBM

The TCGA RNA-seq data and clinical information were to explore the correlation between ASB3 expression and clinical features in GBM patients. The results shown that the expression level of ASB3 was lower in IDH wild-type patients (Figure S2A). ASB3 expression in classical and neural subtypes of GBM are higher than mesenchymal and proneural subtypes (Figure S2B). The expression of ASB3 is not related to radiotherapy, MGMT methylation, chemotherapy and age (Figures S2C–F).

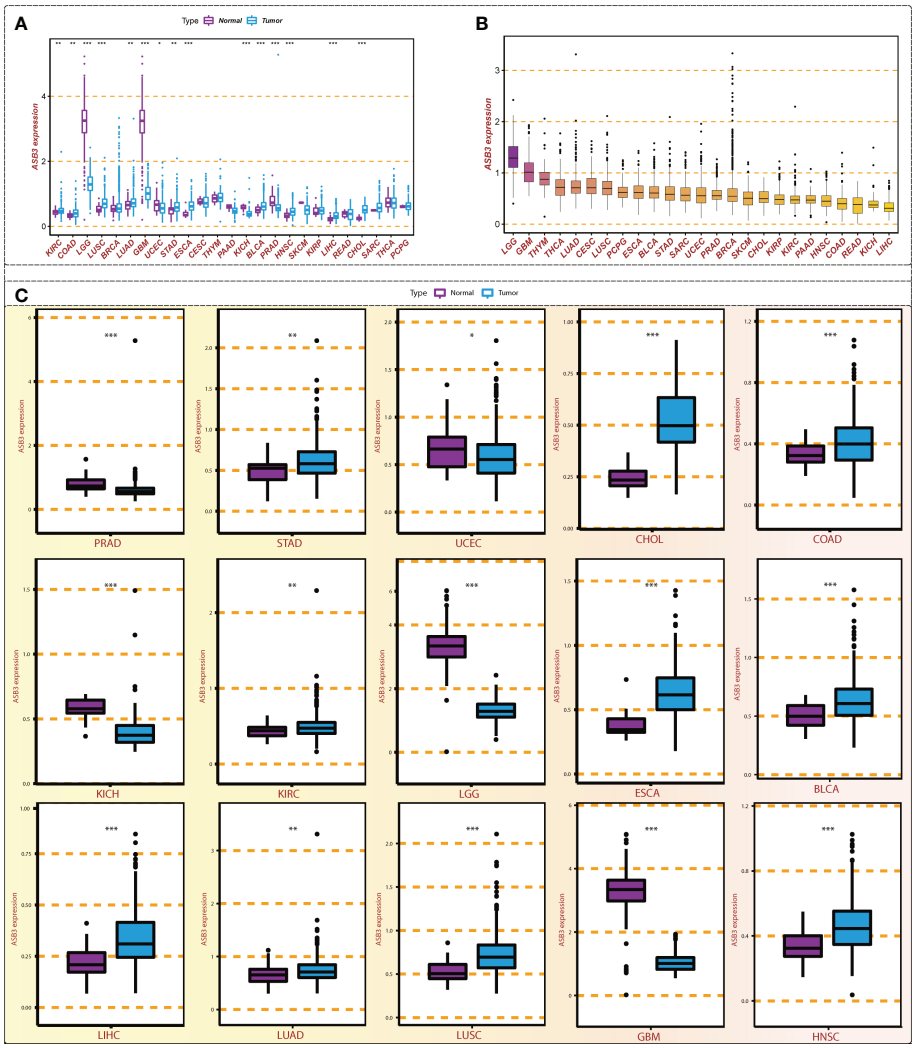

FIGURE 2
Expression level of ASB3 in pan-cancer. **(A)** ASB3 is abnormally expressed in different cancer types, up-regulated in 10 cancer types and down-regulated in 5 cancer types. **(B)** The level of ASB3 in pan-cancer, LGG and GBM have the highest level. **(C)** Box plots showing the significant different expression distribution of ASB3 across tumor and normal samples in 15 cancer types. *$P < 0.05$, **$P < 0.01$, ***$P < 0.001$.

Correlation between ASB3 and immune microenvironment of GBM

The correlation between ASB3 and pan-cancer immune microenvironment was shown by heat map (Figures S3A, S4A). In GBM, ASB3 was positively related with effector memory T cells (TEM) (r = 0.24), and negatively related with regulatory T cells (Tregs) (r = -0.379) (Figures S3B, C). ASB3 was negatively correlated with immunosuppressors TGFB1 (Transforming Growth Factor Beta 1) (r = -0.411) and PD-1 (Programmed Cell Death 1) (r = -0.263) (Figures S4B, C). The expression of ASB3 was negatively correlated with FOXP3 both in TCGA (r = -0.345) and CGGA (r = -0.216) (Figures 5A, B). ASB3 level was significantly negatively associated with Tregs and cancer-associated fibroblasts (CAFs) (Figure 5C). More than that, the results of ESTIMATE analysis demonstrated ASB3 in GBM were negatively correlated with immune score (r = -0.24) and stromal score (r = -0.35) in TCGA (Figures 6A, B). With data from our own RNA-seq, ASB3 was also negatively correlated with immune score (r = -0.61) and stromal score (r = -0.54) (Figures 6C, D). We were surprised to find that renal cell carcinoma patients with high ASB3 expression were more responsive to anti-PD-1 targeted therapy (Figure S7).

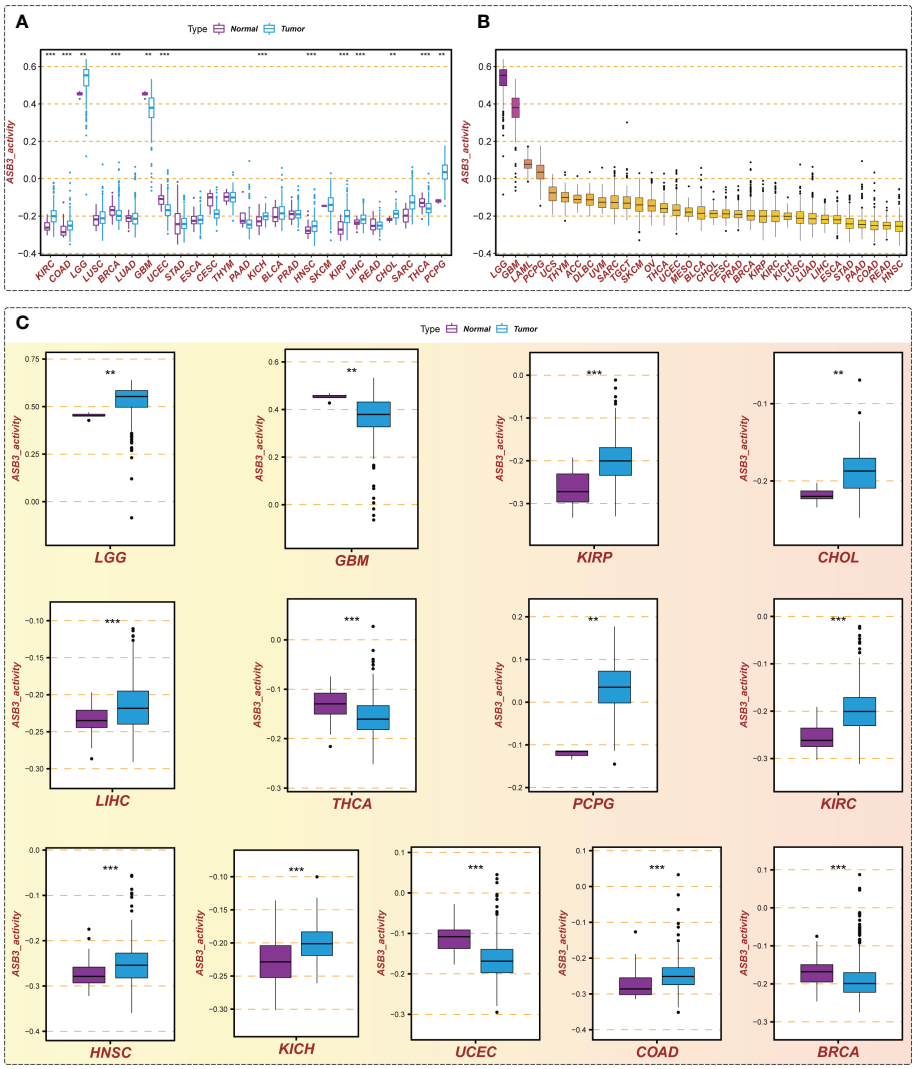

FIGURE 3
Gene activity of ASB3 in pan-cancer. **(A)** Comparison of ASB3 gene activity in a variety of cancers, increased in 9 cancer types and decreased in 4 cancer types. **(B)** The gene activity level of ASB3 in pan-cancer, LGG and GBM have the highest gene activity level. **(C)** Box plots showing the significant different activity of ASB3 across tumor and normal sample in 13 cancer types. $^{**}P < 0.01$, $^{***}P < 0.001$.

Functional enrichment analysis of ASB3 in GBM

In the GSEA analysis of ASB3 related signaling pathways, we defined the ASB3 high expression group as 'benign' and the low expression group as 'malignant'. The results showed that Oxidative Phosphorylation, Chemokine Activity, T Cell Differentiation, Immune Receptor Activity, Extracellular Matrix Structural Constituent and Collagen Fibril Organization were significantly enriched in GSEA GO terms (Figure 7). Focal Adhesion, Antigen Processing and Presentation, JAK STAT Signaling Pathway, Chemokine Signaling Pathway, Oxidative Phosphorylation and Cytokine-Cytokine Receptor Interaction were significantly enriched in GSEA KEGG terms (Figure 8). With data from our own RNA-seq, GSEA GO analysis demonstrated that B Cell Mediated Immunity, Cytokine Activity, Immunoglobulin Receptor Binding, Humoral Immune Response Mediated by Circulating Immunoglobulin, Antigen Binding and Complement Activation were significantly enriched (Figure S5). Toll Like Receptor Signaling Pathway, Lysosome, Chemokine Signaling Pathway, Cytokine-Cytokine Receptor Interaction, Cell Adhesion Molecules CAMS and Primary

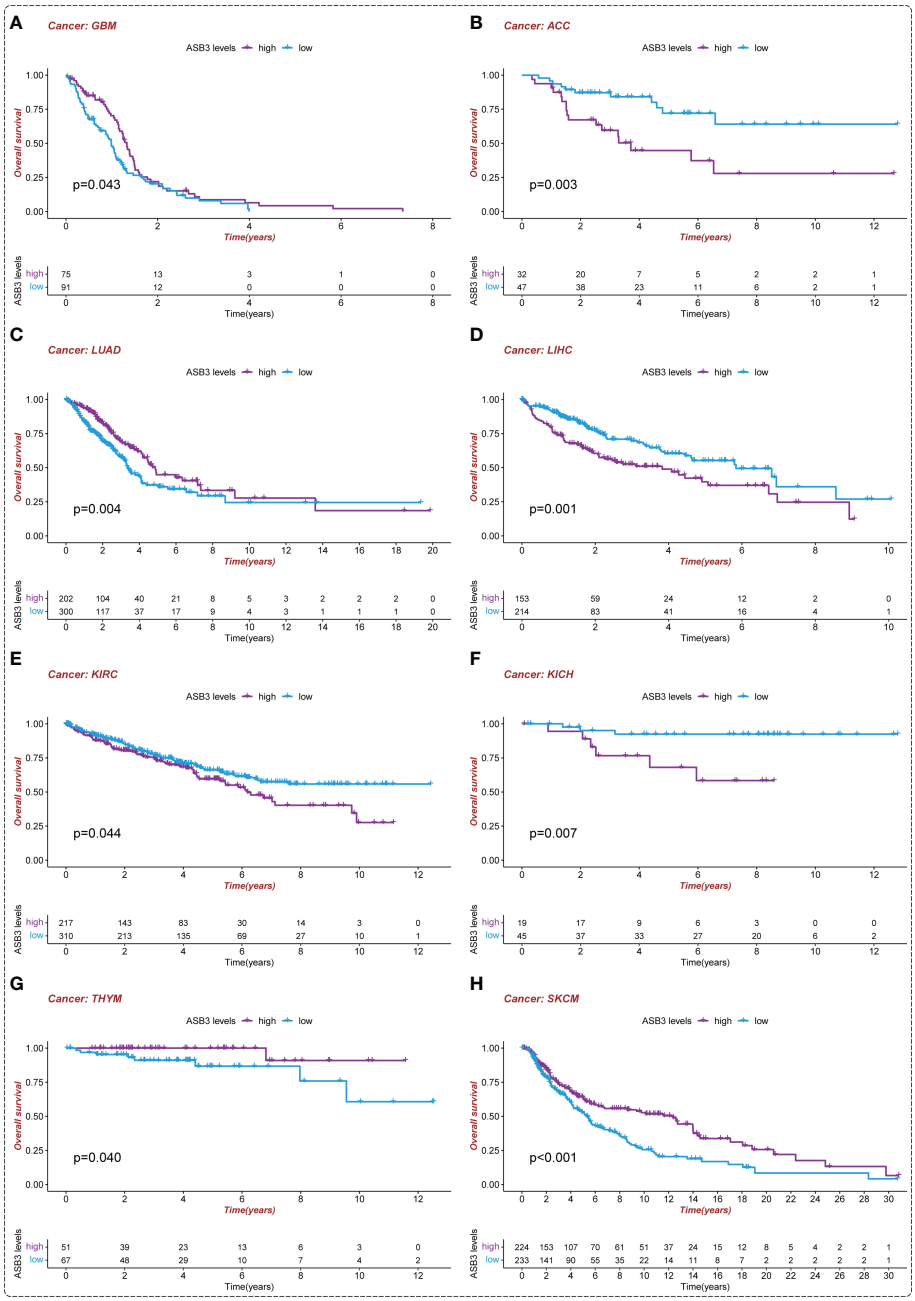

FIGURE 4
Kaplan-Meier survival analysis of ASB3 in pan-cancer. **(A)** The overall Kaplan-Meier survival analysis for ASB3 in GBM, **(B)** ACC, **(C)** LUAD, **(D)** LIHC, **(E)** KIRC, **(F)** KICH, **(G)** THYM and **(H)** SKCM.

Immunodeficiency were significantly enriched in GSEA KEGG analysis (Figure S6). Gene functions such as Regulation of Cell Adhesion, Cytokine Signaling in Immune System and Extracellular Matrix Organization were identified by PPI (Figures 9A, B). PPI network and MCODE components designed by the gene lists were shown in Figures 9C, D.

ASB3 overexpression reduced the proportion of Tregs *in vivo*

We constructed ASB3 overexpression lentiviral plasmid to obtain stable ASB3 overexpression GL261 cell line. The overexpression was verified by RT-qPCR, western blotting and

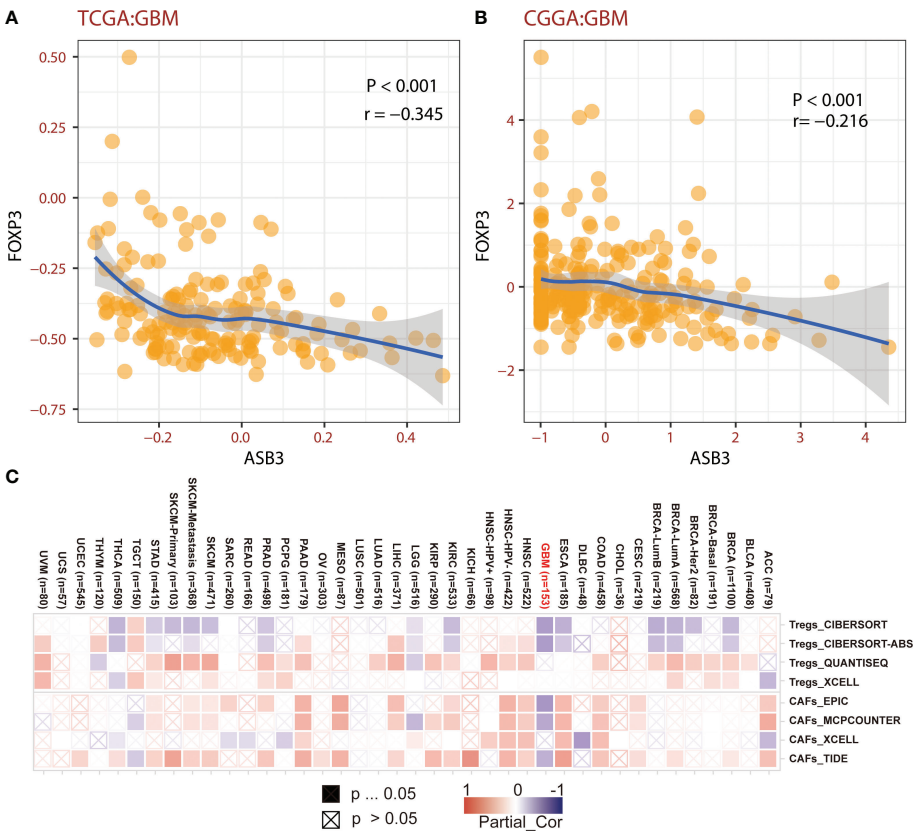

FIGURE 5
The correlation of ASB3 and Tregs. **(A)** Correlation coefficient of ASB3 and FOXP3 in TCGA GBM data. **(B)** Correlation coefficient of ASB3 and FOXP3 in CGGA GBM data. **(C)** Correlation heatmap of ASB3 and Tregs or CAFs in pan-cancer.

immunohistochemistry (Figures 10A, B, D). Orthotopic tumor models were established using normal GL261 cells and ASB3 overexpression GL261 cells, respectively. At the end of survival, tumors were analyzed by immunohistochemistry and TILs were harvested for flow cytometry (Figure 10C). We found that the Tregs/Tconv and Tregs/$CD8^+$ ratios were significantly decreased in ASB3 overexpression cell model (Figures 10E, F). The negative correlation between ASB3 expression and Tregs was confirmed with *in vivo* experiments.

Discussion

Targeting protein degradation has been proven to be a valid strategy for cancer treatment, several components of the UPS have shown to be potential anticancer targets (22). E3s are pivotal components in ubiquitination reactions because they strictly control substrate specificity and affinity (23). E3s are closely related to tumorigenesis owing to they regulate tumor suppressors and oncogenes (24). Therefore, the substrate specificity of E3s indicates that they are promising targets of anticancer drugs (25). The association between ASB family proteins and cancers has been reported previously. Inhibition of ASB4 in PLC and MHCC97-L HCC cells hindered cell migration and invasion, when ASB4 regulated by miR-200a was ectopically expressed in Hep3B HCC cells, the enhanced migration rate was measured (26). Transfection with hASB-8 cDNA truncation mutant lacking SOCS box could suppress the cell growth of SPC-A1 cells, which indicates that this gene might be related to the development of lung adenocarcinoma (27). ASB9 expression status was an independent prognostic factor for CRC overall survival in multivariate analysis and its siRNA transfected cells showed significant high invasiveness (28).

Previous research has shown that ASB3 is a biomarker for HCC and CRC (12, 13), but little is known about its role in other cancer types to date. In this study, we performed a comprehensive

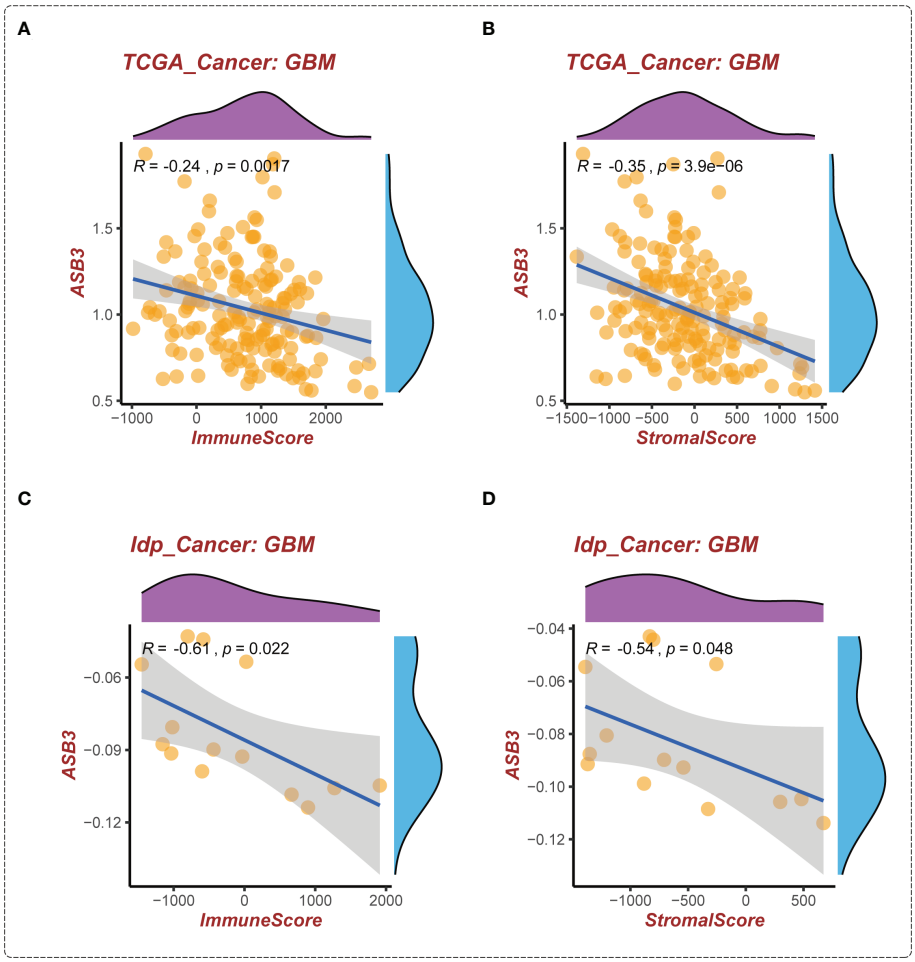

FIGURE 6
The correlation of ASB3 expression and TME in GBM. **(A)** Correlation between ASB3 and immune score in TCGA GBM data. **(B)** Correlation between ASB3 and stromal score in TCGA GBM data. **(C)** Correlation between ASB3 and immune score in independent GBM data. **(D)** Correlation between ASB3 and stromal score in independent GBM data.

bioinformatics analysis using patient data from different databases to determine the functional role of ASB3 in a variety of cancers. Among the 25 cancer types containing normal tissues, the expression of ASB3 in 15 cancer types between normal tissues and tumors was statistically significant. We found that the expression trend of ASB3 in multiple tumors was inconsistent. This situation also widely exists in other genes, which may be related to tissue specificity and TME (29, 30). ASB3 has the highest gene expression and activity in both LGG and GBM in this analysis. The KM survival curve of GBM using TCGA data clearly demonstrated that low ASB3 expression was linked to poor prognosis. We also explored the effect of ASB3 on the GBM clinical features, and the results showed that the expression of ASB3 in GBM patients with IDH mutations was higher than those with IDH wild-type, while the IDH mutations were considered to be crucial for better determining the prognosis (31). Moreover, the level of ASB3 was also distinctness in different pathological subtypes of GBM. The above results are sufficient to illustrate that ASB3 was a potential prognostic biomarker in various cancers types, especially in GBM.

In recent years, cancer immunotherapy has shown prominent clinical effects by recovering the ability of the immune system to recognize and destruct tumor cells, but only for a few tumors (32). Tumor-infiltrating immune cells play important roles in the TME, which not only provide a suitable microenvironment for the survival of tumor cells, but also are connected to the regulation of tumor immune surveillance and the response of tumor treatment (33, 34). Due to the crucial role of the immune system in protecting and battling tumors, we concentrated on the effect of ASB3 on

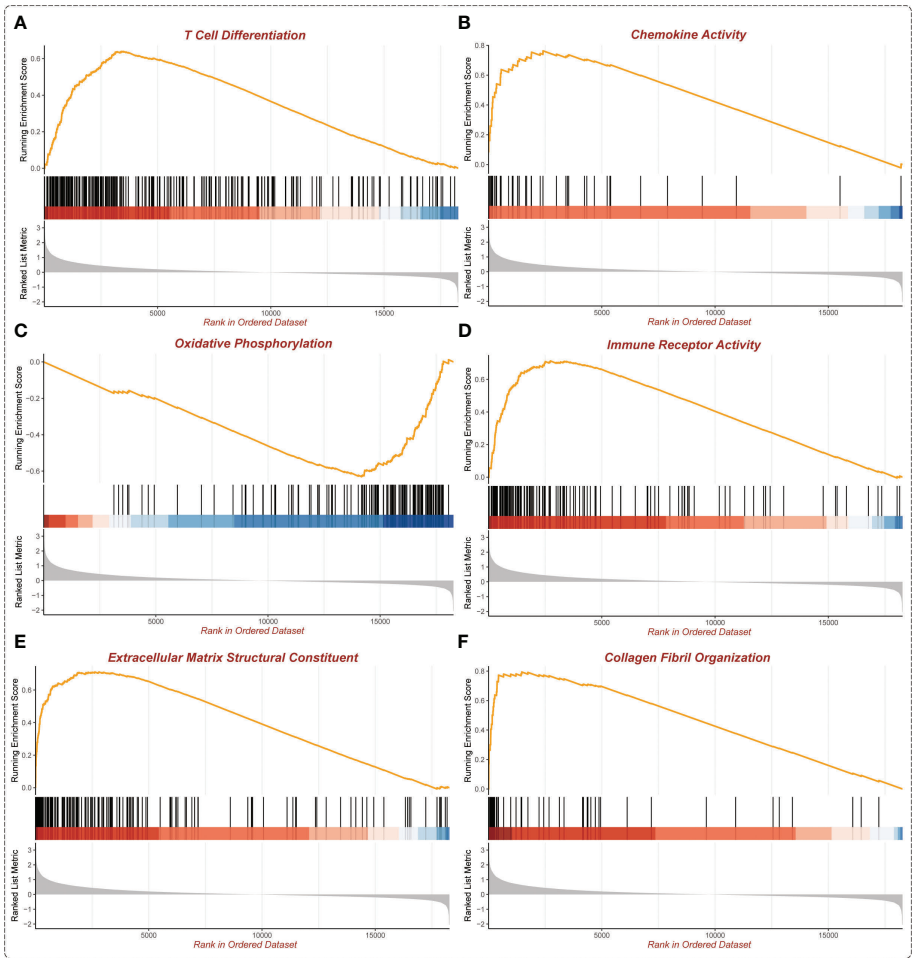

FIGURE 7
Enrichment plots from GSEA GO (TCGA). **(A)** T Cell Differentiation. **(B)** Chemokine Activity. **(C)** Oxidative Phosphorylation. **(D)** Immune Receptor Activity. **(E)** Extracellular Matrix Structural Constituent. **(F)** Collagen Fibril Organization.

immunity. TMB is a promising pan-cancer immunotherapeutic predictive biomarker and can lead immunotherapy to the era of precision medicine (35, 36). MSI can predict sensitivity to ICIs therapy, especially PD-1/PD-L1 inhibitors (37). Our analysis showed that ASB3 expression was correlated with TMB in 8 cancer types and with MSI in 12 cancer types. The results indicated that ASB3 have a regulatory effect on tumor immunity of several cancer types. Consequently, ASB3 may be a potential biomarker to predict the response to immunotherapy in patients with malignant tumors.

GBM is a 'cold' tumor due to the low number of immunoregulatory cells and high levels of immunosuppressive cells, thus it is considered to be highly resistant to immunotherapy (38). Due to the particularity of TIME, the research of GBM immunotherapy has become a major topic. By the analysis of multiple databases, we found that ASB3 was negatively correlated with Tregs, CAFs, TGFB1 and PD-1 in GBM. These factors produce a marked effect on inhibiting anti-tumor immune response and promoting tumor genesis and development in the TME. Tregs are recognized immunosuppressive cells, which can hamper protective immunosurveillance of neoplasia and hinder the effective anti-tumor immune response of tumor hosts, thereby promoting the development and progression of tumors (39, 40). Animal experiment results showed that ASB3 overexpression could reduce the proportion of Tregs in TILs. The mechanism may be related to the inhibition of TNFR2, which needs further study (14, 41). CAFs are a stromal cell population and the most important parts of the TME, activated CAFs can promote tumor growth, angiogenesis, invasion and metastasis, along with extracellular

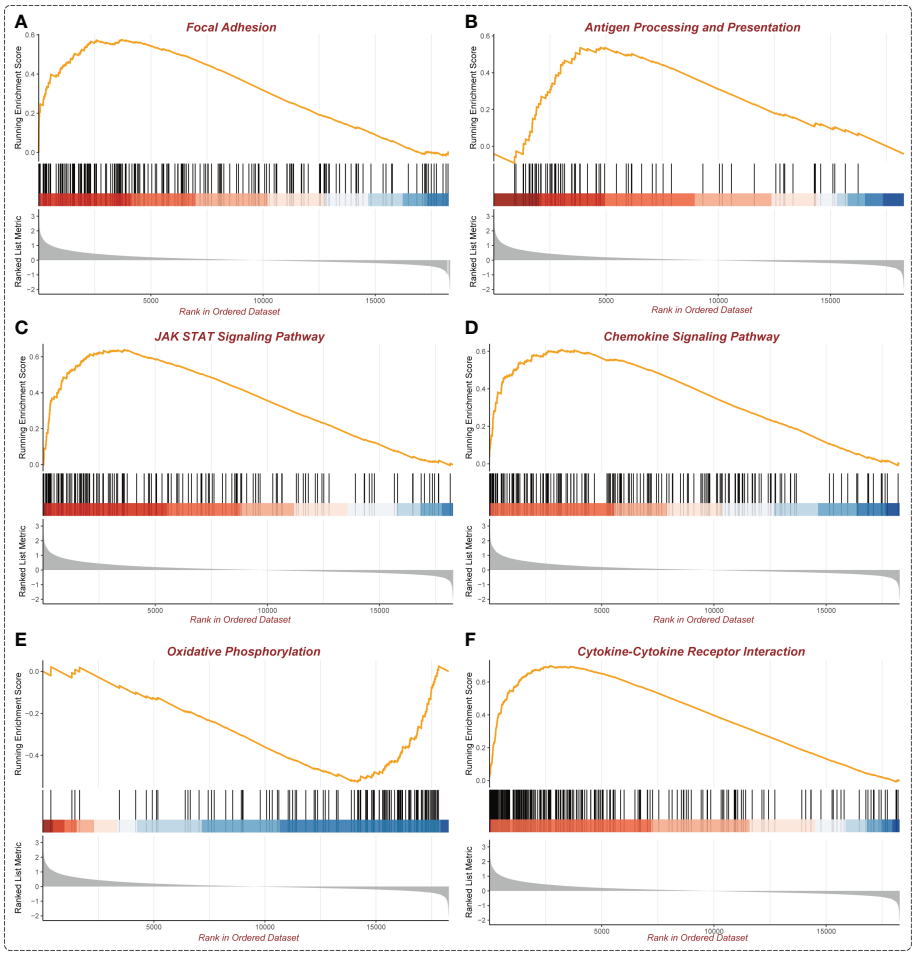

FIGURE 8
Enrichment plots from GSEA KEGG (TCGA). **(A)** Focal Adhesion. **(B)** Antigen Processing and Presentation. **(C)** JAK STAT Signaling Pathway. **(D)** Chemokine Signaling Pathway. **(E)** Oxidative Phosphorylation. **(F)** Cytokine-Cytokine Receptor interaction.

matrix (ECM) remodeling and even chemical resistance (42, 43). TGFB1 can suppress the generation, differentiation and function of effector T cells, induce Tregs to enter the TME and prevent the maturation of Dendritic cells (DCs) (44, 45). Antibodies targeting PD-1 or its ligand PD-L1 rescue T cells from exhausted status and restore immune response against cancer cells (46, 47). Ubiquitination and deubiquitination of PD-1/PD-L1 play important roles in the regulation of PD-1/PD-L1 protein stability and dynamics (48). To sum up, it can be inferred that ASB3 can be used as a potential indicator for GBM immunotherapy, which is helpful for individualized treatment.

The GSEA results suggested that ASB3 was closely linked to many important cancer and immune signaling pathways, mainly including cytokine, chemokine, antigen processing and presentation, focal adhesion and oxidative phosphorylation. The complex and dynamic interactions of the secreted cytokines, chemokines, growth factors, and their receptors mediate chronic inflammation and immunosuppressive TME, which contributes to the progression, metastasis and reduced response to treatment of tumors include GBM (49, 50). Antigen processing and presentation is a complex process that can be used by tumors to escape immune recognition. These mechanisms include the regulation of antigen expression, the surface level of HLA-I, and the changes of antigen processing and presentation mechanism in tumor cells (51, 52). Focal adhesion is a multifunctional organelle that mediates cell ECM adhesion, cytoskeleton regulation and signal transduction (53). Focal adhesion kinase (FAK) is a protein that mainly regulates adhesion signal transduction and cell migration. Researchers found that the activity of FAK was elevated in PDAC, and

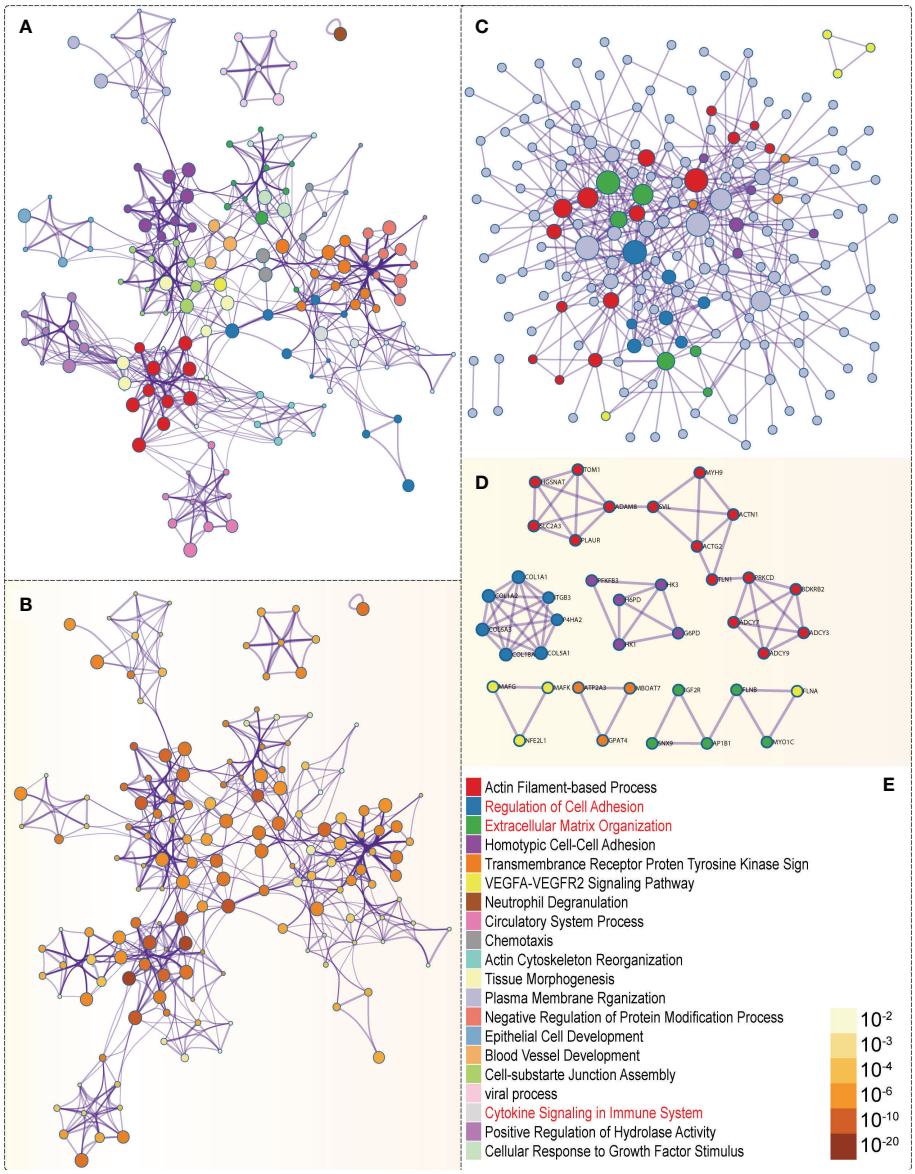

FIGURE 9
PPI network and mRNA enrichment terms negatively correlated with ASB3. **(A)** Colored by cluster ID. **(B)** Colored by P-value. **(C)** PPI network. **(D)** MCODE components. **(E)** Legend of Figure 9.

related with low $CD8^+$ T cell infiltration and high fibrosis (54, 55). Previous study has found that HIF-1α acts as a metabolic switch for Tregs between glycolytic-driven migration and oxidative phosphorylation-driven immunosuppression in GBM (56). Our study discovered that the level of oxidative phosphorylation in 'malignant' group decreased. This implies that the effect of ASB3 on immune microenvironment might be *via* regulating metabolism.

In summary, our results indicated that ASB3 was aberrantly expressed in various cancers and significantly correlated with the prognosis of cancer patients. For different cancers, ASB3 expression will bring different prognosis outcomes, which is necessary to further study the specific role of ASB3 in each cancer. The level of ASB3 was related to the TMB, MSI and immune cell infiltration in some cancer types. ASB3 expression showed closely connect with the

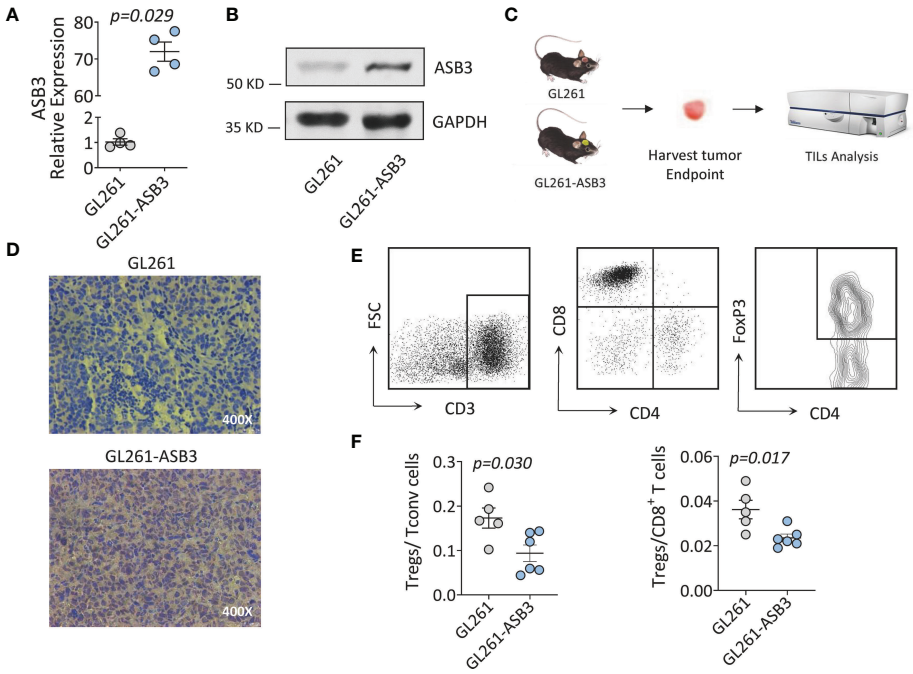

FIGURE 10
The Immunological functions of ASB3 *in vivo*. **(A)** ASB3 overexpression verification at mRNA level in GL261. **(B)** ASB3 overexpression verification at protein level in GL261. **(C)** Flow chart of mice experiments. Harvesting tumor derived TILs at the end of survival period for flow cytometry analysis. **(D)** ASB3 expression was detected by immunohistochemical in mice tumors at the end of survival. **(E)** Lymphocyte grouping in TILs. Phenotypical analysis was carried out by sequentially gating live cells, $CD3^+$ T cells, $CD8^+$ T cells, $CD4^+$ T cells and $FOXP3^+$ T cells. **(F)** The ratios of Tregs ($CD3^+$ $CD4^+$ $FOXP3^+$)/Tconv ($CD3^+$ $CD4^+$ $FOXP3^-$) and Tregs ($CD3^+$ $CD4^+$ $FOXP3^+$)/$CD8^+$ T cells in TILs.

infiltration of immune cells into the TME in GBM, and it had been preliminarily verified in the mice model. ASB3 was identified as a promising biomarker for the prognosis prediction of GBM, and it could provide a reference for the realization of more precise and individualized immunotherapy in the future.

Data availability statement

The datasets presented in this study can be found in online repositories. The names of the repository/repositories and accession number(s) can be found in the article/Supplementary Material.

Ethics statement

The studies involving human participants were reviewed and approved by the Ethics Committee of the First Affiliated Hospital of Harbin Medical University. The patients/participants provided their written informed consent to participate in this study. Written informed consent was obtained from the individual(s) for the publication of any potentially identifiable images or data included in this article.

Author contributions

ZH and SY jointly performed the analysis of the bioinformatics section. LM and AW collected the glioma samples and performed the cell and animal experiments. DC participated in the design of the follow-up experimental scheme and language correction of the article. SK, YG, LX and AL took part in data analysis and figure drawing. YL and RS designed the experiment and participated in all parts of this study. All authors contributed to the article and approved the submitted version.

Funding

This study was supported by the National Natural Science Foundation of China (Grant No. 82002644 and 82001131), the Natural Science Foundation of Heilongjiang Province (Grant No. YQ2021H018), Outstanding Medical Fund for Young Scholar of the First Affiliated Hospital of Harbin Medical University (Grant No. HYD2020YQ0016 and HYD2020YQ0022), Medical and Health Research Program of Heilongjiang Province (Grant No. 2020-129), Young Innovative Talents Fund of the Regular Institutions of Higher Education of Heilongjiang Province (Grant No. UNPYSCT-2020158) and the Heilongjiang Postdoctoral Foundation (Grant No. LBH-Z19189).

Acknowledgments

The authors would like to acknowledge Dr. Nagheme Thomas for her valuable help on this manuscript.

Conflict of interest

The authors declare that the research was conducted in the absence of any commercial or financial relationships that could be construed as a potential conflict of interest.

The reviewer MG declared a shared parent affiliation with the authors ZH, SY, AW, YG, LM, LX, AL, RS, and YL to the handling editor at the time of the review.

Publisher's note

All claims expressed in this article are solely those of the authors and do not necessarily represent those of their affiliated organizations, or those of the publisher, the editors and the reviewers. Any product that may be evaluated in this article, or claim that may be made by its manufacturer, is not guaranteed or endorsed by the publisher.

Supplementary material

The Supplementary Material for this article can be found online at: https://www.frontiersin.org/articles/10.3389/fimmu.2022.842524/full#supplementary-material

SUPPLEMENTARY FIGURE 1
The correlation of ASB3 expression and TMB or MSI in pan-cancer. **(A)** Correlation coefficient between ASB3 expression and TMB, positively in 5 cancer types and negatively in 3 cancer types. **(B)** Correlation coefficient between ASB3 expression and MSI, positively in 7 cancer types and negatively in 5 cancer types. $*P < 0.05$, $**P < 0.01$, $***P < 0.001$.

SUPPLEMENTARY FIGURE 2
The correlation analysis between ASB3 expression and clinical features of GBM. **(A)** IDH mutation status. **(B)** Subtypes of GBM. **(C)** Radiotherapy status. **(D)** MGMT promoter methylation status. **(E)** Chemotherapy status. **(F)** Age.

SUPPLEMENTARY FIGURE 3
The correlation of ASB3 expression and immune cell infiltration. **(A)** Correlation heatmap between ASB3 and immune cell infiltration in pan-cancer. **(B)** Spearman correlation test of ASB3 expression and TEM in GBM. **(C)** Spearman correlation test of ASB3 expression and Tregs in GBM.

SUPPLEMENTARY FIGURE 4
The correlation of ASB3 expression and immunosuppressors. **(A)** Correlation heatmap between ASB3 and immunosuppressors in pan-cancer. **(B)** Spearman correlation test of ASB3 expression and TGFB1 in GBM. **(C)** Spearman correlation test of ASB3 expression and PD-1 in GBM.

SUPPLEMENTARY FIGURE 5
Enrichment plots from GSEA GO (Independent cohort). **(A)** B Cell Mediated Immunity. **(B)** Cytokine Activity. **(C)** Immunoglobulin Receptor Binding. **(D)** Humoral Immune Response Mediated by Circulating Immunoglobulin. **(E)** Antigen Binding. **(F)** Complement Activation.

SUPPLEMENTARY FIGURE 6
Enrichment plots from GSEA KEGG (Independent cohort). **(A)** Toll Like Receptor Signaling Pathway. **(B)** Lysosome. **(C)** Chemokine Signaling Pathway. **(D)** Cytokine-Cytokine Receptor Interaction. **(E)** Cell Adhesion Molecules CAMS. **(F)** Primary Immunodeficiency.

SUPPLEMENTARY FIGURE 7
Correlation of ASB3 expression and immunotherapy response in human renal cell carcinoma.

References

1. Bray F, Laversanne M, Weiderpass E, Soerjomataram I. The ever-increasing importance of cancer as a leading cause of premature death worldwide. *Cancer* (2021) 127(16):3029–30. doi: 10.1002/cncr.33587

2. Siegel RL, Miller KD, Fuchs HE, Jemal A. Cancer statistics, 2022. *CA Cancer J Clin* (2022) 72(1):7–33. doi: 10.3322/caac.21708

3. Low JT, Ostrom QT, Cioffi G, Neff C, Waite KA, Kruchko C, et al. Primary brain and other central nervous system tumors in the united states (2014-2018): A summary of the cbtrus statistical report for clinicians. *Neurooncol Pract* (2022) 9 (3):165–82. doi: 10.1093/nop/npac015

4. Tan AC, Ashley DM, Lopez GY, Malinzak M, Friedman HS, Khasraw M. Management of glioblastoma: State of the art and future directions. *CA Cancer J Clin* (2020) 70(4):299–312. doi: 10.3322/caac.21613

5. Ribas A, Wolchok JD. Cancer immunotherapy using checkpoint blockade. *Science* (2018) 359(6382):1350–5. doi: 10.1126/science.aar4060

6. Li MO, Wolf N, Raulet DH, Akkari L, Pittet MJ, Rodriguez PC, et al. Innate immune cells in the tumor microenvironment. *Cancer Cell* (2021) 39(6):725–9. doi: 10.1016/j.ccell.2021.05.016

7. Bagchi S, Yuan R, Engleman EG. Immune checkpoint inhibitors for the treatment of cancer: Clinical impact and mechanisms of response and resistance. *Annu Rev Pathol* (2021) 16:223–49. doi: 10.1146/annurev-pathol-042020-042741

8. Sampson JH, Gunn MD, Fecci PE, Ashley DM. Brain immunology and immunotherapy in brain tumours. *Nat Rev Cancer* (2020) 20(1):12–25. doi: 10.1038/s41568-019-0224-7

9. Jin WL, Mao XY, Qiu GZ. Targeting deubiquitinating enzymes in glioblastoma multiforme: Expectations and challenges. *Med Res Rev* (2017) 37 (3):627–61. doi: 10.1002/med.21421

10. Kohroki J, Nishiyama T, Nakamura T, Masuho Y. Asb proteins interact with Cullin5 and Rbx2 to form E3 ubiquitin ligase complexes. *FEBS Lett* (2005) 579 (30):6796–802. doi: 10.1016/j.febslet.2005.11.016

11. Kile BT, Viney EM, Willson TA, Brodnicki TC, Cancilla MR, Herlihy AS, et al. Cloning and characterization of the genes encoding the ankyrin repeat and socs box-containing proteins asb-1, asb-2, asb-3 and asb-4. *Gene* (2000) 258(1-2):31–41. doi: 10.1016/s0378-1119(00)00402-9

12. Zhang W, Liu F, Che Z, Wu M, Tang Z, Liu J, et al. Asb3 knockdown promotes mitochondrial apoptosis *via* activating the interdependent cleavage of Beclin1 and caspase-8 in hepatocellular carcinoma. *Sci China Life Sci* (2019) 62 (12):1692–702. doi: 10.1007/s11427-018-9505-0

13. Du WY, Lu ZH, Ye W, Fu X, Zhou Y, Kuang CM, et al. The loss-of-Function mutations and down-regulated expression of Asb3 gene promote the growth and metastasis of colorectal cancer cells. *Chin J Cancer* (2017) 36(1):11. doi: 10.1186/s40880-017-0180-0

14. Chung AS, Guan YJ, Yuan ZL, Albina JE, Chin YE. Ankyrin repeat and socs box 3 (Asb3) mediates ubiquitination and degradation of tumor necrosis factor receptor ii. *Mol Cell Biol* (2005) 25(11):4716–26. doi: 10.1128/MCB.25.11.4716-4726.2005

15. Gao T, Liu Z, Wang Y, Cheng H, Yang Q, Guo A, et al. Uucd: A family-based database of ubiquitin and ubiquitin-like conjugation. *Nucleic Acids Res* (2013) 41(Database issue):D445–51. doi: 10.1093/nar/gks1103

16. Zhou J, Xu Y, Lin S, Guo Y, Deng W, Zhang Y, et al. Iuucd 2.0: An update with rich annotations for ubiquitin and ubiquitin-like conjugations. *Nucleic Acids Res* (2018) 46(D1):D447–D53. doi: 10.1093/nar/gkx1041

17. Yoshihara K, Shahmoradgoli M, Martinez E, Vegesna R, Kim H, Torres-Garcia W, et al. Inferring tumour purity and stromal and immune cell admixture from expression data. *Nat Commun* (2013) 4:2612. doi: 10.1038/ncomms3612

18. Ru B, Wong CN, Tong Y, Zhong JY, Zhong SSW, Wu WC, et al. Tisidb: An integrated repository portal for tumor-immune system interactions. *Bioinformatics* (2019) 35(20):4200–2. doi: 10.1093/bioinformatics/btz210

19. Li T, Fan J, Wang B, Traugh N, Chen Q, Liu JS, et al. Timer: A web server for comprehensive analysis of tumor-infiltrating immune cells. *Cancer Res* (2017) 77 (21):e108–e10. doi: 10.1158/0008-5472.CAN-17-0307

20. Subramanian A, Tamayo P, Mootha VK, Mukherjee S, Ebert BL, Gillette MA, et al. Gene set enrichment analysis: A knowledge-based approach for interpreting genome-wide expression profiles. *Proc Natl Acad Sci U.S.A.* (2005) 102(43):15545–50. doi: 10.1073/pnas.0506580102

21. Mootha VK, Lindgren CM, Eriksson KF, Subramanian A, Sihag S, Lehar J, et al. Pgc-1alpha-Responsive genes involved in oxidative phosphorylation are coordinately downregulated in human diabetes. *Nat Genet* (2003) 34(3):267–73. doi: 10.1038/ng1180

22. Yang H, Chen X, Li K, Cheaito H, Yang Q, Wu G, et al. Repurposing old drugs as new inhibitors of the ubiquitin-proteasome pathway for cancer treatment. *Semin Cancer Biol* (2021) 68:105–22. doi: 10.1016/j.semcancer.2019.12.013

23. Zheng N, Shabek N. Ubiquitin ligases: Structure, function, and regulation. *Annu Rev Biochem* (2017) 86:129–57. doi: 10.1146/annurev-biochem-060815-014922

24. Senft D, Qi J, Ronai ZA. Ubiquitin ligases in oncogenic transformation and cancer therapy. *Nat Rev Cancer* (2018) 18(2):69–88. doi: 10.1038/nrc.2017.105

25. Wang D, Ma L, Wang B, Liu J, Wei W. E3 ubiquitin ligases in cancer and implications for therapies. *Cancer Metastasis Rev* (2017) 36(4):683–702. doi: 10.1007/s10555-017-9703-z

26. Au V, Tsang FH, Man K, Fan ST, Poon RT, Lee NP. Expression of ankyrin repeat and socs box containing 4 (Asb4) confers migration and invasion properties of hepatocellular carcinoma cells. *Biosci Trends* (2014) 8(2):101–10. doi: 10.5582/bst.8.101

27. Liu Y, Li J, Zhang F, Qin W, Yao G, He X, et al. Molecular cloning and characterization of the human asb-8 gene encoding a novel member of ankyrin repeat and socs box containing protein family. *Biochem Biophys Res Commun* (2003) 300(4):972–9. doi: 10.1016/s0006-291x(02)02971-6

28. Tokuoka M, Miyoshi N, Hitora T, Mimori K, Tanaka F, Shibata K, et al. Clinical significance of Asb9 in human colorectal cancer. *Int J Oncol* (2010) 37 (5):1105–11. doi: 10.3892/ijo_00000762

29. Lou W, Wang W, Chen J, Wang S, Huang Y. Ncrnas-mediated high expression of Sema3f correlates with poor prognosis and tumor immune infiltration of hepatocellular carcinoma. *Mol Ther Nucleic Acids* (2021) 24:845–55. doi: 10.1016/j.omtn.2021.03.014

30. Gobin E, Bagwell K, Wagner J, Mysona D, Sandirasegarane S, Smith N, et al. A pan-cancer perspective of matrix metalloproteases (Mmp) gene expression profile and their Diagnostic/Prognostic potential. *BMC Cancer* (2019) 19(1):581. doi: 10.1186/s12885-019-5768-0

31. D'Alessio A, Proietti G, Sica G, Scicchitano BM. Pathological and molecular features of glioblastoma and its peritumoral tissue. *Cancers (Basel)* (2019) 11 (4):469. doi: 10.3390/cancers11040469

32. Wang ZL, Wang Z, Li GZ, Wang QW, Bao ZS, Zhang CB, et al. Immune cytolytic activity is associated with genetic and clinical properties of glioma. *Front Immunol* (2019) 10:1756. doi: 10.3389/fimmu.2019.01756

33. Bader JE, Voss K, Rathmell JC. Targeting metabolism to improve the tumor microenvironment for cancer immunotherapy. *Mol Cell* (2020) 78(6):1019–33. doi: 10.1016/j.molcel.2020.05.034

34. Zeng D, Li M, Zhou R, Zhang J, Sun H, Shi M, et al. Tumor microenvironment characterization in gastric cancer identifies prognostic and immunotherapeutically relevant gene signatures. *Cancer Immunol Res* (2019) 7 (5):737–50. doi: 10.1158/2326-6066.CIR-18-0436

35. Fumet JD, Truntzer C, Yarchoan M, Ghiringhelli F. Tumour mutational burden as a biomarker for immunotherapy: Current data and emerging concepts. *Eur J Cancer* (2020) 131:40–50. doi: 10.1016/j.ejca.2020.02.038

36. Steuer CE, Ramalingam SS. Tumor mutation burden: Leading immunotherapy to the era of precision medicine? *J Clin Oncol* (2018) 36(7):631–2. doi: 10.1200/JCO.2017.76.8770

37. Amato M, Franco R, Facchini G, Addeo R, Ciardiello F, Berretta M, et al. Microsatellite instability: From the implementation of the detection to a prognostic and predictive role in cancers. *Int J Mol Sci* (2022) 23(15):8726. doi: 10.3390/ijms23158726

38. Salemizadeh Parizi M, Salemizadeh Parizi F, Abdolhosseini S, Vanaei S, Manzouri A, Ebrahimzadeh F. Myeloid-derived suppressor cells (Mdscs) in brain cancer: Challenges and therapeutic strategies. *Inflammopharmacology* (2021) 29 (6):1613–24. doi: 10.1007/s10787-021-00878-9

39. Togashi Y, Shitara K, Nishikawa H. Regulatory T cells in cancer immunosuppression - implications for anticancer therapy. *Nat Rev Clin Oncol* (2019) 16(6):356–71. doi: 10.1038/s41571-019-0175-7

40. Tanaka A, Sakaguchi S. Regulatory T cells in cancer immunotherapy. *Cell Res* (2017) 27(1):109–18. doi: 10.1038/cr.2016.151

41. Moatti A, Debesset A, Pilon C, Beldi-Ferchiou A, Leclerc M, Redjoul R, et al. Tnfr2 blockade of regulatory T cells unleashes an antitumor immune response after hematopoietic stem-cell transplantation. *J Immunother Cancer* (2022) 10(4): e003508. doi: 10.1136/jitc-2021-003508

42. Mao X, Xu J, Wang W, Liang C, Hua J, Liu J, et al. Crosstalk between cancer-associated fibroblasts and immune cells in the tumor microenvironment: New findings and future perspectives. *Mol Cancer* (2021) 20(1):131. doi: 10.1186/s12943-021-01428-1

43. Chen X, Song E. Turning foes to friends: Targeting cancer-associated fibroblasts. *Nat Rev Drug Discovery* (2019) 18(2):99–115. doi: 10.1038/s41573-018-0004-1

44. Woo SR, Corrales L, Gajewski TF. Innate immune recognition of cancer. *Annu Rev Immunol* (2015) 33:445–74. doi: 10.1146/annurev-immunol-032414-112043

45. de Streel G, Lucas S. Targeting immunosuppression by tgf-Beta1 for cancer immunotherapy. *Biochem Pharmacol* (2021) 192:114697. doi: 10.1016/j.bcp.2021.114697

46. Yi M, Zheng X, Niu M, Zhu S, Ge H, Wu K. Combination strategies with pd-1/Pd-L1 blockade: Current advances and future directions. *Mol Cancer* (2022) 21 (1):28. doi: 10.1186/s12943-021-01489-2

47. Zhang H, Dai Z, Wu W, Wang Z, Zhang N, Zhang L, et al. Regulatory mechanisms of immune checkpoints pd-L1 and ctla-4 in cancer. *J Exp Clin Cancer Res* (2021) 40(1):184. doi: 10.1186/s13046-021-01987-7

48. Hu X, Wang J, Chu M, Liu Y, Wang ZW, Zhu X. Emerging role of ubiquitination in the regulation of pd-1/Pd-L1 in cancer immunotherapy. *Mol Ther* (2021) 29(3):908–19. doi: 10.1016/j.ymthe.2020.12.032

49. Bhat AA, Nisar S, Maacha S, Carneiro-Lobo TC, Akhtar S, Siveen KS, et al. Cytokine-chemokine network driven metastasis in esophageal cancer; promising avenue for targeted therapy. *Mol Cancer* (2021) 20(1):2. doi: 10.1186/s12943-020-01294-3

50. Broekman ML, Maas SLN, Abels ER, Mempel TR, Krichevsky AM, Breakefield XO. Multidimensional communication in the microenvirons of glioblastoma. *Nat Rev Neurol* (2018) 14(8):482–95. doi: 10.1038/s41582-018-0025-8

51. Jhunjhunwala S, Hammer C, Delamarre L. Antigen presentation in cancer: Insights into tumour immunogenicity and immune evasion. *Nat Rev Cancer* (2021) 21(5):298–312. doi: 10.1038/s41568-021-00339-z

52. Lee MY, Jeon JW, Sievers C, Allen CT. Antigen processing and presentation in cancer immunotherapy. *J Immunother Cancer* (2020) 8(2):e001111. doi: 10.1136/jitc-2020-001111

53. Kanchanawong P, Shtengel G, Pasapera AM, Ramko EB, Davidson MW, Hess HF, et al. Nanoscale architecture of integrin-based cell adhesions. *Nature* (2010) 468(7323):580–4. doi: 10.1038/nature09621

54. Dawson JC, Serrels A, Stupack DG, Schlaepfer DD, Frame MC. Targeting fak in anticancer combination therapies. *Nat Rev Cancer* (2021) 21(5):313–24. doi: 10.1038/s41568-021-00340-6

55. Jiang H, Hegde S, Knolhoff BL, Zhu Y, Herndon JM, Meyer MA, et al. Targeting focal adhesion kinase renders pancreatic cancers responsive to checkpoint immunotherapy. *Nat Med* (2016) 22(8):851–60. doi: 10.1038/nm.4123

56. Miska J, Lee-Chang C, Rashidi A, Muroski ME, Chang AL, Lopez-Rosas A, et al. Hif-1alpha is a metabolic switch between glycolytic-driven migration and oxidative phosphorylation-driven immunosuppression of tregs in glioblastoma. *Cell Rep* (2019) 27(1):226–37 e4. doi: 10.1016/j.celrep.2019.03.029

Frontiers in Immunology

Explores novel approaches and diagnoses to treat immune disorders.

The official journal of the International Union of Immunological Societies (IUIS) and the most cited in its field, leading the way for research across basic, translational and clinical immunology.

Discover the latest Research Topics

See more →

Frontiers

Avenue du Tribunal-Fédéral 34
1005 Lausanne, Switzerland
frontiersin.org

Contact us

+41 (0)21 510 17 00
frontiersin.org/about/contact